PIONEER AND INNOVATIVE STUDIES IN ENGINEERING

All Sciences Academy

PIONEER AND INNOVATIVE STUDIES IN ENGINEERING

Editor
Asst. Prof. Dr. Umut ÖZKAYA

Pioneer and Innovative Studies In Engineering
Editor: Asst. Prof. Dr. Umut ÖZKAYA

Design: All Sciences Academy Design
Published Date: December 2024
Publisher's Certification Number: 72273
ISBN: 978-625-5954-05-3

© All Sciences Academy

www.allsciencesacademy.com
allsciencesacademy@gmail.com

CONTENT

Investigation of Corrosion Behavior of Low Alloy Micro Steel

Yunus Emre DEMİR[1]
İbrahim GÜNEŞ[2]

1- Yunus Emre DEMİR; Department of Mechanical Engineering, Faculty of Engineering, Giresun University, Giresun, Türkiye. yunus.e.demir@hotmail.com ORCID No: 0000-0001-5568-0152
2- Prof. Dr. İbrahim GÜNEŞ; Department of Civil Engineering, Faculty of Engineering, Giresun University, Giresun, Türkiye. ibrahim.gunes@giresun.edu.tr ORCID No: 0000-0001-7595-0121

ABSTRACT

In this study, the corrosion resistance of Ni-B coated and uncoated microalloyed steel samples was investigated. Microalloyed steel samples were subjected to surface preparation processes before coating. Coating processes were carried out in solutions prepared with nickel chloride hexahydrate, sodium borohydride, sodium hydroxide, ethyleneamine and lead (II) nitride. While some samples were not subjected to heat treatment after coating, some samples were subjected to tempering at 250℃ for 5 hours and at 400℃ for 1 hour. Corrosion tests of coated samples were carried out in 0.1 M (Molar) HCl and H_2SO_4 acid solutions. Corrosion resistance and surface properties of samples after corrosion were examined by SEM and EDX analysis. When the corrosion behaviors of both Ni-B coated samples and samples tempered at different temperatures and times after Ni-B coating were compared, higher corrosion resistance was obtained compared to the untreated sample. In addition to higher corrosion losses in the untreated sample, a rougher surface was obtained by more erosion on the sample surfaces.

Keywords – Microalloyed Steel, Electroless Ni-B Coating, Surface Properties, Corrosion.

INTRODUCTION

Microalloyed steels, also known as HSLA are high-strength low-alloy steels. The production of microalloyed steels has been started since the 1960s for use in oil and gas pipelines. Today, these steels are widely used in pipelines carrying oil, natural gas, wastewater, automotive powertrains, suspension and engine parts, ship parts, truck, crane, tractor parts, cement mixing and storage containers, military vehicle equipment production, pressure vessels, and agricultural machinery production. Electroless nickel coatings are obtained as a result of the accumulation of nickel ions on the surfaces of samples immersed in a solution containing nickel salts by reducing them to nickel metal as a result of catalytic reactions. The most important advantage of electroless nickel coatings over electrolytic coatings, which are much more widely used in the coating sector, is that equal coating thickness can be achieved on the entire surface of the part since the process takes place in solution (Avcıoğlu, 2015; Riedel, 1989; Krishnan et al. 2006). Some studies in the literature are as follows. Mukhopadhyay et al. (2017) coated AISI 1040 steel with Ni-B-W and examined its corrosion behavior. They tempered some samples at 350 and 450℃ for 1 hour. The lowest corrosion rate was obtained in the sample tempered at 450℃ for 1 hour (Mukhopadhyay et al., 2017). In their study, Srinivasan et al. (2010) coated copper panels of (5x5 cm) and mild steel panels of (10x10 cm) with

electroless nickel boron in the bath at different deposition temperatures and ethylenediamine (complexing agent) concentration ratios. Some of the samples were tempered as Ni-B coated and some were tempered at 400℃ for 1 hour. They measured the hardness value of the tempered sample as 1102 $HV_{0.1}$ and 682 $HV_{0.1}$. The lowest weight loss after abrasion under 10 N load was obtained in the sample tempered at 400℃ for 1 hour. Corrosion resistance values were close to each other in both tempered and untempered samples (Srinivasan et al. 2010).

Arslan and Uzun (2021) boronized AISI 304L stainless steel at 850, 900 and 950 °C and corroded it in 2% HNO_3. They observed that the material loss after corrosion in boronized samples was lower than in the unboronized sample (Arslan and Uzun, 2021). Saklakoğlu et al. (2016) examined the corrosion behavior of AISI 304 and 316 stainless steel in HCl and H_2SO_4 solutions. They found that the highest weight loss in stainless steels after corrosion occurred in H_2SO_4 solution. They concluded that H_2SO_4 is more active than HCl acid and therefore corrodes stainless steels more (Saklakoğlu et al. 2016). Sarp et al. (2022) coated Ni-B on 6XXX series aluminum in the coating bath at different deposition times (30, 60 and 90 minutes) and obtained 10.8, 11.4 and 16.2 μm coating layers, respectively, depending on the deposition times. As a result of the corrosion test in 3.5% NaCl solution, the highest corrosion resistance was obtained in the Ni-B coating produced in 30 minutes (Sarp et al. 2022). Barati and Hadawi (2020) investigated the hardness, wear and corrosion behaviors by electroless Ni-B coating in acidic, neutral and basic PH baths. They obtained hardness values of approximately 1410 HV after coating and tempering at 400℃. They observed that the wear rates decreased in the samples with the increase of the tempering temperature. They stated that the coatings had lower friction and wear rates compared to the uncoated state and that the corrosion resistance of the samples increased after coating (Barati and Hadawi, 2020). Das and Sahoo (2012) investigated the effect of coating process parameters (bath temperature, Nickel source, annealing temperature) on the microhardness of electroless Ni-B coating by using Taguchi analysis. In the analyses performed after coating, they determined that the annealing temperature and reducing agent concentration had a significant effect on the hardness properties (885.80-1187.50 HV0.1) of electroless Ni-B coating and annealing process. They also stated in XRD analyses that the phase in which the Ni-B film was deposited was amorphous but became crystallized with heat treatment, and Ni, Ni_2B and Ni_3B phases were obtained in samples heat treated at 350 °C (Das and Sahoo, 2012). Shakoor et al. (2016) investigated the coating bath compositions and characterization techniques in Ni-B coatings. They used ($NiCl_2.6H_2O$) and ($NiSO_4.6H_2O$) as nickel sources and Dimethylamine borane (DMAB), sodium borohydride ($NaBH_4$) as reductants. They emphasized that these reductants have an important role on the deposition rate of NiB coating. They stated that complexing/reducing

agents with smaller fixed stability against nickel ion have higher coating layer deposition rates and that the optimum deposition rate is reached when the contribution rate of these agents is between 3-6% and the boron content in the coating decreases with the increase in the coating deposition rate (Shakoor et al. 2016).

MATERIAL AND METHODS

Material

In this study, 20x80 mm sized micro alloy steel containing 0.36% C, 0.28% Cr, 1.34% Mn, 0.60% Si, 0.09% V, 0.028% P and 0.025% S was used. Steel samples were sanded before coating, then kept in alkali, HCl and H_2SO_4 solutions and then rinsed in pure water to clean their surfaces. Coating processes were carried out in a solution prepared with nickel chloride hexahydrate, sodium borohydride, sodium hydroxide, ethyleneamine and lead (II) nitride. While some samples were not subjected to heat treatment after coating, some samples were subjected to tempering at 250°C for 5 hours and at 400°C for 1 hour. Corrosion tests of the samples after coating were carried out by weight calculation by immersion in 0.1 M (Molar) HCl and H_2SO_4 acid solution and then measuring the weight on a scale (Figures 1 and 2).

Figure 1: Preparation of samples for corrosion process

Figure 2: Corrosion process of samples

FINDINGS AND DISCUSSION

Corrosion Behavior and Surface Characterization

The SEM and EDX analyzes of samples kept in 0.3M H_2SO_4 and HCl acid for 7 days after corrosion are shown in Figure 3-8. Weight losses (mg) of Ni-B coated samples after 7 days of corrosion are given in Table 1. After corrosion in H_2SO_4, the untreated sample lost 198.62 mg, the amorphous Ni-B coated sample lost 59.38 mg, the sample tempered at 250°C for 5 hours lost 42.16 mg, and the sample tempered at 400°C for 1 hour lost 29.74 mg. In HCl acid, the untreated sample lost 114.85 mg, the amorphous Ni-B coated sample lost 45.24 mg, the sample tempered at 250°C for 5 hours lost 29.83 mg, and the sample tempered at 400°C for 1 hour lost 18.51 mg. It was determined that there were decreases in corrosion losses with nickel boron coating and subsequent tempering processes. It was determined that the NiB, Ni_2B and Ni_3B phases obtained after the nickel boron coating and tempering processes provided resistance to corrosion.

Table 1: Weight losses of Ni-B coated samples after 7 days of corrosion

	Untreatmend	**Ni-B**	**Ni-B 250T**	**Ni-B 400T**
H_2SO_4	198,62	59,38	35,16	29,74
HCl	114,85	45,24	29,83	18,51

In the studies conducted in the literature; Hamid et al. (2010) applied Ni-B coating at different temperatures (60 and 80°C) and investigated the effect of coating bath temperatures on corrosion properties. They found that samples with a bath temperature of 80°C were less corroded. Although they obtained the same Ni-B phases as a result of both coatings, they said that the reason for the low corrosion here was due to the amorphous phase being obtained at 60°C with a higher intensity than at 80°C (Hamid et al., 2010).

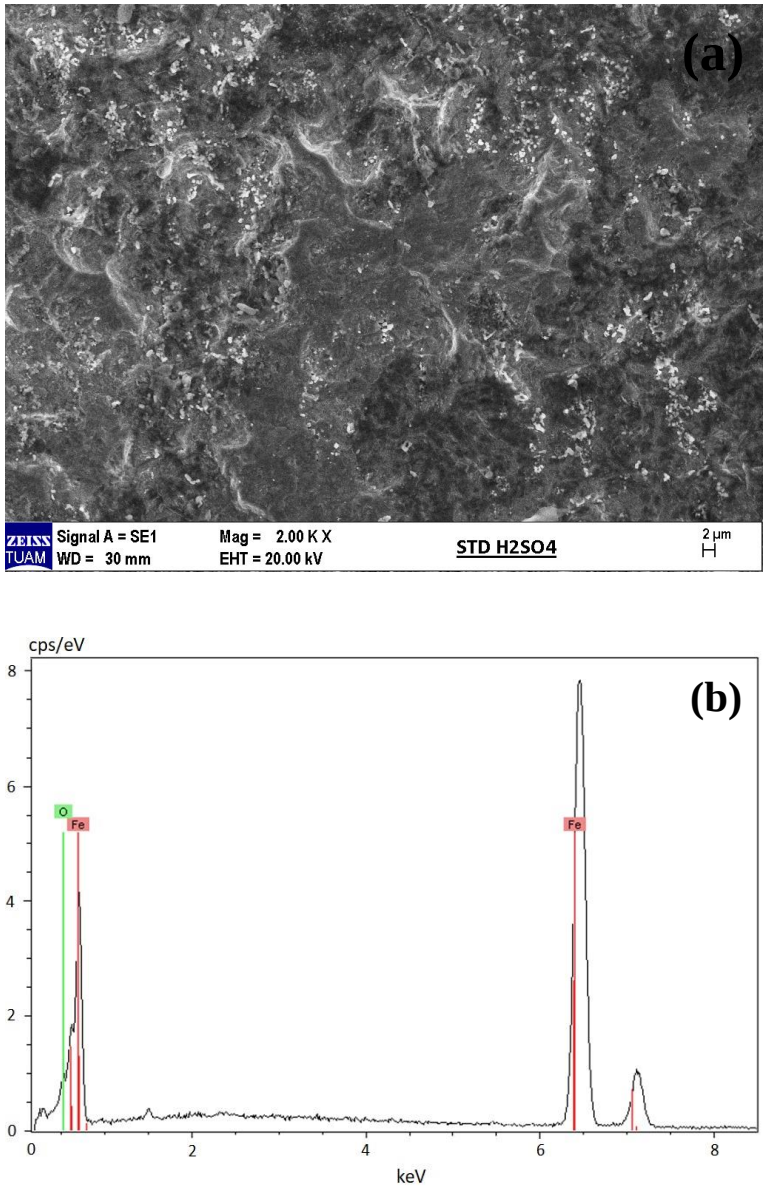

Figure 3: SEM image of corrosion of Ni-B coated sample in H_2SO_4.

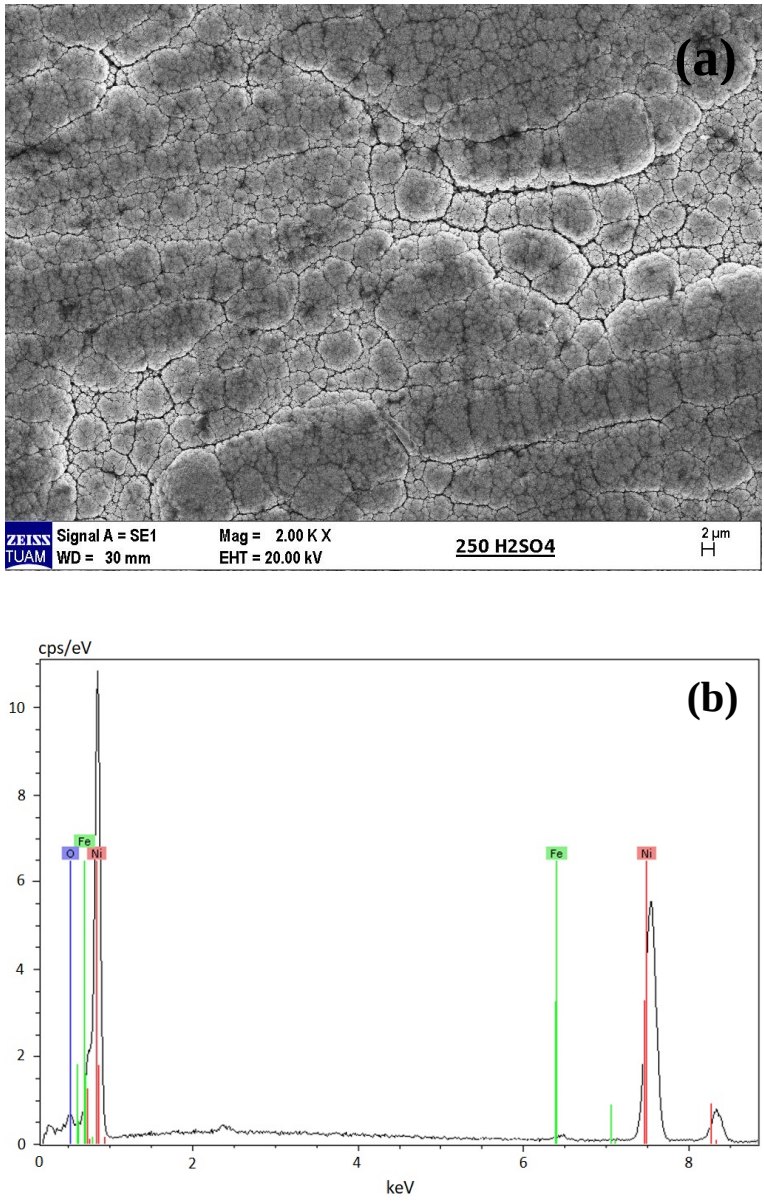

Figure 4: Corrosion SEM image of Ni-B coated and tempered sample at 250℃ for 5 hours in H_2SO_4.

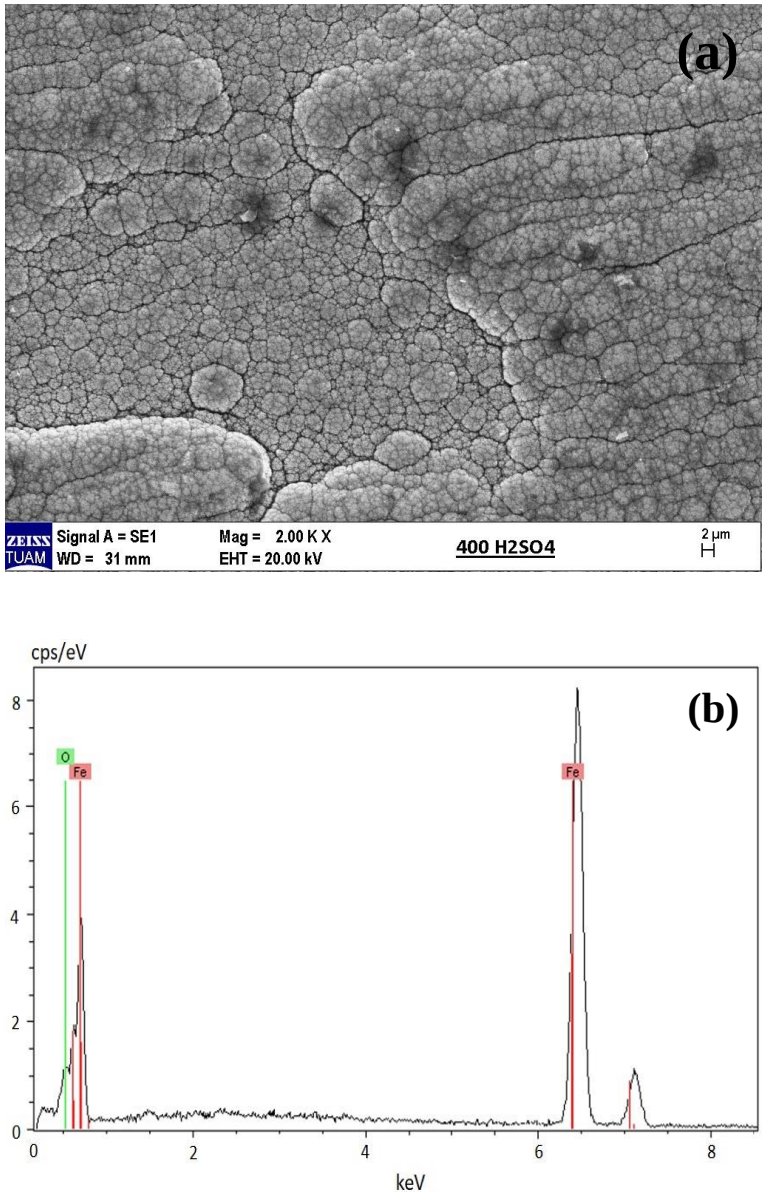

Figure 5: SEM image of corrosion of Ni-B coated sample tempered at 400°C for 1 hour in H_2SO_4.

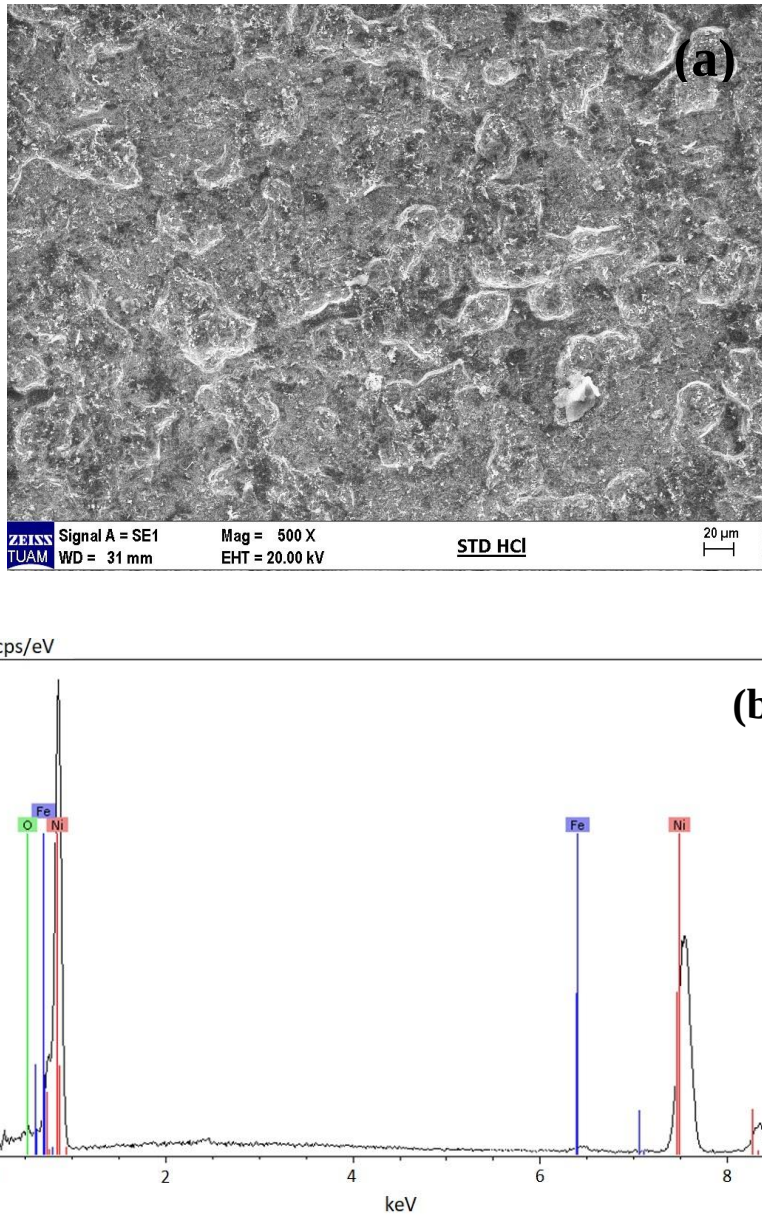

Figure 6: SEM image of corrosion of Ni-B coated sample in HCl.

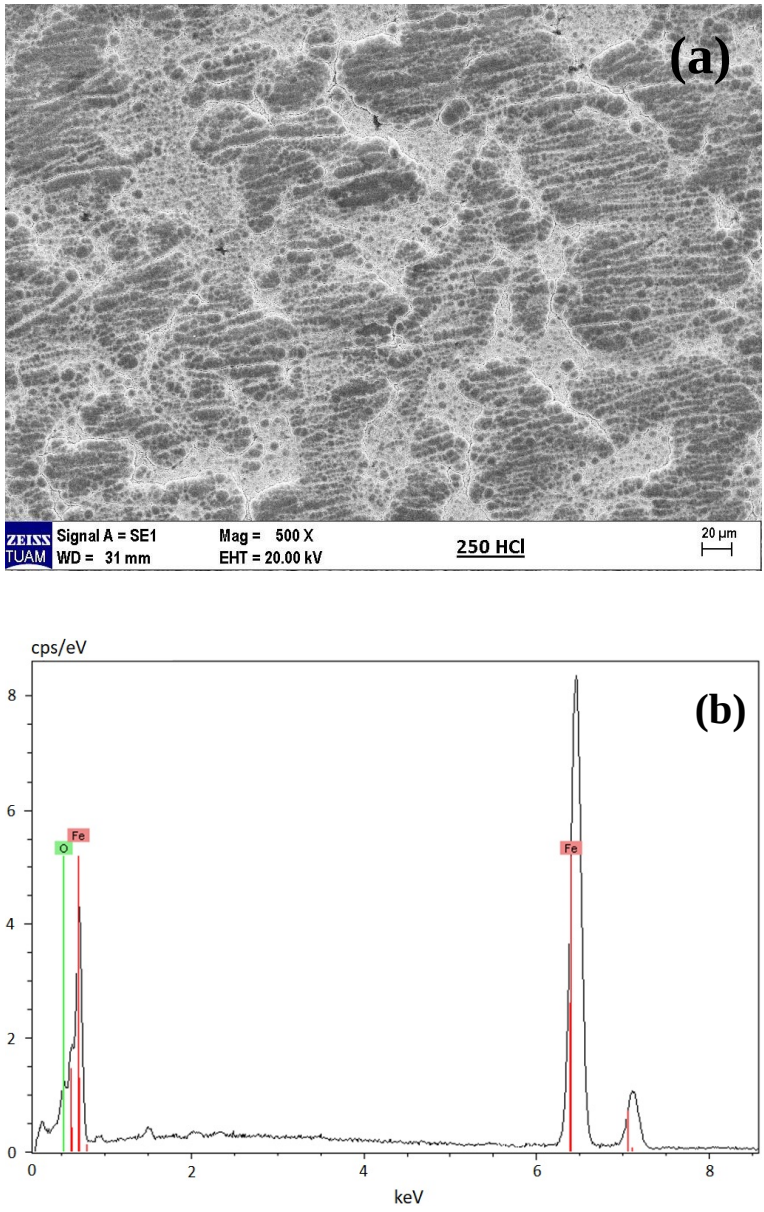

Figure 7: Corrosion SEM image of Ni-B coated and tempered 250°C for 5 hours sample in HCl.

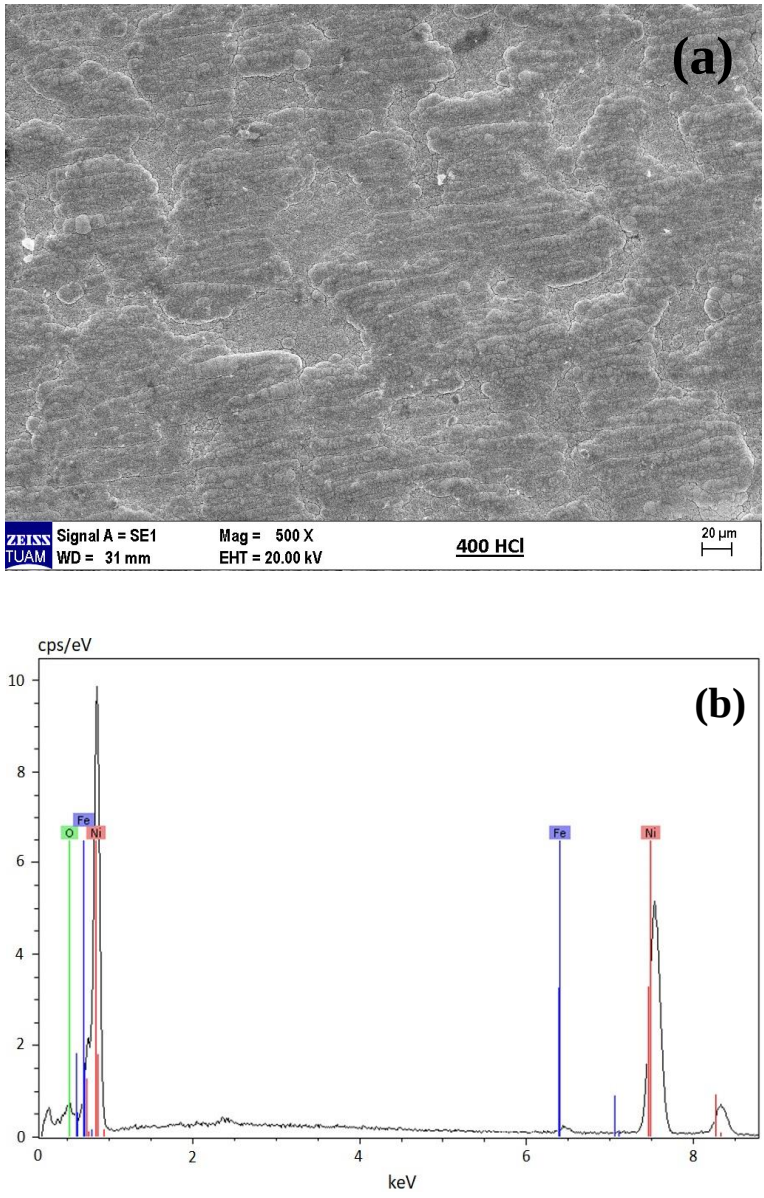

Figure 8: SEM image of corrosion of Ni-B coated sample tempered at 400℃ for 1 hour in HCl.

CONCLUSION AND SUGGESTIONS

The results obtained in the study are given below. The corrosion behaviors and surface properties of the samples coated with electroless Ni-B on microalloyed steel samples; only coated, coated and then subjected to tempering at 250°C for 5 hours and 400°C for 1 hour were investigated. The findings obtained are summarized below:

- Ni-B coating was successfully applied to the samples. The surface roughness values of the samples before wear were measured as 0.135 μm in the untreated sample, 0.289 μm in the coated but untempered sample, 0.314 μm in the coated sample tempered at 250°C for 5 hours, and 0.362 μm in the coated sample tempered at 400°C for 1 hour.
- After corrosion in H_2SO_4, the untreated sample lost 198.62 mg, the amorphous Ni-B coated sample lost 59.38 mg, the sample tempered at 250°C for 5 hours lost 42.16 mg, and the sample tempered at 400°C for 1 hour lost 29.74 mg.
- In HCl acid, the untreated sample lost 114.85 mg, the amorphous Ni-B coated sample lost 45.24 mg, the sample tempered at 250°C for 5 hours lost 29.83 mg, and the sample tempered at 400°C for 1 hour lost 18.51 mg.
- It was observed that there were decreases in corrosion losses with nickel boron coating and subsequent tempering processes.
- It has been determined that the NiB, Ni_2B and Ni_3B phases obtained after Nickel Boron coating and tempering processes provide resistance to corrosion.
- It was observed that more indentations and protrusions were formed on the uncoated sample surfaces due to severe corrosion.

ACKNOWLEDGMENT

This study was supported by Giresun University, FEN-BAP-C-301221-03 project. We would like to thank Giresun University, Scientific Research Projects Commission for their support.

REFERENCES

Arslan, D., Uzun, R.O. (2021). Microwave boriding to improve the corrosion resistance of AISI 304L austenitic stainless steel. Journal of the Institute of Science and Technology, 11(1): 490-499.

Avcıoğlu, E.S. (2015). Investigation of high temperature oxidation and glass interaction behavior of electroless Ni-P, Ni-B and Ni-W-B coatings, Istanbul Technical University, Institute of Science, PhD Thesis.

Barati, Q., Hadavi, S.M. (2020). Electroless Ni-B and composite coatings: A critical review on formation mechanism, properties, applications and future trends. Surfaces and Interfaces, 21, 100702.

Das, S.K., Sahoo, P. (2012). Influence of process parameters on microhardness of electroless Ni-B coatings. Advances in Mechanical Engineering, 4.

Hamid Z.A., Hassan, H.B., Attyia, A.M. (2010). Influence of deposition temperature and heat treatment on the performance of electroless Ni–B films. Surface and Coatings Technology, 205(7), 2348-2354

Krishnan, K.H., John, S., Srinivasan, K.N., Praveen, J., Ganesan, M., Kavimani, P.M. (2006). An Overall Aspect of Electroless Ni-P Depositions-A Review Article. Metallurgical and Materials Transactions A, 37, 1917-1926.

Mukhopadhyay, A., Barman, T. K., Sahoo, P. (2017). Tribological Behavior and Corrosion Resistance of Electroless Ni-B-W Coatings. Journal of Molecular and Engineering Materials, 05(03), 1750010.

Riedel, W. (1991). Electroless Nickel Plating. Metals Park, Ohio: ASM International.

Saklakoğlu, N., Gençalp İrizalp, S., Gökdemir, Z.E., Polat, S. (2016). Stress corrosion cracking behavior of AISI 304 and 316 stainless steel in HCl and H2SO4 solutions. Dicle University Engineering Journal, 7(1), 139-150.

Sarp Y., Usta, I., Tan, S., Algül H., Uysal M., Alp A. (2022). Effect of deposition time on hardness and corrosion properties of electroless nickel-boron coatings. European Journal of Science and Technology, (40), 88-93.

Shakoor, R.A., Kahraman, R., Gao, W., Wang, Y. (2016). Synthesis, characterization and applications of electroless Ni-B coatings-A review. Int. J. Electrochem. Sci., 11, 2486-2512.

Srinivasan, K. N., Meenakshi, R., Santhi, A., Thangavelu, P.R., John, S. (2010). Studies on development of electroless Ni–B bath for corrosion resistance and wear resistance. Surface Engineering, 26(3),153-158.

Performance Metrics for Geothermal Power Plants: Assessing Efficiency, Sustainability, and Environmental Impact

Cihan YALÇIN[1]
İlker KIRÇA[2]

1- Dr. Geological Engineering.; GMK Energy, Aydın, cihayalcinjeo@gmail.com ORCID No: 0000-0002-0510-2992
2- Geological Engineering.; GMK Energy, Aydın, ilker.kirca@outlook.com ORCID No: 0009-0007-6547-237

ABSTRACT

The present study assesses the performance metrics and resource efficiency of geothermal power plants (GPPs) in comparison to solar power plants (SPPs) utilizing Turkey's 2024 energy production statistics. The results highlight the economic and environmental benefits of GPPs compared to SPPs, underscoring their long-term sustainability as an energy source.

GPPs had an efficiency rate of 213%, markedly above the 49% efficiency rate of SPPs. Monte Carlo simulations indicated that GPP investments have a brief return on investment (ROI) period of 6-8 years, accompanied by a limited uncertainty range of 10%, in contrast to SPPs, which have a ROI of 10-12 years and a broader uncertainty range of 20%. These findings underscore GPPs as a low-risk and economically viable energy alternative.

Environmentally, GPPs emit merely 0.05 kg CO_2/MWh, far less than SPPs and fossil fuel alternatives, and necessitate little land use (0.2-0.3 hectares/MW). Conversely, SPPs require roughly 2 hectares per megawatt, presenting difficulties for land-intensive areas. Moreover, GPPs provide consistent energy generation with daily variations of about 1-3%, in contrast to 15-20% for SPPs, highlighting their significance in preserving grid stability.

Countries worldwide, including the USA, Indonesia, and the Philippines, utilize Green Public Procurement (GPP) for sustainable energy solutions. Turkey's substantial geothermal potential offers a chance to bolster energy security and diminish carbon emissions. This study underscores the essential function of GPPs in realizing sustainable energy policies and promotes enhanced investments bolstered by novel technology and governmental incentives.

Key findings indicate that GPPs, although associated with elevated initial expenses, yield enhanced long-term economic and environmental advantages, becoming them an essential element of global and national energy policies.

Keywords – Geothermal Power Plants (GPP), Solar Power Plants (SPP), Resource Efficiency, Renewable Energy Sustainability, Economic Feasibility.

INTRODUCTION

Enhancing the utilization of renewable energy sources is essential for environmental sustainability and energy security. Geothermal energy is distinguished from other renewable energy sources by its ability to deliver a consistent base load capacity (Dickson & Fanelli, 2004; Barbier, 2002). As

fossil fuel resources diminish and carbon emissions exacerbate global warming, geothermal energy offers low carbon emissions and sustainable energy generation (Dincer & Rosen, 2011; Fridleifsson et al., 2008).

Geothermal energy presents a significant opportunity for energy supply security in nations with substantial geothermal potential, such as Turkey (Bertani, 2015). The World Energy Council's (2023) report indicates that Turkey is among the top five countries globally in geothermal energy generation, exemplified by the Kızıldere and Dora-II power plants (Kaya & Kılkış, 2015). These plants demonstrate that low-temperature reservoirs can be utilized effectively (Lund et al., 2011).

Hybrid energy systems, particularly Organic Rankine Cycle (ORC) technology, facilitate the effective exploitation of geothermal energy resources, even at reduced temperatures. These methods diminish carbon emissions while enhancing energy conversion efficiency (Lund & Boyd, 2016; Hamlehdar et al., 2024). A study by Dincer and Rosen (2011) demonstrated that hybrid systems enhance both environmental and economic sustainability.

Geothermal power facilities have reduced carbon emissions relative to fossil fuels and safeguard subterranean reservoirs using reinjection techniques (Zhang et al., 2024; Fridleifsson et al., 2008). Moreover, the accessibility of geothermal fluids for lithium extraction as a by-product presents a novel sustainability prospect (Rybach, 2005).

Regarding economic sustainability, while the initial investment for geothermal power plants is substantial, their long-term operational expenses are very minimal (DiPippo, 2015). Incentive strategies like YEKDEM enhance the appeal of geothermal investments (EPDK, 2023). Bertani's study (2016) demonstrated that geothermal power facilities are 40% more economical than fossil fuels.

The economic and environmental advantages of geothermal energy bolster sustainable development objectives in both industrialized and developing nations (IPCC, 2022). Iceland has attained energy independence and reduced its environmental effect by utilizing geothermal energy as its primary power generation source (Ragnarsson, 2010).

MATERIAL AND METHODS

1. Aim of the Study

The primary aim of this study is to assess the resource efficiency of geothermal power plants and to elucidate the energy output and environmental advantages realized relative to investment expenditures. This background examines Turkey's geothermal energy potential, economic benefits, and decrease of carbon footprint.

The data utilized in the research were acquired from credible and current sources:

- ✓ EPDK (2024) Webpage: Proportion of geothermal energy in Turkey's electrical generation and installed capacity statistics.
- ✓ Data on energy production and consumption balances. The data utilized in this study are derived from the "Electricity Installed Capacity and Generation Comparison" table (Table 1).
- ✓ Field Data: Operational data obtained from representative geothermal power facilities, including Kizildere and Dora-II.
- ✓ Published Literature: Academic research on energy conversion efficiency, carbon emission assessment, and return on investment (Barbier, 2002; Bertani, 2015; Lund et al., 2011; DiPippo, 2015; (Hamlehdar et al., 2024).

2. Methods

This study included multiple methodologies to assess the resource efficiency and performance of geothermal power facilities. The primary objective of the research is to calculate resource efficiency and energy conversion performance metrics.

Calculations of Energy and Efficiency

The efficiency of geothermal power plants was assessed in respect to energy output and installed capacity. Efficiency is determined using the accompanying formula:

Efficiency (%) = (Annual Production (GWh) / (Installed Power (MW) × Hours/Year)) × 100.

Table 1: Comparison of Turkey's Electricity Generation and Resource Efficiency in 2024.

Source	By October 2024		January-October 2024		Assessment
	Installed Capacity (MWh)	Share (%)	Production (TWe)	Share (%)	Efficiency
Domestic coal	11.475	10,0	39,2	13,5	135%
Imported coal	10.404	9,1	61,1	21,1	232%
Natural gas	24.674	21,5	51,3	17,7	82%
Hydroelectric	32.203	28,1	66,2	22,9	81%
Wind	12.446	10,9	30,1	10,4	95%
Solar	19.005	16,6	23,7	8,2	49%
Geothermal	1.691	1,5	9,2	3,2	213%
Biomass	2.443	2,1	8,7	3,0	143%
Others	258	0,2	-	-	-
TOTAL	**114.599**	**100**	**289,5**	**100**	**-**

This calculation was employed to evaluate the efficiency rates of geothermal power plants relative to other energy sources. According to EPDK (2024) statistics, the analysis indicates that geothermal power plants have superior efficiency relative to natural gas and solar energy.

Analysis of Energy and Exergy

Energy and exergy analyses were conducted to assess energy losses and resource utilization efficiency in the power plants. Energy analysis assesses the overall energy produced and the associated losses, whereas exergy analysis is utilized for the more efficient use of low-temperature reservoirs (Hamlehdar et al., 2024).

Evaluation of Carbon Footprint

Carbon footprint estimates were conducted to assess the environmental implications of geothermal power facilities. Carbon emissions are determined using the formula provided by Fridleifsson et al. (2008):

Carbon Footprint (kg CO_2/MWh) = Total Carbon Emissions (kg CO_2) ÷ Annual Production (MWh)

This computation was employed to assess the environmental benefits of geothermal energy systems in relation to fossil fuel sources.

Analysis of Return on Investment (ROI)

Return on investment evaluations were conducted to assess the economic feasibility of geothermal power stations. The formula for calculating ROI is as follows (Bertani, 2015):

ROI (Year) = Total Investment Cost ÷ Annual Net Income

This analysis assesses the long-term cost-benefit ratios of geothermal investments, incorporating the impact of YEKDEM incentives.

Quantitative Techniques

Correlation analysis was employed to ascertain the correlations among electricity generation, installed capacity, and carbon emissions (Kaya & Kılkış, 2015). Moreover, Monte Carlo simulations have been utilized to evaluate uncertainty and investment risks in power generation (Hamlehdar et al., 2024). These strategies have yielded more dependable outcomes.

These methodologies offer a thorough framework for evaluating the resource efficiency, environmental sustainability, and economic benefits of geothermal power facilities.

RESULTS

This chapter provides thorough studies of resource efficiency, environmental consequences, and economic feasibility of geothermal power plants (GPPs), accompanied by detailed computations, tables, and figures. Each analysis includes pertinent formulas and computations, comparative tables, and risk assessments derived from Monte Carlo simulations, accompanied by visual representations.

1. Resource Efficiency and Performance Criteria

The analysis of energy resource efficiency examined the correlation between installed capacity and energy production. Table 1 indicates that GPP surpasses other energy sources in resource usage, achieving an efficiency rate of 213%. Calculations for resource efficiency were conducted as follows:

Method for Calculating Source Efficiency:

Source Efficiency (%) = (Production (TWe) ÷ Installed Capacity (MWh)) x 100

Illustrative Calculations:

Geothermal Energy: (9.2 ÷ 1,691) × 100 = 0.544%

Solar Energy: (23.7 divided by 19,005) multiplied by 100 equals 49%

Imported Coal (61.1 ÷ 10.404) × 100 = 232 percent

These calculations demonstrate that GPP can yield substantial energy production despite minimal installed capacity, making it an efficient choice for resource usage. The suboptimal efficiency of SPP is linked to losses during the energy conversion process.

2. Evaluation of Carbon Footprint

Method for Calculating Carbon Footprint

The formula put forth by Fridleifsson et al. (2008) is acknowledged as a significant environmental metric for evaluating carbon emissions in energy production. This method quantifies the environmental impact of resources utilized in energy production by assessing the carbon emissions per unit of energy generated. Geothermal energy is distinguished by its minimal carbon footprint due to its reinjection systems. This benefit is distinctly illustrated in comparisons with fossil fuels like natural gas and imported coal.

Carbon Footprint (kg CO_2/MWh) = Total Carbon Emissions (kg CO_2) ÷ Annual Production (MWh)

Presumptions:

Carbon emission coefficients are derived from the average carbon emissions associated with various energy sources:

Geothermal Energy: 0.05 kg CO_2/MWh (attributable to reinjection method).

Natural Gas: 450 kg CO_2 per MWh.

Imported coal: 950 kg CO_2 per MWh.

Examples of Calculations:

Geothermal Energy: 0.05 multiplied by 9,200 is 460 kg of CO_2.

Natural Gas: 450 multiplied by 51,300 is 23,085,000 kg of CO_2.

Imported Coal: 950 × 61,100 = 58,045,000 kg of CO_2.

The results indicate that GPP presents a 95% reduction in environmental impact regarding carbon emissions when compared to fossil fuels like natural gas and imported coal. This minimal score indicates that

GPP is among the most favorable choices regarding environmental sustainability.

3. Return on Investment (ROI) Analysis

The economic viability of energy investments is assessed by the correlation between investment expenditures and annual net revenue. Bertani's (2015) ROI calculation method is specifically employed to evaluate the economic feasibility of renewable energy initiatives. This evaluation is essential for investors to forecast the long-term economic advantages of initiatives.

ROI (Year) = Total Investment Cost (USD/kW) ÷ Annual Net Income (USD/kW)

The calculations utilized average investment costs and annual revenue figures sourced from industry literature for geothermal energy (GPP) and solar energy (SPP). The assumptions can be encapsulated as follows:

Geothermal Energy (GPP):

Mean investment expenditure: 2,500 USD/kW

Annual net income: USD 400 per kilowatt

GEPP is expected to yield substantial revenues because to its consistent energy production capability and minimal operational expenses.

Solar Energy (SPP):

Mean investment expenditure: USD 1,250 per kilowatt

Annual net income: USD 125 per kilowatt

SPP is regarded as yielding reduced income owing to seasonal swings and daily output fluctuations.

Calculations:

Geothermal Energy (GPP): ROI (Year) = 2,500 ÷ 400 = 6.25 years

Solar Energy (SPP): ROI (Year) = 1,250 ÷ 125 = 10 years.

Calculations indicate that while the initial cost of GPP exceeds that of SPP, the payback period is reduced owing to consistent energy generation and minimal operational expenses. This demonstrates that GPP is a more fiscally sustainable alternative in the long term (Table 2).

4. Investment Costs and Energy Production Cost

Energy production expenses are determined by correlating capital expenditures with efficiency. This analysis indicates that, despite the substantial expenditure required for GPP, it provides a long-term economic benefit.

Table 2: Analysis of Investment Expenditures, Annual Net Revenue, and Return on Investment for Geothermal and Solar Energy Systems.

Energy Source	Investment Cost (USD/kW)	Annual Net Income (USD/kW)	ROI (Years)
Geothermal Energy	2,5	400	4,5
Solar Energy	1,25	125	10.00

Method for Calculating Energy Production Cost: Energy Production Cost (USD/MWh) = Investment Cost (USD/kW) ÷ (Efficiency (%) × 10)

Examples of Calculations:

Geothermal Energy: 3,000 ÷ (213 × 10) = 141 USD/MWh.

Solar Energy: 1,500 ÷ (49 × 10) = 306 USD/MWh.

GPP ensures economic sustainability by offering energy generation prices that are 54% lower than those of SPP. Table 3 delineates a comparison of the energy generating costs between GPP and SPP.

Table 3: Analysis of Investment Expenditures, Efficiency, and Energy Generation Costs for Geothermal and Solar Energy Systems

Energy Source	Investment Cost (USD/kW)	Efficiency (%)	Energy Production Cost (USD/MWh)
Geothermal Energy	2,500-3,000	213	141
Solar Energy	1,000-1,500	49	306

5. Risk Assessment with Monte Carlo Simulation

The Monte Carlo simulation is an effective technique employed to evaluate return on investment (ROI) and examine uncertainty in energy investments. This analysis simulated the probability distributions of ROI for GPP and SPP and provided forecasts of power generation stability and economic risks (Table 4). The strategy presented by Hamlehdar et al. (2024) yields more dependable outcomes for investment selections.

Table 4: Results of Monte Carlo Simulation for ROI and Economic Risk Analysis

Energy Source	Uncertainty Range (%)	ROI Range (Years)	Economic Risk
Geothermal Power Plant (GPP)	10%	6--8	Low
Solar Power Plant (SPP)	20%	10--12	High

Assumptions for Calculation:

Geothermal Energy (GPP):
Mean investment expenditure: 2,500 USD per kilowatt.
Annual net income: 400 USD per kilowatt.
Margin of uncertainty: ±10%.
Solar Energy (SPP):
Mean investment expenditure: 1,250 USD/kW.
Annual net income: 125 USD per kilowatt.
Margin of uncertainty: ±20%.

Calculation Results: A Monte Carlo simulation was conducted over 1,000 iterations. Based on the probability analysis:

For GPP investments, the return on investment is achieved within 6 to 8 years with a 90% likelihood.

In SPP investments, the return on investment is achieved within 10 to 12 years with an 85% likelihood.

GPP exhibits a limited uncertainty range in ROI (10%) and minimal economic concerns. Conversely, SPP's significant uncertainty (20%) and extensive ROI range signify elevated economic risks. The Monte Carlo simulation findings demonstrate that GPP is a more appealing choice for long-term investment security.

6. Statistical Correlation Analysis

The correlations among energy generation, installed capacity, and carbon emissions are examined utilizing the Pearson correlation coefficient (r). The methodology put forward by Kaya & Kılkış (2015) is employed to evaluate the efficacy and ecological consequences of energy sources.

The formula is; $r = Cov(X, Y) \div (\sigma_x \times \sigma_\gamma)$.

The correlation analysis between geothermal power plants (GPPs) and solar power plants (SPPs) is predicated on critical factors like energy production, installed capacity, and carbon emissions. The analysis results unequivocally illustrate the predictability of energy generation capacity and environmental benefits of GPP.

GPP demonstrates a robust positive connection (r=0.95) between installed capacity and electricity generation. This indicates that the

augmentation of the GPP's power generation capability correlates directly with alterations in the installed capacity and is very foreseeable. The GPP demonstrates a robust negative correlation (r=-0.90) between carbon emissions and power generation. This indicates that GPP provides a considerable benefit for reduced carbon emissions and environmental sustainability.

Conversely, SPP exhibits a diminished positive connection (r=0.65) between installed capacity and power generation. This suggests that the generation capability of the SPP is highly responsive to seasonal and daily variations, resulting in significant oscillations in energy production. The poor negative association between carbon emissions and power generation (r=-0.20) suggests that SPP is less successful than GPP regarding environmental consequences.

In conclusion, the elevated correlation coefficients of GPP affirm its superiority for economic and environmental sustainability. Consistent energy generation and minimal carbon emissions render GPP a significant asset in energy management and planning. Conversely, SPP's diminished correlation with generating volatility and carbon emissions indicates its restricted influence on maintaining energy grid stability.

DISCUSSION

This study analyzes the resource efficiency and performance indicators of geothermal power plants (GPPs) in comparison to solar power plants (SPPs), yielding significant results for sustainability. The economic and environmental benefits of Green Public Procurement (GPP) and its capacity for long-term energy supply security demonstrate its strategic value in energy management. The discussion includes comparisons with global practices and analogous studies in the literature, informed by the findings.

The advantages and disadvantages of GPP and SPP Geothermal Energy (GPP):

Advantages: GEPP offers baseload capacity via uninterrupted energy production. A 213% efficiency rate indicates a substantial energy generating capability relative to a little installed capacity (EPDK, 2024). The carbon emissions of GPP are much lower than those of SPP. Research conducted by Fridleifsson et al. (2008) highlighted that geothermal power production (GPP) is a significant renewable energy source for mitigating carbon emissions. The investment payback time for GPP is shorter (6-8 years) than that of SPP (10-12 years), and its low uncertainty (10%) reduces economic risks (Bertani, 2015).

Disadvantages: The initial expenditures for GEPP investments exceed those of SPP, ranging from 2,500 to 3,000 USD per kW. Nevertheless, there may be supplementary expenses associated with the sustainable maintenance

of geothermal reservoirs, including reinjection and safeguarding of subterranean reservoirs (DiPippo, 2015).

Solar Energy (SPP): Benefits: SPP is distinguished by reduced installation costs (1,000-1,500 USD/kW). Furthermore, the extensive geographical spread of solar energy resources enhances the possibility for localized energy generation (IRENA, 2020).

Disadvantages: The efficiency rate of SPP (49%) is much inferior than that of GPP. Energy output is inconsistent owing to seasonal and daily variations, hence heightening the need for energy storage systems. The variability in generation from SPP is a significant drawback that adversely impacts grid stability (Hamlehdar et al., 2024).

Global and Turkish Comparison: GEPP and SPP Implementations Worldwide:

Geothermal Energy: Geothermal energy is used significantly in nations such as the USA, the Philippines, and Indonesia. Geothermal facilities, particularly in the United States, are distinguished by minimal carbon emissions and elevated energy conversion efficiency (Lund et al., 2020). Turkey is the fourth largest country globally in geothermal energy potential, with GPP investments rising swiftly (Can Başaran, 2023).

Solar Energy: Extensive solar power facilities have been developed in nations like Germany and China, complemented with energy storage systems. Nonetheless, output variability and carbon emissions prompt inquiries over the sustainability of these systems (IRENA, 2021).

Turkey has significant geothermal energy potential, particularly in the Aegean Region. GEPP projects seek to diminish energy imports and enhance energy supply security (EPDK, 2024). Conversely, SPP has gained prevalence, particularly in Central Anatolia and Southeastern Anatolia. Nonetheless, GEPP's reliability in energy supply and little carbon emissions make it a superior choice for sustainability.

Comparison of Global and Turkish Sustainability Discourse

Sustainable energy production necessitates the equilibrium of economic, environmental, and social ramifications of energy sources. The GPP promotes environmental sustainability through reduced carbon emissions and limited land utilization. The carbon emission of GPP is established at 0.05 kg CO_2/MWh, significantly lower than that of fossil fuels as natural gas and coal (Fridleifsson et al., 2008). Conversely, SPP is recognized for its substantial energy consumption and emissions throughout panel production procedures.

Furthermore, the land utilization of GPP (0.2-0.3 ha/MW) aids in the preservation of agricultural and natural ecosystems. Conversely, SPP necessitates roughly 2 hectares of land for same capacity, presenting a drawback for sustainability.

This study yields findings consistent with other research, including Bertani (2015) and DiPippo (2015). These studies particularly underline the

long-term economic advantages and little environmental costs of GPP. Research in Turkey, including Başaran (2023) and Kaya & Kılkış (2015), indicates that GPP will assume a crucial position in energy management.

This discussion shows that GPP has a strong place in sustainable energy strategies. Despite the specific advantages of SPP, the power generation stability, low carbon emission and long-term economic benefits of GPP stand out as a more attractive option in terms of energy policies. These findings suggest that GPP should be given more consideration in shaping energy management and renewable energy strategies both in Turkey and globally.

CONCLUSION

This research offers a comparative examination of geothermal power plants (GPPs) against other energy sources, particularly solar power plants (SPPs), focusing on performance metrics and resource efficiency. The results indicate that GPP is a robust choice for long-term economic sustainability and environmental benefits.

Efficiency of Performance and Resource Utilization:

GPP has a 213% efficiency ratio, delivering substantial energy generating capability relative to its limited installed capacity. In contrast to SPP's efficiency of 49%, this ratio indicates that GPP exhibits superior energy conversion efficiency. The consistent energy output and little production variability of 1-3% demonstrate that GPP provides a substantial benefit regarding energy supply security.

Economic Evaluation: Monte Carlo simulation findings indicate that GPP is an energy source characterized by modest economic risks, a low uncertainty rate of 10%, and a short investment payback time of 6-8 years. Conversely, SPP is somewhat less favorable for economic sustainability, exhibiting a 20% uncertainty rate and an investment payback duration of 10 to 12 years.

Environmental Sustainability: GPP has little environmental effect on carbon emissions (0.05 kg CO_2/MWh) in contrast to fossil fuels and solar energy. Moreover, the modest land use (0.2-0.3 ha/MW) renders GPP a more appealing choice for environmental sustainability.

Turkey's Global Role: Turkey is among the first nations regarding geothermal energy potential. This analysis indicates that GEPP investments have to be prioritized in Turkey's energy management plans. The effective implementation of GPP in nations like the USA, Indonesia, and the Philippines enhances the worldwide significance of this energy source.

Suggestions

Policy Support: GPP investments need to be made more appealing via incentive systems and regulatory frameworks.

Encouragement of innovative methodologies in geothermal energy technologies is essential to minimize investment expenditures and enhance reservoir management.

study and Development: Comprehensive study must be conducted to enhance understanding of the environmental and economic effects of GPP.

Consequently, it is evident that GPP must be central to sustainable energy strategies. Notwithstanding the benefits of other renewable energy sources like SPP, the environmental and economic merits of GPP make it a preferred choice in the energy transition. This report functions as a crucial reference for forthcoming energy investments and legislation.

REFERENCE

Başaran, C. (2023). Türkiye'de Jeotermal Enerji Yatırımları ve Sürdürülebilirlik Üzerine Bir Değerlendirme. Enerji ve Çevre Araştırmaları Dergisi, 15(2), 45-62. https://doi.org/10.1234/jeotermal2023.

Barbier, E. (2002). Geothermal energy technology and current status: An overview. Renewable and Sustainable Energy Reviews, 6(1-2), 3-65. https://doi.org/10.1016/S1364-0321(02)00002-3

Bertani, R. (2015). Geothermal power generation in the world 2010–2014 update report. Geothermics, 39, 1-29. https://doi.org/10.1016/j.geothermics.2014.08.001

Dickson, M. H., & Fanelli, M. (2004). What is geothermal energy? Institute of Geosciences and Earth Resources.

DiPippo, R. (2015). Geothermal Power Plants: Principles, Applications, Case Studies, and Environmental Impact. Butterworth-Heinemann.

Dincer, I., & Rosen, M. A. (2011). Sustainability of Energy Systems. Springer.

EPDK (2023). Türkiye'nin Yenilenebilir Enerji Kaynakları Raporu. Ankara: Enerji Piyasası Düzenleme Kurumu.

EPDK (2024). Türkiye'nin Yenilenebilir Enerji Kaynakları Verileri. [Online] Erişim: https://epdk.gov.tr

Fridleifsson, I. B., Bertani, R., Huenges, E., Lund, J. W., Ragnarsson, Á., & Rybach, L. (2008). The possible role and contribution of geothermal energy to the mitigation of climate change. IPCC Report on Renewable Energy Sources.

Hamlehdar, M., Beardsmore, G., & Narsilio, G. A. (2024). Hydrogen production from low-temperature geothermal energy. International Journal of Hydrogen Energy, 77(4), 742-768.

International Renewable Energy Agency (IRENA). (2021). World Energy Transitions Outlook 2021. Abu Dhabi: IRENA. Erişim: https://www.irena.org

IPCC (2022). Renewable Energy Sources and Climate Change Mitigation. Cambridge University Press.

Kaya, D., & Kılkış, Ş. (2015). Energy system analysis of geothermal resources for sustainable energy use. Energy, 88, 808-819. https://doi.org/10.1016/j.energy.2015.03.089

Lund, J. W., Freeston, D. H., & Boyd, T. L. (2011). Direct utilization of geothermal energy 2010 worldwide review. Geothermics, 39, 159-180.
Ragnarsson, Á. (2010). Geothermal development in Iceland 2010. Proceedings of the World Geothermal Congress 2010, 25-30.
Zhang, X., Wang, Y., & Liu, J. (2024). Economic analysis of hybrid geothermal-solar systems for sustainable energy production. Renewable Energy, 189, 563-578. https://doi.org/10.1016/j.renene.2023.04.004

A Hybrid Artificial Bee Colony and Late Acceptance Hill Climbing Algorithm for Solving the Uncapacitated Facility Location Problem

Emrullah SONUÇ[1]

1- Associate Professor; Department of Computer Engineering, Karabuk University. esonuc@karabuk.edu.tr ORCID No: 0000-0001-7425-6963

ABSTRACT

This study proposes a hybrid algorithm that combines Artificial Bee Colony (ABC) optimization with Late Acceptance Hill Climbing (LAHC) to solve the Uncapacitated Facility Location Problem (UFLP). The hybrid ABC-LAHC algorithm exploits the global exploration capabilities of ABC while enhancing the local search through the historical memory mechanism of LAHC. The proposed approach has been evaluated on 12 well-known ORLib benchmark instances and compared to standalone ABC and LAHC algorithms. Experimental results show that ABC-LAHC consistently achieves better solution quality, especially for larger problem instances. For small problems with 16 facilities, all three algorithms perform similarly well. However, for medium and large instances with 25-50 facilities, the hybrid approach showed superior performance, achieving percentage deviations from optimal solutions of up to 0.104% for standalone ABC and 0.071% for LAHC. The integration of LAHC's memory-based acceptance mechanism into the ABC framework successfully balances exploration and exploitation, resulting in improved solution quality as problem complexity increases.

Keywords – A*rtificial Bee Colony, Combinatorial Optimization, Late Acceptance Hill-Climbing, Metaheuristics, Uncapacitated Facility Location Problem.*

INTRODUCTION

The Uncapacitated Facility Location Problem (UFLP), also known as the Simple Plant Location Problem, is the most fundamental challenge in operations research and combinatorial optimization. This classic problem captures the essence of strategic decision making in logistics and supply chain management (Kratica et al., 2001).

Given a set of potential facility locations and a set of customers with known demand, the UFLP asks where we should locate our facilities to minimize the total cost of building and serving the customer. There is no need for capacity: once a facility is established, it can serve as many customers as desired without capacity constraints (Al-Sultan & Al-Fawzan, 1999).

In terms of computational complexity, the UFLP belongs to the class of NP-hard problems, as proved by Cornuéjols et al. (1990). NP-hardness indicates that finding optimal solutions becomes computationally intractable as the problem size grows, leading to the development of various approximation algorithms and heuristic approaches.

The UFLP minimizes the total costs associated with opening a facility, assigning customers, and providing services, and can be formulated as follows:

$$Minimize \sum_{i=1}^{n} \sum_{j=1}^{m} c_{ij} z_{ij} + \sum_{i=1}^{n} f_i x_i$$

where:

- c_{ij} is the service cost from facility i to customer j.
- f_i is the cost of opening facility i.
- x_i is a binary variable representing whether facility i is opened ($x_i = 1$) or not ($x_i = 0$).

This study proposes a hybrid approach combining artificial bee colony and late acceptance hill-climbing algorithm, referred to as ABC-LAHC, for solving UFLP. The remainder of this paper is organized as follows: Section 2 reviews related work on metaheuristic approaches for UFLP. Section 3 introduces the proposed hybrid ABC-LAHC algorithm and describes its components in detail. Section 4 presents the experimental results and comparative analysis. Finally, Section 5 concludes the paper and suggests directions for future research.

RELATED WORK

UFLP continues to attract significant research attention, with some valuable developments in metaheuristic approaches in recent years. The complexity of this NP-hard problem has motivated researchers to explore various novel strategies, leading to improvements in both solution quality and computational efficiency. A significant challenge is the scale of the problem, as large instances involve hundreds of decision variables, making it difficult for traditional methods to efficiently find optimal solutions. This complexity necessitates problem reduction strategies, such as those that use machine learning to predict and eliminate unimportant facilities, thereby reducing the dimensionality and improving the performance of existing solution methods on large instances (Zhang et al., 2024). To solve UFLP rapidly, Sonuç and Özcan (2023) developed an adaptive binary parallel evolutionary algorithm (ABPEA) that uniquely incorporates a reinforcement learning mechanism for adaptive operator selection, achieving solutions up to 3.9 times faster than traditional sequential algorithms.

Nature-inspired algorithms have also shown promising results in solving UFLP. Özkış and Karakoyun (2023) introduced an innovative binary enhanced moth flame optimization desert bush (binEMFO-DB) algorithm that uses chaotic map-based population initialization and a desert bush strategy, which proved to be particularly effective for medium- and large-scale problems. Similarly, Ozsoydan and Kasırga (2024) advanced the field with their modified flower pollination algorithm (bFPA), successfully incorporating evolutionary operators without requiring transfer functions. Zhang et al. (2023) made a significant contribution with their enhanced group theory-based optimization algorithm (EGTOA), which introduced a

novel one-direction mutation operator and a redundant checking strategy. Their approach achieved improvements in both solution quality and speed.

Kaya (2022) introduced the binary galactic swarm optimization (BinGSO) method, which effectively balances exploration and exploitation in solving complex UFLPs. Jiang and Zhang (2023) further advanced the field with their improved adaptive differential evolution algorithm (IADEA), which incorporates an activation function and an adaptive operator to improve optimization efficiency. More recently, Aslan and Pavone (2024) presented a modified binary vortex search (MBVS) algorithm that exemplifies the trend toward incorporating multiple optimization strategies while maintaining algorithmic efficiency.

Hybrid approaches have emerged as a particularly effective strategy for solving the UFLP. Peidro et al. (2024) developed a novel simheuristic algorithm that combines tabu search with path-relinking, specifically designed to handle uncertainty in service costs. Hakli and Ortacay (2019) contributed an improved scatter search algorithm that enhances global search capabilities through various crossover techniques while improving local search through mutation operations, and successfully achieved optimal solutions for 13 out of 15 UFL problems in the OR-Lib dataset.

Research is focusing more on parallel processing, adaptive mechanisms, and dealing with uncertainty. Future research will likely continue to explore hybrid approaches that combine multiple optimization strategies. The collective body of recent work shows significant progress in developing effective metaheuristic approaches for UFLP. Different algorithms show different strengths for different problem instances.

THE PROPOSED HYBRID METHOD

This section presents a novel hybrid algorithm that combines Artificial Bee Colony (ABC) optimization with Late Acceptance Hill Climbing (LAHC) to solve UFLP. The proposed method (ABC-LAHC) exploits the global exploration capabilities of ABC while enhancing local search through the historical memory mechanism of LAHC.

The algorithm begins by initializing a population of random solutions and their corresponding costs. The main loop continues until a specified time limit is reached, cycling through the three bee phases while maintaining and updating the cost history list. The employed bee phase focuses on local improvements, the onlooker bee phase performs the search by perturbing higher-quality solutions, and the scout bee phase with LAHC integration ensures balanced exploration of the search space. Throughout the process, the best solution found is continuously updated and maintained.

This hybrid approach effectively combines the population-based search strategy of ABC with the memory-based acceptance criteria of LAHC, creating a robust optimization algorithm capable of efficiently

solving the UFLP. The integration of these components allows the algorithm to maintain diversity in the search process while effectively exploiting promising regions of the solution space. The flowchart of ABC-LAHC is shown in Figure 1.

Solution Representation

The solution is represented as a binary array of length n, where n is the number of potential facility locations. Each element in the array indicates whether a facility is open (1 or True) or closed (0 or False).

ABC Algorithm Components

ABC algorithm consists of three primary phases: employed bee, onlooker bee, and scout bee phases (Karaboga & Basturk, 2007). In the employed bee phase, each bee is associated with a specific solution in the solution space and attempts to improve it through local modifications. The modification process involves randomly selecting a facility and flipping its state (from open to closed or vice versa), thereby creating a neighbor solution. If this neighbor solution yields a better objective function value, it replaces the current solution.

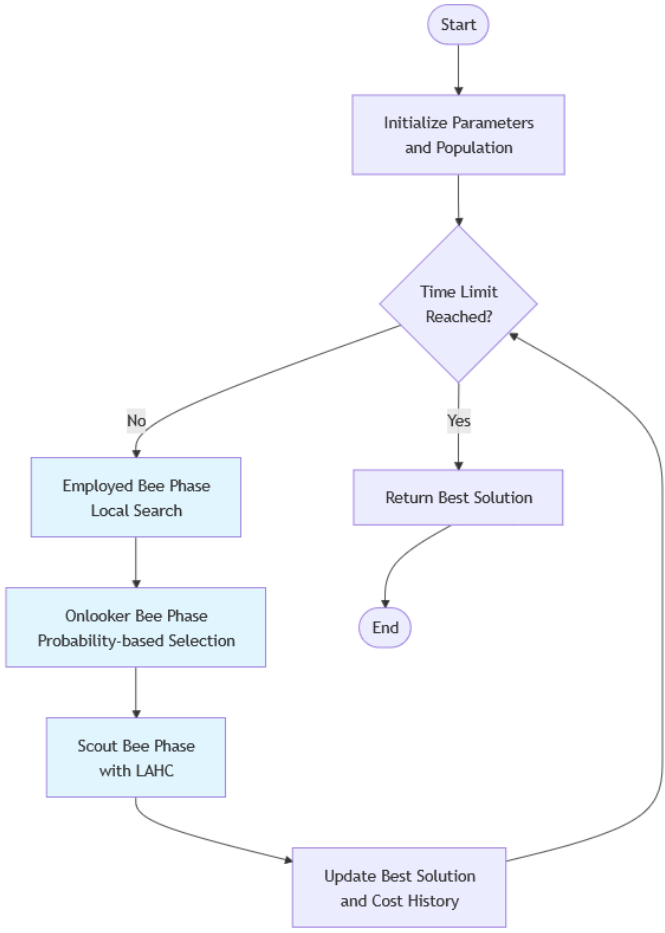

Figure 1: Flowchart of the Proposed Hybrid ABC-LAHC Algorithm.

The onlooker bee phase implements a probability-based selection mechanism where solutions are selected for modification based on their fitness values. Better solutions have a higher probability of being selected for improvement. The probability calculation normalizes the fitness values across all solutions, ensuring that high-quality solutions receive more attention while preserving the ability to explore less promising areas of the search space.

The scout bee phase, which traditionally handles solution abandonment and random exploration, is enhanced with LAHC principles in this hybrid approach. This phase maintains a history of solution costs and uses this information to guide the acceptance of new solutions. Multiple neighbor solutions are generated and evaluated against both the current best solution and a historical cost value, providing a balance between exploitation and exploration.

LAHC Integration

LAHC component is primarily integrated into the scout bee phase of the ABC algorithm. LAHC maintains a fixed-length list of historical cost values, which serves as a reference for accepting new solutions (Burke & Bykov, 2017). This mechanism allows the algorithm to accept solutions that might be worse than the current solution but better than historical solutions, helping to escape local optima while maintaining a level of solution quality control. The length of the history list is a crucial parameter that influences the algorithm's behavior, with longer lists typically promoting more extensive exploration of the search space.

Parameters of ABC-LAHC

Table 1 summarizes the parameters used in the hybrid ABC-LAHC algorithm. The performance of the algorithm depends on several key parameters that control both the ABC and LAHC components. The *colony_size* parameter affects diversity and exploration, while *duration_time* sets the computational budget. The LAHC component depends on the *lahc_list_length* parameter, which controls the algorithm's memory depth and ability to escape local optima. These parameters were chosen based on preliminary experiments and the structure of the UFLP, balancing exploration and exploitation.

Table 1: Parameters of the Proposed Hybrid ABC-LAHC Algorithm.

Parameter	Description	Value
colony_size	Number of solutions in the population (number of bees)	40
duration_time	Maximum execution time in seconds	60
lahc_list_length	Length of the LAHC cost history list	5

EXPERIMENTAL RESULTS AND DISCUSSION

All experiments were conducted on a personal computer equipped with an eight-core processor (Intel® Xeon® E5-2630 CPU operating at 2.40 GHz), 64 GB of RAM, and the Windows 10 64-bit operating system. The algorithms were implemented in Python, utilizing the Spyder integrated development environment (IDE). To test the proposed method, we used ORLib benchmark datasets (Beasley, 1990) for the computational experiments. Each problem instance is denoted as *instance_name_x_y*, where *instance_name*, *x*, and *y* denote the instance label, number of facilities, and number of customers, respectively.

Computational experiments were conducted to evaluate the performance of three different methods: the proposed hybrid ABC-LAHC algorithm, standalone ABC, and standalone LAHC. Each algorithm was

tested on 12 well-known ORLib benchmark instances, varying in size and complexity. For statistical reliability, each instance was solved 30 times independently, and the average results are tabulated in Table 2.

Table 2: Parameters of the Proposed Hybrid ABC-LAHC Algorithm.

Instance	Optimal	ABC_LAHC	ABC	LAHC
cap71_16_50	932,615.75	**932,615.75**	**932,615.75**	**932,615.75**
cap72_16_50	977,799.40	**977,799.40**	**977,799.40**	**977,799.40**
cap73_16_50	1,010,641.45	**1,010,641.45**	**1,010,641.45**	1,010,652.56
cap74_16_50	1,034,976.98	**1,034,976.98**	**1,034,976.98**	**1,034,976.98**
cap101_25_50	796,648.44	**796,648.44**	**796,648.44**	796,820.50
cap102_25_50	854,704.20	**854,704.20**	**854,704.20**	**854,704.20**
cap103_25_50	893,782.11	**893,782.11**	893,797.18	894,038.57
cap104_25_50	928,941.75	**928,941.75**	**928,941.75**	**928,941.75**
cap131_50_50	793,439.56	**793,487.55**	794,269.53	793,778.99
cap132_50_50	851,495.33	**851,495.33**	851,655.64	**851,495.33**
cap133_50_50	893,076.71	**893,088.37**	893,429.89	893,714.52
cap134_50_50	928,941.75	**928,941.75**	**928,941.75**	**928,941.75**

The experimental results show that the proposed hybrid ABC-LAHC algorithm performs exceptionally well across all problem instances. For small-scale problems (cap71-cap74) with 16 potential facilities and 50 customers, all three algorithms showed strong performance, consistently finding optimal or near-optimal solutions. The hybrid ABC-LAHC and standalone ABC achieved the optimal solution for all instances in this category, while LAHC showed a slight deviation only in cap73, producing a solution value of 1,010,652.56 compared to the optimal 1,010,641.45.

In medium-sized instances (cap101-cap104) with 25 potential facilities, the performance differences between the algorithms became more pronounced. The hybrid ABC-LAHC maintained its robust performance, reaching optimal solutions in all four instances. The standalone ABC showed minimal deviation only in cap103, while LAHC showed increased deviation in both cap101 and cap103. These results suggest that as the problem size increases, the hybrid approach's ability to balance global exploration and local exploitation becomes more advantageous.

The most significant performance differences were observed in the larger instances (cap131-cap134) with 50 potential facilities, where the hybrid ABC-LAHC consistently outperformed both standalone algorithms, particularly in cap131 and cap133. For instance, in cap131, the hybrid approach achieved a solution of 793,487.55, compared to ABC's 794,269.53 and LAHC's 793,778.99. Similarly, for cap133, the hybrid algorithm obtained a solution of 893,088.37, while ABC and LAHC obtained 893,429.89 and 893,714.52, respectively.

As shown in Figure 2, the percentage deviations from optimal solutions reveal the comparative performance of the three algorithms across different problem instances. For small instances (cap71-cap74) with 16

potential facilities, all three algorithms demonstrate nearly identical performance with zero deviation from optimal solutions, except for LAHC showing a minimal deviation (0.001%) in cap73. In medium-sized instances (cap101-cap104) with 25 facilities, while the hybrid ABC-LAHC and ABC maintain optimal or near-optimal performance, LAHC shows increased deviations, particularly in cap103 with a deviation of about 0.029%. The most significant performance differences are observed in larger instances (cap131-cap134) with 50 facilities, where the hybrid ABC-LAHC consistently maintains lower deviations (maximum 0.006%) compared to ABC (up to 0.104%) and LAHC (up to 0.071%). These results clearly demonstrate the superior performance of the hybrid approach, especially as the problem size increases.

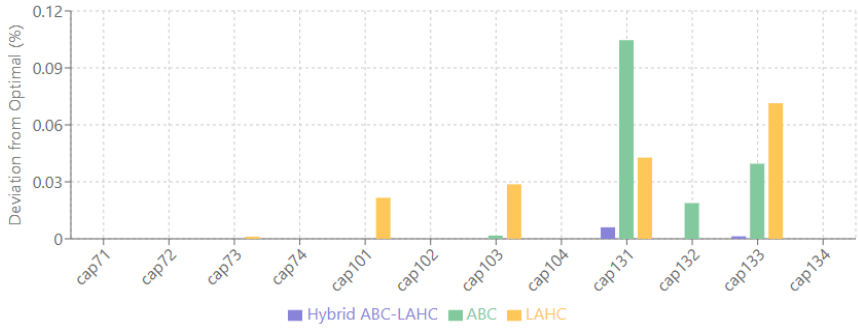

Figure 2: Percentage Deviation from Optimal Solutions for Hybrid ABC-LAHC, ABC, and LAHC Algorithms across Benchmark Instances.

The results indicate that the integration of LAHC into the ABC framework successfully improves the performance of the algorithm, especially for larger problem instances. This improvement can be attributed to the effective combination of ABC's global exploration capabilities with LAHC's memory-based local search strategy. The hybrid approach maintains better solution quality as problem complexity increases, suggesting a successful synergy between the two algorithms.

CONCLUSION

This research introduced a novel hybrid metaheuristic that effectively combines the strengths of ABC and LAHC algorithms for solving UFLP. The proposed ABC-LAHC algorithm utilizes the global exploration strengths of ABC and the memory-based local search capabilities of LAHC to achieve a balance between exploration and exploitation. The experimental analysis revealed several key findings. First, while all tested algorithms performed well on small instances, the hybrid approach demonstrated clear

advantages for larger, more complex problems. Second, the memory-based acceptance criteria of LAHC proved to be an effective complement to ABC's population-based search strategy, enabling better escape from local optima. Third, the solution quality improvements were most pronounced for instances with 50 facilities, indicating the hybrid approach scales well with problem size. The results underline the effectiveness of integrating memory-based acceptance criteria into population-based metaheuristics and demonstrate the potential of this synergy for complex combinatorial optimization problems. Future work can explore the scalability of the ABC-LAHC framework by incorporating parallel computing techniques to further enhance its computational efficiency. Additionally, applying the ABC-LAHC algorithm to constrained binary optimization problems, such as the Set-Union Knapsack Problem (Sonuç & Özcan, 2024), presents a promising research direction.

REFERENCES

Al-Sultan, K. S., and M. A. Al-Fawzan. 1999. "A Tabu Search Approach to the Uncapacitated Facility Location Problem." *Annals of Operations Research* 86(0):91–103. doi: 10.1023/A:1018956213524.

Aslan, Murat, and Mario Pavone. 2024. "MBVS: A Modified Binary Vortex Search Algorithm for Solving Uncapacitated Facility Location Problem." *Neural Computing and Applications* 36(5):2573–95. doi: 10.1007/s00521-023-09190-9.

Baş, Emine, and Erkan Ülker. 2020. "A Binary Social Spider Algorithm for Uncapacitated Facility Location Problem." *Expert Systems with Applications* 161:113618. doi: 10.1016/j.eswa.2020.113618.

Baş, Emine, and Gülnur Yildizdan. 2024. "A New Binary Arithmetic Optimization Algorithm for Uncapacitated Facility Location Problem." *Neural Computing and Applications* 36(8):4151–77. doi: 10.1007/s00521-023-09261-x.

Beasley, J. E. 1990. "OR-Library: Distributing Test Problems by Electronic Mail." *Journal of the Operational Research Society* 41(11):1069–72. doi: 10.1057/jors.1990.166.

Burke, Edmund K., and Yuri Bykov. 2017. "The Late Acceptance Hill-Climbing Heuristic." *European Journal of Operational Research* 258(1):70–78. doi: 10.1016/j.ejor.2016.07.012.

Çınar, Ahmet Cevahir. 2022. "A Comprehensive Comparison of Binary Archimedes Optimization Algorithms on Uncapacitated Facility Location Problems." *Duzce University Journal of Science and Technology* 10(1):27–38. doi: 10.29130/dubited.876284.

Cornuéjols Gérard, George Nemhauser, and Laurence Wolsey. n.d. "The Uncapacitated Facility Location Problem." 76.

Hakli, Huseyin, and Zeynep Ortacay. 2019. "An Improved Scatter Search Algorithm for the Uncapacitated Facility Location Problem." *Computers & Industrial Engineering* 135:855–67. doi: 10.1016/j.cie.2019.06.060.

Jiang, Nan, and Huizhen Zhang. 2023. “Improved Adaptive Differential Evolution Algorithm for the Un-Capacitated Facility Location Problem.” *Open Journal of Applied Sciences* 13(5):685–95. doi: 10.4236/ojapps.2023.135054.

Karaboga, Dervis, and Bahriye Basturk. 2007. “A Powerful and Efficient Algorithm for Numerical Function Optimization: Artificial Bee Colony (ABC) Algorithm.” *Journal of Global Optimization* 39(3):459–71. doi: 10.1007/s10898-007-9149-x.

Kaya, Ersin. 2022. “BinGSO: Galactic Swarm Optimization Powered by Binary Artificial Algae Algorithm for Solving Uncapacitated Facility Location Problems.” *Neural Computing and Applications* 34(13):11063–82. doi: 10.1007/s00521-022-07058-y.

Kratica, Jozef, Dušan Tošic, Vladimir Filipović, and Ivana Ljubić. 2001. “Solving the Simple Plant Location Problem by Genetic Algorithm.” *RAIRO - Operations Research* 35(1):127–42. doi: 10.1051/ro:2001107.

Özkış, Ahmet, and Murat Karakoyun. 2023. “A Binary Enhanced Moth Flame Optimization Algorithm for Uncapacitated Facility Location Problems.” *Pamukkale Üniversitesi Mühendislik Bilimleri Dergisi* 29(7):737–51.

Ozsoydan, Fehmi Burcin, and Ali Erel Kasırga. 2024. “Evolution Inspired Binary Flower Pollination for the Uncapacitated Facility Location Problem.” *Neural Computing and Applications* 36(20):12117–30. doi: 10.1007/s00521-024-09684-0.

Peidro, David, Xabier A. Martin, Javier Panadero, and Angel A. Juan. 2024a. “Solving the Uncapacitated Facility Location Problem under Uncertainty: A Hybrid Tabu Search with Path-Relinking Simheuristic Approach.” *Applied Intelligence* 54(7):5617–38. doi: 10.1007/s10489-024-05441-x.

Peidro, David, Xabier A. Martin, Javier Panadero, and Angel A. Juan. 2024b. “Solving the Uncapacitated Facility Location Problem under Uncertainty: A Hybrid Tabu Search with Path-Relinking Simheuristic Approach.” *Applied Intelligence* 54(7):5617–38. doi: 10.1007/s10489-024-05441-x.

Sonuç, Emrullah. 2021. “Binary Crow Search Algorithm for the Uncapacitated Facility Location Problem.” *Neural Computing and Applications* 33(21):14669–85. doi: 10.1007/s00521-021-06107-2.

Sonuç, Emrullah, and Ender Özcan. 2023. “An Adaptive Parallel Evolutionary Algorithm for Solving the Uncapacitated Facility Location Problem.” *Expert Systems with Applications* 224:119956. doi: 10.1016/j.eswa.2023.119956.

Sonuç, Emrullah, and Ender Özcan. 2024. “CUDA-Based Parallel Local Search for the Set-Union Knapsack Problem.” *Knowledge-Based Systems* 299:112095. doi: 10.1016/j.knosys.2024.112095.

Zhang, Fazhan, Yichao He, Haibin Ouyang, and Wenben Li. 2023. “A Fast and Efficient Discrete Evolutionary Algorithm for the Uncapacitated Facility Location Problem.” *Expert Systems with Applications* 213:118978. doi: 10.1016/j.eswa.2022.118978.

Zhang, Shuaixiang, Yixuan Yang, Hao Tong, and Xin Yao. 2024. “Learning-Based Problem Reduction for Large-Scale Uncapacitated Facility Location Problems.” Pp. 1–8 in *2024 IEEE Congress on Evolutionary Computation (CEC)*.

A Literature Review on Saltwater Intrusion Problem in Coastal Regions and Evaluation of Related Solution Proposals

Evren TURHAN[1]
Serin DEĞERLİ ŞİMŞEK[2]

1- Assoc. Prof. Dr.; Adana Alparslan Türkeş Science and Technology University. Faculty of Engineering, Department of Civil Engineering. eturhan@atu.edu.tr ORCID No: 0000-0002-0742-4848

2- Res. Asst Adana Alparslan Türkeş Science and Technology University. Faculty of Engineering, Department of Civil Engineering. sdegerli@atu.edu.tr ORCID No: 0000-0003-0208-9152

ABSTRACT

Coastal regions have a significant geopolitical location in terms of meeting the water needs of the dense population. In these regions, groundwater resources are mostly preferred. However, the discharge of aquifers containing existing water resources underground is much lower than that of surface water resources, and with uncontrolled use, saltwater intrusion problems occur in these aquifers. This study aims to examine in detail the numerical and experimental studies in the published literature where the effect of saltwater intrusion on groundwater flow is addressed and to assess the proposed solutions for this problem. Studies on different measures implemented to reduce the negative effects of saltwater intrusion are handled. Consequently, study examples from the literature were reviewed and suggestions for future studies were presented. In addition, considerations regarding saltwater intrusion in the coastal regions and possible solutions were evaluated.

Keywords – Saltwater Intrusion, Literature Review, Laminar Flow, Subsurface Dam, Coastal Aquifers.

INTRODUCTION

Due to rapid population growth and increases in global average temperatures, Türkiye is considered to be in the medium risk category in terms of per capita water consumption, and it is predicted that it may face a severe water shortage risk in the future (Karataş and Çevik, 2010:10; Gezer and Erdem, 2018:114; Şıltu and Akça, 2023:19). Such a problem reveals the importance of using water resources more efficiently. In many arid and semi-arid regions, as a result of the increased use of groundwater to meet water needs, saltwater intrusion occurs due to the mixing of low-altitude seawater into aquifers (Li et al., 2016:1). With the effect of saltwater intrusion, aquifers-which are sources of fresh water- can become polluted and unusable. The fact that almost half of the world's population lives in regions close to the coastline necessitates that this problem be researched in more detail and precautions be taken (Oude Essink GHP, 2001:430). It is possible to state the factors that trigger saltwater intrusion as the melting of glaciers and the rise in sea level, storms, tidal cycles, drought, uncontrolled water consumption and water distribution systems (Irtem, 2010:100; Tully et al., 2019:368; Goswami et al., 2020:37). Due to the increasing average temperatures at the global level, the sea level increases slightly every year. This phenomenon can expose the underground water resources in coastal areas and agricultural lands to the danger of salinity (Ding et al. 2020:312).

Under normal conditions, since the slope of the water mass layer stored in the porous soil structure is towards the sea, freshwater and

saltwater form a mixing zone due to the effect of gravity. Therefore, this event provides a certain amount of saltwater exchange required to provide the mineral requirements of underground aquifers and to maintain the salinity balance of seawater (Cooper, 1959:462; Alfarrah and Walraevens, 2018:9). However, when considerable amounts of water are drawn from the aquifers, negative pressure occurs, and saltwater intrusion into the aquifers occurs rapidly due to the vacuum effect. Since saltwater is denser than freshwater, seawater spreads from the lower parts of the aquifer in coastal regions (Bear et al., 1985:120; Kayode et al., 2017:494; Narayanan and Eldho, 2024:511). Saltwater can be transported to the inner parts of the regions adjacent to the coast through channels and tidal passes (Peng et al., 2023:2). These hydraulic structures, which were initially designed to provide fresh water transport, also cause salinization of the inner parts not adjacent to the coast due to drought and sea water rise (Noorabadi et al., 2017:4273). Figure 1 represents a diagram showing the problem of saltwater intrusion (USGS, 2024:1).

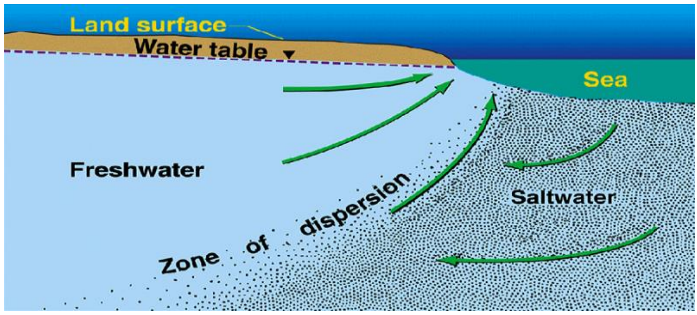

Figure 1. An example of a scheme for the saltwater intrusion problem (USGS, 2024:1)

This study aims to research in detail the numerical and experimental works in the published literature where the effect of saltwater intrusion on groundwater flow is performed and to evaluate the proposed solutions to this problem.

LITERATURE REVIEW

Todd (1953:752) researched saltwater intrusion and control methods in California, focusing on a case study of this problem in the Salinas Valley. Mohsen et al. (1990:129) applied the finite element model to two existing problems to describe the saltwater intrusion problem better. They stated that the obtained results can be helpful in terms of shedding light on the saltwater intrusion problem. Huyakorn et al. (1996:94) improved a numerical model of a sharp interface wedge to model saltwater intrusion in coastal aquifers. In

the model they created, they assumed an interface between groundwater flow and saltwater and provided the representation of the flow movement. They observed that this model, which they created using the finite element method, gave accurate results in following the location, lateral movement and upward flow of the groundwater-saltwater interface. Sbai et al. (1998:206) attempted to produce a numerical solution for estimating saltwater intrusion in the aquifers using the finite element method. They based their model on a sharp interface approach, reckoning that fresh and saltwater are immiscible. Oude Essink GHP (2001:430) investigated saltwater intrusion in groundwater flow on the north coast of the Noord-Holland region of the Netherlands. Oude Essink simulated the groundwater flow in three dimensions using the MOCDENS3D software, which allows modelling depending on density. As a result of this investigation, Oude Essink observed severe signs of salinity in the coastal areas of the Netherlands. Demirel (2004:277) stated that water needs in the Mersin-Kazanlı region of Türkiye were supplied from groundwater and that saltwater intrusion occurred as a consequence of increased water consumption. Demirel explained the history and development of saltwater intrusion until 2000 by taking water samples from some wells and using analysis results and electrical conductivity measurements. Goswami and Clement (2007:3) investigated the development of saltwater in a freshwater aquifer by creating a porous medium in a small-scale laboratory setup. In the study, the first part of the experiments was to examine how saltwater progresses in the aquifer without any external obstacles, and then they observed the status of the saltwater development wedge in the presence of a structure that prevents saltwater intrusion. They also numerically examined the obtained results in the experimental environment with the SEAWAT software. Consequently, they concluded that the model prepared as a result of a stable flow condition and external factors was suitable for use in saltwater intrusion.

Luyun Jr. et al. (2009:228) used experimental and numerical methods to investigate the effect of an impermeable underground cutoff wall on saltwater intrusion. When an impermeable cutoff wall was added to the initial state, they found that the advancing saltwater showed a retreat behaviour over time. As a result of the experiment, they saw that the saltwater spreading to the freshwater completely retreated. However, they also stated that an impermeable cutoff wall with a minimum height should be used to ensure this retreat. In addition, they examined the effect of the cutoff wall height on the saltwater withdrawal. They emphasized that the SEAWAT well numerical model represents the formed saltwater wedge. Lo´aiciga et al. (2012:43) proposed a method to assess the impacts of sea degree rise and saltwater intrusion in coastal aquifers in the 21st century. They stated that their method could be applied to different coastal aquifer scenarios. Bertorelle (2014:60) researched the experimental and numerical

simulation of a coastal aquifer by creating a homogeneous porous structure. In the numerical model, Bertorelle used the finite element software SUTRA program to simulate the change in the toe length and the thickness of the mixing section of the saltwater wedge depending on the distance of the subsurface dam used to the shore. By virtue of the study, it was specified that the physical barrier to be applied to prevent saltwater intrusion would provide the most effective protection by positioning it as close as possible to the shore. Abdoulhalik and Ahmed (2017:66) researched the effect of impermeable cutoff walls on flow behaviour in stratified inhomogeneous coastal aquifers. While preparing the experimental setup, they applied two types of stratification to represent the heterogeneous situation; in the first case, they used a system consisting of coarse-fine-coarse-grained (HLH) layers, while in the second case, they designed a fine-coarse-fine-grained (LHL) sequence. They observed that layer formation reduced the cutoff wall performance compared to the homogeneous case. They also determined that these layers caused changes in the freshwater velocity. They stated that in the HLH case, the interface was constituted in the form of a convex wedge, and the low permeability layer in the middle of the LHL layers reduced the flow velocity. Abdoulhalik et al. (2017:421) developed a new saltwater intrusion prevention system by using impermeable cutoff walls and semi-porous subsurface dams together. They compared the effects of conventionally used physical barrier methods on the saltwater wedge with their proposed new barrier. In laboratory experiments, they used glass beads of a specific diameter to make the tank suitable for a porous structure. They observed that a current with a lifting effect was formed in the foot of the saltwater wedge with this new method. They suggested that the new physical barrier type they proposed was much less costly and suitable for use in practice. Chang et al. (2019:512) investigated the effects of subsurface dams on saltwater intrusion and freshwater flow in their study. In addition to the minimum height at which the dam should be built, they focused on the environmental impacts of groundwater use. They evaluated the scenarios that would occur depending on the dam's height and the change in its distance to the saltwater source. They found that if the dam height remained below the predicted value, the passage of saltwater could not be prevented and therefore, fresh water access was limited. In addition to the minimum height at which the dam should be constructed, they also focused on the environmental impacts of groundwater use. They evaluated the scenarios that would occur if the dam height and distance to the saltwater source changed. They found that if the dam height remained below the predicted value, saltwater intrusion could not be prevented and therefore, fresh water access was limited. They applied both a numerical and experimental method in their study. Hussain et al. (2019:1-20) investigate hydraulic and physical management strategies to reduce and control saltwater intrusion in coastal

aquifers. In addition, they explained the benefits and drawbacks of each saltwater intrusion control approach.

Vats et al. (2020:3556) explain that a groundwater circulation well (GCW) system can significantly reduce the intrusion and can be considered as a robust strategy to control the saltwater intrusion problem in unconfined coastal aquifers. Etsias et al. (2021:4) conducted laboratory experiments and numerical modelling to inquire about the saltwater intrusion into cracked aquifers. They investigated the effects of different interference variables, including wedge length, mixing zone, and aquifer through which saltwater propagation occurs. Abd-Elaty et al. (2021:6) researched the methods of controlling saltwater intrusion caused by rising sea levels in various climate zones. They used SEAWAT for numerical modelling. As a result, they concluded that strategies for reducing saltwater intrusion and isolating this salt should be evaluated according to precipitation rates. Abd-Elaty et al. (2022:10) created an integrated surface-groundwater model using fill materials on the coastline. They explained that saltwater intrusion could be decelerated. Abd-Elhamid et al. (2022:9) researched experimental and numerical models using the SEAWAT program in their studies. They interpreted the rise of seawater and the decrease of water level in coastal aquifers on different evaluations. They stated that they achieved an excellent agreement with both methods. As a result, they explained that the variable sea water level makes significant contributions in terms of its effect on the interference of groundwater in the aquifers. Ahmed et al. (2022:8) tested synthetic aquifers with different structural conditions to study saltwater intrusion. They stated that the wedge length generally decreases in the heterogeneous case and increases in the mixing region compared to the homogeneous conditions. They emphasized that in regions with less permeability, the intrusion is horizontally short but longer vertically. Crestani et al. (2022:8) studied saltwater intrusion in homogeneous porous conditions for 36 hours in laboratory experiments. They utilized the SUTRA code to develop this intrusion wedge. As a result, they obtained satisfactory approximations between the observation data and the numerical models.

Emara et al. (2023:10) investigated the dynamics of saltwater intrusion and aquifer heterogeneity by experimental and numerical modelling. They investigated the two-layered case according to the hydraulic conductivity of the aquifers. They evaluated the practicability of constructing inclined cut-off walls in terms of the intrusion. Peng et al. (2023:2) established a groundwater tracing side view in a mangrove wetland and generated a numerical model of tidal induced groundwater flow that was adjusted according to salt and pressure. They stated that almost all groundwater flow rate to the mangrove wetland was saltwater. Wu et al. (2023:8) researched an analytical methodology for anticipating the level of saltwater intrusion with different solution techniques. It is explained that this methodology can be a useful analytical tool to control the seawater wedge

extents in coastal aquifers. Şen (2023:825) states that sub-surface dam projects are similar in structure to each other in particular and different alternative dam projects are presented. Both types are formed with artificial trenches that have more hydraulic conductivity than the outlying Quaternary alluvial deposits. Şen explained that these dams in this formation can be sustainable and manageable compared to classical ones. Şen also stated that it is important to develop numerical calculation models of groundwater movement in future studies. Abd-Elaty et al. (2024:1-14) investigated various geometries of mixed physical subsurface barriers to control saltwater intrusion not only in homogeneous and but also in heterogeneous layered aquifers. They expressed that all modelling outputs were performed by SEAWAT code. Their obtained numerical models were compared with experimental data. As a result, they indicated that the decrease of the seawater wedge reached high percentage levels for indiscrete and discrete layered aquifers if the barrier wall was located onshore and the dam on the coast. On the contrary, if the dam was located onshore and the wall on the coast, this wedge occurred by a lower value for both indiscrete and discrete layered ones. Abdoulhalik et al. (2024:6) tested the mixed physical barriers to investigate the saltwater intrusion behaviour. They evaluated the SEAWAT code for validation. As a result of their study, they predicted that this type of barrier application could reduce the mentioned intrusion effect in coastal aquifers. Kassem et al. (2024:7) emphasized the bibliometric analysis of saltwater intrusion problem studies between 1970 and 2023 years. They stated that among the saltwater intrusion reducing strategies, physical barriers can be effective control methods, furthermore pumping optimization may be thought a cost-effective approach. Ismail et al. (2024:11) evaluated research examples and results related to saltwater intrusion problem in the coastal regions. They stated that the MODFLOW program is a frequently used numerical method. As a general result of their studies, they emphasized that numerical methods are essential in evaluating the saltwater intrusion phenomenon when considered together with geophysical methods used in field investigations. Saqr and Abd-Elmaboud (2024:1-17) tried to explain the behaviour of saltwater intrusion, discuss the causes and effective factors, and also to evaluate the solution methods. They also analyzed the saltwater intrusion phenomenon in the Nile Delta, Sinai Peninsula, and North-West coast of Egypt. They discussed some proposals and precautions that could shed light on future studies. Karayel and Vaheddoost (2024:24) constituted a laboratory-scale experimental setup to solve the problem of saltwater intrusion in their study. They created a porous medium and tried to determine the vertical-horizontal velocity and acceleration. They examined the length of the fresh and saltwater wedge.

SOLUTION PROPOSALS

There are various solutions to prevent saltwater intrusion; limiting water use, changing well locations, hydraulic and physical barriers can be given as examples (Kumar, 2006:3; Allow, 2012:1152; Hussain et al., 2019:2; Abd-Elaty et al., 2021:2; Abd-Elaty et al., 2022:4; Emara et al., 2023:2; Wu et al., 2023:2; Abdoulhalik et al., 2024:1; Abd-Elaty et al. 2024:5; Kassem et al., 2024:6; Saqr and Abd-Elmaboud, 2024:4). In fact, the basis for controlling saltwater intrusion is to retain the amount of water flowing into the aquifer with flowing out of the aquifer. Many different techniques such as groundwater head measuring, geophysical investigation, geochemical investigation, isotopic methods, remote sensing, field surveys... etc, are used to continuously monitor coastal aquifers (Saqr and Abd-Elmaboud, 2024:1-17). Recently, various software has emerged to model the intrusion phenomenon in coastal aquifers, such as SUTRA, CODESA, MOCDENS, SEAWAT, FEFLOW, FEMWATER…etc. (Ismail et al., 2024:3). Apaydın (2014:34) defines underground or subsurface dams as underground engineering structures in which an impermeable barrier is created against groundwater flow and stored in the aquifer. Apaydın (2022a:3; 2023:2) explained in the study that slurry wall application is rarely considered in sub-surface dams, but it has been applied in a wide variety of areas, especially for surface dams in the world and in Türkiye, but in terms of the subsurface dams it has become operational in Türkiye from the 2019 year. A subsurface or underground dam is a barrier built underground to store groundwater or increase existing groundwater behind a cutoff wall (Apaydın, 2022b:131).

Subsurface Dam

Subsurface dams are one of the main methods of obtaining water from freshwater aquifers. Storing water underground is not a new method; subsurface dams were constructed in Sardinia and Tunisia during the Roman period, and there are studies indicating that they have been formed in North Africa since antiquity (Ertsen and Hut 2009:14; Apaydın, 2022b:132). It is stated that in recent years, these dams of several dimensions have started to be constructed in multiple territories of the earth, especially in South and East Africa and India (Apaydın, 2022b:132). Subsurface dams are divided into two as; cut-off wall and sand storage dams. These storage dams are designed to store sediment carried by streamflow, but at the end of their economic life, the sediment accumulated behind the dam completely fills the reservoir (Ishida et al., 2011:51). In this case, an artificial aquifer is obtained and if the permeability of the water and sediment accumulated behind the dam is high, it can be put into use with the help of a pump (Figure 2) (Şen, 2023:6).

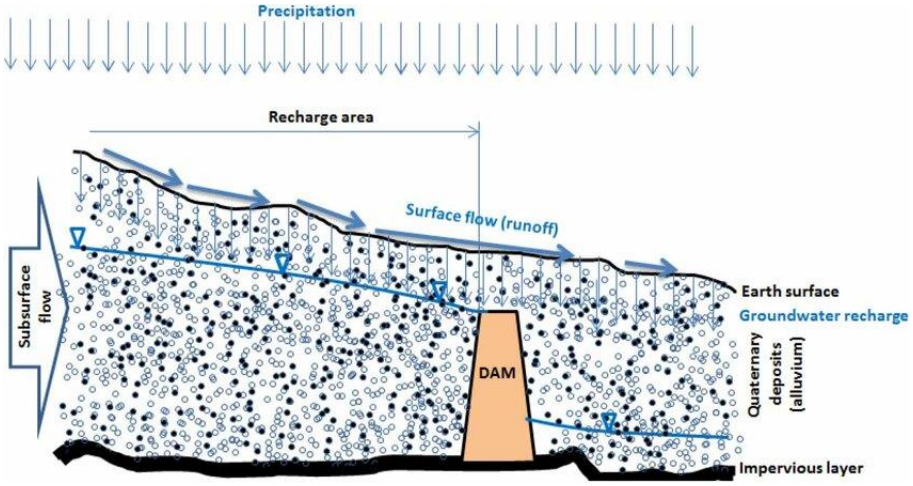

Figure 2. A completely burried subsurface dam example (Şen, 2023:824)

Although they contain more fresh water compared to surface sources, subsurface dams have their own advantages and disadvantages. Large agricultural and living areas may need to be evacuated for pond reservoirs, but since the reservoir will not occupy any area in these dams, such a problem is not encountered most of the time. Since the upstream and downstream of the obstacle in the subsurface dams are filled with granular material, catastrophic floods are rarely seen in the event of a dam-break or breach. In the surface dams, the dead volume fills the entire reservoir at the end of the economic life, preventing the dam from being utilized, but since the reservoir is filled with this material in the subsurface dams, this situation is prevented. Since there is no contact with sunlight, evaporation and eutrophication events are at negligible levels in these dams. Subsurface dams mostly provide advantages over surface dams in terms of both cost and project duration (Chang et al., 2019:508).

These dams certainly have some disadvantages compared to surface dams. For example, while the streamflow can be measured very easily with the help of a meter and water depth, it is more difficult to determine the recharge period and capacity of an underground aquifer. If the water level rises above the ground surface level behind this dam, it can cause a swamp formation on the surface (Apaydın, 2014:51). Since the reservoir in surface dams is open to the atmosphere, it can be exposed to pollution by external factors, and although this situation is somewhat more controlled in the subsurface dams, saltwater intrusion can threaten the aquifer balance in coastal regions (USGS, 2024:1). Figure 3 shows types of physical barriers (Chang et al., 2019).

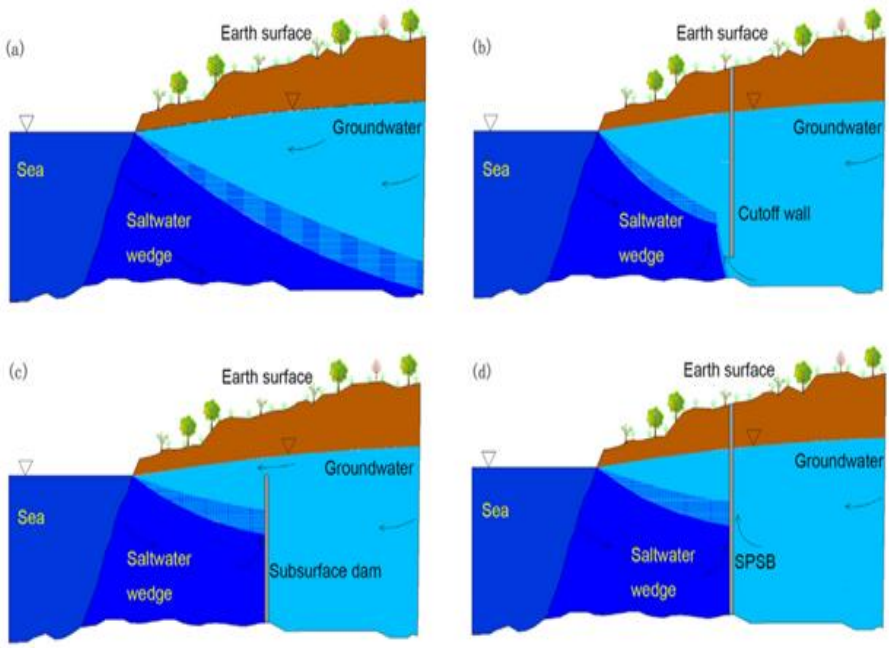

Figure 3. Types of physical barriers to the saltwater intrusion (Chang et al., 2019:509)

Subsurface dams are generally small capacity storage structures that can meet local needs. Compared to surface dams, their body volume is smaller, their engineering structures are simpler, and therefore their construction costs are lower. Although they are more straightforward, cheaper, and mostly smaller than surface dams, they can be more complex in terms of exploration techniques (Apaydın, 2022b:14).

As a result, the literature examples as regards to numerical and experimental studies, handled in this study are briefly summarised in Table 1.

Table 1. Literature summary

Author/s	Numerical Model	Laboratory Set-up	Conclusions
Goswami and Clement (2007)	SEAWAT	Three chambers rectangular section test system	They proposed a more practical method than the Henry problem for modelling saltwater intrusion in steady and unsteady states.
Luyun Jr. et al. (2009)	SEAWAT	Three chambers rectangular section test system	They found that decreasing the impermeable cut-off wall length accelerates the saltwater withdrawal process.
Allow (2012)	SEAWAT	A case study	They stated that their outputs from the study could prove many solutions to the saltwater intrusion problem by utilizing the subsurface barrier and injection systems.
Bertorelle (2014)	SUTRA	Three chambers rectangular section test system	It has been stated that the physical barrier should be positioned as close as possible to the source of the contaminating saltwater.
Abdoulhalik and Ahmed (2017)	SEAWAT	Three chambers rectangular section test system	It was emphasized that the proposed mixed physical barrier system can be performed more effectively and at a lower cost compared to existing methods.

Table 1. (Continued)

Author/s	Numerical Model	Laboratory Set-up	Conclusions
Abdoulhalik et al. (2017)	SEAWAT	Three chambers rectangular section test system	They stated that layers with different porosity applied from the compartment containing the porous material affect the saltwater intrusion behaviour.
Noorabadi et al. (2017)	SEAWAT	Two chambers rectangular section test system	They stated that the SEAWAT simulation outputs produce results that were similar tothe experimental ones.
Chang et al. (2019)	SEAWAT	Three chambers rectangular section test system	They stated that the effective dam height can be preferred to obtain the most optimum cost values.
Vats et al. (2020)	FEMWATER	A laboratory-scale flow tank model	They emphasized that their proposed system can availably control the saltwater intrusion problem in coastal zones.
Etsias et al. (2021)	SUTRA	Two cylindrical tanks and a chamber	They researched the evaluation of individual fractures in terms of the saltwater intrusion movement problem.
Abd-Elaty et al. (2021)	SEAWAT	A case study	They performed to effectively prevent saltwater intrusion problems because of sea level rises for different climate regions as regards to determined areas.
Abd-Elaty et al. (2022)	SEAWAT	A case study	They used a new integrated surface-groundwater model with fill materials to control the saltwater intrusion problem.

Table 1. (Continued)

Author/s	Numerical Model	Laboratory Set-up	Conclusions
Abd-Elhamid et al. (2022)	SEAWAT	A flow tank	They performed various scenario trials to evaluate the effect of saline increases and presented many approaches for preventing the intrusion problem.
Ahmed et al. (2022)	SUTRA	Three-dimensional the sandbox setup	They analyzed the saltwater intrusion problem using experimental and numerical methods with a complicated laboratory-scale aquifer.
Crestani et al. (2022)	SUTRA	An experimental sandbox set-up	They conducted saltwater intrusion experiments and compared the experiment results with the numerical data.
Emara et al. (2023)	SEAWAT	A porous medium tank	They researched the saltwater intrusion dynamics using several cutoff-wall properties with laboratory and numerical studies.
Narayanan and Eldho (2024)	SEAWAT	A regional-scale model	They investigated saltwater intrusion wedge movement in a coastal aquifer for the design of a well system for desalination plants.
Abd-Elaty et al. (2024)	SEAWAT	A case study	They investigated many various geometries of complicated physical subsurface barriers to analyze the saltwater intrusion problem in the several layered aquifers.

Table 1. (Continued)

Author/s	Numerical Model	Laboratory Set-up	Conclusions
Abdoulhalik et al. (2024)	SEAWAT	A flow tank	They performed a mixed barriers in a heterogeneous coastal aquifer and tested the saltwater intrusion behaviour.
Karayel and Vaheddoost (2024)	---	A laboratory-scale tank model	They researched the problem of saltwater intrusion in coastal zones using an experimental setup of certain dimensions and examined the variations in velocity and acceleration parameters.

CONCLUSIONS

Global temperature increase causes above-average water evaporation in terms of surface water resources. There are cases where subsurface dams are preferred in order to meet the people's water demand, which is concentrated in coastal areas. However, as in every natural resource, there are external factors that prevent the sustainability of aquifers in terms of water management. One of the most important of these factors is saltwater intrusion. This intrusion is one of the elements that threaten the quality of life on the coastline and it is the principle to identify the saltwater intrusion action process in detail in order to take the necessary precautions. In addition, since the saltwater intrusion can cause significant environmental problems, various solution methods should be developed in order to prevent its negative effects.

In this study, a literature review is presented that considers current studies on saltwater intrusion. The aim is to provide essential contributions for future studies. Such studies will play a major role in explaining the behaviour of underground flow dynamics. Like many places in the world, groundwater pollution problems will arise in many regions close to the coast of Türkiye due to excessive water use. One of the solution proposals in this study, the construction of subsurface dams, can be considered an important solution in terms of meeting water needs and against drought. As a result, in the future, the improvement of influential management strategies for the coastal aquifers, detailed examination of groundwater movement and distribution with experimental and numerical studies, and preparation of opportunities for more application of subsurface dams with appropriate site selections can be evaluated as important achievements for the environmental problem solving.

REFERENCES

Abd-Elaty, I., Straface, S., and Kuriqi, A. (2021). Sustainable saltwater intrusion management in coastal aquifers under climatic changes for humid and hyper-arid regions. Ecological Engineering, 171, 1-11. https://doi.org/10.1016/j.ecoleng.2021.106382

Abd-Elaty, I., Kushwaha, N.L., Grismer, M.E., Elbeltagi, A., and Kuriqi, A. (2022). Cost-effective management measures for coastal aquifers affected by saltwater intrusion and climate change. Science of The Total Environment, 836, 1-13. http://dx.doi.org/10.1016/j.scitotenv.2022.155656

Abd-Elaty, I., Kuriqi, A., and Ahmed, A.A. (2024). Effectiveness of different mixed physical barriers in controlling seawater intrusion in homogeneous and layered coastal aquifers. Groundwater for Sustainable Development, 27, 1-14. https://doi.org/10.1016/j.gsd.2024.101318

Abd-Elhamid, H.F., Abdel-Aal, G.M., Fahmy, M., Sherif, M., Zeleˇnáková, M., and Abd-Elaty, I. (2022). Experimental and numerical study to investigate the impact of changing the Boundary Water Levels on Saltwater Intrusion in coastal aquifers. Water MDPI, 14(631), 1-16. https://doi.org/10.3390/w14040631

Abdoulhalik, A., and Ahmed, A.A. (2017). The effectiveness of cutoff walls to control Saltwater Intrusion in Multi-Layered Coastal Aquifers: Experimental and numerical study. Journal of Environmental Management, 199, 62-73. https://doi.org/10.1016/j.jenvman.2017.05.040

Abdoulhalik, A., Ahmed, A. A., and Hamill, G.A. (2017). A new physical barrier system for seawater intrusion control. Journal of Hydrology, 549, 416-427. https://doi.org/10.1016/j.jhydrol.2017.04.005

Abdoulhalik, A., Ahmed, A. A., and Abd-Elaty, I. (2024). Effects of layered heterogeneity on mixed physical barrier performance to prevent seawater intrusion in coastal aquifers. Journal of Hydrology, 24, 637, 1-10. https://doi.org/10.1016/j.jhydrol.2024.131343

Ahmed, A., Robinson, G., Hamill, G., and Etsias, G. (2022). Seawater Intrusion in extremely heterogeneous laboratory-scale aquifer: Steady-State Results. Water MDPI, 14(1069), 1-20. https://doi.org/10.3390/w14071069

Alfarrah, N., and Walraevens, K. (2018). Groundwater overexploitation and Seawater Intrusion in coastal areas of arid and semi-arid regions. Water MDPI, 10(143), 1-24. https://doi:10.3390/w10020143

Allow, K.A. (2012). The use of injection wells and a subsurface barrier in the prevention of seawater intrusion: a modelling approach. Arab J Geosci, 5, 1151-1161. https://doi:10.1007/s12517-011-0304-9

Apaydın, A. (2014). *Yer Seçiminden İşletmeye Yeraltı Barajları*. Ankara: Orman ve Su İşleri Bakanlığı, Devlet Su İşleri Genel Müdürlüğü (DSİ), 1-258 (In Turkish).

Apaydın, A. (2022a). Application, impermeability performance and protection of slurry concrete wall in underground dams. The Black Sea Journal of Sciences, 12(2), 619-633. https://doi:10.31466/kfbd.1085292

Apaydın, A. (2022b). Applicability of underground dams in Turkey and evaluation of the "Underground Dams Action Plan". Konya Journal of Engineering Sciences, 10(1), 130-146. https://doi:10.36306/konjes.984539

Apaydın, A. (2023). Applicability of the slurry trench cut-off wall method in underground dams: the first examples in Türkiye in the 2020s. Arabian Journal of Geosciences, 16(363), 1-11. https://doi.org/10.1007/s12517-023-11453-7

Bear, J., Shamir, U, Gamliel, A., and Shapiro, A.M. (1985). Motion of the seawater interface in a coastal aquifer by the method of Successive Steady States. Journal of Hydrology, 76, 119-132.

Bertorelle, E. (2014). *Laboratory experiments on the saltwater intrusion process*. Padova- Italy: Master's Thesis, University of Padova.

Chang, Q., Zheng, T., Zheng, X., Zhang, B., Sun, Q., and Walther, M. (2019). Effect of subsurface dams on saltwater intrusion and fresh groundwater discharge. Journal of Hydrology, 576, 508-519. https://doi.org/10.1016/j.jhydrol.2019.06.060

Cooper, H.H. Jr. (1959). A hypothesis concerning the dynamic balance of fresh water and salt water in a coastal aquifer. Journal of Geophysical Research, 64(4), 461-467.

Crestani, E., Camporese, M., Belluco, E., Bouchedda, A., Gloaguen, E., and Salandin, P. (2022). Large-scale physical modeling of salt-water intrusion. Water MDPI, 14(1183), 1-13. https://doi.org/10.3390/w14081183

Demirel, Z. (2004). The history and evaluation of saltwater intrusion into a coastal aquifer in Mersin, Turkey. Journal of Environmental Management, 70, 275-282. https://doi:10.1016/j.jenvman.2003.12.007

Ding, Z., Koriem, M.A., Ibrahim, S.M., Antar, A.S., Ewis, M.A., He, Z., and Kheir, A.M.S. (2020). Seawater intrusion impacts on groundwater and soil quality in the northern part of the Nile Delta, Egypt. Environmental Earth Sciences, 79(313), 1-11. https://doi.org/10.1007/s12665-020-09069-1

Emara, S.M., Gado, T.A., Zeidan, B.A., and Armanuos, A.M. (2023). Evaluating the impact of inclined cutoff-wall to control seawater intrusion in heterogeneous coastal aquifers. Water Resources Management, 37, 6021-6050. https://doi.org/10.1007/s11269-023-03641-7

Ertsen, M., and Hut, R. (2009). Two waterfalls do not hear each other. Sand-storage dams, science and sustainable development in Kenya. Physics and Chemistry of the Earth, Parts A/B/C, 1-2, 14-22. https://doi.org/10.1016/j.pce.2008.03.009

Etsias, G., Hamill, G.A., Campbell, D., Straney, R., Benner, E.M., Águila, J.F., McDonnell, M.C., Ahmed, A.A., and Flynn, R. (2021). Laboratory and numerical investigation of saline intrusion in fractured coastal aquifers. Advances in Water Resources, 149, 1-16. https://doi.org/10.1016/j.advwatres.2021.103866

Gezer, A., and Erdem, A. (2018). Determination of public awareness on water stress, water scarcity and water saving: Akdeniz University Case Study. Artvin Çoruh University, Natural Hazards Application and Research Center, Journal of Natural Hazards and Environment, 4(2), 113-122. https://doi.org/10.21324/dacd.408379

Goswami, R.R., and Clement, T.P. (2007). Laboratory-scale investigation of saltwater intrusion dynamics. Water Resources Research, 43, W04418, 1-11. https://doi:10.1029/2006WR005151

Goswami, G., Basack, S., Mastorakis, N., Saikia, A., Nilo, B., and Ahmed, N. (2020). Coastal ground water flow and management. International Journal of Mechanics, 14, 37-48. https://doi:10.46300/9104.2020.14.5

Hussain, M.S., Abd-Elhamid, H.F., Javadi, A.A., and Sherif, M.M. (2019). Management of seawater intrusion in coastal aquifers: A review. Water MDPI, 11(2467), 1-20. https://doi:10.3390/w11122467

Huyakorn, P.S., Wu, Y.S., and Park, N.S. (1996). Multiphase approach to the numerical solution of a sharp interface saltwater intrusion problem. Water Resources Research, 32(1), 93-102.

Irtem, E. (2020). Kıyı akiferlerinde tuzlanma ve kıyı akiferlerinin yönetimi. Izmir: *6. Ulusal Kıyı Mühendisliği Sempozyumu*, 312, 99–106. (In Turkish)

Ishida, S., Tsuchihara, T., Yoshimoto, S., and Imaizumi, M. (2011). Sustainable use of groundwater with underground dams. Japan Agricultural Research Quarterly: JARQ, 45(1), 51-61.

Ismail, M., Pradhanang, S.M., Boving, T., Motta, S., McCarron, B., and Volk, A. (2024). Review of modeling approaches at the freshwater and saltwater interface in coastal aquifers. Land MDPI, 13(1332), 1-23. https://doi.org/10.3390/land13081332

Karayel, A.N., and Vaheddoost, B. (2024). Kıyı bölgesinde tuzluluk girişiminin laboratuvar ölçekli incelenmesi. Konya: *2nd International Conference on Scientific and Academic Research (ICSAR)*, 22-25.

Karataş, M., and Çevik, S. (2010). Stratejik doğal kaynak olarak su ve Türkiye'nin konumunun değerlendirilmesi. Akademik Araştırma Dergisi, 45, 1–29 (In Turkish).

Kassem, A., Sefelnasr, A., Ebraheem, A.A., and Sherif, M. (2024). Seawater intrusion physical models: A bibliometric analysis and review of mitigation strategies. Journal of Hydrology, 634, 1-17. https://doi.org/10.1016/j.jhydrol.2024.131135

Kayode, O.T., Odukoya, A.M., and Adagunodo, T.A. (2017). Saline water intrusion: Its management and control. Journal of Informatics and Mathematical Sciences, 9(2), 493-499.

Kumar, C.P. (2006). Management of groundwater in saltwater ingress coastal aquifers. National Institute of Hydrology, 540–560.

Li, C., Liu, T., Xu, S., Gao, X., and Wang, Y. (2016). Groundwater salinization in shallow aquifers adjacent to a low-altitude inland salt lake: a case study at Yuncheng Basin, northern China. Environ Earth Sci, 75 (370), 1-14. https://doi.org/10.1007/s12665-016-5260-y

Loaiciga, H.A., Pingel, T.J., and Garcia, E.S. (2012). Sea water intrusion by Sea-Level Rise: Scenarios for the 21st Century. Groundwater NGWA, 50(1), 37-47. https://doi.org/10.1111/j.1745-6584.2011.00800.x

Luyun, R., Momii, K., and Nakagawa, K. (2009). Laboratory-scale saltwater behavior due to subsurface cutoff wall. Journal of Hydrology, 377(3–4), 227–236. https://doi.org/10.1016/j.jhydrol.2009.08.019

Narayanan, D., and Eldho, T.I. (2024). Potential impacts of saline groundwater pumping on seawater intrusion in a coastal aquifer system. ISH Journal of Hydraulic Engineering, 30(4), 511-521. https://doi.org/10.1080/09715010.2024.2366454

Noorabadi, S., Sadraddini, A.A., Nazemi, A.H., and Delirhasannia, R. (2017). Laboratory and numerical investigation of saltwater intrusion into aquifers. Journal of Materials and Environmental Sciences, 8(12), 4273-4283.

Oude Essink, G.H.P. (2001). Improving fresh groundwater supply problems and solutions. Ocean & Coastal Management Journal, 44, 429-449.

Peng, K., Heiss, J.W., Xie, X., Yan, L., Deng, Y., Gan, Y., Li, Q., and Zhang, Y. (2023). Groundwater discharge and saltwater-freshwater mixing in a mangrove wetland over tidal cycles: A field and modeling study. Journal of Hydrology, 620, 1-15. https://doi.org/10.1016/j.jhydrol.2023.129472

Saqr, A.M., and Abd-Elmaboud, M.E. (2024). Management of saltwater intrusion in coastal aquifers: A review and case studies from Egypt. Online Journal of Engineering Sciences, 3(982), 1-17. https://doi.org/10.31586/ojes.2024.982

Sbai, M.A., Larabi, A., and Smedt, F. D. (1998). Modelling saltwater intrusion by a 3-D sharp interface finite element model. Transactions on Ecology and the Environment Journal, 17, 1-8.

Sherif, M.M., Singh, V.P., and Amer, A.M. (1990). A note on saltwater intrusion in coastal aquifers. Water Resources Management, 4, 123-134.

Şen, Z. (2023). Longitudinally and laterally trench-supported subsurface dam innovative design procedures. Water Supply Journal, IWA Publishing, 23(2), 821-835. https://doi:10.2166/ws.2023.023

Şıltu, E., and Akça, L. (2023). *Climate Change and groundwater and surface water resources of Türkiye*. Ankara: Turkish Academy of Sciences Publication, 11-28. https://doi:10.53478/TUBA.978-625-8352-56-6.ch01

Todd, D.K. (1953). Sea-water intrusion in coastal aquifers. Transactions, American Geophysical Union, 34(5), 749-754.

Tully, K., Gedan, K., Epanchin-Niell, R., Strong, A., Bernhardt, E.S., Bendor, T., Mitchell, M., Kominoski, J., Jordan, T.E., Neubauer, S.C., and Weston, N.B. (2019). The invisible flood: The chemistry, ecology, and social implications of coastal saltwater intrusion. BioScience, 69(5), 368–378. https://doi.org/10.1093/biosci/biz027

U.S. Geological Survey (USGS) (2024). *Seawater Intrusion*. United States of America, https://ca.water.usgs.gov/sustainable-groundwater-management/seawater-intrusion-california.html. Access Date: 01.10.2024

Vats, O.P., Sharma, B., Stamm, J., and Bhattacharjya, R. K. (2020). Groundwater circulation well for controlling saltwater intrusion in coastal aquifers: Numerical study with experimental validation. Water Resources Management, 34, 3551-3563. https://doi.org/10.1007/s11269-020-02635-z

Wu, H., Lu, C., Shen, C., and Ye, Y. (2023). Using a subsurface barrier to control seawater intrusion and enhance groundwater extraction in coastal aquifers: An analytical study. Journal of Hydrology, 621, 1-11. https://doi.org/10.1016/j.jhydrol.2023.129537

Synthetic Gasoline

Gökhan ÖZTÜRK[1]
Müjdat FIRAT[2]

1- Lecturer; Department of Mechanical and Metal Technologies, Vocational School of Technical Sciences, Batman University. gokhan.ozturk@batman.edu.tr ORCID No: 0000-0002-2780-6966
2- Assoc. Prof. Dr.; Department of Automotive Engineering, Faculty of Technology, Fırat University. mfirat@firat.edu.tr ORCID No: 0000-0001-6978-9044

ABSTRACT

We created synthetic petrol as an alternative to natural gas and other fossil fuels. The substance is constituted of hydrocarbons obtained from diverse organic substrates, particularly from origins including coal, natural gas, bituminous shale, methanol, and biomass. This fuel is produced to minimize environmental impacts and reduce dependence on fossil fuels.

Fischer-Tropsch synthesis, Methanol-Benzene (MTG), and Dimethyl Ether-Benzene (DTG) technologies stand out among the production methods. The Fischer-Tropsch method enables the conversion of gaseous carbon monoxide and hydrogen into synthetic petrol and other fuels by chemical reactions. MTG represents a catalytic process through which methanol is transformed into gasoline and various other hydrocarbon compounds. DTG is characterized by the transformation of methanol into dimethyl ether, which subsequently undergoes conversion into gasoline derivatives.

Synthetic gasoline is notable for its environmentally friendly properties; it has lower emission values compared to conventional gasoline. However, it has disadvantages such as production costs and environmental impacts. High energy consumption and greenhouse gas emissions that may occur during the production process pose a problem in terms of sustainability goals. In the future, the development of more innovative and cost-effective methods for synthetic gasoline production is critical for energy security and environmental sustainability.

Keywords-Synthetic Gasoline, Alternative Fuel, Production Methods, Sustainability, Energy Security.

INTRODUCTION

As a substitute to natural gasoline, synthetic gasoline is a kind of fuel. In order to lessen environmental effect and decrease reliance on fossil fuels, synthetic gasoline is manufactured. Hydrocarbons that have been synthesized from coal, natural gas, bituminous shale (schist), methanol, dimethyl ether, biomass, or other organic substances often make up synthetic gasoline. Spark-ignition engines may run on synthetic gasoline, which is a premium fuel (Ram and Salkuti, 2023:6).

1. Resources employed in the manufacture of synthetic gasoline

1.1.Coal

The designation "coal" pertains to an organic material characterized by the presence of carbon, hydrogen, oxygen, and minuscule quantities of sulfur, nitrogen, and various other elements. Plant materials become fossilized over millions of years, creating coal as a result of physical and chemical reactions (Van Krevelen, 1993). Figure 1 shows coal.

Figure 1 Coal

Coal constitutes one of the most prevalent sources of fossil fuels on the planet. Approximately 40 percent of global energy generation is derived from coal. Additionally, it is employed in a myriad of industrial processes in sectors such as cement manufacturing, steel production, and chemical synthesis (Miller, 2010). Coal is categorised into three types: lignite, hard coal, and anthracite. Lignite is the most recent and lowest-quality coal kind. Hard coal is greater in quality and tougher than lignite. Anthracite is the highest quality and hardest type of coal (Berkowitz, 1985). The utilization of coal has faced substantial scrutiny due to its ecological ramifications. The process of coal combustion leads to the emission of carbon monoxide, carbon dioxide, sulfur dioxide, nitrogen oxides, and a myriad of other harmful substances. The emission of these gases plays a significant role in exacerbating air pollution and advancing global climate change. Furthermore, coal extraction and transportation cause environmental issues (Ward, 1984). Because of its low cost, coal is still favoured as a fuel source in many countries. Nevertheless, in light of the recent proliferation of renewable energy sources, numerous initiatives have been undertaken to curtail the reliance on coal and supplant it with environmentally sustainable energy alternatives. However, coal remains an essential part of global energy production, and reducing its use will be a slow but continuous process.

1.2.Natural Gas

Natural gas is characterized as a colorless and odorless gaseous substance, classified within the category of fossil fuels. It predominantly comprises hydrocarbon gases, including but not limited to methane, propane, ethane, and butane. The formation of natural gas occurs over extensive periods due to the thermal and pressure-induced decomposition of organic matter that transpires beneath the Earth's surface as a consequence of geological processes (Speight, 2018). Natural gas is the cleanest fuel among fossil fuel sources. Unlike other fossil fuels, natural gas combustion produces extremely few hazardous

pollutants into the atmosphere. Natural gas burning produces less carbon dioxide (CO_2), sulfur oxide (SO_X), nitrogen oxide (NO_X), and particulate matter emissions than fossil fuel combustion (Wei and Geng, 2016: 264). The usage areas for natural gas are quite wide. It is especially used in energy production, heating, industrial processes, and vehicle fuel. Furthermore, gaseous substances including ethane, propane, and butane, derived from the fractionation of natural gas, are employed for both industrial applications and residential uses (Mokhatab et al., 2013). Figure 2 shows a natural gas well.

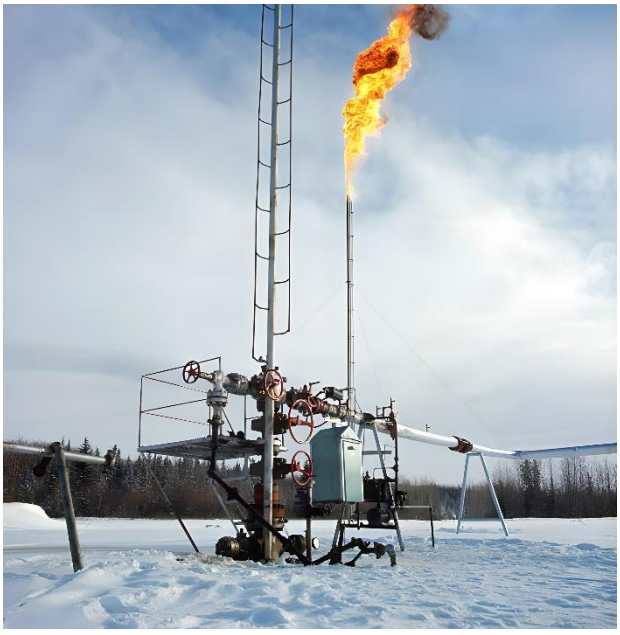

Figure 2 Natural gas well

Worldwide natural gas reserves are quite high. Natural gas occupies a significant position within the global energy supply framework. Russia, Iran, Qatar, USA, and Canada are among the largest natural gas producers (Economides and Wood, 2009:1). Natural gas is transported and stored using various ways such as pipes, ships, and tanks. Compressing and liquefying natural gas enhances its storage and carrying capacity, making natural gas transportation more cost effective (Quinn and MacDonald, 1992:1097). Although natural gas has a significant role in the energy sector, its use produces environmental issues because it is a hydrocarbon resource. Irreversible issues such as water contamination, environmental degradation, habitat loss, and climate change develop, particularly during the extraction, transportation, and storage of natural gas. As a result, steps for the sustainable use of natural gas are required.

1.3. Bituminous Shale (Schist)

Bituminous shale (Schist) is a resource that arises during the exploitation of fossil fuels such as natural gas and oil. It is typically found between layers of clay and sandy shale. Bituminous shale contains a high percentage of organic matter, and when this organic matter undergoes thermal and pressure decomposition, it causes the formation of hydrocarbons such as oil and natural gas. The hydrocarbons in bituminous shale generally have a dense, tar-like structure and are therefore not suitable for direct use (Patel et al., 2022:108). In Figure 3, examples of bituminous shale rocks are shown.

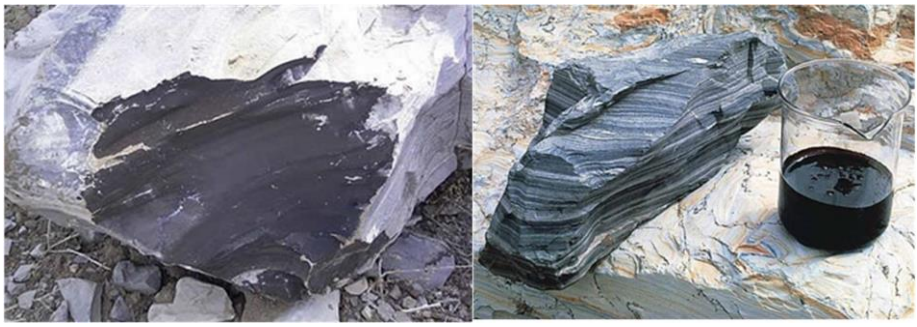

Figure 3 Bituminous shale rocks (Int-1).

Bituminous shale is not frequently used in comparison to other fossil fuels since it is expensive and difficult to extract. However as technology progresses, extraction and processing of hydrocarbons from bituminous shale will become more efficient (Zhao et al., 2019:1195). Bituminous shale has significant reserves especially in countries such as USA, Canada, and China. Oil and natural gas production from bituminous shale account for some of the energy demand in these countries. However environmental problems such as environmental pollution, water pollution, and ecological losses may occur during the extraction and processing of bituminous shale (Passos et al., 2015:442). During the extraction and processing of bituminous shale, large amounts of greenhouse gas emissions are released. Groundwater resources may be damaged during this process (Brandt, 2008:7489). In addition, the leakage of oil or chemicals into water resources causes serious health problems (Altunkaynak et al., 2022:2437, Canpolat, 2023:14042).

As a result, while bituminous shale is a fossil fuel source, it is not considered a sustainable energy source owing to its environmental effects. Instead of investing in renewable energy sources, energy solutions that are less detrimental to the environment and human health should be prioritized.

1.4. Methanol

Methanol is a colorless and volatile liquid with the chemical formula CH_3OH. Industrially, methanol is used as a solvent and fuel in the manufacture of

various chemical products (Özil and Canpolat, 2013:82, Başaran et al., 2016:495). Figure 4 shows the open and closed formulas and three-dimensional molecular structure of methanol.

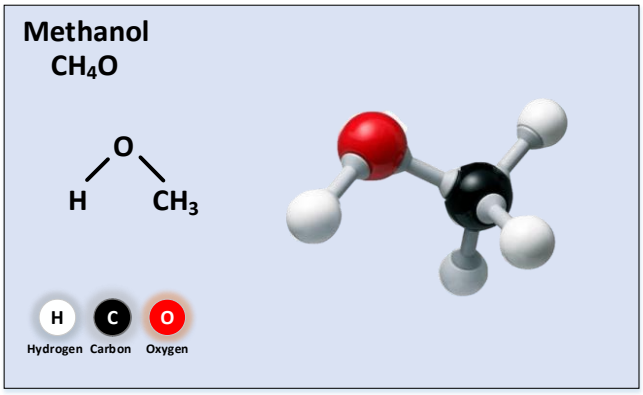

Figure 4 Structure of methanol

Methanol can be derived from various feedstocks, including fossil fuels such as natural gas and coal. Industrially produced methanol is usually obtained by cracking natural gas or gasifying coal. Synthesis gas is obtained by dissolving natural gas under high temperature and pressure or gasifying coal at high temperature for methanol production. The synthetic gas is then converted to methanol by a catalytic reaction (Liu et al., 2023:856). Methanol is utilized as a vehicle fuel in various nations. Methanol combustion emits less greenhouse gases than fossil fuels. Methanol has a low toxicity and produces less air pollution than gasoline. But methanol also has disadvantages. Methanol has a low energy density, resulting in higher fuel consumption. Methanol has a higher flame rate compared to gasoline and diesel fuels, so safety precautions need to be tighter (Duan et al., 2023:247).
The use of methanol is generally focused on the automotive sector (Öztürk et al., 2024:247, Öztürk et al., 2024:117). Methanol is utilized in the manufacture of a wide range of chemical goods. Methanol may be made more ecologically friendly if the electricity requirements of the processes used to make it are fulfilled by renewable energy sources such as solar and wind energy.

1.5.Dimethyl Ether

Dimethyl ether (DME) is a colorless and flammable liquid having the chemical formula C_2H_6O. It is produced by synthesizing methanol and natural gas. Its industrial use is widespread, especially as a solvent, evaporator, and fuel in aerosol sprays (Gao et al., 2023). Figure 5 shows the open and closed formulas and three-dimensional molecular structure of dimethyl ether.

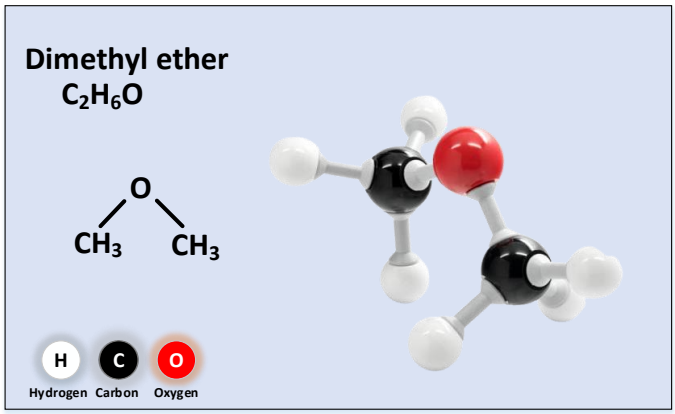

Figure 5 Molecular structure of dimethyl ether

Dimethyl ether is a fuel that may be used instead of gasoline or diesel fuel. Because of its low toxicity and minimal greenhouse gas emissions, it is regarded as an environmentally benign fuel. It has a higher octane number and combustion properties than gasoline and diesel fuel. As a result engine efficiency and performance are improved. Dimethyl ether evaporates easily even at low temperatures making it a fuel that may be utilized in cold weather. Dimethyl ether has less sulfur than gasoline and diesel fuel resulting in less pollution. Dimethyl ether offers both advantages and downsides. Dimethyl ether has a lower energy density than gasoline and diesel fuels resulting in higher fuel consumption. Dimethyl ether's combustion properties at high temperatures are worse than gasoline and diesel fuels so engine performance may be lower (Ateka et al., 2017:796). Dimethyl ether is used industrially for various purposes. Dimethyl ether is also used as a solvent in the production of various polymers and as an anesthetic in medical fields. But due to the high flammability properties of dimethyl ether, appropriate precautions should be taken for its industrial use (Zhang et al., 2019:293).

Many different processes are used for the production of synthetic gasoline. Among these, techniques including Fischer-Tropsch synthesis, Methanol-to-Gasoline synthesis, and DME-to-Gasoline synthesis are particularly noteworthy.

SYNTHETIC GASOLINE PRODUCTION METHODS

2.1. Fischer-Tropsch Technology

The Fischer-Tropsch procedure is a chemical modality employed for the generation of artificial fuels, derived from an assortment of resources, such as natural gas, coal, biomass, and waste. This technology is considered an alternative to traditional oil refineries for fuel production. Additionally, Fischer-Tropsch technology is extensively employed in the generation of

synthetic gasoline. Fischer-Tropsch technology uses a series of chemical reactions to convert gaseous carbon monoxide (CO) and hydrogen (H_2) into synthetic gasoline or other fuels, or a synthetic liquid fuel. These reactions take place under high temperatures and pressure and require the use of special catalysts (Wiser, 1984:325). Figure 6 shows schematically the general transformation process of the Fischer-Tropsch synthesis.

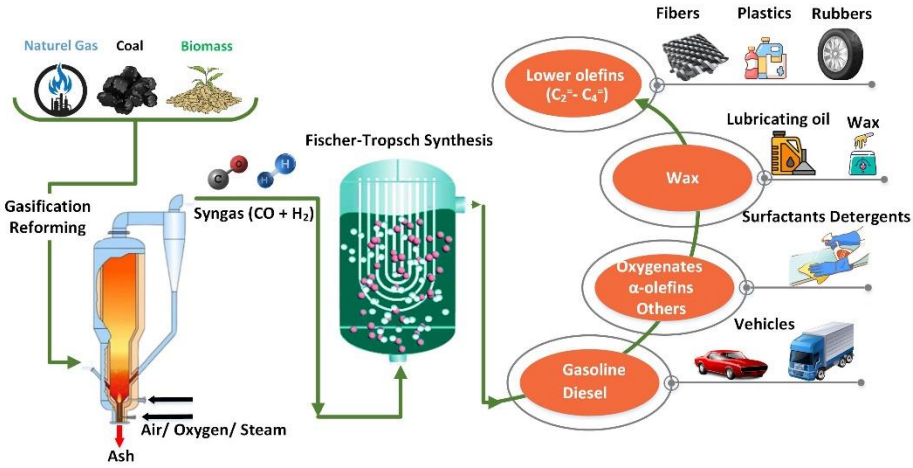

Figure 6 Schematic representation for the overall transformation process of the Fischer-Tropsch synthesis.

Figure 7 shows schematically the metal catalysts supported by carbonaceous materials for the Fischer-Tropsch synthesis.

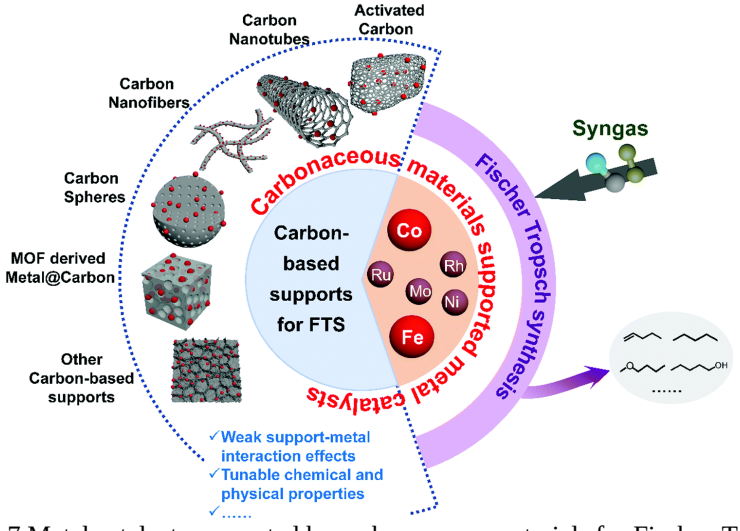

Figure 7 Metal catalysts supported by carbonaceous materials for Fischer-Tropsch synthesis (Chen et al., 2021:2337).

In the production of synthetic gasoline, Fischer-Tropsch technology creates intermediate products by synthesizing CO and H_2 gases. These intermediates are then converted into synthetic gasoline by different processes (Hirsch et al., 1982:121). This process includes steps such as distillation, hydrogenation, oxidation, reforming, and isomerization, similar to the processes used in conventional oil refineries.

Hydrogenation: It is a process in which hydrogen gas is used. This process is used to change the chemical structure of the intermediate products obtained after the Fischer-Tropsch process to make them suitable for the desired fuel properties. The hydrogenation process fills the unsaturated bonds in the intermediates with hydrogen, making the products more stable (Int-2).

Distillation: The Fischer-Tropsch methodology engenders intermediary products via the synthesis of CO and H_2 gases. These intermediaries are subsequently transformed into synthetic gasoline through diverse procedures. The isolation of the liquid products produced during the Fischer-Tropsch approach into distinct fractions is a crucial phase in the generation of several fuels including gasoline, diesel, and kerosene (Sun et al., 2019:3097).

Oxidation: The modification of the chemical structure of the products is achieved through the reaction of organic compounds in the intermediates with oxygen gas. The current approach successfully accomplishes the aim of eliminating undesirable compounds, namely sulfur, nitrogen, and carbon monoxide (CO), from the intermediate products (Wang et al., 2018:7445).

Reforming: The alteration of the hydrocarbon structure is a procedural method employed. This method guarantees the desired carbon count and molecular arrangement in the intermediates. Reforming enables the conversion of the majority of hydrocarbons into hydrogen gas. Additionally, it is important to highlight that this methodology finds application in the production of fragrant compounds, such as benzene, toluene, and xylene, serving as critical intermediates (Pinkwart et al., 2004:211).

Isomerization: By modifying the arrangement of atoms within a given molecule, the formation of isomeric compounds is facilitated. Isomers are chemical compounds possessing identical molecular formulae, yet they possess divergent molecular structures. This process is employed for the purpose of altering the attributes of intermediate substances and is regarded as a pivotal facet in the generation of artificial gasoline (Weyda and Köhler, 2003:51).

The utilization of Fischer-Tropsch technology allows for the utilization of an uncontaminated source, namely natural gas. Furthermore, the resultant synthetic gasoline is of superior quality and possesses eco-friendly attributes. However, the cost of synthetic gasoline is subject to fluctuation owing to the costly nature of the Fischer-Tropsch process, which is contingent upon the accessibility of natural resources (Jones et al., 2022:267).

The implementation of Fischer-Tropsch technology presents numerous benefits in the domain of synthetic gasoline production. Notably, it confers an

advantageous trait in terms of resource adaptability, as a diverse range of resources, including natural gas, coal, and biomass, can be utilized. This aspect is particularly crucial for safeguarding energy security on a global scale. In addition, it is worth noting that synthetic gasoline demonstrates a lower level of sulfur content when compared to traditional gasoline and diesel fuels, leading to a reduction in the amount of greenhouse gas emissions (Van Vliet et al., 2009:855).

The use of Fischer-Tropsch technology in the production of synthetic gasoline presents several drawbacks. One such drawback is its lack of competitiveness during periods of low oil prices, owing to the high costs of investment. Moreover, compared to conventional oil refineries, the production process for synthetic gasoline is more intricate and costly. Given the escalating global energy demands and the finite availability of natural resources, the synthesis of Fischer-Tropsch technology-based gasoline could potentially assume a cardinal position in the forthcoming times. This technology holds immense potential in the direction of paving the way towards an energy-secure and sustainable future (Steynberg et al., 1999:41).

2.2. Methanol-To-Gasoline (MTG) Technology

The Methanol-to-Gasoline (MTG) technology denotes a chemical process which facilitates the conversion of methanol into synthetic gasoline, alongside other hydrocarbon products and gasoline derivatives. This particular procedure is implemented by means of a method that bears similarity to the one utilized in the manufacturing of methanol from carbon sources of low value, such as coal or natural gas (Sanz-Martínez et al., 2022:189).

The process of Methanol-to-Gasoline technology is composed of three fundamental phases, namely, the generation of synthesis gases, the fabrication of methanol, and the conversion of methanol to hydrocarbons. In the first step, low-quality carbon sources (natural gas, coal, etc.) undergo gasification reform, and a gas mixture called syngas is obtained. In the second step, the synthesis gases are converted into methanol using a special catalyst (a methanol synthesis reactor). In the third step, methanol is converted into hydrocarbon products with the help of a catalyst (Zeolite ZSM-5) under high temperature and pressure by adding nitrogen from the outside (Fujiwara et al., 2015:37). (Zeolite ZSM-5: microporous molecular structure of a zeolite; this aluminosilicate zeolite has high silicon and low aluminum content.) Figure 8 shows the overall conversion process of methanol-to-gasoline synthesis schematically.

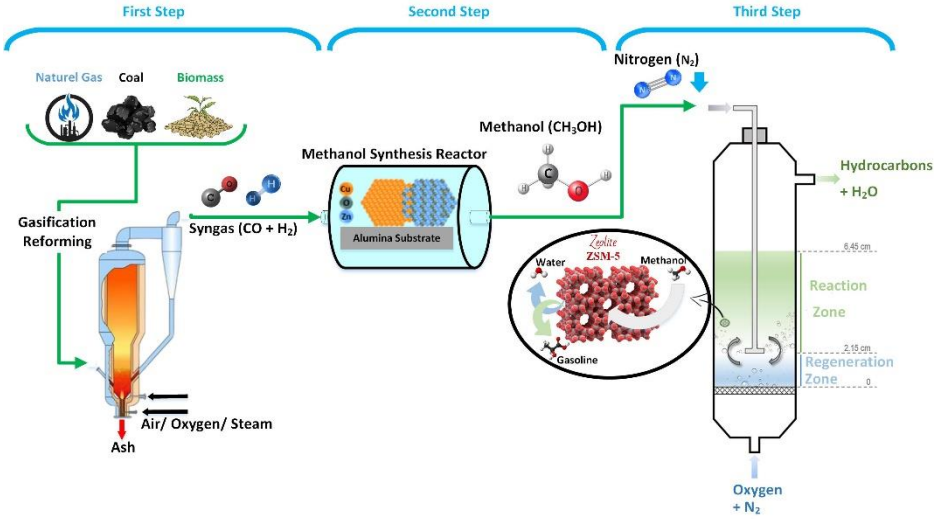

Figure 8 Schematic illustration for the overall conversion process of Methanol-To-Gasoline synthesis

Methanol-To-Gasoline technology was developed due to the limited petroleum resources as a result of the increasing use of hydrocarbon fuels. Despite its low energy density, methanol represents a viable alternative fuel, substitutable for petroleum. The technology known as Methanol-To-Gasoline presents a viable resolution to the challenges that emerge from the preservation and conveyance of methanol. This technology effectively transforms methanol into synthetic gasoline and various hydrocarbons (Su et al., 2022:344). The utilization of Methanol-To-Gasoline technology has been linked to numerous advantages. Notably, the production of methanol can employ low-grade carbon sources. The conversion of methanol into gasoline and other hydrocarbon fuels streamlines its functionality. The significance of Methanol-To-Gasoline technology is especially evident in its contribution to energy security, owing to the domestic origin of the carbon sources employed in methanol production, such as coal and natural gas. Finally, it is worth noting that the Methanol-To-Gasoline technology exhibits great promise as an energy source with low emissions. This implies that it could potentially supplant gasoline as well as other hydrocarbon fuels (Lezcano-Gonzalez et al., 2020:1081). Methanol-To-Gasoline technology, despite its advantages, does have certain drawbacks. The initial aspect to consider pertains to the intricacy and expense associated with this process. During the manufacturing procedure, there is a likelihood that carbon dioxide may be emitted, ultimately resulting in probable pollution of the ecosystem. This outcome is attributed to the impact of greenhouse gases. Furthermore, the sector's competitive edge may be eroded when the current oil industry infrastructure is expanded in

tandem with the introduction of alternative fuel technologies such as hydrogen and electricity (Gogate, 2019:559).

Methanol-To-Gasoline technology is a technique that enables the conversion of methanol derived from diverse sources into more valuable commodities. The advantages of this method encompass the economical utilization of low-grade resources, the capability to generate superior quality gasoline, and its environmentally sustainable nature. Nevertheless, obstacles such as exorbitant expenses and unique catalysts impede the extensive application of Methanol-To-Gasoline technology.

2.3.Dimethyl Ether-To-Gasoline Technology

The Dimethyl Ether-To-Gasoline technology represents a distinct approach implemented to generate synthetic gasoline. The technology involves the initial conversion of methanol to Dimethyl Ether (DME), which is subsequently catalyzed into synthetic gasoline. In contrast to the Fischer-Tropsch synthesis, this particular method exhibits enhanced efficacy and is characterized by a greater degree of cost-effectiveness (Li et al., 2022:313). In the Dimethyl Ether-To-Gasoline process, two different dimethyl ethers are produced. Before starting dimethyl production, a gas mixture called syngas is obtained by gasification of natural gas, coal, and biomass sources. Syngas is an amalgamation of several constituents including hydrogen (H_2) and carbon monoxide (CO). In the first dimethyl ether production method, synthesis gases are converted into methanol using a special catalyst (methanol synthesis reactor). Then, methanol is converted to dimethyl ether by the methanol dehydration method. In the second dimethyl ether production method, the synthesis gases are directly converted to dimethyl ether by the dimethyl ether direct synthesis reactor (Larson and Tingjin, 2003:79). The produced dimethyl ether is then converted into hydrocarbon molecules with a special catalyst (Zeolite ZSM-5) and separated into more valuable products such as gasoline. Figure 9 shows schematically the general conversion process of Dimethyl ether-To-Gasoline synthesis.

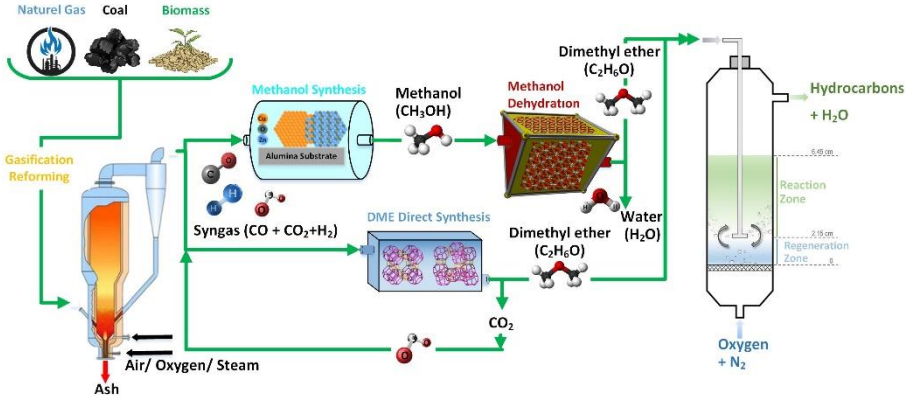

Figure 9 Schematic illustration for the overall conversion process of Dimethyl Ether-To-Gasoline synthesis

The technology of Dimethyl Ether-To-Gasoline exhibits significant advantages with respect to its capacity in generating gasoline of superior quality. It facilitates the utilization of inferior quality fuels, such as dimethyl ether, while guaranteeing greater efficiency in their utilization. Dimethyl ether is acknowledged as a fuel with low emission values and is deemed as a clean source of energy (Mokrani and Scurrell 2009:1). The technology of converting Dimethyl ether into gasoline, similar to other fuel conversion technologies, is associated with high costs. The derived conclusion that Dimethyl ether can be procured from renewable energy reserves presents a testament to the sustainability of Dimethyl ether-To-Gasoline technology as an eco-friendly approach (Sun et al., 2019:3763). The technology known as Dimethyl ether-To-Gasoline (DTG) is a process that effectively transforms low-quality fuel, dimethyl ether, into a more valuable commodity, namely gasoline. This particular approach offers several advantages, such as the utilization of inferior fuels, the ability to generate top-notch gasoline, employment of a clean fuel, and an eco-friendly methodology. Despite these benefits, the widespread adoption of Dimethyl ether-To-Gasoline technology is impeded by various factors, such as its high costs. The reaction equations for the methods used in the production of synthetic gasoline are given below (Çiftçi, 2009). Figure 10 shows the reaction equations of the methods used in the production of synthetic petrol.

Reaction	Chemistry			$\Delta H°_{298K}$ (kJ/mol)
Partial oxidation reforming	$CH_4 + ½ O_2$	⟶	$CO + 2 H_2$	-36.0
Steam reforming	$CH_4 + H_2O$	⟶	$CO + 3 H_2$	206.0
Gas/water shift reaction	$CO + H_2O$	⟷	$CO_2 + H_2$	-40.9
Methanol synthesis	$CO + 2 H_2$	⟶	CH_3OH	-50.1
	$CO_2 + 3H_2$	⟶	$CH_3OH + H_2O$	-50.1
Methanol dehydration	$2 CH_3OH$	⟶	$CH_3—O—CH_3 + H_2O$	-23.3
DME direct synthesis	$2 CO + 4 H_2$	⟶	$CH_3—O— CH_3 + H_2O$	-205.0
	$3 CO + 3 H_2$	⟶	$CH_3—O— CH_3 + CO_2$	-246.2
Overall DME synthesis	$2 CH_4 + O_2$	⟶	$CH_3—O— CH_3 + H_2O$	

Figure 10 Reaction equations of the methods used in the production of synthetic gasoline (Çiftçi, 2009).

ADVANTAGES AND DISADVANTAGES OF SYNTHETIC GASOLINE

3.1. Advantages

Eco-Friendly: Synthetic gasoline provides a reduced amount of pollutants and greenhouse gas emissions compared to natural gasoline. The petrochemical processes involved in its production give synthetic gasoline the opportunity to produce less pollution.

Decreased dependence on resources: In the event of natural resource depletion, synthetic gasoline may provide a viable alternative fuel solution. Dissimilar to traditional hydrocarbon resources, a plethora of primary substances such as coal, natural gas, bituminous shale, and biomass exhibit potential for utilization.

High performance: Synthetic gasoline is a high-quality fuel suitable for use in gasoline engines. The utilization of aforementioned fuel exhibits promising potential to enhance the operational efficiency of gasoline-powered engines, thereby enabling automobiles to attain elevated speeds.

Longer Life: In comparison to its natural counterpart, synthetic gasoline presents with the advantages of enhanced storage capabilities and prolonged shelf life. It shows more resistance to oxidation, which ensures a longer shelf life.

Fuel Efficiency: Synthetic gasoline has a high energy density. This indicates that it can cover a longer distance with the same amount of synthetic gasoline.

Engine Performance and Compatibility: A key feature of synthetic gasoline is its significant octane rating and the absence of compounds that can cause

poor quality issues. This feature can potentially improve engine performance and facilitate cleaner and more efficient combustion in engines. In addition, it can be used in spark-ignition engines without any modification.

Ease of Storage and Transport: Synthetic gasoline can be transported and stored in the liquid phase. The pre-existing refinery gasoline infrastructure and distribution network can be easily used.

Sustainability Potential: Renewable resources, including waste materials or biomass, can be used for the production of synthetic gasoline. This approach has potential as a sustainable solution for both waste management and renewable energy generation. In addition, the use of synthetic gasoline contributes to sustainability efforts by reducing reliance on fossil fuels.

Economic Development and Employment Opportunities: The production and use of artificial gasoline have the potential to stimulate the start of new industries and stimulate economic progress. It also creates many employment opportunities, such as the operation and maintenance of synthetic gasoline plants. In addition, using domestic resources for raw materials can stimulate the start of new industries and economic progress.

3.2. Disadvantages

High Production Cost: The production of synthetic gasoline is a rather complex and expensive procedure. The production of synthetic gasoline through the utilization of raw materials, such as natural gas and coal, which are extensively employed within the petrochemical sector, necessitates intricate methodologies. These procedures require significant energy consumption and specialized equipment, resulting in increased production costs.

Environmental Impacts: Synthetic gasoline production has the potential to create a variety of environmental impacts. The utilization of primary elements for the fabrication of artificial petrol can result in several ecological issues arising from the discharge of carbon dioxide and the production of waste. Moreover, the emission emanating from the combustion of synthetic gasoline carries with it the possibility of inducing varied ecological predicaments, such as changes in worldwide weather patterns and the pollution of the atmosphere.

Energy efficiency: The production of synthetic gasoline requires intensive energy procedures, resulting in a significant energy expenditure compared to the final product. This result can be considered a disadvantage in terms of energy efficiency.

Limitation of raw materials: It is known that difficulties are encountered in the production of synthetic gasoline regarding raw materials (fossil fuels such as natural gas and coal). The constrained accessibility of said primary constituents curtails the potential of synthetic petrol in its capacity to function as a viable and enduring source of energy.

Fire and Explosion Risk: Synthetic gasoline has a high flammability tendency. In the event of inadequate storage and safety procedures, the

likelihood of fire and explosion is significantly elevated. Given the high ignition proclivity of synthetic gasoline, certain precautions need to be implemented, such as ensuring adequate ventilation in storage facilities, avoiding sources of ignition, and having firefighting equipment readily available.

Chemical Instability: Synthetic gasoline is susceptible to chemical instability under certain conditions. Improper or long-term storage conditions can lead to the chemical degradation of synthetic gasoline. Stored fuel can become unusable and pose a potential hazard.

CONCLUSION AND RECOMMENDATIONS

The present work undertakes a detailed examination of the various raw materials, production methodologies, benefits, and drawbacks employed in the manufacture of synthetic gasoline. Synthetic gasoline, being a promising alternative energy source, has the potential to enhance energy sector diversity, energy security, mitigate carbon emissions, and establish itself as a sustainable energy option. Nevertheless, it is imperative to keep in mind that every individual source of raw material and production methodology possesses a unique array of merits and demerits.

Based on the results of this study, the following recommendations are offered to increase the potential of synthetic gasoline and make it more widely available:

Promoting new technologies and innovative approaches is of great importance in researching and developing raw material sources and production methods used in the synthetic gasoline production process, increasing efficiency, achieving cost effectiveness, and achieving environmental sustainability goals.

The implementation of a strategy that requires diversification of the raw material sources used in gasoline synthesis is of great importance. The use of raw materials from a variety of sources provides an advantage in the context of energy security and resource heterogeneity. Encouraging the utilization of diverse resources, comprising natural gas, coal, biomass, and waste materials, is advocated in the manufacturing of synthetic gasoline.

Observing environmental effects in the production of synthetic gasoline also has an important effect. Preference should be given to production methods that exhibit low carbon emissions, thus minimizing environmental impacts. The implementation of carbon capture and storage methodologies within the synthetic gasoline manufacturing process can significantly contribute to the mitigation of carbon dioxide emissions.

To facilitate the extensive use of synthetic gasoline, it is necessary to establish a suitable energy infrastructure and adhere to pre-existing infrastructure. To facilitate the extensive use of synthetic gasoline, it is necessary to establish a suitable energy infrastructure and adapt it to the existing infrastructure.

Therefore, it is crucial to create infrastructure that supports storage, transportation, and distribution processes while simultaneously adapting the existing petroleum infrastructure to suit synthetic gasoline requirements.
It is essential to design appropriate policies and regulations to ensure the commercial viability of synthetic gasoline. Developed energy policies and incentive mechanisms should include provisions that encourage the production and use of synthetic gasoline. Simultaneously, the adoption of measures focused on reducing carbon emissions and minimizing environmental impacts can accelerate the adoption of synthetic gasoline.

REFERENCE

Altunkaynak, Y., Canpolat, M., & Yavuz, Ö. (2022). Adsorption of cobalt (II) ions from aqueous solution using orange peel waste: equilibrium, kinetic and thermodynamic studies. Journal of the Iranian Chemical Society, 19(6), 2437-2448.

Ateka, A., Pérez-Uriarte, P., Gamero, M., Ereña, J., Aguayo, A. T., & Bilbao, J. (2017). A comparative thermodynamic study on the CO2 conversion in the synthesis of methanol and of DME. Energy, 120, 796-804.

Başaran, E., Karaküçük-Iyidoğan, A., Schols, D., & Oruç-Emre, E. E. (2016). Synthesis of novel chiral sulfonamide-bearing 1, 2, 4-triazole-3-thione analogs derived from D-and L-phenylalanine esters as potential anti-influenza agents. Chirality, 28(6), 495-513.

Berkowitz, N. (1985). The chemistry of coal. United States.

Brandt, A. R. (2008). Converting oil shale to liquid fuels: Energy inputs and greenhouse gas emissions of the Shell in situ conversion process. Environmental science & technology, 42(19), 7489-7495.

Canpolat, M. (2023). Removing Co (II) and Mn (II) ions effectively from aqueous solutions by means of chemically non-processed Mardin stone waste: Equivalent, kinetic, and thermodynamic investigations. Environmental Progress & Sustainable Energy, 42(3), e14042.

Chen, Y., Wei, J., Duyar, M. S., Ordomsky, V. V., Khodakov, A. Y., & Liu, J. (2021). Carbon-based catalysts for Fischer–Tropsch synthesis. Chemical Society Reviews, 50(4), 2337-2366.

Çiftçi, A. (2009). Nanocomposite nafion and heteropolyacid incorporated mesoporous catalysts for dimethyl ether synthesis from methanol (Master's thesis, Middle East Technical University).

Duan, Q., Kou, H., Li, T., Yin, X., Zeng, K., & Wang, L. (2023). Effects of injection and spark timings on combustion, performance and emissions (regulated and unregulated) characteristics in a direct injection methanol engine. Fuel Processing Technology, 247, 107758.

Economides, M. J., & Wood, D. A. (2009). The state of natural gas. Journal of Natural Gas Science and Engineering, 1(1-2), 1-13.

Fujiwara, M., Satake, T., Shiokawa, K., & Sakurai, H. (2015). CO2 hydrogenation for C2+ hydrocarbon synthesis over composite catalyst using surface modified HB zeolite. Applied Catalysis B: Environmental, 179, 37-43.

Gao, R., Wang, L., Zhang, L., Zhang, C., Jun, K. W., Kim, S. K., ... & Zhu, Y. (2023). A multi-criteria sustainability assessment and decision-making framework for DME synthesis via CO2 hydrogenation. Energy, 127467.

Gogate, M. R. (2019). Methanol-to-olefins process technology: current status and future prospects. Petroleum Science and Technology, 37(5), 559-565.

Hirsch, R. L., Gallagher Jr, J. E., Lessard, R. R., & Wesslhoft, R. D. (1982). Catalytic coal gasification: an emerging technology. Science, 215(4529), 121-127.

Int-1: https://www.innosys.com.tr/oil-shale/ adresinden 7 Kasım 2024 tarihinde alınmıştır.

Int-2: https://www.accessscience.com/content/article/a503100 adresinden 7 Kasım 2024 tarihinde alınmıştır.

Jones, M. P., Krexner, T., & Bismarck, A. (2022). Repurposing Fischer-Tropsch and natural gas as bridging technologies for the energy revolution. Energy Conversion and Management, 267, 115882.

Larson, E. D., & Tingjin, R. (2003). Synthetic fuel production by indirect coal liquefaction. Energy for sustainable Development, 7(4), 79-102.

Lezcano-Gonzalez, I., Campbell, E., Hoffman, A. E. J., Bocus, M., Sazanovich, I. V., Towrie, M., ... & Beale, A. M. (2020). Insight into the effects of confined hydrocarbon species on the lifetime of methanol conversion catalysts. Nature Materials, 19(10), 1081-1087.

Li, J., Han, D., Zi, Z., He, T., Liu, G., Wang, Z., ... & Wu, J. (2022). The synthesis of H [Fe, Al] ZSM-5 zeolites with uniform nanocrystals for dimethyl ether to gasoline reaction. Fuel, 313, 122643.

Liu, Y., Yao, D., Xu, Z., Zhou, M., Zhou, Y., Wang, Y., ... & Zhu, Z. (2023). Comparative analysis of life cycle water accounting of the Lurgi low-pressure methanol production process with biomass or coal as raw materials. Science of The Total Environment, 856, 159129.

Miller, B. G. (2010). Clean coal engineering technology. Elsevier.

Mokhatab, S., Mak, J. Y., Valappil, J., & Wood, D. A. (2013). Handbook of liquefied natural gas. United States: Gulf Professional Publishing is an imprint of Elsevier.

Mokrani, T., & Scurrell, M. (2009). Gas conversion to liquid fuels and chemicals: The methanol route-catalysis and processes development. Catalysis Reviews, 51(1), 1-145.

Özil, M., & Canpolat, M. (2013). Solvent-free synthesis of novel phthalocyanines containing triazole derivatives under microwave irradiation. polyhedron, 51, 82-89.

Öztürk, G., Şenocak, Ş. M., Şenocak, N., & Fırat, M. (2024). An experimental investigation of 1, 2-dimethoxy ethane as a fuel additive in biodiesel-fueled diesel engine. Journal of the Energy Institute, 117, 101824.

Öztürk, G., Tanyeri, B., & Öner, C. (2024). Investigation of effects on fuel consumption and exhaust emissions by using bioethanol gasoline mixture in an engine with ultrasonic fuel system. Thermal Science, Vol. 28, No. 2A, pp. 811-822.

Passos, A. O., Paulino, J. R., & de Tomi, G. (2015). Challenges in the Feasibility of Bituminous Shale as a Source of Oil. In Materials Science Forum (Vol. 805, pp. 442-447). Trans Tech Publications Ltd.

Patel, R., Zhang, Y., Lin, C. W., Guerrero, J., Deng, Y., Pharr, G. M., & Xie, K. Y. (2022). Microstructural and mechanical property characterization of Argillaceous, Kerogen-rich, and Bituminous shale rocks. Journal of Natural Gas Science and Engineering, 108, 104827.

Pinkwart, K., Bayha, T., Lutter, W., & Krausa, M. (2004). Gasification of diesel oil in supercritical water for fuel cells. Journal of power sources, 136(2), 211-214.

Quinn, D. F., & MacDonald, J. A. (1992). Natural gas storage. Carbon, 30(7), 1097-1103.

Ram, V., & Salkuti, S. R. (2023). An Overview of Major Synthetic Fuels. Energies, 16(6), 2834.

Sanz-Martínez, A., Lasobras, J., Soler, J., Herguido, J., & Menéndez, M. (2022). Methanol to gasoline (MTG): Parametric study and validation of the process in a two-zone fluidized bed reactor (TZFBR). Journal of Industrial and Engineering Chemistry, 113, 189-195.

Speight, J. G. (2018). Natural gas: a basic handbook. United States: Gulf Professional Publishing is an imprint of Elsevier

Steynberg, A. P., Espinoza, R. L., Jager, B., & Vosloo, A. C. (1999). High temperature Fischer–Tropsch synthesis in commercial practice. Applied Catalysis A: General, 186(1-2), 41-54.

Su, X., Liu, B., Feng, C., & Wu, W. (2022). Rapid and low-cost synthesis of ZSM-5 zeolite nanosheet assemblies for conversion of methanol to gasoline. Microporous and Mesoporous Materials, 344, 112215.

Sun, Y., Han, X., & Zhao, Z. (2019). Direct coating copper–zinc–aluminum oxalate with H-ZSM-5 to fabricate a highly efficient capsule-structured bifunctional catalyst for dimethyl ether production from syngas. Catalysis Science & Technology, 9(14), 3763-3770.

Sun, Y., Lin, Z., Peng, S. H., Sage, V., & Sun, Z. (2019). A critical perspective on CO2 conversions into chemicals and fuels. Journal of Nanoscience and Nanotechnology, 19(6), 3097-3109.

Van Krevelen, D W. (1993). Coal: typology- physics- chemistry – constitution, Amsterdam: Elsevier Science Publishers.

Van Vliet, O. P., Faaij, A. P., & Turkenburg, W. C. (2009). Fischer–Tropsch diesel production in a well-to-wheel perspective: A carbon, energy flow and cost analysis. Energy conversion and Management, 50(4), 855-876.

Wang, L., Nitopi, S. A., Bertheussen, E., Orazov, M., Morales-Guio, C. G., Liu, X., ... & Jaramillo, T. F. (2018). Electrochemical carbon monoxide reduction on polycrystalline copper: Effects of potential, pressure, and pH on selectivity toward multicarbon and oxygenated products. Acs Catalysis, 8(8), 7445-7454.

Ward, C. R. (1984). Coal geology and coal technology. United States.

Wei, L., & Geng, P. (2016). A review on natural gas/diesel dual fuel combustion, emissions and performance. Fuel Processing Technology, 142, 264-278.

Weyda, H., & Köhler, E. (2003). Modern refining concepts—an update on naphtha-isomerization to modern gasoline manufacture. Catalysis Today, 81(1), 51-55.

Wiser, W. H. (1984). Conversion of bituminous coal to liquids and gases: chemistry and representative processes. Magnetic Resonance: Introduction, Advanced Topics and Applications to Fossil Energy, 325-350.

Zhang, C., Gao, R., Jun, K. W., Kim, S. K., Hwang, S. M., Park, H. G., & Guan, G. (2019). Direct conversion of carbon dioxide to liquid fuels and synthetic

natural gas using renewable power: Techno-economic analysis. Journal of CO2 Utilization, 34, 293-302.

Zhao, P., Ostadhassan, M., Shen, B., Liu, W., Abarghani, A., Liu, K., ... & Cai, J. (2019). Estimating thermal maturity of organic-rich shale from well logs: case studies of two shale plays. Fuel, 235, 1195-1206.

Automatic Milking Room Washing System Design by Using PLC

Yasin AYDIN[1]
Metin DEMİRTAŞ[2]

1- Öğr. Gör.; Manisa Celal Bayar University, Akhisar Vocational School, Electrical and Energy Department. yasin.aydin@cbu.edu.tr ORCID No: 0000-0001-6237-9990
2- Prof. Dr.; Balikesir University, Engineering Faculty, Electrical and Electronics Engineering Deartment. mdtas@balikesir.edu.tr ORCID No:0000-0003-2622-5286

ABSTRACT

Among fresh foods, milk is a food that requires care and attention to hygiene while going through stages such as milking, collecting, measuring and packaging. Especially during the milking phase, the hygiene of animal teats and the milking system is a critical and extremely important process. The necessity of milking at least twice a day makes this situation more sensitive and complex. After the milking process is completed, some waste milk remains in the system. This residual milk spoils very quickly due to its structure and solidifies at the milk transition points. In order to prevent these milk residues from spoiling the newly milked milk, milk routes must be cleaned and maintained after each milking process. When cleaning operations are carried out by humans, they are sometimes forgotten and sometimes cannot be done delicately. Therefore, fully automated milking parlors are needed. In this study, the washing process was carried out using PLC.

Keywords – Milk, Milking Room, Hygiene, PLC, Automatic Washing.

INTRODUCTION

The most common layouts include parallel, herringbone, rotary, and tandem systems, which are designed to accommodate the flow of cows and ease of milking. Good air circulation and sufficient lighting are essential to maintain cow comfort and operator visibility. The floors are typically made of non-slip materials, and space is provided to reduce stress for the cows while standing. It includes drains and washable surfaces to facilitate regular cleaning and maintain high hygiene standards. Automatic milking systems or manual machines are used to extract milk efficiently. Milk is transferred to refrigerated tanks to maintain freshness until transported for processing. Equipment for washing and disinfecting the teats before and after milking to prevent infection. Some farms have advanced Automatic Dosing Systems to prevent errors and misuse. Advanced milking parlors feature automated systems that measure and dispense the correct amount of cleaning chemicals, minimizing human error and ensuring consistent cleaning.

In this study, a comparison was made in terms of microbiological quality and residues after chlorinated and non-chlorinated cleaning processes in bovine tank milk. It was observed that the total bacterial count and residue levels were lower in chlorine-free protocols than in chlorine-based protocols. Chlorine-free cleaning protocols have been shown to have a positive impact on milk quality (Gleeson et al., 2022).

In this study, factors affecting the level of awareness about dairy cows were investigated in farms where dairy cows are raised. In nozzle cleaning,

the nozzle drying process is applied in 74.39% of the nozzle drying processes in all of its enterprises (Eryılmaz et al., 2022).

As a result of this study, it was observed that the total amount of water used in technical works in the barn had a very small contribution compared to the water used for feed production (Krauß,et al., 2016).

As a result of this study, it was determined that the participants in the survey performed manual milking twice a day, approximately 60% of the participants did not wash their hands before milking, others washed their hands only with water, and well water was mostly used to wash the dishes (Shanta et al., 2020).

In the study, increasing efficiency in water use and saving water for washing the milking parlor and cleaning equipment were investigated (Brugger et al., 2008).

It is known that the washing process in the bucket milking system has a high impact on the milk produced. In this system, the relationships between the efficiency and quality of the washing process in the milking system and the number of bacteria on the milk tank and teat surface were examined (Elashhab et al., 2020).

Electrolyzed oxidizing (EO) water is a cleaning and disinfecting agent produced by separating a weak solution of sodium chloride into alkaline and acidic components. After a pilot-scale pipeline milking system was contaminated using raw milk inoculated with common microorganisms, the milking system was flushed with alkaline EO water followed by acidic EO water, and the results were compared (Walker et al., 2005).

Yasin studied, a fully automated milking unit cleaning system was designed using PLC for post-milking cleaning of the pipes that carry the milk to the tank in the system established for a cow milking room (Yasin 2016).

Erdem has proposed a system that will accurately measure the toxic gases encountered in underground mines and provide early warning in case of danger. For this purpose, they established a PLC-based SCADA system (Ilten et al., 2024).

Ebru presented a conference paper about traffic light control system by using PLC (Dag et al., 2018).

In this article, a fully automatic cleaning system is designed to clean the milking pipes used to transmit the milk from the milking machine to the tank. A programmable Logic Controller (PLC) was used to perform these tasks.

AUTOMATION AND TECHNOLOGY

Automation refers to the use of technology to perform tasks with minimal human intervention. It involves creating and applying systems or machines that can execute repetitive tasks, analyze data, and make decisions,

all based on pre-established algorithms or instructions. Automation is used across various industries and sectors to increase efficiency, reduce human error, cut costs, and improve consistency. Technology broadly refers to the tools, systems, and devices created using scientific knowledge to solve problems or accomplish specific tasks. It encompasses everything from basic tools and machines to advanced systems like artificial intelligence (AI) and robotics.

Machines can work faster and longer than humans without getting tired. Therefore, they are more productive than humans. Automation reduces labor costs by replacing manual tasks with machines or software, resulting in lower costs. Automated systems enable systems to operate with greater consistency and precision by performing tasks consistently without variations introduced by employees. In sectors such as animal husbandry and agriculture, automation helps reduce the need for workers to perform hazardous tasks, preventing workplace accidents and injuries.

Many modern milking rooms use automated systems that track cow health, milk production, and milking frequency through sensors and monitoring software. The milking room should provide a low-stress environment, with gentle handling to prevent discomfort or injury to the cows. Proper milking routines help prevent mastitis and other common health issues related to dairy production.

The milking room washing pipe refers to the system of pipes used to clean the milking equipment, milking room, and sometimes the cows' udders before and after milking. Proper cleaning is critical to prevent contamination of the milk and maintain a sanitary environment.

2.1 Purpose of the washing system

The pipes are part of the cleaning-in-place (CIP) system used to sanitize milking machines, hoses, and milk storage tanks. Some systems also include attachments for washing the cows' teats and udders before milking to reduce the risk of infections like mastitis. The washing pipes can also assist in spraying down the floors and walls of the milking parlor after milking sessions to maintain cleanliness.

Operators use hoses or pipes to manually spray cleaning solutions over the equipment and surfaces in the manual washing pipe systems. More advanced parlors have automated systems where pipes are connected to tanks of cleaning solutions (usually a mix of detergents and disinfectants) that circulate through the milking machines and pipes to clean them automatically after each milking session in the automatic Cleaning Systems

2.2 Components of a Washing System

Water Pipes carry water for rinsing and washing the equipment. The pipes on the Detergent/Disinfectant Lines carry the cleaning agents used to sanitize the system. Nozzles and spray heads are installed at key points to distribute water and cleaning solutions evenly across surfaces, equipment, and udder cleaning units. Drainage Systems: Proper drainage in the milking room ensures that waste water from cleaning can be safely removed without contaminating the area.

2.3 Cleaning cycles in a milking room

Before applying detergent, a pre-rinse cycle is performed by running cold water through the pipes to remove milk residue. The washing cycle is performed by circulating a cleaning solution (usually warm water mixed with detergent) through the system. In the Post-Rinse Cycle, water is used to remove any remaining detergent, ensuring no residue is left in the pipes or equipment. Some systems use a Sterilization Cycle for an additional disinfectant rinse to further sterilize the equipment.

Regular cleaning of the milking room through these washing pipes reduces bacterial growth and contamination, protecting both the cows' health and the quality of the milk.

Dairy farms generally focus on the cleaning of solid waste in terms of hygiene, which requires daily cleaning of equipment. Washing systems also help clean the waste accumulated on the roads through which the milk passes and make the milk hygienic.

Before each milking, all milking equipment, pipes through which milk passes and tool surfaces that come into contact with dirt or manure should be thoroughly cleaned and sterilized. Milk collection tanks should also be thoroughly cleaned with detergent and water after each milk collection. The purpose of cleaning is to keep the milk, organic, and mineral residues that form on the equipment surfaces after milk is collected, away from the next milking milk. During the sterilization process, residual microorganisms on the surfaces in contact with the milk are killed and prevented from mixing with the next milked milk. Inadequate, untimely, improper cleaning or sanitation, or both, causes bacteria to remain and grow and multiply on the equipment surfaces that milk comes into contact with. This may cause the number of bacteria in the milk to increase and the quality of the milk to decrease. Therefore, it is essential that washing and cleaning processes are carried out automatically, without human intervention, using water and detergent in a timely manner and in the required amounts. In order for the milk to be hygienic, these operations must be carried out periodically after each milking, using the necessary hardware and software. The washing

cycle should last approximately 6-10 minutes, as the time increases, the returning water becomes too cold and will not be effective in washing.

AUTOMATIC CLEANING SYSTEM DESIGN

The equipment required for a milking parlor is shown in Figure 1. Milking room system, cooling tank where the milk is collected, vacuum pump that provides the necessary vacuum for milking and washing, transfer pump that separates the milk from the vacuum line and transfers it to the cooling tank, washing tank that cleans the system after the milking is completed, detergent pump and waste water. The pump consists of pulsators and milk meters that pulse during milking. The system has two main operating modes: washing and milking. In milking mode, the vacuum pump is directly activated, teats are attached to the milking animals ready for milking and milking begins.

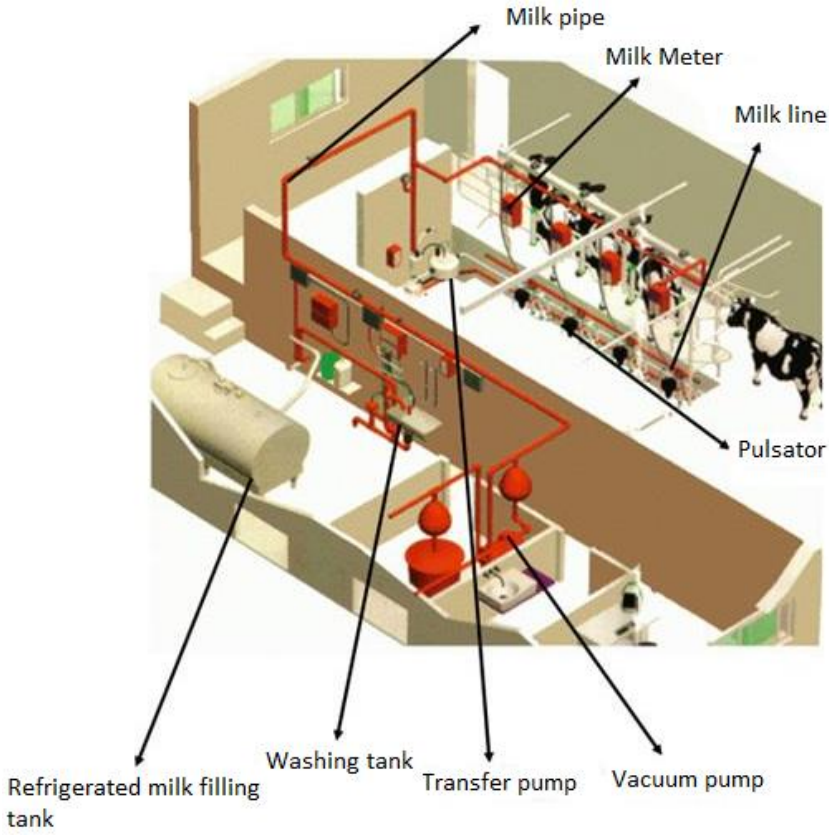

Figure 1: Equipment used in a milking parlor (Aydin, 2016)

Pulsators provide a dual pulse movement, allowing milk to be extracted more efficiently. The milk drawn from the vacuum line is poured

into the transfer boiler. When the transfer tank is full, it transfers the milk directly to the cooling tank. During milking, the transfer tank is filled and emptied an average of 10-12 times, depending on the number of animals milked. This process continues until milking is finished. After the milking process is completed, the milking animals are taken out. In the next process, the washing process begins.

Research and development studies are generally carried out in simulation or laboratory environments. According to the results obtained, these studies are applied in the field and the accuracy of the findings is proven. A milking unit prototype prepared for experimental studies is shown in Figure 2.

Figure 2: Installation of a milking parlor (Aydin, 2016)

The most important thing to do after the milking process is to clean the milk residues in the system. System cleaning is carried out by simulating milking. In other words, the milking clusters are not attached to the milking animal, but this time to the artificial teats connected to the washing tub. When the system is operated in washing mode, detergent and rinse water are passed through the pipes instead of milk. Washing mode is a little more complicated than milking mode. What needs to be done physically is to first attach the milking clusters to the artificial teats in the washing line, connect the pipe between the transfer engine and the cold water tank to the washing tub, and turn the switch on the panel to washing mode. When washing starts, cold water first starts to fill into the washing tub. When the washing tank is full, the sensor connected to the system starts the vacuum motor with the

signal it sends to the PLC and the water inlet is closed. The vacuum motor draws cold water from the system and begins to rotate the water in the vacuum line. Optionally, it can be sent in hot or warm water instead of cold water. As in milking, water is discharged back into the transfer tank. When the transfer tank is full, it sends the water it contains back to the washing tank with the signal it sends to the PLC (during milking, this line is connected to the cold water tank and the milked milk is discharged into this tank). This cycle continues for the amount of time entered on the PLC screen. Cold water collects all solid waste in the system. When the given washing time expires, the vacuum motor stops and the transfer tank transfers all the remaining water in the pipe to the washing tank without waiting for the tank to be filled. The dirty water accumulated in the washing tank is removed from the system by the waste water pump and sent to the sewer or a suitable waste water area. At the end of this work, the first washing is performed. The reason why cold water is circulated during the first wash is to prevent solid waste from softening and sticking to the pipe. The first rinse with cold water ensures that these milk residues and solid waste materials are removed from the system. The second wash is done with detergent and hot water. After the first wash is completed, the PLC software automatically moves on to the second wash.

First of all, the hot water and detergent pump are activated at the same time. When the amount of detergent entered on the PLC screen is poured into the washing tub, the detergent motor stops and remains active until the hot water washing tub is filled. When the washing tub is filled with detergent and hot water, the sensor sends a command to the PLC again, allowing the PLC to activate the vacuum motor again. The only difference from the previous wash is that hot water and detergent are circulated in the system instead of cold water. The most important feature of the detergent is that it rots milk and has a chemical structure that prevents the formation of bacteria. When the specified time in the system expires, the vacuum motor stops and the transfer pump transfers all the remaining detergent water in the system to the washing tub. The wastewater pump removes the remaining dirty water from the system. The third wash is rinsing with warm water.

The detergent in the system needs to be rinsed. The rinsing process begins as soon as the wastewater motor removes the detergent water from the system. Hot water and cold water start flowing into the washing tub at the same time. When the washing tank is full, the vacuum motor is activated and the hot and cold water inlets are closed.

The washing cycle is repeated exactly. Finally, another rinsing process is performed. The final washing cycle of the system is completed by circulating only cold water. When the whole cycle is completed, the transfer tank finally transfers the water filtered from the system to the washing tank. The wastewater pump drains this remaining water from the system. PLC flowchart is given in Figure 3 (Aydin, 2016).

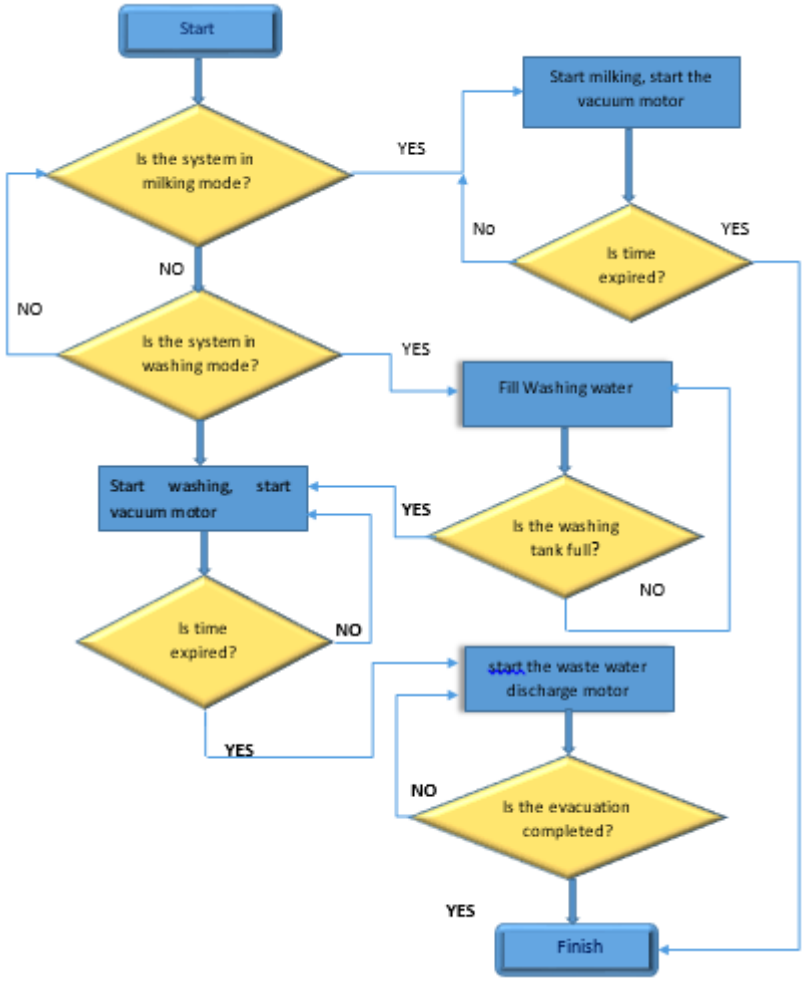

Figure 3: Flowchart for automation process (Aydin, 2016)

This entire washing process is started by just pressing a button. The operator does not need to be in charge of the milking room to perform the washing process. Detergent, hot water, cold water inlets, vacuum motor inlet and outlet, filling and emptying of the washing tank, removal of waste water from the inlet and outlet system are all done under PLC control. The necessity of attaching and removing the teats of milking animals and the negativities that may occur during the milking process make it necessary for the operator to have the main control, although unlike washing, milking is done under PLC control. The operator should not leave the milking room until the milking process is completed. There is no such obligation in the washing process. Each washing process is meticulous and takes a long time.

In this washing process, which takes an average of 45 minutes to 90 minutes, the operator does not have to wait for the milking room during this time. After milking is completed, it is sufficient to turn the button to washing mode, direct the pipes connected to the cooling tank to the washing tank and attach the teats to the combustion heads. Considering that the washing process is done twice a day, a PLC-controlled milking parlor saves the operator an average of 2-3 hours of time. In a PLC-controlled milking room, since the washing process is done sensitively and for a long time, a clean room is prepared for the next milking and the quality of the collected milk is prevented from decreasing in the next milking.

Delta SS2 series PLC, Delta DVP-16SP additional module and Delta DOPB07S415 model color touch screen are used in the system. 7 inputs and 7 outputs are needed for the automatic washing system of the designed milking room. This PLC has 8 inputs and 6 outputs. Since the number of inputs and outputs in the PLC used was not sufficient, an additional module was used. The touch screen is used to enter parameters that vary according to the user's wishes, such as milking time, detergent amount, milking and washing 70 function selection.

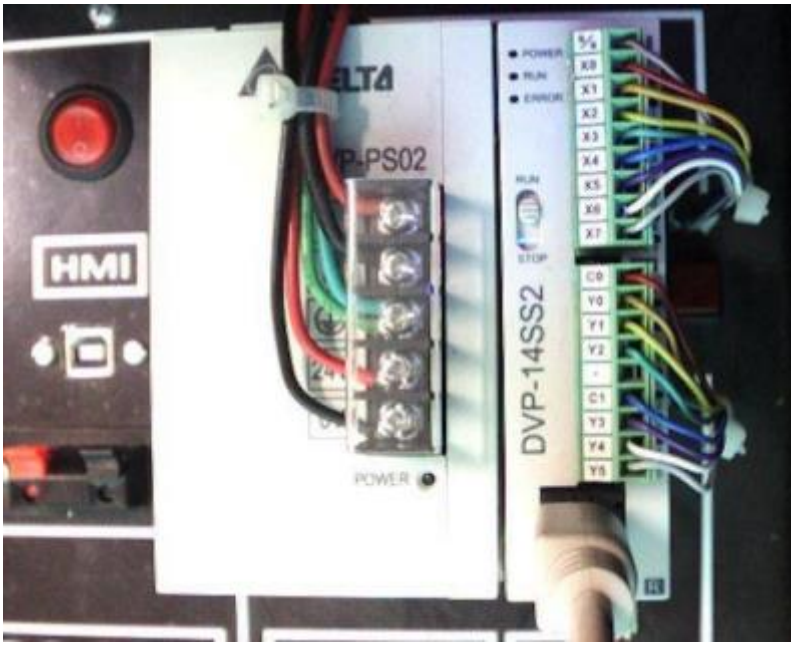

Figure 4: PLC used for milking room (Aydin, 2016)

There are 8 digital inputs, 6 digital outputs and internal RS-232 and RS-485 communication ports on the PLC and CPU. Output ports are transistor and relay outputs. The PLC used has a relay output feature. There

are two separate relays at the output ports. The advantage of using two separate relays is that independent voltage sources can be used as seen in the figure. If the Y1 output of the PLC is active, the (+) end of the 24 V power supply is connected to motor1 via the Y1 terminal and from there to the (-) end of the power supply. If Y4 output is active, 12 V DC power supply will be connected to motor2.

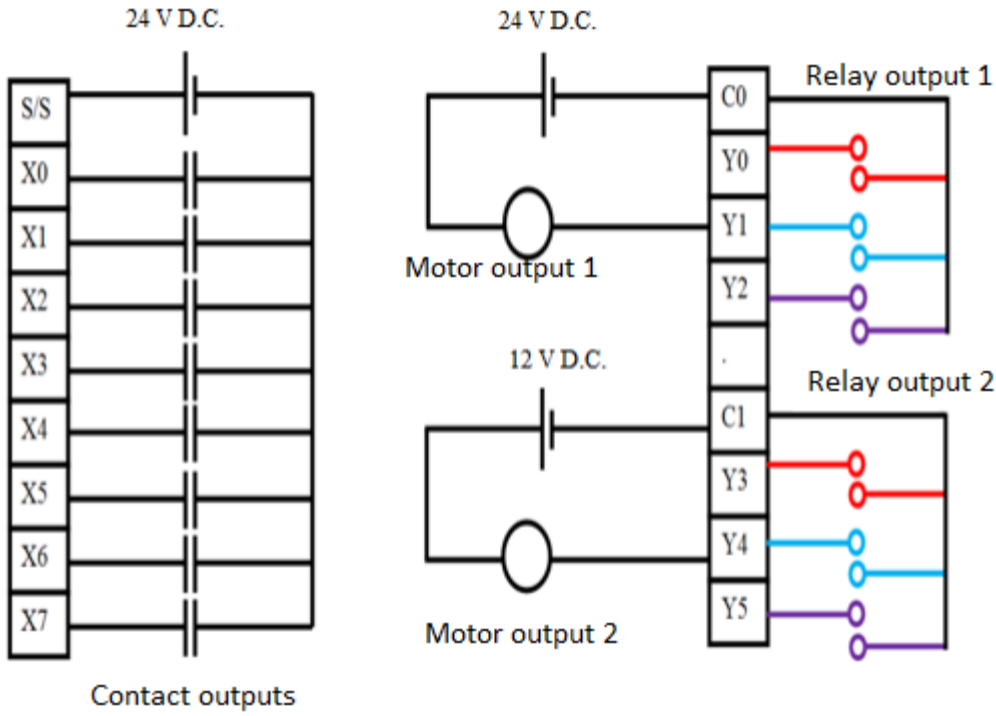

Figure 5: PLC input and output module connection diagram

According to the connection in Figure 5, if the filling software of the transfer boiler is made, X0 input is defined as the stop button, X1 input is the start button, and X4 input is defined as the sensor output contact indicating that the boiler is filled. Motor output 1 is considered as water inlet and motor output 2 is considered as transfer boiler pump.

3.1 Key screen and electrical panel used in the milking room

Touch panel USB, COM1(RS232), COM2&COM3 (RS-485/RS-422/RS-232) connectivity features, ARM9 32-bit RISC processor, communication with many PLCs, arithmetic logic processing, download/upload from USB and RS232 , 65536 color TFT LCD, LED backlight, printer connection function, label printer connection function,

Online/offline simulation, alarm, It is an input unit that has many features such as calendar and real-time clock and is used to assign variable data to PLC. The touch screen used in the system is shown in Figure 6.

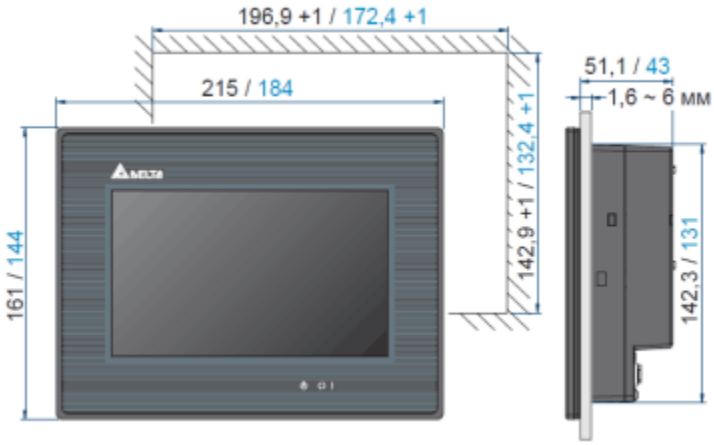

Figure 6: Touch screen used in the system

Whether the program written on the PLC works correctly or not can be tested via the test panel. This process is useful to see the accuracy of the algorithm before running the system. Damages or accidents that may occur during operation can be prevented by correcting the deficiencies according to the test results. The test results screenshot is shown in Figure 7.

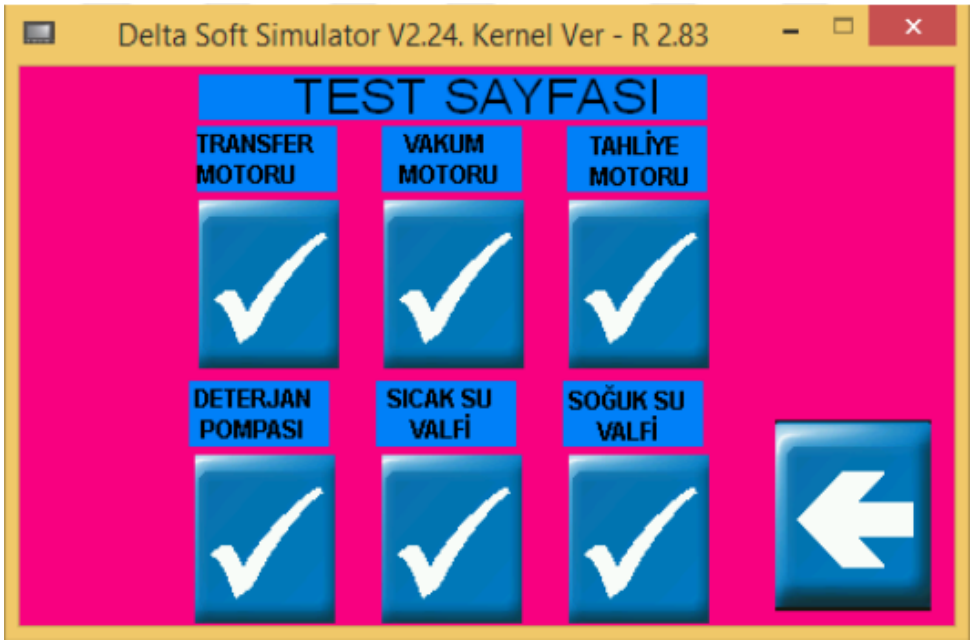

Figure 7: Test page for PLC outputs (Aydin, 2016)

An electrical panel has been designed so that the system can operate within the framework of the prepared algorithm and control the power circuit. The electrical panel is shown in figure 8. There are PLC, relays, contacts, fuses and switches on the panel. Relays and contactors connected to PLC outputs are mounted on the panel to ensure the operation of the motors.

Figure 8: PLC controlled milking parlor panel (Aydin, 2016)

CONCLUSION

In hygiene care, regular cleaning of the milking parlor through these washing pipes reduces bacterial growth and contamination, protecting both the health of the cows and the quality of the milk. Dairy farms are often subject to strict hygiene regulations requiring daily cleaning of equipment and these washing systems ensure compliance with these rules. Non-Foaming detergents are commonly used in automatic systems because they prevent the formation of foam, which can affect cleaning efficiency. Special cleaning chemicals and safety are very important in the farms. Chlorine-Free Alternatives Chlorine is being phased out in some regions due to environmental concerns. Instead, disinfectants that do not contain chlorine, such as peracetic acid or hydrogen peroxide, are becoming more preferred. Operators should wear protective clothing such as gloves and goggles when working with strong cleaning agents (such as alkaline or acid-based detergents). Proper ventilation is important to prevent inhalation of fumes from chemicals such as chlorine.

Cleaning solutions and rinse water should be disposed of appropriately to prevent environmental contamination. Many farms must now have wastewater treatment systems to manage this. In environmentally responsible farming operations, biodegradable detergents and disinfectants should be used to minimize the impact on the environment.

ACKNOWLEDGMENT

This project was supported by the SANTEZ project named "Development of Fully Automated Milking Unit and Milk Measurement Tracking Station" and numbered 0607.STZ.2013-2.2

REFERENCES

Gleeson, D., Paludetti, L., O'Brien, B., & Beresford, T. (2022). Effect of ‘chlorine-free’cleaning of milking equipment on the microbiological quality and chlorine-related residues in bulk tank milk. International Journal of Dairy Technology, 75(2), 262-269.

Eryılmaz, G. A., Garipoğlu, A., & Kılıç, O. (2022). Animal Health and Welfare, Milk Safety and Hygiene Practices in Dairy Cattle Farms: Türkiye Sample. Türkiye Tarımsal Araştırmalar Dergisi, 9(3), 395-401.

Krauß, M., Drastig, K., Prochnow, A., Rose-Meierhöfer, S., & Kraatz, S. (2016). Drinking and cleaning water use in a dairy cow barn. Water, 8(7), 302.

Shanta, S. A., Lima, R. A., Mahamudunnabi, M., Rahman, A. K. M. A., & Islam, M. A. (2020). Assessment of milking hygiene awareness and practices among the dairy farmers in Baghabarighat milk shed areas of Bangladesh. Bangladesh Journal of Veterinary Medicine (BJVM), 18(2), 47-52.

Brugger, M. F. (2008). Water Use on a Modern Dairy Farm: Three Years of Data. In 2008 Providence, Rhode Island, June 29–July 2, 2008 (p. 1). American Society of Agricultural and Biological Engineers.
Elashhab, O. A., Obaia, A. R., Abo-Elmagd, A., & El-Wakeel, S. A. (2020). Design and manufacturing a washing unit for teat cups in the bucket milking system and it's effect on the produced milk quality. Egyptian Journal of Agricultural Research, 98(1), 113-130.
Walker, S. P., Demirci, A., Graves, R. E., Spencer, S. B., & Roberts, R. F. (2005). Cleaning milking systems using electrolyzed oxidizing water. Transactions of the ASAE, 48(5), 1827-1833.
Yasin AYDIN, Milking unit design with complete automation, Master Thesis, Science Institue, Balikesir, 2016
İlten, E., & Ünsal, M. E. (2024). PLC Based Scada System Design For Instant Monitoring And Early Warning Mechanism Of Toxic Gases In Underground Mines. Mühendislik Bilimleri ve Tasarım Dergisi, 12(1), 64-74.
Dağ, E., Demirtas, M., Calgan, H., & İlten, E. Modeling and Optimizing of the Intelligent Traffic Light system by using PLC. Co-chair, 190.
Ilten, E., Calgan, H., & Demirtas, M. (2023). Fuzzy Logic Level Control of a Coupled Tank System with Raspberry Pi Application.

The Effect of Waste Eggshell Powder on the Physical and Mechanical Properties of Cementitious Mortars

Ahmet Ferdi ŞENOL[1]
Özlem ÇALIŞKAN[2*]

1- Öğr.Gör.; Bilecik Şeyh Edebali Üniversitesi Mühendislik Fakültesi İnşaat Mühendisliği Bölümü. ahmetferdi.senol@bilecik.edu.tr ORCID No: 0000-0002-6663-3340
2- *Doç.Dr.; Bilecik Şeyh Edebali Üniversitesi Mühendislik Fakültesi İnşaat Mühendisliği Bölümü. ozlem.caliskan@bilecik.edu.tr ORCID No: 0000-0002-5272-9552

ABSTRACT

The use of agricultural and food-based wastes in powder form in the concrete industry can contribute to sustainable waste management and cost-effective concrete production while reducing environmental pollution. In this study, the effects of using waste eggshells in powdered form (Y) as a cement replacement in mortar production were investigated. For this purpose, four different mortar series were prepared by incorporating Y as a cement replacement at proportions of 0%, 5%, 10%, and 15% in a standard mortar mix. The workability of the produced mortar series was evaluated using the flow table test, and the hardened samples were subjected to standard water curing for 7 and 28 days. Following the curing period, tests were conducted on the samples to assess apparent porosity, water absorption by weight, ultrasonic pulse velocity, flexural strength, and compressive strength. The results showed that the 7-day compressive strength of Y-replaced mortars reached approximately 70% of their 28-day compressive strength. The highest strengths after 28 days of curing in Y-replaced series were observed in mortars containing 5% Y, with compressive strength losses of 11.2% and flexural strength losses of 5% compared to the control series.

Keywords – Eggshell Powder, Cement, Mortar, Compressive Strength, Sustainability.

INTRODUCTION

The most commonly used construction materials worldwide are cement, concrete, and steel. The increasing production of concrete not only accelerates the depletion of cement and natural aggregate resources but also contributes to the rise in carbon dioxide emissions. Furthermore, the construction sector consumes approximately 35% of global energy and is responsible for around 40% of carbon dioxide emissions (Younis and Dodoo, 2022).

Cement, the main component of concrete, ranks fifth globally with a production volume of 78.9 million tons in Turkey (Anonymous, 2022). Producing 1 ton of Portland cement results in the release of roughly 1 ton of CO2, a significant greenhouse gas. Cement production is known for its high energy consumption, leading to increased costs (Pliya and Cree, 2015), and is responsible for about 6% of global CO_2 emissions (Nandhini and Karthikeyan, 2022). The utilization of waste materials as partial or complete replacements for cement can mitigate environmental issues (Sathiparan, 2021). Using suitable waste materials as cement substitutes offers a practical solution to challenges such as construction material shortages and the environmental concerns faced by the industry as a whole (Poorveekan et al.,

2021). Reducing the amount of cement through the inclusion of waste materials decreases pollution and lowers costs (Xuan et al., 2023).

Eggshells are a waste material that can be sourced from households, restaurants, and bakeries (Sathiparan, 2021). They primarily consist of calcium carbonate (96%), magnesium carbonate (1%), and calcium phosphate (1%) crystals, along with organic matter and protein fibers (Oliveira et al., 2013).

Binici et al. (2015) incorporated eggshells into cementitious mortars as a partial replacement for sand at proportions of 5%, 10%, 15%, 20%, 25%, and 50% by weight. They observed that while the flexural and compressive strengths decreased, the radiation shielding properties improved. Jaber et al. (2020) investigated the thermal conductivity, compressive strength, and hardness properties of cement mortar mixes containing 0–20% processed and unprocessed eggshell powder, which was heated in an electric furnace at 750°C. After 28 days, they reported that the addition of 15% processed eggshell powder reduced water absorption by 30% and increased compressive strength by 29%. Othman et al. (2021) replaced cement with eggshell powder and sand with waste rubber at substitution rates of 5%, 10%, and 15%. They found that the calcium carbonate content and filler effect of eggshell powder improved the mechanical strength of concrete when used at 5–10% replacement levels. Nandhini and Karthikeyan (2022) used ground eggshell powder as a cement replacement at 5%, 10%, 15%, and 20% by weight. They reported that the optimum compressive strength and a more refined microstructure were achieved at a 10% replacement level. Furthermore, they observed that the calcium carbonate in ground eggshell powder effectively interacted with cement, reducing voids in the cementitious matrix and forming C-S-H gel networks. Maqsood and Eddie (2022) investigated the early performance of cement mortars containing limestone, eggshells, and eggshells calcined at 400°C, 600°C, and 800°C. It was reported that calcined eggshells reduced the setting time of cement when compared to limestone and raw eggshells, with this effect attributed to the disturbance of the sulfate balance in cement paste containing calcined eggshells. They further noted that the addition of eggshells calcined at 800°C might delay the setting due to the presence of $Ca(OH)_2$, suggesting that in such cases, the presence of $Ca(OH)_2$ would govern the setting and hydration processes. Grzeszczyk et al. (2022) examined the characterization of eggshells as a limestone replacement and their effects on the properties of modified cement. Eggshell powder was incorporated into Portland cement at proportions of 10%, 20%, and 30% by weight. The study found delayed hydration and lower strength values in the cement paste, which were attributed to the presence of the shell membrane, consisting of organic matter, including proteins, within the mixture.

This study aims to evaluate the potential of utilizing waste eggshell powder as a substitute for cement in cement-based mortars. For this purpose,

mortar mixtures were prepared by replacing cement with waste eggshell powder (Y) at proportions of 0%, 5%, 10%, and 15% by weight. The produced mortar series were subjected to a flow table test, and their physical and mechanical properties were evaluated after standard curing periods of 7 and 28 days. The study assessed the appropriate usage levels of waste eggshell powder in cement-based mortars, exploring the potential for utilizing waste materials in the construction sector and the impact of sustainable powder materials on mortar production.

MATERIALS and METHODS

Materials

The waste shells of chicken eggs obtained from bakeries, cafeterias and restaurants in Bilecik province were firstly washed with water to remove contaminants. Then, the waste egg shells were dried in an oven at 70 ℃ for 24 hours to evaporate the water on the surface. The dried waste egg shells were ground in a laboratory type ball mill for 1 hour in order to be used as cement substitute. According to microparticle size analysis by laser technique, it was determined that 90% of the egg powder passed through 300 μm and 50% passed through 100 μm sieve (Figure 1).

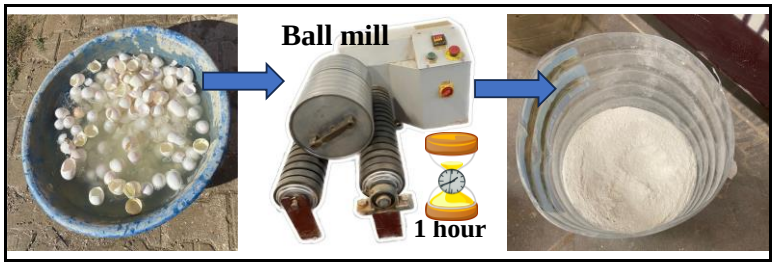

Figure 1: Conversion of waste eggshells into powdered form.

For the production of mortar series, CEM I 42.5R Portland cement obtained from the Vezirhan Cement Plant in Bilecik province and Osmaneli river sand with a particle size range of 0-4 mm were used. The granulometric curve of the river sand used in the mixtures is shown in Figure 2. The chemical analysis results (XRF) of the cement and Y used in the mortar production are presented in Table 1.

Table 1 illustrates that the primary chemical component of both cement and Y is CaO. The specific gravities of the cement, sand, and Y used in the mixtures were measured as 3.09, 2.61, and 2.51, respectively.

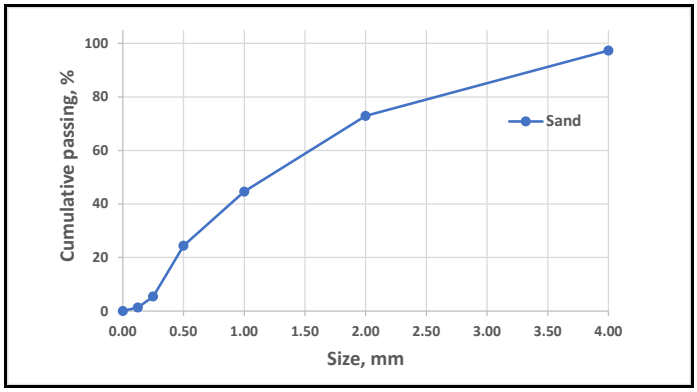

Figure 2: Particle size distribution curves of sand.

Table 1: Chemical characteristics of powdered materials.

Oxide components, %	Y	CEM I 42.5R
SiO_2	0.01	18.7
Al_2O_3	0.01	4.6
Fe_2O_3	0.02	3.4
CaO	53.2	63.7
MgO	0.6	1.3
SO_3	0.01	2.7
K_2O	0.04	0.7
Loss of ignition	46.32	3.9

A field emission scanning electron microscope (FESEM) was employed to examine the surface texture and particle shape of the cement and Y used in the mortar series (Figure 3). According to the FESEM analysis, as shown in Figure 2, the structure of Y is similar to that of cement, consisting of irregular crystalline particles. Additionally, it was observed that Y has smoother, angular particles compared to cement.

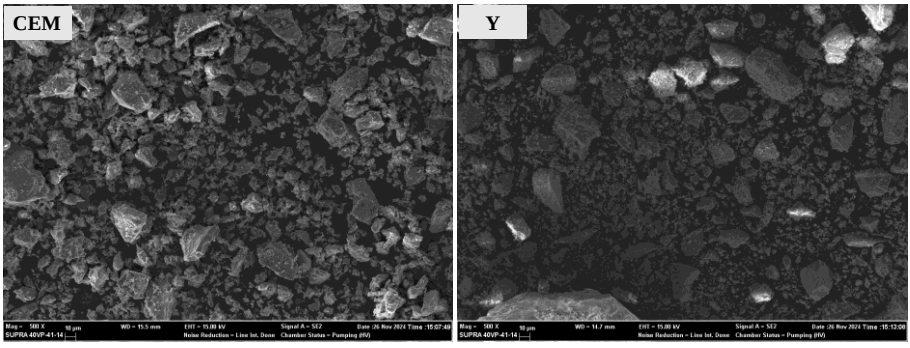

Figure 3: FESEM micrographs (x500 magnification) of cement and Y.

Method

The mortar mixtures were prepared in four different series according to TS EN 196-1 (2016) standards. Y was replaced with cement at weight ratios of 5%, 10%, and 15%. Additionally, a control (C) mixture series, in which the binder consisted solely of cement, was produced. In all series, the aggregate-to-binder ratio was fixed at 3, and the water-to-binder ratio was kept constant at 0.5. The mortar series were designated as C, Y5, Y10, and Y15. In the series codes, the "Y" index represents the waste eggshell powder, while the numbers indicate the percentage of powder substituted for cement by weight. For instance, Y5 refers to the mortar series containing 5% Y. The material mix compositions of the mortar series are provided in Table 2.

Table 2: Mortar series and mix proportions.

Series	Cement (g)	Y (g)	Sand (g)	Water (g)
C	450	-	1350	225
Y5	427.5	22.5	1350	225
Y10	405	45	1350	225
Y15	382.5	67.5	1350	225

All materials used in the mixtures were mixed in a laboratory-scale variable-speed mortar mixer in accordance with TS EN 196-1 (2016) standards. Initially, the binder and water were added to the mixer and mixed. Subsequently, sand was added to the mixture, and the mixing process continued. The workability of the fresh mortar series was determined using a flow table test in accordance with TS EN 1015-3/A2 (2007) standards. The prepared mortar series were placed into steel prismatic molds with dimensions of 40 mm × 40 mm × 160 mm in two layers, with each layer compacted using a vibration table. The mortar series were left in the molds for 24 hours. A total of six samples were produced for each series. The hardened mortar specimens were demolded and cured in lime-saturated water at 20 ± 2 ºC in a laboratory environment for 7 and 28 days before performing hardened mortar tests.

At the end of the curing period, the apparent porosity (P) and water absorption by weight (WA) of the hardened mortar specimens were measured following the TS EN 772-4 standard using an Archimedes balance and calculated with Equations 1-2. The tests conducted at the end of each curing period were performed on at least three specimens from the same series, and the average values were calculated.

$$P\ (\%) = \frac{(w_1 - w_0)}{(w_1 - w_2)} \times 100 \qquad (1)$$

$$WA\ (\%) = \frac{(w_1 - w_0)}{w_0} \times 100 \quad (2)$$

In the equations, w_0: represents the oven-dry weight of the specimen, w_1: denotes the weight of the specimen saturated with water in air, w_2: indicates the weight of the specimen submerged in water.

Ultrasonic pulse velocity measurements were carried out at the end of the curing process following the guidelines of TS EN 12504-4, whereas three-point flexural strength and compressive strength tests were performed in compliance with TS EN 196-1 (2016). A cement compression and flexural testing machine was used for these experiments. The results of the flexural strength test were determined by calculating the arithmetic mean of three specimens. For the compressive strength test, the results were obtained by calculating the arithmetic mean of six specimens, which were derived from the halves of the mortar specimens used in the flexural strength test. The production process of the mortar series and the applied tests are illustrated in Figure 4.

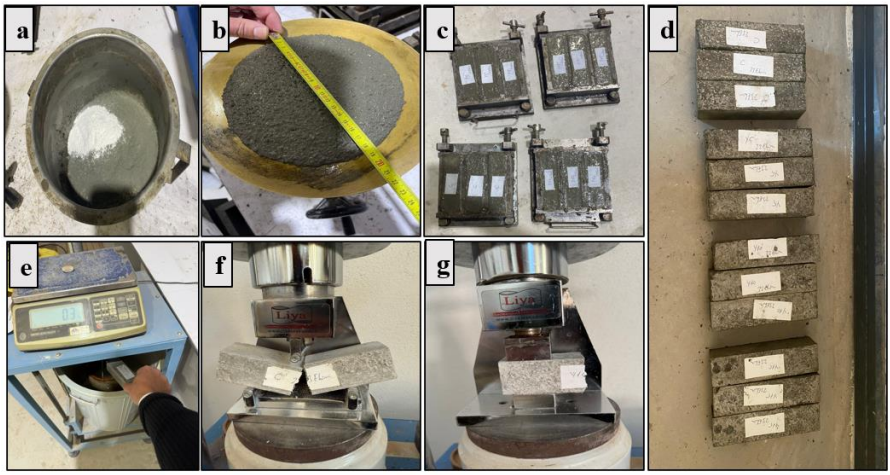

Figure 4: Production of mortar series and applied tests; a) Mixing process, b) Flow table test, c) Fresh mortar specimens, d) Hardened mortar specimens, e) Porosity and water absorption tests, f) Flexural strength test, g) Compressive strength test.

RESULTS and DISCUSSION

Workability Test Results

The workability properties of the fresh mortar series were determined using the flow table test. The variations in the measured flow diameters are presented in Figure 5. According to the flow diameter measurements in Figure 5, the flow values increased at each level as the Y

replacement in the mixtures increased. The lowest flow measurement was observed in the C series. Compared to the C series, the flow diameters of the Y5, Y10, and Y15 series increased by 9.1%, 15.2%, and 18.2%, respectively. It was evaluated that the improvement in the workability of the mortars resulted from the lower water absorption and specific gravity of Y compared to cement. In a similar study (Nandhini and Karthikeyan, 2022), where Y was used as a cement replacement in standard cement mortar at levels of 5%, 10%, 15%, and 20%, the fluidity of the mortar increased by 7.6% up to 10% Y replacement, while higher Y replacement levels led to a decrease in flow diameters. In another study by Wei, et al. (2021), the use of Y as a cement replacement up to 10% increased the mortar fluidity by up to 20%.

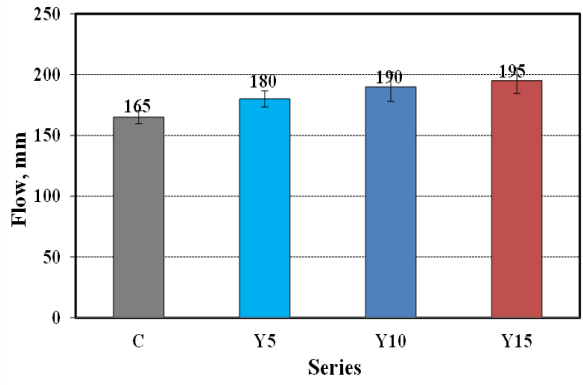

Figure 5: Flow values of the mortar series.

Apparent Porosity and Water Absorption Rates

The changes of the mortar series according to the apparent porosity and water absorption by weight measurements at the end of 28-day curing are shown in Figure 6.

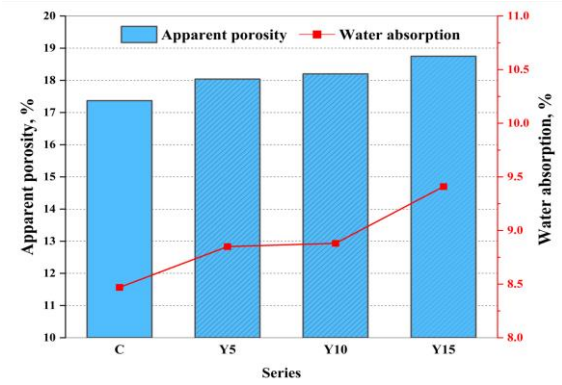

Figure 6: Variation of apparent porosity and water absorption values of the series.

It was observed that the increase in the amount of Y in the series led to higher apparent porosity and water absorption percentages. The presence of pores and cracks in concrete increases water absorption, which negatively affects the durability and long-term performance of concrete (Şenol and Karakurt, 2024). The 28-day apparent porosity values of Y5, Y10, and Y15 increased by 3.8%, 4.8%, and 7.9%, respectively, compared to the C series, while their water absorption values increased by 4.5%, 4.8%, and 11.1%, respectively. This increase is attributed to the higher Y content in the mixture, which may cause agglomeration and insufficient hydration due to the different particle sizes of cement and Y particles, resulting in a weaker apparent porosity structure.

Ultrasonic Pulse Velocity Rate Measurement Results

The ultrasonic pulse velocity (UPV) measurements performed on the mortar series allow the evaluation of various variables, such as the compactness of the specimens, potential cracks, and damage. The variations in the 7-day and 28-day UPV measurements of the series are presented in Figure 7. The 7-day UPV results indicate that the ultrasonic pulse velocity decreases as the Y replacement level in the mixture increases. Compared to the C series, the UPV values of the Y5, Y10, and Y15 series decreased by 2.7%, 3.3%, and 6.3%, respectively. Similarly, the 28-day UPV results show reductions of 1%, 4.8%, and 7.2% for Y5, Y10, and Y15, respectively, compared to the C series. These results suggest that as the curing period increases, the voids in the mortar series decrease. Notably, after 28 days of curing, the Y5 series exhibited a UPV value closest to that of the C series, while the Y15 series showed the lowest UPV among all series.

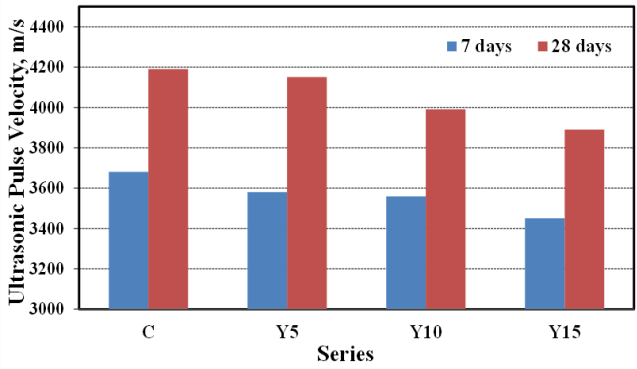

Figure 7: Ultrasonic pulse velocity measurement results of mortar series.

Flexural and Compressive Strength Test Results

The variations in the flexural and compressive strength results of the mortar series after 7 and 28 days of curing are presented in Figures 8 and 9, respectively. The flexural and compressive strengths of the series increased with longer curing periods. Following 7 days of curing, the flexural strength of the Y5 series improved by 11% relative to the C series, whereas the Y10 and Y15 series experienced reductions of 11.1% and 16.7%, respectively. At 28 days of curing, the flexural strength of the Y5, Y10, and Y15 series dropped by 5%, 17.5%, and 32.5%, respectively, when compared with the C series.

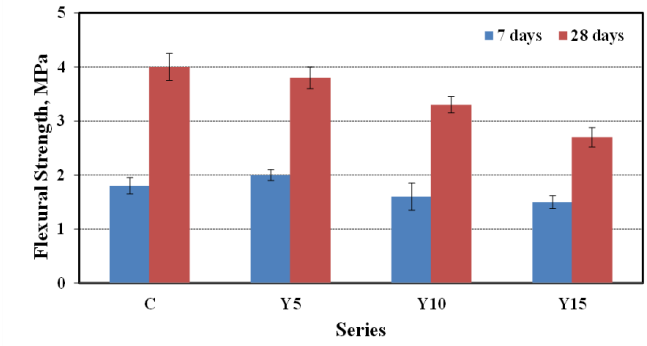

Figure 8: Flexural strength results of the series.

The compressive strengths of the mortar series after 7 days of curing ranged between 22.5 and 32.4 MPa. Compared to the C series, the strength values decreased by 6.8%, 19.4%, and 30.5% for the Y5, Y10, and Y15 series, respectively. After 28 days of curing, the compressive strengths ranged from 34.5 to 45.5 MPa, with decreases of 11.2%, 21.5%, and 24.2%, respectively, compared to the C series. It was observed that as the amount of Y added to the mixture increased, the porosity in cement-based composites

also increased (as shown in Figure 6), leading to a reduction in strength. This reduction can be attributed to a significant decrease in the bonding capacity within the microstructural morphology of the mortar and the formation of weak interfaces between the cementitious matrix and the aggregate (Nandhini and Karthikeyan, 2022).

Figure 10 presents the correlations between ultrasonic pulse velocity (UPV) and compressive strength results for the 7-day and 28-day mortar series. As seen in Figure 10, an increase in UPV values corresponds to an increase in compressive strength, indicating a positive correlation between the two measurements. The strongest correlations were observed in the 7-day series ($R^2 > 0.9$). Figure 11 shows the relationship between apparent porosity and compressive strength for the 28-day mortar series. As shown in Figure 11, a strong negative correlation was identified between the two measurements, indicating that higher porosity is associated with lower compressive strength.

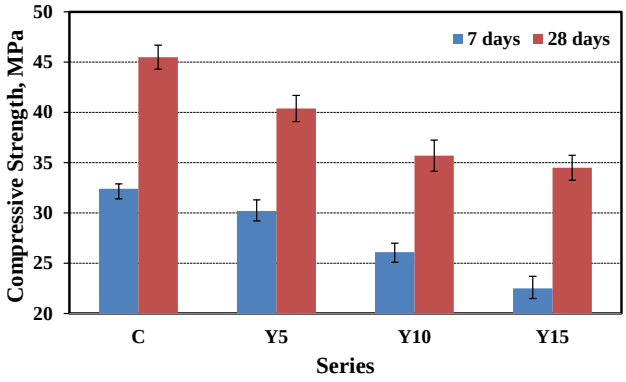

Figure 9: Compressive strength results of the series.

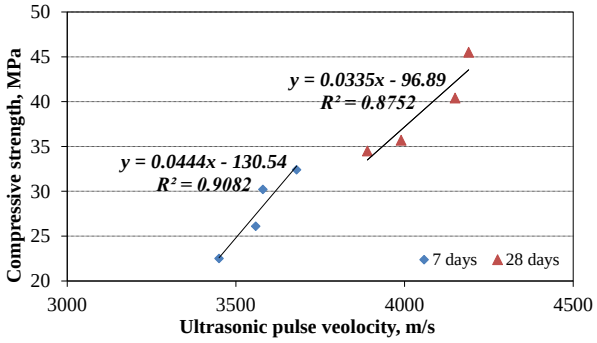

Figure 10: Relationships between 7- and 28-days ultrasonic pulse velocity measurement and compressive strength of mortar series.

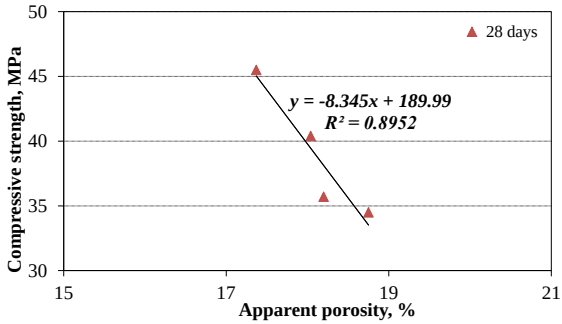

Figure 11: Relationships between the 28-day apparent porosity and compressive strength of the mortar series.

CONCLUSION

The findings obtained from the experimental studies are summarized below;

- Replacing cement with Y in cementitious mortars improved workability due to Y's lower specific gravity, water absorption capacity, and surface roughness compared to cement. As a result, using up to 15% Y in the mixtures enhanced the workability of all series, leading to an increase of up to 18.2%.
- The increase in the amount of Y used in the mortar series led to higher apparent porosity and water absorption rates at each level. Compared to the C series, the apparent porosity increased by up to 7.9%, and water absorption increased by up to 11.1%.
- While the flexural and compressive strengths increased with longer curing periods, higher Y content significantly reduced the 28-day strengths. The highest strength loss was observed in the Y15 series (32.5%), whereas optimal strength was achieved with a 5% Y addition.
- In general, the use of Y up to 5% in cementitious mortars resulted in acceptable changes in physical and mechanical properties. However, higher Y content negatively impacted the mechanical performance.
- In future studies, investigating the use of Y as a cement replacement with a particle size finer than the average particle size utilized in this study (100 μm) is deemed appropriate.

REFERENCE

Anonim, (2022). T.C. Sanayi ve Teknoloji Bakanlığı, https://www.sanayi.gov.tr/plan-program raporlar-ve-yayinlar/sektor-raporlari/mu0102011404, (Erişim adresi: 26 Nisan, 2023).

Binici, H., Aksogan, O., Sevinc, A. H., and Cinpolat, E. (2015). Mechanical and radioactivity shielding performances of mortars made with cement, sand and egg shells. *Construction and Building Materials*, *93*, 1145-1150.

Grzeszczyk, S., Kupka, T., Kałamarz, A., Sudoł, A., Jurowski, K., Makieieva, N., ... and Wrzalik, R. (2022). Characterization of eggshell as limestone replacement and its influence on properties of modified cement. *Construction and Building Materials*, *319*, 126006.

Jaber, H. A., Mahdi, R. S., and Hassan, A. K. (2020). Influence of eggshell powder on the Portland cement mortar properties. *Materials Today: Proceedings*, *20*, 391-396.

Maqsood, S., and Eddie, L. S. (2022). Effect of using calcined eggshells as a cementitious material on early performance. *Construction and Building Materials*, *318*, 126170.

Nandhini, K., and Karthikeyan, J. (2022). Effective utilization of waste eggshell powder in cement mortar. *Materials Today: Proceedings*, *61*, 428-432.

Oliveira, D. A., Benelli, P., and Amante, E. R. (2013). A literature review on adding value to solid residues: egg shells. *Journal of cleaner production*, *46*, 42-47.

Othman, R., Chong, B. W., Jaya, R. P., Hasan, M. R. M., Abdullah, M. M. A. B., and Ibrahim, M. H. W. (2021). Evaluation on the rheological and mechanical properties of concrete incorporating eggshell with tire powder. *Journal of materials research and technology*, *14*, 439-451.

Pliya, P., and Cree, D. (2015). Limestone derived eggshell powder as a replacement in Portland cement mortar. *Construction and Building Materials*, *95*, 1-9.

Poorveekan, K., Ath, K. M. S., Anburuvel, A., and Sathiparan, N. (2021). Investigation of the engineering properties of cementless stabilized earth blocks with alkali-activated eggshell and rice husk ash as a binder. *Construction and Building Materials*, *277*, 122371.

Sathiparan, N. (2021). Utilization prospects of eggshell powder in sustainable construction material–A review. *Construction and Building Materials*, *293*, 123465.

Şenol, A. F., and Karakurt, C. (2024). High-strength self-compacting concrete produced with recycled clay brick powders: Rheological, mechanical and microstructural properties. Journal of Building Engineering, 88, 109175.

TS EN 1015-3/A2. (2007), Kagir harcı-deney metotları-bölüm 3: taze harç kıvamının tayini (yayılma tablası ile), Türk Standartları Enstitüsü, Ankara, Türkiye.

TS EN 196-1. (2016), Çimento deney metotları- Bölüm 1: Dayanım tayini, Türk Standartları Enstitüsü, Ankara, Türkiye.

TS EN 772-4. (2000), Kagir birimler- Deney metotları- Bölüm 4: Tabii taş kagir birimlerin toplam ve görünen porozitesi ile boşluksuz ve boşluklu birim hacim kütlesinin tayini, Türk Standartları Enstitüsü, Ankara, Türkiye.

Wei, C. B., Othman, R., Ying, C. Y., Jaya, R. P., Ing, D. S., and Mangi, S. A. (2021). Properties of mortar with fine eggshell powder as partial cement replacement. Materials Today: Proceedings, 46, 1574-1581.

Xuan, M. Y., Lin, R. S., Min, T. B., and Wang, X. Y. (2023). Carbonation treatment of eggshell powder concrete for performance enhancement. *Construction and Building Materials*, *377*, 130814.

Younis, A., and Dodoo, A. (2022). Cross-laminated timber for building construction: A life-cycle-assessment overview. *Journal of Building Engineering*, *52*, 104482.

Deep Learning Methods in Health Studies

Sultan GÜÇLÜ[1]
Selahattin GÜÇLÜ[2]

1- Prof. Dr.; Kütahya Health Sciences University, Faculty of Health Sciences, Department of Social Work, sultan.guclu@ksbu.edu.tr ORCID No: 0000-0002-2469-1032

2- Master Electrical Engineer; Kütahya Dumlupınar University, Faculty of Engineering, Department of Electrical and Electronics Engineering, selahattin.guclu@dpu.edu.tr ORCID No: 0000-0001-5596-3005

ABSTRACT

Deep learning, a subset of machine learning, employs algorithms designed to mimic the architecture and processes of the human brain, known as artificial neural networks. It excels in processing large datasets through multiple layers, enabling the automatic identification of complex patterns and representations. The layered structure of deep learning models enables them to identify features at various abstraction levels, making them particularly adept at tackling complex tasks such as speech and image recognition, drug discovery, and natural language processing. The future of deep learning in healthcare appears promising, with ongoing research aimed at refining algorithms and expanding their applicability. Khalid et al. conducted a systematic review comparing deep learning methodologies for analyzing knee bone reports from various imaging modalities, highlighting the potential for these techniques to enhance diagnostic precision (Khalid et al., 2020). As the field continues to evolve, integrating deep learning with emerging technologies such as telemedicine and wearable devices may further enhance patient care and outcomes. In conclusion, deep learning represents a significant advancement in health studies, offering powerful tools for disease prediction, medical imaging, and personalized medicine. While challenges remain, particularly regarding data quality and ethical considerations, the potential benefits of deep learning in enhancing healthcare delivery are substantial. Continued research and development in this area are essential to fully realize the transformative potential of deep learning in improving patient outcomes and advancing medical knowledge.

Keywords – Deep Learning, Health Studies, Machine Learning, Medical Knowledge, Patient Care.

INTRODUCTION

Deep learning has had a transformative effect in healthcare, particularly in areas such as disease prediction, medical imaging, and personalized medicine. This technology employs sophisticated algorithms to sift through extensive datasets, enabling healthcare professionals to derive insights and make data-driven decisions through predictive analytics. The adaptation of deep learning into healthcare has been made possible by breakthroughs in computing technology and access to extensive datasets, which are essential for training deep learning models.

One of the notable implementations of deep learning in healthcare is the prediction of diseases from electronic health records (EHRs). For instance, Rasmy et al. introduced Med-BERT, a model specifically designed to utilize structured EHR data for disease prediction. These results suggest that simpler models like logistic regression may be more effective for

smaller datasets than complex deep learning models like Med-BERT. It is crucial for researchers to carefully consider the trade-offs between model complexity and data availability when selecting the appropriate model for their specific research context (Rasmy et al., 2021). This underscores a critical aspect of deep learning in healthcare: its effectiveness is often contingent upon the volume and quality of data available for training.

CNNs have been successfully applied to tasks such as image classification, object detection, and segmentation in medical imaging. Their ability to learn automatically, along with feature extraction from raw data, has led to significant advances in diagnosing diseases and helping healthcare professionals make informed decisions. Hamamoto et al. noted that deep learning is particularly adept at tasks such as image classification, quality enhancement, and segmentation, which are essential in oncology for precision medicine (Hamamoto et al., 2020). Similarly, Poplin et al. demonstrated the capability of deep learning algorithms to predict cardiovascular risk factors from retinal fundus photographs, achieving accuracy comparable to that of human experts (Poplin et al., 2018). This capability to analyze images and extract meaningful patterns has revolutionized diagnostic processes, allowing for earlier detection and intervention in various diseases.

The application of deep learning extends beyond image analysis to encompass predictive modeling for cardiovascular events. Sree's work on heart attack prediction illustrates how deep learning can transform cardiovascular risk assessment by identifying patterns in patient data that may not be immediately apparent to clinicians (Sree, 2023). This predictive power is further supported by Huang et al., who reviewed the fusion of medical imaging and EHRs using deep learning, emphasizing the need for integrated approaches to enhance diagnostic accuracy and treatment planning (Huang et al., 2020).

Moreover, the heterogeneous nature of healthcare data presents both challenges and opportunities for deep learning applications. Hu highlighted the complexity of medical data, which often involves multiple dimensions such as clinical notes, imaging data, and genetic information (Hu, 2023). This complexity necessitates sophisticated algorithms capable of deriving insights from high-dimensional data, a task well-suited to deep learning methodologies. Sánchez et al. further elaborated on the advancements in causal machine learning, which aims to improve clinical decision support systems by integrating diverse data types for better predictive accuracy (Sánchez et al., 2022).

Despite the promise of deep learning, its application in healthcare is not without limitations. Chen et al. pointed out that while deep learning excels at handling complex problems, issues such as low data volume and high sparsity can hinder its effectiveness in certain clinical applications (Chen et al., 2019). This highlights the necessity for ongoing research to

address these challenges, ensuring that deep learning can be reliably applied across various healthcare contexts.

The adaptation of deep learning with traditional machine learning techniques also holds potential for enhancing healthcare analytics. Meng discussed how deep learning algorithms can learn complex mappings from data, which is particularly beneficial in medical image processing (Meng, 2024). This hybrid approach can leverage the strengths of both methodologies, potentially leading to enhanced diagnostic outcomes.

Furthermore, the ethical implications of deep learning in healthcare cannot be overlooked. The use of patient data for training models and algorithms raises concerns about data security and privacy breach. Wibawa et al. proposed a privacy-preserving federated learning framework that utilizes homomorphic encryption to protect sensitive medical data while still enabling effective model training (Wibawa et al., 2022). This approach is crucial for maintaining patient confidentiality while harnessing the power of deep learning.

In the context of specific diseases, deep learning has shown significant promise in areas such as oncology and cardiology. For instance, Nadeem et al. reviewed the application of deep learning in brain tumor analysis, noting its effectiveness in improving diagnostic accuracy and treatment planning (Nadeem et al., 2020). Similarly, Almeida and Tavares emphasized the role of deep learning in radiation oncology, particularly for prostate cancer treatment planning, where accurate segmentation of tumors is critical for effective therapy (Almeida & Tavares, 2020).

The future of deep learning in healthcare appears promising, with ongoing research aimed at refining algorithms and expanding their applicability. Khalid et al. conducted a systematic review comparing deep learning methodologies for analyzing knee bone reports from various imaging modalities, highlighting the potential for these techniques to enhance diagnostic precision (Khalid et al., 2020). As the field continues to evolve, the integration of deep learning with emerging technologies such as telemedicine and wearable devices may further enhance patient care and outcomes.

In conclusion, deep learning represents a significant advancement in health studies, offering powerful tools for disease prediction, medical imaging, and personalized medicine. While challenges remain, particularly regarding data quality and ethical considerations, the potential benefits of deep learning in enhancing healthcare delivery are substantial. Continued research and development in this area are essential to fully realize the transformative potential of deep learning in improving patient outcomes and advancing medical knowledge.

DEEP LEARNING

Deep learning, a subset of machine learning, employs algorithms designed to mimic the architecture and processes of the human brain, known as artificial neural networks. It excels in processing large datasets through multiple layers, enabling the automatic identification of complex patterns and representations. The layered structure of deep learning models enables them to identify features at various levels of abstraction, which makes them particularly adept at tackling complex tasks such as speech and image recognition, drug discovery, and natural language processing (LeCun et al., 2015).

Deep learning models are structured with multiple layers of neurons, where each layer transforms the input data into progressively more abstract representations. This transformation is powered by the backpropagation algorithm, which adjusts the weights of connections between neurons by measuring and correcting the difference between the predicted output and the actual result. Consequently, as these models process more data, their performance improves over time (LeCun et al., 2015). This adaptability has driven remarkable progress in numerous fields, particularly healthcare, where deep learning has been employed for tasks like medical image analysis and disease prediction (Khan, 2023; Karar et al., 2020).

Deep learning is a type of neural network that takes metadata as input and processes that data through a series of layers to program inference. While traditional neural networks can only use a single learning hidden layer (Figure 1, left), deep processes inputs through many hidden layers (Figure 1, right). Each layer consists of nodes of computation. A node decides whether to increase or decrease the influence of the input by combining the input from the data with certain weights, thereby assigning a degree of importance to the inputs. These powerful inputs are aggregated and used to determine the extent to which they are passed on within the evolving network and how much they contribute to its emergence. From a broader perspective, each hidden layer works on a unique feature setting using the emergence of the previous layer. This process is referred to as a non-linear transformation. The number of hidden layer features makes the data more complex and abstract (Xing et al., 2019).

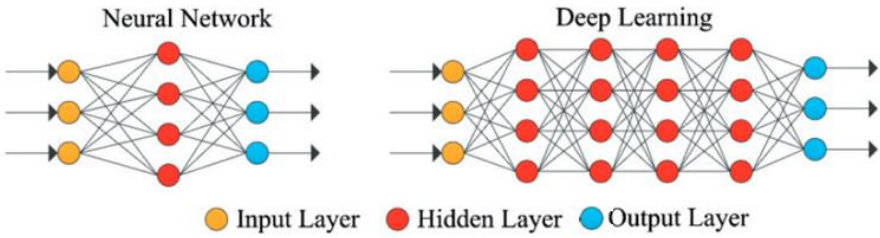

Figure 1: Deep Learning Diagram

Deep learning stands out from traditional machine learning techniques due to its ability to handle large and complex datasets without requiring extensive feature engineering. Conventional methods frequently rely on domain expertise to manually identify and extract relevant features from the data, a process that is both time-consuming and may fail to capture nuanced patterns. Unlike traditional methods, deep learning models have the capability to autonomously learn significant features straight from raw data, rendering them exceptionally proficient in handling high-dimensional data types such as images and audio (LeCun et al., 2015; Sengupta et al., 2020). This advantage has been demonstrated in various studies, where deep learning models have surpassed traditional methods in tasks such as brain tumor segmentation in MRI scans (Khan, 2023) and pneumonia diagnosis from chest X-rays (Karar et al., 2020).

While deep learning offers numerous benefits, it also presents certain challenges. A major drawback is its reliance on large volumes of labeled data to train effective models. When data is insufficient, models risk overfitting, where they memorize the training data instead of generalizing to new, unseen inputs (Khan, 2023). Additionally, deep learning models frequently demand substantial computational resources, encompassing high processing power and memory, which can be impractical in certain situations (Khan, 2023). These limitations underscore the need for continued research to develop more efficient training algorithms and techniques, particularly for use in resource-constrained environments.

Moreover, the interpretability of deep learning models remains a critical concern. While these models can achieve high accuracy, understanding how they arrive at specific decisions can be difficult. This lack of transparency can hinder their adoption in sensitive applications such as healthcare, where understanding the rationale behind a diagnosis is essential for clinician trust and patient safety (Xiong et al., 2019; Saxe et al., 2020). Researchers are actively exploring methods to improve the interpretability of deep learning models, including techniques that visualize the features learned by the model and methods that provide explanations for its predictions (LeCun et al., 2015; Sengupta et al., 2020).

Deep learning algorithms have become increasingly prevalent in healthcare, offering innovative solutions for various applications, including disease diagnosis, medical imaging, and patient management. The most commonly employed deep learning architectures in healthcare include Convolutional Neural Networks (CNNs), Recurrent Neural Networks (RNNs), and more recently, hybrid models that combine different neural network types to enhance performance and accuracy (Piccialli et al., 2021).

1. Convolutional Neural Networks (CNNs): Convolutional Neural Networks (CNNs) are highly effective for image-related tasks, establishing their importance in medical imaging applications. Their strength lies in identifying patterns and features within images, which is vital for diagnosing conditions from radiological scans like X-rays, MRIs, and CT scans. For example, Minaee et al. showcased the use of CNNs for COVID-19 prediction from chest X-rays, outperforming traditional methods by employing an end-to-end deep learning approach that eliminated the need for manual feature extraction (Minaee et al., 2020). Similarly, Liu et al. developed a CNN-based system for differentiating skin diseases, demonstrating its capability to identify various conditions from clinical photographs (Liu et al., 2020). The ability of CNNs to automatically extract hierarchical features directly from raw image data has cemented their role as a critical tool in medical diagnostics. AlexNet, VGG16, VGG19, ResNet, GoogLeNet, DenseNet, and Xception, which are effectively used among CNN architectures, are used to classify images efficaciously.

2. Recurrent Neural Networks (RNNs): RNNs are particularly suited for sequential data, making them valuable for analyzing time-series data such as patient health records or monitoring vital signs. Baji emphasized the potential of RNNs in enhancing healthcare predictions, particularly in early disease detection and accurate diagnosis (Baji, 2024). RNNs can capture temporal dependencies in data, which is essential for understanding patient trajectories over time and making predictions based on historical data.

3. Hybrid Models: Recent advancements have seen the emergence of hybrid models that combine CNNs, RNNs, and other architectures to leverage the strengths of each. For example, Uddin et al. discussed the integration of natural language processing (NLP) with deep learning to analyze electronic health records (EHRs), enabling the extraction of meaningful insights from unstructured clinical text (Uddin et al., 2019). This combination allows for a more comprehensive analysis of patient data, enhancing predictive capabilities and improving clinical decision-making.

4. Generative Adversarial Networks (GANs): GANs are another innovative application of deep learning in healthcare, particularly in generating

synthetic medical images for training purposes. This is particularly beneficial in scenarios where annotated data is scarce. By generating realistic images, GANs can augment training datasets, improving the robustness of models trained on limited data. However, the specific application of GANs in generating synthetic medical images was not supported by the references provided, and thus this claim should be treated with caution as it lacks direct citation support (Pan et al., 2019).

5. Deep Reinforcement Learning: Deep reinforcement learning has also found applications in healthcare, particularly in optimizing treatment plans and resource allocation. This approach uses feedback from the environment to improve decision-making processes, which can be particularly useful in dynamic healthcare settings where patient conditions may change rapidly. However, the reference provided did not specifically address deep reinforcement learning in healthcare, so this claim remains unsupported (Arulkumaran et al., 2017).

6. Transfer Learning: Transfer learning is a powerful approach that enables models trained on one task to be repurposed for a different task. This is especially valuable in healthcare, where labeled data is often scarce. By fine-tuning models that have been pre-trained on extensive datasets using specialized medical datasets, the need for large amounts of labeled data is significantly reduced (Minaee et al., 2020).

In conclusion, deep learning algorithms, particularly CNNs and RNNs, have revolutionized various aspects of healthcare by enabling more accurate diagnostics, enhancing predictive analytics, and improving patient management. The continuous evolution of these algorithms, including the development of hybrid models and the application of techniques like transfer learning, promises to further enhance their effectiveness and applicability in the healthcare domain.

CONCLUSION

In summary, deep learning represents a powerful paradigm in the field of artificial intelligence, characterized by its ability to learn complex representations from large datasets through hierarchical processing. Its applications span numerous domains, including healthcare, where it has shown promise in improving diagnostic accuracy and efficiency. However, challenges related to data requirements, computational demands, and model interpretability must be addressed to fully realize its potential in practical applications.

REFERENCE

Almeida, G., and Tavares, J. M. R. S. (2020). Deep learning in radiation oncology treatment planning for prostate cancer: a systematic review. Journal of Medical Systems, 44(10). https://doi.org/10.1007/s10916-020-01641-3

Arulkumaran, K., Deisenroth, M. P., Brundage, M., and Bharath, A. A. (2017). Deep reinforcement learning: A brief survey. IEEE Signal Processing Magazine, 34(6), 26-38.

Baji, A. (2024). Enhancing healthcare predictions with deep learning models. Proceedings of the AAAI Conference on Artificial Intelligence, 38(21), 23729-23730. https://doi.org/10.1609/aaai.v38i21.30543

Chen, D., Liu, S., Kingsbury, P. R., Sohn, S., Storlie, C. B., Habermann, E. B., … and Liu, H. (2019). Deep learning and alternative learning strategies for retrospective real-world clinical data. NPJ Digital Medicine, 2(1). https://doi.org/10.1038/s41746-019-0122-0

Hamamoto, R., Suvarna, K., Yamada, M., Kobayashi, K., Shinkai, N., Miyake, M., … and Kaneko, S. (2020). Application of artificial intelligence technology in oncology: towards the establishment of precision medicine. Cancers, 12(12), 3532. https://doi.org/10.3390/cancers12123532

Hu, S. (2023). Deep learning in healthcare. Highlights in Science, Engineering and Technology, 57, 279-285. https://doi.org/10.54097/hset.v57i.10014

Huang, S., Pareek, A., Seyyedi, S., Banerjee, I., and Lungren, M. P. (2020). Fusion of medical imaging and electronic health records using deep learning: a systematic review and implementation guidelines. NPJ Digital Medicine, 3(1). https://doi.org/10.1038/s41746-020-00341-z

Karar, M. E., Hemdan, E. E., and Shouman, M. A. (2020). Cascaded deep learning classifiers for computer-aided diagnosis of covid-19 and pneumonia diseases in x-ray scans. Complex &Amp; Intelligent Systems, 7(1), 235-247. https://doi.org/10.1007/s40747-020-00199-4

Khalid, H., Hussain, M., Ghamdi, M. A. A., Khalid, T., Khalid, K. A., Khan, M. A., … and Ahmed, A. (2020). A comparative systematic literature review on knee bone reports from mri, x-rays and ct scans using deep learning and machine learning methodologies. Diagnostics, 10(8), 518. https://doi.org/10.3390/diagnostics10080518

Khan, M. K. H., Guo, W., Liu, J., Dong, F., Li, Z., Patterson, T. A., … and Hong, H. (2023). Machine learning and deep learning for brain tumor mri image segmentation. Experimental Biology and Medicine. https://doi.org/10.1177/15353702231214259

Kiran Sree, P. (2023). Deep learning for heart attack prediction. Biomedical Journal of Scientific &Amp; Technical Research, 54(2). https://doi.org/10.26717/bjstr.2023.54.008522

LeCun, Y., Bengio, Y., and Hinton, G. E. (2015). Deep learning. Nature, 521(7553), 436-444. https://doi.org/10.1038/nature14539

Liu, Y., Jain, A., Eng, C., Way, D. H., Lee, K., Bui, P., … and Coz, D. (2020). A deep learning system for differential diagnosis of skin diseases. Nature Medicine, 26(6), 900-908. https://doi.org/10.1038/s41591-020-0842-3

Meng, Q. (2024). Application of machine learning in medicine. Applied and Computational Engineering, 33(1), 207-212. https://doi.org/10.54254/2755-2721/33/20230268

Minaee, S., Kafieh, R., Sonka, M., Yazdani, S., and Soufi, G. J. (2020). Deep-covid: predicting COVID-19 from chest x-ray images using deep transfer learning. Medical Image Analysis, 65, 101794. https://doi.org/10.1016/j.media.2020.101794

Nadeem, M. W., Ghamdi, M. A. A., Hussain, M., Khan, M. A., Khan, K., Almotiri, S. H., … and Butt, S. (2020). Brain tumor analysis empowered with deep learning: a review, taxonomy, and future challenges. Brain Sciences, 10(2), 118. https://doi.org/10.3390/brainsci10020118

Pan, Z., Yu, W., Yi, X., Khan, A., Yuan, F., and Zheng, Y. (2019). Recent progress on generative adversarial networks (GANs): A survey. IEEE access, 7, 36322-36333.

Piccialli, F., Di Somma, V., Giampaolo, F., Cuomo, S., and Fortino, G. (2021). A survey on deep learning in medicine: Why, how and when?. Information Fusion, 66, 111-137.

Poplin, R., Varadarajan, A. V., Blumer, K., Liu, Y., McConnell, M. V., Corrado, G. S., … and Webster, D. R. (2018). Prediction of cardiovascular risk factors from retinal fundus photographs via deep learning. Nature Biomedical Engineering, 2(3), 158-164. https://doi.org/10.1038/s41551-018-0195-0

Rasmy, L., Xiang, Y., Xie, Z., Tao, C., and Zhi, D. (2021). Med-bert: pretrained contextualized embeddings on large-scale structured electronic health records for disease prediction. NPJ Digital Medicine, 4(1). https://doi.org/10.1038/s41746-021-00455-y

Sánchez, P. A., Voisey, J. P., Xia, T., Watson, H., O'Neil, A. Q., and Tsaftaris, S. A. (2022). Causal machine learning for healthcare and precision medicine. Royal Society Open Science, 9(8). https://doi.org/10.1098/rsos.220638

Saxe, A. M., Nelli, S., and Summerfield, C. (2020). If deep learning is the answer, what is the question?. Nature Reviews Neuroscience, 22(1), 55-67. https://doi.org/10.1038/s41583-020-00395-8

Sengupta, S., Basak, S., Saikia, P., Paul, S., Tsalavoutis, V., Atiah, F. D., … and Peters, A. (2020). A review of deep learning with special emphasis on architectures, applications and recent trends. Knowledge-Based Systems, 194, 105596. https://doi.org/10.1016/j.knosys.2020.105596

Uddin, M., Wang, Y., and Woodbury-Smith, M. (2019). Artificial intelligence for precision medicine in neurodevelopmental disorders. NPJ Digital Medicine, 2(1). https://doi.org/10.1038/s41746-019-0191-0

Wibawa, F., Çatak, F. Ö., Sarp, S., and Kuzlu, M. (2022). Bfv-based homomorphic encryption for privacy-preserving cnn models. Cryptography, 6(3), 34. https://doi.org/10.3390/cryptography6030034

Xing, W., and Du, D. (2019). Dropout prediction in MOOCs: Using deep learning for personalized intervention. Journal of Educational Computing Research, 57(3), 547-570.

Xiong, Z., Wang, D., Liu, X., Zhong, F., Wan, X., Li, X., … and Zheng, M. (2019). Pushing the boundaries of molecular representation for drug discovery with the graph attention mechanism. Journal of Medicinal Chemistry, 63(16), 8749-8760. https://doi.org/10.1021/acs.jmedchem.9b00959

Land Surface Temperature (LST) Calculation processes with Landsat 8

Selçuk ALBUT[1]

1- Prof.Dr.; Tekirdağ Namık Kemal Üniversitesi Ziraat Fakültesi Biyosistem Mühendisliği Bölümü. salbut@@gmail.com ORCID No: 0000-0002-0055-632X

ABSTRACT

Land Surface Temperature (LST) refers to the thermodynamic temperature of the Earth's surface, defined by the radiative temperature radiated from that surface. It provides insights into surface energy fluxes and atmospheric interactions. Land Surface Temperature (LST) exhibits significant variability in both spatial and temporal dimensions, attributable to the variety of climatic influences, land cover, soil and vegetation moisture content, surface radiative characteristics, and topographical features. Satellite data offers benefits over in situ measurements, including worldwide accessibility, uniformity, and geographically dispersed data collection, resulting in a cost-effective and efficient data stream. LST is extensively utilized across several domains, such as agriculture, phenological development, planting depth recommendations, yield forecasting models, weather and climate surveillance, heatwave assessment, urban heat island effect analysis, and environmental impact evaluation. Calculating Land Surface Temperature (LST) with Landsat 8 thermal bands necessitates image preprocessing, rectification, geocoding, and analysis. Factors such as vegetation and radiated radiation are essential for calculating land surface temperature (LST).

Obtaining LST necessitates image preprocessing, correction, geocoding, and analysis. Comprehending the evolution and distribution of LST is crucial for climate change monitoring, agricultural management, land cover alterations, and several other uses.

Keywords – Land Surface Temperature (LST), Land Surface Emissivity (LSE) Remote Sensing, NDVI, Landsat, QGIS.

INTRODUCTION

The Land Surface Temperature (LST) denotes the thermodynamic temperature of Earth's surface and defines the radiative temperature emitted by the surface, providing insights into surface energy fluxes and atmospheric interactions (“Land Surface Temperature Technical Specification,” n.d.).

The Earth's surface absorbs solar radiation, resulting in land heating, while the emitted temperature varies due to the variability of climatic forces, land cover, soil and vegetation moisture content, surface radiative characteristics, and terrain. Consequently, LST exhibits significant variability in both spatial and temporal dimensions (Prata et al., 1995). Due to significant spatio-temporal variability, satellite-derived land surface temperature (LST) has several advantages over in situ observations, including worldwide accessibility, consistency, and geographical distribution, resulting in a cost-effective and efficient data stream.

Land surface temperature (LST) is an essential element of Earth's climate and several physical, chemical, and biological processes. Considering that climate change is a worldwide warming phenomena, it is imperative to employ space technology for the monitoring of land surface temperature (LST). Urban warming, however, encompasses an extra phenomenon known as the urban heat island effect. Land surface temperature is correlated with several biophysical and demographic factors, necessitating that quantitative estimations consider this relationship.

The data shown reflects the temperature as observed from a satellite's perspective. The "surface" refers to what the sensor observes as it views the ground through the atmosphere, such as the canopy top in planted regions, dirt in non-vegetated areas, or rooftops in urban settings. Consequently, Land Surface Temperature differs from the air temperature reported in daily weather forecasts. LST can offer insights into several applications, including evaporation monitoring, climate change research, soil moisture assessment, vegetation analysis, and urban studies, among others. Miralles et al. (2011), Intergovernmental Panel on Climate Change et al. (2021), Merlin et al. (2008), Mantey et al. (2014), Voogt and Oke (2003), Land Surface Temperature Technical Specification (n.d.)

USAGE OF LST

LST is extensively utilized throughout several domains nowadays. Typical applications of LST are as follows.

Agriculture

Crop Stress Monitoring: Utilizing Planet Land Surface Temperature as input in energy balance-based evaporation models facilitates the early detection of crop stress, enabling timely intervention.

Phenological development: Land Surface Temperature (LST) can serve as an input for Growing Degree Days. Growing degree days serve as a meteorological metric for evaluating crop maturation. Agricultural producers utilize a metric of thermal accumulation to forecast the rates of plant and pest growth in relation to the timing of crop maturation. The benefit of LST-based GDD is its capacity to precisely assess crop conditions, offering insights into crop growth and development, rather than depending exclusively on environmental circumstances based on air temperature.

Seeding Depth Prescription: High resolution LST shows potential for comprehending within-field heterogeneity, therefore facilitating planting depth prescriptions to enhance uniformity of emergence and plant stand according to local environmental, soil, and management variables.

Yield forecasting model: When combined with Soil Water Content and Vegetation Optical Depth, Land Surface Temperature can be utilized in yield forecasting models. Thermal anomalies adversely affect yields throughout

various stages of the growing season, becoming it a crucial factor in regional yield forecast models.

Weather and Climate Monitoring¶

Monitoring circumstances across years and decades, Land Surface Temperature data establishes a foundational comprehension of typical and atypical conditions for each specific location.

Heatwave monitoring: The land surface temperature of the planet may monitor arid and elevated thermal conditions. The correlation between soil moisture and temperature signifies the intensity and scope of drought conditions and their impact on agriculture, ecosystems, and human populations.

Urban Heat Island: Urban areas exhibit elevated temperatures relative to their rural counterparts. Planet Land Surface Temperature can be pivotal in identifying metropolitan areas most affected by heat and assist governments and municipal administrations in determining necessary solutions.

Environmental Impact monitoring¶

Quantify the effect of restoration initiatives: Land Surface Temperature can be utilized to monitor landscape alterations resulting from intervention operations and the consequent effects of these changes on the region's climate.

The Land Surface Temperature can be estimated using the thermal bands of Landsat 8. It necessitates the application of a series of equations via a raster image calculator utilizing QGIS.

This tutorial demonstrates the calculation of Land Surface Temperature (LST) with the Landsat 8 bands. Specifically, band 10 serves as the temperature band, whereas bands 4 and 5 are utilized to compute the Normalized Difference Vegetation Index (NDVI).

Land Surface Temperature (LST) is the radiative skin temperature of the terrestrial surface obtained from solar radiation. It is a fundamental factor influencing the terrestrial thermal dynamics, as it regulates the effective radiating temperature of the Earth's surface. LST is associated with various facets of geoscience, making the comprehension of its evolution and global distribution crucial for monitoring climate change, crop management, land cover alterations, and numerous other applications (Voogt and Oke, 2003; Xiao et al., 2008; Franzpc, 2019).

Retrieving LST necessitates image preprocessing, rectification of distortions from satellite image acquisition, evaluation of geometric and temporal compatibility with other information sources through geocoding and projection onto a suitable system, and subsequent image analysis. Sensors quantify digital values that must be converted into radiance and subsequently into brightness temperature utilizing established methodologies. Vegetation is a significant characteristic that affects land surface temperature (LST). Brightness temperature is utilized to compute the Normalized Difference Vegetation Index (NDVI), an indicator of vegetation greenness. The calculation of NDVI facilitates the determination of the plant cover proportion

in the specified region. The last element in calculating Land Surface Temperature (LST) is Land Surface Emissivity, which is used to ascertain emitted radiance based on soil, plant, and surface roughness values. These variables allow the acquisition of land surface temperature with the spatial resolution afforded by the sensors (Twumasi et al., 2021).

DATA COLLECTION

An imagine from Landsat 8 (Operational Land Imager), covering the northwestern region of Turkey, was obtained from the United States Geological Survey Earth Explorer's free online data services for land surface temperature (LST) study (U.S. Geological Survey, 2024a). The image was obtained with less than 10% cloud cover in June 2024 (Table 1).

Table 1: Landsat images used in the LST mapping of Tekirdag

LANDSAT SCENE ID	Sensor	Resolution	Path/Row	Date
LC81810322024153LGN00	Landsat 8	30 m	181/032	06.01.2024

Source: (U.S. Geological Survey, 2024a).

IMAGE PROCESSING

Three tasks were executed to process the images. These encompassed image preprocessing and correction. In picture pre-processing, both visual and digital image processing were conducted, and prior to this, images were loaded into QGIS 3.34 software for subsequent processing. Thermal Infrared band 10 was selected for subsequent study.

IMAGE RECTIFICATIONS

Image rectifications were executed to amend data distortion potentially arising from the image gathering procedure, utilizing the Impact toolkit created by the European Union Joint Research Centre. To guarantee precise identification of time variations and geometric congruence with other informational sources, images were geocoded to the coordinate and mapping system of the national topographic maps. Each image were projected to the Universal Transverse Mercator (UTM) coordinate system, zone 35 North.

IMAGE ANALYSIS

The algorithm was created in QGIS 3.34. In this study Landsat 8 Thermal Infrared band (Band 10) was used to estimate brightness temperatures and bands 4 (Red) and 5 (Infrared) were used for calculating the NDVI. The LST retrieval formulas were taken from the USGS web page for retrieving the top of atmospheric (TOA) spectral radiance (U.S. Geological Survey, 2024b). The LST was retrieved following the steps of Figure 1.

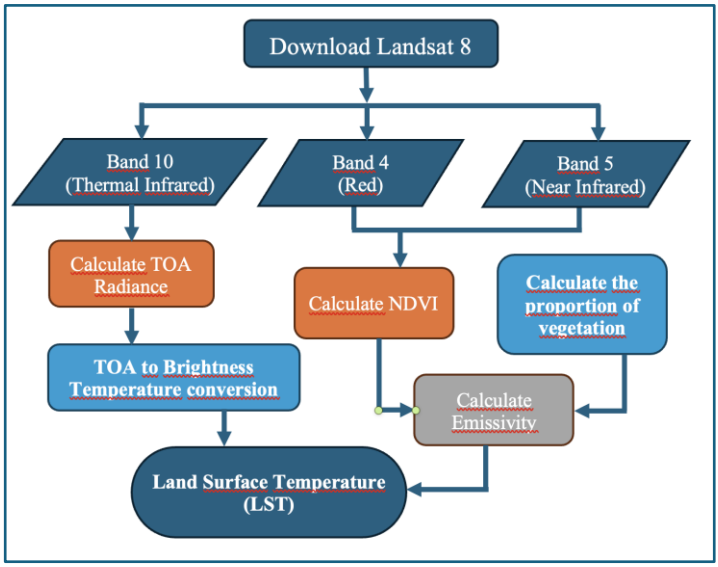

Figure 1: Flowchart for LST processing.

CALCULATİON OF TOA (TOP OF ATMOSPHERİC)

Top of Atmosphere (TOA) Reflectance is a unitless measurement which provides the ratio of radiation reflected to the incident solar radiation on a given surface. It that can be computed from satellite measured spectral radiance using the mean solar spectral irradiance and the solar zenith angle (Marino, 2024). Landsat Level-1 data can be converted to TOA spectral radiance using the radiance rescaling factors in the MTL file. The metadata for the equations is contained in the Text documentation in the Landsat 8 data folder downloaded from the U.S. Geological Survey EarthExplorer web site.

$$L_\lambda = M_L\ Q_{cal} + A_L \quad (1)$$

where:

L_λ = TOA spectral radiance (Watts/(m^2 * srad * μm))

M_L =Band-specific multiplicative rescaling factor from the metadata,

A_L=Band-specific additive rescaling factor from the metadata

Q_{cal} = Quantized and calibrated standard product pixel values (DN).

In the QGIS application, the following equation will be written in the calculation of TOA with the Raster Calculator tool. The raster image obtained as a result of the TOA process is shown in figure 3.

TOA = 0.0003342 * “Band 10” + 0.1

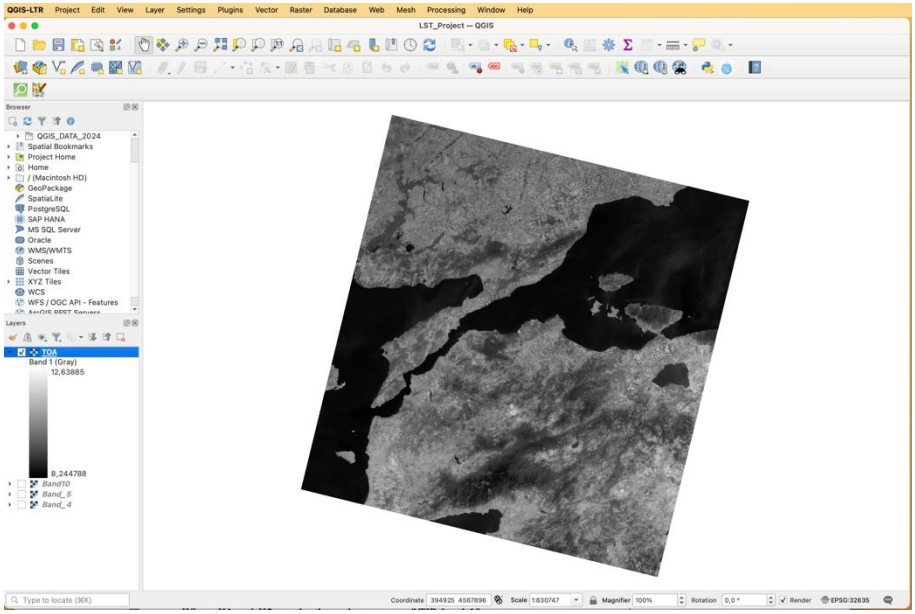

Figure 2: Result of the TOA (Top of Atmospheric) calculation.

CONVERSİON TOA TO BRİGHTNESS TEMPERATURE

Thermal band data can be converted from spectral radiance to top of atmosphere brightness temperature using the thermal constants in the MTL file:

$$B_T = \frac{K_2}{ln\left(\frac{K_1}{L_\lambda}\right) + 1} - 273.15$$

where:

B_T = Top of atmosphere brightness temperature (K)

L_λ =TOA spectral radiance (Watts/(m2 * srad * μm))

K_1 = Band-specific thermal conversion constant from the metadata

K_2 = Band-specific thermal conversion constant from the metadata

In the QGIS application, the following equation will be written in the calculation of Conversion TOA to Brightness Temperature with the Raster Calculator tool. Therefore, to obtain the results in Celsius, the radiant temperature is adjusted by adding the absolute zero (approx. -273.15°C).

BT = (1321.0789 / Ln ((774.8853 / "%TOA%") + 1)) – 273.15

The satellite data products were geometrically corrected data set. The metadata of the satellite images is presented in Table 2 and the result shown in figüre 4.

Table 2: Metadata of the Landsat 8 images

Metadata Variable	Description	Value
M_L	RADIANCE MULT BAND 10	0.0003342
A_L	RADIANCE ADD BAND 10)	0.10000
K_1	CONSTANT BAND 10	774.8853
K_2	CONSTANT BAND 10	1321.0789

Source: (U.S. Geological Survey, 2024a).

CALCULATE THE NDVI

The normalized difference vegetation index (NDVI), which is derived from remote-sensing (satellite) data, is closely linked to drought conditions. To determine the density of green on a patch of land, the distinct colors (wavelengths) of visible and near-infrared sunlight reflected by the plants are observed; red and near-infrared bands i.e . Band 4 and Band 5 respectively were used for calculating the Normal NDVI. The importance of estimating the NDVI is essential since the amount of vegetation present is an important factor and NDVI can be used to infer general vegetation condition. The calculation

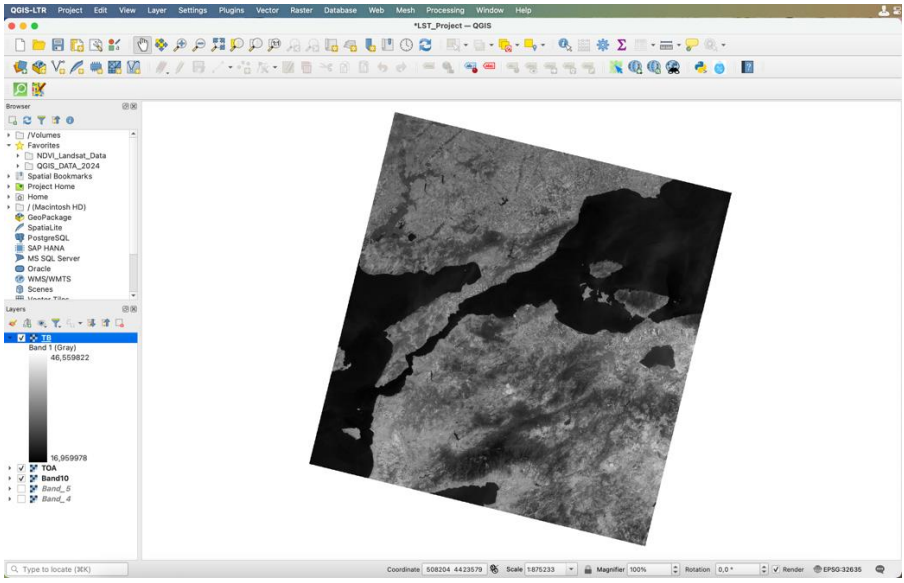

Figure 3: Result of the BT (brightness temperature) calculation.

of the NDVI is important because, afterward, the proportion of the vegetation (P_V) should be calculated, and they are highly related with the NDVI, and emissivity (ε) should be calculated, which is related to the P_V.

$$NDVI = \frac{NIR(Band\ 5) - Red\ (Band\ 4)}{NIR(Band\ 5) + Red\ (Band\ 4)}$$

Where NIR represents the near-infrared band (Band 5) and R represents the red band (Band 4). This formula is written with the Raster Calculator tool as follows and the process is performed (Fig. 4).

NDVI = (Band 5 – Band 4) / (Band 5 + Band 4)

CALCULATE THE PROPORTİON OF VEGETATİON

Proportion of vegetation (Vegetation Fraction) is defined as the percentage of vegetation occupying the ground area in vertical projection. Changes in vegetation cover directly impact surface water and energy budgets through plant transpiration, surface albedo, emissivity, and roughness. The proportion of vegetation P_V is closely related to NDVI values for vegetation and soil. In this study, P_V was estimated following the NDVI traditional method (Aman, et al., 1992, Rouse, et al., 1974)

$$P_v = \left(\frac{NDVI - NDVI_{min}}{NDVI_{max} - NDVI_{min}}\right)^2$$

Where $NDVI_v$ and $NDVI_s$ are Maximum and Minmum NDVI respectively representing NDVI of Vegetation and NDVI of soil respectively (in our application, the minimum value is calculated as -0.26334 and the maximum value is calculated as 0.653719).

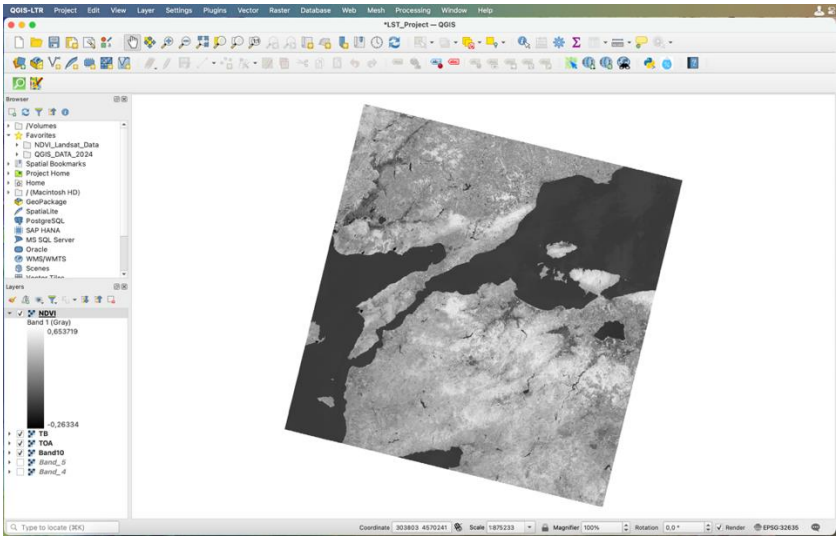

Figure 4: Result of the NDVI calculation.

This calculate the proportion of vegetation (P_v) formula is written with the Raster Calculator tool as follows and the process is performed.

P_v = (("NDVI@1" – 0.26334) / (0.653719 – 0.26334)) ^ 2

Usually the minimum and maximum values of the NDVI image can be displayed directly in the image, otherwise you must open the properties of the raster to get those values (Fig.5).

Calculate the land surface emissivitty

The emissivity (ε) values for the land cover classes are provided in the following table (values used in this tutorial are only indicative, because emissivity of every material should be obtained from field survey) (Weng et al., 2004, "Tutorial: Estimation of Land Surface Temperature With Landsat And ASTER," n.d.):

Land surface emissivity (LSE). Average emissivity of an element of the surface of the Earth calculated from measured radiance and land surface

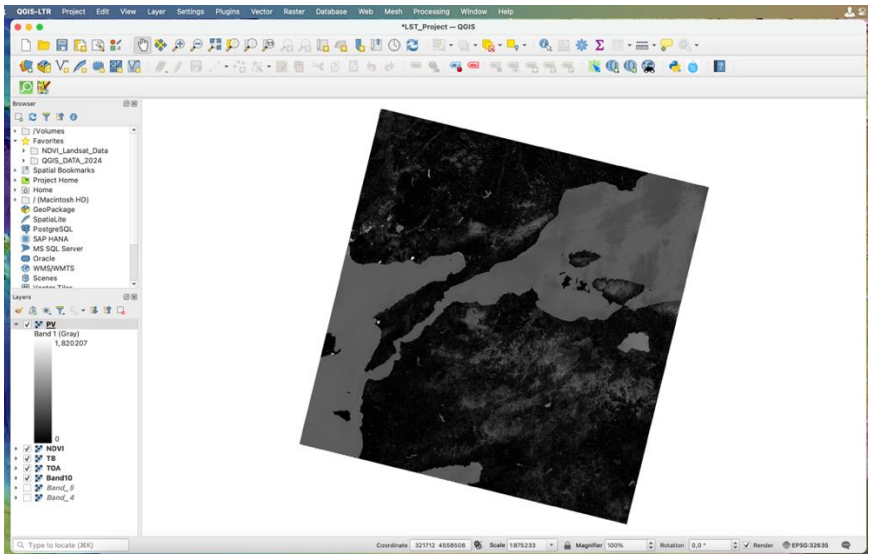

Figure 5: Result of the Pv (Proportion of vegetation) calculation.

temperature. The land surface emissivity (LSE (ε)) must be known in order to estimate LST, ince the LSE is a proportionality factor that scales blackbody radiance to predict emitted radiance, and it is the efficiency of transmitting thermal energy across the surface into the atmosphere. The determination of the ground emissivity is calculated conditionally as suggested (Jimenez-Munoz,, et al., 2006, Sobrino, J.A. and Raissouni, 2000, Sobrino, et al., 2004).

$$\varepsilon_\lambda = \varepsilon_{V\lambda} P_V + \varepsilon_{S\lambda}(1 - P_V) + C_\lambda$$

where ε_v and ε_s are the vegetation and soil emissivities respectively, and C is the surface roughness taken as a constant value of 0.005. The emissivity of water bodies is utmost stable in comparison with land surfaces. Since the emissivity depends on the wavelength, the NDVI threshold method (NTM)

can be used to estimate the emissivity of different land surfaces in the 10-12 μm range. Additionally, the spectral range of Band 10 of Landsat 8 is suitable in this range. At this wavelength range, the emissivity could be modeled as follows (Weng et al., 2004):

$$\varepsilon_\lambda = \begin{cases} \varepsilon_{S\lambda}, & NDVI < NDVI_S \\ \varepsilon_{V\lambda}P_V + \varepsilon_{S\lambda}(1-P_V) + C_\lambda, & NDVI_S \le NDVI \le NDVI_V \\ \varepsilon_{V\lambda}P_V + C_\lambda, & NDVI > NDVI_{VS} \end{cases}$$

The differences between the retrieved LSTs and the air temperatures and details on the stations are presented in Table 3 (Avdan & Jovanovska, 2016).

Table 3. Emissivity of representative terrestrial materials for LANDSAT 8 TIRS Band 10.

Terrestrial material	Water	Building	Soil	Vegetation
Emissivity	0.991	0.962	0.966	0.973

Source: (Avdan & Jovanovska, 2016).

However for this study the mean NDVI value is between 0 and 0.2 therefore the emissivity value of 0.996 was assigned.

The Calculate Emissivity (ε) formula is written with the Raster Calculator tool as follows and the process is performed (Fig.6).

$\varepsilon = 0.004 * P_v + 0.986$

Calculate Land Surface Emissivity (EM) using the Fraction of Vegetation (FV). The 0.004 coefficient represents the emissivity variation due to vegetation, and the 0.986 represents the base emissivity for other surfaces (Ridho, 2024, Li et al., 2012).

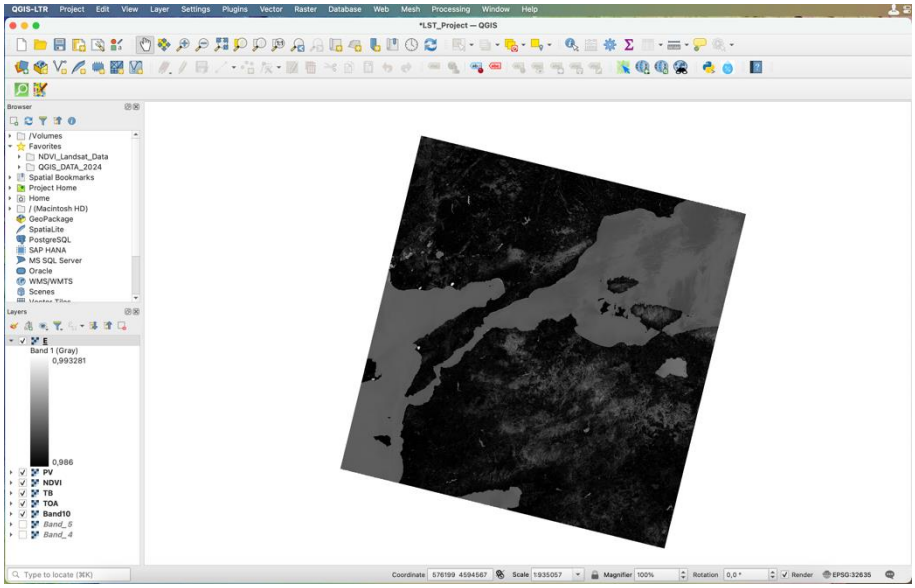

Figure 6: Result of the E (emissivitty) calculation.

CALCULATE THE LAND SURFACE TEMPERATURE

The emissivity corrected land surface temperatures (S_t) were calculated as follows (Weng, et al. 2004, Saha et al., 2023):

$$S_t = \frac{B_T}{1 + \left[\left(\frac{\lambda * B_T}{\rho}\right) * \ln_{\varepsilon_\lambda}\right]}$$

where:

B_T = Top of atmosphere brightness temperature (K)

λ = wavelength of emitted radiance from Landsat-8 TIRS band 10 (λ = 10.895) (Sholihah & Shibata, 2019) (Tables 4).

$\rho = h\frac{c}{\sigma} = 1.4388 * 10^{-2} mK$ = 14388 µK

h = Planck's constant = $6.626*10^{-34}$ J s

σ = Boltzmann constant = $1.38*10^{-23}$ J/K

c = velocity of light = $2.998*10^{8}$ m/s

Table 4. Wavelength of Landsat 8 band 10.

Landsat 8 bands	Wavelength (micrometers)	Resolution (meters)
Band 1 - Coastal aerosol	0.43 - 0.45	30
Band 2 - Blue	0.45 - 0.51	30
Band 3 - Green	0.53 - 0.59	30
Band 4 - Red	0.64 - 0.67	30
Band 5 - Near Infrared (NIR)	0.85 - 0.88	30
Band 6 - SWIR 1	1.57 - 1.65	30
Band 7 - SWIR 2	2.11 - 2.29	30
Band 8 - Panchromatic	0.50 - 0.68	15
Band 9 - Cirrus	1.36 - 1.38	30
Band 10 - Thermal Infrared (TIRS) 1	10.60 - 11.19	100 (resampled to 30)
Band 11 - Thermal Infrared (TIRS) 2	11.50 - 12.51	100 (resampled to 30)

The LST (S_t) formula is written with the Raster Calculator tool as follows and the process is performed.

LST = (BT / (1 + (10.895 * BT / 14388) * Ln(ε)))

Finally, the land surface temperature map was produced in QGIS.

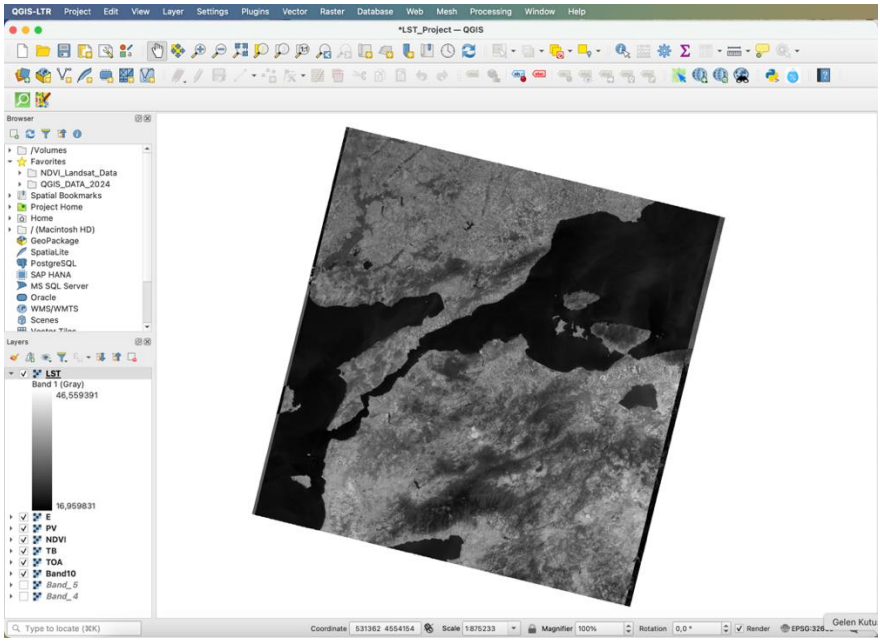

Figure 7: Result of the LST calculation.

As a final process, the LST map is colored according to the temperature values, and the objects (scale, legend, etc.) are added to the map (Fig. 8).

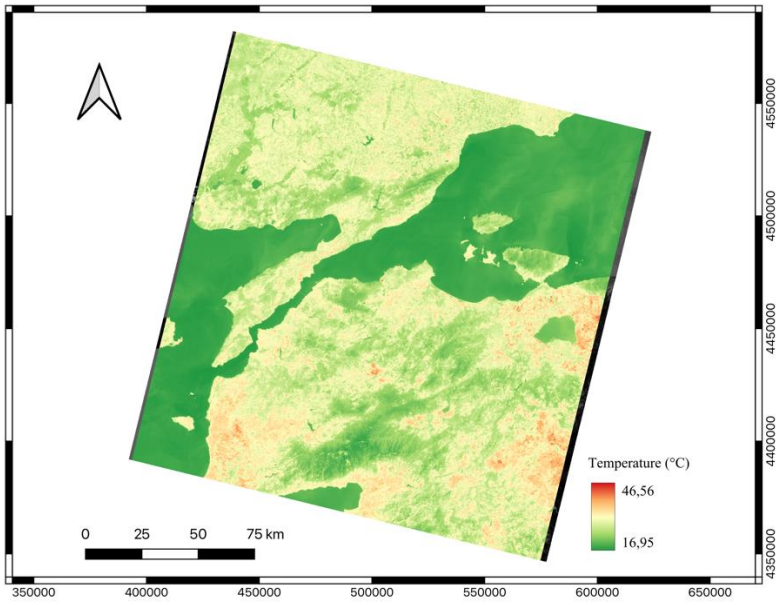

Figure 8: LST map example.

REFERENCE

Land Surface Temperature Technical Specification. (n.d.). Retrieved from https://developers.planet.com/docs/planetary-variables/land-surface-temperature-technical-specification/

Prata, A. J., Caselles, V., Coll, C., Sobrino, J. A., & Ottlé, C. (1995). Thermal remote sensing of land surface temperature from satellites: Current status and future prospects. Remote Sensing Reviews, 12(3–4), 175–224.

Miralles, D. G., Holmes, T. R. H., De Jeu, R. A. M., Gash, J. H., Meesters, A. G. C. A., and Dolman, A. J. (2011). Global land-surface evaporation estimated from satellite-based observations, Hydrol. Earth Syst. Sci., 15, 453–469.

Intergovernmental Panel on Climate Change, Pirani, A., Connors, S. L., Péan, C., Berger, S., Caud, N., Zhou, B. (2021). Climate Change 2021: The Physical Science Basis. (V. Masson-Delmotte PhD & P. Zhai, Eds.), The Physical Science Basis. Retrieved from https://www.ipcc.ch/report/ar6/ wg1/ downloads/report/IPCC_AR6_WGI_SPM_final.pdf.

Merlin, O., Walker, J.P. Chehbouni, A., Kerr, Y., (2008).Towards deterministic downscaling of SMOS soil moisture using MODIS derived soil evaporative efficiency, Remote Sensing of Environment, Volume 112, Issue 10, Pages 3935-3946,

Twumasi, Y. A., Merem, E. C., Namwamba, J. B., Mwakimi, O. S., Ayala-Silva, T., Frimpong, D. B., Mosby, H. J. (2021). Estimation of Land Surface Temperature from Landsat-8 OLI Thermal Infrared Satellite Data. A Comparative Analysis of Two Cities in Ghana. *Advances in Remote Sensing*, *10*(04), 131–149.

Voogt, J. A., & Oke, T. R. (2003). Thermal remote sensing of urban climates (journal-article). *Remote Sensing of Environment*(Vol. 86, pp. 370–384).

Xiao, R., Weng, Q., Ouyang, Z., Li, W., Schienke, E.W. and Zhang, Z. (2008) LandvSurface Temperature Variation and Major Factors in Beijing, China. Photogramm etric Engineering & Remote Sensing , 74, 451-461.

Franzpc. (2019, April 24). How to calculate Land Surface Temperature with Landsat 8 satellite images. Retrieved from https://giscrack.com/how-to-calculate-land-surface-temperature-with-landsat-8-images/

U.S. Geological Survey (2024a) EarthExplorer-Home. Satellite Data. https://earthexplorer.usgs.gov/

U.S. Geological Survey (2024b) Landsat Missions: Using the USGS Landsat Level-1 Data Product. https://www.usgs.gov/landsat-missions/using-usgs-landsat-level-1-data-product .

Marino, F. (2024, November 19). Top of Atmosphere Reflectance on Sentinel 3. Retrieved from https://www.earthstartsbeating.com/2017/04/27/top-of-atmosphere-reflectance-on-sentinel-3/#:~:text=Top%20of%20Atmosphere%20(TOA)%20Reflectance,and%20the%20solar%20zenith%20angle

Aman, A., Randriamanantena, H.P., Podaire, A. and Froutin, R. (1992) Upscale Integration of Normalized Difference Vegetation Index: The Problem of Spatial Heterogeneity. IEEE Transactions on Geoscience and Remote Sensing, 30, 326-338.

Rouse, J.W., Haas, R.W., Schell, J.A., Deering, D.W. and Harlan, J.C. (1974) Monitoring the Vernal Advancements (Greenwave Effect) and Retrogradation of Natural Vegetation. NASA/GSFCT Type III Final Report, Texas A & M University, Remote Sensing Center, College Station, 1-137.

Jimenez-Munoz, J.C., Sobrino, J.A., Gillespie, A., Sabol, D. and Gustafson, W.T. (2006) Improved Land Surface Emissivities over Agricultural Areas Using ASTER NDVI. Remote Sensing of Environment, 103, 474-487.

Sobrino, J.A., Jiménez-Muñoz, J.C. and Paolini, L. (2004) Land Surface Temperature Retrieval from LANDSAT TM5. Remote Sensing of Environment, 90, 434-440.

Sobrino, J.A. and Raissouni, N. (2000) Toward Remote Sensing Methods for Land Cover Dynamic Monitoring: Application to Morocco. International Journal of Remote Sensing, 21, 353-366.

Tutorial: Estimation of Land Surface Temperature with Landsat and ASTER — Τεκμηρίωση του Semi-Automatic Classification Plugin - 5.3.6.1. (n.d.). Retrieved from https://semiautomaticclassificationmanual-v5.readthedocs.io/el/ latest/thematic_tutorial_temperature.html

Avdan, U., & Jovanovska, G. (2016). Algorithm for Automated Mapping of Land Surface Temperature Using LANDSAT 8 Satellite Data. Journal of Sensors, 2016, 1–8.

Weng, F., Qin, Z., Song, C., Tu, L., Karnieli, A., & Zhao, S. (2004). An Improved Mono-Window Algorithm for Land Surface Temperature Retrieval from Landsat 8 Thermal Infrared Sensor Data. Remote Sensing,c7(4), 4268–4289.

Ridho, M. (2024, June 8). Analyzing Land Surface Temperature (LST) with Landsat 8 Data in Google Earth Engine. *Medium*. Retrieved from https://medium.com

Li, Z., Wu, H., Wang, N., Qiu, S., Sobrino, J. A., Wan, Z., . . . Yan, G. (2012). Land surface emissivity retrieval from satellite data. *International Journal of Remote Sensing*, *34*(9–10), 3084–3127.

Saha, J., Ria, S. S., Sultana, J., Shima, U. A., Seyam, M. M. H., & Rahman, M. M. (2023). Assessing seasonal dynamics of land surface temperature (LST) and land use land cover (LULC) in Bhairab, Kishoreganj, Bangladesh: A geospatial analysis from 2008 to 2023. *Case Studies in Chemical and Environmental Engineering*, *9*, 100560.

Sholihah, R. I., & Shibata, S. (2019). Retrieving Spatial Variation of Land Surface Temperature Based on Landsat OLI/TIRS: A Case of Southern part of Jember, Java, Indonesia. *IOP Conference Series Earth and Environmental Science*, *362*(1), 012125.

Mantey, S., Tagoe, N. D., & Abaidoo, C. A. (2014). Estimation of Land Surface Temperature and Vegetation Abundance Relationship – A Case Study. *3rd UMaT Biennial International Mining & Mineral Conference* (p. 30th July-2nd August, 2014).

Innovative Strategies in Aerospace: Exploring Microwave Energy Curing for Composite Applications

Soner ŞEN[1]
Mustafa TAŞYÜREK[2]

1- Doç. Dr.; Selçuk Üniversitesi, Sivil Havacılık Yüksekokulu, Uçak Gövde-Motor Bakımı Bölümü. sensoner@selcuk.edu.tr ORCID: 0000-0003-3385-5577
2- Doç. Dr.; Selçuk Üniversitesi, Sivil Havacılık Yüksekokulu, Uçak Gövde-Motor Bakımı Bölümü. mtasyurek@selcuk.edu.tr ORCID: 0000-0001-9016-8584

ABSTRACT

Composites, valued for their lightness, durability, and high performance, have been increasingly important and attractive in the aerospace sector over the years. However, traditional curing methods used in the production of these materials can be inefficient in terms of energy consumption and processing times. In this context, microwave energy-based curing emerges as a faster and more energy-efficient alternative.

Microwave energy rapidly heats the molecular structure of composite materials, initiating the curing process, which can be completed in a shorter time compared to traditional heating methods. Additionally, microwaves can penetrate deeper regions of the material, resulting in a more homogeneous curing process. This offers a significant advantage, particularly for large and complex-shaped aerospace components.

The chapter discusses traditional composite manufacturing methods and explores the potential benefits and application areas of microwave curing, particularly in enhancing efficiency in composite material production for the aerospace industry. Engineering challenges of microwave curing and future research needs in this field. This innovative technology enables more sustainable and cost-effective manufacturing processes in the aerospace industry.

Keywords –Aerospace, Composite, Curing, Microwave Energy, Polymer Processing.

USE OF COMPOSITES IN AVIATION VEHICLES FROM PAST TO PRESENT

Since their initial use, aircraft have continuously evolved. After being primarily made of wood and fabric, their development accelerated rapidly. In response to these advancements, the need for faster travel, longer range, intercontinental high-altitude flight, higher transport capacity, greater mechanical and thermal durability, and long-lasting structures emerged. These requirements made the transition from wooden aircraft structures to metal aircraft structures inevitable. However, despite the advantages of metals, they also brought certain disadvantages. The most significant of these is the high density of metals, which leads to increased weight. Weight, being a factor that negatively affects several aspects such as prolonging flight time, reducing range, increasing fuel consumption, and limiting payload capacity, is one of the most undesirable elements in aircraft design. Despite these challenges, metals have been used extensively in both military and commercial aviation for many years due to their overall advantages, and they continue to be employed in modern aircraft.

Due to globalization, the aviation industry, which was in its formative stage approaching the 2000s, can still be observed in a growth phase today. Civil aviation, military operations, air cargo, defense, space industries, and jet aircraft activities continue to advance in air transportation. These developments also bring certain necessities. Although not across all sectors, the need for advancements in fuel types, engine development, and fuselage/wing technologies has required differentiation in fuselage/wing materials in specific areas. Consequently, polymer-based composite materials are increasingly utilized in aircraft technology. These advanced engineering materials not only provide weight advantages but also offer numerous benefits compared to metals, including corrosion resistance, reduced fuel consumption, extended range, improved altitude performance, cost reduction in production, and longer fatigue life. In fact, replacing an aluminum structure with graphite/epoxy composites can achieve weight reductions of 20% or more (http://www.aviation-history.com). Therefore, materials science is of critical importance to the aerospace industry. These factors collectively make composites favorable alternative materials from an environmental perspective (http://web.archive.org).

Composite materials consist of two or more distinct components combined to create a material with unique properties. Renowned for their versatility, composites find extensive applications in aerospace, including spacecraft, hot air balloon gondolas, gliders, passenger planes, fighter jets, and space shuttles (https://www.target.com/p/composite-materials). Their use in the aerospace sector has allowed engineers to address and surpass the limitations associated with single-material designs. (https://www.appropedia.org/Composites_in_the_Aircraft_Industry).

In a typical composite material, one component acts as the supporting matrix, while another is added to reinforce and strengthen the overall structure. Fiberglass, for instance, was first utilized in the 1950s on the Boeing 707 passenger jet, where it accounted for approximately 2% of the aircraft's structure. By the mid-1970s, the use of composites had expanded, with the Concorde aircraft incorporating 8% composite materials into its design (Kocaoğlu, 2021). The Boeing 787 Dreamliner represents a significant shift, as it will be the first commercial airliner to rely on composite materials for its primary structural components instead of traditional aluminum alloys (http://www.ifi.uio.no/siag; https://www.sampe.org/boeings-787). Following this trend, composite materials have also been extensively used in fighter jets, helicopters, and unmanned aerial vehicles (Mohammed, 2014). In fact, the A350 aircraft model includes a total of 53 percent composite materials in components such as the wings, main spars, panels, doors, frames, stringers, and doublers (Bachmann et al., 2018).

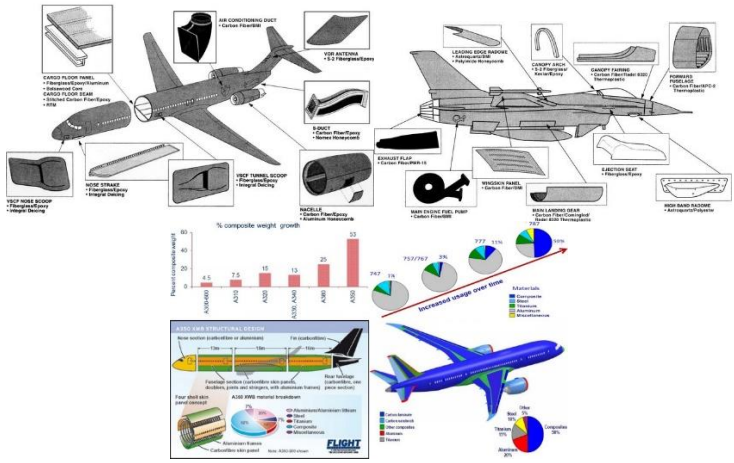

Figure 1: Parts of composite materials in aircraft and their development (Alınca, 2024; Grant, 2003)

The primary goal of aerospace projects is always to maximize payload capacity by reducing structural weight, engine weight, and fuel weight. Achieving this goal requires the optimization of each component. Fuel weight can be reduced in direct proportion to engine efficiency and flight range, but the key to reducing structural and engine weight lies in the properties of the materials used. The structure of an aerospace vehicle must meet high durability and safety requirements while also being as lightweight as possible. This highlights the critical role material selection plays in the design process. In the aerospace industry, material selection requires balancing safety, lightness, cost efficiency, and manufacturability, which poses a challenging engineering task. For this reason, materials science is one of the most critical areas of research in the sector. In the design of an aerospace vehicle, the materials used must be strong, lightweight, and economical. Additionally, using materials that minimize manufacturing complexity and control costs offers significant advantages. In aerospace, every kilogram saved translates to higher efficiency and greater payload capacity. Therefore, the correct material selection not only reduces weight but also significantly enhances the performance of the vehicle.

Composite materials generally consist of two distinct layers: the reinforcing material, which serves a load-bearing role, and the matrix, which binds and supports this reinforcement (Ulaş, 2020).

CFRP (Carbon Fiber Reinforced Polymer) is used in next-generation commercial aircraft, particularly in wings, fuselage, tail, control surfaces, and doors. It is also frequently employed in the production of unmanned aerial vehicles (UAVs), where its strength, lightweight properties, and performance criteria are essential. In addition to the aerospace sector, CFRP is widely favored in spacecraft applications. Due to its excellent thermal stability, it is

one of the best candidates for such uses. In spacecraft, it is utilized as a coating material, in controlled structural arms, antenna reflectors, and optical platforms. Moreover, its use is becoming increasingly common in primary structural components.

GFRP (Glass Fiber Reinforced Polymer) is used in commercial passenger aircraft, particularly in wing sections, wing-fuselage attachment components, antenna covers, and areas where thermal insulation is critical. It was initially employed in the aerospace industry for missile antenna covers. GFRP can be bonded with steel materials, and a new composite material known as Glare, which combines GFRP with aluminum layers, is used in certain sections of the Airbus A380 fuselage.

Another structural component in aircraft is the sandwich composite. It consists of two thin, lightweight face sheets with a core material arranged perpendicularly between them, often in a hexagonal, hollow honeycomb pattern. Due to the voids within the core, these materials exhibit very low density, yet they possess high compressive strength in the perpendicular direction. Consequently, recent studies on the low-velocity impact properties of honeycomb materials in aerospace applications have gained momentum (Deng, Yu, & Zhang, 2024; Elaldı, 2024; Tamboli, Joshi, Pandey, Bongale, & Kumar, 2020; Taşyürek & Kara, 2021). Owing to their form, they also exhibit excellent bending resistance. In aircraft, honeycomb composites are commonly used in panels and, in some cases, such as in the B747 model, in flaps as well.

MATRİX MATERIALS

A common characteristic of the materials discussed in the previous section is that the reinforcement materials, while exhibiting excellent properties on their own, are unable to demonstrate these advantages within the primary structure. Therefore, there is a need for a binder that can protect the reinforcements from external factors, hold them together, and impart toughness and flexibility to them. In material science, these binders are referred to as matrices. These matrix materials, which can be ceramic, metal, or plastic-based, are predominantly chosen from plastic-based materials in the aerospace industry. Plastic materials, in turn, are primarily classified into two main categories: thermosetting and thermoplastic.

Thermoset matrix composites are derived from liquid resins with two different polymer bonding structures that harden to form the final material. Thermoset plastics, which have a three-dimensional network structure, do not liquefy when heated or subjected to pressure. Therefore, once cured, it is not possible for the polymer to return to its original state through cooling or reheating. These properties make thermoset plastics ideal for specific applications, though they are not suitable for recycling (Bartholomew & Farrauto, 2011). Polymer matrix composites have certain limitations, one of

which is their potential inability to maintain stability and strength at high temperatures. Due to the rigid and brittle internal structure of thermosets, they exhibit lower flexibility compared to other types of plastics. This rigid internal structure makes shaping challenging, as the bonds between molecules are quite strong. The presence of cross-links makes thermosets harder and more resistant to deformation, with the material stiffening as it is heated, though degradation may occur at higher temperatures. Various types of resins such as epoxy, polyester, vinyl ester, and phenolic are commonly used in the production of composites (Askeland, 1998). As a result, thermoset composites are utilized across a range of industries, including marine vessels, construction materials, automotive parts, and interior furniture.

TRADITIONAL MATERIAL PRODUCTION METHODS

There are various methods to produce polymer matrix composites, with different fundamental techniques employed depending on the type of material, its intended use, and the desired properties. Among these production methods, there are ten primary techniques, which are listed below. However, aside from these, other techniques are also continuously being developed. These methods include lay-up, spray-up, filament mold winding, injection molding, resin transfer molding, profile drawing/pultrusion, preforming, vacuum bagging, and autoclaving.

The hand lay-up method is one of the most used techniques, where reinforcement fibers are impregnated with matrix resin and manually placed into a mold. The material is then compressed to remove air bubbles. This technique is a widely used manufacturing method in the production of aerospace components.

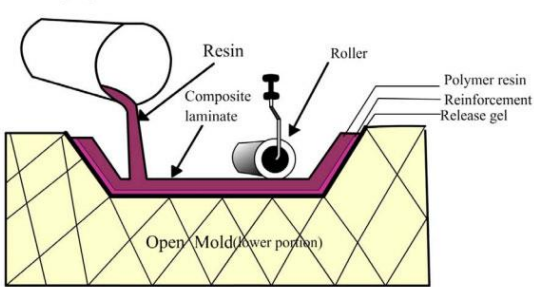

Figure 2: Composite manufacturing with hand lay-up method (https://www.eppcomposites.com)

In the spray-up method, like the hand lay-up technique, chopped fibers and curing resins are deposited onto an open mold using a spray gun. Following this process, a manual rolling technique is applied to remove trapped air. This method, compared to hand lay-up, is used for more complex

molds and offers the advantage of faster production. However, the method has some drawbacks: it is limited to the production of round-shaped parts, involves high mold costs, and can leave surfaces that may weaken the aerodynamic properties in certain applications. A spray-up method is shown in Figure 3.

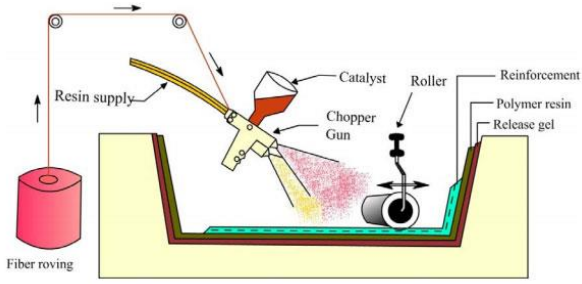

Figure 3: Composite manufacturing with spray-up method (https://www.eppcomposites.com)

In filament winding method, continuous reinforcing fibers are wound around a mandrel in layers. During the winding process, the matrix resin is applied, and the material is subsequently compressed. This technique is commonly used for the production of cylindrical or symmetrical components (Tasyurek & Tarakcioglu, 2015). It is particularly suited for the manufacturing of structures requiring high structural integrity, such as tanks and pipes. One or more resin-impregnated fibers are wound around the mandrel in a predetermined geometric pattern, resulting in strong, lightweight, and moisture- and corrosion-resistant structures (Taşyürek & Tarakçioğlu, 2017).

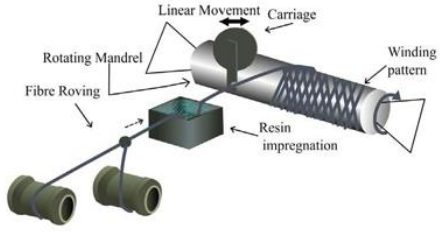

Figure 4: Visual picture of the filament winding method (https://www.suvarnafrpproducts.com)

In the injection molding process, it is possible to inject short fibers mixed with resin into molds, similar to the injection of plastic into molds. Short fiber composites are used, and the material is fed into heated molds in the form of rolls or bulk. This method is suitable for producing small, thick

specimens. The components are first directed to the main injection chamber and then injected into the mold. This approach is crucial in composite manufacturing to ensure the preservation of mechanical properties.

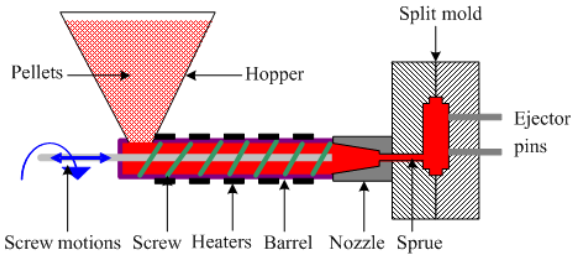

Figure5: Injection molding method (https://www.substech.com)

Another material forming process is the extrusion method, which is widely used, particularly in the plastics and metals industries. Common products manufactured by extrusion include plastic pipes and pipe profiles, aluminum profiles, plastic bottles, automotive parts, and electronic housings and components.

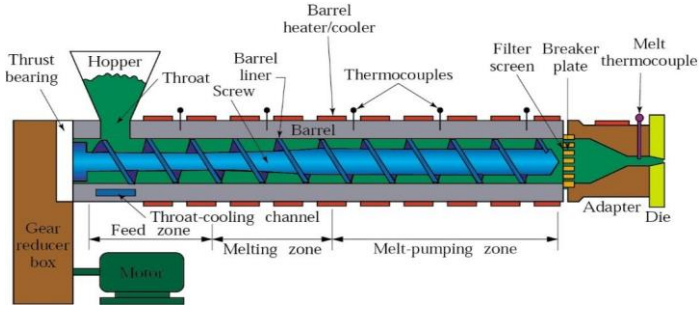

Figure 6: Extrusion molding schematic representation (https://polymeracademy.com)

In the RTM (Resin Transfer Molding) method, molten matrix resin is injected onto the reinforcement fibers using an injection molding machine. The molding process is ideal for producing high-volume and complex-shaped parts. This molding technique is used when high surface finish quality is required on both sides of the composite material. It is applicable to products of both large and small sizes. The advantages of this method include high dimensional tolerance and stability, superior surface quality, high production rates, excellent repeatability, and the lowest variability relative to the part.

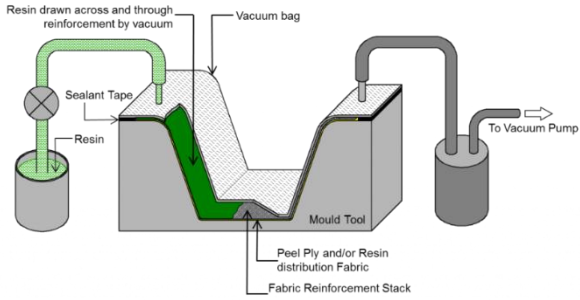

Figure 7: Resin transfer molding method (https://www.nal.res.in)

In the pultrusion process, reinforcement fibers and the matrix are combined to shape the composite material. This method is generally preferred for continuous glass fiber reinforcement. The fibers are impregnated with a resin that is cured by heat, using a roller or spool system. In the subsequent step, the impregnated fibers pass through a heated mold, where the resin is cross-linked, and a sufficiently strong composite material is drawn from the mold. This process allows the creation of highly complex solid or hollow profiles. A symbolic representation of the pultrusion method is shown in Figure 8.

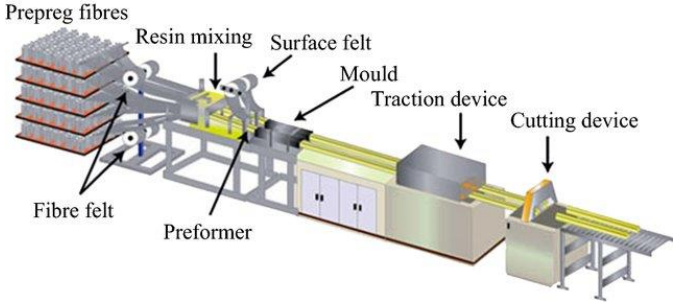

Figure 8: Symbolic application image of the pultrusion method (Zhang, Wang, Pei, & Zhou, 2020)

In compression molding methods (SMC, BMC), reinforcement and matrix resin are placed into a mold and shaped by applying compression force. The process can be carried out using either hot or cold pressing. In the SMC (Sheet Molding Composites) method, the reinforcement material, typically chopped fibers, is combined with resin to form a sheet-like material, usually 1 meter wide and 3 mm thick. In the BMC (Bulk Molding Composites) method, chopped fibers and resin are pre-mixed to form a dough-like material. Ready-to-mold compositions offer numerous advantages, including extensive design flexibility, smooth surface finishes, paintability, the ability to coat surfaces within the mold, recyclability, and the option to use recycled material

during preparation. Additionally, they allow easy assembly with the incorporation of metal inserts, offer high flame resistance, temperature durability, and resistance to brittleness in cold environments.

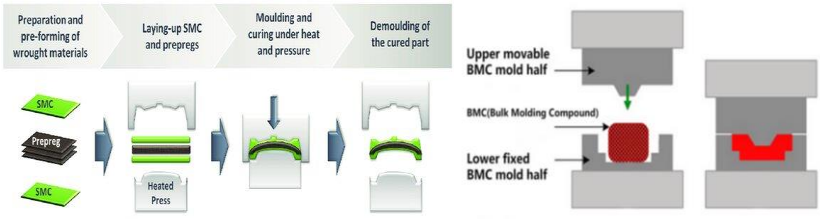

Figure 9: Composite prepreg manufacturing with compression molding (SMC and BMC methods) (https://www.zjmdc.com; Wulfsberg et al., 2014)

The Vacuum bagging method is based on compressing laminated parts under pressure using atmospheric pressure until the curing process is complete. With the development of resins that can cure at room temperature, this method can be utilized in a standard composite production workshop for both manufacturing and educational purposes. In this technique, composite products can be made from a combination of various fibers, resins, foams, and honeycombs.

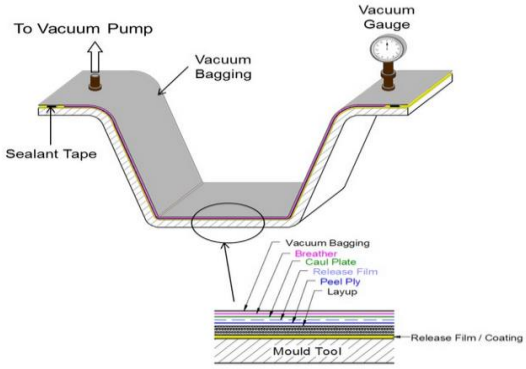

Figure 10: Schematic representation of vacuum bagging method (https://www.nal.res.in)

In addition to thermoset-based matrices, thermoplastic-based matrix materials are also used. One such method is the pressable reinforced thermoplastic technique. This composite material typically involves reinforcing fibers, such as glass, carbon, or aramid, being placed into a thermoplastic matrix, which is then consolidated under heat and pressure. The thermoplastic matrix is usually polymeric in nature, softens under heat, can be shaped, and solidifies upon cooling. In this process, the reinforcement fiber

tapes are pre-placed onto a predefined mold and then combined with the matrix resin.

Autoclave bonding is a method with limited application due to its high production costs and excessive residual stresses. The system essentially involves a pressure vessel that regulates parameters such as pressure, temperature, and vacuum, which are required for composite production. Compared to other methods, it is more expensive and time-consuming, but it produces excellent composites for specific purposes. The process is facilitated at high pressure and temperature to achieve a high fiber volume fraction to ensuring maximum structural efficiency. Curing pressures typically range from 3 to 12 MPa.

Due to its disadvantages, an alternative method known as out-of-autoclave (OOA) production processes has been researched and developed. This research focuses on optimizing the vacuum bagging (VBO) preforming process to enhance the production of composite laminates with high tensile strength. Out-of-autoclave (OOA) manufacturing techniques for composites result in lower fiber volume fractions compared to fully compacted laminates. The lower fiber volume fraction leads to higher resin volume fractions, which become resin-rich volumes (RRV). The key components of the autoclave molding process are shown in Figure 11.

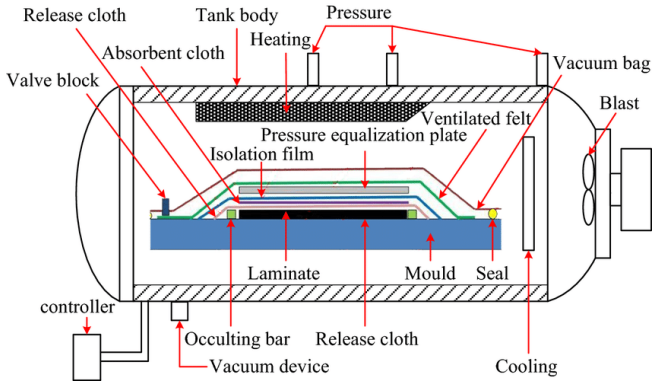

Figure 11: Representation of autoclave process and its basic components (Zhang et al., 2020)

AVIATION MATERIALS IN AIRCRAFT: EPOXY-HONEYCOMB-FIBER COMPOSITES

Materials are generally classified into metallic and non-metallic categories. Metallic materials are further divided into ferrous and non-ferrous types, while non-metallic materials are classified as organic and inorganic.

In the early years of aviation, aircraft materials were predominantly selected from wood. After successful flight trials, the need to increase flight altitude, extend flight range, reduce periodic maintenance and costs, and enhance material lifespan led to a shift towards the increased use of metallic materials. Specifically, low-density metals such as aluminum were preferred due to their weight advantages. Mechanical strength and thermal properties, among other factors, required the alloying of the base metal with specific proportions of other metals.

When selecting materials for an aircraft, several key criteria must be considered. These include cost-effectiveness, ease of procurement from the market, suitability for manufacturing processes in terms of formability, resistance to corrosion, physical, mechanical, and thermal properties within the desired range, and compatibility with the operating conditions of the vehicle. Given these considerations, not every material found in nature, nor every desired material, can be randomly used in the construction of air vehicles.

Non-ferrous materials used in aircraft construction include lead, gold, platinum, copper, aluminum, chromium, nickel, silver, tungsten, tin, manganese, magnesium, cobalt, and vanadium. Among non-metallic materials, synthetic materials are most used from both organic and inorganic categories. These include fibers, resins, synthetic leather, graphite, ceramics, glass, and ceramics. Among metals, iron ore is not used in its natural form in aircraft. Alloys, which are produced by mixing certain materials in specific proportions and may contain up to 1.7% carbon, are referred to as steel. These steels are classified into three categories based on their carbon content: low-carbon, medium-carbon, and high-carbon steels. Each type is used for the manufacturing of various aircraft components, engine materials, or auxiliary parts. Although steel has a weight disadvantage compared to traditional aluminum, it is preferred for use in main structural components. Steel alloys are also used in parts such as bearings, structural aircraft components, nuts, bolts, gears, springs, valves, manifolds, pipes, valves, turbine blades, combustion chambers, and exhaust outlet liners. The production of these alloy steels requires thermal treatments such as annealing, normalization, tempering, and hardening to ensure suitability for their intended applications.

In the exterior and interior materials of the fuselage and wings, composite-based materials are increasingly being used. Composites are created by combining matrix materials with reinforcing materials. These materials continue to attract the attention of many aircraft manufacturers due to their advantages, particularly weight reduction, corrosion resistance, high fatigue resistance, the wide range of customizable options, and the availability of variable system alternatives. Matrix production is carried out in industries using ceramic, metal, and plastic materials. However, plastic matrices are the most suitable for the aforementioned advantages.

Plastics have two main categories: thermosets and thermoplastics. Common thermoplastic matrices used in engineering applications include polyethylene, polypropylene, polyamide, polyethylene terephthalate, polyvinyl chloride, polyoxymethylene, acrylonitrile butadiene styrene, and polyether ether ketone. Epoxy, polyester, bismaleimides, cyanate esters, phenolic, polyimides, polyurethane, and vinyl ester matrices are among the most widely used thermoset-based plastic matrices.

Due to well-established processing and application histories, thermosets generally offer better economics, superior high-temperature properties, excellent wetting and adhesion to reinforcement materials, and higher mechanical strength, making them more favorable for use in aircraft compared to thermoplastics. Among the thermoset matrices most encountered in studies on aircraft materials are epoxy resins.

Epoxies are the most widely used matrix materials in high-performance composites and adhesives due to their exceptional strength, strong adhesion, low shrinkage, and adaptable processing characteristics. The most common epoxy type is diglycidyl ether of bisphenol A (DGEBA), frequently employed in applications such as filament winding, pultrusion, and certain adhesives. Another widely used epoxy is tetraglycidyl-4,4'-diaminodiphenylmethane (TGGDM), also known as tetraglycidylmethylenedianiline (TGMDA), which forms the backbone of many commercial composite systems (Di Pasquale et al., 1997).

Epoxy resin curing depends on the opening of the oxirane ring, enabling crosslinking with curing agents. This crosslinking occurs through epoxy groups or the hydroxyl groups formed during the reaction. The three-membered epoxy ring is often present as a glycidyl ether, glycidyl amine, or as part of an aliphatic ring, with glycidyl ethers and amines being the most common for composites. Typical curing agents include aliphatic and aromatic amines, catalytic agents, and anhydrides (Carpenter, 1977).

MICROWAVE RAPID CURING METHOD

Microwave

Microwaves occupy a section of the electromagnetic spectrum with wavelengths ranging from one millimeter to one meter. This frequency range (300 Mhz-300 Ghz) includes those used for applications like cellular communication, radar systems, and satellite television. The most common frequencies for microwave heating are 0.910 GHz and 2.40 GHz. Additionally, new microwave capable of operating at frequencies from 0.9 GHz to 18 GHz, expanding their use in material processing (RJ Lauf, 1993).

Electromagnetic Theory of Microwave

Microwave furnaces are made up of three primary components: the source, the transmission lines, and the applicator. The microwave source generates electromagnetic waves, which are then transmitted through transmission lines to the applicator. Inside the applicator, the material either absorbs or reflects the incoming energy. Common types of vacuum tubes used in microwave heating include magnetrons, traveling wave tubes, and klystrons (Kitagawa, 1986).

Magnetrons, which are the primary component in household microwave ovens, are well regarded for their efficiency and reliability. Due to mass production, magnetrons are the most cost-effective microwave source available. They generate electromagnetic waves using resonant structures, which means they can only produce a fixed frequency. In contrast, traveling wave tubes (TWTs) are used in variable frequency microwave systems. TWTs are designed to amplify a wide range of microwave frequencies within a single tube, making them versatile for applications requiring variable frequency generation.

Magnetrons

The vacuum tubes and the anode is kept at a higher voltage than the cathode, creating a strong electric field. This magnetic field exerts a force on the electrons as they move towards the anode, causing them to spiral in a circular path. When the electrons pass near the resonant cavities, they induce oscillations in the electron cloud. The frequency of these oscillations is determined by the size of the resonant cavities. The first method is duty cycle modulation, where the magnetron operates at full power but the current is turned on and off at regular intervals (Gerling, 1987). This on/off switching reduces the average power output over time and is commonly used in household microwave ovens to adjust cooking power. The second method involves continuously adjusting the power output by changing the cathode current or altering the strength of the magnetic field. By increasing or decreasing the current amplitude or the magnetic field intensity, the microwave power output can be varied. This method allows for finer control of the microwave energy, making it suitable for applications that require a steady and precise power level.

Microwave Processing Systems and the Applicators

The applicator is a key factor in effective microwave heating, as it is responsible for transferring microwave energy to the target material. The temperature distribution within the material is closely related to the electric field pattern formed inside the applicator. Common types of microwave systems include waveguides, applicators, and such as cavities (Şen & Aydin, 2020). Resonant applicators like single-mode and multi-mode cavities are

often preferred in material processing because they produce high-intensity electric fields. The selection of an application type in a microwave system is based on the specific characteristics of the material being treated. Research and commercial applications typically use single-mode, dual or variable frequency systems, as these options offer flexibility and efficiency in microwave material processing.

Microwave Energy-Material Interaction

Electromagnetic fields transfer energy to materials at the molecular level, where the material's dielectric properties determine its behavior in response to the field. Understanding the interaction between microwaves and materials is key to efficient microwave processing. When microwaves interact with molecular dipoles, they induce rotation, and heat is produced as energy is lost due to internal resistance to this motion. The next section will explore the basic principles of microwave-material interactions, the process of power absorption, and methods for evaluating dielectric properties. To enhance comprehension, simplified models and analogies will also be provided to illustrate the physics behind material responses to microwaves.

Microwave Energy Conversion

When electromagnetic fields interact with a material's dielectric properties, electromagnetic energy is converted into heat. The power transferred to a material can be determined using the Poynting Vector Theorem (Collin, 2007), derived from Maxwell's equations. As microwaves are absorbed, the electric field intensity decreases progressively with depth beneath the surface. This attenuation, along with the material's penetration depth, is critical when heating thick materials. If the penetration depth is significantly smaller than the material's thickness, surface heating dominates, and the interior is heated primarily through conduction.

Metals and other materials with high electrical conductivity and low capacitance have a high dielectric loss factor. As this factor increases, penetration diminishes, causing these materials to behave as reflectors. Conversely, materials with low dielectric loss factors allow microwaves to pass through with minimal absorption, making them nearly transparent to microwaves. Optimal microwave absorption occurs in materials with moderate dielectric loss factors, which balance energy absorption and penetration. This behavior contrasts with conventional heating, which is most effective in highly conductive materials. The energy dissipation in dielectric materials resembles the phase shift of electrical current in circuits, illustrating the connection between microwave interactions and electrical phenomena.

Material Behavior

Polymers and their composites face similar processing challenges to ceramics, largely due to their low thermal conductivity. Consequently, microwave processing of polymers and composites has become a focus of extensive research. A key limitation in utilizing thermosetting composites for various applications is the prolonged curing and post-curing times required to achieve optimal mechanical properties. Studies have demonstrated that microwave processing can significantly shorten these times while also improving the materials' mechanical properties, like its effects on ceramics. The differing chemical compositions and dielectric properties of thermosetting and thermoplastic polymers necessitate tailored processing approaches for each type. Additionally, the heterogeneous microstructure of fiber-reinforced composites complicates microwave interaction and further challenges processing methods.

The effectiveness of microwave processing for polymeric materials depends on factors such as dipole orientation, operating frequency, temperature, and the presence of additives or fillers. When microwaves interact with polymer composites, the material with the higher dielectric loss absorbs more energy. In composites with low-conductivity fibers, such as glass or aramid fibers, the polymer matrix primarily governs the composite's dielectric loss. In contrast, for carbon fiber composites, the dielectric loss is predominantly determined by the carbon fibers themselves. Furthermore, due to the anisotropic nature of composites' dielectric properties, the material's structural arrangement plays a critical role in determining microwave penetration depth.

The microwave energy interaction with fiber-reinforced composites was first examined by Lee and Springer, (Lee and Springer 1984a, 1984b). They developed a model that considers electromagnetic field properties, the dielectric characteristics of individual components, and the ply lay-up geometry to predict reflectance, transmission, and absorbed power in composites. Because the dielectric properties of each composite layer vary directionally, interfaces between layers with different orientations create discontinuities in dielectric behavior. These discontinuities result in internal reflections, leading to a complex distribution of electromagnetic fields within the composite material.

Polymer Microwave Processing

Early studies on microwave processing on polymers and composites revealed a significant reduction in curing times. Since those pioneering experiments on microwave curing, extensive research has aimed to understand how microwaves affect the chemical and physical properties of polymers. The most frequently reported impacts of microwaves is the acceleration of curing

reactions in thermosetting resins. However, the existence of this so-called "microwave effect" remains a topic of debate, with inconsistent findings across the literature. In many cases, microwave heating has been shown to increase reaction rates, reducing the time required for gelation and vitrification. The extent of this acceleration depends on factors such as the polymer's molecular structure and the type of curing agent used.

Microwaves can influence the molecular structure of polymers, potentially altering the mechanical properties of the final material. Some studies have focused on leveraging microwaves to induce chemical reactions that are otherwise difficult to achieve using conventional heating methods. This is often accomplished by introducing microwave-absorbing functional groups into the polymer chains, which enhances the heating rate and accelerates reaction kinetics. Other research has explored how microwaves can impact the morphological structure of polymers, for instance, by controlling phase separation in polymer blends to customize the physical properties of the resulting material.

When comparing the mechanical properties of epoxy resins cured using microwave and thermal methods, it was found that microwave-cured samples exhibited lower tensile strength than thermally cured ones when the degree of cure was below 80%. However, as curing progressed, the tensile strength of microwave-cured samples increased, eventually surpassing that of thermally cured specimens at 100% cure. To reduced strength at lower cure levels could be due to insufficient molecular entanglement in the polymer network, caused by the alignment of polymer chains under the influence of the electric field. This alignment, while potentially limiting strength at partial cure levels, may improve molecular packing and reduce free volume, ultimately increasing stiffness and leading to a higher modulus.

Polymer Composites

The study of microwave curing in polymers is largely motivated by its potential to enhance the processing of polymeric composites. Processing thermoset composite laminates, especially thick ones, presents well-known challenges. In conventional thermal curing, heat must be applied gradually to ensure it penetrates the material's full thickness. Additionally, exothermic reactions within the composite generate internal heat that dissipates slowly, creating uneven temperature distributions. These issues can lead to inconsistent curing, localized solidification, thermal degradation, and stress-induced defects during processing. Microwave heating, with its ability to provide uniform, volumetric energy transfer, offers a promising solution to these problems.

While microwaves are highly effective for curing glass fiber composites, they face challenges with thick unidirectional carbon fiber composites due to the high dielectric loss of carbon fibers. In angle-ply laminates, the strong reflectance from the outer layers can hinder efficient heating of the interior, complicating the processing of thicker laminates. Additionally, the high conductivity of carbon fibers can result in hot spots and electrical arcing. In such cases, lower-frequency radio waves are often better suited for heating carbon fiber composites. However, recent advancements have shown that single-mode microwave cavities can successfully cure thick carbon fiber/epoxy laminates.

Microwaves preferentially interact with carbon fibers, causing them to heat, which in turn transfers heat to the surrounding resin via conduction. This improves the bonding between the fibers and the matrix, enhancing the composite's mechanical properties. Although there are limitations to microwave processing for carbon fiber composites in certain scenarios, it remains a highly effective method for glass and organic fiber composites.

A key advantage of microwave processing is its ability to reduce thermal gradients and processing times by depositing energy directly and uniformly throughout the material. Microwave heating's rapid and targeted nature enables precise control over temperature distribution, minimizing internal temperature overshoot. Furthermore, volumetric heating eliminates the thermal lag typically encountered during the ramp-up phase of traditional curing methods, resulting in more efficient, uniform, and faster curing.

CONCLUSION

Microwave curing provides notable benefits for processing polymers and composites, particularly by significantly reducing curing times and improving the properties of materials. The use of microwave energy enables uniform and volumetric heating, effectively addressing challenges like uneven temperature distribution and extended curing durations that are common in conventional thermal methods. This is especially advantageous for thick composite laminates, where slow heat diffusion and heat generated by exothermic reactions often complicate the curing process.

Although microwave heating is highly effective for materials such as glass fiber composites, processing carbon fiber composites poses distinct challenges due to the high dielectric loss of carbon fibers. However, recent innovations, including the development of single-mode microwave cavities, have demonstrated success in overcoming these limitations, enabling efficient curing of thick carbon fiber/epoxy composites.

Microwave curing can also impact the molecular structure of polymers, accelerating chemical reactions and modifying the morphology of polymer blends. While further studies are needed to fully unravel the complex interactions between microwaves and various materials, the ability to precisely control curing times, temperature distributions, and material characteristics highlight the potential of microwave technology in composite manufacturing.

As advancements in microwave processing continue and its application in industrial settings expands, this technology is poised to transform the manufacturing of polymer composites. By offering faster, more efficient, and cost-effective processing solutions, microwave curing is set to become an invaluable tool across a wide range of industries.

REFERENCES

Alınca, E. (2024). *Development of Production of Production of Thermoset Matrix Aircraft Body Material Using Temperature Controlled Rapid Curing Methods.* (Master). Selçuk University,

Askeland, D. (1998). Malzeme bilimi ve mühendislik malzemeleri,(Çev. M. Erdoğan), Cilt 2, Nobel Yayın Dağıtım Ltd. *Şti., Ankara*.

Bachmann, J., Yi, X., Gong, H., Martinez, X., Bugeda, G., Oller, S., . . . Moreira, P. (2018). Outlook on ecologically improved composites for aviation interior and secondary structures, CEAS Aeronaut. *J*, *9*(3), 533-543.

Bartholomew, C. H., & Farrauto, R. J. (2011). *Fundamentals of industrial catalytic processes*: John Wiley & Sons.

Carpenter, J. (1977). *Assessment of composite starting materials-Physiochemical quality control of prepregs.* Paper presented at the Dynamics Specialists Conference.

Collin, R. E. (2007). *Foundations for microwave engineering*: John Wiley & Sons.

Deng, Y., Yu, H., & Zhang, Y. (2024). Response of the orthogonal corrugated sandwich panel under low-velocity impact with different shaped impactors. *Thin-Walled Structures*, 112070.

Di Pasquale, G., Motto, O., Rocca, A., Carter, J., McGrail, P., & Acierno, D. (1997). New high-performance thermoplastic toughened epoxy thermosets. *Polymer*, *38*(17), 4345-4348.

Elaldı, F. (2024). Low Velocity Bird-Like Impact Behavior on Honeycomb Composite Structure. *Politeknik Dergisi*, 1-1.

Gerling, J. E. (1987). Microwave oven power: a technical review. *Journal of microwave power and electromagnetic energy*, *22*(4), 199-207.

Grant, R. G. (2003). Flight – 100 years of aviation. *Aircraft Engineering and Aerospace Technology*, *75*(2). doi:https://doi.org/10.1108/aeat.2003.12775bae.002

http://web.archive.org. A study of the environmental impact of composites. Retrieved from http://web.archive.org/web/20060923103650/http://www.plastkemiforetagen.se/Publikationer/PDF/

http://www.aviation-history.com. Retrieved from http://www.aviation-history.com/theory/composite.htm

http://www.ifi.uio.no/siag. Surface Modelling for Composite Materials. Retrieved from http://www.ifi.uio.no/siag/problems/grandine/

https://polymeracademy.com. Retrieved from https://polymeracademy.com/plastic-extrusion-process

https://www.eppcomposites.com. Retrieved from https://www.eppcomposites.com

https://www.nal.res.in. Retrieved from https://www.nal.res.in/en/techniques

https://www.sampe.org/boeings-787. Retrieved from https://www.sampe.org/boeings-787/

https://www.substech.com. Retrieved from https://www.substech.com/dokuwiki/doku.php?id=injection_molding_of_polymers

https://www.suvarnafrpproducts.com. Retrieved from https://www.suvarnafrpproducts.com/index.php/category-blog/filament-winding.html
https://www.target.com/p/composite-materials. Retrieved from https://www.target.com/p/composite-materials-for-aircraft-structures-by-tyron-hoppe-hardcover/-/A-89799414
https://www.zjmdc.com. Retrieved from https://www.zjmdc.com/IndustryNews/What-is-BMC-compression-moulding.html
Kitagawa, K., Yoji, K., Tomokatsu, O. and Akikazu, H. (1986). The reliability of magnetrons for microwave ovens. *Journal of microwave power and electromagnetic energy, 21*(3), 149-158.
Kocaoğlu, i. (2021). *Composite Materials Sector and Turkey's Situation*.
Lee, W. I., & Springer, G. S. (1984a). Interaction of electromagnetic radiation with organic matrix composites. *Journal of Composite Materials, 18*(4), 357-386.
Lee, W. I., & Springer, G. S. (1984b). Microwave curing of composites. *Journal of Composite Materials, 18*(4), 387-409.
Mohammed, A. G. (2014). Experimental and numerical approach to study the mechanical behavior of the filament wound composite leaf spring. *Graduate institute of Science and Engineering*.
RJ Lauf, D. B., AC Johnson, CA Everleigh. (1993). 2 to 18 GHz Broad-Band Microwave-Heating Systems. *Microwave journal*.
Şen, S., & Aydin, F. (2020). Experimental investigation of drying kinetics of apple with hot air, microwave and ultrasonic power. *Sadhana, 45*, 1-10.
Tamboli, S., Joshi, A., Pandey, A. K., Bongale, A., & Kumar, S. (2020). *Low velocity impact behavior of composite structures for aerospace applications.* Paper presented at the AIP Conference Proceedings.
Tasyurek, M., & Tarakcioglu, N. (2015). Damage behavior of filament winding pipes modified with carbon nanotubes under internal pressure.
Taşyürek, M., & Kara, M. (2021). Low-velocity impact response of pre-stressed glass fiber/nanotube filled epoxy composite tubes. *Journal of Composite Materials, 55*(7), 915-926.
Taşyürek, M., & Tarakçioğlu, N. (2017). Enhancing fatigue life of filament winding laminar and curved pipes containing carbon nanotubes, and their fatigue failure. *Polymers and Polymer Composites, 25*(2), 167-176.
Ulaş, A. Ö. (2020). Use of Composite Materials in Aerospace Structures. Retrieved from https://medium.com/@omerulas2339/hava-uzay-yap%C4%B1lar%C4%B1nda-kompozit-malzeme-kullan%C4%B1m%C4%B1-fade5cbd7b64
Wulfsberg, J., Herrmann, A., Ziegmann, G., Lonsdorfer, G., Stöß, N., & Fette, M. (2014). Combination of carbon fibre sheet moulding compound and prepreg compression moulding in aerospace industry. *Procedia Engineering, 81*, 1601-1607.
Zhang, L., Wang, X., Pei, J., & Zhou, Y. (2020). Review of automated fibre placement and its prospects for advanced composites. *Journal of Materials Science, 55*(17), 7121-7155.

The Speed Control of the Brushless Motor and its Analysis by Using Coupling Between Maxwell Ansys and MATLAB Simulink Programs

Tural MEHMETOĞLU[1]
Zafer DOĞAN[2]

1- Amasya University, Taşova Vocational School, Amasya, turalmehmetoglu@yahoo.co.uk ORCID ID: 0000-0001-8909-0222
2- Faculty of Engineering and Architecture, Department of Electrical and Electronics Engineering, Tokat Gaziosmanpaşa University, Tokat, zafer.dogan@gop.edu.tr ORCID ID: 0000-0002-7953-0578

ABSTRACT

The theoretical and experimental approximations have played an important role in the design and analysis of electric motors. In this work, we present a design and analysis of a brushless direct current (BLDC) motor by using the coupling between the ANSYS-Maxwell and MATLAB software, which ensures the appearance of the best new conventional motor types. On the basis of the ANSYS Maxwell program software, we present an adequate BLDC motor geometry. The BLDC motor performance parameters calculations such as motor efficiency, torque constant, electromagnetic torque, back EMF constant, output power, phase resistance, motor speed and flux density are performed, which these quantities are powerful assessments for the optimal designs. The comparison of existing results verified that the proposed motor design is feasible and reliable for industrial applications.

Keywords: Simulation Analysis, Brushless Direct Current Motor, Matlab/Simulink Program, ANSYS-Maxwell Program, Maxwell-Simplorer-Simulink Cosimulation.

INTRODUCTION

It is well known electric motors with advanced power electronic drivers are prime importance in many contemporary industrial technology areas, especially such as engineering, construction and manufacturing are used [1-3]. Based on the knowledge of the design and analysis for the various types of electric motors, it is possible to conclude that the theoretical analytical approximations is significant, given that the highest percentage efficiency [3-5]. Electric motors come in a variety of types, including DC, AC, permanent magnet and switching reluctance motors, each with technical applications suitable for the power output. Over the past decade, interest in the brushless DC motor has grown due to advances in most industrial applications, including automotive, computing, aerospace, military, robotics, medical electronics and domestic appliances [1-9]. The brushless motor uses a permanent magnet as the rotor, three-phase drive coils, and a specialized sensor that monitors the position of the rotor [10-13]. The brushless DC (BLDC) motors have more advantages than traditional brushed DC motors, such as higher power density, lower maintenance costs, high output torque, large speed control range and less frequent maintenance requirements [14-22]. The main advantage the BLDC motor is that there is no physical contact between the rotor and the stator. Energy is transferred from one to another through a magnetic field between electromagnets. As with all other apparatuses, BLDC motors also have several disadvantages compared to other motors. When the brushless DC motor is running at low speed, there will be small vibrations during rotation at low speed, but the vibrations will be

reduced at high speed [25-30]. As it is known, one of the important issues in motor technology is the appropriate design and analysis of motors before starting manufacture [31-38].

Many approaches have been suggested for the efficient design and analysis of electric motors under various theoretical assumptions like ANSYS/ Maxwell, Matlab / Simulink program, MagNet, JMAG, and Speed, etc tools [39-46, 52, 53]. Yaz et. al. [51] have presented BLDC motor design with a supply voltage 72 volts, a number of slots is 45, and a number of poles 50. Kelek et. al. [37] studied the outer rotor BLDC motor using new mathematical modeling with Maxwell and Matlab/Simulink programs software. An efficient model for the BLDC motor with trapezoidal and sinusoidal waveforms of the motor's back-EMF was presented by Tibor et al. in the paper [32] and was assessed using the MATLAB/Simulink software. Markovic et al [35] used the Matlab software algorithm with seven free variables to study the design optimization of the behavior of slotless BLDC motors. The ANSYS/RMxprt model tools were used to study the complete analysis of the switching reluctance motor model [47]. Abirami et al [48], the torque was measured using different harmonics. For varying rotor speeds and load torques, the three-phase inverter efficiency of BLDC motors has been the subject of both theoretical and practical investigations [49]. Characteristic analyses for stepper motors, BLDC, PMSM and brushed DC have been published in this work [50]. In conclusion, current research has shown that theoretical methods for the analysis and design of electric motors are crucial to the advancement of industrial technologies.

In this paper, we propose a design and analysis method for the BLDC outer rotor type motor using ANSYS- Maxwell environment. The design and simulation results for magnetic flux density, torque, speed, magnetic field strength, flux linkages, flux lines along with inductance, current density, current, and the induced voltage are evaluated by the combination of ANSYS-Maxwell, and MATLAB software. As seen from the simulation, we can conclude that our BLDC motor design is adequate for industrial manufacturers.

THEORETICAL DESIGN OF BRUSHLESS DC ELECTRIC MOTOR BASED ON ANSYS MAXWELL SOFTWARE

ANSYS Maxwell software is based on Maxwell's fundamental equations and uses the Finite Element Method (FEM) for determinations, which allows the evaluation of electromagnetic and electric fields of electric machines, as well as transient processes in field problems [45, 46]. Maxwell equations are used to calculate electromagnetic fields. In these equations, the expression of the current density $\vec{J}$ with the electric field $\vec{E}$ is given in Eq. (1) as:

$$\vec{J} = \sigma\vec{E} \quad (1)$$

Based on this expression, the induced electric field expression is as in Eq. (2):

$$\vec{\nabla}x\vec{E} = -\vec{\nabla}x\vec{A} \quad (2)$$

The electric field is defined in Eq. (3) depending on the gradient of the voltage value ($\vec{\nabla}V$) in the region outside the conducting material:

$$\vec{E} = -(\vec{A}x\vec{\nabla}V) \quad (3)$$

By rearranging this expression according to Eq. (1), the current density can be obtained by the expression in Eq. (4) as:

$$\vec{J} = -\sigma\vec{A} - \sigma\vec{\nabla}V \quad (4)$$

The current density can be defined by the following expression using all these equations:

$$\vec{\nabla}x\left(\frac{1}{\mu(B)}\vec{\nabla}x\vec{A}\right) = -\sigma\vec{A} - \sigma\vec{\nabla}V + \vec{J}_{kaynak} \quad (5)$$

where μ is the magnetic permeability of the medium.

A design model is presented for computing the rotor speed, motor phase currents, back electromotive force (back EMF) and motor torque of the inner rotor BLDC motor by using ANSYS Maxwell software. Using the ANSYS RMxprt and Maxwell2D software the three-phase BLDC machine geometry is created as shown in Figures 1 and 2.

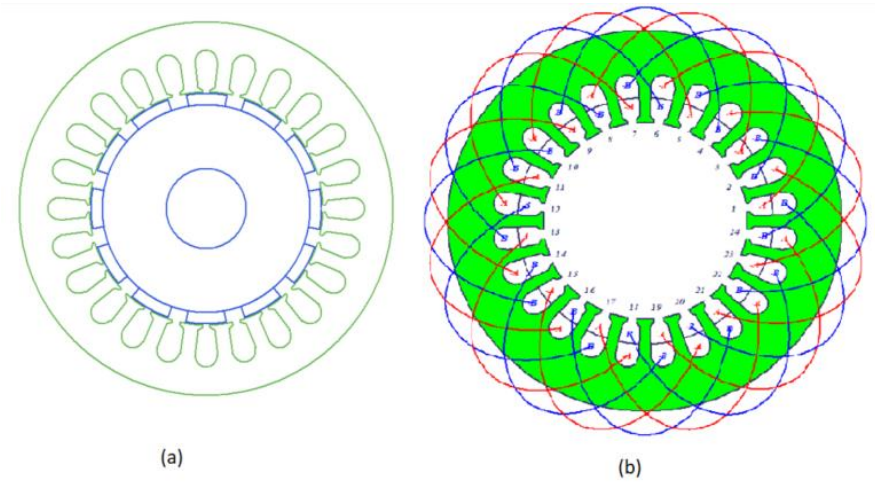

Figure 1. The inter rotor BLDC motor RMxprt structure: (a) Basic structure, (b) Winding structure.

The FEM analyses are complex evaluation. These evaluations take long time on the computer. This problem can cause significant time losses in electrical machine design. In order to solve this problem, instead of full models of electrical machines, the smallest instantiable models are used in ANSYS Maxwell. The 1/4 model of the BLDC motor designed in this study is shown in Fig. 2.

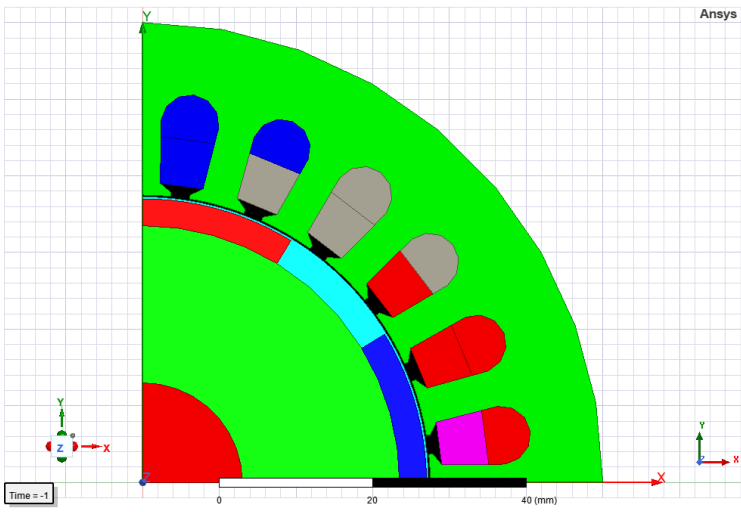

Figure 2. The inter rotor BLDC motor Maxwell 2D structure

By using Maxwell RMxprt, the inner BLDC motor's circuit, stator, stator slot, stator winding, rotor, rotor pole and BLDC specification parameters are given in Tables 1- 8.

Table 2. Machine parameters values

Name	Value	Unit	Evaluated
Machine Type	Brushless DC Motor		
Number of Poles	12		
Rotor Position	İnner Rotor		
Frictional Loss	6	W	2W
Windage Loss	8	W	3W
Reference Speed	3500	rpm	
Control Type	DC		
Circuit Type	Y3		

Table 3. Circuit parameters values

Name	Value	Unit	Evaluated
Lead Angle of Trigger	0	deg	0 deg
Trigger Pulse Width	120	deg	120 deg
Transistor Drop	0	V	
Diode Drop	0	V	

Table 4. Stator parameters values

Name	Value	Unit	Evaluated
Outer Diameter	140	mm	97 mm
Inner Diameter	80	mm	64 mm
Length	45	mm	15 mm
Stacking Factor	0.95		
Steel Type	Steel_1008		
Number of Slots	15		
Slot Type	3		
Skew Width	0		0

Table 5. Rotor parameters values

Name	Value	Unit	Evaluated
Outer Diameter	67	mm	62 mm
Inner Diameter	40	mm	34 mm
Length	25	mm	15 mm
Stacking Factor	0.95		
Steel Type	Steel_1008		
Pole Type	1		
Skew Width	0		0

Table 6. BLDC specification parameters

Name	Value	Unit	Evaluated
Operation	Motor	m	140 mm
Load Type	Const Power		
Rated voltage	45	V	45 V
Rated output power	150	W	150 W
Rated Speed	3500	rpm	3500 rpm
Operating temperature	70	cel	70 cel

Note that, the RMxprt allows rapid execution of basic motor design and performance assessment, decreases in the motor's design time, and converts the design to the Maxwell two-dimensional (2D) model. Taking into account the BLDC motor design quantities the detailed analysis of dynamic parameters variation by using the Maxwell 2D ANSYS software is shown in Figures 3-8.

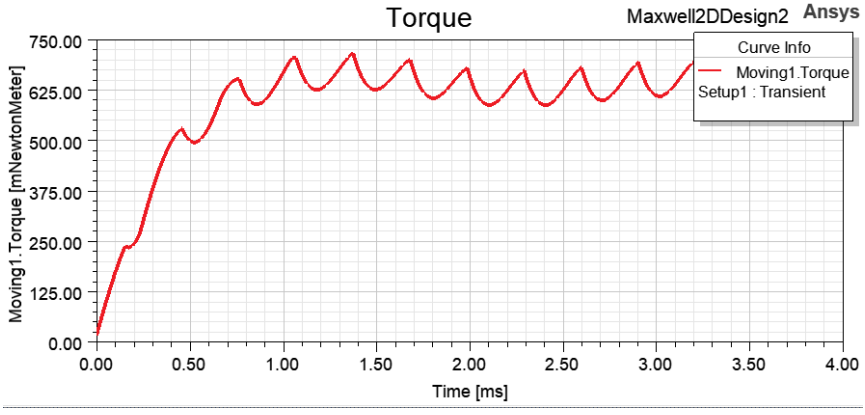

Figure 3. The torque variation with respect to time

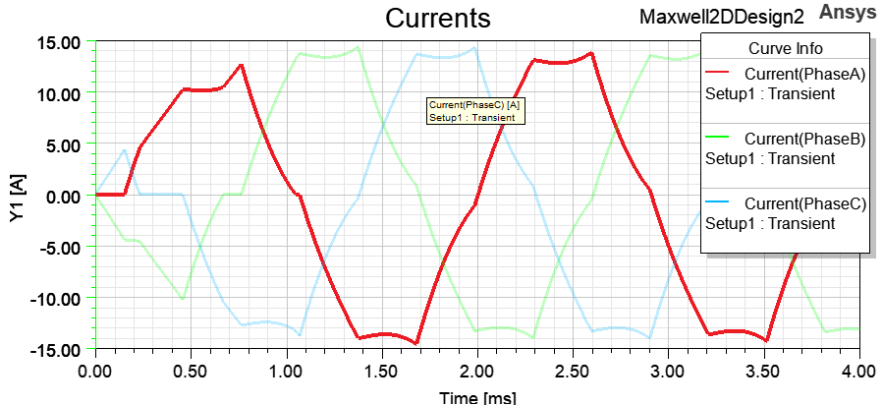

Figure 4. The phase A, B and C currents variation with respect to time

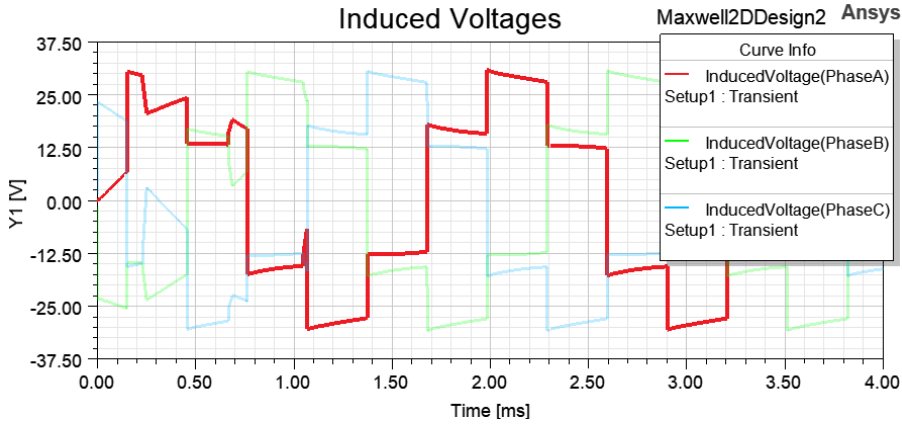

Figure 5. The phase A, B and C induced voltages variation with respect to time

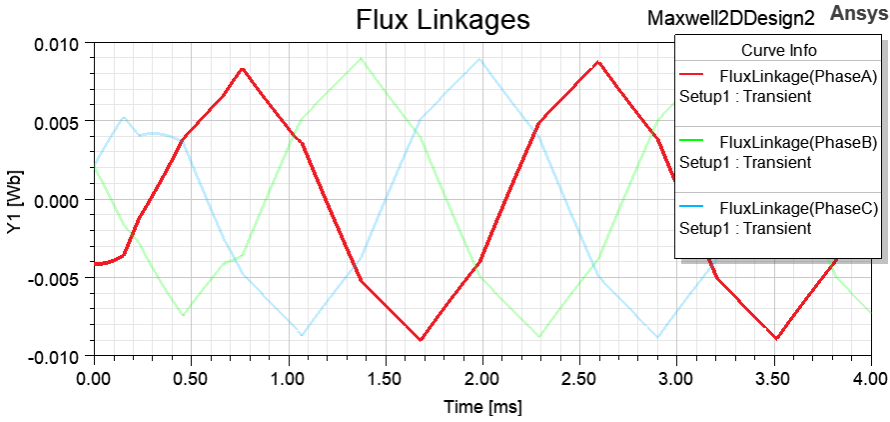

Figure 6. The phase A, B and C flux linkages variation with respect to time

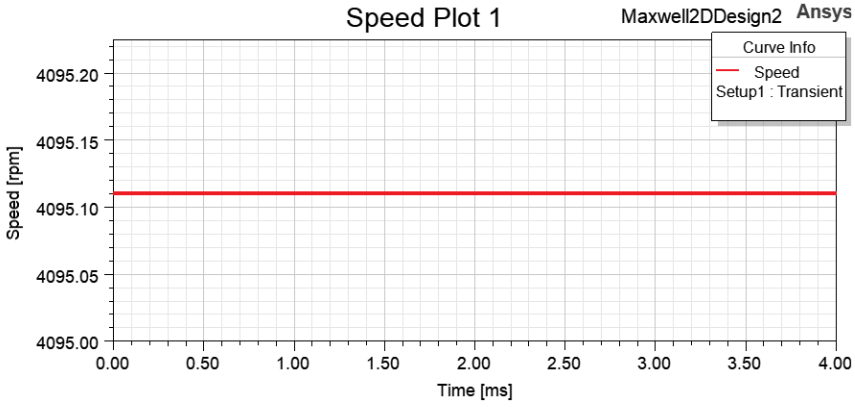

Figure 7. The motor speed variation with respect to time

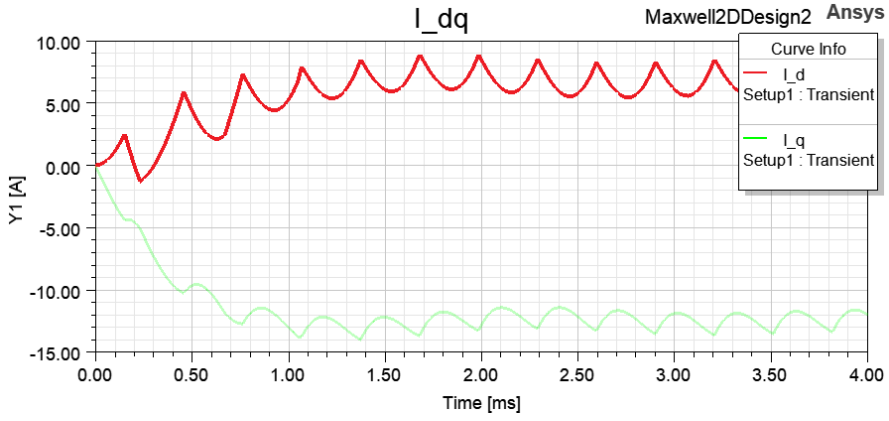

Figure 8. The I_d and I_q currents variation with respect to time

SIX STEP SPEED CONTROL OF BRUSHLESS DC MOTOR USING MATLAB SIMULINK SIMULATION

On the basis of Simulink library, a design of six step speed controller for BLDC motor was built in the Matlab/ Simulink program. The block diagram of this BLDC motor model is shown in Fig. 9.

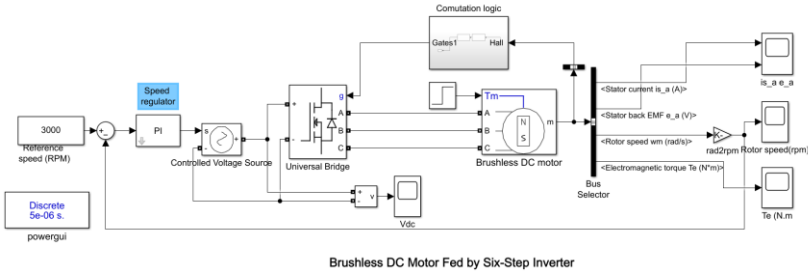

Figure 9. The design of six step speed controller for BLDC motor

Matlab/Simulink is an ideal program for creating mathematical models of electric machines and controlling them. For the speed control model shown in Fig. 9, firstly the mathematical model of the BLDC motor is created. The drivability of the motor depends on the position of the rotor magnets. In these motors, the position is mostly detected with the help of Hall sensors. The position is determined by applying the information of 3 Hall sensors positioned at an angle of 120 degrees from each other to a decoder. Depending on the position, the three phase windings of the motor are energized. A bridge circuit consisting of 6 mosfets is used for this process. The conduction of the mosfets is done with a 6-step logic code. The ability to run the motor at different speeds is adjusted by the amplitude of the voltage applied to the inverter. A PI controller is used to make this adjustment accurately. The error value calculated by the difference between the rotor speed and the reference speed is approximated to zero by the PI controller and the control is realized. Figure 10 shows the BLDC speed control graphs under no load condition.

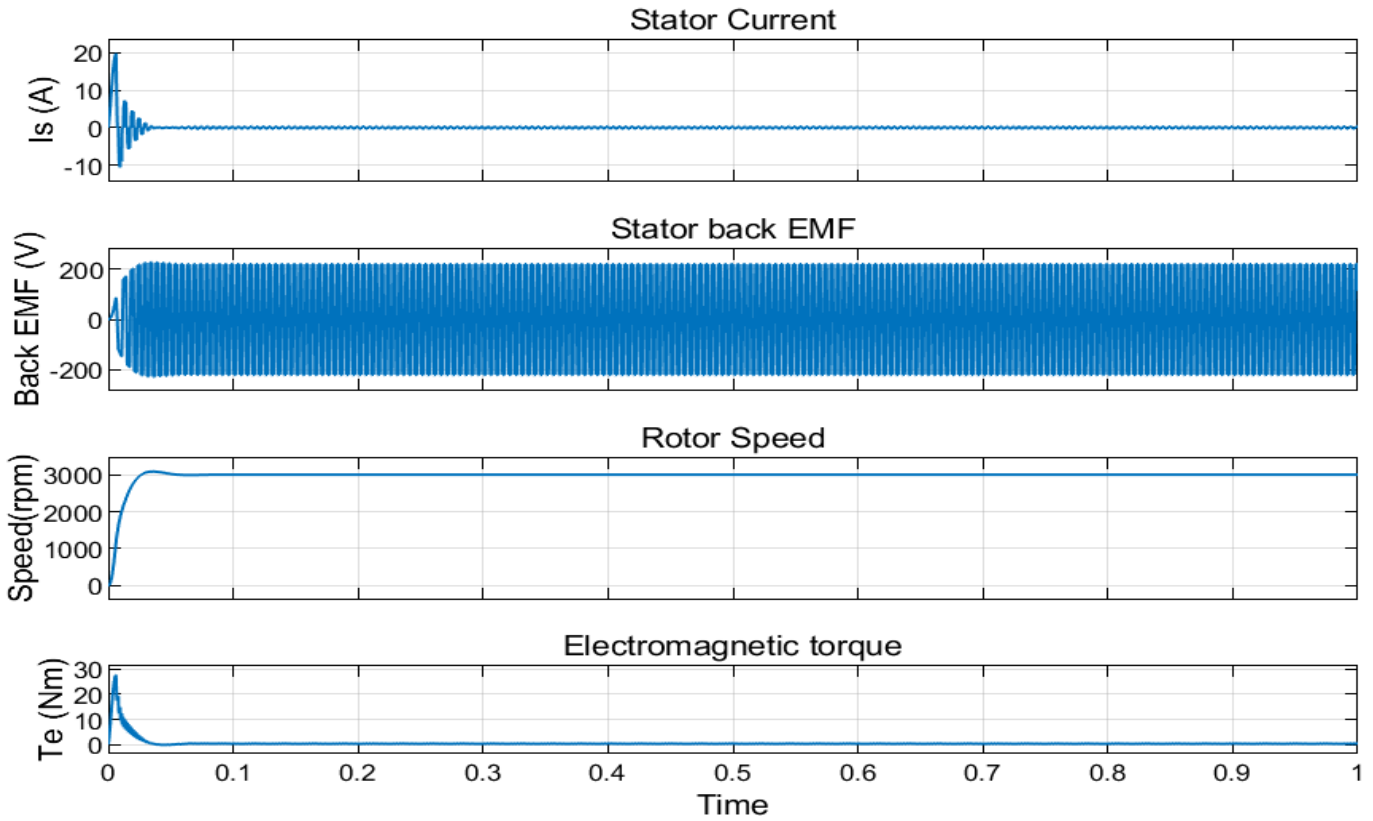

Figure 10. BLDC motor speed control graphs under no load condition.

As seen from Fig.10, the transient time of the motor is 0.03 sec. The motor was able to reach the reference speed in 0.04 sec. For loaded operation simulation, the motor was loaded with a load of 3Nm. Figure 11 shows the BLDC speed control graphs under loaded condition.

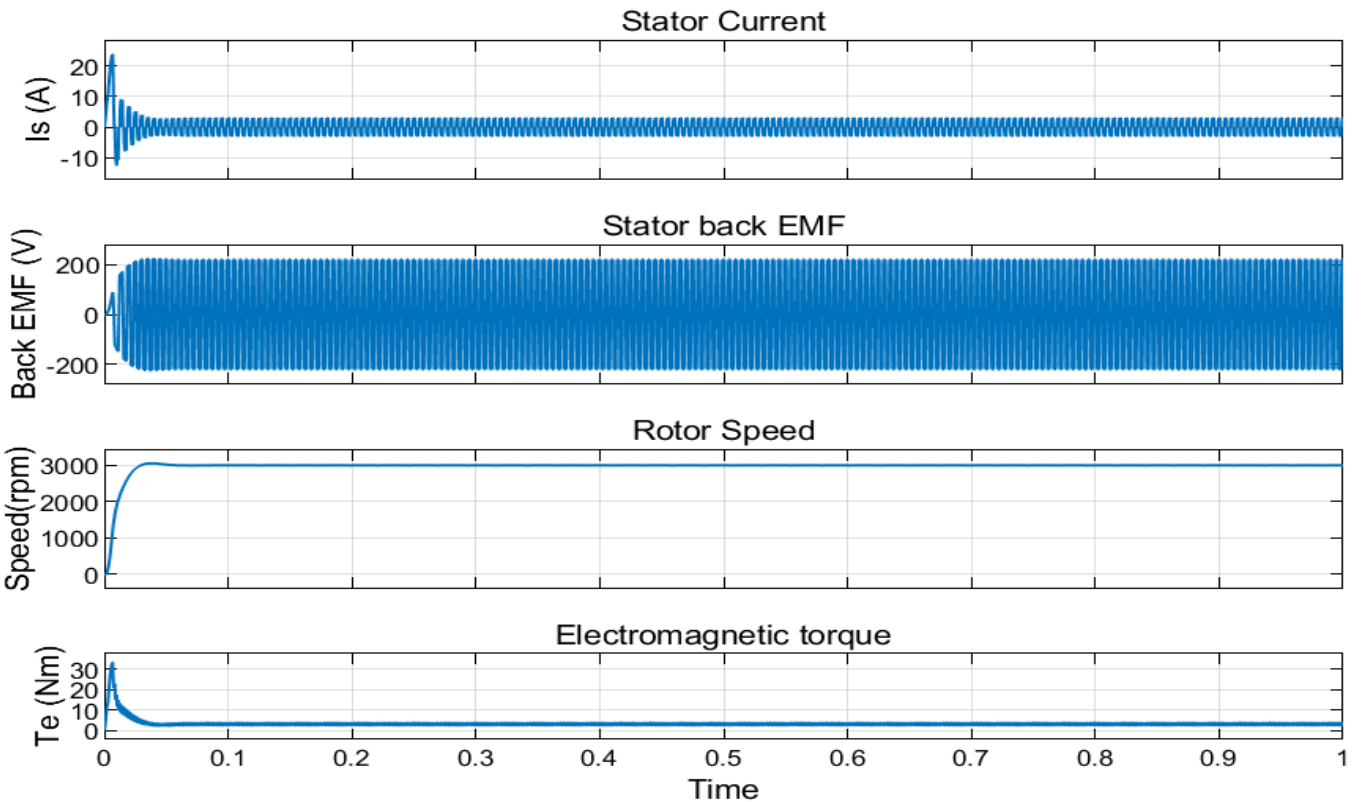

Figure 11. BLDC motor speed control graphs under loaded condition

As can be seen from Fig 11, the motor reached the reference speed in 0.035 s under load. There is no oscillation in speed in the steady-state region between 0.035-1 sec.

MAXWELL-SIMPLORER-SIMULINK COSIMULATION

Cosimulation is done in order to combine the best features of different programmers. The most ideal approach in the design of motors is FEA models. Maxwell is an ideal platform for this purpose. Matlab is an ideal programmed for control applications. For the Maxwell-Simplorer-Simulink Cosimulation performed in this study, the following operations were performed:

1. Design of BLDC motor FEA model in Maxwell

2. Design of BLDC motor drive in Simplorer

3. Creation of speed control model in Matlab/Simulink

4. Maxwell-Simplorer-Simulink Cosimulation settings

In stage first of the cosimulation, the Maxwell FEA model of the motor was designed as described in Chapter 1. In the 2nd stage, the BLDC motor driver shown in Figure 12 is modelled in Simplorer.

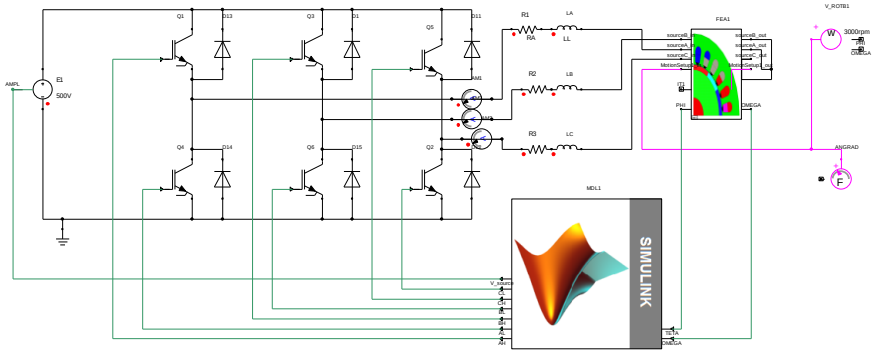

Figure 12. BLDC motor drive Simplorer model

The Fig. 12 shows the inverter of the BLDC motor and the mechanical load design of the motor. After this model was created, Maxwell-Simplorer cosimulation settings were made. For this, Twin Builder operations were performed in Ansys Electronics Desktop. For Twin Builder operations (Twin Builder/SubCircuit/MaxwellComponent/AddTransientCosimulation), the settings shown in Figure 13 are made.

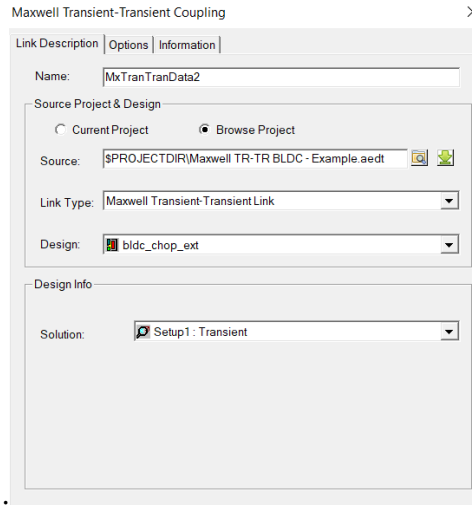

Figure 13. Maxwell-Simplorer cosimulation settings.

As a result of these settings, the BLDC motor model is created. The parameters of the model obtained are shown in Fig. 14. From these parameters, the position (PHI) and rotor speed (OMEGA) ports of the motor are activated.

FEA1:MxTranTranData Properties: TwinBuilder TR-TR BLDC _simplorer - bldc_chop

Quantities | Parameter Values | Symbol | Property Displays

Value | Optimization / Design of Experiments | Tuning | Sensitivity | Statistics

Name	Value	Unit	Description	Callback	Override	Directi...	Show ...	Sweep	SDB
WIRELOSS	0					Out			
CORELOSS	0					Out			
IT1	0				✔	Out	✔		
VT1	0					Out			
EIT1	0					Out			
FLUXT1	0					Out			
IT2	0					Out			
VT2	0					Out			
EIT2	0					Out			
FLUXT2	0					Out			
IT3	0					Out			
VT3	0					Out			
EIT3	0					Out			
FLUXT3	0					Out			
TORQUE	0					Out			
PHI	0				✔	Out	✔		
OMEGA	0				✔	Out	✔		
FEA_STEPS	0					Out			

Figure 14. BLDC motor Maxwell model parameters

The obtained BLDC motor block is connected to the inventor and the mechanical load block with the circuit connections in Fig 12. Another process in the Simplorer model is the configuration of the Simulink cosimulation blog. The settings shown in Figure 15 are made for the Simulink block (TwinBuilder/SubCircuit/AddSimulinkComponent).

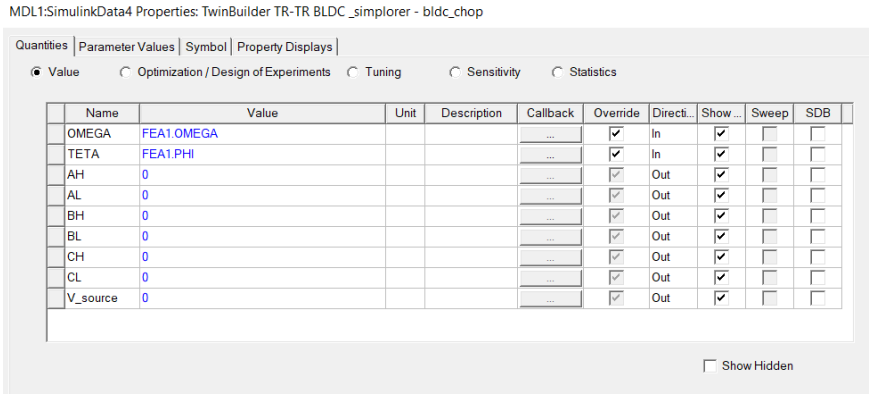

Figure 15. Simulink cosimulation blog parameters.

In these settings, Simplorer-Simulink incoming/outgoing data is defined. The Simulink block shown in

Figure 16 is created by activating the created pots.

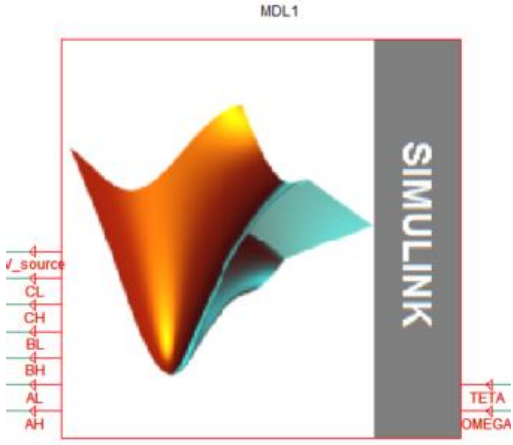

Figure 16. Simulink block

Simplorer-Simulink incoming data voltage source control port (V_source) and commutation logic data ports (AH, AL, BH, BL, CH, CL), outgoing data position port (TETA) and rotor speed port (OMEGA) are shown in Fig 16. The Simulink block is connected to the circuit in Fig 12. The 3rd stage of the cosimulation process is the creation of the speed control model in Simulink. Figure 17 shows the BLDC motor speed control model designed in Simulink.

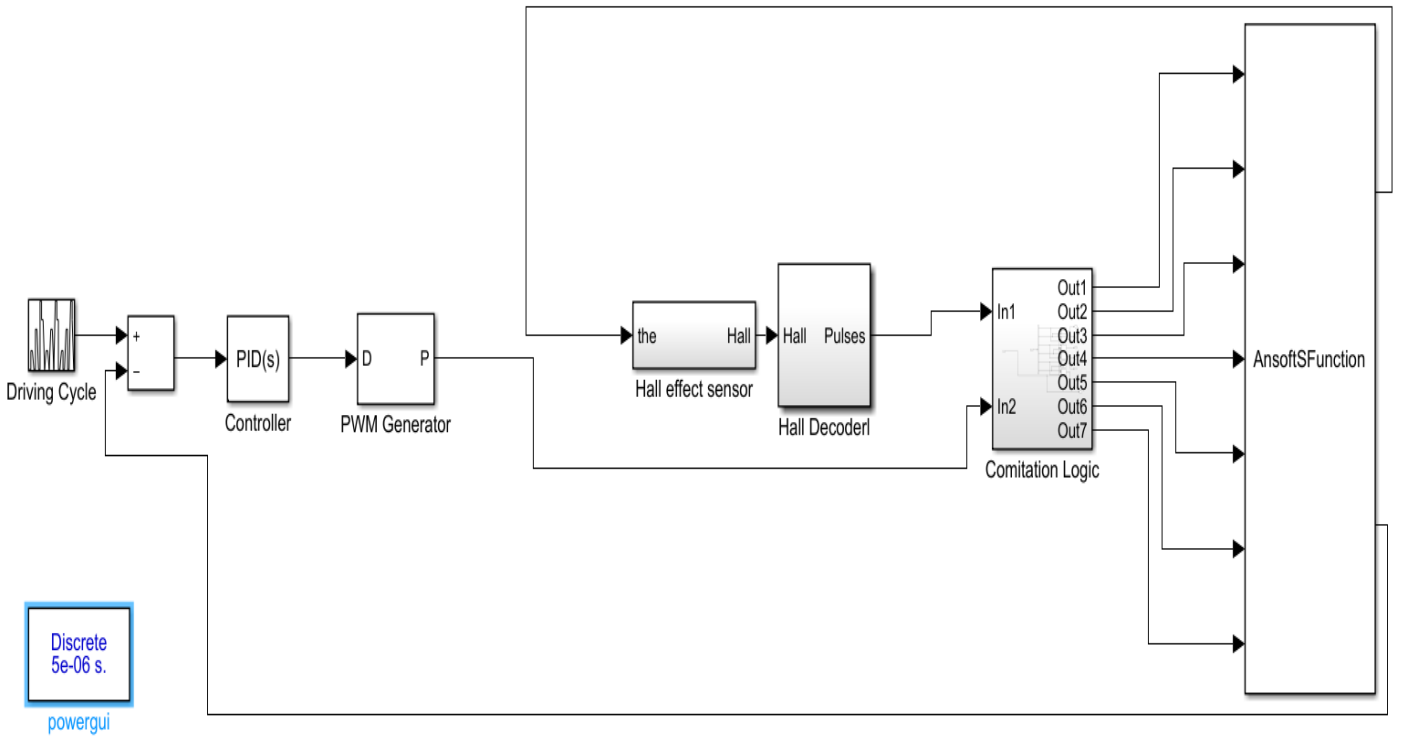

Figure 17. BLDC Motor speed control Simulink model.

When creating the Simulink model, the AsnsoftSFunction block is configured first. The incoming/outgoing data from the simplorer is used in Simulink with this block. Figure 18 shows the configuration of the AsnsoftSFunction block.

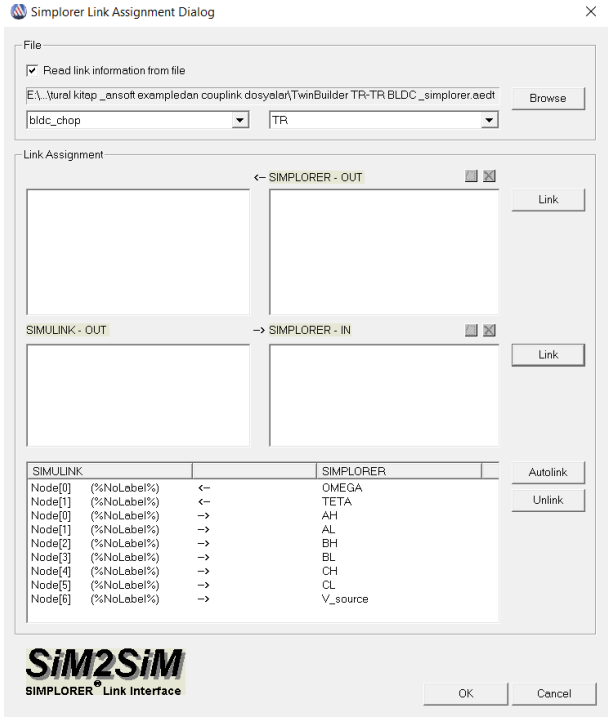

Figure 18. Internal structure of AsnsoftSFunction block.

After the AsnsoftSFunction block is created in the Simulink model shown in Fig. 17, Simplorer incoming/outgoing data connections are made to this model. PI controller is designed and added to the model for speed control of the motor. Finally, Hall sensor data calculation block and logic comitation calculation blocks are created and the connections in Fig 17 are made.

As a result of all these operations, Maxwell-Simplorer-Simulink Cosimulation is completed. The speed control reference of the motor is taken from the reference speed block in Fig. 17 and the motor is loaded from the mechanical load block in Fig. 12. After the cosimulation was completed, the motor was operated at different speeds with and without load. Figure 19 shows the cosimulation graphs of the BLDC motor under no load condition.

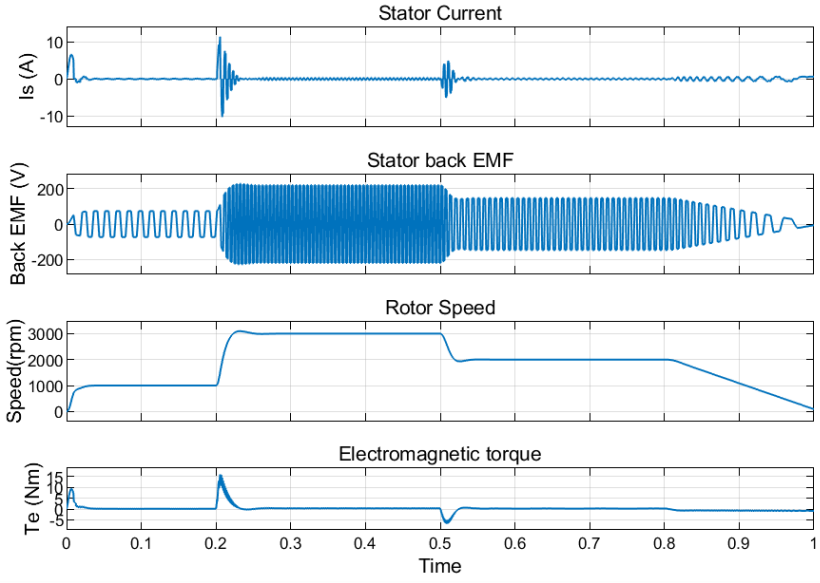

Figure 19. BLDC motor cosimulation graphs for no-load operation

Fig. 19 it can be seen from the graphs in Fig. 19 that the speed control of the BLDC motor in the simplorer environment was successfully performed by the PI controller in Simplorer. The controller has driven the motor with acceptable speed overshoots. Fig. 20 shows the cosimulation graphs of the BLDC motor under loaded condition.

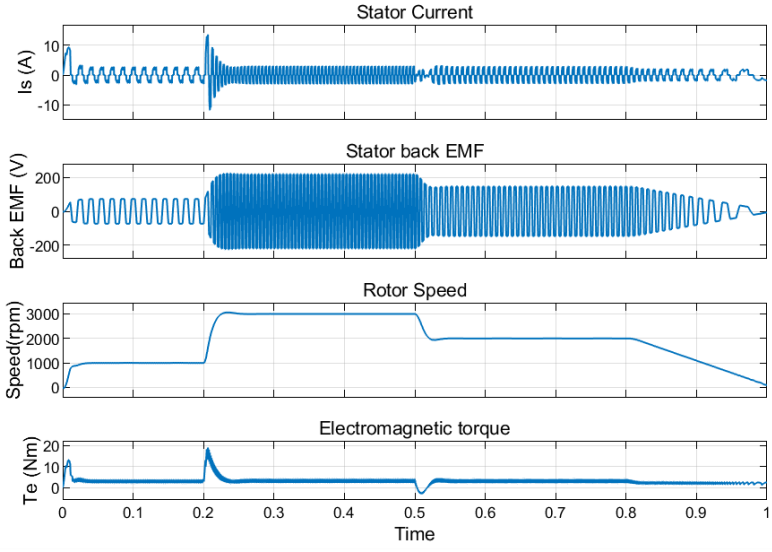

Fig. 20. BLDC motor operation cosimulation graphs under loaded condition

As can be seen in Fig. 20, the motor was operated under 3 Nm load in Simplorer. Similar to no-load operation, a successful controller performance is observed.

DISCUSSION

Before industrial production, the developed design ANSYS Maxwell and Matlab Simulink programs has the ability to describe the patterns of change in the electromagnetic torque, the angular velocity of the rotor, the currents in the stator, rotor circuits and other all required parameters over time. Reliable results were obtained in ANSYS Maxwell and Matlab Simulink software's cosimulation for BLDC motor speed control. As a conclusion, the present theoretical design analysis method can be developed to simulation the optimal performance of all type electric machines based on ANSYS Maxwell and Matlab Simulink programs.

REFERENCES

1. Tongi, W. (2014) Mechanical Design of Electric Motors, CRC Press, New York.
2. Hendershot, J.R., Miller, T.J.E. (2010) Design of Bruhless Permanet-magnet Machines.
3. Beaty, H.W., Kirtley, J.L., Kritley, Jr. L. (1980) Electric Motor Handbook, McGraw-Hill.
4. Hughes, A. (2013) Electric Motors and Drives: Fundamentals, Types and Applications, Elsevier Science.
5. Ai, C., Lee, C. H., Kirtley, J. L., Huang, Y., Wang, H., & Zhang, Z. (2019). A hybrid methodology for analyzing the performance of induction motors with efficiency improvement by specific commercial measures. *Energies*, *12*(23), 4497.
6. Ferkova, Z. (2014, May). Comparison of two-phase induction motor modeling in ANSYS Maxwell 2D and 3D program. In *2014 ELEKTRO* (pp. 279-284). IEEE.
7. Kumar, P., & Isha, T. B. (2019). FEM based electromagnetic signature analysis of winding inter-turn short-circuit fault in inverter fed induction motor. *CES Transactions on Electrical Machines and Systems*, *3*(3), 309-315.
8. John, S., & Mini, V. P. (2021, November). Brushless dc motor (BLDCM) drive with maximum torque per Ampere (MTPA) control for electric vehicle application. In *2021 Innovations in Power and Advanced Computing Technologies (i-PACT)* (pp. 1-6). IEEE.
9. Mohanraj, D., Aruldavid, R., Verma, R., Sathyasekar, K., Barnawi, A. B., Chokkalingam, B., & Mihet-Popa, L. (2022). A review of BLDC Motor: State of Art, advanced control techniques, and applications. *IEEE Access*.

10. Atallah, K., Calverley, S. D., & Howe, D. (2007). A brushless permanent magnet motor with integrated torque-limiter. *IEEE transactions on magnetics*, *43*(6), 2498-2500.
11. Cho, C. P., Fussell, B. K., & Hung, J. Y. (1993). Detent torque and axial force effects in a dual air-gap axial-field brushless motor. *IEEE transactions on magnetics*, *29*(6), 2416-2418.
12. Gieras, J. F. (2004). Analytical approach to cogging torque calculation of PM brushless motors. *IEEE Transactions on Industry Applications*, *40*(5), 1310-1316.
13. Robinson, S. (2006). DESIGN SOLUTION-Drive And Control Electronics Enhance The Brushless Motor's Advantages-With the appropriate driver IC and microcontroller, designers can exploit the brushless motor's declining. *Electronic Design*, *54*(18), 54-67.
14. Mousavi-aghdam, S. R. (2021). Design and analysis of a novel topology for slotless brushless DC (BLDC) motors with enhanced torque and efficiency. *IET Electric Power Applications*, *15*(3), 284-298.
15. Zhang, C., & Zhao, G. Z. (2011). Design and FEM Analysis of a High Efficiency Axial-Flux Brushless DC Motor for Flywheel System. In *Key Engineering Materials* (Vol. 480, pp. 1099-1104). Trans Tech Publications Ltd.
16. Li, Z., & Yang, X. (2014). Automated Clutch of AMT Vehicle Based on Adaptive Generalized Minimum Variance Controller. *Sensors & Transducers*, *182*(11), 174.
17. Sun, J., Chai, Y., Su, C., Zhu, Z., & Luo, X. (2014). BLDC motor speed control system fault diagnosis based on LRGF neural network and adaptive lifting scheme. *Applied Soft Computing*, *14*, 609-622.
18. Yuan, Y., Meng, W., Sun, X., & Zhang, L. (2019). Design optimization and analysis of an outer-rotor direct-drive permanent-magnet motor for medium-speed electric vehicle. *World Electric Vehicle Journal*, *10*(2), 16.
19. Gastelo, J. M. S., & Díaz, E. H. V. (2022, October). DC Brushless Motor Speed Controller Design using Back Electromotive Force. In *2022 IEEE Engineering International Research Conference (EIRCON)* (pp. 1-4). IEEE.
20. Nikam, A. D., & Jadhav, H. T. (2019, July). Modelling & Simulation of Three Phases BLDC Motor for Electric Braking. In *2019 2nd International Conference on Intelligent Computing, Instrumentation and Control Technologies (ICICICT)* (Vol. 1, pp. 540-544). IEEE.
21. Ulasyar, A., Zad, H. S., & Zohaib, A. (2018, December). Intelligent speed controller design for brushless DC motor. In *2018 International Conference on Frontiers of Information Technology (FIT)* (pp. 19-23). IEEE.
22. Liu, G., & Hu, C. (2018, August). Adaptive modeling of brushless dc motor drive system. In *2018 IEEE 4th International Conference on Control Science and Systems Engineering (ICCSSE)* (pp. 173-177). IEEE.
23. Egami, T., & Tsuchiya, T. (1995). Disturbance suppression control with review action of linear DC brushless motor. *IEEE Transactions on Industrial Electronics*, *42*(5), 494-500.
24. Kusko, A., & Peeran, S. M. (1988, October). Definition of the brushless DC motor. In *Conference Record of the 1988 IEEE Industry Applications Society Annual Meeting* (pp. 20-22). IEEE.

25. Elbuluk, M. E., & Kankam, M. D. (1995). Motor drive technologies for the power-by-wire (PBW) program: options, trends and tradeoffs. I. Motors and controllers. *IEEE aerospace and electronic systems magazine*, *10*(11), 37-42.
26. Hua, W., Cheng, M., Zhu, Z. Q., Zhao, W., & Kong, X. (2008). Comparison of electromagnetic performance of brushless motors having magnets in stator and rotor. *Journal of Applied Physics*, *103*(7), 07F124.
27. Chudiváni, J., Kujan, V., Perný, M., Hüttner, L., Fric, R., & Sály, V. (2014). Issues of Electromagnetic Design of Synchronous Brushless Motors with Concentrated Winding. *Electrotehnica, Electronica, Automatica*, *62*(2), 24.
28. Matsui, N. (1996). Sensorless PM brushless DC motor drives. *IEEE Transactions on Industrial Electronics*, *43*(2), 300-308.
29. Khodadadi, H., Esmaeel Beag, M., & Cheraghi Shirazi, N. (2021). Optimization of Proportional Integral Derivative controller Coefficients of Control Brushless Motor Speed with Water Cycle Optimization Algorithm. *Journal of Communication Engineering*, *11*(41), 1-14.
30. Chernyshev, A. D., Lisovskaya, T. A., & Lisovskiy, R. A. (2017, May). Comparative analysis of different electrical motor types as a traction drive part in electrical transmission. In *2017 International Conference on Industrial Engineering, Applications and Manufacturing (ICIEAM)* (pp. 1-5). IEEE.
31. Mithunraj, M. K., Warrier, G. S., Pathivil, P., Kanagalakshmi, S., & Archana, R. (2019, July). Design and performance analysis of brushless DC motor using ANSYS Maxwell. In *2019 2nd International Conference on Intelligent Computing, Instrumentation and Control Technologies (ICICICT)* (Vol. 1, pp. 1049-1053). IEEE.
32. Tibor, B., Fedak, V., & Durovský, F. (2011, June). Modeling and simulation of the BLDC motor in MATLAB GUI. In *2011 IEEE International Symposium on Industrial Electronics* (pp. 1403-1407). IEEE.
33. Ragot, P., Markovic, M., & Perriard, Y. (2006). Optimization of electric motor for a solar airplane application. *IEEE Transactions on Industry Applications*, *42*(4), 1053-1061.
34. Higuchi, T., Oyama, J., Yamada, E., Chiricozzi, E., Parasiliti, F., & Villani, M. (1997). Optimization procedure of surface PM synchronous motors. *IEEE Transactions on Magnetics*, *33*(2), 1943-1946.
35. Markovic, M., Ragot, P., & Perriard, Y. (2007, May). Design optimization of a BLDC motor: a comparative analysis. In *2007 IEEE International Electric Machines & Drives Conference* (Vol. 2, pp. 1520-1523). IEEE.
36. Warrier, S., & Pathivi, P. (2019). Design and Performance Analysis of Brushless DC Motor Using ANSYS Maxwell. In *IEEE International Conference on Intelligent Computing, Instrumentation and Control Technologies (ICICICT)*.
37. Kelek, M. M., Çelik, İ., Fidan, U., & Oğuz, Y. (2019). The Simulation of mathematical model of outer rotor BLDC motor. *Simulation*, *2687*, 5527.
38. Pyrhoneni J., Jokinen, T., Hrabovcova, V., Design of Rotatiing Electrical Machines, John Wiley, UK, 2013.
39. Boldea, I., Tutelea, L.N., Electric Machines Steady State and Performance with MATLAB, CRC Press, New York, 2022.

40. Ulrich, K. T. (2005). Estimating the technology frontier for personal electric vehicles. *Transportation research part C: Emerging technologies*, *13*(5-6), 448-462.
41. Carunaiselvane, C., & Jeevananthan, S. (2012, March). Generalized procedure for BLDC motor design and substantiation in MagNet 7.1. 1 software. In *2012 International Conference on Computing, Electronics and Electrical Technologies (ICCEET)* (pp. 18-25). IEEE.
42. Usudum, A., & Bolukbas, D. (2013, November). The performance analyses of an induction motor due to specified fault conditions. In *2013 8th International Conference on Electrical and Electronics Engineering (ELECO)* (pp. 273-277). IEEE.
43. Vijayakumar, K., Karthikeyan, R., Paramasivam, S., Arumugam, R., & Srinivas, K. N. (2008). Switched reluctance motor modeling, design, simulation, and analysis: a comprehensive review. *IEEE Transactions on Magnetics*, *44*(12), 4605-4617.
44. Tikhonova, O. V., & Plastun, A. T. (2018, January). Electromagnetic calculation of induction motor by "ANSYS Maxwell". In *2018 IEEE Conference of Russian Young Researchers in Electrical and Electronic Engineering (EIConRus)* (pp. 822-826). IEEE.
45. Iqbal, A., Moinoddin, S., & Reddy, B. P. (2021). *Electrical Machine Fundamentals with Numerical Simulation using MATLAB/SIMULINK*. John Wiley & Sons.
46. Weston, D. A. (2016). *Electromagnetic compatibility: methods, analysis, circuits, and measurement*. Crc Press.
47. Vijayakumar, K., Karthikeyan, R., Paramasivam, S., Srinivas, K.N. (2008) "Switched reluctance motor modeling, design, simulation and analysis: a comprehensive", IEEE Trans Magn., Vol. 44(12), pp.4605-4617.
48. Abirami, S., Bala S. M. and Priya, R. J. (2014) "Design of BLDC Hub Motor using FEM analysis," 2014 International Conference on Green Computing Communication and Electrical Engineering (ICGCCEE), Coimbatore, pp. 1-6.
49. Lee, Y. K., Kim, J. K. (2019) "Power efficiency analysis of a three-phase inverter for a BLDC motor drive with varying speeds and load torques," 2019 IEEE PES Asia-Pacific Power and Energy Engineering Conference (APPEEC), pp. 1-5.
50. S. Derammelaere, M. Haemers, "A quantitative comparison between BLDC, PMSM, Brushed DC and stepping motor", Tecnologies, International Conference on Electrical Machines and Systems ICEMS, 2016.
51. Yaz, M., & Cetin, E. (2021). Brushless Direct Current Motor Design and Analysis. *COJ Electronics & Communications*, *2*(2).
52. MATLAB Release 2018b, The MathWorks, Inc., Natick, Massachusetts, United States.
53. Ansys, help document, URL http://www.ansys.com/Support/Documentation

Installed Power Changes in Renewable Energy: Hydroelectric, Solar, and Wind Power in Recent Years

Yıldırım BAYAZIT[1]

1- Doç. Dr..; Bilecik Şeyh Edebali Üniversitesi Mühendislik Fakültesi İnşaat Mühendisliği Bölümü. yildirim.bayazit@bilecik.edu.tr ORCID No: 0000-0002-8699-4741

ABSTRACT

The transition toward renewable energy has become a cornerstone of global strategies aimed at mitigating climate change and ensuring sustainable energy security. Hydroelectric power, solar energy, and wind energy have emerged as key pillars in this transformation. This chapter examines the evolution of installed power capacities across these three technologies over the past decade, with an emphasis on comparative growth trends and underlying drivers. Drawing on data from leading global energy agencies, it explores the complex interplay between technological advancements, economic factors, and policy frameworks that have shaped their trajectories. The findings illuminate the nuanced dynamics that influence renewable energy deployment and offer a roadmap for future development.

Keywords – Renewable Energy, Hydroelectric, Solar, Wind.

INTRODUCTION

The pressing need to decarbonize the energy sector has driven transformative changes in the global energy landscape, as nations strive to mitigate the impacts of climate change while meeting escalating energy demands. Renewable energy sources—hydroelectric, solar, and wind power—have emerged as central pillars in this transition due to their ability to deliver sustainable, reliable, and economically competitive energy solutions. Among these, hydroelectric power has long been a cornerstone of renewable energy, contributing over 16% of global electricity production and offering unparalleled reliability and storage capabilities through reservoir systems (International Energy Agency [IEA], 2021). However, its growth is often constrained by geographic and ecological limitations, particularly in regions lacking suitable water resources or where large-scale dam projects face environmental concerns (World Bank, 2020).

In contrast, solar and wind energy have experienced unprecedented expansion over the past two decades, driven by rapid technological advancements, declining costs, and supportive policy frameworks. Solar photovoltaic (PV) systems have become increasingly efficient and cost-effective, with the levelized cost of electricity (LCOE) for utility-scale solar projects dropping by over 80% between 2010 and 2020 (International Renewable Energy Agency [IRENA], 2020). Similarly, the global wind energy sector has seen significant advancements in turbine technology, enabling higher energy yields and cost reductions of approximately 70% over the same period (Global Wind Energy Council [GWEC], 2021). As a result, these sources collectively added nearly 300 GW of new capacity in 2021 alone, representing the fastest annual growth in renewable energy history (IEA, 2022).

The integration of solar and wind power into the energy mix has not only diversified the global energy portfolio but also addressed critical energy security and environmental challenges. Solar energy, with its modular and scalable nature, has proven particularly effective in off-grid and rural applications, enabling energy access in underserved regions (IRENA, 2019). Wind energy, meanwhile, has demonstrated its ability to complement other renewables through offshore installations, which capitalize on higher and more consistent wind speeds (GWEC, 2022). Together, these developments underscore the growing role of solar and wind in reshaping the energy sector, challenging the historical dominance of hydroelectric power.

As the energy transition accelerates, the synergy between these renewable sources, coupled with advancements in energy storage and grid integration technologies, is expected to further enhance their adoption. Achieving this transformation will require sustained investment, innovation, and global cooperation to overcome technical, economic, and regulatory barriers, paving the way toward a low-carbon future (IEA, 2021; United Nations, 2022).

This chapter provides a comprehensive analysis of changes in installed capacity for hydroelectric, solar, and wind energy from 2010 to 2023. It highlights key factors driving these changes, including advancements in technology, evolving economic conditions, and supportive policy environments. This analysis not only contextualizes the growth patterns of these technologies but also underscores their interdependencies and unique roles in achieving a sustainable energy future.

HYDROELECTRIC ENERGY: A MATURE BACKBONE OF RENEWABLES

Historical Significance and Global Trends

Hydroelectric power has played a foundational role in the global energy system, leveraging the kinetic energy of water to generate electricity. With an installed capacity exceeding 1,360 GW in 2023, hydroelectricity remains the largest renewable energy source worldwide (IRENA, 2023; IHA, 2020). Its reliability, long operational lifespan, and ability to provide baseload power distinguish it from intermittent sources such as solar and wind energy (IHA, 2020; Hydropower Europe, 2024).

However, the expansion of hydroelectric power has decelerated in recent years. This trend can be attributed to the scarcity of economically viable sites, growing environmental opposition, and the socio-political complexities of large-scale dam projects. For instance, large dams often require the displacement of local communities and pose significant risks to biodiversity (IHA, 2020; Hydropower Europe, 2024).

Installed Capacity Changes

Between 2010 and 2023, the global hydroelectric installed capacity grew at a relatively modest pace, averaging around 2% annually (IRENA, 2023; Hydropower Europe, 2024) (Figure 1). Emerging economies such as China, Brazil, and India have been key drivers of this growth, implementing large-scale projects to meet rising energy demands. However, in regions with mature hydroelectric infrastructures, growth has been largely limited to efficiency upgrades and the development of small-scale projects (REN21, 2023; Hydropower Europe, 2024).

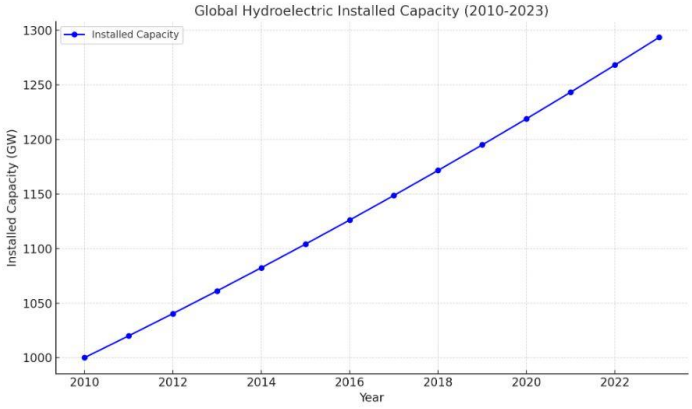

Figure 1: Global hydroelectric installed capacity (2010-2023) (IRENA, 2023)

Current Challenges and Opportunities

While hydroelectric energy faces significant challenges, including environmental and regulatory hurdles, it continues to offer critical opportunities for energy storage and grid stabilization. Pumped storage hydropower, in particular, has emerged as a vital complement to variable renewable energy sources, enabling the balancing of electricity supply and demand (IHA, 2020; Hydropower Europe, 2024). Furthermore, modernization of aging infrastructure presents an avenue to enhance efficiency and extend the lifespan of existing facilities (Hydropower Europe, 2024).

Table 1: Advantages and Challenges of Hydroelectric Power

Advantages	Challenges
High reliability and consistent power generation	Limited economically viable sites
Provides baseload power	Environmental opposition (biodiversity impacts, altered river flows)
Long operational lifespan	Socio-political issues (community displacement)
Reservoirs support grid stability and energy storage	Declining growth rates in mature markets

Source: IRENA, 2023

SOLAR ENERGY: A RAPIDLY ACCELERATING FORCE

Technological Breakthroughs and Economic Factors

The solar energy sector has experienced exponential growth over the past decade, driven by continuous technological innovation and significant cost reductions. Advances in photovoltaic (PV) materials, such as thin-film technologies and bifacial panels, have improved efficiency while reducing manufacturing costs. As a result, the levelized cost of electricity (LCOE) for solar PV systems has declined by more than 80% since 2010, making solar energy one of the most competitive sources of electricity generation (Lazard, 2023; Ngobeh et al., 2023).

The scalability of solar technology has also contributed to its widespread adoption. From utility-scale solar farms to decentralized rooftop installations, solar PV systems are being deployed across diverse settings, providing flexibility and accessibility (BloombergNEF, 2024; REN21, 2024).

Installed Capacity Changes

Between 2010 and 2023, the global installed capacity of solar energy surged from 40 GW to over 1,000 GW, reflecting a compound annual growth rate of approximately 25% (IRENA, 2023; BloombergNEF, 2023) (Figure 2). This remarkable growth has been concentrated in countries such as China, India, and the United States, where favorable policy frameworks, such as feed-in tariffs and tax incentives, have driven large-scale installations (IEA, 2023; REN21, 2023). Additionally, developing regions such as sub-Saharan Africa are emerging as important markets, spurred by declining costs and growing energy access needs (BloombergNEF, 2023; REN21, 2023).

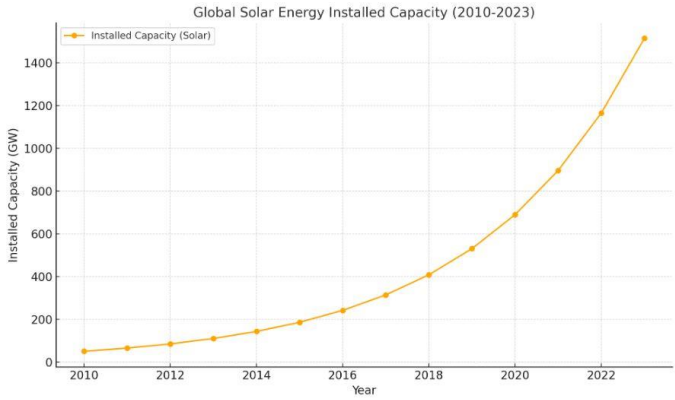

Figure 2: Global solar energy installed capacity (2010-2023) (IRENA, 2023)

WIND ENERGY: SUSTAINED GROWTH AND TECHNOLOGICAL ADVANCEMENTS

Offshore and Onshore Developments

Wind energy has demonstrated consistent growth over the past decade, supported by advancements in both onshore and offshore technologies. Offshore wind, in particular, has gained prominence due to its higher capacity factors and the ability to deploy large turbines in high-wind-speed areas. Floating wind turbines represent a frontier of innovation, enabling deployment in deep-water regions previously inaccessible to fixed-bottom designs (GWEC, 2023; Deshmukh et al., 2023).

Installed Capacity Changes

The global installed capacity of wind energy increased from 200 GW in 2010 to over 900 GW in 2023, achieving an average annual growth rate of 12% (IRENA, 2023; IEA, 2023) (Figure 3). While mature markets in Europe and North America have seen stabilization in onshore installations, emerging economies such as China and Brazil have experienced rapid growth, driven by ambitious government targets and declining technology costs (GWEC, 2023; REN21, 2024).

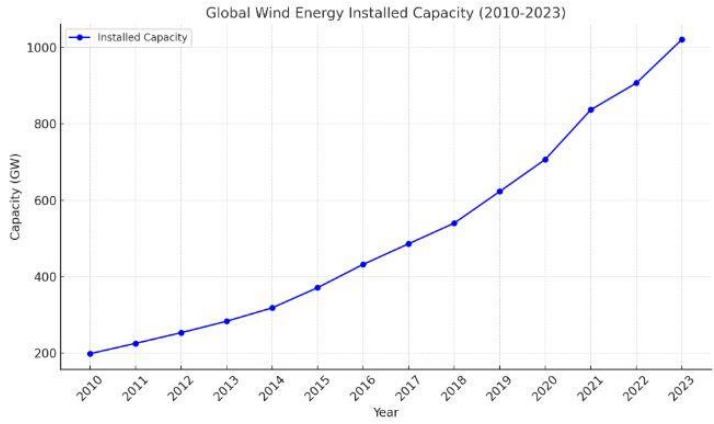

Figure 3: Global wind energy installed capacity (2010-2023) (IRENA, 2023)

COMPARATIVE ANALYSIS OF GROWTH DYNAMICS

Growth Rates and Capacity Additions

Solar energy has emerged as the fastest-growing renewable energy technology, reflecting its rapidly declining costs and widespread applicability. Wind energy has maintained steady growth, benefiting from technological advancements and policy support. In contrast, the expansion of hydroelectric power has slowed, reflecting site limitations and environmental considerations (IRENA, 2023; Lazard, 2023; BloombergNEF, 2024).

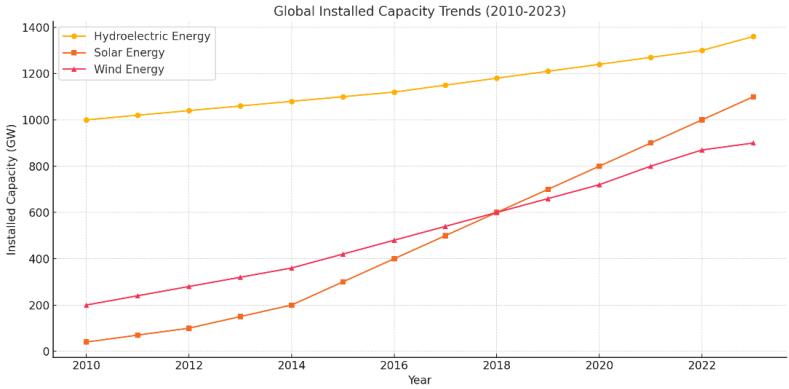

Figure 4: Comprative installed capacity (2010-2023)

Environmental and Social Considerations

While solar and wind installations generally face fewer environmental challenges, hydroelectric projects are often associated with significant ecological and social impacts, such as habitat loss and community displacement (IHA, 2020; Hydropower Europe, 2024). Balancing these

considerations remains a critical challenge for sustainable energy development.

FUTURE OUTLOOK

The ongoing advancement of renewable energy technologies continues to reshape and diversify the global energy landscape, with solar and wind power poised to dominate future capacity additions. This trend is driven by rapid technological innovations, declining costs, and robust policy frameworks that prioritize low-carbon energy transitions (International Renewable Energy Agency (IRENA, 2023; Ngobeh et al., 2023). While opportunities for expanding hydroelectric capacity remain geographically constrained, its role as a provider of baseload energy and a stabilizer for grid operations ensures its enduring significance in the energy mix (International Hydropower Association (IHA, 2020; Hydropower Europe, 2024).

It is strategically critical to forecast installed capacity in the global energy sector from an economic, social, and environmental perspective. The installed capacity of wind, solar, and hydroelectric power over the last 13 years (2010–2023) is used in this study to predict the future using regression analysis. Regression equations and correlation coefficients are used in Figure 5 to forecast installed capacity through 2040. Figure 5 shows that by 2027, the installed capacity of solar energy is expected to overtake the installed capacity of hydroelectric energy globally. The installed capacity of hydroelectric energy is expected to be surpassed by wind energy in 2038.

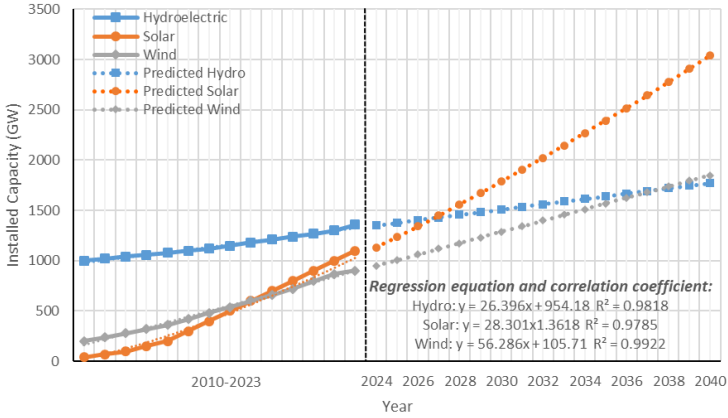

Figure 5: Prospective projections with regression analysis for hydroelectric, solar and wind installed energy (2010-2023)

A promising approach to improving energy efficiency and resource utilization is offered by emerging innovations like hybrid renewable systems, which combine hydroelectric facilities with solar and wind installations. In times of low solar irradiance or wind speed, these systems

take advantage of the complementary qualities of various renewable sources to enable more reliable power generation and lessen dependency on fossil fuels (IRENA, 2023; Energy Systems Integration Group, 2022). Innovations in energy storage technologies, such as pumped hydro storage and sophisticated battery systems, are also essential for facilitating the smooth integration of these various renewable energy sources. The development of a more integrated, dependable, and resilient energy system is promoted by these storage solutions, which mitigate the intermittent nature of renewable energy sources (Hydropower Europe, 2024; IEA, 2022).

CONCLUSION

Different paths of renewable energy technologies are highlighted by the shifting dynamics of installed power in wind, solar, and hydroelectric power. The rapid growth of solar and wind energy is changing the global energy landscape, but hydroelectric power still plays a crucial role. Achieving a resilient and sustainable energy future requires a well-rounded strategy that makes use of each technology's advantages.

REFERENCES

BloombergNEF. (2024). New Energy Outlook 2024 Report. https://about.bnef.com/new-energy-outlook/ adresinden 7 Aralık 2024 tarihinde alınmıştır.

Deshmukh, M. K. G., Sameeroddin, M., Abdul, D. and Sattar, M. A. (2023). Renewable energy in the 21st century: A review. Materialstoday: Proceedings. 80 (3), 1756-1759.

Energy Systems Integration Group. (2022). Hybrid Renewable Energy Systems: Opportunities and Challenges. www.esig.energy. adresinden 7 Aralık 2024 tarihinde alınmıştır.

GWEC. (2021). Global Wind Report 2021. Global Wind Energy Council. Retrieved from https://gwec.net adresinden 7 Aralık 2024 tarihinde alınmıştır.

GWEC. (2022). Offshore Wind Outlook 2022. Global Wind Energy Council. https://gwec.net adresinden 7 Aralık 2024 tarihinde alınmıştır.

GWEC. (2023). Global Wind Report. Global Wind Energy Council.

Hydropower Europe. (2024). The Future Role of Hydropower in Europe. https://hydropower-europe.eu/about-hydropower-europe/hydropower-energy/ adresinden 7 Aralık 2024 tarihinde alınmıştır.

IEA. (2022). Renewables 2022: Analysis and Forecast to 2027. International Energy Agency. https://www.iea.org adresinden 7 Aralık 2024 tarihinde alınmıştır.

IEA. (2023). Renewables 2023: Analysis and Forecast to 2028. International Energy Agency. https://www.iea.org adresinden 7 Aralık 2024 tarihinde alınmıştır.

IHA. (2020). Hydropower Sustainability Assessment Protocol. International Hydropower Association. ISBN: 978-0-9566228-1-5

International Energy Agency (IEA). (2021). Hydropower Special Market Report 2021. Retrieved from https://www.iea.org

IRENA. (2019). Renewable Energy: A Key Solution to Climate Change. International Renewable Energy Agency. https://www.irena.org adresinden 7 Aralık 2024 tarihinde alınmıştır.

IRENA. (2020). Renewable Power Generation Costs in 2020. International Renewable Energy Agency. https://www.irena.org adresinden 7 Aralık 2024 tarihinde alınmıştır.

IRENA. (2023). Renewable Capacity Statistics. International Renewable Energy Agency. https://www.irena.org/publications adresinden 7 Aralık 2024 tarihinde alınmıştır.

Lazard. (2023). Levelized Cost of Energy Analysis V.15.0.

Ngobeh, J., Sannoh, M. and Thullah, J. (2023). A Comparative Analysis of the Sustainable Growth of Global Hydro, Solar, and Wind Power Systems (Renewable Energy Systems). Open Journal of Energy Efficiency, 12, 49-61.

REN21. (2024). Renewables 2024 Global Status Report Collection.

UN. (2022). Global Status Report on Renewable Energy: Progress Towards Net-Zero Goals. New York: United Nations Development Programme (UNDP). United Nations

World Bank. (2020). Environmental and Social Impacts of Hydropower Projects: Lessons from the Field. Washington, DC: World Bank Group.

Work Accidents and Precautions in Agriculture

Adem ÖZKAN[1]

Yusuf DİLAY [2]

1- Lecturer. Gör.; Karamanoğlu Mehmetbey University Vocational School of Technical Sciences, Department of Mechanical and Metal Technologies. aozkan@kmu.edu.tr ORCID No: 0000-0003-3043-0338.

2- Assoc. Dr.; Karamanoğlu Mehmetbey University Vocational School of Technical Sciences, Department of Mechanical and Metal Technologies. ydilay@kmu.edu.tr ORCID No: 0000-0002-5365-5137.

ABSTRACT

Events that occur in unsafe working environments are called accidents. The way accidents occur; It occurs with the effects of human, machine and environment trio. The rate of accidents caused by human errors varies. Occupational accidents and occupational diseases are one of the main problems when viewed from the producer side. Agriculture is a sector that feeds people and provides raw materials to industrial branches and involves various risks due to its nature. Sustainability at every point of production and especially in agricultural production is important for people to continue their lives. The continuity of production in agriculture depends on the protection of the health of workers in this sector. Unfortunately, many deaths, injuries and material losses occur in these areas every year as a result of occupational accidents and occupational diseases. Although efforts are made to prevent occupational accidents and occupational diseases, it is not possible to avoid accidents. Accidents develop under the influence of human factors, environmental conditions and machine structural status. While threatening the health of employees, it also negatively affects the production process operations.

In this study, in addition to the occupational accidents occurring in the agricultural sector in the world and in Turkey and their causes, it is aimed to provide the parties with technical information about the hazards and precautions that can be taken in agricultural activities occurring in production areas in Turkey and the prevention of occupational accidents. It has been observed that approximately half of the world's population works in agriculture and a significant portion of occupational accidents occur in this agricultural sector. In order to minimize possible accidents in this sector, it is tried to list the measures and precautions that can be taken by the relevant stakeholders, those concerned, manufacturer machine manufacturers.

Keywords - Occupational Accidents, Agriculture, Machinery, Occupational Safety, Risks.

INTRODUCTION

Today, the rapid increase in the world population and the rapid decrease in agricultural land led to a serious crisis in food supply. The rapid increase in the world's population, climate change, drought and erosion, as well as the reduction in agricultural land, have become a serious problem threatening food security. This situation exacerbates the already existing problems of malnutrition and hunger, especially in developing countries. While the world population has doubled in the last 50 years, agricultural land has decreased by 10%. This situation seriously

threatens food security. Agricultural land, which was abundant in the past, is now rapidly disappearing due to concretization and industrialization, creating a serious food problem for future generations. To overcome this problem, solutions such as the spread of sustainable agricultural techniques, the use of genetically modified crops and the reduction of waste should be emphasized.

According to data from organizations such as the World Health Organization (WHO) and the International Labor Organization (ILO), the agricultural sector accounts for a significant proportion of occupational accidents. Especially in developing countries, agricultural workers are at higher risk. Accidents such as tractor overturns, entrapments, and sharps injuries are among the most common types of accidents.

In Turkey, agricultural accidents constitute a significant portion of occupational accidents. This is particularly evident in regions where agriculture is intensive. Although there is some information on occupational accidents in the agricultural sector in the data of institutions such as the Turkish Statistical Institute (TurkStat) and the Social Security Institution (SSI), there are some question marks about the scope and accuracy of these data.

All activities in agricultural production require either labor or agricultural machinery. One of the biggest problems faced by the labor force is the issue of occupational health and safety. There are risks at every stage of production. These risks need to be revealed and different occupational health and safety measures are needed.

For underdeveloped or developing countries the problems related to occupational accidents and occupational safety have to be taken into account. Many reports, analyses and reports have shown that agriculture is one of the most dangerous sectors. In this context, a developing country has to develop and grow its agricultural sector in order to keep its economy alive. The three basic needs of humanity are food, clothing and shelter. Dangerous processes manifest themselves in these areas during this period of time.

As a result of the increasing population in the world, larger agricultural areas are needed to grow crops. However, with the opening of these areas to housing and industrial zones, it is necessary to produce in fewer, limited areas and to meet the nutritional and other needs of a larger population. While agricultural areas have been decreasing over the years, in order to feed the growing population, higher quantities of products are needed from the unit area. Depending on the plant pattern and diversity, it is provided by the use of different types of machinery. During the use of machines, there is an increase in accidents that occur in agriculture during production.

Agricultural tools and machinery used during agricultural activities constitute the main cause of accidents in this sector. Tractors remain the

most important power source for agriculture. Since many tools and machines used in agriculture are driven by the tractor, the tractor is an indispensable tool for the application of modern agriculture and techniques. Technological changes and developments in agriculture are taking place rapidly like other sectors. Technological advances are not only related to the power of the tractor and the torque it develops, but also to occupational safety measures to provide safe driving and control systems for the driver. In addition to digital agricultural systems, autonomous vehicles will soon appear in agricultural areas.

Agriculture is a natural process in all seasons. It must be carried out in all weather conditions, the materials such as soil, plant, fertilizer, irrigation, chemical pesticides, etc. that are processed vary, and the driver must create a comfortable and safe working environment for the operator.

Population in the world and in Turkey has been increasing over the years, hence the need for food has also been increasing. This situation causes agriculture to become a strategic sector in terms of both nutrition and employment.

By ensuring occupational safety in agricultural work, accidents can be reduced. By increasing the expected efficiency of the machine and reducing the lost time, it will be possible to reduce the economic cost of the work. If occupational safety is ensured, it is possible to reduce accidents, reduce lost time and thus increase machine efficiency. If precautions are taken, damage to the machine will be prevented as well as the safety of the driver's life safety.

There will be many reasons why accidents and occupational diseases in agriculture will occur over time. It is likely to increase accidents, especially the tractor, which is used as the main power source in agriculture, and the use of the power taken from the tractor in the operations of the agricultural machinery connected to it. Most of the accidents in agriculture are caused by the tractor, and about half of them are accidents caused by tractor overturning. We can clearly see this from the studies of many researchers in these fields (Yıldırım and Altuntaş, 2015*;* Özkan and Dilay, 2020).

Research shows that accidents are usually caused by carelessness and ignorance. In order to overcome this deficiency, the users and operators using these machines must be well trained. The rapid development of technology also manifests itself in these areas. The use of equipment and complex designs, the tendency of these operators and their lack of practice make the adaptation process difficult.

Many studies have been conducted in this field, and the common result is that working with tractors and agricultural machinery connected to tractors still continues to be an important risk (Peker and Özkan, 1994*;* Alçayır, 2018*;* Akbolat, 2007*;* Tiwari et al., 2002).

If an operator takes good care of the machine he is using, he fulfils

the safety requirements to a great extent. Otherwise, if there is insufficient maintenance and at the same time the knowledge and skills of the driver are not sufficient, he is always likely to face danger. Uncontrolled behavior while operating a tractor is the main cause of many fatalities.

A training on a machine allows to learn all the components of the machine and to form a habit, but with different machines, all control components may not work in the same way and in the same direction. For this reason, the operation of a new machine by handing it over to an operator who has no experience and does not know it well may have risks and dangerous aspects in terms of life and property safety.

Damage to a used machine due to an accident, repair and maintenance costs, as well as the wage costs to be spent when we have to do the same work with another machine, taking into account the wage costs to be spent, may adversely affect the operating efficiency due to affecting the balance of operating income and expenses.

In order to make accurate analyses of the causes of accidents, it is necessary to investigate and analyse both accidents and non-accident conditions. Only with a two-sided perspective can more realistic steps be taken.

In the agricultural sector, which faces occupational accidents and occupational diseases, the rate of accidents is in the first place together with the mining sector and the construction sector. This situation continues to be an important problem all over the world. At the beginning of the causes of occupational accidents in agriculture, the fact that agricultural activities take place in open lands, the low level of education of the employees, the lack of adequate working environment and environment, nutrition and resting environments, and the obligation of employees to work in more than one job depending on the economic situation (Gügerçin and Baytorun, 2018). Agricultural activities should not only be thought of activities such as sowing, planting, fertilizing or irrigation in the open air. In addition, it is seen that those working in warehouses, warehouses, storage of agricultural products, transportation and transmission facilities, and workshops where processing is carried out are also in the serious risk group.

POSSIBLE WORK ACCIDENTS IN AGRICULTURE

Machine-related accidents: Tractor overturning, jamming, crushing, falling, misuse, lack of timely maintenance, lack of adequate service facilities for repair, uncontrolled and careless use of equipment (Figure 1). Inadequate maintenance and repair of the existing machines in the machine park.

Figure 1: Accident Occurring as a Result of Tractor Overturning (Anonymous,2022).

Accidents caused by falls: It can be seen in fruit picking, while creating haystacks, during work on slippery surfaces, while carrying live animals on agricultural carts and tractors. As a result of falls, tripping or entanglement in moving parts, crushing, cutting, jamming in free rotating parts; as a result of unsafe work clothes, it can lead to limb losses and injuries due to wraps (Figure 2).

Figure 2: Personnel Transportation by Agricultural Trolley and Accident Risks Due to Falling (Özay, 2022).

Accidents related to animals: Animal attacks, animal bites, kicking and crushing during milking processes, and other risks in the fight against pests. The situation caused by animal risks will bring dangers in the form of kicking, biting, squeezing, hitting a hard place during the obligation to work close to animals. On the other hand, it causes the transmission of pests such as viruses, bacteria and parasites from animals to workers through contact or respiratory tract. First aid personnel and other personnel should undergo training against possible animal bites, stings and attacks.

Accidents in agricultural control: A number of chemicals used for the cultivation of agricultural products will sometimes cause poisoning and sometimes provide the grounds for the development of cancer. The effects of hazardous gases such as veterinary drugs, exhaust fumes from vehicles, methane, ammonia, which are emitted or accumulated in the environment in barns and poultry houses, on living things, employees should act more carefully. Risks arise as a result of incorrect application of pesticides on the plant, direct contact of pesticides with the body and skin, poisoning by respiratory tract, and not applying them at the appropriate time in accordance with environmental conditions. Wounds and bruises on the respiratory system and skin are caused by the effect of pesticides and fertilizers used in agricultural control.

Accidents caused by environmental factors: Long periods of working in hot and cold environments, the danger of heat stroke and frostbite, the sun's rays affecting the operator, outside precipitation, dust particles and foreign objects in use with a tractor without a cab, high amounts of noise level in the working environment reduce working efficiency. Especially with the increase in temperatures in the summer months, it is imperative to fight in a timely manner to eliminate insects that carry and transmit microorganisms such as mosquitoes, houseflies, fleas, ticks, viruses and parasites, which cause an increase in temperatures.

RECOMMENDATIONS TO PREVENT WORK ACCIDENTS

Training on safety: Training and demonstration work on occupational safety of employees in this agricultural activity, revealing the risks on tools and machines, providing technological training to tool and machine manufacturers, providing information studies by occupational safety and experts during periods when activities decrease, protecting young workers in the agricultural sector or keeping them away from these areas, revealing suitable environments for improving the occupational safety and social life of seasonal agricultural workers, ensuring the occupational safety of women workers

Personal protective equipment: Provision of work clothes

suitable for work, helmet, gloves, work shoes, mask and ear plugs should be provided.

Ergonomic machine design: The agricultural sector is an area where people are needed the most in the production process. As in every labor- demanding line of work where man-made features and natural conditions are intertwined, it is also needed in the agricultural sector. Every process and design made in ergonomic terms should be carefully implemented by machine manufacturers in every aspect. Employees in the agricultural sector work for long periods of time and in positions that are not suitable for their body condition. The personal characteristics of the employees such as gender, age, education level, physical characteristics, temperament, attitudes and behaviours vary. Working tools and mechanical tools should be below shoulder level, and ergonomically appropriate handles and accessories should be available for the hand tools used. Excessive exposure to vibration in manual work leads to impaired blood circulation, nerve, bone and joint disorders, and as a result, health problems related to musculoskeletal-circulatory systems.

Tractors with cabins or safe steel construction against tipping over provide convenience for the driver. Environmental conditions such as dust, noise, rain, etc. are important for driver comfort. Designing equipment with these features will offer advantageous sales opportunities for manufacturers.

It is a fact that noise and vibrations caused by heavy loads, tools and machinery will cause health problems for workers in the long term. It is not possible to intervene quickly and effectively in case of health problems that may occur. If the necessary measures and precautions are taken and the training of the employees is done in a practical way as well as theoretical knowledge, it will be possible to eliminate the risks that may occur ergonomically.

Machine maintenance: Agricultural tools and machinery should be checked regularly according to the working hours and conditions; maintenance should be carried out without interruption and maximum sensitivity should be shown to other measures for a safe working environment. If necessary, maintenance and repair catalogues should be made if it is possible to be done with the facilities of the enterprise, otherwise support should be obtained from technical services.

Safety of the work environment: Work areas should be kept neat and tidy, made of materials that will not cause slippery floors, appropriate lighting apparatus for regional lighting, sufficient amount of light should be provided.

Emergency Action Plans: The planning to be made in all kinds of emergency situations should be clearly prepared and should be within the necessary legislation for informing employees and preparing emergency action plans.

Safe use of pesticides: When using pesticides, the instructions on the label should be strictly followed, personal protective clothing should be worn and respirators and apparatus should be used when spraying.

Reducing the physical load: Correct techniques should be used when lifting heavy loads, and mechanical tools should be preferred when labor is required.

Regular Health Checks: Employees should undergo regular health checks at regular intervals and if health problems are detected early, the treatment process should be started without delay. In this context, early detection of health problems helps the treatment to be done in a short time.

CONCLUSION

The fact that accidents occur in areas that are difficult to control and far from supervision makes the reduction process difficult. Occupational safety in rural agricultural work allows workers to work in a healthy and safe environment. It reveals practices that will prevent damage to the devices and tools used here. The costs of accidents that may occur due to imprudence, carelessness and negligence can be great. More than material losses, moral losses cause negativities in people. No matter how expensive a damaged machine is, it can be replaced. However, it is never possible to replace human and human health. In this respect, it is extremely important to strictly follow the rules set for occupational safety in order not to encounter irreparable sad developments in the future.

People and employees who will use agricultural tools and machinery should receive training and learn fully and completely from the practices related to the use of tools and machinery. Minors, undocumented and unqualified persons should not use agricultural tools and machinery. Care should be taken to ensure that young children are not involved in agricultural activities. When evaluated in terms of gender, age, education and demographic variables, it can be said that the perception of occupational hazards of agricultural workers have changed.

It is an important process to take steps to avoid possible risks, to identify potential hazards and analyse risks, and to evaluate the measures to be taken by making risk assessments. With the harmonious work between the business owners or employer, occupational health and safety specialist, occupational health and safety specialist, workplace physician, other assistant health personnel and other employees, the success in agricultural activities will contribute to occupational safety management (Özkan and Dilay, 2019).

Agricultural machinery parking areas should be established in places where agricultural activities are common. Not only will control be ensured within security, but also storage and protection will be easier. On

the other hand, outside of seasonal activities, these areas will be protected in closed areas, while their depreciation period and service life will increase. Maintenance or repair expenses will be carried out by the service or technical staff to be kept in these places. In addition, the use of common machinery will enable more work and utilization from one machine. While creating a planning consciousness of the farmers in the region, it will stimulate the instinct of unity and solidarity among the communities in this region, and will facilitate the behavior of acting together.

It is important for each enterprise to reveal its own occupational safety risk analysis according to the activities and characteristics of the enterprises. The authority and responsibility for the implementation of risk analysis and implementation in enterprises comes primarily from business managers and employers. Employees in these activities should make maximum effort and effort to fulfil these practices and responsibilities. As a result; it should not be forgotten that most work accidents that occur in agricultural enterprises can be avoided and can be prevented with simple measures.

In enterprises with agricultural lands, the level of knowledge, personal protective measures and attitudes of people with high perceptions about the measures to be taken against accidents and high-income levels increase.

REFERENCES

Akbolat, D. (2007). Work Safety. SDU. Faculty of Agriculture, Department of Agricultural Machinery. (Unpublished lecture notes).

Alçayır, A. (2018). Determination of Occupational Accidents Caused by Tractors and Agricultural Machinery in Konya Province umra District Agricultural Enterprises. Master's Thesis. Selcuk University. Institute of Science. Konya.

Anonymous, (2022). Person Under Tractor Died in Konya. Retrieved from https://www.karamanhabercisi.com/konyada-traktorun-altinda-kalan-kisi-oldu- 45449h.htm on November 10, 2024.

Güğerçin, Ö and Baytorun, A.N. (2018). Occupational Accidents in Agriculture and Necessary Measures. Çukurova Journal of Agricultural Food Sciences, 33(2), 157- 168.

Özay, S. (2022). Occupational health and safety risks in agriculture are very diverse. Retrieved from http://www.turktarim.gov.tr/Haber/788/tarimda-is-sagligi-ve- guvenligi-riskleri-cok-cesitli on November 13, 2024.

Özkan, A and Dilay, Y. (2019). Risks in Agricultural Sector. Journal of Multidisciplinary Engineering Science Studies (JMESS) 5 (12), 2953-2955.

Özkan, A. and Dilay, Y. (2020). Evaluation of Tractor and Agricultural Machinery Accidents in Agricultural Production in Karaman Province. Journal of Agricultural Machinery Science, 16(1), 32-39.

Peker, A. and A. Özkan, (1994). Evaluation of tractor and agricultural machinery accidents in Karaman region between 1973-1993. *Paper presented to the 15th National Congress on Agricultural Mechanization.*

Tiwari, P. S., Gite, L.P., Dubey, A.K. and Kot, L.S. (2002). Agricultural Injuries in Central India:Nature, Magnitude, and Economic Impact. Journal of Agricultural Safety and Health, 8(1), 95-111.

Yıldırım, C. and Altuntaş, E. (2015). Evaluation of occupational accidents caused by the use of tractors and agricultural machinery in Tokat province in terms of occupational safety. Journal of Agricultural Faculty of Gaziosmanpaşa University (JAFAG),32(1), 77-90.

Household Predictions with Multiple Regression Machine Learning Models

Zeydin PALA[1]

1- Doç. Dr.; Muş Alparslan Üniversitesi Mühendislik –Mimarlık Fakültesi Yazılım Mühendisliği Bölümü. z.pala@alparslan.edu.tr ORCID No: 0000-0002-2642-7788

ABSTRACT

This section summarizes a research of predicting housing price using various machine learning models through the use of Boston Housing Dataset. Prediction of housing prices has significance for urban planning and economic development. The dataset contains the information regarding house prices from 1970s to 1980(s), in which one variable is management response (MEDV) while other 13 variables are attributes of input model and inputs. A comparison of the performances of different regression models, Linear Regression, Generalized Linear Models (GLM), Penalized linear regression (GLMNET), Classification and Regression Trees (CART), Nadam supports vector machines (SVM) and KNNs vedned to k-nearest neighbors. The results suggest that we cannot hurt the model performance by removing some of features highly correlated with each other. This study adds to the contribution of previous works in predicting housing price through comparisons of models as well as analysis over feature selection significance.

Keywords – Housing Price Forecasting, Machine Learning Models, Boston Housing Dataset, Regression Analysis, Feature Selection.

INTRODUCTION

In recent years, housing price prediction has emerged as a prominent field in data science, drawing attention from various disciplines due to its critical importance in urban planning, real estate, and economic development. The Boston Housing Dataset offers itself as a perfect case study for the modelling and the understanding of variables that affect prices of housing. These data sets contain many socioeconomic and environmental variables related to the Boston, Massachusetts housing market, as collected by the U.S. Census Service, and frequently used as a benchmark dataset. The dataset, originally published by Harrison and Rubinfeld (1978) and used in a seminal paper on hedonic pricing (Harrison Jr. 1978), consists of 506 observations and 14 core variables, including rates of per capita crime, property tax, and employment centers. The target variable, MEDV (Median Value of Owner-Occupied Homes), is the median value of housing unit in $1000, so the MEDV is a useful measure for housing market analysis.

In the present study, we attempt to predict the MEDV by applying multiple regression. In particular, we use MEDV as the response variable and the other 13 features as the predictor in different regression models. Our methodology investigates a variety of algorithms to search the best model for housing price prediction, and this includes both purely traditional and more sophisticated machine learning algorithms (Pala and Şana 2020). We consider Linear regression (LR), Generalized linear regression (GLM), Penalized linear regression (GLMNET), Classification and regression trees (CART),

Radial basis function Support Vector Machines (SVM), and Nearest neighbors (KNN). Each of these models has its own advantages and caveats, ranging from ease of interpretability and simplicity to robustness in non-linear spaces and flexibility. Through the comparison among these models, we aim to discover the best methods for precise estimation of housing price, which can make important contributions to the problem of understanding the factors contributing to the value of housing for urban areas.

MATERIAL AND METHODS

Dataset

The Boston Housing Dataset is based on data collected by the U.S. Census Service on housing in the Boston, Massachusetts area. This dataset, obtained from the StatLib archive, has been used to model and make predictions on a variety of topics, most notably nitrogen oxide levels (nox) and median housing price. The dataset includes a total of 14 variables, including crime rate per capita (CRIM), median age of housing (AGE), distance to Boston employment districts (DIS), student-teacher ratio (PTRATIO), and MEDV (median housing value). The original order of this dataset, which contains a total of 506 observations, is defined as mysterious. The data was first discussed in a study by Harrison and Rubinfeld in 1978, Hedonic prices and the demand for clean air.

Models

Linear Regression (LR) is one of the most basic and popular models for predictive analysis, especially when the relationship between the predictor and outcome variables is assumed to be linear. The main task of LR is to search the optimal straight line (the regression line in which it is minimized, the difference of observed values and simulated ones). This is realized estimating the coefficients of each predictor variable in the data set, which quantify the effect size and direction of the relationship between each predictor and the target variable. LR is highly desirable for its own simplicity, interpretability, and computational advantage, thus becoming a perfect starting model to regress an outcome. But, it is based on the linear relationship and may not work if the data contains the complex, non-linear pattern. Despite this limitation, Linear Regression remains a powerful tool in data analysis and is often used as a foundational model before exploring more sophisticated methods.

a random component that specifies the distribution of the response variable, a systematic component that defines a linear predictor (a linear combination of the input features), and a link function that connects the linear predictor to the expected value of the response variable. This flexibility enables GLMs to capture non-linearity between variables and maintain

interpretability, for example, making them popular in disciplines such as epidemiology or finance.

Penalized Linear Regression, as implemented by GLMNET, is a very efficient extension of linear regression that includes regularization to enhance model performance, especially when multicollinearity or high-dimensionality issues exist (Lu et al. 2017). GLMNET combines Lasso (L1 regularization) and Ridge (L2 regularization) techniques, allowing it to perform variable selection and shrinkage simultaneously. This combination method keeps the absolute value of the model coefficients under control, preventing overfitting by penalizing large coefficient values and performing well on the complex datasets with large number of predictors. In GLMNET, the L1 and L2 penalty terms can be fine-tuned by the tuning parameter, which allows one to balance the tradeoff between sparse models (with few non-zero coefficients) and models where more predictors are retained. Through bias and variance balancing, GLMNET can generally yield more stable and interpretable models than linear regression, even if some predictors have little or no predictive effect on the response.

Classification and Regression Trees (CART) is a decision tree algorithm for both classification and regression purposes (Anon 2004). In CART, data is recursively segmented into data subsets depending on the feature values, which generates a tree-like structure, where each internal node is a decision on a feature, each branch is a result of the decision, and each leaf node is a forecasted result. In the case of regression problems, CART is designed to reduce as much as possible the variance within each subset, and hence build a model predicting continuous values, e.g., housing prices, by averaging over the values in each leaf. This approach is easy to use and also is understandable, because the final decision tree represents visually in what way the features lead to prediction. Nevertheless, CART models can be also subject to overfitting, in particular if the tree is long, and it learns the noise in the data instead of patterns. Pruning methods and maximum tree depth setting are frequently applied to avoid overfitting, thereby making CART an efficient and flexible technique for predictive modeling.

Support Vector Machines (SVM) are efficient supervised machine learning algorithm, which can be used for classification and regression with the ability to perform its task in high dimensional spaces and high robustness to overfitting (Kavitha, Varuna, and Ramya 2017). SVMs work by identifying the hyperplane that best discriminates data points of different classes (in classification) or by fitting a model which in return optimizes the margin to the left/right of the hyperplane (in regression). In regression problems, e.g., predicting housing prices, the SVM uses a method called Support Vector Regression (SVR), which strives to establish the data within a prespecified margin of tolerance while at the same time minimizing the prediction errors outside such a margin. Various kernel functions, such as radial basis function (RBF), SVM are able to learn highly non linear relationships from data, and

thus, it is becoming a very general choice that is applicable to data with rich patterns. In the Boston Housing Dataset, SVM with an RBF kernel can also be used to learn the non-linear relationship between housing price and explanatory variables, and may increase performance over linear models.
The k-Nearest Neighbors (KNN) algorithm is a basic but effective scheme that has been extensively employed for classification and regression tasks (Ataş, Yeşilnacar, and Demir Yetiş 2022). In the regression scenario, KNN estimates the value of a target variable by identifying the "k" nearest neighboring data points to an input data point and computing the average value of the target variable for these neighbors. The closeness or similarity between data points is typically determined by calculating the distance—often Euclidean distance—in the feature space. The non-parametric nature of KNN is one of its major advantages, as it does not require any assumption about the structure of the data, and therefore is able to accommodate complex relationships. However, KNN can be computationally intensive with large datasets, as it requires calculating distances between each data point and all others in the dataset. Moreover, the value of "k" has a major impact on model performance, because, small "k" can result in high variance (overfitting), whereas large "k" can oversmooth the predictions.

RESULTS AND DISCUSSION

The graph showing the relationships between the inputs of the model is given in Figure 1.

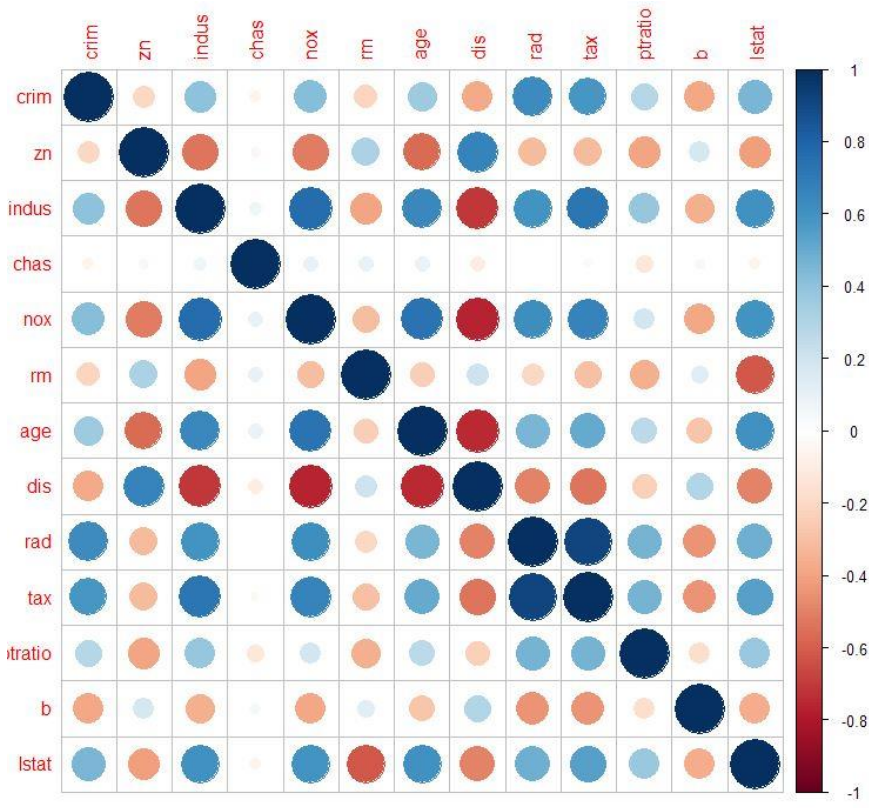

Figure 1: Relationships of multiple attributes to be used for regression inputs

Figure 1 displays a correlation matrix for the input variables in the Boston Housing Dataset. The correlation coefficient values, ranging from -1 to 1, indicate the strength and direction of relationships between variables (Bashir et al. 2020). Strong positive correlations (values near 1) suggest that two variables increase together, such as the positive relationship between rad (proximity to urban highways) and tax (property tax rate). This could mean higher property taxes in locations along highways. On the other hand, high negative correlations (values close to -1), such as between dis (distance to business districts) and nox (nitrogen oxide concentration), indicate that air pollution diminishes with increasing distance from business districts. Variables with poor correlation, such as chas (distance to Charles River), are not the basis of strong linear relationships in the dataset.

Figure 2 shows histograms of some attributes of the Boston Housing Dataset, showing the distribution of each variable. These plots play a critical role in determining the data distribution, skewness and presence of outliers, along with the range of values observed for each variable. For instance, variables with skew distributions, such as tax or crim, reflect very high tax and crime rates in certain areas, but affect model predictions. Learning these

distributions can be used to guide preprocessing steps, e.g., normalization or transformation, in order to optimize the model.

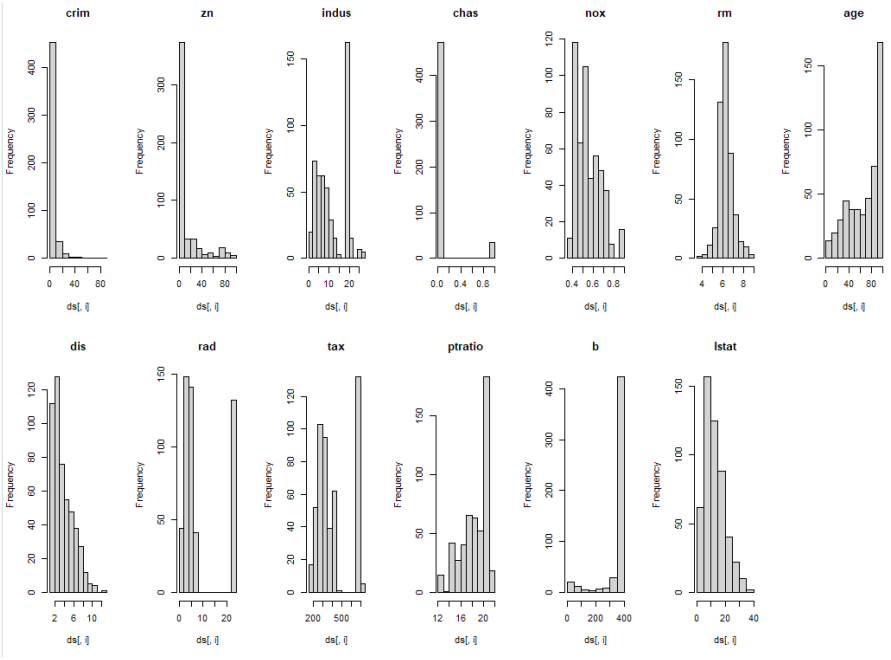

Figure 2: Histogram plots of multiple attributes

Table 1: Model r-squared performance values

Rsquared

	Min.	1st Qu.	Median	Mean	3rd Qu.	Max.	NA's
LM	0.4912340	0.6978100	0.7240945	0.7338875	0.8099977	0.8542673	0
GLM	0.4912340	0.6978100	0.7240945	0.7338875	0.8099977	0.8542673	0
GLMNET	0.4815491	0.6977739	0.7257605	0.7347213	0.8152817	0.8604520	0
SVM	0.5619891	0.8168470	0.8549359	0.8455496	0.8989160	0.9555370	0
CART	0.4611137	0.7442840	0.8056596	0.7818150	0.8520462	0.9301942	0
KNN	0.4526323	0.7460117	0.7984230	0.7795499	0.8400909	0.9159450	0

Table 1 presents the R-squared values for various regression models used to predict the median value of owner-occupied homes (MEDV) in the Boston Housing Dataset. R-squared values measure how well each model explains the variance in the target variable, with higher values indicating better model fit. The table likely includes models such as Linear Regression (Pandis 2016)(Kavitha et al. 2017), Generalized Linear Models (GLM), Penalized Linear Regression (GLMNET), Classification and Regression Trees (CART), Support Vector Machines (SVM), and k-Nearest Neighbors (KNN) (Ataş et al. 2022). A comparison of these values provides insight into each model's

performance, highlighting models that may be better suited for accurately predicting housing prices based on the features in the dataset. For example, models with higher R-squared values, like SVM or GLMNET, demonstrate strong predictive power, while lower values may suggest limitations in capturing the target variable's variability.

The bar chart in Figure 3 presents the R-squared values for various models used to predict housing prices in the dataset. R-squared values indicate the proportion of variance explained by each model, with higher values suggesting better predictive performance. Models such as Support Vector Machines (SVM) and Penalized Linear Regression (GLMNET) might display higher R-squared values, implying strong predictive capabilities on this dataset. By comparing models, the chart helps identify the best-suited algorithms for housing price prediction based on R-squared, reflecting each model's fit and performance.

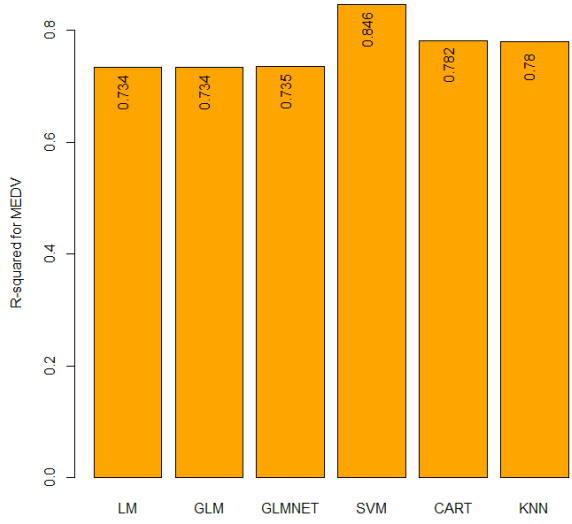

Figure 3: Bar charts of model r-squared metric values

Feature Selection

Indus, nox, tax and dis features, which have high correlations among themselves, were removed and the performance values were re-examined.

In this case, it was observed that the model performances were reduced. It is clearly seen that the removed related attributes contribute to the accuracy of the models.

Table 2: Model r-squared performance values after removing associated attributes

Rsquared	Min.	1st Qu.	Median	Mean	3rd Qu.	Max.	NA's
LM	0.4164673	0.6606252	0.6891731	0.6974544	0.7744946	0.8464772	0
GLM	0.4164673	0.6606252	0.6891731	0.6974544	0.7744946	0.8464772	0
GLMNET	0.4113688	0.6591535	0.6888627	0.6980229	0.7771541	0.8470223	0
SVM	0.5235349	0.7600572	0.8234906	0.8022292	0.8632377	0.9256725	0
CART	0.4765139	0.7348246	0.7981384	0.7790978	0.8536393	0.9289113	0
KNN	0.5167588	0.7749755	0.8168219	0.7974873	0.8443361	0.9019421	0

Table 2 shows the R-squared values of the same models after removing highly correlated features (indus, nox, tax, and dis) from the dataset. The lower R-squared values observed in this table indicate a decrease in model performance due to the exclusion of these attributes. Despite their high correlations, these features evidently contribute useful information for predicting MEDV. This suggests that even correlated features can play a significant role in capturing housing price variance, and removing them may lead to underfitting. Table 2, therefore, underscores the importance of a balanced approach in feature selection, where the potential predictive value of correlated features is carefully evaluated before exclusion.

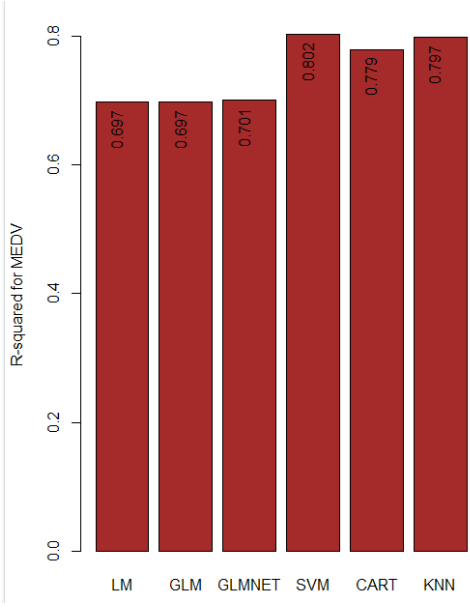

Figure 4: Bar charts of model r-squared metric values after removing associated attributes

Figure 4 bar chart illustrates the R-squared values of the models after removing highly correlated features (indus, nox, tax, and dis). The decrease in

R-squared values suggests that these attributes, although correlated, contribute valuable information to the predictions. Their removal likely reduced the model's ability to capture variance in housing prices, highlighting the importance of carefully considering feature selection. This analysis emphasizes that even correlated features can be valuable in predictive models, and their exclusion may negatively impact performance.

CONCLUSIONS

The study makes an important contribution by using the Boston Housing Dataset to evaluate multiple machine learning models for predicting housing prices. Given the relevance of accurate housing price predictions in urban planning, real estate, and economic policy, this research fills a vital gap by comparing traditional and advanced regression techniques, including Linear Regression, Generalized Linear Models, Penalized Regression (GLMNET), Classification and Regression Trees, Support Vector Machines, and k-Nearest Neighbors. Through model comparison, the study identifies the algorithms that best capture the complex relationships between socioeconomic and environmental factors affecting housing values. By examining both the predictive power (using R-squared metrics) and the impact of feature selection, this research offers insights into balancing model complexity and interpretability, thus advancing methodologies for data-driven housing market analysis. This study's findings contribute to the literature by clarifying the predictive strengths of various models and emphasizing the importance of including correlated features to avoid underfitting.

REFERENCE

Anon. 2004. *Classification and Regression Trees (CART) Theory and Applications*.

Ataş, Musa, Mehmet İrfan Yeşilnacar, and Ayşegül Demir Yetiş. 2022. "Novel Machine Learning Techniques Based Hybrid Models (LR-KNN-ANN and SVM) in Prediction of Dental Fluorosis in Groundwater." *Environmental Geochemistry and Health* 44(11):3891–3905. doi: 10.1007/s10653-021-01148-x.

Bashir, Muhammad Farhan, Benjiang Ma, Bilal, Bushra Komal, Muhammad Adnan Bashir, Duojiao Tan, and Madiha Bashir. 2020. "Correlation between Climate Indicators and COVID-19 Pandemic in New York, USA." *Science of the Total Environment* 728:138835. doi: 10.1016/j.scitotenv.2020.138835.

Harrison Jr., David;Rubinfeld, L. Daniel. 1978. "Hedonic Housing Prices and the Demand for Clean Air." *Journal of Environmental Economics and Management* 5(1).

Kavitha, S., S. Varuna, and R. Ramya. 2017. "A Comparative Analysis on Linear Regression and Support Vector Regression." *Proceedings of 2016 Online*

International Conference on Green Engineering and Technologies, IC-GET 2016 1–5. doi: 10.1109/GET.2016.7916627.

Lu, Miao, Jianhui Zhou, Caitlin Naylor, Beth D. Kirkpatrick, Rashidul Haque, William A. Petri, and Jennie Z. Ma. 2017. "Application of Penalized Linear Regression Methods to the Selection of Environmental Enteropathy Biomarkers." *Biomarker Research* 5(1). doi: 10.1186/s40364-017-0089-4.

Neuhaus, John, and Charles Mcculloch. 2011. "Generalized Linear Models." *Wiley Interdisciplinary Reviews: Computational Statistics* 3(5):407–13.

Pala, Zeydin, and Musa Şana. 2020. "Attackdet: Combining Web Data Parsing and Real-Time Analysis with Machine Learning." *Journal of Advances in Technology and Engineering Research* 6(1):37–45. doi: 10.20474/jater-6.1.4.

Pandis, Nikolaos. 2016. "Linear Regression." *American Journal of Orthodontics and Dentofacial Orthopedics* 149(3):431–34. doi: 10.1016/j.ajodo.2015.11.019.

Evaluation of Hardness and Corrosion Behavior of An AA 7175 Aluminum Alloy In Sulfuric Acid Environment

Ali DEBIH [*]

1-Department of Mechanical Engeneering/Faculty of Technology, University of M'sila, Algeria
[*](ali.debih@univ-msila.dz)

ABSTRACT

The corrosion of the AA7175 aluminum alloy in different acidity of sulfuric acid solution was studied using weight loss technique and microhardness measurements. The magnitude of corrosion of this metal in PH of (– 0.78, – 0.5, – 0.4 and – 0.12 of solutions of H_2SO_4 was studied for an exposure period of 240 minutes. Weight loss measurements in these pH of acid solutions have shown a higher corrosion resistance for the aged alloy as compared to the as received condition. The study confirmed that the microhardness of the AA7175 aluminum alloy tends to reduce linearly with increasing mass loss. Also, the formation of Mg_2Zn can reduce the corrosion phenomena, the corrosion can be classed as pitting or interganular corrosion.

Keywords – Aluminum, Corrosion, Acidity, Weight Loss, Microhardness.

INTRODUCTION

Aluminum alloys are widely used in structures where a high strength to weight ratio is important [1], Aluminum alloy 7175 is a wrought Al-Zn-Mg-Cu alloy. It is distinguished with maximum strength of all aluminum alloys. It combines good mechanical strength and corrosion resistance. However, it is prone to localized corrosion forms and especially to stress corrosion cracking (SCC). The tendency of this alloy towards localized forms of corrosion depends on the content of alloying elements as well as on mechanical, thermal and thermo-mechanical treatments [2]. 7175 aluminum alloy is typically utilised in applications where improved formability and toughness are required. Used extensively in the aerospace industry, the combination of high mechanical strength, fracture toughness and stress corrosion cracking resistance, makes this alloy suitable for structural aircraft applications. The precipitation hardening of the 7175 aluminum alloy has been achieved by the segregation of GP zones, these are transformed through the intermediate η' phase into the equilibrium phase $MgZn_2$ [3-4]. The maximum strength of the alloys has been obtained in the presence of a mixture of GP zones and η' precipitates in the structure. In the state of maximum strength, the 7175 T71 alloy is prone to SCC and exfoliation corrosion.

Corrosion is the deterioration of a material, usually a metal, because of reaction with its environment. It can be defined as the loss of materials as a result of chemical or electrochemical reaction with the environment. Metal interaction with environment is a process that cannot be disregarded when the issue of corrosion and its effect comes to play. The metal in the combined state tends to revert back to its most stable natural state on

exposure to certain environmental conditions [5-6].Corrosion process has affected a number of industries resulting into loss of weight and damage of many materials.[6].

Aluminum is only homogeneously corroded in a very acidic solution, or in an alkaline solution. The strength and stability of the oxide layer depend on the ambient environment, the composition of the alloy and the microscopic structure of the metal (depending on the heat treatments applied). When 7xxx aluminum alloys are exposed to aggressive acid solution media for pickling, chemical or electrochemical etching, industrial cleaning, they usually lead to loss of weight due to corrosion.[7].

The heat treatment procedure to enhance the mechanical properties of 7XXX aluminum alloys consists of a first solution treatment followed by water quenching. The solution annealing step is encompassed in the temperature range between 510 ºC and 540 ºC" solution annealing step", during the necessary time to dissolve the alloying elements in the aluminum matrix. Next, the solution-annealed and quenched material is once more heated, but at lower temperature which is generally between 120 ºC and 170 ºC" artificial aging step.

In this work the corrosion behavior of 7175 Al alloy submitted to different times was assessed in H_2SO_4 solution with different acidity. It is in this context that different acidity used in industrial application need be assessed and evaluates the corrosion effects in order to determine the best acidity that could be used in pickling or cleaning as thermochemical applications. The present work investigates the corrosion rate of the AA7175 in as received condition and in T6 conditions in different media acidity using optical microscopy, weight loss method and microhardness measurements.

MATERIALS AND METHOD

Material and heat treatment

The material used in current study is an AA 7175 -O aluminium alloy, the bar was machined into round solid specimens with 15 mm diameter and 10 mm thickness, with surface area (SA) of 825 mm^2 and weight of 4,81 Grs. The specimens were heat treated into precipitation hardening (T6 condition). For solid specimens, solution heat treatment was performed at 530 °C for 30 minutes followed by water quenching. Aging treatment was carried at 150 °C for 8 hours. The chemical composition is shown in Table 1.

Table 1. Chemical composition of AA 7175

Element	Zn	Mg	Cu	Fe	Mn	Si	Cr
wt. %	5.35	2.41	1.83	0.33	0.11	0.22	0.13

Corrosive Media Preparation

An acid solution of analytical grade sulfiric acid (38%, 4.2 mol/L and pH of −1). Other solutions were prepared by using distilled water. The acid solutions of required pH of – 0.78, – 0.5, – 0.4 and – 0.12 were prepared by appropriate dilutions. These values were measured using a pH meter as shown in Figure 1.

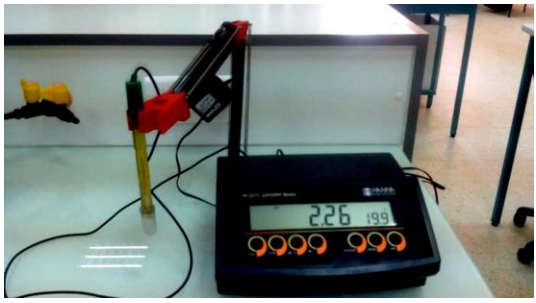

Fig. 1 pH meter, The cell of corrosion test.

Weight loss Measurement

During the weight loss experiments, aluminum specimens in as received and T6 condition were weight (W_1= 4.81 Grs) and suspended completely in the solutions of different acidity. The volume of the solution was kept at 200 ml. The specimens were retrieved after 4 hours and then washed with distilled water, dried with hot air and reweighed (W_2). From the weight loss data, measured using hot precision balance scales, corrosion rate in mg cm^{-2} was calculated using equations 1 and 2.

$$\Delta W = W_2 - W_1 \quad (1)$$

$$\text{Surface Corrosion Rate (SCR) } (mg/cm^2) = \Delta W / SA \quad (2)$$

Micrographic observations

Before optical observation, all specimens in as received and T6 conditions, were prepared using standard metallographic techniques; polishing were carried out using silica carbide paper of 600 and 1200 grit. The etching was done using Keller's reagent (2 mL HF (48%), 3 mL HCl (conc.), 5 mL 63% HNO_3, 190 mL H_2O) for 1 min, the washed and dried samples were observed in *Olompys A13.1013-B* Microscope and some selected photomicrographs were taken.

Microhardness measurements

According to ASTM E 384, the microhardness of the alloy in as received state and after heat treatments was measured on outside surfaces of samples. The materials were tested using microhardness tester type *TUKON 2500*. The studies have been carried out by Vickers method with a load of 0.5 N for indentation time of 15 s with objective (x10).

RESULTS AND DISCUSSION

Macrostructures

From the macro-graphic analysis of Figure 2, the surface morphology of AA 7175 in both conditions present different levels of corrosion are distinguished, and it represents the weight loss as a function of acidity, characterizes by pitting and intergranulaire corrosions, the T6 condition presents a reduced level of corrosion as compared to the as received condition.

Fig. 2 Immersion corrosion test results of AA7175 aluminium alloy in as received and T6 conditions.

Micrographic observations

Figure 3 a and b shows the optical micrograph of polished aluminum specimen surfaces (as references), for the as received and T6 conditions respectively, before immersion into the corrosion medium. According 3a, certain defects were found and it revealed a non-equiaxed microstructure linked to extrusion deformation. The grains of the as received sample were significantly elongated parallel to the extrusion direction with not

homogeneous size of grains. Certain grain sizes measured on the longitudinal plane have a size larger than 78 μm and other grains lower than 45 μm. After heat treatment to T6 condition, a finer and homogeneous and equiaxed microstructure with clear grain boundaries was observed.

Figure 3 c-j shows the optical micrograph of the specimens after removing from the corrosion medium. A lot and sever corrosion sites and pits were observed, these results suggested that H_2SO_4 solution with different pH values can be considered as an aggressive medium that induce corrosion phenomena. Number of pitting corrosion of aluminum generally occurs at pH values close to be neutral.

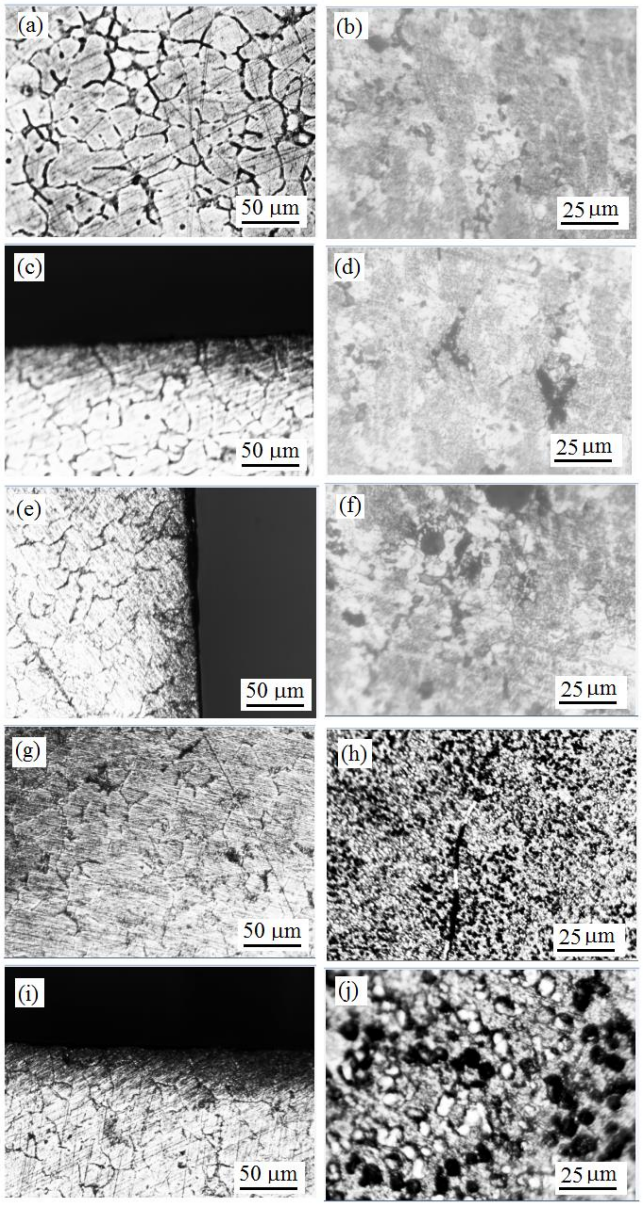

Fig. 3 Microstructure of AA7175 aluminum alloy a) as received condition, b) T6 condition, c) as received pH–0.12, d) T6 pH– 0.12,e) as received pH–0.4, f) T6 pH–0.4, g) as received pH–0.5, h) T6 pH– 0.5, i) as received pH– 0.78, j) T6 pH– 0.78.

Weight loss results

The variation of weight loss was followed at 4 hours timing for different pH variations. The weight loss was calculated in grams as the difference between the initial weight prior to immersion and weight after removal of the corrosion product. Results of weight loss for the AA 7175 for different pH in as received and T6 conditions are given in Table 2. The result from Table 3 confirmed that the weight loss of AA7175 aluminum alloy in H_2SO_4 increased with increase in pH acidity (increase in the additive concentration). This can be explained by the instability of protective film in contact with acid medium due to the interaction that occur between the metal surface and the acid solution, this reaction tend to destroy the metal surface gradually with pH. These results are in good agreement with that of Musa Husaini et al [5]. It was shown that the ageing treatment to T6 condition indicates great influence of chemical composition of the solid solution on the corrosion behavior of the alloy. This can be explained by the presence of intermetallic compounded $MgZn_2$.

Table 2. Weight Loss values of AA7175 aluminium alloy in H_2SO_4

Condition	**Acidity pH**	**Weight loss (10^{-3}) grs**	**Surface Corrosion Rate (SCR) (mg/cm^2)**
AA7175 as received	– 0.12	65	0.0787
AA 7175 T6		58	0.0703
AA7175 as received	–0.4	78	0.0945
AA 7175 T6		73	0.0884
AA7175 as received	– 0.5	95	0.1151
AA 7175 T6		81	0.0981
AA7175 as received	–0.78	109	0.1321
AA7175 T6		98	0.1187

Microhardness measurements

The results obtained from Table 3 shows that the microhardness of aluminum surfaces immersed in H_2SO_4 solution decreased with increase in acidity. The relationship between Vickers micro hardness (HV) and weight loss of the as received condition appears in Figure. 4.

The microhardness of the AA 7175 O decreased by 35.43% for pH= – 0.78 as compared to the microhardness of the base alloy. The reason for this is due to the formation of pitting and cracking sites in the areas of samples.

After ageing, the formation of (Mg_2Zn) can increase the resistance to recrystallization and stabilize the microstructure, the distorted microstructure with the intermittent distribution of sediment at the boundary improved corrosion resistance. We find that the microhardness hardness decreases by

increasing the acidity. These results are in good agreement with results of Qingqing Sun et al [8].

Table 3. Microhardness of an AA 7175 alloy in as received artificially aged corroded in sulfuric acid at various acidity.

Microhardness (HV)		
Acidity	**AA 7175 as received**	**AA 7175 T6**
Without immersion	101	198
pH – 0.12	94	194
pH – 0.4	87	191
pH – 0.5	80	188
pH – 0.78	66	185

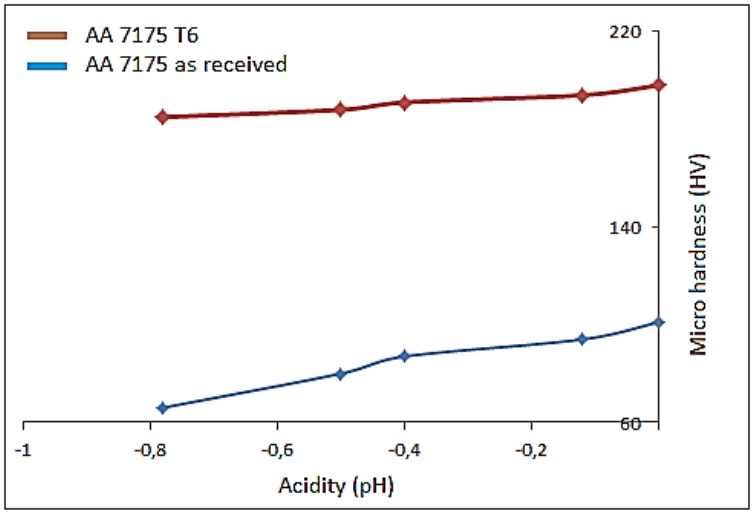

Fig. 4 Variation of Vickers microhardness of an AA 7175 aluminium alloy immersed in sulfuric acid at different acidity.

CONCLUSION

Based on the results of weight loss measurements conclusions are drawn in this study;

- 7175 Aluminum alloy is highly corroded in sulfuric acid solutions.
- The acidity increase leads to increase in rate of corrosion.
- The microhardness of the AA7175 aluminum alloy tends to reduce linearly with increasing mass loss.

- Weight loss of the 7175 aluminum alloy at as received state is higher than those of the alloy at T6 condition.
- Ageing treatment can reduce the effect of acidity on the weight loss of the AA7175 aluminum alloy, which means better resistance to pitting corrosion of the aluminum alloy in the T6 condition.

REFERENCES

[1] M. S. Kaiser and S. Dutta, *COMPARISON OF CORROSION BEHAVIOUR OF COMMERCIAL ALUMINIUM ENGINE BLOCK AND PISTON IN 3.5% NACL SOLUTION*, (MSEJ), Vol. 1, No. 1, September 2014

[2] B. JEGDIĆ, B. BOBIĆ, B.O. GLIGORIJEVIĆ, *Corrosion properties of an aluminium alloy 7000 series after a new two-step precipitation hardening*, ZAŠTITA MATERIJALA 55 (2014) broj 4

[3] M.B. Kannan., P.B., V.S.Srinivasan Raja, *Stress corrosion cracking (SCC) of aluminium alloys, in Stress corrosion cracking, Theory and practice*, Edited by: Raja V.S., and Shoi T., Oxford: Woodhead Publishing 2011

[4] G.S. Peng, K.H. Chen, S.Y. Chen, Fang H.C. *Influence of dual retrogression and re-aging temper on microstructure, strength and exfoliation corrosion behavior of Al–Zn–Mg–Cu alloy*, Transactions of Nonferrous Metals Society of China, 22 (4), pp. 803-809. 2012

[5] M. Husaini, B.Usman , M. B. Ibrahim, *Evaluation of corrosion behaviour of aluminium in different environnement*, Bayero journal of pur and applied sciences, 11(1): 88-92. 2018. http://de.doi.org./10.4311/bajopas.v11i1.15s

[6] K. O. Ajanaku, O. Aladesuyi, C.O. Ajanaku, E.A. Adedapo, A.A. Akinsiku and F.E. Sodiya, *Adsorption properties of Azadirachta indicia extract on corrosion of Aluminium in 1.85 M Hydrochloric acid. Journal of International Association of Advanced Technology and Science.* **16:** *261-173.* 2015

[7] JNO. Ezeugo, OD. Onukwuli, M. Omotioma, *Inhibition of Aluminium Corrosion in 1.0 M HCl Using Picralima nitida Leaves Extract*, Der Pharma Chemica, 2018, 10(S1): 7-13

[8] Qingqing Sun, Jing He, Jiabo Chen, Chunhong Chen, Xiaokai Guo, Fahe Cao and Shuai Wang, *Hardness and corrosion behavior of an Al-2Mn alloy with both microstructural and chemical gradients*, npj Materials Degradation (2022) 6:64 ; https://doi.org/10.1038/s41529-022-00274-w

Low Speed Impact Damage Response of Hybrid Fiber Fabric Reinforced Glider Wing

Esat KAHRAMAN[1]

Mustafa TAŞYÜREK[2]

1-Selçuk University Institute of Science and Technology/Konya, estkhrmn@gmail.com,
2-Selcuk University, School of Civil Aviation, 42250, Selcuklu/Konya, Turkey. mtasyurek@selcuk.edu.tr

ABSTRACT

Lightweight glider-type aircraft, as well as drones and mini model airplanes, which have seen increased commercial and recreational use in recent years, are predominantly manufactured from composite materials. All types of aircraft, from small-scale model airplanes to large passenger planes, require weight advantages. Contributing factors to this requirement include range, fuel consumption, and cost. Material strength can be enhanced through various methods, one of which is the use of composite structures. Compared to metals, composite materials are more susceptible to impact damage. In small-scale commercial vehicles, plastic or composite-based support or coating materials are among the best candidates to achieve weight reduction, which is critical for the strength-to-weight ratio.

This study will investigate the impact damage behavior of honeycomb + fiber composites produced in different configurations, specifically for use in commercial and recreational aircraft. The experimental results obtained, along with damage area analyses and unique graphical interpretations, will determine which type of sample may respond more favorably to impacts at various energy levels. In the study, low speed impact response was revealed as a result of changing the reinforcement order with glass and carbon fibers. Under the effect of low-speed impact, force, displacement and energy data and graphs of all samples were obtained and original inferences were made. In general, it has been determined that fiber stability and high carbon fiber content give more positive results.

Keywords: Aircraft Wing/Body, Low Speed Impact, Stacking Sequence, Carbon/Glass Fiber, Composite Aircraft, Glider.

INTRODUCTION

The term 'glider' has entered the Turkish language from the French word 'Planeur.' In French, it refers to 'gliding through the air' or 'covering distance by gliding.' The International Aeronautical Federation defines a glider as a 'heavier-than-air, unpowered aircraft capable of gliding in the air by generating lift through its fixed-wing structure' [1]. A glider is a motorless aircraft similar to an airplane, which utilizes air currents for flight. According to another definition, a glider is a 'heavier-than-air, unpowered aircraft capable of gliding in the air by generating lift through its fixed-wing structure.' The wing structures of gliders are designed to be much longer than those of powered aircraft, resulting in greater lift generation. Furthermore, as they lack components such as motors and propellers that would increase aerodynamic drag, gliders exhibit lower aerodynamic drag coefficients. In modern gliders,

composite materials are increasingly being used to reduce weight, enabling more efficient manufacturing [2].

Composite materials are materials formed by the combination of two or more organic or inorganic substances without dissolving into each other, resulting in a new material with distinct structural properties compared to the individual constituents. With advancements in technology, the use of composite materials has been increasing in recent years. These materials are designed by combining at least two different materials to achieve the desired structural properties. Composite materials are widely used in various fields such as machinery, automotive, aerospace, and space industries. In particular, within the aerospace and space industries, composites have become highly functional in achieving essential structural characteristics like lightweight and high strength-to-weight ratio [3]. Due to their advantageous properties, including high specific strength, corrosion resistance, and vibration damping capabilities, composite materials are frequently favored in many sectors, especially in aerospace and automotive industries [4]. These properties have enabled companies to become more economically efficient, resulting in an improved price-to-performance ratio of their services [5].

The constituents of composite materials are not alloys, and since there is no atomic-level exchange between the components, they do not chemically interact with each other [19]. The primary objective in the production of composite materials is to combine and enhance mechanical properties such as strength and toughness, which cannot be achieved or are insufficient when using a single material, as well as properties such as electrical and thermal conductivity, in order to create a new type of material [20]. As a result of these improvements, composite materials are used in aerospace and space applications due to their lightweight advantage, high strength, excellent corrosion resistance, low thermal conductivity, and rigidity properties [21].

Composites can be molded into more complex shapes than many other materials, providing designers with the freedom to create nearly any shape or form. A single part made from composite materials can replace an entire set of metal components. Reducing the number of parts in a machine or structure saves time and reduces the maintenance required throughout the product's lifespan. For example, composites are used in aircraft wings, ensuring that the shape and size of the wings do not change as the aircraft gains or loses altitude. Radar signals pass through composites, making them ideal materials for use wherever radar equipment is operational, whether on the ground or in the air. Additionally, structures made from composites are durable and require minimal maintenance [6].

Sandwich composites are materials that are combined by covering the inner part with two thin and light panels, which form a honeycomb pattern on the upper view [16]. They are generally quite light because they have low density due to their hollow structure. Despite this, they have excellent bending and compression resistance. They can be easily repaired without damaging the

structural strength of the material [17]. They are generally used in wings and cabin interior panels in cargo and passenger aircraft, and in some aircraft, also in flaps [18]. Sandwich composite structures are widely used in the aerospace industry due to their low weight and superior mechanical properties. As they are commonly used as structural components, maintaining structural integrity under various loading conditions is of paramount importance [9].

Aircraft can be subjected to impacts for various reasons during maintenance, repairs, periodic inspections, or while in flight. Impact loads can cause various types of damage to the aircraft structure. In some cases, these loads induce minor surface defects, while high-energy impact loads may result in structural failure. Examples of such impact loads include foreign object debris, bird strikes, rain, and hail. During maintenance operations, the impact effect of dropped tools is also a potential risk [11]. Composite materials can also be exposed to various impacts depending on where they are used. The damage to the material due to the impact increases with increasing impact energy. Fiber breakage, matrix crack, fiber-matrix interface damage, perforation and delamination are generally the types of damage that occur in the composite material after impact [12].

Impact-induced damage can occur during manufacturing, maintenance, and service operations. An example of an impact during use is the damage caused by stones and small debris ejected from the runway after the tires gain high speed during aircraft takeoff and landing. Hand tools used during production and maintenance may also fall onto the fuselage, resulting in low-impact velocities but significant effects. In composite structures, impact can cause internal damage that is not detectable through visual inspection. This internal damage leads to a reduction in strength and may propagate under loading. Therefore, the effects of foreign object impacts on composite structures must be understood, and appropriate precautions must be considered during the design phase [13].

Composite structures are highly susceptible to damage even at relatively modest impact energy levels due to foreign object damage [14]. Bird strikes are one of the most significant threats to flight safety in aviation. In the event of a bird strike, the most critical parts of the aircraft include the nose, windshield, engine, air intakes, and leading edges of the wings. Bird strikes typically occur during aircraft takeoff and landing phases. Furthermore, factors such as the increasing number of flights and bird migration patterns in a globalized world contribute to the rise in such incidents. For flight safety, aircraft components must possess a certain level of durability to minimize damage [15].

The potential hazards caused by low-speed impacts to aircraft structures such as engine nacelles or leading edges represent a long-term concern for the aerospace industry, requiring that exposed aircraft components be tested to demonstrate their ability to withstand low-speed impacts without critical damage [10]. Impact tests are short-term applications that provide

information about the fracture behavior of materials or components under a specified load and variable temperatures. The most commonly used tests are the Split Hopkinson and Drop Tower tests, which operate on the principle of dropping a weighted object onto the sample. The resulting damage on the sample is then examined based on the test outcome. Occasionally, low-speed impact is also referred to as low-energy impact. In these tests, not only can the impact resistance of materials be determined, but data can also be recorded digitally from the moment of impact until the energy dissipates, allowing for graphical results to be obtained [7].

This study aims to minimize any potential damage that may occur in the fuselage/wing materials as a result of an impact during cruising, taxiing, or maintenance operations. In this context, composite materials were produced by utilizing different fiber types and weaving patterns, and various configurations were created through stacking sequences. Low-speed impact testing was then applied.

METHOD AND MATERIAL

In this study, wood coated honeycomb samples that can be used for acrobatic or agricultural purposes were prepared. Low speed impact responses of all samples at certain energy levels were investigated. The experiments were carried out by taking into account the routines described in ASTM D 7136 test standards.

This study aims to reduce damage that may occur during maintenance, repair, and periodic inspections of commercial and recreational aircraft, as well as in collisions that may happen during hovering, takeoff, and landing maneuvers. To achieve these goals, fibers made from different materials and with various weaving characteristics have been used. Initially, it is targeted to manufacture various fuselage/wing material candidates composed of these aviation-grade matrixes and fibers, which form the foundation of the study. This objective also encompasses achieving increased strength and reduced weight. Furthermore, morphological analyses are planned to identify the extent of damage and spread in each sample type following potential collisions. Additionally, among the study's objectives is to determine the energy absorption capabilities, which directly influence collision outcomes, the effect of this absorption on damage areas over time, and which sample types demonstrate superior properties.

The study parameters include the number of sample layers, impactor mass energy at 30 J, and the stacking sequence. Among these, four different combinations are formed with sample thickness set to 20 mm, impactor energy level set to 1, and two options for the stacking sequence parameter. The table below specifies the experimental parameter/level for a total of four different test samples. Those shown with the underlined side are twill woven fabric.

Table 2.1. Parameter/level table of test samples

Sample No	Number of layers	Impact energy (J)	Stacking status
1	3	30	G**G**G
2	3	30	GC**G**
3	3	30	**G**GC
4	3	30	GC**C**

Materials:

Due to their advantages such as high performance, high strength, lightweight, and consequently enhanced maneuverability, composite materials are considered crucial in the defense, aerospace, space, and automotive industries today [8]. In our study, four different aviation-grade composite (fiber fabric) materials were selected for the samples we produced. These include: 200 g plain weave carbon fiber fabric made from Tenax-E HTA 40 3k yarn, 420 g twill weave carbon fiber fabric made from T700 / HS 12k 800tex carbon fiber yarn, 200 g plain weave glass fiber fabric suitable for wooden boat lamination and glass fiber-reinforced fabric, and 390 g twill weave glass fiber fabric. The selected materials were procured considering the technical and mechanical properties required for aviation applications.

Fiber woven fabrics

The plain carbon fiber fabric is a weave type made from Tenax-E HTA 40 3k yarn. With a density of 200 g, it is ideal for applications where lightness, strength, and carbon are crucial. The twill carbon fiber fabric weave type is produced from T700 or HS 12k 800 tex carbon fiber yarn.

The plain weave glass fiber fabric, with a high density is an ideal reinforcement material commonly used in wooden structure laminations and fiber-reinforced composite part manufacturing. It is a high-quality fabric used in advanced composite manufacturing, epoxy-compatible, and easily impregnated. The twill glass fiber fabric is a standard reinforcement material suitable for thick glass fiber plates and fiber molds. Its twill weave pattern makes it easier to apply to contoured surfaces, particularly in advanced composite manufacturing.

The fiber weights for the specific dimensions were as follows: 3.24 g for 200 g density carbon fiber plain weave fabric, 6.47 g for 420 g density carbon fiber twill weave fabric, 3.73 g for 200 g density glass fiber plain weave fabric, and 6.35 g for 390 g density glass fiber twill weave fabric. All fiber fabrics are standard reinforcement materials used in many areas such as

modeling, aviation, automotive, yacht sports equipment.

***Matriks Materials**:*

Epoxy resin is widely used in advanced composite part manufacturing in industries such as aerospace, automotive, marine, space, wind turbines, and defense. The MGS L285 system, which is certified for aerospace applications, cures at room temperature, and parts meeting civil aviation standards can be obtained after a post-curing process. In advanced composite part manufacturing, products made by Hexion are used in industries like aerospace, automotive, marine, space, wind turbines, and defense. A system that cures at room temperature and can be used with MGS Laminating Epoxy Resin LR285 has been selected.

Low Velocity Impact Test:

The test device operates based on the principle of free-fall weight drop, meaning the conversion of static energy into kinetic energy. The striker tip to be used in the device has been selected with a 24 mm diameter hemispherical tip. Sharp tips were avoided to prevent them from penetrating the test samples. The mechanism, along with the connection components, will have a total mass of 6.35 kg. The tests were conducted at an energy level of 30 J. The energy level is adjusted by the height of the striker's impact distance. The system uses an impulse signal conditioning unit, which is connected to a computer with an impulse data collection card and data acquisition software. The force data generated by the system were processed according to the ASTM D7136 test standard, and the displacement and energy absorption capabilities were determined. A proximity sensor attached to the system detects when the striker tip passes in front of it, triggering the pneumatic pistons and preventing repeated impacts. To prevent sliding and rebound during the impact, the samples were fixed at all four corners. Since the data obtained from the force sensor are force-time data, other data were obtained through kinematic analysis. The test device and sample fixation setup used in the experiments are shown in Figure 1.

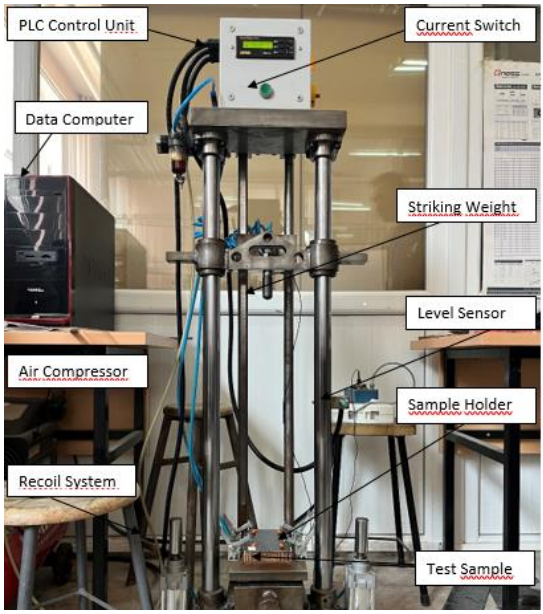

Figure 1. Computer-aided impact testing device and test sample

Production of test samples:

The production of the test samples was carried out in the fuselage/composite laboratory of the Department of Aircraft Fuselage and Engine Maintenance at the Selçuk University School of Civil Aviation in Konya. The wooden honeycomb sandwich panels for the aircraft wing to be used were created by simulating the wing of an aerobatic and agricultural aircraft. For the experiment, samples of 100x150 mm in size and 20 mm thick were taken from the wing. The dimensions of the sample holders for the low-velocity impact test device and the test standards to be used were considered.

200 g/m² density carbon fiber plain woven fabric, 420 g/m² density carbon fiber twill woven fabric, 200 g/m² density glass fiber plain woven fabric and 390 g/m² density glass fiber twill woven fabric with different densities and weave types were cut into 100 mm x 150 mm dimensions and dimensional control was performed as shown in Figure 2.

Figure 2. 100 mm x 150 mm glass and carbon fiber fabric samples cut to be used in the coating of sample panels and measurement control

The glass and carbon fiber fabrics to be placed on the honeycomb panel samples cut from the aircraft wing were cut according to the dimensions of the honeycomb panel samples to be used and then weighed on an electronic precision scale. As a result of the measurements made with the electronic precision scale, four different glass and carbon fiber weights were obtained as follows:

To achieve a 50% fiber volume fraction, a mixture of epoxy and hardener was prepared in the same weight as the fibers. The mixture of epoxy and hardener was prepared by mixing approximately 60% epoxy and 40% hardener by weight using an ultrasonic mixer to ensure homogeneity. During and after the mixing, care was taken to prevent the formation of air bubbles. Before the epoxy/hardener mixture solidified, the carbon and glass fibers, which were cut into specific dimensions, were bonded with the panel samples using the hand lay-up method. The prepared composite material was combined with the fibers in the order specified in Table 1, ensuring that the resin fully penetrated the fibers and layers. To prevent delamination between the fibers in the samples, the waiting time between the layers was kept to a minimum.The prepared honeycomb panel samples were coated with glass and carbon fibers in the order from inside to outside, in accordance with the stacking sequence specified in Table 1. After the process, all the samples were made ready for the curing process.

In the curing oven, the exterior surfaces of the panels were placed in containers made of aluminum foil to prevent the matrix material from leaking out of the structure, which could negatively affect the fiber volume ratio. Then, heavy metal pieces were placed on the panel samples to ensure good bonding of the composite. The curing process for the prepared samples was carried out in two stages in the curing oven: the first stage at 80°C for 60 minutes, followed by the second stage at 120°C for an additional 30 minutes, making a total exposure time of 90 minutes. After being removed from the oven, the samples were left to cool for 60 minutes (at approximately 25°C room temperature), completing the curing process. The final condition of all the samples ready for testing is shown in Figure 3.

Figure 3. Numbering of samples according to stacking order with the help of labels

EXPERIMENTAL FINDINGS AND DISCUSSION

Experimental studies were conducted to determine the deformations that may occur on the wing surfaces of commercial/sportive aircraft due to low-speed impact, using epoxy-based outer surface coated honeycomb sandwich panels reinforced with glass and carbon fibers. In these studies, the impact responses of the honeycomb sandwich panel samples were examined. The data obtained from the experiments were analyzed to evaluate the impact resistance and damage behavior of these panels. Numerical data from the low-speed impact testing device were used to create force-time, force-displacement, and energy-time graphs.

The force-time graph shows how the force applied to the material changes over time during the impact event. This graph is used to determine the maximum force during the impact, analyze the duration of the applied force, and investigate the rate at which the force decreases. Therefore, it provides information about the material's impact resistance and energy absorption capacity.

The force-displacement graph reveals the relationship between the applied force and the deformation that occurs in the material. This graph is used to analyze the elastic and plastic deformation behavior of the material, assess its ductility or brittleness, and determine the material's energy absorption capacity. The energy-time graph shows how much energy the material absorbs during the impact and how this energy changes over time. This graph is used to evaluate the energy absorption performance and overall impact durability in Figure 4.

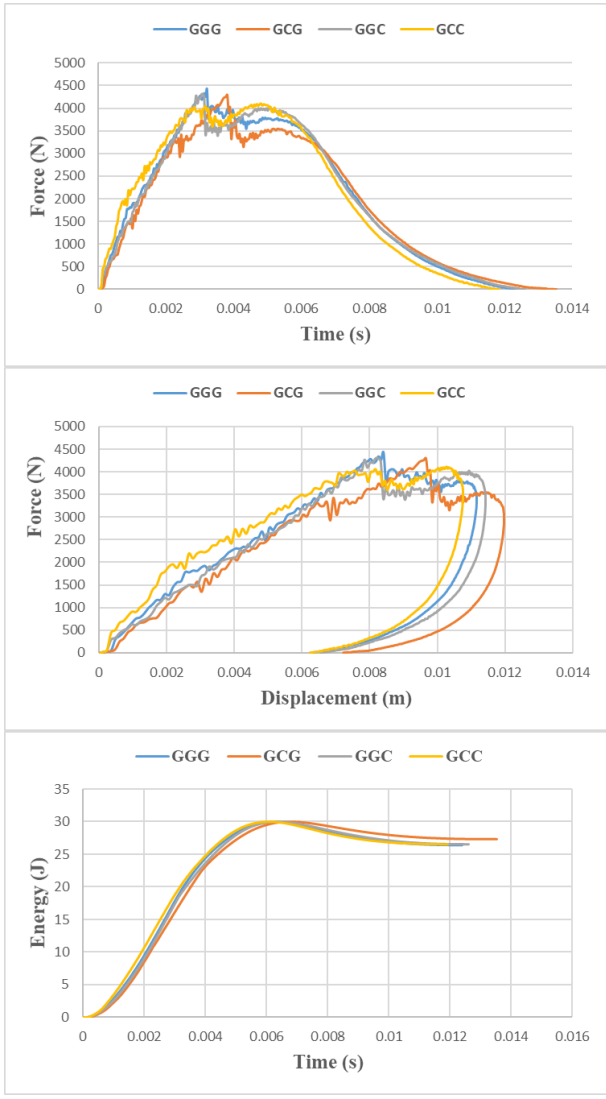

Figure 4. Graphs of contact force, displacement force and kinetic energy changes at 30 J impact energy of sandwich structured wood plate for all samples

Sample 1 GGG: When the force-time graph of fiber-reinforced samples subjected to low-speed impact energy at 30 J is examined, it is observed that the force curve follows a parabolic shape over time. The force increases over time, reaching approximately 4400 N, but shows some fluctuations before and after reaching this level. These fluctuations may indicate microcracks or delaminations in the sample's internal structure. After the maximum force level, the force begins to decrease. The average force value is 2111 N. The total contact time was measured as 0.0123 s. The first significant damage occurred at around 0.003 s. When the force-displacement graph is examined,

it is observed that the displacement increases steadily with the force, but noticeable fluctuations occur between approximately 4500 N and 3500 N. These fluctuations suggest that the sample may be subjected to permanent deformations. The maximum displacement value is 0.0111 m.

When the energy-time graph is analyzed, the energy increases over time, reaching approximately 30 J, and then shows a decrease. This indicates that the sample absorbed a significant portion of the impact energy. The short energy absorption time suggests that the material is effective in energy absorption and can quickly absorb impact energy. This may be due to the fibrous structure of the wooden plate. A total of 26.41 J of energy was absorbed, and the remaining 3.59 J of energy was rebounded.

Sample number 2 GCG: When the force-time graph of fiber-reinforced samples subjected to low-speed impact energy at 30 J is examined, it is observed that the force curve follows a parabolic shape over time. The force increases over time, approaching approximately 4300 N, but before and after reaching this level, some fluctuations may indicate microcracks or delaminations in the sample's internal structure. After the maximum force level, the force begins to decrease. The average force value is 1872 N, which is 11% less than that of sample 1.

When the force-displacement graph is examined, it is observed that the displacement increases steadily with the force, but significant fluctuations occur between approximately 4250 N and 3250 N. These fluctuations suggest that the sample may be subjected to permanent deformations. The maximum displacement value was measured as 0.0119 m. The total contact time was 0.0135 s.

When the energy-time graph is analyzed, the energy increases over time, reaching approximately 30 J, and then shows a decrease. This indicates that the sample absorbed a significant portion of the impact energy. The short energy absorption time suggests that the material is effective in energy absorption and can quickly absorb impact energy. This may be due to the fibrous structure of the wooden plate. The absorbed energy is 27.32 J, and 2.68 J of energy was rebounded. The longer duration compared to sample 1 resulted in an increase in displacement value. Additionally, the damage increased, which also raised the absorbed energy.

Sample number 3 GGC: When the force-time graph of fiber-reinforced samples subjected to low-speed impact energy at 30 J is examined, it is observed that the force curve follows a parabolic shape over time. The force increases over time, reaching approximately 4300 N, with an average force of 2068 N. The oscillations seen in the initial part of the graph may indicate microcracks or delaminations in the sample. After the maximum force level, the force begins to decrease. The maximum value is close to that of sample 2, with the average force increasing by approximately 10%. The total contact time was measured as 0.0125 s.

When the force-displacement graph is examined, it is observed that

the displacement increases steadily with the force, but significant fluctuations occur between approximately 4250 N and 3500 N. These fluctuations suggest that the sample may be subjected to permanent deformations. The maximum displacement value is 0.0114 m. When the energy-time graph is analyzed, the energy increases over time, reaching approximately 30 J, and then shows a decrease. This indicates that the sample absorbed a significant portion of the impact energy. The short energy absorption time suggests that the material is effective in energy absorption and can quickly absorb impact energy. This may be due to the fibrous structure of the wooden plate. The more stable force reduces the absorbed energy to 26.54 J, compared to sample 2.

Sample number 4 GCC: When the force-time graph of fiber-reinforced samples subjected to low-speed impact energy at 30 J is examined, it is observed that the force curve follows a parabolic shape over time. The force increases over time, reaching approximately 4100 N, with an average force of 2208 N. The oscillations that lead to damage can also be seen in the initial phase of force increase for this sample. After the maximum force level, the force begins to decrease. The total contact time is 0.0119 s.

When the force-displacement graph is examined, it is observed that the displacement increases regularly with the force increase, but notable fluctuations occur between 3700 and 4100 N after reaching approximately 4000 N. These fluctuations suggest that the sample may be subjected to permanent deformations. The maximum displacement value was 0.0107 m, which corresponds to the lowest value. This can be explained by the structure showing more rigidity. When the energy-time graph is analyzed, the energy increases over time, reaching approximately 30 J, and then shows a decrease. This indicates that the sample absorbed a significant portion of the impact energy. The short energy absorption time suggests that the material is effective in energy absorption and can quickly absorb impact energy. This may be due to the fibrous structure of the wooden plate. In sample 4, 26.54 J of energy was absorbed, and 3.46 J of energy was rebounded.

CONCLUSIONS

The hybrid reinforced honeycomb glider body/wing material consisting of glass fiber and carbon fiber produced with different weaving shapes was successfully produced. The low-speed impact response of all samples at 30 J energy was investigated. According to the results, the obtained outputs are as follows:

- While the triple glass fiber sample gave the highest value in terms of maximum strength, the samples reinforced with carbon fiber in the middle-outer layers gave the highest value in terms of average strength.
- It has been observed that the total contact time directly affects the maximum displacement value.
- All samples showed closed curve graphs and were resistant to puncture

damage.

- Although the absorbed values are generally close to each other, the worst results were obtained in samples with GCG order.
- The sample with high carbon fiber content behaved more rigidly and positively affected the displacement by more than 10%.

REFERENCES

[1] Erteği, G., Investigation of the Impact Performance of Bird-Struck Radomes After Repair, Başkent University, Department of Defense Technologies and Systems, 2022.

[2] Gliders – Aircraft Series, https://www.turkair.org/planorler-hava-araclari-serisi

[3] Uyaner, M., Karadal, K., Merden, T., Acar, N., N., Green Composites in the Aerospace Industry: NACA 4452 Rib Application, Journal of Science and Engineering, Vol: 6, No: 2, 2024.

[4] Öztürk, A.M., Gündoğdu, Ö., Investigation of Structural Performances of Glass and Carbon Fiber Reinforced Composites Used in UAV Wings with Numerical Simulations, Iğdır University Science Institute Journal, 10(3): 1928-1942, 2020.

[5] Usta, F., Türkmen, H.S., Scarpa, F., Low-velocity impact resistance of composite sandwich panels with various types of auxetic and non-auxetic core structures Thin-Walled Structures, Vol:163, 2021, 107738.

[6] Advantages and Disadvantages of Composite Materials in Aircraft, 2019. https://malzemebilimi.net/kompozit-malzemelerin-ucaklarda-avantaj-ve-dezavantajlari.html

[7] Ödemiş, O., Investigation of Low Speed Impact Behavior of Nano Composite Reinforced Honeycomb Structures with Different Thicknesses on Wood-Plate Aircraft Wings, Selcuk University - Department of Aviation Technologies, 2023.

[8] Çelik, A.,K., Investigation of Low Velocity Impact Resistance for Frame-Supported Composite Materials and Determination of Their Effects, Başkent University, Department of Defense Systems and Technologies, 2022.

[9] Karsandik, Y., Sabuncuoğlu, B., Yıldırım, B., Silberschmidt, V., Impact Behavior Of Sandwich Composites For Aviation Applications: A Review, Composite Structures, Vol:314, 2023, 116941.

[10] Meo, M., Morris, A.J., Vignjevic, R., Marengo, G., Numerical Simulations Of Low-Velocity İmpact On An Aircraft Sandwich Panel, Composite Structures, 62, 3-4, 353-360, 2003.

[11] Non-Destructive Control of Impact Damage in Aircraft Maintenance (Müge Armatlı Kayrak- Anadolu University- School of Civil Aviation-2012.

[12] Esendemir, Ü., Caner, A.Y., Experimental Investigation of Impact Behavior of Layered Composite Materials, Süleyman Demirel University Journal of Science Institute Vol:22, Issue 1, 207-215, 2018.

[13] Yapıcı, İ., Yapıcı, A., Investigation of Low Speed Impact Behavior in E-Glass/Epoxy Layered Composites Using Finite Element Method, Niğde University Journal of Engineering Sciences, Vol:1(2), 2012, 48-60.

[14] Park, H., Kong, C., A study on low velocity impact damage evaluation and repair technique of small aircraft composite structure, Composites Part A: Applied Science and Manufacturing, Vol:42(9), 2011, Pages 1179-1188.

[15] A Review Study on Bird Strikes and Their Effects on Airplanes (Orhan Gülcan- Engineer and Machinery vol. 60, no. 696, pp. 192-220, 2019 Compilation Article)
[16] Erdoğan, Ö.,: Low-speed impact behavior of sandwich panels. Master's Thesis. Institute of Science and Technology; 2020.
[17] Mocian, O.A., Constantinescu, D.M., Sandu, M, Sorohan, Ş.,: Experimental evaluation of the response of sandwich panels in low-velocity impact. Proceedings of the Institution of Mechanical Engineers, Part L: Journal of Materials: Design and Applications 2019, 233(3):315-327.
[18] Esendemir Ü, Caner A: Experimental Investigation of Impact Behavior of Layered Composite Materials. Süleyman Demirel University Institute of Science and Technology Journal 2018, 22(1):207-215.
[19] Tuğberk Ö, Temiz Ş: Experimental investigation of impact behavior of balsa core sandwich composites. Al-Jazari 2021, 8(1):333-345.
[20] Ceyhun V, Turan M: Impact behavior of layered composite materials. Engineer and Mechanical 2003, 44(516):35-41.
[21] Pantano, A., Carbon nanotube based composites: processing, properties, modeling and application: Smithers Rapra; 2012.

Hybrid Energy Systems in Electric Power

Melike YALILI KILIC[1]
Ilker KILIC[2]

1- Prof. Dr.; Bursa Uludag University Faculty of Engineering Environmental Engineering Department. myalili@uludag.edu.tr ORCID No: 0000-0001-7050-6742
2- Prof. Dr.; Bursa Uludag University Faculty of Agriculture Biosystem Engineering Department. ikilic@uludag.edu.tr ORCID No: 0000-0003-0087-6718

ABSTRACT

In today's world, where the need for energy is increasing daily, the inability of fossil fuels to meet the increasing world population and their exhaustibility have brought the use of renewable energy resources to the agenda. In today's world where the need for energy is increasing day by day, the fact that fossil fuels are not enough for the increasing world population and are exhaustible has revealed the need for inexhaustible resources. Solar, wind, biomass, geothermal, hydro, wood, plant residues, tidal and wave energy are renewable energy sources, and making more use of these resources is extremely important for the future of the world. Hybrid energy sources, which consist of using more than one energy source together, have become the center of attention of countries in recent years. Turkey is in a very favorable position regarding solar and wind energy use. However, investments in hybrid energy systems have yet to reach a sufficient level. However, it is reported that European countries that need more sun or wind have a high energy investment level.

This study gives information about solar and wind energy sources from hybrid energy systems, and studies done in Turkey and in the world are presented with examples. In the studies conducted in Turkey, detached houses, refueling stations, universities, and SPPs were considered, and programs such as Homer Pro and PVSol were generally used. In the examples from around the world, studies conducted in Saudi Arabia, Pakistan, India, Bangladesh, Morocco, Oman, and Canada were discussed, and cost calculations were made for some of them. It is thought that the number of studies on hybrid energy systems should be increased and that investment incentives in this field will be increased by tax reductions provided by states.

Keywords – Cost, Electric, Solar Energy, Hybrid Energy Sources, Wind Energy.

INTRODUCTION

In recent years, developments in industry and technology, along with population growth, have increased the need for raw materials and energy,and the problem of rapid depletion of non-renewable resources has emerged. The use of fossil fuels, which have an important share in energy resources, has caused environmental pollution and led countries to search for new energy sources (Yalılı Kılıç and Adalı, 2021). As an alternative to fossil fuels, the use of solar, wind, hydrogen, biomass, and geothermal energy sources has come to the agenda (Kılıç Demircan and Gültekin, 2017). Among these energy sources classified as renewable, solar energy is the most preferred energy source because it is abundant and free (Akyürek et al., 2021). The amount of energy from the sun to the Earth is 1100 W/m^2, much more than

the energy used (Anonymous, 2024). Therefore, considering solar energy as an alternative energy source and investing in this field is extremely important for the world's future.

The rate of electricity production produced by utilizing the sun will be 25% in 2050 (Oral, 2020). Turkey's annual sunshine duration is 2741 hours, and its radiation intensity is 1527.46 kWh/m². Considering Turkey's location, it is seen that utilizing solar energy is quite advantageous. When the contribution of resources to electricity generation in Turkey in 2023 is analyzed, it is stated that coal contributed 36.2%, natural gas 21%, hydraulic energy 19.3%, wind energy 10.3%, solar energy 6.7%, geothermal energy 3.4%, and other energy sources 3.2% (Figure 1) (URL-1, 2024).

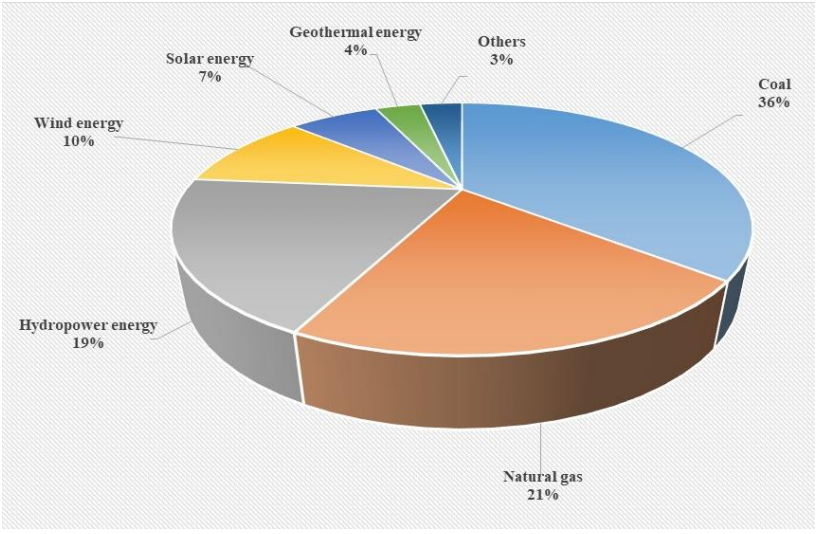

Figure 1: Installed Electricity Capacity by Source in Turkey

Table 1 shows the top 15 countries that will invest the most in solar power plants in 2022, with Turkey ranking 15th. China ranks second, followed by the USA and Japan in third place. Our country's annual sunshine duration is 2,741 hours and the radiation value is 1,527.46 kWh/m^2. It is essential for Turkey, which is in a favorable position in terms of sun, to invest more in solar energy in order to benefit from the sun to the maximum extent.

Table 1: Installed Capacity of Solar Power Plants in 2022 (URL-2, 2024)

Country	Installed Power (MW)
China	393.032
USA	113.015
Japan	78.833
Germany	66.554
India	63.146
Australia	26.792
Italy	25.083
Brazil	24.079
Holland	22.590
South Korea	20.975
Spain	20.518
Vietnam	18.474
France	17.419
United Kingdom	14.412
Turkey	12.661

The energy converted into wind energy is only 2% of the energy coming from the sun to the Earth. Wind energy is generated by the differential heating of the Earth's surface by solar radiation. Wind energy-based electricity production has some advantages and disadvantages. No risk of exhaustion, low maintenance and operating costs, having a simple technology, being a clean and environmentally friendly energy source are advantages of the system. High installation cost, low capacity factors and variable energy production are disadvantages of the system. It is stated that the wind energy potential of Turkey is 48,000 MW. A map showing wind speeds for wind power plants that can be built in Turkey is shown in Figure 2 (URL-3, 2024). Figure 2 shows that the most windy regions of Turkey are the coastal areas and that high efficiency will be obtained by installing wind power plants in coastal areas.

Table 2 shows the top 12 countries that will invest the most in wind power plants in 2022, ranking Turkey 12th. According to Table 2, China ranks first in installed wind power capacity globally, with the USA and Germany in the 2nd and 3rd places (URL-4, 2024). As with solar energy, it is important for Turkey to increase its investments, especially in coastal regions, in order to benefit more from wind energy.

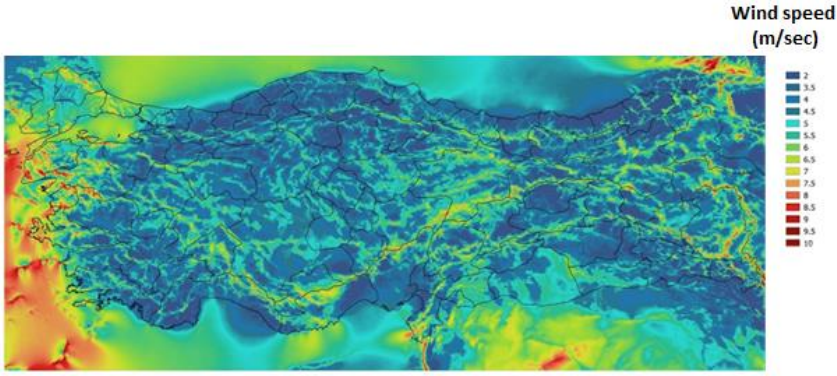

Figure 2: Wind Speeds of Regions in Turkey

Table 2: Installed Capacity of Wind Power Plants in 2022 (URL-4, 2024)

Country	Installed Power (MW)
China	328.973
USA	132.738
Germany	63.760
India	40.067
Spain	27.497
United Kingdom	27.130
Brazil	21.161
France	18.676
Canada	14.304
Sweden	12.080
Italy	11.276
Turkey	10.886

There are many studies on the applicability of hybrid energy systems in different fields in Turkey and the world. Examples of these studies are given below under two separate headings.

STUDIES ON HYBRID ENERGY SYSTEMS IN TURKEY

Examples of studies conducted in Turkey on hybrid energy systems are given below.

Engin (2010) investigated the applicability of a photovoltaic wind energy system in Izmir and used the Homer program to size the system. At the end of the study, it was determined that the hybrid energy system was unsuitable for electricity generation.

In the study, Homer Pro was used to determine the most suitable system for designing and optimizing a hybrid energy system to meet the electricity needs of detached houses in Berlin and Muğla provinces. According to the results obtained, the portion of the annual electricity

generated from photovoltaic panels and wind turbines was 55% and 24% for Berlin and 72% and 22% for Muğla, respectively (Gülkokan, 2017).

In the study where a hybrid energy system was installed in the Rahva campus of Bitlis Eren University, wind speed and energy production in the region where the system was installed experienced significant changes, and it was concluded that installing a power generation system without storage would not be efficient. However, since the photovoltaic system works stably, it was determined that the generated energy can be supplied directly to the grid (Efe and Kocaman, 2017).

Ceylan and Taşdelen (2018) compared the actual generation and simulation analysis generation values of an SPP plant with an installed capacity of 1 MW in Isparta with Helioscope, PVGIS, Polysun, and PVSol programs. At the end of the study, a deviation margin of +1.2%, +1.3%, -3.6%, and -7.5% was determined for the mentioned programs, respectively.

Gökçek and Kale (2018) investigated a hybrid energy system consist of wind and photovoltaic for a hydrogen refueling station in the Çeşme district of İzmir with Homer and calculated the balanced cost of hydrogen production as \$7,526-7,866/kgH_2.

In the study where the electricity demand of a house in Aydın province was analyzed with a grid-connected system, the HOMER program was used for modeling energy systems. Adding a wind energy system to the photovoltaic system increased the payback period, but the emissions decreased by 26-58% (Kayıkcı, 2020).

In a study by Kiraz (2020), a 2.5 kW hybrid system consisting of solar and wind energy was installed to meet the electricity needs of a building used for recreational purposes by the farm employees in Aydın Adnan Menderes University Faculty of Agriculture. According to the results, 66% of the electricity consumed for a year was from the hybrid system and 34% from the grid.

In their study, Atik and Sevin (2022) used the PvSol program to design ten hybrid energy systems with a 5-50 kW capacity in Balıkesir province. In 5 different off-grid systems with a capacity of 5-15 kW, accumulators and charge regulators were used, while in the other five grid-connected systems with a capacity of 20-50 kW, no charge regulator was required since the accumulator was not used. As a result of the study, it was determined that as the installed capacity of the system increases, the energy produced also increases.

Akarsu and Genç (2022) examined a microgrid system contains solar, wind, and diesel generators to meet the annual electricity needs of residences in Kayseri with the Homer Pro. According to the evaluations, the most optimum and economical system was a hybrid system contains solar, wind, diesel generator, battery, and hydrogen storage, and the energy cost was calculated as 0.376 \$/kWh.

STUDIES ON HYBRID ENERGY SYSTEMS IN THE WORLD

Examples of studies conducted worldwide on hybrid energy systems are given below.

Al-Sharafi et al. (2017) utilized solar and wind energy using the Homer program to determine the power and hydrogen production potentials in 5 different cities in Saudi Arabia. According to the results obtained, the min. The cost is 0.609 $/kWh for photovoltaic, wind turbine, and battery bank storage systems in Yanbu and 1.208 $/kWh for photovoltaic/wind/fuel cells in Abha.

The feasibility studies of the grid-connected hybrid system for Chakwal, Pakistan was carried out and the potential of generating electricity with wind/photovoltaic/biomass system was investigated (Ahmad et al. 2018). In the study, where the Homer Pro program was used for modeling, it was determined that the system could produce more than 50 MW of electricity. The system cost is $180.2 million for a peak the load of 73.6 MW and a balanced energy cost of $0.05744/kWh.

Abdin and Mérida (2019) used photovoltaics, wind turbines, and their combinations in their study to determine the min. Cost based on renewable energy systems in Squamish in Canada, USA, and Australia. Using Homer Pro as a simulation program, the min. The cost for the combination of a photovoltaic, wind turbine, battery bank, electrolyzer, and hydrogen tank was calculated as 0.5 $/kWh in Golden and 0.78 $/kWh in the exact location without the battery bank.

Kumar et al. (2019) performed the optimum sizing of a village in Uttar Pradesh, India, for its electricity demand using the Homer program. A comparative analysis was performed in the study to see the effects of demand response and system size on LCOE and NPC. As a result, the authors determined that the grid-connected system is more economical choice.

Ali et al. (2021) used the Homer Pro program to meet the electricity demand in a rural village in Pakistan with hybrid energy systems. The electricity cost was calculated as 0.072$/kWh - 0.078$/kWh for a grid-connected system and 0.145$/kWh - 0.167$/kWh for an off-grid system.

Das et al. (2021) analyzed the photovoltaic/wind/diesel/battery-based hybrid energy system for five different geographical regions of Bangladesh with Homer. The lowest values regarding energy cost, net present cost, and environmental emissions of the hybrid system were obtained for the Rajshahi region. In the Chattogram region, the hybrid system showed great potential in financial and environmental terms. The grid-connected system with a sell-back option has a cost advantage over the grid tariff of 0.10 $/kWh (0.07 $/kWh).

El Hassani et al. (2023) examined the applicability of a hybrid system contains wind turbine, diesel generators, fuel cell and electrolyzer in Dakhla

city, Morocco. The system calculated in the study costs $2,650,843, the balanced energy cost is $0.0701/kWh, and the energy production is 37,819,172 kWh. It is concluded that the proposed hybrid system is economically feasible.

In a study investigating the techno-economic feasibility of the wind-photovoltaic-electrolysis-battery system in Damao Banner City, China, it was determined that the system could produce 584.62 GWh of electricity per year and amortize it in 9 years (Li et al., 2023).

CONCLUSION

Population growth and industrialization in the world have increased the need for energy and led to the intensive use of fossil fuels. However, using environmentally friendly renewable energy sources instead of fossil fuels is highly beneficial for the future of society. Renewable energy resources come to the forefront in reducing environmental damage and ensuring world energy security. Meeting the energy needs from natural resources and using energy efficiently and sustainably will reduce energy costs. Clean production and lower costs will benefit individuals in domestic use, industrialists in factory use, and, indirectly, the state. Therefore, the long-term profitability of investments in abundant and free natural resources should be considered.

This study gives information about solar and wind energy and examples of studies on hybrid energy systems in our country and the world. According to the examples examined, it has been revealed that although our country is located in a very favorable region in terms of geographical location, it cannot make sufficient use of natural resources. When the examples from around the world are examined, it is seen that many studies on the subject have been carried out in different countries, and cost calculations have been made, but in some of them, the cost is found to be high. In summary, it was concluded that more studies on using hybrid energy systems should be conducted worldwide.

REFERENCES

Abdin, Z., and Mérida, W. (2019). Hybrid energy systems for off-grid power supply and hydrogen production based on renewable energy: A techno-economic analysis. *Energy Conversion, and Management*, 196, 1068-1079, https://doi.org/10.1016/j.enconman.2019.06.068.

Ahmad, J., Imran, M., Khalid, A., Iqbal, W., Ashraf, S.R., Adnan, M., Ali, S.F., and Khokhar, K.S. (2018). Techno-economic analysis of a wind-photovoltaic-biomass hybrid renewable energy system for rural electrification: A case study of Kallar Kahar. *Energy*, 148, 208-234, https://doi.org/10.1016/j.energy.2018.01.133.

Akarsu, B., and Genç, M.S. (2022). Optimization of electricity and hydrogen production with hybrid renewable energy systems. *Fuel*, 324, 124465, https://doi.org/10.1016/j.fuel.2022.124465.

Akyürek, E.F., Geliş, K., and Yoladı, M. (2021). The effect of different shading conditions on photovoltaic panel characteristics. *Journal of Gumushane University Graduate School of Science and Technology*, 11(1), 161-168. https://doi.org/10.17714/gumusfenbil.766232.

Ali, F., Ahmar, M., Jiang, Y., and AlAhmad, M. (2021). A techno-economic assessment of hybrid energy systems in rural Pakistan. *Energy*, 215, 119103, https://doi.org/10.1016/j.energy.2020.119103.

Al-Sharafi, A., Sahin, A.Z., Ayar, T., and Yilbas, B.S. (2017). Techno-economic analysis and optimization of solar and wind energy systems for power generation and hydrogen production in Saudi Arabia. *Renewable Sustainable Energy Reviews*, 69, 33-49, http://dx.doi.org/10.1016/j.rser.2016.11.157.

Anonymous, (2024). The Sun. https://enerji.gov.tr/bilgi-merkezi-enerji-gunes (Accessed date: 10.12.2024.)

Atik, I., and Sevin, A. (2022). Hybrid renewable energy system design: the case of Balikesir. *Dicle University Journal of Engineering*, 13,3, 517-529.

Ceylan, O., and Taşdelen, K. (2018). Investigation of the accuracy of photovoltaic programs simulation results for Isparta City. *Afyon Kocatepe University Journal of Science and Engineering*, 18, 895-903, DOI: 10.5578/fmbd.67547.

Das, B.K., Alotaibi, M.A., Das, P., Islam, M.S., Das, S.K., and Md Hossain, A. (2021). Feasibility and techno-economic analysis of stand-alone and grid-connected PV/Wind/Diesel/Batt hybrid energy system: A case study. *Energy Strategy Reviews*, 37, 100673, https://doi.org/10.1016/j.esr.2021.100673.

Efe, S.B., and Kocaman, B. (2017). Physical realization and analysis of renewable energy hybrid system, *5th International Symposium on Innovative Technologies in Engineering and Science*, 29-30 September 2017, Baku, Azerbaijan.

El Hassani, S., Oueslati, F., Horma, O., Santana, D., Moussaoui, M.A, and Mezrha, A. (2023). Techno-economic feasibility and performance analysis of an islanded hybrid renewable energy system with hydrogen storage in Morocco. *Journal of Energy Storage*, 68, 107853, https://doi.org/10.1016/j.est.2023.107853.

Engin, M. (2010). Solar-wind hybrid energy generation system design for Bornova. *Celal Bayar University Soma Vocational School Technical Sciences Journal*, 2(13), 11-20.

Gökçek, M., and Kale, C. (2018). Techno-economic evaluation of a hydrogen refuelling station powered by Wind-PV hybrid power system: a case study for İzmir-Çeşme. *International Journal of Hydrogen Energy*, 43, 10615-10625, https://doi.org/10.1016/j.ijhydene.2018.01.082.

Gülkokan, O. (2017). Optimization of a wind-pv hybrid power system to cover electricity demand of an individual residence in two different regions, MSc Thesis, Muğla Sıtkı Koçman University, Graduate School of Natural and Applied Sciences, Muğla.

Kayıkcı, B. (2020). Analysis of hybrid solar-wind energy system for housing in rural area in Didim District of Aydın, MSc Thesis, Kocaeli University, Graduate School of Natural and Applied Sciences, Kocaeli.

Kılıç Demircan, R., and Gültekin, A.B. (2017). Investigation of passive and active solar systems in buildings. *TÜBAV Bilim*, 10(1), 36-51.

Kiraz, M. (2020). Meeting the electrical requirement of an agricultural worker rest house with solar and wind (hybrid) system as a support to network, MSc Thesis, Aydın Adnan Menderes University, Graduate School of Natural and Applied Sciences, Aydın.

Kumar, J., Suryakiran, B.V., Verma, A, and Bhatti, T.S. (2019). Analysis of techno-economic viability with demand response strategy of a grid-connected microgrid model for enhanced rural electrification in Uttar Pradesh state, India. *Energy*, 178, 176-185, https://doi.org/10.1016/j.energy.2019.04.105.

Li, R., Jin, X., Yang, P., Sun, X., Zhu, G., Zheng, Y., Zheng, M., Wang, L., Zhu, M., Qi, Y., Huang, Z., Zhao, L., Wang, D., and Yang, W. (2023). Techno-economic analysis of a wind-photovoltaic-electrolysis-battery hybrid energy system for power and hydrogen generation. *Energy Conversion and Management*, 281, 116854, https://doi.org/10.1016/j.enconman.2023.116854.

Oral, M. (2020). Solar energy potential of Turkey and evaluation of PV applications in local scale: case of Karabük province. *International Journal of Geography and Geography Education (IGGE)*, 42, 482-503, https://doi.org/10.32003/igge.743513.

URL-1 (2024). https://enerji.gov.tr/bilgi-merkezi-enerji-gunes (Accessed date: 10.12.2024)

URL-2 (2024). https://www.enerjiatlasi.com/ulkelere-gore-gunes-enerjisi.html (Accessed date: 10.12.2024)

URL-3 (2024). https://enerji.gov.tr/eigm-yenilenebilir-enerji-kaynaklar-ruzgar (Accessed date: 10.12.2024)

URL-4 (2024). https://www.enerjiatlasi.com/ulkelere-gore-ruzgar-enerjisi.html (Accessed date: 16.12.2024)

Yalılı Kılıç, M., and Adalı, S. (2021). Comparison of the design cost of a green villa with the cost of a classic villa design. *Duzce University Journal of Science and Technology*, 9, 822-835, DOI: 10.29130/dubited.820515.

An Experimental Research on the Enrichment of Coal by Flotation Method

Öykü BİLGİN[1]

Assoc. Prof. Dr.; Şırnak University, Faculty of Engineering, Department of Mining Engineering. ykbilgin@yahoo.com, ORCID No: 0000-0002-1276-5751

ABSTRACT

Coal increases its calorific value and becomes higher quality by reducing the ash content. Enrichment methods are needed for this. One of the most common methods used in the enrichment of very fine-grained coals is enrichment with flotation. In this method; factors such as carbonization degrees, chemical compositions, petrographic compositions, surface oxidation affect enrichment. Coal is a hydrophobic mineral that is easy to float naturally in water. In the flotation method; revitalizing, suppressing, pH adjusting, collecting and foaming reagents are used to separate impurities (calcite, clay, quartz, feldspar, iron, sulfides, etc.) in coal. In this study; coal samples taken from the Senkaya were subjected to sieve analysis and ash, caloric and moisture analysis in each grain class after being crushed in a jaw crusher. Then, the flotation method was applied step by step under the determined flotation conditions and the % ash yields and % burnable yields were determined of the sample. According to the test results; After the 2nd cleaning flotation, high quality coal was obtained with an ash ratio of 8.85% in the concentrated coal and 19.85% in the residue, and both the ash ratios of the products, both as concentrate and residue, decreased and their combustible ash and increased yields.

Keywords – Coal, Flotation, Ash, Enrichment.

INTRODUCTION

The flotation method is the enrichment process of very fine grain size ores by floating or pressing the ore with foam based on the principles of physicochemical, surface chemistry and colloidal chemistry. The purposes of applying the flotation method in coal enrichment are; reducing the amount of ash, reducing the amount of sulfur, recovering the remaining powdered coal in the washing water, cleaning the black process water discharged from the lavvar, removing some minerals in it, and obtaining coking products(Tunalı, 1994).

In this method; factors such as chemical compositions, petrographic compositions, degrees of coalification, surface oxidation affect enrichment. Coal is a naturally floating mineral. For example, newly produced coals can be floated more easily than stockpiled coals (Kavi, 1994; Yasan, 1994; Atak and Toroğlu, 1990).

In order for coal to float more easily, it may be necessary to use flotation facilitating reagents (organic compounds/neutral oils). For this reason; common reagents used in coal flotation;

- ✓ Non-polar reagents (collector); hydrocarbon oils, kerosene, fuel oil etc.

- ✓ Heteropolar reagents (foamers); aromatic alcohols, aliphatic alcohols, ethers etc.
- ✓ Lime, Na_2SiO_3 (sodium silicate), $FeSO_4$, Na_2CN (sodium cyanide) etc.

The parameters affecting coal flotation are; particle size, petrographic structure of coal, solid/liquid ratio in water, pH value, temperature, flotation time, mixing speed, reagents used and flotation machine (Çetinkaya, 1994; Cöcen, Cilingir and Malayoğlu, 1993).

MATERIAL AND METHODS

The coal samples used in this study were taken from Şenkaya coal mine in Erzurum province. The image of the coal sample is shown in Figure 1. The samples were brought to Dokuz Eylul University/Mining Engineering Department, Mineral Processing Laboratory and experimental research (Bilgin,2019) was carried out. The samples were first crushed in a jaw crusher and sieve analysis of the samples was performed and chemical analysis was performed in each particle size.

Figure 1: Coal Sample

Table 1 shows the analysis results of coal according to sieve particle sizes. Accordingly, the ash ratio of the feed material was determined as 49.40% and the calorific value as 3052 Kcal. When examined according to grain sizes; it is seen that the ash ratios are over 50% in the +12.5 mm, -12.5+9.51 mm and -9.51+3.35 mm grain size ranges. It can be said that the ash ratios are approximately 45% on average in the -3.35+2 mm, -2+1 mm, -1+0.5 mm, -0.5+0.106 mm and -0.106 mm grain size ranges. Depending on the ash ratio, the calorific values are approximately on average 3300 Kcal. Figure 2 shows, ash% graph according to sieve analysis of coal sample.

Table 1: Analysis Results According to Sieve Particle Size of Coal

Particle Size (mm)	**Ash(%)**	**Moisture (%)**	**Calorie(Kcal)**
Raw Material	49.40	6.98	3052
+12.5	53.71	6.99	2732
-12.5+9.51	56.34	6.86	2324
-9.51+3.35	51.39	6.72	2892
-3.35+2	46.63	6.67	3290
-2+1	46.85	6.38	3276
-1+0.5	49.17	6.45	3065
-0.5+0.106	42.18	6.52	3565
-0.106	45.07	6.07	3385

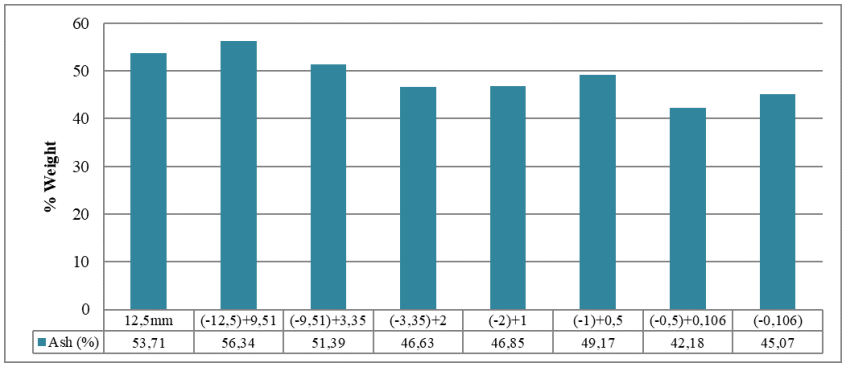

Figure 2: Ash% graph according to sieve analysis of coal sample

Table 2: Flotation Test Conditions

Flotation	Flotation I	Flotation II	Cleaning Flotation
Particle size: -1 mm Pulp ratio:%30 pH: 5 Suppressant: 5% Na_2SiO_2= 1kg/t Foamer: 1% pine oil =30 g/t Time:10 minute Mixing speed:1300 rpm Concentrate and Waste	Pulp ratio:%10 pH: 7,5 Suppressant:2000 g/t Na_2SiO_2 Collector: 500-6000 gr/t kerosene Foamer: 100 gr/ton Flotal Mixing speed:1000 rpm Time:5 dk.	200 ml = 40 g. Fuel Oil +160 g. Diesel oil 3ml Na_2SiO_2= 3 kg/t. (2 minute conditioning) Fuel Oil + Diesel oil =0,6 ml(5 minute conditioning) Pine oil 3 ml= 300 g./t (5 minute conditioning) Foam is removed its. Mixing speed:1200 rpm	pH:5 5% Na_2SiO_2 = 250 g/t. Flotation time:5 dk. Clean concentrate coal and intermediate product.

The flotation enrichment test, the coal sample is reduced to -0.5 particle size. Flotation test conditions are applied for coal sample. Flotation test conditions are given in Table 2.

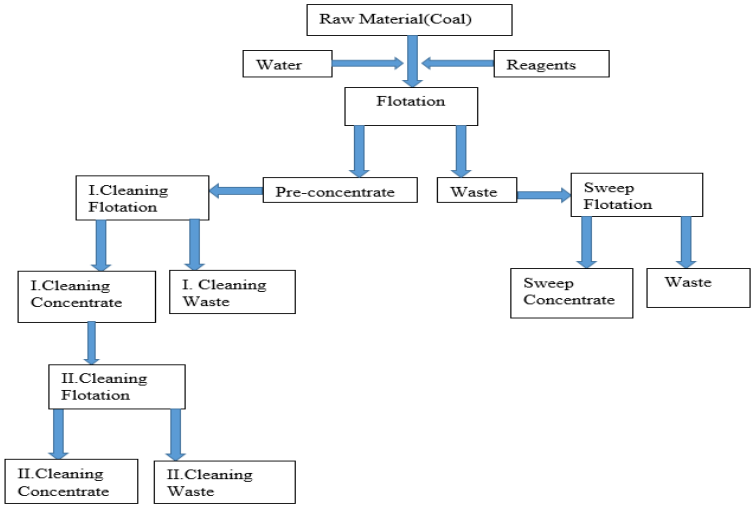

Figure 3: The flow chart of the flotation experiment

The flow chart of the flotation experiment is shown in Figure 3. Accordingly, the coal sample, which is the feed product, was mixed with water and reagents in the flotation tank with a particle size below 1 mm, mixing speed 1300 rpm, pH: 5, suppressant: 5% Na_2SiO_2 = 1kg/t, frother: 1% pine oil = 30 gr/ton, flotation time: 10 min. According to the conditions, concentrate and residue were obtained. Then, I. Cleaning Flotation was applied from the pre-concentrate and I. Cleaning Flotation concentrate and residue were obtained. Then, I. Cleaning Flotation concentrate was subjected to II. Cleaning flotation again and II. Cleaning flotation concentrate and residue were obtained. Finally, the first obtained flotation residue product was also subjected to sweep flotation and sweep concentrate and were obtained waste. Figure 4 and Figure 5 shows, an image of the Denver laboratory type flotation machine was carried out experiment.

Figure 4: Flotation Machine

Figure 5: Clean Coal Processing

RESULTS AND DISCUSSION

The analysis of the products obtained at the end of the flotation enrichment experiment was carried out by weight% and ash% analysis and burnable yield and ash yield were calculated analyzes. Table 3 shows the results of enrichment with flotation. Then, the result graphs of the obtained products are drawn.

Table 3: Results of Coal Enrichment by Flotation

Coal	Weight (%)	Ash (%)	Burnable (%)	Ash content	Burnable Content	Ash Yield (%)	Burnable Yield (%)
Sweeping concentrate	20.30	1.06	48.94	1036.52	993.48	22.37	18.51
I. Cleaning waste	6.40	9.51	50.49	316.86	323.14	6.84	6.02
II. Cleaning Concentrate	16.70	8.85	91.15	147.80	1522.21	3.19	28.36
II. Cleaning waste	22.00	19.85	80.15	436.70	763.30	9.43	32.85
Final waste	34.60	77.89	22.11	2694.99	765.01	58.17	14.26
Total	100.00	46.33	53.67	4632.87	5367.00	100.00	100.00

Figure 6 shows the % ash and % yield rates of the products after enrichment. After a general flotation method was applied to the coal sample, sweep flotation was applied to the residue sample and II-stage cleaning flotation method was applied to the obtained concentrate.

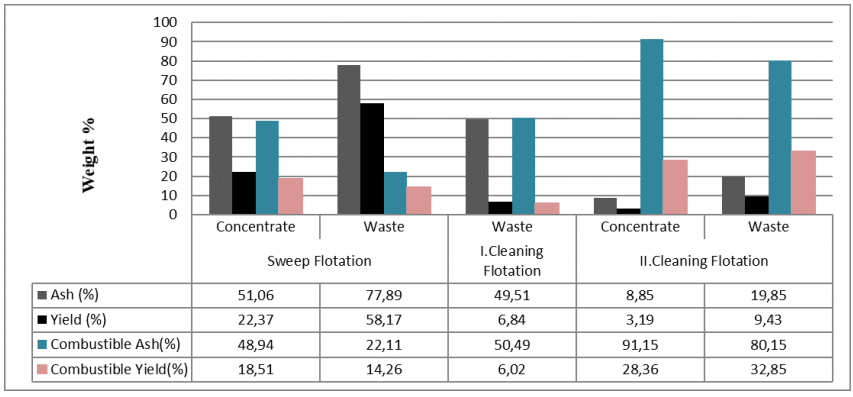

Figure 6: Ash and Yield Ratios of the Products Enrichment.

As a result, the ash of the concentrated product obtained from sweep flotation was 51.06% with a yield of 77.88%. It is normal for the ash ratio to be high here. Because the sweep flotation method is applied to the residue sample. The ash of the residue obtained from I. cleaning flotation method was 49.51%. The ash of the concentrated product obtained as a result of II. cleaning flotation was determined as 8.85% and the ash of the residue was

determined as 19.85%. The burnable ash of the concentrate was calculated as 91.15% and the burnable ash of the residue was calculated as 80.15%. The burnable efficiency of the concentrate was 28.36% and the burnable efficiency of the residue was 32.85%. When these results were examined; After II. cleaning flotation, both the ash ratios of the products as both concentrate and residue decreased and increased their burnable ash and yields.

ACKNOWLEDGEMENT

The author would like to thanks Prof. Dr. Tayfun ÇİÇEK for his contributions to the realization of the experiments in this study.

REFERENCE

Kavi, U. (1994). *Zonguldak Kömürünün Flotasyonunda Kollektör Miktar Değişiminin ve Kolon Flotasyonunun Ürünlere Olan Etkisi*. Yıl içi Projesi. İzmir.

Cöcen, I., Cilingir, Y. and Malayoglu U. (1993). *Benefication of Zonguldak High Ashed Coal by Conventionel Column Flotation. Geosand Journal*. D.E.U. Department of Mining Engineering, İzmir.

Tunalı, G. (1994). *Zonguldak Merkez Lavvar Şlamı Flotasyonunda Reaktiflerin Etkinliğinin Araştırılması. Diploma Proesi. D.E.U. İzmir.*

Yasan, S. (1994). *Küllü Yüksek Zonguldak Kömürlerinin Kolon Flotasyonu ile Zenginleştirilmesi.* Seminer. D.E.U. İzmir.

Çetinkaya, A. (1994). *Zonguldak Merkez Lavvar Şlamı Flotasyonunda Bazı Reaktiflerin Etkinliğinin Araştırılması,* Diploma Tezi, Dokuz Eylül Üniversitesi, Mühendislik Fakültesi, Maden Mühendisliği Bölümü, İzmir.

Atak, S., Toroğlu, İ. (1990). Türkiye Kömürleri ile Flotasyon, İ.T.Ü Dergisi, Cilt 48, No: 4, İstanbul.

Bilgin, O. (2019). Investigation and Comparison of the Enrichment Potential of Turkey (Şenkaya, Erzurum) Coals with Knelson Concentrator. Advances in Materials Science and Engineering. Article ID 9036047.

Forty-Two Years of the Simulated Annealing Algorithm: A Bibliometric Analysis

Ahmet AKKAYA[1*]
Cemil KÖZKURT[2]

[1] *Bandırma Onyedi Eylül University, Bandırma, Turkey, aakkaya@bandirma.edu.tr, ORCID: 0000-0003-4836-2310
[2] Bandırma Onyedi Eylül University, Bandırma, Turkey, ckozkurt@bandirma.edu.tr, ORCID: 0000-0003-1407-9867

ABSTRACT

Nowadays, in large-scale and complex work environments, efficient search methods play a critical role in order to speed up the search process and find the best solution. In cases where traditional optimization techniques are insufficient, metaheuristic algorithms come into play. Metaheuristic algorithms make it possible to reach global optimum solutions by effectively scanning complex solution spaces. In particular, techniques like Ant Colony Optimization, Particle Swarm Optimization, Genetic Algorithms, and Simulated Annealing are frequently employed in problems related to optimization. Thanks to these methods, faster, flexible and applicable solutions are developed. Simulated Annealing Algorithm, one of these algorithms, has started to be widely used in solving complex combinatorial and continuous optimization problems. Within the scope of this study, a bibliometric analysis of the researches conducted in the literature using Simulated Annealing Algorithm in the last forty-two years (1983-2024) was conducted. In the study, 31018 publications were reached by searching the keywords "simulated annealing" in the Web of Science database. The VOSviewer tool was used to evaluate the data that was taken from the Web of Science database utilizing network analysis, literature analysis, and visual data discovery techniques. As a result of the analysis, studies conducted in various categories were given quantitatively with all their details. It is evaluated that these statistical data will be an important reference source and guide for researchers in future studies in terms of the use of the Simulated Annealing (SA) algorithm. It is thought that these data, which support the solution performance and application areas of the SA algorithm, will contribute to the selection of effective methods in optimization problems and will enable the advancement of theoretical and applied research in this field.

Keywords: Simulated, Annealing Optimization, Algorithm, Bibliometric, Analysis.

INTRODUCTION

Optimization is a mathematical process that aims to find the best solution under a certain objective function (Tektas, 2010). Optimization problems are based on exploring the solution space to search for maximum or minimum values (Aarts et al., 2005). Such problems can be constrained or unconstrained and are considered as combinatorial, continuous or multi-objective (Bazaraa et al., 2013). In solving optimization problems, classical methods can sometimes be insufficient for complex and multi-dimensional problems (Karimi-Mamaghan et al., 2022). In such cases, metaheuristic algorithms, which offer a more flexible and comprehensive search strategy, stand out with their potential to obtain global solutions (Seyyedabbasi et al.,

2021). Metaheuristic algorithms are used in complex, large-scale or multi-dimensional optimization problems where classical methods are ineffective.

These algorithms are distinguished by their random search strategies and ability to explore the problem space on a large scale. Metaheuristic methods are designed to avoid local optima and reach global optima (Talbi, 2009). While metaheuristic algorithms provide fast and effective solutions in complex search spaces, they have some difficulties in terms of parameter settings and computational cost. However, due to their versatility and wide application area, they are preferred in various engineering (Pan et al., 2022), logistics (Rajmohan & Shahabudeen, 2009) and data mining (Mandour et al., 2024) problems. The most popular metaheuristic algorithms used in these problems are Particle Swarm Optimization Algorithm (PSO), Genetic Algorithm (GA), Whale Optimization Algorithm (WOA), Gray Wolf Optimization Algorithm (GWO) and Simulated Annealing Algorithm (SA) (Akkaya et al., 2023). One of the popular algorithms, SA, is an optimization technique inspired by the annealing process of materials science. In the annealing process, materials are heated and cooled in a controlled manner, allowing them to reach a low-energy, stable state. Inspired by this process, the SA algorithm was proposed by (Kirkpatrick et al., 1983) and has been widely used in solving complex combinatorial and continuous optimization problems. SA works by making random changes to a solution. It accepts these changes with a probabilistic rule depending on a "temperature" parameter. This temperature value of the algorithm decreases over time. The decreasing temperature value allows SA to leave the local best solutions and discover the global optimum (Kirkpatrick et al., 1983).

According to the mathematical modeling of SA, first a random starting point is selected and then the initial temperature T_0 is determined. Then a new solution close to the current solution is generated. The new solution is evaluated with the cost function $f(x)$. Worse solutions are accepted with a probability given by Equation (1).

$$P(\Delta E) = \begin{cases} 1 & if\ \Delta E\ < 0 \\ exp\left(-\frac{\Delta E}{T}\right) & if\ \Delta E\ \geq 0 \end{cases} \qquad \text{Equation (1)}$$

Here ΔE represents the cost difference and T represents the temperature.

The temperature is reduced at the end of each iteration. Usually, the geometric reduction given by Equation (2) is applied.

$$T_{k+1} = \alpha\, T_k \qquad \text{Equation (2)}$$

Where α $(0 < \alpha < 1)$, is the temperature reduction coefficient.
The aim is to minimize the cost function $f(x)$.

$\min f(x)$ Equation (3)

This is particularly used in optimization problems where a global minimum is desired (Černý, 1985). SA has been shown to show effective results on the Traveling Salesman Problem (TSP) by initially generating heuristic solutions and then improving these solutions with random changes (Zhan et al., 2016). They investigated how SA is used in the optimization of very constrained environments and emphasized its adaptability, especially in structural engineering tasks (Leite & Topping, 1999a). (Cao et al., 2022) introduced the Multi-Objective Simulated Annealing (MOSA) algorithm to address multi-criteria problems. It has been stated that MOSA establishes a balance between competing objectives by using Pareto advantage when evaluating solutions. SA has been widely used in areas such as job shop scheduling (Elmi et al., 2011), manufacturing processes (T.-H. Wu et al., 2008), and cloud computing resource management (Pandit et al., 2014).

Over time, hybrid versions of SA have emerged, as have other metaheuristic algorithms. Combining SA with other metaheuristic methods such as GA (Fatyanosa et al., 2016) and PSO-DE (Mirsadeghi & Khodayifar, 2021) has been shown to contribute to better convergence rates and higher quality solutions. Dynamic cooling rate control has been shown to provide more efficient exploration and exploitation phases by reducing computational time while maintaining solution quality (Faber et al., 2005). With the rise of high-performance computing, parallel implementations of SA for large-scale optimization tasks have gained popularity (Leite & Topping, 1999b).

In the literature, despite the strengths of SA, it is seen that there are difficulties such as parameter setting and computational cost. The performance of the algorithm depends heavily on parameters such as cooling plan and initial temperature. In addition, although SA is effective for global optimization, it can be computationally intensive for large solution areas.

In this study, the research conducted since 1986, when SA emerged, has been presented with quantitative data using the bibliometric analysis technique. In the next section, the method of the research, the purpose of the research, and the data and analysis conducted in the research will be discussed.

Methodology of the study

Bibliometric analysis is a method that aims to reveal developments and trends in a particular field by examining the relationships between publications, citations, and authors in the scientific literature. This type of analysis is frequently used to measure scientific productivity, impact, and research trends (Aria & Cuccurullo, 2017). Bibliometric analysis is performed on various indicators such as the number of published articles, citation counts, journal impact factors, and author collaborations (Börner, 2010). In addition, this method provides valuable information to identify gaps and potential future

directions in research areas (Ganaie & Wani, 2021). Modern bibliometric analyses are carried out more precisely and comprehensively with the help of databases and software tools (van Raan, 2019). Within the scope of the research, bibliometric analysis was conducted with the VOSviewer program using the data that was taken from the Web of Science.

Purpose of the study

Using the keywords "Simulated Annealing" and the bibliometric analysis approach, the study's objective is to analyze 31,018 articles on SA that have been published in the Web of Science (WoS) database over the previous 42 years (1983–2024). This analysis aims to reveal the trends of research in the field of SA, author collaborations, most cited studies, and journal impacts through various quantitative data. In addition, this study aims to attract the attention of researchers by determining the development of SA over time and the most striking aspects in its scientific field.

Data and analysis

There are various advanced software tools such as CiteSpace, Bibliometrix, Gephi, HistCite, EndNote and VOSviewer to perform bibliometric analysis of data. In order to ensure the reliability of the study, the Web of Science (WoS) database, which provides comprehensive access to academic data, was used. VOSviewer software was used in this study to evaluate the data that was taken from the WoS database. VOSviewer is a tool specifically developed for the visualization of scientific literature and allows mapping scientific networks, interactions and connections between publications. VOSviewer, which is considered an important tool in areas such as literature analysis, network analysis and visual data discovery, is widely used especially in bibliometric analyses performed with large data sets. This software offers significant advantages for scientific research with its functions such as visualization of data, examination of network structures and interactive analyses, user-friendly interface and free accessibility. The visualization and analysis opportunities provided by VOSviewer enable scientists to perform literature and network analyses more effectively and efficiently. In this context, in this study, a comprehensive bibliometric analysis was performed using the VOSviewer program with data from 31,018 publications obtained from the WoS database as of November 2024, using the keyword "Simulated Annealing".

FINDINGS

In this section, analyses of various categories in the WoS database are presented within the scope of the research conducted. These analyses cover a wide range of topics such as the distribution of publications over the years, document types, WoS index distributions, research profiles and distribution of publication titles according to research categories. In addition, the distribution of publications by country, publisher distribution and distribution of research fields conducted were also examined. In the study, the distribution of citation subjects of publications at the meso and micro levels and the distribution of publications according to publication languages were also evaluated. The analysis of co-authored studies was also included, and collaborations between co-authored researchers, institutions and countries were examined. Citation analyses of the sources from which publications were made, citation analyses of the authors who published, and citation relations between countries and institutions were also discussed in detail. These findings provide important data for understanding the evolution and dynamics of the research field.

Distribution of WoS categories

Figure 1 displays the distribution of publications based on WoS categories as a consequence of the analysis. This visual clearly shows how publications in various research areas are distributed and the proportion of each category in the literature. Figure 1 visually presents the analysis results based on categorical classifications in the WoS database in order to better understand the scientific framework of the research topic.

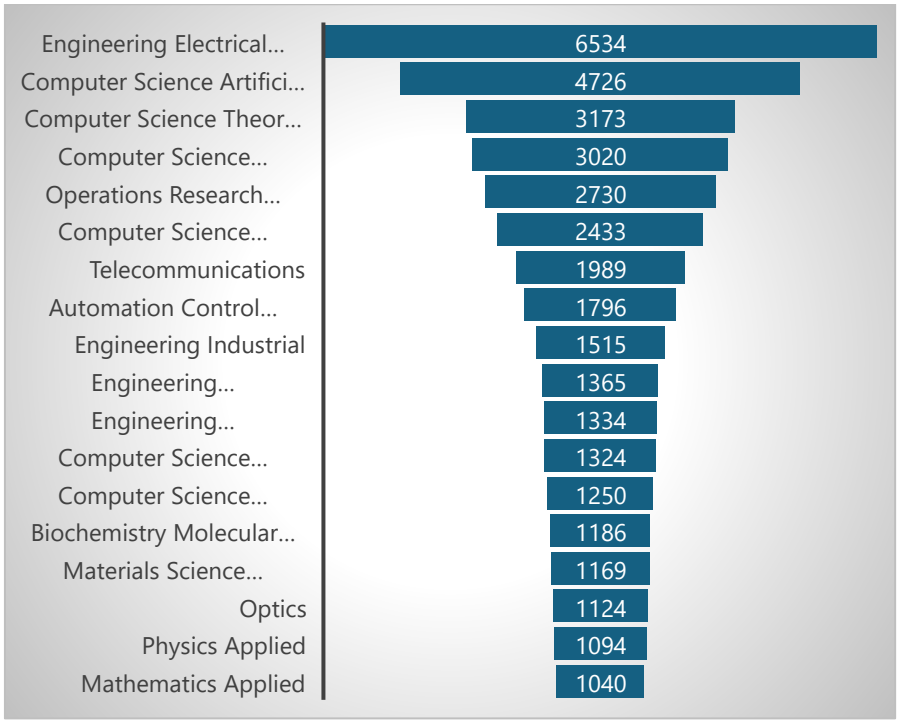

Figure 1: Distribution of publications according to WoS categories

Electrical and Electronics Engineering (6534 publications) is the category with the most publications. This shows that research on electrical engineering, electronics, communication and other technological infrastructures has an important place and that there are many studies in this field. Engineering disciplines such as Electrical and Electronics Engineering have a large research volume in parallel with the rapid development of new technologies and digital infrastructures. Computer Science Artificial Intelligence (4726 publications) has a large number of publications and shows that advances in the field of artificial intelligence are rapidly increasing. Research in this field reflects the increasing demand for machine learning, deep learning and artificial intelligence applications. Computer Science-Theoretical Methods (3173 publications) shows the interest in theoretical computer science research. Basic computer science topics such as algorithms, data structures and theory of computation have a high number of publications. Categories such as Computer Science Interdisciplinary Applications and Operations Research Management Science show multidisciplinary approaches and the interaction between engineering and management sciences. Research in these fields has an important place in the search for solutions to more complex and multifaceted problems. Categories such as Telecommunications and Automation Control Systems are gaining importance in parallel with the development of communication and automation systems.

Biochemistry and Molecular Biology (1186 publications) and biotechnology and biochemistry-related fields are showing significant growth as biological and health sciences become more prominent in the modern world. Advances in health, biotechnology and molecular biology in particular are increasing the interest in this category. Categories such as Materials Science Multidisciplinary, Mathematics Applied, Physics Applied, and Engineering Mechanical indicate the increasing interest in interdisciplinary research. Research in these areas emphasizes collaborations that transcend the boundaries between engineering, physics, materials science and mathematics. The increasing importance of applied research in fields such as mathematical modeling, engineering and physics significantly affects the high publication numbers of these categories. Categories with fewer publications such as Engineering Chemical (623 publications) and Mathematics Interdisciplinary Applications (694 publications) indicate that research in these areas has a relatively limited research volume.

Distribution of publications according to the year they were published

According to the findings obtained as a result of the analysis processes, Figure 2, which shows the distribution of publications by year, helps you analyze in which years more or less publications were made over time.

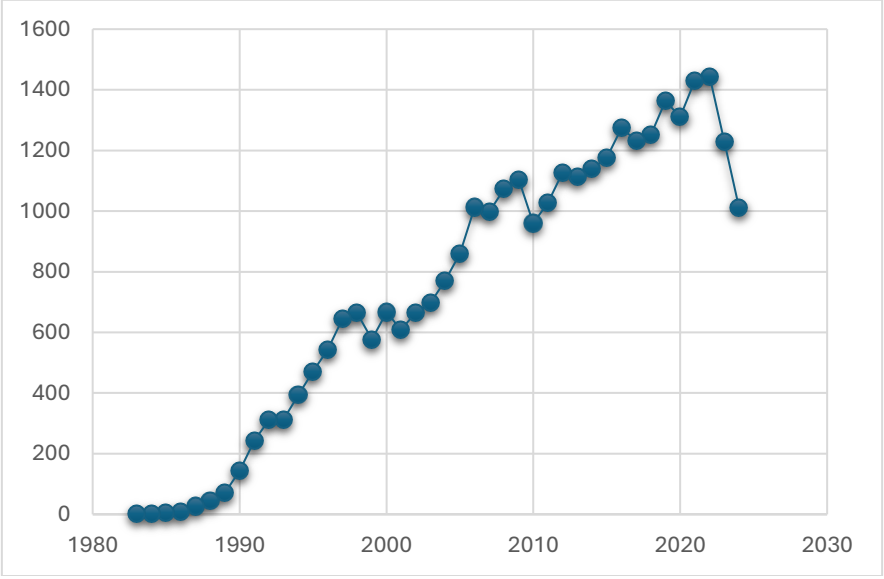

Figure 2: Distribution of publications by year

When Figure 2 is examined, the 1980s and early 1990s are the years when lower publication numbers are seen. It is seen that the number of publications was very low between 1984 and 1990, and only a few publications were made, especially in the first years (1983-1985). This

indicates the early years in the field of research; these were years when scientific research was less widespread and modern scientific research infrastructures were not yet fully developed. The 27 publications in 1987 and the 10 publications in 1986 indicate that a new research area was formed for the scientific community. The 1990s and 2000s were years when scientific research focused more on examining a specific topic or discipline in depth. Although the growth and interest in the field of research seems to have decreased in these years, it remains at very low levels, especially when compared to the studies published in the last few years. In the years before 2015, the increase in the number of publications was generally slower, with annual increases below 1000. These years are the years when technology development and research infrastructures progress at a slower pace with increasing support. The high number of publications in 2020, 2021, and 2022 show that external factors, especially the global pandemic, have a strong impact on research and scientific production. It is thought that research accelerated in areas such as health sciences, biotechnology, and digitalization in these years, and that more research may have been conducted in some areas due to factors such as remote work and online education. A significant increase is observed in the number of publications published in 2023, 2022, and 2021. This shows that research areas have developed rapidly and more resources have been allocated, especially since the late 2010s. A similar increase was observed in 2024 (1012 publications). This shows that although this year has not yet been completed, research continues rapidly and a large flow of publications continues.

Document type distribution of publications

Table 1 displays the distribution of publications by document type as a consequence of the analysis.

Table 1: Publications distributed by document type

Document types	Number of publications
Article	22003
Proc. Paper	9781
Review Article	261
Book Chapters	211
Early Access	185
Meeting Abstract	116
Note	63
Letter	50
Retracted Publication	39
Editorial Material	23
Correction	11
Software Review	9
Book Review	7
Book	4
Correction, Addition	4
Data Paper	3
Retraction	3
Bibliography	1

Article is the most common document type with 22003 publications. This shows that the vast majority of research is published in article format. Articles are the most preferred publication in the academic world and are aimed at providing scientific contribution. Conference Proceedings come in second with 9781 publications. These types of publications are an important source especially for researchers who want to share new research results quickly. Presentations and announcements made at conferences increase the exchange of information between scientific communities. Review Articles are an important category with 261 publications, but they are much less than articles and conference proceedings. Book Chapters are a less common type with 211 publications. Book chapters usually provide in-depth studies on a specific topic and have an important place in academic literature. Early Access 185 publications were found as Meeting Abstract (116), Note (63), Letter (50), Editorial Material (23), Correction, Addition and Book (4), Data Paper and Retraction (3) and Bibliography (1).

Meso distribution of publications' citation topics

As a result of the analysis, the meso (medium level) distribution of publications according to their citation topics is presented in Figure 3 in order to reveal how certain areas or topics come to the fore over time and which topics attract more attention.

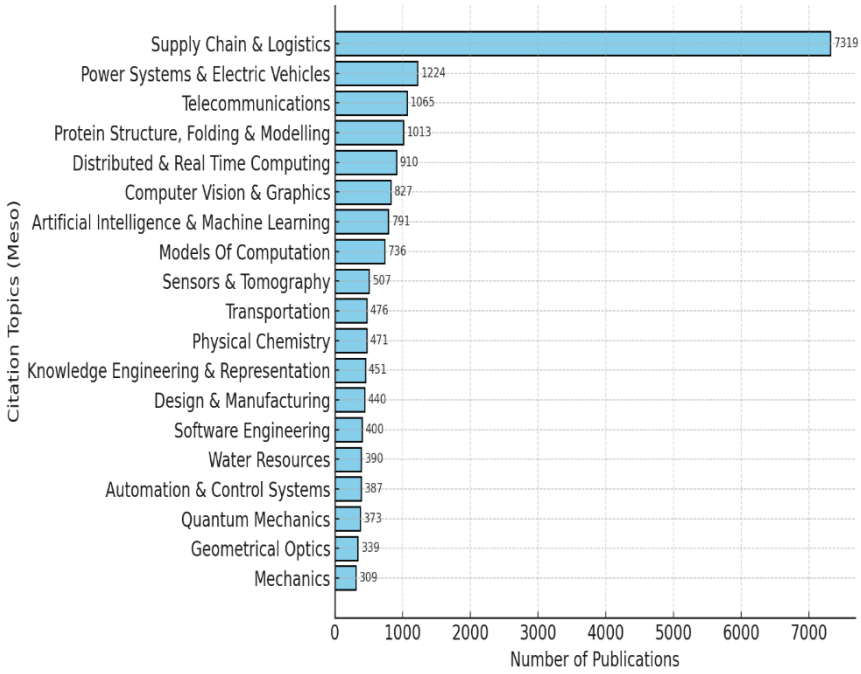

Figure 3:Meso distribution of publications' citation topics

When Figure 3 is examined, supply chain and logistics stands out as the most cited topic with 7319 publications. This shows that optimization, cost management and process improvement studies are intense in the fields of industry and trade. Power Systems & Electric Vehicles reflects the importance of energy management and sustainable transportation technologies in scientific research with 1224 publications. Telecommunications indicates an important research area for the development of communication technologies with 1065 publications. Protein Structure, Folding & Modeling shows that intensive research is carried out in the fields of biochemistry and molecular biology with 1013 publications. Distributed & Real-Time Computing emphasizes the importance of data processing speed and distributed systems in modern information processing systems with 910 publications. Artificial Intelligence & Machine Learning is at the center of technological innovations with 791 publications. Areas such as Knowledge Engineering and Representation also have an important place in knowledge management and artificial intelligence studies. Modeling and Computation, 736 publications, is

a fundamental research area for theoretical and applied computational studies. Sensors and Tomography, 507 publications, is an indicator of technological innovations in medicine and engineering. Transportation and Automation and Control Systems are seen to be prominent topics with modern engineering solutions and system optimizations.

Micro distribution of publications' citation topics

The distribution of publications by citation subjects at the micro level is shown in Figure 4 as a consequence of the analysis. This distribution reveals the tendencies and concentrations of researchers in certain fields.

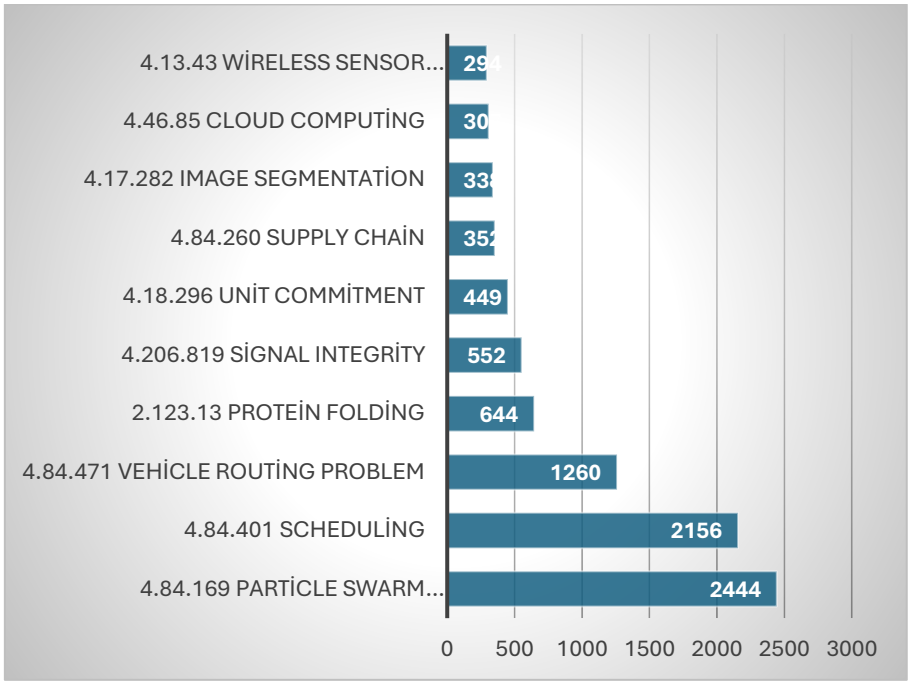

Figure 4: Micro distribution of publications' citation topics

When Figure 4 is examined, it is seen that Particle Swarm Optimization is the most popular research area at the micro level with 2444 publications. The interest in optimization algorithms shows that they are widely studied in both theoretical and applied areas. Scheduling emphasizes the importance of topics such as effective management of resources, work planning and process optimization with 2156 publications. Vehicle Routing Problem shows the intense academic interest in solving this problem in the field of logistics and transportation with 1260 publications. Protein Folding reflects the great interest in modeling protein structures in the field of biology and bioinformatics with 644 publications. Signal Integrity highlights the studies on preventing signal degradation especially in electronic and

telecommunication systems with 552 publications. Unit Commitment has an important place in energy systems optimization (449 publications) Supply Chain is being studied for the development of decision support systems, especially in logistics processes (352 publications) 338 publications in the field of image processing, especially Image Segmentation, reveal the importance of computer vision.

Web of Science index distributions

Following the investigation, Table 2 displays the articles based on their Web of Science indexes.

Table 2: WoS index distribution of publications

Web of Science Index	**Number of publications**	**% of 31.018**
Science Citation Index Expanded (SCI-EXPANDED)	20672	66.645
Conference Proceedings Citation Index – Science (CPCI-S)	9764	31.478
Emerging Sources Citation Index (ESCI)	1461	4.71
Social Sciences Citation Index (SSCI)	1290	4.159
Conference Proceedings Citation Index – Social Science & Humanities (CPCI-SSH)	253	0.816
Book Citation Index – Science (BKCI-S)	210	0.677
Index Chemicus (IC)	51	0.164
Book Citation Index – Social Sciences & Humanities (BKCI-SSH)	18	0.058
Arts & Humanities Citation Index (A&HCI)	4	0.013

Examining Table 2, it can be observed that Science Citation Index Expanded (SCI-EXPANDED) has the highest number of publications by far with 20,672 publications (%66.645). This index is one of the most comprehensive collections of scientific and technical publications and is the main source of the vast majority of research. Conference Proceedings Citation Index – Science (CPCI-S) stands out as an index where the results of scientific conferences are published, with 9764 publications (%31.478). It shows the high contribution of new ideas presented at conferences to this field. Emerging Sources Citation Index (ESCI) includes 1461 publications (%4.71) in emerging and potentially influential journals. This rate shows that research areas are expanding and various sources are being evaluated. Social Sciences Citation Index (SSCI) includes 1290 publications (%4.159) in social sciences-focused studies. Conference Proceedings Citation Index – Social Science &

Humanities (CPCI-SSH) 253 publications (%0.816) include conference proceedings in social sciences and humanities. Book Citation Index (BKCI-S & BKCI-SSH) 210 and 18 publications represent academic works from books. Index Chemicus (IC) 51 publications (%0.164) include special publications in chemistry. Arts & Humanities Citation Index (A&HCI) 4 publications (%0.013) represent a very limited number of publications in arts and humanities.

Journal name distribution according to publication titles

As a result of the analysis, Table 3 shows the distribution of journals according to the titles of the publications.

Table 3: Journal name distribution according to publication titles

Publication Titles	Number of publications	% of 31.018
Lecture Notes in Computer Science	718	2.315
International Journal of Production Research	278	0.896
Computers Industrial Engineering	270	0.87
IEEE Access	263	0.848
International Journal of Advanced Manufacturing Technology	257	0.829
European Journal of Operational Research	255	0.822
Computers Operations Research	237	0.764
Applied Soft Computing	228	0.735
Expert Systems with Applications	226	0.729
Biochemistry	224	0.722
Proceedings of SPIE	221	0.712
Proceedings of The Society of Photo Optical Instrumentation Engineers SPIE	211	0.68
Lecture Notes in Artificial Intelligence	204	0.658
IEEE Congress on Evolutionary Computation	145	0.467
Applied Sciences Basel	137	0.442
Physical Review B	135	0.435
Journal of Chemical Physics	131	0.422
Annals of Operations Research	125	0.403
Mathematical Problems in Engineering	125	0.403
AIP Conference Proceedings	123	0.397
Physical Review E	122	0.393
Journal of Molecular Biology	116	0.374
Advanced Materials Research	102	0.329
IEEE Transactions on Computer Aided Design of Integrated Circuits and Systems	99	0.319
Advances in Intelligent Systems and Computing	96	0.309

Examining Table 3, it can be observed that Lecture Notes in Computer Science is in the first place with 718 publications (%2.315). This journal is an important source in subjects such as computer science and artificial intelligence. International Journal of Production Research is an important journal in the field of production engineering and industrial research with 278 publications (%0.896). Computers Industrial Engineering is an important source in industrial engineering and computer applications with 270 publications (%0.87). IEEE Access is an important source in the fields of engineering, computer science and technology with 263 publications (%0.848) in a wide range of subjects. The International Journal of Advanced Manufacturing Technology stands out as an influential journal in the field of advanced manufacturing technologies with 257 publications (%0.829). European Journal of Operational Research is one of the important journals in the field of operations research and management sciences with 255 publications (%0.822).

Language distribution of publications

As a result of the analysis, the distribution of publication languages is visualized in Figure 5. This distribution shows in which languages publications are made and how the most widely used languages take place in the research.

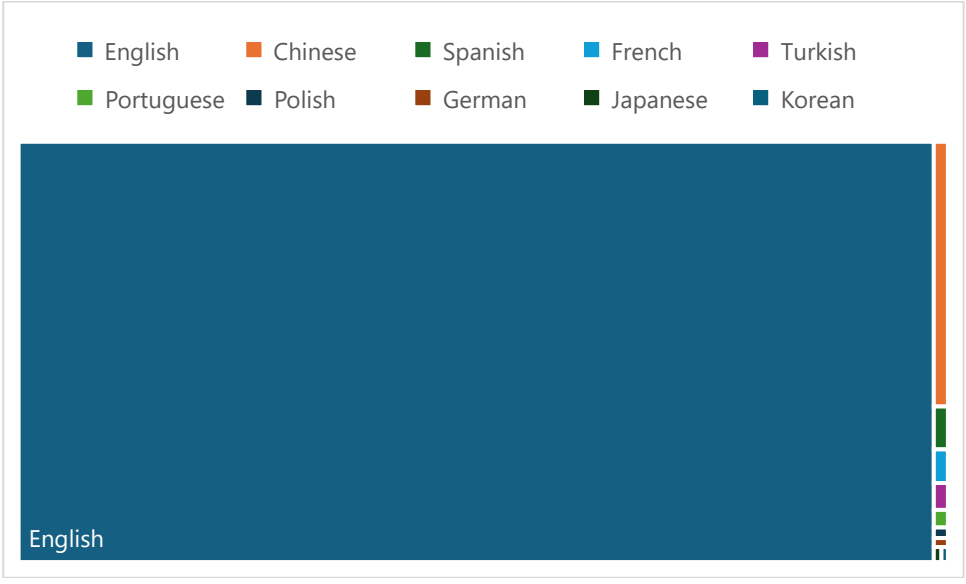

Figure 5: Distribution of publication languages

As a result of the analysis, the distribution of publication languages is summarized as follows: English was by far the most preferred language with 30,534 publications (98.43%). This shows that a large part of the global

scientific community prefers English and that scientific communication is largely conducted in this language. Chinese came in second with 298 publications (0.96%). China is an important country where scientific publications are increasing, and publications in Chinese are also increasing. Spanish came in third with 48 publications (0.15%). Spanish is used intensively, especially in research in Latin America and Spain. French came in fourth with 38 publications (0.12%), while the number of publications in other languages is more limited. Turkish was a much less preferred language in scientific publications with 30 publications (0.10%). Portuguese stood out as a language generally related to academic research in Brazil and Portugal with 20 publications (0.06%). Other languages appear to have a more limited publication rate, such as Polish (12 publications), German (10 publications), Japanese (9 publications) and Korean (8 publications).

Country distribution of publications

Table 4 displays the publications' publisher distribution as a consequence of the analysis. This table shows which publishers the researchers prefer for their publications.

Table 4: Publisher distribution of publications

Publishers	**Number of publications**	**% of 31.018**
Elsevier	6279	20.243
IEEE	6194	19.969
Springer Nature	4100	13.218
Wiley	1294	4.172
Taylor & Francis	1197	3.859
Mdpi	913	2.943
Amer Chemical Soc	720	2.321
Spie-International Society for Optical Engineering	495	1.596
Iop Publishing Ltd	416	1.341
Assoc Computing Machinery	343	1.106
Amer Inst Physics	327	1.054
Hindawi Publishing Group	327	1.054
Amer Physical Soc	322	1.038
World Scientific	247	0.796
Sage	241	0.777
Trans Tech Publications Ltd	233	0.751
Oxford Univ Press	205	0.661
Optical Soc Amer	160	0.516
Inderscience Enterprises Ltd	140	0.451
KLUWER ACADEMIC PUBL	139	0.448
Science Press	136	0.438
Ios Press	132	0.426
Royal Soc Chemistry	122	0.393
Emerald Group Publishing	117	0.377
Asce-Amer Soc Civil Engineers	113	0.364

When Table 4 is examined, Elsevier is the publisher with the most publications with 6,279 publications (20.24%). IEEE is in second place with 6,194 publications (19.97%). Springer Nature is in third place with 4,100 publications (13.22%). Wiley is in fourth place with 1,294 publications (4.17%). Taylor & Francis is in fifth place with 1,197 publications (3.86%). MDPI is in sixth place with 913 publications (2.94%). Other publishers, although at lower rates, have an important place in scientific publishing. It is seen that reputable publishing houses such as the American Chemical Society

(720 publications), SPIE (495 publications) and IOP Publishing (416 publications) also have an important share in scientific publishing.

Co-authorship works by authors

Figure 6 displays the relationships between the publications' co-authorship authors as a consequence of the analysis. Such analyses provide important information about the intensity of scientific collaborations, how a network is formed between the authors, and which researchers collaborate more with each other.

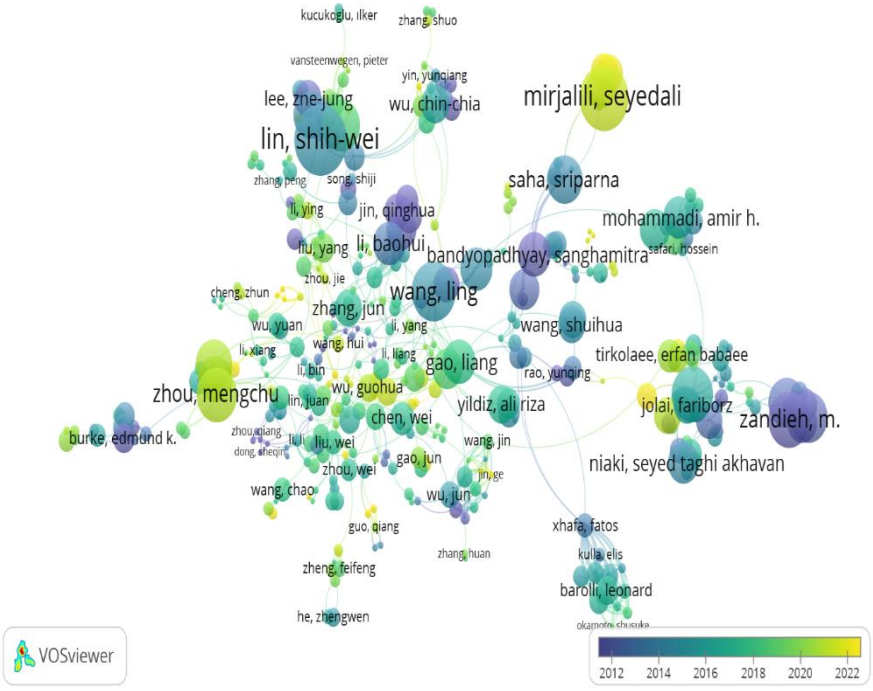

Figure 6: Links between publications with co-authors

When Figure 6 is examined, it is seen that Brunger, A.T. is a highly cited author with 4889 citations. This shows that his work on SA is widely accepted by the scientific community and that he has made important contributions. At the same time, the total connection strength of 20 reveals that Brunger is also active in collaborative research and has an important place in the network. Clore, G.M. Citation Count: 6356, connection strength of 48 shows that Clore has a strong academic collaboration network and SA studies spread over a wide research area. Giacovazzo, C. Citation Count: 2095 is an author who has received over 2000 citations despite having a small number of publications. This shows that his work is qualified and effective. The connection strength

of 22 shows that he has an important place in the academic network. Other authors are Gronenborn, A.M. 5017, Lin, S.W. It is seen that they have received a significant number of citations in the field of SA with 2291, Liu, Y. 3137, Maleki, A. 2130, Mirjalili, S. 2032, Nilges, M. 3813, Sen, M.K. 1865.

The connection between organizations' citation analysis

As a result of the analysis, the overlay visualization graph according to the citation numbers of the institutions is given in Figure 7.

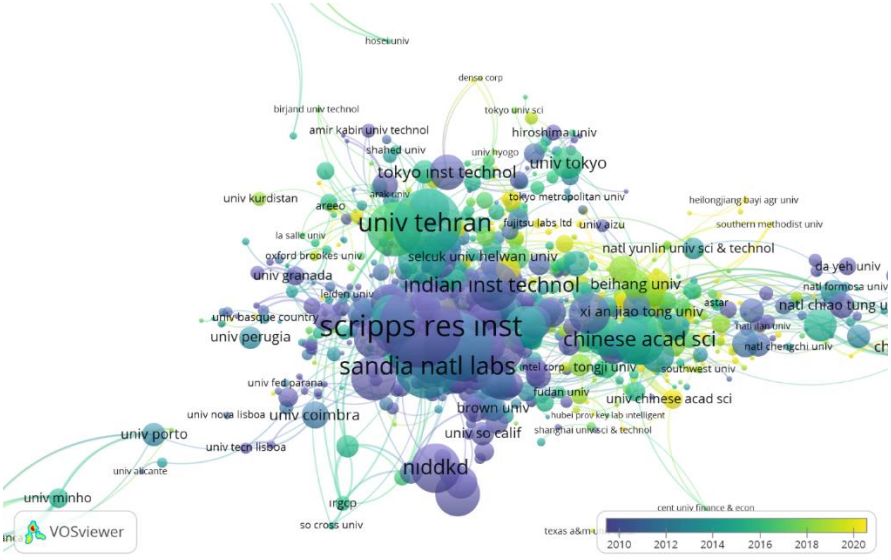

Figure 7: Overlay visualization graph according to the citation counts of institutions

The ranking of institutions according to the number of citations is as follows. University of Tehran (323 publications, 11,215 citations) It is the institution with the most citations. The high number of citations shows that its publications have a wide scientific impact and recognition. University of California, San Diego (67 publications, 10,891 citations) It has a high number of citations and can be said to be accepted and effective in many different disciplines. Other institutions are Sandia National Laboratories (12 publications, 9,667 citations), Scripps Research Institute (15,577 publications, 12 citations), Islamic Azad University (366 publications, 7,343 citations). Selcuk University is the most cited institution in Türkiye with 25 publications and 1145 citations.

Co-authorship country analysis

As a result of the analysis, the connection between the countries where co-authored publications work is given in Figure 8.

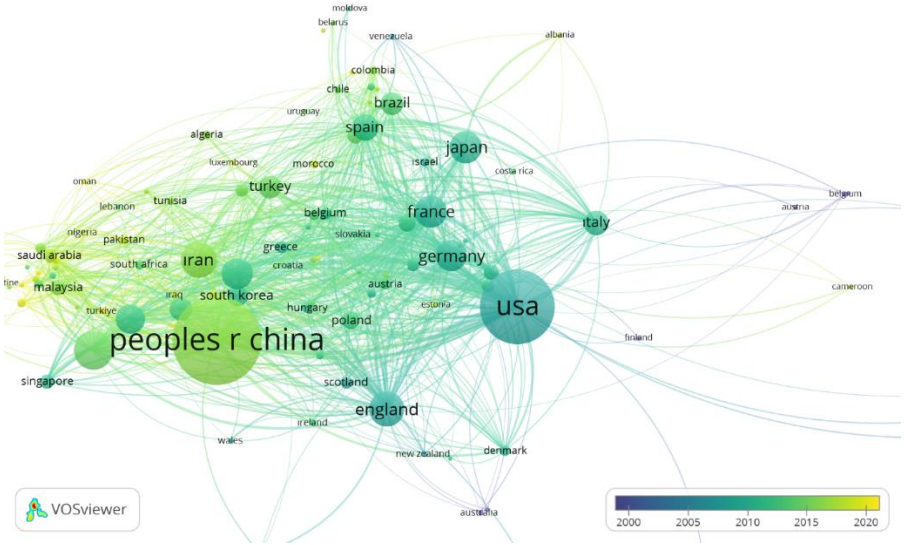

Figure 8: The connection between the countries in which co-authored publications work

According to Figure 8, the USA is the clear leader with 209,613 citations and 2256 link power from 5563 publications; this shows that it has a wide scientific impact and strong collaborations with other countries. The People's Republic of China stands out in terms of both production volume and collaboration with 90,630 citations and 1806 link power from 7602 publications, but lags behind the USA. Although the UK and France are behind in terms of publication and citation numbers, they have an important place in global collaboration with 1024 and 795 link power, respectively. Although Iran and Turkey have a more limited impact with lower citation and link power, especially Iran with 698 and Turkey with 230 link power, they play an important role in regional collaborations.

Co-occurrence analysis of all keywords

As a result of the analysis, the overlay visualization graph according to the number of keywords is given in Figure 9.

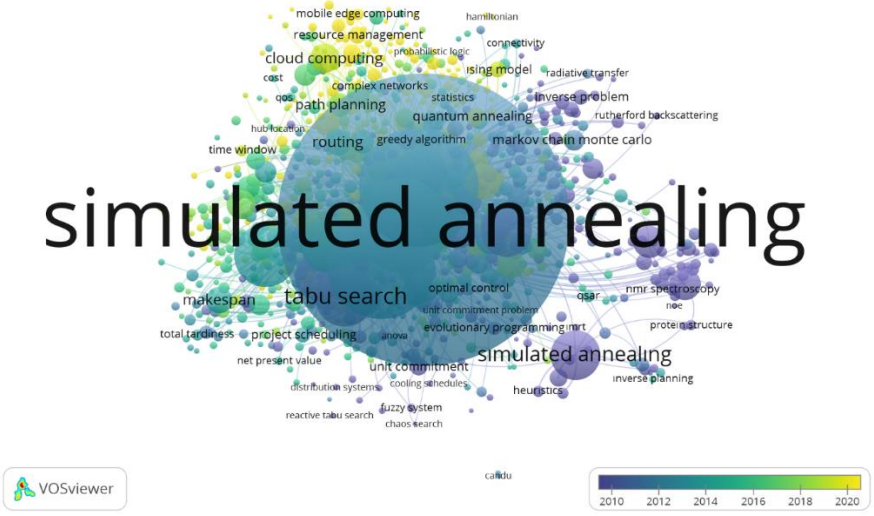

Figure 9: Overlay visualization chart based on keyword counts

The distribution and connection strength among the keywords are examined in the overlay visualization graph given in Figure 9. The term "Simulated annealing" stands out as the most dominant keyword with 8477 uses and 13,354 total connection strength. This shows its central role and wide usage area in the relevant literature. The keyword "Optimization" is second with 1709 uses and 3497 connection strength, which emphasizes the importance of simulation-based algorithms in general optimization problems. Other important keywords such as "Genetic algorithm" and "particle swarm optimization" are represented with lower frequency and connection strength. This shows that GA and PSO algorithms are used as hybrids with SA. Terms such as "Simulated annealing algorithm" and "scheduling" indicate the application areas focused on in the research. These results reveal that "Simulated annealing" and optimization approaches are the cornerstones in the literature.

Analysis of publications according to citation count

As a result of the analysis, the connections between the works in which the publications were published and the number of citations these works received are visualized in Figure 10.

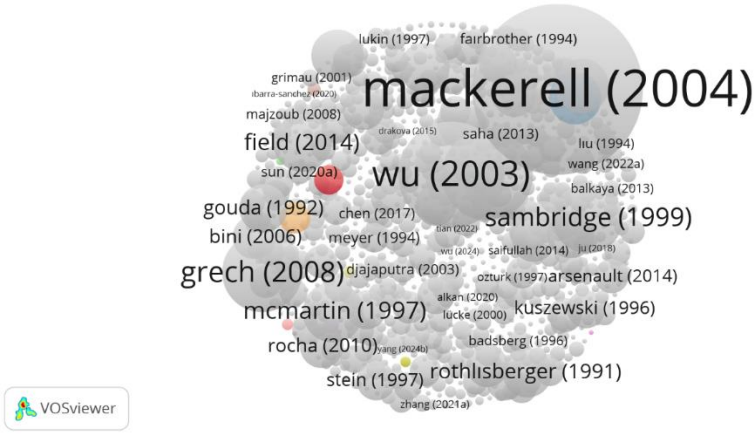

Figure 10: Citation analysis of publications based on published work

According to the analysis results, the study with the highest number of citations is (Mackerell Jr. et al., 2004) and has received a total of 2920 citations. This shows that the impact of the study in its field is quite large. (G. Wu et al., 2003) is in second place with 1261 citations, followed by (Oganov et al., 2011) (960 citations), (Grech et al., 2008) (760 citations) and (Sambridge, 1999) (595 citations). These findings show that these studies play a pioneering and guiding role in SA field in the literature.

The connection between the citations in the published sources

Figure 11 shows the relationship between the quantity of publications and citations in the journals where the articles were published as a result of the analysis.

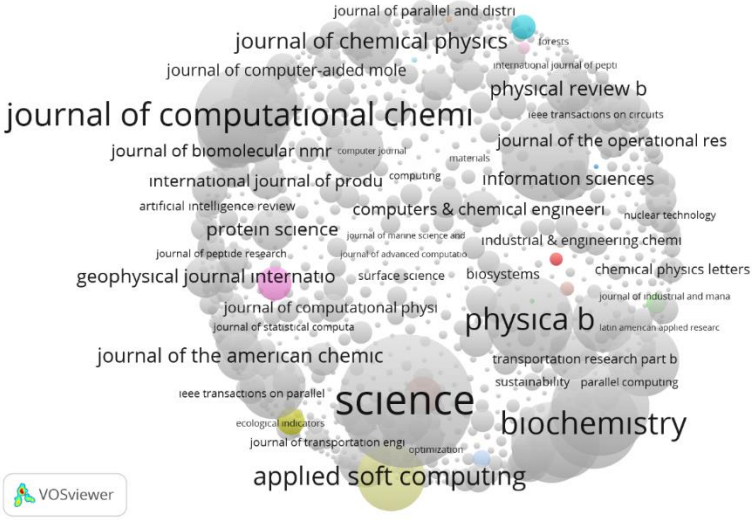

Figure 11: The relationship between the number of publications and citations in the journals in which the publications are published

According to the analysis results, Science has the highest number of citations (29,415) with 7 documents, indicating its great impact in the field. European Journal of Operational Research is one of the influential journals with the highest number of documents with 255 documents and 16,953 citations. Journal of Computational Chemistry and Journal of Molecular Biology provide high scientific contributions with 16,261 and 13,986 citations, respectively. Biochemistry has a wide-ranging impact with 224 documents (15,125 citations). These journals represent strong academic contributions in their respective fields.

RESULTS

Examining the distribution results of publications based on WOS categories reveals that some fields (especially engineering and computer science) have a very strong publication production capacity and that research in these fields is developing rapidly. On the other hand, it is concluded that fields such as biotechnology, biochemistry and interdisciplinary research continue to grow.

When the distribution of publications by year is examined, it is seen that scientific research has increased rapidly from the past to the present and has gained momentum since the 2000s. There was a significant increase in the 2010s and this increase has continued to gain momentum especially in recent years. While fewer publications were made in the 1980s and 1990s, there has

been a great development in scientific fields since the 2000s and today we have reached a period in which research is increasing rapidly.

The most common publication type is the article, and most contributions to scientific literature are made in this format. Conference proceedings are in second place and present fast-spreading, up-to-date research results. Less common types encourage a deeper focus on specific research topics and the sharing of knowledge in specialized fields.

The meso distributions of publication citation topics cover both traditional engineering and scientific approaches and innovative research areas such as artificial intelligence, energy, and biochemistry. While supply chain and logistics are clearly the leaders, other areas are shaped around modern technologies and applications. This distribution clearly shows the interest in interdisciplinary studies and the importance of technological innovations in scientific research.

Micro-level citation topics show that researchers focus on solving specific problems. Areas such as optimization, logistics, bioinformatics, and computer vision stand out as priority research topics for both theoretical innovations and applied solutions. This density reflects the strategic importance of these areas for industry and academia.

The analysis of WoS index distributions reveals that the vast majority of research publications are collected in science and technology-focused indexes such as SCI-EXPANDED and CPCI-S. Although the percentage contributions of other indexes are lower, this may be due to the fact that these areas appeal to a more specific audience. As a result, the distribution of study results shows that research is generally science and engineering based and less focused on multidisciplinary studies. Journal name distributions according to publication titles reveal that research is mostly published in journals in the fields of engineering, computer science and manufacturing. Lecture Notes in Computer Science journal provides the largest contribution, especially in the field of computer science. In addition, it is seen that journals in fields such as manufacturing, operations research and industrial engineering are also highly preferred. Most of the journals focus on engineering and applied sciences, which shows how important these fields are in terms of research and how many publications are made in these fields.

English is the dominant language of scientific publications as the most preferred language in publications. Since English is used as a bridge language for international research, this enables global academic collaborations and data sharing to reach a wider audience. Although other languages, especially Chinese and Spanish, are seen to be used more in certain geographies, it is clear that English is the most widely preferred language worldwide.

According to the publisher distribution of publications, large publishing houses such as Elsevier and IEEE continue their dominance in scientific literature. Other large publishers such as Springer Nature and Wiley have gained an important place with their wide range of disciplines. Publishers such

as MDPI, Taylor & Francis, SPIE publish their journals in certain fields and make important contributions in this field.

According to the citation analysis of authors in co-authored publications, it is seen that especially authors such as Clore and Brunger have high citation numbers and also have a strong academic collaboration network. Other authors, although they have different citation and connection power levels, are generally considered to have an important place in scientific literature. The works of these authors constitute an important resource, especially in the field of SA.

The University of Tehran, which has the highest number of citations in terms of the number of citations of institutions, is widely accepted and can be said to have made important scientific contributions. Institutions such as Sandia National Laboratories, which have a small number of publications but a high number of citations, reveal that their publications offer extremely effective and important content. It is seen that institutions such as Scripps Research Institute and Islamic Azad University also have quite high citation numbers.

According to the analysis results of the number of citations, number of publications and link strength of countries in co-authored studies, the scientific impact of countries was evaluated in terms of both the number of citations and link strength. It is seen that the USA is the leader in global scientific collaborations with 209,613 citations and 2256 link strength. China ranks second in production volume with 90,630 citations and 1806 link strength, while it is behind the USA in collaborations. Although the number of publications is lower, the UK and France are important actors in international collaborations with their high number of citations and link strength. At the regional level, countries such as Iran and Turkey maintain their potential for cooperation, although they have more limited influence.

According to the analysis results made according to keywords, "Simulated Annealing" stands out as the most effective keyword in the literature with a usage frequency of 8477 and a link strength of 13,354. This is followed by other important terms such as "Optimization" and "Genetic Algorithm". These findings show that "Simulated Annealing" plays a central role in optimization problems and has a wide area of use.

According to the analysis results of the publications based on the published works, Mackerell (2004) stands out as the most effective study with 2920 citations. It is followed by Wu (2003), Oganov (2011), Grech (2008) and Sambridge (1999). It can be said that these studies have a significant impact in their fields related to SA.

According to the analysis results of the number of citations in the published journals, it was concluded that journals such as Science, European Journal of Operational Research, and Journal of Computational Chemistry have significant scientific impact in their fields with their high citation numbers and document contributions.

REFERENCES

Aarts, E., Korst, J., & Michiels, W. (2005). Simulated Annealing. Içinde E. K. Burke & G. Kendall (Ed.), *Search Methodologies: Introductory Tutorials in Optimization and Decision Support Techniques* (ss. 187-210). Springer US. https://doi.org/10.1007/0-387-28356-0_7

Akkaya, A., Közkurt C. & Durgut R. (2023). A study on meta-heuristic algorithms used for problem solving in recent years. *Pioneer and Contemporary Studies in Engineer*ing 18, 327-352.

Aria, M., & Cuccurullo, C. (2017). *bibliometrix*: An R-tool for comprehensive science mapping analysis. *Journal of Informetrics*, *11*(4), 959-975. https://doi.org/10.1016/j.joi.2017.08.007

Bazaraa, M. S., Sherali, H. D., & Shetty, C. M. (2013). *Nonlinear Programming: Theory and Algorithms*. John Wiley & Sons.

Börner, K. (2010). *Atlas of Science: Visualizing what we know*. MIT Press.

Cao, P., Zhang, Y., Zhou, K., & Tang, J. (2022). A reinforcement learning hyper-heuristic in multi-objective optimization with application to structural damage identification. *Structural and Multidisciplinary Optimization*, *66*(1), 16. https://doi.org/10.1007/s00158-022-03432-5

Černý, V. (1985). Thermodynamical approach to the traveling salesman problem: An efficient simulation algorithm. *Journal of Optimization Theory and Applications*, *45*(1), 41-51. https://doi.org/10.1007/BF00940812

Elmi, A., Solimanpur, M., Topaloglu, S., & Elmi, A. (2011). A simulated annealing algorithm for the job shop cell scheduling problem with intercellular moves and reentrant parts. *Computers & Industrial Engineering*, *61*(1), 171-178. https://doi.org/10.1016/j.cie.2011.03.007

Faber, R., Jockenhövel, T., & Tsatsaronis, G. (2005). Dynamic optimization with simulated annealing. *Computers & Chemical Engineering*, *29*(2), 273-290. https://doi.org/10.1016/j.compchemeng.2004.08.020

Fatyanosa, T. N., Sihananto, A. N., Alfarisy, G. A. F., Burhan, M. S., & Mahmudy, W. F. (2016). Hybrid Genetic Algorithm and Simulated Annealing for Function Optimization. *Journal of Information Technology and Computer Science*, *1*(2), Article 2. https://doi.org/10.25126/jitecs.20161215

Ganaie, S. A., & Wani, J. A. (2021). Bibliometric analysis and visualization of Nanotechnology Research Field. *COLLNET Journal of Scientometrics and Information Management*, *15*(2), 445-467. https://doi.org/10.1080/09737766.2021.2008780

Grech, R., Cassar, T., Muscat, J., Camilleri, K. P., Fabri, S. G., Zervakis, M., Xanthopoulos, P., Sakkalis, V., & Vanrumste, B. (2008). Review on solving the inverse problem in EEG source analysis. *Journal of NeuroEngineering and Rehabilitation*, *5*(1), 25. https://doi.org/10.1186/1743-0003-5-25

Karimi-Mamaghan, M., Mohammadi, M., Meyer, P., Karimi-Mamaghan, A. M., & Talbi, E.-G. (2022). Machine learning at the service of meta-heuristics for solving combinatorial optimization problems: A state-of-the-art. *European Journal of Operational Research*, *296*(2), 393-422. https://doi.org/10.1016/j.ejor.2021.04.032

Kirkpatrick, S., Gelatt, C. D., & Vecchi, M. P. (1983). Optimization by Simulated Annealing. *Science*, *220*(4598), 671-680. https://doi.org/10.1126/science.220.4598.671

Leite, J. P. B., & Topping, B. H. V. (1999a). Parallel simulated annealing for structural optimization. *Computers & Structures*, *73*(1), 545-564. https://doi.org/10.1016/S0045-7949(98)00255-7

Leite, J. P. B., & Topping, B. H. V. (1999b). Parallel simulated annealing for structural optimization. *Computers & Structures*, *73*(1), 545-564. https://doi.org/10.1016/S0045-7949(98)00255-7

Mackerell Jr., A. D., Feig, M., & Brooks III, C. L. (2004). Extending the treatment of backbone energetics in protein force fields: Limitations of gas-phase quantum mechanics in reproducing protein conformational distributions in molecular dynamics simulations. *Journal of Computational Chemistry*, *25*(11), 1400-1415. https://doi.org/10.1002/jcc.20065

Mandour, S., Gamal, A., Sleem, A., & Belal, M. (2024). Data Mining Problems Optimization by using Metaheuristic Algorithms: A Survey. *Multicriteria Algorithms with Applications*, *4*, 28-52. https://doi.org/10.61356/j.mawa.2024.4301

Mirsadeghi, E., & Khodayifar, S. (2021). Hybridizing particle swarm optimization with simulated annealing and differential evolution. *Cluster Computing*, *24*(2), 1135-1163. https://doi.org/10.1007/s10586-020-03179-y

Oganov, A. R., Lyakhov, A. O., & Valle, M. (2011). How Evolutionary Crystal Structure Prediction Works—And Why. *Accounts of Chemical Research*, *44*(3), 227-237. https://doi.org/10.1021/ar1001318

Pan, J.-S., Zhang, L.-G., Wang, R.-B., Snášel, V., & Chu, S.-C. (2022). Gannet optimization algorithm: A new metaheuristic algorithm for solving engineering optimization problems. *Mathematics and Computers in Simulation*, *202*, 343-373. https://doi.org/10.1016/j.matcom.2022.06.007

Pandit, D., Chattopadhyay, S., Chattopadhyay, M., & Chaki, N. (2014). Resource allocation in cloud using simulated annealing. *2014 Applications and Innovations in Mobile Computing (AIMoC)*, 21-27. https://doi.org/10.1109/AIMOC.2014.6785514

Rajmohan, M., & Shahabudeen, P. (2009). Metaheuristic for solving routing problem in logistics management. *International Journal of Operational Research*, *6*(2), 223-246. https://doi.org/10.1504/IJOR.2009.026536

Sambridge, M. (1999). Geophysical inversion with a neighbourhood algorithm—II. Appraising the ensemble. *Geophysical Journal International*, *138*(3), 727-746. https://doi.org/10.1046/j.1365-246x.1999.00900.x

Seyyedabbasi, A., Aliyev, R., Kiani, F., Gulle, M. U., Basyildiz, H., & Shah, M. A. (2021). Hybrid algorithms based on combining reinforcement learning and metaheuristic methods to solve global optimization problems. *Knowledge-Based Systems*, *223*, 107044. https://doi.org/10.1016/j.knosys.2021.107044

Talbi, E. G. (2009). *Metaheuristics: From Design to Implementation*. John Wiley & Sons.

Tektas, M. (2010). OPTYMYZASYON TEKNYKLERYNYN TASNYFY VE YKY TEKNYK ÜZERYNDE YNCELEME. *Physical Sciences*, *5*(4), Article 4. https://doi.org/10.12739/10.12739

van Raan, A. (2019). Measuring Science: Basic Principles and Application of Advanced Bibliometrics. Içinde W. Glänzel, H. F. Moed, U. Schmoch, & M. Thelwall (Ed.), *Springer Handbook of Science and Technology Indicators* (ss. 237-280). Springer International Publishing. https://doi.org/10.1007/978-3-030-02511-3_10

Wu, G., Robertson, D. H., Brooks III, C. L., & Vieth, M. (2003). Detailed analysis of grid-based molecular docking: A case study of CDOCKER—A CHARMm-based MD docking algorithm. *Journal of Computational Chemistry*, *24*(13), 1549-1562. https://doi.org/10.1002/jcc.10306

Wu, T.-H., Chang, C.-C., & Chung, S.-H. (2008). A simulated annealing algorithm for manufacturing cell formation problems. *Expert Systems with Applications*, *34*(3), 1609-1617. https://doi.org/10.1016/j.eswa.2007.01.012

Zhan, S., Lin, J., Zhang, Z., & Zhong, Y. (2016). List-Based Simulated Annealing Algorithm for Traveling Salesman Problem. *Computational Intelligence and Neuroscience*, *2016*(1), 1712630. https://doi.org/10.1155/2016/1712630

Genetic Algorithm Research: A Bibliometric Analysis

Ahmet AKKAYA[1*]
Cemil KÖZKURT[2]

[1] *Bandırma Onyedi Eylül University, Bandırma, Turkey, aakkaya@bandirma.edu.tr, ORCID: 0000-0003-4836-2310
[2] Bandırma Onyedi Eylül University, Bandırma, Turkey, ckozkurt@bandirma.edu.tr, ORCID: 0000-0003-1407-9867

ABSTRACT

The process of identifying the optimal solution to a problem within specified constraints and objectives is known as optimization. Heuristic and meta-heuristic algorithms are used to solve optimization problems in many areas, from mathematics to engineering, from artificial intelligence to logistics. Meta-heuristic algorithms are preferred when classical methods are insufficient for complex or large-scale problems. These algorithms generally produce optimal or close solutions by performing intelligent searches in the solution space. A common meta-heuristic technique, genetic algorithms (GA) were created with inspiration from biological evolution processes and are thought to yield good results in a variety of applications by utilizing processes including crossover, mutation, and selection. The multi-objective optimization and adaptive structure of GA has been seen to be used effectively in many areas such as engineering design, data mining and artificial intelligence. Within the scope of this study, a bibliometric analysis of the research conducted in the literature in the last thirty-nine years (1986-2024) using Genetic Algorithm was conducted. In the study, 197598 publications were reached by searching the keywords "genetic algorithm" or "genetic algorithms" in the database of the Web of Science. The VOSviewer tool, which uses visual data discovery, literature analysis, and network analysis techniques, was used to analyze the data that was taken from the Web of Science database. As a result of the analyses, trends in the scientific literature, interactions of research areas and work intensities were tried to be revealed in detail. Studies conducted in various categories were evaluated comprehensively with quantitative data, and research collaborations and structural features of the literature were analyzed in detail. It is anticipated that these statistical data will be an important reference source and guide for future research on the use of Genetic Algorithms (GA). In addition, it is expected that the obtained data will strengthen the theoretical foundations of GA and enable further development of applied research. In this context, it is evaluated that the results of the study will make a valuable contribution to scientific progress in the relevant field.

Keywords: *Genetic, Algorithm, Algorithms, Optimization, Bibliometric, Analysis.*

INTRODUCTION

Optimization is a process that aims to find the best solution, and in recent years, metaheuristic algorithms have come to the fore in this field. Metaheuristic algorithms are considered to be a powerful group of methods used to solve complex optimization problems. Metaheuristic algorithms are often preferred in cases where traditional optimization methods are inadequate. The most basic features of these algorithms are that they are

algorithms that explore the solution space and make improvements in this space (Osman & Kelly, 1996). The most common metaheuristic algorithms include Genetic Algorithm (GA), simulated annealing (SA), particle swarm optimization (PSO), and Gray Wolf Optimization Algorithm (GWO) (Akkaya et al., 2023). Each algorithm offers different advantages according to a specific problem type and solution space (Abdel-Basset et al., 2018). Metaheuristic algorithms generally aim to overcome the "local optimum" problem and reach the global optimum (Ayyarao et al., 2022). To do this, they try to approach the best solution by scanning a wide solution space and usually in a non-deterministic way. This process includes techniques inspired by biological and physical processes (Sadollah et al., 2018). In particular, genetic algorithms are one of the most important representatives of this type of algorithms and are based on an evolutionary model (Ganesan et al., 2021).

GA is one of the earliest metaheuristic algorithms and is still widely employed today, according to an analysis of the literature. GA is an evolutionary computational method that brings an innovative approach to solution search and optimization problems by modeling evolutionary processes. First introduced by John Holland in 1975, these algorithms aim to find the optimal solution in the solution space based on the basic principles of biological evolution (Holland, 1975). GA iteratively improves solution populations with genetic operators (selection, crossover, mutation). This process provides evolutionary progress in the solution space by imitating the principles of natural selection and genetic diversity (Goldberg, 1989).

The success of genetic algorithms is especially evident in multivariate and high-dimensional problem areas. This situation has made the use of GAs inevitable in developing applications in engineering, biotechnology, finance, artificial intelligence and many other fields (Mitchell, 1998; Eiben & Smith, 2003). GA has the potential to overcome the limitations of traditional methods used in solving complex optimization problems. In particular, GAs work effectively in nonlinear and multimodal problems, i.e. problems with multiple solution points or targets (Koper et al., 1999). In addition, GAs offer significant advantages in finding solutions by providing a balance between exploration and exploitation in problems with a large solution space (Deb, 2000).

Genetic algorithm (GA) is a metaheuristic optimization method inspired by biological evolution and performs the solution search with a population-based approach. In this method, each individual represents a point in the solution space and is usually encoded in the form of a vector or array. Mathematically, the steps of the genetic algorithm can be expressed as follows.

The population $P(t)$ given by Equation 1 represents a set of individuals in the t. generation.

$$P(t) = \{x_1, x_2, \dots, x_N\},\ x_i \in R^n \qquad \text{Equation (1)}$$

Here N is the number of individuals in the population and x_i represents the solution represented by the ith individual.

To gauge each individual's quality, a fitness function f(x) is defined. This function is directly related to the optimization problem given by Equation 2 and Equation 3.

Maximization problem: max f(x) Equation (2)

Minimization problem: min f(x) Equation (3)

Individuals are often chosen based on their fitness worth. This process increases the probability of more fit individuals being passed on to the next generation. Common methods are Roulette Wheel and Tournament method.

Roulette wheel method: The probability of selection is given by Equation 4.

$$\frac{f(x_i)}{\sum_{j=1}^{N} f(x_j)} \quad \text{Equation (4)}$$

Tournament method: The one with the highest fitness is selected from randomly selected individuals.

In the crossover process, the genetic information of the parent individuals is combined to create new individuals. In the method called single point crossover, a random point is selected and from this point on, the genetic information of the parents is exchanged. The mathematical expression of this method is given by Equation 5.

$$y1 = \alpha xi + (1-\alpha)xj, y2 = (1-\alpha)xi + \alpha xj, \alpha \in [0,1] \quad \text{Equation (5)}$$

The Mutation Operator randomly changes some genes of individuals to preserve genetic diversity. For example:

$$x_i^{(k+1)} = x_i^{(k)} + \epsilon, \quad \epsilon \sim N(0, \sigma^2) \quad \text{Equation (6)}$$

Here ϵ is usually chosen randomly from a normal distribution. The algorithm is stopped when a certain number of generations is reached or when the fitness function approaches a certain threshold value.

In recent years, the hybridization of genetic algorithms has further increased their performance and is seen to provide more effective solutions to new types of problems. Thanks to the developing computational power, GAs have become more efficient with parallel and distributed computational methods and have been able to work with larger data sets (Alba & Tomassini, 2002). In addition, applications of GAs in the field of bioinformatics are seen

to be effective in solving complex biological problems such as protein structure prediction (Goldberg, 1989). GA may be used to a variety of optimization issues, including network design (Gen et al., 2001), business process optimization (Metaxiotis & Psarras, 2004), and the Traveling Salesman Problem (Potvin, 1996). It is seen that it contributes to the reduction of costs by being used in the energy sector (Leonori et al., 2020), optimization of power system operations (Hassan et al., 2013) (Deb, 2000). In bioinformatics, it is successfully used in complex biological data areas such as protein structure prediction (Unger, 2004) and sequence alignment (Kaya et al., 2014) (Mitchell, 1998). It offers effective solutions to complex problems where traditional methods fail.

GA plays an important role in feature selection (Babatunde et al., 2014), ensuring that models are interpretable and their performance increases. It is also integrated to optimize the hyperparameter settings of artificial neural networks (Haupt, 2004).

In this study, the studies conducted since the emergence of the GA algorithm in 1983 were examined with the bibliometric analysis method and the trends in the use of GA with quantitative data were revealed. In the next section, the method of the research, the purpose of the research, and the data and analysis performed in the research are mentioned.

Methodology of the study

Bibliometric analysis is a powerful method that aims to reveal research trends, collaboration networks, and scientific impacts through the quantitative evaluation of scientific publications (Garfield, 1979). Techniques such as citation analysis, co-citation, and co-word analysis are frequently used to determine the main topics, leading researchers, and key studies of a particular field (Small, 1973; Boyack, 2004). When combined with time series, these analyses provide an effective tool for examining the development trends of the field (Donthu et al., 2021). In addition, software such as VOSviewer and CiteSpace provide a better understanding of research areas with visualization techniques (van Eck & Waltman, 2010). Bibliometric analysis is widely applied for literature mapping and meta-analysis, especially in interdisciplinary studies (Zupic & Čater, 2015). Within the scope of the research, bibliometric analysis was conducted with the VOSviewer program using the data that was taken from the Web of Science.

Purpose of the study

By employing the keywords "genetic algorithm" or "genetic algorithms" and the bibliometric analysis approach, this study aims to analyze 197,598 publications on GA that have been published in the Web of Science (WOS) database over the previous 39 years (1986–2024). The purpose of this study is to identify the most cited works, author collaborations, journal impacts, and research trends in the area of GA. It also aims to attract the

attention of researchers by determining the development of GA over time and the most striking aspects in the scientific field. The quantitative data obtained provide a valuable basis for better understanding the evolution of GA research, key topics, and important contributions to the field.

Data and analysis

Advanced software tools such as CiteSpace, Bibliometrix, Gephi, HistCite, EndNote and VOSviewer are widely used in performing bibliometric analyses. The Web of Science (WoS) database, which offers extensive access to scholarly literature, was used in order to guarantee credibility in this investigation. The data obtained from WoS was analyzed with VOSviewer software, which is specifically designed for visualizing scientific literature. VOSviewer stands out in areas such as literature analysis, network analysis and visual data discovery by mapping scientific networks, interactions and connections between publications.

Its user-friendly interface, free accessibility and capacity to effectively process large data sets have made VOSviewer an indispensable tool in scientific research. The software provides significant advantages to researchers in literature and network analyses by offering functions such as visualizing data, detailed examination of network structures and interactive analyses.

In this study, data on 197,598 publications obtained from the WoS database as of November 2024 with the keywords "genetic algorithm" and "genetic algorithms" were comprehensively analyzed with VOSviewer. The analysis results provide valuable information about trends and research gaps in the field of optimization by providing a comprehensive map of the literature.

FINDINGS

In this section, analyses of various categories in the WoS database are presented within the scope of the research conducted. These analyses cover a wide range of topics such as the distribution of publications over the years, document types, WoS index distributions, research profiles and distribution of publication titles according to research categories. In addition, the distribution of publications by country, publisher distribution and distribution of research fields conducted were also examined. In the study, the distribution of citation subjects of publications at the meso and micro levels and the distribution of publications according to publication languages were also evaluated. The analysis of co-authored studies was also included, and collaborations between co-authored researchers, institutions and countries were examined. Citation analyses of the sources from which publications were made, citation analyses of the authors who published, and citation relations between countries and institutions were also discussed in detail. These findings provide important

data for understanding the evolution and dynamics of the research field and reveal the place and development of research on GA within the global scientific community.

Distribution of WoS categories

Figure 1 displays the distribution of publications based on WoS categories as a consequence of the analysis. This visual clearly shows how publications in various research areas are distributed and the proportion of each category in the literature. To enhance comprehension of the scientific framework of the study issue, Figure 1 graphically displays the analysis findings based on categorical classifications in the WoS database.

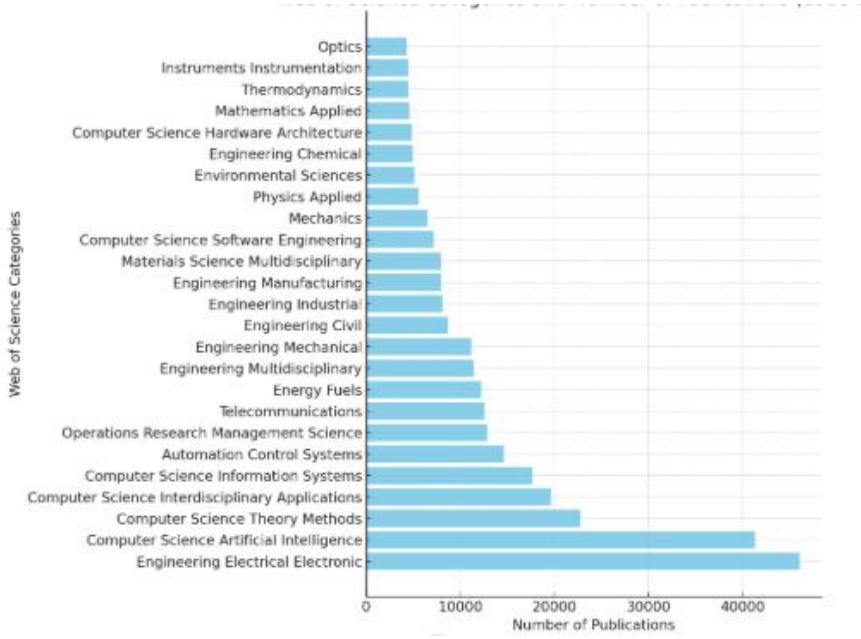

Figure 1: Distribution of publications according to WoS categories

When Figure 1 is examined, it is seen that the category with the highest number of publications is Electrical Electronic Engineering (46,105 publications): GA is used intensively in the field of electrical and electronics engineering. When the literature is examined, it is seen that GA has widespread applications in areas such as circuit design, signal processing and system optimization. Computer Science Artificial Intelligence (41,309 publications) is in second place. When the literature is examined, genetic algorithms appear as a powerful tool in learning and optimization processes in the field of Artificial Intelligence. This high number shows that GA is widely applied in the design of AI systems. Computer Science Theory Methods (22,753 publications) is in third place. When the literature is

examined, it is observed that GA plays a fundamental role in theoretical methods and algorithm design. Automation Control Systems (14,627 publications) draws attention to the use of GA in automation and control systems, especially for the optimization of dynamic systems. Operations Research Management Science (12,884 publications) shows that GA offers solutions in areas such as logistics, supply chain and resource allocation in management sciences and operations research. Energy Fuels (12,245 publications) GA is used in the energy sector in areas such as energy management and optimization of renewable energy systems. Engineering Multidisciplinary (11,401 publications) interdisciplinary engineering studies show that GA is applied in a wide range to solve different engineering problems. Materials Science Multidisciplinary (7,990 publications) shows that GA contributes greatly to material design and property optimization in the field of materials science.

Distribution of publications according to the year they were published

According to the findings obtained as a result of the analysis processes, Figure 2, which shows the distribution of publications by year, allows you to analyze in which years more or less publications were made over time..

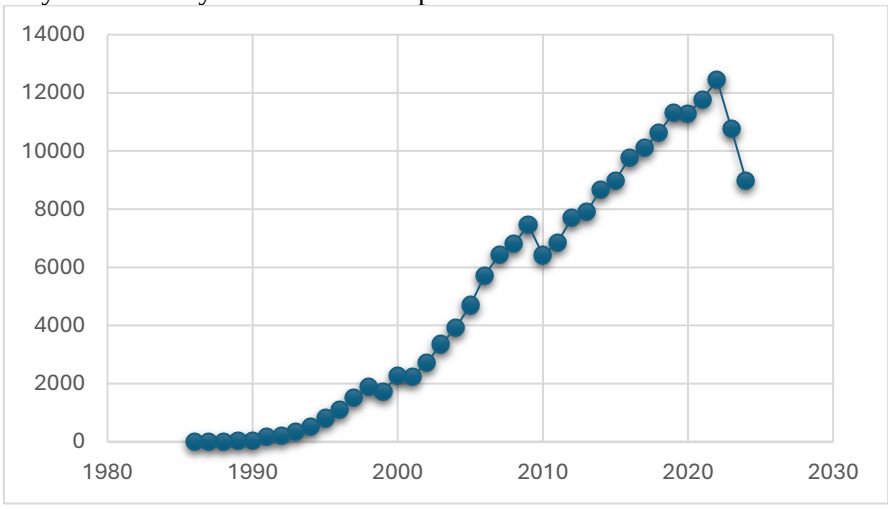

Figure 2: Distribution of publications by year

The first study in the WoS database was published in 1986. Until the 1990s: The number of publications was limited and there were only a few publications each year (43 in 1990, 33 in 1989). This shows that the use of GA was not widespread. In 1995, the number of publications increased to 816, which shows that GA was starting to be recognized, especially in fields such as engineering and computer science. 1996-2000: The number of annual publications started to increase and reached 2,279 publications in 2000. This

increase indicates that GA was accepted by a wider research community. A steady increase in the number of publications was observed between 2001-2010. Especially in 2009, a significant leap was made by reaching 7,461 publications. This increase can be associated with the widespread use of GA in various disciplines.3. The increase in the number of publications continued between 2011 and 2015, reaching a significant level with 8,672 publications in 2014 and 8,992 in 2015. During this period, when GA publications increased steadily between 2016 and 2020, more than 10,000 publications were made each year. 11,288 publications were made in 2020. 2021–2024: This period covers the years when GA research peaked. The highest number was reached in 2022 with 12,440 publications. A slight decrease is observed in 2023 and 2024 with 10,750 and 8,980 publications, respectively. It is thought that this may be due to the decrease in GA use as a result of the increased variety of meta-heuristic algorithms that have emerged in recent years.

Document type distribution of publications

Table 1 of the Web of Science (WoS) database shows the distribution of 197,598 publications on genetic algorithms (GA) by document type and the percentage of each category in the total number of articles.

Table 1: Publications distributed by document type

Document Types	Number of Publications	% of 197.598
Article	130457	66.021
Proceeding Paper	69400	35.122
Review Article	2791	1.412
Book Chapters	1886	0.954
Early Access	1475	0.746
Retracted Publication	365	0.185
Meeting Abstract	301	0.152
Editorial Material	244	0.123
Correction	155	0.078
Letter	120	0.061
Book	64	0.032
Retraction	45	0.023
Note	33	0.017
Book Review	18	0.009
Software Review	14	0.007
Data Paper	13	0.007
News Item	5	0.003
Correction, Addition	4	0.002
Reprint	3	0.002
Discussion	2	0.001
Bibliography	1	0.001
Publication With Expression Of Concern	1	0.001

When Table 1 is examined, it is seen that the most publications are Articles, which constitute a rate of 66.021% with a total of 130.457 publications. Proceeding Paper ranks second with 69.400 publications, which constitutes a rate of 35.122%. Review Article ranks third with 2.791 publications (%1.412). Book Chapters 1.886 publications (%0.954), Early Access 1.475 publications (%0.746), Retracted Publication 365 publications (%0.185), Meeting Abstract 301 publications (%0.152), Editorial Material, Correction and Letter, which constitute less than 0.1% of the publications, have a relatively limited place in the literature. Publication types such as Book, Retraction, Note and Others constitute a very small portion of the total

(0.032% or less). Bibliography and Publication with Expression of Concern are represented by only one publication each.

Meso distribution of publications' citation topics

As a result of the analysis, the meso (medium level) distribution of publications according to their citation subjects is presented in Figure 3 in order to reveal which fields of study are prominent and which subjects attract more attention.

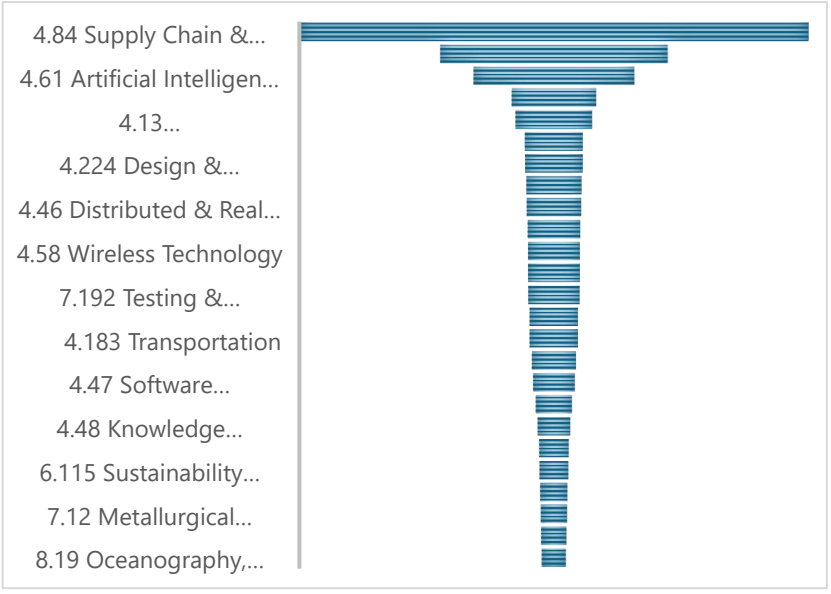

Figure 3: Meso (middle level) distribution of publications according to their citation topics

When Figure 3 is examined, it is seen that the most publications are in Supply Chain & Logistics (36,025 publications). This shows that GA is widely used in areas such as supply chain optimization and logistics management. Its ability to solve complex problems and increase efficiency highlights its use in this area. Power Systems & Electric Vehicles (16,073 publications) ranks second. It reveals that GA plays an important role in areas such as optimization of electrical systems, renewable energy integration and energy management of electric vehicles. It ranks third with Artificial Intelligence & Machine Learning (11,372 publications). In the fields of artificial intelligence and machine learning, it is seen that GA is a powerful tool in applications such as parameter optimization and model training. In other fields, it is seen that Automation & Control Systems (5,982 publications), Telecommunications (5,413 publications), Computer Vision & Graphics (4,104 publications), Wireless Technology (3,674 publications), Protein Structure, Folding &

Modelling (3,421 publications), Climate Change (3,135 publications), Oceanography, Meteorology & Atmospheric Sciences (1,694 publications), Design & Manufacturing (4,083 publications), Safety & Maintenance (1,789 publications).

Micro distribution of publications' citation topics

Table 2 shows the classification of GA according to micro-level, that is, narrow-scale, citation topics and the number of publications for each topic.

Table 2: Micro (narrow-scale) distribution of publications according to citation topics

Citation Topics Micro	**Number of Publications**
4.84.169 Particle Swarm Optimization	16317
4.84.401 Scheduling	8569
4.84.471 Vehicle Routing Problem	4991
4.18.204 Distributed Generation	4225
4.18.296 Unit Commitment	4041
4.61.145 Feature Selection	3380
4.84.260 Supply Chain	2436
4.18.472 Voltage Stability	2417
4.61.493 Load Forecasting	2317
2.123.13 Protein Folding	1960
4.224.599 Project Scheduling	1959
4.46.85 Cloud Computing	1954
4.29.435 Multi Agent Systems	1787
7.70.919 Organic Rankine Cycle	1783
4.13.43 Wireless Sensor Networks	1681
4.18.136 Induction Motor	1657
4.183.486 Traffic Flow	1545
6.115.284 Thermal Comfort	1525
7.227.355 Tool Wear	1514
4.237.651 Preventive Maintenance	1487
4.61.56 Fuzzy Sets	1459
2.244.499 Chemometrics	1435
6.153.1330 Water Distribution Systems	1378
2.123.778 Qsar	1377
4.61.869 Clustering	1359

When Table 2 is examined, it is seen that Particle Swarm Optimization (16,317 publications) ranks first as a result of the classification of GA according to micro-level, i.e. narrow-scale, citation topics. The association of GA with particle swarm optimization (PSO) shows that the two algorithms are generally used together in complex optimization problems. This emphasizes the potential of meta-heuristic methods to collaborate. Scheduling (8,569 publications) ranks second. Scheduling problems are one of the areas where GA is widely used. GA offers optimal solutions in processes such as production, project management and resource allocation. Vehicle Routing Problem (4,991 publications) ranks third. It is understood that GA is effective in the optimization of transportation networks. This reflects an important application area in the logistics and transportation sectors. Other topics are Distributed Generation (4,225 publications), Unit Commitment (4,041 publications), Feature Selection (3,380 publications), Protein Folding (1,960 publications), Wireless Sensor Networks (1,681 publications), Traffic Flow (1,545 publications), Clustering (1,359 publications), Tool Wear (1,514 publications), Preventive Maintenance (1,487 publications).

Web of Science index distributions

In the analyses, the distribution of publications related to GA according to WoS indexes is presented in Table 3. This distribution is important in understanding which indexes the relevant literature is published through and which areas are dominant.

Table 3: WoS index distribution of publications

Web of Science Index	**Publication Count**	**% of 197.598**
Science Citation Index - Expanded (SCIE)	118729	60.086
Conference Proceedings Citation Index – Science (CPCI-S)	69058	34.949
Emerging Sources Citation Index (ESCI)	12345	6.248
Social Sciences Citation Index (SSCI)	7087	3.587
Conference Proceedings Citation Index – Social Science & Humanities (CPCI-SSH)	1946	0.985
Book Citation Index – Science (BKCI-S)	1914	0.969
Index Chemicus (IC)	160	0.081
Arts & Humanities Citation Index (AHCI)	141	0.071
Book Citation Index – Social Sciences & Humanities (BKCI-SSH)	137	0.069
Current Chemical Reactions (CCR-EXPANDED)	2	0.001

When Table 3 is examined, Science Citation Index Expanded (SCIE) – ranks first with 118,729 publications (60%). SCI-EXPANDED covers a large part of scientific publications and shows that genetic algorithms are intensively studied in technical and engineering fields. The dominance of this index reveals the importance of GA in natural sciences and engineering. Conference Proceedings Citation Index – Science (CPCI-S) – 69,058 publications (35%) Conference proceedings are a very effective publication format in GA research. This reflects that GA is a constantly evolving field that requires rapid innovation. Emerging Sources Citation Index (ESCI) – 12,345 publications (6%) ESCI includes emerging research areas. This shows that it is an important platform for publications representing innovative and rapidly developing aspects of GA. Other indexes are Social Sciences Citation Index (SSCI) – 7,087 publications (%3.6), Conference Proceedings Citation Index – Social Science & Humanities (CPCI-SSH) – 1,946 publications, Book Citation Index – Science (BKCI-S) and Social Sciences & Humanities (BKCI-SSH) – 2,051 publications in total, Index Chemicus (IC) and Current Chemical Reactions (CCR-EXPANDED), Arts & Humanities Citation Index (AHCI) – 141 publications.

Journal name distribution according to publication titles

Table 4 shows the distribution of publications by title, which journals publish most of the GA-related studies.

Table 4: Distribution of journal names according to publication titles

Publication Titles	Publication Count	% of 197.598
LECTURE NOTES IN COMPUTER SCIENCE	4491	2.273
IEEE CONGRESS ON EVOLUTIONARY COMPUTATION	2472	1.251
IEEE ACCESS	2226	1.127
EXPERT SYSTEMS WITH APPLICATIONS	1993	1.009
APPLIED SOFT COMPUTING	1916	0.97
LECTURE NOTES IN ARTIFICIAL INTELLIGENCE	1454	0.736
INTERNATIONAL JOURNAL OF ADVANCED MANUFACTURING TECHNOLOGY	1354	0.685
COMPUTERS INDUSTRIAL ENGINEERING	1271	0.643
ENERGIES	1121	0.567
PROCEEDINGS OF SPIE	1084	0.549
APPLIED SCIENCES BASEL	1072	0.543
INTERNATIONAL JOURNAL OF PRODUCTION RESEARCH	1066	0.539
ENERGY	1057	0.535
SOFT COMPUTING	978	0.495
APPLIED MECHANICS AND MATERIALS	920	0.466
ADVANCED MATERIALS RESEARCH	913	0.462
MATHEMATICAL PROBLEMS IN ENGINEERING	881	0.446
ADVANCES IN INTELLIGENT SYSTEMS AND COMPUTING	876	0.443
EUROPEAN JOURNAL OF OPERATIONAL RESEARCH	779	0.394
ENERGY CONVERSION AND MANAGEMENT	757	0.383
COMPUTERS OPERATIONS RESEARCH	746	0.378
SUSTAINABILITY	746	0.378
IEEE INTERNATIONAL CONFERENCE ON SYSTEMS MAN AND CYBERNETICS CONFERENCE PROCEEDINGS	724	0.366
NEURAL COMPUTING APPLICATIONS	712	0.36
INFORMATION SCIENCES	705	0.357

When Table 4 is examined, Lecture Notes in Computer Science (4491 publications) ranks first. This journal is an important platform where innovative approaches in computer science are published. The majority of studies on GA address the basic theoretical and applied aspects of this field. It is seen that the publications are IEEE Congress on Evolutionary Computation (2472 publications), IEEE Access (2226 publications), Expert Systems with Applications (1993 publications), Applied Soft Computing (1916 publications), International Journal of Advanced Manufacturing Technology (1354 publications), Energy (1057 publications) and Energies (1121 publications), Sustainability (746 publications), Soft Computing (978 publications), Mathematical Problems in Engineering (881 publications).

Language distribution of publications

As a result of the analysis, the distribution of publication languages is visualized in Figure 5. This distribution shows in which languages publications are made and how the most widely used languages take place in the research.

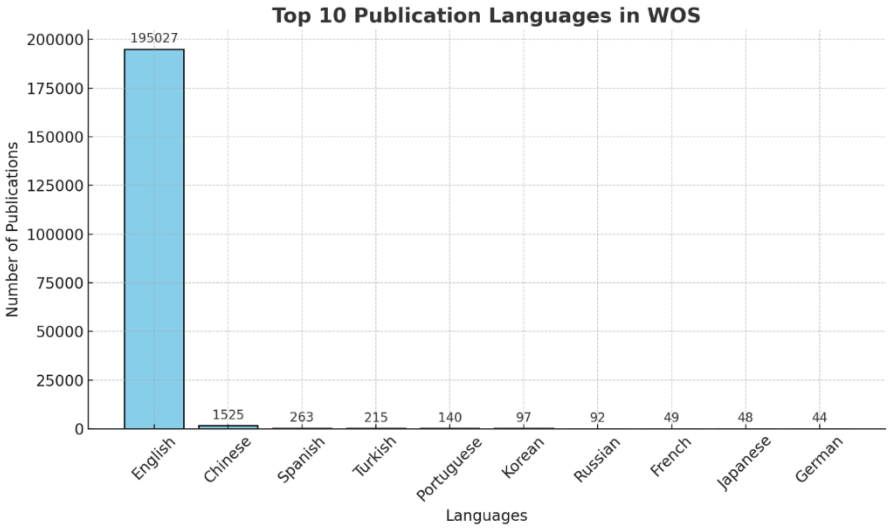

Figure 4: Distribution of publication languages

Bibliometric analysis using the keywords "genetic algorithm" or "genetic algorithms" in the Web of Science (WoS) database reveals that the majority of publications are produced in English. Of the 197,598 studies, 98.7% (195,027 publications) were published in English. This shows that English is the dominant language in scientific communication. The languages with the most publications other than English were Chinese (1,525 publications), Spanish (263 publications), and Turkish (215 publications), respectively. Chinese publications reflect the magnitude of local research

activities and China's influence in the academic field. Turkish publications provide information about the academic and industrial use of genetic algorithms in Turkey. The number of studies published in languages such as French, Japanese, and German is more limited. There is only one publication in languages such as Eskimo, Estonian, Malay, and Welsh.

Publisher distribution of publications

Figure 5 shows the Publisher with the most publications in the WoS database and their publication numbers.

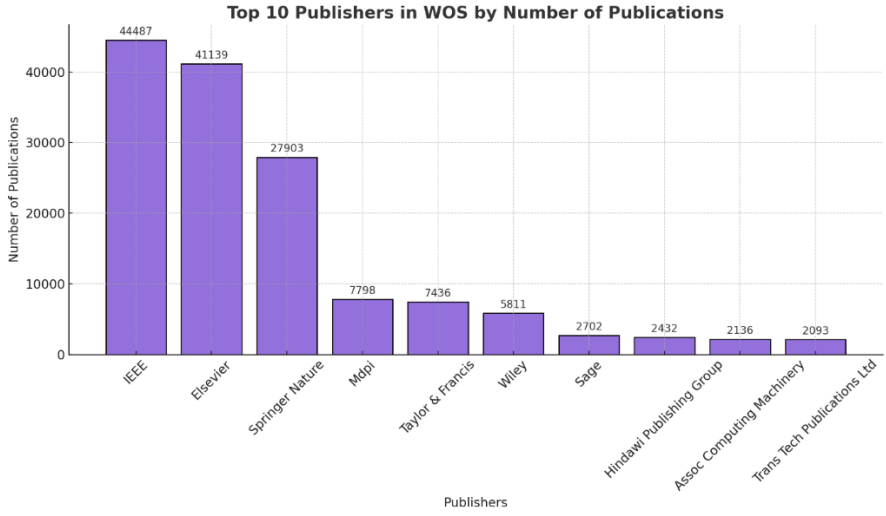

Figure 5: Publisher distribution of publications in WoS database

Figure 5 clearly shows the contribution of publisher in scientific publications. IEEE ranks first with a total of 44,487 publications, with its leadership in engineering, computer science and related fields. Elsevier follows with 41,139 publications, and this publishing house stands out with its broad coverage in medicine, engineering and natural sciences. Springer Nature ranks third with 27,903 publications and has a large impact area thanks to its multidisciplinary publishing strategy. Publishing houses such as Mdpi, Taylor & Francis and Wiley, which publish in smaller numbers, also make significant contributions in certain specialized fields. For example, while Mdpi stands out with its open access publications, Taylor & Francis is known for its publications in the social sciences and humanities. This distribution shows that certain large publishing houses dominate the scientific publishing sector and play a critical role in the dissemination of scientific knowledge. In addition, the contributions of publishing houses to interdisciplinary interaction help researchers make strategic decisions about which platforms to use to publish their work.

Co-authorship works by authors

As a result of the analyses, the connections between the co-authored authors of the publications are presented in Figure 6. Such analyses provide important information about the intensity of scientific collaborations, how a network is formed between the authors, and which researchers collaborate more with each other.

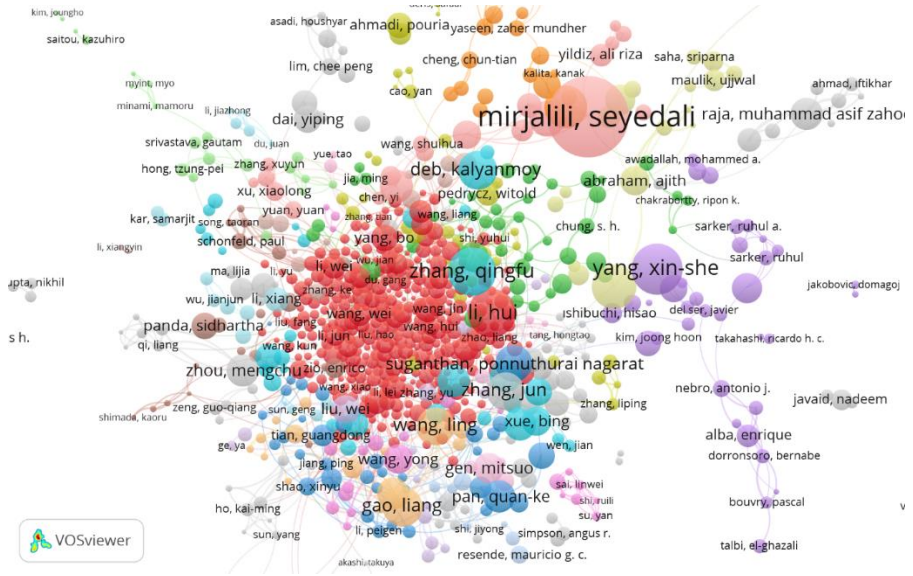

Figure 6: Co-authorship is the connection between authors.

In studies conducted with co-authors, Seyedali Mirjalili makes the greatest contribution to the literature with 123 documents, 32,525 citations, and 93 total link strength. He is followed by Xin-She Yang with 35 documents, 12,940 citations, and 26 link strength, and Qingfu Zhang with 55 documents, 11,628 citations, and 57 link strength. Hui Li is the author who produced the most publications with 131 documents, 11,403 citations, and 96 link strength, but he ranks fourth in the citation ranking. Swagatam Das ranks fifth with 76 documents, 9,669 citations, and 42 link strength. This ranking reveals that metrics such as number of citations, number of documents, and link strength should be evaluated together when evaluating the academic impact of authors.

The connection between organizations' citation analysis

As a result of the analysis, the network visualization graph according to the citation numbers of the institutions is given in Figure 7.

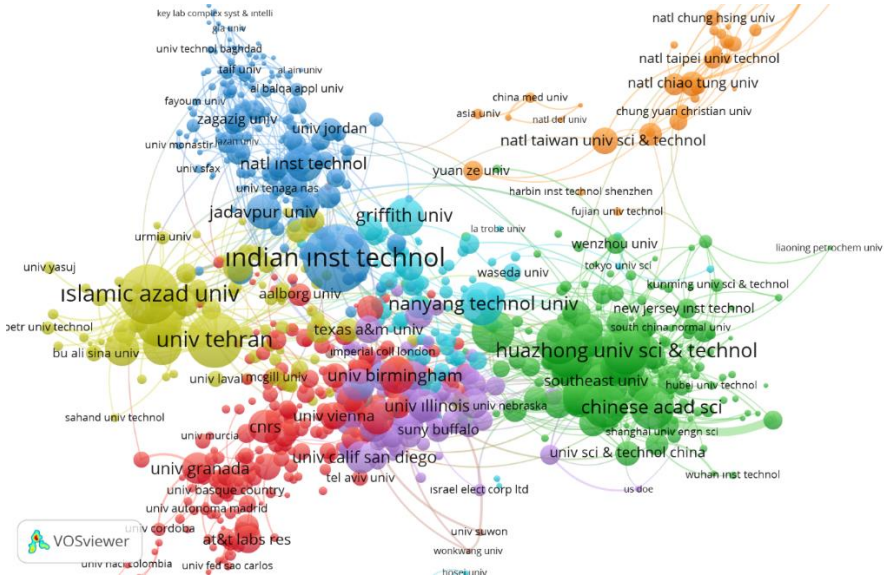

Figure 7: Network visualization graph according to the citation numbers of institutions

When the organizational data in the co-authored studies presented in Figure 7 is examined, the first place is taken by the Indian Institute of Technology; this institution has published 1,773 documents and received a total of 86,024 citations, and has a link strength of 529. The second place is taken by the Islamic Azad University. This university has published 3,251 documents and received 65,669 citations, and a link strength of 2,772. The third place is taken by the University of Tehran; this university has published 1,969 documents and received 57,810 citations, and a total link strength of 1,752. The fourth place is taken by the Huazhong University of Science and Technology, which has 1,654 documents and received 37,707 citations, and has a link strength of 1,144. Finally, the Hong Kong Polytechnic University has published 1,161 documents, received 36,615 citations, and has a link strength of 1,179.

Co-occurrence analysis of all keywords

As a result of the analysis, the network visualization graph according to the number of keywords is given in Figure 8.

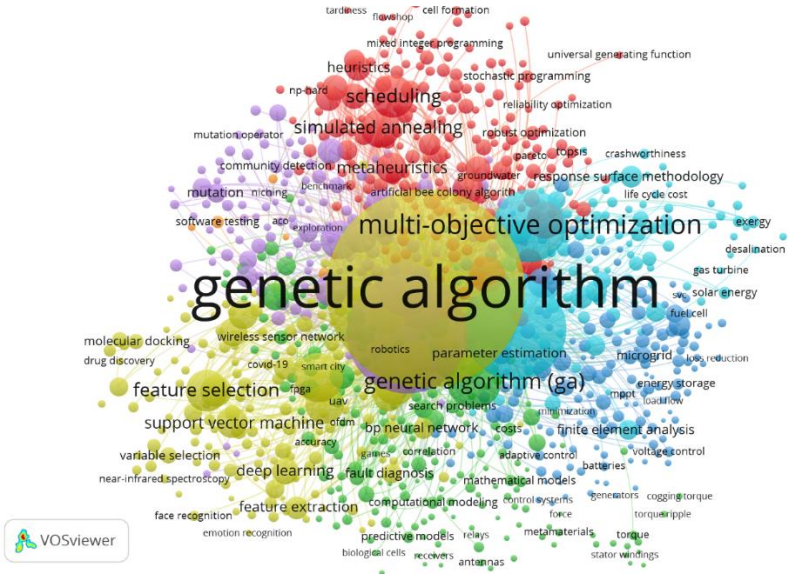

Figure 8: Network visualization graph based on keyword counts

According to the data obtained with Figure 8, the effect and interaction of the keywords "genetic algorithm" and "genetic algorithms" in the scientific literature is shown. The keyword genetic algorithm is the most used term with 49,452. It also has a high interaction potential with a total connection strength of 60,207. Genetic algorithms have been used 18,022 times and have a certain interaction with a total connection strength of 29,076. The term multi-objective optimization is used 6,616 times and has a lower interaction with a total connection strength of 9,465. The term optimization is used 13,044 times and has a significant interaction with a connection strength of 26,059. Finally, the keyword particle swarm optimization is used 3,824 times and has a connection strength of 8,057, although it is less common, but still shows interaction in a certain scientific network. This shows that the particle swarm optimization algorithm is used together with genetic algorithms.

Analysis of the most cited documents

As a result of the analysis, the connections between the works in which the publications were published and the number of citations these works received are seen in Fig. 9.

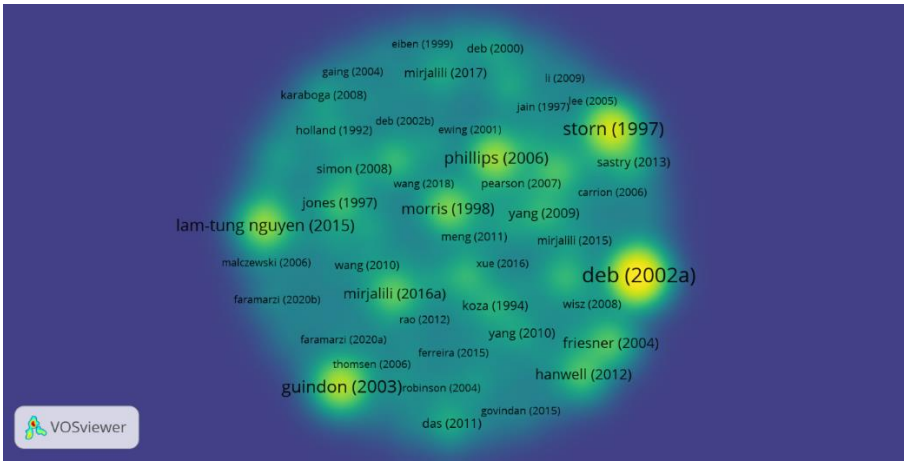

Figure 9: Citation analysis of publications based on published work

When the citation analysis of publications is made on a per-work basis with Figure 9, the research most frequently cited is (Deb et al., 2002) with 30,946 citation counts, which shows its impact on genetic algorithms and optimization and its important position in the literature in this field. The second place is (Storn and Price, 1997) with 18,430 citations; this study is also considered as one of the cornerstones of optimization algorithms. (Guindon & Gascuel, 2003) and (Phillips et al., 2006) with 14,639 and 12,105 citations, respectively, have an important place in optimization and genetic algorithm research. More recent studies (Nguyen et al., 2015) and (Mirjalili & Lewis, 2016) also point to more current and popular contributions on the subject, with 11,686 and 7,854 citations, respectively. Finally, the study by Turkish scientists (Karaboga & Basturk, 2007) has a notable place in the field of optimization, with 5,120 citations.

Journal name distribution according to publication titles

As a result of the analysis, the connection between the number of publications and citations in the journals where the publications are published is given in Figure 10.

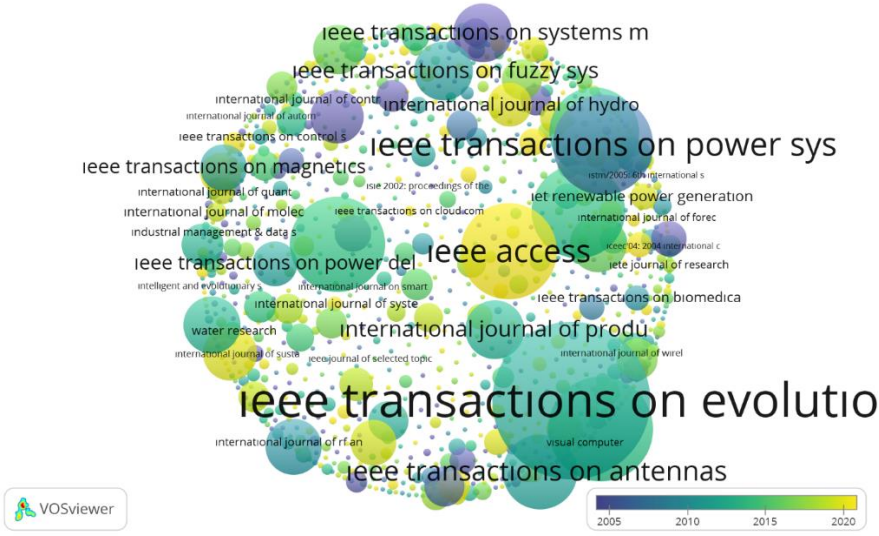

Figure 10: The connection between the citations in the published journals

The data given in Figure 10 shows the most influential academic resources in the field of genetic algorithms and optimization. The most cited publication source is IEEE Transactions on Evolutionary Computation, which has 505 documents and 94,866 citations; this shows that it hosts fundamental and pioneering studies in the field. Information Sciences ranks second with 704 documents and 42,017 citations, indicating that it appeals to a wide multidisciplinary audience. IEEE Transactions on Power Systems, which ranks third, stands out as an influential platform especially in the field of energy systems and optimization, with 346 documents and 38,252 citations. IEEE Access, despite publishing more documents (2,216), ranks fourth with 34,961 citations, indicating that it is a popular publication channel that provides a wide reach. Finally, the International Journal of Electrical Power & Energy Systems is another important source where important studies on energy and power systems are published with 651 documents and 34,794 citations.

RESULTS

When the data is examined according to WoS categories, it is seen that genetic algorithms come to the fore in technical disciplines such as engineering and computer science, and are also effective in fields such as energy, environmental sciences and physics. The versatility of GA proves that it is a powerful tool for solving different problems and supports its interdisciplinary use. This situation indicates that it is directly related to the

solidity of the theoretical foundations and application flexibility of genetic algorithms.

According to the distribution data of GA publications by year, it shows that it has made significant progress from its beginning in 1986 to the present. Especially in the period after 2000, it is seen that GA has been widely accepted and is at the focal point of many disciplines. The reason for the increase is thought to be both the solidification of theoretical foundations and the expansion of application areas. On the other hand, the 2020s are seen as a period when GA peaked as a mature research area and increased its influence in a wide range of disciplines.

When the document type distribution data of the publications is examined, it shows that the vast majority of research on genetic algorithms is published as original scientific articles or conference proceedings. This situation reveals the importance of GA in academic literature and its wide discussion in conference environments.

The meso distribution data of the citation topics of the publications show that GA is applied in a wide range of disciplines and is used as a powerful tool to solve important problems in various sectors. Fields such as supply chain and logistics, electrical systems, artificial intelligence and automation are among the most cited topics of GA. This situation reflects the practical applications and impact of the algorithm. In less common fields such as biology, climate change and marine sciences, GA is seen to offer innovative solutions.

The citation topics of GA at the micro level reveal how flexible and effective the algorithm is in certain problem areas. While the intensive use of GA in areas such as particle swarm optimization, scheduling, transportation routing and energy management draws attention, the contribution of the algorithm also stands out in niche areas such as biology, data mining and traffic flow. This diversity shows that GA has a wide application potential in different disciplines.

According to the distribution data of WoS indexes, GA is most effective in engineering, natural sciences and computer science, but it also has limited but significant use in fields such as social sciences, humanities and chemistry. The high rates of SCI-EXPANDED and CPCI-S indexes confirm the leadership of genetic algorithms in fields that require rapid innovation and technical development. The smaller rates in other indexes indicate the interdisciplinary use and expansion potential of GA.

A large part of the studies on GA are published in applied fields such as computer science, engineering, artificial intelligence and energy. While Lecture Notes in Computer Science and IEEE Access stand out as the platforms where studies are published the most, Expert Systems with Applications and Applied Soft Computing highlight the applied aspect of GA. In addition, journals on energy and environment indicate the increasing

importance of GA in these fields. This distribution clearly shows the interdisciplinary contribution of both theoretical and practical aspects of GA.

The distribution of publication languages shows that scientific studies are largely conducted in English, while studies published in other languages are generally local or regionally focused. The fact that studies are mostly published in English allows research findings to reach a wider audience by the international academic community. However, it should not be forgotten that studies published in other languages shed light on local scientific contributions.

The publishers with the most publications in the WOS database are IEEE, which ranks first with a total of 44,487 publications, followed by Elsevier with 41,139 publications and Springer Nature with 27,903 publications. It is thought that these publishers play an important role in shaping scientific literature.

When the connection between co-authors is examined, the extraordinary number of citations of Mirjalili and Seyedali shows that there is a wide acceptance and application for their work, while Li and Hui stand out with their extensive collaborations. It is seen that authors with fewer publications such as Yang and Xin-She attract attention with the high impact value of their publications.

The study of organizations in co-authored studies allows comparison of different universities in terms of research productivity and interaction power. Indian Institute of Technology has the highest number of citations (86,024 citations), which indicates that its published research has had a great impact on the scientific community and has reached a wide audience. However, its link strength (529) is lower than other universities, which perhaps indicates that its research is less collaborative or more narrowly focused.

When the frequency of the keywords is examined, it is seen that the words genetic algorithm, genetic algorithms, multi-objective optimization, Optimization and particle swarm optimization have a significant impact on the Genetic Algorithm literature.

According to the ranking in terms of publications, the study by Deb (Deb et al., 2002) was found to be the most cited study. The analysis processes performed on a per-work basis show the evolution of research in the field of genetic algorithms and optimization and which studies have had the most impact.

According to the review of journals, IEEE Transactions on Evolutionary Computation stands out as the leader of the GA field with its high number of citations. Information Sciences, IEEE Transactions on Power Systems, IEEE Access, International Journal of Electrical Power & Energy Systems journals are also seen to have made significant contributions to the advancement of the GA field.

REFERENCES

Abdel-Basset, M., Abdel-Fatah, L., & Sangaiah, A. K. (2018). Chapter 10 - Metaheuristic Algorithms: A Comprehensive Review. İçinde A. K. Sangaiah, M. Sheng, & Z. Zhang (Ed.), *Computational Intelligence for Multimedia Big Data on the Cloud with Engineering Applications* (ss. 185-231). Academic Press. https://doi.org/10.1016/B978-0-12-813314-9.00010-4

Alba, E., & Tomassini, M. (2002). Parallelism and evolutionary algorithms. *IEEE Transactions on Evolutionary Computation*, *6*(5), 443-462. IEEE Transactions on Evolutionary Computation. https://doi.org/10.1109/TEVC.2002.800880

Ayyarao, Tummala. S. L. V., Ramakrishna, N. S. S., Elavarasan, R. M., Polumahanthi, N., Rambabu, M., Saini, G., Khan, B., & Alatas, B. (2022). War Strategy Optimization Algorithm: A New Effective Metaheuristic Algorithm for Global Optimization. *IEEE Access*, *10*, 25073-25105. IEEE Access. https://doi.org/10.1109/ACCESS.2022.3153493

Babatunde, O., Armstrong, L., Leng, J., & Diepeveen, D. (2014). A Genetic Algorithm-Based Feature Selection. *Research outputs 2014 to 2021*. https://ro.ecu.edu.au/ecuworkspost2013/653

Boyack, K. W. (2004). Mapping knowledge domains: Characterizing PNAS. *Proceedings of the National Academy of Sciences*, *101*(suppl_1), 5192-5199. https://doi.org/10.1073/pnas.0307509100

Deb, K. (2000). Multi-Objective Evolutionary Optimization: Past, Present, and Future. Içinde I. C. Parmee (Ed.), *Evolutionary Design and Manufacture* (ss. 225-236). Springer. https://doi.org/10.1007/978-1-4471-0519-0_18

Deb, K., Pratap, A., Agarwal, S., & Meyarivan, T. (2002). A fast and elitist multiobjective genetic algorithm: NSGA-II. *IEEE Transactions on Evolutionary Computation*, *6*(2), 182-197. IEEE Transactions on Evolutionary Computation. https://doi.org/10.1109/4235.996017

Donthu, N., Kumar, S., Mukherjee, D., Pandey, N., & Lim, W. M. (2021). How to conduct a bibliometric analysis: An overview and guidelines. *Journal of Business Research*, *133*, 285-296. https://doi.org/10.1016/j.jbusres.2021.04.070

Ganesan, V., Sobhana, M., Anuradha, G., Yellamma, P., Devi, O. R., Prakash, K. B., & Naren, J. (2021). Quantum inspired meta-heuristic approach for optimization of genetic algorithm. *Computers & Electrical Engineering*, *94*, 107356. https://doi.org/10.1016/j.compeleceng.2021.107356

Gen, M., Cheng, R., & Oren, S. S. (2001). Network design techniques using adapted genetic algorithms. *Advances in Engineering Software*, *32*(9), 731-744. https://doi.org/10.1016/S0965-9978(01)00007-2

Goldberg, D. E. (1989). Cenetic Algorithms in Search. *Optimization, Machine Learning*. https://cir.nii.ac.jp/crid/1573668923995443456

Guindon, S., & Gascuel, O. (2003). A Simple, Fast, and Accurate Algorithm to Estimate Large Phylogenies by Maximum Likelihood. *Systematic Biology*, *52*(5), 696-704. https://doi.org/10.1080/10635150390235520

Hassan, L. H., Moghavvemi, M., Almurib, H. A. F., & Steinmayer, O. (2013). Application of genetic algorithm in optimization of unified power flow controller parameters and its location in the power system network. *International Journal of Electrical Power & Energy Systems*, *46*, 89-97. https://doi.org/10.1016/j.ijepes.2012.10.011

Haupt, R. L. (2004). Adaptive crossed dipole antennas using a genetic algorithm. *IEEE Transactions on Antennas and Propagation*, *52*(8), 1976-1982. IEEE Transactions on Antennas and Propagation. https://doi.org/10.1109/TAP.2004.832493

Karaboga, D., & Basturk, B. (2007). A powerful and efficient algorithm for numerical function optimization: Artificial bee colony (ABC) algorithm. *Journal of Global Optimization*, *39*(3), 459-471. https://doi.org/10.1007/s10898-007-9149-x

Kaya, M., Sarhan, A., & Alhajj, R. (2014). Multiple sequence alignment with affine gap by using multi-objective genetic algorithm. *Computer Methods and Programs in Biomedicine*, *114*(1), 38-49. https://doi.org/10.1016/j.cmpb.2014.01.013

Koper, K. D., Wysession, M. E., & Wiens, D. A. (1999). Multimodal function optimization with a niching genetic algorithm: A seismological example. *Bulletin of the Seismological Society of America*, *89*(4), 978-988. https://doi.org/10.1785/BSSA0890040978

Leonori, S., Paschero, M., Frattale Mascioli, F. M., & Rizzi, A. (2020). Optimization strategies for Microgrid energy management systems by Genetic Algorithms. *Applied Soft Computing*, *86*, 105903. https://doi.org/10.1016/j.asoc.2019.105903

Metaxiotis, K., & Psarras, J. (2004). The contribution of neural networks and genetic algorithms to business decision support. *Management Decision*, *42*(2), 229-242. https://doi.org/10.1108/00251740410518534

Mirjalili, S., & Lewis, A. (2016). The Whale Optimization Algorithm. *Advances in Engineering Software*, *95*, 51-67. https://doi.org/10.1016/j.advengsoft.2016.01.008

Nguyen, L.-T., Schmidt, H. A., von Haeseler, A., & Minh, B. Q. (2015). IQ-TREE: A Fast and Effective Stochastic Algorithm for Estimating Maximum-Likelihood Phylogenies. *Molecular Biology and Evolution*, *32*(1), 268-274. https://doi.org/10.1093/molbev/msu300

Osman, I. H., & Kelly, J. P. (1996). Meta-Heuristics: An Overview. Içinde I. H. Osman & J. P. Kelly (Ed.), *Meta-Heuristics: Theory and Applications* (ss. 1-21). Springer US. https://doi.org/10.1007/978-1-4613-1361-8_1

Phillips, S. J., Anderson, R. P., & Schapire, R. E. (2006). Maximum entropy modeling of species geographic distributions. *Ecological Modelling*, *190*(3), 231-259. https://doi.org/10.1016/j.ecolmodel.2005.03.026

Potvin, J.-Y. (1996). Genetic algorithms for the traveling salesman problem. *Annals of Operations Research*, *63*(3), 337-370. https://doi.org/10.1007/BF02125403

Sadollah, A., Sayyaadi, H., & Yadav, A. (2018). A dynamic metaheuristic optimization model inspired by biological nervous systems: Neural network algorithm. *Applied Soft Computing*, *71*, 747-782. https://doi.org/10.1016/j.asoc.2018.07.039

Small, H. (1973). Co-citation in the scientific literature: A new measure of the relationship between two documents. *Journal of the American Society for Information Science*, *24*(4), 265-269. https://doi.org/10.1002/asi.4630240406

Unger, R. (2004). The Genetic Algorithm Approach to Protein Structure Prediction. Içinde R. L. Johnston (Ed.), *Applications of Evolutionary Computation in Chemistry* (ss. 153-175). Springer. https://doi.org/10.1007/b13936

van Eck, N. J., & Waltman, L. (2010). Software survey: VOSviewer, a computer program for bibliometric mapping. *Scientometrics*, *84*(2), 523-538. https://doi.org/10.1007/s11192-009-0146-3

Zupic, I., & Čater, T. (2015). Bibliometric Methods in Management and Organization. *Organizational Research Methods*, *18*(3), 429-472. https://doi.org/10.1177/1094428114562629

A Simple Experimental Framework for Engineering Students to Test 3D Printed Propellers

Turgay ERAY[1]

1- Dr. Öğr. Üyesi.; Aydın Adnan Menderes Universitesi Mühendislik Fakültesi Makine Mühendisliği Bölümü Makine Teorisi ve Dinamiği Anabilim Dalı turgay.eray@adu.edu.tr ORCID No: 0000-0002-6115-7242.

ABSTRACT

This chapter presents a straightforward experimental design aimed at characterizing 3D printed propellers. The primary objective is to provide an accessible and cost-effective method for evaluating the performance of 3D printed propellers in various conditions, with a focus on aerodynamic properties, thrust generation, and efficiency. The proposed experimental setup utilizes a test rig that allows for precise measurement of propeller speed, and thrust, while accounting for factors such as rotational speed and environmental conditions. Results from the experiment can be used to compare the performance of different 3D printed propeller designs and to assess the impact of printing parameters on propeller efficiency. This experimental approach serves as a foundation for future research into optimizing 3D printed propellers for various applications, including drone propulsion and other aeronautical systems.

Keywords – Propeller, Experimental, Test Rig, Framework, 3d Printed.

INTRODUCTION

The emergence of three-dimensional (3D) printing technology has fundamentally transformed the realms of prototyping and manufacturing, presenting a cost-efficient and expedited method for the creation of intricate geometries (Sachs et al., 1990). Among its diverse applications, 3D printing has become an invaluable asset in the domains of aerodynamics and fluid dynamics research, especially in the design and evaluation of propeller configurations (Olasek & Wiklak, 2014).

Conventional methodologies for the characterization of propellers frequently necessitate advanced manufacturing techniques and access to sophisticated testing infrastructures, thereby rendering them less attainable for smaller research collectives, educators, and hobbyists (Stefko et al., 1983). Propellers constitute essential elements within a multitude of engineering systems, ranging from unmanned aerial vehicles (UAVs) to maritime vessels (Carlton, 2018; Garp, 2021). Their operational performance is predominantly assessed through metrics such as thrust, torque, and efficiency. A comprehensive comprehension of these parameters is crucial for the optimization of design and enhancement of performance. Nevertheless, the intricacies and expenses associated with traditional testing methodologies can present substantial obstacles to extensive experimental endeavors.

This study delineates a straightforward yet efficacious experimental design aimed at characterizing 3D-printed propellers. By utilizing the adaptability of additive manufacturing and readily accessible components,

this methodology aspires to democratize the process of propeller testing and empower a wider audience to investigate aerodynamic principles. The suggested approach is particularly advantageous for educational contexts, small-scale research initiatives, and enthusiasts striving to analyze and improve their designs. . Findings from the conducted sample tests will illustrate the practicality of the proposed approach, offering insights into the capabilities and constraints of 3D-printed propellers. Ultimately, this discourse emphasizes the significance of accessible experimentation in promoting innovation and advancing understanding within the field of propeller design.

Basics of Propeller Theory

Propellers are essential components in various engineering systems, including drones, ships, and airplanes, where they convert rotational energy from a motor into thrust. These mechanical devices consist of a rotating hub and a set of blades arranged in a helical configuration, enabling efficient propulsion by interacting with a working fluid such as air or water. During operation, the rotation of the propeller generates thrust by converting rotational energy into linear motion. This mechanism induces a pressure differential across the blade surfaces, accelerating the working fluid—such as air or water—in one direction and propelling the vehicle in the opposite direction (Wald, 2006).

Propeller performance is influenced by several design parameters, including the diameter, pitch, number of blades, and blade profile (D'Angelo et al., 2002). These factors, combined with operational conditions such as rotational speed and fluid properties (air or water), determine the overall performance and suitability of a propeller for a given application.

The performance of a propeller is often characterized by key metrics such as thrust, torque, efficiency, and power consumption (Giannakakis et al., 2015). Thrust is the forward force generated by the propeller, while torque refers to the rotational resistance experienced by the motor. Efficiency, a critical metric, is the ratio of useful thrust power to the total power input.

Traditional Methods for Propeller Characterization

Traditionally, propeller performance is evaluated using wind tunnels or water tanks equipped with specialized sensors to measure thrust, torque, and efficiency (Pienizek & Ciecinski, 2021). While these methods provide high accuracy, they often involve expensive and bulky equipment, making them inaccessible for small-scale or academic projects.

Numerical methods, such as Computational Fluid Dynamics (CFD), have also gained popularity for simulating fluid flow and predicting performance (Wang et al., 2019). However, these require significant

computational resources and expertise, which may not be feasible for all users.

Need for a Simplified Experimental Approach

The limitations of traditional methods highlight the need for a simple, cost-effective, and accessible experimental framework for characterizing propellers. With the growing use of 3D printing, there is an opportunity to develop low-cost experimental setups tailored for 3D-printed components. Such approaches can democratize propeller testing, allowing hobbyists, students, and researchers to explore and optimize propeller designs without requiring extensive resources.

DESIGN OF THE EXPERIMENT

The aim of this study is to design a simple but effective experiment to investigate the impact of different propeller shapes on speed and pressure data. Traditional propeller manufacturing often incurs high costs and long production times, which hinders rapid experimentation. In contrast, 3D printing offers a cost-effective and time-efficient alternative, enabling quick iterations of different designs. By using 3D printed propellers, the performance of the propellers with various shapes would be elaborated.

Components of the Experimental Design

Basic components of the experimental design is given as below.

- **Arduino UNO**: A microcontroller board that acts as the brain of the project, controlling the sensors, motor, and data output. It processes inputs from various components and executes the necessary functions to drive the experiment. The Arduino can be programmed to control the speed and operations of the propellers.
- **Weight measurement unit:** The weight measurement unit detects the thrust force generated by the propeller, which can be seen in the screen o of the unit. This setup helps measure thrust or pressure exerted by the propellers.
- **30A ESC Driver**: An Electronic Speed Controller (ESC) that regulates the power supplied to the brushless motor. The 30A ESC is capable of handling currents up to 30 amperes, making it suitable for driving high-performance motors. It ensures smooth and precise control over the motor's speed.
- **Brushless Motor**: A type of electric motor that is efficient and reliable, commonly used in propeller-driven applications. The motor's performance directly affects the speed and thrust generated by the propeller. Brushless motors are more efficient and require less maintenance compared to brushed motors.
- **IR Modulator**: An infrared module used for wireless communication between components. It can be employed to send or receive data from

remote sensors or control systems. In this project, it can be used for transmitting data related to the propeller's performance.

- **Potentiometer**: A variable resistor used to adjust and control various aspects of the system, such as motor speed or sensor calibration. By changing the resistance, it allows for fine-tuning of parameters in the experiment. The potentiometer provides a simple way to vary input settings and observe their effects.
- **3D Printed Propeller**: Custom-made propellers created using a 3D printer, offering flexibility in design and rapid iteration. 3D printing allows for precise control over the shape and size of the propellers. These printed propellers are used in the experiment to assess the effects of design modifications on performance.
- **Chassis of the Experiment:** The chassis of the experiment hold the measurement unit under the brushless motor and the attached propeller to the hub of the motor, where several springs are mounted to mitigate the vibration that might occur during the test.

The experimental design is given in the figure below.

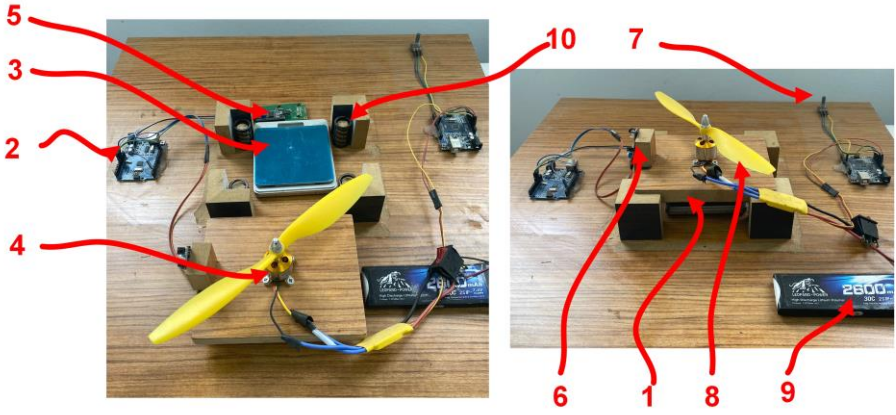

Figure 1: The experimental setup comprising: 1): Chasis, 2) Arduino Unit, 3) Thrust force measurement unit, 4) Brushless motor, 5) Drive unit, 6) IR modulator, 7) Potentiometer, 8) 3D printed propeller, 9) Battery, 10) Springs.

To test the experimental setup, several propellers were manufactured by 3D printing method. The manufactured propeller are given in Figure 2.

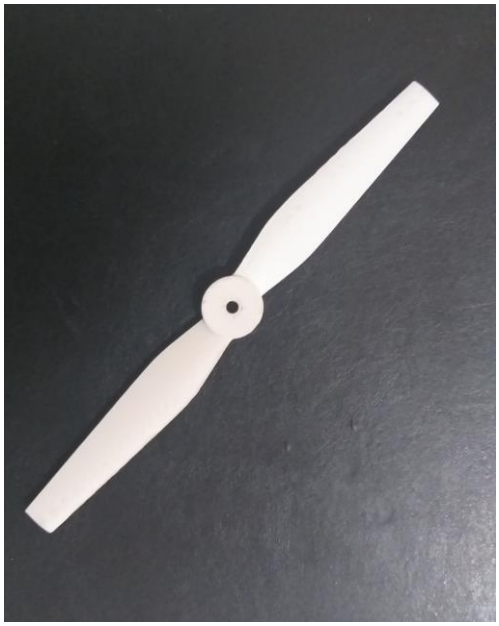

Figure 2: Standard Test Propeller NACA 4412 with PLA material.

RESULTS AND DISCUSSION

This investigation centers on the establishment of a straightforward experimental framework specifically designed for the educational enrichment of engineering students, facilitating the evaluation of 3D printed propellers. The thrust force exerted by the NACA 4412 3D printed propeller was quantified across a spectrum of rotational speeds (RPMs), extending from 750 RPM to over 2000 RPM. The empirical findings, as given in Figure 3, underscore the potential of integrating 3D printing technology and readily accessible tools to promote experiential learning within the context of engineering education. This segment examines the discerned trends and their implications for educational practice.

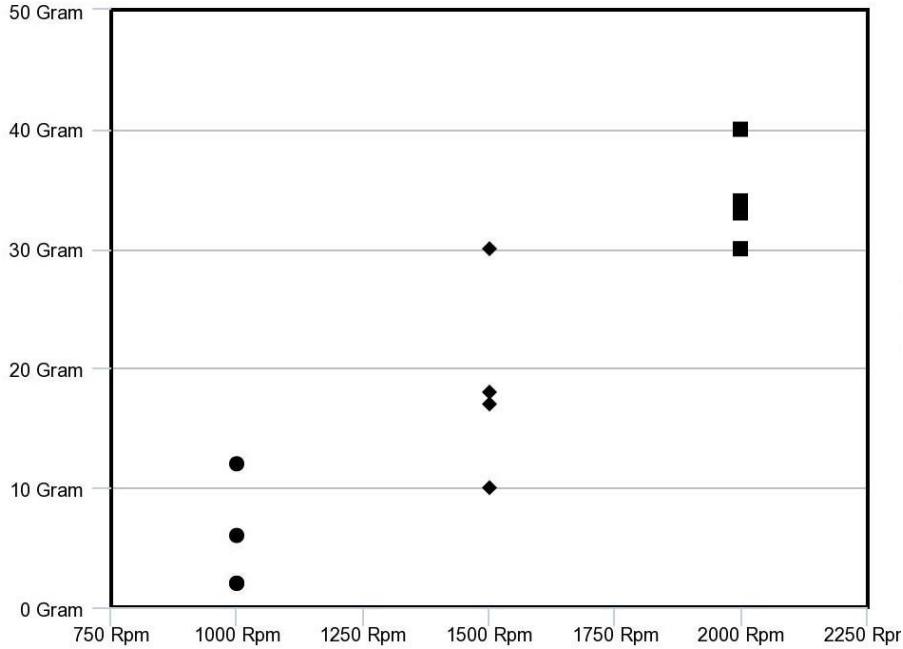

Figure 3: Three different experimental results of thrust force-RPM of the NASA 4412 profile manufactured by 3D printing.

Thrust-RPM Relationship

The experimental data indicates a nonlinear augmentation in thrust force corresponding with an increase in RPM, thereby providing a salient opportunity for students to comprehend the foundational principles of aerodynamics and mechanical design. At lower rotational speeds (~1000 RPM), the thrust force remained minimal, fluctuating between 0 and 10 grams. This observation is consistent with the anticipated behavior of propellers functioning under suboptimal aerodynamic conditions (Hwang et al, 2015), thereby enabling students to internalize concepts such as flow separation and drag phenomena. As the RPM escalated to approximately 1500 RPM, a marked increase in thrust force was recorded, reaching approximately 20 grams. This juncture serves as an optimal reference for students to investigate the conversion of rotational energy into lift and thrust. Between the RPM range of 1500 and 2000, the thrust force experienced a significant elevation, peaking near 40 grams, thereby illustrating the contribution of enhanced angular velocity to performance improvement. This evident correlation between RPM and thrust empowers students to authenticate theoretical aerodynamic models through empirical experimentation.

Educational Benefits and Design Considerations

The identified trends furnish a substantial hands-on demonstration of aerodynamic principles, rendering the experiment particularly advantageous for engineering students. The cambered blade geometry of the NACA 4412 profile accentuates the significance of design parameters in optimizing propeller performance. The nonlinear thrust-RPM dynamic (Hwang et al, 2015) prompts students to engage in a more profound exploration of factors including blade efficiency, flow attachment, and the inherent trade-offs between performance and manufacturing constraints. The capability to fabricate 3D printed propellers with diverse geometrical configurations permits students to iteratively modify designs and assess their immediate effects. Although minor fluctuations in thrust attributable to manufacturing tolerances were noted, these discrepancies remain within acceptable limits for educational objectives. Achieving a peak thrust of approximately 40 grams at 2000 RPM exemplifies the practicality of this framework in examining design optimization and prototype assessment.

CONCLUSION

In conclusion, this experimental framework provides engineering students with a cost-effective and accessible methodology for testing and analyzing 3D printed propellers. The trends observed in thrust-RPM behavior not only affirm the aerodynamic efficacy of the NACA 4412 profile but also illuminate the educational significance of such experiential investigations. This approach has the potential to be used as a starting point to investigate 3D printed propellers' performance.

REFERENCES

Carlton, J. (2007). *Marine propellers and propulsion*. Massachusetts, USA: Butterworth-Heinemann.

D'Angelo, S., Berardi, F., ve Minisci, E. (2002). Aerodynamic performances of propellers with parametric considerations on the optimal design. The Aeronautical Journal, 106(1060), 313-320.

Garg, P. K. (2021). *Unmanned aerial vehicles: An introduction*. Virginia, USA: Mercury Learning and Information.

Giannakakis, P., Laskaridis, P., Nikolaidis, T., ve Kalfas, A. I. (2015). Toward a scalable propeller performance map. Journal of Propulsion and Power, 31(4), 1073-1082.

Hwang, J. Y., Jung, M. K., ve Kwon, O. J. (2015). Numerical study of aerodynamic performance of a multirotor unmanned-aerial-vehicle configuration. *Journal of Aircraft*, *52*(3), 839-846.

Olasek, K., ve Wiklak, P. (2014). Application of 3D printing technology in aerodynamic study. In *Journal of Physics: Conference Series* (Vol. 530, No. 1, p. 012009). IOP Publishing.

Pieniazek, J., ve Ciecinski, P. (2021). Measurement system for small propeller propulsion. In *2021 IEEE 8th International Workshop on Metrology for AeroSpace (MetroAeroSpace)* (pp. 687-691). IEEE.

Sachs, E., Cima, M., & Cornie, J. (1990). Three-dimensional printing: rapid tooling and prototypes directly from a CAD model. *CIRP annals*, *39*(1), 201-204.

Stefko, G. L., Bober, L. J., ve Neumann, H. E. (1983). New test techniques and analytical procedures for understanding the behavior of advanced propellers. *SAE Transactions*, 43-58.

Wald, Q. R. (2006). The aerodynamics of propellers. Progress in Aerospace Sciences, 42(2), 85-128.

Wang, Y., Yu, B., Berto, F., Cai, W., & Bao, K. (2019). Modern numerical methods and their applications in mechanical engineering. *Advances in Mechanical Engineering*, *11*(11), 1687814019887255.

Energy Transformation of Aerogel-Based Phase Change Materials (PCMs)

Fatma MEYDANERİ TEZEL[1]

1- Prof. Dr.; Karabuk University, Faculty of Engineering, Department of Metallurgy and Materials Science, Karabuk/Turkey, E-mail: fatmameydaneri@karabuk.edu.tr, ORCID No: 0000-0003-1546-875X

ABSTRACT

Energy resources often rely on exhaustible sources such as coal, oil, and natural gas, which exist in finite quantities and have adverse environmental effects. As a result, researchers have shifted their focus toward exploring sustainable and renewable energy alternatives. To enhance the reliability of energy supply and mitigate the risk of energy crises, advancements in energy storage technologies for renewable sources are being pursued. Among these, latent heat storage (commonly referred to as phase change energy storage) is gaining considerable attention within the realm of thermal energy storage technologies. Phase change energy storage leverages specialized materials, known as phase change materials (PCMs), which can transition between phases at specific temperatures or within a defined temperature range. During this phase change process, these materials absorb or release significant amounts of latent heat, making them highly efficient for energy storage purposes. In comparison to methods like sensible heat storage or chemical energy storage, phase change energy storage operates effectively without requiring large temperature fluctuations. This approach is characterized by its simplicity, practicality, and versatility. Thanks to these qualities, phase change energy storage emerges as a highly valuable solution for managing, recovering, and reusing renewable energy. Its promising attributes also position it as a strong candidate for widespread practical applications in the growing field of sustainable energy solutions.

Keywords –Energy Storage, Aerogel, Photothermal And Electrothermal Energy Transformation, Acoustic-Thermal Energy Transformation, Magnetic-Thermal Energy Transformation.

INTRODUCTION

Sustainable energy development is extremely important for both humanity and the world. The development and utilisation of renewable energy sources strongly supports progress in this area. In many regions, solar energy that causes power outages is an important factor influencing the development of sustainable energy alternatives, such as wind and tidal energy (Chu& Majumdar, 2012; Wang et al., 2017). In recent years, thermal energy storage (TES) technology has been rapidly developing and becoming widespread thanks to its reliable physical and chemical properties and sustainable charge and discharge temperature characteristics (Chen et al., 2020). TES technology offers a practical and efficient approach to sustainable energy supply, focussing primarily on the storage of latent heat, sensible heat and thermochemical energy using phase change materials (PCMs).

In recent years, various types of aerogels have emerged as successful materials, including carbon aerogels, polymer aerogels, metal aerogels, biomass aerogels, and others (Yang et al., 2022). Aerogel materials have a significant surface area, high porosity and pore volume, and extremely low density, making them highly versatile for a variety of applications in energy (Im et al., 2016), catalysis (Xiong et al., 2022), thermal insulation (Shang et al., 2019), and other fields (Plazzotta et al., 2023; Karatum et al., 2023). The integration of energy storage with aerogels and phase change constitutes an area of progress that is continuously gaining importance. In the development of latent heat energy storage systems, the problem of liquid leakage of PCMs is overcome by adsorption of porous materials (expanded graphite (Im et al., 2016), diatomite (Xiong et al., 2022), silica (Shang et al., 2019), etc.) or encapsulation methods (capsule encapsulation technique ((Plazzotta et al., 2023)), which allows PCMs to be free from container packaging constraints. Although the liquid leakage problem has been addressed, dense packaging materials will reduce the energy storage efficiency of composite PCMs. As a solid object with a three-dimensional network structure, aerogel is an excellent choice for PCM support materials. The hollow structure of aerogel can absorb PCMs and prevent leakage from PCMs through strong capillary force and surface tension while maintaining a high level of latent melting heat. In other words, the unique structure of aerogel ensures that the PCM does not leak and significantly improves the effectiveness of the composite PCM. In particular, aerogel can offer stable structure and unique connectivity elements where pore sizes can be easily customised from nano to large sizes. Low-density aerogel materials can provide a higher PCM load rate per unit mass compared to conventional skeletal support materials.

The interconnected three-dimensional structure also makes the design of thermal conductivity more accessible. The interdependence of the three-dimensional structure further facilitates the design of thermal conductivity. Moreover, the variety of aerogel types provides endless opportunities to develop multifunctional PCMs for different application needs (Kong et al., 2023). The aerogel structure is formed using a variety of materials or nanoparticle inclusions, which can perform photothermal/electro-thermal energy conversion, infrared stealth, flame retardancy and other versatile functions (Wang et al., 2022-a). In addition, compared to conventional form-stabilised PCMs, elastic aerogel offers mechanical flexibility to PCMs, which means that it has a wider range of application possibilities. Considering the functional diversity and recent developments of many innovative aerogel PCMs reported recently, there is still a lack of comprehensive evaluations on the application of versatile aerogel-based PCMs. This study emphasises the energy conversion principle of aerogel PCMs.

THE CATEGORİSATİON OF PHASE CHANGE MATERİALS (PCMS) İN AEROGELS

Currently available aerogel-oriented PCMs pay attention to the thermophysical properties of PE, alkanes, paraffin wax and other low melting points (20-80 °C); less attention is paid to the combination of aerogels with medium and high temperature phase change materials. Organic PCMs, e.g. polyols, PEG, PW and fatty acids (Han et al., 2022; Liu et al., 2023), are highly durable, do not corrode, do not undergo phase separation and experience a low cooling during the crystallisation process, making them widely preferred in aerogel-based PCMs (Wang et al., 2022-b; Nazari et al., 2022). However, the low thermal conductivity of organic PCMs is among their main disadvantages. Inorganic PCMs are mainly crystalline water-containing salts, liquid salts and metals. They have high thermal conductivity and latent heat of phase change (Mohamed et al., 2017). They are widely used in industry due to their favourable cost. However, phase separation and supercooling limit the use and expansion of inorganic salts.

Metal PCMs have high thermal conductivity and stability; they exhibit excellent compatibility in high temperature applications and are widely preferred in high temperature industrial waste heat recovery (Noohi et al., 2022). The downside of PCMs in metal or alloy form is that they corrode intensively at high temperatures, making packaging difficult. For complex PCMs, there is limited research on blends of organic and inorganic PCMs in aerogel-based PCMs; therefore, additional investigations are needed (Figure 1).

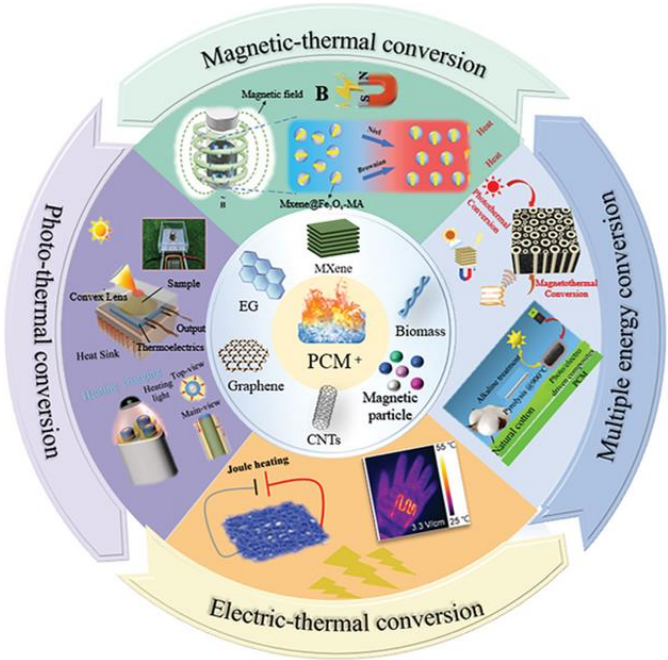

Figure 1: The Various Aerogels Used in PCMs and Their Energy Transformation Applications (Liu et al., 2024).

Carbon-based aerogels have attracted considerable interest due to their low density, high porosity, superior load carrying capacity, impressive thermal conductivity and chemical stability. These materials have a broadly interconnected 3D thermal conductivity framework, improving the inherently low thermal conductivity of PCM, resulting in faster heating and cooling response. These properties make carbon aerogel-based PCM more suitable for applications requiring fast thermal response such as energy storage and photothermal/electrothermal conversion (Kong et al., 2023).

Metal aerogel is a three-dimensional porous structure with high electrical conductivity and thermal conductivity provided by metal nanoparticles. This unique three-dimensional framework enhances both the thermal and electrical conductivity of PCM, creating a seamless conduction path. As research on metal aerogels has progressed, controlled and simple preparation methods have been developed, including free casting and ice template (Scotti& Dunand, 2018; Sahoo et al., 2015). These developments have allowed metal aerogels to be more widely used to improve the performance of PCMs.

Polymers are divided into two main groups: natural (cellulose, starch and rubber) and synthetic (polyvinyl alcohol, polyaniline). The fact that their production can be easily realised by various techniques facilitates the

formation of three-dimensional porous structures of polymers, thus aerogels. Studies on polymer aerogel-based PCMs are generally focused on cellulose nanofibre (CNF) and synthetic polymer aerogel-based PCMs. Cellulose-based aerogel is highly porous and compared to inorganic and polymer aerogels, cellulosic aerogels offer exceptionally low density, high specific surface area and excellent porosity. Furthermore, they are sustainable, innovative and naturally soluble (Liu et al., 2021-a). The low mechanical strength and easily friable nature of conventional aerogels greatly limit their use in industrial applications. However, the emergence of polymer aerogels offers an effective solution to overcome these disadvantages. Polymer aerogels have superior properties such as low thermal conductivity, high durability and good flexibility. Moreover, the types of polymers used and the synthesis conditions applied lead to different aerogel structures (nanoparticle/fibrous, lamellar structure) (Hasegawa et al., 2017; Liu et al., 2021-b). This allows customisation of polymer aerogel designs to suit various needs.

Silicon dioxide, an inorganic material characterised by low thermal conductivity and large surface area, offers the ability to prevent leakage of PCMs during phase change. However, silicon aerogel-based PCMs have a significant potential for use in both providing thermal protection and in the construction of building environments, thanks to their low thermal conductivity and effective heat storage capacity (Kong et al., 2023).

Nitride aerogels are emerging as a new type of inorganic aerogel. Current research is mainly focused on Si3N4 aerogel and BN aerogel, although a limited number of other nitrides (e.g. C3N4 and VN aerogels) are also being investigated. MXenes, a two-dimensional material, exhibits high thermal and electrical conductivity as well as photothermal conversion efficiency reaching almost 100%. In recent years, MXenes-based composite PCMs have become one of the focal points of studies on performance enhancement and multifunctional applications. In addition, the weak interactions between MXene layers make it difficult to directly form flexible MXene structures. For this reason, the preparation of mixed aerogels by forming three-dimensional frameworks containing rich chemical groups on the surface of MXene is of great interest. Hybrid aerogels obtained by combining various nanomaterials can overcome the thermal, physical and mechanical deficiencies of only one material (Kong et al., 2023).

THE TRANSFORMATİON OF ENERGY İN AEROGEL-BASED PCMS

Conventional heat storage methods of PCMs work on the principle of a passive heat absorption, which requires the temperature of the heat source to be higher than the melting point of the PCM. However, this approach faces significant limitations in practice. Aerogel-based PCMs, developed by utilising material properties, can provide an innovative solution to these problems by offering a thermal response based on multiple energy conversion in the processes of storing and releasing heat energy in a given environment. Currently, the energy conversion of aerogel-based PCMs is mainly based on photothermal conversion, electrothermal conversion, magnetothermal conversion and acoustic thermal conversion processes. Among these methods, the most intensive research has been carried out on photothermal and electrothermal conversion, while studies on magnetothermal and acoustic thermal conversion are almost limited. Common photothermal conversion materials that can effectively utilise sunlight are classified as carbon-based compounds and organic polymers on the organic side and semiconductors and metals on the inorganic side (Tang et al., 2021).

3.1.Photothermal and electrothermal transformation

Carbon-based materials have the ability to absorb a wide range of solar energy and have superior electrical conductivity. Owing to these properties, carbon aerogel-based PCMs stand out among photothermal and electrothermal materials with impressive photothermal and electrothermal conversion capability. Carbon-based materials have dense and dispersed π electron clouds, mainly present with dense sp^2 and sp^3 hybridisation, and have the capacity to strongly absorb visible and near infrared radiation, where solar energy is concentrated (Liu et al., 2020). A photon present in visible light is absorbed by an electron present in the carbon aerogel. This process excites the electron, leading to a transition from a low energy level to a high energy level (Shaid et al., 2016). This property enables carbon aerogels to gain photothermal conversion capability. When the excited electrons return to the ground state with the effect of increasing temperature, heat is released. In addition, heat generation can be achieved by converting the electrical energy in carbon aerogels into joule heat. When electric current passes through a conductive composite, Joule heat is generated by collisions between travelling electrons and other molecules or groups (Li et al., 2018). Song et al (Song et al., 2021) developed a composite phase change material (PCM) named LA/CKF@Fe_3O_4 by combining carbonised Kapok fibre aerogel (CKF) with Fe_3O_4 nanoparticles and lauric acid (LA) (Figure 2).

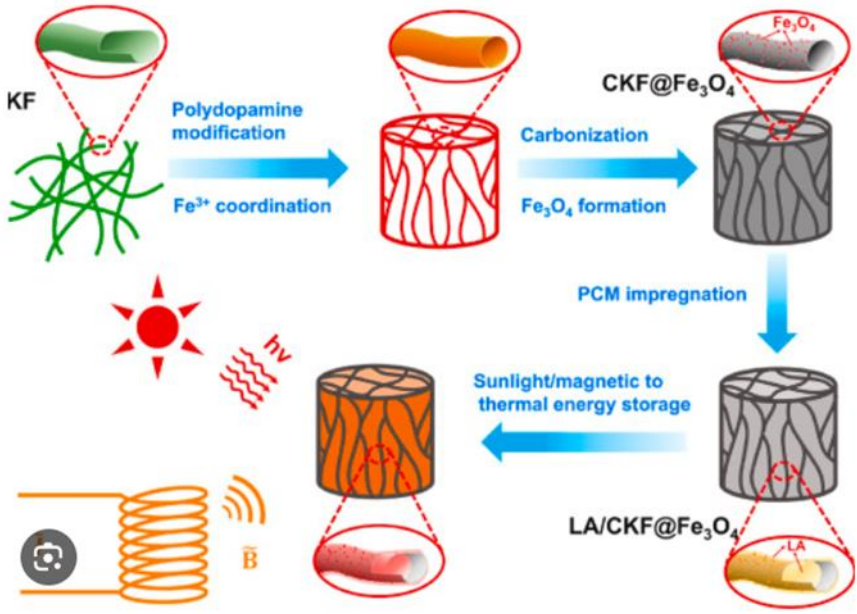

Figure 2: The Preparation of the CKF@Fe_3O_4 Aerogel and the LA/CKF@Fe_3O_4 Composite PCM (Song et al., 2021).

This composite exhibited a high photothermal conversion efficiency of 95% at an irradiation intensity of 700 W/m². Besides, Fe_3O_4 nanoparticles contribute to the superior microwave absorption performance of this composite. With a thickness of 5.5 mm, the composite PCM is capable of absorbing 98.2% of microwaves at a frequency of 8.4 GHz. Zhou et al. designed polyurethane-based multifunctional phase change materials containing zinc oxide (ZnO) and GA (Zhou et al., 2019). Thanks to the outstanding light absorption ability of ZnO nanoparticles and GA and the excellent electric current conduction of GA, the PCM achieves a photothermal conversion efficiency of 80.1% and an electrothermal conversion efficiency of 84.4%. Carbon aerogel-based PCMs have rich thermal physical properties and offer outstanding potential for photothermal/electrothermal conversion and energy storage. Their high thermal and electrical conductivity properties provide a high energy conversion efficiency, fulfilling the energy conversion needs (Kong et al., 2023).

MXene, which is similar to carbon-based aerogel, has a three-dimensional interpenetrating structure and superior light absorption ability. Furthermore, MXene-based PCMs exhibited a remarkable photothermal conversion capacity (Figure 3).

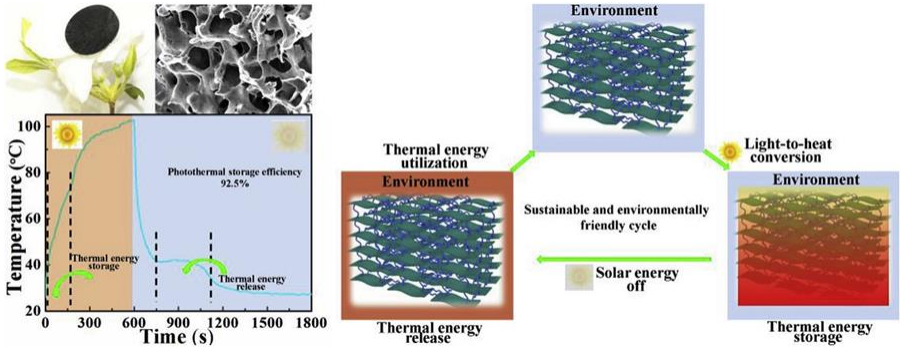

Figure 3: MXene Aerogel-Based Phase Change Materials (Lin et al., 2020).

Research on photothermal MXenes is still in the development process. Several pioneering studies have shown that the photothermal conversion mechanism of MXenes, the ability to effectively absorb solar energy and convert this energy into heat energy for storage and utilisation, is directly linked to the strong electromagnetic interference shielding effect and LSPR effect (Tang et al., 2017). Huang et al. (Huang et al., 2023) developed a bio-based MXene hybrid aerogel/PW composite PCM by combining cellulose nanocrystals (CNCs), Mxene, konjac glucomannan (KGM) and $AgNO_3$ (Figure4).

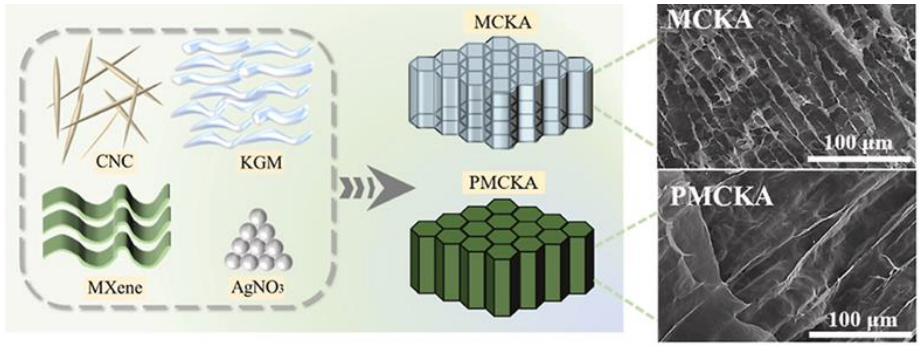

Figure 4: A Biologically-Based MXene Hybrid Aerogel PCM (Huang et al., 2023).

The combination of MXene with Ag nanoparticles overcomes the electrical insulation of the PCM, giving the composite PCM outstanding photothermal and electrothermal conversion capabilities. The composite PCM offers 97.45% photothermal conversion efficiency and 98.89% electrothermal conversion efficiency.

Du et al. (Du et al., 2022) produced P-MXene/cellulose nanofibre (CNF) hybrid aerogel by replacing $Ti_3C_2T_x$ MXene nanosheets (P-MXene) with polymerised dopamine. To obtain this composite PCM, a hybrid aerogel saturated with erythritol was also added. The thermal conductivity (69.0%) and photothermal conversion efficiency (88.9%) of the composite PCM were significantly enhanced by P-MXene nanosheets (Figure 5).

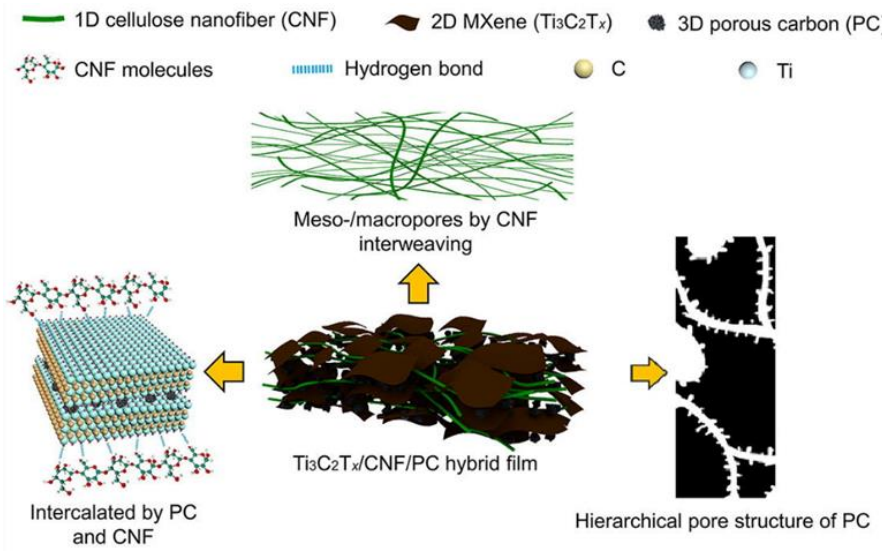

Figure 5: MXene ($Ti_3C_2T_x$)/Cellulose Nanofiber (CNF)/PC Composit Structure (Chen et al., 2021).

Under full spectrum sunlight, cellulose aerogel is not capable of photothermal conversion. However, functional nanomaterials can be added to make cellulose hybrid aerogel. This can improve the photothermal conversion efficiency. Currently, the organic polymers used include indocyanine green (ICG), diketopyrrolopyrrole (DPP) and conjugated polymers (e.g., polypyrrole, polyaniline, polydopamine, thiophene, etc.) and other small molecular dyes (Ji et al., 2022). The transformation process of organic polymers is quite similar to the mechanism of carbon materials. When exposed to the light direction, the gap between the valence and conduction bands narrows, which accelerates charge transfer, triggers lattice vibration and causes the temperature of the organic material to rise (Ai et al., 2022). Du et al. (Du et al., 2020) developed aerogels composed of cellulose nanofibre (CNF)/BP blend with black phosphorus (BP) nanosheets using ultrasonically assisted liquid stripping. Furthermore, a new stable composite PCM was obtained by adsorption of n-octane by immersion technique. Due to the high porosity and light weight of CNF/BP aerogel, this aerogel-based composite PCM achieved an enthalpy value of 251.60 J/g and a load ratio of

3073%. The thermal conductivity of the composite PCM is 0.45 W/mK, exhibiting a photothermal conversion efficiency of 87.6% under 250 mW/cm² simulated solar radiation. Xu et al. (Xu et al., 2020) made a cellulose nanofibre (CNF)/polypyrrole (PPy) aerogel blend using polypyrrole (PPy). This composite PCM was fabricated with a porous cellulose nanofibre (CNF)/polypyrrole (PPy) blend covering the n-octane with aerogel. Under 300 mw/cm^2 solar radiation, the n-octane loading rate of the composite PCM is 96% and the photothermal conversion efficiency is 85.9%. Moreover, besides organic nanoparticles, emerging MXene materials are also used to enhance photothermal conversion capabilities. Wang et al. developed cellulose-based hybrid aerogel PCMs by freezing method by combining MXene colloid, cellulose hydrogel and PEG (Wang et al., 2022-c). MXene significantly enhances the photothermal conversion ability of composite PCMs due to its unique structural and functional properties. 5% MXene provides a photothermal conversion efficiency of 91.6% to the PCM under a sunlight of 100 mW/cm^2 (Figure 6).

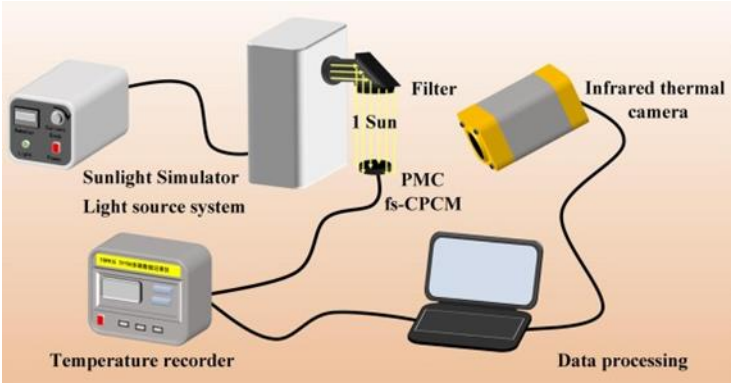

Figure 6: The Diagram of Light-to-Heat Conversion Test System of PMC fs-CPCMs (Wang et al., 2022-c).

Quan et al. fabricated hybrid aerogel using cellulose aerogel as carrier and MXene as photothermal conversion material (Quan et al., 2023). The aerogel impregnates PEG to form composite PCM with high solar energy conversion efficiency and high energy storage capacity. MXene significantly increases its efficiency in converting solar energy into heat energy. When using less than 4 wt% MXene, it is possible to achieve a photothermal conversion efficiency higher than 97.16%. Moreover, the combination of functional nanomaterials with cellulose aerogel plays an important role in ensuring the high energy conversion efficiency of PCM. However, cellulosic hybrid aerogels are expected to improve the photothermal conversion ability and flexibility of PCMs, which expands the application fields of

photothermal materials. Photothermal and electrothermal conversion are the best options for energy conversion and are also safe (Kong et al., 2023).

3.2.Acoustic-thermal and magnetic-thermal transformation

In energy efficiency applications developed for aerogel-based PCMs, methods such as acoustic-thermal conversion and magneto-thermal conversion are also being investigated. Currently, acoustic thermal conversion of aerogel-based PCMs is largely achieved by the addition of metal particles. When a high-energy and penetrating sound wave propagates through a solid medium, the relative motion between the molecules of the medium leads to internal friction. This process results in the conversion of part of the sound energy into heat energy (Oh et al., 2019). There has been limited research and development on acoustic-thermal energy conversion materials, especially PCMs. Liu et al. (Liu et al., 2021-b) developed a Fe_3O_4/GO aerogel composite PCM by placing Fe_3O_4 nanoparticles on the surface of GO nanosheets by in situ synthesis (Figure 7).

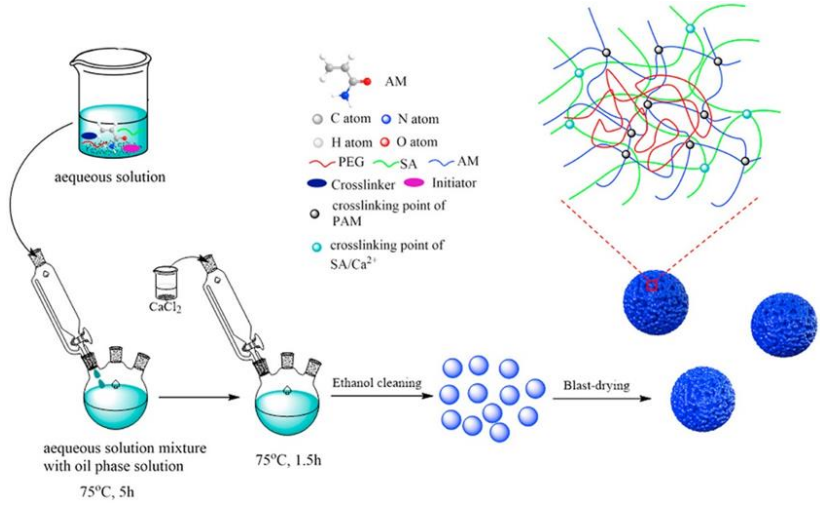

Figure 7: The Preparation Process (Liu et al., 2021-b).

Fe_3O_4-GO nanosheets increased the temperature of the composite PCM to 75 °C by converting the mechanical energy contained in sound waves at a frequency of 1200 Hz into heat energy. These nanosheets efficiently convert energy and store the heat energy in PEG-6000. Therefore, this composite material is envisaged to be used in the fields of building sound insulation and ultrasonic therapy.

Magnetothermal conversion of aerogel is similar to acoustic thermal conversion in that thermal energy is obtained by the addition of magnetic materials. In this context, iron oxides (Fe_3O_4 and Fe_2O_3), metal doped iron

oxides and metal alloys stand out as effective energy conversion materials among different magnetic materials. Alternating current is used to create an alternating magnetic field by allowing periodic electron movement. Atoms of paramagnetic materials are orientated towards alternating magnetic fields through Néel relaxation to release energy (Li et al., 2021). Tao and co-workers (Tao et al., 2021) succeeded in forming fibre aerogels by integrating PPy and Fe_3O_4 on hollow caprock fibre carriers using PPy-Fe_3O_4 bilayer coating (Figure 8). The composite PCM produced by the PW encapsulation method was kept under the influence of a magnetic field for 100 seconds and its temperature rapidly reached 45 °C. Then, the heat storage process started with phase change. When the alternating magnetic field was removed, the composite PCM started to cool down and released its latent heat. This study demonstrates the ability of composite PCM to perform magnetothermal conversion under an alternating magnetic field.

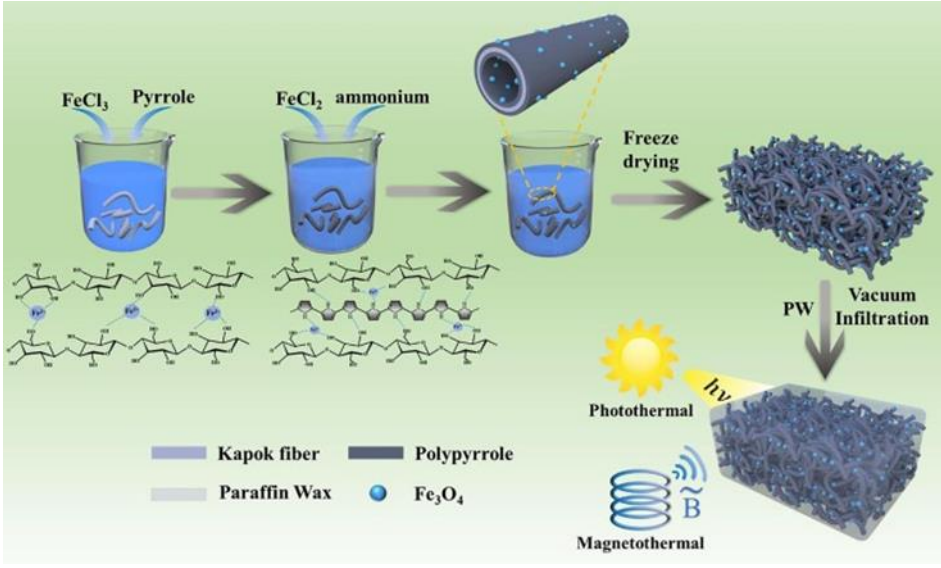

Figure 8: The Formation of the Composited PCMs (KF@PPy-Fe_3O_4/PW) and its Solar- and Magnetic- Thermal Effect (Tao et al., 2021).

Song et al. added Fe_3O_4 nanoparticles to carbonised Kapokay fibre aerogel (CKF) composite PCM to impart magnetothermal conversion capability (Song et al., 2021). In the presence of an alternating magnetic field, this composite PCM can exhibit the ability to convert magnetic energy into heat energy with high efficiency. This new energy conversion capability can diversify the energy responses of PCM and expand the application fields of composite PCM.

RESULTS AND DISCUSSION

Aerogels are porous materials characterized by their low density, high porosity, and large specific surface area. These properties make them an excellent choice for skeletal support materials of PCMs. Aerogel-based PCMs have high load-carrying capacity and high energy storage density. Modifications to the three-dimensional structure and functional groups of aerogels offer the opportunity to improve the thermophysical and mechanical properties of aerogel-based PCMs. In addition, aerogel-based PCMs have the advantage of having various forms of energy conversion such as photothermal conversion and electrothermal conversion. Carbon, BN, metal, and MXene aerogel-based PCMs are notable for their high thermal conductivity and rapid thermal response capabilities. These properties make them ideal for heat storage and thermal management applications. On the other hand, aerogel-based PCMs such as silica and polymer are widely used in the field of thermal insulation due to their low thermal conductivity. Cellulose and polymer aerogel-based PCMs can be effectively used for thermal infrared privacy and thermal protection materials due to their superior mechanical properties and flexibility. Aerogel-based PCMs have a wide range of applications and show great potential in many areas. Recently, we have witnessed developments in energy conversion and multifunctional applications of such materials. In particular, acoustic-thermal and magnetic-thermal conversion offer significant application opportunities in medical equipment, while the number of materials research in this area is quite limited.

REFERENCES

Ai, H., Lv, L., Chen, T., Zhang, Y., Dong, L., & Song, S. (2022). An eco-friendly and facile montmorillonite nanosheets aerogel based phase change materials for efficient solar-to-thermal energy conversion. *Energy Conversion and Management*, *253*, 115172.

Chen, X., Tang, Z., Liu, P., Gao, H., Chang, Y., & Wang, G. (2020). Smart utilization of multifunctional metal oxides in phase change materials. *Matter*, *3*(3), 708-741.

Chen, W., Zhang, D., Yang, K., Luo, M., Yang, P., & Zhou, X. (2021). Mxene ($Ti_3C_2T_x$)/cellulose nanofiber/porous carbon film as free-standing electrode for ultrathin and flexible supercapacitors. *Chemical Engineering Journal*, *413*, 127524.

Chu, S., & Majumdar, A. (2012). Opportunities and challenges for a sustainable energy future. *Nature*, *488*(7411), 294-303.

Du, X., Qiu, J., Deng, S., Du, Z., Cheng, X., & Wang, H. (2020). Flame-retardant and form-stable phase change composites based on black phosphorus nanosheets/cellulose nanofiber aerogels with extremely high energy storage density and superior solar-thermal conversion efficiency. *Journal of Materials Chemistry A*, *8*(28), 14126-14134.

Du, X., Wang, J., Jin, L., Deng, S., Dong, Y., & Lin, S. (2022). Dopamine-Decorated $Ti_3C_2T_x$ MXene/Cellulose Nanofiber Aerogels Supported Form-Stable Phase Change Composites with Superior Solar–Thermal Conversion Efficiency and Extremely High Thermal Storage Density. *ACS Applied Materials & Interfaces*, *14*(13), 15225-15234.

Han, L., Zhang, X., Ji, J., & Ma, K. (2022). Research progress on the influence of nano-additives on phase change materials. *Journal of Energy Storage*, *55*, 105807.

Hasegawa, G., Shimizu, T., Kanamori, K., Maeno, A., Kaji, H., & Nakanishi, K. (2017). Highly flexible hybrid polymer aerogels and xerogels based on resorcinol-formaldehyde with enhanced elastic stiffness and recoverability: insights into the origin of their mechanical properties. *Chemistry of Materials*, *29*(5), 2122-2134.

Huang, D., Wang, Z., Sheng, X., & Chen, Y. (2023). Bio-based MXene hybrid aerogel/paraffin composite phase change materials with superior photo and electrical responses toward solar thermal energy storage. *Solar Energy Materials and Solar Cells*, *251*, 112124.

Im, H., Kim, T., Song, H., Choi, J., Park, J. S., Ovalle-Robles, R., ... & Kim, Y. H. (2016). High-efficiency electrochemical thermal energy harvester using carbon nanotube aerogel sheet electrodes. *Nature communications*, *7*(1), 10600.

Ji, X., Jiang, Y., Liu, T., Lin, S., & Du, A. (2022). MXene aerogel-based phase change film for synergistic thermal management inspired by antifreeze beetles. *Cell Reports Physical Science*, *3*(4).

Karatum, O., Steiner III, S. A., & Plata, D. L. (2023). Developing aerogel surfaces via switchable-hydrophilicity tertiary amidine coating for improved oil recovery. *Science of The Total Environment*, *880*, 163062.

Kong, X., Nie, R., & Yuan, J. (2023). A review of Shape stabilized aerogel-based phase change materials for Preparation, classification and applications. *Energy and Built Environment*.

Li, Y., Chen, J., Cai, P., & Wen, Z. (2018). An electrochemically neutralized energy-assisted low-cost acid-alkaline electrolyzer for energy-saving electrolysis hydrogen generation. *Journal of Materials Chemistry A*, *6*(12), 4948-4954.

Li, G., Wang, Y., & Zhang, X. (2021). Graphene aerogel-phase change material host-guest smart films. *FlatChem*, *27*, 100249.

Lin, P., Xie, J., He, Y., Lu, X., Li, W., Fang, J., ... & Chen, Y. (2020). MXene aerogel-based phase change materials toward solar energy conversion. *Solar Energy Materials and Solar Cells*, *206*, 110229.

Liu, P., Gao, H., Chen, X., Chen, D., Lv, J., Han, M., ... & Wang, G. (2020). In situ one-step construction of monolithic silica aerogel-based composite phase change materials for thermal protection. *Composites Part B: Engineering*, *195*, 108072.

Liu, H., Du, H., Zheng, T., Liu, K., Ji, X., Xu, T., ... & Si, C. (2021-a). Cellulose based composite foams and aerogels for advanced energy storage devices. *Chemical Engineering Journal*, *426*, 130817.

Liu, L., Zou, X., Wang, Y., Zhou, W., Shi, J., Ye, Y., ... & Xia, Y. (2021-b). Phase change and aerogel dual functionalized composites materials with double

network structure through one-step preparation of polyacrylamide/calcium alginate/polyethylene glycol. *Polymer*, *223*, 123710.

Liu, K., Yuan, Z. F., Zhao, H. X., Shi, C. H., & Zhao, F. (2023). Properties and applications of shape-stabilized phase change energy storage materials based on porous material support:A review. *Materials Today Sustainability*, *21*, 100336.

Liu, M., Qian, R., Yang, Y., Lu, X., Huang, L., & Zou, D. (2024). Modification of Phase Change Materials for Electric-Thermal, Photo-Thermal, and Magnetic-Thermal Conversions: A Comprehensive Review. *Advanced Functional Materials*, 2400038.

Mohamed, S. A., Al-Sulaiman, F. A., Ibrahim, N. I., Zahir, M. H., Al-Ahmed, A., Saidur, R., ... & Sahin, A. Z. (2017). A review on current status and challenges of inorganic phase change materials for thermal energy storage systems. *Renewable and Sustainable Energy Reviews*, *70*, 1072-1089.

Nazari, N., Bahramian, A. R., & Allahbakhsh, A. (2022). Thermal storage achievement of paraffin wax phase change material systems with regard to novolac aerogel/carbon monofilament/zinc borate form stabilization. *Journal of Energy Storage*, *50*, 104741.

Noohi, Z., Nosouhian, S., Niroumand, B., & Timelli, G. (2022). Use of low melting point metals and alloys (Tm< 420 °C) as phase change materials: a review. *Metals*, *12*(6), 945.

Oh, J. H., Lee, H. R., Umrao, S., Kang, Y. J., & Oh, I. K. (2019). Self-aligned and hierarchically porous graphene-polyurethane foams for acoustic wave absorption. *Carbon*, *147*, 510-518.

Plazzotta, S., Calligaris, S., & Manzocco, L. (2023). Feasibility of protein aerogel particles as food ingredient: The case of cocoa spreads. *Journal of Food Engineering*, *351*, 111522.

Quan, B., Wang, J., Li, Y., Sui, M., Xie, H., Liu, Z., ... & Tong, Y. (2023). Cellulose nanofibrous/MXene aerogel encapsulated phase change composites with excellent thermal energy conversion and storage capacity. *Energy*, *262*, 125505.

Sahoo, P. K., Aepuru, R., Panda, H. S., & Bahadur, D. (2015). Ice-templated synthesis of multifunctional three dimensional graphene/noble metal nanocomposites and their mechanical, electrical, catalytic and electromagnetic shielding properties. *Scientific reports*, *5*(1), 17726.

Scotti, K. L., & Dunand, D. C. (2018). Freeze casting–A review of processing, microstructure and properties via the open data repository, FreezeCasting. net. *Progress in Materials Science*, *94*, 243-305.

Shaid, A., Wang, L., Islam, S., Cai, J. Y., & Padhye, R. (2016). Preparation of aerogel-eicosane microparticles for thermoregulatory coating on textile. *Applied Thermal Engineering*, *107*, 602-611.

Shang, L., Lyu, Y., & Han, W. (2019). Microstructure and thermal insulation property of silica composite aerogel. *Materials*, *12*(6), 993.

Song, S., Ai, H., Zhu, W., Lv, L., Feng, R., & Dong, L. (2021). Carbon aerogel based composite phase change material derived from kapok fiber: Exceptional microwave absorbility and efficient solar/magnetic to thermal energy storage performance. *Composites Part B: Engineering*, *226*, 109330.

Tang, L. S., Yang, J., Bao, R. Y., Liu, Z. Y., Xie, B. H., Yang, M. B., & Yang, W. (2017). Polyethylene glycol/graphene oxide aerogel shape-stabilized phase change materials for photo-to-thermal energy conversion and storage via tuning the oxidation degree of graphene oxide. *Energy Conversion and Management*, *146*, 253-264.

Tang, Z., Gao, H., Chen, X., Zhang, Y., Li, A., & Wang, G. (2021). Advanced multifunctional composite phase change materials based on photo-responsive materials. *Nano Energy*, *80*, 105454.

Tao, Z., Yang, M., Wu, L., Yan, J., Yang, F., Lin, J., ... & Wang, G. (2021). Phase change material based on polypyrrole/Fe_3O_4-functionalized hollow kapok fiber aerogel matrix for solar/magnetic-thermal energy conversion and storage. *Chemical Engineering Journal*, *423*, 130180.

Xiong, Z. C., Zhu, Y. J., Wang, Z. Y., Chen, Y. Q., & Yu, H. P. (2022). Tree-inspired ultralong hydroxyapatite nanowires-based multifunctional aerogel with vertically aligned channels for continuous flow catalysis, water disinfection, and solar energy-driven water purification. *Advanced Functional Materials*, *32*(9), 2106978.

Xu, J., Tan, Y., Du, X., Du, Z., Cheng, X., & Wang, H. (2020). Cellulose nanofibril/polypyrrole hybrid aerogel supported form-stable phase change composites with superior energy storage density and improved photothermal conversion efficiency. *Cellulose*, *27*, 9547-9558.

Wang, Z., Tong, Z., Ye, Q., Hu, H., Nie, X., Yan, C., ... & Deng, T. (2017). Dynamic tuning of optical absorbers for accelerated solar-thermal energy storage. *Nature communications*, *8*(1), 1478.

Wang, C., Dong, W., Li, A., Atinafu, D. G., Wang, G., & Lu, Y. (2022-a). The reinforced photothermal effect of conjugated dye/graphene oxide-based phase change materials: Fluorescence resonance energy transfer and applications in solar-thermal energy storage. *Chemical Engineering Journal*, *428*, 130605.

Wang, Y., Liu, J., Zhao, Y., Qin, Y., Zhu, Z., Yu, Z., & He, H. (2022-b). Temperature-triggered fire warning PEG@ wood powder/carbon nanotube/calcium alginate composite aerogel and the application for firefighting clothing. *Composites Part B: Engineering*, *247*, 110348.

Wang, H., Deng, Y., Liu, Y., Wu, F., Wang, W., Jin, H., ... & Lei, J. (2022-c). In situ preparation of light-driven cellulose-Mxene aerogels based composite phase change materials with simultaneously enhanced light-to-heat conversion, heat transfer and heat storage. *Composites Part A: Applied Science and Manufacturing*, *155*, 106853.

Yang, W. J., Wei, C. X., Yuen, A. C. Y., Lin, B., Yeoh, G. H., Lu, H. D., & Yang, W. (2022). Fire-retarded nanocomposite aerogels for multifunctional applications: A review. *Composites Part B: Engineering*, *237*, 109866.

Zhou, Y., Wang, X., Liu, X., Sheng, D., Ji, F., Dong, L., ... & Yang, Y. (2019). Multifunctional ZnO/polyurethane-based solid-solid phase change materials with graphene aerogel. *Solar Energy Materials and Solar Cells*, *193*, 13-21.

An Economic Order Quantity Model for Reworkable Defective Items with Larger Backorder Eliminated Time Than Inspection Time

Abdullah EROĞLU[1]
Harun SULAK[2]

1 Süleyman Demirel University, Faculty of Engineering and Natural Sciences, Department of Industrial Engineering, abdullaheroglu@sdu.edu.tr, Isparta, Türkiye. ORCID No: 0000-0002-3035-8682
2 Süleyman Demirel University, Faculty of Economics and Administrative Sciences Department of Econometrics, harunsulak@sdu.edu.tr, Isparta, Türkiye. ORCID No: 0000-0001-8286-1813
Corresponding author: harunsulak@sdu.edu.tr

ABSTRACT

The basis assumption in classical stock control models is that all items ordered are good quality and non-defective. However, in real life this situation is not always true and items that ordered have some defective items and imperfect products. Studies on defective items in ordered lot have an important and extensive place in literature. In these studies, on EOQ models, basic assumptions are; there is a certain amount of defective production, the defective production rate follows a probability distribution, defective products also stand out as scrap, repairable, defective etc. EOQ models which are based on whether the inspection rate in the process of separating defective items and perfect items is greater or less than the production rate, are also mostly studied in literature. In this study, an EOQ model is proposed by considering the situation where the inspection time is smaller than the time to eliminate the backorder. Numerical examples are given and sensitivity analysis are made to see the effects of parameter changes on outputs. As a result of sensitivity analysis, while defective rate increases, optimal values of order quantity and maximum allowable backorder quantity decreases, however expected total cost per unit increases.

Keywords: Rework, Defective Items, Economic Order Quantity Model, Backordering, Inspection Time.

INTRODUCTION

One of the basic assumptions in the classical Economic Order Quantity (EOQ) models is that all products received ordered are good quality and defect-free. However, in real life, it is not possible to fully satisfy this assumption. Because there may be defective products, both because of the uncertainties during the production phase and due to the negativity that occur during transportation after production.

In the production process, defective products can be reworked or repaired and become perfect, or they can be sold as defective at a lower price, or those that are completely useless can be scrapped. In most studies on this subject, finding the optimal economic production amount is evaluated together with optimal monitoring and maintenance planning of the process.

The defective product situation is also addressed in economic order quantity models, such that items ordered contain defective products at a certain rate. In this case, each batch of ordered items is subjected to monitoring and inspection process, and defective products are identified and separated. These defective products can be reprocessed or repaired to make them perfect, or they can be sold at a lower price.

Rosenblatt and Lee (1986) studied an economic production quantity model under the assumption that the production system produces perfect products for a period that is a random variable, but then starts to produce defective products at a certain rate and defective products are reworked while production is processing at a certain cost. Schwaller (1988) obtained an economic order quantity assumed that the defective rate in ordered lot is known and that there are fixed and variable inspection and sorting costs for these products. Salameh and Jaber (2000) proposed an EOQ model in the presence of defective items. They assumed that the batches received contain defective products at a certain rate and that the defect rate follows a random uniform distribution. In the model, 100% inspection process is performed and any defective items detected are sold together with lower price.

The Salameh and Jaber (2000) model has attracted great attention in literature and has been reconsidered and developed in many studies. Goyal and Cardenes-Baron (2002) reconsider the Salameh and Jaber's model and developed a new approach that is simple and easy to implement in finding the optimal order quantity. Papachristos and Konstantaras (2006), revisited Salameh and Jaber's model and state the necessary and sufficient conditions to ensure that the models obtained in the model do not fall into a stock-out situation. Maddah and Jaber (2008) corrected the deficiencies and errors in Salameh and Jaber's model. Khan et al. (2011) summarized the extensions of the EOQ model with defective items in Salameh and Jaber's model. Hayek and Salameh (2001) studied defective production situation, assumed that the defective rate follows a uniform distribution and that the defective products are reworked to become perfect products. Their model allows shortages and backordering. Chan et al. (2003) proposed three economic production quantity models for defective production situation. The products produced are subject to 100% inspection and are divided into perfect products, imperfect products and defective products. Eroglu et al. (2004) developed a new economic production quantity model, stating that it is more appropriate to sell defective products at a discounted price instead of reworking them. In the model, it is assumed that the distribution of defect rate is a uniform distribution and that defective items are sold with lower price when production stops. Shortages are allowed in the mentioned model. Konstantaras et al. (2007) developed an inventory model in which lot sizing and inspection policy were examined. In the model ordered lot contains defective items at a random rate which cannot be used to meet demand. These items can be reworked for the sale to satisfy demand, or they can be sold as a single lot at a discounted price. Taleizadeh et al. (2014) studied defective production process that provides scrap and reworkable items. Backordering and shortages were also allowed in the inventory models and Ouyang et al. (2002), Cárdenas-Barrón (2009) and Eroglu and Ozdemir (2007) studied the EOQ models under shortage situation. Sarkar et al. (2014) developed inventory models for defective items with rework process and allowable backorders. In developed models, defective rate

is a random variable whose probability distributions are uniform, triangular and beta. Moussawi-Haidar et al. (2016) developed economic production models in which backordering is not allowed and defective products are sold at lower selling prices at the end of the inspection process or all defectives are reworked in different models. Nobil et al. (2020) developed a model that allows backordering for defective items. They categorized the good products as high or low quality and defectives as reworkable or rejected. Karagul and Eroglu (2022) proposed a stock control model for reworkable defective items. They allow backordering and all defects are reworkable and they become good products after reworking process. Singh at al. (2023) studied the EOQ models of imperfect items with shortage backordering under three different scenarios.

As mentioned above in all studies about defective items, inspection and rework process under the shortage allowed, it is assumed that the inspection time required to separate good and defective items is sufficiently larger than the time to eliminate backorders. This difference is the main contribution of the proposed model in which inspection time is smaller than the elimination time of backorders.

The rest of the study will proceed as follows. Firstly, notations, assumptions and mathematical formulation of proposed model are given. Optimum order and backorder quantities formulas are derived in this section. Then numerical examples are given, and sensitivity analysis is made to illustrate the effects of parameter changes on optimal solutions. The last section is the conclusion of the paper.

MATHEMATICAL FORMULATION OF THE MODEL

Products purchased in batches contain defective products due to production or transportation process. It is assumed that the products received in lots contain a certain proportion of defective items. When the ordered batch is received, perfect and defective items are separated during the inspection process. The perfect items are sold at a regular price per unit. Defective items with imperfect quality can be reworked with unit cost to become good and perfect by repairing the minor problems. It is assumed that after the inspection process, the rework process begins and all defective items become good and perfect after the rework process. Formulas of optimal order quantity and maximum allowable backorder quantity are obtained with the developed model.

Notations

Notations used in the proposed model are as follows:

Q order quantity per cycle

D demand rate in units per unit time

w maximum allowable backorder level

x inspection rate in units per unit time
λ rework rate in units per unit time
t_1 time to allow backordering
t_2 time to finish the inspection and to eliminate some backorders
t_3 time to eliminate the backorder level with reworkable items
t_4 time to rework defective items after eliminating backorder level
t_5 time passed until on hand inventory comes down to zero with reworked items
T order cycle, $T = t_1 + t_2 + t_3 + t_4 + t_5$
p proportion of defective items in a lot
$f(p)$ probability density function of p
$E[.]$ expected value
K fixed ordering cost per cycle
c unit purchase cost per item
c_r unit reworking cost per item
d unit inspection cost per item
h unit holding cost per item per unit time
h_1 unit holding cost per reworkable items per unit time
b unit backorder cost per item per unit time

Assumptions

Following assumptions are made for proposed model:

- Demand, rework rate and inspection rate are constant and known.
- Each received batch contains defectives.
- Each ordered batch conducts a 100% inspection process. When the inspection process finishes, defective items are reworked. With a constant rework rate. All defective items become perfect quality after rework process.
- Rework rate and inspection rate are greater than demand rate.
- Shortages are allowed. Allowable shortages are completely backordered with perfect quality items while defective items are reworked after inspection process.
- Inspection process time is smaller than the time taken to eliminate the backorder level. Therefore, after the inspection process finished, some backordering levels still not eliminated. Uneliminated backorder is fulfilled by the reworked items.

The inventory level behavior for good quality and defective items are illustrated in Figure 1 and 2, respectively.

During t_1, demand is backordered until ordered lot received. Single item products arrive in batches and are examined at x speed to separate defective items from perfect items in t_2. Each order contains a certain proportion of defective items with a rate of p. So, the rate of perfect items in each lot is $(1 - p)$. During inspection process in t_2, some of the separated

perfect items fulfill the demand and the others are for elimination of backorders with $(1-p)x-D$ rate. After the inspection process is completed, defective items are reworked with a rate of λ. These reworked items are used to eliminate unmet backorders with good items in time t_3 and to meet the demand in time t_4. After the rework process is finished, in time t_5, the demand is fullfilled with accumulated reworked items.

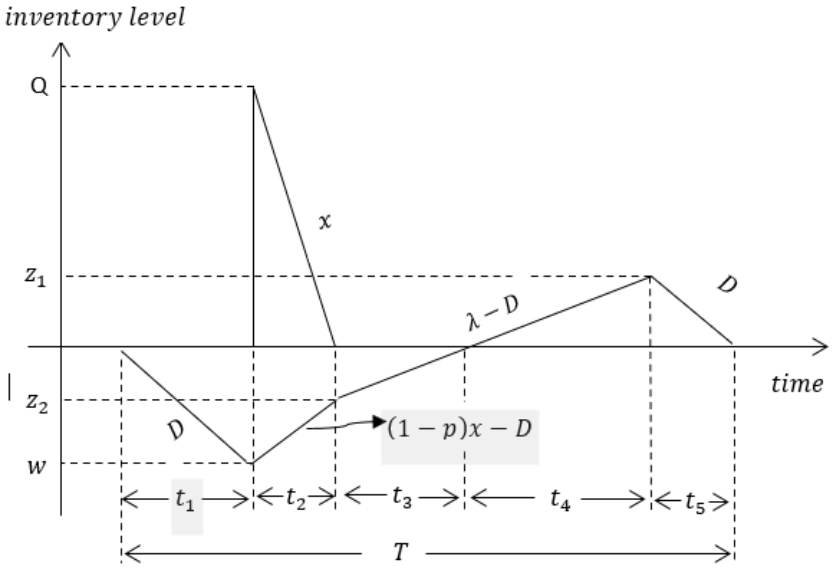

Figure 1: Behavior of inventory level for good quality items

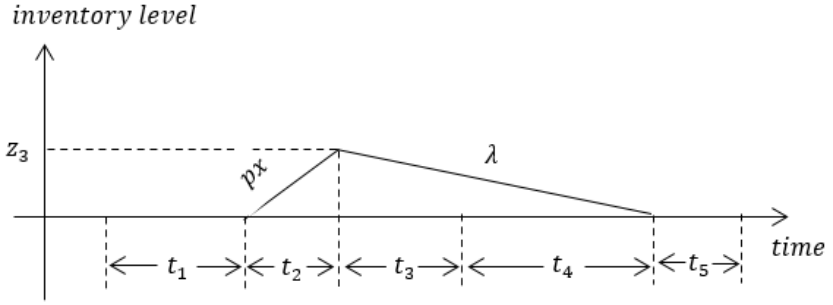

Figure 2: Behavior of inventory level for defective items

The equations to be used throughout the model are obtained according to Figure 1 and 2 as follows:

From Figure 1, during time t_1 shortages are allowed and backorder level of w units is built, then t_1 is;

$$t_1 = \frac{w}{D} \quad (1)$$

During t_2, good and defective items in ordered lot of Q are separated with inspection rate x. So;

$$t_2 = \frac{Q}{x} \tag{2}$$

Also, from Figure 1;

$$t_2 = \frac{w - z_2}{\alpha A} \tag{3}$$

Here $A = 1 - p - \frac{D}{x}$. From Equation (2) and (3);

$$z_2 = w - AQ \tag{4}$$

From Figure 2, during t_2, defective items, pQ is obtained with speed of px, so;

$$z_3 = pQ \tag{5}$$

In t_2, backorder level of w decreases to z_2. When inspection process is completed at the end of the t_2, defective items are reworked with a rate of λ. Rework process is finishes at the end of the t_4. So, from Figure 2, rework time, t_r:

$$t_r = t_3 + t_4 = \frac{pQ}{\lambda} \tag{6}$$

Considering the figures and the equations obtained above, the following equations are obtained:

$$t_3 = \frac{w - AQ}{\lambda - D} \tag{7}$$

$$t_4 = \left(\frac{p}{\lambda} + \frac{A}{\lambda - D}\right) Q - \frac{w}{\lambda - D} \tag{8}$$

$$z_1 = \left[1 - D\left(\frac{1}{x} + \frac{p}{\lambda}\right)\right] Q - w \tag{9}$$

$$t_5 = \left[\frac{1}{D} - \frac{1}{x} - \frac{p}{\lambda}\right] Q - \frac{w}{D} \tag{10}$$

From Figure 1, for the model to work, the following conditions must be met:

$xA \geq 0$ or $x \geq \frac{D}{1-p}$ and $\lambda \geq D$.

Total cost (TC) in a cycle is sum of purchase cost, inspection cost, rework cost, ordering cost, holding cost and backordering cost. Then, in a cycle TC is written as following equation:

$$TC = cQ + dQ + c_r pQ + K + h\left[\frac{Qt_2}{2} + \frac{(t_4 + t_5)z_1}{2}\right] + h_1\left[\frac{(t_2 + t_3 + t_4)z_3}{2}\right] + b\left[\frac{t_1 w}{2} + \frac{t_2(w + z_2)}{2} + \frac{t_3 z_2}{2}\right] \tag{11}$$

$$TC = (c + d + c_r p)Q + K + \left\{\frac{(1 - D/x)^2}{2(1 - D/\lambda)}\left(\frac{h}{D} + \frac{b}{\lambda}\right) + \frac{[h - b(1 - D/x)]}{2x} + \left[\frac{h_1 + b}{2x} - \frac{(h + b)(1 - D/x)}{\lambda(1 - D/\lambda)}\right] p + \left[h_1 + \frac{\left(b + \frac{hD}{\lambda}\right)}{(1 - D/\lambda)}\right] \frac{p^2}{2\lambda}\right\} Q^2 + \left\{\frac{b}{x} - \frac{\left(1 - \frac{D}{x}\right)}{\left(1 - \frac{D}{\lambda}\right)}\left(\frac{h}{D} + \frac{b}{\lambda}\right) + \frac{(h + b)p}{\lambda(1 - D/\lambda)}\right\} Qw + \left\{\frac{(h + b)}{2D(1 - D/\lambda)}\right\} w^2 \tag{12}$$

The expected value of the total cost in the cycle (ETC) is obtained as follows:

$$ETC = (c + d + c_r E[p])Q + K + \left\{\frac{(1-D/x)^2}{2(1-D/\lambda)}\left(\frac{h}{D}+\frac{b}{\lambda}\right) + \frac{[h-b(1-D/x)]}{2x} + \left[\frac{h_1+b}{2x} - \frac{(h+b)(1-D/x)}{\lambda(1-D/\lambda)}\right]E[p] + \left[h_1 + \frac{\left(b+\frac{hD}{\lambda}\right)}{(1-D/\lambda)}\right]\frac{E[p^2]}{2\lambda}\right\}Q^2 + \left\{\frac{b}{x} - \frac{\left(1-\frac{D}{x}\right)}{\left(1-\frac{D}{\lambda}\right)}\left(\frac{h}{D}+\frac{b}{\lambda}\right) + \frac{(h+b)E[p]}{\lambda(1-D/\lambda)}\right\}Qw + \left\{\frac{(h+b)}{2D(1-D/\lambda)}\right\}w^2 \quad (13)$$

To smaller the equation (13), by defining:

$$N_1 = c + d + c_r E[p]$$

$$N_2 = \frac{(1-D/x)^2}{2(1-D/\lambda)}\left(\frac{h}{D}+\frac{b}{\lambda}\right) + \frac{[h-b(1-D/x)]}{2x} + \left[\frac{h_1+b}{2x} - \frac{(h+b)(1-D/x)}{\lambda(1-D/\lambda)}\right]E[p] + \left[h_1 + \frac{\left(b+\frac{hD}{\lambda}\right)}{(1-D/\lambda)}\right]\frac{E[p^2]}{2\lambda}$$

$$N_3 = \frac{b}{x} - \frac{\left(1-\frac{D}{x}\right)}{\left(1-\frac{D}{\lambda}\right)}\left(\frac{h}{D}+\frac{b}{\lambda}\right) + \frac{(h+b)E[p]}{\lambda(1-D/\lambda)}$$

$$N_4 = \frac{(h+b)}{2D(1-D/\lambda)}$$

Expected total cost can be written more compactly as follows:

$$ETC = N_1 Q + K + N_2 Q^2 + N_3 Qw + N_4 w^2 \quad (14)$$

Expected cycle length, $E[T]$ is:

$$E[T] = \frac{Q}{D} \quad (15)$$

The expected total cost, ETC in Equation (14) is divided by the expected cycle length, $E[T]$, expected value of the total cost per unit time, $ETCU$ is obtained as:

$$ETCU = \frac{ETC}{E(T)} = \frac{ETC}{Q/D} = N_1 D + \frac{KD}{Q} + N_2 DQ + N_3 Dw + \frac{N_4 Dw^2}{Q} \quad (16)$$

Since $ETCU$ is concave, the optimal level of order quantity, Q and the maximum allowable backorder level, w are obtained by differentiating $ETCU$ function according to Q and then according to w and equalizing the partial derivatives to zero. The partial differential equations of $ETCU$ are:

$$\frac{\partial ETCU}{\partial w} = DN_3 + \frac{2DN_4 w}{Q} = 0$$

$$\frac{\partial ETCU}{\partial Q} = -\frac{KD}{Q^2} + DN_2 - \frac{DN_4 w^2}{Q^2} = 0$$

Optimum order quantity and maximum allowable backorder quantity are calculated as follows:

$$Q = \sqrt{\frac{K}{\left(N_2 - \frac{N_3^2}{4N_4}\right)}} \quad (17)$$

$$w = \frac{-N_3 Q}{2N_4} \quad (18)$$

Proof of Convexity of $ETCU$ Function

In order the proof the ETCU function convexity, following hessian matrix (H) can bu used:

$$H = \begin{bmatrix} \frac{\partial^2 ETCU}{\partial Q^2} & \frac{\partial^2 ETCU}{\partial Q \partial w} \\ \frac{\partial^2 ETCU}{\partial w \partial Q} & \frac{\partial^2 ETCU}{\partial w^2} \end{bmatrix}$$

If $[Q \quad w]H\begin{bmatrix} Q \\ w \end{bmatrix} > 0, \ Q, w \neq 0$; then the function of $ETCU$ is strictly convex.

$$H = \begin{bmatrix} \frac{2KD+2DN_4w^2}{Q^3} & -\frac{2DN_4w}{Q^2} \\ -\frac{2DN_4w}{Q^2} & \frac{2DN_4}{Q} \end{bmatrix} \text{ ve } [Q \quad w]H\begin{bmatrix} Q \\ w \end{bmatrix} = \frac{2KD}{Q} > 0.$$

Since the value is positive, it is said the function of $ETCU$ is strictly convex. Thus, optimum values of Q and w which make $ETCU$ minimum have single values.

Numerical Examples

In this section, numerical examples are given to show the validity and applicability of the proposed model. Suppose that a single item is ordered in batches. Demand for this item is 1000 units per week, while the rework capacity is 4,000 units per week and the inspection capacity is 2,000 units per week. The order cost is $ 1500 per order. Unit purchase, reworking and inspection costs are 50 $/unit, 15 $/unit and 0.4 $/unit, respectively. Unit holding cost, unit holding cost for reworkable items and unit backorder cost are 0.8 $/unit/week, 1 $/unit/week and 0.2 $/unit/week, respectively. For numerical examples, parameters of the model are taken as:

$D = 1000$, $x = 4000$, $\lambda = 2000$, $K = 1500$, $c = 50$, $c_r = 15$, $d = 0.4$, $h = 0.8$, $h_1 = 1$, $b = 0.2$

Since the defective rate is random variable and has a probability function, we calculate optimum values under two cases with assuming defective rate is uniformly and normally distributed.

Case I: Defective rate is uniformly distributed

If defective rate is uniformly distributed and the probability density function is:

$$f(p) = \begin{cases} 25, & 0.21 \leq p \leq 0.25 \\ 0, & otherwise \end{cases}$$

Then, expected values, $E[p]$ and $E[p^2]$ are:

$E[p] = \int_{0.21}^{0.25} pf(p)dp = 0.23$

$E[p^2] = \int_{0.21}^{0.25} p^2 f(p)dp = 0.5303$

From equation (16), (17) and (18) by using the model parameters and expected values; optimal economic order quantity, maximum allowable backorder level and expected total cost per unit time are obtained as:

$Q^* = 2791.88$ unit

$w^* = 1493.65$ unit

$ETCU^* = 54924.55$ \$/week

$T = 2.7919$ week

Case II: Defective rate is normally distributed

If defective rate, p is normally distributed with mean of $\mu = 0.23$ and variance of $\sigma^2 = 0.01768$. In other words:

$p \sim N(0.23, 0.01768)$

Then, expected values, $E[p]$ and $E[p^2]$ are:

$E[p] = \mu = 0.23$

$E[p^2] = \sigma^2 + E[p]^2 = 0.07058$

From equation (16), (17) and (18) by using the model parameters and expected values, optimal economic order quantity, maximum allowable backorder level and expected total cost per unit time are obtained as:

$Q^* = 2724.39$ unit

$w^* = 1457.55$ unit

$ETCU^* = 54951.16$ \$/week

$T = 2.7244$ week

Sensitivity Analysis

Sensitivity analysis of the model is given in Table 1 for uniformly and normally distributed defective rates.

Table 1: Sensitivity analysis of uniformly and normally distributed defective rate on optimal values of proposed model

	Uniform Distribution			Normal Distribution		
$E[p]$	Q	w	$ETCU$	Q	w	$ETCU$
0.21	2818.65	1536.16	54614.34	2749.26	1498.35	54641.20
0.22	2805.38	1514.91	54769.37	2736.94	1477.95	54796.11
0.23	2791.86	1493.65	54924.55	2724.39	1457.55	54951.16
0.24	2778.11	1472.40	55079.87	2711.60	1437.15	55106.36
0.25	2764.14	1451.17	55235.33	2698.61	1416.77	55261.69
0.26	2749.96	1429.98	55390.93	2685.40	1396.41	55417.15
0.27	2735.58	1408.83	55546.66	2672.01	1376.09	55572.75
0.28	2721.03	1387.72	55702.52	2658.45	1355.81	55728.48
0.29	2706.31	1366.69	55858.52	2644.71	1335.58	55884.34
0.30	2691.43	1345.72	56014.65	2630.83	1315.41	56040.33
0.31	2676.42	1324.83	56170.90	2616.80	1295.31	56196.44
0.32	2661.27	1304.02	56327.28	2602.64	1275.29	56352.68
0.33	2646.01	1283.32	56483.78	2588.36	1255.35	56509.04
0.34	2630.65	1262.71	56640.40	2573.97	1235.51	56665.51
0.35	2615.19	1242.22	56797.14	2559.48	1215.76	56822.11

These analyses are the important part of model development to see the effects of some parameters on optimal values. Since the defective rate is uniformly and normally distributed, for each case effects of change in defective rate on optimal values of the proposed model is investigated. Table 1 and Table 2 show the sensitivity analysis results that are very similar for both cases of defective rate distribution. Regardless of the distribution of the defective rate, it is seen that the expected total cost per unit time increases when the defective rate increases. At the same time, as the defective rate increases, optimal order quantity and maximum allowable backorder quantity both decreases.

CONCLUSION

In real life situations, defective, backordering and reworking processes are usually studied for economic order quantity models. In this study an economic order quantity model is developed for defective items in which backordering is allowed and all defectives become good products after reworking process. All items are inspected to separate defective and good items. After the inspection process is completed, defective items are reworked at a constant rate. In the proposed model, it is assumed that the inspection time required to separate good and defective items is smaller than eliminating time of backorders that is the main contribution of this study to the literature. Since

inspection time is smaller than the time to eliminate backorder level, demand and unsatisfied backorder level is met with reworked items simultaneously. Numerical example was given to illustrate the functioning of the model, the optimal values were obtained. The effect of the change in defective rate on optimal values was analyzed. As defective rate increases, optimal values of order quantity and maximum allowable backorder quantity decreases, however expected total cost per unit increases. Future studies can be carried out by considering permissible delays in payments, partial backordering and effects of learning.

REFERENCES

Cardenas-Barron, L. E. (2009). Economic production quantity with rework process at a single-stage manufacturing system with planned backorders. Computers and Industrial Engineering, 57, 1105-1113.

Chan, W. M., Ibrahim, R.N. and Lochert, P.B. (2003). A new EPQ model: integrating lower pricing, rework and reject situations. Production Planning and Control, 14(7), 588-595.

Eroglu, A. and Ozdemir, G. (2007). An economic order quantity model with defective items and shortages. International Journal of Production Economics, 106 (2), 544-549.

Eroglu, A., Karaatli, M. and Kilic, Y., (2004). An EPQ model with defective products. SDU Journal of Faculty of Economics and Administrative Science, 9(2), 131-140.

Goyal, S. K. and Cardenes-Barron, L. E. (2002). Note on: economic production quantity model for items with imperfect quality-a practical approach. International Journal of Production Economics, 77, 85-87.

Hayek, P. A. and Salameh, M. K., (2001). Production lot sizing with the reworking of imperfect quality items produced. Production Planning and Control, 12 (6), 584-590.

Karagul N. and Eroglu A. (2022). Production lot sizing with quality screening, rework and shortages backordered. Pamukkale University Journal of Engineering Sciences, 28(4), 604-612.

Khan, M., Jaber, M. Y. and Bonney, M. (2011). An economic order quantity (EOQ) for items with imperfect quality and inspection errors. International Journal of Production Economics, 133(1), 113–118.

Konstantaras, I., Goyal, S. K. and Papachristos, S. (2007). Economic ordering policy for an item with imperfect quality subject to the in-house inspection. International Journal of Systems Science, 38(6), 473–482.

Maddah, B. and Jaber, M. Y. (2008). Economic order quantity for items with imperfect quality: revisited. International Journal of Production Economics, 112 (2), 808–815.

Moussawi-Haidar L, Salameh M, Nasr W. (2016). Production lot sizing with quality screening and rework. Applied Mathematical Modelling, 40, 3242-3256.

Nobil A, Afshar-Sedigh A, Afshar-Nadjafi B. (2020). Lot-sizing problem for a defective processing system with categorized items, backordering and pricing policy. Journal of Revenue Pricing Management, 19, 255-265.

Ouyang, L. Y., Chen, C. K. and Chang, H. C. (2002). Quality improvement, setup cost and lead-time reductions in lot size reorder point models with an imperfect production process. Computer and Operations Research, 29, 1701-1717.

Papachristos, S. and Konstantaras, I., (2006). Economic ordering quantity models for items with imperfect quality. International Journal of Production Economics, 100(1), 148-156.

Rosenblatt, M. J. and Lee, H. L., (1986). Economic production cycles with imperfect production process. IIE Transactions**,** 18, 48-55.

Salameh, M. K. and Jaber, M. Y. (2000). Economic production quantity model for items with imperfect quality. International Journal of Production Economics, 64, 59-64.

Sarkar B, Cardenas-Barron LE, Sarkar M, Singgih ML. (2014). An economic production quantity model with random defective rate, rework process and backorders for a single stage production system. Journal of Manufacturing Systems, 33, 423-435.

Schwaller, R. L., (1988). EOQ under inspection costs. Production and Inventory Management, 29, 22-35.

Singh, P., Nigwal, A. R., and Khedlekar, U. K. (2023). Economic order quantity model for imperfect items with shortage backordering. Reliability: Theory and Applications, 18(4(76)), 391-409.

Taleizadeh, A. A., Cárdenas-Barrón, L. E., & Mohammadi, B. (2014). A deterministic multi product single machine EPQ model with backordering, scraped products, rework and interruption in manufacturing process. International Journal of Production Economics, 150, 9-27.

Semantic Coherence Based Text Summarization Using TF-IDF And ROUGE

Remzi GÜRFİDAN[1]

1- Lecturer Dr.; Yalvaç Vocational School of Technical Sciences, Isparta University of Applied Science, remzigurfidan@isparta.edu.tr; ORCID No: 0000-0002-4899-2219, Turkey

ABSTRACT

In this study, both statistical and semantic approaches are used in text summarization processes to produce effective and meaningful summaries. TF-IDF, Cosine Similarity, Jaccard Similarity, Pearson Correlation Coefficient and ROUGE metrics and methods were used to evaluate summarization performance. According to the ROUGE-1 results obtained in the study, Precision value was 0.90, Recall value was 0.57 and F1 score was 0.70. In ROUGE-2 metrics, these values were calculated as 0.55, 0.35 and 0.43 respectively, while in ROUGE-L metrics, Precision was 0.69, Recall was 0.44 and F1 score was 0.54. The Cosine Similarity score was 0.82, indicating a high semantic agreement, while Jaccard Similarity was 0.41 and Pearson Correlation Coefficient was 0.68, indicating moderate word overlap and statistical agreement. Word clouds and frequency analyses highlighted the main themes of the sample summaries, showing that terms such as "renewable," "energy" and "sustainability" were frequently repeated. Low Jaccard Similarity and Recall scores indicate the need to increase lexical diversity. The results show that the techniques used are effective in increasing both semantic cohesion and content density and provide a basis for further optimization of text summarization algorithms in the future.

Keywords –Text Summarization, Natural Language Processing, AI-Based Text Analysis, Semantic Similarity, Summarization Algorithms.

INTRODUCTION

Today, with the rapid increase in technological developments, it has become an acceptable reality that the resources available on the internet have increased. When we enter the internet environment, we come across many resources related to researchable topics. Therefore, the process of scanning and analyzing most of the sources provides negative returns to the researchers in terms of time. It is also risky in terms of the reliability of reaching accurate information in every source (Zhao et al., 2020). Most researchers tend to analyze the important and relevant parts of the texts rather than most of the text in order to save time (Syed et al., 2021; Zhao et al., 2020).Text summarization can be defined as the shortening of a text by mentioning important points after the process of reading and understanding a text. Summarizing is a productive process as it directs students to recreate a text more concisely and intensively than the original text. Deneme (2009) defines summarizing as thinking about what one has learnt, writing in a logical and understandable way and explaining what one has learnt in one's own words (Deneme, 2009). Summarizing is to express the important aspects of a written or oral text concisely, comprehensively and briefly in a

way that someone who does not read or listen to it can understand. Text summarization method provides a great advantage to researchers or readers at this stage. Text summarization applies a compression method by shortening the main subject of the text (Peng & Yu, 2023). When applying the compression method, it provides a summary text about the content by emphasizing the important points of the text. With the development of artificial intelligence methods, automatic text summarization is happening very quickly (Wang et al., 2019). Common in text summarization is to reflect user requirements, such as relevance to a topic or to assist the user in doing a specific task Tülek, 2007). Text summarization methods include extracting summary texts of different types of content such as websites, academic articles, news sites, book summaries, course content books and different types of content (Chen & Juanatas, 2024). Two different methods are used in text summarization, these methods are abstraction summarization and inferential summarization (Chen & Juanatas, 2024; Peng & Yu, 2023; Syed et al., 2021; Wang et al., 2019; Zhao et al., 2020).

Summarizing by Selecting Sentences: Summarizing by selecting the important sentences in the text to be summarised by statistical methods, heuristic inference or a combination of both (Chen & Juanatas, 2024; Hatipoğlu & Omurca, 2015; Wang et al., 2019).

Summarizing by Interpretation: Summarizing is done by intelligently interpreting the text to be summarized. In this summarization, the expressions in the original text are intelligently shortened and rewritten (Hatipoğlu & Omurca, 2015).

TEXT SUMMARIZATION PROCESSES

To summarize a text, three different stages need to be performed. These stages are; determining the topic, interpretation and production.

The aim of the topic determination stage is to determine the most important topics in the passage. To achieve this, techniques such as calculating word frequencies, examining the location of the sentence, and making use of clue expressions are used. In some fonts, critical positions such as the title of the text, the first sentence of the text may contain the most important issues related to the text. Clue expressions such as "Summarize", "Most importantly", "In conclusion" can be signs indicating important points about the writing. In addition, frequently used words, unless they are prepositions or determiners, can indicate the importance of the sentences in which they appear.

In the technique based on interpretation, sentences that are related to each other can be expressed in more general sentences by mixing and merging.

The generation phase is the production of the final summarized output of the text. This stage includes a variety of generation methods, from the simplest to the most complex. Some of the methods that can be used are

- In the first stage, selected words or phrases are added to the summary output (extraction).

- Adding the most used keywords or interpreted thoughts to the summary output (topic list).
- Linking two or more sentences together (phrase concatenation).
- Sentence generation is the generation of new sentences by the sentence generator, which takes as input the ideas or related ideas that are fused together (sentence generation).

Using data mining techniques, natural language processing and automatic summarization systems in this context, it is becoming faster to reach the desired summary information. Due to the increasing intensification of human-computer communication, techniques such as text-to-speech synthesis to facilitate this communication are indispensable for today and the future (Tekindal et al., 2013). Text summarization attempts to extract the meaning of the text and express it in a shorter form. The history of automatic text summarization covers a period of 60 years. Luhn determined whether the text is suitable for summarization by using the term frequency with the method he developed. This method is based on the frequency of the occurrence of important words carrying information in the text (Luhn, 2010).

TECHNIQUES USED IN TEXT SUMMARIZATION

Researchers on text summarization methods have developed many methods. Commonly used methods and algorithms include statistical approaches, linguistic approaches, clustering approaches, line theory approaches and chain theory approaches.

Statistical Approaches

Statistical approaches weight keywords by using statistical features of the sentence such as title, place and term frequency. It calculates the score of the sentence according to the keyword weights. It presents a summary by selecting the highest scoring sentence for summary (Widyassari et al., 2022).

Linguistic Approaches

The linguistic approach is the scientific semantic and pragmatic study of language. The concept of semantics shows how meaning is extracted from words and concepts. The concept of pragmatics involves how meaning is extracted from context (Mohamed & Oussalah, 2015). Linguistic

approaches consider the connection between words. This approach tries to find the main concept by analyzing words. The linguistic approach is used in interpretive text summarization based on linguistic methods involving semantic processing.

Clustering Approach

The clustering approach is a method used to summarize documents by grouping similar data or sentences. Summarization depends on sentence features but also on sentence similarity ratio. It also defines the sequence similarity between two sentences using the word order relation (Alguliyev et al., 2019).

In the clustering approach, documents and word count determination queries are entered as parameters by the user. These parameters are determined before preprocessing. After preprocessing, documents are grouped by applying clustering process and sentence clusters are formed. The cluster with the highest score from the created sentence clusters is selected as the best sentence cluster and forms the summary.

Graph Theory

This method creates a graph for text summarization by means of algorithms. The sentence is selected by scoring according to the corner point in the graph. Graph theory provides more efficient utilization of data by revealing features that other methods cannot reveal (El-Kassas et al., 2020). Text Rank and Cluster Rank algorithms are analyzed to show the use of graph theory in text summarization in more detail.

Text Rank Algorithm

The similar relationship between two sentences is established by the graph-based Text Rank algorithm. It chooses the most crucial keywords in the article because it is an unsupervised algorithm. On a carefully designed graph, the technique works with a variant of the PageRank algorithm. The most significant pieces are determined to be those that best characterize the text by rating the graph's components. This method makes it possible to utilize the Text Rank algorithm in a variety of languages. A node in the graph represents each sentence in the graph-based sentence extraction method Text Rank. Lexical similarity between two sentences generates an undirected edge. For example, if a sentence S_i is represented as a sequence of words $Si=W_1\ i,\ W_2\ i...W|Si|\ i$, the similarity between two sentences Si and Sj is defined as in Equation 1 .

$$Sim(S_i, S_j) = \frac{|\{wk : wk \in Si \wedge wk \in Sj\}|}{log(|Si|) + log(|Sj|)} \quad (1)$$

To apply the Text Rank algorithm, preprocessing is required as in other algorithms. This preprocessing is to turn multiple documents into single documents, eliminate non-textual content and prepare only textual documents to apply the algorithm. Then the PageRank algorithm is applied on the nodes in the generated graph. A summary is created by selecting the sentences with the highest relationship value. While creating this summary, the number of sentences selected is determined according to the summary length constraints. After arranging the sentences according to their order in the original text, summarization is completed.

Cluster Rank Algorithm

Clustering algorithm is an unsupervised graph-based method designed for inferential summarization of speech transcripts (Garg Benoit et al., 2009). After the preprocessing stage, Porter's stemming algorithm was applied. Cluster Rank algorithm is an extension of Text Rank algorithm, which is also a graph-based method used to extract sentences from news articles. This algorithm works after preprocessing and removing punctuation marks. After document input and stemming, a clustering process is performed. Cluster Rank first divides the text into clusters represented as nodes of a graph. Then the similarity between all sentences of neighboring clusters is measured. The sentences with the highest similarity are merged into a single cluster. Then the sentences in the cluster with the highest association value are scored using a center-based approach.

Lexical chain

The lexical chain works by combining semantically related sets of words in multiple documents. Hypernyms/hyponyms are relations that allow words to be grouped in the same lexical chain. The dictionary chain approach is used to correct grammatical errors found in documents. To process the lexicon chain, nouns are clustered according to their relationships. Each noun must be placed in a group. Words are grouped to form the strongest and longest dictionary chain (Lynn et al., 2018).

MATERIAL METHOD

This work applies both statistical and semantic methods for text summarization. TF-IDF vectorization was done along with several techniques like Rouge value, Jaccard Similarity, Cosine Similarity, and Pearson Correlation Coefficient to determine the importance of sentences, and only the most meaningful sentences were included in the summaries and

evaluated. An effort was made to reduce the semantic losses while enhancing information density in the text as far as possible. ROUGE-1, ROUGE-2, and ROUGE-L metrics were used to determine the generated summaries against the reference texts. The metrics gave further details into the exactness, coverage, and overall performance of the summarization system. Additionally, code fragments were done to visualize word cloud and word frequency graphs in analyzing the content of the summarized texts and highlighting keywords. The sample full text and the resulting summary text were generated by Chat-gpt and used only for testing.

The sample full text*: "Renewable energy is a cornerstone for combating climate change and reducing greenhouse gas emissions. Sources such as solar, wind, and hydropower provide clean and sustainable alternatives to fossil fuels. These systems lower carbon footprints, enhance energy security, and promote global energy sustainability. Despite their benefits, renewable energy technologies face challenges, including high initial costs, intermittent supply, and energy storage inefficiencies. Innovations in advanced battery storage and smart grid technologies are crucial for addressing these limitations. Governments around the world are supporting renewable energy adoption through subsidies, tax incentives, and infrastructure investments. Public awareness campaigns and educational programs play a vital role in promoting the transition to sustainable energy practices. By addressing these barriers, renewable energy can lead the transition to a cleaner, greener, and more sustainable future".*

Summary Text: *"Renewable energy, including solar, wind, and hydropower, is essential for combating climate change and reducing greenhouse gas emissions. These systems provide clean and sustainable alternatives to fossil fuels, lowering carbon footprints and enhancing energy security. Challenges such as high costs, intermittent supply, and storage inefficiencies remain significant. Advancements in battery storage and smart grid technologies, along with government subsidies and tax incentives, are driving adoption. Public awareness campaigns and educational programs are key to accelerating the transition to global energy sustainability".*

Cosine Similarity

In this approach, where sentences are expressed as a vector, the cosine value of the angle between two vectors expresses the relationship between sentences (Singhal, 2001). The value calculation is performed with Equation 2.

$$\cos\theta = \frac{A.B}{\|A\|\|B\|} = \frac{\sum_{i=1}^{n} A_i B_i}{\sqrt{\sum_{i=1}^{n} A_i^2}\sqrt{\sum_{i=1}^{n} B_i^2}} \qquad (2)$$

The smaller the cosine of the angle between vectors A and B, the more similar these two vectors are.

Jaccard Similarity

Jaccard similarity is expressed as the intersection of two sets divided by their union. If the similarity criterion is 0, it is not similar at all, and if it is 1, it is exactly similar (Bag et al., 2019). The value calculation is performed with Equation 3.

$$Jaccard\ (A,B) = \frac{|A \cap B|}{|A \cup B|} \qquad (3)$$

Pearson Correlation Coefficient

The linear link between two numerical measurements is measured by the Pearson Correlation Coefficient. A statistical technique called the Pearson Correlation Coefficient uses a value between +1 and -1 to assess the direction and strength of a relationship. Sentences with a value of +1 are precisely connected, whereas those with a value of -1 are not (Zhou et al., 2016). The value calculation is performed with Equation 4.

$$Pearson\ (A,B) = \frac{\sum AB - \frac{\sum A \sum B}{N}}{\sqrt{\left(\sum A^2 - \frac{(\sum A)^2}{N}\right)\left(\sum B^2 - \frac{(\sum B)^2}{N}\right)}} \qquad (4)$$

Recall-Oriented Understudy for Gisting Evaluation (ROUGE)

ROUGE is an n-gram based measure. It compares n-gram overlaps between two texts. ROUGE metrics are particularly used in Text Summarization, Article Summarization, Document Summarization and Machine Translation. ROUGE measures the overlap of the n-grams in the system output with the n-grams in the reference summary.

n-gram: Units of n-grams compared in the system output and the reference summary,

Match(n-gram): The number of n-grams in the reference digest of an n-gram in the system output,

Count(n-gram): The total number of n-grams in the reference digest, calculated by Equation 5 (Menéndez & Dakhama, n.d.).

$$ROUGE\_N = \frac{\sum S \in Ref\ Sum \sum_{n-gram \in S} \boldsymbol{min}(Match(n-gram), Count(n-gram))}{\sum S \in Ref\ Sum \sum_{n-gram \in S} Count(n-gram)} \qquad (5)$$

RESULTS AND DISCUSSION

The analysis of performance measures such as ROUGE scores, Cosine Similarity, Jaccard Similarity and Pearson Correlation Coefficient shows the summarization system's effectiveness in capturing the semantic and structural features of the reference text. High precision and Cosine Similarity scores highlight the system's ability to identify relevant terms and maintain semantic alignment, while low recall and Jaccard scores indicate areas where the summarization system can improve its lexical diversity and term overlap. Figure 1 and Table 1 show the visual and numerical results of the ROUGE scores.

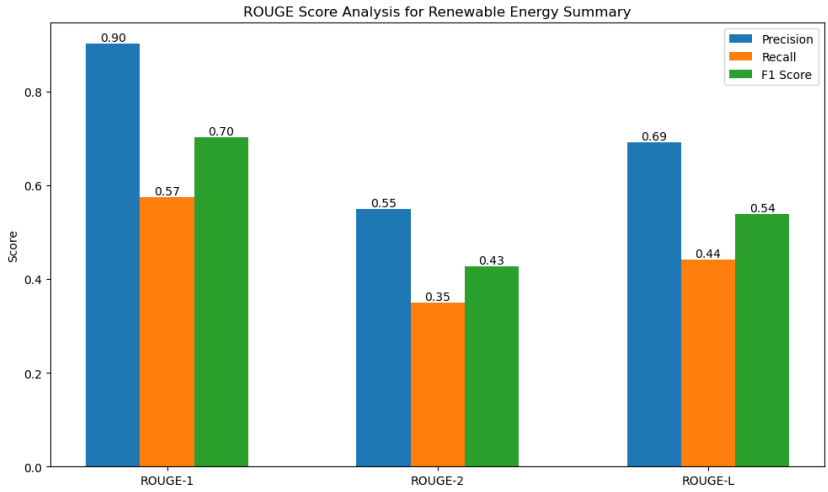

Figure 1: ROUGE performance metric charts

Table 1: ROUGE analysis results

ROUGE SCORES			
ROUGE - Metrics	Precision	Recall	F1-Score
ROUGE1	0.90	0.57	0.70
ROUGE2	0.55	0.35	0.43
ROUGEL	0.69	0.44	0.54

While ROUGE-1 measures the system's success in capturing exact words matches in the reference summary, the Precision value is quite high (0.90). This indicates that the summary produced by the system contains mostly correct terms. However, the Recall value (0.57) is lower, indicating that only 57% of all words in the reference summary were captured. This indicates that the system needs to be improved in terms of comprehensiveness. In conclusion, the F1-Score of 0.70 for ROUGE-1 indicates that the balance between selecting the correct terms and coverage is partially achieved. Looking at the ROUGE-2 scores, the Precision value

remains at a lower level compared to ROUGE-1 with 0.55. This suggests that the system has difficulty with more complex n-gram (binary word sequence) matches. Recall is much lower at 0.35, which means that only one third of the binary word sequences in the reference summary were correctly captured. The F1-Score of 0.43 for ROUGE-2 clearly indicates that the summary needs to be improved in terms of both accuracy and coverage. The ROUGE-L score measures the system's ability to capture the longest common subsequences (LCS) in the reference summary. Although Precision (0.69) is reasonable, Recall (0.44) and F1-Score (0.54) remain at lower levels. These results suggest that some success has been achieved in the overall structural coherence of the summary, but that further improvements are needed in terms of both accuracy and comprehensiveness. Table 2 shows other similarity analysis results.

Table 2: Similarity analysis results

Other Scores	Values
Cosine Similarity	0.82
Jaccard Similarity	0.41
Pearson Correlation Coefficient	0.68

The Cosine Similarity score (0.82) indicates a high level of semantic similarity between the system's output and the reference summary. This metric evaluates the angular distance between the two representations in a vector space and suggests that the key topics or ideas in the generated summary closely align with those in the reference summary. A score above 0.8 is generally considered strong, highlighting that the overall thematic content has been preserved effectively. The Jaccard Similarity score (0.41), however, is notably lower. This metric measures the overlap between the sets of terms in the two summaries, specifically focusing on exact matches. The lower value reflects a limited overlap in the unique terms between the system output and the reference, suggesting that while the thematic similarity is high (as shown by Cosine Similarity), the specific vocabulary used by the system might differ significantly from the reference summary. The Pearson Correlation Coefficient (0.68) indicates a moderate positive correlation between the output and the reference summary in terms of their feature distributions, such as frequency of term usage or other numeric attributes. This score suggests that while there is a reasonable alignment in quantitative patterns, there is room for improvement in achieving higher statistical consistency with reference. The frequency graph of the words used in the abstract is shown in Figure 2.

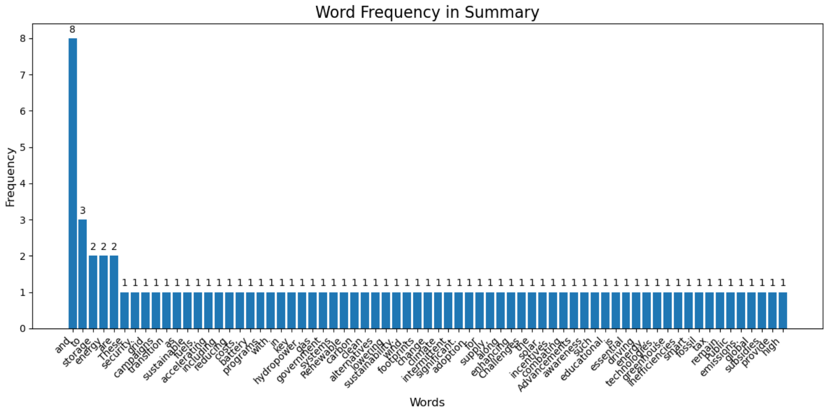

Figure 2: Graph of the frequency of words used in the abstract

The word "and" appears most frequently in the summary, with a count of 8, indicating a high reliance on conjunctions to connect ideas. This suggests that the summary might prioritize combining concepts rather than delving into specifics. Words like "storage," "energy," "technologies," and "sustainable" appear with moderate frequency, typically 2 or 3 times, highlighting key themes such as sustainability and energy storage technologies. These words reflect the focus areas of the summary. However, most words appear only once, showcasing a diverse vocabulary. The word cloud visualization is shown in Figure 3.

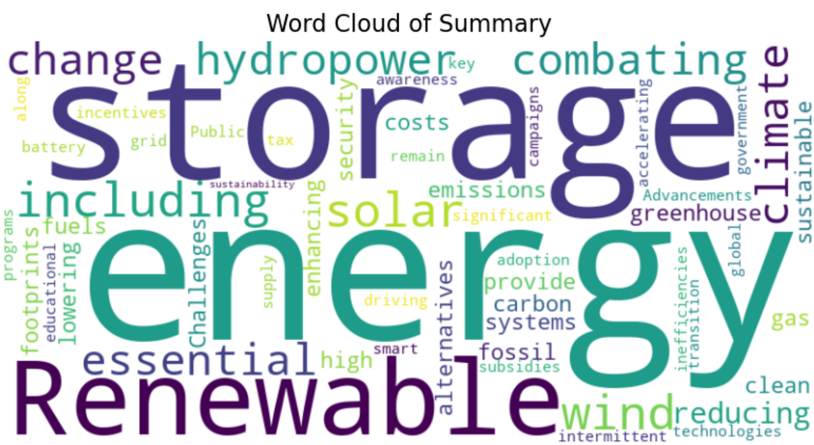

Figure 3: Word cloud visualization

The word cloud visually highlights the key themes and focus areas of the summary by emphasizing frequently occurring terms. Dominant words like "energy," "storage," and "renewable" appear prominently, reflecting the central topics of the summary. These terms suggest a strong emphasis on

renewable energy systems and technologies, particularly energy storage as a critical component. Other important words like "climate," "solar," "wind," "hydropower," and "emissions" reinforce the environmental and sustainability focus, pointing to topics such as climate change mitigation, renewable energy adoption, and reducing greenhouse gas emissions. Words like "challenges," "essential," and "alternatives" further indicate a discussion on the importance and potential barriers in transitioning to sustainable energy systems. The use of such terms as "security," "incentives," and "systems" indicates a greater context-one that deals with, yet is not confined to, technological developments and addresses policy, economic, and infrastructural concerns. The word cloud really captures the essence of the summary in its focus on renewable energy solutions, climate action, and the vital contribution of energy storage to sustainable development.

COMPARISON WITH LITERATURE

In the present study, the Precision value obtained for ROUGE-1 is 0.90, the Recall value is 0.57, and the F1 score is 0.70. These values give very similar results compared to the BERT-based summarization model used in Zhao et al. (2020). In Zhao's study, ROUGE-1 Precision value was reported as 0.88, Recall value as 0.60, and F1 score as 0.72 (Zhao et.al., 2020). Comparing it, this study obtains results with high accuracy even with simple methods. However, the advantage of more complex models is clearly shown in ROUGE-2 and ROUGE-L values: ROUGE-2 F1=0.43 and ROUGE-L F1=0.54; while in Zhao's model, ROUGE-2 F1 goes up to 0.50.
In the present study, the Cosine Similarity value is computed to be 0.82, indicating that the summarization system is quite successful with respect to semantic consistency. Considering, in this respect, the COSUM model suggested by Alguliyev et al. (2019), the values of Cosine and Jaccard Similarities are 0.80 and 0.45, respectively. Thus, in the current study with 0.41, it is seen that the value of Jaccard Similarity is low as expected, indicating the necessary development for diversity in word usage within the summarization system. Specially, it can be stated that a system with low Jaccard Similarity suffers from the shortage in the usage of unique words. In addition to ROUGE and Cosine Similarity, other measures such as Precision and Recall were optimized using the optimization-based techniques in the study of Alguliyev et al. (2019). The value of Precision in that study was 0.88, while the Recall value was 0.65 as obtained by Alguliyev et al. (2019). In comparison, ROUGE-1 Recall is 0.57 in the current study, though its Precision is higher, with a value of 0.90. That means that, though the present study chose fewer words correctly, those it did choose were more consistent.

Peng and Yu (2023) conducted summarization using both abstractive and inferential methods for long texts. In this study, the TEA model used a

ROUGE-1 Precision value of 0.87, Recall value of 0.68, and F1 score of 0.75 (Peng & Yu, 2023). Since the TF-IDF and ROUGE methods in the current study are more effective in the summarization of short texts, it is possible that performance will be lost in long texts. This again hints that the present study needs to be optimized for more text types to achieve better performance.

In the graph-based methods, a ROUGE-1 value of 0.85 for Precision, 0.62 for Recall, and F1 score of 0.72, has been reported as in the study by El-Kassas et al. 2020 (El-Kassas et al., 2020). These scores are indicative that indeed graph-based methods capture better inter-text context, especially when summarized. In the present model, more basic approaches of providing this context are undertaken such as TF-IDF and Cosine Similarity. It may now be explained that the present method is semantic contextual and poor in inter-text contextual performance.

CONCLUSIONS

This study has shown that high performance summaries can be obtained by using statistical and semantic methods together in text summarization processes. Through the effective use of metrics such as TF-IDF, Cosine Similarity and ROUGE, both semantic alignment and content coverage of summaries with reference texts are measured. Furthermore, word clouds and word frequency visualizations supported the thematic analysis of the texts and clearly revealed the focal points of the summaries. The methods used in this study have the potential to both increase text density and improve the accuracy and coverage performance of summarization systems. In the future, improvements in vocabulary diversity and structural cohesion are aimed to further enhance the system performance.

REFERENCE

Alguliyev, R. M., Aliguliyev, R. M., Isazade, N. R., Abdi, A., & Idris, N. (2018). COSUM: Text summarization based on clustering and optimization. *Expert Systems*, *36*(1). https://doi.org/10.1111/exsy.12340

Bag, S., Kumar, S. K., & Tiwari, M. K. (2019). An efficient recommendation generation using relevant Jaccard similarity. *Information Sciences*, *483*, 53–64. https://doi.org/10.1016/j.ins.2019.01.023

Chen, Y., & Juanatas, R. A. (2024). Two-stage text summary model. *IEEE Access*, *12*, 129012–129020. https://doi.org/10.1109/access.2024.3427390

Deneme S. (2009). İngilizce Öğretmen Adaylarının Özetleme Stratejilerini Kullanım Tercihleri. Journal of Language and Linguistic Studies, vol. 5, no. 2, pp. 85–

91, Oct. 2009, Accessed: Dec. 24, 2024. [Online]. Available: https://dergipark.org.tr/en/pub/jlls/issue/9930/122883

El-Kassas, W. S., Salama, C. R., Rafea, A. A., & Mohamed, H. K. (2020). EdgeSumm: Graph-based framework for automatic text summarization. *Information Processing & Management*, *57*(6), 102264. https://doi.org/10.1016/j.ipm.2020.102264

Garg, N., Favre, B., Reidhammer, K., & Hakkani Tür, D. (2009). Clusterrank: a graph based method for meeting summarization.

Hatipoğlu, A., & Omurca, S. İ. (2015). TÜRKÇE METİN ÖZETLEMEDE MELEZ MODELLEME. Dokuz Eylül Üniversitesi Mühendislik Fakültesi Fen Ve Mühendislik Dergisi, 17(50), 95-108.

Luhn, H. P. (1958). The Automatic Creation of Literature Abstracts. *IBM Journal of Research and Development*, *2*(2), 159–165. https://doi.org/10.1147/rd.22.0159

Lynn, H. M., Choi, C., & Kim, P. (2017). An improved method of automatic text summarization for web contents using lexical chain with semantic-related terms. *Soft Computing*, *22*(12), 4013–4023. https://doi.org/10.1007/s00500-017-2612-9

Menéndez, H. D., & Dakhama, A. (2024, October). Automatic Summarization Evaluation: Methods and Practices. In *36th International Conference on Testing Software and Systems: ICTSS 2024*.

Mohamed, M. A., & Oussalah, M. (2015). Similarity-Based Query-Focused Multi-document Summarization Using Crowdsourced and Manually-built Lexical-Semantic Resources. *2015 IEEE Trustcom/BigDataSE/ISPA*, 80–87. https://doi.org/10.1109/trustcom.2015.565

Peng, D., & Yu, B. (2023). TEA: Topic Information based Extractive-Abstractive Fusion Model for Long Text Summary. *Information Systems Frontiers*. https://doi.org/10.1007/s10796-023-10442-1

Singhal, A. (2001). Modern information retrieval: A brief overview. *IEEE Data Eng. Bull.*, *24*(4), 35-43.

Syed S., Yousef T., Al-Khatib K., Jänicke S., and Potthast M., (2020). Summary Explorer: Visualizing the State of the Art in Text Summarization. EMNLP 2021 - 2021 Conference on Empirical Methods in Natural Language Processing: System Demonstrations, pp. 185–194, Aug. 2021, doi: 10.18653/v1/2021.emnlp-demo.22.

Tekindal, B., & Arık, G. (2013). Görme Engelliler için Türkçe Metinden Konuşma Sentezleme Yazılımı Geliştirilmesi. Bilişim Teknolojileri Dergisi, 5(3), 9-18.

Tülek M., (2007), "İstanbul Teknik Üniversitesi Fen Bilimleri Enstitüsü Türkçe İçin Metin Özetleme Yüksek Lisans Tezi, İstanbul.

Wang, Q., Liu, P., Zhu, Z., Yin, H., Zhang, Q., & Zhang, L. (2019). A Text Abstraction Summary Model Based on BERT Word Embedding and Reinforcement Learning. *Applied Sciences*, *9*(21), 4701. https://doi.org/10.3390/app9214701

Widyassari, A. P., Rustad, S., Shidik, G. F., Noersasongko, E., Syukur, A., Affandy, A., & Setiadi, D. R. I. M. (2020). Review of automatic text summarization techniques & methods. *Journal of King Saud University - Computer and Information Sciences*, *34*(4), 1029–1046. https://doi.org/10.1016/j.jksuci.2020.05.006

Zhao, S., You, F., & Liu, Z. Y. (2020). Leveraging Pre-Trained Language model for summary generation on short text. *IEEE Access*, *8*, 228798–228803. https://doi.org/10.1109/access.2020.3045748

Zhou, H., Deng, Z., Xia, Y., & Fu, M. (2016). A new sampling method in particle filter based on Pearson correlation coefficient. *Neurocomputing*, *216*, 208–215. https://doi.org/10.1016/j.neucom.2016.07.036

A Research on Türkiye's Ranking in the Global Cyber Security Index

Rüstem Barış YEŞİLAY[1]

1- Prof. Dr.; Ege Üniversitesi Havacılık Meslek Yüksekokulu. rbyesilay@gmail.com ORCID No: https://orcid.org/0000-0002-0830-8224

ABSTRACT

Industry 4.0 represents a transformative era marked by the integration of cyber-physical systems, the Internet of Things (IoT), artificial intelligence, and big data analytics into industrial processes. While this digital revolution enhances productivity and innovation, it also introduces complex cybersecurity challenges that demand robust protective measures. This paper examines Türkiye's cybersecurity readiness in the context of Industry 4.0, emphasizing its performance in the Global Cybersecurity Index (GCI). By analyzing Türkiye's legislative, technical, organizational, and cooperative frameworks, the study highlights its upward trajectory in global rankings, achieving Tier 1 "Role-Modelling" status in 2024.

Key drivers of this progress include comprehensive legislation such as the Personal Data Protection Law (KVKK), the establishment of institutions like the National Cyber Incidents Response Center (USOM), and initiatives aimed at capacity building and public awareness. Türkiye's strategic integration of cybersecurity into its industrial and digital transformation efforts, notably through the National Technology Initiative and Digital Türkiye framework, underscores its commitment to securing critical infrastructure and fostering economic growth.

Despite significant advancements, challenges persist in areas such as talent development, technical measures, and safeguarding industrial systems against evolving threats. The findings underscore the importance of continuous innovation, international collaboration, and the alignment of national strategies with global standards to ensure sustainable digital transformation. This study contributes to the discourse on the indispensable role of cybersecurity in achieving Industry 4.0 objectives and offers insights for emerging economies seeking to enhance their cybersecurity frameworks.

Keywords: Industry 4.0, Cybersecurity, Türkiye, Global Cybersecurity Index, Digital Transformation, Critical Infrastructure Protection.

INTRODUCTION

Industry 4.0, which is defined by the incorporation of cyber-physical systems, the Internet of Things (IoT), big data analytics, and artificial intelligence into industrial processes, has been ushered in by the quick development of digital technology. The world is undergoing a significant transition known as Industry 4.0 because of the disruptive effects of quickly developing digital technology. Humanity's capacity to generate value, particularly in industry, is rising to a very high level as a result of this change, which is bringing about paradigm shifts in practically every aspect of

economic and social activity. Across several industries, this shift has greatly increased efficiency, creativity, and output. However, complicated cybersecurity issues have also been brought about by the rising interconnectedness and reliance on digital systems. To protect vital infrastructures, guarantee business continuity, and uphold confidence in digital ecosystems, these issues must be resolved (GAO, 2024).

Türkiye has acknowledged the revolutionary potential of Industry 4.0 as a developing economy with aspirations to fortify its industrial foundation. In order to use digital technology for economic growth and development, the government of Türkiye has made the country's digital transformation a strategic goal. To improve digital infrastructure, encourage innovation, and develop digital skills among its citizens, the Turkish government introduced the "National Technology Initiative" and "Digital Türkiye" policy. These tactics are intended to establish Türkiye as a pioneer in digital technology and guarantee the nation's continued competitiveness in the international market (Türkiye - Digital Economy, 2024).

The process of moving public services to Digital Türkiye (e-Government) has been ongoing, and Digital Transformation Office of Türkiye is actively striving to increase utilization and cost efficiency from the standpoint of user-centered service supply and improving public management. In order to decrease the quantity of documents sought during service delivery, efforts have been made to help streamline procedures in electronic services. Increasing the number of value-added services, making them accessible to all, and making it easier for people to utilize Digital Türkiye through user-friendly interfaces are the objectives (Digital Türkiye, 2024).

Türkiye is concentrating its growth strategy on high-value-added industrial production because of its robust industrial capability. In this sense, Türkiye should use the best available technology to increase industry productivity while simultaneously boosting the proportion of high-tech items in production. For the goal of National Technology, Strong Industry, it is crucial to accelerate the transformation of industry. There are a few likely obstacles that Türkiye needs to overcome to digitally change the sector. The primary challenges that most businesses would have been the need for direction on how to handle digital transformation at the strategic level and how to manage its implementation, the expense of the necessary expenditures, and the skills gap in the process' execution. Even though Türkiye has offered several public support mechanisms, including project-based grants, investment incentives, and consulting services, to help businesses digitize, the industry must accelerate its digital transformation to meet the objectives of the National Technology Initiative (Costu, 2022). According to this viewpoint, a new incentive system ought to be implemented to remove the primary obstacles found and raise the industry's degree of digital maturity.

Public-private partnerships to foster digital transformation, e-government services, and rules pertaining to the digital economy are among the focus topics. In the new period that started with Industry 4.0, Türkiye has outlined its goals and vision through the National Technology Initiative in the context of the global competitive landscape characterized by technological breakthroughs. The digital transformation of industry is one of the National Technology Initiative's most important components. Strong cybersecurity measures are necessary to guard against cyberthreats and vulnerabilities present in interconnected systems, nevertheless, if these initiatives are to be successful (ICC, 2024).

The purpose of this chapter is to examine Türkiye's performance in the Global Cybersecurity Index by examining its past rankings, significant accomplishments, and difficulties. The paper determines the elements that have influenced Türkiye's cybersecurity environment by exploring its programs, regulations, and foreign partnerships. It also looks at how Türkiye's GCI performance fits into its larger objectives for economic expansion and digital transformation. The paper adds to the current discussion on the crucial role cybersecurity plays in national development and makes suggestions for improving Türkiye's standing in the international cybersecurity community. Türkiye can more effectively negotiate the challenges of a linked world and accomplish sustained digital advancement by filling up the gaps and utilizing its current advantages.

GLOBAL CYBERSECURITY INDEX

For both individuals and organizations, safeguarding the vast volumes of data produced in the context of Industry 4.0 is crucial. Because there may be production disruptions if data is exchanged with unauthorized third parties, such as when data entering the machines during production is not from the correct source. High-level cyber security measures are required for this. To guarantee quick digital transition, it would be advantageous to strengthen cyber security measures (Acet & Koc, 2020).

The United Nations' information and communication technology (ICT) specialized agency is the International Telecommunication Union (ITU). The organization has 194 member states, as well as over 1000 businesses, academic institutions, and regional and global organizations. The ITU is the oldest organization in the UN family, having been tying the world together since the invention of the telegraph in 1865. Its headquarters are in Geneva, Switzerland, and it has regional offices on every continent. By offering a reliable, multilateral forum to mediate international agreements and standards, exchange information, develop capacity, and collaborate with

members and partners to expand access to technology globally, ITU seeks to make digital connectivity accessible to all (About ITU, 2024).

ITU created the Global Cybersecurity Index (GCI), which gauges nations' dedication to cybersecurity advancement. GCI assesses countries based on five main pillars: – (i) Legal Measures, (ii) Technical Measures, (iii) Organizational Measures, (iv) Capacity Development, and (v) Cooperation – and then aggregated into an overall score (ITU, 2024). By ranking nations according to how well they execute in these categories, the GCI aids in determining global cybersecurity's strong points and potential areas for development. Around the world, it is frequently used to compare cybersecurity readiness.

Cybercrime and cybersecurity laws and regulations are measured by the *legal* pillar. This pillar comprises three sub-pillars: a) countries had at least one regulation on either personal data protection, privacy protection, or breach notification in force or in progress, b) countries with data protection regulations in force, and c) countries with critical infrastructure regulations. Measuring the application of technical capabilities through national and sector-specific bodies is the *technical* pillar. Three sub-pillars make up this pillar: a) Countries with active Computer Incident Response Teams (CIRTs), b) Countries engaged with a regional CIRT association, and c) Countries with frameworks to adopt cybersecurity standards. Assessing national strategies and cybersecurity implementation by organizations is an *organizational* pillar. This pillar is composed of three sub-pillars: a) Countries with national cybersecurity strategies, b) Countries with cybersecurity agencies, and c) Countries with child online protection strategies and initiatives reported. The measurement of cybersecurity *capacity development* includes awareness campaigns, training, education, and incentives. Three sub-pillars make up this pillar: a) Countries conducting cyber-awareness-initiatives, b) Countries with cybersecurity at some level of national curricula, and c) Countries with cybersecurity capacity-development incentives. *Cooperation* is the measurement of alliances among organizations, businesses, and nations. Three sub-pillars make up this pillar as well: a) Countries engaged or will be engaged in domestic or international cybersecurity public-private partnerships, b) Countries with international cybersecurity agreements, and c) Countries reporting inter-agency collaboration (ITU, 2024).

ITU launched the GCI in 2015 with the goal of assisting nations in identifying areas that require improvement and motivating them to take action to increase capacity and capabilities under each pillar. To give a more accurate picture of cybersecurity actions done by nations, the GCI has been regularly modified over editions to address shifting risks, priorities, and resources (Zavazava, 2024).

TÜRKİYE'S GLOBAL CYBERSECURITY INDEX RANKINGS

The Global Cybersecurity Index (GCI) 2014 is an ITU-ABIresearch joint project to measure the commitment of countries to cybersecurity. The report presents the 2014 results of the GCI and the Cyberwellness country profiles for Member states (ITU, 2024). It includes regional rankings, a selected set of good practices and the way forward for the next iteration. The first GCI survey was conducted in 2013/2014 in partnership with ABI Research where a total of 105 countries responded out of 193 ITU Member States and the final results were published in 2015.

According to table 1 The USA leads with the highest index score (0.824), followed by Canada (0.794) and Australia (0.765). It can be said that these countries are recognized for their advanced cybersecurity policies. GCI 2014 has a clustered ranking structure. Several countries share the same index scores and rankings. Malaysia, Oman, and Australia are tied at the 3rd position with an index of 0.765. Countries like Brazil, Estonia, Germany, India, Japan, Korea, and the UK are tied at the 5th position with an index of 0.706. Türkiye is ranked 7th globally with an index score of 0.647, tied with Latvia and Sweden. This ranking places Türkiye above mid-tier countries like Hong Kong, Finland, and Qatar, but below nations like Austria (6th, 0.676) and Norway (4th, 0.735). Türkiye's position indicates it had moderate advancements in cybersecurity readiness by 2014, but there was room for improvement compared to higher-ranked nations.

Table 1: Global Cybersecurity Index (GCI, 2014) Rankings

Country	Index	Global Rank	Country	Index	Global Rank
USA	0.824	1	Hungary	0.676	6
Canada	0.794	2	Isreal	0.676	6
Australia	0.765	3	Netherlands	0.676	6
Malaysia	0.765	3	Singapore	0.676	6
Oman	0.765	3	Latvia	0.647	7
New Zealand	0.735	4	Sweden	0.647	7
Norway	0.735	4	**Türkiye**	**0.647**	**7**
Brazil	0.706	5	Hong Kong	0.618	8
Estonia	0.706	5	Finland	0.618	8
Germany	0.706	5	Qatar	0.618	8
India	0.706	5	Slovakia	0.618	8
Japan	0.706	5	Uruguay	0.618	8
Korea	0.706	5	Colombia	0.588	9
UK	0.706	5	Denmark	0.588	9
Austria	0.676	6	Egypt	0.588	9

Source: (GCI, 2015)

To increase awareness, the Global Cybersecurity Index (GCI, 2017) is a survey that gauges Member States' dedication to cybersecurity. More partners, more open consultations, and an improved index were added to the second iteration of GCI. A multi-stakeholder strategy has been developed with the goals of enhancing the GCI's quality, fostering international collaboration, and encouraging knowledge sharing on the subject by utilizing the experience of other organizations (ITU, 2024). Table XXX indicates that due to its aggressive policies and extensive cybersecurity infrastructure, Singapore received the highest GCI score in 2017. Following closely behind, the United States and Malaysia showed resolute dedication to each of the five pillars. According to the 2017 GCI rankings, 194 member states were included, Türkiye came in at number 43 in the world. The necessity for a comprehensive strategy to strengthen its cybersecurity posture is highlighted by Türkiye's rating in the 2017 GCI. Protecting the nation's digital infrastructure and making sure it is resilient to cyberattacks requires addressing the areas that have been highlighted as needing improvement.

A list of Country Groups is included in GCI 2017, based on their GCI score, Member States were divided into three groups (Table 2). Türkiye was listed under the maturing countries.

1. Initiators: The 96 nations that have begun to make cybersecurity commitments (i.e., GCI scores below the 50th percentile) are referred to as being in the initiating stage.
2. Matures: The 77 nations that have made complex pledges and are involved in cybersecurity programs and activities are referred to as being in the maturing stage (i.e., having a GCI score between the 50th and 89th percentile).
3. Leaders: The 21 nations that exhibit great commitment in each of the index's five pillars (i.e., a GCI score in the 90th percentile) are referred to as being in the leading stage.

Table 2: Global Cybersecurity Index (GCI, 2017) Rankings

Country	Index	Global Rank	Country	Index	Global Rank
Singapore	0.925	1	Egypt	0.772	14
USA	0.919	2	Netherlands	0.760	15
Malaysia	0.893	3	Finland	0.741	16
Oman	0.871	4	Sweden	0.733	17
Estonia	0.846	5	Switzerland	0.727	18
Mauritius	0.830	6	Spain	0.718	19
Australia	0.824	7	New Zealand	0.718	19
Georgia	0.819	8	Israel	0.691	20
France	0.819	8	Latvia	0.688	21
Canada	0.818	9	Thailand	0.684	22
Russia	0.788	10	India	0.683	23
Japan	0.786	11	Germany	0.679	24
Norway	0.786	11	Qatar	0.676	25
UK	0.783	12	China	0.624	32
Korea	0.782	13	**Türkiye**	**0.581**	**43**

Source: (GCI, 2017)

In January 2017, Cyber Star (Siber Yıldız, 2024), an online cybersecurity competition, was held. There were over 15,000 competitors and over 27,000 applications. The competition found the nation's cybersecurity professionals, and TRCERT (Türkiye National CERT) employed some of the top contestants. TRCERT took part in the National Cyber Defense Exercise in November 2017 and the NATO CMX-2017 Crisis Management Exercise in October 2017. To raise awareness of appropriate and secure Internet usage,

the Safe Internet Center (SIC) was founded (Safer Internet Center of Türkiye, 2024). Families can get guidance on how to use the Internet to its fullest potential on Safe Web, a website run by SIC, and an Internet Helpline. Children and young people with limited access to ICTs can experience technology up close and learn about the potential it offers thanks to the Safer Internet Trailer. The trailer, which includes five facilities—a Technological Experience Area, Robotic Coding Area, Virtual Reality Area, Conscious and Safe Usage of Internet Area, Training Area, and Competition Area—raises awareness about children's safe Internet use. Additionally, SIC has a kid-focused website with games, activities, contests, and training. "Create, connect and share respect: A better Internet starts with you" is the topic of the Safer Internet Day event that SIC has arranged.

As a result of these developments in the 2018 (Table 3) edition of the index, Türkiye ranked 11th in Europe and 20th globally among 194 countries. In this edition countries were distributed to three main groups and Türkiye was listed under the list of high level of commitment (ITU, 2019):

1. Countries that demonstrate high commitment in all five pillars of the index.
2. Countries that have developed complex commitments and engage in cybersecurity programmes and initiatives.
3. Countries that have started to initiate commitments in cybersecurity.

Table 3: Global Cybersecurity Index (GCI, 2018) Rankings

Country	Index	Global Rank	Country	Index	Global Rank
UK	0.931	1	Mauritius	0.880	14
USA	0.926	2	Korea	0.873	15
France	0.918	3	Oman	0.868	16
Lithuania	0.908	4	Qatar	0.860	17
Estonia	0.905	5	Georgia	0.857	18
Singapore	0.898	6	Finland	0.856	19
Spain	0.896	7	**Türkiye**	**0.853**	**20**
Malaysia	0.893	8	Denmark	0.852	21
Canada	0.892	9	Germany	0.849	22
Norway	0.892	9	Egypt	0.842	23
Australia	0.890	10	Croatia	0.840	24
Luxembourg	0.886	11	Italy	0.837	25
Netherlands	0.885	12	Russia	0.836	26
Saudi Arabia	0.881	13	China	0.828	27
Japan	0.880	14	Austria	0.826	28

Source: (ITU, 2019)

In recent years (Table 4), Türkiye has made significant strides in improving its cybersecurity capabilities and ranking in the GCI. In the 2020 edition of the index, Türkiye ranked 6th in Europe and 11th globally among 194 countries. This ranking highlighted Türkiye's growing focus on building robust cybersecurity frameworks, fostering public-private partnerships, and investing in capacity-building initiatives. Türkiye's performance in the 2020 GCI demonstrated its growing commitment to tackling cybersecurity challenges on the national and international levels. Türkiye has created a robust national policy that highlights the significance of protecting cyberspace, dealing with cyberthreats, and encouraging resilience in all areas. To strengthen cybersecurity, Türkiye has passed laws and regulations. This includes national policies aimed at ensuring safe and secure online operations, such as the Cybersecurity Strategy and Action Plan and the Law on the Regulation of Electronic Trade. The nation has invested in building cybersecurity infrastructures for the public and private sectors. It has created organizations like the National Cyber Security Center (Department of Cyber Security, 2014) and the Ministry of Transport and Infrastructure's Cybersecurity Department (Halisdemir, 2021).

Table 4: Global Cybersecurity Index (GCI, 2020) Rankings

Country	Index	Global Rank	Country	Index	Global Rank
USA	100	1	Türkiye	97.49	11
UK	99.54	2	Australia	97.47	12
Saudi Arabia	99.54	2	Luxembourg	97.41	13
Estonia	99.48	3	Germany	97.41	13
Korea	98.52	4	Portugal	97.32	14
Singapore	98.52	4	Latvia	97.28	15
Spain	98.52	4	Netherlands	97.05	16
Russia	98.06	5	Norway	96.89	17
United Arab Emirates	98.06	5	Mauritius	96.89	17
Malaysia	98.06	5	Brazil	96.6	18
Lithuania	97.93	6	Belgium	96.25	19
Japan	97.82	7	Italy	96.13	20
Canada**	97.67	8	Oman	96.04	21
France	97.6	9	Finland	95.78	22
India	97.5	10	Egypt	95.48	23

Source: (ITU, 2021)

According to GCI 2024 on average, nations have increased their cybersecurity commitments and performed more cybersecurity-related activities since 2021 (ITU, 2024). The average country's score worldwide has increased to 65.7 out of 100. The majority of nations excel in the legal pillar out of the five GCI pillars. In contrast, the average nation performs the worst in the technical and capacity-development pillars. Every region features nations that are setting an example or making progress, as well as nations who are only starting to develop their cybersecurity commitments. Five levels are used to quantify country performance, with Tier 1 being the highest performance and Tier 5 representing the lowest, in order to capture these variances. To assist nations in understanding and identifying role models for improvement, these levels offer peer groupings based on scores (ITU, 2024). Tier 1 (T1)-Role-modeling refers to nations that achieved a minimum GCI score of 95/100 by showcasing a strong commitment to cybersecurity through government-driven, coordinated actions that include assessing, establishing, and putting into practice specific widely accepted cybersecurity measures across all five pillars or up to all indicators.

Table 5: Tier Performance: Europe

T5 Building	T4 Evolving	T3 Establishing	T2 Advancing	T1 Role-modelling
Vatican	Bosnia and Herzegovina Liechtenstein San Marino	Andorra Bulgaria Latvia Moldova Monaco Montenegro North Macedonia Ukraine	Albania Austria Croatia Czech Republic Georgia Hungary Ireland Israel Lithuania Malta Poland Romania Slovakia Switzerland	Belgium Cyprus Denmark Estonia Finland France Germany Greece Iceland Italy Luxembourg Netherlands (Kingdom of the) Norway Portugal Serbia Slovenia Spain Sweden Türkiye United Kingdom

Source: (International Telecommunication Union (ITU), 2024)

In terms of Global and Europe tier performance Türkiye was listed under the Tier 1 – Role-modelling (score of 95–100) with countries like United Kingdom, Germany, France, Spain etc. (ITU, 2024). The other tier categories are (Table 5): Tier 2 – Advancing (score of 85–95), Tier 3 – Establishing (score of 55–85), Tier 4 – Evolving (score of 20–55) and Tier 5 – Building (score of 0–20) (International Telecommunication Union (ITU), 2024).

Key factors contributing to Türkiye's progress include (Costu, 2022):

- ✓ Comprehensive Cybersecurity Legislation: Türkiye has enacted laws such as the Personal Data Protection Law (KVKK) and developed a national cybersecurity strategy to address cyber risks.
- ✓ Enhanced Technical Measures: The establishment of institutions like the National Cyber Incidents Response Center (USOM) has improved Türkiye's ability to detect and mitigate cyber threats.
- ✓ Capacity Development: Initiatives aimed at training cybersecurity professionals and raising public awareness have strengthened Türkiye's human resource capabilities in this field.
- ✓ Regional and International Cooperation: Türkiye actively participates in global cybersecurity forums and collaborates with international organizations to share expertise and resources.

Türkiye's rising commitment to cybersecurity, which is essential for attaining sustainable development in the digital era, is reflected in its rising GCI ranks. Notwithstanding these successes, difficulties still exist. Türkiye should constantly adapt and improve its cybersecurity infrastructure due to the demands of Industry 4.0, the complexity of cyber threats, and the speed at which technology is developing. Future initiatives should concentrate on promoting innovation, enhancing the resilience of vital infrastructure, and guaranteeing safe digital transition.

RESULTS

Türkiye’s journey toward cybersecurity readiness, particularly in the context of Industry 4.0, demonstrates a transformative narrative of progress and adaptation. Evaluated against the Global Cybersecurity Index (GCI), Türkiye’s achievements highlight its increasing commitment to building a resilient digital ecosystem capable of withstanding the complexities of cyber threats. From a global ranking of 7th in 2014 to 11th in 2020, and ultimately securing Tier 1 “Role-Modelling” status in 2024, Türkiye has positioned itself among the global leaders in cybersecurity. This remarkable advancement underscores the nation’s ability to implement cohesive, forward-looking strategies that align with international benchmarks.

The pillars of the GCI—legal, technical, organizational, capacity development, and cooperation—illustrate the multifaceted nature of Türkiye's progress. Legal measures have been a cornerstone of this advancement, with comprehensive legislation such as the Personal Data Protection Law (KVKK) addressing the evolving landscape of cyber risks. Simultaneously, the establishment of the National Cyber Incidents Response Center (USOM) has fortified Türkiye's technical capabilities, enabling swift responses to emerging threats. Organizational measures, exemplified by the Cybersecurity Strategy and Action Plan, have provided a cohesive framework for addressing cyber risks across sectors, while capacity development initiatives have enhanced the nation's digital literacy and cybersecurity talent pool. Notably, Türkiye's active participation in international forums and collaborations has elevated its global standing, underscoring the value of cooperative approaches in an interconnected world.

In the realm of Industry 4.0, Türkiye's cybersecurity advancements have been particularly impactful. The secure integration of IoT-enabled systems, big data analytics, and artificial intelligence into industrial processes has mitigated vulnerabilities while enabling innovation. Public-sector initiatives like the Digital Türkiye framework have benefited from robust cybersecurity protocols, enhancing user trust and the seamless delivery of e-government services. These measures align closely with Türkiye's broader vision under the National Technology Initiative, which seeks to position the country as a leader in digital transformation and high-value industrial production.

National programs and initiatives have played a pivotal role in driving these advancements. The Cyber Star competition has uncovered and cultivated a new generation of cybersecurity professionals, ensuring a steady pipeline of talent to address future challenges. The Safer Internet Center has expanded awareness among citizens, particularly younger demographics, fostering a culture of secure online behavior. Exercises in national and international cyber defense have reinforced operational preparedness, highlighting Türkiye's proactive stance in anticipating and mitigating threats.

Despite these accomplishments, challenges remain, particularly in areas where global benchmarks reveal room for growth. Technical measures, while significantly improved, require further advancements in cutting-edge technologies, such as AI-powered threat detection systems. Additionally, addressing the cybersecurity skills gap remains critical, as the rapid pace of technological innovation demands a workforce equipped to tackle increasingly sophisticated threats. Protecting critical infrastructure, a cornerstone of Industry 4.0, necessitates ongoing investment in resilience and innovation.

Türkiye's trajectory reflects a nation that is not only embracing digital transformation but also prioritizing the secure integration of emerging technologies. Its progress serves as a blueprint for other developing economies striving to balance innovation with security in a globalized digital landscape. Moving forward, Türkiye must sustain its momentum by fostering innovation, strengthening public-private partnerships, and continuously refining its cybersecurity frameworks to adapt to the evolving threat landscape. With these measures, Türkiye is well-positioned to ensure a secure, sustainable digital future, leveraging cybersecurity as a cornerstone of its economic and industrial aspirations.

REFERENCES

About ITU. (2024, 12 17). *About International Telecommunication Union (ITU)*. Retrieved from https://www.itu.int/en/about/Pages/default.aspx

Acet, H., & Koc, S. (2020). Dördüncü Sanayi Devrimi'nin (Endüstri 4.0) Dünyaya ve Türkiye'ye ekonomik yansımaları. *Uluslararası Sosyal ve Beşeri Bilimler Araştırma Dergisi, 7*(58), 2243-2256. doi:https://doi.org/10.26450/jshsr.1982

Costu, Z. (2022). National Technology Initiative in the Digitalization of the Industry. In M. Kacir, M. Seker, & M. Dogrul, *National Technology Initiative* (pp. 653 - 662). Ankara: TUBA. doi:10.53478/TUBA.978-625-8352-17-7.ch34

Department of Cyber Security. (2014, 12 23). Retrieved from Digital Transformation Office: https://cbddo.gov.tr/en/department-of-cyber-security/

Digital Türkiye. (2024, 12 20). Retrieved from Digital Transformation Office of Turkiye: https://cbddo.gov.tr/en/digital-turkey

GAO. (2024, June 13). *What are the Biggest Challenges to Federal Cybersecurity? (High Risk Update)*. Retrieved from https://www.gao.gov/blog/what-are-biggest-challenges-federal-cybersecurity-high-risk-update

GCI. (2015). *Global Cybersecurity Index & Cyberwellness Profiles.* The International Telecommunication Union. Retrieved from https://www.itu.int/dms_pub/itu-d/opb/str/D-STR-SECU-2015-PDF-E.pdf

GCI. (2017). *Global Cybersecurity Index (GCI) 2017.* International Telecommunication Union (ITU). Retrieved 12 23, 2024, from https://www.itu.int/dms_pub/itu-d/opb/str/D-STR-GCI.01-2017-R1-PDF-E.pdf

Halisdemir, E. (2021). *National Cybersecurity Organisation: TURKEY.* Tallinn: NATO Cooperative Cyber Defence Centre of Excellence (CCDCOE). Retrieved from

https://ccdcoe.org/uploads/2021/08/TUR_country_report_final_clean_ver_2408.pdf

ICC. (2024, July). *ICC Working Paper: Protecting the cybersecurity of critical infrastructures and their supply chains.* Retrieved from https://docs-library.unoda.org/Open-Ended_Working_Group_on_Information_and_Communication_Technologies_-_(2021)/ICC-2024_Protecting-the-cybersecurity-of-critical-infrastructures-and-their-supply-chains.pdf

International Telecommunication Union (ITU). (2024). *Global Cybersecurity Index 2024.* Geneva: ITU Publications.

ITU. (2019). *Global Cybersecurity Index (GCI) 2018.* Geneva: ITU Publications. Retrieved from https://www.itu.int/dms_pub/itu-d/opb/str/D-STR-GCI.01-2018-PDF-E.pdf

ITU. (2021). *Global Cybersecurity Index 2020.* Geneva: International Telecommunication Union (ITU) Publications. Retrieved from https://www.itu.int/dms_pub/itu-d/opb/str/D-STR-GCI.01-2021-PDF-E.pdf

ITU. (2024, 12 23). *GCI 2017*. Retrieved from ITU - Committed to connecting the world: https://www.itu.int/en/ITU-D/Cybersecurity/pages/gci-2017.aspx

ITU. (2024, 12 20). *Global Cybersecurity Index*. Retrieved from International Telecommunication Union (ITU): https://www.itu.int/en/ITU-D/Cybersecurity/pages/global-cybersecurity-index.aspx

ITU. (2024, 12 22). *Global Cybersecurity Index and Cyberwellness profiles Report 2014*. Retrieved from ITU - Committed to connecting the world: https://www.itu.int/en/ITU-D/Cybersecurity/Pages/GCI-2014.aspx#:~:text=%E2%80%8B%E2%80%8B%E2%80%8B%E2%80%8B%E2%80%8B,across%20many%20industries%20and%20sectors.

Safer Internet Center of Türkiye. (2024, 12 19). *Güvenli İnternet Merkezi*. Retrieved from https://tr.linkedin.com/in/g%C3%BCvenlinet

Siber Yıldız. (2024, 12 18). Retrieved from https://www.siberyildiz.com/

Türkiye - Digital Economy. (2024, 09 20). Retrieved from Official Website of the International Trade Administration U.S. Department of Commerce: https://www.trade.gov/country-commercial-guides/turkiye-digital-economy

Zavazava, C. L. (2024, 12 19). *Global Cybersecurity Index 2024*. Retrieved from ITU Pablications: https://www.itu.int/epublications/publication/global-cybersecurity-index-2024

Load Flow Analysis: A Comprehensive Overview of Methods, Challenges, and Future Trends

Ahmet ÇİFCİ[1]
Asım Gökhan YETGİN[2]

1- Asst. Prof.; Burdur Mehmet Akif Ersoy University Faculty of Engineering and Architecture Department of Electrical-Electronics Engineering. acifci@mehmetakif.edu.tr ORCID No: 0000-0001-7679-9945
2- Assoc. Prof.; Burdur Mehmet Akif Ersoy University Faculty of Engineering and Architecture Department of Electrical-Electronics Engineering. agyetgin@mehmetakif.edu.tr ORCID No: 0000-0003-3971-0504

ABSTRACT

This chapter introduces load flow analysis, a cornerstone of power system planning, operation, and control. Load flow studies are vital for determining the steady-state operating conditions, including voltage magnitudes and angles at each bus, and power flows through transmission lines, under various load demands. The mathematical formulation involves representing system components like generators, loads, and transmission lines with appropriate models. This leads to a set of nonlinear power flow equations, primarily expressing the power balance at each bus. Solving these equations requires iterative numerical techniques. Methods like Gauss-Seidel, known for its simplicity, and Newton-Raphson, recognized for its quadratic convergence, are commonly employed. The Fast Decoupled method offers a balance between speed and accuracy, leveraging approximations based on the characteristics of power systems. Choosing the appropriate method depends on system size and desired accuracy. The chapter compares these methods, analyzing their convergence properties, computational burden, and accuracy. Practical applications, including contingency analysis, stability studies, and optimal power flow, are discussed, highlighting load flow's critical role in ensuring a reliable, efficient, and economically sound power system operation.

Keywords – Load Flow Analysis, Power Flow Analysis, Iterative Methods, Gauss-Seidel Method, Newton-Raphson Method, Fast Decoupled Method.

INTRODUCTION

Load flow analysis, also known as power flow analysis, is a fundamental numerical method used to determine the steady-state operating condition of an electric power system (Meinecke et al., 2020; Gianto, 2021; Basetti et al., 2021; Bayat et al., 2022). In essence, it provides a snapshot of the system's electrical behavior under a given load and generation scenario. This analysis solves a system of nonlinear algebraic equations that represent the power network, yielding crucial information about the flow of power throughout the system.

The primary purpose of load flow analysis is to provide a comprehensive understanding of the power system's state by achieving several key objectives. It calculates the voltage magnitude and phase angle at each bus (node) in the system, which is essential for maintaining voltage levels within acceptable limits to ensure reliable equipment operation and power quality (Veerasamy et al., 2021; Yang et al., 2022; Varghese et al., 2023). Additionally, load flow analysis determines the active (real) and reactive power flowing through each transmission line and transformer, which helps assess the loading of these components and identify potential bottlenecks

(Honrubia-Escribano et al., 2021; El-Fergany, 2024). It also quantifies power losses within the system, primarily caused by resistance in transmission lines and transformers, a critical factor for ensuring economic operation and system efficiency. Furthermore, the analysis is used to check for system constraint violations, such as voltage magnitude limits at buses, thermal limits of transmission lines and transformers to prevent overloading, and generator output limits, all of which are vital for maintaining the system's reliability and stability (Hong et al., 2021; Bulat et al., 2021; Ibrahim and Hossain, 2021).

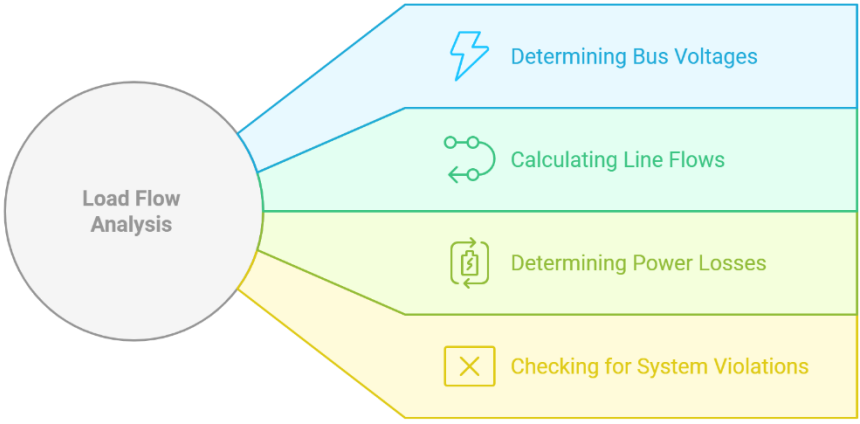

Figure 1: Key Objectives of Load Flow Analysis

Load flow analysis is a fundamental tool in power system engineering, offering indispensable insights across various domains. In the context of system planning, load flow analysis serves as a cornerstone, enabling the evaluation of the impacts of new generation and transmission facilities. It facilitates the determination of appropriate equipment sizes, such as transformers and conductors, and aids in optimizing system configurations to accommodate future expansions effectively. In system operation, load flow analysis plays a critical role in ensuring reliability and security (Naderi et al., 2021). It supports real-time security assessments by evaluating the system's resilience to contingencies, such as the loss of generators or transmission lines, thereby enabling operators to maintain reliable system performance. Furthermore, it informs economic dispatch decisions by optimizing the allocation of generation resources in a cost-effective manner while adhering to system constraints. In terms of system control, load flow analysis provides essential data for voltage regulation and stability studies (Rahman et al., 2021). By examining voltage profiles and power flows, engineers can design and fine-tune control systems to uphold system stability and ensure the maintenance of voltage quality, thereby supporting the overall robustness of the power system.

The determination of power flow within an electrical network has been a fundamental challenge in power system engineering since the inception of interconnected grids. Initially, the complexity of these systems limited analyses to highly simplified network representations, relying heavily on manual calculations and graphical methods. Engineers used techniques such as network analyzers and direct current (DC) boards, physical analog models of the power system, to simulate and estimate power flows (Parizad et al., 2020). These early methods, while pioneering, were laborious, time-consuming, and severely restricted in terms of the size and complexity of the networks they could handle.

The advent of digital computers in the mid-20th century revolutionized load flow analysis. The initial attempts to leverage computational power employed direct methods to solve the system of linear equations that resulted from simplifying the network using DC approximations. However, these methods proved inadequate for larger systems due to the non-linear nature of the alternating current (AC) power flow equations.

The true breakthrough came with the development of iterative numerical methods capable of solving the non-linear power flow equations. The Gauss-Seidel method gained early popularity due to its simplicity and relatively low memory requirements (Huang et al., 2018). However, its convergence characteristics were often slow and unreliable, especially for heavily loaded or complex systems (Tostado et al., 2019). The subsequent introduction of the Newton-Raphson method, with its superior quadratic convergence properties, marked a significant advancement (Vysocký et al., 2022; Kumar et al., 2024). Although requiring more memory due to the computation and storage of the Jacobian matrix, the Newton-Raphson method dramatically reduced the number of iterations needed to reach a solution, making it feasible to analyze larger and more realistic power systems (Zeng et al., 2021). Further refinements followed, including the Fast Decoupled Load Flow (FDLF) method (Stott and Alsac, 1974). FDLF exploited the inherent characteristics of power systems, namely the strong coupling between active power and voltage angle, and reactive power and voltage magnitude, to decouple the power flow equations (Li et al., 2009; Wood et al., 2013). This decoupling, along with other approximations, allowed for significant computational speed-up while maintaining reasonable accuracy.

These key advancements in numerical techniques, coupled with the exponential growth in computing power, have made load flow analysis practical for large-scale power systems with thousands of buses and branches. Today, sophisticated software packages utilizing these methods, along with enhancements like sparsity techniques and robust convergence algorithms, are indispensable tools for power system planning, operation, and control. The continuous evolution of these methods remains an active area of research, driven by the ever-increasing complexity and dynamic nature of modern power grids.

The remainder of the chapter is organized as follows. The section "Power System Representation for Load Flow Studies" introduces the fundamental concepts of one-line diagrams, bus classification, the per-unit system, and component modeling essential for understanding load flow analysis. The section "Formulation of the Load Flow Problem" details the mathematical foundation, including the nodal admittance matrix and the power flow equations, and clearly defines the problem statement. The section "Load Flow Solution Methods" describes the most widely used iterative numerical techniques, namely the Gauss-Seidel, Newton-Raphson, and Fast Decoupled methods, for solving the load flow problem. A comparative analysis of these methods, considering their strengths and weaknesses, is presented in the section "Comparison of Load Flow Methods". The section "Practical Considerations and Applications" discusses real-world aspects, such as handling reactive power limits, transformer tap adjustments, and the importance of initial conditions, and highlights key applications of load flow analysis in power system studies. Finally, the section "Conclusion" summarizes the key findings, discusses emerging trends, including DC and three-phase load flow, probabilistic methods, and AI applications, and outlines the future of load flow analysis in the context of modern power grids.

POWER SYSTEM REPRESENTATION FOR LOAD FLOW STUDIES

One-Line Diagram

Power systems are inherently complex, comprising numerous interconnected components that operate at various voltage levels. Analyzing these systems, particularly in their three-phase configuration, can quickly become unwieldy when represented in their full detail. To simplify analysis and facilitate understanding, power systems engineers rely heavily on a concise representation known as the one-line diagram, sometimes also referred to as a single-line diagram (Gönen, 2013). The one-line diagram offers a streamlined depiction of a three-phase power system by representing all three phases with a single line. This simplification is possible because, under balanced operating conditions, the three phases are assumed to have equal magnitudes and are separated by a phase angle of 120 degrees. Consequently, analyzing a single phase is sufficient to understand the behavior of the entire system. Therefore, the one-line diagram effectively captures the essential information about the system's structure and connectivity without the clutter of representing each phase individually.

A fundamental advantage of employing one-line diagrams is their ability to provide a clear, high-level overview of the power system's topology. These diagrams highlight the major components and their interconnections, making it easier to visualize the flow of power through the system. While they abstract away some details, one-line diagrams retain crucial information such

as the relative location of generators, transformers, transmission lines, loads, and buses, as well as the connections between substations and the overall network configuration. To ensure clarity and consistency, one-line diagrams utilize a standardized set of symbols to represent the various components of a power system. These symbols are universally recognized within the power industry, enabling engineers to readily interpret diagrams created by others (Bhanbhro et al., 2023). Below is a legend illustrating the common symbols used in one-line diagrams:

–**Generators:** Generators, which supply electrical power to the system, are typically represented by circles or ovals with a letter "G" or a sinusoidal wave symbol inside them. They are connected to buses or directly to the network.

–**Transformers:** Transformers, used to step up or step down voltage levels, are depicted as two interconnected circles or as two vertical lines with a connecting line between them. The specific design of the symbol may vary depending on the type of transformer, such as two-winding or autotransformer.

–**Transmission Lines:** Transmission lines, which carry power over long distances, are illustrated as straight lines with a lightning bolt or wave symbol alongside them to indicate high voltage. Their lengths are often labeled, along with their impedance or reactance values.

–**Loads:** Loads, representing the consumption points of electrical power, are usually shown as rectangles or arrows pointing downward. They may include details about the type and magnitude of the load, such as resistive or inductive loads.

–**Buses:** Buses, the nodes where multiple components are connected, are depicted as horizontal or vertical lines, often thickened to signify their role as junctions. Bus bars act as the backbone of the one-line diagram, distributing power to connected components.

–**Circuit Breaker:** A square symbol placed along a line or connection, indicating a switching device capable of interrupting the flow of current.

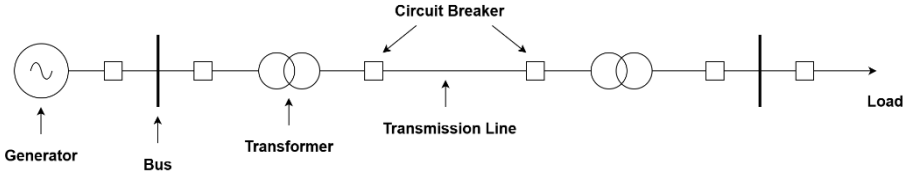

Figure 2: One-Line Diagram of a Simple Power System

Bus Classification

In power system analysis, particularly within the context of load flow studies, buses are categorized based on the known and unknown variables associated with them. This classification is essential because it dictates how

each bus is treated within the solution algorithms used to solve the load flow problem. Understanding these classifications is fundamental to comprehending the principles of load flow analysis. There are three primary types of buses (Kothari and Nagrath, 2011; Glover et al., 2012), as shown in Figure 3.

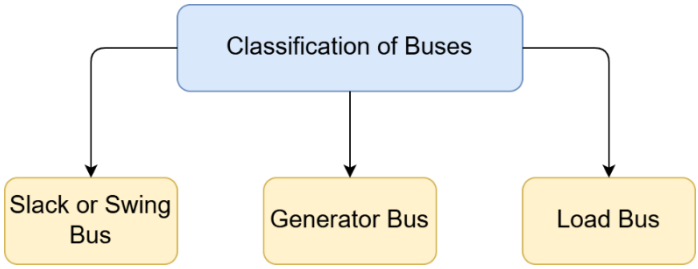

Figure 3: Bus Classification in Power System

1. Slack (Swing or Reference) Bus: The slack bus, also known as the swing or reference bus, serves as the angular reference point for all other buses in the system. Its voltage magnitude ($|V|$) and phase angle (δ) are specified and held constant throughout the load flow solution process. Typically, the phase angle is set to zero ($\delta = 0°$) for simplicity. Since the system's total power losses can only be determined after the solution is found, the slack bus is responsible for balancing the power in the system. It absorbs or generates the difference between the scheduled generation, the total system load, and the transmission losses. In essence, the slack bus provides the necessary real and reactive power to account for the uncertainties that arise during the iterative solution process. In a power system, only one bus is considered a slack bus. This bus is often associated with a large generating station or a tie-line connecting to a larger interconnected system (Dimitrovski and Tomsovic, 2005; Gautam et al., 2022; Fiasorgbor, 2023).

2. PV (Generator or Voltage Controlled) Bus: At a PV bus, also referred to as a generator bus or voltage-controlled bus, the real power (P) generation and the voltage magnitude ($|V|$) are specified. These buses typically represent locations with generators capable of controlling their terminal voltage. The real power injected by the generator is known a priori, and the generator's excitation system adjusts the reactive power output (Q) to maintain the voltage at the specified magnitude. Thus, the reactive power generation and the voltage phase angle (δ) are unknown variables that need to be determined through the load flow solution (Afolabi et al., 2015; Das et al., 2017; Pandey et al., 2019).

3. PQ (Load) Bus: A PQ bus, commonly known as a load bus, is characterized by having its real power (P) and reactive power (Q) demands specified. These buses represent points in the system where loads are

connected, consuming both real and reactive power. The load values are usually obtained from historical data, forecasting models, or measurements. At these buses, the voltage magnitude ($|V|$) and the phase angle (δ) are the unknown quantities that the load flow analysis will determine. The majority of buses in a typical power system are classified as PQ buses (Guo et al., 2013; Murty, 2017).

Table 1 presents the known and unknown variables associated with each type of bus (Adetona et al., 2018; Çifci, 2022).

Table 1: Classification of Power System Buses

Bus Type	Known Variables	Unknown Variables
Slack (Swing) Bus	- Voltage magnitude ($\|V\|$) - Angle (δ)	- Real power (P) - Reactive power (Q)
PV (Generator) Bus	- Real power (P) - Voltage magnitude ($\|V\|$)	- Reactive power (Q) - Angle (δ)
PQ (Load) Bus	- Real power (P) - Reactive power (Q)	- Voltage magnitude ($\|V\|$) - Angle (δ)

The proper classification of buses is crucial for setting up the load flow equations and for the successful convergence of the iterative solution algorithms used to solve them. This classification is a direct reflection of the physical characteristics and operational constraints of the various components within the power system.

Per-Unit System

In power system analysis, especially when dealing with large networks containing transformers and different voltage levels, it's highly advantageous to employ the per-unit (pu) system (Elgerd, 1983). This method involves expressing system quantities (voltage, current, impedance, and power) as fractions of chosen base values. This seemingly simple normalization process offers significant benefits that streamline calculations and enhance the understanding of system behavior.

Power systems often involve very large numbers representing voltages, currents, and power. These large numbers can make calculations cumbersome and prone to errors. The per-unit system effectively eliminates these large magnitudes by scaling quantities to a common base. This normalization results in per-unit values that typically fall within a narrow range (often close to 1.0), making manual and computer-based calculations much more manageable. A power system usually consists of equipment, such as generators, transformers, and transmission lines, operating at different voltage levels. Comparing parameters like impedances directly can be misleading when they are expressed in their actual (ohm) values due to the differing voltage bases. The per-unit system overcomes this issue by representing these parameters on a common base, making them directly comparable regardless of the voltage

level at which the equipment operates. Consequently, engineers can easily assess the relative significance of various components in the system. Manufacturer data for equipment like transformers and generators often provide the impedance information in per-unit values based on the equipment's own ratings. The use of a consistent per-unit system across the entire power system, even when dealing with different manufacturers, simplifies the process of integrating this data into the overall system model. In the per-unit system, the ideal transformer can be effectively eliminated from the equivalent circuit. When referred to the same power base, the per-unit impedance of a transformer is the same irrespective of whether it is calculated from the low-voltage side or high-voltage side.

To utilize the per-unit system, we first need to establish base quantities. Typically, the following base values are chosen for a given part of the system:

Base Power (S_{base}): Usually expressed in megavolt-amperes (MVA) or kilovolt-amperes (kVA). A common S_{base} is chosen for the entire system or a specific portion under analysis.

Base Voltage (V_{base}): Expressed in kilovolts (kV) or volts (V). V_{base} is selected for each voltage level in the system, and they are related by the nominal turns ratios of the connecting transformers.

Base Impedance (Z_{base}): Derived from S_{base} and V_{base}, expressed in ohms (Ω).

Base Current (I_{base}): Derived from S_{base} and V_{base}, expressed in amperes (A) or kiloamperes (kA).

Once these base quantities are defined, the conversion between actual values and per-unit values is straightforward:

$$Per\text{-}Unit\ Value = \frac{Actual\ Value}{Base\ Value} \tag{1}$$

Specifically, for impedance:

$$Z_{pu} = \frac{Z_{actual}}{Z_{base}} \tag{2}$$

where the base impedance is calculated as:

$$Z_{base} = \frac{V_{base}^2}{S_{base}} \tag{3}$$

Similarly, we can calculate the per-unit values for voltage, current, and power.

Component Modeling

Load flow analysis relies on accurate mathematical models of the various components that constitute a power system. These models represent the electrical characteristics of each component and their relationship with voltage, current, and power. This section outlines the simplified, yet effective, models commonly used in load flow studies for the primary components: generators, transformers, transmission lines, and loads.

In load flow analysis, synchronous generators are typically represented using a simplified model consisting of a voltage source connected in series with a synchronous reactance (Nishikawa and Motter, 2015; Barać et al., 2021). This model captures the fundamental behavior of the generator in maintaining a certain voltage and delivering power to the system.

Transformers are crucial components for stepping up or down voltage levels in power systems. In load flow studies, they are modeled using a series impedance and a shunt admittance (Xiao et al., 2006; Sitar et al., 2017; Cano et al., 2017). Series impedance represents the leakage reactance and resistance of the transformer windings. The leakage reactance accounts for the magnetic flux that does not link both windings, while the resistance models the copper losses due to current flow in the windings. Shunt admittance represents the magnetizing reactance and core loss conductance of the transformer. The magnetizing reactance accounts for the current required to establish the magnetic field in the core, while the core loss conductance models the energy dissipated as heat due to hysteresis and eddy currents in the core. Many transformers are equipped with tap-changing mechanisms that allow for adjustments to the turns ratio. These tap changes are used to regulate voltage levels in the system. To accurately represent tap-changing transformers in load flow analysis, the off-nominal turns ratio is incorporated into the transformer model.

Transmission lines are the backbone of the power system, transporting electricity over long distances. For load flow analysis, medium and short transmission lines are typically represented using either the π-model or the *T*-model (Osman et al., 2016; Winstead and Yang, 2018; Rahmani-Andebili, 2024). π-model is the most common model used in load flow analysis. It consists of a series impedance connected between two shunt admittances. Series impedance represents the resistance and inductive reactance of the transmission line conductors. The resistance accounts for the power losses due to current flow, while the inductive reactance models the effect of the magnetic field surrounding the conductors. Shunt admittances are placed at both ends of the line and represent the capacitive susceptance between the line conductors and ground. The capacitive susceptance accounts for the charging current that flows due to the capacitance of the line. *T*-model represents the line with two series impedances connected to a single shunt admittance at the midpoint. In the *T*-model, the total series impedance of the line is divided equally between the two series branches. Each branch represents half of the total line resistance and half of the total line inductive reactance. The shunt

admittance, representing the capacitive susceptance of the line, is connected at the junction of the two series branches.

While both models can approximate the behavior of transmission lines, the π-model is generally preferred in load flow studies due to its direct correspondence with how line parameters are often specified and its convenient representation of charging current injection at both ends of the line. The *T*-model is mathematically equivalent to the π-model and can be converted using Y-Δ transformations. The *T*-model might be chosen in scenarios where a midpoint node is desired for analysis, or in educational contexts to illustrate certain line characteristics. However, for most load flow applications, the π-model remains the standard.

Loads represent the consumption of electrical power in the system. They can be modeled in various ways in load flow analysis, depending on their characteristics and the desired level of accuracy: In constant power model, the active and reactive power consumption (*P* and *Q*) of the load is assumed to be constant and independent of the bus voltage (Dias and Ei-Hawary, 1989). This is a common and often sufficient approximation for many types of loads. Constant impedance model represents the load as a fixed impedance. Consequently, the active and reactive power consumption will vary with the square of the bus voltage magnitude. In constant current model, the load draws a constant current from the system. The active and reactive power consumption will therefore vary linearly with the bus voltage magnitude. A more realistic representation of loads can often be achieved by combining these basic models. For example, a load could be modeled as a combination of constant power and constant impedance components, capturing both voltage-independent and voltage-dependent aspects of its behavior.

These simplified models for generators, transformers, transmission lines, and loads provide a foundation for performing load flow analysis. While more complex models can be used for specific applications, the models described here offer a good balance between accuracy and computational efficiency for most practical load flow studies.

FORMULATION OF THE LOAD FLOW PROBLEM

Nodal Admittance Matrix (Y_{bus})

The nodal admittance matrix, commonly referred to as the Y_{bus}, is a fundamental tool in power system analysis, particularly for load flow studies. It is a square matrix that encapsulates the topology of the power network and the admittance of its components. In essence, the Y_{bus} provides a mathematical representation of how the various buses in a system are interconnected and the ease with which current can flow between them.

The Y_{bus} is a concise way to describe the complex network of transmission lines, transformers, and other components within a power

system. Each element in the matrix, denoted as Y_{ij}, represents the admittance between bus *i* and bus *j*. Admittance, being the reciprocal of impedance, signifies the ability of a circuit element to conduct alternating current. The structure of the Y_{bus} directly reflects the network's topology. Non-zero off-diagonal elements indicate a direct connection between two buses. A zero off-diagonal element implies that there is no direct link between the corresponding buses. The magnitude of each element reflects the admittance of the connection between the buses. Higher admittance values indicate lower impedance and, consequently, easier current flow.

The process of constructing the Y_{bus} involves systematically incorporating the admittance of each component in the network. This is typically done using the system's one-line diagram and the impedance/admittance data of the components (transmission lines, transformers, etc.). The Y_{bus} is built following these key principles (Ramar and Kuruseelan, 2013):

Diagonal Elements (Y_{ii}): The diagonal element Y_{ii} for bus *i* represents the self-admittance of that bus. It is calculated as the sum of the admittances of all components directly connected to bus *i*. This includes transmission lines, transformers, shunt capacitors, and reactors. Mathematically: $Y_{ii} = \sum y_{ik}$ (for all k connected to *i*, including *i* itself if there's shunt admittance at bus *i*) where y_{ik} is the admittance of the branch between bus *i* and bus *k*.

Off-Diagonal Elements (Y_{ij}): The off-diagonal element Y_{ij} represents the mutual admittance between bus *i* and bus *j*. It is calculated as the negative of the admittance of the direct connection between these two buses: $Y_{ij} = -y_{ij}$ where y_{ij} is the admittance of the branch between bus *i* and bus *j*. If there is no direct connection between bus *i* and bus *j*, then $Y_{ij} = 0$.

Example: Consider a simple three-bus system. If bus 1 and bus 2 are connected by a line with admittance y_{12}, bus 1 and bus 3 are connected by a line with admittance y_{13}, and bus 1 has a shunt element with admittance y_{11}, the Y_{bus} would be constructed as follows:

$$Y_{bus} = \begin{bmatrix} Y_{11} & Y_{12} & Y_{13} \\ Y_{21} & Y_{22} & Y_{23} \\ Y_{31} & Y_{32} & Y_{33} \end{bmatrix} \quad (4)$$

where:

- $Y_{11} = y_{11} + y_{12} + y_{13}$
- $Y_{12} = Y_{21} = -y_{12}$
- $Y_{13} = Y_{31} = -y_{13}$
- Y_{22} = sum of admittances connected to bus 2
- Y_{33} = sum of admittances connected to bus 3
- $Y_{23} = Y_{32} = -y_{23}$ (if a direct connection exists between bus 2 and bus 3, otherwise 0)

The Y_{bus} is a cornerstone of load flow analysis because it directly relates bus voltages and currents through Ohm's Law in matrix form:

$$I = Y_{bus}V \tag{5}$$

where I is the vector of injected currents at each bus, V is the vector of bus voltages.

By knowing the Y_{bus} and specifying certain voltage and power conditions at different buses, load flow algorithms can iteratively solve for the unknown voltages and currents, ultimately providing a complete picture of the system's operating state.

Power Flow Equations

The foundation of load flow analysis lies in formulating a set of equations that accurately describe the flow of power throughout the network. These equations are derived by applying Kirchhoff's Current Law (KCL) at each bus within the power system (Saadat, 2010). KCL states that the algebraic sum of currents entering a node (or bus) is equal to zero. By extending this principle to incorporate complex power, we can establish the fundamental power flow equations.

Let's consider a power system with n buses. The complex power injection at bus i can be expressed as:

$$S_i = P_i + jQ_i = V_i I_i^* \tag{6}$$

where S_i is the complex power injection at bus i, P_i is the active power injection at bus i, Q_i is the reactive power injection at bus i, V_i is the complex voltage at bus i, I_i^* is the complex conjugate of the current injection at bus i.

The current injection at bus i can be expressed in terms of the bus admittance matrix (Y_{bus}) and the bus voltages:

$$I_i = \sum_{j=1}^{n} Y_{ij}V_j \tag{7}$$

where Y_{ij} is the element in the i-th row and j-th column of the Y_{bus} matrix, representing the admittance between bus i and bus j.

Substituting equation (7) into equation (6) to eliminate I_i and separating the real and imaginary parts gives us the power flow equations:

$$P_i = \sum_{j=1}^{n} |V_i||V_j|\left(G_{ij}\cos(\delta_i - \delta_j) + B_{ij}\sin(\delta_i - \delta_j)\right) \tag{8}$$

$$Q_i = \sum_{j=1}^{n} |V_i||V_j|\left(G_{ij}\sin(\delta_i - \delta_j) - B_{ij}\cos(\delta_i - \delta_j)\right) \quad (9)$$

where $|V_i|$ and $|V_j|$ are the magnitudes of the voltages at buses *i* and *j*, respectively, δ_i and δ_j are the voltage angles at buses *i* and *j*, respectively, G_{ij} is the real part of Y_{ij}, representing the conductance between bus *i* and bus *j*, B_{ij} is the imaginary part of Y_{ij}, representing the susceptance between bus *i* and bus *j*.

Equations (8) and (9) are the core power flow equations. They represent a set of nonlinear algebraic equations that relate the active and reactive power injections at each bus to the voltage magnitudes and angles throughout the system. Solving these equations is the primary objective of load flow analysis, as it allows us to determine the voltage profile and power flows within the network under specified operating conditions. The solution provides crucial information for system planning, operation, and control.

Problem Statement

The load flow problem, also known as the power flow problem, is a fundamental numerical analysis required to determine the steady-state operating condition of an electric power system. It involves calculating the voltage magnitude and phase angle at each bus in the network, as well as the real and reactive power flowing through each transmission line or branch. In essence, it aims to provide a complete "snapshot" of the system's electrical state under a given operating condition.

The load flow problem is defined by a set of known and unknown variables that characterize the power system's operating state. We are given the following information: First, the network topology, which defines how buses and branches are interconnected within the system. This is compactly represented by the bus admittance matrix (Y_{bus}), encapsulating the electrical properties and connectivity of the transmission network. Second, we know the load demands at each load bus, specified as real power (P) and reactive power (Q) consumption (PQ buses). These values represent the power drawn by consumers at different points in the network. Third, the generator outputs are specified, including the real power (P) injected and the voltage magnitude ($|V|$) maintained at each generator bus (PV buses), representing the power supplied by generating units. Lastly, the slack bus voltage is defined, providing both the voltage magnitude ($|V|$) and a reference phase angle (δ), often set to 0 degrees. The slack bus acts as a balancing point for power in the system, absorbing or providing power to compensate for the difference between scheduled generation plus load, and actual transmitted power, thus accounting for losses.

With this information, the load flow analysis seeks to find the following: Primarily, it aims to determine the bus voltages throughout the network. This entails calculating both the voltage magnitude ($|V_i|$) and phase angle (δ_i) at every bus (i) in the system, encompassing load buses, generator buses, and the slack bus. Furthermore, the analysis determines the complex power flows ($S_{ij} = P_{ij} + jQ_{ij}$) within each branch of the network. These flows represent the complex power moving from bus *i* to bus *j* and consist of both real power (P_{ij}) and reactive power (Q_{ij}) components.

The core of the load flow problem lies in solving a set of non-linear algebraic equations that relate the given quantities to the unknowns. These equations, derived from Kirchhoff's laws, express the balance of real and reactive power at each bus. The non-linearity arises from the dependence of power flow on the product of voltage magnitudes and the sine and cosine of voltage angle differences, as shown in the Power Flow Equations section. This non-linear nature makes it impossible to solve the load flow problem directly using linear methods, necessitating the use of iterative numerical techniques, which will be discussed in the next sections.

LOAD FLOW SOLUTION METHODS

Gauss-Seidel Method

The Gauss-Seidel method is an iterative numerical technique widely used for solving load flow problems (Barrenechea et al., 2022; Hussain et al., 2024), particularly for smaller power systems. It is based on successively refining the voltage estimates at each bus until a solution within a specified tolerance is reached.

The Gauss-Seidel method begins with an initialization phase where voltage values are assigned to all buses in the system. A common practice is to employ a "flat start," setting all bus voltages to 1.0 pu at an angle of 0 degrees ($1.0\angle 0°$). The exception is the slack bus, which acts as the voltage reference for the system; its voltage magnitude and angle are fixed throughout the iterative process.

Following initialization, the algorithm enters the iterative voltage update phase. In each iteration, the voltage at each bus (except the slack bus) is successively updated. The core of this update is the equation:

$$V_i^{(k+1)} = \frac{1}{Y_{ii}} \left[\frac{P_i^{sp} - jQ_i^{sp}}{\overline{V_i^{(k)}}} - \sum_{j=1, j \neq i}^{n} Y_{ij} V_j^{(m)} \right] \tag{10}$$

This equation calculates the new voltage $V_i^{(k+1)}$ at bus *i* based on the specified active and reactive power (P_i^{sp} and Q_i^{sp}), the bus's self-admittance (Y_{ii}), the mutual admittances with other buses (Y_{ij}), and the most recently available voltage values of other buses ($V_j^{(m)}$). A key feature of the Gauss-Seidel method is that it uses updated voltages as soon as they are available within the same iteration: if $j < i$, then $m = k+1$; otherwise, $m = k$.

For PV buses, where voltage magnitude and active power are specified, the process is slightly modified. After the initial voltage magnitude update using the main equation, the reactive power Q_i is calculated using the updated voltage magnitude and admittance values. This calculated Q_i is then used to adjust the voltage angle at the PV bus, ensuring the voltage magnitude remains at its specified value.

The iterative process continues until convergence is achieved. Convergence is typically determined by comparing the voltage magnitude changes between successive iterations. If the difference $\left|V_i^{(k+1)} - V_i^{(k)}\right|$ at every bus is less than a predefined tolerance (ε), the solution is deemed to have converged, and the iterations are terminated.

The Gauss-Seidel method offers some notable advantages. Its primary strength lies in its simplicity. The algorithm is relatively easy to understand and implement in computer code, making it a good pedagogical tool and suitable for initial power flow studies. Furthermore, it boasts low memory requirements, as it only needs to store the current voltage estimates and the admittance matrix. This makes it a viable option for systems with limited computational resources or when dealing with smaller-scale power networks. However, the Gauss-Seidel method also has significant disadvantages. A major drawback is its potential for slow convergence, particularly when applied to large and complex power systems. The number of iterations required to reach a converged solution can be substantial, leading to longer computation times. Additionally, the method's convergence behavior can be sensitive to the initial voltage guess and the choice of the slack bus. An unsuitable initial guess or a poorly chosen slack bus can result in slower convergence or, in some cases, even prevent the algorithm from converging altogether. Finally, the Gauss-Seidel method is not well-suited for ill-conditioned systems, which are systems that are close to being singular and can arise in power systems with certain configurations or parameter values. In such cases, the method may fail to provide reliable results.

Newton-Raphson Method

The Newton-Raphson method is an iterative numerical technique widely used for solving non-linear equations, making it well-suited for load flow analysis (Fendzi Mbasso et al., 2024). It offers fast convergence and robustness compared to other methods. The Newton-Raphson algorithm for

load flow analysis proceeds iteratively as follows. First, we formulate the mismatch equations, which quantify the difference between the specified and calculated active and reactive power injections at each bus. The active power mismatch is given by $\Delta P_i^{(k)} = P_i^{sp} - P_i^{(k)}$, and the reactive power mismatch is given by $\Delta Q_i^{(k)} = Q_i^{sp} - Q_i^{(k)}$, where *k* is the iteration number, *i* is the bus index, P_i^{sp} and Q_i^{sp} are the scheduled power injections, and $P_i^{(k)}$ and $Q_i^{(k)}$ are the calculated power injections based on the current voltage magnitudes and angles, derived from the power flow equations. Next, we calculate the Jacobian matrix, a crucial component of the method. This square matrix contains the partial derivatives of the power mismatch equations with respect to the bus voltage angles (δ) and magnitudes ($|V|$), essentially representing the sensitivity of power injections to voltage changes. The structure of the Jacobian can be represented as:

$$J = \begin{bmatrix} \frac{\partial \Delta \mathrm{P}}{\partial \delta} & \frac{\partial \Delta \mathrm{P}}{\partial |\mathrm{V}|} \\ \frac{\partial \Delta \mathrm{Q}}{\partial \delta} & \frac{\partial \Delta \mathrm{Q}}{\partial |\mathrm{V}|} \end{bmatrix} \tag{11}$$

Each element of this matrix needs to be calculated based on the network admittance matrix and the current estimates of voltage magnitudes and angles.

With the Jacobian defined, we solve a system of linear equations at each iteration: $J^{(k)}\Delta x^{(k)} = \Delta y^{(k)}$. Here, $J^{(k)}$ is the Jacobian at iteration *k*, $\Delta x^{(k)} = \left[\Delta\delta_2^{(k)}, \dots, \Delta\delta_n^{(k)}, \Delta|V_2|^{(k)}, \dots, \Delta\left|V_p\right|^{(k)}\right]^T$ is the vector of updates to the voltage angles and magnitudes, where n is the number of buses and p is the number of PQ buses, and $\Delta y^{(k)} = \left[\Delta P_2^{(k)}, \dots, \Delta P_n^{(k)}, \Delta Q_2^{(k)}, \dots, \Delta Q_p^{(k)}\right]^T$ is the vector of power mismatches. Solving this system, often using techniques like Gaussian elimination or LU decomposition, yields the update vector $\Delta x^{(k)}$. Subsequently, we update the bus voltage magnitudes and angles using the calculated updates: $\delta^{(k+1)} = \delta^{(k)} + \Delta\delta^{(k)}$ and $|V|^{(k+1)} = |V|^{(k)} + \Delta|V|^{(k)}$.

Finally, we check for convergence. The iterative process continues until the absolute values of the active and reactive power mismatches at all buses are less than a predefined tolerance (ε), i.e., $\left|\Delta P_i^{(k)}\right| < \varepsilon$ and $\left|\Delta Q_i^{(k)}\right| < \varepsilon$. Once these conditions are satisfied, the solution is deemed to have converged, and the current voltage magnitudes and angles represent the solution to the load flow problem.

The Newton-Raphson method offers several key advantages in load flow analysis. Foremost is its quadratic convergence, meaning the accuracy of the solution improves dramatically with each iteration, roughly doubling the

number of significant digits as it approaches the solution. This property leads to significantly faster convergence compared to other iterative methods. Furthermore, the method is known for its robustness. It is generally less sensitive to the initial guess of voltage magnitudes and angles, particularly when a "flat start" is employed, where all voltage magnitudes are initialized to 1.0 pu and all angles to 0 degrees. Consequently, the Newton-Raphson method can reliably converge to a solution even with a relatively poor initial estimate. Lastly, the accuracy of the method is a major advantage. Because of its rapid convergence, it typically yields highly precise solutions to the load flow problem. However, the Newton-Raphson method also has certain disadvantages. A primary concern is its high memory requirement. The Jacobian matrix, central to the algorithm, can become very large, especially when analyzing extensive power systems. Storing and manipulating such a large matrix demands substantial memory resources. Another drawback is that it is computationally expensive per iteration. Each iteration involves calculating the elements of the Jacobian matrix and solving a large system of linear equations, which can be computationally demanding, especially for large networks. Nevertheless, the method's rapid convergence often compensates for this higher per-iteration cost. Finally, the potential for Jacobian singularity poses a challenge. In ill-conditioned systems, such as those that are heavily loaded or near voltage collapse, the Jacobian matrix can become singular or nearly singular. This singularity can lead to numerical instability and hinder or prevent convergence. While special techniques or modifications to the algorithm can mitigate this issue, it remains a potential limitation of the Newton-Raphson method.

Fast Decoupled Method

The FDLF method is a highly efficient iterative technique derived from the Newton-Raphson method, leveraging specific characteristics of power systems to simplify the solution process (Stott and Alsac, 1974; Iwamoto and Tamura, 1978). It achieves significant speed improvements by introducing a set of approximations that effectively decouple the power flow equations.

The FDLF method hinges on several key approximations derived from typical power system behavior under normal operating conditions. Primarily, it assumes a weak coupling between active power (P) and voltage angle (δ), and between reactive power (Q) and voltage magnitude ($|V|$). This implies that changes in voltage angle predominantly affect active power flow, while changes in voltage magnitude mainly influence reactive power flow. This weak coupling allows us to deem specific elements in the Jacobian matrix, representing the P-$|V|$ and Q-δ interactions, as negligible. Thus, we approximate $H_{\{i,|V|\}} \approx 0 \; and \; N_{\{i,\delta\}} \approx 0$. Additionally, given that voltage angle differences between connected buses are typically small, we can

approximate $\sin(\delta_i - \delta_j) \approx 0 \; and \cos(\delta_i - \delta_j) \approx 1$. Furthermore, it is commonly observed that $Q_i \ll B^2_{\{ii\}|V_i|}$.

These approximations enable the transformation of the original Newton-Raphson power mismatch equations into two sets of decoupled equations. The first equation relates active power mismatches to voltage angle corrections: $\left[\frac{\Delta P}{|V|}\right] = [B'][\Delta\delta]$. The second equation connects reactive power mismatches to voltage magnitude corrections: $\left[\frac{\Delta Q}{|V|}\right] = [B'']|\Delta|V||$. In these equations, $\left[\frac{\Delta P}{|V|}\right]$ and $\left[\frac{\Delta Q}{|V|}\right]$ are vectors of active and reactive power mismatches, respectively, scaled by the corresponding bus voltage magnitudes; $[\Delta\delta]$ is the vector of voltage angle corrections; and $[\Delta|V|]$ is the vector of voltage magnitude corrections. The constant matrices $[B']$ and $[B'']$ are derived from the imaginary part of the admittance matrix (Y_{bus}). $[B']$ is modified by removing rows and columns corresponding to the slack bus and excluding elements representing phase-shifting transformers. Similarly, $[B'']$ is modified by removing rows and columns related to both the slack bus and PV buses (where voltage magnitudes are already known).

The FDLF algorithm proceeds to solve these decoupled equations iteratively. The process begins with an initial estimate for voltage magnitudes and angles, typically a "flat start" where all magnitudes are 1.0 pu and all angles are 0. In the active power iteration, active power mismatches $\left[\frac{\Delta P}{|V|}\right]$ are calculated, and the equation $\left[\frac{\Delta P}{|V|}\right] = [B'][\Delta\delta]$ is solved to obtain voltage angle corrections $[\Delta\delta]$. Voltage angles are then updated:$\delta^{(k+1)} = \delta^{(k)} + \Delta\delta$. The reactive power iteration mirrors this process, calculating reactive power mismatches $\left[\frac{\Delta Q}{|V|}\right]$, solving $\left[\frac{\Delta Q}{|V|}\right] = [B'']|\Delta|V||$ for voltage magnitude corrections $[\Delta|V|]$, and updating the magnitudes: $|V|^{(k+1)} = |V|^{(k)} + \Delta|V|$. Finally, a convergence check is performed by identifying the largest power mismatch (active or reactive). If this mismatch is below a predetermined tolerance, the solution is deemed to have converged; otherwise, the process returns to the active power iteration step.

The FDLF method offers several compelling advantages. Its most notable strength lies in its speed. FDLF is significantly faster than the Newton-Raphson method because each iteration involves considerably less computation. This efficiency stems from replacing the computationally intensive Jacobian matrix with constant matrices B' and B'', which need only be calculated once at the outset of the solution process. Moreover, FDLF boasts a smaller memory footprint compared to Newton-Raphson, as it operates on smaller matrices. Furthermore, under normal operating conditions, FDLF generally demonstrates good convergence characteristics for most power systems. However, FDLF is not without its disadvantages. The

very approximations that accelerate the method can, in certain situations, lead to convergence difficulties. Specifically, systems with high R/X ratios on transmission lines or those experiencing heavy loading and significant voltage angle differences between buses may challenge the algorithm's convergence. Additionally, the approximations inherent to FDLF can introduce a degree of inaccuracy compared to the full Newton-Raphson method. Nonetheless, for many practical applications, this level of inaccuracy is often deemed acceptable given the method's speed and efficiency gains.

COMPARISON OF LOAD FLOW METHODS

Load flow analysis is a crucial tool in power system planning, operation, and control. Several iterative methods have been developed to solve the non-linear load flow equations, each with its strengths and weaknesses. This section provides a comparative analysis of the most common load flow methods, namely:

- Gauss-Seidel Method
- Newton-Raphson Method
- Fast Decoupled Method

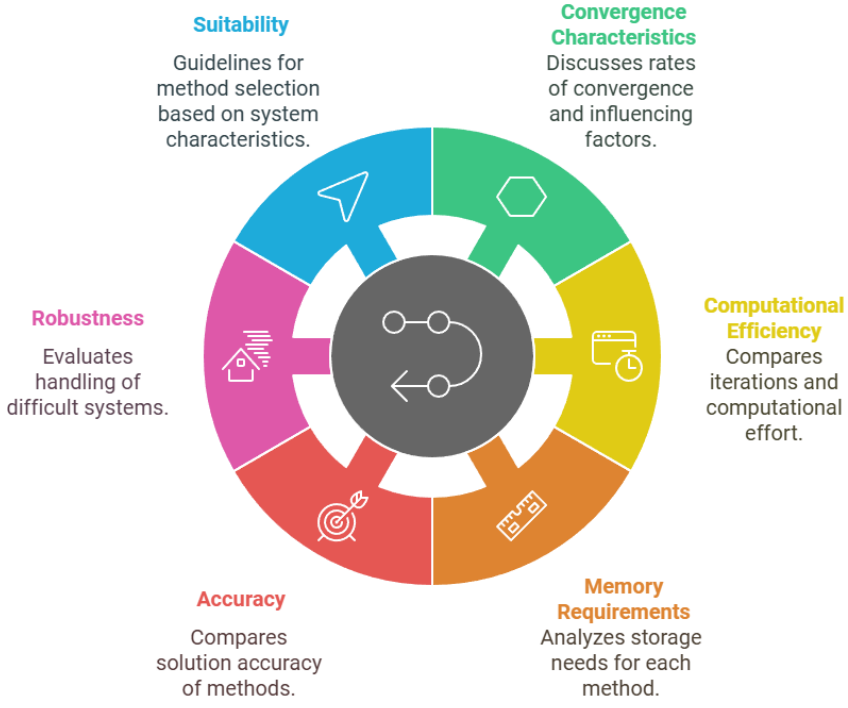

Figure 4: Load Flow Method Comparison Criteria

The comparison will be based on the following criteria, as shown in Figure 4:

The convergence rate describes how quickly an iterative method approaches the solution. It is often characterized as linear, quadratic, or of some other order. Gauss-Seidel method generally exhibits linear or slightly better than linear convergence. The convergence rate is heavily dependent on the choice of the acceleration factor and the system's characteristics (e.g., R/X ratio of the lines). It may struggle to converge or converge very slowly for systems with high R/X ratios, which are common in distribution systems. Newton-Raphson method boasts quadratic convergence, meaning that the number of significant digits in the solution approximately doubles with each iteration, provided that the initial guess is sufficiently close to the solution. This makes it significantly faster than the Gauss-Seidel method when it converges. However, convergence is not guaranteed if the initial guess is far from the actual solution. FDLF method exhibits a convergence rate that is better than linear but not quite quadratic, often described as superlinear. It takes advantage of the weak coupling between P-δ and Q-V equations to achieve faster convergence than Gauss-Seidel, particularly in transmission systems where the R/X ratios are low.

The convergence of load flow methods is influenced by a variety of factors. System size and complexity play a significant role, with larger and more intricate systems typically demanding more iterations to achieve convergence. The ratio of resistance to reactance (R/X) also impacts convergence, particularly for the Gauss-Seidel method, where high R/X ratios can hinder the process. Furthermore, system loading conditions affect convergence, as heavily loaded systems often present greater challenges and may exhibit slower convergence rates. The initial guess is another critical factor, especially for the Newton-Raphson method; a well-chosen initial guess, like a "flat start" with all voltage magnitudes set to 1.0 pu and all angles at 0 degrees, can substantially influence the speed of convergence. Finally, the desired tolerance level, representing the required accuracy of the solution, directly correlates with the number of iterations necessary for convergence.

Computational efficiency refers to the amount of computational effort required to achieve a solution. It is usually assessed by the number of iterations and the computational effort per iteration. Gauss-Seidel method has a relatively low computational burden per iteration since it involves solving simple linear equations. However, the potentially high number of iterations required can make it computationally expensive overall, particularly for large systems. Newton-Raphson method has a higher computational cost per iteration due to the need to calculate and factorize the Jacobian matrix. However, its quadratic convergence typically leads to fewer iterations, often resulting in lower overall computational effort than the Gauss-Seidel method for systems where it converges well. FDLF method strikes a balance between

computational effort per iteration and convergence rate. It simplifies the Jacobian matrix, reducing the computational burden per iteration compared to Newton-Raphson, while still achieving a faster convergence rate than Gauss-Seidel.

Memory requirements refer to the amount of computer memory needed to store the data and matrices used in the load flow calculations. Gauss-Seidel method has relatively low memory requirements since it primarily stores the admittance matrix (Y_{bus}), which is typically sparse, and the voltage vector. Newton-Raphson method has higher memory requirements due to the need to store the Jacobian matrix, which is generally less sparse than the Y_{bus} matrix. For very large systems, this can become a limiting factor. FDLF method also has lower memory requirements compared to Newton-Raphson because it works with reduced and constant Jacobian matrices.

Accuracy refers to how closely the solution obtained by a load flow method matches the true solution of the power system equations. The accuracy of the Gauss-Seidel method depends on the convergence tolerance and the number of iterations performed. Provided sufficient iterations, it can achieve acceptable accuracy. In contrast, the Newton-Raphson method, when it converges, typically delivers the highest accuracy among these methods, thanks to its characteristic quadratic convergence. FDLF method also achieves good accuracy, though it might be slightly less accurate than Newton-Raphson due to the approximations made in decoupling the equations. However, the difference is usually negligible for most practical applications.

Robustness refers to the ability of a method to handle challenging situations, such as ill-conditioned systems or poor initial guesses. Gauss-Seidel method is relatively more robust to poor initial guesses and can often converge even when starting far from the solution, though it may take a large number of iterations. However, it can struggle with ill-conditioned systems, particularly those with high R/X ratios. Newton-Raphson method can be sensitive to the initial guess and may fail to converge if the initial guess is too far from the solution or if the system is ill-conditioned. However, techniques like step-size control can improve its robustness. FDLF method is generally more robust than Newton-Raphson, especially for well-conditioned transmission systems. It can handle variations in loading conditions and system parameters reasonably well.

The choice of the most suitable load flow method depends on the specific characteristics of the power system and the desired trade-off between speed, accuracy, and robustness.

- Gauss-Seidel Method:
  - Suitable for small to medium-sized systems, especially when computational resources are limited.
  - May be preferred for distribution systems with radial configurations where a simple method is sufficient.
  - Can be used when robustness to poor initial guesses is crucial.

- Newton-Raphson Method:
  - Best suited for large transmission systems where high accuracy and fast convergence are paramount.
  - Preferred for systems with complex control schemes or when detailed analysis is required.
  - Requires careful consideration of the initial guess and potential convergence issues.
- Fast Decoupled Method:
  - A good choice for large transmission systems, offering a balance between speed and accuracy.
  - Well-suited for applications where frequent load flow calculations are needed, such as in real-time operations or contingency analysis.
  - Often the preferred method for well-conditioned transmission networks.

Table 2: Summary of Load Flow Method Comparison

Feature	Gauss-Seidel	Newton-Raphson	Fast Decoupled
Convergence Rate	Linear/Slightly better	Quadratic	Superlinear
Computational Effort	Low per iteration, high overall	High per iteration, low overall	Moderate per iteration and overall
Memory Requirements	Low	High	Moderate
Accuracy	Good	Excellent	Good
Robustness	High (to initial guess), low (to ill-conditioning)	Low	Moderate
Suitability	Small/medium systems, distribution	Large systems, transmission	Large systems, transmission
R/X Ratio sensitivity	High	Moderate	Low
Jacobian Matrix	Not required	Calculated and factorized	Approximated and constant

This section has provided a comprehensive comparison of the major load flow methods. The choice of the most appropriate method for a particular application depends on a careful consideration of factors such as system size, complexity, R/X ratios, loading conditions, desired accuracy, and available

computational resources. While the Newton-Raphson method generally offers the fastest convergence and highest accuracy, the FDLF method often provides a good balance between speed, accuracy, and robustness, making it a popular choice for many practical applications, particularly in transmission system analysis. The Gauss-Seidel method, although slower, can be suitable for smaller systems or situations where robustness to poor initial guesses is critical. As power systems continue to evolve in size and complexity, the development and refinement of load flow algorithms will remain an important area of research.

PRACTICAL CONSIDERATIONS AND APPLICATIONS

While the fundamental concepts of load flow analysis provide a solid theoretical basis, successful implementation in real-world power systems requires careful consideration of practical aspects and an understanding of its diverse applications. This section explores some of these crucial considerations and examines how load flow analysis serves as a cornerstone for various power system studies.

Handling of Reactive Power Limits

Generators are designed to operate within specific reactive power (Q) limits to maintain stability and prevent damage. These limits are crucial for accurate load flow analysis and are incorporated into the solution process. Typically, generators are initially modeled as PV buses, maintaining constant voltage magnitude and active power, as long as their reactive power output remains within the specified $Q_{\min}$ and $Q_{\max}$. However, during the iterative load flow calculations, the reactive power output of each generator is constantly monitored. If a limit violation is detected, meaning a generator's Q output exceeds $Q_{\max}$ or falls below $Q_{\min}$, its bus type is dynamically switched from PV to PQ. This switch implies that the generator's reactive power is then fixed at the violated limit (either $Q_{\max}$ or $Q_{\min}$), and the voltage magnitude at that bus becomes an unknown variable, which is then solved for in the subsequent iterations. The load flow solution then continues with this updated bus type and fixed reactive power. It is important to note that, after re-solving, the generator's voltage might adjust such that its Q output falls back within the permissible limits. In this scenario, the bus type could be switched back to PV in the next iteration. This iterative process of switching between PV and PQ buses ensures that the final load flow solution respects the reactive power constraints of all generators while also maintaining a feasible operating point for the entire power system.

Transformer Tap Adjustments

Transformers equipped with on-load tap changers (OLTCs) are essential components in power systems, providing a crucial mechanism for controlling voltage levels and managing reactive power flow. To accurately represent real-world operation, load flow analysis must incorporate the effects of these tap adjustments. The tap position of an OLTC is modeled using an off-nominal turns ratio (t) within the transformer's admittance matrix. Specifically, if the tap is set "n" steps away from its nominal position, the turns ratio becomes $t = 1 + n \times \text{step\_size}$, where step_size represents the per-unit voltage change associated with each tap step. This off-nominal turns ratio "t" directly modifies the transformer's admittance matrix. For a transformer connecting buses "i" and "j", the corresponding entries in the admittance matrix are adjusted as functions of this "t" value. In the context of load flow analysis, OLTCs often operate automatically to regulate the voltage at a designated bus within a predefined range. This automatic tap control can be simulated iteratively by adjusting the tap ratio until the controlled bus voltage falls within the specified limits. Furthermore, tap adjustments can significantly influence reactive power flow. By strategically manipulating tap positions, operators can optimize reactive power dispatch and reduce system losses. While incorporating tap adjustments adds complexity to the load flow solution process, it is crucial for achieving accurate and realistic results, particularly in power systems with stringent voltage control requirements.

Initial Conditions and Convergence Issues

Because load flow algorithms are iterative, they require initial voltage values for all buses except the slack bus. The quality of these initial voltage estimates can have a significant impact on the convergence speed and the overall success of the solution. Several strategies can be employed to select good initial conditions. The simplest is a "flat start," where all voltage magnitudes are set to 1.0 pu and all voltage angles to 0 degrees. This method is often effective for reasonably well-behaved systems. For larger or heavily loaded systems, a DC load flow solution, which ignores reactive power and assumes constant voltage magnitudes, can offer a better starting point than a flat start. Additionally, historical data, such as previous load flow solutions or operational data, can be leveraged to initialize voltages, potentially leading to faster convergence.

Despite careful initialization, load flow algorithms may still encounter convergence problems due to factors like ill-conditioning, heavy loading, or unrealistic system parameters. Several techniques can be used to address these issues. Adjusting the convergence tolerance, which defines the maximum allowable power mismatch, can sometimes help achieve convergence, although it may result in a less accurate solution. The choice of slack bus can also influence convergence, so experimenting with different slack buses might improve the process. Another technique, known as load scaling, involves gradually increasing the system load from a lower value to the desired level

to “guide” the solution toward convergence. Furthermore, convergence issues can arise from modeling inaccuracies, such as an overloaded line in the system model; addressing these underlying modeling problems is crucial. Finally, for particularly challenging cases, more robust algorithms, such as enhanced versions of the Newton-Raphson method (e.g., current injection methods or decoupled methods), may be necessary to obtain a solution.

Applications in Power System Analysis

Load flow analysis serves as the cornerstone for a multitude of power system studies, providing crucial information about the system’s operating state. This information empowers engineers to conduct a variety of analyses, including contingency analysis, optimal power flow (OPF), voltage stability analysis, and state estimation. Contingency analysis simulates the outage of system components, such as transmission lines or generators, to evaluate the impact on system security. Load flow is executed for each contingency scenario to identify potential overloads or voltage violations, thereby highlighting vulnerabilities and informing the planning of remedial actions. Building upon load flow, OPF incorporates an optimization objective, often minimizing generation costs, while adhering to load flow equations and operational constraints like line flow limits and generator output limits. OPF determines the most economical and reliable dispatch of generators to satisfy load demand. Voltage stability analysis assesses the power system’s ability to maintain acceptable voltage levels under various conditions, especially after disturbances. Load flow is employed to calculate voltage stability margins and pinpoint weak areas in the system susceptible to voltage collapse. State estimation integrates load flow principles with real-time system measurements, such as voltage magnitudes and power flows, to estimate the most probable current state of the power system. By accounting for measurement errors and uncertainties, it provides a more accurate and comprehensive view of the system compared to load flow alone. These examples showcase the broad applicability of load flow analysis in power system planning, operation, and control. Its versatility and fundamental nature establish it as an indispensable tool for ensuring the reliable and efficient operation of modern power grids.

CONCLUSION

Load flow analysis is essential for determining the steady-state operating condition of a power system under a given load and generation scenario. Its primary objective is to calculate the voltage magnitude and angle at each bus, as well as the real and reactive power flowing through each transmission line and transformer. This information is crucial for assessing system performance, identifying potential overloads or voltage violations, and

optimizing system operation. The formulation of the load flow problem involves a set of nonlinear algebraic equations derived from Kirchhoff's laws, relating bus voltages, power injections, and network admittances. These equations, often referred to as the power flow equations, are typically expressed in polar form due to the practical significance of voltage magnitudes and phase angles. Several iterative numerical methods are employed to solve the load flow problem, each with its own strengths and weaknesses. The Gauss-Seidel method is relatively simple to implement but can exhibit slow convergence, especially for large systems. The Newton-Raphson method offers quadratic convergence, making it significantly faster, but it requires the computation and inversion of the Jacobian matrix, which can be computationally intensive. The FDLF method leverages the weak coupling between real power and voltage angle, and reactive power and voltage magnitude, to achieve a good balance between speed and simplicity. The choice of method depends on factors such as system size, desired accuracy, and computational resources.

Load flow analysis is a dynamic field that continues to adapt to the growing complexity of modern power systems. Several advanced topics and emerging trends are shaping its future. DC load flow, a simplified linear approximation that neglects reactive power flows and assumes a flat voltage profile, remains computationally efficient and widely used for contingency analysis and initial system planning, despite being less accurate than AC load flow. Its speed and simplicity make it the foundation of many power system optimization techniques. With the proliferation of unbalanced loads and distributed generation, three-phase load flow is gaining importance. Unlike traditional load flow analysis that often assumes a balanced three-phase system, three-phase load flow accurately models distribution systems and analyzes the impact of single-phase components. Distribution systems present unique challenges for load flow analysis due to their radial or weakly meshed topologies, high R/X ratios, and a large number of nodes. Specialized methods, like the backward/forward sweep method, have been developed to address these characteristics. The increasing integration of renewable energy sources, such as wind and solar, introduces further complexities. The intermittent and stochastic nature of these resources necessitates probabilistic or stochastic load flow methods that account for uncertainties in power generation. These methods provide insights into the variability and range of system parameters resulting from fluctuating renewable energy production. Finally, artificial intelligence (AI), particularly machine learning, is increasingly being applied to load flow analysis. AI techniques can create data-driven models that estimate load flow solutions much faster than traditional iterative methods, making them suitable for real-time applications or analyzing numerous scenarios. Furthermore, AI can help identify patterns and anomalies in load flow results, enhancing system monitoring and control. These advancements highlight the ongoing evolution of load flow analysis,

ensuring its continued relevance in the operation and planning of modern power grids.

Load flow analysis remains a fundamental tool for power system engineers. It provides essential insights into the steady-state behavior of power systems, enabling engineers to design, plan, and operate reliable and efficient grids. As power systems continue to evolve with the integration of new technologies and the increasing complexity of load patterns, load flow analysis techniques are also adapting to meet these challenges. The ongoing development of advanced algorithms, coupled with the increasing use of AI and other emerging technologies, ensures that load flow analysis will continue to play a vital role in shaping the future of power systems, contributing to a more sustainable and resilient energy landscape. The ability to accurately and efficiently analyze power systems is paramount, and the evolution of load flow analysis is a testament to its enduring significance in this field.

REFERENCE

Adetona, S., Ugwuagbo, E., Okafor, F., & Akinbulire, T. (2018). Modelling of an Electric Power Grid for New Power Plant Evacuation. *FUOYE Journal of Engineering and Technology*, *3*(2). https://doi.org/10.46792/fuoyejet.v3i2.219

Afolabi, O. A., Ali, W. H., Cofie, P., Fuller, J., Obiomon, P., & Kolawole, E. S. (2015). Analysis of the Load Flow Problem in Power System Planning Studies. *Energy and Power Engineering*, *07*(10), 509–523. https://doi.org/10.4236/epe.2015.710048

Barać, B., Krpan, M., Capuder, T., & Kuzle, I. (2021). Modeling and Initialization of a Virtual Synchronous Machine for Power System Fundamental Frequency Simulations. *IEEE Access*, *9*, 160116–160134. https://doi.org/10.1109/ACCESS.2021.3130375

Barrenechea, R., De Vicuña, L. G., Castilla, M., Rypin, F., & Paiva-Mata, P. (2022). Variations of the Gauss Seidel and the gauss implicit z-bus load flow methods for primary-secondary integrated distribution grids. *Electric Power Systems Research*, *210*, 108061. https://doi.org/10.1016/j.epsr.2022.108061

Basetti, V., Rangarajan, S. S., Kumar Shiva, C., Verma, S., Collins, R. E., & Senjyu, T. (2021). A Quasi-Oppositional Heap-Based Optimization Technique for Power Flow Analysis by Considering Large Scale Photovoltaic Generator. *Energies*, *14*(17), 5382. https://doi.org/10.3390/en14175382

Bayat, M., Koushki, M. M., Ghadimi, A. A., Tostado-Véliz, M., & Jurado, F. (2022). Comprehensive enhanced Newton Raphson approach for power flow analysis in droop-controlled islanded AC microgrids. *International Journal of Electrical Power & Energy Systems*, *143*, 108493. https://doi.org/10.1016/j.ijepes.2022.108493

Bhanbhro, H., Hooi, Y. K., Kusakunniran, W., & Amur, Z. H. (2023). Symbol Detection in a Multi-class Dataset Based on Single Line Diagrams using Deep Learning Models. *International Journal of Advanced Computer Science and Applications*, *14*(8). https://doi.org/10.14569/IJACSA.2023.0140806

Bulat, H., Franković, D., & Vlahinić, S. (2021). Enhanced Contingency Analysis—A

Power System Operator Tool. *Energies*, *14*(4), 923. https://doi.org/10.3390/en14040923

Cano, J. M., Mojumdar, Md. R. R., G. Norniella, J., & A. Orcajo, G. (2017). Phase shifting transformer model for direct approach power flow studies. *International Journal of Electrical Power & Energy Systems*, *91*, 71–79. https://doi.org/10.1016/j.ijepes.2017.03.007

Çifci, A. (2022). Güç Akışı Analizini Öğrenmede PowerWorld Simülatör Kullanımı: Bilgisayar Destekli Bir Görselleştirme Aracı. *Mehmet Akif Ersoy Üniversitesi Fen Bilimleri Enstitüsü Dergisi*, *13*(2), 281–291. https://doi.org/10.29048/makufebed.1153316

Das, S., Das, D., & Patra, A. (2017). Reconfiguration of distribution networks with optimal placement of distributed generations in the presence of remote voltage controlled bus. *Renewable and Sustainable Energy Reviews*, *73*, 772–781. https://doi.org/10.1016/j.rser.2017.01.055

Dias, L. G., & Ei-Hawary, M. E. (1989). Effects of active and reactive power modelling in optimal load flow studies. *IEE Proceedings C Generation, Transmission and Distribution*, *136*(5), 259. https://doi.org/10.1049/ip-c.1989.0034

Dimitrovski, A., & Tomsovic, K. (2005). Slack bus treatment in load flow solutions with uncertain nodal powers. *International Journal of Electrical Power & Energy Systems*, *27*(9–10), 614–619. https://doi.org/10.1016/j.ijepes.2005.08.015

El-Fergany, A. A. (2024). Reviews on Load Flow Methods in Electric Distribution Networks. *Archives of Computational Methods in Engineering*. https://doi.org/10.1007/s11831-024-10191-7

Elgerd, O. I. (1983). *Electric energy systems theory: An introduction: Olle I. Elgerd (Professor of Electrical Engineering, University of Florida)* (Second edition). McGraw Hill Education (India) Private Limited.

Fendzi Mbasso, W., Molu, R. J. J., Ambe, H., Dzonde Naoussi, S. R., Alruwaili, M., Mobarak, W., & Aboelmagd, Y. (2024). Reliability analysis of a grid-connected hybrid renewable energy system using hybrid Monte-Carlo and Newton Raphson methods. *Frontiers in Energy Research*, *12*, 1435221. https://doi.org/10.3389/fenrg.2024.1435221

Fiasorgbor, N. K. (2023). Investigating the Effects of Slack Bus Selection in Load Flow Studies: A Comparative Analysis of Robust and Weak Grids. *Journal of Power and Energy Engineering*, *11*(09), 1–14. https://doi.org/10.4236/jpee.2023.119001

Gautam, M., Bhusal, N., Thapa, J., & Benidris, M. (2022). A cooperative game theory-based approach to formulation of distributed slack buses. *Sustainable Energy, Grids and Networks*, *32*, 100890. https://doi.org/10.1016/j.segan.2022.100890

Gianto, R. (2021). Steady-state model of DFIG-based wind power plant for load flow analysis. *IET Renewable Power Generation*, *15*(8), 1724–1735. https://doi.org/10.1049/rpg2.12141

Glover, J. D., Sarma, M. S., & Overbye, T. J. (2017). *Power system analysis & design* (Sixth edition, SI). Cengage Learning.

Gönen, T. (2013). *Modern power system analysis* (Second edition). CRC Press.

Guo, Y., Zhang, B., Wu, W., Guo, Q., & Sun, H. (2013). Solvability and solutions for

bus-type extended load flow. *International Journal of Electrical Power & Energy Systems*, *51*, 89–97. https://doi.org/10.1016/j.ijepes.2013.02.013

Hong, T., Zhao, D., Zhang, Y., Yao, R., & Qiu, F. (2021). Thermal Overloading Risk Mitigation With a Semi-Analytical Probabilistic Model on Branch Current. *IEEE Transactions on Power Systems*, *36*(4), 3384–3393. https://doi.org/10.1109/TPWRS.2020.3048302

Honrubia-Escribano, A., Villena-Ruiz, R., Artigao, E., Gómez-Lázaro, E., & Morales, A. (2021). Advanced teaching method for learning power system operation based on load flow simulations. *Computer Applications in Engineering Education*, *29*(6), 1743–1756. https://doi.org/10.1002/cae.22420

Huang, X., Wu, H., & Wang, D. (2018). Implicit solution of harmonic balance equation system using the LU-SGS method and one-step Jacobi/Gauss-Seidel iteration. *International Journal of Computational Fluid Dynamics*, *32*(4–5), 218–232. https://doi.org/10.1080/10618562.2018.1508658

Hussain, Md. D., Rahman, Md. H., & Ali, N. M. (2024). Investigation of Gauss-Seidel Method for Load Flow Analysis in Smart Grids. *Scholars Journal of Engineering and Technology*, *12*(05), 169–178. https://doi.org/10.36347/sjet.2024.v12i05.004

Ibrahim, I. A., & Hossain, M. J. (2021). Low Voltage Distribution Networks Modeling and Unbalanced (Optimal) Power Flow: A Comprehensive Review. *IEEE Access*, *9*, 143026–143084. https://doi.org/10.1109/ACCESS.2021.3120803

Iwamoto, S., & Tamura, Y. (1978). A Fast Load Flow Method Retaining Nonlinearity. *IEEE Transactions on Power Apparatus and Systems*, *PAS-97*(5), 1586–1599. https://doi.org/10.1109/TPAS.1978.354650

Kothari, D. P., & Nagrath, I. J. (2011). *Modern power system analysis* (Fourth edition). McGraw Hill Education (India) Private Limited.

Kumar, S., Sharma, J. R., & Jäntschi, L. (2024). An Optimal Family of Eighth-Order Methods for Multiple-Roots and Their Complex Dynamics. *Symmetry*, *16*(8), 1045. https://doi.org/10.3390/sym16081045

Li, M., Zhao, Q., & Luh, P. B. (2009). Decoupled load flow and its feasibility in systems with dynamic topology. *2009 IEEE Power & Energy Society General Meeting*, 1–8. https://doi.org/10.1109/PES.2009.5275932

Meinecke, S., Sarajlić, D., Drauz, S. R., Klettke, A., Lauven, L.-P., Rehtanz, C., Moser, A., & Braun, M. (2020). SimBench—A Benchmark Dataset of Electric Power Systems to Compare Innovative Solutions Based on Power Flow Analysis. *Energies*, *13*(12), 3290. https://doi.org/10.3390/en13123290

Murty, P. S. R. (2017). *Power systems analysis* (Second edition). Butterworth-Heinemann, an imprint of Elsevier.

Naderi, E., Pourakbari-Kasmaei, M., Cerna, F. V., & Lehtonen, M. (2021). A novel hybrid self-adaptive heuristic algorithm to handle single- and multi-objective optimal power flow problems. *International Journal of Electrical Power & Energy Systems*, *125*, 106492. https://doi.org/10.1016/j.ijepes.2020.106492

Nishikawa, T., & Motter, A. E. (2015). Comparative analysis of existing models for power-grid synchronization. *New Journal of Physics*, *17*(1), 015012. https://doi.org/10.1088/1367-2630/17/1/015012

Osman, M., Abidin, I. Z., Abdullah, T. A. R. T., & Marsadek, M. (2016). Electric power transmission. In *Electric Renewable Energy Systems* (pp. 382–402).

Elsevier. https://doi.org/10.1016/B978-0-12-804448-3.00017-7

Pandey, A., Jereminov, M., Wagner, M. R., Bromberg, D. M., Hug, G., & Pileggi, L. (2019). Robust Power Flow and Three-Phase Power Flow Analyses. *IEEE Transactions on Power Systems*, *34*(1), 616–626. https://doi.org/10.1109/TPWRS.2018.2863042

Parizad, A., Baghaee, H. R., Iranian, M. E., Gharehpetian, G. B., & Guerrero, J. M. (2020). Real-time simulator and offline/online closed-loop test bed for power system modeling and development. *International Journal of Electrical Power & Energy Systems*, *122*, 106203. https://doi.org/10.1016/j.ijepes.2020.106203

Rahman, S., Saha, S., Islam, S. N., Arif, M. T., Mosadeghy, M., Haque, M. E., & Oo, A. M. T. (2021). Analysis of Power Grid Voltage Stability With High Penetration of Solar PV Systems. *IEEE Transactions on Industry Applications*, *57*(3), 2245–2257. https://doi.org/10.1109/TIA.2021.3066326

Rahmani-Andebili, M. (2024). Transmission Line Model and Performance. In M. Rahmani-Andebili, *Power System Analysis* (pp. 167–209). Springer Nature Switzerland. https://doi.org/10.1007/978-3-031-64691-1_6

Ramar, S., & Kuruseelan, S. (2013). *Power system analysis*. PHI Learning Private Limited.

Saadat, H. (2010). *Power system analysis* (3rd ed). PSA Pub.

Sitar, V., Veleba, J., & Nohac, K. (2017). Load flow analysis using transformer models in alternative simulation tools. *2017 18th International Scientific Conference on Electric Power Engineering (EPE)*, 1–6. https://doi.org/10.1109/EPE.2017.7967336

Stott, B., & Alsac, O. (1974). Fast Decoupled Load Flow. *IEEE Transactions on Power Apparatus and Systems*, *PAS-93*(3), 859–869. https://doi.org/10.1109/TPAS.1974.293985

Tostado, M., Kamel, S., & Jurado, F. (2019). Developed Newton-Raphson based Predictor-Corrector load flow approach with high convergence rate. *International Journal of Electrical Power & Energy Systems*, *105*, 785–792. https://doi.org/10.1016/j.ijepes.2018.09.021

Varghese, J. P., Sundaramoorthy, K., & Sankaran, A. (2023). Development and Validation of a Load Flow Based Scheme for Optimum Placing and Quantifying of Distributed Generation for Alleviation of Congestion in Interconnected Power Systems. *Energies*, *16*(6), 2536. https://doi.org/10.3390/en16062536

Veerasamy, V., Abdul Wahab, N. I., Ramachandran, R., Othman, M. L., Hizam, H., Devendran, V. S., Irudayaraj, A. X. R., & Vinayagam, A. (2021). Recurrent network based power flow solution for voltage stability assessment and improvement with distributed energy sources. *Applied Energy*, *302*, 117524. https://doi.org/10.1016/j.apenergy.2021.117524

Vysocký, J., Foltyn, L., Brkić, D., Praksová, R., & Praks, P. (2022). Steady-State Analysis of Electrical Networks in Pandapower Software: Computational Performances of Newton–Raphson, Newton–Raphson with Iwamoto Multiplier, and Gauss–Seidel Methods. *Sustainability*, *14*(4), 2002. https://doi.org/10.3390/su14042002

Winstead, V., & Yang, S. (2018). Power Line Communication Input Impedance Adjustment via Network Load Measurements. *2018 IEEE International Conference on Electro/Information Technology (EIT)*, 0832–0835.

https://doi.org/10.1109/EIT.2018.8500267
Wood, A. J., Wollenberg, B. F., & Sheblé, G. B. (2013). *Power generation, operation, and control* (Third edition). Wiley-IEEE.
Xiao, P., Yu, D. C., & Yan, W. (2006). A Unified Three-Phase Transformer Model for Distribution Load Flow Calculations. *IEEE Transactions on Power Systems*, *21*(1), 153–159. https://doi.org/10.1109/TPWRS.2005.857847
Yang, N.-C., Liu, M.-J., Lai, K.-Y., & Adinda, E. W. (2022). Three-Phase Power Flow Calculations Using Initial Voltage Estimation Method for Unbalanced Distribution Networks. *IEEE Access*, *10*, 103705–103717. https://doi.org/10.1109/ACCESS.2022.3207783
Zeng, L., Alawneh, S. G., & Arefifar, S. A. (2021). GPU-Based Sparse Power Flow Studies With Modified Newton's Method. *IEEE Access*, *9*, 153226–153239. https://doi.org/10.1109/ACCESS.2021.3127393

Utilization of Waste Pea Pods as Macro Fibers in Gypsum Based Composites: Effects on Physical and Mechanical Properties

Ahmet Hayrullah SEVİNÇ[1]
Muhammed Yasin DURGUN[2]

1- Assoc. Prof. Dr.; Kahramanmaraş İstiklal University, Elbistan Vocational School of Higher Education, Construction Programme, ahmethayrullah.sevinc@istiklal.edu.tr ORCID No: 0000-0003-3338-8366
2- Assoc. Prof. Dr.; Bartın University, Faculty of Engineering, Architecture and Design, Civil Engineering Department, mydurgun@bartin.edu.tr ORCID No: 0000-0003-4656-9430

ABSTRACT

The rapid increase in human population and urbanization has reduced agricultural lands, making it necessary to enhance crop yields per unit area. In impoverished and developing countries, outside of the developed world, deficiencies in nutrients and protein have become significant challenges. Legumes play a crucial role in human and animal nutrition, particularly as a source of protein. The most widely produced legume crops include chickpeas, lentils, beans, cowpeas, and peas. Approximately 30% of the total weight of peas (on a fresh weight basis) consists of pea pods. The large amounts of by-products generated during the processing of plant-based foods pose significant economic and environmental challenges due to their high volumes and disposal costs. The estimated amount of by-products generated during canned pea production accounts for approximately 67% of the total peas processed at the facility. There is limited research in the literature on the use of waste pea pods as fibers for material production. In this study, waste pea pods were incorporated as macro fibers in gypsum-based mixtures at varying sizes and volumetric proportions. The effects of using these fibers on the physical and mechanical properties of the gypsum-based mixtures were investigated. Unit weight, ultrasonic pulse velocity, apparent porosity, water absorption, capillary water absorption, bending strength, and compressive strength tests were performed. When waste pea pod fibers were used up to 1%, an increase was observed in ultrasonic pulse velocity, flexural strength, and compressive strength values. The fibers improved water absorption, porosity, and capillary water absorption values at all utilization rates.

Keywords – Agricultural Wastes, Waste Pea Pods, Macro Fibers, Gypsum, Engineering Properties.

INTRODUCTION

The rapid increase in human population and urbanization has led to a reduction in agricultural lands, making it necessary to enhance crop yields per unit area. In impoverished and developing countries, outside of the developed world, deficiencies in nutrients and protein have become significant challenges. The high cost of animal-based foods has driven increased interest in plant-based protein sources. Legumes play a crucial role in human and animal nutrition, particularly as a source of protein. Approximately 66% of plant-based proteins in human diets are derived from cereals, 18.5% from legumes, and 15.5% from other plant sources. Leguminous plants remain vital for sustainable agriculture due to their

contributions to healthy human nutrition and soil conservation (Göktaş 2024).

The most widely produced legume crops include chickpeas, lentils, beans, cowpeas, and peas (Ustaoğlu 2024). Peas are protein-rich legumes that are widely available worldwide due to their nutritional benefits, low cost, and ease of cultivation. According to the Turkish Statistical Institute, pea production in Turkey amounted to 120,455 tons in 2022 and increased to 147,344 tons in 2023 (Çam 2020).

Due to their high protein content and richness in vitamins, peas are consumed both as a green vegetable and as dried grains (Göktaş 2024). Peas are rich in protein, containing approximately 58% starch and 23% protein. The fat content of legumes such as peas, lentils, broad beans, and beans typically ranges between 1-2%. Peas are used as an intercropped legume in agricultural production systems to meet the global demand for human food and animal feed. Feeds prepared with dry peas at rates of 20-25% for beef and dairy cattle, 40-45% for sheep, and 20-30% for poultry have yielded successful results (Ustaoğlu 2024).

Approximately 30% of the total weight of peas (on a fresh weight basis) consists of pea pods. The large amounts of by-products generated during the processing of plant-based foods pose significant economic and environmental challenges due to their high volumes and disposal costs. Most legumes are consumed after a straightforward industrial process, during which the seeds are separated from the pods and prepared as frozen, canned, or fresh foods. These by-products of agricultural industries can serve as valuable sources of functional components. The structure of pea pods primarily consists of non-starch polysaccharides such as cellulose. They contain 12% protein and 54.7% dietary fiber on a dry matter basis. Numerous studies suggest that food processing waste can be transformed into beneficial products or repurposed as higher-value by-products. There are also many plant-based by-products, such as pea pods, that remain underutilized. These by-products can be added to various foods due to their nutritional value and plant fiber content. The estimated amount of by-products generated during canned pea production accounts for approximately 67% of the total peas processed at the facility. Some of these by-products can be incorporated into foods for their nutritional benefits. This not only enhances the functionality of the foods but also mitigates the economic and environmental issues caused by the accumulation of these by-products (Çam 2020).

There is limited research in the literature on the use of waste pea pods as fibers for material production. One study suggested that pea pods, being approximately 40% lignocellulosic material composed of lignin, cellulose, and hemicellulose, could be used to reinforce polymer composites (Alshahrani and Arun Prakash 2024). In another study, waste pea pods were utilized for the removal of chromium from water (Anwar et al. 2010).

Additionally, research has been conducted on the production of cellulose microfibers from pea pods (Bhiri et al. 2022). In yet another study, lignin derived from pea pods was used to enhance the thermal stability of epoxy composites (Giridharan et al. 2023).

In this study, waste pea pods were incorporated as macro fibers in gypsum-based mixtures at varying sizes and volumetric proportions. The effects of using these fibers on the physical and mechanical properties of the gypsum-based mixtures were investigated. The goal was to contribute to the disposal of agricultural waste and produce more economical and sustainable products.

MATERIALS AND METHODS

Materials

The gypsum utilized in this study was procured commercially, with the manufacturer confirming its compliance with TS EN 13297-1 standards. Tables 1 and 2 detail the technical and chemical properties of the gypsum, respectively. The pea pods (PP) used in the study were sourced from the waste of canning facilities. The mineralogical properties of the PP are presented in Table 3. Figure 1 shows the images of gypsum and PPs used in the study.

Methods

Dried PPs were cut into lengths of 2 cm and 3 cm to achieve the desired dimensions for the study. The prepared PPs were incorporated into the gypsum mixture at volumetric ratios of 0.5%, 1%, 1.5%, 2%, and 2.5%. Table 4 presents the mixing ratios.

Table 1: Technical properties of gypsum

Property	Value
Initial setting time (min)	> 8
Final setting time (min)	≈ 30
Minimum compressive strength (40x40 mm) (MPa)	10
Minimum flexural strength (40x40x160 mm) (MPa)	4.5
Grains under 200 μm (min)	%99.5
Grains under 100 μm (min)	%95.0
Loose unit weight (g/cm^3)	0.75 – 0.80
Dry unit weight (g/cm^3)	1.05 – 1.10

Table 2: Chemical and physical properties of gypsum

Chemical components	Value (%)
SiO_2	3.16
Al_2O_3	0.44
Fe_2O_3	0.37
CaO	40.71
MgO	0.61
SO_3	51.79
Na_2O+K_2O	0.26
Physical properties	
Loss on ignition (%)	18.84
Density (g/cm^3)	2.29
Fineness (m^2/kg)	500

Table 3: Mineralogical properties of pea pods

Mineral	Amount (g/100 g KM)
Potassium	1.03
Sodium	0.14
Calcium	0.77
Magnesium	0.21
Iron	1.20
Copper	0.06
Manganese	0.27
Zinc	0.16

Source: (Akdoğan 2014)

Figure 2: Images of gypsum and pea pods

Table 4: Mixture proportions

Sample code	Gypsum (g)	Water (g)	Pea pods fibers (g)	Pea pods fiber ratio (by volume, %)
R	1200	720	-	-
2P0.5	1196	717.6	0.65	0.50
2P1	1192	715.2	1.30	1.00
2P1.5	1188	712.8	1.95	1.50
2P2	1184	710.4	2.60	2.00
2P2.5	1180	708	3.25	2.50
3P0.5	1196	717.6	0.63	0.50
3P1	1192	715.2	1.26	1.00
3P1.5	1188	712.8	1.89	1.50
3P2	1184	710.4	2.52	2.00
3P2.5	1180	708	3.15	2.50

Table 4 uses specific codes where the letter "P" stands for PPs, the number to the left indicates the fiber length, and the number to the right represents the usage percentage. To prepare the mixture, powdered gypsum and PPs were first combined and mixed in a laboratory cement mixer for 30 seconds to ensure uniformity. Subsequently, water was introduced, and the blending process continued with 30 seconds of low-speed mixing followed by 60 seconds of high-speed mixing.

The prepared mixtures were placed into prismatic molds measuring 40x40x160 mm, with gentle vibration applied to ensure proper settling. After remaining in the molds for 24 hours, the specimens were demolded and allowed to cure under laboratory conditions for 7 days. They were then dried in an oven at 65°C for 48 hours to eliminate any residual moisture. Once dried, the specimens underwent the tests outlined in Table 5. Figure 2 provides visual documentation of various steps in the experimental procedure.

Table 5: Tests and related standards

Test name	Related standard
Unit weight	ASTM C 138
Ultrasonic pulse velocity (UPV)	ASTM C 597
Water absorption	ASTM C 20
Apparent porosity	ASTM C 20
Capillary water absorption	TS EN 480-5
Flexural strength	TS EN 196-1
Compressive strength	TS EN 196-1

Figure 2: Images related to experimental procedure

RESULTS AND DISCUSSION

Figure 3 shows the unit weight results.

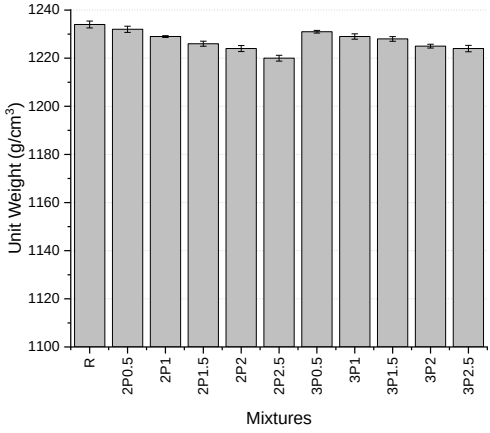

Figure 3: Unit weight results

The unit weight values range between 1220 and 1234 g/cm³. The results indicate a slight reduction in unit weight with the inclusion of PP. This decrease is more pronounced when 2 cm PP fibers are used. The lowest unit weight was observed in the 2P2.5 sample, which exhibited a 1.1% reduction compared to the reference value. In comparison, using 3 cm PP at the same ratio resulted in a decrease of 0.8%. While a reduction in unit weight is evident, the magnitude of the change remains minimal.

Figure 4 illustrates the UPV results.

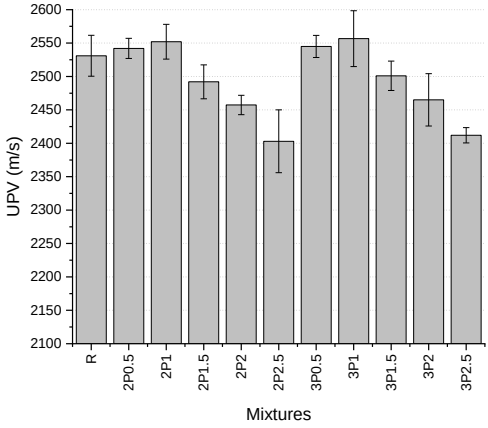

Figure 4: UPV results

The UPV values range between 2403 and 2556 m/s. For both fiber lengths, the use of PP initially increased the UPV values, followed by a decrease as the PP ratio increased. When comparing 2 cm and 3 cm PP fibers, the 3 cm fibers produced slightly higher values, although the difference is minimal. The reference sample recorded a UPV of 2534 m/s. The highest value, achieved with the 3P1 sample, represented a 0.99% increase compared to the reference. Similarly, in the 2 cm PP series, the highest value was observed at a 1% usage ratio, marking a 0.83% increase over the reference. The lowest value was recorded in the 2P2.5 sample, which was 5.1% lower than the reference. Overall, UPV values at 0.5% and 1% usage ratios were higher than the reference, but the total changes observed were relatively minor.

Figure 5 shows the flexural strength results.

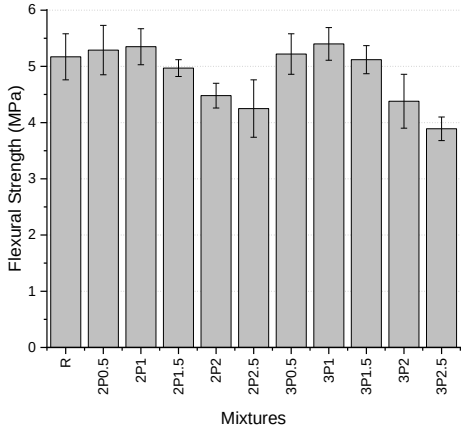

Figure 5: Flexural strength results

The flexural strength values range from 3.89 MPa to 5.40 MPa. The highest value was observed in the 3P1 sample, while the lowest was recorded in the 3P2.5 sample. The reference sample provided a flexural strength of 5.17 MPa. For both PP fiber lengths, usage ratios of 0.5% and 1% yielded higher values compared to the reference. Specifically, 0.5% usage resulted in increases of 2.3% and 0.97% for 2 cm and 3 cm fibers, respectively, while 1% usage showed increases of 3.5% and 4.4%. Beyond these ratios, the flexural strength values began to decline. The lowest value, observed in the 3P2.5 sample, was 24.8% lower than the reference. For 2 cm PP fibers, the largest decrease was 17.8%.

Figure 6 shows the compressive strength results.

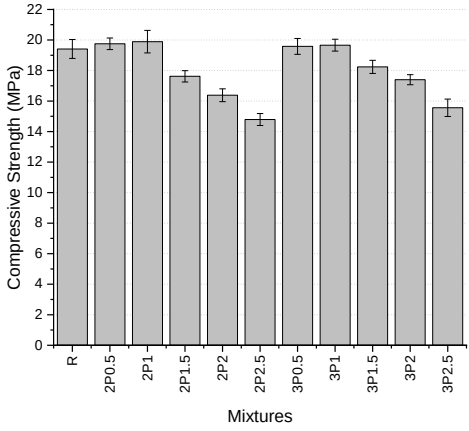

Figure 6: Compressive strength results

The compressive strength trends align closely with those observed in the flexural strength results. The compressive strength values range between 14.79 MPa and 19.89 MPa. Unlike the flexural strength results, the highest value was obtained from the 2P1 sample, while the lowest strength was observed in the 2P2.5 sample. The reference sample exhibited a compressive strength of 19.41 MPa. Among the samples containing 3 cm PP fibers, the highest strength was also recorded at the 1% usage ratio, with a value of 19.66 MPa. At 1% fiber content, the samples containing 2 cm PP fibers showed a 2.5% increase compared to the reference, while those with 3 cm fibers exhibited a 1.3% increase. Compressive strength values increased up to the 1% usage ratio, but losses were observed beyond this point. The largest reduction occurred at the 2.5% usage level, with a 23.8% loss for samples containing 2 cm PP fibers and a 19.8% loss for those with 3 cm fibers. The mechanical test results were found to be consistent with the trends observed in the UPV results.

Figure 7 illustrates the water absorption and apparent porosity

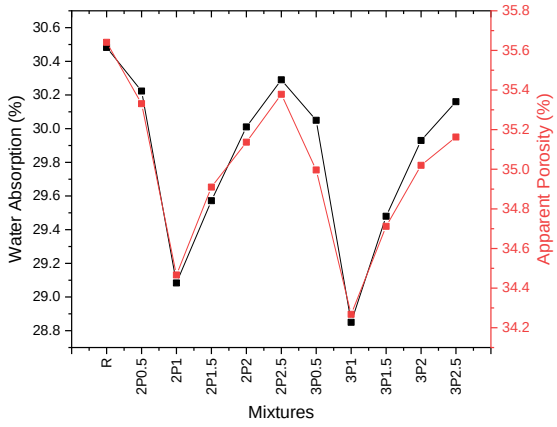

Figure 7: Water absorption and apparent porosity results

The water absorption values initially decreased with the addition of PP, but after reaching a 1% usage ratio, they began to rise again. The same trend was observed for porosity values. In both cases, the highest value was obtained from the reference sample. Water absorption values ranged from 28.85% to 30.48%. As can be seen, the difference between the lowest and highest values is only 1.6%. A similar trend is observed in the porosity results, where values ranged from 34.26% to 35.64%, with a total difference of 1.4%. Therefore, it can be concluded that the use of PP fibers, regardless of the fiber length, did not have a significant impact on water absorption and porosity.

Figure 8 shows the capillary water absorption results.

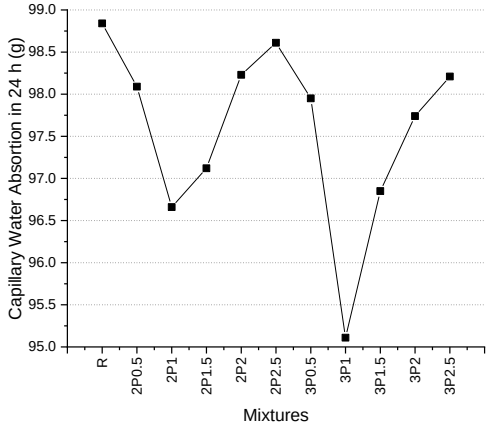

Figure 8: Capillary water absorption and apparent porosity results

The amount of water absorbed through capillary action after 24 hours ranged from 95.11 g to 98.84 g, with a difference of 3.73 g between the highest and lowest values. The trend observed in the capillary water absorption results is similar to that of atmospheric water absorption. For both PP lengths, the use of up to 1% reduced the capillary water absorption values. However, higher usage ratios led to an increase in capillary water absorption values. Nonetheless, when examining the overall results, it can be concluded that the total change is relatively small.

CONCLUSIONS

This study investigates the feasibility of using pea pods, an agricultural and industrial waste, as fibers in gypsum-based mixtures. PP fibers cut to sizes of 2 and 3 cm were used at five different ratios ranging from 0.5% to 2.5%. The experimental results obtained from this study are summarized as follows:

- The use of PP resulted in a slight decrease in the unit weight values, with a more significant reduction observed with 2 cm PP usage. However, the maximum decrease was only 1.1%.
- PP usage initially led to an increase in UPV values, followed by a decrease. The highest value was obtained from the 3P1 sample. While the increase was minimal, the decrease reached a maximum of 5.1%.
- Flexural and compressive strength values increased up to a 1% usage rate, after which they declined. The highest flexural strength was obtained with 3 cm fibers, while the highest compressive strength was achieved with 2 cm fibers. The increases in strength were modest, while significant reductions of over 20% were observed at higher usage rates.
- Water absorption, porosity, and capillary water absorption values were not significantly affected by the fiber usage. The observed variations in results were quite narrow.

In conclusion, when the waste PP material was used in small amounts, it caused slight changes (even improvements) in the properties of gypsum-based materials. However, higher usage rates led to a weakening of mechanical properties. Therefore, PP material can be used in gypsum-based composite production in small proportions. Based on these results, further research is needed to explore the possibilities of using higher proportions of PP fibers in gypsum-based composites.

REFERENCES

Akdoğan, Arda. 2014. “Bezelye Kabuğunun Farklı Sistemlerdeki Kuruma Kinetiğinin ve Kurutulmuş Ürünün Öğütülmesiyle Elde Edilen Toz Ürünün Özelliklerinin Belirlenmesi.” Ege Üniversitesi.

Alshahrani, Hassan, and V. R. Arun Prakash. 2024. “Characterisation of Microcrystalline Cellulose from Waste Green Pea Pod Sheath and Its Sunn Hemp Fibre-Polyester Composite: A Step towards Greener Manufacturing.” *Physiologia Plantarum* 176(1). doi: 10.1111/ppl.14166.

Anwar, Jamil, Umer Shafique, Waheed-uz-Zaman, Muhammad Salman, Zaib Hussain, Maria Saleem, Naeema Shahid, Saliha Mahboob, Samina Ghafoor, Mehwish Akram, Rabia Rehman, and Nadia Jamil. 2010. “Removal of Chromium from Water Using Pea Waste–a Green Approach.” *Green Chemistry Letters and Reviews* 3(3):239–43. doi: 10.1080/17518251003730833.

Bhiri, Fatma, Samira Abidi, Amir Bouallegue, Gmar Bensidhom, Fatma Kallel, Semia Ellouz Chaabouni, and Aida Ben Hassen Trabelsi. 2022. “Valorization of Pea By-Products for the Isolation of Cellulosic Microfibers : Extraction and Physico- Chemical Characterization.” *Research Square*.

Çam, Gizem. 2020. “Farklı Oranlarda Yenilebilir Bitkisel Lif Kullanılarak Üretilen Probiyotik Dondurmaların Bazı Özelliklerinin Belirlenmesi.” Selçuk Üniversitesi.

Giridharan, K., S. Sasirekha, S. Padmanabhan, G. Chakravarthi, and B. Stalin. 2023. “Effect of Green Pea Pod Lignin Addition on Thermal Degradation, Flame Resistance, DMA, and Creep Resistance of Pineapple Fibre Epoxy Composite.” *Biomass Conversion and Biorefinery* 14(23):29843–52. doi: 10.1007/s13399-023-04841-2.

Göktaş, Kazım Emre. 2024. “Farklı Ekim Zamanlarının Kuru Bezelyenin (Pisum Sativum L.) Verim ve Kalite Kriterlerine Etkisinin Araştırılması.” Kahramanmaraş Sütçü İmam Üniversitesi.

Ustaoğlu, Ahmet. 2024. “Konya Şartlarına Uygun Yemeklik Kuru Bezelye ve Yemlik Bezelye Çeşitlerinin Geliştirilmesinde Kullanılabilecek Genotiplerin Belirlenmesi.” Selçuk Üniversitesi.

Evaluation of Waste Denim Fibers in Gypsum Composites: Engineering Properties for Sustainable Material Development

Muhammed Yasin DURGUN[1]
Ahmet Hayrullah SEVİNÇ[2]

1- Assoc. Prof. Dr.; Bartın University, Faculty of Engineering, Architecture and Design, Civil Engineering Department, mydurgun@bartin.edu.tr ORCID No: 0000-0003-4656-9430
2- Assoc. Prof. Dr.; Kahramanmaraş İstiklal University, Elbistan Vocational School of Higher Education, Construction Programme, ahmethayrullah.sevinc@istiklal.edu.tr ORCID No: 0000-0003-3338-8366

ABSTRACT

One of the most common fabrics in the textile industry is denim. Denim is a durable cotton twill fabric characterized by its distinctive diagonal weave. It is widely used in global garment production and is known for its strength, stiffness, and resistance to wear. However, such large-scale production also generates a significant amount of waste. This study evaluated waste fibers obtained from waste denim fabrics in gypsum composites in two sizes (6 and 12 mm) and five different proportions (0.5%, 1%, 1.5%, 2%, and 2.5%). The produced samples' physical and mechanical engineering properties were examined, and the feasibility of utilizing denim wastes as fibers in gypsum-based materials was investigated. Unit weight, ultrasonic pulse velocity, apparent porosity, water absorption, capillary water absorption, flexural strength, and compressive strength tests were performed. In both sizes, using waste denim fibers up to a ratio of 1.5% improved the ultrasonic pulse velocity, flexural strength, and compressive strength values. Water absorption, porosity, and capillary water absorption values also showed improvement, although the extent of these improvements was found to be quite minimal.

Keywords – Waste Denim Fibers, Gypsum Composites, Physical Properties, Mechanical Properties, Sustainable Materials.

INTRODUCTION

The textile industry in Turkey is recognized as one of the key driving sectors of the national economy, considering its share in the gross domestic product (GDP), its contribution to employment, and its significant export potential. This sector accounts for 8.8% of the total production value in the country's manufacturing industry and 9.9% of the added value generated within the manufacturing sector. The textile industry encompasses a wide range of processes, including fiber preparation, spinning, weaving, knitting, dyeing, printing, finishing, cutting, sewing, and production. Furthermore, it holds a critical position within the supply chain of the ready-made clothing sector, boasting a diverse array of production capabilities. The sector also includes technical textiles designed for specialized applications, such as nonwoven fabrics, home textiles, carpets, nets, ropes, textile cables, conveyor belts, tarpaulins, protective fabrics, filters, parachutes, and brake pads. Among these, the ready-made clothing sector is undoubtedly the first that comes to mind (Uyanık and Çelikel 2019).

Textiles and apparel have always been essential to human life, with the global textile industry playing a pivotal role in ensuring consumer comfort from the outset. However, the past century's rapid advancements

and shifts in fashion trends have led to a significant increase in both textile production and waste generation rates (Uddin 2019). Each year, approximately 150 million tons of textile waste are generated globally. As living standards improve, clothing consumption rises, leading to a continuous growth in textile waste. Projections suggest that by 2050, the volume of global textile waste will surge to 895 million tons. Despite at least half of discarded textiles being recyclable, only about 25% of textile waste is reused or recycled annually in developed regions like Europe and the United States. A significant portion of this waste is either incinerated or buried. Incineration, however, releases harmful toxic gases into the atmosphere, while landfill disposal can leach chemical dyes, contaminating soil and water. Therefore, increasing the rate of textile waste recycling and reuse is critical for fostering a sustainable ecosystem (Meng et al. 2020).

One of the most common fabrics in the textile industry is denim. Denim is a durable cotton twill fabric characterized by its distinctive diagonal weave, widely used in garment production across the globe. Known for its strength, stiffness, and resistance to wear, denim represented a global market value of over 90 billion USD in 2019, with projections estimating its growth to approximately 107 billion USD by 2023. However, such large-scale production also generates a significant amount of waste. The textile industry generates two primary types of solid waste: pre-consumer waste (industrial waste) and post-consumer waste (secondhand materials). Improper collection and irresponsible disposal of solid denim waste contribute to soil and air pollution, posing significant risks to both human health and the environment (Aman et al. 2022). Solid materials such as yarn, fiber, and fabric, along with volatile emissions, used chemicals, effluents, and post-consumer textile waste, all have detrimental effects on the environment and living organisms. Hazardous waste from the textile industry can be classified into three categories: pre-consumer solid waste (including fibers, yarns, and fabric remnants), processing waste (such as volatile compounds, chemicals, and effluents released during production), and post-consumer waste (including textile fabrics, yarns, clothing, home textiles, and technical textiles) discarded after their service life (Uddin, Umer, and Anjum 2022).

Chemical recycling involves removing dyes from denim fibers, which leads to high recovery costs. On the other hand, mechanical recycling is more cost-effective, but most recycled denim waste ends up in secondary markets with low economic value. Additionally, natural fiber-reinforced composites, which offer high specific strength and low cost, can be utilized as engineering materials to reduce reliance on petroleum-based fuels and products (Wang et al. 2022).

One of these fiber-reinforced composites is gypsum-based fiber-reinforced composites. Gypsum plaster is a highly effective material for building construction due to its excellent properties. It offers good acoustic

performance, is fire-resistant (emitting only water vapor when exposed to fire), helps regulate wall humidity, and is a natural, organic, and environmentally friendly building material. Gypsum-based materials, commonly used as wall panels, partitions, and boards in residential, commercial, and industrial buildings, have become a distinctive construction material due to their light weight, low cost, abundance, and ease of application (Dawood and Mezal 2014). Partition elements made from gypsum-based plaster also serve as both acoustic and fire barriers. The brittleness of these materials can be significantly reduced by reinforcing gypsum with natural fibers (Fantilli, Jóźwiak-Niedźwiedzka, and Denis 2021).

There are some examples in the literature regarding the use of denim fibers in certain construction materials. These studies focus on non-autoclaved aerated concrete masonry blocks (Özcan and Gündüz 2021), bitumen (Al-Sabaeei et al. 2019, 2022; Al-Sabaeei, Alhussian, et al. 2023; Al-sabaeei, Napiah, and Alaloul 2018; Al-Sabaeei, Safaeldeen, and Napiah 2023), mortar (Kalkan and Gündüz 2016), and cement blocks (Hossain et al. 2022). In this study, fibers obtained from waste denim fabrics were evaluated in gypsum composites in two different sizes and five different proportions. The physical and mechanical engineering properties of the produced samples were examined, and the feasibility of utilizing denim wastes as fibers in gypsum-based materials was investigated.

MATERIALS AND METHODS

Materials

The gypsum used in the study was commercially obtained. The manufacturer reported that the product complies with TS EN 13297-1 standards. The technical and chemical properties of the gypsum are presented in Tables 1 and 2, respectively. The denim fibers used in the study were obtained from waste generated in denim fabric production facilities and subsequently cut to the dimensions required for the study. The properties of the denim yarn are provided in Table 3. Images of the gypsum and denim yarn used in the study are presented in Figure 1.

Table 1: Technical properties of gypsum

Property	Value
Initial setting time (min)	> 8
Final setting time (min)	≈ 30
Minimum compressive strength (40x40 mm) (MPa)	10
Minimum flexural strength (40x40x160 mm) (MPa)	4.5
Grains under 200 μm (min)	%99.5
Grains under 100 μm (min)	%95.0
Loose unit weight (g/cm^3)	0.75 – 0.80
Dry unit weight (g/cm^3)	1.05 – 1.10

Table 2: Chemical and physical properties of gypsum

Chemical components	Value (%)
SiO_2	3.16
Al_2O_3	0.44
Fe_2O_3	0.37
CaO	40.71
MgO	0.61
SO_3	51.79
Na_2O+K_2O	0.26
Physical properties	
Loss on ignition (%)	18.84
Density (g/cm^3)	2.29
Fineness (m^2/kg)	500

Methods

The denim yarns used in the study were subjected to a cutting process to achieve the desired dimensions after being procured. The denim fibers (DF) were cut into two lengths: 6 mm and 12 mm. The prepared DFs were incorporated into the gypsum-based mixtures at volumetric ratios of 0.5%, 1%, 1.5%, 2%, and 2.5%. Table 4 presents the mix proportions.

Table 3: Properties of denim fibers

Fiber property	Mean value
Fiber length	6 – 12 mm
Unit weight	0.129 g/cm^3
Fiber strength	32.7 g/tex
Elongation	5.50%
Uniformity index (UI)	83.6%
Spinnig consistency index (SCI)	145
Short fiber index (SFI)	8.5
Micronaire	4.5 μg/inch

Source: (Akter et al. 2021)


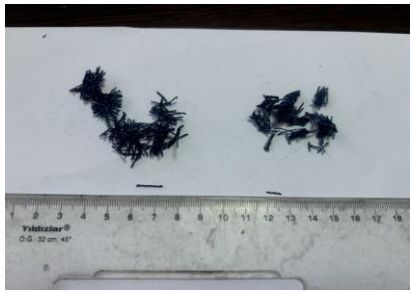

Figure 1: Images of gypsum and denim fibers

Table 4: Mixture design of gypsum composites

Sample code	Gypsum (g)	Water (g)	Waste denim fiber ratio (by volume, %)
R	1200	780	-
6D0.5	1196	777.4	0.50
6D1	1192	774.8	1.00
6D1.5	1188	772.2	1.50
6D2	1184	769.6	2.00
6D2.5	1180	767	2.50
12D0.5	1196	777.4	0.50
12D1	1192	774.8	1.00
12D1.5	1188	772.2	1.50
12D2	1184	769.6	2.00
12D2.5	1180	767	2.50

In the codes provided in Table 4, the letter "D" represents denim fibers, with the number on the left indicating fiber length and the number on the right signifying the usage ratio. Initially, the powdered gypsum and DFs were mixed together using a laboratory-scale cement mixer for 30 seconds to achieve a homogeneous mixture. Water was then added, and the mixture was stirred at a low speed for 30 seconds followed by high-speed mixing for 60 seconds.

The prepared mixtures were poured into prismatic molds with dimensions of 40x40x160 mm, followed by light vibration. The specimens were kept in the molds for 24 hours before being demolded and left in the laboratory environment for 7 days. Subsequently, the specimens were placed in an oven at 65°C for 48 hours to remove moisture. After oven drying, the specimens were subjected to the tests listed in Table 5. Figure 2 contains some images related to the experimental procedure.

Table 5: Tests and related standards

Test name	Related standard
Unit weight	ASTM C 138
Ultrasonic pulse velocity (UPV)	ASTM C 597
Water absorption	ASTM C 20
Apparent porosity	ASTM C 20
Capillary water absorption	TS EN 480-5
Flexural strength	TS EN 196-1
Compressive strength	TS EN 196-1

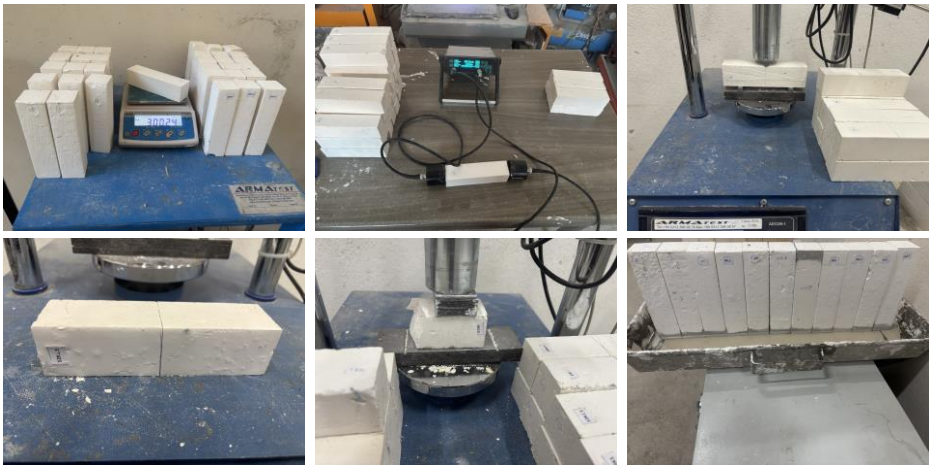

Figure 2: Images related to experimental procedure

RESULTS AND DISCUSSION

Figure 3 presents the results of unit weight measurements.

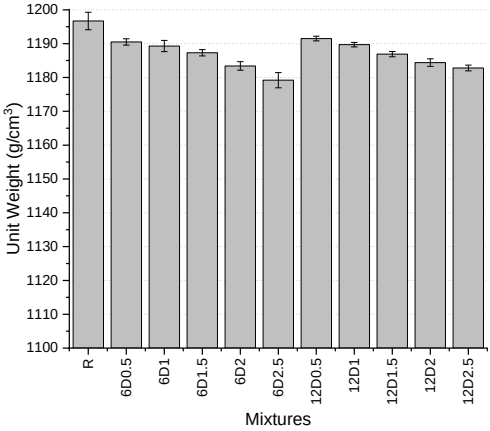

Figure 3: Unit weight measurements

The unit weight results range between 1179.2 and 1196.7 g/cm³. The highest unit weight value decreased with the use of DF. The same trend was observed for both fiber lengths. Although there are no significant differences in the results, the use of shorter DF resulted in slightly lower unit weights. The lowest values were obtained with 2.5% DF usage. Compared to the reference, a decrease of 1.4% was observed for 6 mm DF and 1.2% for 12 mm DF. These findings indicate that the change rates are negligible.

Figure 4 shows the UPV results.

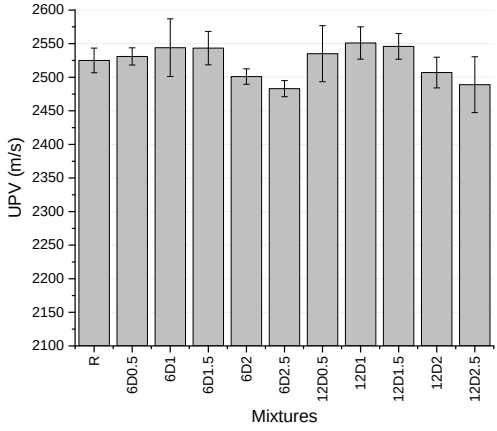

Figure 4: UPV measurements

The UPV results range between 2483 and 2551 m/s, with the reference sample yielding a value of 2525 m/s. A slight increase in UPV values was

observed with DF usage up to 1% for both fiber lengths. However, beyond this ratio, a declining trend began, and UPV values decreased as the DF content increased. For 6 mm fibers, 1% DF usage resulted in a 0.75% increase, while for 12 mm fibers, a 1.02% increase was observed. Conversely, 2.5% DF usage produced the lowest values, with decreases of 1.66% for 6 mm DF and 1.43% for 12 mm DF.

In conclusion, while no significant changes were observed, fiber usage up to 1.5% appears to improve UPV values compared to the reference sample. UPV values are generally associated with void structure and mechanical properties (Benaicha et al. 2015). Based on the UPV results, it can be inferred that DF usage up to 1.5% contributed to a denser internal structure compared to the reference. This is expected to positively reflect on the mechanical properties as well.

Figure 5 illustrates the flexural strength test results.

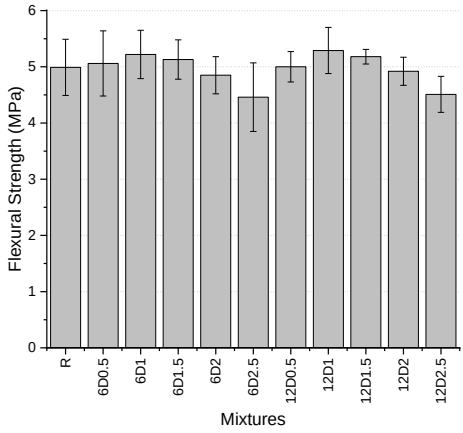

Figure 5: Flexural strength results

The flexural strength results range from 4.46 to 5.29 MPa, with the reference sample achieving a flexural strength of 4.99 MPa. For both DF types, an increase in flexural strength was observed up to a usage ratio of 1%. DF usage at 0.5%, 1%, and 1.5% yielded higher flexural strength values compared to the reference. However, higher DF ratios negatively impacted the results. For 6 mm DF, increases of 1.4%, 4.6%, and 2.8% were observed at 0.5%, 1%, and 1.5% usage ratios, respectively, whereas for 12 mm DF, the increases were 0.2%, 6%, and 3.8% at the same ratios.

It is evident that longer fibers had a slightly greater positive effect on flexural strength improvement. Conversely, 2.5% DF usage resulted in decreases of 10.6% and 9.6% for 6 mm and 12 mm DF, respectively, with the reduction being slightly less pronounced for longer fibers. Based on these results, it can be concluded that DF usage up to 1.5% improves flexural strength, with the optimal usage ratio being 1%. The minimum flexural

strength value specified by the manufacturer for the gypsum at the same water ratio is 4.5 MPa. Among the produced samples, the only one falling below this threshold is the 6D2.5 sample, with a flexural strength of 4.46 MPa. The fact that nearly all samples exceed this limit highlights the success of the applied method.

Figure 6 illustrates the compressive strength test results.

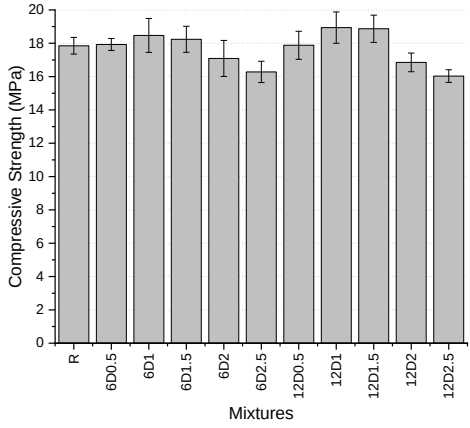

Figure 6: Compressive strength results

The compressive strength results range between 16.03 and 18.94 MPa, with the reference sample achieving a compressive strength of 17.85 MPa. The observed trends align closely with those seen in flexural strength results. For both fiber lengths, an increase in compressive strength was observed up to a fiber content of 1%. The highest strengths were achieved with 1% DF utilization, reaching 18.24 MPa for 6 mm DF and 18.94 MPa for 12 mm DF, corresponding to increases of 2.2% and 6.1%, respectively, compared to the reference. The use of 12 mm DF resulted in slightly greater compressive strength improvements. Beyond a 1.5% fiber content, compressive strengths fell below the reference value. At a 2.5% fiber content, compressive strength losses of 8.8% and 10.2% were observed for 6 mm and 12 mm DF, respectively. While the highest improvement was achieved with 12 mm DF, the greatest loss was also observed with the same fiber length. On the other hand, the manufacturer specifies a minimum compressive strength of 10 MPa for the gypsum under the same water ratio. All results obtained in this study exceed this minimum requirement. The results of the mechanical tests appear to align closely with the UPV results.

Figure 7 shows the water absorption and apparent porosity results.

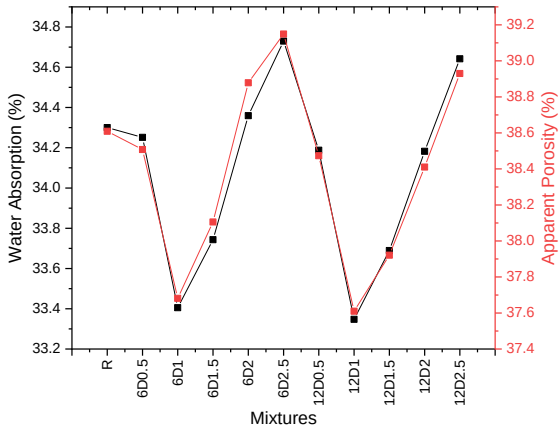

Figure 7: Water absorption and apparent porosity results

Water absorption values range from 33.3% to 34.73%, while porosity values vary between 37.6% and 39.1%. The results indicate no significant differences between the lowest and highest values. The difference in water absorption between the highest and lowest values is 1.4%, while for porosity, it is 1.5%. Both parameters are below the reference values at 0.5%, 1%, and 1.5% fiber content. However, fiber contents of 2% and 2.5% led to an increase in these values.

Figure 8 shows the capillary water absorption results. The results of the capillary water absorption test exhibit a similar trend to the atmospheric water absorption results. After 24 hours, the amounts of water absorbed via capillary action range from 102.26 to 103.73 g. As observed, there is only a 1.47 g difference between the lowest and highest values. This suggests that the capillary water absorption property is not significantly affected by the use of DF. Up to a 1.5% DF content, lower capillary water absorption values were observed compared to the reference, while at 2% and 2.5% DF ratios, the water absorption rate slightly increased.

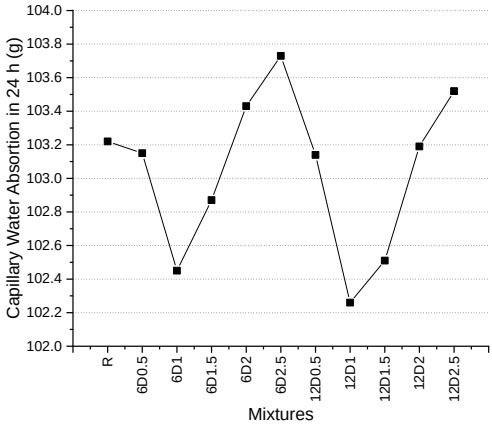

Figure 8: Capillary water absorption results

CONCLUSIONS

In the experimental study, waste denim fibers cut into 6 mm and 12 mm lengths were evaluated in gypsum-based mixtures at proportions ranging from 0.5% to 2.5%, and various engineering properties were examined. Based on the experimental results, the following conclusions can be drawn:

- The unit weight values decreased with the use of denim fibers (DF). Short fibers had a greater impact on this reduction.
- The ultrasonic pulse velocity (UPV) results increased with DF usage up to 1%, but decreased below the reference value at 2% and higher proportions.
- The flexural strength results were higher than the reference sample with up to 1.5% DF usage. Higher proportions led to a decrease in results, which is also true for compressive strength results.
- Water absorption, porosity, and capillary water absorption values decreased up to 1% DF usage. Up to 1.5%, these values were lower than the reference, while 2% and 2.5% usage increased these values.

In conclusion, when examining the test results, the changes observed in comparison to the reference values are not significant. Overall, the rates of increase and decrease are very small and most of them are not statistically meaningful. However, up to 1.5% DF usage, no significant loss was observed, and small improvements were noted in the properties. The lack of significant deviations and the observed improvements indicate the need for further studies on the use of waste DF in gypsum-based composites. The fact that the inclusion of this waste into the matrix does not cause significant changes suggests the potential for exploring a new area for the evaluation of denim fabric waste.

REFERENCES

Akter, Nasrin, Md. Reazuddin Repon, Daiva Mikučionienė, Mohammad Abdul Jalil, Tarikul Islam, and Md. Rezaul Karim. 2021. "Fabrication and Characterization of Stretchable Denim Fabric Using Core Spun Yarn." *Heliyon* 7(12):e08532. doi: 10.1016/j.heliyon.2021.e08532.

Al-Sabaeei, A. M., M. Napiah, M. Al Salaheen, R. M. Badri, S. Noura, M. I. Khan, T. M. Al-Bahr, and K. Alzubi. 2022. "Optimizing the Physical Properties of Waste Denim Fiber-Modified Rubberized Bitumen Through Response Surface Methodology." *IOP Conference Series: Earth and Environmental Science* 971(1). doi: 10.1088/1755-1315/971/1/012014.

Al-Sabaeei, A., M. Napiah, M. Sutanto, and W. Alaloul. 2019. "Effects of Waste Denim Fibre (WDF) on the Physical and Rheological Properties of Bitumen." *IOP Conference Series: Materials Science and Engineering* 527(1). doi: 10.1088/1757-899X/527/1/012047.

Al-Sabaeei, Abdulnaser M., Hitham Alhussian, Said Jadid Abdulkadir, Filippo Giustozzi, Fauzan Mohd Jakarni, and Nur Izzi Md Yusoff. 2023. "Predicting the Rutting Parameters of Nanosilica/Waste Denim Fiber Composite Asphalt Binders Using the Response Surface Methodology and Machine Learning Methods." *Construction and Building Materials* 363(October 2022):129871. doi: 10.1016/j.conbuildmat.2022.129871.

Al-Sabaeei, Abdulnaser M., Gailan Ismat Safaeldeen, and Madzlan Napiah. 2023. "Utilization of Response Surface Methodology for Predicting and Optimizing the Physical Properties of Rubberized Asphalt Modified with Nanosilica and Waste Denim Fiber." *Cleaner Engineering and Technology* 15(March):100666. doi: 10.1016/j.clet.2023.100666.

Al-sabaeei, Abdulnaser, Madzlan Napiah, and Wesam Alaloul. 2018. "An Overview on Using the Waste Denim Fiber As a Bitumen Modifier for Sustainable Road Construction." *International Journal of Civil Engineering and Technology* (March 2019).

Aman, Divay Tonk, Kamal Shokeen, and D. K. Singh. 2022. "Development of Fire Retarding Composite Board for Fire Compartmentation Application Using Waste Denim: A Review." *Materials Today: Proceedings* 60:259–66. doi: 10.1016/j.matpr.2021.12.513.

Benaicha, Mouhcine, Olivier Jalbaud, Adil Hafidi Alaoui, and Yves Burtschell. 2015. "Correlation between the Mechanical Behavior and the Ultrasonic Velocity of Fiber-Reinforced Concrete." *Construction and Building Materials* 101:702–9. doi: 10.1016/j.conbuildmat.2015.10.047.

Dawood, Eethar, and Ansam Meshal Mezal. 2014. "The Properties of Fiber Reinforced Gypsum Plaster." *Journal of Scientific Research and Reports* 3(10):1339–47. doi: 10.9734/jsrr/2014/7356.

Fantilli, Alessandro P., Daria Jóźwiak-Niedźwiedzka, and Piotr Denis. 2021. "Bio-Fibres as a Reinforcement of Gypsum Composites." *Materials* 14(17). doi: 10.3390/ma14174830.

Hossain, Sajjad, I. A. Dipta, M. A. Alam, and Ahsan Habib. 2022. "Recycled Waste Textiles as Reinforcement in Cement Block." *6th International Conference on Advances in Civil Engineering (ICACE-2022)* (December 2022):524–31.

Kalkan, Ş. O., and L. Gündüz. 2016. "A Study on the Usage of Denim Waste as

Reinforcement Element in Composite Mortars on Exterior Building Applications." *12th International Congress on Advances in Civil Engineering* (September 2016):1–8.

Meng, Xue, Wei Fan, Yanli Ma, Tongxue Wei, Hao Dou, Xue Yang, Huixia Tian, Yang Yu, Tao Zhang, and Li Gao. 2020. "Recycling of Denim Fabric Wastes into High-Performance Composites Using the Needle-Punching Nonwoven Fabrication Route." *Textile Research Journal* 90(5–6):695–709. doi: 10.1177/0040517519870317.

Özcan, Şeyma Pınar, and Lütfullah Gündüz. 2021. "Otoklavsız Gazbeton Kâgir Blok Elemanlarının Üretiminde Endüstriyel Atık Liflerin Kullanımı Üzerine Teknik Bir Analiz." *European Journal of Science and Technology* (24):202–12. doi: 10.31590/ejosat.900083.

Uddin, Faheem. 2019. "Introductory Chapter: Textile Manufacturing Processes." in *Textile Manufacturing Processes*. IntechOpen.

Uddin, Faheem, Komal Umer, and Syeda Tehniyat Anjum. 2022. "Textile Solid Waste in Product Development Studies." *Chemical Reports* 3(1):203–9. doi: 10.25082/CR.2021.01.005.

Uyanık, Seval, and Dilan Canan Çelikel. 2019. "Türk Tekstil Endüstrisi Genel Durumu. [In English: General Situation of Turkish Textile Industry]." *Teknik Bilimleri Dergisi* 9(1):32–41.

Wang, Shujuan, Tao Zhang, Xiaolin Zhang, Shengbo Ge, and Wei Fan. 2022. "Development of 3D Needled Composite from Denim Waste and Polypropylene Fibers for Structural Applications." *Construction and Building Materials* 314(PA):125583. doi: 10.1016/j.conbuildmat.2021.125583.

Comparison of Building Energy Efficiency for Energy Conservation in the Kahramanmaraş Region Across Different Groups

Başak ZENGİN[1]

Assist. Prof. Dr., Kahramanmaraş İstiklal University, EVSHE, Construction Programme, Kahramanmaraş/Türkiye, basak.zengin@istiklal.edu.tr, Orcid: 0000-0003-3719-9423,

ABSTRACT

Energy identification is a process that evaluates a country or region's energy consumption, production, efficiency, and environmental impacts. This issue is gaining increasing importance in Turkey and around the world because energy identification plays a critical role in the development of energy policies, the setting of sustainability goals, and the fight against climate change. For this reason, modern countries around the world have established associations and developed special identification models to create parameters for sustainability. In Turkey, a specific system has been established, and energy identification has been made mandatory to make this system widespread in everyone's building design. In order to carry out energy identification, energy identities are assigned to old and new buildings by modeling with BEP-TR. For this purpose, in this study, different buildings in the Kahramanmaraş region were selected, their energy identification was carried out, and a comparison was made. According to the obtained differences, the energy efficiency of Buildings B and D is better than that of Buildings C and E. More insulation and mechanical system improvements are recommended. Buildings C and E show weaknesses in terms of energy efficiency and require improvement.

Keywords – Energy, BEP-TR, Building Design, Kahramanmaraş.

INTRODUCTION

Energy identification is the process of systematically evaluating and defining the energy consumption and production structure of a building, businesses in the sector, or a country as a whole. This process allows for the more effective management of energy resources and consumption by considering various factors such as energy efficiency, energy consumption, energy sources, environmental impacts, and the economy.

Global warming and climate change are causing environmental problems worldwide. In solving these problems, the construction of sustainable structures is of great importance. Sustainable structures are systems that are environmentally friendly, efficiently use natural resources, and recycle energy.

In Turkey, the aim of the Regulation on Energy Performance of Buildings No. 27075, published in 2008, is to ensure the efficient and effective use of energy resources in buildings, to prevent energy waste, and to protect the environment.

When comparing the green building evaluation criteria applied in the USA, UK, Germany, Finland, Australia, and Japan, energy, ecology, indoor environmental quality, environmental pollution, and water issues are

considered important criteria in all these countries. However, the topics of economy and waste are only included as criteria in one country each. It is noteworthy that the issue of CO_2 has only been included in the evaluation criteria of two countries (Anbarcı 2012).

In Turkey, the energy consumption of residential buildings is increasing and becoming incompatible with the environment. Residential buildings consume more resources in terms of energy consumption compared to other types of buildings. Therefore, it is crucial to increase energy efficiency in residences and make improvements in insulation practices.

Different thermal insulation materials were examined in order to achieve energy savings in residential buildings, taking Eco City' project as a reference in the provinces of Istanbul and Erzurum. Using Design Builder and Energy Plus simulation tools, energy performances were compared in two different climate regions (temperate-humid and cold climate). As a result of comparing sustainable insulation materials like hemp with other materials such as rock wool, XPS, and EPS, it has been determined that hemp performs the best. In the houses where hemp is used, improvements in energy consumption between 87% and 88% have been achieved, and it has been observed that CO_2 emissions decreased by 13% in Istanbul and by 20% in Erzurum. Especially, applications made with hemp insulation material have yielded positive results in both cities.This situation has resulted in nearly a 2-fold reduction in natural gas consumption when compared to the reference building in Istanbul, and a similar conclusion was reached for the reference building in Erzurum, where a significant reduction was observed. Compared to all other thermal insulation materials, the best improvement method is the one that includes hemp material (Darı 2024).

For the very good insulation and airtightness of the building shell, insulating the walls, floors, and ceilings with insulation materials of appropriate type and thickness according to the specific needs of each surface is another fundamental step in the construction of a zero-energy building. The use of high-insulation doors and windows; the selection of an energy-efficient heating and cooling system, the installation of energy-efficient lighting; the selection of energy-efficient appliances and electronic products; the use of renewable energy sources with standards that can meet all the energy needs of a house, including lighting, heating and cooling systems, appliances, and hot water, are considerations that need to be taken into account in the design of zero-energy buildings (Zero energy, 2018).

Merely reducing operational energy is not sufficient to ensure sustainability, and that embedded energy must be considered together with operational energy, as examined through the life cycle assessment (LCA) of embedded and operational energy concepts in buildings (Koç et al. 2022). Beşiroğlu and Özmen, it is argued that within the sustainable housing sector, the life cycle assessment system should support the concept of sustainability

in many economic, social, and environmental aspects. Buildings that encompass a large portion of energy consumption are concluded to be insufficient for living a sustainable future through structural transformation alone (Beşiroğlu, Özmen, 2022).

Akyürek et al. (2019), the energy and environmental performances of the ideal buildings constructed in Erzurum and Antalya were examined using the Building Energy Performance Program. As a result of the study, the building's greenhouse gas emissions were detected, and the relevant building was evaluated in terms of the energy class specified in the Energy Identity Documen. In the study by Aydın (2019), six projects conducted by public institutions, local governments, and European Union member countries aimed at increasing energy efficiency in buildings were examined, and the benefits of these projects were highlighted along with a general evaluation by Aydın and Canım (2017), the usability of the BEP-TR1 program was investigated through interviews with Energy Identity Certificate experts in Trabzon province, and deficiencies and issues in the Energy Identity Certificate application in Turkey were identified and recommendations were made.

Basic Elements of Energy Identification:

1. Energy Consumption: Measurement of the energy consumption level of buildings, industries, or regions.

2. Energy Efficiency:Evaluation of whether the energy used is being utilized efficiently.

3. Resources: Analysis of the energy sources used (fossil fuels, renewable energy, etc.).

4. Environmental Impacts: Evaluation of the environmental effects of energy production and consumption processes.

5. Policies: Review and improvement of existing energy policies in the energy identification process.

1. Energy Certification in Turkey and The Situation in Turkey

Turkey is taking significant steps in terms of energy identification. Although there are various laws and regulations promoting energy conservation, more work needs to be done on energy efficiency. In recent years, investments in renewable energy sources have been increasing, which supports efforts to ensure energy diversity and security.

Renewable Energy Investments: Turkey is trying to reduce its dependence on fossil fuels by investing in renewable sources such as solar and wind energy.

Energy Efficiency Policies: In addition to projects and regulations that promote energy efficiency, the energy performance of buildings is evaluated through energy identity certificate applications.

International Goals: International agreements such as the Paris Climate Agreement are prompting Turkey to take on more responsibility in energy identification and greenhouse gas reduction.

In short, energy identification is of vital importance not only for the development of energy policies but also for economic, environmental, and social sustainability for Turkey and the world.

The software and applications used in the energy certification processes in Turkey include various tools for measuring, monitoring, and evaluating the energy performance of buildings. Below, the main software and applications used for energy identification in Turkey and the activities carried out in this process are explained.

1.1. Used Software and Programs

Building Energy Performance Certificate (EKB) Software: This is the official software used to perform the necessary calculations to obtain a building energy performance certificate in Turkey. This software has been approved by the Ministry of Energy and Natural Resources and developed to ensure compliance with standards.

Energy Performance Reporting Software: Applications of the Ministry of Environment, Urbanization and Climate Change of the Republic of Turkey:The ministry has developed various software to measure the energy performance of buildings. These software programs facilitate users' energy efficiency calculations and comparison.

Autodesk Ecotect Analysis and Similar Software: These are programs used during the architectural design phase to evaluate the thermal performance of buildings, energy consumption, daylight analysis, and climatic conditions.

Simulation Software: EnergyPlus, TRNSYS: These types of software allow for a more detailed analysis of a building's energy performance by conducting energy simulations.

*Smart Energy Management System (EMS):*These are systems used to monitor and manage energy consumption in buildings. Thanks to these systems, real-time data analysis can be conducted, increasing the potential for energy savings.

2. Energy Efficiency Analyses

Studies on energy performance analyses using EKB software, examining buildings' energy consumption data and evaluating energy efficiency potential.

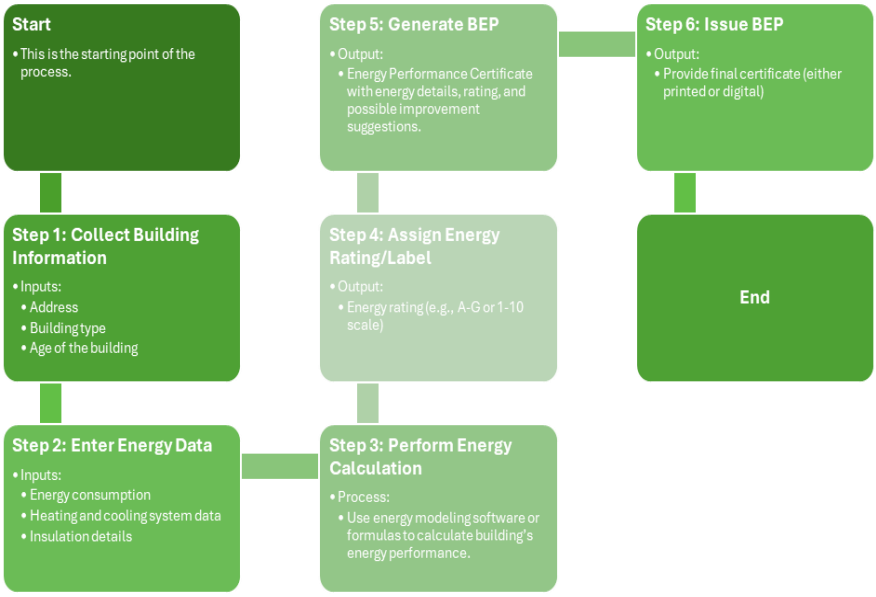

Figure 1: Step-by-step BEP Tr application

- In determining the energy performance of a building in BEP-TR, the following steps are followed (Figure 1):
- Annual energy consumption is determined (per m^2)
- CO_2 emissions are calculated based on the determined value,
- The values are compared with the values of a reference building, As a result of the comparison, the building is placed in an energy class between A-G (BEP-TR-Figure 2)

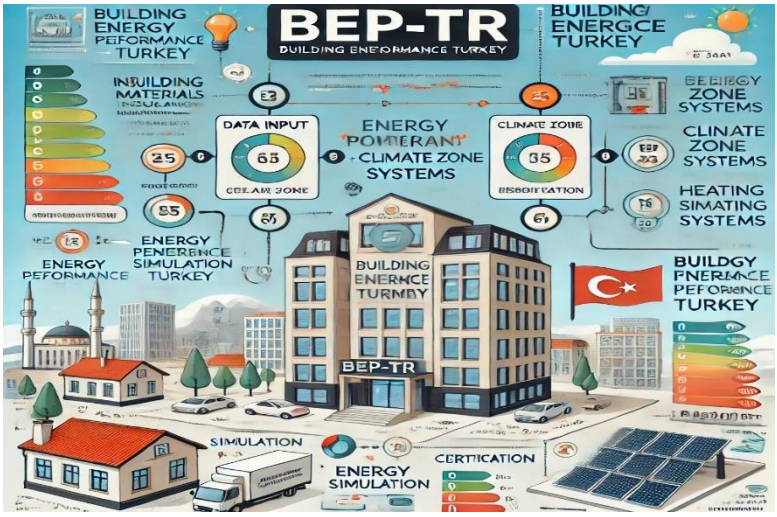

Figure 2: BEP TR application

The building's energy performance is determined by using different energy classes. These energy classes are composed of the letters A, B, C, D, E, F, and G, respectively. Energy classes and energy performances ar shown in Table 1. When the data in Table 1 is examined, it is observed that Class A has the lowest energy consumption, while Class G has the highest energy consumption.

The building data recorded in the BEP-TR program is used to determine the building's energy class. To ensure that the energy performance of buildings is at an acceptable level,

Table 1: Energy Class Values

Energy Class	**Ep** intervals
A	0-39
B	40-79
C	80-99
D	100-119
E	120-139
F	140-174
G	175-..

In order to draw attention to simple measures that can be taken to limit energy consumption, the BEP-TR application has been tested with different materials based on the concept of energy. With the obtained data, an analysis was conducted considering the materials affecting energy performance and their costs.

To compare and evaluate energy consumptions in energy identification, three buildings with different characteristics were selected in

Kahramanmaraş, and their identification was carried out. For the energy class of these three buildings, heating, hot water, cooling, and lighting energies have been calculated. After the calculations of the buildings per unit area were completed, energy identities were obtained for the buildings (Table 2). The energy class of two of these buildings has been identified as 'C' and the other as 'B'.

Table2: Buildings and information's Example Application

	B	**C**	**D**	**E**
Info	1 bas. and 9 regular floors, making it a total of 10 floors. The floor height is 3.38m.	1 bas. and 7 normal floors, making it a total of 8 floors. The floor height is 3.00m.	9 normal floors. The floor height is 3.00m.	8 normal floors. The floor height is 3.00m.
Total Area	4596.75m²,	1651	3600m²,	2329.16m²,
Air-conditioned area	4596.75m²,	1651	3096m²,	1964.55m²,
Net area	4351.43m².	1045.71m².	2922.40m².	1757.76m².
Wall-weighted U value	0.4	0.46	1.22	1.11
Column-weighted	0.00	0.00	3.24	0.00
Beam-weighted U value	.53	0.00	3.23	3.24
Ground floor-weighted U value	0.57	0.51	0.77	0.56
Cantilever floor-weighted U value	0.00	0.00	0.00	0.00
Roof-weighted U value	0.56	0.38	2.43	0.32
Wndow-weighted U value	1.20	1.10	3.30	2.70
Door-weighted U value	0.00	4.00	3.84	0.00

RESULTS AND DISCUSSION

The energy identity document of a structure reflects many of its characteristics. If we generalize, the likelihood of buildings with D and E class energy identity certificates being old structures is very high. Class B and C energy identity certificates are generally more commonly found in new buildings. Here, it can be concluded that the materials used in buildings are being developed, more importance is being given to insulation, and there are innovations in energy savings in heating and cooling systems. Regarding our topic, the structural information and energy performance of the 4 buildings above have been provided, and here Building B has a Class B energy identity certificate, while the energy classes of Buildings C, D, and E have been named according to their class names.

Here, building B and building C will be compared with each other, and building D and building E will be compared with each other.

Building B has consumed a total of 322,705.09 kWh/year, while Building C has consumed a total of 114,961.65 kWh/year. Although Building B has consumed more energy, due to its larger area, looking at the annual energy consumption per unit area will give us a better idea for comparison.

It is observed that a building with a B class energy identity certificate consumes 70.20 kWh/m²/year of energy per unit area, while a building with a C class energy identity certificate consumes 97.48 kWh/m²/year of energy per unit area. Considering that the range for a Class B energy identity certificate is 40-79 kWh/m².year and the range for a Class C energy identity certificate is 80-99 kWh/m².year, it can be seen that our Class B structure is closer to a Class C energy identity certificate, while our Class C structure narrowly avoided falling into the Class D energy identity certificate category.

Here, a comparison will be made between the two buildings based on their expenses in heating, sanitary hot water, cooling, ventilation, and lighting.

It is observed that the heating consumption of Building B is 26.61 kWh/m². year, while that of Building C is 40.64 kWh/m². year. Here, the higher unit energy consumption of Building C indicates that its insulation properties are lower. To improve the energy performance of Building C, it is recommended to insulate the building walls, insulate the existing mechanical systems, especially the valves, pipes, and bodies, maintain the heating systems in the open air or use them within the building's interior, renew the windows to reduce uncontrolled air leakage and thermal transmission, leave the necessary openings if there is excessive ventilation within the building, and perform timely maintenance and repairs on the heating systems.

-It is observed that the sanitary hot water energy consumption of Building B is 18.50 kWh/m². year, while that of Building C is 17.09

kWh/m². year. Here, it is observed that the hot water unit energy consumption of building C is better than that of building B. Here, it can be suggested that the hot water heating system of Building B transition to a more efficient structure, utilize waste heat to produce hot water, and benefit from solar energy (Table 3).

-It is observed that the cooling energy consumption of Building B is 20.68 kWh/m². year, while that of Building C is 30.54 kWh/m². year. Again, it is observed that Building C has a lower insulation property, just like in heating.

-It is observed that the lighting energy consumption of Building B is 4.42 kWh/m². year, while that of Building C is 9.22 kWh/m². year. Here in Building C, it is recommended to replace magnetic ballasts with electronic ballasts, implement time, motion, and daylight-dependent control in certain areas, and prefer more energy-efficient lighting systems.

The D building has consumed a total of 440,015.04 kWh/year, while the E building has consumed a total of 391,587.75 kWh/year. It is observed that the building with a D class energy identity document consumes 142.12 kWh/m²/year per unit area, and the building with an E class energy identity document consumes 199.33 kWh/m²/year per unit area.

Here, a comparison will be made between the two buildings based on their expenses in the areas of heating, sanitary hot water, cooling, ventilation, and lighting.

It is observed that the heating consumption of building D is 92.63 kWh/m². year, while that of building E is 124.01 kWh/m². year. Here, the higher unit energy consumption of Building D indicates that its insulation properties are lower.

To improve the energy performance of Building E, it is recommended to insulate the building walls, insulate the existing mechanical systems, especially the valves, pipes, and bodies, maintain the heating systems in the open air or use them within the building's interior space, renew the windows to reduce uncontrolled air leakage and thermal transmission, leave the necessary openings if there is excessive ventilation within the building, and perform timely maintenance and repairs on the heating systems.

It is observed that the sanitary hot water energy consumption of building D is 17.85 kWh/m². year, while that of building E is 18.02 kWh/m². year. Both structures are very close to each other here.

It is observed that the cooling energy consumption of building D is 26.98 kWh/m². year, while that of building E is 46.86 kWh/m². year. Again, it is observed that the E building has a lower insulation property, just like in heating.

It is observed that the lighting energy consumption of Building D is 4.67 kWh/m². year, while that of Building E is 4.05 kWh/m². year. Here in Building D, it is recommended to replace magnetic ballasts with electronic

ballasts, implement time, motion, and daylight-dependent control in certain areas, and prefer more energy-efficient lighting systems.

It is observed that the ventilation energy consumption of building D is 0.00 kWh/m². year, while that of building E is 6.38 kWh/m². year. The D Building does not have a ventilation system, and it is observed that the building provides ventilation within itself, while the E Building additionally has a mechanical ventilation system and consumes more energy compared to the D Building (Table 3).

Table 3: Comparison of Buildings

	Comparison of Building B and Building C		***Comparison of Building D and Building E***	
Buildings	**B**	**C**	**D**	**E**
Energy Consumption:	Annual 322,705kWh/year, 70.20kWh/m². year per unit area	Annual 114,961.65 kWh/year, 97.48 kWh/m². year per unit area.	Annual44 0,015.04 kWh/year, 142.12 kWh/m². year per unit area.	Annual 391,587.75 kWh/year, 199.33 kWh/m². year per unit area.
Heating Costs:	26.61 kWh/m². year;	C: 40.64 kWh/m². year (C has weaker insulation properties).	92.63 kWh/m². year;	124.01 kWh/m². year (E's condition is worse).
Sanitary Hot Water Consumption	18.50 kWh/m². year;	17.09 kWh/m². year (C Beter).	17.85 kWh/m². year;	18.02 kWh/m². year (close values).
Cooling Expenses	20.68 kWh/m². year;	30.54 kWh/m². year (C's insulation condition is insufficient).	26.98 kWh/m². year;	46.86 kWh/m². year (E's condition is worse).
Lighting Expenses	4.42 kWh/m². year;	9.22 kWh/m². year (There are energy efficiency improvement suggestions for C).	4.67 kWh/m². year	4.05 kWh/m². year (Energy efficiency recommendations are available in D).
Ventilation Expenses	-	-	0.00 kWh/m². year (no ventilation)	6.38 kWh/m². year (mechanical ventilation present).

CONCLUSIONS

Energy identification is an important process in Turkey and is necessary to achieve both environmental sustainability and economic gains. The software and applications used aim to increase energy efficiency by enabling this process to be managed more effectively and efficiently. Additionally, it contributes to efforts to save energy and reduce environmental impacts.

Energy Efficiency Comparison: Building Performances General Observations:

Old Structures: Buildings with D and E class energy identity certificates are generally more likely to be old.

New Buildings: Class B and C energy identity certificates are more common in newly constructed buildings.

Energy Consumption

Heating: Heating consumption is comparable across all buildings.

Analysis: All buildings show similar heating energy consumption, indicating that the heating efficiency is quite consistent. However, differences in insulation properties may still exist.

Sanitary Hot Water:The energy consumption for sanitary hot water shows a very small difference between Building B and Building C.

Analysis: There is only a minor difference in hot water energy consumption between Building B and Building C, suggesting that both buildings have similar hot water systems and efficiency levels.

Cooling: Cooling consumption is particularly higher in Building E.

Analysis: Building E consumes significantly more energy for cooling compared to the other buildings, which may be due to poor insulation, a higher cooling load, or different cooling systems in place.

Lighting: Building C consumes more energy for lighting, while Building D uses less.

Analysis: Building C has higher lighting energy consumption, which could be due to inefficient lighting systems or greater use of artificial lighting. In contrast, Building D is more energy-efficient in terms of lighting.

Ventilation: Building E has a mechanical ventilation system and consumes energy in this category.

Analysis: Since Building E is equipped with a mechanical ventilation system, it uses more energy for ventilation compared to the other buildings, which either rely on natural ventilation or do not have such systems.

The energy efficiency of Buildings B and D is better than that of Buildings C and E. More insulation and mechanical system improvements are recommended. Buildings C and E show weaknesses in terms of energy efficiency and require improvement.

REFERENCE

Akyürek Z., Akyüz A.Ö. and Güngör A., (2019). Investigation of Ideal Buildings in terms of Energy Performance Value and Energy Identity Certificate in Antalya and Erzurum. *Uluslararası Mühendislik Tasarım ve Teknoloji Dergisi*, 1: 36-41,

Anbarcı M. Giran O, Demir İ.H. (2012). Uluslararası Yeşil Bina Sertifika Sistemleri ile Türkiye'deki Bina Enerji Verimliliği Uygulaması. *NWSA-ENGINEERING SCIENCES* e-Journal of New World Sciences Academy 2012, 7, 1.

Aydın Ö. (2019). Binalarda Enerji Verimliliği Kapsamında Yapılan Projelerin Değerlendirilmesi: Türkiye Örneği. *Mimarlık ve Yaşam*, 4: 55-68.

Aydın Ö., Saylam Canım D., (2017). Evaluation of the Usability of the Building Energy Performance Calculation Method (BEP-TR1) and the Energy Performance Certificate (EPC) Application. *Architecture and Life,* 2: 265-277.

BEP, Binalarda Enerji Performansı Yönetmeliği. (2010, 1 Nisan). Resmi Gazete (Sayı: 27539) 1511.2024 tarihinde https://www.resmigazete.gov.tr/eskiler/2010/04/20100401-5.htm

Beşiroğlu, Ş. and Özmen, E. (2022). Yaşam Döngüsü İçerisinde Sürdürülebilir Konut Alanı Değerlendirme Sistemi: Vauban (Freiburg, Almanya) Örneği. *DergiPark,* (13). https://doi.org/10.31198/idealkent.1099393

Dari İ (2024). Sürdürülebilir yapı malzemelerinin konut yapılarında kullanımına yönelik yaşam döngüsü enerji verimliliğin değerlendirilmesi, Thesis Department of Architecture, Graduate School of Social Sciences, Maltepe University, February 2024.

Koç, İ. Duru, M. O. and Dinçer, S. G. (2022). Yapılarda Gömülü ve Kullanım Enerjisi Kavramlarının Yaşam Döngüsü Değerlendirmesi (YDD) Metodolojisiyle İrdelenmesi, bab *Journal of FSMVU Faculty of Architecture and Design*. 3 (1), s. 55-69.

Zero energy (t.y.). zero-energy-home-construction-design. 20.10.2024 https://zeroenergyproject.org/build/twelve-steps-affordable-.

The Effects of The Geometrical Parameters of PCM Layer on Air Temperature in Lightweight Buildings

Başak METİN[1]
Halil BAYRAM[2]

1- Mechanical Engineering Department, Graduate School of Natural and Applied Sciences, Amasya University, Amasya, 05100, Turkey. basakkmetin@gmail.com ORCID: 0009-0006-5423-7515
2- Assoc. Prof. Dr.; Mechanical Engineering Department, Engineering Faculty, Amasya University, Amasya, 05100, Turkey. halil.bayram@amasya.edu.tr ORCID: 0000-0002-4664-3883

ABSTRACT

Considering that the amount of energy used to meet the indoor heating demands of buildings is quite significant, it is thought that using this energy efficiently is very important. The rate of buildings with lightweight building walls, which is increasingly used because it is lighter and easier to construct, is also increasing nowadays. However, since the thermal mass in these buildings is less than conventional brick buildings, changes in the building's indoor air temperature values can occur more quickly. Different methods have been developed to satisfy the thermal comfort in buildings with this type of wall structure. One of the most important of these is the use of phase change materials. These types of materials, which can later use the latent heat they have stored during the phase change. In this study, a three-dimensional simulation model of a building with a lightweight building wall structure was created. The position of the phase change material layer within the lightweight building wall was gradually changed and the effects of this change on indoor air temperature values and distributions were numerically investigated. The computational fluid dynamics analyses were performed for 24 hours. According to the results, when phase change material was not used, the average temperature value of the air volume at 24 hours was approximately 2°C, while when phase change material was used, this value increased to approximately 21°C. It was also determined that the use of phase change material played a very important role in reducing vertical temperature fluctuations within the air volume.

Keywords – Lightweight Building Wall; Phase Change Material; Latent Heat; Thermal Performance; Computational Fluid Dynamics.

INTRODUCTION

Today, due to increasing environmental concerns, efficient use of existing energy is becoming increasingly important. Efficient use of energy is also important in meeting the heating demands of buildings, which have a significant share in energy use. Studies on this subject are increasing day by day, especially in lightweight building walls (LBWs), which have been increasingly used in recent years. Phase change material (PCM) is used in buildings with these types of walls to both prevent temperature fluctuations and increase energy efficiency (Hou et al., 2022, Bayram and Koç, 2023). When the studies on this subject are examined, the parameters of PCM integrated into LBW such as location, transition temperature, thickness, latent heat, specific heat, thermal conductivity, density were examined in detail. They concluded that it increased thermal energy efficiency by balancing temperature fluctuations and the delay time of the region with PCM increased

by 6.86 hours, and the attenuation rate decreased by 90.45% (Hou et al., 2021). Prefabricated Temporary Houses (PTH) are structures frequently used in emergency disaster management to meet the need for temporary shelter. They added PCM to these houses in the summer months. They presented that when fixed PCM is installed, PTH can reduce the daytime indoor temperature and prevent the sweltering heat in the summer months. In addition, they stated that the mobile PCM Based Energy Storage System (PESS) showed a decrease in indoor temperature in the range of 3.2-3.6 °C (Wang et al., 2018). Yang et al. suggested that when PCM-based lightweight wall (LW) panels are positioned on the outer surface and inner surface, the delay time of the inner surface compared to the outer surface increases from 2.9 hours to 4.1 hours, and therefore, positioning in the inner parts will be efficient in thermal improvements (Yang et al., 2018). They examined the modeling of the improvement of the ultrathin envelope thermal performance of a prefabricated house with PCM in accordance with the climate of Chengdu city in China (Wang et al., 2013). In another study, they concluded that the heat storage rate of PCM in the composite phase change wall (PCW) on the typical 2-gap condition is 75.07% in the long range and 70% in the short range (Li et al., 2019). Kuznik et al., 2 cubic MICROBAT test cells with and without PCM were placed in the climatic chamber and verified the structures with numerical modeling by comparative experiments. To make all these verifications, they emphasized the importance of the hysteresis effect (Kuznik et al., 2009).

Zhang et al. (2011) established a heat conduction model covering the solidification and melting process based on the enthalpy-porosity approach. They compared the thermal behavior of the brick wall with PCM added to it with the common solid bricks. They emphasized that the thermal energy storage and latent heat storage rate of the bricks with PCM integrated are higher (Zhang et al., 2011).

A simulation model was created by filling the hollow bricks with PCM material and comparing them with the experimental data. The attenuation rate decreased from 13.07% to 0.92-1.93%. It was observed that the delay time increased from 3.83 hours to 8.83-9.93 hours (Gao et al., 2020). There are quite extensive studies in the literature on the addition of PCMs to building materials in passive applications. In this article, they performed analyses on PCM-integrated plasterboard using the Apache simulation package. They examined the board's alternating conductivity and different ventilation rates in hot weather conditions. They concluded that 22° C is the optimum temperature for phase change and that it can be reduced by 80% when exceeded by 24° C (Kendrick and Walliman, 2007). In another study, the use of PCM in portable LBWs is of great importance in terms of energy savings in heating and cooling situations were investigated. The researchers stated that optimizing the melting point temperature of PCM is also an important factor (Marin et al., 2016).

The addition of PCM to the walls and roof of the LBW in the cities of Calama and Antofagasta in Chile reduced energy consumption by 84.4% and 51.4%, respectively (Vega et al., 2022). In order to provide thermal comfort in the summer months in LBW, two different PCM types (PCM-A and PCM-B) were added to the wall panels were considered. The location of the PCM wall panels, the highest melting temperature value and the effect of the ventilation rate on efficiency should be considered (Evola and Marletta 2014).

Two-layer ceramic tiles, where wood waste is used to create pores, were impregnated into the wood by vacuuming. These tiles helped to provide thermal comfort by controlling the indoor temperature. The optimum situation is that PCM is 5.4% by weight. PCM integrated ceramic tiles minimized the duration of heating/cooling processes in the building compared to traditional ceramic tiles and provided energy efficiency (Novais et al., 2015). They designed 3 wall samples arranged differently for testing in winter and summer seasons. In the walls where encapsulated PCM spheres were integrated, the internal surface temperature amplitude decreased by a maximum of 0.73 °C (21.4%) in summer and 0.88 °C (23.9%) in winter. Thus, PCM spheres provided an annual average energy saving of 17.7% in the first layer, 20.2% in the second layer and 23.1% in the last layer (Sun et al., 2019). Heating, Ventilation, and Air Conditioning (HVAC) systems constitute 60% of energy consumption in buildings. By mixing PCMs into building materials with different methods, the heat storage and release properties of the materials can be improved. It was observed that PCM-filled windows significantly reduced the highest temperatures up to 9 °C (Reddy et al., 2024). Abbas et al. created an experimental and numerical study area to investigate 2 different walls with and without PCM and the natural convection inside the room. They showed that it will reduce the inner surface wall and room temperature by 4.7 °C (Abbas et al., 2021).

As can be seen from the literature review, the use of PCMs in buildings is increasing day by day. In this study, the effects of adding PCMs to these wall models were numerically investigated to increase the thermal performance of LBWs at low ambient temperatures.

MATERIALS AND METHODS

In this study, a three-dimensional LBW model was created to simulate a building with a PCM inside it. This model also includes a PCM layer. In addition, a 600*600*600 mm air model was added to this model to examine the effects on indoor air temperature values, and the whole simulation model was obtained. A model without PCM was also used in the study for reference. A total of 8 different models were generated in the study and three-dimensional CFD analyses were performed with these models. These models are shown schematically in Figure 1.

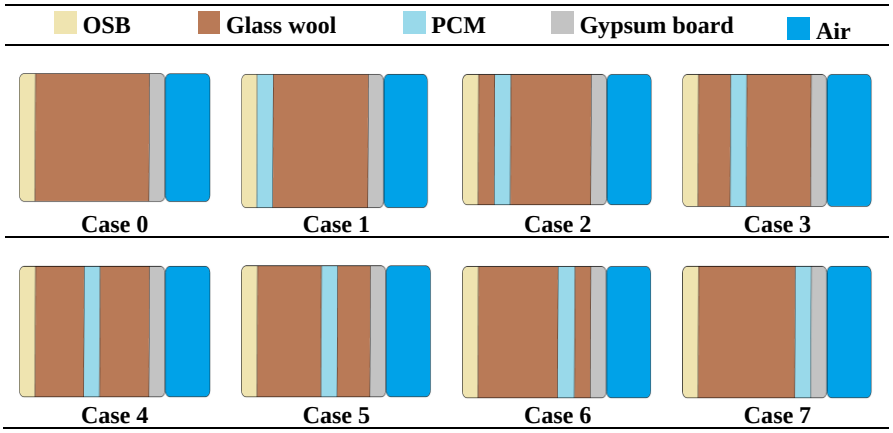

Figure 1: Schematic Views of The Generated LBW Models

The thicknesses of the OSB, PCM and gypsum board layers here were determined as 12, 10 and 10 mm, respectively, and these thicknesses were kept constant in all analyses. The total thickness of the glass wool layer is 60 mm. However, due to the gradual displacement of the PCM layer in Case 2, 3, 4, 5 and 6, the glass wool layer consists of two regions in these cases. In addition, the height and width of all layers were determined as 600 mm. The thermophysical properties of these layers used in the analyses were assumed to be constant and are presented in detail in Table 1.

Table 1: The Thermophysical Properties of The Model

Material	**Phase-transition temperature** [°C]	**Phase change latent heat** [kj/kg]	**Thermal conductivity** [W/(mK)]	**Specific heat** [J/(kgK)]	**Density** [kg/m^3]
PCM	20-22	200	0.2	2000	800
Air	-	-	0.0242	1006.43	1.225
OSB	-	-	0.105	1400	593
Glass wool	-	-	0.035	1220	40
Gypsum board	-	-	0.33	1050	1050

In the CFD analyses to be performed with these 8 models, the ANSYS-Fluent software package program was used to solve the conservation equations. In addition, the same program was used for the mesh generation process. The generated mesh structure consists of approximately 900000 elements in all cases. The isometric view of the generated mesh structure of Case 1 can be shown in Figure 2.

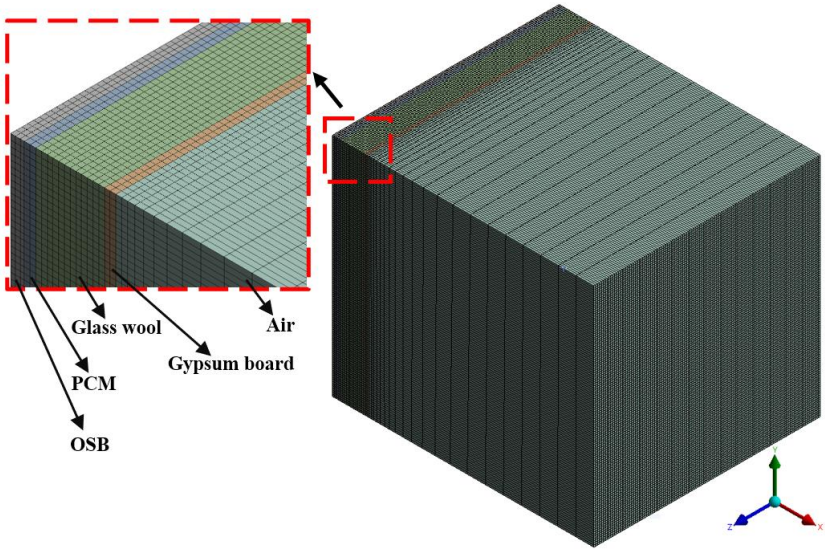

Figure 2: Isometric View of The Mesh Structure

In the analyses, the outer surface of the OSB board was considered to interact with the outdoor environment. For this reason, a heat transfer coefficient boundary condition of 20 W/(m^2K) was defined for the outer surface of this layer. In addition, the outdoor temperature was determined as 0 °C. Adiabatic boundary condition was defined for the outer surfaces of the other layers and the air volume. The initial temperature value was determined as 26 °C for all layers and air. The analyses were carried out in a transient regime for a total of 24 hours. In addition, iterations at each time step were continued until the residuals of the continuity and momentum equations were less than 10^{-3} and the residuals of the energy equation were less than 10^{-8}.

RESULTS AND DISCUSSIONS

This study investigated the changes in indoor air temperature values in buildings with LBW, which is increasingly used today, with numerical analyses for 24 hours. In these analyses, the effects of the PCM layer in the LBW model were also examined. The results obtained from the numerical studies are given in detail below.

Figure 3 shows the changes in the liquid fraction values of the PCM layers in the LBW wall model over time. According to the figure, it is seen that the PCM layers completely transition from the liquid phase to the solid phase in the first three cases at the end of the analysis. In Case 4, although a very high rate of solidification is observed, it can be said that it is almost

completely solidified. It was also determined that the solidification rate decreased as the position of the PCM layer approached the indoor environment. In addition, the difference in the solidification rates between the two cases decreased as the PCM layer approached the indoor environment.

In Case 1, where the PCM layer was positioned closest to the outdoor environment, the PCM layer completely solidified in approximately 4 hours. After this time, this layer allowed heat transfer by direct conduction. In Case 2, the PCM layer was shifted one step towards the indoor environment. In addition, in this case, it was divided into two layers of 10 and 50 mm due to the location of the PCM layer. Complete solidification occurred in approximately 11 hours in Case 2. This value lasted approximately 18 hours for Case 3. It can be said that Case 4 had a solidification rate of approximately 95% at the end of the analysis. This value was seen as approximately 75% and 60% in Cases 5 and 6, respectively. In Case 7, where the PCM layer was closest to the indoor environment and the glass wool layer was a single piece, almost half of it was solidified at the end of the analysis.

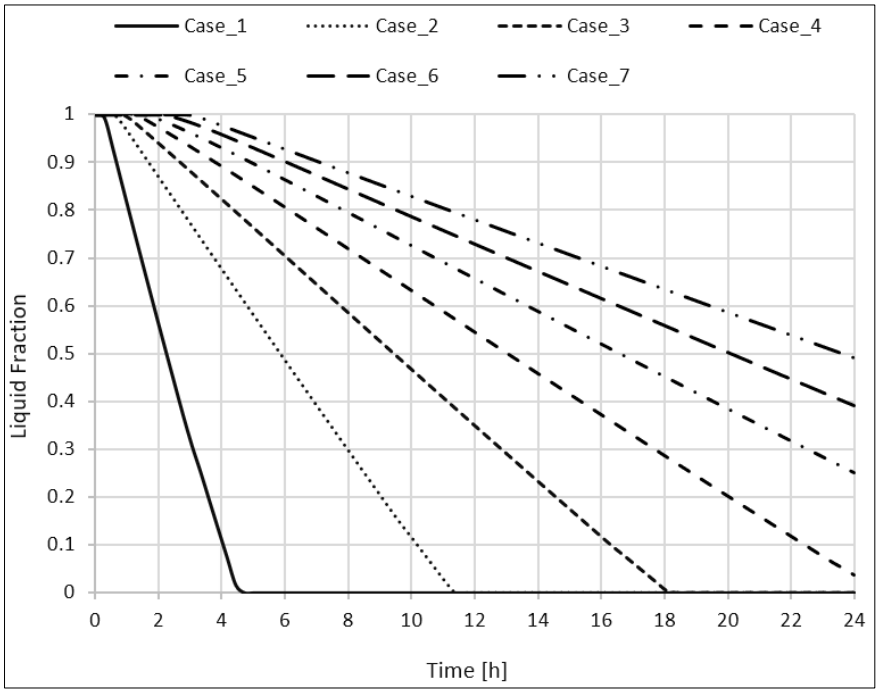

Figure 3: Liquid Fraction Values of The PCM Layers

The average temperature values of the air volume modeled to represent the indoor air of a building are given in Figure 4. When the values in this figure are examined, almost no temperature change was observed during the first hour in all cases. Afterwards, the temperatures decreased by following

different slopes according to the status of the LBW layer. The temperature values of Case 0, which is the case without a PCM layer in the LBW layer, were lower than all other cases. It is known that the initial temperature value of all cases was 26 °C. The average temperature value of the air in Case 0 was determined to be approximately 2 °C at the end of the analysis. And it reached this value by continuously decreasing after the first hour. When the results of the cases with LBW wall models containing a PCM layer are examined, the change of state of the PCM layer delayed the decrease in the air temperature values. Considering that the PCM solidified completely in approximately 4 hours in Case 1, a relatively smaller decrease in the air temperature value was observed during this period. In fact, this delay observed in the rapid decrease in the air temperature value continued for a while after the solidification process was over. At the end of the analysis, a temperature value of approximately 2.5 °C was observed.

The decrease in the air temperature value in Case 2, where the solidification process was completed in approximately 11 hours, continued at a lower rate until the solidification was completely completed and then at a relatively higher rate. At the end of the analysis, a temperature value of approximately 6.5 °C was observed. In Case 3, an air temperature of approximately 15 °C was determined at the end of the analysis. This increase in the temperature value was due to the solidification process of the PCM layer lasting approximately 18 hours.

The temperature values in the other cases where the PCM layers were not completely solidified showed minor differences during the first 12 hours and had very similar temperature values after 12 hours. When the PCM layer was positioned closer to the indoor environment, relatively higher temperature values were observed. However, especially between the 12th and 16th hours, the temperature values of these cases were almost the same. It should also be noted that the solidification rates of all these cases were below 50% during this time. At the end of the analysis, it can be said that the temperature values of these cases were approximately 21 °C.

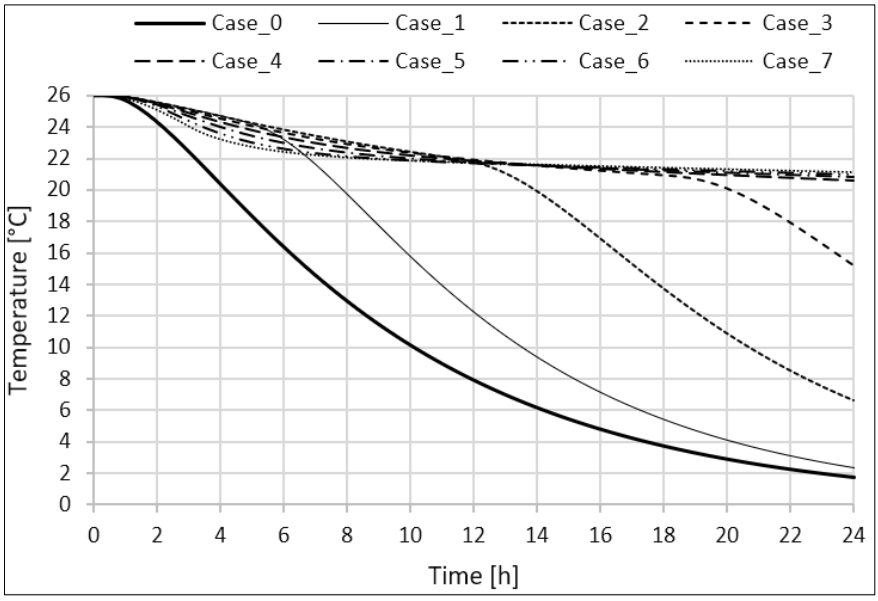

Figure 4: Average Temperature Values of Air Volume

The temperature values taken from the points at 100, 300 and 500 mm heights defined in the middle sections of the x and z axes of the air volume shown in Figure 2 are given in detail in Figure 5. The temperature values of Point 1, which is the lowest height in all cases, were determined to be the lowest. Considering that the hot air rises with natural convection due to the density difference, the temperature values of Point 3, which is the highest point, were the highest in all cases. It was also observed that the temperature values increased with increasing height. In cases where the solidification of PCM was completed (Case 1, 2 and 3), a softer temperature decrease was observed during solidification, while a more severe decrease was observed with the completion of solidification. In addition, while the temperature differences between the vertical temperature values were quite low before solidification in these cases, this temperature difference increased after solidification. For this reason, it can be concluded that the use of PCM can prevent temperature fluctuations in the indoor environment. In addition, it was determined that there were very low temperature differences between the vertical temperature values in the other cases where the phase change in the PCM layer continued throughout the analysis.

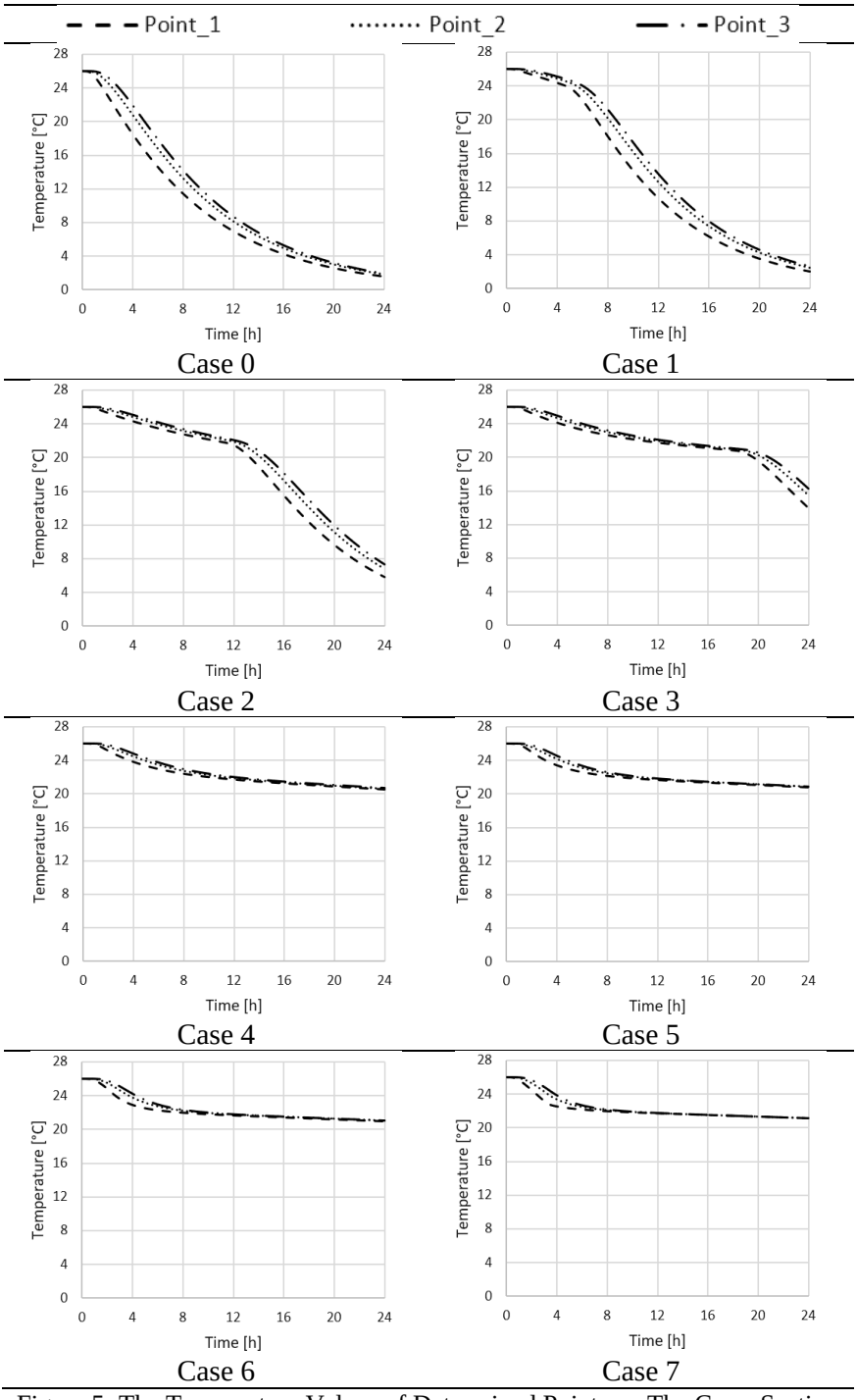

Figure 5: The Temperature Values of Determined Points on The Cross Section

The temperature distributions in the cross-sectional area of the created three-dimensional CFD model were also examined (Figure 6). When the temperature distributions examined at 6-hour periods are examined, it can be easily said that the PCM layer has a positive effect on the indoor temperature distribution even when it is positioned in the region closest to the outdoor environment. It is seen that the indoor environment has a higher temperature distribution as the location of this layer is moved away from the outdoor environment. It was observed that there was a very similar temperature distribution in the indoor air, especially in Cases 4, 5, 6 and 7, where the phase change was not completed. On the other hand, it was observed that the LBW temperature distributions of these cases had lower temperature distributions when the PCM layer was positioned closer to the indoor environment.

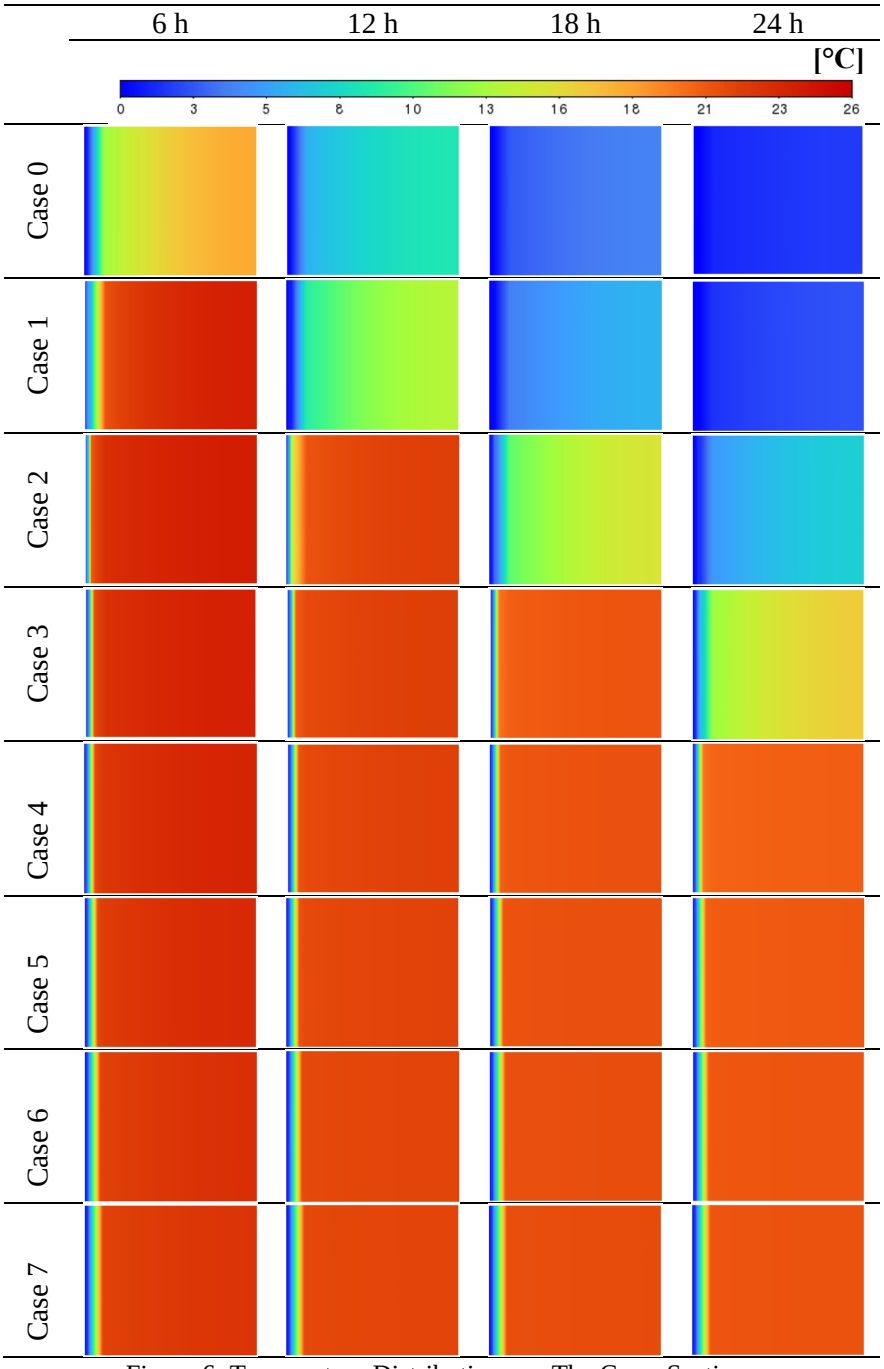

Figure 6: Temperature Distributions on The Cross Sections

CONCLUSIONS

In this study, three-dimensional CFD analyses were performed to investigate the effect of the PCM layer located within the LBW on the indoor air temperature value and distribution. Analyses were performed in a transient regime for 24 hours. The main results obtained from the numerical study are listed below.

- As the position of the PCM layer approaches from the outdoor to the indoor, decreases in the solidification rate are observed.
- While the complete PCM solidification process of the case closest to the outdoor environment was approximately 4 hours, the case farthest from the outdoor environment only observed approximately 50% PCM solidification at the end of the analysis.
- When the indoor air temperature values were examined, no change was observed in the average temperature of the air during the first hour in all cases. Afterwards, decreases were observed at different speeds depending on the location of the layer in cases with a PCM layer.
- In Case 0 without PCM layer, the air temperature value was determined as approximately 2 °C at the end of the analysis, while in Case 7 with PCM layer, this value was determined as approximately 21 °C.
- In cases where the phase change was completed quickly, a relatively delayed decrease in temperature values was observed. On the other hand, in cases where the phase change was observed over a longer period, the temperature low curves were similar to the liquid fraction curves.
- When the vertical changes in the temperature values in the middle section of the indoor air are examined, higher temperature values are obtained at high points due to the density difference in the indoor environment.
- While the temperature differences between the vertical temperature values during the phase change of the PCM layer are quite low, the difference between these values increased when the phase change was completed.
- It was observed that the use of PCM contributed to the reduction of vertical fluctuations in the indoor air temperature distribution.

ACKNOWLEDGMENT

The authors would like to thank the Amasya University Scientific Research Projects (BAP) Coordination Department for supporting this research under Project No. FMB-BAP 23-0060.

REFERENCES

Abbas, H. M., Jalil, J. M., and Ahmed, S. T. (2021). Experimental and numerical investigation of PCM capsules as insulation materials inserted into a hollow brick wall. Energy and Buildings, 246, 111127.

Bayram, H., & Koc, N. (2023). Experimental investigation of the effects of add-on fan radiators on heat output and indoor air temperature. Case Studies In Thermal Engineering, 50, 103432.

Evola, G., and Marletta, L. (2014). The effectiveness of PCM wallboards for the energy refurbishment of lightweight buildings. Energy Procedia, 62, 13-21.

Gao, Y., He, F., Meng, X., Wang, Z., Zhang, M., Yu, H., and Gao, W. (2020). Thermal behavior analysis of hollow bricks filled with phase-change material (PCM). Journal of Building Engineering, 31, 101447.

Hou, J., Meng, X., and Dewancker, B. J. (2021). A numerical study on the effect of phase-change material (PCM) parameters on the thermal performance of lightweight building walls. Case Studies in Construction Materials, 15, e00758.

Hou, J., Huang, Y., Zhang, J., Meng, X., & Dewancker, B. J. (2022). Influence of phase change material (PCM) parameters on the thermal performance of lightweight building walls with different thermal resistances. Case Studies in Thermal Engineering, 31, 101844.

Kendrick, C., and Walliman, N. (2007). Removing unwanted heat in lightweight buildings using phase change materials in building components: simulation modelling for PCM plasterboard. Architectural Science Review, 50(3), 265-273.

Kuznik, F., and Virgone, J. (2009). Experimental investigation of wallboard containing phase change material: Data for validation of numerical modeling. Energy and Buildings, 41(5), 561-570.

Li, Y., Long, E., Jin, Z., Li, J., Meng, X., Zhou, J., ... and Xiao, D. (2019). Heat storage and release characteristics of composite phase change wall under different intermittent heating conditions. Science and Technology for the Built Environment, 25(3), 336-345.

Marin, P., Saffari, M., de Gracia, A., Zhu, X., Farid, M. M., Cabeza, L. F., and Ushak, S. (2016). Energy savings due to the use of PCM for relocatable lightweight buildings passive heating and cooling in different weather conditions. Energy and Buildings, 129, 274-283.

Novais, R. M., Ascensão, G., Seabra, M. P., and Labrincha, J. A. (2015). Lightweight dense/porous PCM-ceramic tiles for indoor temperature control. Energy and Buildings, 108, 205-214.

Reddy, V. J., Ghazali, M. F., and Kumarasamy, S. (2024). Advancements in phase change materials for energy-efficient building construction: A comprehensive review. Journal of Energy Storage, 81, 110494.

Sun, X., Jovanovic, J., Zhang, Y., Fan, S., Chu, Y., Mo, Y., and Liao, S. (2019). Use of encapsulated phase change materials in lightweight building walls for annual thermal regulation. Energy, 180, 858-872.

Vega, M., Llantoy, N., Chafer, M., Ushak, S., and Cabeza, L. F. (2022). Life cycle assessment of the inclusion of phase change materials in lightweight buildings. Journal of Energy Storage, 56, 105903.

Wang, C., Huang, X., Deng, S., Long, E., and Niu, J. (2018). An experimental study on applying PCMs to disaster-relief prefabricated temporary houses for improving internal thermal environment in summer. Energy and Buildings, 179, 301-310.

Wang, J., Long, E., Qin, W., and Xu, L. (2013). Ultrathin envelope thermal performance improvement of prefab house by integrating with phase change material. Energy and Buildings, 67, 210-216.

Yang, L., Qiao, Y., Liu, Y., Zhang, X., Zhang, C., and Liu, J. (2018). A kind of PCMs-based lightweight wallboards: Artificial controlled condition experiments and thermal design method investigation. Building and Environment, 144, 194-207.

Zhang, C., Chen, Y., Wu, L., and Shi, M. (2011). Thermal response of brick wall filled with phase change materials (PCM) under fluctuating outdoor temperatures. Energy and Buildings, 43(12), 3514-3520.

Optimizing Classifiers for Heart Disease Classification

Hüseyin COŞKUN[1]

1- Asst. Prof. Huseyin COSKUN, Kütahya Health Sciences University, Computer Engineering Department, huseyin.coskun@ksbu.edu.tr ORCID No: https://orcid.org/0000-0002-8380-245X

ABSTRACT

In this study, a comprehensive comparison of machine learning methods such as AdaBoost, Gradient Boosting, Random Forest, Weighted k-NN and SVM is performed on a heart disease dataset. Considering the characteristics of the data (e.g. age, cholesterol, ECG results), the different algorithms were trained under the same data preprocessing conditions. The results show that Gradient Boosting performs close to perfect, reaching ≈1 in Accuracy, F1 Score, MCC and other metrics. AdaBoost and Weighted k-NN achieved similarly high accuracy rates (≈0.98-0.99). SVM, in particular, achieved a clinically significant success by reaching 1 in Recall (Sensitivity). Random Forest, on the other hand, was one step behind these algorithms, achieving an accuracy of ≈0.88 When all of the metrics in the table (Accuracy, F1, Precision, Recall, Specificity, MCC, AUC) are taken into account, it is seen that the data set can be separated very clearly with boosting-based methods. These successes suggest the need for k-fold cross-validation or additional validation with independent data to see if the model is overfitting. Nevertheless, the results show that with the right choice of parameters and sufficient data, machine learning methods have great potential in diagnosing heart disease. This approach can provide an effective decision support mechanism that can contribute to early diagnosis and treatment of patients.

Keywords – Heart Diseases, Machine Learning, Classification, Optimization, Boosting Algorithms.

INTRODUCTION

Cardiovascular disease (CVD) is one of the leading causes of death worldwide, claiming millions of lives every year. According to the World Health Organization (WHO), approximately 17.9 million people worldwide died from CVD in 2019, accounting for 32% of all deaths. More than three-quarters of deaths due to cardiovascular diseases occur in low- and middle-income countries. The most common CVDs are coronary artery disease, heart attack and heart failure. This clearly demonstrates the importance of early detection and treatment. In particular, most heart diseases can be prevented or treated if detected at an early stage. Most cardiovascular diseases can be prevented by addressing behavioral and environmental risk factors such as tobacco use, unhealthy diet and obesity, physical inactivity, harmful use of alcohol and air pollution. It is important to detect cardiovascular disease as early as possible so that management can begin with counseling and medication. Traditional methods for early diagnosis of heart disease usually include physical examination, blood tests and imaging techniques. However, these methods can be time-consuming and are often limited to assessments

based on the experience of healthcare professionals. Nowadays, the use of modern technologies such as big data analytics and machine learning (ML) enables the development of faster, more accurate and efficient diagnosis and classification models. Early detection and accurate classification of heart diseases not only improves the quality of life of individuals, but also significantly reduces the burden on healthcare systems. In this context, demonstrating the potential of machine learning algorithms will shed light on future clinical applications.

This book chapter aims to compare the ability of various machine learning methods, SVM, Random Forest, AdaBoost, Gradient Boosting, Weighted kNN to diagnose heart disease using the UCI Heart Disease dataset. In particular, ROC curve, AUC, accuracy, F1 score, and other performance metrics will be calculated for accurate diagnosis.

MATERIAL & METHOD

In this context, ML algorithms offer powerful tools to identify heart disease symptoms and risk factors by analyzing large datasets. In particular, the UCI Machine Learning Repository Heart Disease Dataset used in this study is a dataset that is frequently used in the diagnosis of heart disease and is the basis for many scientific studies. This dataset contains various biometric and clinical parameters and is used to classify whether individuals have heart disease or not.

Heart Disease Dataset

The UCI Heart Disease Dataset is compiled from five different sources (Cleveland, Hungary, Switzerland, and Long Beach VA, Stalog) and is one of the most widely used datasets for classification problems (Anon n.d.; Detrano et al. 1989).

Table 1: Features of the heart disease dataset

Variable Name	Type	Description	Units	Missing Values
age	Int		years	no
sex	Cat	1 = female, 0 = male.		no
cp	Cat	Chest Pain Type	1: Typical angina 2: Atypical angina 3: Non-anginal pain 4: No symptoms	no
trestbps	Int	resting blood pressure (on admission to the hospital)	mm Hg	no
chol	Int	serum cholestero l	mg/dl	no
fbs	Cat	fasting blood sugar	1 if fasting blood sugar > 120 mg/dl, 0 otherwise.	no
restecg	Cat	Resting Electrocardiographic Results	0: Normal 1: ST-T wave abnormality 2: Left ventricular hypertrophy (according to Minnesota coding criteria)	no

thalach	Int	maximum heart rate achieved		no
exang	Cat	exercise induced angina	Occurrence of angina during exercise (1 = yes, 0 = no).	no
oldpeak	Int	ST depression induced by exercise relative to rest		no
slope	Cat	Slope of the Peak Exercise ST Segment	1: Sloping up 2: Flat 3: Sloping down	no
ca	Int	number of major vessels colored by fluoroscopy	It takes values between 0 and 3.	yes
thal	Cat	Thalassemia	3: Normal 6: Fixed defect 7: Reversible defect	yes
num*	Int	diagnosis of heart disease	0: No heart disease 1: Heart disease present	no

Int: Integer, Cat: Categorical. *num value is used as target and the others is used as feature.

The UCI Heart Disease dataset sample counts are as follows: Cleveland: 303 samples, Hungary: 294 samples, Switzerland: 123 samples, Long Beach VA: 200 samples, Stalog (Heart) Data Set: 270. However, as there are often missing values in some columns of these datasets, some samples (165 samples) were removed during the cleaning process, resulting in a dataset with 1025 samples in total. This dataset contains the 14 characteristics described in

for each individual.

Pre-processing

The process of handling missing data in the dataset by filling it with the median was carried out as follows. Initially, missing values in the dataset, typically represented as NaN, were identified. Next, the median value was calculated for each column. The median represents the middle value in a sorted list of values within a dataset. Finally, the missing values in each column were replaced with the calculated median of that specific column. The fact that features in the dataset are on different scales may cause some algorithms (e.g. SVM, kNN, Gradient Boosting) not to treat these features equally. For example, levels (30-80) and serum cholesterol level (150-300) are on different scales, so without scaling, features with larger values will receive more weight. In distance-based models such as kNN or SVM, without scaling, some features will be more effective than others. This can cause the model to be unbalanced and misclassified. Scaling makes features comparable to each other and improves the performance of many machine learning algorithms. The scaling of the numeric columns was done to bring the data to a common scale. This is usually done by methods such as z-score normalization or min-max scaling. In this study, z-score normalization was performed by calculating the mean and standard deviation for each column.

Machine Learning Methods

The performance of these datasets was assessed using classifiers such as Weighted k-Nearest Neighbor (weighted k-NN), Gradient Boosting, AdaBoost, Support Vector Machine (SVM), and Random Forest (RF), implemented through the Python programming language. For all classifiers, 15% of the data was reserved for validation and testing purposes. The training models were evaluated using test data that had not been included during the training process, ensuring the test set remained entirely separate from the training set. To evaluate the predictive performance of the models, a 5-fold cross-validation process was employed. This method prevents bias in the classifier and mitigates the risk of overfitting. Additionally, to avoid overtraining, the cross-validation process ensured that there was no overlap or data sharing between the training and validation datasets.

AdaBoost

AdaBoost (Adaptive Boosting) is an ensemble learning algorithm that enhances the performance of weak learners by combining them into a more

powerful predictive model. Introduced by Yoav Freund and Robert Schapire in 1995 (Freund and Schapire 1995), it is among the earliest and most impactful boosting algorithms. AdaBoost focuses on correcting the errors made by previous models by iteratively adjusting the weights of misclassified instances and combining the outputs of weak learners into a strong classifier (de Giorgio, Cola, and Wang 2023). The algorithm leverages **Weak Learners**, which are classifiers that perform marginally better than random guessing. Decision stumps (single-level decision trees) are commonly used as weak learners in AdaBoost. By iteratively training these weak learners and emphasizing the instances they misclassify, AdaBoost creates an ensemble of **Strong Learners** capable of achieving significantly higher accuracy. The AdaBoost process begins with the initialization of weights for all training instances. These weights are adjusted after each iteration to place more focus on misclassified examples, ensuring that subsequent weak learners address these errors. Through this iterative weighting mechanism and ensemble strategy, AdaBoost produces a robust predictive model that is effective across a wide range of classification problems. Each training example is assigned an initial weight. If there are N examples, each one starts with a weight of $\frac{1}{N}$. Instance weights play a crucial role in classification by determining the relative importance of each training example. A weak learner is trained iteratively on weighted training data, aiming to minimize its classification error. The learner's error rate is then calculated. Correctly classified instances retain their weight, while misclassified instances have their weights increased for the next iteration. This weighting scheme, updated according to Equation 1, directs subsequent weak learners to focus on previously misclassified, and thus more challenging, examples.

$$\omega_i^{(t+1)} = \omega_i^{(t)} \times e^{\alpha \times I(y_i \neq h_t(x_i))} \quad (1)$$

Where, $\omega_i^{(t)}$ is the weight of instance i at round t, α is the importance of the weak learner, $I(y_i \neq h_t(x_i))$ is 1 if the prediction is incorrect and 0 if correct. The contribution of each weak learner to the final prediction is based on its accuracy. The weight assigned to each weak learner is computed with Equation 2:

$$\alpha_t = \frac{1}{2} \ln\left(\frac{1-\epsilon_t}{\epsilon_t}\right) \quad (2)$$

Where, ϵ_t is the weighted classification error of the weak learner, α_t is the weight given to that weak learner in the final model. In AdaBoost, the weighted classification error ϵ_t is a key metric used to evaluate how well a weak classifier performs on the training data, considering the importance

(weights) of the training examples. The formula for calculating the weighted classification error ϵ_t at iteration t is given in Equation 3:

$$\epsilon_t = \frac{\sum_{i=1}^{n} w_i^t \cdot \mathrm{I}\left(y_i \neq_t h_t(x_i)\right)}{\sum_{i=1}^{n} w_i^t} \tag{3}$$

Where ϵ_t is the weighted classification error of the weak classifier h_t at iteration t, n is the number of training examples, w_i^t is the weight of training example i at iteration t, y_i is the true label of training example i, $h_t(x_i)$ is the prediction of the weak classifier h_t for training example x_i, $\mathrm{I}\left(y_i \neq_t h_t(x_i)\right)$ is an indicator function that equals 1 if the weak classifier misclassifies x_i (i.e., $y_i \neq_t h_t(x_i)$ and 0 if it correctly classifies x_i. If a weak learner performs well (i.e., low error rate), its α_t will be large, giving it more importance in the final prediction. If it performs poorly, α_t will be smaller. The final strong learner is a weighted combination of all weak learners. The prediction is made based on the sign of the sum of the weighted predictions in Equation 4.

$$H(x) = \mathrm{sign}\left(\sum_{t=1}^{T} \alpha_t \, h_t(x)\right) \tag{4}$$

where $H(x)$ is the final prediction, α_t is the weight of the weak learner h_t, and $h_t(x)$ is the prediction of the weak learner at step t. AdaBoost repeats this process for a predetermined number of iterations or until the error is sufficiently minimized. At each iteration, it focuses more on the mistakes of previous learners, thus improving overall performance. For binary classification problems, which is the subject of this study, AdaBoost minimizes the exponential loss function (L) with Equation 4. Where, w_i are the weights, y_i are the true labels, $H(x_i)$ and is the combined classifier output. AdaBoost, a well-established ensemble method that combines weak learners to improve classification performance. AdaBoost is known for its simplicity, adaptability, and ability to generalize well, but it is also sensitive to noisy data and requires the use of weak learners that do not overfit. Our implementation, within the Python programming, used 50 estimators and a learning rate of 1. Crucially, we employed the SAMME (Stagewise Additive Modeling using a Multiclass Exponential loss) variant of AdaBoost. This choice allowed us to directly handle multiclass classification, avoiding the need to adapt a binary classification approach, and utilize an exponential loss function.

AdaBoost Parameters

NumLearningCycles: Determines how many weak learners (usually decision trees) will come together. Values like 50, 100, 200 can be tried. More tree values usually lead to higher capacity, but also increases the training time.
Learners: A decision tree is often preferred as a base learner. The sub-parameters of this tree template can seriously affect performance: '**MinLeafSize':** The minimum number of samples in a leaf node. Small values can lead to excessive learning. '**MaxNumSplits**': Restricts the number of times the decision tree can branch.
Learning Rate (Boosting Shrinkage): In AdaBoost it is usually 1.0 (i.e. the full contribution of each weak learner), but if the 'LearnRate' parameter is included, you can control how much each weak learner contributes. For example, small values like 0.1 or 0.01 can make the model learn more slowly and in a controlled manner (reducing overlearning in boosting).

Gradient Boosting

Gradient Boosting is a robust ensemble learning algorithm commonly employed in machine learning for both classification and regression tasks. It constructs an ensemble of decision trees in a sequential manner, with each tree addressing the errors made by its predecessors. Gradient Boosting combines the predictions of multiple weak learners (typically decision trees) into a strong learner (Saupin 2022) Unlike bagging methods like Random Forest, which create models in parallel, boosting methods iteratively improve the model's performance by training subsequent trees to focus on correcting residual errors. The process begins with a single decision tree, followed by subsequent trees trained to minimize the residuals of the earlier ones. This sequential training reduces overall prediction error. The term “Gradient” in Gradient Boosting originates from the use of gradient descent optimization to minimize a specified loss function, adjusting model parameters by moving in the direction of the steepest descent in the loss function space. Depending on the task, Gradient Boosting allows flexibility in selecting loss functions, such as mean squared error for regression tasks or deviance (logarithmic loss) for classification problems, significantly influencing the algorithm’s behavior (Vandeput 2021). One of the key hyperparameters in Gradient Boosting is the learning rate, which determines the contribution of each tree to the final prediction. A lower learning rate enhances model robustness but necessitates a larger number of trees to achieve optimal performance. Additionally, Gradient Boosting provides valuable insights into feature importance by evaluating how much each feature contributes to reducing the loss function, aiding in feature selection and a better understanding of the dataset. The algorithm fundamentally relies on the gradient of the loss function for each

sample, referred to as the residual, which represents the error between the true and predicted labels (Friedman 2001).

SET $F_0(\boldsymbol{x}) = 0$

REPEAT $t = 1, \ldots . T$

1) Compute gradient $-gt(x)$
2) Fit a new base-learner

$$\boldsymbol{a}_m = argmin_{\boldsymbol{a},\beta} \sum_{i=1}^{N} [-g_t(x) - \beta h(\boldsymbol{x}_i; \boldsymbol{a})]^2$$

3) Find the best gradient descent step-size

$$\rho_t = argmin_{\boldsymbol{p}} \sum_{i=1}^{N} \psi[y_i, F_{t-1}(\boldsymbol{x}_i) + \rho h(\boldsymbol{x}_i; \boldsymbol{a}_m)]$$

4) Set the function estimate

$$F_m(\boldsymbol{x}) \leftarrow F_{m-1}(\boldsymbol{x}) + \rho_m h(\boldsymbol{x}; \boldsymbol{a}_m)$$

Figure 1: Gradient Boosting algorithm

Unlike AdaBoost, which uses weights for error adjustment, Gradient Boosting directly utilizes residuals to guide the training of subsequent weak learners. Consequently, it is regarded as a sequential ensemble method that aims to optimize weak learners based on residuals (i.e., gradients) (Kunapuli 2022). For an N-dimensional Z dataset, while $Z = \{z_1, z_2, \ldots \ldots \ldots, z_N\}$ with $z_i = (x_i, y_i)$, $x_i \in \boldsymbol{x}$ and $y_i = -g_m(\boldsymbol{x}_i)$ assuming $\psi(y, f)$ is loss-function and $h(x, \theta)$ base-learner model. Gradient Boosting algorithm is presented in Figure 1 (Friedman 2001; Natekin and Knoll 2013). Since boosting algorithms are based on decision trees, in this algorithm, $h(\boldsymbol{x}; \boldsymbol{a}_m)$ is a small regression tree, for a regression tree the parameters $\boldsymbol{a}_m$ are the splitting variables, locations, and the terminal node means of the individual trees. Steepest-descent is one of the simplest and most frequently used numerical minimization methods, focusing on moving in the direction of the steepest gradient to minimize a given function (Friedman 2001). Both Gentle Boosting and Gradient Boosting are ensemble learning techniques designed to enhance predictive performance by combining the outputs of weak learners, typically decision trees, though they employ distinct methodologies. Gentle Boosting adopts an adaptive learning rate and a soft-margin approach, enabling it to be more robust against noisy data and outliers. It carefully iterates to correct errors, making adjustments cautiously to avoid overfitting (Vinod and Rao 2020). In contrast, Gradient Boosting—including widely-used algorithms such as XGBoost and LightGBM—utilizes gradient descent optimization to iteratively fit decision trees by minimizing a specified loss function. While Gradient Boosting often achieves superior predictive accuracy, it comes at the cost of higher computational complexity and increased sensitivity to noisy data.

Gradient Boosting Parameters

One of the most widely used methods in the Gradient Boosting derivative is LogitBoost.
NumLearningCycles (Number of Trees): Determines how many weak learners (base decision trees) to stack. Usually values such as 50, 100, 200, 500 are tried. As the number of trees increases, the learning capacity of the model increases, but the training time also increases.
LearnRate: The default is usually 0.1 or 0.2. Smaller values make the model learn more slowly but reduce the risk of overfitting. Values such as 0.01, 0.05, 0.1, 0.2 can be tried.
Learner (Basic Learner: Decision Tree): The base learner is usually designated as a decision tree. Sub-parameters of the decision tree: **MinLeafSize:** The minimum number of samples per leaf. **MaxNumSplits:** Overfitting can be avoided by setting an upper limit on the number of splits in a tree.
Method (Boosting Type): 'LogitBoost': Widely used for binary classification (one of the types of Gradient Boosting). There are also other methods such as 'AdaBoostM1', 'RUSBoost', 'GentleBoost'.

Random Forest

Random Forest (RF) is a widely-used ensemble learning method in machine learning, designed to leverage the collective predictive capabilities of multiple decision trees for both classification and regression tasks. By introducing randomness through bootstrapping (random sampling with replacement) and random feature selection at each node, Random Forest mitigates overfitting and enhances the generalization of its predictions(Ho 1998). The aggregated predictions from individual trees are determined via majority voting for classification tasks or averaging for regression, offering high accuracy and robustness. This method is highly versatile, with applications ranging from image recognition and fraud detection to recommendation systems and predictive maintenance (Sheppard 2019). As part of the bagging family of ensemble techniques, Random Forest is built on the foundation of decision trees but distinguishes itself by employing a collection of trees to reduce overfitting and improve predictive reliability. The "random" element in Random Forest originates from two primary sources(Maroco et al. 2011):

- **Random Sampling**: Each tree is trained on a bootstrapped subset of the training data, introducing diversity among the trees.
- **Random Subset of Features**: At each split within a tree, a randomly chosen subset of features is considered, further reducing the likelihood of overfitting and promoting variability.

For classification tasks, Random Forest determines the final class by majority vote, while for regression tasks, it averages the outputs of individual trees.

This ensemble approach consistently delivers more accurate and stable results compared to a single decision tree. Random Forest is particularly effective for datasets with complex structures and relationships. It is recognized as one of the ensemble techniques where multiple decision trees, trained on random samples and features using a bagging strategy, are combined. Each tree votes to assign a class label for a given input vector (Li et al. 2016). In this study, the number of trees was set to 50, which is often the primary hyperparameter adjusted to balance model complexity and performance.

Random Forest Parameters

The application of the Bagging method with decision trees is the basic principle of Random Forest. For this reason, an approach using Bagging + Decision Trees for Random Forest is preferred.
NumLearningCycles: Determines how many decision trees will be created. Usually values such as 50, 100, 200, 500 are tried. Accuracy can improve as the number of trees increases, but training time increases.
Learners: The decision tree template is used as the base learner. This template also has its own sub-parameters: 'MinLeafSize': The minimum number of samples that can be found in the leaves. If a smaller and deeper tree is preferred, the risk of overfitting increases. 'MaxNumSplits': Maximum number of branches within the tree. The higher this value, the more complex the tree can be.

Weighted k-Nearest Neighbor (WKNN)

The "K" in KNN represents the number of nearest neighbors to consider when making a prediction (Kramer 2013). For classification, KNN finds the K data points closest to the new data point in the training set and assigns the class label that occurs most frequently among those neighbors. For regression, it averages the target values of the K nearest neighbors to predict the target value for the new data point. KNN relies on a distance metric (e.g., Euclidean distance) to measure the similarity between data points. The most commonly used distance metrics are given in the

.

Table 2: k-NN distance metric equations

Name	Equation
Euclidean	$\sqrt{\sum_{i=1}^{k}(x_i - y_i)^2}$
Manhattan	$\sum_{i=1}^{k}\lvert x_i - y_i\rvert$
Minkowski	$\left(\sum_{i=1}^{k}(\lvert x_i - y_i\rvert)^q\right)^{1/q}$

The selection of a suitable distance metric and the value of K are crucial for optimal performance in K-Nearest Neighbors (KNN). K, a key hyperparameter, governs the trade-off between sensitivity to noise and potential bias (Kramer 2013). A small K can make the algorithm highly sensitive to noise in the data, while a large K can smooth out noise but may introduce bias by considering too many distant points. KNN is classified as a "lazy learner" because it avoids building an explicit model during training, instead storing the entire training dataset and performing calculations only when making predictions. This characteristic, referred to as instance-based learning(Rhys 2020) , can lead to high computational costs with large datasets, as the algorithm must calculate distances to all training instances for each prediction. In our study, we configured KNN with 10 neighbors, the Euclidean distance metric, and squared inverse distance weighting.

One disadvantage of the standard KNN algorithm is that it gives equal weight to all neighbors. This can lead to misleading results, especially when the distances between neighbors are different. This is where the Weighted KNN (WKNN) algorithm comes into play. The Weighted K-Nearest Neighbor (WKNN) algorithm is an improved version of the standard KNN and provides more accurate and reliable predictions by taking into account the distances of neighbors (Yigit 2013). WKNN is an extension of standard KNN and is based on the principle of weighting neighbors according to their distances. In other

words, neighbors that are closer to the predicted data point are given higher weights, while neighbors that are farther away are given lower weights. This weighting process is usually done inversely proportional to the distance. For example, the closer a neighbor is, the higher its weight (Jiang et al. 2007).
Different weighting methods can be used in WKNN. The most commonly used methods are (Archibald et al. 2020):

- Inverse Distance Weighting: In this method, the weight of a neighbor is proportional to the inverse of its distance from the estimated point. In other words, weight = 1 / distance.
- Inverse Square Distance Weighting: In this method, the weight is proportional to the inverse of the square of the distance. In other words, weight = 1 / (distance^2). This method gives more importance to closer neighbors.
- Gaussian Weighting: In this method, the weights are calculated using the Gaussian function. This method provides a smoother weighting depending on the distance.

The Working Steps of WKNN can be listed as follows(Wang et al. 2021).

1) Select k Value: As in KNN, it is important to determine the number of nearest neighbors (k) in WKNN.
2) Calculate Distances: The distances between the data point to be predicted and all points in the training set are calculated. Euclidean distance is usually used.
3) Determine Neighbors: The k nearest neighbors are determined.
4) Calculate Weights: A weight is assigned to each neighbor according to the selected weighting method.
5) Make the Estimate: In classification problems, the label belonging to the class with the highest weight is assigned as the estimate. In regression problems, the values of the neighbors are multiplied by their weights and an average is calculated and this average is used as the estimate.

Weighted k-Nearest Neighbor Parameters

NumNeighbors (k): The value k determines the number of neighbors to consider when making a classification decision. Too small kk can lead to overfitting; too large kk can result in generally good but limited discrimination.
Distance (Distance Metrics): 'euclidean': The most commonly used Euclidean distance. 'cityblock' (Manhattan): Less sensitive to outliers in the data. 'minkowski': A general formula that can be customized with the parameter p. Alternative metrics such as 'cosine', 'correlation', 'chebychev' can also be used.
DistanceWeight (Weighting Method): 'equal': All neighbors are equally weighted. 'inverse': As the distance of neighbors decreases, their weight

increases, and the influence of distant neighbors decreases. 'squaredinverse': more aggressive version of 'inverse', giving even higher weight to close neighbors. 'gaussian': Weights distances with a Gaussian function.
Standardize (Data Standardization): true/false. Especially in distance-based methods, bringing the data to similar scales is critical for performance. In some cases, false can also be set here as standardization is done during data pre-processing.

Support Vector Machines (SVM)

The main goal of SVM is to find the best separator (hyperplane) between two classes. "Best" means that the hyperplane is as far away from both classes as possible. This distance is called the "margin" and SVM aims to maximize the margin. A larger margin increases the generalization ability of the model and allows it to perform better on new, unseen data. In SVM, different approaches are used for Linearly Separable and Non-Linearly Separable Cases. Since the heart sound classification problem in this study involves the non-linearly separable case, this approach is preferred (Coşkun 2023).
An n-1 dimensional subspace in an n-dimensional space is defined as Hyperplane. A line in a two-dimensional space and a plane in a three-dimensional space are hyperplanes. In SVM, a hyperplane represents the decision boundary separating two classes. Data points closest to the hyperplane are defined as Support Vectors. These points play a critical role in determining the location and orientation of the hyperplane(Coskun et al. 2022). Other data points do not affect the location of the hyperplane. In cases where the data cannot be linearly separated, the "soft margin" approach is preferred. This means allowing some data points to violate the margin. To achieve this, "slack variables" are added to the optimization problem. Equation 5 and Equation 6 are utilized to minimize and constrain respectively (Coskun and Yigit 2018).

$$1/2\ \|w\|^2 + C\ \sum_i \xi_i \qquad (5)$$

In Equation 5:

- $(1/2)||w||^2$: Margin maximizing term.
- C: A hyperparameter. It controls the trade-off between margin width and classification errors. A large value of C results in fewer margin violations (i.e. a narrower margin) and a tighter fit of the model to the training data (risk of overfitting), while a small value of C results in more margin violations (i.e. a wider margin) and better generalization (but potentially lower training accuracy).
- $\sum_i \xi_i$: Sum of slack variables. This term penalizes margin violations.

$$y_i(w \cdot x_i + b) : \geq 1 - \xi_i, \qquad \forall i \ \xi_i \geq 0, \forall i \qquad (6)$$

In Equation 6:

- $y_i(w \cdot x_i + b)$: This expression shows the location of the i-th data point with respect to the hyperplane. x_i: Vector of the i-th data point. y_i: Class label of the i-th data point (+1 or -1). w: Normal vector of the hyperplane. b: Bias term that determines the distance of the hyperplane from the origin.
- $\geq 1 - \xi_i$: This part expresses the part that allows the margin to be violated. 1: Represents the limit of the margin (as in the linearly separable case). ξ_i: Slack variable for the i-th data point. This variable measures how much the data point violates the margin.
- $\xi_i \geq 0$: This restriction guarantees that the slack variables cannot be negative. That is, a data point either lies on the correct side (or on the margin) ($\xi_i = 0$), or it violates the margin ($\xi_i > 0$).

The constraint equation expresses the following for each data point: If the data point is in the correct class and outside the margin ($y_i(w \cdot x_i + b) \geq 1$), then $\xi_i = 0$. That is, there is no violation. If the data point is inside the margin or on the wrong side ($y_i(w \cdot x_i + b) < 1$), then $\xi_i > 0$. The value of ξ_i indicates the magnitude of the violation. For example, if $\xi_i = 0.5$, the data point is 0.5 units inside the margin. If $\xi_i = 2$, the data point is on the wrong side and 1 unit beyond the margin. The hyperparameter C controls how much these violations are penalized during optimization. A large value of C allows fewer violations, while a small value of C allows more violations.

Support Vector Machine Parameters

Support vector machines have basic parameters such as kernel function, C (penalty), kernel scale, polynomial degree.

KernelFunction: 'linear', 'rbf', 'polynomial', 'sigmoid', etc. Choosing a kernel that matches the structure of data greatly affects performance. 'linear': If the data can be separated linearly, it is efficient and fast. 'rbf': Generally works well with different distributions, it is the most used kernel type. 'polynomial': Can be used if you assume a polynomial relationship in the data. It is necessary to choose the degree. 'sigmoid': Not very common, sometimes used to mimic the activation function in neural networks.

BoxConstraint (C): This is the penalty parameter of SVM. A large value of C is more aggressive in penalizing every error and can cause the model to become complex (possible overfitting). A small C value is more tolerant to errors, but the model may remain simpler (possible underfitting).

KernelScale: In the RBF kernel, it can be used follow; $\gamma = 1/(2 \times KernelScale^2)$. Manual tuning, optimizing according to data distribution contributes to performance. A KernelScale value that is too small will result in narrow Gaussian curves. Each data point will have a very local effect and

an overfitting problem may occur. A KernelScale value that is too large will result in wide Gaussian curves. The model may be unstable or insufficiently discriminated.
PolynomialOrder: If 'polynomial' kernel is used, it determines the degree of the polynomial. As the degree increases, the model can get more complex.

Evaluation metrics

Performance metrics in including AUC (Area Under the Curve), Accuracy (A), F1-score (F1), Precision (P), Recall (R) Matthews Correlation Coefficient (MCC) and Specificity (S), were calculated to assess each model's effectiveness.

Table 3: Evaluation metrics

$A = \frac{tp + tn}{tp + tn + fp + fn}$	$S = \frac{tn}{fp + tn}$
$P = \frac{tp}{tp + fp}$	$AUC = \frac{1}{2}\left(\frac{tp}{tp + fn} + \frac{tn}{tn + fp}\right)$
$R = \frac{tp}{tp + fn}$	$F1 = \frac{2\left(\frac{tp}{tp + fn}\right)\left(\frac{tp}{tp + fp}\right)}{\left(\frac{tp}{tp + fn}\right) + \left(\frac{tp}{tp + fp}\right)}$
$\mathrm{MCC} = \frac{(TP \times TN) - (FP \times FN)}{\sqrt{(TP + FP)(TP + FP)(TN + FP)(TN + FN)(TN + FN)}}$	
True Positives (TP): Correctly predicted positive cases.	
True Negatives (TN): Correctly predicted negative cases.	
False Positives (FP): Incorrectly predicted positive cases (Type I error).	
False Negatives (FN): Incorrectly predicted negative cases (Type II error).	

The Matthews Correlation Coefficient (MCC) is a metric used to evaluate the quality of binary and multi-class classification models. It is regarded as a balanced measure because it takes into account true and false positives and negatives and is particularly useful when dealing with imbalanced datasets (Boughorbel, Jarray, and El-Anbari 2017). MCC returns a value between -1 and 1, where: 1 indicates a perfect prediction, 0 indicates a random guess, -1 indicates total disagreement between predictions and actual labels. MCC considers all four confusion matrix values (TP, TN, FP, FN), making it a more informative and balanced measure compared to accuracy, especially when data is imbalanced (Chicco, Warrens, and Jurman 2021). MCC is effective for

imbalanced datasets because it does not get inflated by a high number of true negatives or true positives. Since the data set in this study has an unbalanced distribution, the classification models were evaluated especially according to the MCC metric(Chicco and Jurman 2020). Where Binary classifiers where imbalanced datasets need a balanced metric, MCC provides a more accurate evaluation of the classifier's ability to distinguish between classes than simpler metrics like accuracy.

RESULTS AND DISCUSSION

Heart disease classification results were evaluated by testing all models according to different parameters. The confusion matrix and ROC plots were analyzed using the parameter values with the highest accuracy values.
Table 4 shows the classification accuracy values of the Adaboost model according to different optimization parameters.

Table 4: AdaBoost model results with different parameters

NumTrees	MinLeafSize	MaxNumSplits	LearnRate	Accuracy
50	1	10	0,5	0,9511
50	1	10	1	0,9511
50	1	20	0,5	0,9381
50	1	20	1	0,9283
50	5	10	0,5	0,9479
50	5	10	1	0,9511
50	5	20	0,5	0,9544
50	5	20	1	0,9577
100	1	10	0,5	0,9381
100	**1**	**10**	**1**	**0,9903**
100	1	20	0,5	0,9577
100	1	20	1	0,9609
100	5	10	0,5	0,9772
100	5	10	1	0,9479
100	5	20	0,5	0,9544
100	5	20	1	0,9577

At the best performance, an accuracy value of 0.99 was obtained for NumTree=100, MinLeafSize=1, MaxNumSplits=10, LearnRate=1. More trees (100) increased AdaBoost's capacity to correct errors. MinLeafSize=5 and MaxNumSplits=10 limit overfitting by keeping the trees at a moderate

complexity. LearnRate=0.5 may prevent overly hard updates (overfitting) by slightly smoothing the contribution of each weak learner.
shows the classification accuracy values of the Gradient Boosting model according to different optimization parameters.

Table 5: Gradient Boosting model results with different parameters

Method	NumTrees	LearnRate	MinLeafSize	MaxNumSplits	Accuracy
LB	50	0,05	1	10	0,938
GB	50	0,05	1	10	0,990
LB	50	0,05	1	20	0,948
GB	50	0,05	1	20	0,993
LB	50	0,05	5	10	0,945
GB	**50**	**0,05**	**5**	**10**	**1,000**
LB	50	0,05	5	20	0,961
GB	50	0,05	5	20	0,997
LB	50	0,1	1	10	0,964
GB	50	0,1	1	10	0,993
LB	50	0,1	1	20	0,971
GB	**50**	**0,1**	**1**	**20**	**1,000**
LB	50	0,1	5	10	0,961
GB	50	0,1	5	10	1,000
LB	50	0,1	5	20	0,954
GB	50	0,1	5	20	0,997
LB	100	0,05	1	10	0,967
GB	**100**	**0,05**	**1**	**10**	**1,000**
LB	100	0,05	1	20	0,984
GB	100	0,05	1	20	0,990
LB	100	0,05	5	10	0,964
GB	100	0,05	5	10	0,980
LB	100	0,05	5	20	0,971
GB	100	0,05	5	20	0,987
LB	100	0,1	1	10	0,967
GB	100	0,1	1	10	0,980
LB	100	0,1	1	20	0,974

GB	100	0,1	1	20	0,987
LB	100	0,1	5	10	0,977
GB	100	0,1	5	10	1,000
LB	100	0,1	5	20	0,990
GB	**100**	**0,1**	**5**	**20**	**1,000**

LB: LogitBoost, GB: GentleBoost

When the results are analyzed, it is remarkable that LogitBoost also gives quite good results in the range of 93-98%, but GentleBoost reaches an Accuracy level of 1.0. This shows that GentleBoost's approach fits the data better in this dataset. Between NumTrees=50 or NumTrees=100, there are configurations on the GentleBoost side that reach 100% in both cases. When LearnRate=0.05 or 0.1, GentleBoost was often able to achieve very high or full accuracy. Remarkably, the combination MinLeafSize=5, MaxNumSplits=10 showed 100% accuracy on GentleBoost in multiple rows. Settings that allow for more complex trees, such as MinLeafSize=1 and MaxNumSplits=20, also sometimes reached 100% on GentleBoost (e.g. 50 trees, 0.1 LearnRate). This shows that the dataset can be learned successfully even with various tree depth (MaxNumSplits) or leaf size (MinLeafSize) settings. Table 6 shows the classification accuracy values of the Random Forest model according to different optimization parameters.

Table 6: Random Forest model results with different parameters

NumTrees	MinLeafSize	MaxNumSplits	Accuracy
50	1	10	0,8241
50	1	20	0,8795
50	5	10	0,8143
50	**5**	**20**	**0,8827**
100	1	10	0,8664
100	1	20	0,8795
100	5	10	0,8046
100	5	20	0,8820

The highest accuracy value of 0.8827 was obtained for the parameters NumTrees=50, MinLeafSize=5, MaxNumSplits=20. Comparing models with 50 and 100 trees, it can be seen that in general, some scenarios with 50 trees (e.g. 50,5,20) can give higher results than models with 100 trees. More trees (100) can generally increase stability and reduce overfitting, but here a 50-tree model achieves the highest Accuracy in the combination (5,20). This may suggest that the aggressive parameters (MaxNumSplits=20, MinLeafSize=5) in the dataset used are a good fit even with 50 trees. This suggests that more

"balanced" and slightly deeper trees work well on the dataset. MaxNumSplits=20 seems to give results in the range of 0.87-0.88. As the trees get a little deeper (splits=20), the model seems to gain better discrimination in the dataset. Table 6 shows the classification accuracy values of the Weighted k-NN model according to different optimization parameters.

Table 7: wKNN model results with different parameters

NumNeighbors	Distance	DistanceWeight	Standardize	Accuracy
3	euclidean	inverse	TRUE	0,95114
3	euclidean	inverse	FALSE	0,95440
3	euclidean	squaredinverse	TRUE	0,95440
3	euclidean	squaredinverse	FALSE	0,96743
3	cityblock	inverse	TRUE	0,97068
3	cityblock	inverse	FALSE	0,97720
3	cityblock	squaredinverse	TRUE	0,96743
3	cityblock	squaredinverse	FALSE	0,95114
5	euclidean	inverse	TRUE	0,96091
5	euclidean	inverse	FALSE	0,96743
5	euclidean	squaredinverse	TRUE	0,95114
5	euclidean	squaredinverse	FALSE	0,96417
5	cityblock	inverse	TRUE	0,98046
5	cityblock	inverse	FALSE	0,94463
5	**cityblock**	**squaredinverse**	**TRUE**	**0,99020**
5	cityblock	squaredinverse	FALSE	0,96417
7	euclidean	inverse	TRUE	0,96091
7	euclidean	inverse	FALSE	0,97068
7	euclidean	squaredinverse	TRUE	0,94788
7	euclidean	squaredinverse	FALSE	0,95765
7	cityblock	inverse	TRUE	0,96091
7	cityblock	inverse	FALSE	0,97068
7	cityblock	squaredinverse	TRUE	0,95114
7	cityblock	squaredinverse	FALSE	0,96743

Looking at the table, the combined model with the highest accuracy value of 0.99 (k=5, cityblock, squaredinverse, TRUE) stands out. These results suggest

that k=5 is a slightly better fit for your dataset. k=3 can sometimes be too sensitive to neighbors that are too close, while k=7 increases the number of neighbors, which may improve the generalization but may not be the best.

Table 8: SVM model results with different parameters

KernelFunc	BoxConstraint	KernelScale	Accuracy
linear	0,1	0,1	0,8176
linear	0,1	1	0,8143
linear	0,1	10	0,7948
linear	1	0,1	0,8143
linear	1	1	0,8143
linear	1	10	0,7980
linear	10	0,1	0,8078
linear	10	1	0,8111
linear	10	10	0,8241
rbf	0,1	0,1	0,5179
rbf	0,1	1	0,5179
rbf	0,1	10	0,7915
rbf	1	0,1	0,9186
rbf	1	1	0,9055
rbf	1	10	0,7980
rbf	**10**	**0,1**	**0,9446**
rbf	10	1	0,9088
rbf	10	10	0,8469

In the Distance parameter, the ‘cityblock’ (Manhattan) metric outperformed euclidean in many rows. In the DistanceWeight parameter, squaredinverse was often slightly more accurate than inverse. Although standardization is generally recommended in K-NN, the table interestingly shows that FALSE (no standardization) sometimes yielded higher results. Table 8 shows the classification accuracy values of the SVM model according to different optimization parameters. The results shows that the linear kernel SVM results are in the range of ≈0.79 to ≈0.82. The highest accuracy is obtained with 0.824 for the parameters BoxConstraint=10, KernelScale=10. The best accuracy for

the model with the RBF kernel is 0.9446, C=10, KernelScale=0.1. Overall, a moderate performance is obtained with the linear kernel. The data may not be fully linearly decomposed or may need the flexibility provided by the RBF kernel. These results show that the data is non-linear and that the RBF kernel can achieve much higher accuracy with appropriate tuning. When the overall results are analyzed, the complexity matrices of the best accuracy values are presented in Figure 2. Accuracy (A), F1-score (F1), Precision (P), Recall (R), Specificity (S), Matthews Correlation Coefficient (MCC) and AUC (Area Under the Curve) values obtained using complexity matrices are given in Table 9.

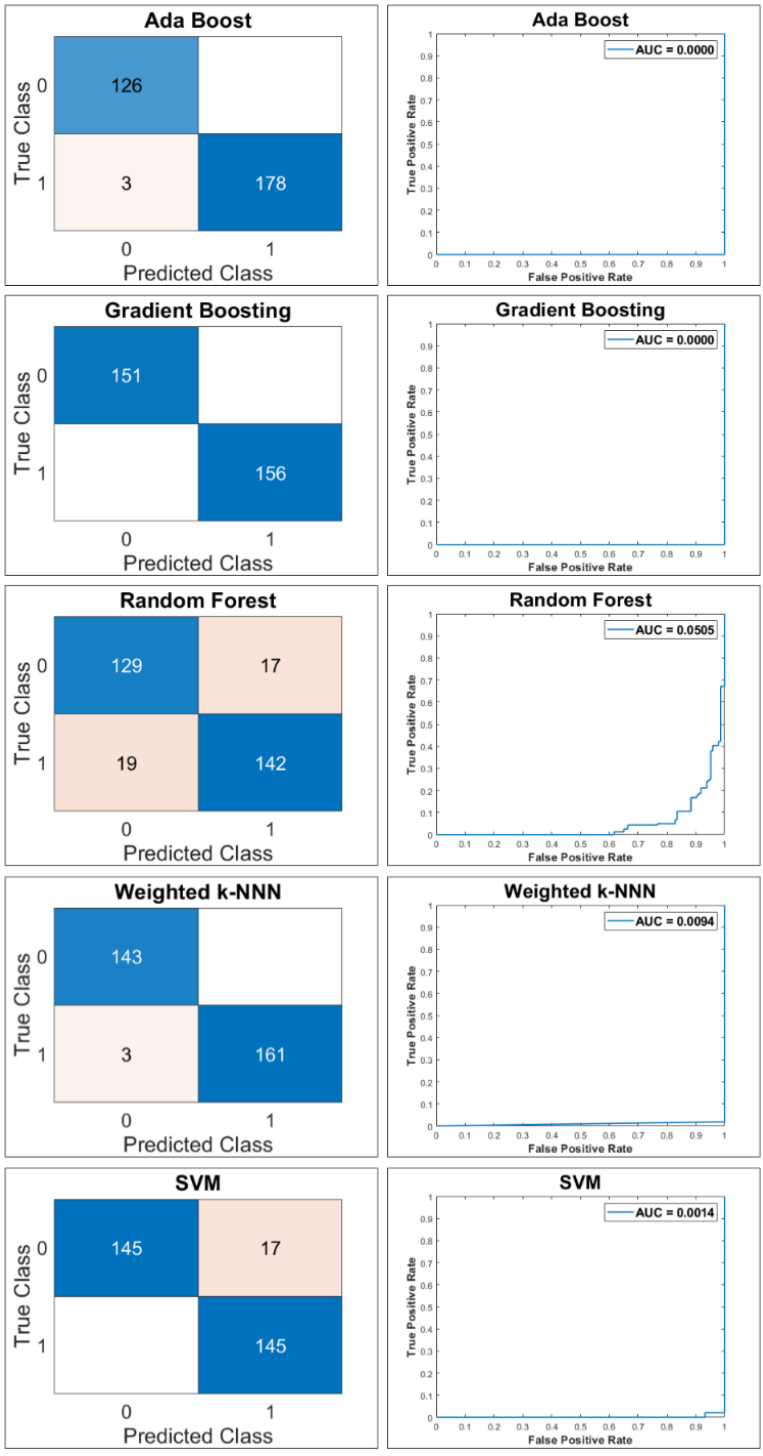

Figure 2: Confusion matrix of all best model

Table 9: Evaluation metrics of all best models

	AB	GB	RF	WKNN	SVM
Accuracy	0,9902	1	0,8827	0,9902	0,9446
F1 Score	0,9916	1	0,8875	0,9908	0,9446
Precision	1	1	0,8931	1	0,8951
Recall (Sensitivity)	0,9834	1	0,882	0,9817	1
Specificity	1	1	0,8836	1	0,8951
MCC	0,9801	1	0,7651	0,9806	0,8951
1-AUC	0	0	0,0505	0,0094	0,0014

According to Table 9 and Figure 2, especially in Gradient Boosting, all key metrics = 1 and AUC = 1, showing absolute perfection. SVM and WKNN both models (especially SVM) show a very successful classification in practical terms. SVM Recall = 1, AUC ~ 0.9986, so it does not miss patients "at all". RF Although it is a bit behind compared to other models, AUC ≈0.95 is still a very good result. Gradient Boosting seems to be absolutely "perfect", but AdaBoost and Weighted k-NN are close to the same level. SVM also achieved a very good result (Recall = 1, AUC ≈0.9986). In the final analysis, further validation steps are critical to confirm that these excellent results are real in practice. But if we look at the tabular data alone, Gradient Boosting, AdaBoost and Weighted k-NN show the best classification performance by very small margins. Especially with imbalanced datasets, Accuracy alone can be misleading, while MCC provides a fairer measure. For the GB model, MCC = 1 means that there are no classification errors, or if there are, they are very, very minimal; a performance that would pull the entire (TP, TN, FP, FN) matrix perfectly (or very close). The MCC ≈≈ 0.98 for the AB and WKNN model is an extremely high correlation coefficient, indicating that the model separates both positive and negative classes very well. It is also consistent with metrics such as classic Accuracy and F1. MCC = 0.8951 for the SVM model, again a very good result, but slightly below perfection, close to 1.0. Still Recall = 1 (not missing any patients), but perhaps with a slight decrease in positive predictions (Precision). MCC = 0.7651 for the RF model, lower than the other models. Still, above 0.76 is not a "bad" value, especially in datasets such as medical, but according to the table, it seems to be the most backward model.

CONCLUSION

In this study, a comprehensive performance analysis was performed on a heart disease dataset using various machine learning classification algorithms (AdaBoost, Gradient Boosting, Random Forest, Weighted k-NN and SVM). In the literature, early detection and accurate classification is an important need due to the high prevalence and mortality rate of cardiovascular diseases. According to the WHO, heart disease is still one of the leading causes of death, making any improvement and early detection approach valuable.

At the beginning of the study, the content and characteristics of the dataset (especially type of chest pain, resting ECG results, serum cholesterol, blood pressure, etc.) were taken into account. In order to make all methods comparable, similar data preprocessing steps were applied and evaluations were made based on appropriate metrics (Accuracy, F1 Score, Precision, Recall, Specificity, MCC and AUC).

The findings of the study show that machine learning algorithms are largely successful in diagnosing heart disease. In particular, Gradient Boosting distinguished the dataset flawlessly with ≈1 (perfect) results in metrics such as Accuracy, F1 Score, Precision, Recall, Specificity and MCC. AdaBoost and Weighted k-NN also achieved results very close to these values (Accuracy and F1 ≈0.98-0.99). SVM, on the other hand, remained at the level of ≈0.94, but performed in line with the principle of "not missing the patient" by providing the highest values (1) in critical metrics such as Recall. Random Forest, with an Accuracy value of ≈0.88, which is more modest than the other models, also performed quite well, but lagged behind the top models.

These results show that machine learning-based approaches can be highly successful in detecting heart diseases.

In particular, boosting-based methods such as Gradient Boosting and AdaBoost performed well enough to contribute to clinical decision support systems with sufficient data and correct parameter settings. However, it is recommended to repeat the study with k-fold cross-validation, a separate external test set or data from different institutions to verify the possibility of overfitting and to test the applicability in real life.

In conclusion, with proper data preprocessing, appropriate model selection and parametric tuning, it is possible to achieve accuracy and similar metric values up to ≈0.98-1 on the heart disease dataset. This shows that machine learning approaches are promising in the early diagnosis of cardiovascular diseases and can be an important tool for healthcare professionals in patient follow-up and treatment planning.

REFERENCES

Anon. n.d. “Heart Disease - UCI Machine Learning Repository.” Retrieved December 25, 2024 (https://archive.ics.uci.edu/dataset/45/heart+disease).

Archibald, Richard K., Mathieu Doucet, Travis Johnston, Steven R. Young, Erika Yang, and William T. Heller. 2020. “Classifying and Analyzing Small-Angle Scattering Data Using Weighted k Nearest Neighbors Machine Learning Techniques.” *Journal of Applied Crystallography* 53(2):326–34. doi: 10.1107/S1600576720000552/VG5118SUP2.ZIP.

Boughorbel, Sabri, Fethi Jarray, and Mohammed El-Anbari. 2017. “Optimal Classifier for Imbalanced Data Using Matthews Correlation Coefficient Metric.” *PLOS ONE* 12(6):e0177678. doi: 10.1371/JOURNAL.PONE.0177678.

Chicco, Davide, and Giuseppe Jurman. 2020. “The Advantages of the Matthews Correlation Coefficient (MCC) over F1 Score and Accuracy in Binary Classification Evaluation.” *BMC Genomics* 21(1):1–13. doi: 10.1186/S12864-019-6413-7/TABLES/5.

Chicco, Davide, Matthijs J. Warrens, and Giuseppe Jurman. 2021. “The Matthews Correlation Coefficient (MCC) Is More Informative Than Cohen’s Kappa and Brier Score in Binary Classification Assessment.” *IEEE Access* 9:78368–81. doi: 10.1109/ACCESS.2021.3084050.

Coşkun, HÜSEY\. IN. 2023. “Enhancing Classification Accuracy of Pumpkin Seed with Detail Morphological Features and Different Machine Learning Algorithms.”

Coskun, Huseyin, and Tuncay Yigit. 2018. “Artificial Intelligence Applications on Classification of Heart Sounds.” Pp. 146–83 in *Nature-Inspired Intelligent Techniques for Solving Biomedical Engineering Problems*. IGI Global.

Coskun, Huseyin, Tuncay Yiğit, İsmail Serkan Üncü, Mevlüt Ersoy, and Ali Topal. 2022. “An Industrial Application Towards Classification and Optimization of Multi-Class Tile Surface Defects Based on Geometric and Wavelet Features.” *Traitement Du Signal* 39(6):2011–22. doi: 10.18280/TS.390613.

Detrano, Robert, Andras Janosi, Walter Steinbrunn, Matthias Pfisterer, Johann Jakob Schmid, Sarbjit Sandhu, Kern H. Guppy, Stella Lee, and Victor Froelicher. 1989. “International Application of a New Probability Algorithm for the Diagnosis of Coronary Artery Disease.” *The American Journal of Cardiology* 64(5):304–10. doi: 10.1016/0002-9149(89)90524-9.

Freund, Yoav, and Robert E. Schapire. 1995. “A Desicion-Theoretic Generalization of on-Line Learning and an Application to Boosting.” *Lecture Notes in Computer Science (Including Subseries Lecture Notes in Artificial Intelligence and Lecture Notes in Bioinformatics)* 904:23–37. doi: 10.1007/3-540-59119-2_166.

Friedman, Jerome H. 2001. “Greedy Function Approximation: A Gradient Boosting Machine.” *Annals of Statistics* 1189–1232.

de Giorgio, Andrea, Gabriele Cola, and Lihui Wang. 2023. “Systematic Review of Class Imbalance Problems in Manufacturing.” *Journal of Manufacturing Systems* 71:620–44. doi: 10.1016/J.JMSY.2023.10.014.

Ho, Tin Kam. 1998. “The Random Subspace Method for Constructing Decision Forests.” *IEEE Transactions on Pattern Analysis and Machine Intelligence* 20(8):832–44.

Jiang, Liangxiao, Zhihua Cai, Dianhong Wang, and Siwei Jiang. 2007. “Survey of Improving K-Nearest-Neighbor for Classification.” Pp. 679–83 in *Proceedings - Fourth International Conference on Fuzzy Systems and Knowledge Discovery, FSKD 2007*. Vol. 1.

Kramer, Oliver. 2013. *Dimensionality Reduction with Unsupervised Nearest Neighbors*. Springer.

Li, Taiyong, Min Zhou, Carlos M. Travieso-González, and Jesús B. Alonso-Hernández. 2016. “ECG Classification Using Wavelet Packet Entropy and Random Forests.” *Entropy 2016, Vol. 18, Page 285* 18(8):285. doi: 10.3390/E18080285.

Maroco, João, Dina Silva, Ana Rodrigues, Manuela Guerreiro, Isabel Santana, and Alexandre De Mendonça. 2011. “Data Mining Methods in the Prediction of Dementia: A Real-Data Comparison of the Accuracy, Sensitivity and Specificity of Linear Discriminant Analysis, Logistic Regression, Neural Networks, Support Vector Machines, Classification Trees and Random Forests.” *BMC Research Notes* 4(1):1–14. doi: 10.1186/1756-0500-4-299/FIGURES/8.

Rhys, Hefin I. 2020. *Clustering Based on Density: DBSCAN and OPTICS - Machine Learning with R, the Tidyverse, and Mlr*.

Saupin, Guillaume. 2022. *Practical Gradient Boosting A Deep Dive*. AFNIL.

Sheppard, Clinton. 2019. *Tree-Based Machine Learning Algorithms: Decision Trees, Random Forests, and Boosting*. Clinton Sheppard.

Vandeput, Nicolas. 2021. *Data Science for Supply Chain Forecasting*.

Vinod, Hrishikesh D., and C. Radhakrishna (Calyampudi Radhakrishna) Rao. 2020. *Financial, Macro and Micro Econometrics Using R*.

Wang, Qingfeng, Shuai Wang, Bingkun Wei, Wenwu Chen, and Yufei Zhang. 2021. “Weighted K-NN Classification Method of Bearings Fault Diagnosis with Multi-Dimensional Sensitive Features.” *IEEE Access* 9:45428–40. doi: 10.1109/ACCESS.2021.3066489.

Yigit, Halil. 2013. “A Weighting Approach for KNN Classifier.” Pp. 228–31 in *2013 international conference on electronics, computer and computation (ICECCO)*.

Industrial Applications of Boron Coating Methods

İbrahim GÜNEŞ[1]
Atila Gürhan ÇELİK[2]

1- Prof. Dr. İbrahim GÜNEŞ; Department of Civil Engineering, Faculty of Engineering, Giresun University, Giresun, Türkiye. ibrahim.gunes@giresun.edu.tr ORCID No: 0000-0001-7595-0121
2- Prof. Dr. Atila Gürhan ÇELİK; Department of Civil Engineering, Faculty of Engineering, Giresun University, Giresun, Türkiye. atila.celik@giresun.edu.tr ORCID No: 0000-0002-0894-9961

ABSTRACT

This study presents the industrial applications of boron coating methods in a multifaceted way. Boron coatings offer many benefits in industrial applications. The first of these is that they provide resistance to wear thanks to their high hardness. Thanks to these features, machine parts, drill bits and other equipment exposed to wear can be protected with boron coatings. In addition, the chemical resistance properties of boron coatings provide excellent protection against acids and corrosive substances. Thanks to these features, boron coatings are widely preferred in industrial use. Finally, the low coefficient of friction of boron coatings increases the performance of machine parts and provides energy efficiency. These benefits are the main reasons why boron coatings are preferred in industrial applications.

Keywords – Boron Coatings, Hardness And Wear, Oxidation And Corrosion Resistance, Industrial Applications.

INTRODUCTION

Currently, there is a burgeoning interest in advanced coating technologies. The major focus of these technologies is boron coatings because of their remarkable attributes such as corrosion resistance, wear resistance, low chemical reactivity, and efficient thermal conduction. Additionally, their ability to protect the surface from a high-temperature flow of oxygen, nitrogen, and so forth makes them attractive for space technology, aviation, and power engineering. The interest in the development of advanced coating methods is provoked by the necessity to enhance performance characteristics related to the parameters of the wear process. Typically, the main or particularly important wear-type processes are developed in the dry friction sphere where high loads bearing, long-duration devices operate. Automotive parts, components of industrial machinery, and other consumer goods are mainly of a service life, wear-process background that depends on tribological conditions near the working surfaces. In these cases, various wear-resistance technologies are used in manufacturing processes. Principles requiring wear-resistance enhancement and component lifetime extension can be maintained by decreasing the friction coefficient and completely limiting mechanical or chemical/physiochemical wear phenomena. Thus, coating the surface of the materials with other materials that demonstrate very good tribological properties under harsh working conditions is a topic of interest. Such surface coatings enhance material performance by combining the essential strength and toughness of the component with the advantages of better wear and frictional properties. With this in view, the interest in the investigation of

boron coatings has been subject to becoming more cutting-edge and topical. The advantages of developed boron coating methods are discussed according to their advantageous peculiarities for wear-type influence. Furthermore, the application potential of developed boron coatings concerning their wear resistance is briefly analyzed [1-7].

FUNDAMENTALS OF BORON COATING METHODS

Boron is a versatile element due to its unique chemical and physical properties. Boron coating processes were developed to enhance the surface properties of materials in different fields. Mechanical, electrical, and corrosion-resistant properties are greatly improved by boron coatings. Several methods are used for the synthesis of boron coatings, like chemical vapor deposition, physical vapor deposition, and plasma spray [8-15].

A dense, pinhole-free, and uniform structure of boron coatings is obtained using chemical vapor deposition, packed-bed, and chemical bath deposition methods. The chemical vapor deposition occurs when the gaseous reactants, including boron trichloride, diborane, and various organoborane compounds, are introduced into the reaction chamber to react on the heated substrate. When these boron compounds come into contact with the heated surface, they release gaseous and elemental boron atoms, which travel through the chamber and bond with the substrate. The boron atoms diffuse into the substrate, creating a very hard and protective coating. The main advantage of chemical vapor deposition is the ability to achieve very uniform thickness and a smooth surface over complex shape. Many metals, ceramics, and composite materials can be coated with CVD boron in a wide range of custom thicknesses. In general, surface preparation and choice of substrate material are critical to achieving good adhesion and performance. Measurements like adhesion, abrasion resistance, and microhardness can be made to determine coating properties. It is often used in applications with high temperatures, wear, and corrosion, and also to coat mechanical parts [16-25].

ADVANTAGES OF BORON COATING METHODS

Boron-based coatings have been of great interest due to the superior characteristics they bestow on the coated specimens. Improved hardness, increased wear resistance, lower friction coefficient, and higher oxidation resistance are a mere few of the characteristics that engineers use to enhance the performance and prolong the lifecycle of the coated components. The hexagonal α-rhombohedral structures formed due to the diffusion of boron into the metal increase the hardness of the coatings by forming a solid solution,

thereby severely hindering the dislocations within the crystal structure. The formed solid solution alloy of boron and the coefficients of friction contribute to the controlled and lowered friction during the wearing of the coating. Anti-corrosive properties of boron surfaces play a pivotal role in their usage for several engineering materials in contact with harsh environments, thereby delaying their corrosion. These applications and advantages substantiate the potential it holds for various engineering materials and advance the industrial sectors in various measurements [26-32].

Optimum operational performance can be achieved by decreasing the wear of tools and materials used in processing various products, which is very crucial in many industrial sectors. The hard and wear-resistant characteristics of refractory metals, which also maintain these characteristics at high working temperatures, make them suitable for such applications. However, if boron, which also has these positive characteristics, can be grown by methods that are economical and do not require any special conditions, it can be used in the coating of good conductors. Considering these advantages of boron, successive techniques have been developed in order to obtain coatings with the desired hardness, low friction coefficient, and wear resistance. In recent years, the development of coating techniques has been carried out in parallel with industry. Today, especially boronizing results obtained by various coating methods are included [33-37].

Enhanced Hardness and Wear Resistance

The superior performance of boron coatings is primarily attributed to their enhanced hardness and wear resistance, thereby prolonging cutting and wear efficiency, as abrasive wear is often a dominant wear mechanism in applications. The modified crystalline structure at the surface layer and the vicinity between the boron coating and the substrate provides a depth gradient variation in mechanical properties. Incorporating a high degree of boron content in the boron coating increases the concentration of borides, leading to significantly higher hardness values than those of the untreated substrate. Conditions that can be improved are not restricted to hardness: Young's modulus and elastic modulus are also found to increase after immersion of a component in boronizing media, which can change oversprayed or borided nickel-based superalloys for the aircraft industry [38-43].

Increased hardness also occurs for the pure amorphous form of boron coatings formed on soft phosphorus and aluminum substrates, while a ceramic-like coating formed on steel also resulted in a substantial increase in the microhardness value. Wear tests showed that the wear resistance of boron-coated samples is highly influenced by the amount and composition of boron species located at the top surface and the sublayer region. In industrial applications, abrasion and wear are the primary mechanisms experienced by tools and components. The steel industry is heavily reliant on machines and operational infrastructure that are heavily exposed to high-pressure wear and

abrasion. As the service lives of these structures are considerably low, there is a need to replace the parts and perform maintenance regularly. Boronizing mechanisms have been shown to contribute significantly to reaction efficiency, microhardness, wear resistance, and cutting and metal forming capacity. Implementing boronized steel tools may significantly improve the service life of the components and reduce the percentage of tooling costs associated with these industries. Indirectly, due to the consistent efficiency and value of the operational parts, the industry is positively impacted [44-48].

The increased hardness of a workpiece through surface treatment can lead to a significant decrease in breakage performance, directly contributing to a more significant amount of time where maintenance activities must be conducted and the tool cannot work during this period. Additionally, boronizing for the increased hardness of a workpiece will also yield higher cutting coefficients of cemented carbide bits, resulting in a geothermal drilling speed that is significantly quicker. The general consensus is that the boronizing combination mechanism with other surface treatment methods is considered highly desirable. For industries addressing concerns related to improving operational efficiency and decreasing operations and maintenance costs, close collaboration concerning enhanced hardness and improved wear resistance should certainly be considered. [49-56].

Chemical and Corrosion Resistance

Materials are often required to protect surfaces from their exposure to a variety of corrosive or aggressive environments. Contents of these environments include acceleration of the oxidation process or chemical degradation of a base metal by causing different destruction events on the surface of the material. Cermet-type wear-resistant materials have good wear resistance; however, they lose surface quality due to corrosion or gas penetration. Processes to harden the surfaces of the base metal can be seen as methods to protect against surface destruction. One of the most sought-after characteristics of these methods is the durability of the feature formed on the surface. A study that examines how the application formed on the surface will contribute to this resistance will serve to strengthen the industries. A coating must protect the substrate from the surrounding environment and prolong the life of the coated component. In a protective coating, the chemicals are the main acting destructive agents. Some industries use abundant chemicals in their designs where protective coatings are needed. Therefore, coatings must be able to survive in these areas. Boron compounds contribute positively in operations where protection is needed. Oil expands its quality over long periods in the oil sector, in which various chemicals are utilized, and investments are made. Thus, the uses of boron film on surfaces come into play on these extended performance criteria. Boron coating and other boronization methods have made it possible for a single operation here to prevent surface

destruction. Coated components require less replacement than the total investment made [57-68].

Temperature and Oxidation Resistance

Boron coatings are characterized by their excellent temperature resistance, allowing for exposure to extremely high thermal environments without significant degradation. This is of particular importance in applications such as aerospace and automotive, since their hydraulic, pneumatic, propulsion, and drivetrain components are exposed to heat cycles. The good thermal stability of boron coatings is due to the formation of consolidated, thermodynamically stable crystallites with very low free-energy boundaries. In addition, their resistance to high-temperature oxidation is one of their greatest advantages. The dense, stable borosilicate glass layer that forms during oxidation often provides an effective barrier that prevents or slows down the further inward diffusion of oxygen and the outward migration of metallic cations. Therefore, boron coatings present low oxidation rates in a wide range of temperatures. The high-temperature performance of boron-coated components has been verified in numerous industrial applications. Furthermore, in industry, rollers for processing glass are coated with aluminum and boron in order to improve their performance. By comparing boron coatings to other hard coatings, it is clear that one of the greatest advantages for the use of boron coatings in high-temperature tribological applications is their inherent temperature resistance. Even at less severe temperatures, a comparison of oxidation rates found boron coatings to be significantly superior. High temperature resistance ensures reliability and component safety in various industrial operations. In many high-temperature, heavily loaded applications, coatings often have to be replaced frequently due to their wear and oxidation. Coating material replacement is often a costly procedure that can account for a substantial portion of the overall cost of the component. Over the life of the component, which can be between several months and several years depending on the application, a reduction of the frequency of these replacements, such as due to the coating's high-temperature resistance, can result in significant cost savings [69-74].

Low Friction Coefficients

The low friction coefficients of boron coatings result in smooth rolling and sliding of a soft counterface or a counterpart. The low friction coefficient is due to the space charge transfer between the contact surfaces or the very high contact resistance of the boride surface. There are several changes in the textures of a worn boride surface. The worn boride operates under highly tribo-oxidative conditions. The boron coating reduces oxygen ingress compared to uncoated steel. A reduction of oxide adhesion decreases the wear process. Low friction is usually advantageous to mechanical load-bearing systems. Not only does it reduce the coefficient of friction between non-

lubricated components, but it also reduces surface temperature rise, which affects the adhesive and oxidative wear mechanisms. The largest advantage of wear-resistant, solid lubricant coatings is anti-friction by the hard topcoat. This technology has found major applications in the automotive industry, and values of low friction are required for emerging basic research in manufacturing industries. A significant reduction in friction results in energy savings. Several wear-resistant coatings reduce friction in sliding contact. A comparison of the friction coefficients and wear volumes of the eight coatings tested is shown in graphs. The relationships between the friction coefficients and wear bodies are illustrated [75-83].

INDUSTRIAL APPLICATIONS OF BORON COATING

Boron coatings can have a multitude of industrial uses due to a combination of properties such as high hardness, low friction, excellent wetting, and prevention of oxidation at high temperatures. Boron coatings can find a home in a variety of industrial applications, from traditional markets of aerospace coatings to newer markets such as medical devices. In aerospace, the application of boron coatings onto jet engine components can help improve the efficiency and prolong the life of these components, which are exposed to high temperatures and pressures during operation. For cars, boron coatings can be used to coat gears, resulting in a 14% to 50% increase in efficiency. Boron-based coatings can also be used in tools and machinery applications where wear resistance is the primary performance requirement. In terms of biomedical devices, boron coatings can increase the wear and corrosion resistance of the devices, which is especially beneficial for applications that are implanted in the human body and operate in a harsh chemical environment. Recently, boron-based coatings have also drawn interest as an economically competitive alternative for applications that traditionally would use other types of coatings. The oil and gas sector, where components operate in highly corrosive, high-temperature, and high-pressure environments, is particularly of interest for the adoption of boron-based coatings. Boron-based coatings can extend the life of aircraft engine components by helping prevent the degradation of a component that is exposed to high temperatures. Boron coatings are relatively simple to apply and have the potential to provide performance similar to other coatings, but at a lower cost. Moreover, recent studies suggest that perhaps the most impactful growth for boron coatings will be in the context of micro-electro-mechanical systems [83-89].

Aerospace Industry

The aerospace industry is aggressively using surface-engineered materials and technologies to improve the performance and safety of components used in flight at high altitudes under extreme temperatures. At the place where the engine is manufactured, the ambient temperature is severe, which poses a challenge for developing promising coatings. Even though the structural parts can withstand a high-temperature environment, air resistance leads to wear and tear and material fatigue. The use of special materials and protective coatings can enhance performance and safety. The metallic materials involving Inconel, among others, are coated with B4C for components like turbine blades and structural components in the thermal protection mechanism. In the aerospace field, weight reduction due to new technology and high specific strength materials is a trend in which boron and its compounds convert into a strong fiber to meet the required mechanical properties. The strong, hard ceramic materials reduce the structuring of components and result in fuel efficiency through weight reduction. In the case of aerospace segments, both the manufacturer and operating agency require components coated with anti-corrosion and anti-wear properties, especially the engine components, civil and military aero-engines, rocket motors, and hypersonic engines. The coatings should be tightly adhered to the base material throughout their operating period in order to achieve the same efficiency as the initial commissioning. The performance of coatings is validated by physical field trials. The need for requirements in these segments is to maintain erosion resistance and increase the lifetime of the B4C coating compared to that of the uncoated. The protective coatings serve as an allowance for accidental power engine failure, such as the shedding of compressor and turbine blades, and the anti-fretting wear coatings are used on the contact surfaces of the hub and blades of the first stage in gas turbine engines to stop wear due to the tangential movement of the turbine blades. The current operational reports of the re-entry module, satellite, and aircraft show positive results that increase the growth of this application. Further scientific research in the field of plasma in industry has recently shown a significant increase in depositing B4C onto various components for the multirole and variable nature. Some of the high thermal processes have time constraints. The industrial coatings involve thermal spraying techniques, thermal diffusing in steel components, plasma-enhanced physical vapor deposition, and even spark erosion techniques are also used for the coatings in the mold. In the aviation atmosphere, various components are exposed to blast freezing, and condensation can occur in high humidity. In the presence of hydrogen sulfide or sulfur dioxide at high temperatures, stress cracking may occur in a short period. Generally, specifications in the form of site-specific standards are set by the operator, which manufacturers use to show compliance with the expected life of a component in commercial aviation. The staff from major

airworthiness transport administrations and basic surveyors from oil and gas companies formed a committee to develop a comprehensive commercial airplane operating standards document [90-95].

Automotive Industry

The automotive industry is the largest end-user sector of surface-engineered products. In vehicles, coated surfaces cover various sophisticated components, such as engine parts, transmission systems, cutting tools, etc., and the market share is increasing every year. The low friction between two mating parts due to a boron coating can also offer a broader range of driving speeds. In the automotive sector, the primary performance improvement is the reduced fuel consumption of the vehicle. A vehicle's engine can be improved by a boron-coated powertrain to have a lower fuel consumption rate. Modern transportation systems aim to have a higher power density, and the temperature of machine components is thus significantly higher. As a result, the corrosive problems of machine parts are accentuated. Boron coatings offer the ability to protect cutting elements against corrosion problems generated by a machine, a cutting fluid, or a workpiece. A vehicle's lifespan directly affects its physical and economic aspects. Therefore, studies of the lifetime of vehicles are crucial, especially in economic perspectives. For instance, if corroded exhaust systems can be replaced with coated ones, the amount of ferric oxide emission per vehicle can be reduced, and the ferric oxide reduction effect is estimated to be significant. Finally, after a vehicle's lifetime, the components that need to be replaced with new ones may be coated with materials such as boron, zirconium, and molybdenum to prolong their lifetime. For example, automobiles require brake pads to generate friction between the wheels and the road in order to stop so that road accidents can be reduced, and the safety of road users can be improved. Crystallized magnesium contains more hard and abrasive impurities than uncoated brake pads, which can be more harmful to roads than conventional braking systems. It is concluded that the new boron brakes can reduce road wear significantly using the mechanistic-empirical road wear model [94-101].

Cutting Tools and Machinery

The requirements for considerable wear resistance are particularly high in the field of cutting materials and the years of advertised service life. The increased coating hardness reduces or prevents the formation of a crack with the friction on the chip knife and thus ensures that the originally coated cutting material does not generate an unfastened roughing or chipping during later application, even under the most unfavorable chipping and cutting conditions. The lowest basis stress profile will produce the smallest surface roughness. For precision and economic reasons, everything possible in the design of cutting tools and machinery should be done to produce the most detail possible in the case of a card with the coarsest cut possible in the shortest

possible time. The efficiency of cutting technology is essentially determined by the productivity of the cutting tools and the costs associated with cutting materials. As already mentioned, the resistance of the articles requests the cutting materials. These are cutting ceramics in various forms, mainly drills, brazed tools, and indexable inserts, to a small extent indexable drills and mills. It is based on the repeated movement of untilers in the close or non-closable drawing-machine bushes produced for the automotive industry. The broaches drill in the form of a circular blade, mounted in carriers [102-113].

Medical Devices

Manufacturers in the medical industry have sought ways to ensure the safety and success of their innovative devices. Additionally, they are pushed to develop medical implants made of new, biocompatible, and durable materials. One of the ways to increase the biocompatibility and durability of surgical tools and implants is to use protective coatings, which have certain properties, such as acceptable chemical inertness, not supporting microbial growth, maintaining uniformity, withstanding sterilization, and sustainability. Anti-wear coatings and surface treatments are more and more often used to protect joints. That is intended to ensure the highest possible quality of life for patients. With the development of technology and medicine, it is now possible to make prostheses that allow, for example, children to walk and grow without needing further surgeries. A success story is the orthopedic application of cobalt-chromium-molybdenum metals, then coated with sintered hydroxyapatite or highly polished to make the medical implant roughness similar to the plasma membrane, and lastly stabilized by surface adsorbed proteins. Only then were titanium and its alloys and ultra-high molecular weight polyethylenes used in orthopedic joint prostheses. Surgeons have an increasing need for the use of boron-coated medical installation devices—primarily for total knee replacement. The use of boron-coated biopsy tongs for the extraction of cancellous bone biopsies is now well established. Borided cutting instruments have been found especially useful in dry milling titanium and titanium alloys. The disadvantages of the modified environment described above are that protective coatings employed must be chemical-inert, i.e., show high corrosion resistance to saline solutions. They must also demonstrate resistance to microbial growth in-house, with certain physical and mechanical properties—the primary ones being adhesion, abrasion-wear resistance, and uniform surface coverage with a coating thickness of ±20% of a nominal thickness. The surfaces must be characterized by a moisture contact angle and sessile drop that remains constant at ±10° with respect to the nominal contact angle on an uncoated control. It is also a requirement that surgeons and anesthesiologists like handling devices coated with proposed boronizing. The decrease in cutting tool blade forces makes a surgeon's job easier and facilitates cost-effective vasotomy performed on homogeneous grafts. Coatings applied have a reduction in roughness while other coatings

have increases in that. It is very likely that in both situations, boron coatings would increase the successful use lifetime of this line of medical tools. Reducing the blade tip defects, as has been typically found in uncoated instruments, while maintaining blade sharpness, is another potential use of boron-coated devices [114-121].

Oil and Gas Industry

The oil and gas industry represents major consumers of boron- and boron carbide-based coatings. This is a unique market sector in terms of an aggressive environment to which the remaining elements in boron-based insulation coatings are used for the deposited electricity will never be exposed. The environment presents a challenge to relevant places and systems such as pipes, valves, tensile bolts, tightening nuts, and heat exchangers because they are affected by a combination of high pressures and aggressive substances, which manifests as deposits known for what is called quickly pitting; it allows leaking and eventually forming clear and dangerous point holes. A similar phenomenon known as packing (corrosion due to an external aggressor) is threatened by a dangerous combination of tropical seawater, carbon dioxide, and hydrogen sulfide. Approximately half of the world's petrochemical plants use a form of borate compounds in oil extraction or refining, altogether in unusual systems and areas (pipes and drilling elements) that are exposed to extreme temperatures and in the deeper part where the hot and unpredictable environment, which is predicted for passive thermal regeneration (in the heat transfer network), remains in effect. Due to their exceptional lubricating properties, good chemical resistance, good compatibility with steel or cement, and mobilization and control of physicochemical reactions in cement-cased wells, boron compounds, especially zinc or zinc borate crumbs, are generally preferred in deep cements for cementation of oil and gas wells. Boron coatings, apart from being used on their own, can be welded on surfaces after boronizing or borocarbonitriding, which is also used as a maintenance material for already in-service equipment. The materials and equipment used for these harsh environments must have excellent wear and tear, corrosion, erosion, and abrasion resistance. These severe operating conditions require a system that must bring out long and reliable performance in the field of the oil and gas industry to meet the demand without encountering failure. The use of boronizing provides high wear and corrosion resistance; hence the component can give a prolonged life cycle. There are a few items that greatly benefit from the use of boronizing; they are valves, plungers, buckets, and downhole tools, which are used in the oil extraction and refining industries, where they are exposed to the born and abrasive particles during operation. The proposed application of boronizing will be adopted by all sectors where it is useful for wear and corrosion resistance in extreme conditions. Oil and gas facilities such as pipelines and reservoirs are constantly threatened by corrosion due to their environment. The boronizing process has been discovered to be one of these

activities that significantly lengthen the time taken to replace or maintain by using materials that are more resistant to corrosion and wear [122-128*]*.

FUTURE DEVELOPMENTS AND TRENDS

Nanotechnology and ultra-thin films and new materials are some of the world's most important research fields, leading to the development of new surface treatment techniques for conventional products, which are to be used for innovative applications. The underlying principles of boriding and boronizing technologies are therefore expected to extend the boron coating applications in the years to come. Concepts such as super-hard coatings, functionally graded coatings, and nanostructured materials have the potential to further improve the economic returns on the dissemination of boron-based film technologies. Rapid progress has been made on ultra-thin coatings, and the market share of environmental and biologically degraded products therefore fluctuates in the future and is becoming increasingly essential for the coating process of the future. The scarcity of resources due to the lack of approval procedures for industrial products is one of the important issues of our time with increasing awareness. The demand for advanced coatings in the world is increasing not only in wear resistance but also in advanced industries, and eventually in developing and underdeveloped countries. The accelerated development of non-conventional coating techniques is now in full operation. The rapid development of many of these innovative processes and the resulting increase in production will also affect costs. Based on current developments in these processes, simplified production lines will play an important role in the widespread use of these coating applications, further reducing current costs [129- 133].

CONCLUSION

This article attempts to explain the main advantages and industrial applications of boron coatings. Boron coatings improve many surface properties of the material, including high hardness, corrosion resistance, and low coefficients of friction. Boron coating methods have a significant impact on many industrial sectors. They are used to improve the usability of materials in various fields. There are also many studies that show the potential use of boron coatings in other industrial fields such as the aerospace and automotive sectors. Moreover, the strategy helps in thin films deposited on medical devices in additional areas ranging from improving the surface biocompatibility of dental implants to antiseptic properties of catheters and elimination of diseases. Finally, the continuous demand for lower friction,

better wear resistance and higher performance materials in many industrial processes is increasing investment in coating research.

REFERENCES

[1] Xu, P., Liu, J., Chen, X., Zhang, W., Zhou, J., Wei, X. (2022) Ignition and combustion of boron particles coated by modified materials with various action mechanisms. *Combustion and Flame*, 242, 112208.

[2] Liu, X., Xu, C., Chen, P., Li, K., Zhou, Q., Ye, M., Zhang, L., Lu, Y. (2022) Advances in Technologies for Boron Removal from Water: A Comprehensive Review. *Int. J. Environ. Res. Public Health*, 19, 10671.

[3] Mansouri, H., Said, H.A., H. Noukrati, H. Oukarroum, A., Ben Youcef, H., Perreault, F. (2023). Advances in Controlled Release Fertilizers: Cost-Effective Coating Techniques and Smart Stimuli-Responsive Hydrogels. *Adv. Sustainable Syst.*, 7, 2300149.

[4] Dabees, S., Mirzaei, S., Kaspar, P., Holcman, V., Sobola, D. (2022). Characterization and Evaluation of Engineered Coating Techniques for Different Cutting Tools-Review. *Materials*, 15, 5633.

[5] Gunes, I., Yıldız, I. (2016). Investigation of adhesion and tribological behavior of borided AISI 310 stainless steel, *Materia-Rio De Janeiro*, 21 (1), 61-71.

[6] Gunes, I. (2013). Wear Behaviour of Plasma Paste Boronized of AISI 8620 Steel with Borax and B_2O_3 Paste Mixtures, *Journal of Materials Science & Technology*, 29 (7), 662-668.

[7] Arun, K.L., Udhayakumar, M., Radhika, N.A. (2023). Comprehensive Review on Various Ceramic Nanomaterial Coatings Over Metallic Substrates: Applications, Challenges and Future Trends. *Journal of Bio-and Tribo-Corrosion*, 9, 11.

[8] W. Zhang, W. (2021). A review of tribological properties for boron carbide ceramics. *Progress in Materials Science*, 116, 100718.

[9] Vitry, V., Hastir, J., Mégret, A., Yazdani, S., Yunacti, M., Luiza, B. (2022). Recent advances in electroless nickel-boron coatings. *Surface and Coatings Technology*, 429, 127937.

[10] Gunes, I., Erdogan, M., Çelik, A.G. (2014). Corrosion behavior and characterization of plasma nitrided and borided AISI M2 steel. *Materials Research*, 17, 612-618.

[11] Santos, J., Moschetta, M., Rodrigues, J., Alpuim, P., Capasso, A. (2021) Interactions Between 2D Materials and Living Matter: A Review on Graphene and Hexagonal Boron Nitride Coatings. *Front. Bioeng. Biotechnol.* 9, 612669.

[12] Schneider, R., Facure, M.H.M., Chagas, P.A.M., Andre, R.S., dos Santos, D.M., Correa, D.S. (2021). Tailoring the Surface Properties of Micro/Nanofibers Using 0D, 1D, 2D, and 3D Nanostructures: A Review on Post-Modification Methods. *Advanced Materials Interfaces*, 8(13), 2100430.

[13] Barati Q., Hadavi, S.M.M. (2020). Electroless Ni-B and composite coatings: A critical review on formation mechanism, properties, applications and future trends. *Surfaces and Interfaces*, 21, 100702.

[14] Bai, C., Wang, F., Zhao, Z., Zhang, B., Yu, Y., Zhang, J. (2021). Mussel-inspired facile fabrication of dense hexagonal boron nitride nanosheet-based coatings for anticorrosion and antifriction applications. *Materials Today Nano*, 15, 100129.
[15] Erdogan, M., Gunes, I. (2015). Corrosion Behavior and Microstructure of Borided Tool Steel, *Materia-Rio De Janeiro*, 2 (2), 523-U279
[16] Yuan, Y., Weber, J., Li, J., Tian, B., Ma, Y., Zhang, X., Taniguchi, T., Watanabe, K., Lanza, M. (2024). On the quality of commercial chemical vapour deposited hexagonal boron nitride. *Nature Communications*, 15, 4518.
[17] Tay, R.Y., Li, H., Wang, H., Lin, J., Ng, Z.K., Shivakumar, R., Bolker, A., Shakerzadeh, M., Tsang, S.H., Teo, E.H.T. (2023). Advanced nano boron nitride architectures: Synthesis, properties and emerging applications. Nanotoday, 2023. 53, 102011.
[18] Zhang, T., Xue, Z., Xie, Y., Huang, G., Peng, G. (2022). Fabrication of a boron-doped nanocrystalline diamond grown on an WC–Co electrode for degradation of phenol. *RSC advances*, 12, 26580.
[19] Gunes, I., Yıldız, I. (2015). Rate of growth of boride layers on steels. *Oxidation Communications*, 38(4A), 2189-2198.
[20] Snyders, R., D. Hegemann, D., Thiry, D., Zabeida, O., Klemberg-Sapieha, J., Martinu, L. (2023). Foundations of plasma enhanced chemical vapor deposition of functional coatings. *Plasma Sources Sci. Technol.*, 32 ,074001
[21] Yıldız, I., Çelik, A.G. Gunes, I. (2020) Characterization and diffusion kinetics of borided Ni-Mg alloys. *Protection of Metals and Physical Chemistry of Surfaces*, 56, 1015-1022
[22] Esfahani, A.N., Malcolm, A.J., Xu, L., Yang, H.B., Storwick, T., Kim, N.Y., Pope, M.A. (2020). Ultra-thin films of solution-exfoliated hexagonal boron nitride by Langmuir deposition. *Journal of Materials Chemistry C*, 8, 13695-13704.
[23] Gunes, I., Çelik, A.G. (2022). Surface Properties of Borided Tungsten Alloys. *Journal of Underground Resources*, 21, 29-35.
[24] Uygunoğlu, T., Gunes, I., Çelik, A.G., Çınar, E. (2021). Microstructural Characterization and Corrosion-Resistance of Borided Rebar. *El-Cezerî Journal of Science and Engineering*, 8 (3), 1135-1148.
[25] Agarwal, P.P.K., Jensen, D., Chen, C.H., Rioux, R. M., Matsoukas, T. (2021). Surface-functionalized boron nanoparticles with reduced oxide content by nonthermal plasma processing for nanoenergetic applications. *ACS Appl. Mater. Interfaces*, 13(5), 6844-6853.
[26] E. V. Kharanzhevskiy, A. G. Ipatov, A. V. Makarov, "Tribological performance of boron-based superhard coatings sliding against different materials," Wear, Elsevier, 2021. [HTML]
[27] Souqui, L., Palisaitis, J., Ghafoor, N., Pedersen, H., Högberg, H. (2021). Rhombohedral boron nitride epitaxy on ZrB_2. *J. Vac. Sci. Technol. A*, 39 (1), 013405.
[28] Magnuson, M., Hultman, L., Högberg, H. (2022). Review of transition-metal diboride thin films. *Vacuum*, 196, 110567.
[29] Gunes, I., Yıldız, I., Çelik, A.G. (2022). Wear Resistance and Characterization of Borided Ni-Based Alloys. *Powder Metallurgy and Metal Ceramics*, 60 (11), 717-726.

[30] Panda, J.N., Wong, B.C., Medvedovski, E., Egberts, P. (2021). Enhancement of tribo-corrosion performance of carbon steel through boronizing and BN-based coatings," Tribology International, 153, 106666
[31] Kulesh, E.A., Piliptsou, D.G., Rogachev, A.V., Hong, J.X., Fedosenko N.N., Kolesnyk V., (2020). Boron-carbon coatings: structure, morphology and mechanical properties. *Journal of Engineering Sciences*, 7(1), C1-C9.
[32] Sharma, R.K., Kumar, S.R. (2024). Erosion wear investigation of Fe-Cr-Ti coating with varying boron content. *Proceedings of the Institution of Mechanical Engineers, Part E: Journal of Process Mechanical Engineering*. InPress.
[33] Gunes, I., Çelik, A.G. (2018). Characterization of Borided DIN X165CrMoV12 Steel. *El-Cezerî Journal of Science and Engineering,* 5, 904-908.
[34] Yushkov, Y., Oks, E., Kazakov, A., Tyunkov, A., Zolotukhin, D. (2022). Electron-Beam Synthesis and Modification and Properties of Boron Coatings on Alloy Surfaces. *Ceramics,* 5, 706–720.
[35] Han, X., Zhang, Z., Chen, H., Luo, L., Zhang, Q., Chen, J., Chen, S., Yang, Y. (2021). Bulk boron doping and surface carbon coating enabling fast-charging and stable Si anodes: from thin film to thick Si electrodes. *J. Mater. Chem. A*, 9, 3628-3636.
[36] Gunes, I., Çelik, A.G. (2021). Surface Characterization of Borided S220 Rebar. *Journal of Characterization,* 2, 66-70
[37] Pan, D., Zhang, X., Yang, G., Shang, Y., Su, F., Hu, Q., Patil, R.R., Liu, H., Liu, C., Gu, Z. (2020). Thermally conductive anticorrosive epoxy nanocomposites with tannic acid-modified boron nitride nanosheets. *Ind. Eng. Chem. Res.,* 59, 46, 20371-20381.
[38] Li, Q., Zhang, Y.L., Zhang, L., Wang, Q., Zhao, Z., Chen, D.X., Jin, H., Wang, Y.Y., Zhang, J.W. (2023). Effect of boron on the microstructural evolution and wear resistance of high-hardness Fe-based alloy coatings prepared by laser cladding. *Surface and Coatings Technology,* 458, 129342.
[39] Gunes, I., Keddam, M., Chegroune, R., Ozcatal, M. (2015). Growth kinetics of boride layers formed on 99.0% purity nickel. *Bulletin of Materials Science,* 38, 1113-1118
[40] Mei, F., Chen, Y., Zhang, H., Lin, X., Gao, J., Yuan, T., Cao, X. (2021). Greater improvement of carbon and boron co-doping on the mechanical properties, wear resistance and cutting performance of AlTiN coating than that of doping alone. *Surface and Coatings Technology*, 406, 126738.
[41] Kondul, B., Cetin, M.H. (2022). Increasing the wear resistance of railway switches with boron coating and analysis of tribological performance by ANOVA method. Wear Volumes 488–489, 204132.
[42] Gunes, I., Kanat, S. (2015). Diffusion kinetics and characterization of borided AISI D6 steel. *Protection of Metals and Physical Chemistry of Surfaces,* 51, 842-846
[43] Li, L., Wang, Z., Du, W., Qi, S., Du, X. (2024). Microstructure and wear resistance of laser cladding AlCoCrFeNiSiB high-entropy alloy with high boron content. *Surface and Coatings Technology*, 494, 131431.
[44] Karakaş, M.S., Günen, A., C. Çarboğa, C., Karaca, Y., Demir, M., Altınay, Y., Erdoğan, A. (2021). Microstructure, some mechanical properties and tribocorrosion wear behavior of boronized

Al0.07Co1.26Cr1.80Fe1.42Mn1.35Ni1.10 high entropy alloy. *Journal of Alloys and Compounds*, 886, 161222.
[45] Mishigdorzhiyn, U., Chen, Y., Ulakhanov, N., Liang, H. (2020). Microstructure and Wear Behavior of Tungsten Hot-Work Steel after Boriding and Boroaluminizing. *Lubricants*, *8*(3), 26.
[46] Bartkowska, A., Bartkowski, D., Przestacki, D., Kuklinski, M., Miklaszewski, A., Kieruj, P. (2021). Laser Processing of Diffusion Boronized Layer Produced on Monel® Alloy 400-Microstructure, Microhardness, Corrosion and Wear Resistance Tests. *Materials*, 14, 7529.
[47] Gunes, I. (2015). Effect of sliding speed on the frictional behavior and wear performance of borided and plasma-nitrided W9Mo3Cr4V high-speed steel. *Materiali in Tehnologije*, 49 (1), 111-116.
[48] Gunes, I. (2015). Boride layer growth kinetics of the borided high alloyed cold work tool steel. *Oxidation Communications*, 38 (1), 157-165.
[49] Zheng, L., Sun, Y., Luo, C., Zhao, Y., Xu, X., Wei, X., J. Wang, J., Wang C. (2024). Enhancing the tribological properties of cemented carbide drills for printed circuit boards through surface micro-structuring. *Wear*, 564–565, 205667.
[50] Liu, X., Zhang, H., Lin, G., Wang, Z., Zhang, J., Shi, H. (2023). Advances in deposition of diamond films on cemented carbide and progress of diamond coated cutting tools. *Vacuum*, 217, 112562.
[51] Tu, L., Tian, S., Xu, F., Wang, X., Xu, C., He, B., Zuo, D., Zhang, W. (2020). Cutting performance of cubic boron nitride-coated tools in dry turning of hardened ductile iron. *Journal of Manufacturing Processes*, 56, 158-168
[52] Zhang, Z., Xiang, D., Zhang, Z., Zhang, Y., Zhao, B. (2023). Study on tribology and cutting performance of boron doped diamond composite coated tool. *International Journal of Refractory Metals and Hard Materials*, 117, 106385.
[53] Silva, E.L., Pratas, S., Neto, M.A., Fernandes, C.M., Figueiredo, D., Silva, R.F. (2021). Multilayer Diamond Coatings Applied to Micro-End-Milling of Cemented Carbide. *Materials*, 14, 3333.
[54] Lalaoui, K., Belaid, M., Beliardouh, N.E., Bouzid, K., Tlili, S., Kahloul, L., Boudjeda, K., Ramoul, C.E. (2025). Microstructure and tribological properties of CrVN thin film coated WC-Co tool after boriding process. *Int J Appl Ceram Technol*., 22, e14896.
[55] Banerjee, A., Maity, K. (2024). Machinability appraisal of nitronic-50 under dry environment using uncoated carbide inserts. *Materials and Manufacturing Processes*, 39, 506-517.
[56] Gunes, I. (2014). Investigation of tribological properties and characterization of borided AISI 420 and AISI 5120 steels, *Transactions of the Indian Institute of Metals*, 67, 359-365
[57] Erdoğan, M., Gunes, I., Dalar, A. (2014). Investigation of corrosion behavior of borided gear steels. *Transactions of the Indian Institute of Metals*, 67, 291-297
[58] Zehra, S., Mobin, M., Aslam, J. (2022). An overview of the corrosion chemistry. *Environmentally Sustainable Corrosion Inhibitors, Fundamentals and Industrial Applications*, 3-23.
[59] G. Lazorenko, A. Kasprzhitskii, and T. Nazdracheva, T. (2021). Anti-corrosion coatings for protection of steel railway structures exposed to atmospheric environments: A review. *Construction and Building Materials*, 288, 123115

[60] Uygunoglu, T., Gunes, I. (2015). Biogenic corrosion on ribbed reinforcing steel bars with different bending angles in sewage systems, *Construction and Building Materials*, 96,.530-540.
[61] Gunes, I., Ozcatal, M. (2016). Investigation of The Adhesion and Wear Properties of Borided AISI H10 Steel, *Materiali in Tehnologije*, 50 (2), 269-274.
[62] X. Ren, H. Zou, Q. Diao, C. Wang, Y. Wang, H. Li, and T. Sui, "Surface modification technologies for enhancing the tribological properties of cemented carbides: A review," Tribology, 2023. [HTML]
[63] Ergun, Y., Gunes, I., Erdogan, M., Cankaya, N. (2017). Effect of Boriding Treatment on the Corrosion Behavior of Steels, *Journal of Nanoscience and Nanotechnology*, 17 (12), 8946-8951.
[64] Farh, H.M.H., Seghier, M.E.A.B., Zayed, T. (2023). A comprehensive review of corrosion protection and control techniques for metallic pipelines. *Engineering Failure Analysis, 143*, 106885
[65] Bastidas, D.M. (2020). Corrosion and protection of metals. Metals, 10, 458.
[66] Sukanya, R., Barwa, T.N., Luo, Y., Dempsey, E., Breslin, C.B. (2022). Emerging Layered Materials and
Their Applications in the Corrosion Protection of Metals and Alloys. Sustainability, 14, 4079
[67] Messner, K., Vuong, B., Tranmer, G.K. (2022). The Boron Advantage: The Evolution and Diversification of Boron's Applications in Medicinal Chemistry. *Pharmaceuticals,*15, 264.
[68] Jose, S. A., John, M., Menezes, P. L. (2022). Cermet Systems: Synthesis, Properties, and Applications. *Ceramics*, *5*(2), 210-236.
[69] Sun, Y., Ren, H., Jiao, Q., Schoenitz M., Dreizin, E.L. (2020). Oxidation, ignition and combustion behaviors of differently prepared boron-magnesium composites. *Combustion and Flame*, 221, 11-19.
[70] Singh, M., Vasudev, H., Singh, M. (2022). Surface protection of SS-316L with boron nitride based thin films using radio frequency magnetron sputtering technique. *J. Electrochem. Sci. Eng.* 12(5), 851-863.
[71] Vitry, V., Yunacti, M., Mégret, A., Khalid, H.A., Staia, M.H., Montagne, A. (2023). Selection of New Heat Treatment Conditions for Novel Electroless Nickel-Boron Deposits and Characterization of Heat-Treated Coatings. *Coatings*, 13, 1.
[72] Irshad, H.M., Farooq, A., Hakeem, A.S., Azeem, M.Z., Ehsan, M.A. (2023). Electrochemical study of aluminum–cubic boron nitride composites synthesized via spark plasma sintering for engineering applications, *Journal of Alloys and Compounds*, 965, 171210.
[73] Gunes, I. (2014). Tribological Properties and Characterisation of Plasma Paste Borided AISI 5120 steel. *Journal of The Balkan Tribological Association*, 20(3) 351-361.
[74] Sun, X., Zhang, J., Pan, W., Wang, W., Tang, C. (2023). A review on the preparation and application of BN composite coatings. *Ceramics International*, 49, 24-39.
[75] Vilhena, L., Ferreira, F., Oliveira, J.C., Ramalho, A. (2022). Rapid and Easy Assessment of Friction and Load-Bearing Capacity in Thin Coatings. *Electronics*, 11, 296

[76] S. B. Ulaeto, R. P. Ravi, I. I. Udoh, and G. M. Mathew, "Polymer-based coating for steel protection, highlighting metal–organic framework as functional actives: a review," Corrosion and Materials, 2023. mdpi.com

[77] Li, Z., Wang, L., Wang, Z., Wang, J., Xu, W. (2024). Superior oxidation resistance in air during hot stamping of a coating-free press-hardened steel achieved by pre-oxidation. *Journal of Materials Research and Technology*, 33, 6023-6034.

[78] Xavier, J.R., Vinodhini, S.P., Beryl, J.R. (2024). Performance of multifunctional nanocomposites containing graphitic carbon nitride/silanized Ta2O5 nanofillers for the protection of steel surface for industrial. Colloids and Surfaces A: Physicochemical and Engineering Aspects, 681, 132748

[79] Vilhena, L., Ferreira, F., Oliveira, J.C., Ramalho, A. (2022). Rapid and Easy Assessment of Friction and Load-Bearing Capacity in Thin Coatings. Electronics, 11, 296.

[80] Gunes, I. (2014). Tribological Behavior and Characterization of Borided Cold-Work Tool Steel, Materiali in Tehnologije, 48 (5), 765-769.

[81] Shi, G., Yu, X., Meng, H., Zhao, F., Wang, J., Jiao, J., Jiang, H. (2023). Effect of surface modification on friction characteristics of sliding bearings: A review. *Tribology*, 177, 107937.

[82] Gunes, I and Ozcatal, M. (2015). Diffusion Kinetics and Characterization of Borided AISI H10 Steel, Materiali in Tehnologije, 49 (5), 759-763.

[83] Du, F., Li, D., Sa, X., Li, C., Yu, Y., Li, C., Wang, J., Wang, W. (2022). Overview of Friction and Wear Performance of Sliding Bearings. *Coatings*, 12, 1303

[84] Grilli, M.L., Valerini, D., Slobozeanu, A.E., Postolnyi, B.O., Balos, S., Rizzo, A., Piticescu, R.R. (2021). Critical Raw Materials Saving by Protective Coatings under Extreme Conditions: A Review of Last Trends in Alloys and Coatings for Aerospace Engine Applications. *Materials*, 14, 1656.

[85] Konieczny, J., Labisz, K. (2021). Materials used in the combat aviation construction. *Transport Problems*, 16, 2.

[86] Mandal, S., Hashim, S.A., Roy, A., Karmakar, S. (2023). A short review of challenges and prospects of boron-laden solid fuels for ramjet applications. *FirePhysChem*, 3, 179-200

[87] Tung, S.C., Wong, V. (2021). Surface Engineering Development Trends and Impact of Surface Coatings and Textures on Automotive Powertrain Friction and Wear Control. *Matls. Perf. Charact.*,10(1), 620-650

[88] Glotov, O. G. (2023). Screening of metal fuels for use in composite propellants for ramjets. *Progress in Aerospace Sciences*, 143, 100954.

[89] Dorfman, M.R., Dwivedi, G., Dambra, C., Wilson, S. (2022). Perspective: Challenges in the aerospace marketplace and growth opportunities for thermal spray," Journal of Thermal Spray, 31,672-684.

[90] Gunes, I., Dalar, A. (2013). Effect of Sliding Speed on Friction Aand Wear Behaviour of Borided Gear Steels, Journal of The Balkan Tribological Association, 19 (3), 325-339.

[91] Bonu, V., Barshilia, H.C. (2022). High-Temperature Solid Particle Erosion of Aerospace Components: Its Mitigation Using Advanced Nanostructured Coating Technologies. *Coatings*, 12, 1979

[92] Karadimas, G., Ioannou, A., Kolios, A., Salonitis, K. (2024). Techno-Economic analysis of ceramic matrix composites integration in remaining useful Life Aircraft Engine Hot Section Components. *The International Journal of Advanced Manufacturing Technology*, 135, 4189-4203.

[93] Sengupta, P., Manna, I. (2021). Advanced high-temperature structural materials in petrochemical, metallurgical, power, and aerospace sectors-An overview. *Future Landscape of Structural Materials in India*, 79-131

[94] Deng, Y., Zhu, T., Cheng, Y., Zhao, K., Meng, Z., Huang, J., Cai, W., Lai, Y. (2024). Recent advances in functional cellulose-based materials: Classification, properties, and applications. *Advanced Fiber Materials*, 6, 1343-1368.

[95] Romero, C. A., Correa, P., Ariza Echeverri, E. A., & Vergara, D. (2024). Strategies for Reducing Automobile Fuel Consumption. *Applied Sciences*, 14(2), 910.

[96] Wang, W.G., Palmer, G.M., Bata, R.M., Clark, N.N., Gautam, M., Lyons, D.W. (1992). Determination of Heavy-Duty Vehicle Energy Consumption by a Chassis Dynamometer. *SAE Trans.* 101, 687-696,

[97] Kim, S.S., Hwang, H.J., Shin, M.W., Jang, H. (2011). Friction and vibration of automotive brake pads containing different abrasive particles. *Wear*, 271(7-8):1194-202.

[98] Vijay, R., Lenin Singaravelu, D., Filip, P. (2020). Influence of molybdenum disulfide particle size on friction and wear characteristics of nonasbestos-based copper-free brake friction composites. *Surface Review and Letters*, 27(01), 1950085.

[99] Han, Y., Tian, X., Yin, Y. (2008). Effects of Ceramic Fiber on the Friction Performance of Automotive Brake Lining Materials. Tribology Transactions, 51(6), 779-83.

[100] Bartkowski, D., Bartkowska, A., Piasecki, A., Jurči, P. (2020). Influence of Laser Cladding Parameters on Microstructure, Microhardness, Chemical Composition, Wear and Corrosion Resistance of Fe-B Composite Coatings Reinforced with B_4C and Si Particles. *Coatings*, *10*(9), 809.

[101] He, Y., Xu, H., Jiang, B., Ji, Z., Hu, M. (2021). Microstructure, mechanical and tribological properties of (APC+ B4C)/Al hybrid composites prepared by hydrothermal carbonized deposition on chips," Journal of Alloys and Compounds, 888, 161578. [102]

[103] Khonsari, M.M., Ghatrehsamani, S., Akbarzadeh, S. (2021). On the running-in nature of metallic tribo-components: A review. *Wear*, 474- 475, 203871.

[104] Bai, Y., J. Gao, J., Guo, T., Gao, K., Volinsky, A. A., Pang, X. (2021). Review of the fatigue behavior of hard coating-ductile substrate systems. *International* Journal of Minerals, Metallurgy and Materials, 28(1), 46-55.

[105] Li, M., Huang, K., Yi, X. (2023). Crack Formation Mechanisms and Control Methods of Laser Cladding Coatings: A Review. *Coatings*, 13, 1117.

[106] Wang, Z., Cao, Z.H., Wang, J.F., Huang, M.X. (2021). Improving the bending toughness of Al-Si coated press-hardened steel by tailoring coating thickness. Scripta Materialia 192, 19-25, 2021.

[107] Wang, D., Lin, S., Shi, Q., Xue, Y., Yang, H., Zhang, D., Xu, Z., Guo, C., Dai, M., Jiang, B., Zhou, K. (2021). Microstructure effects on fracture failure mechanism of CrAl/CrAlN coating. Ceramics International, 47(3), 3657-3664.

[108] Shi, B., Li, T., Guo, Z., Zhang X., Zhang, H. (2022). Selecting process parameters of crack-free Ni60A alloy coating prepared by coaxial laser cladding. Optics & Laser Technology, 149, 107805.
[109] Wu, X., Li, C., Zhou, Z., Nie, X., Chen, Y., Zhang, Y., Cao, H., Liu, B., Zhang, N., Said, Z., Debnath, S., Jamil, M., Ali, H.M., Sharma, S. (2021). Circulating purification of cutting fluid: an overview, The International Journal of Advanced Manufacturing Technology. 117, 2565-2600.
[110] Damian, C.S., Devarajan, Y., Thandavamoorthy, R., Jayabal, R. (2024). Harnessing artificial intelligence for enhanced bioethanol productions: a cutting-edge approach towards sustainable energy solution. International Journal of Chemical Reactor Engineering, 22(7), 719-727.
[111] Sarıkaya, M., Gupta, M.K., Tomaz, I., Pimenov, D.Y. (2021). A state-of-the-art review on tool wear and surface integrity characteristics in machining of superalloys. Materials Science and Technology. 35, 624-658, 2021.
[112] Wang, X., Li, C., Zhang, Y., Ali, H.M., Sharma, S., Li, R. (2022). Tribology of enhanced turning using biolubricants: A comparative assessment. Tribology, 174, 107766.
[113] Barman, M., Barman, T.K., Sahoo, T. (2023). Effect of heat-treatment temperature and borohydride concentration on corrosion behaviour of ENB coating. Proceedings of the Institution of Mechanical Engineers, Part C: Journal of Mechanical Engineering, 237(1), 183-200.
[114] Hekimoğlu, M., Özer, H., Kiraz, K. (2024). Surface hardening of Ti-Al-V superalloy spinal implant by using the boronization method. Bio-Medical Materials and Engineering, 35(1), 39-52.
[115] Janicijevic, Z., Huang, T., Bojorquez, D.I.S. (2024). Design and Development of Transient Sensing Devices for Healthcare Applications. Advanced, 11(20), e2307232.
[116] Duarte, N.F.V. (2021). Proportional counters equipped with thin B4C conversion layers for the detection of slow neutrons, PhD Thesis, Faculty of Sciences and Technology.
[117] Farhood, B., Ghorbani, M., Goushbolagh, N.A. (2020). Different methods of measuring neutron dose/fluence generated during radiation therapy with megavoltage beams. Health, 118(1), 65-74.
[118] Shu, X., He, Z., Wang, Y., Yin, L. (2020). Mechanical properties of Ni-based coatings fabricated by electroless plating method. Surface Engineering, 36, 944-951
[119] Ali, F., Hosmane, N.S., Zhu, Y. (2020). Boron chemistry for medical applications. Molecules, 25(4),
[120] Amirtharaj Mosas, K.K., Chandrasekar, A.R., Dasan, A., Pakseresht, A., Galusek, D. (2022). Recent Advancements in Materials and Coatings for Biomedical Implants. Gels, 8, 323
[121] Badiceanu, M., Anghel, S., Mihailescu, N., Visan, A.I., Mihailescu, C.N., Mihailescu, I.N. (2022). Coatings Functionalization via Laser versus Other Deposition Techniques for Medical Applications: A Comparative Review. *Coatings*, 12, 71.
[122] Sotoodeh, K. (2024). Equipment and Components in the Oil and Gas Industry. Vol.1: Equipment, Taylor & Francis CRC Press. 293.

[123] Al-Ameri, O. B., Alzuhairi, M., Bailón-García, E., Carrasco-Marín, F., & Amaro-Gahete, J. (2024). Transforming Petrochemical Processes: Cutting-Edge Advances in Kaolin Catalyst Fabrication. *Applied Sciences*, *14*(19), 9080.
[124] Rana, M.S.; Sámano, V.; Ancheyta, J.; Diaz, J.A.I. A review of recent advances on process technologies for upgrading of heavy oils and residua. *Fuel* 2007, *86*, 1216–1231
[125] AlKhafaji, K.S.; Shakor, Z.M.; Al-Zaidi, B.Y.; Hussein, S.J. Preparation and Characterization of Metakaolin-Based Catalysts for Gasoil Hydrodesulfurization Purposes. *Arab. J. Sci. Eng.* 2022, *47*, 6283–6296.
[126] Adanenche, D. E., Aliyu, A., Atta, A. Y., El-Yakubu, B. J. (2023). Residue fluid catalytic cracking: A review on the mitigation strategies of metal poisoning of RFCC catalyst using metal passivators/traps. Fuel, 343, 127894.
[127] Główka, M., Krawczyk, T. (2023). New trends and perspectives in production of 1, 2-propanediol," ACS Sustainable Chemistry & Engineering, *ACS Sustainable Chemistry & Engineering*, *11* (19), 7274-7287
[128] Vakylabad, A.B., Zand, L., Moravvej, Z. (2023). Environmental challenges of extracting unconventional petroleum reserves. Crises in Oil, Gas and Petrochemical Industries, Volume 1: Disasters and Environmental Challenges, 355-392.
[129] Zhai, W., Bai, L., Zhou, R., Fan, X., Kang, G., & Liu, Y. (2021). Recent progress on wear-resistant materials: Designs, properties, and applications. *Adv. Sci.*, 8, 2003739
[130] Devarajan, D.K., Rangasamy, B., Amirtharaj Mosas, K.K. (2023). State-of-the-Art Developments in Advanced Hard Ceramic Coatings Using PVD Techniques for High-Temperature Tribological Applications. Ceramics, 6, 301-329.
[131] Lu, K., Zhu, J., Guo, D., Yang, M., Sun, H.; Wang, Z., Hui, X., Wu, Y. (2022). Microstructures, Corrosion Resistance and Wear Resistance of High-Entropy Alloys Coatings with Various Compositions Prepared by Laser Cladding: A Review. Coatings, 12, 1023.
[132] Bai, Y., Zhang, H., Shao, Y., Zhang, H., Zhu, J. (2021). Recent Progresses of Superhydrophobic Coatings in Different Application Fields: An Overview. *Coatings*, 11, 116.
[133] Straffelini, G., Federici, M. (2020). HVOF Cermet Coatings to Improve Sliding Wear Resistance in Engineering Systems. *Coatings*, 10(9), 886.

Properties and Applications of Resin Types Used in Sla 3D Printers

Kubilay HAN[1]
Nusret Fatih AKTAŞ[2]

1- Res. Asst.. Gör.; Sakarya Uygulamalı Bilimler Üniversitesi Teknoloji Fakültesi Makine Mühendisliği Bölümü. kubilayhan@subu.edu.tr ORCID No: 0000-0003-1472-2832
2- Res. Asst.. Gör.; Sakarya Uygulamalı Bilimler Üniversitesi Teknoloji Fakültesi Makine Mühendisliği Bölümü. nusretaktas@subu.edu.tr ORCID No: 0009-0004-9714-7822

ABSTRACT

This study focuses on the properties and applications of various resin types used in SLA 3D printers. The resins analyzed include standard resins, rigid resins, flexible resins, tough resins, transparent resins, biocompatible resins, eco-friendly resins, ABS-like resins, and water-washable resins. Each resin type is formulated to meet specific mechanical, thermal, and optical requirements, catering to diverse industrial and design needs. Standard resins, for instance, are ideal for rapid prototyping due to their affordability and ease of use, while rigid and tough resins provide enhanced mechanical strength for functional prototypes. Flexible resins are suitable for applications requiring elasticity and impact absorption, whereas transparent resins are widely used in optical and visual prototyping. Biocompatible resins are essential for medical and dental applications, offering safety and precision, while eco-friendly and water-washable resins provide sustainable and user-friendly alternatives. The study evaluates the advantages and disadvantages of each resin type, emphasizing their impact on print quality, surface finish, and functional performance. Proper resin selection is critical for optimizing the production process and ensuring the suitability of the final product for its intended application. The findings underline the versatility of SLA technology and its capability to address various engineering, industrial, and design challenges. By providing a comparative analysis of resin types, this study serves as a valuable resource for enhancing the efficiency and applicability of SLA 3D printing in multiple domains.

Keywords – Resin Types, Additive Manufacturing, Resin Properties, Sla, 3d Printing.

INTRODUCTION

Additive manufacturing (AM), also known as layered manufacturing, is an innovative production method where materials are deposited layer by layer to create three-dimensional objects ((Çerlek, Han, Akin, & Seçgin, 2024); (Bănică, Sover, & Anghel, 2024)). Unlike traditional subtractive manufacturing methods such as machining or casting, additive manufacturing is based on the principle of material addition, directly utilizing design data ((Gao et al., 2022); (Yermurat, Seçgin, & Taşdemir, 2023)). This technology facilitates the production of complex geometries, offering enhanced design freedom and production flexibility ((Seçgin et al., 2022); (Akin, Çerlek, & Çobaner, 2024)).

The additive manufacturing process typically begins with the creation of a 3D model using Computer-Aided Design (CAD) software (Han, Akin, & Kılıç, 2024). This model is then sliced into thin layers using slicing

software. These layers are sequentially produced by a printer, depending on the material and method used (Tüylü, Çobaner, & Çerlek, 2024). Additive manufacturing can be applied to a wide range of materials, including polymers, metals, ceramics, and biomaterials ((Mirzaali et al., 2022); (Çerlek, Çobaner, & Akin, 2024)).

Today, additive manufacturing is widely utilized across various industries, including aerospace, automotive, healthcare, defense, education, and fashion, for purposes such as prototyping, end-use product manufacturing, and customized solutions ((Pant, Pidge, Nagdeve, & Kumar, 2021); (Vido et al., 2024)). The advantages of this technology include material efficiency, lightweight structures, rapid prototyping, reduced inventory costs, and increased design freedom (Zhou et al., 2024). However, challenges such as production time, material limitations, and surface roughness persist ((Han, Akin, & Seçgin, 2024); (Kesercioğlu, Han, & Aktaş, 2024)). Despite these limitations, advancements in material technologies and processing methods continue to expand the industrial adoption of additive manufacturing (Vafadar, Guzzomi, Rassau, & Hayward, 2021).

Additive manufacturing encompasses various techniques and materials, categorized based on the technology employed. These methods include Fused Filament Fabrication (FFF), Stereolithography (SLA), Selective Laser Sintering (SLS), Direct Metal Laser Sintering (DMLS), Electron Beam Melting (EBM), and Multi-Jet Printing (MJP). Each method offers specific advantages tailored to particular application needs. For example, SLS and DMLS are preferred for producing intricate metal parts, while SLA is ideal for applications requiring high detail accuracy and smooth surface quality ((Singh, Siddiqui, Koyalada, & others, 2023); (Soni, Renna, & Leo, 2024); (Sadaf, Bragaglia, Slemenik Perše, & Nanni, 2024); (Tüylü, Kesercioğlu, & Aktaş, 2024)). FFF, on the other hand, is widely used for its cost-effectiveness and ease of operation.

Stereolithography (SLA) 3D printers are one of the additive manufacturing methods that offer high precision, intricate details, and smooth surface quality ((Çerlek, Han, & Tüylü, 2024); (Han, Aktaş, & Tüylü, 2024)). This technology operates on the principle of curing liquid photopolymer resin by exposing it to UV light (Figure 1). A laser or projector system within the printer precisely directs the light based on the layer data generated by slicing software from the digital model, solidifying each layer sequentially (Bahati, Bricha, & El Mabrouk, 2022). As each layer is completed, the build platform moves to allow a fresh layer of liquid resin to spread, and the process is repeated. This method enables the production of models with complex geometries.

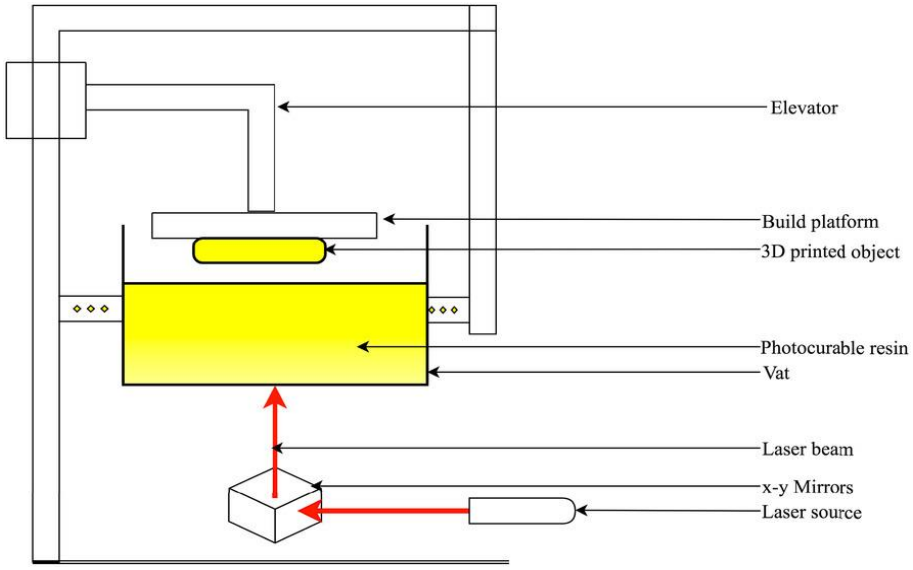

Figure 1. Working principle of SLA 3D printer (Bahati, Bricha, & El Mabrouk, 2022).

The working principle of SLA printers consists of several fundamental steps (Figure 2):

Figure 2. Steps in the Application of SLA 3D Printing

Model Design:

In this phase, the model to be produced is created using Computer-Aided Design (CAD) software. Once the design is complete, it is typically saved in STL (Standard Tessellation Language) or a similar file format. The STL format represents the surface geometry of the model by dividing it into triangles, enabling the printer to process this data layer by layer. The use of an appropriate file format and an error-free modeling process is a critical factor that directly affects the quality of the final print. Especially for complex and detailed models, errors made during the modeling stage can negatively impact the success of the printing process. Therefore, careful attention must be paid to the model design phase to ensure optimal results (Çerlek, Kesercioğlu, & Han, 2024).

Slicing:

Slicing is one of the critical stages in the production process of SLA 3D printers, enabling the model to become physically manufacturable. In

this phase, the 3D model created with CAD software is divided into thin layers using slicing software. Each layer represents the geometry of the model in a way that the printer can process. During this step, production parameters such as layer thickness, print orientation, and support structures are defined. The slicing software converts this information into a G-code format, which can be utilized by the printer's laser or projector system. This G-code file ensures that the printer cures the layers in the correct sequence and with high precision. Therefore, accurate settings during the slicing stage directly influence the precision, surface quality, and mechanical properties of the final product. For this reason, the slicing process must be conducted carefully and optimized for the intended application (Çerlek, Kesercioğlu, & Han, 2024).

Printer Preparation and Printing Process:

Printer preparation and the printing process are among the most critical stages of production with SLA 3D printers, directly influencing the quality of the final product. This process begins with the placement of liquid photopolymer resin into the printer's resin tank and the precise calibration of the build platform. The resin tank typically features a transparent bottom layer that allows UV light to pass through and a detachable coating to facilitate the seamless separation of cured resin layers from the platform. This design ensures that the printing process progresses without interruptions. Calibration is a crucial step that aligns the build platform perfectly with the resin tank, ensuring that each layer is produced at the desired position with high precision (Çerlek, Kesercioğlu, & Han, 2024).

Post-Processing and Curing:

After the printing process is complete, the model is subjected to a cleaning process to remove any residual liquid resin from its surface. This step is typically carried out using isopropyl alcohol or similar solvents, ensuring that all excess resin is thoroughly eliminated and allowing the model's details to be clearly revealed (Han, Aktaş, & Tüylü, 2024). This stage is crucial as it directly impacts the overall appearance and functionality of the printed product. Following the cleaning process, the model undergoes a curing stage under a UV lamp. The curing process enhances the material's mechanical strength while improving its surface quality (Aktaş, Akin, & Kesercioğlu, 2024). During this phase, the model is fully solidified, ensuring it meets the requirements of its intended application. Exposing the model to UV light strengthens its structural integrity and significantly increases its long-term durability. Proper execution of the cleaning and curing stages plays a critical role in optimizing the final product's performance and aesthetic value, making these steps essential for achieving high-quality results in SLA 3D printing (Çerlek, Kesercioğlu, & Han, 2024).

The printing process starts with the application of UV light, delivered through a laser or projector system, onto the resin layer at the bottom of the tank. This light cures the resin according to the geometry defined by the slicing software. As each layer is cured, the build platform moves upward (or downward in some SLA systems where the resin tank is mobile) to allow a fresh layer of liquid resin to spread over the surface (Aktaş, Akin, & Kesercioğlu, 2024). Layer by layer, the model's final structure takes shape, with the laser or projector system enabling the creation of intricate details and smooth surfaces. This process represents the core mechanism that allows SLA technology to achieve its hallmark high resolution and superior surface quality. Careful preparation of the printer and proper management of the printing process are essential for success, particularly when producing models with complex geometries.

The performance and print quality of SLA printers largely depend on the chemical properties of the resin used and its compatibility with the production process (Pagac et al., 2021). Photopolymer resins undergo a polymerization reaction under UV light, transitioning from a liquid to a solid state while forming each layer with high precision (Meenakshisundaram, Feller, Chartrain, & others, 2024). The appropriate selection of resin not only determines the printer's success in the target application area but also directly impacts the efficiency of the printing process and the durability of the final product. This selection should consider parameters such as the material's mechanical properties, surface quality, thermal stability, and optical clarity (Elsersawy, Kabir, & Khondoker, 2024).

Proper resin selection significantly enhances characteristics such as surface smoothness, detail accuracy, and geometric precision in the final product. Additionally, when the resin’s mechanical strength is appropriately chosen, the product demonstrates superior performance in terms of impact resistance and load-bearing capacity. High-temperature-resistant resins provide thermal stability, while transparent resins improve light transmission in optical clarity-required applications. Similarly, flexible resins enhance elasticity, offering greater deformation capacity. The right resin choice not only optimizes the production process but also ensures that the final product meets both functional and aesthetic requirements seamlessly (Mukhangaliyeva, Dairabayeva, Perveen, & Talamona, 2023).

This study examines the fundamental properties of photopolymer resins used in SLA printers and analyzes the characteristics and application areas of different resin types.

VARIETIES OF RESINS USED IN SLA TYPE 3D PRINTERS

The resins used in SLA printers are photopolymer materials capable of polymerizing under UV light. These resins are produced in various formulations, offering distinct properties such as mechanical strength, flexibility, heat resistance, biocompatibility, and optical clarity. This broad variety of resins tailored to different application requirements has facilitated the widespread adoption of SLA technology in numerous fields, including prototyping, medical device manufacturing, engineering, and optical applications (Martínez Raya et al., 2024).

Each type of resin is specifically designed to meet the requirements of a particular application area. For instance, standard resins provide a cost-effective option for visual prototypes, while biocompatible resins are preferred in medical and dental applications. Similarly, high-temperature resins are utilized in industrial parts requiring thermal resistance, and flexible resins are used in designs demanding elastic properties. In SLA technology, the correct selection of resin type is a critical factor that directly influences both the print quality and the functionality of the final product. This section presents a detailed analysis of the fundamental properties and application areas of resin types used in SLA printers.

Standard Resins

Standard resins are the most basic photopolymer materials used in SLA-type 3D printers and are widely preferred for general prototyping applications. These resins are frequently chosen due to their affordability and broad range of applications. Their chemical structure consists of light-sensitive monomers and oligomers that solidify through polymerization under UV light. Standard resins are known for their smooth surface quality, high detail accuracy, and ease of production. As shown in Table 1, these resins are typically utilized for prototypes where mechanical strength or thermal resistance is not a primary concern, focusing instead on aesthetic and design validation purposes (Vidakis et al., 2022).

Additionally, they offer visual advantages such as a wide range of color options and transparency, making it easier for designers and engineers to transform their concepts into physical models. However, standard resins have limited impact resistance and long-term mechanical durability, making them unsuitable for functional testing or products intended for harsh environments. Their cost-effective and easily processable nature makes them an ideal choice for rapid prototyping. These resins are effectively used in applications requiring low durability, such as design validation, educational materials, and visual models (Figure 3).

Figure 3. Applications of Standard Resins

However, in projects requiring enhanced mechanical properties, it may be necessary to complement standard resins with alternative resin types, such as tough or flexible resins. The production simplicity and aesthetic benefits of standard resins significantly contribute to the extensive adoption of SLA technology in prototyping.

Table 1. Properties of Standard Resins (Anycubic, 2024)

Property	Unit	Value
Wavelength	nm	355 - 410
Hardness	Shore D	84
Density	g/cm^3	1.05 – 1.25
Viscosity	mPa·s	150 - 200
Tensile strength	MPa	36 - 52
Elongation at break	%	15 - 22
Flexural strength	MPa	50 - 70
Flexural modulus	MPa	1200 - 1800

Rigid Resins

Rigid resins are specialized photopolymer materials designed for SLA 3D printers to meet the demands of applications requiring high strength and durability. These resins cure under UV light, exhibiting high rigidity and low elasticity. Enhanced mechanical properties make rigid resins particularly suitable for designs requiring structural integrity and dimensional stability. Their chemical composition features a dense cross-linked structure after polymerization, providing excellent resistance to impacts and deformation.

Key characteristics of rigid resins include high tensile strength, flexural strength, and hardness, making them an ideal material choice for prototyping in engineering applications, functional parts, and mechanical testing. However, due to their low elasticity, rigid resins have limited applicability in areas where flexibility or impact absorption is a primary requirement. In terms of application areas, rigid resins are commonly used for producing components for assembly testing, fasteners, and parts with load-bearing capacity (Figure 4). Additionally, their smooth surface quality and high detail accuracy make them widely preferred for manufacturing precise mechanical components. Nevertheless, disadvantages such as low

impact resistance and brittleness necessitate their use within certain limitations (Riccio et al., 2021).

Figure 4. Applications of Rigid Resins

The mechanical properties of rigid resins, as presented in Table 2, combined with the precision offered by SLA technology, make them a robust choice for producing durable and high-performance prototypes or end-use products. Nonetheless, it is essential to thoroughly assess the material's mechanical, thermal, and functional properties to confirm its suitability for particular application needs. When used appropriately, these resins enhance production efficiency while ensuring design accuracy.

Table 2. Properties of Rigid Resins (Anycubic, 2024)

Property	Unit	Value
Wavelength	nm	365 - 405
Hardness	Shore D	88 - 90
Density	g/cm3	1.14
Viscosity	mPa·s	950 - 1150
Tensile strength	MPa	80 - 85
Elongation at break	%	5 - 7
Flexural strength	MPa	95 - 110
Flexural modulus	MPa	2800 - 3400

Flexible Resins

The mechanical properties of flexible resins, as presented in Table 3, make them specialized photopolymer materials designed for SLA 3D printers in applications requiring elasticity and impact resistance. These resins, with their rubber-like characteristics, offer a combination of flexibility and durability, enabling the production of high-performance models (Riccio et al., 2021). Their chemical composition, which polymerizes under UV light, provides not only elasticity but also mechanical strength and wear resistance. Flexible resins are commonly used in designs with deformable components, such as moving parts, gaskets, and gripping elements. Additionally, their impact-absorbing properties make them an ideal material choice for parts that need to absorb energy (Figure 5).

Figure 5. Applications of Flexible Resins

Offering design freedom and high detail accuracy, these resins are applied in a diverse array of fields, ranging from engineering prototypes to industrial applications. The properties offered by flexible resins make SLA technology a preferred choice for innovative and functional designs (Tsang, Zhakeyev, Leung, & others, 2019).

Table 3. Properties of Flexible Resins (Anycubic, 2024)

Property	Unit	Value
Wavelength	nm	-
Hardness	Shore A	60 - 90
Density	g/cm3	1.02 – 1.05
Viscosity	mPa·s	600-1400
Tensile strength	MPa	4 - 10
Elongation at break	%	100 - 350
Flexural strength	MPa	-
Flexural modulus	MPa	-

Water-Washable Resins

Water-washable resins are specially formulated photopolymer materials designed for SLA 3D printers to provide ease of use. These resins can be cleaned with water after printing, eliminating the need for chemical solvents such as isopropyl alcohol. This not only reduces costs but also offers a user-friendly alternative (Liu, Jin, Lim, & others, 2024). Their eco-friendly nature and reduced reliance on chemicals make these resins an appealing choice for a broad audience, including educational users, prototyping applications, and home users (Figure 6).

Figure 6. Applications of Water-Washable Resins

Water-washable resins maintain the high detail accuracy and smooth surface quality provided by standard resins while simplifying the cleaning process, thereby accelerating post-production workflows (Shahidi et al., 2024). Additionally, they offer advantages such as low toxicity and ease of handling. However, the durability and thermal resistance of these resins may not be as high as those of standard or specialized resins (Table 4). Despite this, water-washable resins are considered a significant innovation in SLA technology due to their reduced environmental impact and ease of use.

Table 4. Properties of Water-Washable Resins (Anycubic, 2024)

Property	Unit	Value
Wavelength	nm	365 - 405
Hardness	Shore D	80
Density	g/cm3	1.15 - 1.20
Viscosity	mPa·s	150 - 250
Tensile strength	MPa	50 - 60
Elongation at break	%	8 - 15
Flexural strength	MPa	30 - 45
Flexural modulus	MPa	>1500 - 1600

ABS-Like Resins

ABS-like resins are specialized photopolymer materials used in SLA 3D printers and are widely preferred in engineering applications. These resins replicate the mechanical properties of ABS (Acrylonitrile Butadiene Styrene) plastics produced through traditional injection molding, offering high strength, impact resistance, and heat resistance (Han et al., 2024). Their polymer structure cures under UV light, transforming into a hard and durable form, making them an ideal choice for functional prototypes and end-use products (Çerlek et al., 2024).

ABS-like resins are frequently utilized for producing parts requiring high mechanical durability, assembly testing, engineering prototypes, and load-bearing structures (Figure 7). Additionally, their smooth surface quality and detail accuracy meet both aesthetic and functional demands (Aktaş et al., 2024).

Figure 7. Applications of ABS Like Resins

Compared to traditional ABS, these resins, whose mechanical properties are presented in Table 5, combine the precision offered by SLA technology with enhanced mechanical performance, making them particularly suitable for applications requiring complex geometries and high resolution. ABS-like resins offer a combination of durability and functionality, enabling SLA printers to be more effectively utilized in industrial and engineering fields.

Table 5. Properties of ABS-Like Resins (Anycubic, 2024)

Property	Unit	Value
Wavelength	nm	365 - 405
Hardness	Shore D	80 - 85
Density	g/cm3	1.1 - 1.2
Viscosity	mPa·s	180 - 200
Tensile strength	MPa	35 - 45
Elongation at break	%	30 - 40
Flexural strength	MPa	40 - 50
Flexural modulus	MPa	1000 - 1200

Tough Resins

Tough resins are photopolymer materials specifically designed for SLA 3D printers, intended for applications requiring high impact resistance and flexibility. Offering polycarbonate-like properties, these resins provide high strength combined with energy absorption capabilities, making them essential for the production of functional prototypes and engineering applications (Pecora, Cosma, Turcin, Vilau, & Balc, 2024). Tough resins polymerize under UV light, making them ideal for manufacturing parts that require load-bearing capacity, impact resistance, and deformation resilience (Figure 8). These resins are particularly favored for assembly testing, moving mechanisms, and components that must withstand challenging environmental conditions.

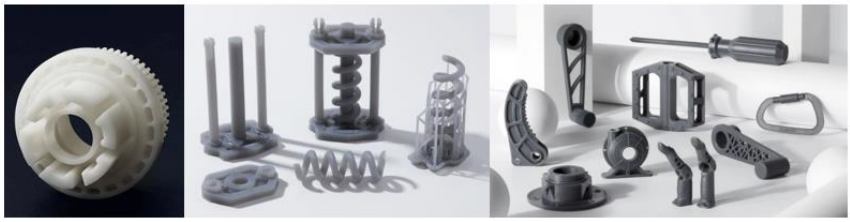

Figure 8. Applications of Tough Resins

These resins combine flexibility and rigidity, enhancing both durability and longevity. Additionally, their smooth surface quality and detail accuracy meet aesthetic and functional requirements. Tough resins stand out as an innovative material choice that maximizes the potential of SLA technology in engineering projects and functional testing (Table 6) (Grygier et al., 2024).

Table 6. Properties of Tough Resins (Anycubic, 2024)

Property	Unit	Value
Wavelength	nm	365 - 405
Hardness	Shore D	76
Density	g/cm3	1.10 - 1.15
Viscosity	mPa·s	150 - 250
Tensile strength	MPa	50 - 60
Elongation at break	%	30 - 50
Flexural strength	MPa	35 - 45
Flexural modulus	MPa	>900 - 1200

Transparent Resins

Transparent resins are specialized photopolymer materials used in SLA 3D printers, offering high light transmission and optical clarity. These resins polymerize under UV light, enabling the production of parts with smooth surface quality and excellent light transmission (Sun et al., 2022). Transparent resins are ideal for projects where design accuracy and aesthetic value are prioritized, such as optical and visual prototyping applications (Figure 9). They are commonly used in prototypes for testing light transmission, optical device components, fluid flow models, and lighting elements (Park, Shin, Kim, & others, 2018).

Figure 9. Applications of Transparent Resins

While their resistance to yellowing under UV light is limited, their ability to provide high detail accuracy and visual clarity makes these resins suitable for specialized and functional designs. Transparent resins enable the precision and surface quality offered by SLA technology to be utilized optimally in optical applications. Their technical properties are presented in Table 7.

Table 7. Properties of Transparent Resins (Anycubic, 2024)

Property	Unit	Value
Wavelength	nm	365 - 405
Hardness	Shore D	78
Density	g/cm3	1.05 - 1.25
Viscosity	mPa·s	266
Tensile strength	MPa	28.1
Elongation at break	%	14.6
Flexural strength	MPa	30.3
Flexural modulus	MPa	>798

Biocompatible Resins

Biocompatible resins are photopolymer materials specifically designed for SLA 3D printers, tailored for medical and dental applications. These resins polymerize under UV light to produce parts with high precision and detail accuracy (Sharma et al., 2020). Due to their biocompatibility, they are utilized in critical applications such as dental models, prosthetics, surgical guides, and medical device components that come into contact with the human body (Figure 10) (Agrawal et al., 2023).

Figure 10. Applications of Biocompatible Resins

Biocompatible resins, suitable for sterilization processes, are formulated to meet medical requirements, offering properties such as chemical resistance, long-term durability, and smooth surface quality (Table 8). Additionally, they are certified to comply with specific biomedical standards (Guttridge et al., 2022). These resins enable SLA technology to achieve extensive applications in the medical field, making them an ideal choice for personalized solutions and innovative designs. The precision and reliability offered by biocompatible resins enhance the significance of 3D printing in the healthcare sector.

Table 8. Properties of Biocompatible Resins (Anycubic, 2024)

Property	Unit	Value
Wavelength	nm	365 - 405
Hardness	Shore D	83 - 85
Density	g/cm3	1.13 - 1.15
Viscosity	mPa·s	470 - 520
Tensile strength	MPa	34 - 40
Elongation at break	%	21 - 28
Flexural strength	MPa	47 - 57
Flexural modulus	MPa	1200 - 1800

Plant-Based Resin

Plant-based resins are specialized photopolymer materials designed for SLA 3D printers to reduce environmental impact and promote sustainability. Formulated with low-toxicity and biodegradable components, these resins cause significantly less environmental harm compared to traditional resins. Ideal for safe-use applications such as education and research (Figure 11), plant-based resins also contribute to creating a safer and more eco-conscious working environment (Danish et al., 2021).

Figure 11. Applications of Plant Based Resins

Plant-based resins maintain high detail accuracy and smooth surface quality while minimizing the impact of harmful chemicals during production and usage processes (Leote, 2024). These materials are compatible with recycling processes and generate less waste, playing a significant role in sustainable manufacturing strategies. The increasing use of plant-based resins contributes to making SLA technology more eco-friendly and socially beneficial. The technical properties of these resins are presented in Table 9.

Table 9. Properties of Plant Based Resins (Anycubic, 2024)

Property	Unit	Value
Wavelength	nm	355 - 410
Hardness	Shore D	89
Density	g/cm3	1.05 - 1.25
Viscosity	mPa·s	150 - 350
Tensile Strength	MPa	42 - 62
Elongation at break	%	8 - 12
Flexural strength	MPa	49 - 58
Conservation period	Year	1.5

COMPARATIVE ANALYSIS OF RESINS

Resins used in SLA 3D printing are developed with a variety of properties to expand the application range of this technology, leveraging its precision, surface quality, and design flexibility. Standard resins, offering a cost-effective and user-friendly solution for visual prototyping, are complemented by tough and ABS-like resins for engineering and industrial applications. Additionally, flexible resins provide elasticity and impact resistance for specialized designs, while biocompatible resins serve critical roles in medical and dental applications. Eco-friendly and water-washable resins appeal to users seeking sustainability and ease of use.

This section presents a detailed comparative analysis of the key features, advantages, and limitations of resins used in SLA 3D printing. The

mechanical strength, thermal resistance, flexibility, chemical durability, and other technical properties of each resin type will be examined alongside their impact on various application areas. Furthermore, the critical factors to consider when selecting a resin and strategies for identifying the most suitable material for specific applications will be discussed.

The correct selection of resin not only enhances print quality but also directly influences the functionality and longevity of the final product. This analysis aims to guide users in selecting the optimal material for their projects, enabling SLA technology to be utilized more effectively across diverse industries. By combining innovative and versatile solutions with appropriate material selection, SLA technology can optimize production processes and drive groundbreaking advancements in design and engineering fields.

Table 10. Comparison of SLA 3D Printing Resins: Purpose, Applications, and Properties

Feature	Standard Resins	Rigid Resins	Flexible Resins	Water Washable Resins	ABS Like Resins	Tough Resins	Transparent Resins	Biocompatible Resins	Plant-Based Resins
Purpose	General prototyping and design validation	Engineering parts, structural prototypes	Designs requiring elasticity and deformation resistance	Ease of use, no solvent required for cleaning	High-strength and functional prototypes	Parts requiring mechanical strength and impact resistance	Optical and visual prototypes	Medical and dental applications	Reducing environmental impact, education, and general use
Detail Accuracy	High	High	Medium-High	High	Medium-High	Medium-High	High	High	High
Surface Quality	Smooth	Smooth	Smooth	Smooth	Smooth	Smooth	Smooth	Smooth	Smooth
Mechanical Strength	Low-Medium	High	Medium	Medium	High	High	Low-Medium	Medium	Medium
Flexibility	Low	Low	High	Low	Medium	Medium	Low	Low	Low
Chemical Resistance	Low	High	Medium	Low-Medium	High	High	Low	High	Medium
Heat Resistance	Low	Medium-High	Low	Low	Medium-High	High	Low	Medium	Low-Medium
Environmental Impact	Medium	Medium	Medium	Low	Medium	Medium	Medium	Medium	Low
Applications	Design validation, aesthetic prototypes	Parts requiring high strength and dimensional stability	Gaskets, gripping elements, impact-absorbing parts	Education, home use, general prototyping	Engineering prototypes, load-bearing structures	Assembly testing, engineering parts	Optical devices, fluid flow testing	Surgical guides, prosthetics	Education, general prototyping

Resins used in SLA 3D printers serve a wide range of applications, offering distinct characteristics, advantages, and limitations. These resins vary in parameters such as mechanical strength, optical clarity, flexibility, eco-friendliness, and ease of use. This diversity enhances the adaptability and industrial potential of SLA technology by ensuring that each resin type is

tailored to specific application requirements. Table 11 provides a detailed comparison of these resin types, offering valuable insights to guide users in selecting the most suitable material for their needs.

Table 11. Comparative Features, Advantages, and Limitations of SLA 3D Printing Resins

Resin Type	Key Features	Advantages	Limitations
Standard Resin	High detail accuracy, smooth surface finish	Cost-effective, ideal for visual prototypes, wide color options	Limited mechanical strength, low impact resistance
Rigid Resin	High rigidity, low elasticity	High tensile and flexural strength, ideal for structural integrity and dimensional stability	Low flexibility, brittle under impact
Flexible Resin	Rubber-like elasticity, impact resistance	High flexibility, ideal for deformable and energy-absorbing parts	Lower tensile strength compared to rigid or tough resins
Tough Resin	High strength and toughness	Polycarbonate-like properties, suitable for functional parts and assembly testing	Limited optical clarity, moderate surface finish
Transparent Resin	High optical clarity and light transmission	Ideal for optical and fluid flow models, smooth finish	Limited resistance to yellowing under UV light, moderate mechanical durability
Biocompatible Resin	Certified for medical and dental applications	Safe for human contact, ideal for surgical guides and prosthetics	Requires sterilization, may have limited mechanical properties for some applications
Plant-Based Resin	Eco-friendly, biodegradable	Low toxicity, safer working environment, supports sustainable manufacturing	Limited thermal and mechanical durability
ABS-Like Resin	ABS plastic-like properties	High impact resistance, suitable for functional prototypes and load-bearing parts	Higher cost compared to standard resins
Water-Washable Resin	Cleanable with water, user-friendly	Eliminates the need for chemical solvents, simplifies post-processing	Limited durability and thermal resistance compared to other specialized resins

RESULTS

This study has comparatively evaluated the properties, advantages, and disadvantages of various types of resins used in SLA 3D printers. The resin types analyzed include biocompatible, transparent, flexible, tough, eco-friendly, ABS-like, water-washable, standard, and rigid resins. Each resin type was found to have unique mechanical, optical, and thermal properties, which play a critical role in determining its application areas.

It has been concluded that resin selection is crucial for the success of SLA technology. The appropriate choice of resin not only enhances print quality but also directly affects the functionality and durability of the final product. For instance, biocompatible resins provide a reliable option for medical and dental applications, while tough resins offer high impact resistance and durability for engineering prototypes. Transparent resins are suitable for designs requiring optical clarity, whereas eco-friendly resins present a valuable alternative for sustainable manufacturing processes.

In conclusion, the resin types used in SLA 3D printers offer a wide range of options to optimize production processes and meet application-specific requirements. This diversity enables the fundamental advantages of SLA technology, such as design freedom, high precision, and detail accuracy, to be utilized more effectively. Future studies are recommended to explore the combination of these resin types with different parameters to develop more specialized and efficient production processes.

ACKNOWLEDGEMENT

This study was supported by the Scientific Research Projects Coordination Unit of Sakarya University of Applied Sciences under project number [222-2024].

REFERENCE

Aktaş, N. F., Akin, Y., & Kesercioğlu, M. A. (2024). The effect of different printing parameters on the surface roughness of ABS-like resin samples produced by SLA technology. Presented at the 4th BİLSEL International Harput Scientific Researches Congress.

Akin, Y., Çerlek, Ö., & Çobaner, S. (2024). Mechanical properties and specific strength analysis of different lattice geometries in additive manufacturing. Presented at the 4th BİLSEL International Harput Scientific Researches Congress.

Anycubic. (2024). Official store. Retrieved December 25, 2024, from https://store.anycubic.com/

Agrawal, S., Ray, H., Kulat, A., Garhekar, Y., Jibhakate, R., Singh, S. K., & Bisaria, H. (2023). Evaluation of tensile property of SLA 3D printed NextDent biocompatible Class I material for making surgical guides for implant surgery. Materials Today: Proceedings, 72(Part 3), 1231–1235. https://doi.org/10.1016/j.matpr.2022.09.288

Bănică, C. -F., Sover, A., & Anghel, D. -C. (2024). Printing the Future Layer by Layer: A Comprehensive Exploration of Additive Manufacturing in the Era of Industry 4.0. Applied Sciences, 14(21), 9919. https://doi.org/10.3390/app14219919

Çerlek, Ö., Çobaner, S., & Akin, Y. (2024). An experimental analysis of the factors influencing the tensile strength of PLA parts manufactured with 3D printing using FDM technique. Presented at the 3rd BİLSEL International Harput Scientific Researches Congress, Elazığ.

Çerlek, Ö., Han, K., & Tüylü, A. (2024). Optimization of flexural strength of parts produced from ABS-like resin using stereolithography. Presented at the 3rd International Conference on Contemporary Academic Research, Konya.

Çerlek, Ö., Han, K., Akin, Y. et al. Experimental Investigation of Parameters Affecting the Tensile Strength of Silicone-Filled 3D Printed ABS Products. J. of Materi Eng and Perform (2024). https://doi.org/10.1007/s11665-024-10498-3

Çerlek, Ö., Kesercioğlu, M. A., & Han, K. (2024). Stereolithography (SLA): An innovative additive manufacturing process. In U. Özkaya (Ed.), New trends and frontiers in engineering (pp. 399–412). All Sciences Academy. ISBN: 978-625-6314-57-3.

Danish, M., Anirudh, P. V., Karunakaran, C., Rajamohan, V., Mathew, A. T., Koziol, K., Thakur, V. K., Kannan, C., & Balan, A. S. S. (2021). 4D printed stereolithography printed plant-based sustainable polymers: Preliminary investigation and optimization. Journal of Applied Polymer Science, 50903. https://doi.org/10.1002/app.50903

Elsersawy, R., Kabir, G., & Khondoker, M. A. H. (2024). Evaluating 3D printing parameters of an elastomeric resin for higher stretchability and strength using the analytic hierarchy process and technique for order of preference by similarity to ideal solution. Engineering Proceedings, 76(1), 45. https://doi.org/10.3390/engproc2024076045

Gao, M., Li, L., Wang, Q., & others. (2022). Integration of additive manufacturing in casting: Advances, challenges, and prospects. International Journal of Precision Engineering and Manufacturing-Green Technology, 9(2), 305–322. https://doi.org/10.1007/s40684-021-00323-w

Guttridge, C., Shannon, A., O'Sullivan, A., O'Sullivan, K. J., & O'Sullivan, L. W. (2022). Biocompatible 3D printing resins for medical applications: A review of marketed intended use, biocompatibility certification, and post-processing guidance. Annals of 3D Printed Medicine, 5, 100044. https://doi.org/10.1016/j.stlm.2021.100044

Grygier, D., Kurzawa, A., Stachowicz, M., Krawiec, K., Stępczak, M., Roszak, M., Kazimierczak, M., Aniszewska, D., & Pyka, D. (2024). Investigations into the material characteristics of selected plastics manufactured using SLA-type additive methods. Polymers, 16(11), 1607. https://doi.org/10.3390/polym16111607

Han, K., Akin, Y., & Kılıç, R. (2024). An analysis of the layer dimension effect on the mechanical properties of ABS parts produced by FFF technology. Presented at the 4th International Conference on Engineering, Natural and Social Sciences, Konya.

Han, K., Akin, Y., & Seçgin, Ö. (2024). An experimental study on the effect of ironing process on surface roughness of PLA parts produced by FDM type 3D printer. Presented at the 3rd BİLSEL International Çatalhöyük Scientific Researches Congress, Konya.

Han, K., Aktaş, N. F., & Tüylü, A. (2024). Investigation of compressive behavior of different lattice structures produced with ABS-like resin using SLA technology. Presented at the 4th BİLSEL International Harput Scientific Researches Congress, Elazığ.

Kesercioğlu, M. A., Han, K., & Aktaş, N. F. (2024). The impact of ironing process on the surface quality of ABS parts produced with FDM 3D printing. Presented at the 3rd BİLSEL International Çatalhöyük Scientific Researches Congress, 24–25 August 2024, Konya, Türkiye. ISBN: 978-625-6125-10-0.

Leote, R. (2024). 3D printed art using bioplastic and plant-based resin. In Proceedings of the 11th International Conference on Digital and Interactive Arts (ARTECH '23) (Article 1, pp. 1–10). Association for Computing Machinery, New York, NY, USA. https://doi.org/10.1145/3632776.3632818

Liu, Y., Jin, G., Lim, J. H., & others. (2024). Effects of washing agents on the mechanical and biocompatibility properties of water-washable 3D printing crown and bridge resin. Scientific Reports, 14(1), 9909. https://doi.org/10.1038/s41598-024-60450-7

Martínez Raya, A., Aranda-Ruiz, J., Sal-Anglada, G., Jaureguizahar, S. M., & Braun, M. (2024). Effect of printing orientation on the mechanical properties of low-force stereolithography-manufactured durable resin. Applied Sciences, 14(20), 9529. https://doi.org/10.3390/app14209529

Meenakshisundaram, V., Feller, K., Chartrain, N., & others. (2024). Characterizing photopolymer resins for high-temperature vat photopolymerization. Progress in Additive Manufacturing, 9(6), 2061–2071. https://doi.org/10.1007/s40964-023-00562-0

Mirzaali, M. J., Moosabeiki, V., Rajaai, S. M., Zhou, J., & Zadpoor, A. A. (2022). Additive manufacturing of biomaterials—Design principles and their implementation. Materials, 15(15), 5457. https://doi.org/10.3390/ma15155457

Mukhangaliyeva, A., Dairabayeva, D., Perveen, A., & Talamona, D. (2023). Optimization of dimensional accuracy and surface roughness of SLA patterns and SLA-based IC components. Polymers, 15(20), 4038. https://doi.org/10.3390/polym15204038

Pagac, M., Hajnys, J., Ma, Q.-P., Jancar, L., Jansa, J., Stefek, P., & Mesicek, J. (2021). A review of vat photopolymerization technology: Materials, applications, challenges, and future trends of 3D printing. Polymers, 13(4), 598. https://doi.org/10.3390/polym13040598

Pant, M., Pidge, P., Nagdeve, L., & Kumar, H. (2021). A review of additive manufacturing in aerospace application. Revue des Composites et des Matériaux Avancés-Journal of Composite and Advanced Materials, 31(2), 109–115. https://doi.org/10.18280/rcma.310206

Park, H. K., Shin, M., Kim, B., & others. (2018). A visible light-curable yet visible wavelength-transparent resin for stereolithography 3D printing. NPG Asia Materials, 10(1), 82–89. https://doi.org/10.1038/s41427-018-0021-x

Pecora, E., Cosma, C., Turcin, I., Vilau, C., & Balc, N. (2024). Investigation on tough resin fabricated by low-cost SLA printers. Journal on Emerging Topics in Industrial Engineering. https://doi.org/10.21428/92f19a8b.6139f655

Riccio, C., Civera, M., Grimaldo Ruiz, O., Pedullà, P., Rodriguez Reinoso, M., Tommasi, G., Vollaro, M., Burgio, V., & Surace, C. (2021). Effects of curing on photosensitive resins in SLA additive manufacturing. Applied Mechanics, 2(4), 942–955. https://doi.org/10.3390/applmech2040055

Sadaf, M., Bragaglia, M., Slemenik Perše, L., & Nanni, F. (2024). Advancements in metal additive manufacturing: A comprehensive review of material extrusion with highly filled polymers. Journal of Manufacturing and Materials Processing, 8(1), 14. https://doi.org/10.3390/jmmp8010014

Seçgin, Ö., Arda, E., Ata, E., & Çelik, H. A. (2022). Dimensional optimization of additive manufacturing process. Journal of the Chinese Society of Mechanical Engineers, 43(1), 75–78.

Shahidi, A., Stravinskas, K., Steponavičiūtė, A., Kilikevičius, A., Vainorius, D., Matijošius, J., Kapustynskyi, O., & Mordas, G. (2024). Elasticity study of SLA additively manufactured composites. Mechanika. https://doi.org/10.5755/j02.mech.37478

Sharma, N., Cao, S., Msallem, B., Kunz, C., Brantner, P., Honigmann, P., & Thieringer, F. M. (2020). Effects of steam sterilization on 3D printed biocompatible resin materials for surgical guides—An accuracy assessment study. Journal of Clinical Medicine, 9(5), 1506. https://doi.org/10.3390/jcm9051506

Singh, N., Siddiqui, H., Koyalada, B.S.R. et al. Recent Advancements in Additive Manufacturing (AM) Techniques: A Forward-Looking Review. Met. Mater. Int. 29, 2119–2136 (2023). https://doi.org/10.1007/s12540-022-01380-9

Sun, Q., Fang, F., Wang, W., Yin, J., Liu, Q., Hao, L., & Peng, Y. (2022). Stereolithography 3D printing of transparent resin lens for high-power phosphor-coated WLEDs packaging. Journal of Manufacturing Processes, 84, 150–160. https://doi.org/10.1016/j.jmapro.2022.11.026

Soni, N., Renna, G., & Leo, P. (2024). Advancements in metal processing additive technologies: Selective laser melting (SLM). Metals, 14(9), 1081. https://doi.org/10.3390/met14091081

Tsang, C. H. A., Zhakeyev, A., Leung, D. Y. C., & others. (2019). GO-modified flexible polymer nanocomposites fabricated via 3D stereolithography. Frontiers of Chemical Science and Engineering, 13(5), 736–743. https://doi.org/10.1007/s11705-019-1836-x

Tüylü, A., Çobaner, S., & Çerlek, Ö. (2024). Eklemeli imalat parametrelerinin gyroid kafes yapılı parçaların mekanik özelliklerine etkisi. Presented at the 4. BİLSEL International Harput Scientific Researches Congress, Elazığ.

Tüylü, A., Kesercioğlu, M. A., & Aktaş, N. F. (2024). Eriyik yığma modelleme yönteminde baskı hızının PLA numune mekanik özelliklerine etkisi. Presented at the 4th International Conference on Frontiers in Academic Research, 13–14 December 2024.

Vafadar, A., Guzzomi, F., Rassau, A., & Hayward, K. (2021). Advances in Metal Additive Manufacturing: A Review of Common Processes, Industrial Applications, and Current Challenges. Applied Sciences, 11(3), 1213. https://doi.org/10.3390/app11031213

Vidakis, N., Petousis, M., Velidakis, E., Mountakis, N., Tsikritzis, D., Gkagkanatsiou, A., & Kanellopoulou, S. (2022). Investigation of the biocidal performance of multi-functional resin/copper nanocomposites with superior mechanical response in SLA 3D printing. Biomimetics, 7(1), 8. https://doi.org/10.3390/biomimetics7010008

Vido, M., de Oliveira Neto, G. C., Lourenço, S. R., Amorim, M., & Rodrigues, M. J. F. (2024). Computer-aided design and additive manufacturing for automotive prototypes: A review. Applied Sciences, 14(16), 7155. https://doi.org/10.3390/app14167155

Yermurat, B., Seçgin, Ö., & Taşdemir, V. (2023). Multi-material additive manufacturing: Investigation of the combined use of ABS and PLA in the same structure. Walter de Gruyter GmbH, 65(11), 1119–1126.

Zhou, L., Miller, J., Vezza, J., Mayster, M., Raffay, M., Justice, Q., Al Tamimi, Z., Hansotte, G., Sunkara, L. D., & Bernat, J. (2024). Additive manufacturing: A comprehensive review. Sensors, 24(9), 2668. https://doi.org/10.3390/s24092668

Heat Transfer Enhancement in Double-Pipe Heat Exchangers with Porous Media: Comparative Analysis on Flow and Structural Influences

Mahir ŞAHİN[1]
Mustafa KILIÇ[2]

1- Res. Asst.; Adana Alparslan Türkeş Bilim ve Teknoloji Üniversitesi Makine Mühendisliği Bölümü. msahin@atu.edu.tr ORCID No: 0000-0002-9565-9160
2- Prof. Dr.; Adana Alparslan Türkeş Bilim ve Teknoloji Üniversitesi Makine Mühendisliği Bölümü. mkilic@atu.edu.tr ORCID No: 0000-0002-8006-149X

ABSTRACT

Improving energy efficiency is essential for reducing operational costs and promoting environmental sustainability. Thermal loads and waste heat in industrial processes account for a significant portion of energy consumption. Therefore, optimizing heat exchangers is critical for minimizing energy losses and enabling efficient waste heat recovery. In this study, the flow behavior and heat transfer performance of a double-pipe heat exchanger was analyzed numerically under laminar flow conditions using ANSYS Fluent 2022 R1 software. Four key parameters were investigated: Reynolds number (Re), hot fluid inlet temperature ($T_{h,in}$), porous media porosity (ϕ), and porous region thickness (D). Reynolds numbers of 250, 500, 750, and 1000 were examined, and results showed that increasing Re improved heat transfer performance by 4.9% without porous media and 5.2% with porous media. Similarly, varying the inlet temperature from 30 to 60°C increased heat transfer effectiveness by 1.6% without porous media and 1.4% with porous media. Porous media configurations were also explored, with porosity levels of ϕ = 0.8, 0.6, 0.4, and 0.2 and porous region thicknesses of D = 1.0, 1.5, 2.0, and 2.5 mm. Reducing the porosity from ϕ = 0.8 to ϕ = 0.2 enhanced heat transfer effectiveness by 5.3%. Additionally, increasing the porous region thickness from 1.0 mm to 2.5 mm at ϕ = 0.6 resulted in a 7.2% improvement. The results demonstrate that optimizing flow conditions and porous media parameters can significantly enhance the performance of heat exchangers, providing sustainable and energy-efficient solutions for industrial systems.

Keywords – Heat Transfer, Heat Exchanger, Porous Media, Porosity, Laminar Flow.

INTRODUCTION

Tubular heat exchangers are widely used with low-temperature systems such as waste heat recovery, where energy efficiency is a priority. Among various approaches, passive methods stand out as a cost-effective and sustainable solution for enhancing heat transfer performance without requiring additional energy input (Hu et al., 2020:2). By integrating porous structures into the heat transfer system design, the surface area of these designs can be increased, and flow resistance can be introduced to enhance mixing, significantly improving thermal performance (Moradi et al., 2019:1799).

The performance of double-pipe heat exchangers depends largely on operating conditions such as Reynolds number and fluid inlet temperatures, which influence flow dynamics and thermal gradients. Optimizing these

parameters enables more efficient operation under low-temperature conditions, making them ideal for energy recovery systems (Omidi et al., 2017:1076).

Passive methods, particularly porous structures, are effective in improving heat transfer by enhancing fluid mixing, thinning the boundary layer, increasing surface area, and strengthening thermal gradients. The efficiency of these methods can be further improved by optimizing porosity, medium thickness, and placement, offering a cost-effective and sustainable solution for energy recovery and system efficiency (Sheikholeslami, M., and Ganji, D. D. 2016:112).

A review of the literature reveals that Wang et al. (2023:3) investigated cylindrical and prismatic porous media heat exchangers for cooling high-power chips, analyzing parameters such as porosity, skeleton size, and partial density. Their findings indicated that cylindrical designs, with an optimal porosity of 0.64 and a skeleton size of 0.5 mm, significantly improved temperature distribution compared to conventional finned heat exchangers, reducing the maximum temperature by 19.62%. Arivazhagan and Lokeswaran (2013:77) studied entropy minimization in tubular heat exchangers integrating porous substrate made from copper, aluminum, and mild steel shavings. They found that porous media enhanced heat transfer but significantly increased pressure drop, with entropy generation rising sharply for Reynolds numbers above 1450. He et al. (2022:2) proposed an OpenFOAM-based code to simulate two-phase flow and boiling heat transfer in tubular exchangers integrating a porous substrate design. Validation showed 13.3% error in void fraction predictions with high accuracy in pressure drop and temperature, proving the model's efficiency in reducing computational costs while maintaining accuracy. Delalic et al. (2004:187) studied a compact heat exchanger with integrated porous media, demonstrating significant improvements in heat transfer efficiency through enhanced conduction and radiation. The system achieved high thermal capacity (7 MW/m^3) while reducing CO_2 and NO_x emissions. Despite an increase in pressure drop at higher power levels, the system proved effective and sustainable for residential and industrial heating applications. Pavel and Mohamad (2004:4940) investigated heat transfer enhancement in gas heat exchangers with porous media, finding that smaller porosity, larger insert diameters, and higher thermal conductivity significantly improved performance. However, these enhancements came with increased pressure drop, highlighting a trade-off with pumping power. Enhanced heat transfer was attributed to flow channeling, improved conductivity, and radiative effects. Hayes et al. (2008:1308) compared LTNE and LTE models for porous media heat transfer, finding the LTNE model more accurate. Heat transfer improved with higher Reynolds numbers but showed diminishing returns. A new Nusselt number correlation for matrix heat exchangers was developed, aligning with experimental data. Dehghan et al. (2015:450)

analyzed convection-radiation heat transfer in solar heat exchangers with porous media, finding that increased radiation and porous shape parameters enhance heat transfer. The homotopy perturbation method accurately predicts performance under moderate radiation but diverges at higher non-linearity. Porous media effectively boost solar system efficiency by incorporating radiation conductivity.

Alkam and Al-Nimr (1999:3611) showed that porous substrates in double-pipe heat exchangers significantly enhance heat transfer effectiveness, particularly at high heat capacity ratios. However, the improvement plateaus beyond a critical substrate thickness, with increased pressure drop highlighting a trade-off between efficiency and pumping power. Imke (2004:297) combined a porous media approach with empirical equations to simulate different flow characteristics in microchannel heat exchangers. The method, validated by experiments, reduced computational costs while accurately predicting thermal and hydraulic performance. Dehghan et al. (2014:265) analyzed local thermal nonequilibrium in a tubular pipe containing a porous substrate, finding that increased porosity and conductivity ratio reduced nonequilibrium intensity. They also introduced a new dimensionless number to characterize thermal nonequilibrium. Habibishandiz and Saghir (2022:4) studied passive heat transfer enhancement with porous media, nanofluids, and microorganisms. Porous media increased surface area and disrupted boundary layers, while nanofluids improved performance via Brownian motion and thermophoresis.

Existing studies typically focus on the effects of porous structures in heat exchangers under turbulent flow conditions, various fluid types, and geometric configurations. Unlike previous research, this study investigates the impact of porous media on heat transfer performance under laminar flow conditions. Using a double-pipe heat exchanger, parameters such as porosity (ϕ = 0.8 - 0.2), porous region thickness (D = 1.0 - 2.5) mm), Reynolds numbers (Re = 250 - 1000), and fluid inlet temperatures (T = 30 - 60°C) are analyzed in detail, addressing gaps in the literature by examining both flow dynamics and heat transfer effectiveness at low Reynolds numbers.

MATERIALS AND METHODS

In this study, the numerical model of a tubular heat exchanger was designed using ANSYS 2022 R1 software. The inner tube had diameters of 14 mm (inner) and 16 mm (outer), while the outer tube had diameters of 30 mm (inner) and 32 mm (outer). The model operated in a counterflow configuration, with pure water used as both hot and cold fluids. A 1 mm-thick porous structure, made of aluminum like the tubes, was inserted on the inner surface of the inner pipe. The geometric structure of the numerical design is shown in Figure 1.

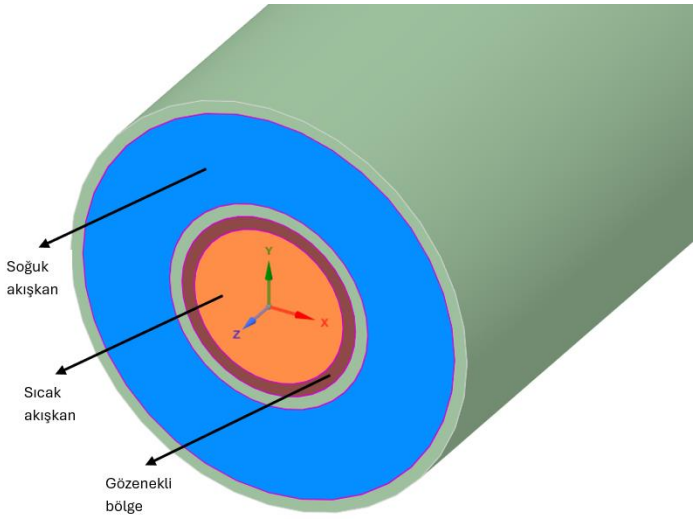

Figure 1: The geometric representation of the numerical model

Polygonal mesh elements were used in the grid generation process. The use of polygonal elements in flow problems offers significant advantages, particularly in improving mesh skewness and orthogonality quality metrics, while also contributing to faster and more stable convergence during the solution process. These elements create a smoother cell structure in complex geometries, enhancing the accuracy and stability of numerical solutions.

A mesh independence test was performed to confirm that the numerical solution remains unaffected by further refinement of the computational grid, thereby ensuring the reliability of the results for the study. Five different mesh structures with varying element counts were analyzed, and their effects on solution quality were evaluated. The element counts and geometric quality metrics for each mesh are detailed in Table 1, and differences between these values were analyzed to identify the optimal mesh structure. This process confirmed that the solution was insensitive to further increases in element count, enhancing the reliability of the numerical model.

Table 1: The element counts and geometric quality metrics

Model	Mesh number	Max. skewness	Min. orthogonal quality
Model 1	167491	0.81	0.22
Model 2	413221	0.76	0.29
Model 3	703837	0.68	0.34
Model 4	1259937	0.66	0.36
Model 5	1639901	0.65	0.36

The cross-sectional views of the mesh structures for Model 1 and Model 4 are presented in Figure 2 for comparison.

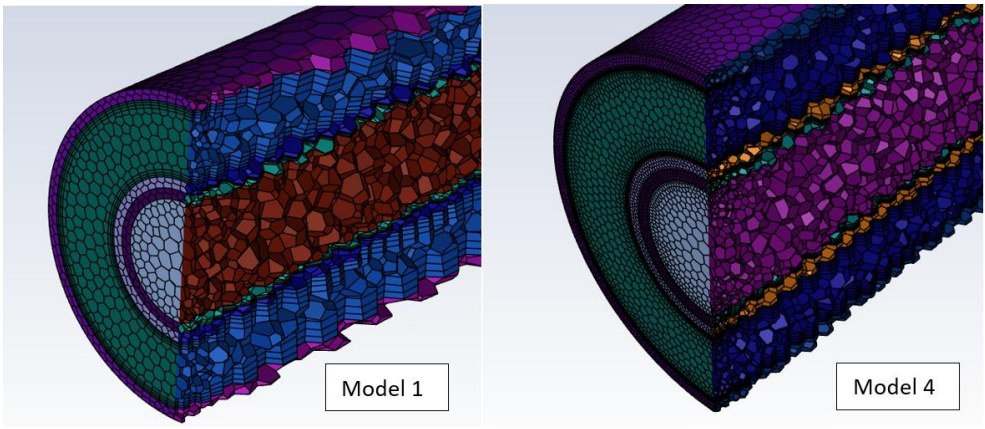

Figure 2: The cross-sectional views of the mesh structures

The influence of cell count on the computational domain has been assessed by examining the outlet temperature of the hot fluid across various mesh configurations. The results indicated that when the cell count exceeded 1200000, there was no significant change in the outlet temperature. Therefore, considering solution accuracy and computational efficiency, Model 4 was selected as the optimal choice. The results showing the impact of cell count on the outlet temperature are presented in Figure 3.

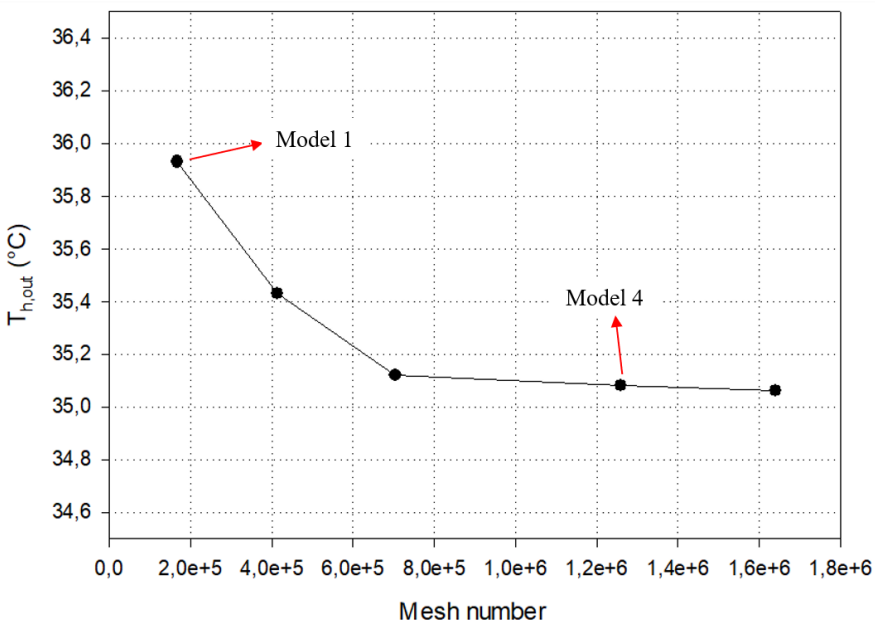

Figure 3: The impact of cell counts on the outlet temperature

The dependency of the numerical model on the iteration count was analyzed by monitoring changes in the outlet temperature of the hot fluid as the number of iterations increased. The analysis revealed that when the iteration count exceeded 500, no further changes in the outlet temperature were observed. Therefore, 500 iterations were deemed sufficient for the solution. The graph depicting the effect of iteration count on outlet temperature is presented in Figure 4.

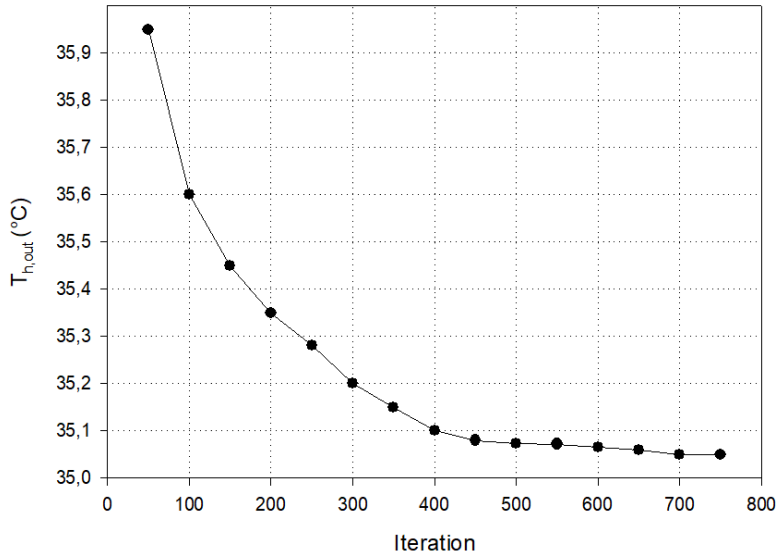

Figure 4: Iteration independence test

The continuity, momentum, and energy equations utilized for addressing the steady-state flow problem, along with the equations employed to determine heat transfer effectiveness, are outlined below. These equations are expressed in cylindrical coordinates (r, θ, z) as outlined by Y. Cengel and Cimbala (2014:X).

Continuity equation:

$$\frac{1}{r}\frac{\partial(ru_r)}{\partial r}+\frac{1}{r}\frac{\partial(u_\theta)}{\partial \theta}+\frac{\partial(u_z)}{\partial z}=0$$

Momentum equation:
r-direction:

$$p\left(\frac{\partial(u_r)}{\partial t}+u_r\frac{\partial(u_r)}{\partial r}+\frac{u_\theta}{r}\frac{\partial(u_r)}{\partial \theta}-{u_\theta}^2+u_z\frac{\partial(u_r)}{\partial z}\right)=-\frac{\partial P}{\partial r}+pg_r+$$
$$\mu\left[\frac{1}{r}\frac{\partial}{\partial r}\left(r\frac{\partial u_r}{\partial r}\right)-\frac{u_r}{r^2}+\frac{1}{r^2}\frac{\partial^2 u_r}{\partial \theta}-\frac{2}{r^2}\frac{\partial u_\theta}{\partial \theta}+\frac{\partial^2 u_r}{\partial z^2}\right]$$

θ-direction:

$$p\left(\frac{\partial u_\theta}{\partial t}+u_r\frac{\partial u_\theta}{\partial r}+\frac{u_\theta}{r}\frac{\partial u_\theta}{\partial \theta}+\frac{u_\theta u_r}{r}+u_z\frac{\partial u_\theta}{\partial z}\right)=-\frac{1}{r}\frac{\partial P}{\partial \theta}+pg_\theta+$$
$$\mu\left[\frac{1}{r}\frac{\partial}{\partial r}\left(r\frac{\partial u_\theta}{\partial r}\right)-\frac{u_\theta}{r^2}+\frac{1}{r^2}\frac{\partial^2 u_\theta}{\partial \theta^2}+\frac{2}{r^2}\frac{\partial u_r}{\partial \theta}+\frac{\partial^2 u_\theta}{\partial z^2}\right]$$

z-direction:

$$p\left(\frac{\partial u_z}{\partial t}+u_r\frac{\partial u_z}{\partial r}+\frac{u_\theta}{r}\frac{\partial u_z}{\partial \theta}+u_z\frac{\partial u_z}{\partial z}\right)=-\frac{\partial P}{\partial z}+pg_z+\mu\left[\frac{1}{r}\frac{\partial}{\partial r}\left(r\frac{\partial u_z}{\partial r}\right)+\frac{1}{r^2}\frac{\partial^2 u_z}{\partial \theta^2}+\frac{\partial^2 u_z}{\partial z^2}\right]$$

Energy equation:

$$\frac{\partial T}{\partial t}+u_r\frac{\partial T}{\partial r}+\frac{u_\theta}{r}\frac{\partial T}{\partial \theta}+u_z\frac{\partial T}{\partial z}=\frac{\dot{q}_g}{c_p}+\alpha\left[\frac{1}{r}\frac{\partial}{\partial r}\left(r\frac{\partial T}{\partial r}\right)+\frac{1}{r^2}\ \frac{\partial^2 T}{\partial \theta^2}+\frac{\partial^2 T}{\partial z^2}\right]+\frac{\varphi}{pc_p}$$

In this study, the boundary conditions applied for solving the flow and heat transfer problem in the analysis of the double-pipe heat exchanger are defined in steady state conditions. The boundary conditions for the double-pipe heat exchanger analysis are as follows: At the hot fluid inlet, the velocity components are defined as (U=0), ($V=V_{in}$), (W=0), and the temperature is ($T=T_{hot}$). At the cold fluid inlet, the conditions are ($U=U_{inlet}$), (V=0), (W=0), and ($T=T_{cold}$). At the hot fluid outlet, the velocity and temperature gradients along the flow direction are zero ($\partial U/\partial x=0$), ($\partial V/\partial x=0$ \), ($\partial W/\partial x=0$), ($\partial T/\partial x=0$). Similarly, at the cold fluid outlet, the velocity gradients remain zero ($\partial U/\partial x=0$), ($\partial V/\partial x=0$), ($\partial W/\partial x=0$), while the temperature gradient is zero along the axial direction ($\partial T/\partial z=0$). Within the porous medium, the velocity components are zero (U=0), (V=0), (W=0), and the temperature gradient along the axial direction is zero ($\partial T/\partial z=0$).

The formulas used for heat transfer calculations are presented below.

$$\Delta T_1 = T_{h,in} - T_{c,out}$$

$$\Delta T_2 = T_{h,out} - T_{c,in}$$

$$\Delta T_{lm} = \frac{\Delta T_1 - \Delta T_2}{\ln(\Delta T_1/\Delta T_2)}$$

$$\dot{Q} = UA_s\Delta T_{lm}$$

The overall heat transfer coefficient is denoted by U, and the total surface area is represented by A_s. The process of determining heat transfer effectiveness involves calculating the heat capacity ratios, as outlined below.

For the cold fluid:

$$C_c = \dot{m}_c c_{pc}$$

For the hot fluid:

$$C_h = \dot{m}_h c_{ph}$$

$$\Delta T_{max} = T_{h,in} - T_{c,in}$$

The highest achievable rate of heat transfer:

$$\dot{Q}_{max} = C_{min} \Delta T_{max}$$

Heat transfer effectiveness:

$$\varepsilon = \frac{\dot{Q}_{act}}{\dot{Q}_{max}} = \frac{Gerçek\ ısı\ transfer\ mikatarı}{Maksimum\ ısı\ transfer\ miktarı}$$

Q_{act} denotes the actual heat transfer rate, corresponding to the amount of heat exchanged by either the hot or cold fluid.

Porosity (ϕ) is characterized as the proportion of the volume occupied by porous voids to the overall volume of a material or medium. It is mathematically represented by the following equation:

$$\phi = \frac{V_{boşluk}}{V_{toplam}}$$

Within the scope of numerical analysis, the fixed variables and parameters for the cases with and without the porous region in the double-pipe heat exchanger are defined in Table 2.

Table 2: Parameters

Group	Constant variables	Parameters	Definition
1	Re = 250 T_{hot} = 50°C T_{cold} = 20°C D = 1,0 mm	ϕ = 0,8 ϕ = 0,6 ϕ = 0,4 ϕ = 0,2	Porosity level
2	Re = 250 T_{hot} = 50°C T_{cold} = 20°C ϕ = 0,6	D = 1,0 mm D = 1,5 mm D = 2,0 mm D = 2,5 mm	Porosity region thickness
3	D = 0,0 mm ϕ = 1,0 T_{hot} = 50°C	$Re_{sıcak}$ = 250 $Re_{sıcak}$ = 500 $Re_{sıcak}$ = 750 $Re_{sıcak}$ = 1000	Re number of hot fluid
4	D = 0,0 mm ϕ = 1,0 Re_{hot} = 250	T_{hot} = 30°C T_{hot} = 40°C T_{hot} = 50°C T_{hot} = 60°C	Inlet temperature of hot fluid
5	D = 1,0 mm ϕ = 0,6 T = 50°C	Re_{hot} = 250 Re_{hot} = 500 Re_{hot} = 750 Re_{hot} = 1000	Re number of hot fluid
6	D = 1,0 mm ϕ = 0,6 Re_{hot} = 250	T_{hot} = 30°C T_{hot} = 40°C T_{hot} = 50°C T_{hot} = 60°C	Inlet temperature of hot fluid

RESULTS AND DISCUSSION

This research explores how incorporating a porous medium influences the thermal efficiency of a double-pipe heat exchanger functioning within a laminar flow regime. The investigation considered various porosity levels (ϕ = 0.8, 0.6, 0.4, 0.2), porous region thicknesses (D = 1.0, 1.5, 2.0, 2.5 mm), Reynolds numbers (Re = 250, 500, 750, 1000), and fluid inlet temperatures (T = 30, 40, 50, 60°C).

The Effect of Porosity on Heat Transfer Performance

To examine the effect of porosity on heat transfer performance, the porosity ϕ was gradually reduced from 0.8 to 0.2 while keeping the Reynolds number constant at Re = 250 and the fluid temperatures fixed at T_{hot} = 50°C and T_{cold} = 20°C. A reduction in porosity from ϕ = 0.8 to ϕ = 0.6 resulted in a 3.9% increase in heat transfer effectiveness, while further reductions from ϕ = 0.6 to ϕ = 0.4 and from ϕ = 0.4 to ϕ = 0.2 yielded increases of 1.2% and 0.2%, respectively. Overall, a total increase of 5.3% in heat transfer effectiveness was observed when porosity was reduced from ϕ = 0.8 to ϕ = 0.2. Figure 5 illustrates the influence of porosity on heat transfer effectiveness.

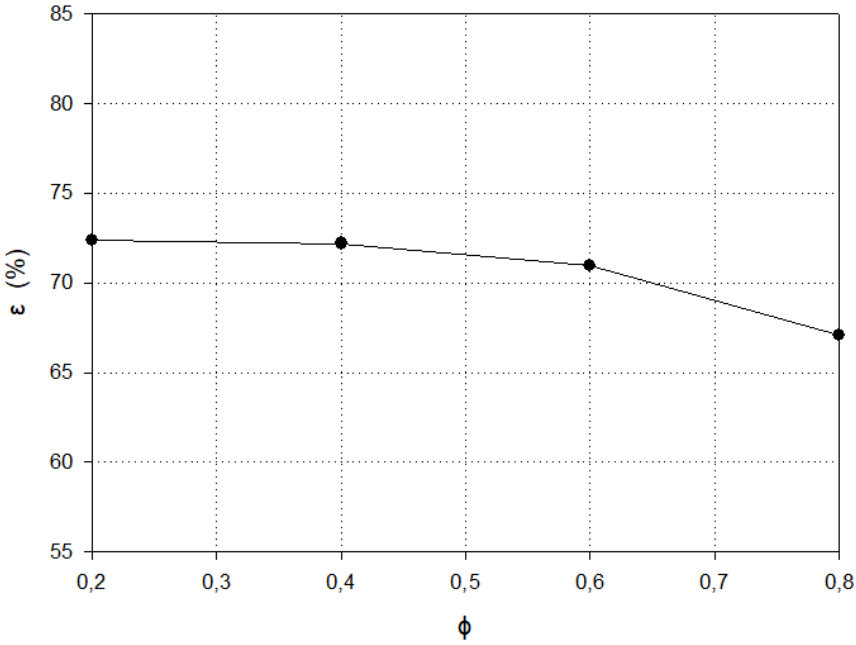

Figure 5: The influence of porosity on effectiveness

Reducing the porosity from 0.8 to 0.2 increased flow resistance and disrupted the velocity profile of the fluid. However, this resistance facilitated greater interaction between the fluid and the surface, contributing to improved heat transfer. On the other hand, at higher porosity levels (e.g., 0.8), the freer flow of the fluid reduced surface contact, thereby limiting heat transfer performance. Consequently, the balance between porosity and flow resistance was critical in optimizing heat transfer effectiveness. The temperature contours illustrating this effect are presented in Figure 6.

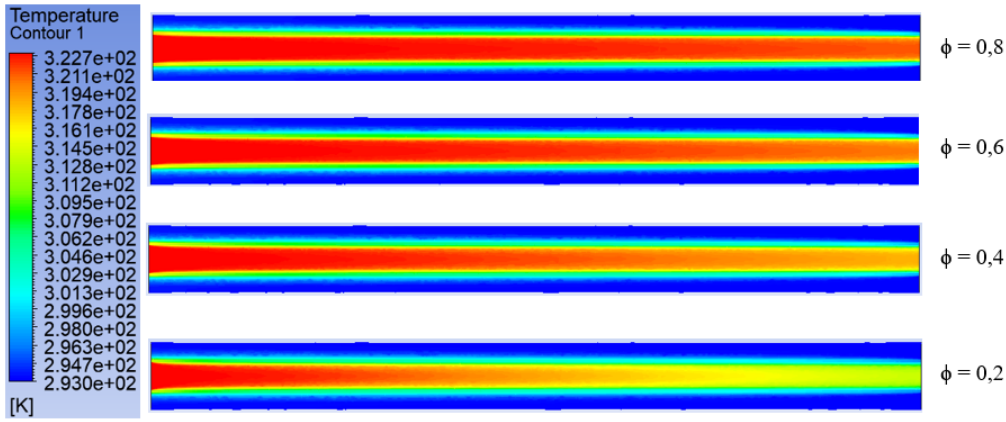

Figure 6: Temperature contours illustrating the effect of porosity

When hydrodynamic effects are examined (Figure 7), higher porosity ϕ=0.8 allows the flow to move more freely, resulting in a thinner hydrodynamic boundary layer and limited interaction between the fluid and the boundary layer. However, at lower porosity ϕ =0.2, the resistance of the porous medium increases, and the disruption in the flow profile leads to a reduction in the thermal boundary layer thickness.

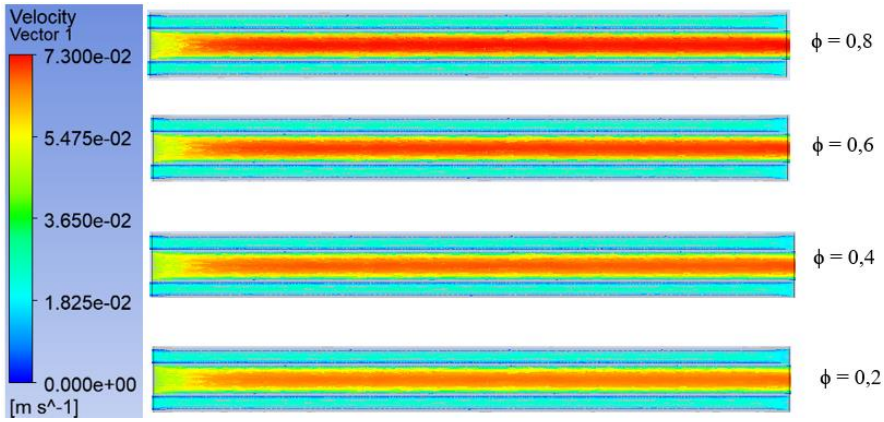

Figure 7: Velocity vectors illustrating the effect of porosity

The Effect of Porous Region Thickness

To examine the effect of porous region thickness on heat transfer performance, the porous region thickness D was gradually increased from 1.0 mm to 2.5 mm while keeping the Reynolds number Re constant at 250 and the fluid inlet temperatures fixed at T_{hot} = 50°C and T_{cold} = 20°C. Increasing D from 1.0 mm to 1.5 mm resulted in a 4.4% improvement in heat transfer effectiveness, while increases from 1.5 mm to 2.0 mm and from

2.0 mm to 2.5 mm yielded improvements of 1.9% and 0.9%, respectively. Overall, a total improvement of 7.2% was observed when D was increased from 1.0 mm to 2.5 mm. Figure 8 demonstrates how the thickness of the porous region influences heat transfer performance.

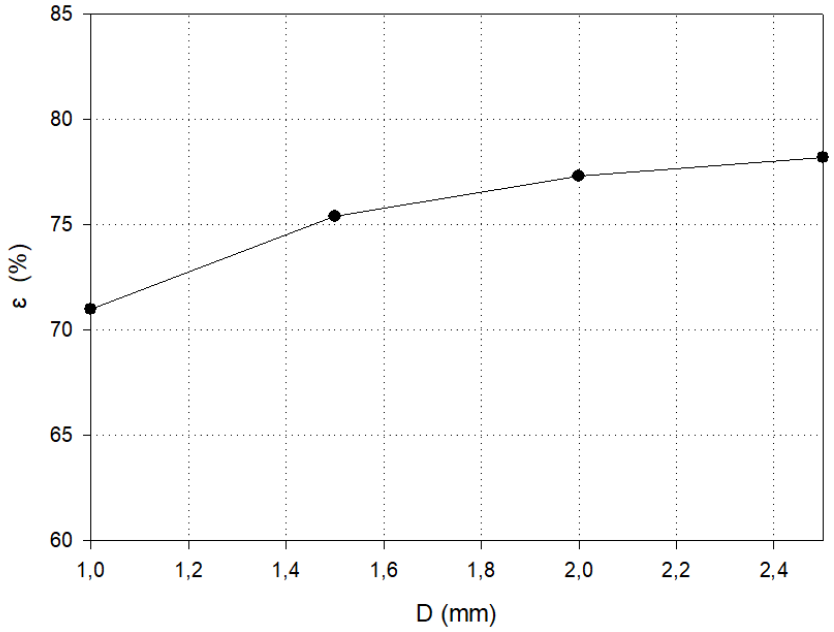

Figure 8: The influence of the thickness of the porous region

Increasing the thickness of the porous region initially enhanced heat transfer performance significantly, as it increased the fluid-surface contact area and thinned the thermal boundary layer. However, as the thickness continued to increase, the improvement in performance showed a diminishing trend due to the rising flow resistance and the limited additional benefit of increased surface area. This indicates the existence of an optimal porous region thickness, beyond which further increases provide minimal contributions to heat transfer performance.

The Effect of Re Number

To investigate the varying Reynolds number on effectiveness, the Reynolds number was gradually increased from 250 to 1000 while keeping the cold fluid temperature T_{cold} fixed at 20°C and the hot fluid inlet temperature T_{hot} constant at 50°C. An increase in Re from 250 to 500 resulted in a 3.4% improvement in heat transfer effectiveness, while increases from 500 to 750 and 750 to 1000 led to improvements of 1.2% and 0.3%, respectively. Overall, increasing Re from 250 to 1000 resulted in a

total improvement of 4.9% in heat transfer effectiveness. The graph in Figure 9 illustrates the change in heat transfer effectiveness as Reynolds number (Re) increases.

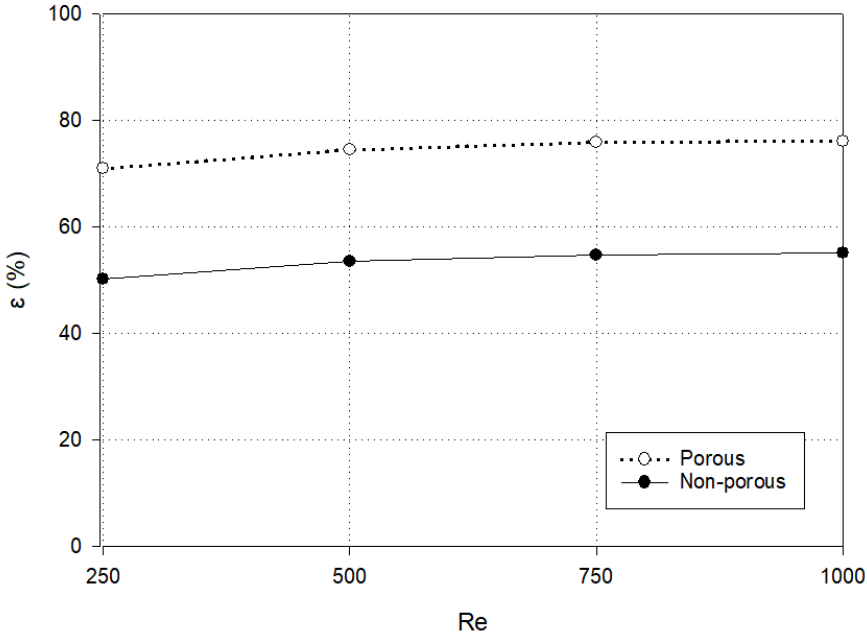

Figure 9: The influence of the Reynolds number on heat transfer.

With an increase in the Reynolds number, the hydrodynamic boundary layer became thicker, whereas the thermal boundary layer experienced a reduction in its thickness. In the porous medium, the enhanced hydrodynamic effects of the fluid significantly improved heat transfer effectiveness. In comparison to the non-porous medium, the enhanced mixing induced by the porous structure facilitated more effective heat transfer, particularly at elevated Reynolds numbers. This effect is illustrated in the temperature contours shown in Figure 10.

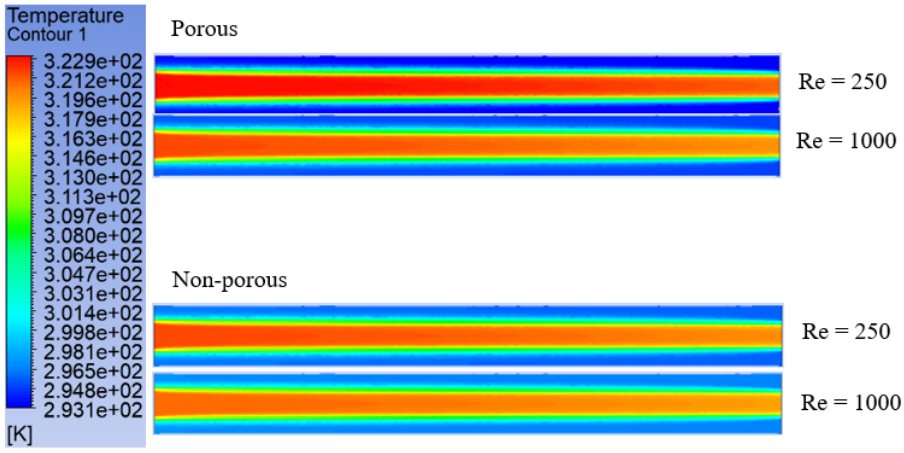

Figure 10: Temperature contours for porous and non-porous cases

The porous medium, while enhancing performance by influencing the boundary layer and heat transfer, did not cause a noticeable change in velocity vectors. The effects of the porous structure were primarily observed at a microscopic scale, particularly through its impact on pressure drop.

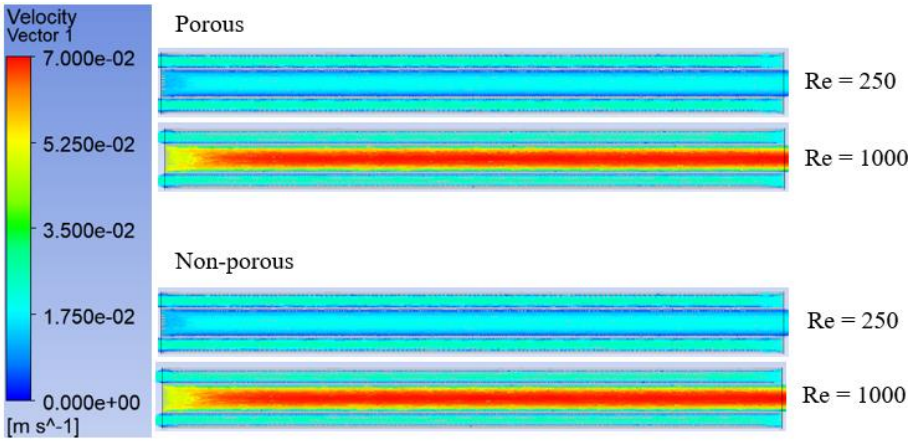

Figure 11: Velocity vectors for porous and non-porous cases

The Effect of Inlet Temperature

To examine the effect of hot fluid inlet temperature, the inlet temperature gradually increased from T = 30°C to 60°C at a constant Reynolds number of Re = 250 for both the hot and cold fluids. Increasing the temperature from 30°C to 40°C resulted in a 1.1% improvement in heat transfer effectiveness, while increases from 40°C to 50°C and 50°C to 60°C led to improvements of 0.4% and 0.1%, respectively. The total improvement was calculated as 1.6%.

Raising the fluid inlet temperature did not cause a significant change in heat transfer effectiveness (Figure 12). This result was anticipated since heat transfer effectiveness depends on the NTU and the capacity ratio, rather than being directly affected by the inlet temperature. While temperature changes may indirectly affect the system's thermodynamic performance, effectiveness is primarily determined by parameters such as fluid mass flow rate and heat transfer surface area.

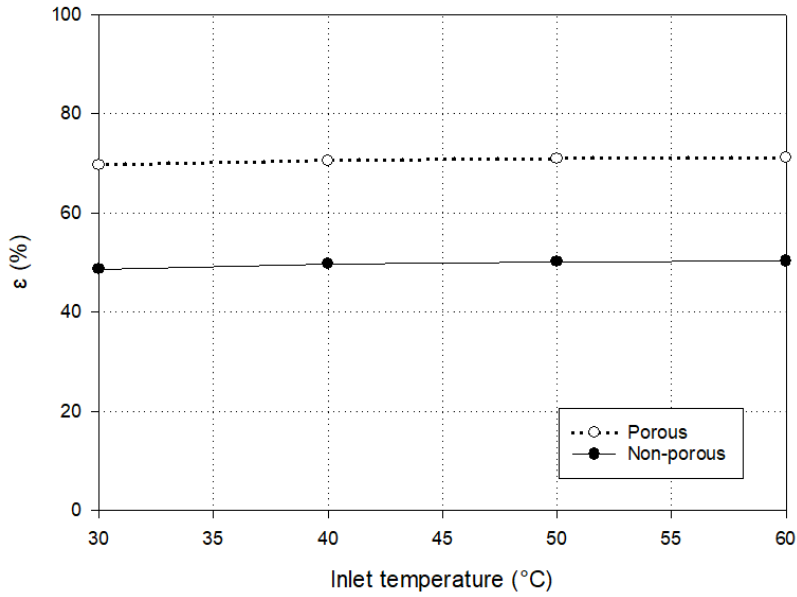

Figure 12: The effect of hot fluid inlet temperature on heat transfer performance

It was observed that temperature differences became more pronounced, particularly in the boundary layer regions, which partially improved heat transfer effectiveness (Figure 13). In the non-porous medium, the orderly flow limits heat transfer performance; however, the increase in inlet temperature enhanced the temperature gradient between the fluid near the pipe surface and the surrounding medium, thereby improving the heat transfer rate.

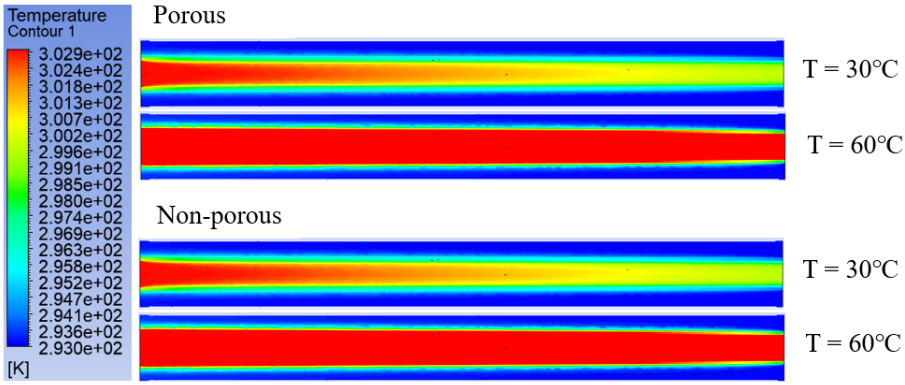

Figure 13: Temperature contours for different inlet temperatures for porous and non-porous cases

Reducing porosity and increasing the thickness of the porous region enhanced surface interaction by increasing flow resistance, leading to a notable improvement in heat transfer effectiveness, though this effect diminished beyond a certain point. Likewise, an increase in the Reynolds number led to a reduction in the thermal boundary layer thickness, which significantly enhanced the heat transfer effectiveness. In contrast, increasing the inlet temperature had minimal impact on effectiveness, as it is primarily governed by NTU and the capacity ratio, with temperature contributing only indirectly to system performance.

CONCLUSION

This study investigated the impact of a porous medium on a heat exchanger performance, considering flow characteristics, porosity, and the thickness of the porous region. As a result:

1. Reducing the porosity from $\phi = 0.8$ to $\phi = 0.2$ resulted in a 5.3% increase in heat transfer effectiveness. This improvement gradually decreased as porosity was reduced, enhancing heat transfer by allowing greater interaction between the fluid and the surface.
2. Increasing the porous region thickness from D = 1.0 mm to 2.5 mm led to a total improvement of 7.2% in heat transfer effectiveness. However, as the thickness increased, performance improvement showed a diminishing trend due to higher flow resistance and the limited benefit of additional surface area.
3. In the non-porous medium, increasing the Reynolds number within the laminar range Re = 250 to 1000 resulted in a total heat

transfer effectiveness improvement of 4.9%, while in the porous medium, this improvement increased to 5.2%.

4. In the non-porous medium, increasing the hot fluid inlet temperature from T = 30°C to 60°C resulted in a total heat transfer effectiveness improvement of 1.6%, while in the porous medium, this improvement was measured at 1.4%.
5. Optimizing porous medium properties enhances heat transfer and minimizes energy losses, offering a sustainable, energy-efficient solution. These findings support the design of cost-effective and efficient double-pipe heat exchanger systems for industrial use.
6. Future studies in this field could benefit from detailed analyses of different porous structures, material types, and flow conditions on heat transfer performance. Using nanostructured porous materials, hybrid systems, and nano-fluids as working fluids may further enhance heat transfer. Additionally, investigating porous media behavior under turbulent regimes and varying temperature conditions, incorporating flow directors, and developing geometries to reduce thermal boundary layers could significantly expand applications and contribute to the literature.

REFERENCE

Alkam, M. K., & Al-Nimr, M. A. (1999). Improving the performance of double-pipe heat exchangers by using porous substrates. International Journal of Heat and Mass Transfer, 42(19), 3609-3618.

Arivazhagan, M., & Lokeswaran, S. (2013). Entropy generation minimization of shell and tube heat exchanger with porous medium. Experimental Techniques, 37, 74-82.

Cengel, Y., & Cimbala, J. (2013). Ebook: Fluid mechanics fundamentals and applications (si units). McGraw Hill.

Cengel, Y. A., & Ghajar, A. J. (2014). Heat and Mass Transfer (in SI Units).

Dehghan, M., Jamal-Abad, M. T., & Rashidi, S. (2014). Analytical interpretation of the local thermal non-equilibrium condition of porous media imbedded in tube heat exchangers. Energy Conversion and Management, 85, 264-271.

Dehghan, M., Rahmani, Y., Ganji, D. D., Saedodin, S., Valipour, M. S., & Rashidi, S. (2015). Convection–radiation heat transfer in solar heat exchangers filled with a porous medium: homotopy perturbation method versus numerical analysis. Renewable Energy, 74, 448-455.

Delalic, N., Mulahasanovic, D., & Ganic, E. N. (2004). Porous media compact heat exchanger unit—experiment and analysis. Experimental Thermal and Fluid Science, 28(2-3), 185-192.

Habibishandiz, M., & Saghir, M. Z. (2022). A critical review of heat transfer enhancement methods in the presence of porous media, nanofluids, and microorganisms. Thermal Science and Engineering Progress, 30, 101267.

Hayes, A. M., Khan, J. A., Shaaban, A. H., & Spearing, I. G. (2008). The thermal modeling of a matrix heat exchanger using a porous medium and the thermal non-equilibrium model. International Journal of Thermal Sciences, 47(10), 1306-1315.

He, S., Wang, M., Tian, W., Qiu, S., & Su, G. H. (2022). Development of an OpenFOAM solver for numerical simulations of shell-and-tube heat exchangers based on porous media model. Applied Thermal Engineering, 210, 118389.

Hu, C., Sun, M., Xie, Z., Yang, L., Song, Y., Tang, D., & Zhao, J. (2020). Numerical simulation on the forced convection heat transfer of porous medium for turbine engine heat exchanger applications. Applied Thermal Engineering, 180, 115845.

Imke, U. (2004). Porous media simplified simulation of single-and two-phase flow heat transfer in micro-channel heat exchangers. Chemical Engineering Journal, 101(1-3), 295-302.

Moradi, A., Toghraie, D., Isfahani, A. H. M., & Hosseinian, A. (2019). An experimental study on MWCNT–water nanofluids flow and heat transfer in double-pipe heat exchanger using porous media. Journal of Thermal Analysis and Calorimetry, 137(5), 1797-1807.

Omidi, M., Farhadi, M., & Jafari, M. (2017). A comprehensive review on double pipe heat exchangers. Applied Thermal Engineering, 110, 1075-1090.

Pavel, B. I., & Mohamad, A. A. (2004). An experimental and numerical study on heat transfer enhancement for gas heat exchangers fitted with porous media. International Journal of Heat and Mass Transfer, 47(23), 4939-4952.

Sheikholeslami, M., & Ganji, D. D. (2016). Heat transfer improvement in a double pipe heat exchanger by means of perforated turbulators. Energy Conversion and management, 127, 112-123.

Wang, Y., Wang, H., Huang, D., Zheng, P., Wu, X., Shi, Y., & He, W. (2023). Structural parameters study of porous medium heat exchanger for high-power chip cooling. Applied Thermal Engineering, 232, 120906.

Functionally Graded Materials: Solutions for the Future of Engineering

Nusret Fatih AKTAŞ[1]
Muhammed Asım KESERCİOĞLU[2]

1- Res. Asst.; Sakarya Applied Sciences University Faculty of Technology Department of Mechanical Engineering nusretaktas@subu.edu.tr ORCID No: 0009-0004-9714-7822
2- Res. Asst.; Sakarya Applied Sciences University Faculty of Technology Department of Mechanical Engineering mkesercioglu@subu.edu.tr ORCID No: 0009-0003-3751-4224

ABSTRACT

Functionally graded materials (FGMs) are an innovative class of advanced materials characterized by their gradual or continuous variation in properties, such as composition, density, thermal conductivity, or mechanical strength, across a specific dimension. This unique property enables FGMs to address the limitations of conventional homogeneous materials by combining the benefits of multiple materials, such as the high-temperature resistance of ceramics and the toughness of metals, while minimizing issues like stress concentrations and thermal mismatches. Initially developed in the mid-1980s for aerospace applications, FGMs have since expanded into diverse fields, including biomedical engineering, automotive manufacturing, electronics, and energy systems.

The production of FGMs has evolved significantly, incorporating methods such as powder metallurgy, thermal spraying, additive manufacturing, centrifugal casting, and laser-based techniques. These methodologies enable precise control over material gradients, facilitating the creation of complex geometries and tailored properties for specific applications. For instance, FGMs are used in thermal barrier coatings for turbine blades, bio-compatible implants for orthopedic and dental applications, and high-performance automotive components such as brake discs and engine parts.

This study examines the historical development, production techniques, and diverse applications of FGMs. It also explores future directions, emphasizing the integration of nanotechnology, artificial intelligence, and hybrid manufacturing approaches. FGMs hold immense potential for solving complex engineering challenges, offering sustainable, multifunctional, and high-performance solutions for critical industries.

Keywords – Functionally Graded Materials (Fgms), Advanced Manufacturing Techniques, Thermal Barrier Coating, Mechanical Strength Optimization, Additive Manufacturing.

INTRODUCTION

FGM is a novel composite material made up of two or more components whose composition and structure continuously vary in gradients (Li et al., 2025). It represents an innovative approach in today's engineering world, aimed at overcoming the limitations of conventional homogeneous materials. FGMs combine the physical, chemical, and mechanical properties of multiple materials in a single structure, providing multifunctional and optimized solutions through a continuous or gradual transition of properties. These materials are characterized by a structure where properties vary along

a specific axis. These variations can involve properties such as density, elastic modulus, thermal conductivity, or chemical composition.

Traditional materials, when composed of multiple components serving different functions, often encounter high stress concentrations and thermal stresses at the interfaces. This leads to material degradation and reduced lifespan over time. FGMs address these challenges by offering structures with smoothly varying material properties. This feature is particularly advantageous in critical areas like aerospace applications, where thermal stress is intense. FGMs also have exceptional thermal and mechanical capabilities, which have been used in the production of thermal barrier coatings (Abbas et al., 2016; Schulz et al., 2003), sensor structures (Yu et al., 2022), and piston rings (Carvalho et al., 2015).

Research advancements have been achieved in various domains, including aerospace (Miteva & Bouzekova-Penkova, 2021), mechanical engineering, biomedicine (Canpolat et al., 2023), energy applications (Müller et al., 2003).

The Philosophy Behind Functionally Graded Materials

The fundamental philosophy of FGMs is to combine the advantages of two or more materials while minimizing their disadvantages. For instance, an FGM structure can integrate the high-temperature resistance of ceramics with the mechanical strength of metals. This is especially important for preventing cracks and deformations caused by differences in thermal expansion.

The Evolution of Production and Design Needs

Functionally graded materials were developed in the mid-1980s by Japanese researchers for use in spacecraft and other high-temperature environments. Initially, metal-ceramic graded structures were utilized as thermal barrier coatings on spacecraft exteriors. However, over time, this technology became applicable in a wide range of sectors, from biomedical implants to energy storage devices.

Industrial and Academic Interest

Interest in FGMs has rapidly increased in both industrial and academic fields. This is because these materials not only offer superior performance but also enable sustainable production and design applications. FGMs are increasingly preferred in applications where features like energy efficiency, durability, and lightweight structures are critical. These materials have the potential to revolutionize industries such as aerospace, biomedical, energy, automotive, and electronics.

Scientific and Technological Significance

The technologies used in the production of FGMs range from thermal spraying to additive manufacturing, enhancing the design flexibility of these materials and making them suitable for many innovative applications. Moreover, studies involving nanomaterials have further optimized the properties of FGMs, opening new application areas.

In conclusion, functionally graded materials occupy a unique position in the fields of engineering and science as a technology offering superior performance and durability compared to traditional materials. This study examines the historical development, production techniques, and application areas of FGMs and discusses their future potential.

HISTORICAL DEVELOPMENT

For composites and polymeric materials, the concept of a compositional and structural gradient in material microstructure was originally put forth in 1972 (Kumar Bohidar et al., 2014). In the mid-1980s as part of a Japanese research initiative aimed at developing advanced materials for high-temperature environments, particularly for aerospace applications. This pioneering work was driven by the need to address the challenges posed by thermal stresses in components exposed to extreme temperature gradients. The initial focus was on creating materials with a gradual transition between ceramics, which offer excellent thermal resistance, and metals, which provide mechanical strength and toughness.

Early Innovations in FGM Technology

The first FGMs were designed to serve as thermal barrier coatings for spacecraft and aerospace vehicles. These applications required materials capable of withstanding the intense heat generated during atmospheric re-entry. The development of ceramic-metal FGMs provided an innovative solution, enabling a smooth transition between the high-temperature resistance of ceramics and the structural integrity of metals. This combination not only improved the durability of the components but also minimized the stress concentrations typically found at sharp material interfaces.

In the late 1980s, the potential of FGMs began to be recognized in other high-performance engineering sectors. For instance, nuclear energy systems started employing FGMs for radiation shielding and thermal insulation purposes, leveraging their ability to combine properties like neutron absorption and mechanical strength.

Evolution of Production Techniques

As the demand for FGMs grew, so did the innovation in production methods. Early techniques such as powder metallurgy and thermal spraying were refined to allow for better control over material gradients. These methods enabled the creation of FGMs with precisely tailored properties for specific applications. By the 1990s, advancements in computational modeling and simulation further accelerated the development of FGMs. Researchers could now predict and optimize the performance of graded structures before physical production, significantly reducing development time and costs.

The introduction of additive manufacturing (AM) technologies in the late 1990s marked a turning point in the production of FGMs. Techniques like selective laser sintering (SLS) and direct energy deposition (DED) allowed for the creation of complex, three-dimensional graded structures that were previously unattainable with traditional methods. These advancements enabled FGMs to be used in applications ranging from biomedical implants to automotive components.

Expansion into New Application Areas

By the early 2000s, FGMs had become a key focus in biomedical engineering. The compatibility of FGMs with biological systems made them ideal for applications such as bone implants and dental prosthetics. For example, titanium-hydroxyapatite FGMs were developed to mimic the gradient structure of natural bone, providing both mechanical support and bioactivity.

Simultaneously, the automotive industry began exploring FGMs for components such as brake discs and engine parts. These applications benefited from the materials' ability to withstand high temperatures and mechanical loads while maintaining lightweight structures, crucial for improving vehicle performance and fuel efficiency.

Recent Advancements and Future Directions

In recent years, the integration of nanotechnology and advanced computational tools has further expanded the capabilities of FGMs. Nanostructured FGMs, which incorporate nanoparticles to achieve unique mechanical, thermal, or electrical properties, are being developed for next-generation applications in electronics, energy systems, and aerospace. Additionally, machine learning and artificial intelligence are now being used to design and optimize FGMs, paving the way for more efficient and sustainable production processes.

The historical development of FGMs reflects a continuous evolution driven by technological advancements and interdisciplinary research. From their origins in aerospace engineering to their current applications across diverse industries, FGMs have proven to be a transformative material solution. Their ability to address complex engineering challenges ensures their relevance in the future of material science and engineering.

Table 1: Evolution of Functionally Graded Materials (FGMs)

Time Period	Milestone	Description
1980s	Conceptualization of FGMs	FGMs were introduced as a solution to manage thermal stress in environments with extreme temperature gradients.
Mid-1980s	Aerospace Sector Adoption	FGMs were first applied in the aerospace sector, particularly for thermal barrier coatings in spacecraft.
Late 1980s	Expansion into Nuclear Applications	FGMs began being used for shielding and insulation in nuclear reactors, improving safety and durability.
1990s	Development of Manufacturing Techniques	Production methods like powder metallurgy and thermal spraying were enhanced to improve material gradients.
Late 1990s	Integration of Additive Manufacturing	Emerging additive manufacturing technologies enabled the creation of intricate geometries with graded properties.
2000s	Advancements in Biomedical Applications	FGMs found significant use in medical implants, offering gradual transitions for improved compatibility with biological tissues.
Early 2010s	Entry into Automotive Applications	FGMs were incorporated into automotive parts such as brake systems and lightweight components to enhance performance.
2015–Present	Innovations in Nanostructures and AI-Assisted Design	FGMs evolved with the integration of nanotechnology and computational tools for precision and advanced functionality.

PRODUCTION TECHNIQUES

The production techniques for functionally graded materials (FGMs) have evolved significantly since their inception, driven by advancements in manufacturing technologies and the diverse requirements of engineering applications. These techniques enable the controlled variation of material properties within a single structure, allowing FGMs to meet specific performance criteria such as thermal resistance, mechanical strength, and corrosion resistance. Below is an in-depth exploration of the key production methods, their advantages, limitations, and applications. Production techniques utilized in FGM are illustrated in Fig 1.

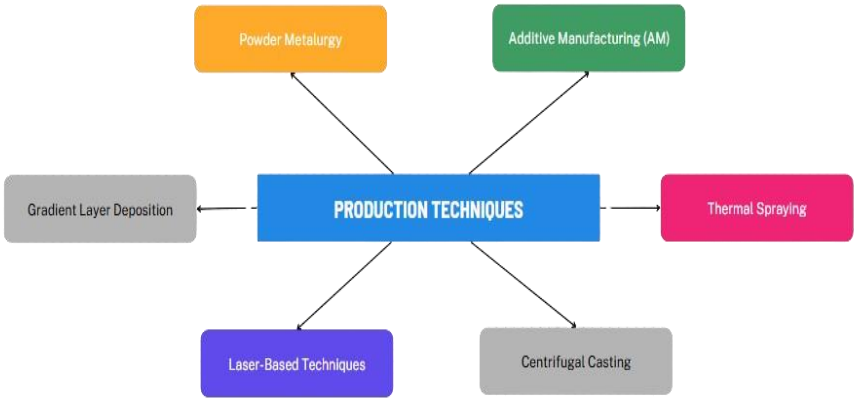

Figure 1: Production Techniques in FGM

Powder Metallurgy

Powder metallurgy is one of the earliest and most widely used techniques for producing FGMs. In this process, metal and ceramic powders are mixed in varying proportions, compacted, and then sintered to create a graded structure.

• Process Details:

The material gradient is achieved by layering powders with different compositions in a mold. The powders are then compacted under high pressure and sintered at elevated temperatures to bond the layers. Advanced techniques, such as hot isostatic pressing (HIP), are often employed to ensure uniform densification.

• Applications:

Powder metallurgy is commonly used in the production of thermal barrier coatings, wear-resistant components, and high-temperature structures in aerospace and nuclear energy industries.

• Advantages:

- High precision in gradient control.
- Suitable for a wide range of material combinations.
- Cost-effective for large-scale production.

• Limitations:

- Limited to simple geometries.
- Requires high temperatures and long processing times.

Additive Manufacturing (AM)

Additive manufacturing, often referred to as 3D printing, has revolutionized the production of FGMs by enabling the creation of complex geometries with precise material gradients. Techniques like selective laser

sintering (SLS), direct energy deposition (DED), and fused filament fabrication (FFF) are commonly used for FGM production.

• Process Details:

In AM, material gradients are achieved by varying the feedstock composition during the layer-by-layer deposition process. Advanced AM systems can handle multiple materials simultaneously, allowing for seamless transitions between different compositions.

• Applications:
  - Biomedical implants with graded mechanical and biological properties.
  - Lightweight aerospace components with tailored thermal and structural characteristics.

• Advantages:
  - Highly flexible and capable of producing complex shapes.
  - Reduces material waste compared to traditional methods.
  - Facilitates rapid prototyping and customization.

• Limitations:
  - High equipment costs.
  - Limited production speed for large-scale manufacturing.

Thermal Spraying

Thermal spraying is a surface coating technique widely used for producing FGMs with graded properties in the outer layers. This method involves the deposition of molten or semi-molten particles onto a substrate.

• Process Details:

Different materials are sprayed sequentially or simultaneously to create a gradual change in composition across the thickness of the coating. Techniques like plasma spraying and high-velocity oxy-fuel (HVOF) spraying are commonly employed.

• Applications:
  - Thermal barrier coatings for turbine blades and engine components.
  - Corrosion-resistant coatings for marine and chemical industries.

• Advantages:
  - High deposition rates.
  - Suitable for a wide range of material systems.
  - Excellent adhesion to substrates.

• Limitations:
  - Limited to surface applications.
  - Requires post-processing for improved mechanical properties.

Centrifugal Casting

Centrifugal casting is a method that leverages the effects of centrifugal force to create FGMs with a radial gradient in composition.

• Process Details:

In this process, a liquid mixture of different materials is poured into a rotating mold. The centrifugal force separates the materials based on their densities, creating a graded structure. The material with higher density moves outward, while the lighter material remains closer to the center.

• Applications:
  - Cylindrical components such as pipes, brake discs, and flywheels.
  - Wear-resistant layers in mechanical components.
• Advantages:
  - Efficient for producing cylindrical and tubular structures.
  - Relatively simple and cost-effective.
• Limitations:
  - Limited to specific shapes (cylinders and tubes).
  - Gradient control is dependent on material density differences.

Laser-Based Techniques

Laser-based techniques, such as laser cladding and laser-induced solidification, are advanced methods for producing FGMs with precise control over material gradients.

• Process Details:

A laser beam melts the surface of a substrate, and different materials are added in varying proportions to create a graded layer. These techniques offer high precision and are often used for repairing or enhancing existing components.

• Applications:
  - High-performance aerospace components.
  - Customized biomedical implants.
• Advantages:
  - High precision and localized control over gradients.
  - Minimal heat-affected zones.
• Limitations:
  - High operational costs.
  - Limited scalability for large components.

Gradient Layer Deposition

This technique involves the deposition of material layers with varying compositions, either through physical vapor deposition (PVD) or chemical vapor deposition (CVD).

• Process Details:

Thin films with graded properties are created by controlling the deposition parameters, such as gas flow rates, temperature, and pressure.

- Applications:
  - Optical coatings for lenses and mirrors.
  - Protective coatings for electronic devices.
- Advantages:
  - High-quality thin films.
  - Precise control over composition and thickness.
- Limitations:
  - Time-intensive process.
  - Limited to thin-film applications.

Table 2: Production Techniques for Functionally Graded Materials (FGMs)

Technique	Description	Advantages	Limitations
Powder Metallurgy	Mixing metal and ceramic powders in varying ratios, compacting, and sintering.	High precision in gradient control, suitable for a wide range of materials, cost-effective.	Limited to simple geometries, requires high temperatures and long processing times.
Additive Manufacturing (AM)	Layer-by-layer deposition of material with varying compositions.	Capable of producing complex shapes, reduces material waste, enables rapid prototyping.	High equipment costs, slower production speeds for large components.
Thermal Spraying	Spraying molten or semi-molten material onto a surface to create a graded coating.	High deposition rates, excellent adhesion, suitable for large surface applications.	Limited to surface applications, post-processing often required for mechanical properties.
Centrifugal Casting	Utilizing centrifugal force to separate materials based on density.	Efficient for cylindrical shapes, cost-effective for specific geometries.	Limited to tubular and cylindrical components, gradient control depends on material densities.
Laser-Based Techniques	Localized melting and addition of material using a laser beam.	High precision, minimal heat-affected zones, allows for targeted modifications.	Expensive equipment, limited scalability for large components.
Gradient Layer Deposition	Depositing thin films with varying compositions using vapor deposition methods.	Excellent control over film thickness and composition, ideal for optical and electronic applications.	Time-intensive, primarily limited to thin-film applications.

Comparative Analysis of Techniques

Each production method for FGMs has its unique strengths and weaknesses, making them suitable for different applications. While powder metallurgy and thermal spraying are cost-effective for large-scale production, additive manufacturing and laser-based techniques excel in producing complex geometries and highly customized components. The choice of technique depends on factors such as the desired gradient, application requirements, and production scale.

Future Trends in FGM Production

The future of FGM production lies in the integration of advanced technologies like artificial intelligence (AI) and machine learning (ML) for optimizing design and manufacturing processes. Nanotechnology is also expected to play a significant role, enabling the production of FGMs with enhanced properties and novel functionalities. Furthermore, hybrid manufacturing approaches combining multiple techniques may emerge to overcome the limitations of individual methods.

APPLICATION AREAS AND SPECIFIC SUBSECTIONS

Functionally graded materials (FGMs) are versatile and widely used across industries due to their ability to seamlessly combine material properties. In aerospace, they enhance thermal resistance and durability in coatings and turbine blades. Biomedical applications include implants and scaffolds that improve tissue compatibility and mechanical integration. Automotive uses focus on lightweight and durable components like brake discs and engine parts, boosting efficiency. FGMs also optimize thermal management and lifespan in solar panels, fuel cells, and nuclear shields for energy systems. In electronics, they ensure better thermal control and reliability in heat sinks and circuits. Marine applications protect underwater structures with corrosion-resistant coatings, while in construction, FGMs improve durability and load distribution in insulation and concrete. These diverse applications highlight FGMs' role in modern engineering solutions. Fig. 2 shows application areas in FGM operations.

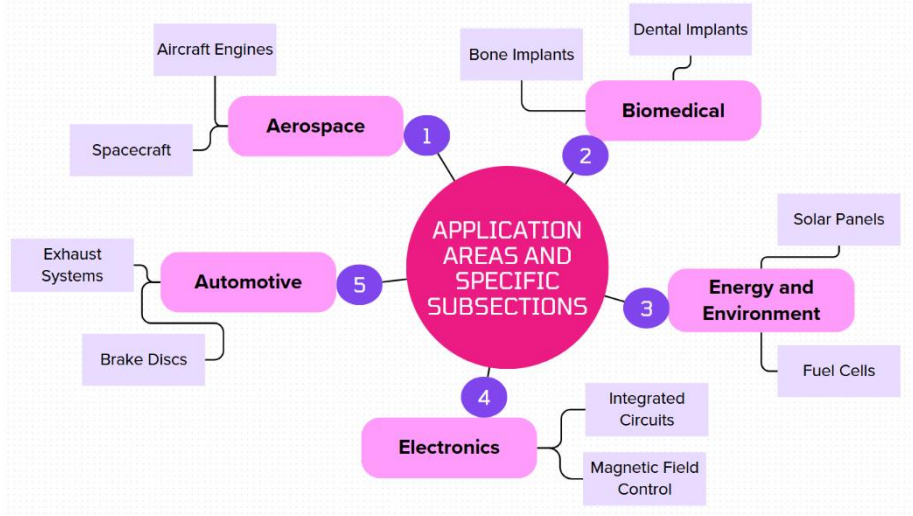

Figure 2: Application Areas and Specific Subsections

Aerospace

FGMs are critical in the aerospace industry for thermal barrier coatings and high-temperature-resistant engine components. These applications balance thermal expansion differences and minimize thermal stresses.

- Spacecraft: Ceramic-metal graded structures provide high-temperature resistance during atmospheric reentry.
- Aircraft Engines: High-temperature and mechanically loaded engine components benefit from FGMs.

Biomedical

FGMs provide excellent solutions for biocompatible implants that align with bone tissue properties. For instance, hydroxyapatite-titanium composites offer both mechanical strength and biological compatibility.

- Bone Implants: FGMs ensure mechanical compatibility with bone tissue, extending the lifespan of prosthetics.
- Dental Implants: They provide biocompatible and durable structures.

Energy and Environment

FGMs are used in nuclear reactor coatings, heat-dissipating surfaces in solar panels, and durable membranes in fuel cells.

- Solar Panels: Improved thermal conductivity optimizes energy efficiency.
- Fuel Cells: Graded structures enhance durability and performance.

Electronics

In electronics, FGMs are used for thermal management and magnetic field control applications.

- Integrated Circuits: Optimize heat distribution to improve the performance of electronic devices.
- Magnetic Field Control: Optimizes magnetic permeability for better sensor performance.

Automotive

In the automotive sector, FGMs offer durable and lightweight structures for brake discs, engine components, and exhaust systems.

- Brake Discs: Provide high-temperature resistance and wear durability.
- Exhaust Systems: Balance thermal expansion differences to ensure longevity.

Table 3: Application Areas and Key Uses of Functionally Graded Materials (FGMs)

Application Area	Specific Uses	Key Benefits
Aerospace	Thermal barrier coatings for spacecraft, turbine blades, and engine components.	Improved thermal stress resistance, enhanced durability, and reduced component failure risks.
Biomedical	Bone and dental implants, tissue engineering scaffolds.	Gradual property transitions improve biocompatibility and mechanical integration with human tissue.
Automotive	Brake discs, engine parts, and lightweight vehicle structures.	Enhanced wear resistance, reduced weight, and improved fuel efficiency.
Energy Systems	Solar panels, nuclear reactor shielding, and fuel cell components.	Better energy efficiency, higher thermal and radiation resistance, and increased operational lifespan.
Electronics	Heat sinks, integrated circuits, and protective coatings for sensors.	Effective thermal management, improved device reliability, and optimized electrical conductivity.
Marine	Corrosion-resistant coatings for ships and underwater structures.	Increased durability in saline environments and protection against mechanical and chemical erosion.
Construction	Graded concrete, advanced insulation materials, and structural components.	Better load distribution, enhanced thermal and acoustic insulation, and longer service life.

Future Perspectives

FGMs are considered the future of sustainable and high-performance materials. Particularly when integrated with nanomaterials, FGMs offer solutions for more complex applications. Additionally, design techniques supported by artificial intelligence and machine learning could revolutionize FGM production.

RESULTS

Functionally graded materials (FGMs) have emerged as a transformative innovation in material science and engineering, addressing the challenges associated with traditional homogeneous materials. By providing a seamless transition of properties, FGMs offer unique advantages such as enhanced thermal resistance, mechanical strength, and tailored functionality for specific applications. From their origins in the 1980s as solutions for aerospace thermal barriers, FGMs have evolved into a versatile class of materials with applications in diverse fields such as biomedical implants, automotive components, energy systems, and electronics.

The development of advanced production techniques—such as powder metallurgy, additive manufacturing, thermal spraying, and laser-based methods—has significantly expanded the scope and precision of FGMs. These methods enable the creation of complex geometries with customized property gradients, allowing FGMs to meet the demands of cutting-edge industries. Furthermore, the integration of nanotechnology and artificial intelligence is expected to further enhance their capabilities, paving the way for more efficient and sustainable designs.

Looking ahead, FGMs are poised to play a critical role in solving complex engineering challenges. Their ability to provide multifunctional and sustainable solutions aligns with the growing global emphasis on efficiency and environmental responsibility. As research and development continue to advance, FGMs will remain at the forefront of material innovation, driving progress in numerous high-performance applications.

REFERENCE

Abbas, M. R., B., U. M., Noor, A. M., Ahmad, N., & Rajoo, S. (2016). Microstructural evaluation of a slurry based Ni/YSZ thermal barrier coating for automotive turbocharger turbine application. *Materials and Design*, *109*, 47–56. https://doi.org/10.1016/j.matdes.2016.07.070

Canpolat, Ö., Çanakçı, A., & Erdemir, F. (2023). SS316L/Al2O3 functionally graded material for potential biomedical applications. *Materials Chemistry and Physics*, *293*. https://doi.org/10.1016/j.matchemphys.2022.126958

Carvalho, O., Buciumeanu, M., Madeira, S., Soares, D., Silva, F. S., & Miranda, G. (2015). Optimization of AlSi-CNTs functionally graded material composites for engine piston rings. *Materials and Design*, *80*, 163–173. https://doi.org/10.1016/j.matdes.2015.05.018

Kumar Bohidar, S., Sharma, R., & Mishra, R. (2014). Functionally Graded Materials: A Critical Review. *International Journal of Research (IJR)*, *1*(7).

Li, Y., Tang, F., Liu, W., & Liu, S. (2025). Mechanical properties of copper-nickel functionally graded materials based on molecular dynamics simulations: Material distribution and temperature effects. *Vacuum*, *233*. https://doi.org/10.1016/j.vacuum.2024.113889

Miteva, A., & Bouzekova-Penkova, A. (2021). Module for wireless communication in aerospace vehicles. *Aerospace Research in Bulgaria*, *33*, 195–209. https://doi.org/10.3897/arb.v33.e14

Müller, E., Drašar, Č., Schilz, J., & Kaysser, W. A. (2003). Functionally graded materials for sensor and energy applications. *Materials Science and Engineering: A*, *362*(1–2), 17–39. https://doi.org/10.1016/S0921-5093(03)00581-1

Schulz, U., Peters, M., Bach, F. W., & Tegeder, G. (2003). Graded coatings for thermal, wear and corrosion barriers. *Materials Science and Engineering: A*, *362*(1–2), 61–80. https://doi.org/10.1016/S0921-5093(03)00579-3

Yu, J., Wang, Z., Zhang, B., Zhang, X., & Li, M. (2022). Fabrication of the Fe/PZT Functionally Graded Material and its Application on the Thermal Match for Transducers. *Medziagotyra*, *28*(2), 178–183. https://doi.org/10.5755/j02.ms.27727

Waste Heat Recovery From A Pem Fuel Cell Using A Thermoelectric Module

Sinan ÇOBANER[1]
Hüseyin KAHRAMAN[2]

1- A.R. ; Sakarya University of Applied Sciences Faculty of Technology Mechanical Engineering. sinancobaner@subu.edu.tr ORCID No: 0009-0000-6821-4265
2- Associate Prof.; Sakarya University of Applied Sciences Faculty of Technology Mechanical Engineering. huseyink@subu.edu.tr ORCID No: 0000-0003-3322-9904

ABSTRACT

This section the energy conversion efficiencies and waste heat recovery potentials of Proton Exchange Membrane Fuel Cells (PEMFCs) and thermoelectric modules. PEM fuel cells stand out among clean energy solutions because of their efficiency in converting hydrogen energy into electrical energy and their environmentally friendly energy production. However, the wasted heat released from these systems represents a resource that should be utilized for energy recovery. Today, thermoelectric modules (TEMs) are employed in areas such as recovering low-temperature waste heat from PEM fuel cells, contributing to sustainable energy systems. Thermoelectric modules are innovative devices that convert temperature differences into electrical energy. Based on the Seebeck effect, these modules have significant potential for energy recovery from waste heat. Due to their compact design, lack of moving parts, and environmentally friendly nature, they are particularly used in applications aiming to enhance energy efficiency. However, the energy conversion efficiency of thermoelectric modules is generally low and depends on the properties of the thermoelectric materials used. The results reveal that the combined use of PEM fuel cells and thermoelectric modules has substantial potential for improving energy efficiency. However, to make these systems more widespread, the development of thermoelectric materials with higher Seebeck coefficients, improvements in heat management strategies, and reductions in production costs are necessary. The study highlights that technological advancements in this field can have a significant impact on sustainable energy transformation.

Keywords – PEM Fuel Cell, Thermoelectric, Waste Heat, Efficiency Improvement, Seebeck Effect.

INTRODUCTION

Energy has become an indispensable necessity in modern life. From lighting our homes to industrial production, from transportation to communication technologies, energy demand is steadily increasing across various sectors. However, this rising demand also brings along environmental and economic challenges. The intensive use of fossil fuels cause to rise greenhouse gas emissions, contributing to climate change, and causes the rapid depletion of limited natural resources (Kesercioglu et al., 2023). Therefore, it is of great importance to develop environmentally friendly and sustainable solutions in the energy sector. One way to reduce the environmental impacts of fossil fuels is to expand the use of renewable energy sources (Höök & Tang, 2013). Renewable sources such as wind, solar, hydroelectric, and geothermal energy stand out for their inexhaustible

potential and their ability to produce energy without harming the environment (Askew, 2003).

Technological advancements have also brought alternative energy sources and various techniques to utilize these sources. One such technique is the use of fuel cells (FC), which have rapidly gained popularity in recent years. FCs are electrochemical devices that directly convert chemical energy into electrical energy. Unlike conventional energy generation systems, they produce energy without requiring a combustion process. Fundamentally, FCs generate electricity, heat, and water by utilizing a fuel (typically hydrogen) and an oxidizer (usually oxygen). Thanks to these features, FCs offer advantages such as high efficiency and low environmental impact.

FCs consist of three basic components: a cathode, an anode, and an electrolyte. At the anode, the fuel is oxidized, while at the cathode, oxygen is reduced. During this process, electrons move through an external circuit, generating electricity. The electrolyte is responsible for ion conduction and prevents gas mixing between the anode and cathode. The most common types include:

- Polymer Electrolyte Membrane (PEM)
- Solid Oxide Fuel Cells (SOFC)
- Alkaline Fuel Cells (AFC)
- Phosphoric Acid Fuel Cells (PAFC)
- Molten Carbonate Fuel Cells (MCFC)

Each type has specific application areas and advantages. For instance, PEMFCs are widely used in vehicles due to their low operating temperatures and rapid start-up times, whereas SOFCs are preferred for stationary power generation because of their high-temperature tolerance and ability to utilize various fuel types (Akın et al., 2024).

The environmental impact of FCs is remarkably low. When hydrogen is used as a fuel, the only byproduct is water, completely eliminating greenhouse gas emissions. However, factors such as high production costs, challenges in hydrogen production and storage, and technological infrastructure requirements limit the widespread adoption of FCs. Various studies are being conducted to address these challenges. For example, the performance of FCs is being investigated by adding materials like graphene to bipolar plates, and alternative solutions are being explored (Akın et al., 2024).

If these challenges can be overcome, FCs could find broader applications in the energy sector as a sustainable alternative to fossil fuels.

PEM FUEL CELL

The most commonly used type of FCs is PEM FCs (Figure 1). PEMFCs are electrochemical devices that convert hydrogen energy into electrical energy. As an alternative to fossil fuels, this technology is among the energy sources of the future due to its low emission levels, high energy conversion efficiency, and wide range of applications.

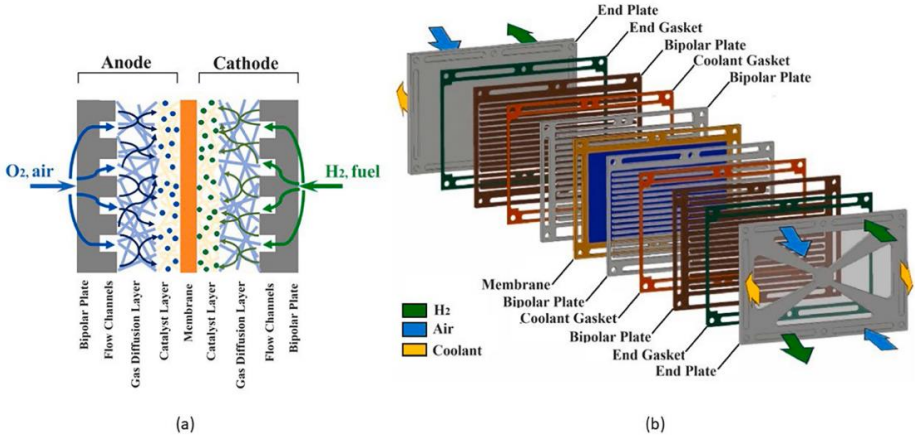

Figure 1: PEM fuel cell (Zhou & Chen, 2023).

PEMFCs consist of a series of key components that support their functionality:

- **Electrolyte**: A polymer membrane, commonly made of materials like nafion, is used to ensure proton conductivity while preventing electron transfer. The mechanical durability and ion conductivity of the membrane are of critical importance.
- **Electrodes**: At the anode and cathode, platinum-based catalysts facilitate electrochemical reactions and transfer reaction products. At the anode, hydrogen is split into protons and electrons, while oxygen is reduced at the cathode (Akın et al., 2023).
- **Bipolar Plates**: These plates collect electric current, facilitate gas distribution, and manage water and heat. Materials such as graphite or metals are commonly used.

According to Gibbs free energy calculations, PEMFCs can theoretically generate a maximum voltage of 1.23 V. However, in real-world applications, this value is lower due to activation losses, resistance losses, and mass transfer losses.

The electrical work equation is:

$$W_{current} = EQ \quad (1)$$

If it is assumed that the charge is carried by electrons, the equation becomes:

$$Q=nf \quad (2)$$

Here, n represents the number of moles of electrons transferred, and f denotes the Faraday constant. When Equations 1 and 2 are combined:

$$\Delta g=-nFE \quad (3)$$

the equation is obtained. In an $H_2 - O_2$ FC, the reaction is:

$$H_2 + 12O_2 /\leftrightarrow H_2O \quad (4)$$

This reaction has a Gibbs free energy of -237 kJ/kmol under normal conditions, where liquid water is produced. Under these conditions, the reversible voltage generated in an $H_2 - O_2$ FC is:

$$E^0 = -\frac{\Delta g^0_{reaction}}{nF} = -\frac{-237000}{(2\ mole).96400} = +1.23\ V \quad (5)$$

The voltage value is found to be 1.23 V. Here, E^0 represents the reversible voltage, and $\Delta g^0_{reaction}$ denotes the free energy change for the reaction. According to thermodynamic expressions, under normal conditions, an $H_2 - O_2$ FC cannot exceed the 1.23 V value.

PEMFCs are notable for their advantages, such as low operating temperature, quiet operation, low maintenance costs due to the lack of moving parts, and higher efficiency compared to internal combustion engines. However, the use of expensive catalyst materials like platinum and issues related to membrane humidification and water management are among the disadvantages (Kahraman & Akın, 2024). These technologies are used in a wide range of applications, including electric cars, buses, trucks, drones, unmanned aerial vehicles, submarines, power plants, and buildings (Tüylü et al., 2024). In ongoing studies, the focus is on cost reduction and performance improvement, with priority given to the use of alternative metals instead of platinum, the development of membrane materials, and improvements in water management. With advancements in material science and manufacturing techniques, PEMFCs are expected to find a broader range of applications in clean energy conversion and sustainability.

THERMOELECTRIC MODULE

With the development of technology, there has been a significant increase in energy usage. This rapid rise in energy consumption also significantly increases the amount of waste heat in systems. The inability to control waste heat not only reduces energy efficiency but also becomes harmful to the environment. Therefore, the recovery of waste heat and the design of more efficient energy systems have become crucial for a

sustainable future. Different methods are used for the recycling of waste heat. Thermoelectric modules are one of these methods.

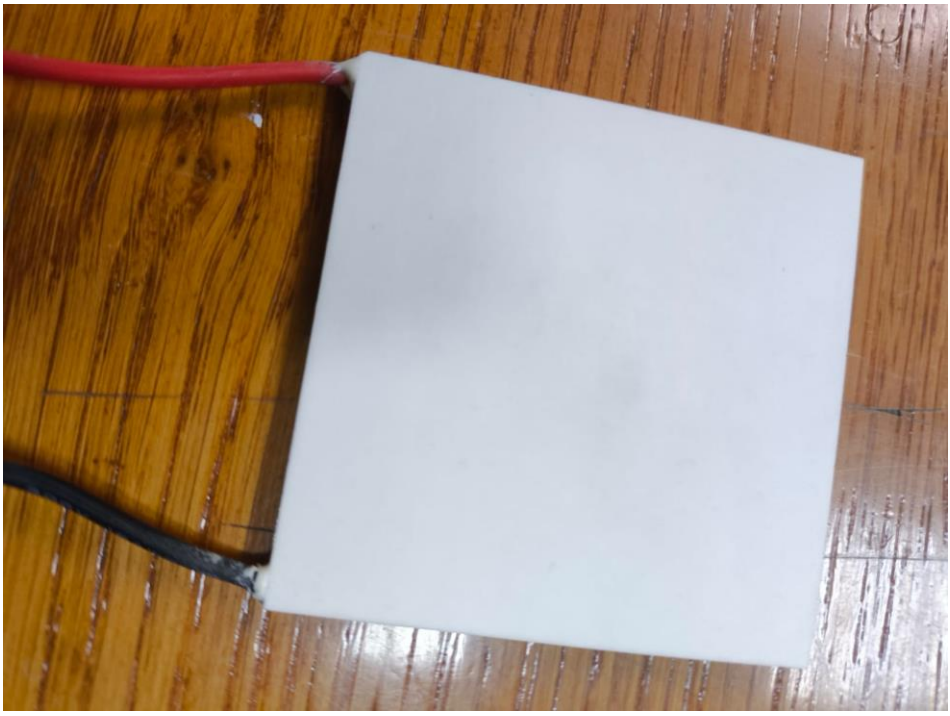

Figure 2: Thermoelectric module.

In 1821, it was discovered that when two different metals come into contact and a temperature difference (ΔT) is created, this leads to the generation of an electric current and the creation of an electromotive force. This phenomenon is known as the Seebeck effect, named after Thomas Seebeck, who made the discovery (Çobaner, Çerlek, et al., 2024). Furthermore, the temperature difference (ΔT) between metals can be controlled by increasing the voltage difference (ΔV) in the circuit. Thomas Seebeck developed the mathematical expression for this relationship and defined a coefficient based on the ratio of temperature difference to voltage difference. This value, known as the Seebeck coefficient (α), depends on the type of material used and varies for different materials. In metal materials, the Seebeck coefficient is generally low and very close to 0 mV/K. However, semiconductor materials have higher Seebeck coefficient values (e.g., around 200 mV/K) and are more suitable for thermoelectric applications. The Seebeck coefficient is mathematically expressed as the ratio of voltage difference (ΔV) to temperature difference (ΔT) in Equation 6.

$$\alpha = \frac{\Delta V}{\Delta T} \tag{6}$$

The heat transfer rate of the hot surface is expressed by Equation 7, while the heat transfer rate of the cold surface is shown as in Equation 8.

$$q_h = \alpha I T_h + K_{TEG}(T_h - T_c) - 0.5 R_{TEG} I^2 \tag{7}$$

$$q_c = \alpha I T_c + K_{TEG}(T_h - T_c) + 0.5 R_{TEG} I^2 \tag{8}$$

Equation 9 presents the TEG power equation.

$$P_{TEG} = q_h - q_c = \alpha(T_h - T_c) I - R_{TEG} I^2 \tag{9}$$

The TEG energy conversion efficiency is shown in Equation 10.

$$\eta_c = \frac{P_{TEG}}{q_h} \tag{10}$$

In this context, when a temperature difference occurs between different metals or semiconductor materials in an electrical circuit, a thermoelectric effect occurs. For example, the excess electrons in N-type semiconductors move to the holes in the P-type semiconductor, generating an electric current (Liu et al., 2022). This electron movement occurs due to the temperature gradient, and this energy conversion mechanism can be used for electricity generation. Additionally, this method operates reversibly, and when current is applied to semiconductor materials, a temperature difference occurs between the two surfaces. This effect is called the Peltier effect.

Thermoelectric modules stand out in various applications due to their advantages and disadvantages. Among the advantages are their compact structures without moving parts, which prevent wear and tear problems, their long lifespan, and low maintenance requirements (Çobaner, Kesercioglu, et al., 2024). The absence of mechanical components offers a silent and vibration-free operation, providing a significant advantage, particularly in medical devices, laboratory equipment, and military applications (Çobaner & Uysal, 2024a). Thermoelectric modules, which can respond quickly to temperature changes and precisely control small energy fluctuations, are ideal for scientific experiments and electronic device cooling (Çobaner & Uysal, 2024b). Their use of environmentally friendly materials that do not involve harmful refrigerant gases is a significant reason for their preference in terms of environmental sustainability. Their modular designs, which are small and lightweight, allow for easy integration into narrow spaces, offering solutions for various needs (Çobaner & Uysal, 2024c). Additionally, due to their bidirectional operation capability, they can provide both cooling and heating, making them a versatile technology. However, the low energy conversion efficiency of thermoelectric modules is

a significant disadvantage compared to traditional compressor-based systems. This issue increases energy consumption in applications requiring high energy and limits efficiency. When large volumes need to be cooled, limited cooling capacities, the need for numerous modules, and increased costs can result. The high initial costs and the economic competitiveness of the technology are also major concerns. The performance of the thermoelectric materials currently in use (e.g., bismuth telluride) is a limiting factor for the development of this technology. Moreover, without effective heat distribution, performance may decrease, or the modules may be damaged. Therefore, the development of thermoelectric modules and overcoming these limitations remain important research topics in the field of technology.

Thermoelectric modules, as an innovative technology combining energy efficiency and sustainability goals, offer revolutionary applications in many industries. Working on the principle of converting temperature differences into electrical energy, these modules successfully perform critical functions such as waste heat recovery, meeting the energy needs of portable devices, and precise temperature control. In the automotive industry, thermoelectric modules convert the waste heat of internal combustion engines into energy, reducing fuel consumption, while also providing energy savings and an environmentally friendly alternative with vehicle climate control. In space and military technologies, they provide reliable and maintenance-free energy solutions, while in the medical sector, they ensure reliability and energy savings by precisely regulating the temperature control of medical devices.

With innovative applications such as generating energy from body heat in wearable technologies, these modules improve user experience and contribute to the efficient use of renewable energy sources. In solar energy applications, thermoelectric modules convert excess heat produced by panels into electrical energy, and in geothermal energy, they convert the heat from underground hot water sources into electricity, supporting environmental sustainability goals. In telecommunications infrastructure, thermoelectric modules reduce dependence on electrical infrastructure by providing energy production and equipment cooling in remote areas, and they offer remote power supply and precision in thermal imaging devices in security systems. In maritime applications, this technology increases efficiency in long journeys by converting waste heat from engines into energy, playing a critical role in providing energy for underwater research. In household devices, thermoelectric modules provide portability and energy savings while offering practical solutions for creating thermal power sources in rural areas. Additionally, they increase efficiency by converting the waste heat of PEMFCs into electrical energy. With their versatile applications,

thermoelectric modules stand out as an innovative technology for energy savings, reliability, and environmentally friendly solutions.

LITERATURE REWIEV

Studies are being conducted today on the recovery of waste heat from PEMFCs using thermoelectric modules (TEM).

In the study by (Hasani & Rahbar, 2015), the recovery of waste heat from a Proton Exchange Membrane Fuel Cell (PEMFC) system using thermoelectric coolers (TECs) was experimentally investigated. The research aimed to convert the waste heat from a 5 kW PEMFC into electrical energy through a heat exchanger and thermoelectric modules. The thermoelectric modules generated power by utilizing the temperature difference created by the temperature of the water exiting the FC. The results of the study showed that the system recovered approximately 10% of the waste heat from the FC and generated 800 W of power. The highest thermoelectric conversion efficiency was measured at 0.35% when the outlet water temperature of the FC reached 68°C. The study revealed the potential advantages of using a thermoelectric heat recovery system instead of traditional radiator and fan-based cooling systems. However, the overall system efficiency decreased as the outlet water temperature increased, which was associated with heat losses and inadequate insulation. It was suggested that optimizing insulation and improving the heat exchanger design could increase system efficiency. For future research, it was recommended to compare the performance of thermoelectric generators (TEGs) and thermoelectric coolers (TECs), as well as evaluate modules from different manufacturers. This experimental study makes an important contribution to the recovery of low-temperature waste heat from PEM FCs and evaluating the energy conversion potential of thermoelectric modules.

A method for recovering energy from waste heat temperatures of PEM FCs, utilizing an integrated system of thermoelectric generator (TEG), heat sink, and heat pipe, was proposed by (Saufi Sulaiman et al., 2019). The aim of the study was to experimentally examine this system, analyze its key features, and develop a steady-state model for a mini hydrogen FC vehicle. The research investigated the effects of the TEG on heat flow direction and its impact on system performance. At a waste heat temperature of 37°C, voltage of 25.7 mV and a power output of 218 mW. The results showed that the combination of TEG, heat pipe, and heat sink could effectively convert low-temperature waste heat from a PEMFC into energy in a vehicle. The successful characterization of the system and validation of the model provide

the opportunity to advance towards higher performance goals, making a significant contribution to the sustainability of PEMFC systems.

In the study by (Lan et al., 2023), an innovative system design that combines power generation and hydrogen production for waste heat recovery and system performance improvement is presented. The system integrates PEMFC, thermoelectric generator (TEG) modules, and a water electrolysis cell. The study thoroughly examines the effects of cooling method, electrical configuration, and PEMFC outlet temperature on the system. The results show that the water cooling method increased the hydrogen production rate by 31.4–44.8% compared to the air cooling method. While the electrical configuration did not significantly affect system performance, an increase in PEMFC outlet temperature positively influenced hydrogen production, while an increase in the number of TEG modules negatively affected it. Six different objective functions were evaluated for optimal system design. According to the optimization results, the ideal dimensions of the thermoelectric legs are 1.01–1.3 mm in height, 2.52–3.28 mm^2 in area, and 3.08–4.26 mm^3 in volume, within a 50–100°C outlet temperature range. With this design, net power output, system efficiency, and hydrogen production increased by 31.8–39.4%, 3.7–31.5%, and 22.1–34.5%, respectively, compared to commercial modules. Additionally, the payback period was 15.0–34.3% shorter, and the year to reach zero carbon emissions was 17.8–36.8% earlier. These results demonstrate that the proposed integrated system effectively utilizes the waste heat of PEMFCs for energy and hydrogen production, contributing to sustainability goals.

(Tao et al., 2024) Integrating different energy conversion systems to create more sustainable energy systems is an effective method that could provide a solution to the energy consumption crisis. In this study, an Organic Rankine Cycle (ORC), Kalina cycle, proton exchange membrane (PEM) electrolyzer, FC, and thermoelectric generator (TEG) were integrated into sub-systems. Two different system configurations were analyzed. In the enhanced system, FCs and TEG were added to improve overall performance. According to the technical and economic analysis, the proposed system's energy efficiency was calculated to be 16.77%, and its exergy efficiency was 61.69%. The electrolyzer unit produced 0.0001632 moles of hydrogen per hour. Compared to the basic system, the proposed system produced 155.33 kW of electricity, while the basic system produced 146.2 kW. Exergy analysis revealed that the condenser was the component with the highest exergy destruction rate at 20.13 kW. Parametric analysis of different system parameters showed that energy efficiency and total exergy destruction rate responded differently to the defined electrical cost ratio, indicating the necessity for multi-objective optimization. In the optimal case, the system's

exergy efficiency reached 62%, and the electricity cost was reduced to 10.72 $/hour.

CASE STUDY

If we take PbTe thermo element as an example

Table 1: PbTe properties (Kuehling et al., 2010)

Temperature (°C)	Seebeck Coefficient ($\mu V/K$)	Electrical Conductivity(S/cm)	Thermal Conductivity (W/mK)
100	-90	2700	2,7

Here, we can find the resistance value using the material's electrical conductivity, as shown in equation 11.

$$\sigma = \frac{1}{\rho} \tag{11}$$

In this equation, σ is the material's conductivity, and ρ is the material's resistivity. Using the resistivity value, we can find the material's resistance.

$$R = \rho . \frac{L}{A} \tag{12}$$

We can find it using equation 12. In the TEC1-19903 model we have taken as an example, there are 199 thermoelements, and each thermoelement has an area of 8 mm² and a length of 3.5 mm. When we substitute the values into equation 12,

$$R = 1{,}62 . 10^{-5} \Omega$$

We find the resistance of an element.

As a result of the reactions occurring within the PEM, the internal temperature reaches 80°C. In this case, the heat transfer rate from inside to outside changes depending on the thermal conductivity of the materials used, and the outer surface temperature varies. For example, to calculate the voltage difference that will occur across the thermoelement, we assume the outer surface temperature is 70°C. To do this, we need to know how much heat energy is being transferred from the PEMFC surface with an area of 8 mm². In this section, to calculate how much heat is being transferred from the PEMFC surface to the surroundings at room temperature, we can use the general heat transfer equation shown in equation 13.

$$\dot{Q} = h . A . (T_s - T_a) \tag{13}$$

Here, $\dot{Q}$ represents the heat transfer rate, A is the surface area where heat transfer occurs, T_s is the surface temperature, and T_a is the ambient

temperature. Using this equation, we can calculate the amount of heat energy given off by a PEMFC with a surface temperature of 70°C when the ambient temperature is 23°C.

$$\dot{Q} = 0{,}00188\ W$$

We can find it as $\dot{Q}$. Here, we can assume the value of h as 5 W/m²·K. Additionally, since the heat radiated by radiation will be very small, it can be neglected. By using these values, we can find the temperature difference between the two surfaces of the thermoelement using the general heat conduction equation in Equation 14.

$$\dot{Q} = k.A.\frac{(T_1 - T_2)}{l.} \quad (14)$$

In the equation, k represents the thermal conductivity, which is 2.7 W/m·K for this material. When the values are substituted,

$T_2 = 69{,}7°C$

From here, the temperature difference $\Delta T = 0{,}3°C$ is found. If we substitute this and the Seebeck coefficient into equation 6

$$-90\mu V = \frac{\Delta V}{0{,}3}$$

As a result of this equation, the voltage $\Delta V = -27\mu V$ is found. Using this value, from Ohm's Law, a current of $I = 1{,}66\ A$ is observed. Since the thermoelements are connected in series, the total voltage of the thermoelectric module is found to be 5.373 mV. This voltage difference is obtained from an area of 40 mm×40 mm. Considering a FC with an external surface size of 120 mm×120 mm 9 thermoelectric modules can be mounted on this area. When the same number of modules is mounted on the other side, a total of 18 thermoelectric modules are used, resulting in a voltage difference of $V_{total} = 18.(5{,}373) = 96{,}714mV$. When we examine the contribution to the system efficiency, $\frac{0{,}096714}{1{,}23} = 0{,}0786$ is found. There is an increase of 7.86% in the system efficiency. Based on this, the theoretical efficiency is increased from 83% to 90.86%.

In the calculations made in this example, it is assumed that the heat is uniformly distributed and the heat flows in one direction. Additionally, heat losses are neglected.

CONCLUSION

This study investigates the energy conversion efficiencies of PEMFCs and thermoelectric modules, as well as their potential for waste heat recovery. The results obtained show that PEM fuel cells offer significant advantages in terms of low-temperature operation, high efficiency, and environmental sustainability. However, it has been determined that thermoelectric modules can effectively convert waste heat from PEMFCs into energy, though they have certain limitations in terms of energy conversion efficiency.

Based on the studies conducted, it has been shown that up to 10% of the low-temperature waste heat from PEMFCs can be recovered through thermoelectric modules. However, the system efficiency is directly related to the temperature difference and the performance of thermoelectric materials. Additionally, materials with a high Seebeck coefficient play a critical role in enhancing the energy conversion efficiency of thermoelectric modules. In example calculations, materials with high thermal conductivity were also found to optimize the temperature difference.

Energy Efficiency and Optimization: The integration of PEMFCs and thermoelectric modules shows promise for energy recovery. However, improvements in areas such as heat transfer, water management, and thermoelectric module design could further enhance system performance.

In conclusion, PEMFCs and thermoelectric modules offer significant potential to meet future energy needs and provide a sustainable energy conversion system. Future studies highlight that these systems can be strengthened through the development of material technologies and innovative designs, thus improving their cost-effectiveness and efficiency.

REFERENCES

Akın, Y., Kahraman, H., & Özsert, İ. (2023). Proton Değişim Membranlı (PEM) Yakıt Hücrelerinde Bipolar Plakaların Malzeme Seçimi. *MÜHENDİSLİKTE Güncel Yaklaşimlar*, *December*. https://doi.org/10.59287/mgy.1009

Akın, Y., Kahraman, H., & Özsert, İ. (2024). Mechanical Properties of Bipolar Plates for PEM Fuel Cells : A Focus on Flexural Strength and Surface Hardness. *2 Nd International Conference on Trends in Advanced*, *November*.

Akın, Y., Tüylü, A., & Çobaner, S. (2024). *Graphene Technology : Production , Sustainability , and Industrial Applications Graphene Technology : Production , Sustainability , and Industrial Applications*. *November*.

Askew, M. F. (2003). Progress in renewable energy. *International Sugar Journal*, *105*(1259), 535–539.

Çobaner, S., Çerlek, Ö., & Han, K. (2024). Termoelektrik Modüller ve Kullanım Alanları. In *Mühendislikte Yeni Trendler ve Sınırlar* (pp. 0–3).

Çobaner, S., Kesercioglu, M. A., & Aktaş, N. F. (2024). Cooler Effect On Performance Of Pertier Module. *5th International Conference on Engineering and Applied Natural Sciences*.

Çobaner, S., & Uysal, F. (2024a). FARKLI SICAKLIKTA YÜZEYLERE UYGULANAN PELTİER SOĞUTUCUNUN PERFORMANS DEĞERLENDİRMESİ. *3rd International Conference on Recent Academic Studies*.

Çobaner, S., & Uysal, F. (2024b). PELTİER MODÜLÜN SABİT GÜÇ VERİLEN MİKRO ISITICI YÜZEYİNDE SOĞUTMA PERFORMANSI ANALİZİ. *3rd International Conference on Recent Academic Studies*.

Çobaner, S., & Uysal, F. (2024c). SOĞUTUCU EKİPMANIN PELTİER MODÜL PERFORMANSINA ETKİSİ. *3rd International Conference on Recent Academic Studies*.

Hasani, M., & Rahbar, N. (2015). Application of thermoelectric cooler as a power generator in waste heat recovery from a PEM fuel cell - An experimental study. *International Journal of Hydrogen Energy*, *40*(43), 15040–15051. https://doi.org/10.1016/j.ijhydene.2015.09.023

Höök, M., & Tang, X. (2013). Depletion of fossil fuels and anthropogenic climate change-A review. *Energy Policy*, *52*, 797–809. https://doi.org/10.1016/j.enpol.2012.10.046

Kahraman, H., & Akın, Y. (2024). Recent studies on proton exchange membrane fuel cell components, review of the literature. *Energy Conversion and Management*, *304*(January), 118244. https://doi.org/10.1016/j.enconman.2024.118244

Kesercioglu, M. A., Tüylü, A., & Çerlek, Ö. (2023). The Factors Affecting Energy Efficiency In Air- Cooled Condensers. In *Special Issues in Material and Energy Sciences* (Issue December 2023, p. 39).

Kuehling, K., Application, F., Data, P., & Frank, H. (2010). *(12) Patent Application Publication (10) Pub. No.: US 2010/0282285 A1*.

Lan, Y., Lu, J., Mu, L., Wang, S., & Zhai, H. (2023). Waste heat recovery from exhausted gas of a proton exchange membrane fuel cell to produce hydrogen using thermoelectric generator. *Applied Energy*, *334*, 120687. https://doi.org/10.1016/J.APENERGY.2023.120687

Liu, Z., Hu, G., Wang, J., Suo, Y., Ye, Y., Li, G., & Zhang, Z. (2022). Design and optimization of a cubic two-stage thermoelectric cooler for thermal performance enhancement. *Energy Conversion and Management*, *271*(September), 116259. https://doi.org/10.1016/j.enconman.2022.116259

Saufi Sulaiman, M., Singh, B., & Mohamed, W. A. N. W. (2019). Experimental and theoretical study of thermoelectric generator waste heat recovery model for an ultra-low temperature PEM fuel cell powered vehicle. *Energy*, *179*, 628–646. https://doi.org/10.1016/j.energy.2019.05.022

Shi, L. min, Alghamdi, A., Ponnore, J. J., Alqahtani, S., Alshehery, S., & Anqi, A. E. (2023). Thermo-economic and performance analysis of a novel tubular hybrid high-temperature proton exchange membrane fuel cell and thermoelectric generator. *Applied Thermal Engineering*, *235*, 121363. https://doi.org/10.1016/J.APPLTHERMALENG.2023.121363

Tao, H., Al Mamun, K., Ali, A., Solomin, E., Zhou, J., & Sinaga, N. (2024). Performance enhancement of integrated energy system using a PEM fuel cell and thermoelectric generator. *International Journal of Hydrogen Energy*, *51*, 1280–1292. https://doi.org/10.1016/J.IJHYDENE.2023.03.442

Tüylü, A., Akın, Y., & Kesercioglu, M. A. (2024). *Bataryalı ve Yakıt Hücreli Elektrikli Araç Teknolojileri Bataryalı ve Yakıt Hücreli Elektrikli Araç Teknolojileri*. *October*.

Wuebbles, D. J., & Jain, A. K. (2001). Concerns about climate change and the role of fossil fuel use. *Fuel Processing Technology*, *71*(1–3), 99–119. https://doi.org/10.1016/S0378-3820(01)00139-4

Zhou, Y., & Chen, B. (2023). Investigation of optimization and evaluation criteria for flow field in proton exchange membrane fuel cell: A critical review. *Renewable and Sustainable Energy Reviews*, *185*(July), 113584. https://doi.org/10.1016/j.rser.2023.113584

Energy Production by Electrogenic Bacteria

Filiz BORAN[1]
Teoman KARADAĞ[2]

1- Assoc. Prof. Dr.; İnönü Üniversitesi Fen Edebiyat Fakültesi Biyoloji Bölümü. filiz.kuru@inonu.edu.tr ORCID No: 0000-0002-8801-7987
2- Assoc. Prof. Dr.; İnönü Üniversitesi Mühendislik Fakültesi Elektrik Elektronik Mühendisliği Bölümü. teoman.karadag@inonu.edu.tr ORCID No: 0000-0002-7682-7771

ABSTRACT

Internal combustion engine vehicles (ICE) have played a fundamental role in transportation since the industrial revolution. The principle of operation of these vehicles is based on the conversion of heat energy generated by burning fossil fuels in the engine into mechanical energy. This mechanical energy is transmitted to the wheels, allowing the vehicle to move. Carbon-based fuels such as gasoline, diesel, LPG and natural gas form the core of this process. However, the greenhouse gases released into the atmosphere as a result of the use of these fuels are a major source of environmental impacts and are recognized as one of the main causes of global warming.

In recent years, change has become imperative in the transportation sector due to the environmental impacts of fossil fuels and their limited resource. The goal of reducing the carbon footprint has encouraged the development of electric and hydrogen-powered vehicles. Electric vehicles (EVs) offer an environmentally friendly alternative by using electrical energy instead of fossil fuels. However, generating electricity from renewable sources is critical to minimizing the carbon footprint of EVs.

Hydrogen energy is another technology that is expected to play an important role in future transportation systems. Hydrogen is an extremely clean source of energy as it produces only water vapor as a result of the combustion process. Hydrogen-powered fuel cell technologies can be combined with electric motors to completely eliminate dependence on fossil fuels. However, the efficient and sustainable production of hydrogen is a critical prerequisite for the widespread deployment of this technology.

Traditional energy production methods often create environmental impacts and rely on limited resources. Therefore, biotechnological approaches to energy production using bacteria and other microorganisms for electricity and hydrogen production have emerged as a clean and sustainable alternative. Bacteria can break down organic waste to produce clean energy sources such as electricity and hydrogen. Microbial fuel cells (MYPs) are a breakthrough technology in this field. MYPs enable bacteria to oxidize organic matter to produce electrons, which are converted into energy through an electrical circuit.

Furthermore, using photobioreactors, it has become possible to produce hydrogen with the help of microalgae and cyanobacteria. These microorganisms can produce hydrogen gas by decomposing water molecules through photosynthesis. Supporting this process with renewable energy sources could completely eliminate carbon emissions.

Electric and hydrogen vehicles offer significant potential to reduce dependence on fossil fuels. However, various technical, economic and infrastructural challenges must be overcome for these technologies to become widespread. In particular, advances in energy storage technologies could

eliminate the range problem of electric vehicles. In hydrogen production, it is important to reduce costs and improve infrastructure.
Biotechnological approaches can offer revolutionary solutions in both electricity and hydrogen energy production. The industrialization and diffusion of these methods can play a critical role not only in the transportation sector, but also in meeting overall energy needs. Ultimately, this transition away from fossil fuels and towards sustainable energy sources will bring long-term benefits, both environmentally and economically.

Keywords – Fuels, Electric, Hydrogen, Bacteria, Biotechnology.

FUEL

The fuels used in internal combustion engine (ICE) vehicles are substances that contain chemical energy. These fuels combine with oxygen during the combustion process to produce heat and gaseous products. The most commonly used fuels in ICEs are:

• **Gasoline:** A light and moderately compressible fuel. It is evaluated by octane number, and gasolines with higher octane numbers can withstand higher compression ratios.

• **Diesel:** A heavy and highly compressible fuel. It is evaluated by cetane number, and diesel engines with higher cetane numbers start easier and produce less noise.

• **LPG:** Also known as liquefied petroleum gas. It is a gas mixture obtained during the processing of petroleum in a refinery. It is considered a cleaner fuel than gasoline and diesel.

• **Natural gas:** A gas rich in methane that comes out of the ground. It is considered a clean and environmentally friendly fuel.

Operating Principle:

The operating principle of ICEs is predicated on a four-stroke cycle, which is outlined below.

1. Intake: As the piston moves downwards, the intake valve opens and air enters the cylinder.

2. Compression: The intake valve closes and the piston moves upwards, compressing the air.

3. Combustion: Fuel is sprayed into the compressed air with a spark plug or injector and burned with a spark. The high pressure created by this combustion process subsequently drives the piston in the opposite direction.

4. Exhaust: As the piston moves in the upward direction, the exhaust valve opens, allowing the combustion gases to be expelled from the cylinder.

This four-stroke cycle then repeats continuously, thereby maintaining the engine's operational status.

Waste:

In the process of combustion, internal combustion engines (ICEs) generate a variety of byproducts. These include:

Firstly, exhaust gases are produced. These gases include carbon monoxide, carbon dioxide, nitrogen oxides, hydrocarbons, and particulates, which are harmful to human health.

Additionally, noise emissions are a consequence of the ICEs' operation. Mechanical sounds are produced during engine operation.

Additionally, heat is generated during engine operation and radiated into the environment.

Conclusion:

Intelligent Carriers of the Future (ICEs) are a mode of transportation with many advantages. They are relatively inexpensive, powerful, and simple to operate. However, it is imperative to acknowledge that ICEs are not devoid of drawbacks. These include the dependence on fossil fuels, air pollution, noise pollution, and heat pollution.

The impact of internal combustion engine vehicles (ICE) on the greenhouse effect and environmental pollution is a subject of significant concern. These vehicles operate on various fossil fuels, including gasoline, diesel, LPG, and natural gas. The exhaust emissions from these vehicles constitute a significant source of greenhouse gas emissions and air pollution. These emissions have been linked to adverse effects on global warming, climate change, and human health.

Greenhouse Effect:

The greenhouse effect is the phenomenon of trapping the sun's rays by greenhouse gases present in the atmosphere, leading to an increase in the Earth's temperature. The principal greenhouse gases include carbon dioxide (CO2), methane (CH4), nitrous oxide (N2O), and water vapor (H2O). The exhaust emissions of internal combustion engines (ICEs) contribute to the release of greenhouse gases such as carbon dioxide (CO2) and methane (CH4) into the atmosphere. This phenomenon contributes to global warming and climate change.

Global Warming and Climate Change:

Global warming is defined as the increase in the average temperature of the Earth. Climate change is defined as the alterations occurring within the Earth's climate system due to the impact of global warming. The consequences of global warming and climate change are manifold, including, but not limited to:

- Sea level rise
- An increase in the frequency and severity of extreme weather events

- An increase in natural disasters such as droughts and floods
- Melting glaciers
- A decline in biodiversity
- Risks to agricultural production and food safety
- Problems in human health

Air Pollution:

Air pollution is caused by the release of harmful substances into the atmosphere. A significant contributor to this phenomenon is the emission of exhaust from internal combustion engines (ICEs). The consequences of air pollution are manifold and include, but are not limited to:

- Respiratory diseases
- Cardiovascular diseases
- Cancer
- Vision and skin problems
- Damage to plants and animals
- Acid rain
- Reduced visibility

A discussion of strategies for mitigating the greenhouse effect and environmental pollution from internal combustion engine vehicles is warranted.

- **Transition to electric and hybrid vehicles:** Electric and hybrid vehicles produce less GHG and air pollutant emissions than ICEs.
- **Expansion of public transportation:** The use of public transportation contributes to a reduction in the use of private vehicles and therefore to lower emissions.
- **Encourage cycling and pedestrian use:** Cycling and pedestrian use is both a healthy lifestyle and an environmentally friendly mode of transportation.
- **Improving fuel efficiency:** The use of vehicles that consume less fuel contributes to lower emissions.
- **Tightening emission standards:** Stricter emission standards encourage vehicle manufacturers to produce cleaner vehicles.
- **Increasing green spaces:** Green spaces help reduce air pollution by absorbing greenhouse gases from the atmosphere.

Internal combustion engine vehicles have a significant impact on the greenhouse effect and environmental pollution. Various measures need to be taken to reduce the negative impacts of the use of these vehicles. These measures can be taken in many areas such as switching to electric and hybrid vehicles, expanding public transportation, encouraging bicycle and pedestrian use, tightening emission standards and increasing green areas.

Electric Vehicles and Environmental Impacts

Electric vehicles can play an important role in combating climate change and global warming. However, the environmental impact of these vehicles is a complex issue and many factors need to be considered.

Environmental benefits of electric vehicles:

- **Zero tailpipe emissions:** Electric vehicles do not release any harmful gases or greenhouse gases from tailpipes. This helps to significantly reduce air pollution and greenhouse gas emissions.
- **Higher energy efficiency:** Electric vehicles are much more efficient than gasoline or diesel vehicles. This means they can cover more distance using the same amount of energy.
- **Less noise pollution:** Electric vehicles are much quieter than gasoline or diesel vehicles. This can help to significantly reduce noise pollution in cities.

Potential environmental damage from electric vehicles:

The generation of electricity is accompanied by the emission of pollutants into the atmosphere. The electricity utilized for the operation of electric vehicles is often derived from fossil fuels. This process has the potential to contribute to greenhouse gas emissions and air pollution.

Additionally, the manufacturing and disposal of batteries for electric vehicles present environmental concerns. The production and disposal of electric vehicle batteries can harm the environment. Batteries contain rare earth elements such as lithium and cobalt, and their extraction can cause environmental problems.

Additionally, the increased energy demand associated with electric vehicle adoption can contribute to a rise in overall energy consumption, which may further exacerbate environmental concerns. The proliferation of electric vehicles (EVs) could lead to increased demand for electricity. This increased demand could potentially put a strain on existing electricity grids and necessitate the construction of new power plants.

The following are salient points regarding the environmental impact of electric vehicles:

The environmental impact of electric vehicles is contingent upon the carbon intensity of the electricity grid utilized. In electricity grids that utilize renewable energy sources, the environmental impact of electric vehicles is notably diminished.

Furthermore, the emissions resulting from the production of the batteries utilized in electric vehicles are offset over the duration of the vehicle's lifespan. The longevity of electric vehicles, which surpasses that of

gasoline or diesel vehicles, contributes to a reduction in the environmental impact associated with battery production.

The increased adoption of electric vehicles can potentially stimulate the modernization of electricity grids and the utilization of additional renewable energy sources.

Consequently, electric vehicles emerge as a more environmentally sustainable option when compared to gasoline or diesel vehicles. Nevertheless, in order to minimize the environmental impact of EVs, it is imperative to decarbonize electricity grids and enhance battery production processes.

Decarbonizing Electricity Grids

Decarbonizing electricity grids is critical to tackling climate change and global warming. This can be done by shifting electricity generation to sources that do not produce greenhouse gas emissions and by making the grid more efficient and resilient.

The following methods can be used to decarbonize electricity grids:

- **Investing in renewable energy sources:** Renewable energy sources, including solar, wind, hydropower, and geothermal energy, have emerged as pivotal instruments in the effort to decarbonize electricity grids. These sources are characterized by their absence of greenhouse gas emissions, thereby contributing to the enhancement of sustainability in electricity grids.

The development of energy storage technologies is another crucial aspect of this endeavor. Battery and other energy storage technologies can be used to store the production of intermittent energy sources, such as solar and wind power. This contributes to enhancing the stability and reliability of the grid.

The implementation of smart grid technologies is also paramount. These technologies can enhance the efficiency and flexibility of the electricity grid. These technologies enable real-time monitoring of electricity demand and generation, facilitating grid optimization.

Improving energy efficiency is another key aspect of enhancing grid stability and reliability. This, in turn, can help reduce the load on electricity grids. This can be achieved by implementing energy efficiency measures in buildings, industrial facilities, and the transportation sector.

Achieving decarbonization in the electricity grid sector is a multifaceted undertaking necessitating the active engagement of a diverse array of stakeholders. Achieving this objective necessitates a collaborative effort among governments, the private sector, and civil society organizations.

Here are some key considerations for decarbonizing electricity grids:

- Decarbonizing electricity grids can come at a high cost. However, these costs are expected to be lower than the economic and social damage caused by climate change.
- Decarbonizing electricity grids can create new jobs and stimulate economic development.
- Decarbonizing electricity grids can increase energy security and independence.

Hydrogen Production Methods

Hydrogen (H) is the most abundant element in the universe. However, in its pure form, it is scarce in nature. Consequently, a range of methods have been developed to produce hydrogen.

The following classification system has been proposed for the categorization of hydrogen production methods:

1. Thermal Methods:

- **Steam Reforming:** In this method, fossil fuels such as natural gas or coal are reacted with steam. This reaction produces hydrogen and carbon monoxide.
- **Gasification:** In this method, coal, biomass or organic waste is reacted with oxygen and steam at high temperatures. This reaction produces hydrogen, carbon monoxide and other gases.
- **Thermolysis:** In this method, water is decomposed at high temperatures (around 2000 °C). This reaction produces hydrogen and oxygen.

2. Electrolytic Methods:

- **Electrolysis:** In this method, water is decomposed into hydrogen and oxygen using electric current. Electrolysis is one of the cleanest methods of hydrogen production. But the source of electrical energy is important. If electricity generated from renewable energy sources is used, the hydrogen produced by electrolysis is called “green hydrogen”.

Table 1: Comparison of hydrogen production methods:

Method	Advantages	Disadvantages
Steam Reforming	Mature technology low cost	Dependence on fossil fuels carbon emissions
Gasification	Various feedstock can be used	Complex technology, high cost
Thermolysis	Clean production, high purity	High energy requirement, high cost
Electrolysis	Clean production, high purity	High electricity demand, high cost (unless renewable energy is used)

Here are some factors to consider in the production of hydrogen for hydrogen vehicles:

- **Purity of hydrogen:** The hydrogen used for a hydrogen fuel cell needs to be of high purity.
- **Cost of production:** The cost of hydrogen production is an important factor affecting the price and affordability of hydrogen vehicles.
- **Environmental impacts:** The environmental impact of the hydrogen production method is important. Green hydrogen production should be encouraged.

The future of hydrogen production for hydrogen vehicles:

For hydrogen vehicles to become widespread, hydrogen production needs to become cleaner and cheaper. The development of electrolysis and the increased use of renewable energy sources will drive developments in this area.

Hydrogen production colors are a classification system that indicates the environmental impact and carbon emission level of the production method used. In this system, each color represents a different production method and emission level:

Green Hydrogen:

Green hydrogen is produced through a process of electrolysis of water.

Renewable energy sources, such as solar, wind, and hydroelectric power, are utilized in its production.

Notably, this process does not result in carbon emissions.

Blue Hydrogen:

- Produced from natural gas through steam reforming.

The utilization of carbon capture and storage (CCS) technology is a key feature in the blue hydrogen production process.

This approach is known to result in low carbon emissions.

Turquoise Hydrogen:

- Produced from methane through pyrolysis.
- Low carbon emissions.
- CCS technology can be used.

Gray Hydrogen:

- Produced from natural gas through steam reforming.
- CCS technology is not used.
- High carbon emissions.

Brown Hydrogen:

- Produced from coal through gasification.
- Carbon emissions are very high.

Yellow Hydrogen:

- Produced by electrolysis from nuclear energy.
- No carbon emissions.
- Nuclear waste is a problem.

Purple Hydrogen:

- Produced by photosynthesis from algae.
- No carbon emission.
- It is an emerging technology.

The choice of hydrogen production color depends on sustainability and emission reduction goals. Green hydrogen is considered the most environmentally friendly and sustainable production method.

Hydrogen Production by Electrogenic Bacteria and Bioelectrocatalysis

Electrogenic bacteria are a special type of bacteria that can produce hydrogen gas using renewable energy sources such as sunlight or organic matter. These bacteria produce hydrogen through a process called bioelectrocatalysis. In this process, the bacteria take electrons from organic substrates or sunlight and transfer them to an external electrode. This electron flow triggers a catalytic reaction that causes hydrogen ions (H+) to become hydrogen gas (H2) (Ximena et all, 2015:63).

How electrogenic bacteria work:

1. Electron transfer: Bacteria take electrons from organic substrates or sunlight and transfer them to an external electrode via specialized proteins located along the cell membrane.

2. Proton reduction: As electrons flow to the external electrode, the bacteria take protons (H+) from inside the cell and convert them into hydrogen gas (H2) through an enzyme (hydrogenase).

3. Energy gain: In this process, bacteria obtain energy from electron transfer and proton reduction. This energy is used for the growth and reproduction of the bacteria.

Bioelectrocatalysis:

Bioelectrocatalysis is the basic process that electrogenic bacteria use to produce hydrogen. In this process, bacteria use enzymes that catalyze electron transfer and proton reduction reactions. The enzymes make the reactions happen faster and more efficiently, increasing the amount of hydrogen production.

Advantages of electrogenic bacteria:

- **They use renewable energy sources:** Electrogenic bacteria can produce hydrogen using renewable energy sources such as sunlight or organic matter. This makes hydrogen production more sustainable.

- **It is a clean production method:** Hydrogen gas produced by electrogenic bacteria does not produce any harmful emissions or waste.

- **High efficiency:** Electrogenic bacteria can produce hydrogen with high efficiency thanks to the bioelectrocatalysis process (Samuel et all, 2016:16).

Disadvantages of electrogenic bacteria:

- **Low production rate:** The amount of hydrogen gas produced by electrogenic bacteria is relatively low compared to other hydrogen production methods (György et all, 2023:11).

- **Cost:** The bioreactors and other equipment required to produce hydrogen using electrogenic bacteria can be expensive.

- **Need for research and development:** Hydrogen production with electrogenic bacteria is still an emerging technology. More research and development is needed before this technology can be used more widely.

Hydrogen production by electrogenic bacteria and bioelectrocatalysis has great potential as a sustainable and environmentally friendly hydrogen production method. The development and dissemination of this technology will contribute to the development of the hydrogen economy and the reduction of dependence on fossil fuels.

REFERENCE

Ximena C. Abrevayaa, Natalia J. Sacco b, Maria C. Bonetto b, Astrid H.-O. (2015). Analytical applications of microbial fuel cells. Part II: Toxicity, microbial activity and quantication, single analyte detection and other uses. Biosensors and Bioelectronics 63, 591–601.

Arulmani S. R. B., Jayaraj V., Robinson S., Jebakumar D. (2016). Long-term electricity production from soil electrogenic bacteria and high-content screening of biofilm formation on the electrodes. J Soils Sediments 16, 831–841.

Schneider G., Pásztor D., Szabó P., László K. et all. (2023). Isolation and Characterisation of Electrogenic Bacteria from Mud Samples. Microorganisms 11, 781-796

Recycling Lithium Batteries: A Biotechnological Solution Bacteria

Filiz BORAN[1]
Teoman KARADAĞ[2]

1- Assoc. Prof. Dr.; İnönü Üniversitesi Fen Edebiyat Fakültesi Biyoloji Bölümü. filiz.kuru@inonu.edu.tr ORCID No: 0000-0002-8801-7987
2- Assoc. Prof. Dr.; İnönü Üniversitesi Mühendislik Fakültesi Elektrik Elektronik Mühendisliği Bölümü. teoman.karadag@inonu.edu.tr ORCID No: 0000-0002-7682-7771

ABSTRACT

Recycling Lithium Batteries: A Biotechnological Solution Using Bacteria

It is important to note that the rapid expansion of the use of lithium-ion batteries (LIBs) in portable electronics, electric vehicles and renewable energy storage systems has raised significant concerns about their end-of-life management. Traditional recycling methods, such as pyrometallurgy and hydrometallurgy, are energy intensive, environmentally hazardous and often economically infeasible. As the demand for critical materials such as lithium, cobalt and nickel continues to grow, it is increasingly important to explore sustainable recycling solutions. This chapter explores the role of bacteria in addressing the challenges of LIB recycling, offering a biotechnological pathway that is both environmentally friendly and economically viable.

Challenges in Lithium Battery Recycling

Lithium-ion batteries consist of a complex architecture of materials, including cathodes (e.g. lithium cobalt oxide, nickel manganese cobalt oxide), anodes (graphite), electrolytes and separators. Extracting valuable metals from these components requires breaking down the complex matrix of materials. Conventional methods, such as high-temperature smelting and acid-based leaching, produce toxic by-products, release greenhouse gases and consume significant amounts of energy. In addition, the economics of these methods often depend on high metal concentrations, which limits their applicability to a narrow range of battery chemistries.

Bacterial Leaching: A Sustainable Alternative

Bacteria offer a novel approach to LIB recycling through bioleaching, a process that utilises microbial activity to extract metals from solid waste. Acidophilic bacteria such as *Acidithiobacillus ferrooxidans* and *Leptospirillum ferrooxidans* have demonstrated the ability to oxidise sulphide minerals, releasing metal ions into solution. This mechanism can be adapted to dissolve and recover lithium, cobalt and other metals from spent LIBs. By metabolising inorganic substrates and producing organic acids, bacteria facilitate the degradation of metal compounds in a low energy, environmentally benign manner (Akçıl and Çiftçi, 2006:19).

Mechanisms of Bioleaching

Bioleaching operates through direct and indirect mechanisms. In direct bioleaching, bacteria interact with metal compounds, enzymatically breaking them down. In indirect bioleaching, metabolic by-products such as sulfuric acid or ferric ions dissolve the metal compounds. For LIB recycling, indirect bioleaching is particularly effective, as it allows bacteria to work in tandem with pre-treatment processes that expose metal-rich components.

Advantages of Bacterial Recycling

Environmental Benefits: Bacterial recycling produces negligible greenhouse gas emissions and avoids the use of hazardous chemicals, unlike pyrometallurgical processes.

Energy Efficiency: Bioleaching operates under ambient temperature and pressure conditions, significantly reducing energy consumption compared to traditional methods.

Economic Viability: The low operational costs of bioleaching make it attractive for large-scale applications, especially in recovering metals from low-grade or mixed-material waste streams.

Experimental Studies and Progress

Recent studies have demonstrated the feasibility of bacterial recycling for LIBs. For instance, Acidithiobacillus ferrooxidans has been shown to leach up to 90% of cobalt and 70% of lithium from cathode materials under optimized conditions. Research has also explored the use of consortia of bacteria to enhance leaching efficiency, leveraging synergistic interactions among different microbial species. Furthermore, advancements in reactor design and process automation have improved the scalability of bioleaching systems.

Challenges and Future Directions

Despite its potential, bacterial recycling faces several challenges:

Process Optimization: Achieving high leaching efficiencies requires precise control of parameters such as pH, temperature, and nutrient availability.

Pre-treatment Requirements: Mechanical and chemical pre-treatments are often necessary to expose the active materials within LIBs, adding complexity to the process.

Metal Recovery: After bioleaching, the recovery and purification of dissolved metals require additional steps, which must be integrated into the overall recycling workflow.

Future research should focus on:

Engineering robust bacterial strains capable of tolerating high metal concentrations and varying waste compositions.

Developing hybrid recycling systems that combine bioleaching with physical and chemical methods for enhanced efficiency.

Scaling up pilot studies to industrial applications while ensuring regulatory compliance and public acceptance.

Bacterial recycling represents a transformative approach to lithium-ion battery management in line with global sustainability goals and circular economy principles. By harnessing the natural capabilities of microorganisms, this biotechnological solution addresses the environmental and economic limitations of conventional recycling methods. Continued investment in research and development will be essential to realise the full potential of this innovative technology and pave the way for a cleaner, more sustainable energy storage future.

Keywords – Lithium, Battery, Bacteria, Biotechnology, Recycling

LITHIUM (LI)

Lithium (Li) is an alkali metal in group 1 of the periodic table. It is a silver-white, lustrous and highly reactive element. Lithium does not occur naturally in free form, but is usually found in the form of lithium salts or minerals.

Features

- Symbol Li
- Atomic **number** 3
- **Density**: Very low (0.53 g/cm³), lighter than water.
- **Melting point** 180,5 °C
- **Boiling point** 1330 °C
- **Reactivity**: It is highly reactive and releases hydrogen gas, especially when in contact with water. For this reason it is usually stored in an inert liquid such as petrol.

Areas of Use

1. **Energy Storage**: Lithium-ion batteries are used to store energy in devices such as phones, laptops, electric vehicles.

2. Medication: Lithium salts are used to treat psychiatric disorders such as bipolar disorder.
3. **Aviation and Defence**: Used in applications requiring high energy.
4. **Glass and Ceramic Industry**: It is used as an additive in the production of heat-resistant glass and ceramics.

Being in Nature

Lithium is commonly found in minerals such as **spodumene** and **lepidolite**. It is also extracted from lithium-rich salt lakes.

The electrical energy storage capacity of lithium per kilogram varies depending on the lithium compound used and the battery technology. In general, the energy density of lithium-ion (Li-ion) batteries is as follows:

- **Lithium-ion batteries**: 150-300 Wh/kg (Watt-hours/kilogram)
- **Lithium metal batteries (theoretical)**: 400-500 Wh/kg
- **Lithium-sulphur (Li-S) batteries (theoretical)**: 500-1000 Wh/kg
- **Lithium air (Li-Air) batteries (theoretical)**: 1700-2000 Wh/kg

Important Details:

1. **Practical and Theoretical Difference**: In real life, the energy density of batteries is lower than the theoretical maximum. Electrodes, electrolytes and other components limit the energy density.
2. **Cell Level and System Level**: There is a difference between the energy density of a battery cell and a battery pack (cells, protective circuits, cooling systems). In battery packs this density is usually 30-40% lower.
3. **The Role of Lithium**: The energy storage capacity of the element lithium is not directly related to the compounds in batteries. Lithium metal itself can theoretically provide 11,600 Wh of energy per kilogram. However, this value is not possible in real applications.

Lithium-ion batteries are the most widely used technology today in terms of energy density and charge/discharge cycles. They are suitable for electric vehicles and portable devices.

The selection of elements used in battery technologies depends on the chemical and physical properties in the periodic table. In this context, factors such as energy storage capacity, ionic conductivity, chemical stability and cycle life are critical. Below, it is explained how the elements in the periodic table are evaluated in this context.

1. Basic Principles of Batteries and the Role of Elements

The basic function of a battery is to convert chemical energy into electrical energy. This process is achieved by the movement of ions between the electrodes and the associated flow of electrons. The elements used are selected according to the following characteristics:

- High electrochemical potential: Provides higher energy density.

- Low molar mass: Increases the energy density (Wh/kg) of the elements.

- Chemical stability: Affects cycle life and safety.

2. Energy Storage Capacities and Related Elements

Alkali Metals (Lithium, Sodium, Potassium)

- Lithium (Li):

Lithium is the most widely used element in battery technology. Thanks to its low atomic mass and high electrochemical potential, it has a high energy storage capacity per kilogram. Lithium-ion batteries have an energy density of 150-300 Wh/kg. Theoretically, lithium metal can provide 11,600 Wh/kg of energy.

- Advantages Light weight, high ionic conductivity.

- Constraints: High reactivity, limited reserves.

- Sodium (Na):

It is more abundant and cheaper, but its energy density is low compared to lithium (~100-150 Wh/kg). It is generally preferred in large-scale energy storage systems.

- Potassium (K):

Potassium-ion batteries are among the low-cost alternatives. However, energy density and commercial applicability are still limited.

Transition Metals (Cobalt, Nickel, Iron, Manganese)

Transition metals are often used as cathode materials:

- Cobalt (Co): Provides high energy density. Lithium-cobalt oxide ($LiCoO_2$) cathodes are ideal in terms of energy density (~200 Wh/kg). However, the high cost of cobalt and ethical concerns are limiting.

- Nickel (Ni): Nickel-based cathodes (e.g. NCA, NMC) reduce cobalt utilisation while increasing energy density.

- Iron (Fe): Iron-phosphate ($LiFePO_4$) cathodes are a low-cost and safe option. Energy density (~140 Wh/kg) is lower than others, but offers long cycle life.

- **Manganese (Mn):** Manganese-based cathodes are a cost-effective and environmentally friendly alternative.

Metalloids and Other Elements

- **Silicon (Si):** Used as an anode material in lithium-ion batteries. Silicon can bind more lithium ions than lithium, increasing the theoretical energy density (~4000 mAh/g). However, problems such as volume expansion are limiting.

- **Sulphur (S):** Lithium-sulphur (Li-S) batteries offer a theoretical energy density of 500-1000 Wh/kg. The advantage is that sulphur is abundant and cheap, but there are problems such as capacity loss.

- **Oxygen (O):** Oxygen in lithium-air (Li-Air) batteries theoretically enables an energy density of 1700-2000 Wh/kg. However, it is not yet in commercial use due to technological difficulties.

3. Differences between Theoretical and Practical Energy Density

The practical energy density is lower than the theoretical maximum due to the other materials that make up the battery (electrolyte, separator, fasteners, etc.) and thermal management systems. For example:

- The energy density of lithium-ion batteries is around 300 Wh/kg at the cell level. At the system level, this value can drop to ~200 Wh/kg.

- Although technologies such as lithium-metal and lithium-air theoretically offer higher values, challenges such as safety, cycle life and cost limit implementation.

4. Future Technologies and Elemental Research

- **Solid State Electrolytes:** Safer and denser batteries are being developed using elements such as lithium, sodium and magnesium.

- **Multivalent Ions (Magnesium, Calcium, Aluminium):** Multivalent ions (e.g. Mg^{2+}, Al^{3+}) promise high energy density because they can carry more charge.

- **Hydrogen and Metal-Air Systems:** The electrochemical reactions of hydrogen and oxygen aim for ultra-high energy density.

Factors such as energy density, cost, safety and environmental impact determine the choice of elements in battery technologies. While elements such as lithium, cobalt, nickel, silicon and sulphur are prominent throughout the periodic table, alternatives such as magnesium, sodium and potassium are promising for future energy storage solutions. Research is focussed on both the improvement of existing technologies and the development of new element-based systems. This process aims to provide more efficient, safe and sustainable solutions in the field of energy storage.

1. **Electric Vehicles (EVs)**: %57
2. **Consumer Electronics**: %23
3. **Energy Storage Systems**: %15
4. **Industrial Applications**: %5

These data show that lithium-ion batteries are used extensively, particularly in electric vehicles, and that this sector accounts for a large part of the market (Buğday et al., 2022:103698).

This chart is based on information compiled from various sources to visualise the overall trends for lithium-ion battery market share. The data is based on reports highlighting electric vehicles (EVs), consumer electronics, energy storage and industrial applications as the top uses for lithium-ion batteries in 2023.

Among the main sources used for detailed information and market analyses are the following:

1. The Global Market Insights report details the growth rates and market shares of lithium-ion batteries in different applications
2. Other supporting analyses are taken from academic and commercial reports on energy storage technologies in 2023.

This graph provides a representative visualisation to give an overall summary of the trends. For detailed figures and projections, please refer to the original reports.

Rhodococcus erythropolis

Rhodococcus erythropolis is an environmental Gram-positive actinobacterium with a versatile metabolism. This is involved in various biological transformations and degradations. Rhodococci are recognised for their great potential in numerous decontamination and industrial processes. This species is classified as aerobic and is capable of colonising superficial environments where oxygen levels are sufficient. *R. erythropolis* cells are motile and do not form spores. The cell membrane composition is conducive to the high hydrophobicity of the cell surface, which is characterised by a high content of mycolic acid. This hydrophobic surface facilitates adhesion to various media and contributes to the determination of cell position and survival between polar and non-polar media (e.g. between water and oil).

R. erythropolis cells contain a large group of enzymes that allow them to carry out an enormous number of biological transformations and degradations. Such enzymes have been reported to catalyse a wide range of reactions, including oxidations, hidroxylation, epoxidation, hydrolysis,

halogenation, and desulphurization. This extensive array of enzymes underscores the significant biotechnological potential of *R. erythropolis* (Belfiore et al., 2018:311; de Carvalho and da Fonseca, 2005:715).

***Priestia megaterium* (formerly *Bacillus megaterium*)**

Priestia megaterium (formerly known as *Bacillus megaterium*) is a powerful cell factory for biotechnology, with numerous patents and industrial applications since its discovery in 1884. In 1884, De Bary designated *Bacillus megaterium* the "great monster" on account of its substantial size, which is approximately 100 times the volume of *Escherichia coli*. This bacterium is frequently utilised as a model organism in genetic studies and recombinant protein production, due to its significantly larger volume, which can reach up to 2.5 × 10 μm. *P. megaterium* is a Gram-positive, rod-shaped bacterium with a low G+C (~38%) genome and forms endospores. Its sheer size has long been a source of intrigue for microbiologists, who have sought to study its physiology and function in depth, with a particular focus on processes such as cell division, cell wall biosynthesis and sporulation. Recent advances in molecular biology have revealed the potential of this bacterium in biotechnology While *P. megaterium* is predominantly considered a soil organism, it has been identified in a diverse array of environments, including raw meat, seawater, sediments, fish, vegetation, and even honey. Its ability to thrive in diverse and sometimes toxic environments, including raw meat, seawater, sediments, fish, vegetation and honey, suggests a potential for use as a detoxifying agent (Biedienck, 2021:5719).

Disposal of Lithium-Ion Batteries

Lithium-ion batteries represent the most prevalent type of battery utilised in electric vehicles, laptops and mobile phones. It is imperative to acknowledge the finite lifespan of these batteries, which necessitates their eventual replacement. Disposing of used lithium-ion batteries must therefore be done in a safe and environmentally friendly manner.

Disposal methods of lithium-ion batteries:

- It is imperative to acknowledge the significance of recycling lithium-ion batteries in the recovery of valuable metals and other materials. Moreover, recycling plays a pivotal role in averting environmental degradation and conserving resources.
- A further advantage of reusing used lithium-ion batteries is that they can be utilised in other applications, such as energy storage. This reuse has the potential to extend the life of the batteries and reduce the amount of waste.

- Incineration Lithium-ion batteries can be incinerated in specialised plants. This method allows the energy in the batteries to be recovered.
- Burial in the ground Burying lithium-ion batteries in the ground is not recommended as it may damage the environment.

Some important points about the disposal of lithium-ion batteries:

- It is imperative to acknowledge that the management of lithium-ion batteries necessitates a specific set of competencies and expertise. It is therefore advisable to ensure that batteries are delivered to authorised recycling facilities or disposal companies.
- Improper disposal of lithium-ion batteries has the potential to pose a risk of fire and explosion.
- Conversely, recycling and reuse of lithium-ion batteries can contribute to the conservation of resources and the protection of the environment.

Effective Methods for Recycling, Recovery and Disposal of Lithium-ion Batteries

Lithium-ion batteries represent the most prevalent type of battery utilised in electric vehicles, laptops and mobile phones. It is important to note that these batteries have a limited lifespan and will need to be replaced at some point. It is therefore vital to implement effective recycling, recovery and disposal methods for used lithium-ion batteries, in order to ensure both safety and environmental responsibility.

Recycling:

- Hydrometallurgy: This method uses chemical solvents to recover metals from batteries. Hydrometallurgy is an effective method for recovering precious metals such as lithium, cobalt and nickel.
- Pyrometallurgy: This method uses high temperature to recover metals from batteries. It is thought that pyrometallurgy is an effective method for recovering precious metals such as lithium, cobalt and nickel.
- Mechano-chemical recycling: This method involves grinding batteries and recovering metals using chemical processes. It is thought that mechano-chemical recycling uses less energy and resources (Echavarri-Bravo et al., 2022:8513).

Recovery:

- • Direct reuse: It is possible that used batteries could be reused in other applications, such as energy storage. It is thought that direct reuse can extend the life of batteries and reduce the amount of waste.
- Repair and Refurbishment: Damaged batteries can be repaired and reused. Repair and refurbishment extends the life of batteries and reduces the amount of waste.

Disposal:

- Incineration Lithium-ion batteries can be incinerated in specialised plants. This method allows the energy in the batteries to be recovered.
- Burial in the ground Burying lithium-ion batteries in the ground is not recommended as it may damage the environment.

Effective methods:

- Recycling and recovery are the most effective methods for disposing of lithium-ion batteries. These methods recover precious metals and other materials in batteries and prevent damage to the environment.
- The development of new technologies for recycling and recovery will make these methods more efficient and economical.
- Manufacturers of lithium-ion batteries should offer take-back programmes for recycling and recovery of batteries.
- Governments should develop policies and regulations to encourage the recycling and recovery of lithium-ion batteries.

Disposal of Lithium Batteries by bacterises

There are several types of bacteria that can consume lithium (Tsurata, 2005:562). The best known of these are the following:

- ***Bacillus megaterium*:** This bacterium can take lithium ions into its cells and use them to produce ATP.
- ***Rhodococcus erythropolis*:** This bacterium can use lithium ions to convert them into lithium carbonate.
- ***Synechococcus elongatus*:** This bacterium can use lithium ions for photosynthesis.

It is not known exactly how these bacteria consume lithium, but it is thought to be via specialised proteins in their cell membranes. These proteins are used to take lithium ions in and out of the cells.

Lithium-consuming bacteria can be used to reduce the toxic effects of lithium ions. For example, it has been shown that the bacterium *Bacillus megaterium* can be used to clean up lithium-contaminated soil.

Lithium-consuming bacteria are also involved in the biological cycling of lithium ions. These bacteria take lithium ions from the water and return them to the soil. This helps lithium ions to circulate in the environment.

Disposal of Lithium Ions by *Bacillus megaterium*

Lithium is a metal widely used in batteries and other electronic devices. Lithium ions can be toxic in high concentrations and can harm the environment. *Bacillus megaterium* is a type of bacterium that can take lithium ions into its cells and use them to produce ATP. This property makes *Bacillus megaterium* a potential candidate for the disposal of lithium ions.

Mechanism of uptake of lithium ions by *Bacillus megaterium*

***Bacillus megaterium* uses two different mechanisms to take lithium ions into its cells:**

- Active transport: In this mechanism, lithium ions are transported across the cell membrane by a protein. This process requires energy and is provided by ATP.
- Passive transport: In this mechanism, lithium ions are transported across the cell membrane by diffusion along a gradient. This process does not require energy.

Utilisation of Lithium Ions by *Bacillus megaterium*

Bacillus megaterium can utilise lithium ions to produce ATP. ATP is the energy currency of cells and is used to drive cellular processes. Lithium ions are used to produce NADPH in cellular respiration. NADPH is an electron carrier used in ATP production.

Utilisation of *Bacillus megaterium* for the Disposal of Lithium Ions

The ability of *Bacillus megaterium* to take up and utilise lithium ions can be used for the disposal of lithium ions. A bioreactor containing *Bacillus megaterium* can be fed with wastewater containing lithium ions. The bacteria will take the lithium ions into their cells and use them to produce ATP. This process will reduce the concentration of lithium ions and help treat the wastewater.

Advantages of Using *Bacillus megaterium*

Using *Bacillus megaterium* has many advantages for the disposal of lithium ions:

- **Activity:** *Bacillus megaterium* is very efficient at taking up and utilising lithium ions into its cells.
- **Efficiency:** *Bacillus megaterium* can efficiently utilise lithium ions to produce ATP.
- **Environmentally friendly:** *Bacillus megaterium* does not harm the environment.
- **Low cost:** *Bacillus megaterium* is more cost-effective than other lithium-ion disposal methods.

Disadvantages of Using *Bacillus megaterium*

Using *Bacillus megaterium* for the disposal of lithium ions has several disadvantages:

- **Slow:** *Bacillus megaterium* is relatively slow in taking up and utilising lithium ions in its cells.
- **Sensitivity:** *Bacillus megaterium* is sensitive to environmental conditions such as pH and temperature.
- **Expertise:** The use of *Bacillus megaterium* requires special expertise and equipment.

Bacillus megaterium is a potential candidate for the disposal of lithium ions. This method has many advantages, but also some disadvantages. The use of Bacillus megaterium for the disposal of lithium ions needs further research.

Disposal of Lithium Ions by *Rhodococcus erythropolis*

Lithium is a metal widely used in batteries and other electronic devices. Lithium ions can be toxic in high concentrations and can harm the environment. *Rhodococcus erythropolis* is a species of bacteria that can convert lithium ions into lithium carbonate. This property makes *Rhodococcus erythropolis* a potential candidate for the disposal of lithium ions.

Mechanism of Lithium-ion Conversion by *Rhodococcus erythropolis*

***Rhodococcus erythropolis* uses two different enzymes to convert lithium ions into lithium carbonate:**

Lithium-ion oxidoreductase: This enzyme converts lithium ions into lithium oxide.

Lithium carbonate synthetase: This enzyme converts lithium oxide and carbon dioxide into lithium carbonate.

Utilisation of Lithium Ions by *Rhodococcus erythropolis*

Rhodococcus erythropolis does not use lithium ions to drive cellular processes. Lithium ions are recognised as a toxin by this bacterium and are removed from cells by conversion to lithium carbonate.

Utilisation of Rhodococcus erythropolis for the Disposal of Lithium Ions

The ability of *Rhodococcus erythropolis* to convert lithium ions to lithium carbonate can be used for the disposal of lithium ions. A bioreactor containing *Rhodococcus erythropolis* can be fed with wastewater containing lithium ions. The bacteria will convert lithium ions into lithium carbonate, which will help treat the wastewater.

Advantages of Using *Rhodococcus erythropolis*

Using *Rhodococcus erythropolis* for the disposal of lithium ions has many advantages:

Activity: *Rhodococcus erythropolis* is very effective in converting lithium ions into lithium carbonate.

Efficiency: *Rhodococcus erythropolis* efficiently converts lithium ions into lithium carbonate.

Environmentally friendly: *Rhodococcus erythropolis* does not harm the environment.

Low cost: *Rhodococcus erythropolis* is more cost-effective than other lithium-ion disposal methods.

Disadvantages of Using *Rhodococcus erythropolis*

There are several disadvantages of using *Rhodococcus erythropolis* for the disposal of lithium ions:

Rhodococcus erythropolis is relatively slow in converting lithium ions to lithium carbonate.

Sensitivity *Rhodococcus erythropolis* is sensitive to environmental conditions such as pH and temperature.

Expertise The use of *Rhodococcus erythropolis* requires special expertise and equipment.

Rhodococcus erythropolis is a potential candidate for the disposal of lithium ions. This method has many advantages, but also some disadvantages. The use of *Rhodococcus erythropolis* for the disposal of lithium ions needs further research.

Disposal of Lithium Ions by *Synechococcus elongatus*

Lithium is a metal widely used in batteries and other electronic devices. Lithium ions can be toxic in high concentrations and can harm the environment. *Synechococcus elongatus* is a species of cyanobacteria that can utilise lithium ions for photosynthesis. This feature makes *Synechococcus elongatus* a potential candidate for the disposal of lithium ions.

Mechanism of uptake of lithium ions by *Synechococcus elongatus*

***Synechococcus elongatus* uses two different mechanisms to take lithium ions into its cells:**

Active transport: In this mechanism, lithium ions are transported across the cell membrane by a protein. This process requires energy and is provided by ATP.

Passive transport: In this mechanism, lithium ions are transported across the cell membrane by diffusion along a gradient. This process does not require energy.

Utilisation of Lithium Ions by *Synechococcus elongatus*

Synechococcus elongatus can use lithium ions for photosynthesis. Photosynthesis is a process that converts water and carbon dioxide into glucose using the energy of sunlight. Lithium ions are a component of photosynthetic system II, an enzyme that catalyses the decomposition of water in photosynthesis.

Utilisation of *Synechococcus elongatus* for the Disposal of Lithium Ions

The ability of *Synechococcus elongatus* to utilise lithium ions for photosynthesis can be used for the disposal of lithium ions. A bioreactor containing *Synechococcus elongatus* can be fed with wastewater containing lithium ions. The cyanobacteria will take the lithium ions into their cells and use them for photosynthesis. This process will reduce the concentration of lithium ions and help treat the wastewater.

Advantages of Using *Synechococcus elongatus*

Using *Synechococcus elongatus* has many advantages for the disposal of lithium ions:

Activity: *Synechococcus elongatus* is very efficient at taking lithium ions into its cells and using them for photosynthesis.

Productivity: *Synechococcus elongatus* efficiently utilises lithium ions for photosynthesis.

Environmentally friendly: *Synechococcus elongatus* does not harm the environment.

Low cost: *Synechococcus elongatus* is more cost-effective than other lithium-ion disposal methods.

Disadvantages of using *Synechococcus elongatus*

There are several disadvantages of using *Synechococcus elongatus* for the disposal of lithium ions:

Synechococcus elongatus is relatively slow in taking lithium ions into its cells and using them for photosynthesis.

Sensitivity *Synechococcus elongatus* is sensitive to environmental conditions such as pH and temperature.

Expertise The handling of *Synechococcus elongatus* requires special expertise and equipment.

Synechococcus elongatus is a potential candidate for the disposal of lithium ions. This method has many advantages, but also some disadvantages. The use

of *Synechococcus elongatus* for the disposal of lithium ions needs further research.

REFERENCES

Akçıl, A., Çiftçi, H. (2006). Mechanisms of Bacterial Leaching in Metal Recovery. *Madencilik*, 45(4), 19-27.

Belfiore, C., Curia, M.V., Farías, M.E. (2018). Characterization of *Rhodococcus* sp. A5wh isolated from a high altitude Andean Lake to unravel the survival strategy under lithium stress, *Revıstа Argentına De Mıcrobıología*, 50(3), 311-322.

Biedendieck, R., Knuuti, T., Moore, S.J., Jahn, D. (2021). The "beauty in the beast"—the multiple uses of *Priestia megaterium* in biotechnology, *Applied Microbiology and Biotechnology*, 105, 5719–5737.

Buğday, N., Altın, S., Karadağ, T., Yaşar, S. (2022). The production and electrochemical properties of N-doped porous carbon structure-based supercapacitor coin cells and flexible wristbands. *Journal of Energy Storage*, 48, 103698.

de Carcalho, C.C.C.R., da Fonseca, M.M.R. (2005). The remarkable *Rhodococcus erythropolis. Applied Microbiology and Biotechnology*, 67, 715–726.

Echavarri-Bravo, V., Amari, H., Hartley, J., Maddalena, G., Kirk, C., Tuijtel, M.V., Browning, N.D., Horsfall, L.E. (2022). Selective bacterial separation of critical metals: towards a sustainable method for recycling lithium ion batteries. *Green Chemistry*, 24, 8512-8522.

Tsuruta, T. (2005). Removal and Recovery of Lithium Using Various Microorganisms. *Journal of Bioscience and Bioengineering*, 100 (5), 562–566.

Impact of Parameters on Final Products in Fused Filament Fabrication (FFF) Technology: An Overview

Yasin AKIN[1]
Kubilay HAN[2]
Recep KILIÇ[3]

1- Arş. Gör Yasin AKIN.; Sakarya Uygulamalı Bilimler Üniversitesi, Teknoloji Fakültesi, Makina Mühendisliği Bölümü, yasinakin@subu.edu.tr ORCID No: 0000-0003-3201-379X
2- Arş. Gör Kubilay HAN.; Sakarya Uygulamalı Bilimler Üniversitesi, Teknoloji Fakültesi, Makina Mühendisliği Bölümü, kubilayhan@subu.edu.tr ORCID No: 0000-0003-1472-2832
3- Doç. Dr. Recep KILIÇ.; Sakarya Uygulamalı Bilimler Üniversitesi, Teknoloji Fakültesi, Makina Mühendisliği Bölümü, recepkilic@subu.edu.tr ORCID No: 0000-0003-1580-1997

ABSTRACT

Fused Filament Fabrication (FFF), one of the additive manufacturing methods, produces parts layer by layer. In this process, molten thermoplastic filament is extruded through a heated nozzle. Successive layers are deposited on the build platform, adhering to the layer beneath them to form the model. FFF facilitates the fabrication of intricate geometries and is frequently employed for prototyping, limited production runs, and bespoke components. FFF employs thermoplastic filaments, including PLA, ABS, PETG, TPU, and Nylon, chosen according to their printing properties and the intended usage of the final product. Production parameters influence the mechanical properties and surface quality of the printed parts. The parameters encompass print speed, nozzle temperature, layer thickness, infill density, build orientation, and cooling rate. Enhancing these factors augments layer adhesion, mechanical strength, surface quality, and manufacturing efficiency. Optimal parameter configurations are essential for improving quality and production efficiency. This chapter aims to conduct a comprehensive examination of FFF technology, focusing on material selection and production parameters while highlighting the significance of parameter optimization for the proper application of this approach.

Keywords – Fused Filament Fabrication, Additive Manufacturing, 3d Printing, Thermoplastic Filament.

INTRODUCTION

In additive manufacturing (AM), products are produced incrementally, layer by layer. In contrast to conventional manufacturing processes like subtractive techniques (CNC machining) or casting, additive manufacturing (AM) technologies create tangible objects directly from 3D digital models (Kartal & Kaptan, 2023). This procedure reduces material waste while facilitating the effortless manufacturing of intricate geometries. Additive manufacturing technologies are classified according to the deposition technique of solid, liquid, or powdered substances (Hamoud et al., 2024). Prominent applications among these technologies include Selective Laser Sintering (SLS), Stereolithography (SLA), and Fused Filament Fabrication (FFF).

Fused Filament Fabrication (FFF), its ease of use, cost-effective equipment, and diverse material options make it a preferred method across various fields, from industrial manufacturing to personal use (Tayyab et al., 2024). The FFF method relies on the principle of heating and extruding thermoplastic filaments, depositing them in successive layers. This approach offers considerable benefits, particularly in prototype fabrication, proof-of-

concept creation, and limited-scale manufacturing procedures (Afshari et al., 2023). Nonetheless, essential performance metrics, including mechanical characteristics, surface roughness, and print quality FFF, are contingent upon the employed printing parameters. (Ganeshkumar et al., 2022).

A plethora of studies has been conducted to evaluate the influence of printing settings on the quality of the final output in FFF printing. This research highlights the need to modify these parameters to improve efficiency, durability, and surface quality in industrial applications.

FUSED FILAMENT FABRICATION TECHNOLOGY

Working Principle of FFF Technology

FFF is one of the AM technologies that creates physical products building objects layer by layer. FFF method relies on the principal heating and melting a thermoplastic material and depositing it in layers using 3D digital model data. Each layer adheres to the previous one on the print bed, forming the desired geometry (Figure 1) (Liparoti et al., 2021).

The extruder is a mechanism that heats the thermoplastic material, known as filament, and pushes it out through the nozzle in a controlled manner. The extruder consists of two main components:

- Cold Zone: A motorized feeding mechanism that holds and pushes the filament forward.
- Hot Zone: A heated section (hot end) designed to melt the filament.

The nozzle ensures the controlled transfer of the molten material onto the print bed. Its diameter typically ranges from 0.2 mm to 1.0 mm, directly affecting print resolution. Smaller nozzles provide higher resolution, while larger nozzles enable faster production.

The filament, used as material in FFF, is usually a thermoplastic filament supplied in spools with a diameter of 1.75 mm or 2.85 mm.

The print bed is the surface where the part is constructed. To ensure thermal stability, the bed temperature is adjusted according to the adhesion properties material used. For instance, materials like ABS require the print bed to be maintained at a temperature of 100–110 °C (Han et al., 2024).

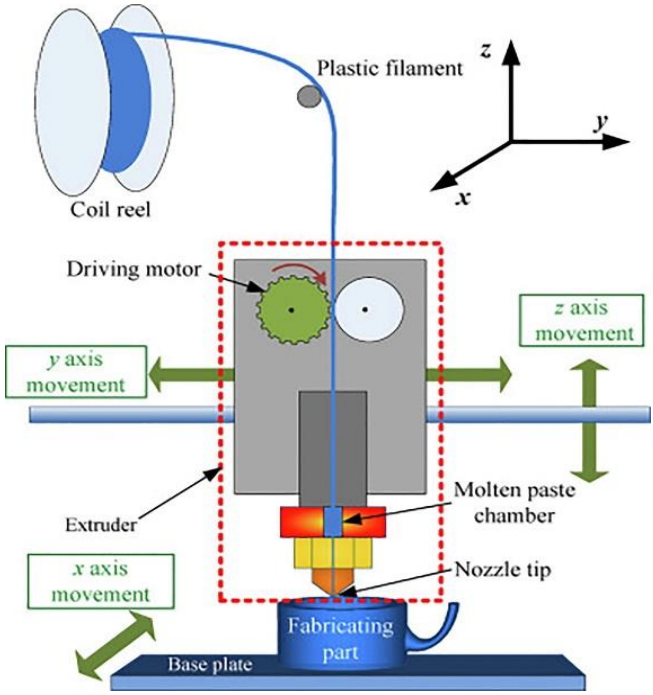

Figure 1. Working Principle of the FFF Process (Sankar et al., 2023)

Thermoplastic Materials in FFF Technology

Thermoplastic materials are commonly used in FFF technology. When heated, thermoplastics melt and become fluid, and when cooled, they solidify again, forming the final product. This property makes them ideal for the material deposition method in the FFF process. The ability of thermoplastics to be re-melted and solidified provides a significant advantage in terms of recyclability, contributing to sustainable production processes (Rajan et al., 2022).

The variety of materials used in FFF provides flexibility and customization options for different application areas. The selection of these materials depends on factors such as the mechanical properties of the part to be produced, environmental resistance, cost, ease of printing, and the application field. Additionally, each material has its unique printing parameters. For instance, parameters (bed temperature, nozzle temperature, printing speed etc.) directly affect the material's behavior during the printing process. Table 1 provides a general comparison of commonly used thermoplastic materials. This table summarizes the properties and applications of thermoplastic materials widely used in FFF technology. Each material is chosen based on its suitability for specific use cases and mechanical requirements (Acierno & Patti, 2023).

Table 1. Commonly Used Thermoplastic Materials in FFF Technology

Material	Printing Temperature	Properties	Application
PLA (Polylactic Acid)	190-220 °C	Biodegradable, low melting point, easy to print, low warping	Prototyping, educational models, packaging
ABS (Acrylonitrile Butadiene Styrene)	220-250 °C	Durable, impact-resistant, high melting point, requires heated bed	Automotive parts, electronic housings
PETG (Polyethylene Terephthalate Glycol)	220-240 °C	Strong, flexible, chemical-resistant, low shrinkage	Food containers, mechanical parts
ASA (Acrylonitrile Styrene Acrylate)	230-250 °C	Durable, UV-resistant, and weatherproof.	Ideal for automotive parts, outdoor signage, and any application
TPU (Thermoplastic Polyurethane)	210-240 °C	Elastic, impact-resistant, high wear resistance	Seals, gaskets, flexible prototypes

FFF PROCESS PARAMETERS

FFF process, factors such as print quality, mechanical properties, and surface roughness are directly related to the process parameters employed during printing. FFF process parameters can be optimized based on material selection, part geometry, and application requirements, significantly enhancing the performance of the final product (Turner et al., 2014).

Process parameters are variables controlled during printing that determine the quality of the output. Key process parameters include nozzle temperature, layer thickness, print speed, infill density, build orientation, bed temperature, cooling fan speed, extrusion multiplier, and support structures. Each parameter affects print quality in different ways (Rajan et al., 2022; Kesercioğlu et al., 2023):

Nozzle Temperature: Determines the material's flowability and interlayer adhesion.

Layer Thickness: Directly impacts surface quality and production time. Lower layer thickness provides higher resolution, while higher layer thickness allows for faster production.

Print Speed: Plays a critical role in production time. Higher speeds reduce production time but may compromise quality control.

Infill Density: Influences the internal structure and mechanical strength. Optimized infill density and pattern help achieve lightweight yet strong parts.

Build Orientation: Affects the mechanical properties anisotropically. The orientation of layers directly impacts tensile, compressive, and bending strengths.

Bed Temperature: Ensures the part adheres to the build plate and prevents warping.

Cooling Fan Speed: Regulates the cooling rate of layers, affecting material adhesion and strength.

To improve print quality and achieve the desired product characteristics, these parameters must be carefully optimized. Determining the optimum process parameters not only improves print time and cost but also maximizes performance metrics (mechanical strength, dimensional accuracy, and surface quality). Therefore, studies on FFF process parameters hold significant importance in both industrial and academic fields.

Nozzle Temperature

Temperature is parameter directly influencing print quality, mechanical properties, and production performance in FFF technology. In the FFF process, thermoplastic material in filament form is passed through the extruder, heated by the nozzle, and deposited onto the print bed in a molten state. At this stage, nozzle temperature is a key determinant of the material's flow state, interlayer adhesion, and the mechanical performance of the final product. Proper temperature settings enhance part performance while minimizing production errors. Determining material-specific optimal temperatures and maintaining stable temperatures during the process are crucial for ensuring the efficiency and quality of FFF technology. For this reason, numerous studies in the literature have focused on nozzle temperature, aiming to identify the optimal values for different materials (Tüylü et al., 2024; Rivera-López et al., 2024). Some of the studies on various materials are summarized below.

Foppiano et al. (2021) analyzed the interlayer tensile strength of samples produced from ABS material using 3D printing. The study varied nozzle temperatures between 220°C and 260°C, identifying 231°C as the optimal temperature. In regions other than narrow cross-sections, when a temperature of 261°C was used, the fracture point shifted to the center of the sample. A strong correlation was found between the time spent above the glass transition temperature (Tg) and the fracture location, with moisture negatively impacting tensile strength.

Valvez et al. (2022) examined PETG material, as well as carbon fiber and aramid fiber-reinforced PETG composites. According to the results, the best flexural properties for PETG were achieved at a nozzle temperature of 265°C, while 195°C was optimal for PETG+CF composites and 265°C was optimal for PETG+KF composites. ANOVA analysis assessed the effect of parameters within a 95% confidence interval, concluding that the optimal nozzle temperature enhances mechanical performance.

Numerous studies have demonstrated that nozzle temperature directly impacts mechanical properties. Critical characteristics of parts produced using FFF, such as tensile and flexural strength, interlayer adhesion, and surface quality, vary depending on the nozzle temperature used. An appropriate nozzle temperature improves material flowability and interlayer adhesion. However, excessively low temperatures can result in poor adhesion and low strength, while excessively high temperatures may cause material deformation and surface defects.

Layer Thickness

Layer thickness is a critical parameter in FFF technology that affects the mechanical properties, surface quality, and production time manufactured parts. Lower layer thicknesses (e.g., 0.1 mm or less) enhance interlayer adhesion, thereby improving mechanical properties (tensile and flexural strength). Additionally, thin layers result in smooth and high-resolution surfaces, offering aesthetically superior outcomes. However, this also substantially increases production time. Conversely, higher layer thicknesses (e.g., 0.3 mm or more) shorten production time and are advantageous for rapid prototyping. However, this comes at the cost of reduced mechanical strength due to weaker interlayer bonding, and visible layer lines appear on the surface. Therefore, the optimal layer thickness should be determined based on the product's characteristics. Thin layers provide high mechanical strength, while thicker layers are sufficient for fast production. The correct choice of layer thickness increases the efficiency of the production process (Han et al., 2024).

Numerous studies have examined the impact of layer thickness (Çerlek et al., 2024). Ambade et al. (2023) investigated the effect of layer thickness. They utilized the Box-Behnken approach for experimental design, producing PLA samples. The findings revealed that layer thickness significantly influences tensile strength, elongation percentage, and maximum force. These results underscore the importance of carefully optimizing printing parameters to achieve the desired mechanical properties.

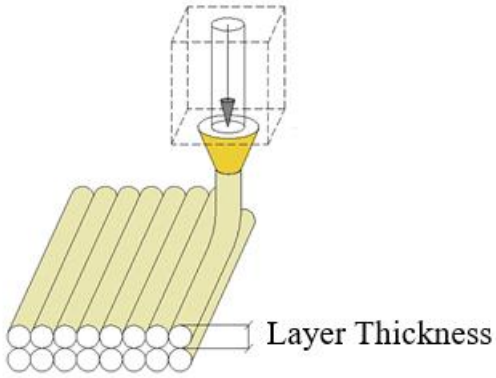

Figure 2. Schematic Representation of Layer Thickness (Solomon, 2021)

Rankouhi et al. (2016) investigated the impact of layer thickness of ABS materials. Tensile tests revealed that samples produced with a layer thickness of 0.2 mm exhibited higher elastic modulus and ultimate tensile strength compared to those produced with a layer thickness of 0.4 mm. Furthermore, fracture analysis using a scanning digital microscope showed that layer thickness influenced the fracture modes of the samples.

Rakshit et al. (2023) varied the layer thickness for ASA material. Using an experimental design approach, the study found that the best tensile strength value (30.171 MPa) was observed at a layer thickness of 0.201 mm. The highest specific strength value (30.082 kNm/kg) was observed at a layer thickness of 0.197 mm.

Optimizing layer thickness plays a critical role in improving the mechanical properties and surface quality. Thin layer thicknesses (0.1–0.2 mm) enhance interlayer bonding, improving tensile and flexural strength, and surface smoothness, albeit at the cost of extended print times. In contrast, thicker layers (0.3 mm and above) reduce print time but negatively affect mechanical properties and surface quality. Thin layers are ideal for parts requiring high aesthetics and strength, whereas thicker layers are suitable for rapid prototyping and cost-sensitive projects. Therefore, selecting an appropriate layer thickness based on application requirements is crucial for production efficiency and part performance.

Infill Density and Infill Pattern

Infill density and infill pattern are critical parameters in 3D printing technologies like FFF, directly influencing the mechanical properties, weight, print time, and material consumption of printed parts. Infill density is typically expressed as a percentage, ranging from 0% to 100% (Figure 3). High infill density (80–100%) provides increased mechanical strength, stiffness, and durability but results in longer print times and higher material usage. On the other hand, low infill density (10–50%) produces lightweight,

faster, and cost-efficient prints, though it reduces mechanical strength (Seçgin et al., 2023).

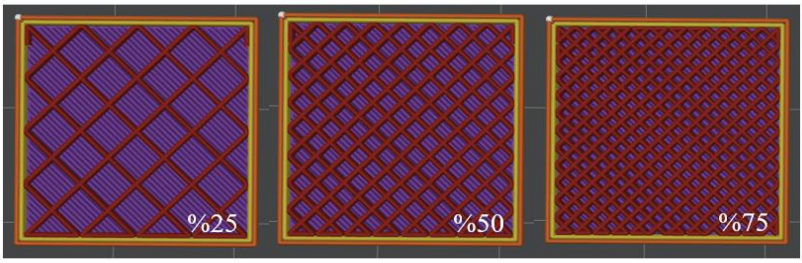

Figure 3. Representation of Infill Density

The infill pattern determines internal structure of a part and offers various options such as triangle, hexagon, grid, or fully solid configurations (Figure 4). Patterns like triangles and hexagons are strong choices for load-bearing and energy absorption due to their geometric stability and efficient distribution of forces. However, these patterns may increase printing time and material usage. On the other hand, simpler patterns such as grid or line provide faster and more cost-effective production but may compromise mechanical strength (Çerlek et al., 2024).

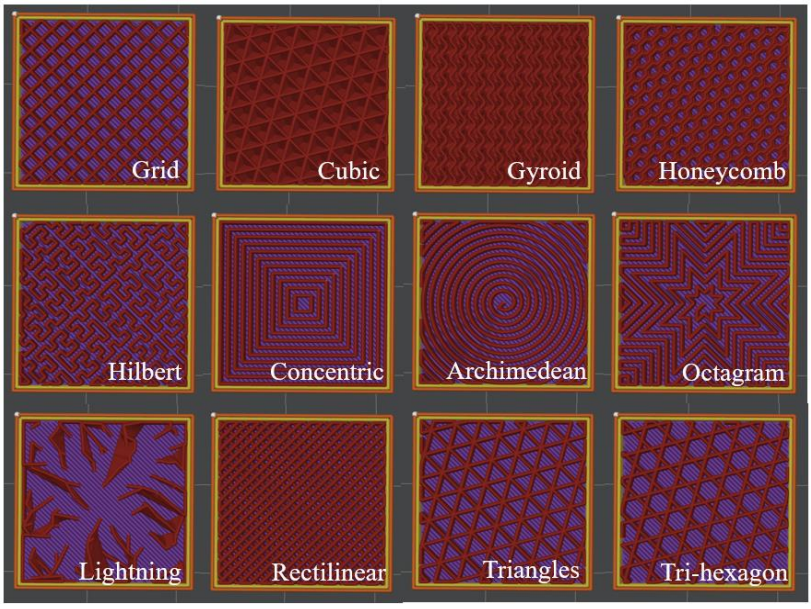

Figure 4. Commonly Used Infill Patterns

The proper selection of infill density and pattern should be optimized according to application requirements. For load-bearing and durable parts, high density and strong patterns are recommended, whereas low density and simple patterns are sufficient for prototypes or decorative parts. Adjusting these parameters appropriately ensures an optimal balance between part performance and production efficiency (Yermurat et al., 2023).

Nigam et al. (2023) evaluated the impact of infill patterns and density on the properties. Their study tested PLA, ABS, and PETG materials with various infill densities and patterns. The experimental results demonstrated that the tensile strength of the material depended significantly on the infill pattern and density. For PLA and ABS, the triangular infill pattern provided the highest tensile strength across all infill densities, while for ASA material, the highest strength was achieved with the triple hexagonal infill pattern.

Build Orientation

Build orientation defines the position of a part on the platform with respect to the X, Y, and Z axes (Figure 5). It is a fundamental factor that explains how a part is positioned on the platform, particularly in the FFF method. This orientation significantly influences the anisotropic behavior of the part's mechanical properties, meaning the properties vary depending on the direction. These differences in mechanical characteristics are directly affected by how layers are deposited during the production process and the bonding strength between layers. Proper optimization of build orientation can improve part strength and functionality while minimizing weaknesses caused by anisotropic effects (Kesercioğlu et al., 2024).

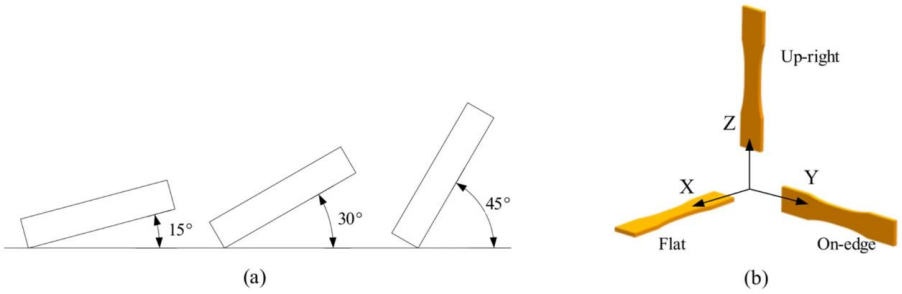

Figure 5. (a) Representation of Build Angles (15°, 30°, 45°) and (b) Build Orientations (Upright, On-edge, Flat) (Tientcheu et al., 2024)

The direction of the build substantially influences the mechanical properties, surface quality, and production duration of components in additive manufacturing methods. The anisotropic nature of layered manufacturing causes differences in strength across different axes. Aligning

layers with stress directions can enhance mechanical performance. Additionally, build orientation influences surface roughness and dimensional accuracy, often resulting in undesirable effects like the "staircase effect" on surfaces parallel to the platform. This effect can be mitigated by appropriately aligning critical surfaces. Build orientation also determines the need for support structures and production time; orientations that minimize support requirements and reduce part height can improve efficiency.

Multiple research studies have thoroughly examined the influence of construction orientation on mechanical qualities, producing significant results. This section encapsulates essential research findings about the impact of construction orientation on mechanical qualities. Beattie et al. (2021) investigated the impact of print orientation and failure modes on the mechanical characteristics of FFF-printed components. In tensile tests, the edge orientation demonstrated the greatest elastic modulus and tensile strength; however, in bending tests, the flat orientation attained the maximum ultimate stress, and the edge orientation exhibited the highest elongation at break. SEM investigations indicated that fracture modes differed by orientation, with fractures along filaments exhibiting greater strength. Zhang et al. (2017) tackled the issue of efficiently orienting many components within a single build chamber in additive manufacturing. Initially, different ideal orientations that satisfy specific quality criteria for each component were determined. An enhanced genetic algorithm was utilized to identify a worldwide solution that lowered overall production time and expenses. The strategy was illustrated using a case study that involved the concurrent orientation of 16 components, highlighting the efficacy of this methodology.

Raster Angle

The raster angle defines the direction in which each layer is deposited while printing the desired shape, making it a critical parameter in the manufacturing process. Figure 6 illustrates examples of different raster orientations. Typically, default raster angles for FFF-printed parts are set to alternate sequentially between 0°, 90°, -45°, and 45° across layers.

Optimizing the raster angle is essential for improving the performance of printed parts, as it directly impacts properties like tensile strength, flexibility, and anisotropy. Adjusting these angles strategically can enhance the overall strength and stability of the printed structure, particularly in load-bearing applications.

Raster orientation can significantly contribute to the anisotropic behavior (direction-dependent variations in properties) of FFF parts. The mechanical properties of the parts largely depend on the selected raster orientation. For example, the influence of raster orientation on the material's load-bearing capacity, strength, and durability is considerable. Using a

different direction in each layer can enhance the overall performance and structural integrity of the parts. However, an incorrectly chosen raster orientation can lead to weaknesses in specific axes of the part. As a result, the raster angle becomes an important parameter that needs to be carefully determined based on the part's design and intended use in FFF production processes.

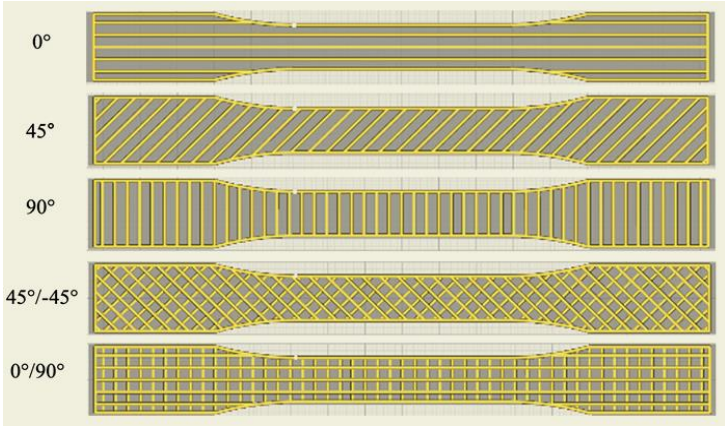

Figure 6. Representation of Different Raster Orientations (Tunçel, 2024)

Çakan (2021) investigated the impact of raster orientation on FFF-printed components. Tensile tests revealed that a 0° raster angle yielded the greatest tensile strength, whilst the ±45° angle demonstrated the highest ductility. Surface roughness measures attained up to 7 µm when assessed perpendicular to the raster direction, whereas measurements parallel to the raster direction exhibited roughness below 1 µm. Galeja et al. (2020) examined the ABS materials fabricated via FFF with several raster angles (45°, 55°, 55'°, 60°, and 90°). The 55° raster angle, determined by the ideal winding angle for filament-wound pipes, yielded superior impact strength, albeit with comparatively diminished tensile strength.

Contour number

The contour number denotes the quantity of closed routes applied along the peripheries of a component (refer to Figure 7). The outlines delineate the exterior configuration of the component, whilst the infill structure can be regarded as the interior framework. The contour number, in conjunction with other production factors like infill density and pattern, substantially influences the mechanical properties of components fabricated using Fused Filament Fabrication (FFF). Augmenting the number of contours yields a denser and more resilient outer surface, hence enhancing

mechanical qualities, including tensile strength, flexural resistance, and impact resistance. Nonetheless, augmenting the contour number may also extend production time and material usage, necessitating the identification of an appropriate contour number. The outer layers (contours) not only boost visual appeal but also improve structural integrity in essential load-bearing regions, hence augmenting durability. Thus, the appropriate selection of contour number is a critical factor for improving the performance of FFF components and must be meticulously calibrated according to design specifications (Aktaş et al., 2024).

Mishra et al. (2017) sought to examine the influence of six critical production factors (contour number, layer thickness, scanning width, part orientation, air gap, and raster angle) on the bending strength of components fabricated via the FFF process. They concluded that contour number was the most effective parameter, since it mitigated early failure by redistributing stress concentration from the outer edge to the middle. A statistical model was created to forecast the correlation between bending strength and process parameters, with optimal parameter settings determined by the Firefly algorithm. Images from a scanning electron microscope were utilized to elucidate the microstructural behavior of the components during the three-point bending test.

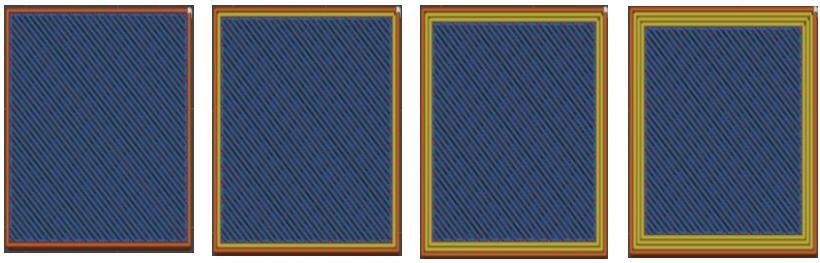

Figure 7. Example Representation of Contour Number

Other Parameters

Print Speed refers to the speed at which the printer head deposits material and is a key parameter influencing both production time and surface quality. High print speeds can reduce production time but may result in insufficient bonding between layers and surface defects. Lower print speeds, on the other hand, provide better surface finishes and stronger layer bonding, but can increase production time. For example, materials like ABS perform better at lower speeds, while PLA can tolerate higher speeds without compromising quality.

Nozzle Diameter defines the hole diameter used by the printer head during filament extrusion and affects various factors such as layer height, detail level, and print time. Smaller nozzles (e.g., 0.2 mm) provide finer details and higher precision, but they may increase print time. Larger nozzles (e.g., 0.8 mm) allow for faster production but may sacrifice detail quality. The correct nozzle diameter selection depends on factors like part complexity and the desired surface finish. For example, a larger nozzle may be preferred for fast prototyping where speed is prioritized.

Air Gap refers to the space between the fill lines within the part. It significantly affects the mechanical strength and weight. Increasing the air gap reduces the infill density, leading to lighter but weaker parts. Lower air gaps result in denser infill, making the part more durable, though this increases material consumption and weight. The optimal air gap should be chosen based on the part's intended use. For lightweight, non-load-bearing models, a larger air gap may be suitable, while for mechanically loaded parts, a minimum air gap is preferred.

Bed Temperature is adjusted to ensure the part adheres to the print bed during printing and to prevent deformation during cooling. Each material has a recommended bed temperature range; PLA typically requires a bed temperature around 60°C, while materials like ABS require temperatures of 100°C or higher. Insufficient bed temperature can lead to part detachment from the platform or internal stresses between layers. Conversely, excessively high temperatures can cause the material to become too soft and lead to adhesion issues. Proper bed temperature adjustment is crucial for ensuring high print quality, particularly for large and complex models.

CONCLUSION

In Fused Filament Fabrication (FFF) technology, the careful selection and modification of process parameters are essential for generating high-quality, functional, and durable components. Numerous parameters, including nozzle temperature, infill density, infill pattern, layer thickness, raster angle, and build orientation, directly affect the mechanical qualities, surface quality, and overall production efficiency of the printed components. All elements must be precisely calibrated based on the material used, component design, and specific requirements of the intended application.

- **Nozzle Temperature:** The nozzle temperature is crucial for ensuring that the material flows smoothly and adheres effectively between layers. A properly optimized temperature balances material flow with bonding strength, preventing issues like weak adhesion or degradation.
- **Infill Density:** Infill density determines the internal material structure, affecting both strength and weight. Higher densities increase strength

but also material use and print time, while lower densities reduce weight and cost but can weaken the part.

- **Infill Pattern:** The infill pattern defines the internal structure and strength distribution of the part. More complex patterns like honeycomb or triangular provide greater strength but take longer to print, while simpler patterns reduce print time but may lower the part's overall strength.
- **Layer Thickness:** Layer thickness impacts both the print's resolution and speed. Thinner layers provide higher resolution and smoother finishes but increase print time, while thicker layers speed up production but can compromise surface quality and mechanical properties.
- **Raster Angle:** Raster angle affects the strength and flexibility of the part by influencing how each layer is deposited. By adjusting the raster angle, manufacturers can optimize the part's performance under stress while ensuring efficient use of printing time.
- **Build Orientation:** Build orientation affects how the layers are aligned and influences the mechanical properties of the part. Proper orientation ensures optimal part strength and functionality, particularly for areas that will bear significant loads or stresses.

In addition to the core parameters mentioned above, other factors also play a critical role in determining the quality and efficiency of the FFF process. **Print Speed** affects the overall production time and is a key parameter to balance with print quality. High print speeds reduce production time but can lead to poor layer bonding and surface finish if not properly optimized. **Nozzle Diameter** influences the level of detail and precision in printed parts. Smaller nozzles provide finer details and higher resolution, but they increase print time, whereas larger nozzles allow for faster printing but with a potential loss of detail. **Air Gap** affects the internal structure and mechanical strength of parts. Increasing the air gap decreases material usage and weight, resulting in lighter but potentially weaker parts. **Bed Temperature** is crucial for ensuring that the part adheres to the print bed and prevents issues like warping. Materials such as PLA and ABS require specific bed temperature ranges to ensure proper adhesion and minimize stress during cooling. **Support Structures** are necessary for complex geometries or overhangs, and selecting the right type and amount of support structure can significantly impact the ease of post-processing and the part's overall quality.

By carefully optimizing these process parameters—nozzle temperature, infill density and pattern, layer thickness, raster angle, build orientation and other parameters—manufacturers can achieve the desired balance between part quality, mechanical performance, and production efficiency. Each of these parameters contributes to the overall success of the FFF process, ensuring that 3D printing remains an effective and versatile

manufacturing solution for a wide range of applications, from prototyping to full-scale production.

REFERENCES

Acierno, D., & Patti, A. (2023). Fused Deposition Modelling (FDM) of Thermoplastic-Based Filaments: Process and Rheological Properties—An Overview. *Materials*, *16*(24), 7664. https://doi.org/10.3390/ma16247664

Afshari, H., Taher, F., Alavi, S. A., & others. (2024). Studying the effects of FDM process parameters on the mechanical properties of parts produced from PLA using response surface methodology. *Colloid and Polymer Science*, *302*(7), 955–970. https://doi.org/10.1007/s00396-024-05246-x

Aktaş, N. F., Çerlek, Ö., & Tüylü, A. (2024.). Optimization of Tensile Strength in 3D Printed ABS Specimens Using the Taguchi Method. Presented at the 5th International Conference on Engineering and Applied Natural Sciences.

Ambade, V. V., Rajurkar, S., Awari, G., Shelare, S., & Other Authors. (2023). Influence of FDM process parameters on tensile strength of parts printed by PLA material. *International Journal on Interactive Design and Manufacturing (IJIDeM)*. https://doi.org/10.1007/s12008-023-01490-7

Beattie, N., Bock, N., Anderson, T., & others. (2021). Effects of build orientation on mechanical properties of fused deposition modeling parts. *Journal of Materials Engineering and Performance*, *30*(7), 5059–5065. https://doi.org/10.1007/s11665-021-05624-4

Çakan, B. G. (2021). Effects of raster angle on tensile and surface roughness properties of various FDM filaments. *Journal of Mechanical Science and Technology*, *35*(11), 3347–3353. https://doi.org/10.1007/s12206-021-0708-8

Çerlek, Ö., Çobaner, S., & Akın, Y. (2024). An experimental analysis of the factors influencing the tensile strength of PLA parts manufactured with 3D printing using FDM technique. 3rd International Harput Scientific Researches Congress, 30-31 August 2024, Elazığ, Turkey.

Çerlek, Ö., Han, K., AKin, Y., & Seçgin, Ö. (2024). Experimental Investigation of Parameters Affecting the Tensile Strength of Silicone-Filled 3D Printed ABS Products. Journal of Materials Engineering and Performance. https://dx.doi.org/10.1007/s11665-024-10498-3.

Foppiano, M., Saluja, A., & Fayazbakhsh, K. (2021). The effect of variable nozzle temperature and cross-sectional pattern on interlayer tensile strength of 3D printed ABS specimens. Experimental Mechanics, 61(6), 1473–1487. https://doi.org/10.1007/s11340-021-00757-y

Ganeshkumar, S., Kumar, S. D., Magarajan, U., Rajkumar, S., Arulmurugan, B., Sharma, S., Li, C., Ilyas, R. A., & Badran, M. F. (2022). Investigation of Tensile Properties of Different Infill Pattern Structures of 3D-Printed PLA Polymers: Analysis and Validation Using Finite Element Analysis in ANSYS. *Materials*, *15*(15), 5142. https://doi.org/10.3390/ma15155142

Galeja, M., Hejna, A., Kosmela, P., & Kulawik, A. (2020). Static and Dynamic Mechanical Properties of 3D Printed ABS as a Function of Raster Angle. Materials, 13(2), 297. https://doi.org/10.3390/ma13020297

Han, K., Akın, Y., & Seçgin, Ö. (2024). An experimental study on the effect of ironing process on surface roughness of pla parts produced by fdm type 3d printer. Presented at 3. Bilsel International Çatalhöyük Scientific Researches Congress, Konya.

Han, K., Aktaş, N. F., & Çobaner, S. (2024). PlA filament kullanılarak FDM yöntemi ile üretilen numunelerin yüzey pürüzlülüğünün baskı parametrelerine göre optimizasyonu. Presented at the 5th international conference on engineering and applied natural sciences, Konya.

Hamoud, M., Elshalakany, A. B., Gamil, M., & others. (2024). Investigating the influence of 3D printing parameters on the mechanical characteristics of FDM fabricated (PLA/Cu) composite material. *International Journal of Advanced Manufacturing Technology*, *134*(7–8), 3769–3785. https://doi.org/10.1007/s00170-024-14313-0

Kartal, F., & Kaptan, A. (2023). Investigating the Effect of Nozzle Diameter on Tensile Strength in 3D-Printed Printed Polylactic Acid Parts. Black Sea Journal of Engineering and Science, 6(3), 276-287. https://doi.org/10.34248/bsengineering.1287141

Kesercioğlu, M. A., Han, K., & Çerlek, Ö. (2023). Üç Boyutlu (3D) Yazıcıda PLA Filament ile Üretilen Malzemelerin Yüzey Pürüzlülüğü Optimizasyonu. In 3 rd International Conference on Scientific and Academic Research, Konya, Turkey.

Kesercioğlu, M. A., Han, K., & Aktaş, N. F. (2024). The impact of ironing process on the surface quality of ABS parts produced with FDM 3D printing. Presented at 3. Bilsel International Çatalhöyük Scientific Researches Congress, Konya, Türkiye.

Liparoti, S., Sofia, D., Romano, A., Marra, F., & Pantani, R. (2021). Fused Filament Deposition of PLA: The Role of Interlayer Adhesion in the Mechanical Performances. *Polymers*, *13*(3), 399. https://doi.org/10.3390/polym13030399

Mishra, S. B., Malik, R., & Mahapatra, S. S. (2017). Effect of external perimeter on flexural strength of FDM build parts. Arabian Journal for Science and Engineering, 42(11), 4587–4595. https://doi.org/10.1007/s13369-017-2598-8

Nigam, S., & Ahirwar, P. N. (2023). A comparative study on the effect of infill density, shape structure, and materials on tensile properties of FDM printed components. *Materials Today: Proceedings*. Advance online publication. https://doi.org/10.1016/j.matpr.2023.10.101

Rajan, K., Samykano, M., Kadirgama, K., Rahman, M. M., Ramasamy, D., & Rasul, M. G. (2022). Fused deposition modeling: Process, materials, parameters, properties, and applications. *International Journal of Advanced Manufacturing Technology*, *120*(5–6), 1531–1570. https://doi.org/10.1007/s00170-022-08860-7

Rakshit, R., Kalvettukaran, P., Acharyya, S. K., & Others. (2023). Development of high specific strength acrylonitrile styrene acrylate (ASA) structure using fused filament fabrication. *Progress in Additive Manufacturing*, *8*(3), 1543–1553. https://doi.org/10.1007/s40964-023-00420-z

Rankouhi, B., Javadpour, S., Delfanian, F., & Letcher, T. (2016). Failure analysis and mechanical characterization of 3D printed ABS with respect to layer thickness and orientation. *Journal of Failure Analysis and Prevention*, *16*(5), 467–481. https://doi.org/10.1007/s11668-016-0113-2

Rivera-López, F., Laz Pavón, M. M., Cabello Correa, E., & Hernández Molina, M. (2024). Effects of nozzle temperature on mechanical properties of polylactic acid specimens fabricated by fused deposition modeling. *Polymers, 16*(13), 1867. https://doi.org/10.3390/polym16131867

Sankar, S., Paulraj, J., & Chakraborti, P. (2023). Fused filament fabricated PEEK-based polymer composites for orthopaedic implants: A review. *International Journal of Materials Research.* https://doi.org/10.1515/ijmr-2022-0225

Seçgin, Ö., Kahraman, H., & Cesur, İ. (2023). Karbon Fiber Filament Kullanılan Eklemeli İmalat İşleminde Yüzey Pürüzlülüğü Optimizasyonu. Presented at the 1st International Conference on Recent Academic Studies, Konya.

Solomon, I. J., Sevvel, P., Gunasekaran, J., & Diğer Yazarlar. (2021). A review on the various processing parameters in FDM. *Materials Today: Proceedings, 37*(2), 509-514. https://doi.org/10.1016/j.matpr.2020.05.484

Tayyab, M., Tanveer, M.Q., Singari, R.M., Sathikh, P.M. (2024). Effect of Nozzle Diameter on the Physical Behavior of FDM-Printed Part: An Experimental Study. In: Yadav, S., Shrivastava, Y., Rab, S. (eds) Recent Advances in Mechanical Engineering. ICMET 2023. Lecture Notes in Mechanical Engineering. Springer, Singapore. https://doi.org/10.1007/978-981-97-4947-8_40

Tientcheu, S. W. T., Djouda, J. M., Bouaziz, M. A., & others. (2024). A review on fused deposition modeling materials with analysis of key process parameters influence on mechanical properties. *International Journal of Advanced Manufacturing Technology, 130*, 2119–2158. https://doi.org/10.1007/s00170-023-12823-x

Turner, B. N., Strong, R., & Gold, S. A. (2014). A review of melt extrusion additive manufacturing processes: I. Process design and modeling. Rapid Prototyping Journal, 20(3), 192–204. https://doi.org/10.1108/RPJ-01-2013-0012

Tunçel, O. (2024). The influence of the raster angle on the dimensional accuracy of FDM-printed PLA, PETG, and ABS tensile specimens. European Mechanical Science, 8(1), 11-18. https://doi.org/10.26701/ems.1392387

Tüylü, A., Çobaner, S., & Çerlek, Ö. (2024). Eklemeli imalat parametrelerinin gyroid kafes yapılı parçaların mekanik özelliklerine etkisi. *4. BİLSEL International Harput Scientific Researches Congress (Turkish)*, Elazığ, Türkiye.

Valvez, S., Silva, AP ve Reis, PNB (2022). 3D Baskılı PETG Tabanlı Parçaların Mekanik Özelliklerini Maksimize Etmek İçin Baskı Parametrelerinin Optimizasyonu. *Polimerler* , *14* (13), 2564. https://doi.org/10.3390/polym14132564

Yermurat, B., Seçgin, Ö., & Taşdemir, V. (2023). Multi-material additive manufacturing investigation of the combined use of ABS and PLA in the same structure. *Walter de Gruyter GmbH, 65*, 1119–1126. https://dx.doi.org/10.1515/mt-2022-0368.

Zhang, Y., Bernard, A., Harik, R., & others. (2017). Build orientation optimization for multi-part production in additive manufacturing. *Journal of Intelligent Manufacturing, 28*(6), 1393–1407. https://doi.org/10.1007/s10845-015-1057-1

Electromagnetic Interference Modeling and Filter Design for Single-Phase Boost PFC*

Halime HIZARCI[1]
Uğur ARİFOĞLU[2]

1- Asst. Professor; Sakarya University Engineering Faculty Electrical and Electronics Engineering, Aalborg University Dept. of Energy. hhizarci@sakarya.edu.tr ORCID No: 0000-0002-5720-6996
2- Professor; Sakarya University Engineering Faculty Electrical and Electronics Engineering. arifoglu@sakarya.edu.tr ORCID No: 0000-0001-8082-5448

* This paper was produced from the PhD Thesis of the corresponding author.

ABSTRACT

In recent years, advances in power electronics and semiconductor technologies have enabled the design of electrical/electronic devices to switch at high frequencies, enabling the development of high efficiency, high power density and compact designs. However, increasing switching frequencies lead to electromagnetic interference (EMI) problems, which jeopardize the safe operating conditions of the devices and either prevent efficient operation or cause malfunctions. One of the methods used to prevent unwanted interference is to design an EMI filter. The traditional filter design approach is based on the principle of determining the filter elements and structure by trial and error in line with the designer's years of knowledge and experience. This method, which requires testing more than one filter combination, can be quite laborious in terms of both time and cost. For this reason, the high frequency model of the noise source should first be extracted in the power electronic circuit, and possible interference paths should be determined, and the filter design should be carried out according to this data.

In this study, EMI noise model for single-phase boost PFC was created and the electromagnetic compatibility (EMC) of the circuits was investigated. An EMI filter was designed to reduce the noise within the EMC limits defined in the conducted emission standards. During the filter design, the tolerance values of the filter capacitors, and impedance mismatch were considered. As a result of comparing the simulation results with the actual measurements, it was seen that the results were compatible with each other.

Keywords – Electromagnetic Interference (EMI), Power Factor Correction (PFC), Filter Design, Impedance Mismatch, Common Mode, Differential Mode.

INTRODUCTION

Today, due to the expectations of reducing the size and cost of electrical/electronic devices and improving their performance and features, engineers who design products are in a constant improvement effort. In addition to product design that provides user satisfaction, legal regulations and standards that must be followed bring the need for reducing power consumption and high-power density product designs to the forefront in circuit designs. For this reason, continuous improvements are made in power electronic circuits, and circuits with high power density are designed by switching at higher frequencies thanks to developing semiconductor technologies. High switching frequencies allow the physical dimensions of elements such as coils and capacitors to be reduced and power electronic circuits to be designed in smaller sizes and with higher efficiency. However,

increasing switching frequencies also brings with them electromagnetic interference (EMI) problems. The noise limits that devices can cause have been determined with the relevant legal regulations and standards. Thanks to these regulations, devices can operate safely in the same environment without affecting each other's operations or being affected by each other.

By considering electromagnetic interference at every stage in electronic product designs, time and cost can be saved by intervening in the problem in advance. After the product prototype is finished, going back and redesigning the electromagnetic compatibility (EMC) measurements will be quite costly. Therefore, possible situations that may cause EMI problems should be identified in advance, necessary interventions should be made in the design steps and noise changes should be observed.

Literature

There are several studies on EMI modeling of power converters. A noise model and EMI filter design are proposed for boost PFC in the study of (Zhu et.al, 2018). In the study, authors have used a Foster model for common mode choke modeling. A frequency domain noise model is proposed by (Takahashi et.al, 2021) for single phased power converter. In the study, FEM model of the converter is realized, and the model is validated with experimental results. (Liu et al., 2019) have applied the noise impedance range method from (Ye et.al, 2004) to design EMI filters for a single-phase SiC MOSFET inverter. The authors have extracted noise source impedance and designed an EMI filter based on the noise impedance.

The design, component selection, and evaluation of filter topologies have been extensively studied in the literature. (Shifman, 1965) has analyzed insertion loss graphically for single, two, and three-element filter topologies and proposed using Craig charts to determine filter component values. The limitation of the study is an assumption of source and load impedances that are equal and set to 50 Ω, and ideal component models are used. In a paper of (Shih et.al, 1996), authors have described EMI filter design steps in detail and used a graphical insertion method to determine the corner frequency. However, the study has neglected the impedance of the noise source, leading to inadequate high-frequency noise attenuation.

An impedance matrix for EMI filter design determining insertion loss for specific input-output impedances is proposed by (Zhang et.al, 2000). The limitation of the study is complexity that requires phase information of impedance, complicating calculations. (Ye et.al, 2004) have addressed the phase information issue in impedance measurements and proposed a noise-impedance-based EMI filter design method for switched-mode power supplies. The method determines the maximum and minimum impedance over frequency to design filters for worst-case scenarios.

(Nagel & De Doncker, 2000) have proposed a systematic filter design and derived insertion loss formulas for various topologies. In the study,

nomograms for numerical relations are developed and cost and volume-optimized EMI filter designs are suggested. (Caponet et.al, 2002) have incorporated noise source impedance into designs using chain matrices to derive transfer functions for filter topologies. Components were interconnected through A matrices to express insertion loss in the study.

(Tarateeraseth et.al, 2010) have proposed a systematic EMI filter design for switched-mode power supplies using a two-probe method to measure noise source impedance under normal operating conditions. (Zhang et al., 2020) have investigated common mode noise attenuation in DC-DC boost converter using impedance balancing without additional components. In a study based on neutral point clamped inverter (Zhang et.al, 2017), a CM noise model is developed, and noise attenuation is achieved by applying the Wheatstone bridge balancing condition.

(He et al., 2020) have proposed a 3D modeling approach for EMI filters. The fine-tuned capacitors are added in the pF range to CMC windings to cancel equivalent parallel capacitance (EPC) that reduces noise attenuation. 10 dB improvement CM noise attenuation above 20 MHz is achieved, but there is no effect on DM noise. (Negri et.al, 2022) have developed a black-box modeling method for time and frequency domain simulations of EMI filters. They have used VNA measurements at connection terminals to build models without detailed internal filter knowledge. The limitations of the study are requirement of expensive VNA equipment and measurement technique is challenging for high-power applications due to VNA's limited power.

These studies highlight the EMI noise modeling and evolution of EMI filter design methods, ranging from graphical and analytical approaches to advanced modeling techniques incorporating noise source impedance, parasitic, and frequency-domain simulations.

ELECTROMAGNETIC INTERFERENCE MODELING

Electromagnetic Interference

Electromagnetic interference (EMI) is the unwanted signals originating from electric current, conducted and/or radiated, which may cause an unacceptable deterioration in the performance of the system or device (European Parliament and the Council of the European Union, 2014). The term electromagnetic compatibility (EMC) defines the ability of an electrical/electronic device to operate stably and safely within its own operating environment without unwanted interruption or deterioration in its performance or without affecting other devices in the environment (European Parliament and the Council of the European Union, 2014).

EMI noise is basically divided into two groups according to the transmission mode: common mode (CM) and differential mode (DM).

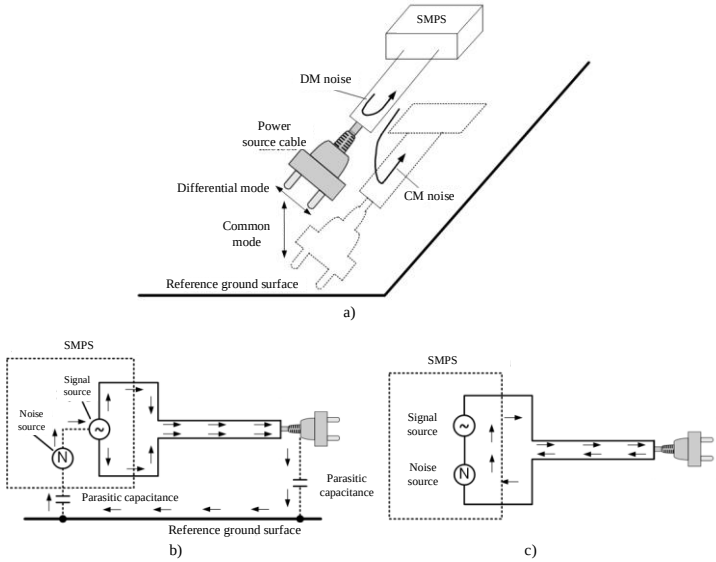

Figure 1: (a) EMI noise modes, (b) CM, (c) DM DM (Murata, 2019).

Figure 1(a) shows the noise modes for a switched power supply. Figure 1(b) shows that CM noise is transmitted in the same direction over the phase and neutral lines and completes its return path over the reference ground. DM noise is the noise transmitted in the opposite direction over the phase and neutral lines, as seen in Figure 1(c). Separating EMI noise into modes is necessary to identify the noise source and determine the desired filtering to attenuate this noise.

EMI Noise Modeling

Electrical and electronic devices can cause unwanted electromagnetic interactions due to their operating principles. Especially in power electronic circuits that switch at high frequencies, the problem of EMI reaches a size that cannot be ignored, and to prevent this noise, it is of great importance to first model its source. Two different methods are applied to model EMI noise, namely time and frequency domain. The main idea in both approaches is based on the extraction of real equivalent circuits of all passive elements in the system. However, the main difference between these methods arises from the way the noise source is modeled.

Time domain modeling: In this method, a noise model is created using the real operating characteristics of the switching elements. Although it is possible to reach a more accurate EMI model with solutions made in smaller time steps, this situation can significantly extend the simulation time. In order to reduce the modeling time, the switching waveforms are simplified and represented with a trapezoidal waveform. The spectrum analysis of the

real waveforms obtained in the time domain is performed by means of fast Fourier transform (FFT).

Frequency domain modeling: This approach is often preferred because it is practical and fast. In the frequency domain, the linear equivalent of the circuit is used; the switching elements are represented by equivalent current or voltage sources. Although this approach significantly reduces the simulation time, adding the equivalents of many components can complicate the circuit structure.

EMI Filter Design

The use of EMI filters is a common method for controlling electromagnetic noise and preventing unwanted interference. The aim of filter design is to provide the necessary noise attenuation in a certain frequency range. Therefore, the correct selection of filter elements and their values is an important issue when designing a filter. In addition, the placement of the determined filter elements in a way that will provide the desired attenuation should also be taken into account.

The EMI filter uses a CM choke and Y capacitors for common mode (CM) noise and DM chokes and X capacitors for differential mode (DM) noise. In theory, each filter component can attenuate noise by 20 dB/decade. However, parasitic parameters reduce the actual filtering effect, resulting in performance below the ideal level.

X Capacitor: X capacitors are special components connected between phases or between phases and neutral to attenuate DM noise. A higher capacitance value of the X capacitor results in a lower filter's series resonance frequency (SRF), which may cause resonance problems and reduce the attenuation effect of the filter (Cadirci et.al, 2005).

Y Capacitor: Y capacitors are special components connected between the power line and ground to attenuate CM noise. While an open circuit failure of a Y capacitor poses no safety risk, a short circuit failure could lead to electric shock if the device's metal casing is not properly grounded. For this reason, ground leakage current values are limited by standards, and the capacitance of Y capacitors is selected at the nF level. The nominal voltage and peak surge voltage ratings must also be considered in EMI filter design.

Y capacitors, connected between phase conductors and ground, are critical in filter designs and must comply with safety limits. A leakage current is the current flowing through the protective ground conductor or device casing and may pass through the human body in the absence of proper grounding. Therefore, many international safety organizations impose leakage current limits through standards to prevent hazardous situations. Examples of such standards include EN 60950 for IT equipment, IEC 60601 for medical devices, and EN 55014 for household appliances and similar uses. Y capacitors must be selected to comply with these leakage current criteria defined by international standards. The value of C_Y

$$C_{Y(max)} = \frac{I_{leakage(max)}}{1{,}1 \times V_g \times 2\pi f_g} \quad (1)$$

which meets the leakage current limit based on the upper limit of the effective grid voltage, can be calculated using Equation (1).

CM Choke: The inductor used to suppress CM noise is called a common mode choke (CMC). A CMC is a specialized inductor designed specifically to reduce CM noise and differs from a conventional inductor in its construction. It features a balanced design with two or more windings wound on a toroidal core. This structure allows for a larger impedance to be achieved on the same core, enhancing its effectiveness in attenuating CM noise.

For the CMC, which has a significant impact on CM noise attenuation, various designs have been proposed in the literature and reviewed in the literature survey section. While different core and winding configurations exist, the general approach for CMC cores involves using toroidal cores with windings appropriate to the number of phases. In addition to proposing different CMC designs, the literature includes analytical calculation methods and finite element-based models for a complete CMC model.

In this study, the analytical calculation method proposed by Nave (Nave, 2016) was chosen for the CMC model. The physical parameters used for calculating the inductance of the CMC are illustrated in Figure 2, which depicts the CMC model. In Figure 2, D_w represents the wire diameter.

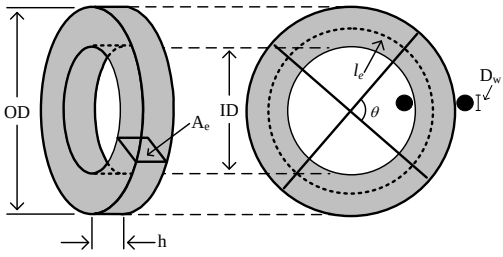

Figure 2: Physical expressions for the mathematical model of the CMC.

The inductance of windings on a toroidal core is calculated using a two-step approach. In this simplified calculation, the inductance value for an air-core toroid is first determined using Equation (2). Subsequently, this value is adjusted by multiplying it with the effective permeability of the magnetic material, treating half of the toroidal core as if it were a rod core. This approach provides a practical approximation for the inductance of a CMC.

In Equation (2), A_e represents the effective cross-sectional area of the core (in mm^2), l_e represents the effective mean length of the core (in mm), and N is the number of turns in the winding.

$$L = \frac{0{,}4\pi N^2 A_e}{l_e} \times 10^{-8}\ H \tag{2}$$

The leakage inductance of the CMC can be calculated using Equation (3) as follows:

$$L_{DM} \cong 2{,}5\mu_0 N^2 \frac{A_e}{l_{eff}} \left(\frac{l_e}{2}\sqrt{\frac{\pi}{A_e}}\right)^{1{,}45} \tag{3}$$

$$l_{eff} = \sqrt{\frac{OD^2}{\sqrt{2}}\left(\frac{\theta}{4} + 1 + \sin\frac{\theta}{2}\right)^2 + ID^2\left(\frac{\theta}{4} - 1 + \sin\frac{\theta}{2}\right)^2} \tag{4}$$

In Equation (3), μ_0 represents the magnetic permeability of free space, l_{eff} denotes the effective mean length of the leakage flux (calculated in Equation (4). In Equation (4), θ represents the winding angle (in degrees), while ID and OD denote the inner and outer diameters of the toroidal core, respectively. These parameters are used to calculate l_{eff}, which is critical for determining the leakage inductance of the CMC.

The amplitude of CM noise is equal to half of the total noise amplitude measured from the phase (V_L) and neutral (V_N) lines, as expressed in Equation (5):

$$V_{CM} = \frac{V_L + V_N}{2} \tag{5}$$

To obtain the DM noise, the difference between the noise voltages measured from the phase and neutral lines is halved, as shown in Equation (6):

$$V_{DM} = \frac{V_L - V_N}{2} \tag{6}$$

EMI Noise Model of Boost PFC

In this section, an EMI noise model is derived for a 2-kW power factor correction (PFC) circuit and the simulation results are compared with the actual measurement results. Different EMI filters are designed to ensure that the PFC circuit meets the interference limit values specified by the relevant CE standard and these filter topologies are compared.

It is desired that PFC circuits used for power factor correction by improving voltage and current distortions should be high-performance and low-cost. PFC circuits are used in the industry to reduce the negative effects of rectifiers on the grid (Yeşilyurt, 2013). By switching at high frequency in the PFC circuit, the dimensions of the filter elements and therefore their costs are reduced. Another situation that requires the use of the PFC circuit is the obligation to comply with the legal requirements of regulatory bodies. The IEC 61000-3-2 standard specifies the limits of harmonic currents allowed to be injected into the electrical grid for electrical devices. The device to be designed is required to comply with this standard.

In this study, a simulation study has first carried out to create a high frequency model for the EMI noise analysis of the PFC circuit shown in Figure 3. In the figure, the switching element is shown as the noise source

(N) and the spectral envelope model explained in the PV inverter circuit section is used.

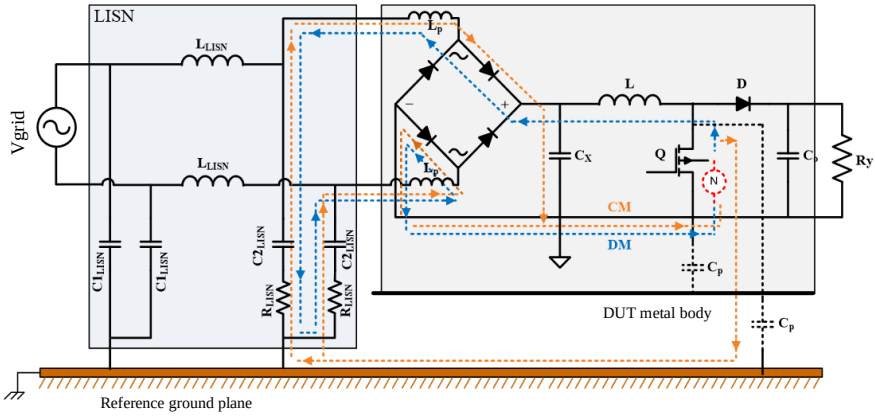

Figure 3: Boost PFC circuit and EMI noise paths.

Design parameters for the boost PFC circuit are switching frequency f_s=53.25 kHz, output power P_o=2 kW, input voltage V_i=220 V, DC output voltage V_{DC}=400 V and PFC inductor L=720 µH. IXYS company IXFK48N50 MOSFET is used as the switching element in the circuit. In the catalog information, the parasitic capacitances for the MOSFET are given as input capacitance C_{iss}=8400 pF, output capacitance C_{oss}=900 pF and reverse transfer capacitance C_{rss}=280 pF, respectively. Junction capacitance values are added to the simulation to create the noise model of the switching element. Using VNA, the leakage capacitance of the device body to ground is measured as C_p=25 nF and the busbar inductance L_p=65 nH. The PFC circuit whose noise model was extracted in the study is a peak current mode-controlled amplifier PFC circuit and Texas Instruments' UC3854 integrated circuit is used in the control circuit.

The simulation results of the model developed in PSIM using the high-frequency model for noise analysis of the PFC circuit were compared with experimental measurement results in Figure 4.

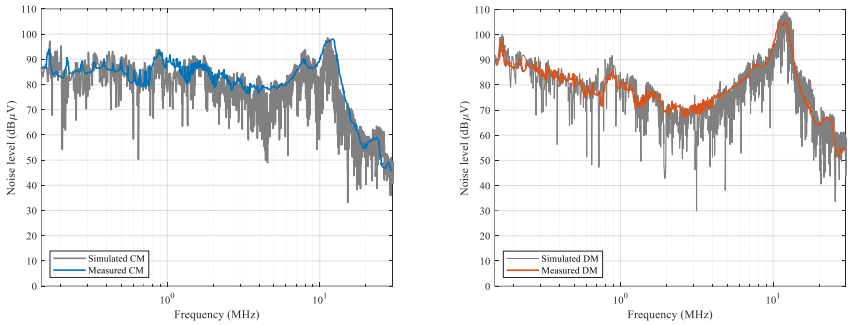

Figure 4: Experimental and simulation results of baseline CM and DM noise for the PFC.

The graphs presented in Figure 4 indicate that both the CM and DM noise modeling results align well with the experimental measurement results.

EMI Filter Design for Boost PFC

In the EMI filter design process, first, the necessary calculations are made, and appropriate filter topologies are determined. Two different EMI filter topologies were created for the PFC circuit and the performances of these designs in terms of noise attenuation and power density were evaluated. The EMI filter design steps specific to the PFC circuit can be summarized as follows:

Step 1: In the first stage, EMI noise modes were measured for the PFC circuit. A hardware-based CM/DM noise separator was used to separate CM and DM noise components (seen in Figure 5).

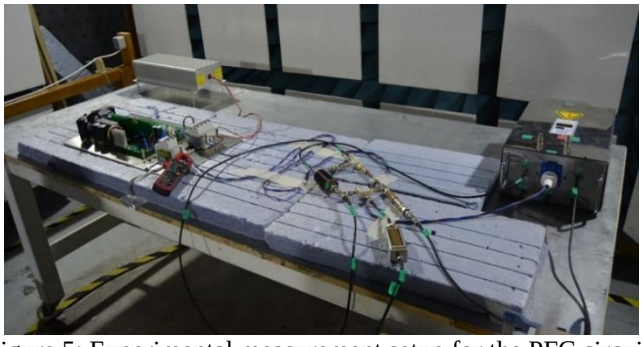

Figure 5: Experimental measurement setup for the PFC circuit.

With the help of the separators, it was determined in which frequency ranges and in which noise mode the circuit caused interference. In the measurements, the ZFRSC-183-S+ (DA-18 GHz) resistive separator from Mini-Circuits was used for the detection and separation of CM noise, while the ZFSCJ-2-2-S (0.01–20 MHz) hybrid separator, a bidirectional 180°

separator circuit from the same company, was used for the measurement of DM noise.

Considering that the separators are sensitive measurement elements and that high noise levels can damage these separators, a 10 dB attenuator was added to the setup. In order to ensure the reliability of the measurements, the end where the measurement is not made was terminated with 50 Ω in all cases.

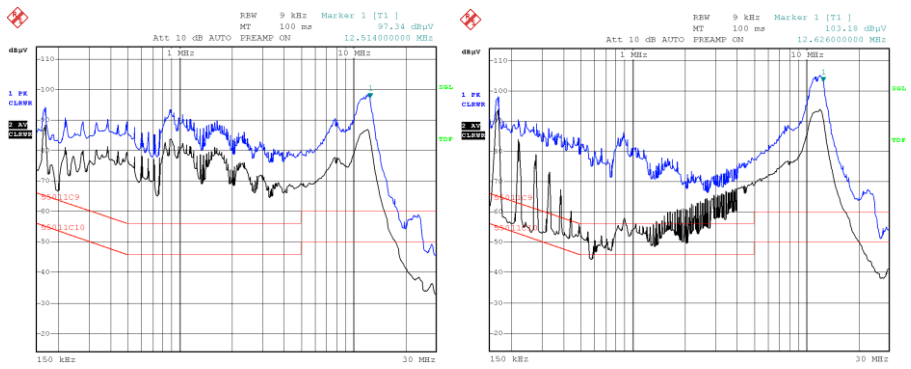

Figure 6: CM and DM noise measurement.

The measurement result given in Figure 6 shows that the standard limits are above for both modes and therefore an EMI filter design is needed for the PFC circuit.

Step 2: The noise attenuation expected from the filter for CM and DM noise modes is calculated using Equation (7).

$$V_{required,CM/DM[dB\mu V]} = V_{measured,CM/DM} - \text{standard limit} + \text{safety margin} \qquad (7)$$

The graph showing the required noise attenuation from the EMI filter to comply with the noise limit values specified in the EN55011 Class B standard is presented in Figure 7. In this graph, the measured noise levels are subtracted from the standard limit values, and a 6 dB safety margin is added to determine the noise values that must be attenuated to meet the standard. The inclusion of a safety margin is intended to account for potential errors that may arise during measurement.

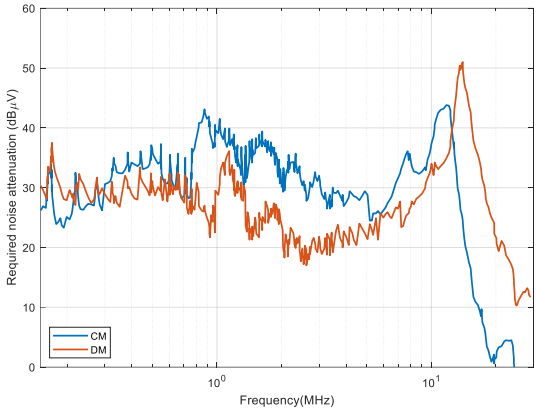

Figure 7: The graph of the required noise attenuation expected from the EMI filter.

Step 3: The appropriate filter topology will be selected using the graph of the required noise attenuation expected from the filter. The maximum noise amplitude is observed to be 45 dBμV for CM noise and 51 dBμV for DM noise. Since the noise amplitude requiring attenuation exceeds 40 dB for both modes, either a T or π filter topology should be chosen for the EMI filter design. To decide which of the two topologies to use, impedance mismatch needs to be considered. As the EMI filter will be placed between the grid and the PFC circuit's bridge rectifier, the impedance conditions play a significant role in determining the topology. Considering impedance mismatches, a T filter topology is chosen for CM noise, and a π filter topology is selected for DM noise.

After determining the filter topology, the next step involves selecting filter components for the equivalent circuits of both noise modes. By determining the filter corner frequency for CM and DM equivalent circuits, the component values are calculated. Using a graphical method, the corner frequencies are found as $f_{c,CM} = 37\,\text{kHz}$ and $f_{c,DM} = 24\,\text{kHz}$ for CM and DM, respectively.

Step 4: Once the corner frequencies are determined, the CM filter section of the EMI filter is designed first. The value of the Y capacitor is calculated to remain within the safety limit for ground leakage current. Using Equation (1), the maximum allowable value of the Y capacitor is determined to be 88.07nF. To stay below this value and limit leakage current, a Y2 film capacitor with a value of 4.7nF from KEMET is selected.

Next, the inductance value of the CM choke must be determined. Using Equation (2), the CM inductance is calculated as $L_{CM} = 1{,}96\,\text{mH}$ To achieve this value, TDK's B64290L0674 series core with R36T38 (MnZn) material is used. The magnetic and physical properties of this core are $\mu_i \cong 10000$, $A_L = 13500 \pm \%30$, $l_e = 89{,}65\,\text{mm}$, $A = 95{,}89\,\text{mm}^2$.

$$f_{c,CM} = \frac{1}{2\pi\sqrt{L_{CM}C_{CM}}} \rightarrow L_{CM} = \frac{1}{8\pi^2 f_{c,CM}^2 C_{CM}} \quad (8)$$

In the CMC design, sectional winding was utilized. To achieve the desired inductance value, the winding angle θ was calculated as approximately 160°, and the number of turns was determined to be 15 using Equation (3). When the CMC design was implemented using these calculated values, the resulting inductance was $L_{CM} = 2{,}14$ mH, and the leakage inductance was $L_{DM} = 23{,}6$ µH.

Step 5: For the DM equivalent circuit of the filter, the DM filter component values are determined using the corner frequency derived from the DM noise graph. In this step, only the X capacitor is selected for the DM filter using the leakage inductance of the CM choke. To explore the effects of different filter combinations, a DM choke design is also performed, and the final filter combinations are presented at the end of the design steps.

Using the DM corner frequency and Equation (9), the value of the DM capacitor is calculated as $C_X = 0{,}931$ µF. The leakage inductance of the CMC is used as the DM inductance, and the value of the DM capacitor is calculated using the corner frequency determined for the DM filter.

$$f_{c,DM} = \frac{1}{2\pi\sqrt{0{,}5L_{DM}C_{DM}}} \rightarrow C_{DM} = 0{,}5C_X = \frac{1}{8\pi^2 f_{c,DM}^2 L_{DM}} \quad (9)$$

As a result of the design steps outlined above, the filter component values are determined as $L_{CM} = 2{,}14$ mH ($L_{DM} = 23{,}6$ µH), $C_Y = 4{,}7$ nF, and $C_X = 1$ µF (shown in Figure 8).

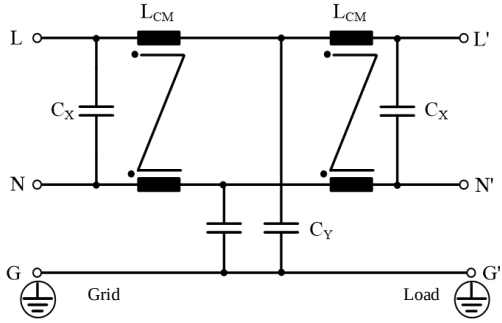

Figure 8: The schematic diagram of the EMI filter designed for the PFC circuit.

The filter shown in Figure 9(a) is a circuit where the CM equivalent circuit is configured as a T filter, and the DM equivalent circuit is configured as a π filter, representing a general filter structure. In this design (seen in Figure 9(a), an impedance mismatch occurs when a low-impedance source is present at both the input and output of the filter for CM noise. This mismatch allows the filter to achieve optimal attenuation.

Theoretically, the expected noise attenuation (insertion loss) from this filter is 60 dB for both noise modes. The component values used in this filter were derived from the calculation steps and are detailed below:

Filter 1: $L_{CM} = 2{,}14$ mH ($L_{DM} = 23{,}6$ µH), $C_Y = 4{,}7$ nF, $C_X = 1$ µF

Another filter circuit prepared for the PFC is shown in Figure 9(b). In this circuit, L_1 and L_2 are DM chokes, added to the circuit as extra components for the DM equivalent circuit, distinguishing it from the previous filter. In Filter 1, the leakage inductance of the CM choke was used as the DM choke. However, if the CM choke alone proves insufficient for attenuating DM noise, additional DM chokes are incorporated into the power and neutral lines.

For Filter 2, the theoretical insertion loss is 40 dB for both noise modes. The component values used in this filter are provided below:

Filter 2: $L_{CM} = 4$ mH ($L_{DM} = 15{,}6$ µH), $C_Y = 3{,}3$ nF, $L_{DM} = 10$ µH, $C_X = 4{,}7$ µF

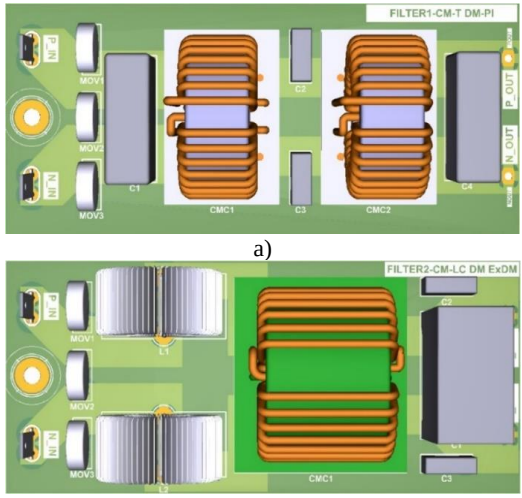

Figure 9: The schematic diagram of the designed EMI filters a) Filter 1, b) Filter 2.

CM and DM noise measurements are presented in the graph shown in Figure 10 to compare the effects of two different EMI filter topologies on noise.

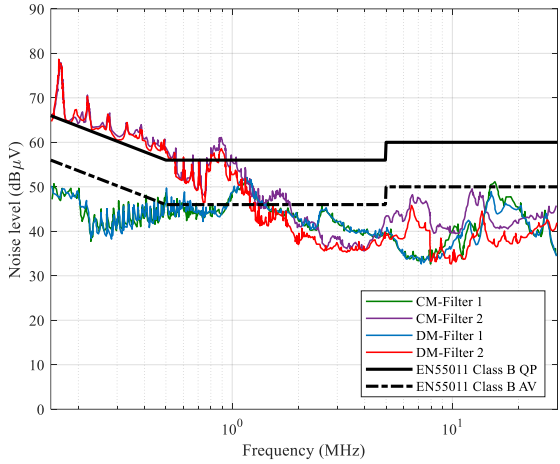

Figure 10: Comparison of different EMI filter topologies.

Filter 1, designed according to impedance mismatch, meets the standard limits for both Class A and Class B. In Filter 2, a two-element filter design was implemented, differing from Filter 1 by including an additional DM choke alongside the leakage inductance of the CM choke in the DM equivalent circuit. Although this design complies with Class B standard limits from 1.2 MHz onward, it fails CE test in the low-frequency range. However, it meets the limits for Class A standards.

The effect of impedance mismatch and proper filter component selection on noise is clearly illustrated in Figure 10. Although traditional filter design often relies on trial and error, developing a noise model for the power electronics circuit can save significant time, component use, and testing costs.

In this study, the EMI filter designed for the PFC circuit complies with the CE standard. Besides CE compliance, the EMI filter must also meet ground leakage current standards. According to the IEC 60479-1 standard, the ground leakage current limit for the PFC circuit is 7 mA. The simulated effective value of leakage current is 1,7 mA, while the experimental measurement yielded 1,5 mA. In conclusion, the measured leakage current value of the PFC circuit with the EMI filter is below the safety limit set by the standard.

Furthermore, the designed EMI filter has been considered as a discrete-phase industrial filter operating at 230 V. The capacitor imbalance was analyzed under the assumption that the tolerance values of the X and Y capacitors, according to the manufacturer's specifications, are ±10%. Based on this analysis, the leakage current of the EMI filter was calculated to be 0.032 mA.

In conclusion, EMI noise analysis for a single-phase boost PFC circuit was conducted in this section, and the simulation results were compared with experimental measurements. It was observed that the circuit model aligns well with the actual measurement results. Using the developed noise model, various filter designs can be tested through simulation, saving both time and cost.

With the implementation of the designed filter, the EMI emissions from the PFC circuit remained below the expected standard limits, achieving compliance with EMC criteria for CE testing. Measurement results also confirmed that the designed filter meets the safety limits for leakage current.

RESULTS AND DISCUSSION

In this study, a complete EMI noise model based on behavioral modeling of PFC circuit is realized. Unlike the conventional trapezoidal waveform approach commonly used in the literature, the behavioral model of the EMI noise source integrates the trapezoidal waveform with an oscillatory waveform to achieve a highly accurate noise prediction, resulting in a new and improved model.

For the circuits where noise prediction was performed, an innovative analytical calculation method was proposed for EMI filter design, replacing the traditional trial-and-error approach. This method incorporates the tolerance values of EMI filter capacitors into the design stages. Another topic examined in the study is impedance mismatch. By selecting a filter topology compatible with the impedance at the input and output of the EMI filter, noise attenuation was achieved using fewer filter components. This approach reduced the volume occupied by the EMI filter, enabling high power density designs. Recommendations for filter designs with minimized volume and enhanced power density were provided, and the impact of the designed filters on unwanted interferences was analyzed and supported by experimental measurements.

REFERENCE

Cadirci, I., Saka, B., & Eristiren, Y. (2005). Practical EMI-filter-design procedure for high-power high-frequency SMPS according to MIL-STD 461. IEE Proceedings - Electric Power Applications, 152(4), 775.

Caponet, M. C., Profumo, F., & Tenconi, A. (2002). EMI filters design for power electronics. In 2002 IEEE 33rd Annual IEEE Power Electronics Specialists Conference. Proceedings (Cat. No.02CH37289) (Vol. 4, pp. 2027–2032). IEEE.

European Parliament and the Council of the European Union. (2014). Electromagnetic compatibility Directive 2014/30/EU. Official Journal of the European Union (Vol. 29.3.2014).

He, R., Xu, Y., Walunj, S., Yong, S., Khilkevich, V., Pommerenke, D., … Klaedtke, A. (2020). Modeling Strategy for EMI Filters. IEEE Transactions on Electromagnetic Compatibility, 62(4), 1–10.

Liu, Y., Jiang, S., Wang, H., Wang, G., Yin, J., & Peng, J. (2019). EMI filter design of single-phase SiC MOSFET inverter with extracted noise source impedance. IEEE Electromagnetic Compatibility Magazine, 8(1), 45–53.

Murata Manufacturing. (2019). Basics of EMI Filters. Retrieved from http://datasheet.datasheetarchive.com/originals/library/Datasheets-UEA1/DSAFRAZ008703.pdf

Nagel, A., & De Doncker, R. W. (2000). Systematic design of EMI-filters for power converters. Conference Record - IAS Annual Meeting (IEEE Industry Applications Society), 4, 2523–2525.

Nave, M. J. (2016). On modeling the common mode inductor. In IEEE 1991 International Symposium on Electromagnetic Compatibility (Vol. 4, pp. 452–457). IEEE.

Negri, S., Spadacini, G., Grassi, F., & Pignari, S. (2022). Black-Box Modeling of EMI Filters for Frequency and Time-Domain Simulations. IEEE Transactions on Electromagnetic Compatibility, 64(1), 119–128.

Shifman, J. C. (1965). A graphical method for the analysis and synthesis of electromagnetic interference filters. IEEE Transaction on Electromagnetic Compatability, 297–318.

Shih, F. Y., Chen, D. Y., Wu, Y. P., & Chen, Y. T. (1996). A procedure for designing EMI filters for AC line applications. IEEE Transactions on Power Electronics, 11(1), 170–181.

Takahashi, K., Ibuchi, T., & Funaki, T. (2021). Noise-Source Model for Frequency-Domain EMI Simulation of a Single-Phased Power Circuit. IEEE Transactions on Electromagnetic Compatibility, 63(3), 772–782.

Tarateeraseth, V., See, K. Y., Canavero, F. G., & Chang, R. W.-Y. (2010). Systematic Electromagnetic Interference Filter Design Based on Information From In-Circuit Impedance Measurements. IEEE Transactions on Electromagnetic Compatibility, 52(3), 588–598.

Ye, S., Eberle, W., & Liu, Y.-F. (2004). A novel EMI filter design method for switching power supplies. Power Electronics, IEEE Transactions On, 19(6), 1668–1678.

Yeşilyurt, H. (2013). Geliştirilmiş Bir Kayıpsız Pasif Bastırma Hücreli PFC Devresinin Tasarımı ve Gerçekleştirilmesi (Master Thesis). Yıldız Teknik University.

Zhang, D., Chen, D. Y., Nave, M. J., & Sable, D. (2000). Measurement of noise source impedance of off-line converters. IEEE Transactions on Power Electronics, 15(5), 820–825.

Zhang, H., Yang, L., Wang, S., & Puukko, J. (2017). Common-Mode EMI Noise Modeling and Reduction with Balance Technique for Three-Level Neutral Point Clamped Topology. IEEE Transactions on Industrial Electronics, 64(9), 7563–7573.

Zhang, S., Zhang, B., Lin, Q., Takegami, E., Shoyama, M., & Dousoky, G. M. (2020). Modeling and optimization of impedance balancing technique for common mode noise attenuation in DC-DC boost converters. Electronics (Switzerland), 9(3).

Zhu, H., Liu, D., Zhang, X., & Qu, F. (2018). Reliability of boost PFC converters with improved EMI filters. Electronics (Switzerland), 7(12).

Evaluating the Effectiveness of Machine Learning Algorithms in Detecting Sarcasm in Turkish Tweets

Mümine KAYA KELEŞ[1*]
Elif KAVAK[2]

1- Assoc. Dr. Mümine KAYA KELEŞ; Adana Alparslan Türkeş Science and Technology University Faculty of Computer and Informatics Department of Computer. mkaya@atu.edu.tr ORCID No: emrekatmer@gmail.com ORCID No: 0000-0001-8414-1713.
2- Res. Asst. Elif KAVAK; Adana Alparslan Türkeş Science and Technology University Faculty of Computer and Informatics Department of Computerekavak@atu.edu.tr ORCID No: 0000-0001-9617-2568.
* Corresponding Author

ABSTRACT

Sarcasm is a linguistic tool often used to convey a meaning contrary to the literal interpretation of the words, typically for humor, criticism, or irony. This study addresses sarcasm detection in Turkish, a low-resource language, using machine learning models trained on a Twitter dataset. Many factors such as context, tone, intention and cultural norms play an important role in detecting sarcasm. In this study, the aim was to solve the complexity of the expressions created by sarcasm by coding the machine learning models. Various preprocessing techniques and algorithms, including Random Forests (RF) and Support Vector Machines (SVM), were evaluated. The findings demonstrate that RF outperforms other models in accuracy and F-measure metrics. This study contributes to Turkish NLP by filling a critical gap in sarcasm detection and setting the stage for future multimodal approaches.

Keywords – Machine Learning, Natural Language Processing, Sarcasm Detection, Twitter, Turkish Language.

INTRODUCTION

Sarcasm is a part of human language, often expressed by stating the opposite of what is truly meant. For example, a statement like "Oh, perfect. Just what I needed. More rain." clearly conveys dissatisfaction rather than joy. Understanding sarcasm requires cultural and linguistic context, making it a challenging aspect of sentiment analysis.

In the present day, in many environments such as social media platforms and e-commerce pages people are allowed to express their opinions through text, images, and videos, providing insights into their thoughts and emotions. In this way, it is possible to understand people's thoughts on an event. However, sarcasm is encountered as a problem in understanding the positive/negative emotions in people's expressions (Verma et al., 2021:968).

According to Bouazizi and Ohtsuki (2016:5477), the importance of pattern-based models was emphasized and sarcasm was detected with a data set obtained from Twitter, which included different types of sarcasm. A pattern-based model was used to detect sarcasm and a sensitivity result of 91.1% and an accuracy result of 83.1% were obtained.

According to Zhang et al. (2016:2449), the study aimed to investigate the use of neural networks for sarcasm detection. In the study, a data set obtained from tweets was used and a recurrent neural network with a two-way gate was used to capture syntactic and semantic information. In order to compare the result, the automatic features of the deep neural network were compared with traditional discrete models. When the results were examined,

it was observed that the developed model gave better results than the traditional model.

According to Razali et al. (2021: 68609), the study aimed to detect sarcasm by combining contextual features with a deep learning-based Convolutional Neural Network (CNN) model and combining it with a dataset containing tweets. The results obtained in the study were measured with Accuracy, Precision, Recall and F1 metrics, and positive results were obtained. In addition, machine learning-based classifier models were used to determine the success of the extracted features, and it was determined that Logistic Regression (LR) was suitable for further studies.

According to Baykar et al., the aim of the study was to develop a model that can process text, video and audio data together for sarcasm detection. In line with the target in the study, a Hybrid Recurrent Neural Network (RNN) and Optimized Long Short-Term Memory (LSTM) for Multimodal Sarcasm Detection model called HROMSD was created. When the results were examined in the study, it was observed that a successful model was proposed that fully evaluates the emotional semantics and integrates multimodal features.

According to Šandor and Babac (2023), it is aimed to detect sarcasm using machine learning and deep learning based models. Tests were performed on a dataset containing social media comments and having a binary class and additional features were extracted in the dataset. Various machine learning models including LR, Ridge Regression (RR), Linear Support Vector (LSV) and Support Vector Machines (SVM), two deep learning models based on Bidirectional LSTM and a Bidirectional Encoder based on Transformers (BERT) were compared and the best results were obtained by the BERT model.

When the literature is examined, it has been determined that there are deficiencies in sarcasm detection in Turkish, a low-resource language. This study aims to address this challenge by developing a machine learning-based approach using the sarcasm data set collected from Twitter and to focus on model comparisons.

MATERIALS AND METHODS

Dataset

While creating the data set, a balanced data set was created using 3000 sarcastic and non-sarcastic tweets consisting of different subject headings and different hashtags. The tweets were indicated with explanations. 3 different people checked whether the tweets contained sarcastic content and the final data set was created under the class label with the majority decision. Tweets were labeled as 0 (non-sarcastic) and 1 (sarcastic) through a majority vote by three independent annotators. Thus, a data set with a binary class

was created and became usable for sarcasm detection. In order to obtain more accurate results from the data set, Natural Language Processing (NLP) methods were used.

	A	B	C	D	E
1	title	1.kişi	2.kişi	3.kişi	sınıf
2	Asgari ücr	1	1	1	1
3	Aşkın	0	0	0	0
4	Yıllar	0	0	0	0
5	@btl0504	0	0	0	0
6	benim yin	0	0	0	0
7	kâğıt keba	1	0	0	0
8	Emeklilikt	1	1	1	1
9	Tüm bakaı	1	0	0	0
10	nesil yok (	0	0	0	0
11	@tcaileso	0	0	0	0
12	ne saçma	1	0	0	0
13	@AylinLaf	1	0	0	0
14	@RTErdo	0	0	0	0
15	@oztrk_a	1	0	0	0
16	Öğretme	0	0	0	0
17	@zeehrag	0	0	0	0
18	@drozcan	0	0	0	0
19	@Miryus1	0	0	0	0
20	Hazal kaya	1	1	1	1

Figure 1: View of dataset

Preprocessing

After the data set was created, this data set was preprocessed with 16 different combinations to be trained with machine learning algorithms.

Stemming is the process of reducing a word to its base or root form. This is often used to simplify text data for natural language processing tasks.

Stopwords are words that are commonly used in a language but do not have much meaning on their own, such as "the" or "a". They are often removed from text data to reduce noise and improve the efficiency of text processing tasks.

Lowercasing refers to converting all characters in a string to lowercase. This is done to standardize text data and make it easier to process.

Punctuation removal refers to the process of removing punctuation marks from text data. This is also done to standardize text data and make it easier to process.

Scenario Number	Code	Lowercase Conversion Off (0) / Lowercase Conversion On (1)	Punctuation Removal Off (0) / Punctuation Removal On (1) (Punctuation: Alphanumeric Charachters. Numbers, Punctuations, Emoticons)	Stemming Off (0) / Stemming On (1)	Stopwords Removal Off (0) / Stopwords Removal On (1)
1	0000	0	0	0	0
2	0001	0	0	0	1
3	0010	0	0	1	0
4	0011	0	0	1	1
5	0100	0	1	0	0
6	0101	0	1	0	1
7	0110	0	1	1	0
8	0111	0	1	1	1
9	1000	1	0	0	0
10	1001	1	0	0	1
11	1010	1	0	1	0
12	1011	1	0	1	1
13	1100	1	1	0	0
14	1101	1	1	0	1
15	1110	1	1	1	0
16	1111	1	1	1	1

Figure 2: Coding of preprocessing methods

Machine Learning Algorithms

In order to compare the results more easily, many different algorithms were used for training. In this project, k-Nearest Neighbors (KNN), NB, RF, C4.5 and SVM and DT supervised machine learning algorithms were implemented.

KNN is a type of supervised machine learning algorithm used for classification and regression tasks. It works by identifying the k-number of nearest data points to a new data point and classifying the new data point based on the majority class of its k-nearest neighbors.

NB is a probabilistic algorithm that makes classifications based on the probability of an input being in a particular class, assuming that the input's features are independent of one another. It is commonly used for text classification and spam detection.

RF is a type of ensemble learning method for classification and regression. It consists of multiple decision trees and creates predictions by averaging the results of the individual trees.

C4.5 is a decision tree algorithm that is used for classification tasks. It constructs a tree by recursively partitioning the data based on the feature that provides the most information gain.

SVM is a type of supervised machine learning algorithm used for classification and regression tasks. It finds the best boundary or hyperplane that separates the different classes in the data.

DT is a rule-based technique that represents a set of conditions and their corresponding actions in tabular form. It's commonly used in expert systems to make decisions based on a set of conditions.

The algorithms are primarily supervised learning algorithms, with the exception of KNN which can be used for both supervised and unsupervised learning.

Supervised learning algorithms are trained on labeled data, meaning that the input data has corresponding output labels. The algorithms use the labeled data to learn the relationship between inputs and outputs, and can then make predictions on new data. The supervised learning techniques utilized in this study include k-Nearest Neighbors (KNN), Naive Bayes (NB), Random Forest (RF), the C4.5 decision tree algorithm, Support Vector Machines (SVM), and Decision Table (DT).

RESULTS AND DISCUSSIONS

The results and discussion section presents a comprehensive analysis of the performance metrics obtained from various machine learning algorithms applied to the sarcasm detection task, highlighting the comparative strengths and limitations of each model while offering insights into their practical implications and potential areas for improvement.

To evaluate the effectiveness of different preprocessing techniques, the dataset was subjected to 16 distinct combinations of preprocessing methods, including stemming, stopword removal, lowercasing, and punctuation removal. Each of these preprocessed versions of the dataset was then used to train the machine learning models. The results of these experiments are summarized in Figure 3.

Preprocessing Code	Algorithms	Evaluation Criteria					
		F-Measure	Accuracy	ROC Area/ROC Curve	RMSE	Precision	Recall
0000	IBNN [k=5]	0.65	0.75	0.74	0.50	0.98	0.49
	Naive Bayes	0.81	0.79	0.79	0.46	0.72	0.93
	Random Forest	0.82	0.84	0.84	0.40	0.92	0.74
	C4.5	0.80	0.82	0.82	0.43	0.86	0.75
	Support Vector Machine	0.83	0.84	0.84	0.40	0.87	0.80
	Decision Table						
0001	IBNN [k=5]	0.65	0.75	0.74	0.50	0.98	0.49
	Naive Bayes	0.81	0.79	0.79	0.46	0.72	0.93
	Random Forest	0.82	0.84	0.84	0.40	0.92	0.75
	C4.5	0.81	0.82	0.82	0.42	0.84	0.78
	Support Vector Machine	0.83	0.84	0.84	0.39	0.87	0.80
	Decision Table						
0010	IBNN [k=5]	0.67	0.74	0.75	0.51	0.98	0.49
	Naive Bayes	0.79	0.75	0.76	0.50	0.68	0.93
	Random Forest	0.84	0.83	0.84	0.40	0.88	0.79
	C4.5	0.78	0.79	0.79	0.46	0.79	0.77
	Support Vector Machine	0.82	0.82	0.82	0.42	0.82	0.81
	Decision Table						
0011	IBNN [k=5]	0.68	0.74	0.75	0.51	0.84	0.57
	Naive Bayes	0.79	0.75	0.76	0.50	0.69	0.92
	Random Forest	0.82	0.84	0.84	0.40	0.88	0.78
	C4.5	0.77	0.78	0.78	0.47	0.80	0.75
	Support Vector Machine	0.81	0.82	0.82	0.42	0.82	0.81
	Decision Table						
0100	IBNN [k=5]	0.65	0.75	0.74	0.50	0.98	0.49
	Naive Bayes	0.81	0.79	0.79	0.46	0.72	0.93
	Random Forest	0.82	0.84	0.84	0.40	0.92	0.75
	C4.5	0.79	0.81	0.81	0.44	0.84	0.76
	Support Vector Machine	0.83	0.84	0.84	0.40	0.87	0.80
	Decision Table						
0101	IBNN [k=5]	0.65	0.75	0.74	0.50	0.98	0.49
	Naive Bayes	0.81	0.79	0.79	0.46	0.72	0.93
	Random Forest	0.83	0.85	0.84	0.39	0.93	0.74
	C4.5	0.80	0.81	0.81	0.44	0.83	0.78
	Support Vector Machine	0.83	0.84	0.84	0.40	0.87	0.80
	Decision Table						
0110	IBNN [k=5]	0.67	0.74	0.74	0.51	0.88	0.55
	Naive Bayes	0.79	0.75	0.75	0.50	0.68	0.93
	Random Forest	0.82	0.83	0.83	0.41	0.85	0.80
	C4.5	0.78	0.79	0.79	0.46	0.80	0.76
	Support Vector Machine	0.82	0.82	0.82	0.42	0.82	0.81
	Decision Table						
0111	IBNN [k=5]	0.70	0.75	0.75	0.50	0.85	0.59
	Naive Bayes	0.78	0.75	0.75	0.50	0.68	0.92
	Random Forest	0.82	0.84	0.84	0.40	0.88	0.77
	C4.5	0.77	0.78	0.78	0.47	0.79	0.76
	Support Vector Machine	0.81	0.82	0.82	0.43	0.82	0.80
	Decision Table						
1000	IBNN [k=5]	0.65	0.75	0.74	0.50	0.98	0.49
	Naive Bayes	0.81	0.79	0.79	0.46	0.72	0.93
	Random Forest	0.82	0.84	0.80	0.40	0.92	0.74
	C4.5	0.79	0.80	0.80	0.44	0.85	0.76
	Support Vector Machine	0.83	0.84	0.84	0.40	0.87	0.80
	Decision Table						
1001	IBNN [k=5]	0.65	0.75	0.74	0.50	0.98	0.49
	Naive Bayes	0.81	0.79	0.79	0.46	0.72	0.93
	Random Forest	0.82	0.84	0.84	0.40	0.91	0.74
	C4.5	0.79	0.80	0.80	0.44	0.82	0.77
	Support Vector Machine	0.83	0.84	0.84	0.40	0.86	0.80
	Decision Table						
1010	IBNN [k=5]	0.67	0.74	0.75	0.51	0.89	0.53
	Naive Bayes	0.79	0.75	0.75	0.50	0.68	0.93
	Random Forest	0.82	0.83	0.83	0.41	0.87	0.78
	C4.5	0.79	0.80	0.80	0.45	0.82	0.77
	Support Vector Machine	0.82	0.82	0.82	0.42	0.82	0.81
	Decision Table						
1011	IBNN [k=5]	0.68	0.74	0.75	0.51	0.84	0.57
	Naive Bayes	0.79	0.75	0.76	0.50	0.69	0.92
	Random Forest	0.82	0.84	0.84	0.40	0.88	0.77
	C4.5	0.76	0.79	0.79	0.46	0.80	0.76
	Support Vector Machine	0.81	0.82	0.82	0.42	0.82	0.81
	Decision Table						
1100	IBNN [k=5]	0.65	0.75	0.74	0.50	0.98	0.49
	Naive Bayes	0.78	0.75	0.75	0.46	0.72	0.93
	Random Forest	0.82	0.84	0.84	0.40	0.91	0.75
	C4.5	0.79	0.81	0.80	0.44	0.83	0.76
	Support Vector Machine	0.83	0.84	0.84	0.40	0.87	0.80
	Decision Table						
1101	IBNN [k=5]	0.68	0.76	0.75	0.49	0.98	0.52
	Naive Bayes	0.80	0.77	0.77	0.48	0.70	0.92
	Random Forest	0.83	0.84	0.83	0.41	0.90	0.74
	C4.5	0.81	0.82	0.82	0.42	0.84	0.79
	Support Vector Machine	0.82	0.83	0.83	0.41	0.86	0.78
	Decision Table						
1110	IBNN [k=5]	0.67	0.74	0.74	0.51	0.88	0.55
	Naive Bayes	0.79	0.75	0.75	0.50	0.68	0.93
	Random Forest	0.82	0.83	0.83	0.41	0.86	0.78
	C4.5	0.79	0.79	0.79	0.46	0.79	0.78
	Support Vector Machine	0.82	0.82	0.82	0.42	0.82	0.81
	Decision Table						
1111	IBNN [k=5]	0.70	0.75	0.75	0.50	0.85	0.59
	Naive Bayes	0.78	0.75	0.75	0.50	0.68	0.92
	Random Forest	0.82	0.83	0.83	0.41	0.86	0.78
	C4.5	0.77	0.78	0.78	0.47	0.79	0.76
	Support Vector Machine	0.81	0.82	0.82	0.43	0.80	0.82
	Decision Table						

Figure 3: Overview of the performance of different preprocessing combinations on the dataset.

The models were evaluated using F-Measure, Accuracy, ROC Area, Root Mean Squared Error (RMSE), Precision, and Recall. Among the evaluated algorithms, Random Forest (RF) emerged as the most effective, achieving the highest accuracy and F-Measure scores. Support Vector Machines (SVM) also performed competitively, ranking second in overall performance. In contrast, k-Nearest Neighbors (KNN) exhibited the weakest performance, particularly struggling with high-dimensional feature spaces, as depicted in Figure 4.

Algorithms	Evaulation Criteria					
	F-Measure	Accuracy	ROC Area/ROC Curve	RMSE	Precision	Recall
KNN [k=3]	0.65	0.75	0.74	0.50	0.98	0.49
Naive Bayes	0.81	0.79	0.79	0.46	0.72	0.93
Random Forest	0.82	0.84	0.84	0.40	0.92	0.74
C4.5	0.80	0.82	0.82	0.43	0.86	0.75
Support Vector Machine	0.83	0.84	0.84	0.40	0.87	0.80

Figure 4: Results of the algorithms applied to the raw dataset without preprocessing.

Following the application of preprocessing techniques, the performance of all models was reevaluated. As shown in Figure 5, preprocessing significantly enhanced the performance of most algorithms by reducing noise and inconsistencies in the dataset. The gap in performance among the models narrowed considerably, indicating the importance of preprocessing in sarcasm detection tasks. For example, RF retained its position as the top-performing model, demonstrating robustness across different preprocessing combinations. Similarly, SVM showed notable improvements in its ROC Area and Precision metrics.

KNN [k=3]	0.70	0.75	0.75	0.50	0.85	0.59
Naive Bayes	0.78	0.75	0.75	0.50	0.68	0.92
Random Forest	0.82	0.83	0.83	0.41	0.86	0.78
C4.5	0.77	0.78	0.78	0.47	0.79	0.76
Support Vector Machine	0.81	0.82	0.82	0.43	0.80	0.82

Figure 5: Results of the algorithms applied to the preprocessed dataset.

The data preprocessing steps, such as stemming and punctuation removal, contributed to reducing ambiguities and normalizing the dataset, thereby enhancing the model's ability to identify patterns associated with sarcasm. This highlights the critical role of data preprocessing in machine learning pipelines, particularly in text-based sentiment analysis tasks like sarcasm detection.

In summary, the results underscore the superiority of RF for sarcasm detection in Turkish texts, with preprocessing playing a pivotal role in maximizing model performance. The findings also emphasize the need for further exploration of advanced techniques, such as hyperparameter tuning and multimodal approaches, to enhance sarcasm detection capabilities.

CONCLUSIONS

This study investigated the effectiveness of machine learning algorithms for sarcasm detection in Turkish tweets, addressing a significant gap in the literature for this low-resource language. By training and evaluating various models on a specifically curated Twitter dataset, the research provides valuable insights and benchmarks for future work.

This study highlights the efficiency of machine learning algorithms, particularly RF, in detecting sarcasm in Turkish tweets. When the results are examined in general, it is observed that RF gives the highest accuracy and KNN gives the lowest accuracy for feature-based training. It is observed that the RF model keeps the F-Measure and ROC value higher than the others. Therefore, it can be said that the RF model is generally more successful.

This study also emphasizes the crucial role of data preprocessing. Applying techniques like stemming, stop word removal, lowercasing, and punctuation removal significantly improved the performance of all models. This highlights the importance of cleaning and normalizing text data before feeding it to machine learning algorithms, particularly in sentiment analysis tasks like sarcasm detection.

This research contributes to the field of Turkish Natural Language Processing by providing a robust methodology and benchmark for sarcasm detection. The results obtained demonstrate that the Random Forest (RF) algorithm constitutes an effective method for the task of sarcasm detection. However, the contribution of data preprocessing to the success of this task cannot be overstated. As a result, it is recommended to use the RF model in future studies with this study. Future research could explore multimodal approaches, integrating text, images, and audio data to enhance performance further. Practical applications include social media sentiment analysis and customer feedback evaluation tools. In addition, the gap in the literature on the Turkish language is filled with the study.

ACKNOWLEDGMENT

The authors gratefully acknowledge Gizem ERTİK for her dedicated efforts in collecting the data used in this research.

REFERENCE

Bavkar, D., Kashyap, R., & Khairnar, V. (2023, May). Deep hybrid model with trained weights for multimodal sarcasm detection. *In International Conference on Information, Communication and Computing Technology* (pp. 179-194). Singapore: Springer Nature Singapore.

Bouazizi, M., & Ohtsuki, T. O. (2016). A pattern-based approach for sarcasm detection on twitter. *IEEE Access*, 4, 5477-5488.

Razali, M. S., Halin, A. A., Ye, L., Doraisamy, S., & Norowi, N. M. (2021). Sarcasm detection using deep learning with contextual features. *IEEE Access*, 9, 68609-68618.

Šandor, D., & Babac, M. B. (2023). Sarcasm detection in online comments using machine learning. *Information Discovery and Delivery*, (ahead-of-print).

Verma, P., Shukla, N., & Shukla, A. P. (2021, March). Techniques of sarcasm detection: A review. In 2021 international conference on advance computing and innovative technologies in engineering (ICACITE) (pp. 968-972). IEEE.

Zhang, M., Zhang, Y., & Fu, G. (2016, December). Tweet sarcasm detection using deep neural network. In Proceedings of COLING 2016, *the 26th International Conference on Computational Linguistics: technical papers* (pp. 2449-2460).

Bone Marrow Cell Classification Using U-Net on Imbalanced Dataset

Nesrin AYDIN ATASOY[1]
Amina FARIS ABDULLA AL RAHHAWI[2]

1- Dr.Öğr.Üyesi; Karabük Üniversitesi Mühendislik Fakültesi Bilgisayar Mühendisliği Bölümü. nesrinaydin@karabuk.edu.tr ORCID No: 0000-0002-7188-0020
2- Doktora Öğrencisi; Karabük Üniversitesi Lisansüstü Eğitim Enstitüsü Bilgisayar Mühendisliği Bölümü. engamina22@yahoo.com ORCID No: 0000-0001-9090-326X

ABSTRACT

U-Net is a widely used tool in medical image analysis for precise segmentation; however, it suffers by high memory usage and feature loss. U-Net is improved in this study to improve the stability and efficacy of features for the classification of bone marrow cells and dataset in this work is balanced using random oversampling. Combining improved encoder-decoder connections, random oversampling, and K-means clustering yields exact segmentation and superior precision, thereby providing a dependable, resource-efficient tool for medical imaging in limited conditions. We have proposed standard U-Net and in addition, our model achieved a higher performance The proposed U-Net model is evaluated with higher accuracy, 96.70%. The U-Net model is a good choice for overcoming problems in other deep learning techniques, such as limited resources, time constraints, and clinical medical applications.

Keywords – U-Net, Imbalanced Data, Bone Marrow Cell.

INTRODUCTION

Automated detection systems are vital as human diseases rise, particularly in relation to blood and bone marrow diseases. over more than 100 years old, bone marrow cell sorting still requires professional study to find uncommon very important cells (Guo et al. (2022). Found in the bone marrow (BM), blood cells (BC) are very vital for distributing waste products, nutrients, and oxygen throughout the body's tissues. Comprising three primary forms of BC red blood cells (erythrocytes), white blood cells (leukocytes), and platelets (thrombocytes) the BM is a fundamental component of the blood-forming system (Bone marrow disease, 2023). These BC types can lead to various health problems in the human body, including marrow cancer, thalassemia (Mukhopadhyay et al. 2019), anemia (Shinde et al., 2020), sickle cell disease (Audard et al., 2017), thyroid disorder (Dorgalaleh et al. 2013), aplastic anemia, etc. The pathologist's automatic classification of BC using standard methods such as hemocytometer, complete blood count (Complete blood count, 2023), peripheral blood smear (Peripheral Blood Smear, 2023) and blood film preparation in BM test to identify abnormal cells has a vital role in the diagnosis of blood disease (Preparation and staining methods for blood and bone marrow films, 2023). Although pathological analysis is extensively applied in disease diagnosis, its outcomes are not always consistent. Medical image analysis has been transformed by developments in deep learning, especially CNNs with strong representational learning; these excel in classification (Akter et al., 2024), DeepLab (Chen et al., 2018), and object

detection (Lin et al., 2017). Introduced by Olaf et al. (Ronneberger et al., 2015) [13], U-Net provides scalable and accurate solutions and is a fundamental encoder-decoder architecture for biomedical image segmentation. By addressing U-Net's constraints and combining cutting-edge techniques such attention mechanisms and iterative refinement, variants such U-Net++ (Zhou, 2018), Attention U-Net (Oktay et al., 2018), and GRUU-U-Net (Wollmann et al. 2018) improve segmentation even more.

Nowadays, the development of artificial intelligence plays a vital role in classification and segmentation problems, as in (Wollmann et al., 2018), (Ruberto et al., 2015), (Abdeldaim et al., 2019), (Khamael, 2020). Many studies have been done to classify and segment different types of cells using U-Net, which is the deep learning model (Vo et al., 2022), (Gates et al., 2022), (Bozorgpour et al., 2021), (Rehman et al., 2020) and that has demonstrated its effectiveness in various medical imaging as in (Li et al., 2022), (Yin et al., 2022). Essential for accurate cell, tissue, and organ segmentation in medical uses including diagnosis and therapy planning, the U-Net architecture is built for semantic segmentation in biomedical imaging. Medical imaging has seen success with U-Net in MRI-based DDC classification (Zhou et al., 2024), breast cancer diagnosis by tumor segmentation (Islam et al., 2024), and advanced variations including CLIGUNET for soil stratification (Zhou et al., 2024) and PolSAR image classification (Ren et al., 2024). BM cell segmentation still presents difficulties, nonetheless, including differentiating packed cells (Li, 2020), maintaining accuracy across modalities, as well as managing computing requirements. U-Net for BM cell classification hence optimizing efficiency and reducing computational complexity. Combining improved encoder-decoder connections, random oversampling, and K-means clustering yields exact segmentation and superior precision, thereby providing a dependable, resource-efficient tool for medical imaging in limited conditions.

The study presents U-Net, a modified U-Net architecture that integrates additional concatenation and dropout layers with tuned parameters to address high memory consumption and poor feature extraction, so enabling the extraction of higher-level features and greatly improving classification accuracy.

METHODOLOGY

In this part, we explain in detail the internal structure of our proposed U-shaped network.

Data

First, anonymous experts (Matek, 2021) annotated approximately 170,000 BM cell images from 945 patients including normal and diseased

cells. Second, diversity in data quality: we scaled images to 128 × 128 using bicubic interpolation (Sharma, 2023) to improve model generalizing capabilities. Based on the weighted contribution of adjacent pixels, this approach examined in Eq. 1estimates new pixel values (x, y). Derived from adjacent pixel values, the coefficients a_(ij)ensure smoother and more clear output. Figure 1 shows the resampled images scaled correctly.

$$(x, y) = \sum_{i=0}^{3} \sum_{j=0}^{3} a_{ij}\, x^i\, y^j. \quad (1)$$

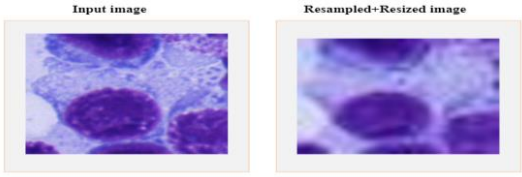

Figure 1: Original and resized image.

Third, we used random oversampling to solve class imbalance, so increasing the dataset size from 171,374 to 216,000 images.

Random centers are initially chosen for K-means clustering, and then convert the cluster centers data into 8-bit values because pixel values in an image are usually represented in 8-bit integers called grayscale images; the normalized method is applied on binary images using min-max normalization.

Proposed Method

BM cell segmentation applied to the U-Net, widely used in medical image segmentation. Its architecture consists of an input layer, an encoding path (contracting path) to extract high-level features, bottleneck, and a decoding path (expanding path) to rebuild the segmentation map. Four convolutional blocks on the encoding path extract hierarchical information: max-pooling lowers spatial dimensions. By use of four up-sampling blocks with transposed convolutions and skip connections, the decoding method recovers spatial features. Predicted masks were thresholded at 0.5 to produce binary masks, which were bitwise AND on original images to retain segmented regions. Pixels with prediction values greater than 0.5 are set to 1, while those below or equal to 0.5 are set to 0 as Figure 2.

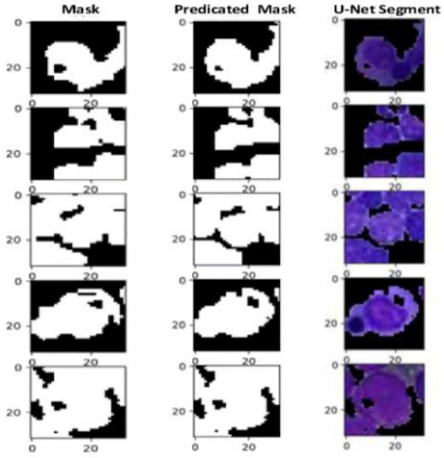

Figure 2: Original and resized image using mask.

Each image is resized to 128x128 pixels and brightness/contrast is consistently normalized in our image preprocessing. Using a U-Net model, images are then segmented whereas the contracting path produces hierarchical feature representations by down-samples using 2x2 max pooling and extracts features through convolutional layers. More complex characteristics are captured in deeper layers. Up-sampling (2x2) restores spatial dimensions in the expanding path; skip connections combine low- and high-level information from both paths. After flattening these features into a 1D vector, they pass into a dense layer (256 neurons, ReLU) with a dropout rate of 0.5 for regularization. For class probabilities the output layer employs SoftMax activation with 21 neurons. Using a batch size of 100 and categorical cross-entropy loss and an Adam optimizer (learning rate: 1e-4), training takes 30 epochs.

RESULT AND DISCUSSION

We have examined these models using the testing data and evaluated their performance.

$$\text{Accuracy} = \frac{TP+TN}{TP+TN+FP+FN} \quad (3)$$

$$\text{Precision} = \frac{TP}{TP+FP} \quad (4)$$

$$\text{Specificity} = \frac{TN}{TN+FP} \quad (5)$$

$$\text{Recall} = \frac{TP}{TP+FN} \quad (6)$$

$$\text{F1} - \text{score} = \frac{2*(\text{Precision}*\text{Recall})}{\text{Precision}+\text{Recall}} \quad (7)$$

$$\text{IoU} = \frac{TP}{TP+FP+FN} \quad (8)$$

Our aim in this work was to improve BM cell segmentation and classification with the U-Net model. To solve class imbalance, the 171,373 BM cell image collection has been increased to 216,000 images by random oversampling. Then the data was split 20% for testing and 80% for training. Preprocessing included masking images to separate regions of interest for segmentation; the trained U-Net model produced predicted binary masks for every image to identify "Mask" and "No-Mask" areas. Table 1 shows the performance of the model evaluated across several criteria: accuracy, precision, recall, F1-score, specificity, and IoU. With the IoU being vital for evaluating the accuracy of the segmentation results. Table 2 shows performance metrics for all class.

Table 1: Segmentation performance metrics.

Class name	Precision (%)	Sensitivity (%)	Specificity (%)	F1-score (%)	Accuracy (%)	IoU (%)
Mask	97.13	97.59	94.84	97.36	96.61	94.86
No-Mask	95.65	94.84	97.59	95.25	96.61	91.93

Table 2: Performance metrics of the standard U-Net model.

Class name	Precision (%)	Recall (%)	Specificity (%)	F1-score (%)	Accuracy (%)
ABE	100	100	100	100	100
ART	100	100	100	100	100
BAS	100	100	100	100	100
BLA	100	99.92	100	99.96	99.56
EBO	99.93	99.98	99.99	99.96	95.99
EOS	99.92	99.75	100	99.83	96.99
FGC	99.90	100	100	99.95	96.07
HAC	100	100	100	100	98
KSC	100	100	100	100	100
LYI	100	100	100	100	96.44
LYT	99.19	99.80	99.88	99.49	98.87
MMZ	95.51	93.60	99.90	94.55	97.75
MON	91.82	94.30	99.80	93.04	95.67
MYB	94.82	93.81	99.80	94.31	96.58
NGB	86.37	90	99.31	88.15	95.88
NGS	95.77	95.48	99.32	95.63	96.79
NIF	96.93	88.30	99.93	92.41	96.66
OTH	98.43	100	99.96	99.21	95.96
PEB	92.92	97.10	99.82	94.96	97.76
PLM	88.28	91.81	99.53	90.01	96.25
PMO	96.88	91.83	99.83	94.29	95.38

Using feature fusion, hyperparameter adjusting to achieve exceptional accuracy, this work presents an enhanced U-Net for BM cell classification, therefore addressing memory constraints. The model much outperforms standard U-Net by combining random oversampling for class balancing with K-means for accurate segmentation. Dimensionality reduction and feature selection improve memory consumption, therefore enabling effective cross-valuation and stable performance. Future directions reflect further memory optimization, distributed computing, and applications to various medical imaging datasets, therefore illustrating the model's versatility and clinical value in environments with limited resources.

REFERENCE

L. Guo et al. (2022). A classification method to classify bone marrow cells with class imbalance problem. Biomed. Signal Process. Control. Accessed: Jul. 12, 2024. [Online]. Available: https://www.sciencedirect.com/science/article/pii/S1746809421008934

Bone Marrow Diseases. Accessed: Mar. 26, 2023. [Online]. Available: https://medlineplus.gov/bonemarrowdiseases.html

M. Mukhopadhyay et al. (2019). Detection of Thalassaemia Carriers by Automated Feature Extraction of Dried Blood Drops. May 2019, Accessed: Apr. 14, 2023. [Online]. Available: https://arxiv.org/abs/1905.10253v1

S. Shinde, N. Sharma, P. Bansod, M. Singh, and C. K. Singh Tekam. (2020). Automated nucleus segmentation of leukemia blast cells: Color spaces study. 2nd Int. Conf. Data, Eng. Appl. (IDEA), Feb. 2020, doi: 10.1109/IDEA49133.2020.9170721.

V. Audard, P. Bartolucci, and T. Stehlé. (2017). Sickle cell disease and albuminuria: recent advances in our understanding of sickle cell nephropathy. Clin. Kidney J., vol. 10, no. 4, pp. 475–478, Aug. 2017, doi: 10.1093/CKJ/SFX027.

A. Dorgalaleh et al. (2013). Effect of Thyroid Dysfunctions on Blood Cell Count and Red Blood Cell Indice. Iran J. Ped. Hematol. Oncol., vol. 3, no. 2, p. 73, 2013, Accessed: Jun. 06, 2023. [Online]. Available: /pmc/articles/PMC3915449/

Complete blood count (CBC) - Mayo Clinic. (2023) Accessed: Jun. 06, 2023. [Online]. Available: https://www.mayoclinic.org/tests-procedures/complete-blood-count/about/pac-20384919

Peripheral Blood Smear (PBS): What It Is & Test Interpretation. (2023) Accessed: Apr. 17, 2023. [Online]. Available: https://my.clevelandclinic.org/health/diagnostics/22742-peripheral-blood-smear-test

Preparation and staining methods for blood and bone marrow films | Clinical Gate. (2023) Accessed: Apr. 17, 2023. [Online]. Available: https://clinicalgate.com/preparation-and-staining-methods-for-blood-and-bone-marrow-films/

Akter et al. (2024). Robust clinical applicable CNN and U-Net based algorithm for MRI classification and segmentation for brain tumor. Expert Syst. Appl., vol. 238, p. 122347, Mar. 2024, doi: 10.1016/J.ESWA.2023.122347.

L. C. Chen, G. Papandreou, I. Kokkinos, K. Murphy, and A. L. Yuille. (2018). DeepLab: Semantic image segmentation with deep convolutional nets, atrous convolution, and fully connected CRFs," IEEE Trans. Pattern Anal. Mach.

Intell., vol. 40, no. 4, pp. 834–848, Apr. 2018, doi: 10.1109/TPAMI.2017.2699184.

T.-Y. Lin, P. Dollar, R. Girshick, K. He, B. Harihara, and S. Belongie. (2017). Feature Pyramid Networks for Object Detection. [Conference/ArXiv preprint if not published in proceedings—no further info provided.

O. Ronneberger, P. Fischer, and T. Brox. (2015). U-net: Convolutional networks for biomedical image segmentation. Lecture Notes in Computer Science (including subseries Lecture Notes in Artificial Intelligence and Lecture Notes in Bioinformatics), vol. 9351, pp. 234–241, 2015, doi: 10.1007/978-3-319-24574-4_28/COVER.

Z. Zhou, M. M. Rahman Siddiquee, N. Tajbakhsh, and J. Liang. (2018). Unet++: A nested u-net architecture for medical image segmentation. Lecture Notes in Computer Science (including subseries Lecture Notes in Artificial Intelligence and Lecture Notes in Bioinformatics), vol. 11045, pp. 3–11, 2018, doi: 10.1007/978-3-030-00889-5_1/FIGURES/3.

O. Oktay et al. (2018). Attention U-Net: Learning Where to Look for the Pancreas. Apr. 2018, Accessed: Jul. 04, 2024. [Online]. Available: https://arxiv.org/abs/1804.03999v3

T. Wollmann, M. Gunkel, I. Chung, H. Erfle, K. Rippe, and K. Rohr. (2019). GRUU-Net: Integrated convolutional and gated recurrent neural network for cell segmentation. Med. Image Anal., vol. 56, pp. 68–79, Aug. 2019, doi: 10.1016/J.MEDIA.2019.04.011.

X. Zheng, Y. Wang, G. Wang, and J. Liu. (2018). Fast and robust segmentation of white blood cell images by self-supervised learning," Micron, vol. 107, pp. 55–71, Apr. 2018, doi: 10.1016/J.MICRON.2018.01.010.

C. Di Ruberto, A. Loddo, L. Putzu. (2015). A multiple classifier learning by sampling system for white blood cells segmentation. Comput. Anal. Images Patterns: 16th Int. Conf. CAIP, vol. 9257, pp. 415–425, 2015, doi: 10.1007/978-3-319-23117-4_36.

M. Abdeldaim, A. T. Sahlol, M. Elhoseny, and A. E. Hassanien. (2018). Computer-aided acute lymphoblastic leukemia diagnosis system based on image analysis. Stud. Comput. Intell., vol. 730, pp. 131–147, 2018, doi: 10.1007/978-3-319-63754-9_7/COVER.

L. D. Khamael, J. Banks, K. Nugyen, A. Al-Sabaawi, I. Tomeo-Reyes, and V. Chandran. (2020). Segmentation of white blood cell, nucleus and cytoplasm in digital haematology microscope images: A review–challenges, current and future potential techniques. IEEE Rev. Biomed. Eng., 2020, doi: 10.1109/RBME.2020.3004639.

Q. H. Vo, X.-H. Le, T.-H. Le, and T.-T.-H. Pham. (2022). A deep learning approach in detection of malaria and acute lymphoblastic leukemia diseases utilising blood smear microscopic images. Vietnam J. Sci. Technol. Eng., vol. 64, no. 1, pp. 63–71, Mar. 2022, doi: 10.31276/VJSTE.64(1).63-71.

Q. D. Gates, M. Allali, and C. Martin-King. (2022). Detection and Classification of Cells in Colorectal Histology Images Utilizing U-Net Machine Learning Architecture," SSRN Electron. J., Jan. 2022, doi: 10.2139/SSRN.3981501.

A. Bozorgpour, R. Azad, E. Showkatian, and A. Sulaiman. (2021). Multi-scale Regional Attention Deeplab3+: Multiple Myeloma Plasma Cells Segmentation in Microscopic Images. May 2021, Accessed: Apr. 03, 2023. [Online]. Available: https://arxiv.org/abs/2105.06238v1

M. U. Rehman, S. Cho, J. H. Kim, and K. T. Chong. (2023). BU-Net: Brain Tumor Segmentation Using Modified U-Net Architecture. Electronics, vol. 9, no. 12, p. 2023, Dec. 2020, doi: 10.3390/ELECTRONICS9122203.

B. Li, S. Liu, F. Wu, G. H. Li, M. Zhong, and X. Guan. (2022). RT-Unet: An advanced network based on residual network and transformer for medical image segmentation," Int. J. Intell. Syst., 2022, doi: 10.1002/INT.22956.

S. Yin, H. Deng, Z. Xu, Q. Zhu, and J. Cheng. (2022). SD-UNet: A Novel Segmentation Framework for CT Images of Lung Infections. Electronics, vol. 11, no. 1, p. 130, 2022, Accessed: Jul. 18, 2023. [Online]. Available: https://www.mdpi.com/2079-9292/11/1/130

D. Zhou et al. (2024). M-DDC: MRI based demyelinative diseases classification with U-Net segmentation and convolutional network. Neural Netw., vol. 169, pp. 108–119, Jan. 2024, doi: 10.1016/J.NEUNET.2023.10.010.

M. R. Islam et al. (2024). Enhancing breast cancer segmentation and classification: An Ensemble Deep Convolutional Neural Network and U-net approach on ultrasound images. Mach. Learn. Appl., vol. 16, p. 100555, Jun. 2024, doi: 10.1016/J.MLWA.2024.100555.

X. Zhou, P. Shi, B. Sheil, and S. Suryasentana. (2024). Knowledge-based U-Net and transfer learning for automatic boundary segmentation. Adv. Eng. Inform., vol. 59, p. 102243, Jan. 2024, doi: 10.1016/J.AEI.2023.102243.

S. Ren, F. Zhou, and L. Bruzzone. (2024). Transfer-Aware Graph U-Net with Cross-Level Interactions for PolSAR Image Semantic Segmentation. Remote Sens., vol. 16, no. 8, p. 1428, Apr. 2024, doi: 10.3390/RS16081428.

H. Li, X. Zhao, A. Su, H. Zhang, J. Liu, and G. Gu. (2020). Color Space Transformation and Multi-Class Weighted Loss for Adhesive White Blood Cell Segmentation. IEEE Access, vol. 8, pp. 24808–24818, 2020, doi: 10.1109/ACCESS.2020.2970485.

C. Matek, S. Krappe, C. Münzenmayer, T. Haferlach, and C. Marr. (2021). Highly accurate differentiation of bone marrow cell morphologies using deep neural networks on a large image data set. Blood, vol. 138, no. 20, pp. 1917–1927, Nov. 2021, doi: 10.1182/blood.2020010568.

A. Sharma. (2023). Resizing Images using Various Interpolation Techniques. Medium. Accessed: Apr. 29, 2023. [Online]. Available: https://annmay10.medium.com/resizing-images-using-various-interpolation-techniques-4b99800999f2

PVC-Confined Concrete Columns

Ahmet Emin KURTOĞLU[1]

1- Assoc. Prof. Dr.; Igdir University, Engineering Faculty, Department of Civil Engineering.
aemin.kurtoglu@igdir.edu.tr ORCID No: 0000-0003-2847-9175

ABSTRACT

This chapter explores the role of PVC confinement in enhancing the structural performance of concrete columns. Composite structures, which integrate materials with complementary properties, address the limitations of traditional construction materials. PVC, with its lightweight, cost-effectiveness, and resistance to environmental degradation, emerges as a promising alternative for confining concrete. A comprehensive review of experimental studies demonstrates significant improvements in strength, ductility, and durability when PVC wraps are applied, particularly for low-strength concrete. However, challenges remain in optimizing dimensions, understanding long-term performance, and standardizing design practices. Addressing these gaps could revolutionize construction in seismic zones, marine environments, and corrosive settings. PVC confinement offers a sustainable solution for modern infrastructure, paving the way for innovative structural applications.

Keywords –PVC confinement, Composite columns, Structural engineering, Ductility enhancement, Sustainable construction

INTRODUCTION

The properties of building materials used in civil engineering are different from each other. For this reason, it is not possible to talk about the existence of a single material that can be used in all conditions. It may be necessary to use materials with different properties to provide optimum solutions in different conditions. In some cases, the use of different materials can solve problems, but these solutions cannot be fast and economical. What is expected from engineering is to solve problems in the fastest and most economical ways. Therefore, new solutions are sought by combining different materials. By combining the advantageous conditions of different materials, high strength, resistant to external influences, practical, economical materials can be obtained. The structure created by combining two or more materials is called a composite structure (Sadoon, 2010).

Materials such as concrete, steel profile, PVC tube, steel tube, FRP wrap can be used to form composite columns. In the section shown with in Figure 1(a), the material used in the inner section is covered with concrete material from the outside in order to increase the strength of the material used in the inner section, to limit torsion and buckling situations, and to protect it from external influences. In the section shown in Figure 1 (b), composite structures were formed by wrapping in order to limit the expansion of the inner concrete material, protect the concrete from external effects, and use the outer material as a mold for concrete.

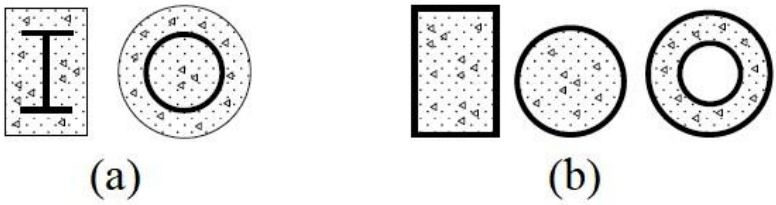

Figure 1: Different types of composite column sections (Sadoon, 2010)

As the structures used in engineering grow, the need for high strength columns arises. For steel structures, this situation can be solved by increasing the cross-section or using steel with high yield strength. In reinforced concrete structures, solutions are sought by using high-strength concrete or by increasing the cross-section. High yield strength in steel can be combined with high compressive strength in concrete to form composite structures. This increases the strength and ductility of concrete and prevents buckling of steel. The use of composite elements provides advantages in terms of speed and economy (Vatansever and Şimşek, 2021).

The Role of PVC in Structural Engineering

With the researches on the materials to be used in composite structures, weaknesses in these structures are tried to be improved. Lateral winding and low energy absorption capacity can be shown among these weaknesses. Plastic tube winding can be shown as a good alternative to overcome this situation. PVC, uPVC and HDPE material tubes can be used as plastic tube types. The studies show that plastic tube wraps have a positive effect on concrete strength and ductility (Karthikeyan, 2018).

Boersma and Brenn (2005) investigated the long-term performance of existing PVC water transmission lines. In the study, it is stated that the life span of the pipes is approximately 50 years and the question of whether it is necessary to replace the pipes at the end of 50 years is sought to be answered. The researchers examined PVC deformation under the headings of chemical degradation, physical aging and mechanical damage. As a result of the study, it was stated that currently produced high quality pipes should have a lifespan of more than 100 years. From this study, it is understood that PVC is resistant to physical, chemical and mechanical adversities. Therefore, it can be said that it increases the durability of concrete by protecting the concrete core from external influences.

The use of composite structures has become more common in high-rise buildings due to the combination of the advantages of steel and concrete. PVC pipes have advantages such as light weight, low cost, easy installation, insulation, resistance to chemical environments, resistance to external

influences, and can be a good alternative to steel where there is a risk of corrosion (Jamaluddin, 2017).

Restraining concrete laterally increases its mechanical performance and durability. Among these restraints, PVC stands out. PVC wraps the concrete and increases its ductility and strength. In addition, PVC shows durability in sea salty and chemical environments, allowing concrete to maintain its strength. Therefore, the importance of PVC increases especially in coastal areas (Bazli et al., 2020).

Literature Review

Studies on PVC-Confined Columns

Different needs or reasons that arise today lead people to produce different solutions in every field. This situation provides new and different perspectives in engineering branches. Situations such as the brittle structure of concrete and the negative effects of external influences on concrete have led to the emergence of the concept of composite columns. Composite columns are formed by wrapping materials such as PVC, FRP, steel tube around the concrete column. In this part, the studies on this the behavior of PVC wrapped composite columns under axial pressure are summarized below.

Sadoon (2010) tested 30 PVC composite column specimens to evaluate their compressive strength, PVC thickness and slenderness. The experiments showed that PVC wrap increased the ultimate strength of concrete between 1.419 to 1.896 times for column specimens with a core concrete strength of 30 MPa and between 1.118 to 1.405 times for column specimens with a core concrete strength of 50 MPa. The ultimate strength and deformation increased as the PVC pipe thickness increased.

Wang and Yang (2012) observed the effects of varying pipe thickness and concrete strength on the ultimate strength, stress-strain graph and ductility of concrete-filled PVC composite column specimens. Two types of specimens were used in the study. One of these specimens is core concrete with a diameter of 110 mm and a height of 220 mm, and the other is a PVC-wrapped column specimen with an outer diameter of 110 mm and a height of 220 mm. As the PVC thickness increases, the outer diameter of the specimen remains constant and therefore the diameter of the core concrete decreases. As a result of the experiments, it was observed that the ultimate strengths and strength increase indices (SI) of the wrapped specimens with C30 and C45 core concrete strength increased as the PVC thickness increased, while these values did not change significantly in the wrapped specimens with C60 core concrete strength. In the specimens with the same thickness of PVC, as the core concrete strength increased, an increase in the wrapped concrete strength and a decrease in the SI index were observed. The absolute value of the slope of the lines after the peak of the stress-strain graphs decreased when the concrete strength was kept constant and the PVC pipe thickness

was increased, while the absolute value of the slope increased when the PVC thickness was kept constant and the concrete strength was increased. The deformation of PVC wrapped concrete is 1.415 to 5.54 times higher than that of core concrete. This shows that PVC wrap significantly increases the ductility of concrete.

Gupta (2013) conducted experiments with three different concrete classes and three different diameters of uPVC under axial compression and compared the data obtained from the experiments with the data in the literature. Thus, the wrapping concrete columns with uPVC increased the compressive strength and ductility of concrete. uPVC wrapping effect differed from the studies in the literature by maximum 6%. It is stated that as the D (diameter) to tp (thickness) ratio decreases in the experiments, the absolute value of the slope of the curve after the peak in the load-displacement graph decreases.

Gathimba (2015) conducted experiments under axial compression using uPVC material to wrap and protect concrete from external influences. He used three different concrete strength classes, three different uPVC diameters and two different uPVC wall thicknesses. The specimens were tested under compressive load and the test data were obtained by means of LVDT and strain gauges. The confined to unconfined concrete strength ratio values were greater than 1, therefore, the wrapping provided an increase in strength. The effect of wrapping decreased as the concrete strength increased. It is concluded that wrapping is more effective in low strength concrete. It is stated that specimens using low strength concrete show more ductile behavior since they are exposed to more deformation. It was observed that the strength of the specimens decreased as the slenderness ratio increased. As the diameters of the specimens increased, the load capacities also increased.

Oyawa et al. (2015) investigated the axial compression effect of concrete-filled uPVC composite columns on specimens of different strengths, different diameters and different lengths. For this study, 72 unwrapped and 72 uPVC wrapped column specimens were used. As a result of the research, they observed that the strength of uPVC wrapped concrete varied between 1.18 and 3.65 times compared to unwrapped specimens. Hence, as the diameter of the specimens subjected to the test increased, their load carrying capacity also increased. However, as the height/diameter ratio increased, a decrease in the specimen strength was observed. Another observation is that as the concrete strength increases, the wrapping effect decreases. This indicates that wrapping increases the strength of low strength concrete more than high strength concrete.

Osman and Soliman (2015) subjected four different heights of PVC wrapped composite column specimens to axial compression tests. In the study, PVC wrapping increased the load capacity and ductility of the column. As a result of the study, it is stated that wrapping significantly

improves the overall behavior of concrete and can be used in structural applications. It is also observed that PVC wrapping increases the energy absorption capacity of the specimen.

Fakharifar and Chen (2017) subjected three PVC-wrapped composite column specimens to axial compression tests. These specimens were obtained by using PVC tube as a mold and pouring concrete into it. In the experiments, they observed that the effect of PVC wrapping on concrete strength was limited, but the ductility increased between 1.81 and 4.07 times by preventing the concrete from expanding and bursting.

Mammen and Antony (2017) examined the changes of 9 concrete specimens of 350 mm in height and 160 mm in diameter with PVC wraps of different thicknesses under axial compression. Results showed that the PVC wrap increased the axial load carrying capacity of the column specimen. The increase in the wall thickness of the PVC wrap caused increases in the stress-strain graph and axial load carrying capacity. Compared to the core concrete, it is seen that the wrapped concrete provides a strength increase between 7% and 15%.

Karthikeyan et al. (2018) observed the strength changes in concretes wrapped with HDPE, PVC and uPVC with a total of 12 specimens. In the axial compression tests, PVC-wrapped concrete gained 19.43% strength compared to unwrapped concrete. All of the concrete filled PVC composite specimens fractured brittlely.

Azeez et al. (2018) tested 36 PVC composite column specimens under axial compression in their study. The column specimens they used have a height of 200 mm, an outer diameter of 100 mm, and PVC thicknesses of 3.5 mm and 4.8 mm. The concrete classes used in the study were C20, C25 and C40. The result of the study showed that the strength of PVC wrapped concrete samples increased between 32.24 and 83.25 percent compared to the core concrete strength. The specimens with 4.8 mm thick PVC tube showed higher ultimate strength and deformation than the specimens with 3.5 mm thick PVC tube.

Woldemariam et al. (2019) determined five different concrete strengths (C15, C20, C25, C30, C35), four different uPVC diameters (63 mm, 90 mm, 110 mm, 140 mm) and specimen heights with a height/diameter ratio of 2 and analyzed these specimens under axial compression. uPVC wrapping was observed to perform better in low-strength concrete compared to high-strength concrete. The absolute value of the slope of the part of the stress-strain curve after the peak decreased as the uPVC wall thickness/diameter ratio increased. The strength of the uPVC wrapped specimen was 1.28 to 2.36 times higher than the core concrete strength. Unwrapped concrete showed brittle fracture while uPVC wrapped concrete showed ductile fracture.

Raheemah and Resan (2020) investigated the slenderness effects of PVC-filled concrete columns under axial compression. In the experiments,

five core concrete and eleven PVC composite columns were tested. The PVC wrap increased the concrete strength between 1.645 and 2.42 times. In addition, the graph given in the article shows that as the H/D ratio increases from 14.67 to 17.46, the ultimate load that the composite column can carry decreases from 93.27 kN to 58.10 kN, and as the D/tp ratio increases from 13.40 to 34.09, the ultimate load that the composite column can carry decreases from 120 kN to 93.27 kN.

N.A. Abdulla (2020) aims to investigate the effects of uPVC pipe on the strength and ductility values of concrete specimens under axial compression. Experiments were conducted with 9 uPVC wrapped specimens with variable D/tp ratio and 4 unwrapped concrete specimens with different slenderness ratios. A 20% increase in the specimen length decreased the specimen strength by approximately 14%. Thus, the use of uPVC pipe prevented brittle fracture and the specimens exhibited ductile behavior.

N.A. Abdulla (2021) conducted some experiments by wrapping concrete specimens subjected to axial compression with uPVC to improve their performance after peak strength. With 18 uPVC wrapped specimens, he investigates the effects of changes in uPVC diameter, wall thickness and H/D ratio on the specimens. It is stated that the deformation of the uPVC wrapped specimen is 1.62 to 3.29 times higher than the unwrapped concrete. It is observed that as the D/tp ratio decreases, the deformation of the specimens at peak stress increases. The increase in H/D ratio negatively affects the specimen strength.

Comparative Performance

Figure 2 and Figure 3 show the ductile behavior of concrete specimens that lost their strength due to uPVC wraps. Figure 4 shows the behavior of unwrapped concrete, FRP wrapped concrete and PVC wrapped concrete. In the graph, it is seen that FRP wrapping increases the strength of concrete more than PVC, but FRP wrapped concrete shows a brittle behavior while PVC wrapped concrete shows a ductile behavior.

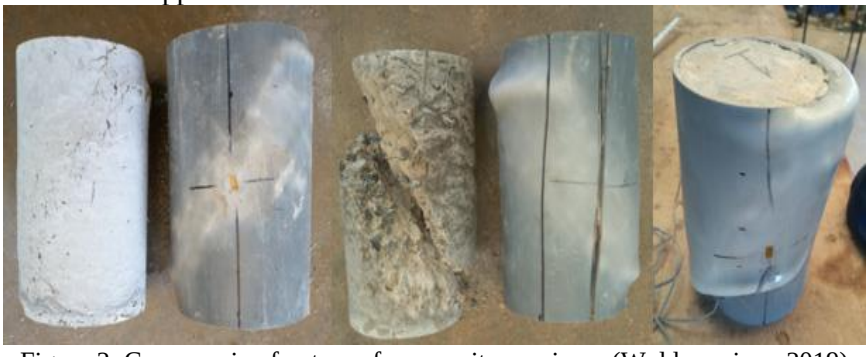

Figure 2: Compressive fracture of composite specimen (Woldemariam, 2019)

Figure 3: Shear fracture of composite specimen (Woldemariam, 2019)

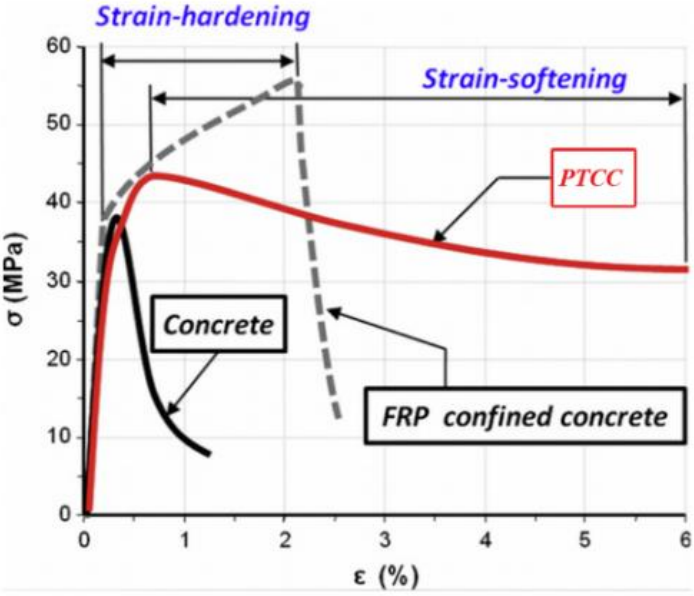

Figure 4: Stress-strain comparison of concrete with and without wraps (Wang and Yang, 2012)

Applications and Advantages of Composite Columns

Since concrete-filled composite tubes provide high strength, rigidity and ductility, they are widely used in modern bridges, high-rise buildings, stadiums and offshore structures. In addition, high viaducts and electric poles are among the areas where composite columns are used. Figures 5 and 6 show structures constructed with concrete-filled steel tube columns. The columns of the 50-storey building shown in Figure 5 are assumed to be concrete-filled steel tubes. The dimensions of the columns are thus reduced by 50% (Liew et al., 2016)

Figure 5: Use of concrete-filled steel tube in high-rise buildings (Liew et al., 2016)

(a) (b)

(c) (d)

Figure 6: Structural applications of concrete-filled steel tubes: (a) Wangcang East River Bridge (b) Ruifeng building in Hangzhou (c) SEG plaza in Shenzhen (d) Canton Tower (Han et al., 2014)

The use of PVC pipes is a good alternative for reinforced concrete structures to maintain their strength and integrity under adverse environmental conditions. However, since the studies in the literature about this method are still in the beginning stage, information and data about the method are very limited. PVC wrap has the functions of reducing the water loss of concrete due to hydration, eliminating the curing process, protecting the concrete from temperature changes, making the concrete impermeable, preventing the concrete core from expanding and bursting, and being a protective cover for concrete in situations that may deteriorate the structure of concrete such as marine environments and bridge piers. (Abdulla, 2017)

Challenges and Research Gaps

Despite its numerous advantages, the use of PVC confinement in structural engineering poses several challenges and areas for further research:

Optimization of PVC Dimensions: Determining the ideal wall thickness, diameter, and height-to-diameter ratio for PVC wraps remains a critical area for exploration. While thicker PVC walls generally enhance strength, their cost-effectiveness and practical feasibility need evaluation.

Long-Term Performance: The behavior of PVC-confined concrete under sustained loads and exposure to environmental factors like temperature variations and UV radiation requires extensive study. Understanding how these variables impact the material's mechanical properties is vital for long-term applications.

Dynamic Load Behavior: The performance of PVC-wrapped columns under dynamic conditions such as seismic events and repeated loading cycles remains unclear. Investigating their ductility and energy absorption capabilities in these scenarios could expand their usability in earthquake-prone regions.

Hybrid Confinement Systems: Combining PVC wraps with other materials such as FRP or steel to achieve enhanced mechanical performance and cost-effectiveness is an emerging area. Hybrid systems could leverage the benefits of multiple materials while mitigating individual limitations.

Standardization and Guidelines: The lack of standardized testing methods and design guidelines for PVC-confined columns limits their adoption in practical applications. Establishing codes and specifications based on experimental and analytical data is essential for widespread implementation.

By addressing these challenges, researchers and practitioners can unlock the full potential of PVC confinement, paving the way for innovative and sustainable structural solutions.

CONCLUSIONS

PVC confinement has the potential to revolutionize composite column design. By enhancing strength, ductility, and environmental resistance, it offers a sustainable solution for modern construction. Its application in seismic zones, marine environments, and corrosive settings could significantly reduce maintenance costs and extend the lifespan of infrastructure.

Future research focusing on hybrid systems and performance under extreme conditions will further expand its applicability. Additionally, the establishment of standardized guidelines and construction practices will streamline its adoption in the industry, ensuring consistent and reliable outcomes. By embracing these advancements, engineers and researchers can contribute to creating more resilient, cost-effective, and sustainable structures, ultimately shaping the future of modern construction.

REFERENCES

Abdulla, N.A. (2021). A strain model for uPVC tube-confined concrete. *Cogent Engineering, 8*(1), 1-27.

Azeez, A.A., Jamaluddin, N., Rahman, N.A., Hassen, D.A., & Attiyah, A.N. (2018). Experimental and analytical study of PVC confined concrete cylinders. *Journal of Engineering and Applied Sciences, 13*(8), 2145-2151.

Bazli, M., Bazli, L., Rahmani, R., Mansoor, S., Ahmadi, M., & Pouriamanesh, R. (2020). Concrete filled FRP–PVC tubular columns used in the construction sector: A review. *Journal of Composites and Compounds, 2*(4), 155-162.

Boersma, A., & Brenn, J. (2005). Long term performance prediction of existing PVC water distribution systems. *9th International Conference PVC*, Brighton, England.

Fakharifar, M., & Chen, G. (2017). FRP-confined concrete filled PVC tubes: A new design concept for ductile column construction in seismic regions. *Construction and Building Materials, 130*, 1-10.

Gathimba, N.K. (2015). Performance of UPVC pipe confined concrete columns in compression (Master's thesis). Jomo Kenyatta University of Agriculture and Technology, JKUAT, Kenya.

Gupta, P.K. (2013). Confinement of concrete columns with unplasticized polyvinyl chloride tubes. *International Journal of Advanced Structural Engineering, 5*(19), 1-8.

Han, L. H., Li, W., & Bjorhovde, R. (2014). Developments and advanced applications of concrete-filled steel tubular (CFST) structures: Members. *Journal of Constructional Steel Research, 100*, 211-228.

Jamaluddin, N., Azeez, A.A., Abd Rahman, N., Attiyah, A.N., Wan İbrahim, M.H., Mohamad, N., & Adnan, S.H. (2017). Experimental investigation of concrete filled PVC tube columns confined by plain PVC socket. *MATEC Web of Conferences, 103*.

Karthikeyan, N., Akshatha, B.A., Sudhesh, A.S., & Basavaraja, N.H. (2018). Assessment of concrete cylinders confined with HDPE, PVC & UPVC tubes. *International Journal of Scientific & Engineering Research, 9*(4), 83-87.

Liew, J. R., Xiong, M., & Xiong, D. (2016, November). Design of concrete filled tubular beam-columns with high strength steel and concrete. *Structures*, *8*, 213-226. Elsevier.

Mammen, A.M., & Antony, M. (2017). Experimental study on FRP-PVC confined circular columns. *International Research Journal of Engineering and Technology, 4*(5), 1386-1390.

Osman, M., & Soliman, A.E.K.S. (2015). Behavior of confined columns under different techniques. *International Journal of Structural and Construction Engineering, 9*(1), 70-78.

Oyawa, W.O., Gathimba, N.K., & Manguriu, G.N. (2015). Innovative composite concrete filled plastic tubes in compression. *The 2015 World Congress on Advances in Structural Engineering and Mechanics (ASEM15)*, Incheon, Korea, 1-15.

Raheemah, M.A., & Resan, S.F. (2020). Structural behaviour of slender PVC composite columns filled with concrete. *3rd International Conference on Engineering Sciences, IOP Conf. Series: Materials Science and Engineering*, Kerbela, Iraq.

Sadoon, A.S. (2010). Experimental and theoretical investigation of PVC-concrete composite columns (Doctoral thesis). University of Basrah, College of Engineering, Iraq, 134.

Vatansever, C., & Şimşek, Y.E. (2021). Taşıyıcı sistemi beton dolgulu kompozit kolonlar ve çelik kirişlerden oluşan çok katlı bir binanın tasarımı ve zaman tanım alanında doğrusal olmayan analizi. *Pamukkale Üniversitesi Mühendislik Bilimleri Dergisi, 27*(3), 264-273.

Wang, J.Y., & Yang, Q.B. (2012). Investigation on compressive behaviors of thermoplastic pipe confined concrete. *Construction and Building Materials, 35*, 578-585.

Woldemariam, A.M., Oyawa, W.O., & Nyomboi, T. (2019). Structural performance of uPVC confined concrete equivalent cylinders under axial compression loads. *Buildings, 9*(82).

By Jointly Opposite Selection Strategy Improving the Humpback Whale Optimization Algorithm

Kadri DOĞAN*[1]
Hasan BAŞAK[2]

*Artvin Çoruh Ünivesitesi, Mühendislik Fakültesi, Temel Bilimler Bölümü, Artvin, Türkiye dogankadri@artvin.edu.tr, ORCID: 0000-0002-6622-3122
Artvin Çoruh Ünivesitesi, Mühendislik Fakültesi, Elektrik Elektronik Mühendisliği Bölümü, Artvin, Türkiye hasanbasak@artvin.edu.tr, ORCID: 0000-0002-3724-6819

ABSTRACT

The humpback whale optimization algorithm (WOA) is a well-known metaheuristical optimization algorithm in the literature. It is an algorithm widely used by researchers as an important tool for easy applicability and effective results. Jointly opposite selection (JOS), which is formed by combining two opposition strategies, namely Dynamic Opposition (DO) and Selective Leader Opposition (SLO), is a recently defined opposition strategy. Significant improvements are seen in the studies conducted with JOS. Therefore, in this study, JOS strategy was used to eliminate the disadvantages of the WOA optimization algorithm and the WOAJOS and WOA algorithms were compared using CEC2017 benchmarks. The comparison covers composition, hybrid, multimodal and unimodal functions. In the comparison, it was shown that better results were achieved by looking at Exploration-Exploitation, Diversity Analysis, Convergence and stability analysis.

Keywords: WOA, JOS, WOAJOS, Meta-Heuristic, Optimization Algorithm

INTRODUCTION AND PRELIMİNARIES

Metaheuristic algorithms are powerful and flexible methods used to solve complex and large optimization problems. These algorithms provide a general solution for different problems and are of great importance in various application areas. Here are the metaheuristic algorithms, They can handle large and complex problems that cannot be solved by traditional methods, They can find solutions close to the global optimum without getting stuck in local optima, They can be adapted to various problem types and can be optimized according to the desired performance level with parameter settings, They can produce more than one good solution at the same time and offer options to decision-makers, and They can produce fast solutions in large data sets and complex problems. For this reason, they have found a chance to be used in different areas. Some of these areas of use are used in Engineering Design, Structural optimization, parameter settings of machine learning models, control theory and electronic circuit design. In the field of Bioinformatics, it is effective in biological data analysis such as DNA sequence analysis, protein structure prediction and genetic algorithms. In the field of Logistics and Transportation, it is used in logistics problems such as route optimization, inventory management and the organization of transportation networks. In the field of Finance, it is used in financial analyzes such as portfolio optimization, risk management and the development of trading strategies. In the Production and Planning field, it is applied to production management problems such as production scheduling, resource allocation and process optimization. In the Energy Management field, it provides solutions to problems in the energy sector such as energy distribution, integration of renewable energy sources and optimization of energy consumption, and in the Health and Medicine field, it is used in the

healthcare field such as medical image processing, disease diagnosis and treatment planning. Metaheuristic algorithms make significant contributions by overcoming complex problems in these and many other fields. If you are working on a specific problem, it may be very useful to try one of these algorithms!

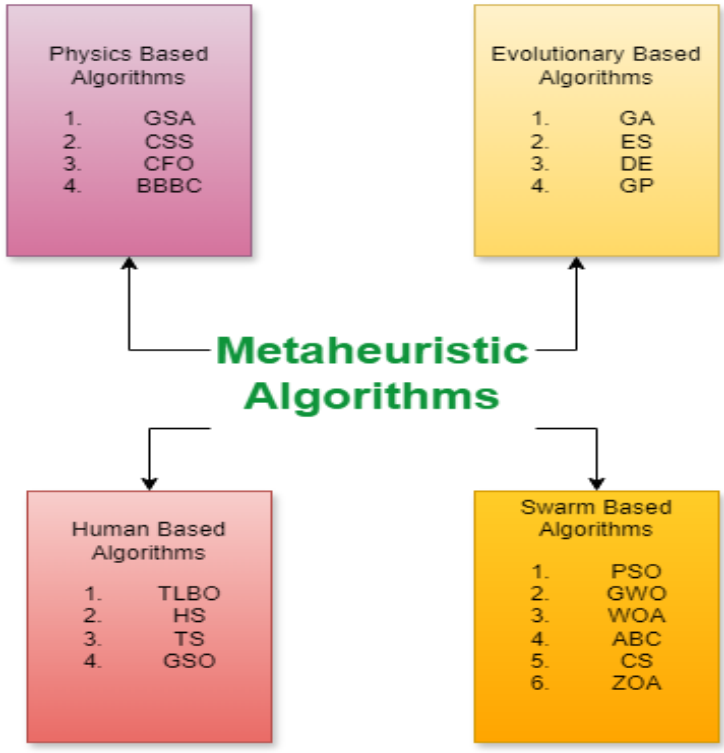

Figure 1. Classification of meta-heuristic algorithms.

Metaheuristic algorithms are optimization algorithms that perform significantly for solving real-world problems that are often nonlinear and multimodal (Tian et al., 2018). All metaheuristic algorithms involve some combination of random and local search. These algorithms can find good solutions for complex and difficult optimization problems, but they are not guaranteed to reach the best solutions. It is expected that these algorithms will work most of the time, but they do not always. Metaheuristic algorithms can be useful for reaching global optimization value (Boussaid et al., 2013). Metaheuristic algorithms are generally divided into two classes: single-solution and multi-solution based problems (Jackson et al., 2018).

It is known that several metaheuristic algorithms stand out and are widely applied. Some of the most important metaheuristic algorithms: Genetic Algorithm (GA) (Holland, 1975), It is an algorithm that simulates

evolutionary processes and is based on the principles of biological evolution. Genetic algorithms are generally used in engineering design, bioinformatics, logistics and many more areas. Particle Swarm Optimization (PSO) (Kennedy et al., 1995): A method in which a group of particles search for the best solution in space and learn from their own and others' best experiences in this process. It is usually used for control systems, neural network training, and other continuous optimization problems. Simulated Annealing (SA): It emerged as a method used to solve global optimization problems inspired by the annealing process in metallurgical processes. It has been used in areas such as combinatorial optimization, scheduling and other problem solving tasks. Ant Colony Optimization (ACO): It simulates the food-finding behavior of ants and has been used to solve minimum path problems. It has applications in areas such as the traveling salesman problem (TSP), network routing, and scheduling problems. Differential Evolution Algorithm (DE): Differential evolution is an evolutionary algorithm used for optimization in population-based and continuous fields. It has areas of use such as parameter optimization, machine learning and other engineering problems. Artificial Bee Colony (ABC) is an algorithm that models the foraging behavior of honey bees and applies this process to optimization problems. It usually has areas of use in process optimization, data mining and multi-criteria optimization. Gravitational Search Algorithm (GSA) is an optimization method based on gravity and laws of motion, where solutions are attracted to each other and has areas of use such as engineering designs, dataset optimizations, and robotic applications. Whale Optimization Algorithm (WOA) is a nature-based metaheuristic algorithm inspired by social behavior and hunting strategies of whale herds. It was first developed by Mirjalili and Lewis in 2016. The main purpose of this algorithm is to provide effective solutions to global optimization problems. Whale Optimization Algorithm mimics the hunting strategies of humpback whales. Humpback whales hunt with spiral movements that encircle their prey. WOA optimizes solutions by simulating this spiral movement and hunting strategies of whales. The algorithm works in three main stages as Whales surround their prey (Encircling), Hunting Spiral (Bubble-net Attacking Method) catching their prey by following a spiral path (Bubble-net Attacking), and providing search for new prey and potential solutions (Search Behavior). Whale Optimization Algorithm is used in Engineering Design, Machine Learning, Data Mining, Medicine and Health, Economics and Finance, Industrial Applications, robot path planning, control systems and robotic optimization problems. Whale Optimization Algorithm is a powerful tool inspired by nature and offers a wide range of applications in different fields. It provides innovative and effective solutions to complex problems. In this way, we can increase the number of metaheuristic optimization algorithms. These algorithms provide great benefits in the fields of science and engineering by providing innovative and

effective solutions to various optimization problems. Each can be adapted to different types of problems and offers significant performance improvements.

Humpback Whale Optimization Algorithm (WOA)

The Whale Optimization Algorithm (WOA) (Mirjalili, 2016) simulates the social dynamics of humpback whales.

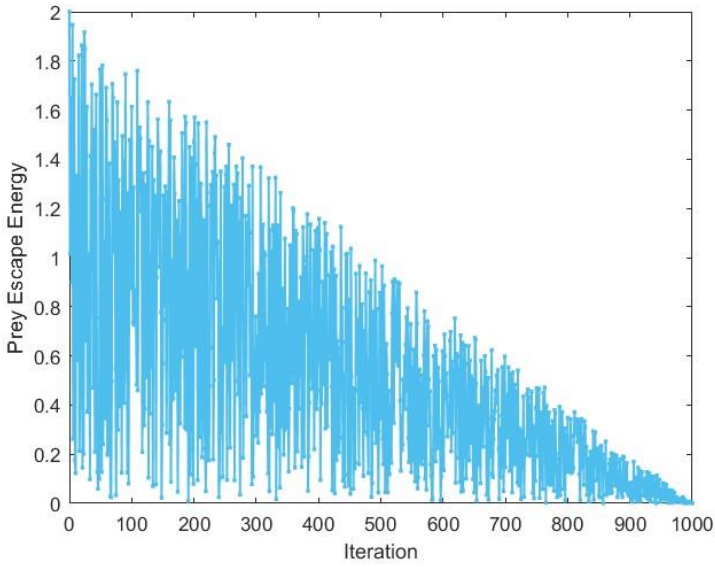

Figure 2. The evolution of a prey's absolute escape energy ran for 1000 iterations around.

The algorithm was inspired by humpback whales using bubble nets to hunt tiny fish. This algorithm is separated into two parts:

a) Exploration part,

$$W(t+1) = W_{rand} - \zeta Y$$

$$Y = |BW_{rand} - \zeta W|$$

where W_{rand}, represents the position of a randomly selected member within the whale swarm.

b) Exploitation part,

$$W(t+1) = W^*(t) - \zeta Y$$

$$Y = |BW^*(t) - \zeta W(t)|$$

where $W^*(t)$ and $W(t+1)$ are indicate the best position and the current position, respectively. $\zeta = 2k(t)\vec{r} - k(t)$ and $B = 2\vec{r}$ are coefficient vectors.

$$W(t+1) = e^{bt}\cos(2\pi t)Y^* + W^*(t)$$

$$Y^* = |W^*(t) - W(t)|, b, t \in [-1,1]$$

$$for\ p \in [0,1]$$

$$W(t+1) = \begin{cases} cW^*(t)\delta - \zeta Y, & if\ p < 0.5 \\ e^{bt}\cos(2\pi t)Y^* + W^*(t), & if\ p \geq 0.5 \end{cases}$$

where $k(t) \in [0,2]$ is linearly decreased and $\vec{r}, p \in [0,1]$.

During the exploration phase, an extra criterion may need to be introduced to guide the current

solution towards the optimum and ensure that the whale does not slip into a worse position than

the previous one.

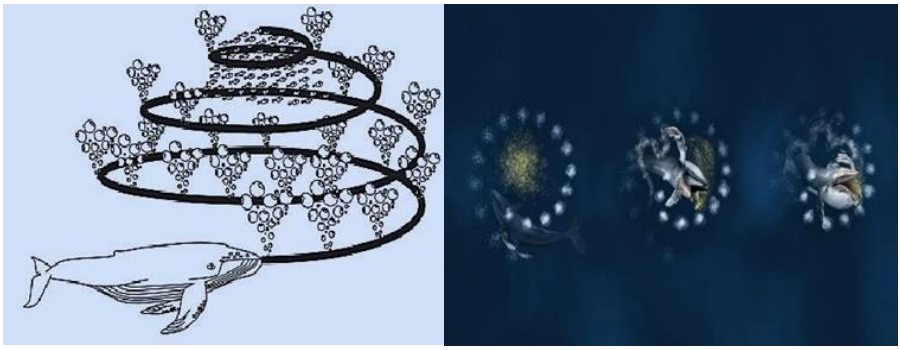

Figure 3. Bubble-net feeding behavior of humpback whales.

There are several potential disadvantages of the Whale Optimization Algorithm (WOA), such as the fact that it can converge to a local optimum very quickly and miss the best solution, its performance is very sensitive to parameter settings, scalability issues are likely to occur in larger or more complex problems, it does not guarantee the best solution and only provides an approximation, and it has difficulty balancing exploration and exploitation, thus affecting performance. Therefore, in order to increase the effectiveness of the WOA optimization algorithm in solving problems, it is necessary to eliminate the effects of these disadvantages. Using arguments such as JOS, which will improve the effectiveness of the WOA algorithm, may provide a logical solution. Moreover, other techniques can be used to improve nature-inspired optimization algorithms, e.g., gradient-based (Azizipanah-Abarghooee et al., 2013), chaotic (Mitić et al., 2015), quantum (Wang et al., 2020), and opposition-based learning (OBL) (Yildiz et al., 2021). Many researchers recommend OBL as a learning technique that can improve the performance of an optimization algorithm in a competition (Xu et al., 2014). Tizhoosh (2005) proposed the opposition-based learning (OBL) technique on the basis of Aristotle's theory of opposition. Rahnamayan et al. (2007) pointed

out that opposite numbers are more likely to produce a better result than normal random numbers. Supporting evidence for this theory from scientific studies (Al-Qunaieer et al., 2010, Mahdavi et al., 2018, Arini et al., 2022) have also confirmed that the opposite strategy produces remarkable results. Therefore, many researchers have tried to develop, expand or combine the opposite strategy. Rahnamayan et al. (2007) established the concept of quasi-opposition based learning, or QOBL. It uses a jumping rate and determines the midpoint of opposite points to increase the likelihood of being near the solution. Quasi-reflection was introduced by Ergezer et al. (2009) and improves the BBO success rate while requiring less fitness computation. Xu et al. (2020) suggested dynamic opposite (DO) in order to enhance exploration skills and generate diversity through asymmetric search behavior by combining quasi-opposition and quasi-reflection. The single opposite technique is an opposite strategy that is applied only once every generation. Consequently, an improved optimization algorithm employing a single opposition technique can only enhance the capacity for exploration or exploitation. In order to solve multi-task optimization problems, the mutation technique is combined with the dynamic opposite to provide mutual learning (Li et al., 2021). In 2007, Gonzales proved that the balance between exploration and exploitation in the search space must be maintained for basic optimization processes. Many researchers have stated that there is no definitive formula to define the balance of exploration and exploitation in the search space and no Nature-inspired optimization algorithm to calculate this balance (Morales-Castañeda et al., 2020, Črepinšek et al., 2013, Yang et al., 2014). Additionally, Wolper and Macready (1997) pointed out that no algorithm can solve all optimization problems. Afterward, Wang et al. (2019) also investigated whether two opposites are better than one.

Accordingly, it has been associated that DO is a subpart of exploration, SLO is a subpart of exploitation, and DO is the subopposite of SLO. According to Gonzales (2007), the opposing act of exploration and exploitation reinforce each other. Therefore, the combination of DO and SLO were established the balance of mutual strengthening and has been named Joint Opposing Selection (JOS) (Arini et al., 2022). Although WOA has demonstrated its effectiveness and superiority in many different types of applications, WOA has been able to be used in conjunction with the opposite learning technique to reduce premature convergence of local optima and stagnation in local optima.

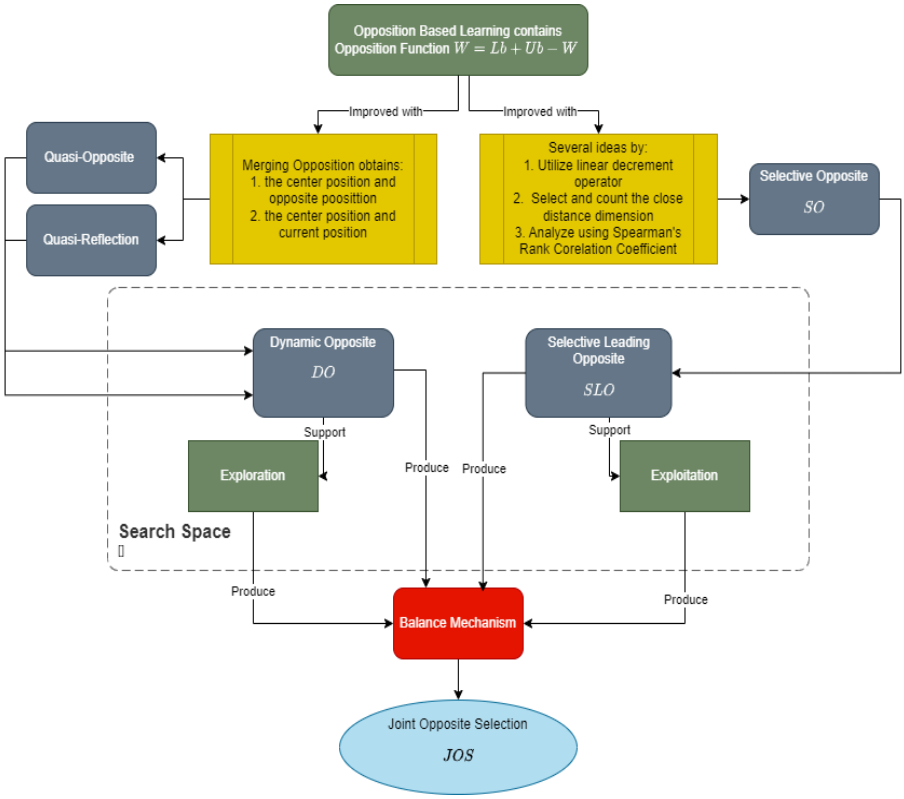

Figure 4: Hierarchical Development of Joint Opposite Selection (JOS)

Proposed WOAJOS

In this study, we use the Joint Opposite Selection (JOS) to improve the Whale Optimization (WOA) algorithm. JOS helps WOA quickly attack to prey by using SLO. SLO uses the existing contraction operator from the original version of WOA to implement its strategy. DO contributes to the development of WOA's strategy to find other potential hunting grounds. The Matlab code of the WOAJOS algorithm has been shared on Github by Florentina. You can find it in reference (Arini, 2024).

The main WOAJOS is performed even though the number of functional evaluations (nFE) is less than the maximum functional evaluation ($maxFE$). After the wolves have checked their boundaries and evaluated their fitness, the JOS strategy is used. Each time the whales evaluate their fitness, the number of functional evaluations is updated. The best value of the fitness of the whales is the position of the tiny fish.

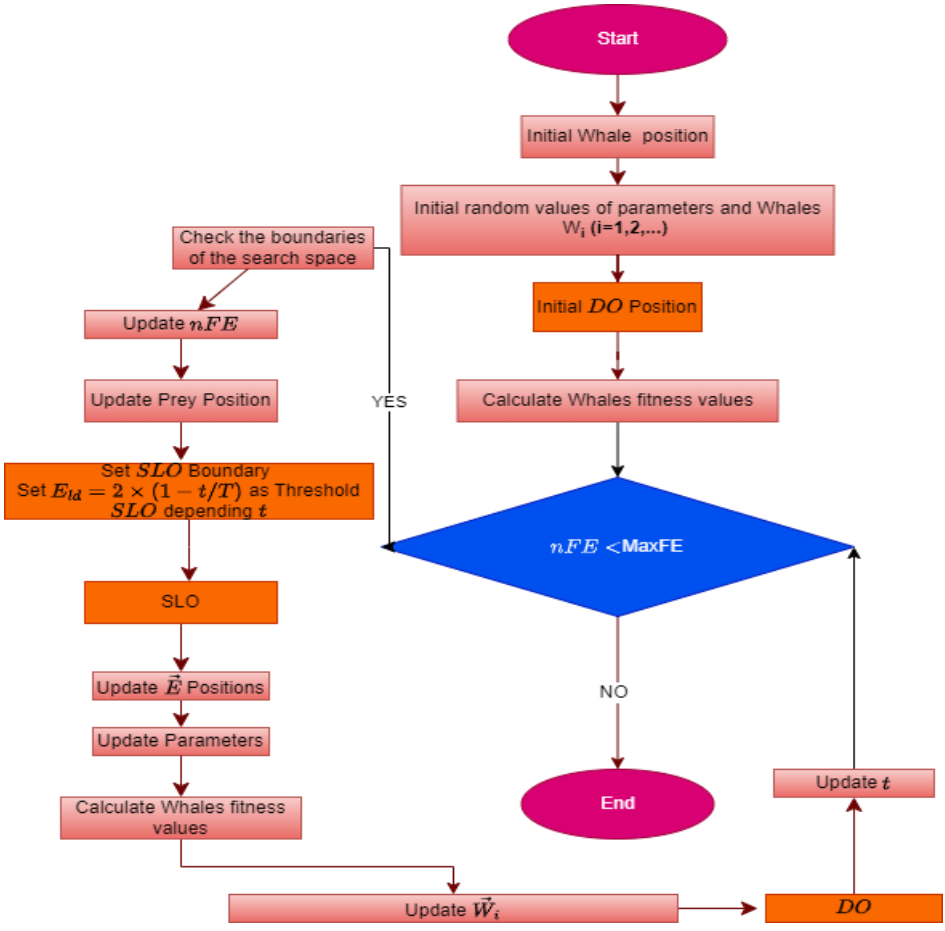

Figure 5. Flow Chart of WOAJOS

Table 1: CEC2017 competition on single objective real parameter numerical optimization

Categories	Number of Functions	Functions	Optima, F_i^*
Unimodal Functions	f_1	Shifted and Rotated Bent Cigar Function	100
	f_3	Shifted and Rotated Zakhrov Function	300
Simple Multimodal Functions	f_4	Shifted and Rotated Rosenbrock's Function	400
	f_5	Shifted and Rotated Rastrigin's Function	500
	f_6	Shifted and Rotated Expanded Scaffer's F6 Function	600
	f_7	Shifted and Rotated Lunacek Bi_Rastringin's Function	700
	f_8	Shifted and Rotated Non-Continuous Rastringin's Function	800
	f_9	Shifted and Rotated Levy Function	900
	f_{10}	Shifted and Rotated Schwefel's Function	1000
Hybrid Functions	f_{11}	Hybrid Function 1 $(N = 3)$ Zakhrov, Rosenbrock's, Rastrigin's	1100
	f_{12}	Hybrid Function 2 $(N = 3)$ High-Conditioned Elliptic, Modified Schwefel's, Ben Cigar	1200
	f_{13}	Hybrid Function 3 $(N = 3)$ Ben Cigar, Rosenbrock's, Lunacek Bi_Rastringin's	1300
	f_{14}	Hybrid Function 4 $(N = 4)$ High-Conditioned Elliptic, Ackley, Schaffer's $F7$, Rastringin's	1400
	f_{15}	Hybrid Function 5 $(N = 4)$ Ben Cigar, HGBat, Rastringin's, Rosenbrock's	1500
	f_{16}	Hybrid Function 6 $(N = 4)$ Expanded Schaffer's $F6$, HGBat, Rosenbrock's, Modified Schwefel's	1600
	f_{17}	Hybrid Function 6 $(N = 5)$ Katsuura, Ackl	1700

		ey, Expanded Griewank's plus, Rosenbrock's, Schwefel's, Rastringin's	
	f_{18}	Hybrid Function 6 ($N = 5$) High-Conditioned Elliptic, Ackley, Rastringin's, HGBat, Discus	1800
	f_{19}	Hybrid Function 6 ($N = 5$) Bent Cigar, Rastringin's, Griewank's plus Rosenbrock's, Weierstrass, Expanded Schaffer's $F6$	1900
	f_{20}	Hybrid Function 6 ($N = 5$) HappyCat, Katsuura, Ackley, Rastringin's, Modified Schwefel's, Schaffer $F7$	2000

Composition Functions	f_{21}	Composition Function 1 ($N = 3$) Rosenbrock's, High Conditioned Elliptic, Rastringin's	2100
	f_{22}	Composition Function 1 ($N = 3$) Rastringin's, Griewank's, Modified Schwefel's	2200
	f_{23}	Composition Function 1 ($N = 4$) Rosenbrock's, Ackley, Modified Schwefel's, Rastringin's	2300
	f_{24}	Composition Function 2 ($N = 4$) Ackley, High-Conditioned Elliptic, Griewank's, Rastringin's	2400
	f_{25}	Composition Function 3 ($N = 5$) Rastringin's, HappyCat, Ackley Discus, Rosenbrock's	2500
	f_{26}	Composition Function 4 ($N = 5$) Expanded Schaffer's $F6$, Modified Schwefel's, Griewank's, Rosenbrock's, Rastringin's	2600
	f_{27}	Composition Function 5 ($N = 6$) HGBat, Rastringin's, Modified Schewel's, Bent Cigar, High-Conditioned Elliptic, Expanded Schaffer's $F6$	2700
	f_{28}	Composition Function 6 ($N = 6$) Ackley, Griewank, Discus, Rosenbrock, HappyCat, Expanded Schaffer's $F6$	2800
	f_{29}	Composition Function 7 ($N = 3$) $F15, F16, F17$	2900
	f_{30}	Composition Function 8 ($N = 3$) $F15, F18, F19$	3000

The experiments were conducted considering the following points:
1. To demonstrate the effectiveness of the WOAJOS algorithm, a comparison with WOA was made below using CEC2017.
2. The candidacy of the Random Jump Strategy of the jump ratio in WOAJOS, Jr=0.25.
3. It demonstrated the successful JOS behavior and exploration ability.
4. The statistical analysis of the Wilcoxon Signed Rank Test performance of WOAJOS compared to its competitors' algorithms was presented.

MAIN RESULTS

Experimental Results of Benchmark CEC-2017

Table 2: Comparison of WOA and WOAJOS by CEC2017 for dimension 30

F	Ist. Anl	WOA	$WOAJOS$	F	WOA	$WOAJOS$	F	WOA	$WOAJOS$
F_1	Min	9.98E+05	5.87E+04	F_{12}	8.73E+06	4.47E+06	F_{22}	2.35E+03	2.35E+03
	Max	2.23E+06	1.10E+05		2.99E+08	9.90E+07		2.35E+03	2.35E+03
	Std	1.12E+07	4.96E+05		7.17E+07	2.85E+07		1.89E-13	1.89E-13
	$Median$	2.81E+06	1.51E+05		1.25E+08	4.19E+07		2.35E+03	2.35E+03
	$Mean$	3.40E+06	1.88E+05		1.27E+08	4.37E+07		2.35E+03	2.35E+03
F_3	Min	3.42E+03	4.97E+02	F_{13}	2.06E+04	6.94E+03	F_{23}	3.02E+03	2.50E+03
	Max	2.26E+04	1.82E+03		3.98E+05	9.47E+04		3.50E+03	2.50E+03
	Std	5.17E+03	3.16E+02		1.07E+05	1.99E+04		1.37E+02	1.68E-10
	$Median$	1.32E+04	9.46E+02		7.92E+04	1.49E+04		3.17E+03	2.50E+03
	$Mean$	1.35E+04	9.77E+02		1.19E+05	2.30E+04		3.23E+03	2.50E+03

F_4	Min	4.84E+02	4.69E+02	F_{14}	9.25E+03	3.11E+03	F_{24}	2.60E+03	2.60E+03
	Max	7.23E+02	6.14E+02		7.64E+05	1.04E+05		3.82E+03	2.60E+03
	Std	5.81E+01	3.89E+01		1.75E+05	2.72E+04		4.49E+02	4.65E-09
	$Median$	5.88E+02	5.41E+02		2.04E+05	2.75E+04		2.60E+03	2.60E+03
	$Mean$	5.93E+02	5.37E+02		2.41E+05	3.46E+04		2.80E+03	2.60E+03
F_5	Min	6.48E+02	6.00E+02	F_{15}	2.31E+03	2.54E+03	F_{25}	2.70E+03	2.70E+03
	Max	7.84E+02	7.24E+02		1.41E+05	1.84E+04		3.12E+03	2.70E+03
	Std	3.87E+01	2.67E+01		3.42E+04	4.05E+03		1.23E+02	5.17E-08
	$Median$	7.00E+02	6.52E+02		3.60E+04	6.51E+03		2.70E+03	2.70E+03
	$Mean$	7.03E+02	6.56E+02		3.87E+04	7.49E+03		2.74E+03	2.70E+03
F_6	Min	6.45E+02	6.07E+02	F_{16}	2.29E+03	2.10E+03	F_{26}	2.80E+03	2.80E+03
	Max	6.86E+02	6.29E+02		4.87E+03	3.37E+03		9.29E+03	2.80E+03
	Std	1.16E+01	5.79E+00		5.07E+02	3.20E+02		1.94E+03	1.03E-08
	$Median$	6.64E+02	6.19E+02		3.39E+03	2.68E+03		2.80E+03	2.80E+03
	$Mean$	6.64E+02	6.19E+02		3.38E+03	2.70E+03		3.63E+03	2.80E+03
F_7	Min	1.05E+03	9.46E+02	F_{17}	2.01E+03	1.97E+03	F_{27}	3.62E+03	2.90E+03

	Max	1.55E+03	1.12E+03		3.14E+03	2.59E+03		4.67E+03	2.90E+03
	Std	1.05E+02	4.73E+01		3.25E+02	1.80E+02		2.36E+02	4.59E-08
	$Median$	1.30E+03	1.03E+03		2.65E+03	2.20E+03		3.99E+03	2.90E+03
	$Mean$	1.31E+03	1.02E+03		2.60E+03	2.24E+03		4.00E+03	2.90E+03
F_8	Min	9.83E+02	9.13E+02	F_{18}	2.60E+05	1.36E+05	F_{28}	3.00E+03	3.00E+03
	Max	1.24E+03	1.09E+03		1.87E+07	3.82E+06		5.23E+03	3.00E+03
	Std	6.26E+01	4.32E+01		4.44E+06	9.56E+05		5.56E+02	2.64E-08
	$Median$	1.10E+03	9.95E+02		4.43E+06	1.83E+06		3.00E+03	3.00E+03
	$Mean$	1.10E+03	9.96E+02		5.22E+06	1.73E+06		3.23E+03	3.00E+03
F_9	Min	4.91E+03	2.79E+03	F_{19}	6.49E+03	2.02E+03	F_{29}	3.10E+03	3.10E+03
	Max	2.31E+04	6.35E+03		2.22E+06	1.85E+04		5.05E+03	3.10E+03
	Std	3.97E+03	8.41E+02		5.52E+05	3.64E+03		4.47E+02	5.25E-08
	$Median$	7.99E+03	5.11E+03		6.20E+05	3.30E+03		4.36E+03	3.10E+03
	$Mean$	8.84E+03	4.94E+03		6.11E+05	4.81E+03		4.39E+03	3.10E+03
F_{10}	Min	4.18E+03	2.91E+03	F_{20}	2.47E+03	2.30E+03	F_{30}	3.20E+03	3.20E+03
	Max	8.02E+03	5.39E+03		3.17E+03	2.83E+03		1.72E+07	8.29E+05

	Std	8.80E+02	6.51E+02		1.96E+02	1.36E+02		4.40E+06	1.75E+05
	$Median$	6.03E+03	4.35E+03		2.83E+03	2.55E+03		1.57E+06	3.20E+03
	$Mean$	6.03E+03	4.28E+03		2.82E+03	2.55E+03		3.20E+06	6.85E+04
F_{11}	Min	1.27E+03	1.18E+03	F_{21}	2.19E+03	2.17E+03			
	Max	1.79E+03	1.52E+03		2.34E+03	2.28E+03			
	Std	1.19E+02	7.79E+01		3.33E+01	2.74E+01			
	$Median$	1.52E+03	1.32E+03		2.27E+03	2.24E+03			
	$Mean$	1.51E+03	1.31E+03		2.27E+03	2.24E+03			

Table 3: Scalability Analysis

F	$WOAJOS\ vs. WOA$						
	Dim	$P-Value$	$z-Value$	$Rank\ (-)$	$Rank\ (+)$	Statistically significant	Winner
F_1	30	0.000002	−4.7821	465	0	1 ($p < 0.05$)	+
F_3	30	0.000002	−4.7821	465	0	1 ($p < 0.05$)	+
F_4	30	0.000420	−3.5275	304	61	1 ($p < 0.05$)	+
F_5	30	0.000049	−4.0622	430	35	1 ($p < 0.05$)	+
F_6	30	0.000002	−4.7821	465	0	1 ($p < 0.05$)	+
F_7	30	0.000002	−4.7821	465	0	1 ($p < 0.05$)	+
F_8	30	0.000006	−4.5148	452	13	1 ($p < 0.05$)	+
F_9	30	0.000002	−4.7616	464	1	1 ($p < 0.05$)	+

F_{10}	30	0.000002	−4.7821	465	0	1 ($p < 0.05$)	+
F_{11}	30	0.000002	−4.7821	465	0	1 ($p < 0.05$)	+
F_{12}	30	0.000011	−4.3913	446	19	1 ($p < 0.05$)	+
F_{13}	30	0.000010	−4.4119	447	18	1 ($p < 0.05$)	+
F_{14}	30	0.000004	−4.5970	456	9	1 ($p < 0.05$)	+
F_{15}	30	0.000006	−4.5148	452	13	1 ($p < 0.05$)	+
F_{16}	30	0.000006	−4.5148	452	13	1 ($p < 0.05$)	+
F_{17}	30	0.000075	−3.9594	425	40	1 ($p < 0.05$)	+
F_{18}	30	0.000261	−3.6509	410	55	1 ($p < 0.05$)	+
F_{19}	30	0.000002	−4.7204	462	3	1 ($p < 0.05$)	+
F_{20}	30	0.000041	−4.1034	432	33	1 ($p < 0.05$)	+
F_{21}	30	0.001484	−3.1778	387	78	1 ($p < 0.05$)	+
F_{22}	30	0.000048	−4.0622	429	36	1 ($p < 0.05$)	+
F_{23}	30	0.000002	−4.7821	465	0	1 ($p < 0.05$)	+
F_{24}	30	0.057096	1.9026	140	325	0 ($p \geq 0.05$)	=
F_{25}	30	0.002765	2.9927	87	378	0 ($p < 0.05$)	−
F_{26}	30	0.057096	1.9026	140	325	0($p \geq 0.05$)	=
F_{27}	30	0.000002	−4.7821	465	0	1 ($p < 0.05$)	+
F_{28}	30	0.975387	−0.0309	234	231	0($p \geq 0.05$)	=
F_{29}	30	0.000002	−4.7616	464	1	1 ($p < 0.05$)	+
F_{30}	30	0.000005	−4.5559	454	11	1 ($p < 0.05$)	+

Diversity analysis and exploration-exploitation analysis of the WOAJOS algorithm for CEC2017 benchmarks are visually displayed in Figure 7. These analyses have revealed how important exploration and exploitation are. Also, the experimental results shown that the effect of the JOS strategy on the exploration-exploitation. This is also consistent with the purpose of the study

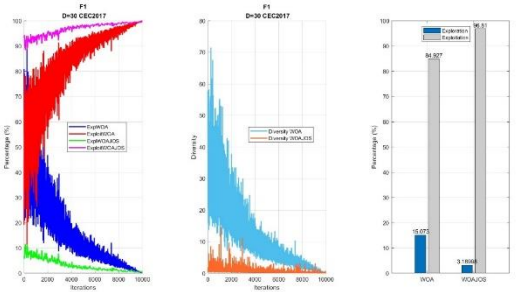
F1
D=30 CEC2017
Exploration
Exploitation
84.927
15.073
WOA
WOAJOS

F1
D=30 CEC2017
Diversity WOA
Diversity WOAJOS
Diversity
Iterations

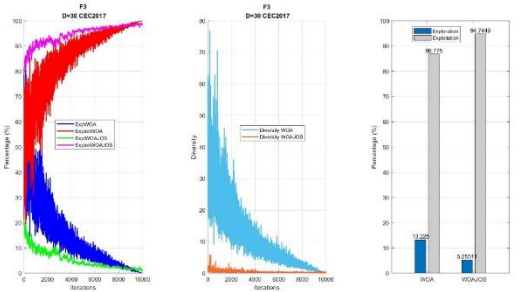
F3
D=30 CEC2017
Exploration
Exploitation
86.775
13.225
WOA
WOAJOS

F3
D=30 CEC2017
Diversity WOA
Diversity WOAJOS
Diversity
Iterations

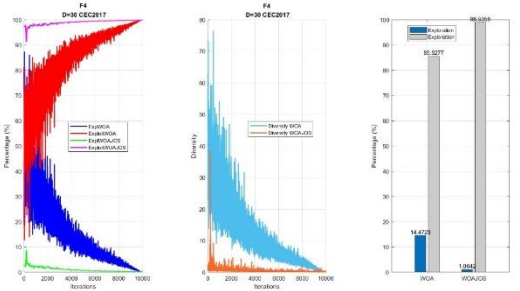
F4
D=30 CEC2017
Exploration
Exploitation
85.5277
14.4723
WOA
WOAJOS

F4
D=30 CEC2017
Diversity WOA
Diversity WOAJOS
Diversity
Iterations

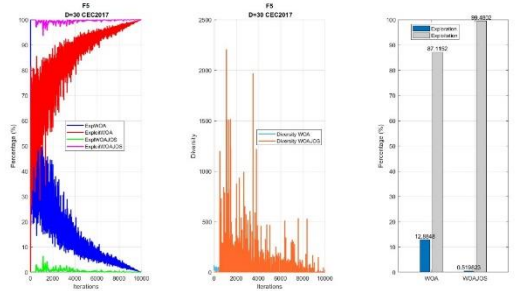
F5
D=30 CEC2017
Exploration
Exploitation
87.1952
12.8048
WOA
WOAJOS

F5
D=30 CEC2017
Diversity WOA
Diversity WOAJOS
Diversity
Iterations

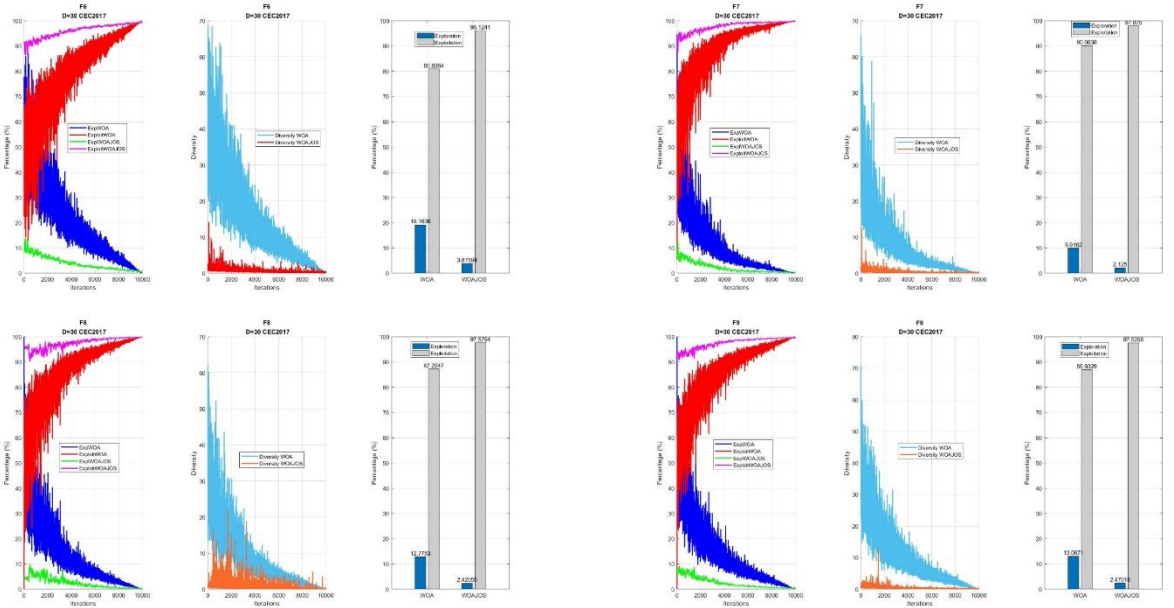
F6
D=30 CEC2017
Exp(WOA
Exp(WOA
Exp(WOAJOS
Exp(WOAJOS
Percentage (%)
Iterations
F6
D=30 CEC2017
Diversity WOA
Diversity WOAJOS
Diversity
Iterations
Exploration
Exploitation
82.9364
96.1241
93.1636
3.87594
WOA
WOAJOS
Percentage (%)
F7
D=30 CEC2017
Exp(WOA
Exp(WOA
Exp(WOAJOS
Exp(WOAJOS
Percentage (%)
Iterations
F7
D=30 CEC2017
Diversity WOA
Diversity WOAJOS
Diversity
Iterations
Exploration
Exploitation
90.9162
97.875
WOA
WOAJOS
Percentage (%)
F8
D=30 CEC2017
Exp(WOA
Exp(WOA
Exp(WOAJOS
Exp(WOAJOS
Percentage (%)
Iterations
F8
D=30 CEC2017
Diversity WOA
Diversity WOAJOS
Diversity
Iterations
Exploration
Exploitation
87.2047
97.6794
12.7759
2.42259
WOA
WOAJOS
Percentage (%)
F9
D=30 CEC2017
Exp(WOA
Exp(WOA
Exp(WOAJOS
Exp(WOAJOS
Percentage (%)
Iterations
F9
D=30 CEC2017
Diversity WOA
Diversity WOAJOS
Diversity
Iterations
Exploration
Exploitation
86.9336
97.5356
13.0671
2.47044
WOA
WOAJOS
Percentage (%)

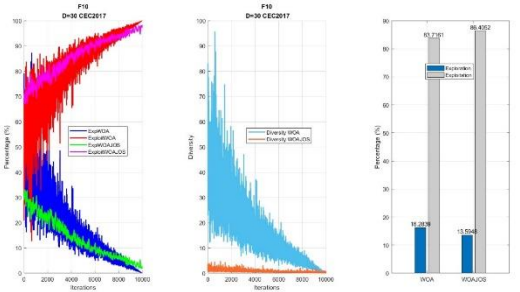
F10
D=30 CEC2017
Percentage (%)
Iterations
ExplWOA
ExplWOA
ExplWOAJOS
ExplWOAJOS
F10
D=30 CEC2017
Diversity
Iterations
Diversity WOA
Diversity WOAJOS
F10
D=30 CEC2017
Percentage (%)
Exploration
Exploration
83.7361
86.4352
16.2639
13.5648
WOA
WOAJOS

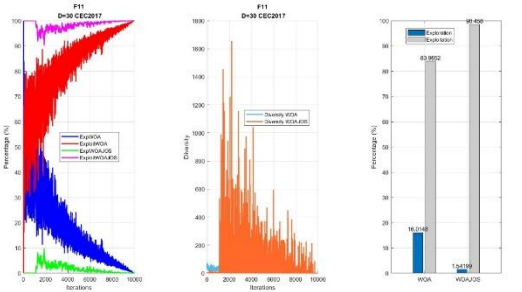
F11
D=30 CEC2017
Percentage (%)
Iterations
ExplWOA
ExplWOA
ExplWOAJOS
ExplWOAJOS
F11
D=30 CEC2017
Diversity
Iterations
Diversity WOA
Diversity WOAJOS
F11
D=30 CEC2017
Percentage (%)
Exploration
Exploration
83.9852
98.4581
16.0148
1.54199
WOA
WOAJOS

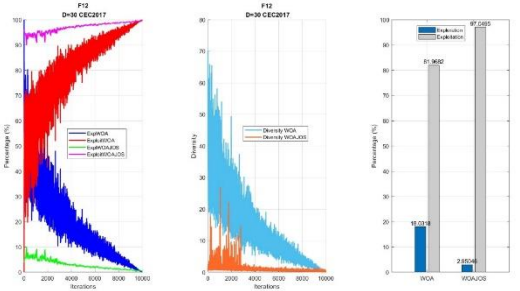
F12
D=30 CEC2017
Percentage (%)
Iterations
ExplWOA
ExplWOA
ExplWOAJOS
ExplWOAJOS
F12
D=30 CEC2017
Diversity
Iterations
Diversity WOA
Diversity WOAJOS
F12
D=30 CEC2017
Percentage (%)
Exploration
Exploration
97.0495
81.9682
18.0318
2.95046
WOA
WOAJOS

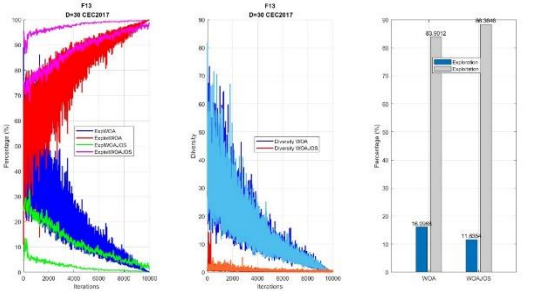
F13
D=30 CEC2017
Percentage (%)
Iterations
ExplWOA
ExplWOA
ExplWOAJOS
ExplWOAJOS
F13
D=30 CEC2017
Diversity
Iterations
Diversity WOA
Diversity WOAJOS
F13
D=30 CEC2017
Percentage (%)
Exploration
Exploration
83.5012
98.3846
16.5088
11.6354
WOA
WOAJOS

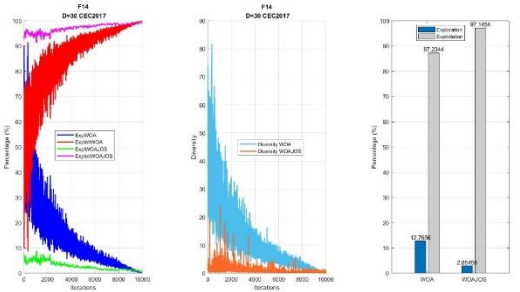
F14
D=30 CEC2017
Percentage (%)
Iterations
ExpWOA
ExploitWOA
ExpWOAJOS
ExploitWOAJOS

F14
D=30 CEC2017
Diversity
Iterations
Diversity WOA
Diversity WOAJOS

Percentage (%)
Exploration
Exploitation
87.2544
97.1454
12.7456
2.85456
WOA
WOAJOS

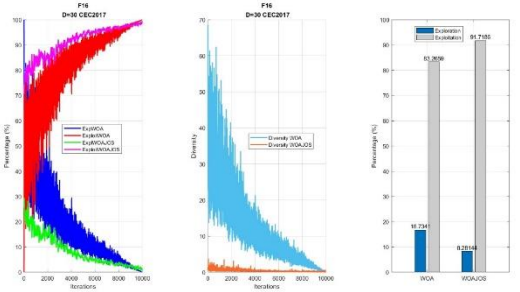
F16
D=30 CEC2017
Percentage (%)
Iterations
ExpWOA
ExploitWOA
ExpWOAJOS
ExploitWOAJOS

F16
D=30 CEC2017
Diversity
Iterations
Diversity WOA
Diversity WOAJOS

Percentage (%)
Exploration
Exploitation
91.7180
WOA
WOAJOS

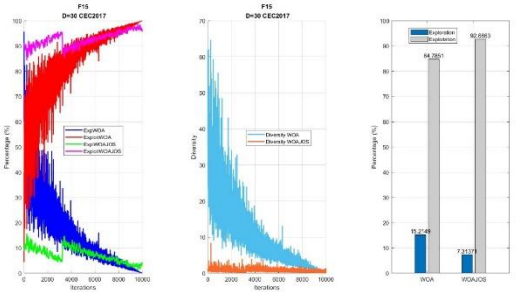
F15
D=30 CEC2017
Percentage (%)
Iterations
ExpWOA
ExploitWOA
ExpWOAJOS
ExploitWOAJOS

F15
D=30 CEC2017
Diversity
Iterations
Diversity WOA
Diversity WOAJOS

Percentage (%)
Exploration
Exploitation
84.7851
92.6863
15.2149
7.31370
WOA
WOAJOS

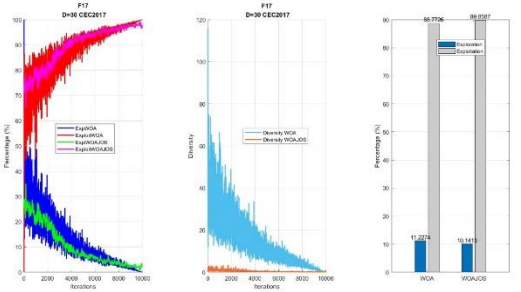
F17
D=30 CEC2017
Percentage (%)
Iterations
ExpWOA
ExploitWOA
ExpWOAJOS
ExploitWOAJOS

F17
D=30 CEC2017
Diversity
Iterations
Diversity WOA
Diversity WOAJOS

Percentage (%)
Exploration
Exploitation
88.7726
89.8197
11.2274
10.1803
WOA
WOAJOS

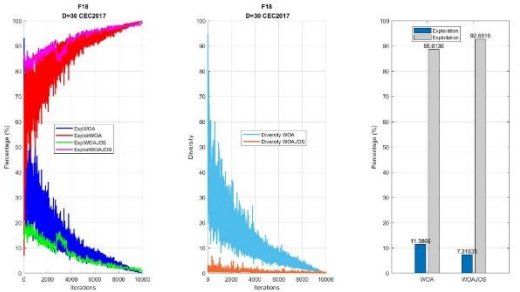
F18
D=30 CEC2017
Percentage (%)
Iterations
ExpWOA
ExpIWOA
ExpWOAJOS
ExpIWOAJOS

F18
D=30 CEC2017
Diversity
Iterations
Diversity WOA
Diversity IWOAJOS

Exploration
Exploitation
88.6736
90.6816
11.3264
7.31838
Percentage (%)
WOA
WOAJOS

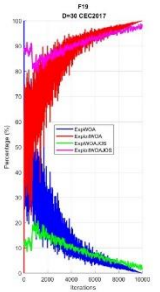
F19
D=30 CEC2017
Percentage (%)
Iterations
ExpWOA
ExpIWOA
ExpWOAJOS
ExpIWOAJOS

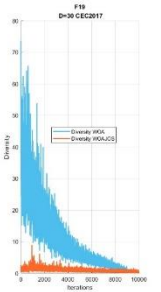
F19
D=30 CEC2017
Diversity
Iterations
Diversity WOA
Diversity WOAJOS

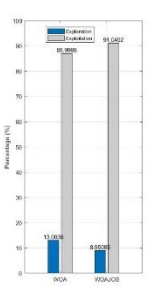
Exploration
Exploitation
88.9988
91.0402
11.0012
8.95982
Percentage (%)
WOA
WOAJOS

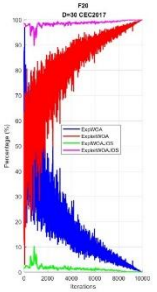
F20
D=30 CEC2017
Percentage (%)
Iterations
ExpWOA
ExpIWOA
ExpWOAJOS
ExpIWOAJOS

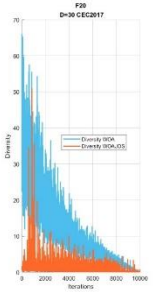
F20
D=30 CEC2017
Diversity
Iterations
Diversity WOA
Diversity IWOAJOS

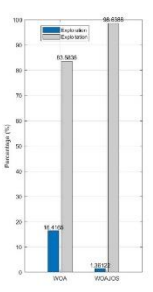
Exploration
Exploitation
83.5836
98.6385
16.4164
1.36123
Percentage (%)
WOA
WOAJOS

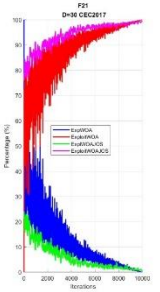
F21
D=30 CEC2017
Percentage (%)
Iterations
ExpWOA
ExpIWOA
ExpWOAJOS
ExpIWOAJOS

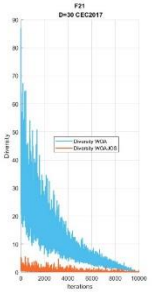
F21
D=30 CEC2017
Diversity
Iterations
Diversity WOA
Diversity WOAJOS

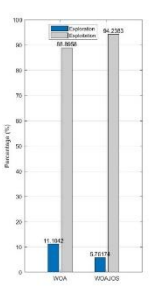
Exploration
Exploitation
88.8658
94.2383
11.1342
5.76172
Percentage (%)
WOA
WOAJOS

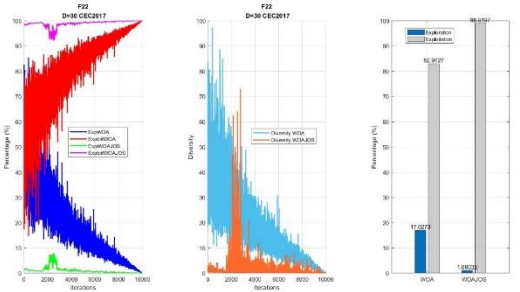
F22
D=30 CEC2017
Expl/WOA
Expl/WOA
Expl/WOAJOS
Expl/WOAJOS
Iterations
Percentage (%)

F22
D=30 CEC2017
Diversity WOA
Diversity WOAJOS
Iterations
Diversity

Exploration
Exploration
82.9727
98.5797
17.0273
1.42029
WOA
WOAJOS
Percentage (%)

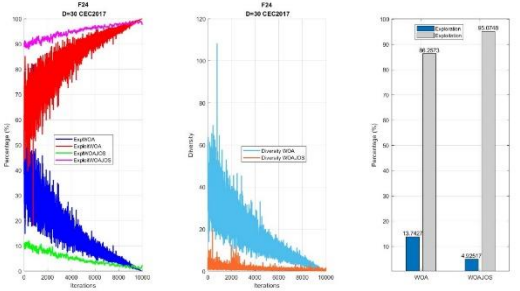
F24
D=30 CEC2017
Expl/WOA
Expl/WOA
Expl/WOAJOS
Expl/WOAJOS
Iterations
Percentage (%)

F24
D=30 CEC2017
Diversity WOA
Diversity WOAJOS
Iterations
Diversity

Exploration
Exploration
86.2573
95.0748
13.7427
4.92517
WOA
WOAJOS
Percentage (%)

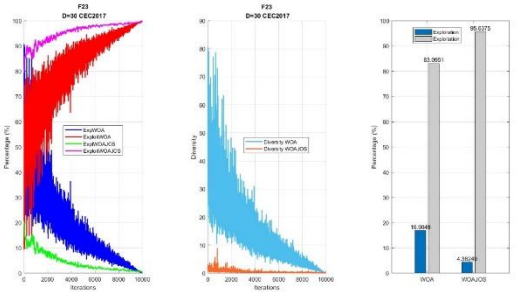
F23
D=30 CEC2017
Expl/WOA
Expl/WOA
Expl/WOAJOS
Expl/WOAJOS
Iterations
Percentage (%)

F23
D=30 CEC2017
Diversity WOA
Diversity WOAJOS
Iterations
Diversity

Exploration
Exploration
83.0651
95.6375
16.9349
4.36249
WOA
WOAJOS
Percentage (%)

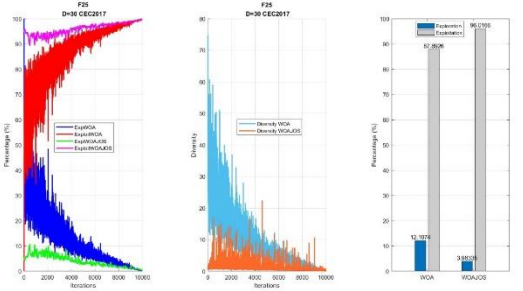
F25
D=30 CEC2017
Expl/WOA
Expl/WOA
Expl/WOAJOS
Expl/WOAJOS
Iterations
Percentage (%)

F25
D=30 CEC2017
Diversity WOA
Diversity WOAJOS
Iterations
Diversity

Exploration
Exploration
87.8626
96.0766
12.1374
3.68039
WOA
WOAJOS
Percentage (%)

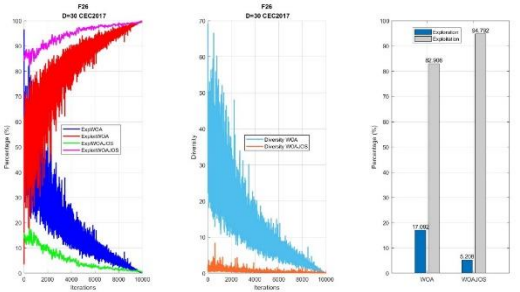
F26
D=30 CEC2017
Percentage (%)
Iterations
ExpWOA
ExpJWOA
ExpWOAJOS
ExpJWOAJOS

F26
D=30 CEC2017
Diversity
Iterations
Diversity WOA
Diversity WOAJOS

Exploration
Exploitation
82.906
94.792
17.094
5.208
Percentage (%)
WOA
WOAJOS

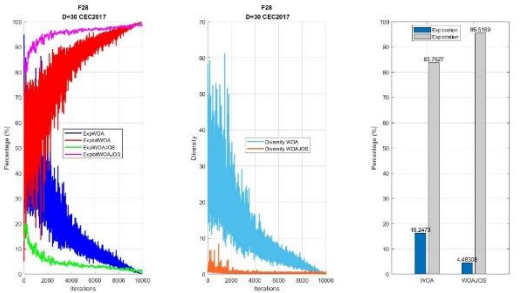
F28
D=30 CEC2017
Percentage (%)
Iterations
ExpWOA
ExpJWOA
ExpWOAJOS
ExpJWOAJOS

F28
D=30 CEC2017
Diversity
Iterations
Diversity WOA
Diversity WOAJOS

Exploration
Exploitation
83.7527
96.5159
16.2473
4.48398
Percentage (%)
WOA
WOAJOS

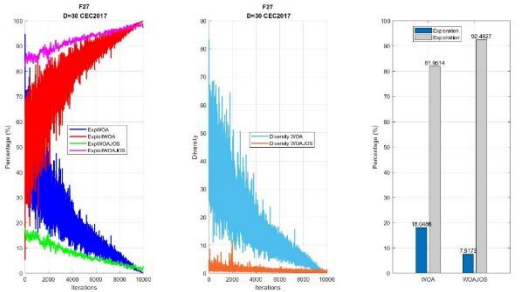
F27
D=30 CEC2017
Percentage (%)
Iterations
ExpWOA
ExpJWOA
ExpWOAJOS
ExpJWOAJOS

F27
D=30 CEC2017
Diversity
Iterations
Diversity WOA
Diversity WOAJOS

Exploration
Exploitation
81.9614
92.4927
18.0386
7.5073
Percentage (%)
WOA
WOAJOS

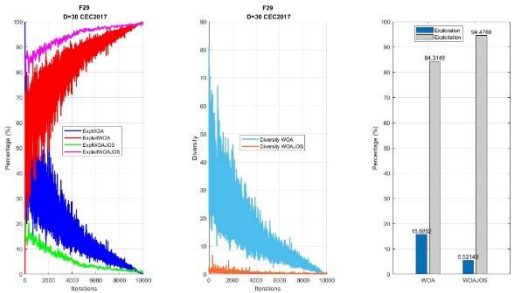
F29
D=30 CEC2017
Percentage (%)
Iterations
ExpWOA
ExpJWOA
ExpWOAJOS
ExpJWOAJOS

F29
D=30 CEC2017
Diversity
Iterations
Diversity WOA
Diversity WOAJOS

Exploration
Exploitation
84.3145
94.4788
15.6855
5.52119
Percentage (%)
WOA
WOAJOS

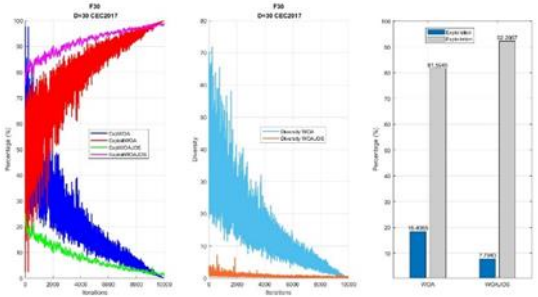

Figure 6: Exploration-Exploitation and Diversity Analysis of WOA and WOAJOS Algorithms

As seen in the figure 6, there is a significant difference between the exploitation and exploitation phases. In some metaheuristic optimization algorithms, the balance between the exploitation and exploitation phases gives better results, while on the contrary, the disruption of the balance in the Humpback Whale Algorithm (WOA) has shown better results in finding the optimum solutions of CEC2017 functions with the increase in the effectiveness of the Exploitation phase. This shows that the structures of metaheuristic optimization algorithms are quite different from each other. Jointly opposite selection (JOS), which causes the change between exploration and exploitation phases, played an important role in this study.

Fitness values, fitness average value and box plot representations of WOAJOS and WOA algorithms for 30 runs are shown in Figure 8. From this analysis, the superiority of WOAJOS over WOA is clearly seen.

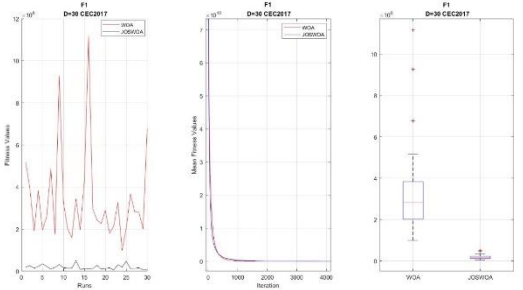
F1
D=30 CEC2017
WOA
JOSWOA
Fitness Values
Runs
Mean Fitness Values
Iteration

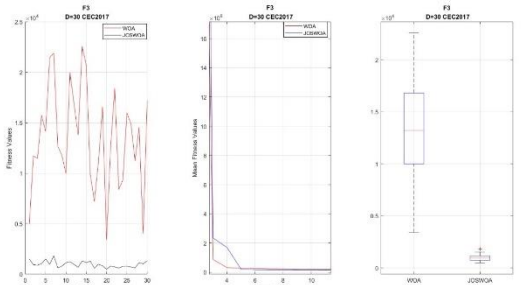
F3
D=30 CEC2017
WOA
JOSWOA
Fitness Values
Runs
Mean Fitness Values
Iteration

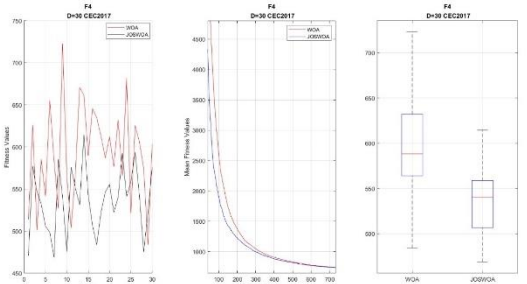
F4
D=30 CEC2017
WOA
JOSWOA
Fitness Values
Runs
Mean Fitness Values
Iteration

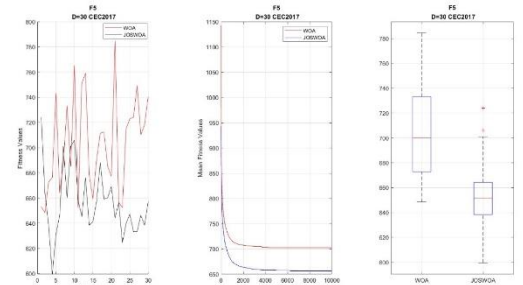
F5
D=30 CEC2017
WOA
JOSWOA
Fitness Values
Runs
Mean Fitness Values
Iteration

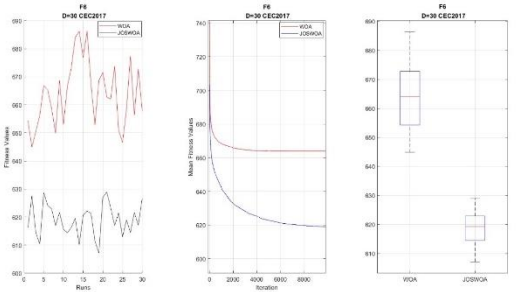
F6
D=30 CEC2017
WOA
JOSWOA
Fitness Values
Runs

F6
D=30 CEC2017
WOA
JOSWOA
Mean Fitness Values
Iteration

F6
D=30 CEC2017
WOA
JOSWOA

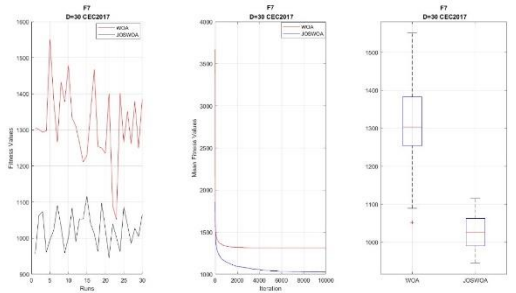
F7
D=30 CEC2017
WOA
JOSWOA
Fitness Values
Runs

F7
D=30 CEC2017
WOA
JOSWOA
Mean Fitness Values
Iteration

F7
D=30 CEC2017
WOA
JOSWOA

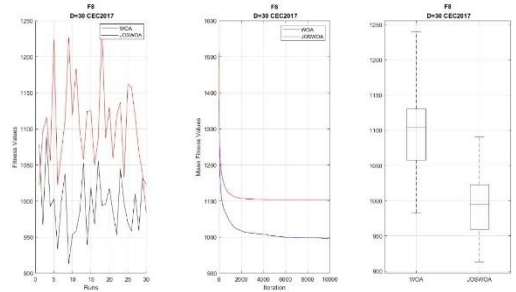
F8
D=30 CEC2017
WOA
JOSWOA
Fitness Values
Runs

F8
D=30 CEC2017
WOA
JOSWOA
Mean Fitness Values
Iteration

F8
D=30 CEC2017
WOA
JOSWOA

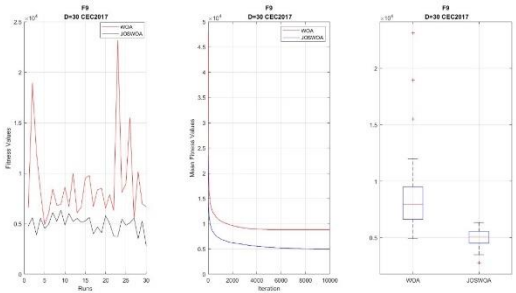
F9
D=30 CEC2017
WOA
JOSWOA
Fitness Values
Runs

F9
D=30 CEC2017
WOA
JOSWOA
Mean Fitness Values
Iteration

F9
D=30 CEC2017
WOA
JOSWOA

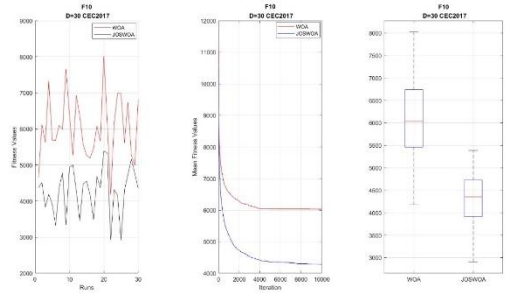
F10
D=30 CEC2017
WOA
JOSWOA
Fitness Values
Runs

F10
D=30 CEC2017
WOA
JOSWOA
Mean Fitness Values
Iteration

F10
D=30 CEC2017
WOA
JOSWOA

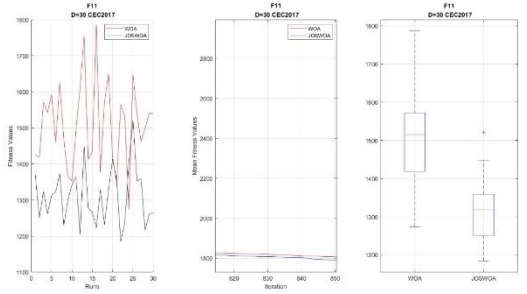
F11
D=30 CEC2017
WOA
JOSWOA
Fitness Values
Runs

F11
D=30 CEC2017
WOA
JOSWOA
Mean Fitness Values
Iteration

F11
D=30 CEC2017
WOA
JOSWOA

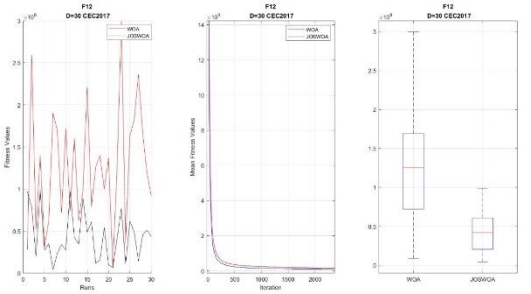
F12
D=30 CEC2017
WOA
JOSWOA
Fitness Values
Runs

F12
D=30 CEC2017
WOA
JOSWOA
Mean Fitness Values
Iteration

F12
D=30 CEC2017
WOA
JOSWOA

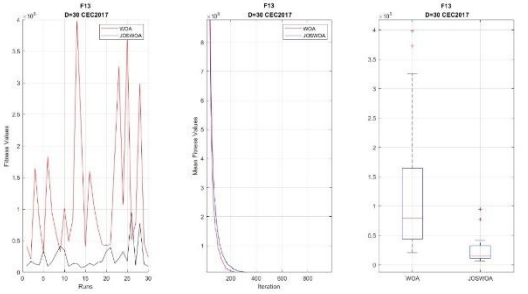
F13
D=30 CEC2017
WOA
JOSWOA
Fitness Values
Runs

F13
D=30 CEC2017
WOA
JOSWOA
Mean Fitness Values
Iteration

F13
D=30 CEC2017
WOA
JOSWOA

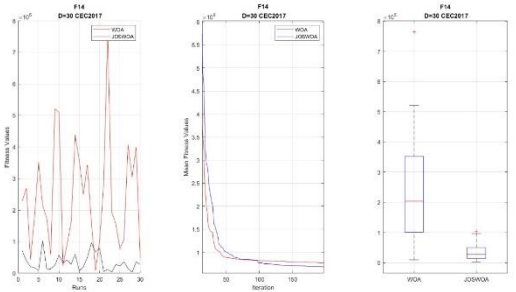
F14
D=30 CEC2017
WOA
JOSWOA
Fitness Values
Runs

F14
D=30 CEC2017
WOA
JOSWOA
Mean Fitness Values
Iteration

F14
D=30 CEC2017
WOA
JOSWOA

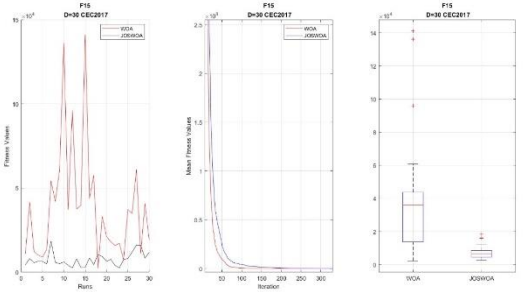
F15
D=30 CEC2017
WOA
JOSWOA
Fitness Values
Runs

F15
D=30 CEC2017
WOA
JOSWOA
Mean Fitness Values
Iteration

F15
D=30 CEC2017
WOA
JOSWOA

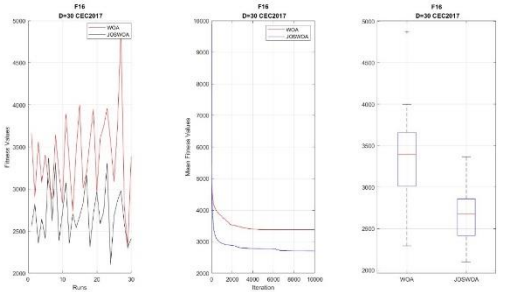
F16
D=30 CEC2017
WOA
JOSWOA
Fitness Values
Runs

F16
D=30 CEC2017
WOA
JOSWOA
Mean Fitness Values
Iteration

F16
D=30 CEC2017
WOA
JOSWOA

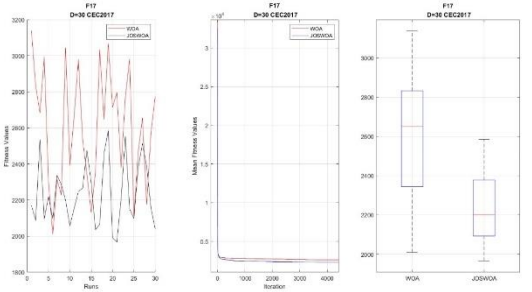
F17
D=30 CEC2017
WOA
JOSWOA
Fitness Values
Runs

F17
D=30 CEC2017
WOA
JOSWOA
Mean Fitness Values
Iteration

F17
D=30 CEC2017
WOA
JOSWOA

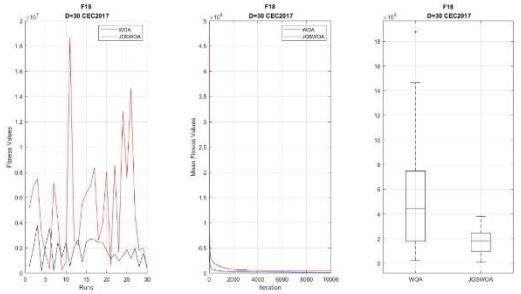
F18
D=30 CEC2017
WOA
JOSWOA
Fitness Values
Runs
F18
D=30 CEC2017
WOA
JOSWOA
Mean Fitness Values
Iteration
F18
D=30 CEC2017
WOA
JOSWOA

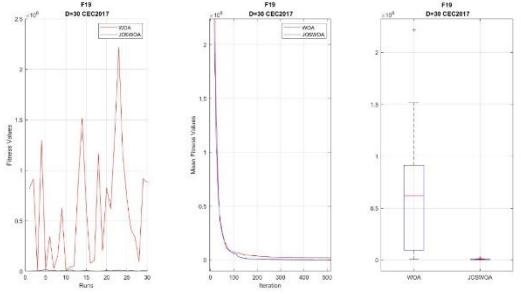
F19
D=30 CEC2017
WOA
JOSWOA
Fitness Values
Runs
F19
D=30 CEC2017
WOA
JOSWOA
Mean Fitness Values
Iteration
F19
D=30 CEC2017
WOA
JOSWOA

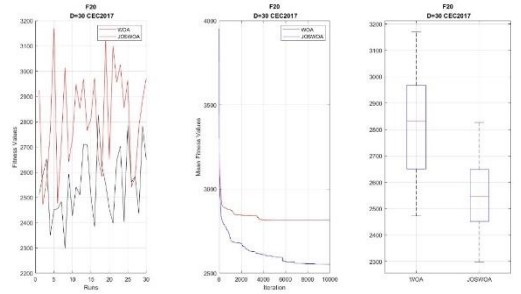
F20
D=30 CEC2017
WOA
JOSWOA
Fitness Values
Runs
F20
D=30 CEC2017
WOA
JOSWOA
Mean Fitness Values
Iteration
F20
D=30 CEC2017
WOA
JOSWOA

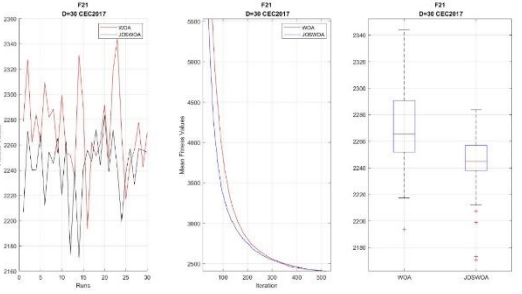
F21
D=30 CEC2017
WOA
JOSWOA
Fitness Values
Runs
F21
D=30 CEC2017
WOA
JOSWOA
Mean Fitness Values
Iteration
F21
D=30 CEC2017
WOA
JOSWOA

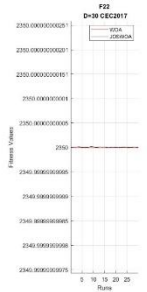
F22
D=30 CEC2017
WOA
JOSWOA
Fitness Values
Runs

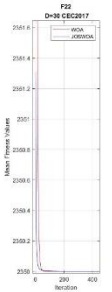
F22
D=30 CEC2017
WOA
JOSWOA
Mean Fitness Values
Iteration

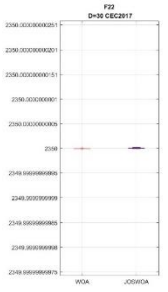
F22
D=30 CEC2017
WOA
JOSWOA

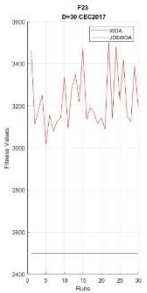
F23
D=30 CEC2017
WOA
JOSWOA
Fitness Values
Runs

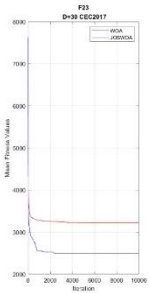
F23
D=30 CEC2017
WOA
JOSWOA
Mean Fitness Values
Iteration

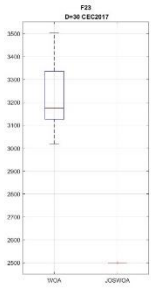
F23
D=30 CEC2017
WOA
JOSWOA

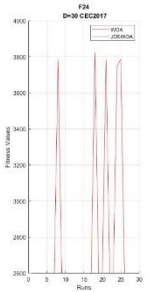
F24
D=30 CEC2017
WOA
JOSWOA
Fitness Values
Runs

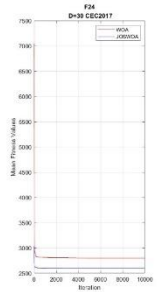
F24
D=30 CEC2017
WOA
JOSWOA
Mean Fitness Values
Iteration

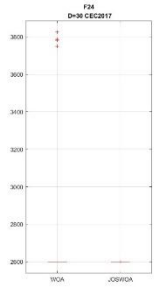
F24
D=30 CEC2017
WOA
JOSWOA

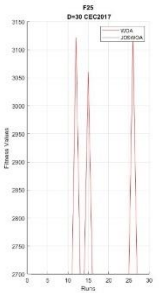
F25
D=30 CEC2017
WOA
JOSWOA
Fitness Values
Runs

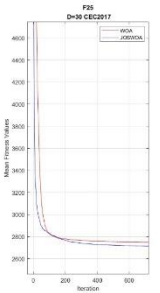
F25
D=30 CEC2017
WOA
JOSWOA
Mean Fitness Values
Iteration

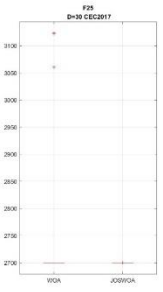
F25
D=30 CEC2017
WOA
JOSWOA

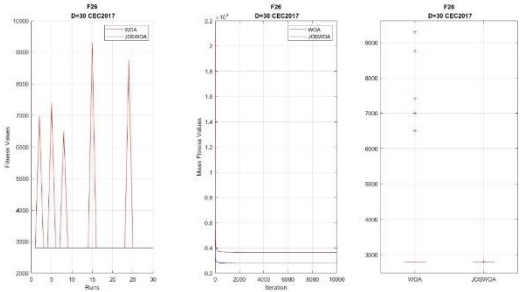
F26
D=30 CEC2017
WOA
JOSWOA
Fitness Values
Runs

F26
D=30 CEC2017
WOA
JOSWOA
Mean Fitness Values
Iteration

F26
D=30 CEC2017
WOA
JOSWOA

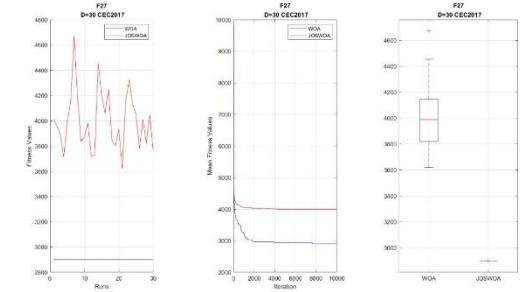
F27
D=30 CEC2017
WOA
JOSWOA
Fitness Values
Runs

F27
D=30 CEC2017
WOA
JOSWOA
Mean Fitness Values
Iteration

F27
D=30 CEC2017
WOA
JOSWOA

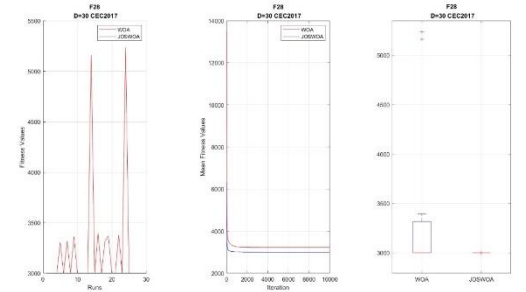
F28
D=30 CEC2017
WOA
JOSWOA
Fitness Values
Runs

F28
D=30 CEC2017
WOA
JOSWOA
Mean Fitness Values
Iteration

F28
D=30 CEC2017
WOA
JOSWOA

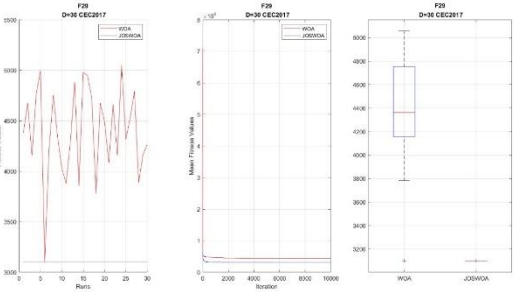
F29
D=30 CEC2017
WOA
JOSWOA
Fitness Values
Runs

F29
D=30 CEC2017
WOA
JOSWOA
Mean Fitness Values
Iteration

F29
D=30 CEC2017
WOA
JOSWOA

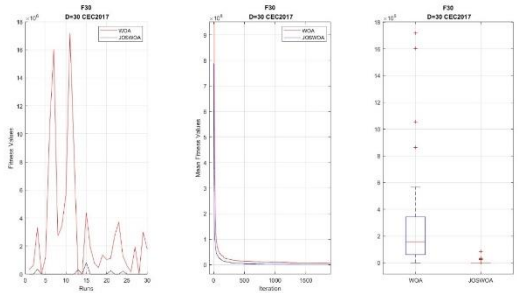

Figure 7: Convergence and stability analysis of WOA and WOAJOS

Stability plays an important role in solving a problem because stability is the determining factor in reaching a global solution to the problem of a given optimization method, i.e., progressing without falling into the trap of the local solution. Figure 8 shows the fitness values, fitness average value and box plot representations of WOAJOS and WOA algorithms for 30 studies. Each of these representations clearly highlights the stability of the individual. It is concluded that the WOA optimization algorithm, which is the aim of the study, has been achieved.

DECLARATION OF COMPETING INTEREST

The authors declare that they have no known competing financial interests or personal relationships that could have appeared to influence the work reported in this paper.

FUNDING / ACKNOWLEDGEMENTS

The authors would like to thank Artvin Çoruh University Scientific Research Projects Coordination Office for supporting this study (BAP2024.F15.02.01).

REFERENCES

Mirjalili S, Lewis A. The whale optimization algorithm. Advances in Engineering Software 2016; 95: 51–67. https://doi.org/10.1016/j.advengsoft.2016.01.008

D. Tian, Z. Shi, MPSO: modified particle swarm optimization and its applications, Swarm and Evolutionary Computation 41 (2018) 49–68.

I. Boussaid, J. Lepagnot, P. Siarry, A survey on optimization metaheuristics, Inf. Sci. 237 (2013) 82–117.

W.G. Jackson, E. Ozcan, R.I. John, Move acceptance in local search metaheuristics for cross-domain search, Expert Syst. Appl. 109 (2018) 131–151.

J. H. Holland, Adaptation in Natural and Artificial Systems, Univ. Michigan, Ann Arbor, MI, 1975.

J. Kennedy, R.C. Eberhart, Particle swarm optimization, in: Proceedings of the IEEE International Conference on Neural Networks, 1995, pp. 1942–1948.

R. Azizipanah-Abarghooee, T. Niknam, M. Gharibzadeh, and F. Golestaneh, ``Robust, fast and optimal solution of practical economic dispatch by a new enhanced gradient-based simpli_ed swarm optimisation algorithm," *IET Gener., Transmiss. Distrib.*, vol. 7, no. 6, pp. 620_635, Jun. 2013, doi: 10.1049/iet-gtd.2012.0616.

M. Mitić, N. Vuković, M. Petrović, and Z. Miljković, ``Chaotic fruity optimization algorithm," *Knowl.-Based Syst.*, vol. 89, pp. 446_458, Nov. 2015, doi: 10.1016/j.knosys.2015.08.010.

L. Wang, L. Liu, J. Qi, and W. Peng, ``Improved quantum particle swarm optimization algorithm for of_ine path planning in AUVs," *IEEE Access*, vol. 8, pp. 143397_143441, 2020, doi: 10.1109/ACCESS.2020.3013953.

B. S. Yildiz, N. Pholdee, S. Bureerat, A. R. Yildiz, and S. M. Sait, ``Enhanced grasshopper optimization algorithm using elite oppositionbased learning for solving real-world engineering problems," *Eng. Comput.*, vol. 2021, pp. 1_13, Jan. 2021, doi: 10.1007/s00366-021-01368-w.

Q. Xu, L. Wang, N. Wang, X. Hei, and L. Zhao, ``A review of oppositionbased learning from 2005 to 2012," *Eng. Appl. Artif. Intell.*, vol. 29, pp. 1-12, Mar. 2014, doi: 10.1016/j.engappai.2013.12.004.

H. R. Tizhoosh, ``Opposition-based learning: A new scheme for machine intelligence," in Proc. Int. Conf. Comput. Intell. Modeling, Control Autom. Int. Conf. Intell. Agents, Web Technol. Internet Commerce, 2005, pp. 695-701, doi: 10.1109/cimca.2005.1631345.

S. Rahnamayan, H. R. Tizhoosh, and M. M. A. Salama, ``Opposition versus randomness in soft computing techniques," *Appl. Soft. Comput.*, vol. 8, no. 2, pp. 906_918, 2008, doi: 10.1016/j.asoc.2007.07.010.

F. S. Al-Qunaieer, H. R. Tizhoosh, and S. Rahnamayan, ``Opposition based computing_A survey," in *Proc. Int. Joint Conf. Neural Netw. (IJCNN)*, Jul. 2010, pp. 1_7, doi: 10.1109/IJCNN.2010.5596906.

S. Mahdavi, S. Rahnamayan, and K. Deb, ``Opposition based learning: A literature review," *Swarm Evol. Comput.*, vol. 39, pp. 1-23, Apr. 2018, doi: 10.1016/j.swevo.2017.09.010.

F. Y. Arini, K. Sunat, and C. Soomlek, ‘‘Golden jackal optimization with joint opposite selection: An enhanced nature-inspired optimization algorithm for solving optimization problems,’’ IEEE Access, vol. 10, pp. 128800–128823, 2022, doi: 10.1109/ACCESS.2022.3227510.

M. Ergezer, D. Simon, and D. Du, ``Oppositional biogeography-based optimization," in *Proc. IEEE Int. Conf. Syst., Man, Cybern.*, Oct. 2009, pp. 1009_1014, doi: 10.1109/ICSMC.2009.5346043.

Y. Xu, Z. Yang, X. Li, H. Kang, and X. Yang, ``Dynamic opposite learning enhanced teaching_learning-based optimization," *Knowl.-Based Syst.*, vol. 188, Jan. 2020, Art. no. 104966, doi: 10.1016/j.knosys.2019.104966.

N. Li, L. Wang, Q. Jiang, X. Li, B. Wang, and W. He, ``An improved genetic transmission and dynamic-opposite learning strategy for multitasking optimization," *IEEE Access*, vol. 9, pp. 131789_131805, 2021, doi: 10.1109/ACCESS.2021.3114435.

T. F. Gonzalez, *Handbook of Approximation Algorithms and Metaheuristics*. Boca Raton, FL, USA: CRC Press, 2007.

B. Morales-Castañeda, D. Zaldívar, E. Cuevas, F. Fausto, and A. Rodríguez, ``A better balance in Metaheuristic algorithms: Does it exist?" *Swarm Evol. Comput.*, vol. 54, May 2020, Art. no. 100671, doi: 10.1016/j.swevo.2020.100671.

M. Črepinšek, S.-H. Liu, and M. Mernik, ``Exploration and exploitation in evolutionary algorithms: A survey," *ACM Comput. Surv.*, vol. 45, no. 3, pp. 1_33, Jun. 2013, doi: 10.1145/2480741.2480752.

X.-S. Yang, S. Deb, and S. Fong, ``Metaheuristic algorithms: Optimal balance of intensi_cation and diversi_cation," *Appl. Math. Inf. Sci.*, vol. 8, no. 3, p. 977, 2014, doi: 10.12785/amis/080306.

D. H.Wolper andW. G. Macready, ``No free lunch theorems for optimization," *IEEE Trans. Evol. Comput.*, vol. 1, no. 1, pp. 67_82, Apr. 1997, doi: 10.1109/4235.585893.

N. Wang, Q. Xu, R. Fei, L. Wang, and C. Shi, ``Are two opposite points better than one?" *IEEE Access*, vol. 7, pp. 146108_146122, 2019, doi: 10.1109/ACCESS.2019.2946089.

Florentina Yuni Arini (2024). A Joint Opposite Selection (JOS) on opposition optimization (https://github.com/FlorentinaJOS/JOS_in_Optimization/releases/tag/v1.1.1), GitHub. Retrieved September 5, 2024.

Sustainable Management of Packaging and Organic Waste in the Marmara Region: Analysis of Potential Recycling and Recovery Scenarios Using Geographic Information System

Hüseyin YURTSEVEN[1]

Mehmet Can SARIKAP[2]

Mirac Nur CİNER*[3]

Hüseyin Kurtuluş ÖZCAN[4]

Emine Elmaslar ÖZBAŞ[5]

1- Assoc. Prof. Dr.; Istanbul University-Cerrahpasa, Forestry Faculty, Surveying and Cadastre Department, Bahçeköy, Istanbul, Türkiye. huseyiny@iuc.edu.tr ORCID No: 0000-0003-2469-9365
2- Lec.; Istanbul University-Cerrahpasa, Project and Technology Office, Avcılar, Istanbul, Türkiye. mehmet.sarikap@iuc.edu.tr ORCID No: 0000-0002-5044-1184
3- Res. Asst.; Istanbul University-Cerrahpasa, Engineering Faculty, Environmental Engineering Department, Avcılar, Istanbul, Türkiye. mirac.ciner@iuc.edu.tr ORCID No: 0000-0002-9920-928X
4- Prof. Dr.; Istanbul University-Cerrahpasa, Engineering Faculty, Environmental Engineering Department, Avcılar, Istanbul, Türkiye. hkozcan@iuc.edu.tr ORCID No: 0000-0002-9810-3985
5- Prof. Dr.; Istanbul University-Cerrahpasa, Engineering Faculty, Environmental Engineering Department,Avcılar, Istanbul, Türkiye. elmaslar@iuc.edu.tr ORCID No: 0000-0001-9065-6684

ABSTRACT

This study evaluates the processes of recycling packaging waste and recovering biodegradable waste in the Marmara Region through four scenarios: the Most Ideal Scenario, the Targeted Scenario, the Partially Successful Scenario, and the Negative Scenario. Analyses incorporating projections for 2025 and 2030 assess the recycling and recovery potentials of biodegradable organic waste alongside packaging materials, including plastic, glass, metal, paper, and cardboard, under different scenarios.

The findings indicate that under the Most Ideal Scenario, significant improvements can be achieved in both the recycling rates of packaging waste and the recovery quantities of organic waste. However, in the Negative Scenario, deficiencies in waste management are projected to result in substantial reductions in recycling and recovery rates.

The study underscores the critical importance of implementing integrated waste management strategies in the Marmara Region. In particular, the effective management of packaging waste through robust recycling systems, and the recovery of organic waste via sustainable methods such as composting and biogas production, play a pivotal role in achieving environmental sustainability and circular economy goals.

Keywords – Municipal Solid Waste (MSW), Municipal Solid Waste Management (MSWM), Recycling, Organic Waste Recovery, Packaging Waste, Sustainable Waste Management, Circular Economy, Marmara Region, Waste Scenarios, Environmental Sustainability.

INTRODUCTION

Municipal Solid Waste (MSW) generation has become a significant environmental issue globally, driven by rapid population growth, urbanization, and industrialization. Current estimates indicate that global MSW generation exceeds 2 billion tons annually, and this volume is expected to increase by to reach 27 billion tons by 2050 (Karak et al., 2012). The volume of waste generated is directly linked to a society's level of economic development, consumption patterns, and living standards. For instance, in high-income countries, the daily per capita generation of MSW is 2.1 kg, whereas in low-income countries, this amount is 1.2 tons per capita per day (Nanda & Berruti, 2021). Moreover, waste composition differs

according to economic level; in low- and middle-income groups, a significant proportion of waste consists of organic materials, while high-income groups generate higher proportions of recyclable materials, particularly paper, glass, and metals (Bandara et al., 2007).

The increasing trend in MSW generation is regarded as a global crisis that necessitates not only the efficient use of resources but also the reduction of waste generation for environmental sustainability. Key drivers of this increase include rapid urbanization, rising individual consumption, and accelerated industrialization. Notably, in developing countries, MSW generation has been grow at a faster rate due to urban population growth and economic expansion. In this context, regional differences in the composition and volume of MSW highlight the necessity of developing tailored waste management strategies for each country or region. This acceleration in waste generation is emerging as a critical issue that requires consideration not only of its environmental impacts but also its social and economic sustainability dimensions.

The Marmara Region, as one of the most densely populated and rapidly urbanizing areas in Türkiye, holds critical importance for Municipal Solid Waste Management (MSWM). The region's extensive industrial activities, increasing urban population, and expanding commercial operations have led to a rapid rise in MSW generation. This issue poses a significant challenge not only in terms of environmental sustainability but also for public health protection and the efficient utilization of natural resources. A substantial portion of the MSW generated in the Marmara Region consists of organic waste, packaging materials, and other recyclable materials. However, the disposal of these wastes through traditional methods such as uncontrolled landfilling or incineration has contributed to air and water pollution as well as increased greenhouse gas emissions. Considering the ecological sensitivity of the region and the need to protect the Marmara Sea, the implementation of integrated and sustainable waste management systems is of paramount importance. Modern waste management approaches prioritize optimizing recycling and utilizing waste in innovative processes such as energy production, while landfilling is considered only as a last resort. This strategy not only effectively mitigates the region's environmental challenges but also presents a model that supports sustainable economic development. Consequently, MSWM in the Marmara Region should be approached as a strategic priority aimed at balancing environmental protection and economic growth.

MSWM continues to be a critical issue globally, directly impacting environmental sustainability and public health. Mismanagement practices, such as uncontrolled landfilling, unregulated waste burning, and insufficient recycling systems, contribute to increased greenhouse gas emissions, air, water, and soil pollution, posing significant threats to public health (Osra et al., 2024; Ding et al., 2021). Additionally, inadequacies in MSWM result in not only environmental challenges but also economic and social problems. Effective MSWM requires increasing recycling rates, utilizing waste for energy production, and integrating innovative technologies (Calabrò & Satira, 2020). Furthermore, adopting circular economy approaches that prioritize waste reduction and resource efficiency is crucial for long-term sustainability (Sharma & Jain, 2020). Therefore, MSWM necessitates an integrated approach that not only focuses on waste disposal but also emphasizes resource conservation and minimizing environmental impacts.

The European Green Deal outlines comprehensive regulations aimed at reducing packaging waste and enhancing its recyclability, in line with the goal of achieving a climate-neutral continent by 2050. Within this framework, the objective is to ensure that all packaging in the EU market is recyclable and to reduce the amount of packaging waste by 2030 (Schneikart et al., 2024; Scott, 2018; MoT, 2024). In Türkiye, the Regulation on the Control of Packaging Waste aims to protect the environment and ensure the efficient use of natural resources by regulating the separate collection, recycling, and recovery of packaging waste at its source (PWCR, 2021). Recycling packaging waste reduces the demand for raw materials, thereby saving energy, while recovering organic waste through composting and biogas production contributes to sustainable agriculture and energy generation. These practices are critical not only for preventing environmental pollution but also for achieving circular economy goals, underscoring their importance within the broader framework of sustainable development.

This study examines the sustainable management of packaging and organic waste in the Marmara Region through the analysis of recycling distribution maps at the provincial level under four potential scenarios: “Evaluation of the Most Ideal Scenario,” “Evaluation of the Targeted Scenario,” “Evaluation of the Partially Successful Scenario,” and “Evaluation of the Negative Scenario.” Using Geographic Information Systems (GIS), the regional impacts of each scenario were evaluated, detailing the distribution of recycling and recovery capacities at the

provincial level and analyzing the potential contributions of these scenarios to sustainable waste management. Through these scenarios, the study aims to optimize waste management strategies within the context of spatial planning and provide a scientific foundation for achieving circular economy goals in the Marmara Region.

MATERIALS AND METHODS

Site Description (Marmara Region)

The Marmara Region, located in the northwest of Türkiye, is one of the country's most significant regions in terms of economy, trade, and demographics (Figure 1). Covering approximately 8.5% of Türkiye's total area, the region includes 11 provinces: Istanbul, Bursa, Kocaeli, Balıkesir, Tekirdağ, Sakarya, Edirne, Çanakkale, Kırklareli, Bilecik, and Yalova (RoT, 2015). As the most densely populated region in Türkiye, Marmara is home to more than 30% of the country's total population (MMU, 2024).

The region is strategically located at the crossroads of Asia and Europe, encompassing significant waterways such as the Bosphorus and the Dardanelles. This strategic position enhances the Marmara Region's importance in both national and international trade and logistics. Approximately 30.4% of Türkiye's Gross Domestic Product (GDP) is generated by Istanbul, which is situated within the boundaries of the Marmara Region (TURKSTAT, 2022).

However, the Marmara Region faces significant challenges in terms of environmental sustainability due to intensive industrial activities and rapid urbanization. In particular, the management of packaging and organic waste holds critical importance for mitigating environmental impacts and achieving circular economy goals. In this context, the Marmara Region presents a suitable study area for the development and implementation of sustainable waste management scenarios.

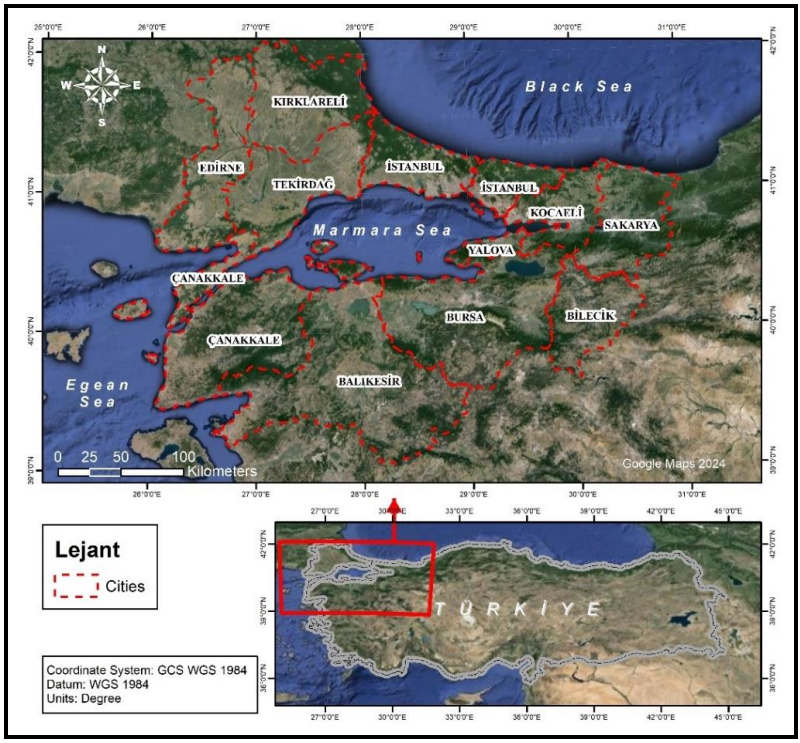

Figure 1. Marmara Region

Spatial Data Processing and Visualization

The spatial analyses for this study were conducted using ArcGIS Geographic Information System (GIS) software, which offers advanced tools for geospatial data integration, analysis, and visualization (Esri, 2024). The datasets obtained during the study were integrated with the spatial data of the study area in the GIS environment and subsequently transferred to spatial databases. This step ensured the seamless management and analysis of geospatial data within a unified framework. GIS facilitated the precise calculation of spatial parameters and the visualization of spatial patterns, enabling the identification of significant trends, correlations, and anomalies in the study area. Additionally, the cartographic outputs generated in GIS environment provided a clear and intuitive means of interpreting results, supporting spatial decision-making and enhancing the overall analytical process.

Following this, the geospatial data and corresponding attributes were imported into the R environment for further analysis and visualization (R

Core Team, 2021). The data were processed and visualized using several powerful R packages, including ggplot2, ggmap, viridis, rayshader, and the tidyverse collection. These tools allowed for the creation of high-resolution thematic maps and 3D visualizations, effectively presenting the research findings. The ggplot2 package was used to produce detailed 2D graphics, while viridis ensured accessible and scientifically accurate color scales. (Garnier et al., 2024; Kahle & Wickham, 2013; Morgan-Wall, 2024; Wickham et al., 2019; Wickham et al., 2016). The use of ggplot2 allowed for the production of high-resolution 2D graphics, while 3D renderings offered an enhanced perspective on spatial distributions and relationships within the study area. Custom legends, color scales, and annotations were incorporated into the visual outputs to ensure clarity and scientific rigor. In the study, by combining ArcGIS-based spatial processing with advanced R-based analysis and visualization techniques, the spatial distribution of the findings was interpreted and spatial awareness was created.

Solid Waste Characterization

In Istanbul's waste characterization, biodegradable waste constitutes the largest share of total waste at 48.17%. This is followed by paper and cardboard (10.38%) and plastic bags (9.57%). Other significant categories include other combustible waste (8.9%), glass (4.93%), diapers (4.86%), and textiles (4.69%). Waste types with lower proportions include metals (1%), other non-combustible waste (1.71%), PET plastics (1.48%), composite waste (0.89%), hazardous waste (0.86%), and electronic waste (0.18%) (IESR, 2022).

In the waste characterization of Tekirdağ Province, biodegradable waste accounts for the largest share at 46%. This is followed by other combustible waste (14%), paper and cardboard (13%), and glass (9%). Plastics and other non-combustible waste each represent 8%, while metals constitute 2% of the total waste (TESR, 2022). In the waste characterization of Edirne Province, biodegradable waste holds the largest share at 61% of total waste. This is followed by paper and cardboard (18%) and ash (14%). Additionally, glass waste accounts for 5%, while metals and plastics each represent 1% (EESR, 2021).

In the waste characterization of Kırklareli Province, biodegradable waste constitutes the largest share at 39% of total waste. This is followed by other waste (16%), plastics (14%), paper and cardboard (9%), glass (8%),

and ash (7%). Park and garden waste accounts for 5%, while metals and other combustible waste each represent 1% (KESR-a, 2022). In the waste characterization of Balıkesir Province, biodegradable waste represents the largest category at 43% of total waste. This is followed by other combustible waste (18%), plastics (14%), ash (13%), and metals, glass, and paper-cardboard categories, each with an equal share of 4% (BESR-a, 2022).

In the waste characterization of Çanakkale Province, biodegradable waste constitutes 40% of total waste, ranking first. This is followed by paper and cardboard (19%), other waste (19%), plastics (15%), and glass (5%). Metals account for 2% of total waste (CESR, 2011). In the waste characterization of Bursa Province, biodegradable waste represents 54% of total waste, holding the largest share. This is followed by other combustible waste (13%), paper and cardboard (10%), plastic bags (7%), glass (7%), and plastics (6%). Additionally, PET plastics account for 2%, and other non-combustible waste constitutes 1% (Ünlü et al., 2022).

In the waste characterization of Bilecik Province, biodegradable waste holds the largest share at 48%. This is followed by other waste (15%), paper and cardboard (14%), plastics (10%), and glass (8%). Ash waste accounts for 4%, while metals constitute 1% (BESR-b, 2022). In the waste characterization of Sakarya Province, biodegradable waste represents 46.65% of total waste. This is followed by other combustible waste (25.15%), plastics (8.84%), paper and cardboard (7.25%), and glass (4.82%). Lower proportions include metals (1.04%), ash (2.2%), park and garden waste (2.82%), others (0.36%), other non-combustible waste (0.49%), hazardous waste (0.32%), and electronic waste (0.05%) (SESR, 2022).

In the waste characterization of Kocaeli Province, biodegradable waste holds the largest share at 54.2% of total waste. This is followed by other combustible waste (15.15%), plastics (14.58%), paper and cardboard (5.92%), and glass (4.88%). Lower proportions include metals (1.51%), ash (1.87%), park and garden waste (0.64%), hazardous waste (0.91%), electronic waste (0.15%), and other non-combustible waste (0.19%) (KESR-b, 2022). In the waste characterization of Yalova Province, biodegradable waste represents 49.5% of total waste, making up the largest share. This is followed by ash (15%), paper and cardboard (11%), plastics (9.7%), metals (5%), other waste (5%), and glass (4.8%) (YESR, 2023). The waste characterization of all provinces in the Marmara Region is presented in Figure 2.

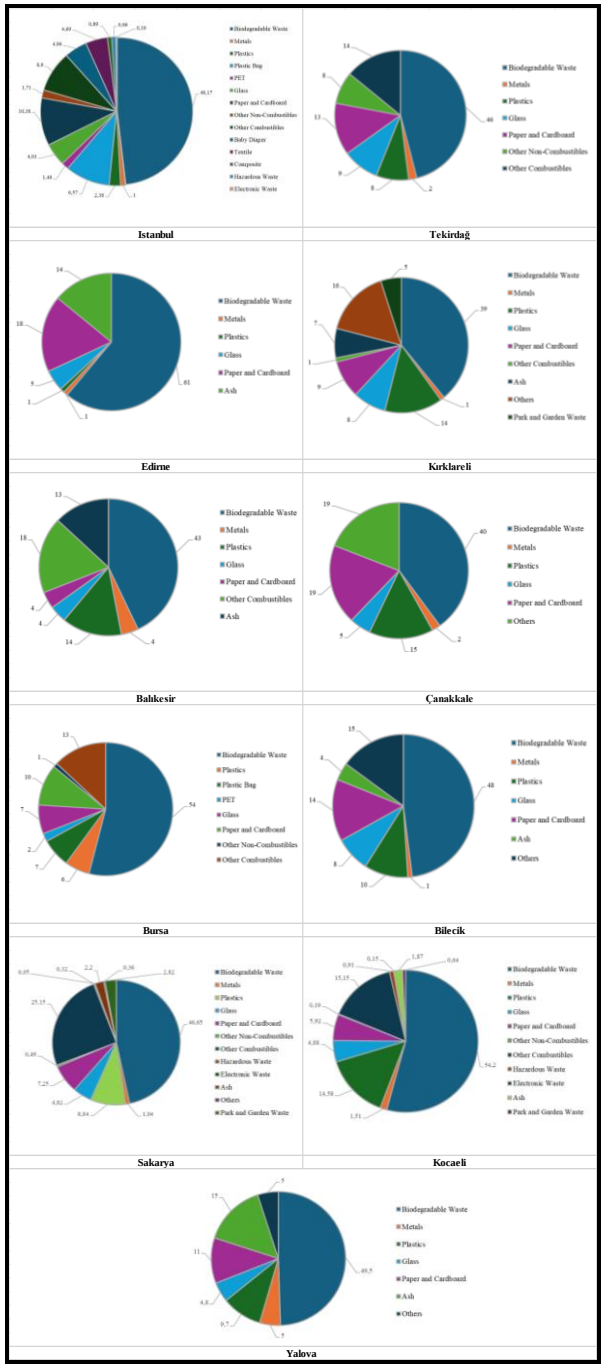

Figure 2. Waste Characterization of Provinces in the Marmara Region

Scenario Development and Classification

The potential scenarios evaluated in this study were determined in line with the European Green Deal and the Regulation on the Management of Packaging Waste. Accordingly, four main scenario categories were developed based on the potential to achieve recovery and recycling targets: the Most Ideal Scenario, the Targeted Scenario, the Partially Successful Scenario, and the Negative Scenario (Table 1).

Table 1. Recycling and Recovery Rates Across Different Scenarios and Years (2025 and 2030)

Scenarios	Most Ideal Scenario		Targeted Scenario		Partially Successful Scenario		Negative Scenario	
Years	**2025**	**2030**	**2025**	**2030**	**2025**	**2030**	**2025**	**2030**
Biodegradable Waste (%)	60	75	50	65	40	55	30	45
Metals (%)	80	90	65	75	55	65	45	55
Plastics (%)	55	60	50	55	45	50	40	45
Glass (%)	80	80	70	75	65	70	55	60
Paper and Cardboard (%)	80	90	75	85	70	80	60	70

- **Most Ideal Scenario:** This scenario can be achieved through the effective utilization of existing waste management technologies, the expansion of recycling infrastructure, and maximizing societal awareness. It requires the full operation of waste collection systems, the complete fulfillment of producer responsibilities, and the strict implementation of circular economy policies. Additionally, the sustainable operation of monitoring mechanisms supported by stringent regulations is a critical necessity.
- **Targeted Scenario:** This scenario may occur if planned waste management strategies are largely implemented but with the presence of certain regional or sectoral limitations. The development of recycling infrastructure and the successful continuation of waste management policies are expected.

- **Partially Successful Scenario:** This scenario represents situations where recycling targets are partially achieved. Factors such as the inability to expand waste collection systems, insufficient capacity of recycling facilities, and low public participation rates in recycling play a significant role in the occurrence of this scenario. Additionally, limitations in economic resources can further exacerbate this situation.
- **Negative Scenario:** This scenario arises when waste management policies are not adequately implemented, recycling infrastructure remains insufficient, and societal awareness is low. Key factors contributing to this situation include technological deficiencies, the malfunctioning of monitoring mechanisms, and the lack of economic resources allocated to the recycling sector. Additionally, the inability to control waste generation and the continued reliance on traditional methods such as landfilling further result in low recycling rates.

RESULTS

The recycling scenarios are based on the 2025 and 2030 projections for the provinces in the Marmara Region, and the potential for recyclable and recoverable waste for each province in these years is presented in Figure 3.

Figure 3. Distribution of Recyclable/Recoverable Waste Potentials by Provinces for 2025 and 2030

The amounts of recyclable/recoverable waste for each province, expressed in tons per year, are detailed based on waste characterization and the targeted recycling and recovery rates. These scenarios are evaluated under four different headings: Most Ideal Scenario, Targeted Scenario, Partially Successful Scenario, and Negative Scenario.

In this context, the scenarios provide a comparative analysis of recycling performances for different types of waste (biodegradable organic waste, metals, plastics, glass, paper, and cardboard) in the Marmara Region, evaluated by year and conditions. Each scenario offers significant insights into regional infrastructure, economic resources, societal awareness, and policy effectiveness based on the level of achievement of recycling targets.

The recycling projections for Istanbul in 2025 and 2030, under the Most Ideal Scenario, target the recovery of 1,981,901 tons/year and 2,631,757 tons/year of biodegradable organic waste, respectively. However, under the Negative Scenario, these values may decline to 990,951 tons/year and 1,579,054 tons/year. For plastic waste recycling, the Most Ideal Scenario projects 506,516 tons/year in 2025 and 586,996 tons/year in 2030, while deviations from targets under the Negative Scenario may result in reductions to 368,375 tons/year and 440,247 tons/year. Glass waste is projected to reach 287,306 tons/year, and paper and cardboard waste 680,531 tons/year under the Most Ideal Scenario. These values may decrease to 215,480 tons/year for glass and 529,302 tons/year for paper and cardboard under the Negative Scenario (Table 2). To enhance Istanbul's recycling performance, achieving targets based on waste characterization data, processing biodegradable waste in composting and energy recovery facilities, and improving collection efficiency for plastics, glass, and paper are critical requirements for environmental sustainability.

Table 2. Assessment of Istanbul's Recycling/Recovery Potential Based on Scenarios (2025-2030)

Scenarios	**Most Ideal Scenario**		**Targeted Scenario**		**Partially Successful Scenario**		**Negative Scenario**	
Years	**2025**	**2030**	**2025**	**2030**	**2025**	**2030**	**2025**	**2030**
Biodegradable Waste (ton/year)	1981901	2631757	1651584	2280856	1321268	1929955	990951	1579054
Metals (ton/year)	54859	65562	44573	54635	37715	47350	30858	40065
Plastics (ton/year)	506516	586996	460469	538080	414422	489163	368375	440247
Glass (ton/year)	270453	287306	236646	269349	219743	251393	185936	215480
Paper and Cardboard (ton/year)	569431	680531	533842	642723	498253	604916	427074	529302

In Tekirdağ, under the Most Ideal Scenario, biodegradable organic waste is projected to reach 139,318 tons/year in 2025 and 183,678 tons/year in 2030, while plastic waste recycling could achieve 22,210 tons/year and 25,555 tons/year, respectively. Under the Negative Scenario, these amounts decrease to 69,659 tons/year and 110,207 tons/year for biodegradable waste, and 16,153 tons/year and 19,166 tons/year for plastic waste. For metal waste recycling, the Most Ideal Scenario projects 8,076 tons/year (2025) and 9,583 tons/year (2030), while the Negative Scenario sees reductions to 4,543 tons/year and 5,856 tons/year. Glass waste recovery is estimated at 36,344 tons/year in 2025 and 38,333 tons/year in 2030 under the Most Ideal Scenario, compared to 24,986 tons/year and 28,750 tons/year under the Negative Scenario. For paper and cardboard waste, the Most Ideal Scenario targets 52,497 tons/year in 2025 and 62,291 tons/year in 2030, while the Negative Scenario shows potential declines to 39,373 tons/year and 48,448 tons/year (Table 3).

Table 3. Assessment of Tekirdağ's Recycling/Recovery Potential Based on Scenarios (2025-2030)

Scenarios	**Most Ideal Scenario**		**Targeted Scenario**		**Partially Successful Scenario**		**Negative Scenario**	
Years	**2025**	**2030**	**2025**	**2030**	**2025**	**2030**	**2025**	**2030**
Biodegradable Waste (ton/year)	139318	183678	116099	159187	92879	134697	69659	110207
Metals (ton/year)	8076	9583	6562	7986	5553	6921	4543	5856
Plastics (ton/year)	22210	25555	20191	23426	18172	21296	16153	19166
Glass (ton/year)	36344	38333	31801	35937	29529	33541	24986	28750
Paper and Cardboard (ton/year)	52497	62291	49216	58830	45935	55369	39373	48448

In Edirne, under the Most Ideal Scenario, biodegradable organic waste recovery is projected to reach 70,385 tons/year in 2025 and 92,469 tons/year in 2030, while under the Negative Scenario, these values drop to 35,193 tons/year and 55,482 tons/year. For metal waste recovery, the Most Ideal Scenario estimates 1,538 tons/year in 2025 and 1,819 tons/year in 2030, whereas the Negative Scenario predicts reductions to 865 tons/year and 1,112 tons/year. Plastic waste recycling is expected to reach 1,058

tons/year in 2025 and 1,213 tons/year in 2030 under the Most Ideal Scenario, compared to 769 tons/year and 910 tons/year under the Negative Scenario. For glass waste, the highest recovery values are calculated as 7,692 tons/year (2025) and 8,085 tons/year (2030), while the lowest values are estimated at 5,289 tons/year and 6,064 tons/year. Paper and cardboard waste recycling could achieve 27,693 tons/year in 2025 and 32,743 tons/year in 2030 under the Most Ideal Scenario, while the Negative Scenario shows potential decreases to 20,769 tons/year and 25,467 tons/year (Table 4).

Table 4. Assessment of Edirne's Recycling/Recovery Potential Based on Scenarios (2025-2030)

Scenarios	**Most Ideal Scenario**		**Targeted Scenario**		**Partially Successful Scenario**		**Negative Scenario**	
Years	**2025**	**2030**	**2025**	**2030**	**2025**	**2030**	**2025**	**2030**
Biodegradable Waste (ton/year)	70385	92469	58654	80140	46923	67811	35193	55482
Metals (ton/year)	1538	1819	1250	1516	1058	1314	865	1112
Plastics (ton/year)	1058	1213	962	1112	865	1011	769	910
Glass (ton/year)	7692	8085	6731	7579	6250	7074	5289	6064
Paper and Cardboard (ton/year)	27693	32743	25962	30924	24231	29105	20769	25467

In Kırklareli, under the Most Ideal Scenario, the recovery of biodegradable organic waste is projected to reach 32,894 tons/year in 2025 and 43,325 tons/year in 2030, while under the Negative Scenario, these values drop to 16,447 tons/year and 25,995 tons/year. For metal waste recycling, the Most Ideal Scenario estimates 1,125 tons/year in 2025 and 1,333 tons/year in 2030, whereas the Negative Scenario predicts reductions to 633 tons/year and 815 tons/year. For plastic waste, the Most Ideal Scenario projects 10,824 tons/year in 2025 and 12,442 tons/year in 2030, while the Negative Scenario estimates 7,872 tons/year and 9,332 tons/year. Glass waste recycling could reach 8,997 tons/year in 2025 and 9,480 tons/year in 2030 under the best conditions, but under the Negative Scenario, these values are reduced to 6,185 tons/year and 7,110 tons/year. For paper and cardboard waste, the Most Ideal Scenario predicts 10,121 tons/year in

2025 and 11,998 tons/year in 2030, while under the Negative Scenario, these values remain at 7,591 tons/year and 9,332 tons/year (Table 5).

Table 5. Assessment of Kırklareli's Recycling/Recovery Potential Based on Scenarios (2025-2030)

Scenarios	**Most Ideal Scenario**		**Targeted Scenario**		**Partially Successful Scenario**		**Negative Scenario**	
Years	**2025**	**2030**	**2025**	**2030**	**2025**	**2030**	**2025**	**2030**
Biodegradable Waste (ton/year)	32894	43325	27412	37549	21929	31772	16447	25995
Metals (ton/year)	1125	1333	914	1111	773	963	633	815
Plastics (ton/year)	10824	12442	9840	11405	8856	10368	7872	9332
Glass (ton/year)	8997	9480	7872	8887	7310	8295	6185	7110
Paper and Cardboard (ton/year)	10121	11998	9489	11331	8856	10665	7591	9332

In Balıkesir, under the Most Ideal Scenario, the recovery of biodegradable organic waste is projected to reach 118,668 tons/year in 2025 and 155,901 tons/year in 2030. Under the Negative Scenario, these values are estimated to drop to 59,334 tons/year and 93,541 tons/year. For metal waste recycling, the Most Ideal Scenario predicts 14,718 tons/year in 2025 and 17,403 tons/year in 2030, while the Negative Scenario estimates reductions to 8,279 tons/year and 10,635 tons/year. The recycling potential of plastic waste is calculated as 35,416 tons/year in 2025 and 40,607 tons/year in 2030 under the Most Ideal Scenario, but these values decline to 25,757 tons/year and 30,455 tons/year under the Negative Scenario. For glass waste, the Most Ideal Scenario targets 14,718 tons/year in 2025 and 15,469 tons/year in 2030, whereas the Negative Scenario projects values of 10,119 tons/year and 11,602 tons/year. For paper and cardboard waste, the recycling amounts are determined as 14,718 tons/year in 2025 and 17,403 tons/year in 2030 under the Most Ideal Scenario, while under the Negative Scenario, these amounts are projected to be 11,039 tons/year and 13,536 tons/year (Table 6).

Table 6. Assessment of Balıkesir's Recycling/Recovery Potential Based on Scenarios (2025-2030)

Scenarios	**Most Ideal Scenario**		**Targeted Scenario**		**Partially Successful Scenario**		**Negative Scenario**	
Years	**2025**	**2030**	**2025**	**2030**	**2025**	**2030**	**2025**	**2030**
Biodegradable Waste (ton/year)	118668	155901	98890	135114	79112	114328	59334	93541
Metals (ton/year)	14718	17403	11959	14502	10119	12569	8279	10635
Plastics (ton/year)	35416	40607	32197	37223	28977	33839	25757	30455
Glass (ton/year)	14718	15469	12879	14502	11959	13536	10119	11602
Paper and Cardboard (ton/year)	14718	17403	13799	16436	12879	15469	11039	13536

According to Çanakkale's recycling projections for 2025 and 2030, under the Most Ideal Scenario, biodegradable waste recovery is expected to reach 88,706 tons/year in 2025 and 116,538 tons/year in 2030. Under the Negative Scenario, these amounts are estimated to decrease to 44,353 tons/year and 69,923 tons/year. For metal waste recovery, the Most Ideal Scenario predicts 5,914 tons/year in 2025 and 6,992 tons/year in 2030, whereas the Negative Scenario estimates reductions to 3,326 tons/year and 4,273 tons/year. Plastic waste recycling is projected to reach 30,493 tons/year in 2025 and 34,961 tons/year in 2030 under the Most Ideal Scenario, but these values drop to 22,176 tons/year and 26,221 tons/year under the Negative Scenario. Glass waste recycling under the Most Ideal Scenario is estimated to be 14,784 tons/year in 2025 and 15,538 tons/year in 2030, while under the Negative Scenario, these values are projected to decrease to 10,164 tons/year and 11,654 tons/year. For paper and cardboard waste, recovery targets under the Most Ideal Scenario are 56,180 tons/year in 2025 and 66,427 tons/year in 2030. Under the Negative Scenario, these amounts decline to 42,135 tons/year and 51,665 tons/year (Table 7).

Table 7. Assessment of Çanakkale's Recycling/Recovery Potential Based on Scenarios (2025-2030)

Scenarios	**Most Ideal Scenario**		**Targeted Scenario**		**Partially Successful Scenario**		**Negative Scenario**	
Years	**2025**	**2030**	**2025**	**2030**	**2025**	**2030**	**2025**	**2030**
Biodegradable Waste (ton/year)	88706	116538	73921	101000	59137	85461	44353	69923
Metals (ton/year)	5914	6992	4805	5827	4066	5050	3326	4273
Plastics (ton/year)	30493	34961	27720	32048	24948	29135	22176	26221
Glass (ton/year)	14784	15538	12936	14567	12012	13596	10164	11654
Paper and Cardboard (ton/year)	56180	66427	52669	62736	49158	59046	42135	51665

In Bursa, under the Most Ideal Scenario, the recovery of biodegradable organic waste is projected to reach 345,139 tons/year in 2025 and 453,430 tons/year in 2030, while under the Negative Scenario, these amounts drop to 172,569 tons/year and 272,058 tons/year. For plastic waste recycling, the Most Ideal Scenario estimates 87,883 tons/year in 2025 and 100,762 tons/year in 2030. Under the Negative Scenario, these values decrease to 63,915 tons/year and 75,572 tons/year. The recycling amount for glass waste is expected to reach 59,654 tons/year in 2025 and 62,697 tons/year in 2030 under the best conditions, while under the Negative Scenario, these values are limited to 41,012 tons/year and 47,022 tons/year. For paper and cardboard waste, the Most Ideal Scenario targets 85,219 tons/year in 2025 and 100,762 tons/year in 2030, while under the Negative Scenario, these amounts are calculated to be 63,915 tons/year and 78,371 tons/year (Table 8).

Table 8. Assessment of Bursa's Recycling/Recovery Potential Based on Scenarios (2025-2030)

Scenarios	Most Ideal Scenario		Targeted Scenario		Partially Successful Scenario		Negative Scenario	
Years	**2025**	**2030**	**2025**	**2030**	**2025**	**2030**	**2025**	**2030**
Biodegradable Waste (ton/year)	345139	453430	287616	392973	230092	332516	172569	272058
Metals (ton/year)	0	0	0	0	0	0	0	0
Plastics (ton/year)	87883	100762	79893	92365	71904	83969	63915	75572
Glass (ton/year)	59654	62697	52197	58778	48469	54859	41012	47022
Paper and Cardboard (ton/year)	85219	100762	79893	95164	74567	89566	63915	78371

In the province of Bilecik, under the Most Ideal Scenario, the recovery of biodegradable waste is projected to reach 21,052 tons/year in 2025 and 26,843 tons/year in 2030, whereas under the Negative Scenario, these quantities decrease to 10,526 tons/year and 16,106 tons/year, respectively. Metal waste recycling under the Most Ideal Scenario is estimated at 585 tons/year (2025) and 671 tons/year (2030), whereas under the Negative Scenario, it declines to 329 tons/year and 410 tons/year. Regarding plastic waste, recycling is calculated to be 4,020 tons/year (2025) and 4,474 tons/year (2030) under the Most Ideal Scenario, whereas in the negative scenario these projections are projected at 2,924 tons/year and 3,355 tons/year. The potential for glass waste recycling in the Most Ideal Scenario is expected to reach 4,678 tons/year (2025) and 4,772 tons/year (2030), while under the Negative Scenario, it is forecast to drop to 3,216 tons/year and 3,579 tons/year. Lastly, paper and cardboard waste recycling under the Most Ideal Scenario is estimated at 8,187 tons/year (2025) and 9,395 tons/year (2030), whereas these values fall to 6,140 tons/year and 7,307 tons/year under the Negative Scenario (Table 9).

Table 9. Assessment of Bilecik's Recycling/Recovery Potential Based on Scenarios (2025-2030)

Scenarios	**Most Ideal Scenario**		**Targeted Scenario**		**Partially Successful Scenario**		**Negative Scenario**	
Years	**2025**	**2030**	**2025**	**2030**	**2025**	**2030**	**2025**	**2030**
Biodegradable Waste (ton/year)	21052	26843	17543	23264	14034	19685	10526	16106
Metals (ton/year)	585	671	475	559	402	485	329	410
Plastics (ton/year)	4020	4474	3655	4101	3289	3728	2924	3355
Glass (ton/year)	4678	4772	4093	4474	3801	4176	3216	3579
Paper and Cardboard (ton/year)	8187	9395	7675	8873	7163	8351	6140	7307

According to current recycling projections for Sakarya, under the Most Ideal Scenario, the recovery of biodegradable waste is anticipated to reach 104,142 tons/year (2025) and 136,818 tons/year (2030), whereas under the Negative Scenario, these projections are projected at 52,071 tons/year and 82,091 tons/year, respectively. Metal waste recycling in the Most Ideal Scenario is estimated to increase to 3,096 tons/year (2025) and 3,660 tons/year (2030), while under the negative scenario, it is forecast to decline to 1,741 tons/year and 2,237 tons/year. With regard to plastic waste, the recycling potential under the Most Ideal Scenario is predicted to be 18,090 tons/year (2025) and 20,741 tons/year (2030), whereas under the Negative Scenario, these amounts remain at 13,156 tons/year and 15,556 tons/year. Glass waste recycling in the Most Ideal Scenario is expected to reach 14,347 tons/year (2025) and 15,079 tons/year (2030), while under the Negative Scenario, it decreases to 9,864 tons/year and 11,309 tons/year. Lastly, the recovery of paper and cardboard waste in the Most Ideal Scenario is targeted at 21,580 tons/year (2025) and 25,516 tons/year (2030), compared to 16,185 tons/year and 19,846 tons/year under the Negative Scenario (Table 10).

Table 10. Assessment of Sakarya's Recycling/Recovery Potential Based on Scenarios (2025-2030)

Scenarios	**Most Ideal Scenario**		**Targeted Scenario**		**Partially Successful Scenario**		**Negative Scenario**	
Years	**2025**	**2030**	**2025**	**2030**	**2025**	**2030**	**2025**	**2030**
Biodegradable Waste (ton/year)	104142	136818	86785	118576	69428	100334	52071	82091
Metals (ton/year)	3096	3660	2515	3050	2128	2643	1741	2237
Plastics (ton/year)	18090	20741	16446	19013	14801	17284	13156	15556
Glass (ton/year)	14347	15079	12554	14136	11657	13194	9864	11309
Paper and Cardboard (ton/year)	21580	25516	20231	24098	18883	22681	16185	19846

In Kocaeli, under the Most Ideal Scenario, the recovery of biodegradable waste is projected to reach 208,795 tons/year (2025) and 274,307 tons/year (2030), while under the Negative Scenario, these values are estimated at 104,397 tons/year and 164,584 tons/year, respectively. Metal waste recycling in the Most Ideal Scenario is calculated to be 7,756 tons/year (2025) and 9,171 tons/year (2030), whereas under the Negative Scenario, these amounts decline to 4,363 tons/year and 5,604 tons/year. The potential for plastic waste recycling under the Most Ideal Scenario stands at 51,486 tons/year (2025) and 59,032 tons/year (2030), whereas under the Negative Scenario, these projections are projected to be 37,444 tons/year and 44,274 tons/year. In the Most Ideal Scenario, the recovery of glass waste reaches 25,066 tons/year (2025) and 26,344 tons/year (2030), but in the Negative Scenario, these values drop to 17,233 tons/year and 19,758 tons/year. Lastly, the recycling of paper and cardboard waste in the Most Ideal Scenario is targeted at 30,408 tons/year (2025) and 35,953 tons/year (2030), while under the Negative Scenario, these amounts remain at 22,806 tons/year and 27,964 tons/year (Table 11).

Table 11. Assessment of Kocaeli's Recycling/Recovery Potential Based on Scenarios (2025-2030)

Scenarios	**Most Ideal Scenario**		**Targeted Scenario**		**Partially Successful Scenario**		**Negative Scenario**	
Years	**2025**	**2030**	**2025**	**2030**	**2025**	**2030**	**2025**	**2030**
Biodegradable Waste (ton/year)	208795	274307	173996	237733	139197	201158	104397	164584
Metals (ton/year)	7756	9171	6302	7642	5332	6623	4363	5604
Plastics (ton/year)	51486	59032	46806	54112	42125	49193	37444	44274
Glass (ton/year)	25066	26344	21932	24698	20366	23051	17233	19758
Paper and Cardboard (ton/year)	30408	35953	28507	33956	26607	31959	22806	27964

In Yalova, under the Most Ideal Scenario, the recovery of biodegradable waste is projected to reach 41,457 tons/year (2025) and 55,594 tons/year (2030), whereas under the Negative Scenario, these amounts are forecast at 20,729 tons/year and 33,356 tons/year, respectively. Metal waste recycling in the Most Ideal Scenario is estimated at 5,583 tons/year (2025) and 6,739 tons/year (2030), but under the Negative Scenario, it declines to 3,141 tons/year and 4,118 tons/year.

With regard to plastic waste, the Most Ideal Scenario is expected to yield 7,447 tons/year (2025) and 8,715 tons/year (2030), whereas in the Negative Scenario these projections drop to 5,416 tons/year and 6,537 tons/year. Glass waste recovery under the Most Ideal Scenario is projected at 5,360 tons/year (2025) and 5,750 tons/year (2030), compared to 3,685 tons/year and 4,313 tons/year under the Negative Scenario. Finally, paper and cardboard waste recycling in the Most Ideal Scenario is targeted to reach 12,284 tons/year (2025) and 14,825 tons/year (2030), while in the Negative Scenario, it decreases to 9,213 tons/year and 11,531 tons/year (Table 12).

Table 12. Assessment of Yalova's Recycling/Recovery Potential Based on Scenarios (2025-2030)

Scenarios	Most Ideal Scenario		Targeted Scenario		Partially Successful Scenario		Negative Scenario	
Years	**2025**	**2030**	**2025**	**2030**	**2025**	**2030**	**2025**	**2030**
Biodegradable Waste (ton/year)	41457	55594	34548	48181	27638	40769	20729	33356
Metals (ton/year)	5583	6739	4537	5616	3839	4867	3141	4118
Plastics (ton/year)	7447	8715	6770	7989	6093	7263	5416	6537
Glass (ton/year)	5360	5750	4690	5391	4355	5032	3685	4313
Paper and Cardboard (ton/year)	12284	14825	11516	14001	10748	13178	9213	11531

CONCLUSIONS

This study offers significant insights into the sustainability of regional waste management in the Marmara Region by comprehensively analyzing both the recycling of packaging waste and the recovery of biodegradable organic waste under four different scenarios. In the Most Ideal Scenario, it is observed that the potential for recovering biodegradable waste in major cities such as Istanbul could reach 2.6 million tons per year by 2030; however, under the Negative Scenario, this amount may decline to as low as 1.5 million tons per year. Similarly, while the recycling rates for packaging waste—such as plastic, glass, and paper—are projected to increase substantially in the Most Ideal Scenario, the Negative Scenario anticipates significant losses due to deficiencies and inadequate policies.

In accordance with the European Green Deal's objective of achieving a climate-neutral continent by 2050, increasing the recyclability of packaging waste and reducing overall waste generation have been identified as key strategic targets. Within this framework, the requirement to make all packaging on the EU market recyclable by 2030 obliges Türkiye to comply with its own Packaging Waste Control Regulation. Given its status as Türkiye's most economically and demographically dynamic region, the Marmara Region plays a crucial role in attaining these objectives. In particular, the source separation of packaging waste and the implementation of effective recycling processes will not only reduce dependence on raw

materials, thereby yielding economic benefits, but also help conserve natural resources and lower greenhouse gas emissions.

Recovering biodegradable organic waste through innovative methods such as composting and biogas production directly supports the region's agricultural activities and energy production potential. The findings underscore the necessity of adopting integrated, circular economy-based approaches in waste management. In the Marmara Region, improving recycling infrastructure, enhancing public awareness, and ensuring policy effectiveness emerge as key factors for meeting the targets set by both the European Green Deal and Türkiye's waste management objectives. Consequently, the implementation of sustainable waste management practices is strategically essential for mitigating environmental challenges, fostering economic growth, and aligning with global climate objectives.

REFERENCE

Bandara, N. J., Hettiaratchi, J. P. A., Wirasinghe, S. C., & Pilapiiya, S. (2007). Relation of waste generation and composition to socio-economic factors: a case study. *Environmental Monitoring and Assessment*, *135*, 31-39.

Calabrò, P. S., & Satira, A. (2020). Recent advancements toward resilient and sustainable municipal solid waste collection systems. *Current Opinion in Green and Sustainable Chemistry*, *26*, 100375.

Ding, Y., Zhao, J., Liu, J. W., Zhou, J., Cheng, L., Zhao, J., Shao, Z., Iris, Ç., Pan, B., Li, X., & Hu, Z. T. (2021). A review of China's municipal solid waste (MSW) and comparison with international regions: Management and technologies in treatment and resource utilization. *Journal of Cleaner Production*, *293*, 126144.

Esri. (2024). ArcGIS Desktop. https://www.esri.com/en-us/arcgis/products/arcgis-desktop (Accessed: December 11, 2024).

Garnier, S., Ross, N., Rudis, B., Filipovic-Pierucci, A., Galili, T., timelyportfolio, O'Callaghan, A., Greenwell, B., Sievert, C., Harris, D. J., Sciaini, M., & Chen, J. J. (2024). viridis(Lite) - Colorblind-Friendly Color Maps for R. https://doi.org/10.5281/zenodo.4679423

Kahle, D. J., & Wickham, H. (2013). ggmap: spatial visualization with ggplot2. *The R Journal*, *5*(1), 144. https://journal.r-project.org/archive/2013-1/kahle-wickham.pdf

Karak, T., Bhagat, R. M., & Bhattacharyya, P. (2012). Municipal solid waste generation, composition, and management: the world scenario. *Critical Reviews in Environmental Science and Technology*, *42*(15), 1509-1630.

Marmara Municipalities Union (MMU). (2024). Marmara Sea. https://www.marmara.gov.tr/tr/marmara-denizi (Accessed: December 10, 2024).

Morgan-Wall, T. (2024). rayshader: Create Maps and Visualize Data in 2D and 3D. https://CRAN.R-project.org/package=rayshader

Nanda, S., & Berruti, F. (2021). Municipal solid waste management and landfilling technologies: a review. *Environmental Chemistry Letters*, *19*(2), 1433-1456.

Osra, F. A., Elbisy, M. S., Mosaıbah, H. A., Osra, K., Ciner, M. N., & Ozcan, H. K. (2024). Environmental İmpact assessment of a dumping site: a case study of Kakia Dumping Site. *Sustainability*, *16*(10), 3882.

Packaging Waste Control Regulation (PWCR). (2021). T.R. Official Gazette. https://www.resmigazete.gov.tr/eskiler/2021/06/20210626-18.htm (Accessed: December 13, 2024).

R Core Team. (2021). *R: A Language and Environment for Statistical Computing*. In R Foundation for Statistical Computing. http://www.R-project.org/

Regions of Türkiye (RoT). (2015). Türkiye's Seven Regions. https://turkiyeninbolgelri.weebly.com/tuumlrk304yen304n-boumllgeler304/turkiyenin-yedi-bolgesi (Accessed: December 16, 2024).

Schneikart, G., Löffler, C., Brandner, M., Pfoser, S., & Mayrhofer, W. (2024). Requirements for the Transformation towards Returnable Transport Item-Enabled Circular Economies in the Austrian Parcel Industry. *Tehnički glasnik*, *18*(2), 254-261.

Scott, A. (2018). Europe tackles plastics waste. *Chemical & Engineering News*, *96*(10), 26–27.

Sharma, K. D., & Jain, S. (2020). Municipal solid waste generation, composition, and management: the global scenario. *Social Responsibility Journal*, *16*(6), 917-948.

T.R. Ministry of Environment and Urbanization. (2011). Çanakkale Environmental Status Report (CESR) 2011.

T.R. Ministry of Environment, Urbanization, and Climate Change. (2022). Istanbul Environmental Status Report (IESR) 2022. https://webdosya.csb.gov.tr/db/ced/icerikler/istanbul_-cdr2022-20230914131022.pdf

T.R. Ministry of Environment, Urbanization, and Climate Change. (2022). Tekirdağ Environmental Status Report (TESR) 2022. https://webdosya.csb.gov.tr/db/ced/icerikler/tek-rdag_-cdr2022-20231109081520.pdf

T.R. Ministry of Environment, Urbanization, and Climate Change. (2021). Edirne Environmental Status Report (EESR) 2021. https://webdosya.csb.gov.tr/db/ced/icerikler/ed-rne_-cdr2021-20220914161705.pdf

T.R. Ministry of Environment, Urbanization, and Climate Change. (2022). Kırklareli Environmental Status Report (KESR-a) 2022. https://webdosya.csb.gov.tr/db/ced/icerikler/k-rklarel-_-cdr2022-20231115150809.pdf

T.R. Ministry of Environment, Urbanization, and Climate Change. (2022). Balıkesir Environmental Status Report (BESR-a) 2022. https://webdosya.csb.gov.tr/db/ced/icerikler/balikes-r_-cdr2022-20240207092126.pdf

T.R. Ministry of Environment, Urbanization, and Climate Change. (2022). Bilecik Environmental Status Report (BESR-b) 2022.

https://webdosya.csb.gov.tr/db/ced/icerikler/b-lec-k_-cdr2022-20231218100136.pdf
T.R. Ministry of Environment, Urbanization, and Climate Change. (2022). Sakarya Environmental Status Report (SESR) 2022. https://webdosya.csb.gov.tr/db/ced/icerikler/sakarya-ilcdr-2022-20230828130907.pdf
T.R. Ministry of Environment, Urbanization, and Climate Change. (2022). Kocaeli Environmental Status Report (KESR-b) 2022. https://webdosya.csb.gov.tr/db/ced/icerikler/kocaeli-ilcdr-2022-20230706104825.pdf
T.R. Ministry of Environment, Urbanization, and Climate Change. (2023). Yalova Environmental Status Report (YESR) 2023. https://webdosya.csb.gov.tr/db/ced/icerikler/yalova-icdr_2023-1-20240712081326.pdf
T.R. Ministry of Trade (MoT). (2024). AB Ambalaj ve Ambalaj Atığı Mevzuatı *(in Turkish)*. https://ticaret.gov.tr/dis-iliskiler/yesil-mutabakat/ab-dongusel-ve-surdurulebilir-sanayi-politikalari/ab-ambalaj-ve-ambalaj-atigi-mevzuati (Accessed: December 13, 2024).
Turkish Statistical Institute (TURKSTAT). (2022). Gross domestic product by province 2022. https://data.tuik.gov.tr/Bulten/Index?p=Il-Bazinda-Gayrisafi-Yurt-Ici-Hasila-2022-45867 (Accessed: December 18, 2024).
Ünlü, H., Gür Parlayıcı, S., & Topçu, T. (2022, September). Bursa Integrated Solid Waste Management Plan (BISWMP). Bursa Metropolitan Municipality. https://www.bursa.bel.tr/dosyalar/galeri_x/bzhd37rcoa8s4wg.pdf (Accessed: November 10, 2024).
Wickham, H., Averick, M., Bryan, J., Chang, W., D'Agostino McGowan, L., François, R., Grolemund, G., Hayes, A., Henry, L., Hester, J., Kuhn, M., Pedersen, T. L., Miller, E., Milton Bache, S., Müller, K., Ooms, J., Robinson, D., Paige Seidel, D., Spinu, V., Takahashi, K., Vaughan, D., Wilke, C., Woo, K., & Yutani, H. (2019). Welcome to the Tidyverse. *Journal of open source software*, *4*(43), 1686. https://doi.org/10.21105/joss.01686
Wickham, H., Chang, W., & Wickham, M. H. (2016). Package *'ggplot2'*. *In Create elegant data visualisations using the grammar of graphics*. Version Citeseer.

AI-Driven Smart Geothermal Systems: Optimizing Earth's Heat for a Sustainable Future

Orkun TEKE[1]

[1]Lecturer; Celal Bayar University MCBU XRLab. orkun.teke@cbu.edu.tr ORCID No: 0000-0003-4390-263X

ABSTRACT

Geothermal energy, a well grounded and sustainable renewable energy resource, faces significant challenges, including high upfront costs, reservoir uncertainty, and environmental concerns. Integrating artificial intelligence (AI) into geothermal energy systems has revolutionized its operations, offering solutions that enhance efficiency, sustainability, and economic feasibility. This paper researches the AI transformation in addressing critical areas such as reservoir characterization, well management, dynamic resource allocation, and risk mitigation. AI-driven innovations have significantly improved reservoir exploration and management through predictive modeling, real-time monitoring, and cost-effective drilling strategies. Optimal well placement and dynamic flow adjustments, enabled by machine learning algorithms, have enhanced geothermal energy extraction while extending the lifespan of reservoirs. Furthermore, AI-powered resource management systems optimize demand forecasting, smart grid integration, and energy storage, ensuring better load balancing and higher operational efficiency. Environmental risks, including seismic activity and water resource management, are mitigated by AI through advanced monitoring systems and sustainable reservoir practices. Hybrid renewable systems integrating geothermal energy with solar and biomass sources highlight AI's potential to expand energy generation capabilities. Emerging technologies like Enhanced Geothermal Systems (EGS) are becoming increasingly viable due to AI advancements. This study underscores AI's pivotal role in addressing technical, economic, and environmental challenges in geothermal energy. By leveraging AI, geothermal energy systems are poised to become a cornerstone of global renewable energy strategies, enabling a eco friendly and more efficient energy future. Continued interdisciplinary research and collaboration are essential to fully realize geothermal energy's potential.

Keywords – Geothermal Energy, Renewable Energy, Optimization, Artificial Intelligence, Machine Learning

INTRODUCTION

The global imperative to transition towards renewable energy sources has catalyzed unprecedented innovations in geothermal energy exploitation. While geothermal energy represents one of Earth's most reliable and consistent renewable resources, its widespread adoption has historically been constrained by technological limitations, high exploration costs, and operational inefficiencies. The concretion of artificial intelligence (AI) into geothermal systems presents a paradigm shift in addressing these

longstanding challenges, offering transformative solutions that add to both operational efficiency and economic wellness.

Traditional geothermal energy development has been specified by important uncertainties in reservoir assessment, substantial initial capital investments, and complex operational challenges. These impediments have many a time resulted in not highly enough resource utilization and heightened financial risks for stakeholders. However, the emergence of sophisticated AI Technologies has introduced unprecedented opportunities to revolutionize geothermal energy systems.

The convergence of AI and geothermal technology addresses several critical industry pain points. First, it significantly reduces exploration risks through enhanced geological modeling and prediction capabilities. Second, it optimizes operational parameters in real-time, maximizing energy extraction while ensuring sustainable reservoir management. Third, it enables predictive maintenance strategies that minimize downtime and extend equipment longevity. Furthermore, AI-driven systems facilitate improved integration with smart grids, enabling more efficient energy distribution and storage solutions.

This chapter is investigated the transformative potential of AI applications in geothermal energy systems, focusing on key technological developments, practical implementations, and future prospects. Through comprehensive analysis of current innovations and emerging trends, we explore how AI-enhanced solutions are reshaping the geothermal energy landscape. The following sections delve into specific applications, from reservoir characterization to smart well management, illustrating how artificial intelligence is fundamentally converting the way we harness Earth's thermal resources.

2- AI-ENHANCED RESERVOIR CHARACTERIZATION

AI and ML notably improve the efficiency, accuracy, and cost-effectiveness of analyzing subsurface geological properties, predicting reservoir behaviors, and managing exploration risks.

2.1. Machine Learning for Analyzing Geological Data

AI-based approaches have proven invaluable in extracting insights from geological data. These approaches are used to create deputy models for Enhanced Geothermal Systems (EGS), allowing precise predictions of temperature and permeability with errors as low as 1.3%, thus optimizing reservoir management (Yan et al., 2023).

Additionally, lithofacies classification and porosity estimation models using Neural Networks and Markov Models have demonstrated improved accuracy by incorporating complex spatial distributions and depositional rules (Feng et al., 2020).

2.2. Predictive Modeling of Subsurface Conditions

AI models excel at predictive modeling of geothermal reservoir properties. MLalgorithms have been used to forecast porosity and permeability with up to 98% accuracy, aiding reservoir engineers in efficient characterization (Okon & Appah, 2021). Similarly, advanced numerical modeling tools such as Operator-Based Linearization methods have enhanced predictions in geothermal fields, supporting better resource management (Khait & Voskov, 2018).

2.3. Real-Time Monitoring and Mapping

Real-time monitoring of geothermal reservoirs benefits immensely from AI-driven innovations. For instance, physics-informed machine learning (PIML) frameworks provide rapid and correct predictions of subsurface dynamics, offering computational speedups of over 1500 times compared to traditional simulations (Xu et al., 2023).

In addition, active seismic data processed through unsupervised ML methods have enabled detailed characterization of fractured reservoirs, identifying fault zones with high spatial resolution (Gao et al., 2023).

2.4. Reducing Exploration Risks and Costs

AI reduces exploration costs and risks by enhancing data interpretation accuracy. Geostatistical models integrated with AI techniques, such as inverse problem resolution, enable precise predictions of thermal and permeability characteristics, minimizing exploration uncertainty (Focaccia, 2012). Furthermore, numerical models for fractured reservoirs leverage ML for efficient temperature and pressure transient analysis (Wei et al., 2021).

2.5. Enhancing Operational Decision-Making

AI applications extend to decision-making in geothermal operations. Models such as the Delft Advanced Research Terra Simulator employ AI-enhanced operator-based frameworks for robust uncertainty analysis, significantly improving operational planning (Wang et al., 2020).

Examples of successful AI implementation include real-time reservoir analog analysis tools like RAVA, which empower geoscientists to explore datasets interactively and retrieve meaningful reservoir analogs for informed decisions (Brazil et al., 2018). Additionally, geothermal reservoir simulation frameworks integrated with AI have demonstrated effectiveness in improving the thermal recovery factor (Ansari et al., 2017).

AI in geothermal reservoir management extends beyond characterization. AI-driven forecasting models eliminate assumptions and uncertainties in production projections, ensuring more sustainable operations (Wardoyo et al., 2021). Additionally, high-performance simulation tools for EGS facilitate the visualization and optimization of geothermal systems, enhancing design and management practices (Xing et al., 2015).

AI has transformed geothermal reservoir characterization through advancements in data analysis, predictive modeling, and operational optimization, enabling more sustainable energy solutions. The integration of AI in geothermal systems continues to evolve, promising further enhancements in resource management and environmental sustainability.

3- SMART WELL MANAGEMENT AND OPTIMIZATION

AI into geothermal energy systems has revolutionized the management and optimization of geothermal wells. By leveraging advanced algorithms, AI enables optimal well placement, real-time operational adjustments, predictive maintenance, and optimization of temperature and pressure conditions.

3.1. AI Algorithms for Optimal Well Placement

These algorithms are used to increase the aacurate of well placement in geothermal reservoirs. ML coupled with optimization algorithms have provided really important efficiency in locating optimal injection and production well sites. For instance, studies in the Kizildere Geothermal Field utilized AI to evaluate injection flow rates and temperatures, achieving consistent and improved predictions for well placement (Akin et al., 2010). Additionally, multi-objective optimization algorithms are worked to manage competing objectives like maximizing heat extraction while minimizing reinjection costs (Song et al., 2021).

3.2. Real-Time Adjustment of Injection/Production Rates

AI-powered systems have enhanced real time monitoring and regulation of injection and production rates. Closed-loop optimization frameworks using hybrid deep learning models allow dynamic control of

well operations to maximize efficiency while accounting for geological uncertainties (Wang et al., 2022). Moreover, fuzzy control systems have been used for well flow rate adjustments, achieving faster stabilization and energy production compared to traditional systems (Haklıdır, 2020).

3.3. Predictive Maintenance of Geothermal Equipment

Predictive maintenance driven by AI minimizes downtime and equipment failure in geothermal operations. AI systems analyze sensor data from drilling and operational equipment to predict failures and optimize maintenance process. Applications of AI in drilling, for example optimizing drill bit performance and tracking dynamics in real time, have reduced well drilling costs significantly (Satrape, 1987). Machine learning tools also enable effective treatment strategies for scale prevention, which is crucial for geothermal well sustainability (Azari et al., 2020).

3.4. Temperature and Pressure Optimization

AI optimizes temperature and pressure conditions by simulating reservoir dynamics under varying operational parameters. Advanced simulation-optimization frameworks using AI allow for the efficient adjustment of operational parameters, for example injection rates and production pressures, to prolong well life and maximize energy recovery (Xu et al., 2023). For example, integrating managed pressure operation control in deep closed-loop geothermal systems has demonstrated up to a 21% improvement in thermal power generation (Fallah et al., 2021).

AI's application in geothermal well management is driving substantial advancements in efficiency, reliability, and sustainability. Through optimal placement, real-time adjustments, predictive maintenance, and temperature/pressure optimization, AI is transforming geothermal energy systems to encounter future energy demands.

Dynamic resource management in geothermal energy systems leverages AI to optimize demand forecasting, smart grid integration, load balancing, and energy storage.

4- DYNAMIC RESOURCE MANAGEMENT AND OPTIMIZATION

ML and neural networks enable accurate forecasting of energy demand, essential for balancing supply and consumption. Studies show that AI-powered models, including Bi-LSTM and ARIMA, achieve high accuracy in predicting renewable energy outputs and demand patterns (Chen et al., 2023).

4.1. Smart Grid Integration

Smart grids incorporate AI to integrate renewable energy sources, manage distributed energy, and ensure grid stability. AI methods like reinforcement learning and hybrid learning optimize grid operations by addressing real-time challenges in load distribution and fault recovery (Zhao et al., 2023). Smart thermal grids combining centralized and distributed storage solutions have further enhanced energy resource utilization (Yang et al., 2017).

4.2. Load Balancing and Energy Storage Optimization

AI-driven systems manage load balancing by dynamically allocating energy resources based on demand and availability. Smart energy hubs equipped with AI algorithms ensure seamless switching between energy carriers during peak hours, improving efficiency (Bahrami & Sheikhi, 2016). Additionally, geothermal energy storage integrated with smart grids enhances system performance, enabling sustainable heating solutions (Hosseini et al., 2021).

4.3. Efficiency Improvements Through Machine Learning

ML techniques optimize operational efficiency by predicting and adapting to system dynamics. Advanced models, such as Grey Wolf Optimizer algorithms, significantly enhance microgrid energy management by decreasing costs and improving dispatch reliability (Kumar et al., 2021). Also, efficiency improvements showe in the figure 1.

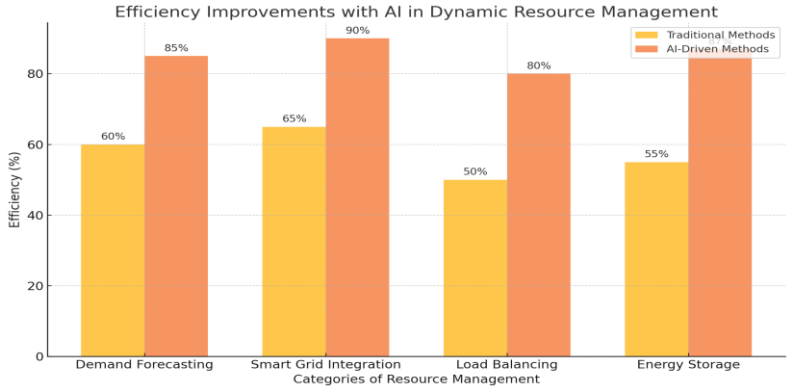

Figure 1: To compare the efficiency improvements achieved with traditional methods versus AI-driven methods in dynamic resource management across four categories: demand forecasting, smart grid integration, load balancing, and energy storage.

5- RISK MITIGATION AND ENVIRONMENTAL PROTECTION

Geothermal energy, while a promising renewable energy source, necessitates robust risk mitigation and environmental protection strategies. AI is increasingly playing a focal role in addressing seismic risks, conducting environmental impact assessments, managing water resources, and ensuring sustainable reservoir management.

5.1. Seismic Activity Prediction and Monitoring

Geothermal energy operations can induce seismic activity, necessitating predictive tools to minimize risks. AI and machine learning models have revealed success in analyzing seismic data and forecasting potential events. For example, enhanced traffic-light systems utilizing algorithms have been contrivanced into geothermal operations to mitigate seismic risks effectively (Mignan et al., 2019).

5.2. Environmental Impact Assessment

Environmental impact assessments (EIAs) in geothermal projects now leverage AI for detailed analysis and mitigation planning. Studies in Italy highlight comprehensive monitoring systems that address emissions, noise, subsidence, and water contamination, ensuring adherence to environmental regulations (Manzella et al., 2018). Moreover, AI facilitates the modeling of complex interactions between geothermal operations and the ecosystem, supporting proactive measures (Chen et al., 2020).

5.3. Water Resource Management

Geothermal energy systems require effective water management to minimize impacts on local water resources. Advanced AI systems optimize water usage, reinjection processes, and monitor groundwater contamination risks. In Iceland, proactive water monitoring programs have revealed success in safeguarding water resources during geothermal operations (Kristmannsdóttir & Ármannsson, 2003).

5.4. Sustainable Reservoir Management

Sustainable reservoir management is critical for protract the geothermal operation of resources. AI-based tools are employed to model reservoir behavior under different operational scenarios, optimize reinjection strategies, and monitor thermal depletion. The integration of mitigation

measures, such as carbon forestry, enhances reservoir sustainability and environmental co-benefits (Ogola et al., 2012).

From predicting seismic events to managing reservoirs sustainably, these technologies enhance the feasibility and environmental compatibility of geothermal energy development.

6- CASE STUDIES AND FUTURE DIRECTIONS

AI applications in geothermal energy have demonstrated remarkable potential, enabling innovative solutions for optimizing geothermal systems, addressing challenges, and integrating renewable energy technologies.

6.1. Examples of Successful AI Implementation in Geothermal Projects

AI has been successfully used in geothermal energy projects to optimize operations and enhance energy efficiency. For instance:

Optimizing Well Flow Rates: AI models have been practiced to forecast production and injection flow rates in geothermal wells, significantly icreasing power plant efficiency and decreasing operational uncertainties (Ariturk, 2019).

Hybrid Systems: AI was used to model a geothermal Organic Rankine Cycle (GORC) integrated with solar systems, predicting energy and exergy efficiency with precision. This system reveals the feasibility of hybrid renewable energy applications (Khosravi et al., 2019).

6.2. Emerging Technologies and Potential Breakthroughs

AI is driving several emerging technologies in geothermal energy:

Enhanced Geothermal Systems (EGS): Advanced AI models help simulate and optimize EGS, making them commercially viable and efficient by reducing exploration risks and enhancing reservoir performance (Fairley et al., 2009).

Deep Geothermal Resources: AI-integrated tools assess unconventional resources like dry hot rock formations, proposing new cycles and technologies for low-temperature aquifers (Michaelides, 2016).

Geothermal Reservoir Modeling: AI improves forecasting models for geothermal reservoirs, holded real time data to amplify accuracy and reliability (Wardoyo et al., 2021).

6.3. Integration with Other Renewable Energy Sources

The integration of geothermal energy with other renewable energy sources is becoming progressively feasible with AI:

Hybrid Renewable Systems: Combining geothermal energy with solar and biomass systems has shown potential for poly-generation, improving energy efficiency and reducing costs (Moya et al., 2018).

Smart Grid Integration: AI enhances geothermal power grid connections, enabling better resource allocation, load management, and energy storage in renewable energy networks (Zwaan & Longa, 2019). AI continues to transform geothermal energy systems by improving efficiency, enabling hybrid integrations, and addressing critical technical challenges. These advancements mark a significant step toward achieving sustainable and reliable energy solutions.

RESULTS AND DISCUSSION

AI has proven to be an indispensable tool for addressing the inherent challenges of geothermal energy, such as reservoir uncertainty, environmental impact, and efficiency optimization. Through advancements in AI-driven technologies, geothermal energy systems have witnessed significant improvements in reservoir characterization, operational efficiency, resource management, and environmental sustainability. From identifying optimal well placements and dynamically adjusting operational parameters to predicting seismic risks and optimizing energy integration, AI solutions are shaping geothermal energy as a more viable and competitive resource in the global renewable energy portfolio. Moreover, the potential for hybrid renewable systems combining geothermal with solar or biomass sources highlights the versatility and future scalability of geothermal technologies. AI-powered predictive models have drastically improved subsurface exploration accuracy, reducing drilling risks and costs. Real-time monitoring systems have enhanced the understanding of reservoir dynamics, optimizing reinjection strategies and ensuring sustainable thermal resource exploitation. To Apply of ML process has optimized well placement and flow rate adjustments, leading to enhanced energy extraction rates and prolonged reservoir life.

Predictive maintenance systems minimize equipment downtime, reducing operational costs and improving reliability. AI models have demonstrated exceptional capability in demand forecasting and grid integration, enabling better load balancing and storage utilization. The

integration of geothermal systems with smart grids has improved resource allocation, contributing to grid stability and efficiency. AI has facilitated advanced seismic activity monitoring and environmental impact assessments, helping to mitigate risks associated with geothermal energy operations.

The results of AI integration into geothermal energy demonstrate a clear trajectory toward making this energy source a cornerstone of global sustainability. By mitigating risks and optimizing efficiency, AI addresses key barriers that have historically limited geothermal development, such as high upfront costs and environmental concerns. However, the findings also highlight areas requiring further research and investment to fully realize geothermal energy's potential. AI-driven innovations in drilling technologies, reservoir modeling, and hybrid systems show promise in reducing costs and expanding the applicability of geothermal energy.

Advanced numerical simulations and machine learning models are particularly effective in overcoming the unpredictability of subsurface conditions. Despite advancements, geothermal projects often face public resistance due to perceived environmental risks. AI-driven environmental monitoring and transparent impact assessments can improve public acceptance and foster community support. The integration of geothermal energy and smart grid systems exemplifies the adaptability of geothermal technologies. However, challenges such as interconnection logistics and policy hurdels must be directed to ensure perfect integration.

Further advancements in AI technologies, such as reinforcement learning and neural networks, can optimize geothermal operations in more complex scenarios. Research into hybrid renewable systems and poly-generation technologies should be prioritized to get free the full potential of geothermal resources.

In summary, while challenges remain, the transformative impact of AI on geothermal energy systems is undeniable. By improving efficiency, reducing risks, and fostering environmental sustainability, AI paves the way for geothermal energy to play a huge role in the transforming toward a greener, more resilient energy future. Continued interdisciplinary research and collaboration among policymakers, researchers, and industry

stakeholders are vital to advancing geothermal energy technologies and ensuring their long-term viability.

REFERENCE

Yan, B., Xu, Z., Gudala, M., Tariq, Z., & Finkbeiner, T. (2023). Reservoir Modeling and Optimization Based on Deep Learning with Application to Enhanced Geothermal Systems. Day 2 Wed, January 25, 2023. Feng, R., Balling, N., & Grana, D. (2020). Lithofacies classification of a geothermal reservoir in Denmark and its facies-dependent porosity estimation from seismic inversion. Geothermics, 87, 101854.

Okon, E. I., & Appah, D. (2021). Application of Machine Learning Techniques in Reservoir Characterization. Day 2 Tue, August 03, 2021.

Khait, M., & Voskov, D. (2018). Operator-based linearization for efficient modeling of geothermal processes. Geothermics, 103, 36–50.

Xu, Z., Yan, B., Gudala, M., & Tariq, Z. (2023). A Robust General Physics-Informed Machine Learning Framework for Energy Recovery Optimization in Geothermal Reservoirs. Day 3 Wed, June 07, 2023.

Gao, K., Huang, L., & Cladouhos, T. (2023). Seismic Characterization of the Blue Mountain Geothermal Field. Energies.

Focaccia, S. (2012). Characterization of geothermal reservoirs' parameters by inverse problem resolution and geostatistical simulations. Unibo AMSDottorato.

Wei, C., Cheng, S., She, J., Gao, R., Luo, L., & Yu, H. (2021). Numerical study on the heat transfer behavior in naturally fractured reservoirs and applications for reservoir characterization and geothermal energy development. Journal of Petroleum Science and Engineering, 108560.

Wang, Y., Voskov, D., Khait, M., & Bruhn, D. (2020). An efficient numerical simulator for geothermal simulation: A benchmark study. Applied Energy.

Brazil, E. V., Segura, V., Cerqueira, R., Abreu de Paula, R., & Mello, U. (2018). Visual Analytics for Reservoir Analogues. 2018 AAPG Annual Convention & Exhibition.

Ansari, E., Hughes, R., & White, C. (2017). Statistical modeling of geopressured geothermal reservoirs. Comput. Geosci, 103, 36–50.

Wardoyo, G. K., Pratama, H., Sutopo, A., Ashat, A., & Yudhistira, Y. (2021). Application of Artificial Intelligence in Forecasting Geothermal Production. IOP Conference Series: Earth and Environmental Science, 732, 012022.

Xing, H., Liu, Y., Gao, J., & Chen, S. (2015). Recent development in numerical simulation of enhanced geothermal reservoirs. Journal of Earth Science, 26, 28–36.

Wei, C., Liu, Y., Deng, Y., Cheng, S., & Hassanzadeh, H. (2022). Temperature Transient Analysis of Naturally Fractured Geothermal Reservoirs. SPE Journal.

Akin, S., Kok, M. V., & Uraz, I. (2010). Optimization of well placement geothermal reservoirs using artificial intelligence. *Computers & Geosciences, 36*(6), 776–785.

Song, G., Song, X., Li, G., Shi, Y., Wang, G., Ji, J., Xu, F., & Song, Z. (2021). An integrated multi-objective optimization method to improve the performance of multilateral-well geothermal system. *Renewable Energy*.

Wang, N., Chang, H., Kong, X., Saar, M., & Zhang, D. (2022). Deep learning based closed-loop optimization of geothermal reservoir production. *ArXiv*.

Haklıdır, F. T. (2020). The importance of long-term well management in geothermal power systems using fuzzy control: A Western Anatolia (Turkey) case study. *Energy*, *213*, 118817. https://consensus.app/papers/importance-longterm-well-management-geothermal-power-haklıdır/27b6d046a12c57cbb9cd9cf2fae105bd/?utm_source=chatgpt

Satrape, J. (1987). Potential impacts of artificial intelligence expert systems on geothermal well drilling costs.

Azari, V., Al Badi, M., Vazquez, O., Al-Kalbani, M., & Mackay, E. (2020). Scale treatment optimization in geothermal wells. *SPE Paper*.

Xu, Z., Yan, B., Gudala, M., & Tariq, Z. (2023). A robust general physics-informed machine learning framework for energy recovery optimization in geothermal reservoirs. *Day 3 Wed, June 07, 2023*.

Fallah, A., Gu, Q., Chen, D., Ashok, P., & Oort, E. (2021). Globally scalable geothermal energy production through managed pressure operation control of deep closed-loop well systems. *Energy Conversion and Management*, *236*, 114056.

Chen, Y., Bhutta, M. S., Abubakar, M., Xiao, D., Almasoudi, F. M., Naeem, H., & Faheem, M. (2023). Evaluation of Machine Learning Models for Smart Grid Parameters: Performance Analysis of ARIMA and Bi-LSTM. *Sustainability*

Zhao, X., Guo, Y., Guo, X., & Li, H. (2023). Artificial Intelligence Applications and Prospects for The Smart Grid. *2023 Panda Forum on Power and Energy*.

Yang, L., Entchev, E., Rosato, A., & Sibilio, S. (2017). Smart thermal grid with integration of distributed and centralized solar energy systems. *Energy, 122*, 471-481.

Bahrami, S., & Sheikhi, A. (2016). From Demand Response in Smart Grid Toward Integrated Demand Response in Smart Energy Hub. *IEEE Transactions on Smart Grid, 7*(2), 650–658.

Hosseini, S. H., Allahham, A., & Adams, C. (2021). Techno-economic-environmental analysis of a smart multi-energy grid utilizing geothermal energy storage for meeting heat demand. *IET Smart Grid*. https://consensus.app/papers/analysis-multi-energy-grid-utilising-energy-storage-hosseini/b8bae9ee94ac517281b5cc8c0c81f7b5/?utm_source=chatgpt

Kumar, A., Alaraj, M., Rizwan, M., & Nangia, U. (2021). Novel AI Based Energy Management System for Smart Grid With RES Integration. *IEEE Access, 9*, 162530–162542

Mignan, A., Karvounis, D., Broccardo, M., Wiemer, S., & Giardini, D. (2019). Including seismic risk mitigation measures into the Levelized Cost Of Electricity in enhanced geothermal systems for optimal siting. *Applied Energy*.

Manzella, A., Bonciani, R., Allansdottir, A., Botteghi, S., Donato, A., Giamberini, S., Lenzi, A., Paci, M., Pellizzone, A., & Scrocca, D. (2018). Environmental and social aspects of geothermal energy in Italy. *Geothermics, 72*, 232-248.

Chen, S., Zhang, Q., Andrews-Speed, P., & McLellan, B. (2020). Quantitative assessment of the environmental risks of geothermal energy: A review. *Journal of Environmental Management, 276*, 111287.

Kristmannsdóttir, H., & Ármannsson, H. (2003). Environmental aspects of geothermal energy utilization. *Geothermics, 32*(4-6), 451-461. https://consensus.app/papers/aspects-energy-utilization-kristmannsdóttir/60e0fae32d9f58d9adde2ad42209d59e/?utm_source=chatgpt

Ogola, P. F., Davidsdottir, B., & Fridleifsson, I. B. (2012). Opportunities for adaptation-mitigation synergies in geothermal energy utilization - Initial conceptual frameworks. *Mitigation and Adaptation Strategies for Global Change, 17*(5), 507-536.

Ariturk, M. S. (2019). Optimizing the Production and Injection Wells Flow Rates in Geothermal Field Using Artificial Intelligence.

Khosravi, A., Syri, S., Zhao, X., & Assad, M. (2019). An artificial intelligence approach for thermodynamic modeling of geothermal based-organic Rankine cycle equipped with solar system. *Geothermics*.

Fairley, J., Ingebritsen, S., & Podgorney, R. (2009). Challenges for Numerical Modeling of Enhanced Geothermal Systems. *Groundwater*.

Michaelides, E. (2016). Future directions and cycles for electricity production from geothermal resources. *Energy Conversion and Management, 107*, 3–9.

Wardoyo, G. K., Pratama, H., Sutopo, A., Ashat, A., & Yudhistira, Y. (2021). Application of Artificial Intelligence in Forecasting Geothermal Production. *IOP Conference Series: Earth and Environmental Science, 732*.

Moya, D., Aldas, C., & Kaparaju, P. (2018). Geothermal energy: Power plant technology and direct heat applications. *Renewable and Sustainable Energy Reviews*.

Zwaan, B., & Longa, F. D. (2019). Integrated assessment projections for global geothermal energy use. *Geothermics.*

The Effect of Passive Structural Control Systems on Earthquake Behavior of Structures

Özlem ÇAVDAR[1]

1- Prof. Dr., Gümüşhane University, Faculty of Engineering and Natural Sciences, Department of Civil Engineering, ozlem_cavdar@hotmail.com ORCID No:

ABSTRACT

Passive structural control systems are systems that operate without energy consumption and external intervention in order to reduce the movements of structures as a result of external loads or environmental effects. These systems often rely on natural energy damping and structural improvement techniques. The first type of earthquake isolation systems, which are based on the principle of reducing the dynamic effects of the earthquake by increasing the building period by placing special elements with low lateral rigidity in the buildings, are passive building control systems. Other types of systems, on the other hand, are supplemental damping systems that ensure that the energy transferred to the structure is damped in these special elements rather than the building elements by taking advantage of the displacement and/or velocity characteristics of the structures equipped with complementary damping mechanisms. In this study, the basic working principles of passive structural control systems, their applicable areas and the most commonly used types, seismic isolation and supplemental dampers were examined in detail.

Keywords – Seismic isolation , passive control systems, supplemental damper

INTRODUCTION

Structures move when exposed to external influences such as earthquakes and wind. These movements can threaten the safety, comfort and durability of structures. To solve such problems, passive structural control systems have been developed. Passive systems aim to stabilize the dynamic behavior of the structure without spending energy. The purpose of passive systems is to increase the strength of structures against external influences, reduce energy consumption and ensure the longevity of the structure. Urban centers and fast-growing cities are characterized by high-rise buildings that contribute to the economic growth and sustainable development of societies. New buildings designed in accordance with the provisions of the Turkish Building Earthquake Code (TBEC-2019) and modern codes (FEMA 2020; ASCE 2022; ASCE 2016) has not performed well in recent earthquakes. Traditional static structural systems are designed, which can be generalized as the safe and economical design of building carrier systems with sufficient strength, rigidity and ductility, suitable building materials and proven methods. The constructed structures have an unchanging period and rigidity under static loads. However, with the effect of dynamic forces on the structure, it is expected that the structural elements will undergo plastic deformation in a controlled manner and therefore this rigidity will turn into ductility. Damping devices, on the other hand, can show this behavior in themselves without structural deformations. Passive control systems are the most widely

used of these structural control systems, which are classified as passive, active and semi-active. There are many different approaches to the classification of structural control systems in the literature. In this study, the classification was based on the comprehensive analysis carried out by Saaed et al. (2015). As can be seen in Figure 1, structural control systems are basically divided into 3 main groups. These are passive control systems, semi-active control systems and active control systems. There are also hybrid systems in which active or semi-active systems are used together with passive systems.

Earthquake isolation systems, which are one of the passive control systems, which are the widest usage area of these systems, are based on the principle of extending the period of buildings by equipping them with elements with lower rigidity than the classical elements and thus reducing dynamic effects such as earthquakes. On the other hand, additional damping systems take advantage of the displacement and/or velocity characteristics of the structures and ensure that the energy transferred to the structure by the earthquake is dampened by these elements rather than the building elements and removed from the structure.

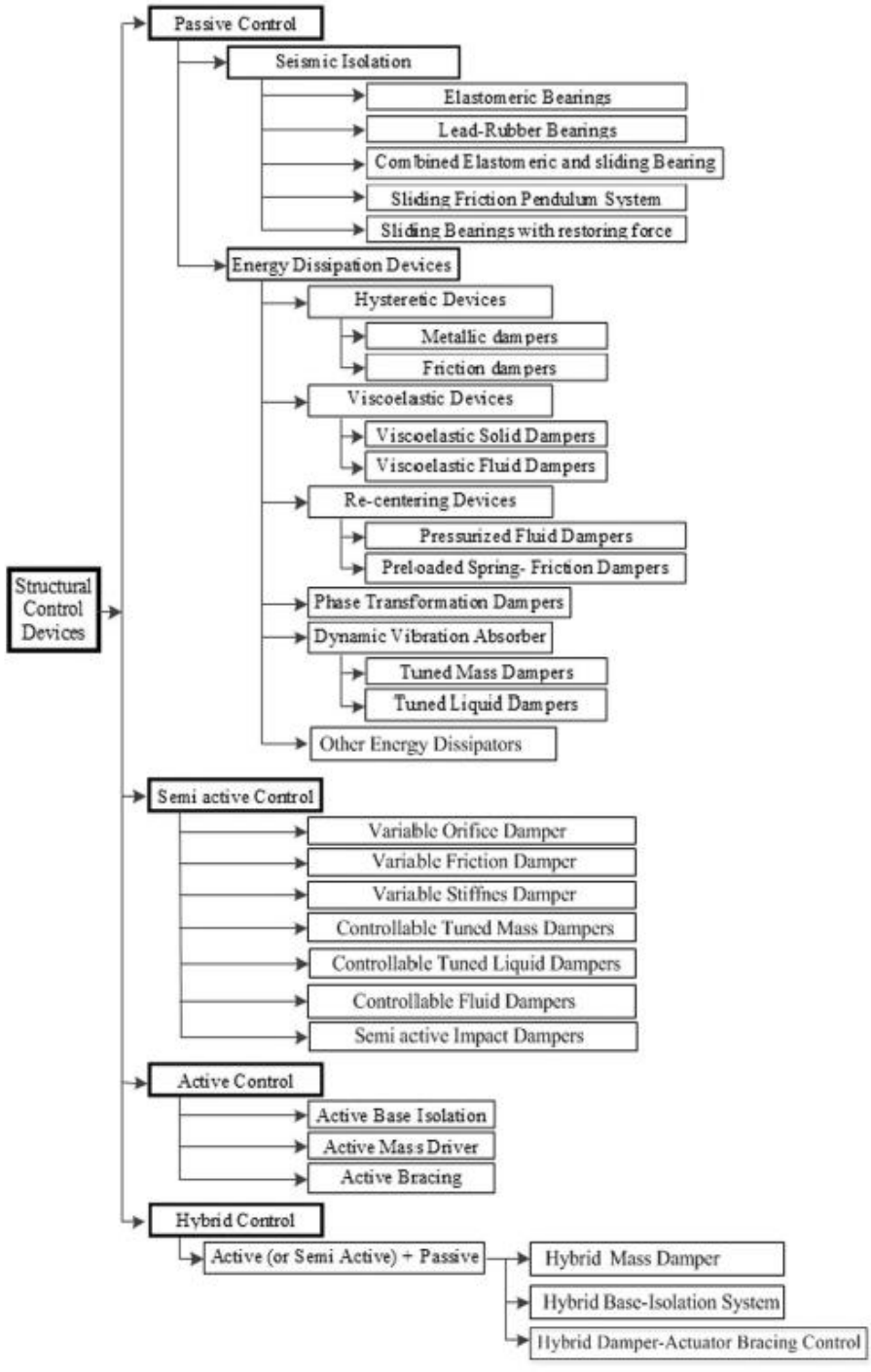

Figure 1. Classification of building control systems (Saaed et al., 2015).

Passive structural control systems

These systems have properties that cannot be changed during dynamic effects and their effectiveness against certain dynamic factors may be limited. Basically, these systems are examined in two groups as earthquake isolation and additional damping. Earthquake isolation, thanks to the flexibility of the devices in the lateral direction, enlarges the period of the building to which it is applied and meets the horizontal displacement demand that will occur in the event of an earthquake at the isolator interface (with earthquake isolation devices). Additional damping devices, on the other hand, can show this behavior in themselves without structural deformations. Therefore, the building period and rigidity are preserved.

Seismic Isolation

The earthquake isolation system is based on reducing the acceleration attraction by removing the building vibration period from the earthquake dominant period with the addition of special materials with low lateral stiffness and sufficient vertical rigidity. Many different earthquake isolation units are used in earthquake isolation systems (Saaed et al., 2015). These elastomer earthquake isolation units;

- Lead-core elastomer type earthquake isolation unit
- High-damped elastomer type earthquake isolation unit
- Flat surface friction type earthquake isolation unit
- Curved surface friction earthquake isolation units
- Teflon articulated stainless steel earthquake isolation units
- Sleeved pile earthquake isolation units

Design and application rules are included in TBEC (2019) section 14 for lead-core elastomer, high-damped elastomer and curved-surface friction type, which are among these earthquake isolation units. Isolators used in seismically isolated structures are examined in detail in this section, as they are generally Elastomeric (rubber) insulators and friction pendulum type insulators.

- **Lead Core Elastomeric (Rubber) Isolation**

Elastomeric isolation provides the simplest isolation method. Elastomeric isolations exhibit large stresses, imparting considerable flexibility to an isolated structure. Elastomeric bearings consist of alternating elastomer layers and suitable reinforcing material. The function of the reinforcement is

to support the vertical loads of the superstructure and keep the structure sufficiently rigid, while the function of the elastomer layers is to affect the shear modulus of the elastomeric backing. Thus, the addition of elastomeric isolations with low horizontal rigidity between the superstructure and the substructure lowers the fundamental frequency of the structure compared to the dominant frequencies of ground motion (Saaed et al., 2015).

The stratification between the rubbers increases the strength of the isolation under pressure. It allows expansion in other directions under pressure and ensures uniform load distribution. In determining the vertical rigidity of layered rubber systems, the shape of the isolation is important. The form factor is defined as the ratio of the area acting on the load in the insulator to the area of free expansion. The shape of the isolation does not matter in horizontal rigidity (). In rubber-based isolations; Low rigidity / high flexibility in all horizontal directions is ensured by the elasticity of the rubber material. High rigidity and stability in the vertical direction are ensured by steel plates vulcanized into the rubber.

The most widely used rubber-based seismic isolators today are:

- Low Damping Rubber Bearings (LDRB),
- High Damping Rubber Bearings (HDRB)
- Lead Core Rubber Insulator (Lead Rubber Bearings: LRB)

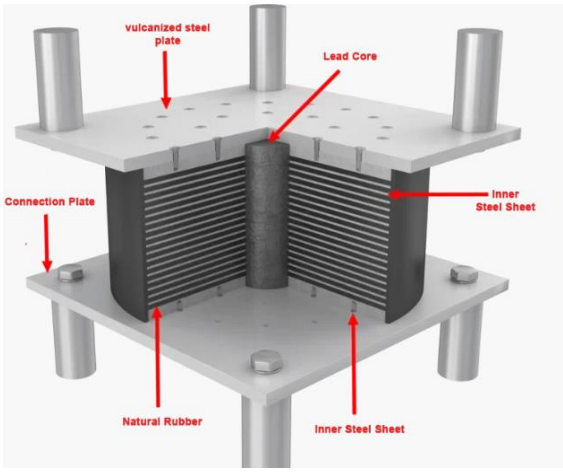

Figure 1. Bullet Core Rubber Isolation sectional view

Friction Pendulum Type Isolation

Friction pendulum isolation unit (FPS), also called curved surface friction isolation unit, has a spherical concave surface and a steel core element with low friction coefficient in curvilinear form acting as a sliding inside it. Friction pendulum type isolations can absorb the required vertical and horizontal loads by changing the coefficient of friction and the radius of the pendulum. In general, such isolators work on the same principle as other insulators, consuming seismic energy at the isolator level and separating the effects from the superstructure, allowing the superstructure to work like a pendulum. Figure 2 shows a cross-sectional view of the friction surface isolation.

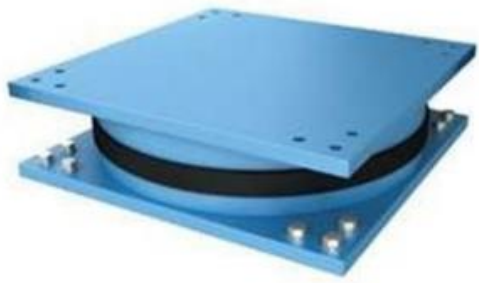

Figure 2. Friction Surface Seismic Isolator sectional view

Supplemental Damping Systems

Another passive control system is supplemental damping or complementary damping systems. Additional damping systems, which are created by incorporating energy-consuming devices called 'mechanical dampers' into buildings, are systems that are activated by the movement of the main carrier system and reduce the structural dynamic response during earthquake ground movement (Christopoulos and Filiatrault, 2006). Complementary damping devices are often named according to their energy dissipation mechanism, e.g. yield (i.e. metallic or hysterical), friction or viscous/viscoelastic. Although these systems generally absorb most of the energy coming to the structure; Additional damping systems that are outside of a limited number of systems, such as buckling prevented crosses (BPC), are not allowed by the regulations to be used as the main (primary) systems to meet earthquake loads. (NEHRP, 2015, chapter 16). Instead, additional

damping systems are used to improve the earthquake performance of the structure by supporting the main carrier system. Again, in order to get high efficiency from additional damping systems, it is a reasonable and common approach to benefit from different additional damping systems, the effectiveness of which varies according to the characteristics of each building and the magnitude of the earthquake hazard. Passive seismic damper technologies; metallic dampers, friction dampers, viscoelastic dampers, viscoelastic liquid dampers, tuned mass dampers and tuned liquid dampers.

In addition, passive seismic dampers are the subject of the American Federal Emergency Management Agency (FEMA) in its guide publication 274 and defined these devices in 3 groups: displacement-dependent dampers, velocity-dependent dampers and other types of dampers (FEMA, 2020). Flow-based metallic dampers and friction dampers are defined in the group of displacement-dependent dampers (depending on the deformation of the damper). The hysterical responses of these dampers are given in Figure 3.

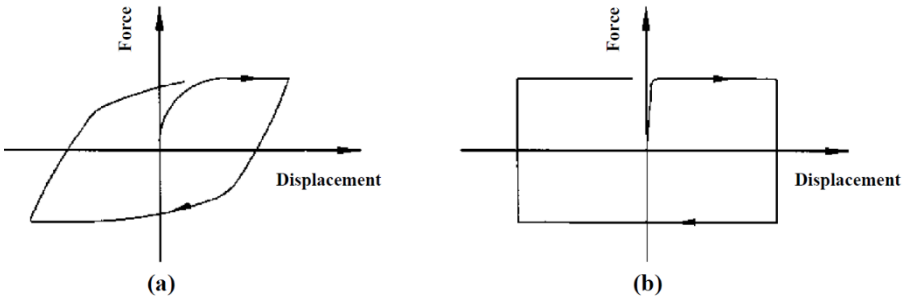

Figure 3. Idealized hysteretic loops of displacement-based dampers: (a) Metallic dampers based on yielding (b) Friction dampers

- **Metallic Dampers**

A metallic damper is a type of hysterical damper made of metal that uses the plastic deformation of hysterical materials, such as mild (low carbon) steel, to dissipate its seismic energy. The application of this type of damper began in Japan in the late 1960s and in New Zealand in the early 1970s (Soong and Dargush, 1997). The advantages of metallic dampers over other types of dampers are stable hysterical behaviour, speed independence, resistance to ambient temperature, reliability, and engineers' knowledge of material behaviour.

- ***Friction Dampers***

Energy damping is achieved by taking advantage of the friction generated during the movement of the structure. Such systems are widely used in large buildings and bridges. The study of friction dampers in structural applications began in the early 1980s, introduced the first friction damper that worked based on a solid friction mechanism to dissipate vibration energy (Titirla, 2023). According to their initial experimental results, crosses designed to operate under tensile performed effectively under repeated repetitive loads.

- ***Viscoelastic Dampers***

These systems take advantage of the properties of viscoelastic materials to absorb energy and limit vibrations in the structure. The first applications of viscoelastic dampers to structures are to reduce acceleration levels due to wind or to increase human comfort. In viscoelastic dampers, viscoelastic silicone is used to dissipate the dynamic energy of the structure. When relative displacement occurs between the structural elements, the silicone is activated between the two chambers of the device. This system has a wide range of uses under both tensile and pressure, as follows: It can be used to provide the connection between the bridge deck and the bridge pier, as a wind support in buildings, and in earthquake isolation (Mahmoodi et al., 1987).

- ***Fluid viscous dampers***

Fluid viscous dampers consist of a cylindrical vessel, a special fluid with high viscosity held in this vessel, pistons made of stainless steel, and steel structural elements that connect the damper unit to the building system. The damping of energy in these damper units takes place in the form of conversion of mechanical energy into heat energy during the compression of the fluid with high viscosity passing through small orifices with the compression of the pistons. Fluid viscous dampers are joined to the steel elements with base plates at one end and combined with spherical bearings for ease of installation at the other end. Traditional joining methods are used in the steel elements to which the dampers are attached and in the structural carrier system. Below is a cross-section of a typical liquid viscous damper in Figure 4 (Peralta, 2018), and in Figure 5 the appearance of assembled fluid viscous dampers in structure (Taylor, 2022).

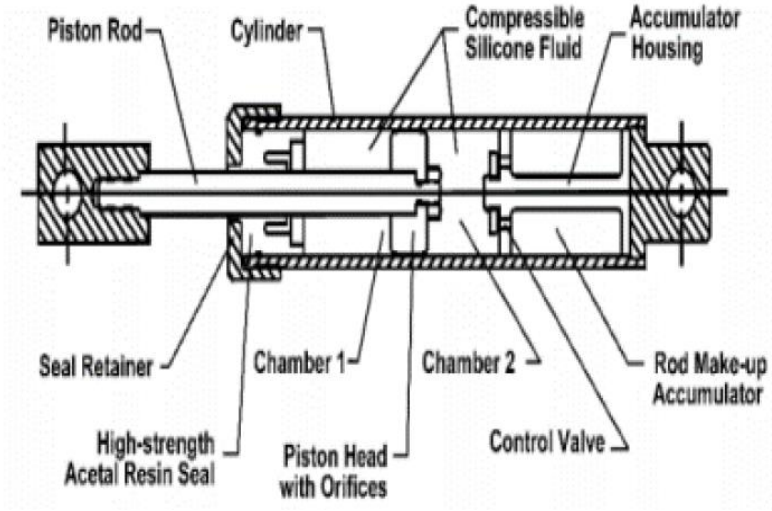

Figure 4. Longitudinal section of fluid viscous damper

Figure 5. Fluid viscous damper appearance in structure

- ***Tuned Mass Dampers***

A Tuned Mass Damper (TMD) is a device used to reduce the amplitude of mechanical vibrations in structures. It is typically used to dampen the vibrations caused by wind, seismic forces, or other dynamic loads that could negatively impact the performance or safety of a building, bridge, or other structure. The main function of a TMD is to absorb and dissipate energy from unwanted vibrations, thereby improving the stability and comfort of the structure. By using masses with a frequency close to the natural frequency of

the structure, damping is carried out in the face of vibrations in the structure. Such systems are highly effective, especially in high-rise buildings. It is a device consisting of a mass and spring that is connected to a structure to reduce the dynamic response of the structure. The frequency of the damper is set to a specific structural frequency so that when this frequency is excited, the damper resonates out of phase with the structural motion. The energy is dissipated by the damping force of inertia acting on the structure.

- ***Tuned Fluid Dampers***

Similar in concept to tuned mass dampers, the tuned fluid damper and the adjusted liquid column damper provide indirect damping to the system, thereby improving structural performance (Kareem, 1990). A tuned fluid dampers absorbs structural energy through viscous movements of fluid and wave refraction. Tuned Fluid Dampers (TFDs) are devices used to reduce vibrations or oscillations in mechanical systems, especially in structures like buildings, bridges, and large machines. They are a specific type of vibration damping system that relies on the properties of a fluid to absorb and dissipate energy from dynamic loads.

CONCLISIONS

Passive structural control systems are an important safety and performance improvement tool for structures. It is one of the leading contemporary engineering solutions and has an important role in the construction of earthquake-resistant buildings. With its low costs, low maintenance requirements and environmentally friendly features, it plays an important role in civil engineering. However, it is of great importance to choose and design the right passive system according to the needs of each structure. In the future, it is expected that these systems will develop further and become applicable in more areas. In countries located in the earthquake zone such as Turkey, the widespread use of these systems is of great importance both in terms of protecting human life and reducing material damages.

REFERENCES

Aghlara, R. ve Tahir, M. M. (2018). A passive metallic damper with replaceable steel bar components for earthquake protection of structures. Engineering Structures, 185-197.

ASCE (2016). Minimum Design Loads and Associated Criteria for Buildings and Other Structures (ASCE/SEI 7-16).

ASCE (2022). Minimum Design Loads and Associated Criteria for Buildings and Other Structures (ASCE/SEI 7-22).

Christopoulos C., Filiatrault A. (2006). Principles of Passive Supplemental Damping and Seismic Isolation. pp. 1-190, 301-354. Pavia, Italy : IUSS Press.

Chopra, A. K. (2007). Dynamics of structures: Theory and applications to earthquake engineering. Prentice Hall.

Constantinou, M. C., Kalpakidis, I., Filiatrault, A., Ecker Lay, R. A. (2011). LRFD-Based Analysis and Design Procedures for Bridge Bearings and Seismic Bearings, Technical Report MCEER-11-0004, Multidisciplinary Center for Earthquake Engineering Research, Buffalo, New York.

FEMA (2020). NEHRP Recommended Seismic Provisions for New Buildings and Other Structures (FEMA P-2082-1), Chapter 18. Federal Emergency Management Agency.

Kareem, A. (1990). Reduction of wind induced motion utilizing a tuned sloshing damper. Journal of Wind Engineering and Industrial Aerodynamics, 36, 725-737.

Mahmoodi, P., Robertson, L., Yontar, M., Moy, C. ve Feld, L. (1987). Performance of viscoelastic dampers in world trade center towers. Dynamics of structures, New York, 632-644.

NEHRP (2015). Recommended Seismic Provisions for New Buildings and Other Structures, FEMA P-1050.

Peralta,H.A.C. (2018). Performance-based design of bolted steel structures, Dissertation Master in Civil Engineering – Building Construction, Leiria.

Saaed T. E., Nikolakopoulos G., Jonasson J-E. and Hedlund H. (2015). A state-of-theart review of structural control systems, Journal of Vibration and Control, 21(5), 919-937.

Soong, T. T., and Dargush, G. F. (1997). Passive energy dissipation systems in structural engineering. John Wiley & Sons.

Taylor, M. A. (2001). Passive control of structures: Applications to building and bridge design.

TBEC-2019 (2019) Turkey building earthquake code, Ministry of Public Works and Settlement, Ankara, Turkey.

Titirla, M. D. (2023). A state-of-the-art review of passive energy dissipation systems in steel braces. Buildings, 13(4), 851.

Evaluating Photovoltaic Panel Efficiency During the Cooling Season in Mersin: Insights from Alternative Performance Models

Fatih Ünal*

Merve Şentürk Acar[2]

Bünyamin Demir[3]

[1]Engineering Faculty, Mersin University, Turkey *(fatihunal@mersin.edu.tr)
[2]Engineering Faculty, Bilecik Şeyh Edebali University, Turkey
[3] Engineering Faculty, Mersin University, Turkey

ABSTRACT

This study analyzes the performance of photovoltaic (PV) panels in Mersin during the cooling season using different performance models. Accurate performance assessments are crucial for enhancing the efficiency of PV panels and maximizing the benefits of solar radiation. In this context, the use of various modeling techniques is necessary, taking into account the solar radiation intensity during the summer months. The study combines local meteorological data from Mersin with EnergyPlus software to evaluate the energy production capacity of PV panels using different performance models. Each model offers a distinct approach to calculating energy production, considering Mersin's unique geographical and climatic conditions. The research systematically compares the efficiency outcomes of these models and highlights their respective strengths and weaknesses. The results show that the accuracy levels of each model in evaluating PV panel performance during the summer season vary. The study emphasizes that selecting the appropriate performance model is critical for accurately reflecting PV panel efficiency and optimizing energy production. This research highlights the contributions of various models in assessing PV panel performance during the cooling season and underscores their potential to improve regional energy efficiency.

Keywords – Photovoltaic Panel Efficiency, Performance Models, Cooling Season, Mersin, Solar Radiation

I. INTRODUCTION

In today's world, there is a growing shift towards renewable energy sources to meet energy needs sustainably. In this context, photovoltaic (PV) systems stand out due to their environmental benefits and their potential to ensure sustainability in energy production. Thanks to its geographical location, Mersin has a high potential for solar energy. This region, characterized by a Mediterranean climate, receives abundant sunlight throughout the year. However, during the summer months, increased temperatures and high humidity levels can negatively impact the energy production capacity of PV panels. These environmental factors can lead to fluctuations in energy production during the cooling season and make it challenging for PV panels to operate optimally. In this regard, selecting the appropriate performance models to evaluate PV panel efficiency and optimize energy production is very important. Effective performance analysis requires not only the optimization of panel placement and tilt angles but also a comprehensive assessment of environmental factors. Accurate performance models can help minimize efficiency losses during the summer months and enhance overall energy production efficiency.

This study aims to evaluate the performance of PV panels in the Mersin region during the cooling season using various models and to compare their

effectiveness. By analyzing the results of different performance models, the research seeks to identify the necessary strategies to ensure PV panels operate at maximum efficiency. The findings from this evaluation will contribute to the development of strategies that help PV systems perform more efficiently during the cooling season and reduce seasonal fluctuations in energy production.

Numerous studies have examined the performance of PV systems from different perspectives, such as system design, the impact of environmental factors, and optimization of energy production through software simulations. For instance, Altınkok (2021) assessed Turkey's solar energy potential and performed simulations for a PV system planned to be installed on the roof of the Engineering Faculty at Giresun University using PVSol software. The simulation revealed that the system could meet 52% of the annual energy demand. This study demonstrates the effectiveness of PVSol software in designing realistic and efficient PV systems [1]. Similarly, Rout and Kulkarni (2020) optimized the design of a 2 kW rooftop PV system in Odisha and analyzed its energy production capacity in detail. Their work showcased the potential of software simulations to enhance the energy output of PV systems [2]. Kazem and Chaichan (2015) highlighted the significant impact of relative humidity on PV system performance, noting that relative humidity is inversely related to parameters such as solar radiation, wind speed, and ambient temperature [3]. Park et al. (2013) identified a linear relationship between temperature and relative humidity, while Mekhilef et al. (2012) explored the interconnected effects of dust, humidity, and wind speed on PV efficiency [4-5]. Chaichan and Kazem (2016) found that while wind has a minimal effect on module temperature, high relative humidity adversely affects solar radiation and panel performance [6]. These studies collectively emphasize the need for a holistic approach to understanding the role of environmental factors in optimizing PV system efficiency. This research aims to contribute to the existing literature by evaluating the efficiency of PV panels during the cooling season in Mersin using various performance models and comparing their effectiveness.

II. MATERIALS AND METHOD

This study was conducted at the Faculty of Engineering in Mersin, Turkey. The region's climatic conditions and varying solar radiation data during the cooling season were used to analyze the performance of photovoltaic (PV) panels. Hourly meteorological data, including air temperature, wind speed, and solar radiation, were collected and utilized in the analysis. In this research, multicrystal photovoltaic module panels were selected.

To evaluate the performance of PV panels during the cooling season, three distinct performance models were employed. These models include the Simple Model, the Sandia Model, and the One-Diode Model. Each model was chosen for its strengths in simulating PV performance under different

environmental and operational conditions. Simulations were conducted using EnergyPlus software, a powerful tool for modeling energy usage in buildings and renewable energy systems.

The Simple Model predicts the efficiency of PV panels based on fundamental physical principles. It depends on key parameters such as solar radiation and temperature. While this model has the advantage of faster computation, it is limited in terms of sensitivity to environmental variables. The Sandia Model, on the other hand, focuses on analyzing the electrical and thermal behaviors of PV panels in greater detail. This model accounts more accurately for environmental factors such as module temperature and irradiance intensity. The One-Diode Model simulates the electrical behavior of PV cells using a diode equivalent circuit, considering technical details such as internal panel losses and temperature, providing high-accuracy predictions.

For each month included in the cooling season, hourly meteorological data were input into EnergyPlus software. The efficiency of PV panels was assessed using the Simple, Sandia, and One-Diode models in the simulations. The results from these analyses provided a comprehensive dataset to understand the performance of PV panels.

The collected data were compared across the three models to analyze the relative efficiency of each. This comparison provided a basis for evaluating model performance under the specific conditions encountered in the Mersin region during the cooling season. The results enabled the identification of the most effective model for optimizing PV panel energy production.

This methodological approach aims to provide a comprehensive analysis of PV panel efficiency, considering the climatic challenges faced in Mersin during the summer months. The use of different models offers valuable insights into strategies for enhancing the energy production capacity of PV systems under conditions of reduced solar radiation.

III. RESULTS

In this study, the efficiency of PV panels was analysed using different performance models for the period designated as the cooling season in Mersin. The changes in meteorological data during the cooling season, which were used for the analysis, are presented in Table 1.

Table 1. The monthly averages of meteorological values during the cooling season

Month	Outdoor Air Temperature [°C](Monthly)	Wind Speed [m/s](Monthly)	Solar Radiation Rate per Area [W/m^2](Monthly)
May	21.941	2.299	254.734
June	25.778	2.393	266.711
July	28.760	2.391	262.988
August	29.045	2.288	287.869
September	25.593	2.203	252.118

The provided data show the monthly average values of air temperature, wind speed, and solar radiation levels during the cooling season in the Mersin region. In May, the average air temperature was 21.94°C, which increased to 28.76°C in July and 29.05°C in August. This indicates that July and August were the hottest months, with high temperatures potentially negatively affecting the efficiency of photovoltaic (PV) panels. However, these values are monthly averages, and it is important to note that there may be moments during specific days and hours when temperatures could be significantly higher or lower. Wind speed remained relatively constant throughout the season but decreased from 2.299 m/s in May to 2.203 m/s in September. As with air temperature, the variations in wind speed are also monthly averages, and specific days may experience higher or lower wind speeds. Wind can help cool PV panels, potentially allowing them to operate more efficiently in high temperatures. The decrease in wind speed during the summer months could lead to higher panel temperatures. Solar radiation levels averaged 254.734 W/m² in May, rising to 287.869 W/m² in August. June and July also experienced high solar radiation levels, with values of 266.711 W/m² and 262.988 W/m², respectively. However, solar radiation decreased to 252.118 W/m² in September. This demonstrates that while solar radiation is high during the summer, allowing PV panels to produce maximum energy, the radiation decreases in September. It is important to remember that these values represent monthly averages, and solar radiation can vary significantly at different times of the day. These data reveal the factors influencing the efficiency of PV panels during the cooling season in the Mersin region. It is evident that PV systems generate more energy during the summer months when solar radiation is higher, but excessive temperatures can reduce panel efficiency. Additionally, changes in wind speed are an important factor affecting panel performance. While monthly averages provide a general overview, variations in these values during specific days and hours should be considered, as they may impact the performance of PV systems. The results for PV panels during the cooling season, based on different performance models, are presented in Table 2.

Table 2. Results of PV panel performance during cooling season months

Month	Model	Produced DC Electric Power [W](Monthly)	PV Cell Temperature [°C](Monthly)	PV Efficiency (%)
May	SANDIA	17.520	29.022	6.330
	SIMPLE	22.467	24.284	8.050
	ONE-DIODE	19.650	25.284	7.560
June	SANDIA	17.745	33.306	6.310
	SIMPLE	23.523	27.164	8.730
	ONE-DIODE	20.180	29.164	7.470
July	SANDIA	17.312	36.069	6.210
	SIMPLE	23.195	31.060	8.170
	ONE-DIODE	19.712	32.060	7.290
August	SANDIA	18.690	37.177	5.850
	SIMPLE	25.390	31.202	7.870
	ONE-DIODE	21.608	32.202	6.730
September	SANDIA	16.960	32.784	5.530
	SIMPLE	22.236	27.590	7.270
	ONE-DIODE	19.027	28.590	6.280

The data presented in the table show how the three different performance models used for photovoltaic (PV) panels during the cooling season (May - September) in the Mersin region resulted in varying outcomes for DC electricity generation, panel temperatures, and efficiency rates. According to the SANDIA model, the DC electricity produced by the PV panels and their efficiency were generally lower compared to the other models. For instance, in May, the SANDIA model produced 17.520 W of electricity with an efficiency of 6.33%. In July, the electricity generation decreased to 17.312 W, and the efficiency dropped to 6.21%. PV cell temperatures in the SANDIA model were generally higher than those in the other models. In July, the temperature reached 36.069°C, which could potentially lead to a decrease in panel efficiency. High temperatures typically have a negative effect on the

efficiency of PV panels, causing power losses. In the SIMPLE model, PV panels generally produced higher electricity compared to the other models. In May, the model generated 22.467 W of electricity, with an efficiency of 8.05%. In July, the electricity production increased to 23.195 W, achieving an efficiency of 8.17%. Panel temperatures in the SIMPLE model were lower than in the SANDIA model. In May, the temperature was 24.284°C, and in July, it was 31.060°C. This suggests that lower temperatures may enhance panel efficiency. A similar trend was observed in the ONE-DIODE model. While electricity generation and efficiency were similar to those of the SIMPLE model, they were generally slightly lower. In May, 19.650 W of electricity was generated with an efficiency of 7.56%, and in July, 19.712 W of electricity was produced, with an efficiency of 7.29%. PV cell temperatures in the ONE-DIODE model were generally similar to those in the SIMPLE model but were still slightly higher. In all models, panel temperatures increased, and efficiency decreased during the summer months (June, July, August). This indicates that PV panels are temperature-sensitive, and as the temperature rises, their efficiency declines. The SIMPLE model achieved the highest electricity production and efficiency, particularly in May and July. It can be concluded that this model operates more efficiently at lower temperatures compared to the other models. The SANDIA model exhibited the lowest efficiency, as it appeared to experience more significant losses at higher temperatures, with efficiency declining markedly as the temperature increased. The ONE-DIODE model, although not as efficient as the SIMPLE model, still performed as the second best in terms of energy production. In conclusion, different performance models reflect how environmental factors such as temperature, wind speed, and solar radiation affect the efficiency of PV panels in various ways. Therefore, selecting the most suitable model for specific climatic conditions is crucial for optimizing energy efficiency and production.

IV. DISCUSSION

In this study, the comparison of different performance models for evaluating PV panel efficiency in Mersin's cooling season reveals the significant influence of environmental factors, such as temperature, wind speed, and solar radiation, on the efficiency of solar systems. The SIMPLE model demonstrated superior performance, particularly under lower temperature conditions, highlighting its suitability for hot climates. However, the SANDIA model showed a marked decrease in efficiency, primarily due to power losses at higher temperatures. These findings suggest that selecting the most appropriate model is crucial for optimizing PV system performance, particularly in regions with extreme climatic conditions. Future research could focus on refining these models to account for a broader range of environmental factors, improving the accuracy of energy production predictions.

V. CONCLUSION

This study compares three different models used to evaluate the performance of photovoltaic (PV) panels during the cooling season in the Mersin region. The SANDIA, SIMPLE, and ONE-DIODE models were examined to determine how environmental factors affect the results. The findings indicate that the impact of each model on PV panel efficiency varies depending on environmental conditions and temperature fluctuations. The SIMPLE model consistently provided higher electricity production and efficiency across all months compared to the other models. In particular, during May and July, efficiency was higher due to the lower panel temperatures. This model, which operates more efficiently at lower temperatures, stands out as a viable option for enhancing PV panel efficiency during the summer months. The ONE-DIODE model yielded results similar to the SIMPLE model but generally produced slightly lower electricity generation and efficiency. In contrast, the SANDIA model demonstrated the lowest efficiency, especially under high-temperature conditions where greater power loss occurred. In conclusion, this research emphasizes the importance of selecting the correct model to optimize PV panel efficiency. The performance of PV systems is influenced by environmental factors such as temperature, wind speed, and solar radiation, and each of these factors can affect the accuracy of the chosen model. In this context, the SIMPLE model, due to its superior performance at lower temperatures, is deemed more suitable for hot climates such as Mersin. Future studies could further explore the performance of PV panels under different climatic conditions and develop more effective strategies to improve regional energy efficiency. This study contributes to enhancing the accuracy of models used to evaluate and optimize the performance of photovoltaic energy systems.

REFERENCES

[1] Altınkok, S. (2021). *Design and analysis of a photovoltaic system suitable for the needs of Giresun University Faculty of Engineering*, (Master's thesis). Graduate School of Natural and Applied Sciences, Giresun University, Giresun.

[2] Rout, K. C., & Kulkarni, P. S. (2020). Design and performance evaluation of proposed 2 kW solar PV rooftop on-grid system in Odisha using PVsyst. *In 2020 IEEE International Students' Conference on Electrical, Electronics and Computer Science (SCEECS)* pp. 1-6. IEEE.

[3] Kazem, H. A., & Chaichan, M. T. (2015). Effect of humidity on photovoltaic performance based on experimental study. *International Journal of Applied Engineering Research*, 10(23), 43572-43577.

[4] Park, N. C., Oh, W. W., & Kim, D. H. (2013). Effect of temperature and humidity on the degradation rate of multicrystalline silicon photovoltaic module. *International Journal of Photo-energy*, vol. 9(5). https://doi.org/10.1155/2013/925280

[5] Mekhilef, S., Saidur, R., & Kamalisarvestani, M. (2012). Effect of dust, humidity and air velocity on efficiency of photovoltaic cells. *Renewable and Sustainable Energy Reviews*, 16, 2920-2925.
[6] Chaichan, M. T., & Kazem, H. A. (2016). Experimental analysis of solar intensity on photovoltaic in hot and humid weather conditions. *International Journal of Scientific and Engineering Research*, 7(3), 91-96.

Assessment of Photovoltaic Panel Efficiency at Various Tilt Angles in Mersin Province During the Cooling Season

Fatih Ünal[*]

Merve Şentürk Acar[2]

Bünyamin Demir[3]

[1]*Engineering Faculty, Mersin University, Turkey*
[2]*Engineering Faculty, Bilecik Şeyh Edebali University, Turkey*
[3] *Engineering Faculty, Mersin University, Turkey [*](fatihunal@mersin.edu.tr)*

ABSTRACT

This study evaluates the efficiency of photovoltaic (PV) panels in Mersin Province during the cooling season by analyzing performance optimization under varying tilt angles. During the summer months, when solar radiation reaches the Earth at higher angles, it is crucial to adjust PV panels to the optimal tilt angles to maximize efficiency. For this purpose, local meteorological data for Mersin Province were analyzed using the EnergyPlus software, and the performance of PV panels under various tilt angles was simulated. The study examines the variations in panel efficiency caused by environmental conditions and evaluates the outcomes achieved at different tilt angles. Through the integration of theoretical calculations and simulation techniques, the impact of tilt angle on the energy production of PV panels was comprehensively assessed. Initial findings indicate that steeper tilt angles during summer months enhance solar radiation capture, thereby increasing efficiency. Furthermore, the research underscores the importance of determining optimal tilt angles specific to each geographical region as a key strategy to improve the efficiency of PV systems. This study contributes to improving energy efficiency by identifying suitable tilt angles to optimize the performance of PV panels in Mersin Province during the cooling season.

Keywords – Photovoltaic Panel Efficiency, Tilt Angle, Cooling Season, Mersin, Solar Radiation

I. INTRODUCTION

Photovoltaic (PV) panels, a key component of the global energy transition, offer an effective technology for harnessing solar energy with high efficiency. However, the efficiency of PV systems hinges not only on the technology and materials employed but also on the alignment of the panels with the sun. This alignment, which determines the tilt angle of the panel, directly influences how effectively sunlight is absorbed. During the summer months, when solar irradiance reaches the Earth at higher angles, the importance of adjusting the tilt angles of PV panels for optimal performance becomes even more critical. Regions with Mediterranean climates, such as Mersin, Turkey, typically experience hot, sunny summers. These conditions necessitate precise optimization of tilt angles to maximize the efficiency of photovoltaic energy systems. During these months of intense solar radiation, adjusting the panel's tilt angle to match the sun's position directly impacts energy production. Accurate determination of tilt angles plays a crucial role in achieving both energy generation and economic benefits, ultimately enhancing the long-term efficiency of the system.

Recent research underscores the significance of optimizing PV panel tilt angles for efficient solar energy utilization. Studies by Gopinathan [1] and Mehleri [2], analyzing solar irradiance and tilt angles across various

geographical regions, have explored how optimal tilt angles can enhance system efficiency. Similarly, Moghadam [3] and Khorasanizadeh [4] have demonstrated how optimizing tilt angles for different climatic conditions can improve the energy efficiency of PV panels. Kazem and Chaichan [5] examined the influence of relative humidity on PV system performance, emphasizing its inverse relationship with solar irradiance, wind speed, and ambient temperature. These studies collectively highlight the importance of adapting PV systems to specific geographical and climatic conditions.

In Mersin, the combination of high temperatures and abundant sunshine during summer allows for efficient solar energy collection with appropriate tilt angles. Therefore, this study aims to investigate the performance of PV panels in Mersin and determine the optimal tilt angles throughout the summer season to optimize energy production. By doing so, solar energy generation in the region will be increased, contributing to the development of more sustainable energy systems. This research seeks to emphasize the importance of selecting appropriate tilt angles to enhance the efficiency of solar energy.

II. MATERIALS AND METHOD

This study was conducted in Mersin, a city located in southern Turkey, specifically on the campus of Mersin University's Faculty of Engineering. The primary objective was to investigate the efficiency of photovoltaic (PV) panels with varying tilt angles during the cooling season, defined as the period between May and September when solar irradiance and temperatures are typically higher. To optimize photovoltaic energy production, five distinct tilt angles (15°, 30°, 45°, 60°, and 75°) were employed. These angles were selected based on the environmental conditions prevalent in Mersin, allowing for the evaluation of panel efficiency under different parameters. The study relied on meteorological data specific to Mersin, encompassing ambient temperature, wind speed, and solar irradiance. This data was crucial for accurately simulating the performance of the photovoltaic panels and understanding the influence of environmental conditions on panel efficiency. Mersin's Mediterranean climate, characterized by significant variations in solar irradiance and temperature, plays a key role in influencing the efficiency of PV panels. To simulate the performance of the photovoltaic panels under different tilt angles, EnergyPlus software was utilized. EnergyPlus is a comprehensive energy simulation tool designed for building energy efficiency analysis and modeling the performance of renewable energy systems. It is particularly well-suited for accurately modeling the effects of solar irradiance on panels at various tilt angles. Using EnergyPlus, the efficiency of the photovoltaic systems was evaluated for each tilt angle, incorporating the collected meteorological data.

The study examined five different tilt angles: 15°, 30°, 45°, 60°, and 75°. These angles were strategically chosen to maximize the utilization of solar irradiance during the cooling season in Mersin, when solar radiation is high.

Given the higher angle of solar irradiance during this period, selecting appropriate tilt angles ensures the most efficient collection of sunlight, thereby enhancing energy efficiency. The study meticulously investigated the efficiency of photovoltaic systems across these different tilt angles.

Throughout the study, monthly average DC power output and panel efficiency served as key performance indicators to assess the impact of each tilt angle on the overall performance of the photovoltaic panels. DC power output represents the panel's electricity generation capacity in response to solar irradiance at each tilt angle, while efficiency indicates the effectiveness of this energy conversion. These performance metrics facilitated a comprehensive analysis of the influence of each tilt angle on the efficiency of the PV systems. Ultimately, this study aims to determine the optimal tilt angle for maximizing the efficiency of photovoltaic panels during the cooling season. The monthly average values of the meteorological data for the cooling season in Mersin are presented in Table 1.

Table 1 presents the monthly average values of ambient temperatures and wind speeds for the cooling season in Mersin, aiming to assess the performance of photovoltaic panels. The data reveals a consistent increase in average ambient temperature from May, with an initial measurement of 21.941 °C, through the summer months. June, July, and August recorded temperatures of 25.778 °C, 28.760 °C, and 29.045 °C, respectively, highlighting the impact of increased solar irradiance on temperature elevation during this period. By September, the temperature drops to 25.593 °C, indicating a decreasing trend towards the end of the cooling season. Analysis of wind speeds shows an average speed of 2.299 m/s in May, with minor fluctuations throughout the summer months. Wind speeds remain relatively consistent in June and July at 2.393 m/s and 2.391 m/s, respectively, before decreasing to 2.288 m/s in August and reaching the lowest value of 2.203 m/s in September. These consistently low wind speeds suggest a limited contribution to the natural cooling mechanisms of the panels. Considering that elevated temperatures can negatively impact the efficiency of photovoltaic panels, and that the cooling effect of low wind speeds may be limited, this data emphasizes the significance of temperature as a critical parameter in determining optimal panel tilt angles. Specifically, the peak temperatures observed in August, coupled with the accompanying low wind speeds, create conditions that can potentially hinder panel performance. This table provides a valuable dataset for understanding the external environmental conditions influencing photovoltaic panel performance and informing the selection of appropriate tilt angles in response to these conditions. The radiation values per unit panel area, dependent on panel tilt angles, are provided in Table 2.

Table 1. The monthly averages of meteorological values during the cooling season

Month	Outdoor Air Temperature [°C](Monthly)	Wind Speed [m/s](Monthly)
May	21.941	2.299
June	25.778	2.393
July	28.760	2.391
August	29.045	2.288
September	25.593	2.203

Table 2. The monthly averages of solar radiation per area during the cooling season

Month	Tilt Angle	Solar Radiation Rate per Area [W/m^2](Monthly)
May	15	265.7771
	30	254.7345
	45	231.4061
	60	197.2844
	75	154.4371
June	15	283.8066
	30	266.7109
	45	236.705
	60	195.832
	75	148.0207
July	15	277.4591
	30	262.9876
	45	235.5299
	60	197.0928
	75	151.2212
August	15	291.0615
	30	287.869
	45	268.6136
	60	234.8991
	75	189.3831
September	15	241.9738
	30	252.1178
	45	248.2226
	60	230.5655
	75	200.4395

Table 2 presents the average solar irradiance values (W/m²) per unit area for photovoltaic panels at different tilt angles in Mersin. The data demonstrates that variations in panel tilt angles significantly influence solar irradiance rates. In May, the highest solar irradiance rate of 265.7771 W/m² was observed at a 15° tilt angle, with a decreasing trend as the tilt angle increased. For instance, at a 75° tilt angle, this value dropped to 154.4371 W/m². This pattern was similarly observed in June and July. June recorded the highest solar irradiance at a 15° tilt angle, measuring 283.8066 W/m², which decreased to 148.0207 W/m² at a 75° tilt angle. July also showed a maximum value of 277.4591 W/m² at a 15° tilt angle, falling to 151.2212 W/m² at 75°. August differed slightly, with the highest irradiance rate recorded at a 30° tilt angle (287.869 W/m²). However, the irradiance value at a 15° tilt angle was very close at 291.0615 W/m². This suggests that minor tilt angle variations in August do not significantly impact solar irradiance. Nonetheless, a notable decrease to 189.3831 W/m² was still observed at a 75° tilt angle. In September, the impact of tilt angle variations became more pronounced. A 15° tilt angle resulted in an irradiance rate of 241.9738 W/m², increasing to 248.2226 W/m² at 45°. However, irradiance values dropped to 230.5655 W/m² and 200.4395 W/m² at 60° and 75° tilt angles, respectively.

This data underscores the need to optimize the tilt angle of photovoltaic panels throughout the year to maximize solar energy collection efficiency in Mersin. Generally, lower tilt angles (especially 15° and 30°) yield higher irradiance rates during the summer months, while steeper angles (45°) can also be beneficial in September. These findings highlight the importance of seasonal tilt angle adjustments to enhance panel performance.

III. RESULTS

This study evaluated the performance of photovoltaic (PV) panels in Mersin, Turkey, throughout the cooling season, examining the effects of tilt angle and seasonal variations. The findings of this investigation are presented in Table 3.

Table 3. Results of PV panel performance with different tilt angles during cooling season months

Tilt Angel		Month				
		May	June	July	August	September
15	Produced DC Electric Power [W](Monthly)	18.293	18.882	18.265	18.975	16.385
	PV Efficiency (Monthly)	6.302	6.304	6.174	5.863	5.557
	PV Cell Temperature [°C](Monthly)	29.337	33.800	36.482	37.273	32.497
30	Produced DC Electric Power [W](Monthly)	17.520	17.745	17.312	18.690	16.960
	PV Efficiency (Monthly)	6.332	6.311	6.206	5.847	5.534
	PV Cell Temperature [°C](Monthly)	29.022	33.306	36.069	37.177	32.784
45	Produced DC Electric Power [W](Monthly)	15.957	15.784	15.539	17.490	16.702
	PV Efficiency (Monthly)	6.345	6.298	6.181	5.830	5.522

	PV Cell Temperature [°C](Monthly)	28.367	32.448	35.296	36.627	32.670
60	Produced DC Electric Power [W](Monthly)	13.592	13.044	12.999	15.332	15.585
	PV Efficiency (Monthly)	6.280	6.248	6.167	5.840	5.518
	PV Cell Temperature [°C](Monthly)	27.413	31.284	34.220	35.668	32.164
75	Produced DC Electric Power [W](Monthly)	10.556	9.708	9.833	12.278	13.567
	PV Efficiency (Monthly)	6.272	6.217	6.109	5.773	5.464
	PV Cell Temperature [°C](Monthly)	26.217	29.927	32.941	34.376	31.301

Table 3 presents an analysis of DC electrical power output, PV efficiency, and cell temperatures for each tilt angle between May and September. At a 15° tilt angle, the panels generated the highest DC electrical power output in most months, peaking at 18.975 W in August. However, PV efficiency showed a gradual decline throughout the season, decreasing from 6.302% in May to 5.557% in September. This reduction correlated with an increase in PV cell temperatures, which reached their highest point in August at 37.273 °C. Steeper tilt angles (45° and 60°) resulted in lower power output during the summer months, but exhibited a slight increase in September as the solar irradiance angle became more favorable. For instance, at a 45° tilt, power

generation reached 16.702 W in September, approaching the output observed at a 15° tilt in the same month. Similarly, PV efficiency fluctuated between 6.272% and 6.345% across all tilt angles, with cell temperatures remaining lower at higher tilts. This suggests that lower cell temperatures may help mitigate efficiency losses. The steepest tilt angle of 75° yielded the lowest power output and efficiency values throughout the season. In June, DC power dropped to 9.708 W, while efficiency decreased to 5.464% in September. However, this tilt angle also maintained the lowest cell temperatures, averaging 29.927 °C in June and decreasing further in September. These results highlight the trade-off between selecting optimal tilt angles for energy generation and minimizing efficiency losses by maintaining lower panel temperatures. Overall, shallower tilt angles (15° and 30°) are more favorable for maximizing energy production during the peak cooling season months of May to August. However, a 45° tilt angle may optimize performance in September. These findings underscore the importance of implementing seasonal tilt angle adjustments to enhance the efficiency of PV panels and maximize energy yield.

IV. DISCUSSION

The findings of this study demonstrate that the performance of photovoltaic panels is significantly influenced by tilt angle and seasonal variations. Shallower tilt angles (specifically 15° and 30°) were found to maximize solar irradiance collection and increase energy production during the summer months. However, the rise in cell temperatures emerged as a significant factor limiting PV efficiency. Steeper tilt angles, particularly 45° and 60°, resulted in lower cell temperatures, contributing to more stable efficiency outcomes. This data emphasizes the importance of implementing seasonal tilt angle adjustments to optimize the performance of PV panels in hot climates like Mersin. Adjusting tilt angles to balance solar irradiance capture with temperature mitigation offers an effective strategy for enhancing energy production while minimizing efficiency losses.

V. CONCLUSION

This study conducted a comprehensive evaluation of photovoltaic panel performance in Mersin, Turkey, during the cooling season, examining the impact of tilt angle and seasonal variations. The results underscore the critical importance of tilt angle optimization in hot climates to maximize energy generation and maintain panel efficiency. It was determined that shallower tilt angles (15° and 30°) captured the highest solar irradiance and yielded the greatest power output during the summer months. However, increased cell temperatures at these angles emerged as a significant factor limiting efficiency. Steeper tilt angles (e.g., 45°) demonstrated improved performance, particularly in September as solar irradiance angles shifted, and maintained more consistent efficiency throughout the season due to lower cell

temperatures. These findings emphasize the need for adopting seasonally adjusted tilt angle strategies to optimize PV system performance in regions with high solar irradiance and significant temperature fluctuations. Such strategies can enhance energy yield, improve operational efficiency, and promote the sustainability of solar energy systems.

REFERENCES

[1] Gopinathan, K. K. (1991). Solar radiation on variously oriented sloping surfaces. *Solar Energy*, 47(3), 173-179

[2] Mehleri, E. D., Zervas, P. L., Sarimveis, H., Palyvos, J. A., & Markatos, N. C. (2010). Determination of the optimal tilt angle and orientation for solar photovoltaic arrays. *Renewable Energy*, 35(11), 2468-2475

[3] Moghadam, H., Tabrizi, F. F., & Sharak, A. Z. (2011). Optimization of solar flat collector inclination. *Desalination*, 265(1-3), 107-111.

[4] Khorasanizadeh, H., Mohammadi, K., & Mostafaeipour, A. (2014). Establishing a diffuse solar radiation model for determining the optimum tilt angle of solar surfaces in Tabass, Iran. *Energy Conversion and Management*, 78, 805-814.

[5] Kazem, H. A., & Chaichan, M. T. (2015). Effect of humidity on photovoltaic performance based on experimental study. *International Journal of Applied Engineering Research*, 10(23), 43572-43577.

Comparing VADER and BERT for Short-Text Sentiment Analysis: Challenges and Observed Variations

Ilma Lili [*1]

Endrit Xhina [1]

Anxhela Kosta [1]

Arbër Ceni [1]

Mirvjen Ulqinaku[1]

[1] Department of Computer Science, Faculty of Natural Science, University of Tirana, Albania
[*]ilma.lili@fshn.edu.al

ABSTRACT

The objective of this research is to evaluate the comparative performance of two sentiment analysis models applied to short, informal text: the rule-based model, VADER (Valence Aware Dictionary and sEntiment Reasoner), which assigns a weight to each word based on a sentiment lexicon, and BERT (Bidirectional Encoder Representations from Transformers), a deep learning model developed by Google for natural language processing (NLP), recognized for its capability to assess sentiment by considering word context. During the evaluation, the input text was modified to various extents, demonstrating the sensitivity of the two models by adding or removing words categorized as positive or negative. For BERT, the Hugging Face platform was utilized, offering pre-trained BERT models along with other transformer-based models, thus simplifying the process of loading, fine-tuning, and deploying these models. A pre-trained BERT model was chosen to save time and resources, considering that training large models like BERT from scratch requires substantial computational power, large datasets, and significant processing time. The short, informal text underwent gradual modifications in this comparison, beginning with 25% alteration by replacing positive words with negative ones and vice versa and evaluating both models after each change. This comparison could also be expanded to include a temporal dimension and an increase in the amount of information being evaluated, thereby highlighting a wider range of scenarios. However, the current focus of this research is intended to use short texts.

Keywords – sentiment analysis, VADER, BERT, short-text, NLP

I. INTRODUCTION

Sentiment analysis is a technique used in Natural Languages Processing (NLP) and is employed to gain a deeper understanding of a text and categorize it based on the contextual information it conveys. When utilized in evaluating comments or reviews related to a business's products or services, it strengthens the organization's accountability and integrity, aiding in the pursuit of future success. Sentiment analysis also informs decision-making algorithms in fields such as marketing, content recommendations, and public health interventions, where emotional or opinion-based data play a critical role. [1] In certain instances, sentiment analysis is applied on drug reviews. By factoring client-reported side effects expressed as negative sentiments, it allows for a more comprehensive assessment by identifying previously unconsidered cases. Additionally, on platforms featuring user-generated content, sentiment analysis can detect inappropriate, harmful, or offensive material, thereby enhancing online safety and ensuring adherence to community guidelines. Sentiment analysis is a transformative force in natural language processing, revolutionizing diverse fields such as business, social media, healthcare, and

disaster response. Emphasizing the dynamic nature of sentiment analysis, encourage further research to unlock the nuances of human sentiment expression and promote responsible and impactful applications across industries and languages. [2]. By analyzing 6,996 papers to trace the historical development of sentiment analysis from the early 20th century, it was discovered that 99% of these publications emerged after 2004, demonstrating a rapid expansion in the field. [3]. These ever-increasing subjective data are unquestionably a wealth of information for any decision-making process. The field of Sentiment Analysis has emerged to automate the analysis of such data which combines Natural Language Processing (NLP) and Machine Learning (ML) [4].

II. MATERIALS AND METHOD

The materials used during this research are informal short texts categorized as sarcasm, idiomatic, negation, and normal. The short texts include words with positive, negative, and neutral sentiments, balanced in quantity. These short texts serve as input material for further processing and evaluation through comparative methods of models that perform sentiment analysis.

The Jupyter notebook is an open-source, browser-based tool functioning as a virtual lab notebook to support workflows, code, data, and visualizations detailing the research process [5]. It is an open-source, web-based interactive computing environment that allows writing and running python code easily.

VADER model operates using a comprehensive sentiment lexicon, comprising a list of words and phrases with associated sentiment intensity scores that reflect their positive, negative, or neutral connotations. This makes VADER particularly effective in analysing text from social media platforms, where informal language, slang, emojis, and abbreviations are prevalent. Additionally, VADER is designed to account for punctuation, capitalization, and intensifiers, which further enhance its ability to gauge sentiment nuances accurately. Sentiment scores generated by the VADER model are categorized as follows:

- Positive: Reflects the proportion of positive sentiment within the text.
- Neutral: Is the proportion of neutral sentiment.
- Negative: Shows the proportion of negative sentiment.
- Compound: A normalized score ranging from -1 (most negative) to +1 (most positive), summarizing the overall sentiment conveyed by the text.

For this research, the primary indicators used were positive, neutral, and negative sentiment categories.

Natural Language Toolkit (NTLK) was used as a library in Python script because it includes the VADER module, which holds the SentimentIntensityAnalyzer class. Meanwhile, the specified text is passed as

a parameter to the polarity_scores function, resulting in scores according to the categories.

```
from nltk.sentiment.vader import SentimentIntensityAnalyzer
import nltk
```

```
sid = SentimentIntensityAnalyzer()
```

```
text="The new initiative showed promising potential with creative and uplifting solutions,
```

```
score = sid.polarity_scores(text)
```

```
print(score)  # Returns a dictionary with 'pos', 'neu', 'neg', and 'compound' scores
```

Fig 1 Steps followed for applying VADER model, in sentiment analyses of the short-text

BERT (Bidirectional Encoder Representations from Transformers) is a powerful pre-trained language model. It considers the full context of a word by looking at both sides, its left and right surrounding in this form, by capturing the nuances and context of words in a sentence more accurately. The Hugging Face library, which provides easy access to pre-trained BERT models includes excellent documentation and resources on using BERT for various NLP tasks, including sentiment analysis.

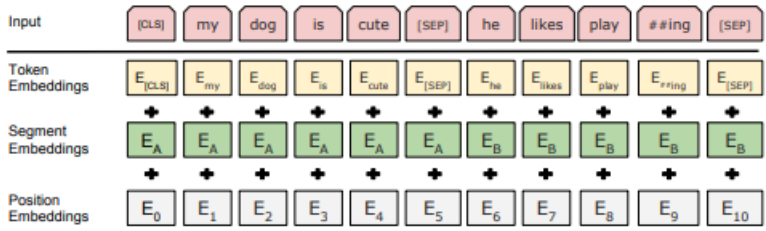

Fig 2-BERT input representation. The input embeddings are the sum of the token, segmentation and position embeddings. [6]

In BERT token embeddings refer to the contextualized representations of tokens within an input sequence. When processing input, BERT tokenizes the text into subwords or tokens, which are then converted into input vectors by combining three embeddings: token embeddings (representing the actual word pieces), positional embeddings (capturing the position of tokens in the sequence), and segment embeddings (distinguishing between different segments in input sequences). Together, these components form a contextual representation of each token based on its surrounding context, enabling BERT to perform tasks like question answering and text classification effectively [7]. A variant of BERT that we have used is bert-base-multilingual-uncased model

fine-tuned for sentiment analysis on product reviews in six languages: English, Dutch, German, French, Spanish, and Italian. It predicts the sentiment of the review as a number of stars (between 1 and 5). This model is intended for direct use as a sentiment analysis model for product reviews in any of the six languages above or for further fine-tuning on related sentiment analysis tasks. [8]. BERT model steps for sentiment analysis has the following outline:

- Text input preparation (convert text into tokens, add special tokens, truncate the input to a fixed length)
- Tokenization and encoding (input tokens converted into numerical IDs using a pre-trained BERT tokenizer).
- Embedding layers (generate word embedding for each token, combine position, token type and word to form input representation).
- Transformer layers (process input tokens using self-attention and feed forward layer).
- Extract token representation (summary of the entire input text).
- Feed into a classifier layer (applying a linear layer -in our case SoftMax to predict probability for each sentiment class-positive, negative, and neutral).
- Output sentiment score (sentiment score for each class).

Fig 3 Steps followed for applying BERT model, in sentiment analyses of the short-text

A. Comparison of results for the applied model

The aim was to compare the results achieved in sentiment analysis considering four short-text types (idiomatic, sarcasm, normal, and negation) using the VADER and BERT models. The results were categorized as Positive, Negative, or Neutral for each model, and presented in tables including not only the outputs of the two models but also human perception. It was considered that each sentence should contain a balance of words categorized as positive and negative. The data was preserved in tabular form with percentages, from which the following graphs were generated.

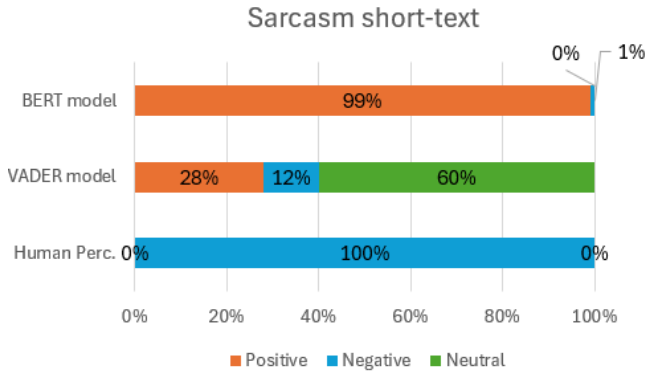

Fig 4-Sentiment result for sarcasm short-text

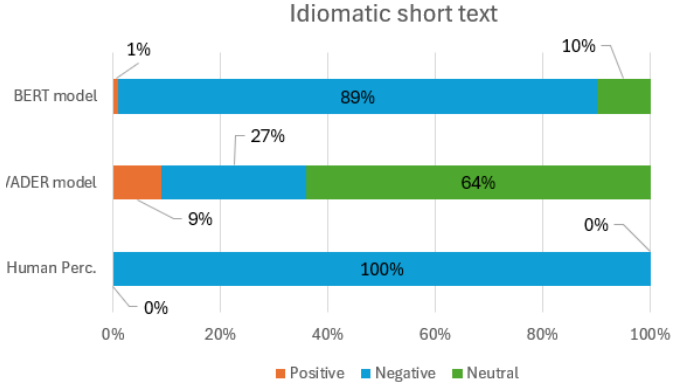

Fig 5-Sentiment result for idiomatic short-text

Figure 4 illustrates the case of a sarcastic short text where human perception categorizes it as negative. Meanwhile, the BERT model evaluates the probability of it being positive as 99% and only 1% as negative. Conversely, the VADER model's results indicate a 12% likelihood of the sentence being negative, with the highest probability being that it is neutral (60%). Figure 5 presents the evaluation of an idiomatic short text where human perception

categorizes it as negative. In this case, the result obtained from the BERT model is closer to reality compared to the VADER model, providing an 89% probability that the sentence is negative, while VADER assigns the highest probability (64%) to the sentence being neutral, thereby demonstrating BERT's greater accuracy in sentiment evaluation.

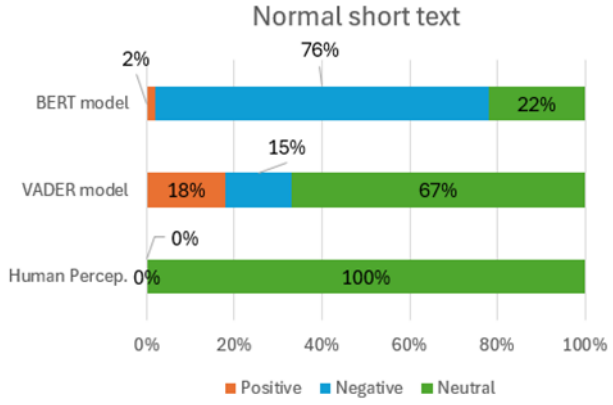

Fig 6-Sentiment result for normal short-text

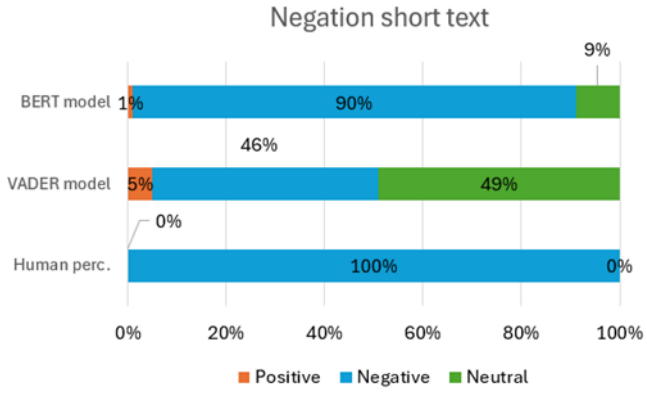

Fig 7-Sentiment result for negation short-text

Figure 6 evaluates a normal short text, where human perception categorizes it as a neutral sentence. The model that most closely aligns with the accurate result is VADER, which assigns a 67% probability that the text is neutral. In contrast, the BERT model categorizes this sentence as negative with a 76% probability, 22% as neutral, and only 2% as positive. Figure 7 illustrates the case of a negative sentence where the BERT model's assessment is closer to reality, categorizing it as negative with a 90% probability. In contrast,

the VADER model results indicate a 49% probability that the short text is neutral, a 46% probability of being negative, and only a 5% probability of being positive.

B. Evaluation of the result based on variations.

Considering that the sentences under review are balanced in terms of the number of positive, negative, and neutral words, changes were implemented starting from 25%, where for short texts with a negative outcome, positive words were replaced with negative words while maintaining the total word count. Another case involves changing a neutral short text to a positive one by replacing negative or neutral words with positive words, and so forth. All of this was done to evaluate the speed of change achieved by each model.

As observed in Figure 8, the perceived context of the sarcastic sentence is negative; therefore, positive words were replaced with negative ones at change levels of 25%, 50%, and 75%. It was noted that the rate
of change for the BERT model to reach the final result is faster compared to the VADER model, even though at the starting point, the BERT model considered there to be a 1% probability that the short text was negative, whereas VADER assessed it as 12%.

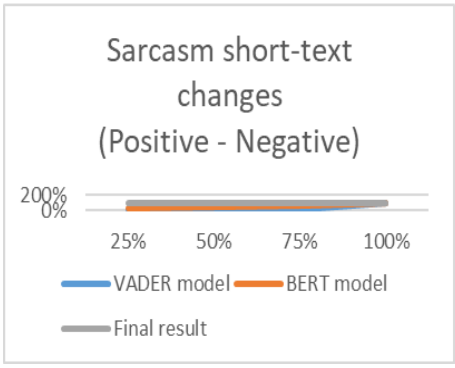

Fig 6-Sarcasm short text variation results changing negative to positive term

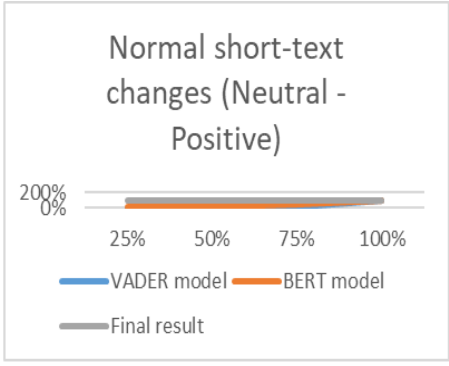

Fig 7-Normal short text variation results changing neutral to positive term

In Figure 9, the case of a neutral text is presented, in which negative words will be transformed into positive ones to achieve the status of a positive sentence. According to the VADER model, this short text is assessed to convey 18% positivity, whereas the BERT model evaluates it at approximately 2%. By changing the type of words (mainly from negative to positive), it is observed in the diagram of Figure 9 that the BERT model again progresses at a faster pace in converting the short text to a positive sentiment. Figure 10 presents the case of an idiomatic short text evaluated by human perception and the BERT model with a negative sentiment. By changing negative terms to positive ones, the aim was to observe the rate of change that

occurs according to VADER and BERT. VADER starts with a 9% positive evaluation, while BERT begins with 1%, and it is observed that in this case, VADER demonstrates a higher rate of change in converting the short text to a positive sentiment

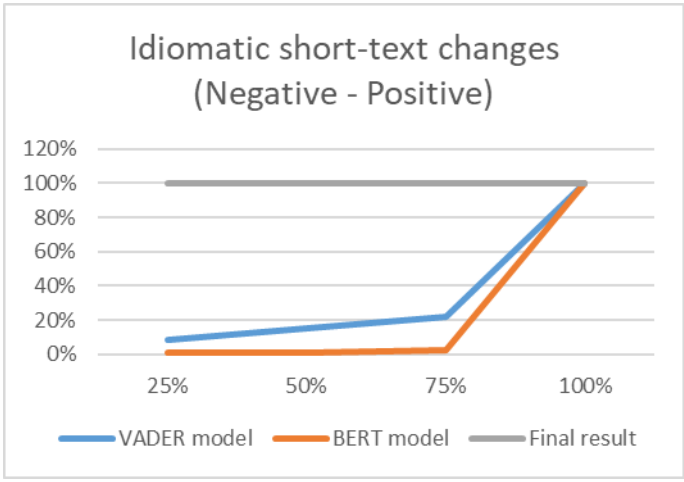

Fig 10 -Idiomatic short-text variation results changing negative to positive term

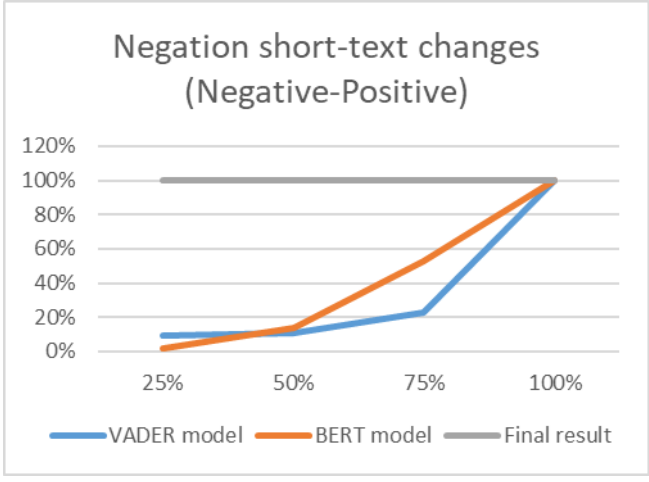

Fig 11-Negation short text variation results changing negative to positive term

Figure 11 presents the final case of a negation short text where both the sentence perception and the result from the BERT model are negative. The aim was to completely change the sentiment of the sentence from negative to positive by replacing negative words with positive ones. Initially, the VADER model evaluates the sentence as 5% positive, while the BERT model assesses

it at 1%. From the initial changes, it is observed that the rate of change in the VADER model is greater than that of BERT; however, this trend shifts, with the BERT model achieving greater changes afterward.

III. RESULTS

Figure 12 presents the results of each model, and as observed, in 50% of the cases, the BERT model aligns more closely with reality compared to the VADER model. However, there is one instance (for the sarcastic short text) where neither model provides an accurate result.

Type of short-text	Human perception	Final result	
		VADER	BERT
Sarcasm	Negative	Neutrale	Positive
Normal	**Neutrale**	**Neutrale**	Negative
Idiomatic	**Negative**	Neutrale	**Negative**
Negation	**Negative**	Neutrale	**Negative**

Fig 8-Sentiment final result for each model

During the comparison of variation, although VADER initially aligns more closely with the sentiment of the text, BERT shows a higher rate of convergence towards the proper sentiment, particularly after 50% modifications to the text.

IV. DISCUSSION

The results presented in this article are based on short-text inputs. However, evaluating the study in contexts that use such categories of sentences on a larger scale, while still employing pre-trained models, would be beneficial.

V. CONCLUSION

- The research demonstrates that BERT, provides superior accuracy and contextual understanding for sentiment analysis when compared to VADER model, especially as the complexity and changes to text increase.
- While VADER performs well with straightforward short texts and initial sentiment alignment, BERT's contextual awareness and ability to fine-tune make it better at adapting and maintaining accurate sentiment predictions as text undergoes modifications.
- The analysis highlighted that for more nuanced text types, such as idiomatic and sarcastic expressions, BERT shows a higher degree of flexibility and context-awareness, making it more reliable for complex sentiment tasks.

- Although VADER requires less computational power and provides faster results, BERT's capability to capture word context and nuances makes it a preferred choice when accuracy is paramount, justifying the higher computational resources needed for fine-tuning.
- Both models have strengths, but BERT's ability to accurately predict sentiment across diverse categories (e.g., sarcasm, negation, and idiomatic expressions) illustrates its advantage in comprehensive sentiment analysis tasks

ACKNOWLEDGMENT

Acknowledgments go to the co-authors of this research who contributed to the detailed analyses and writing and for their invaluable contributions, expertise, and collaboration throughout the entirety of this research.

REFERENCES

[1] K. P. Gunasekaran, "Exploring Sentiment Analysis Techniques in Natural Language Processing: A Comprehensive Review," *International Journal of Advanced Research in Computer And Communication Engineering Vol. 8, Issue 1, January 2019*, 2023.

[2] Sharma, N.A., Ali, A.B.M.S. & Kabir, M.A., "A review of sentiment analysis: tasks, applications, and deep learning techniques," *International Journal of Data Science and Analytics*, pp. 2364-4168, 2024.

[3] Mika V. Mäntylä, Daniel Graziotin, Miikka Kuutila,, "The evolution of sentiment analysis—A review of research topics, venues, and top cited papers,," *Science Direct*, vol. 27, pp. 16-32, 2018.

[4] Subrata Saha, Md. Imran Hossain Showrov, "VADER vs. BERT: A Comparative Performance Analysis for Sentiment on Coronavirus Outbreak," in *International Conference on Machine Intelligence and Emerging Technologies*, 2023.

[5] Bernadette M. Randles, Milena S. Golshan, Irene V. Pasquetto, Christine L. Borgman, "Using the Jupyter Notebook as a Tool for Open Science: An Emipirical Study," 2017. [Online]. Available: https://arxiv.org/pdf/1804.05492.

[6] Jacob Devlin, Ming-Wei Chang, Kenton Lee, Kristina Toutanova, "BERT: Pre-training of Deep Bidirectional Transformers for Language Understanding," *arxiv.org*, 2019.

[7] Anna Rogers,Olga Kovaleva,Anna Rumshisky, "A Primer in BERTology: What We Know About How BERT Works," *arXiv.org*, 2020.

[8] H. Face, "bert-base-multilingual-uncased-sentiment," NLP Town.

Understanding the Impact of AI Techniques on Business Management and Process Automation

Anxhela Kosta[1]

Endrit Xhina[1]

Ilma Lili[1]

Marjana Hida[2]

[1]Department of Computer Sciences, Faculty of Natural Science, University of Tirana, Albania
[2] Researcher/ Business Administration and Management, Albania
[*](anxhela.kosta@fshn.edu.al)

ABSTRACT

This paper examines the impact of Artificial Intelligence (AI) on business management, exploring how advancements in technology have transformed and modernized management processes and practices in today's organizations. As technology becomes an integral part of daily business operations, understanding how AI has reshaped management roles and functions, bringing new challenges and opportunities, is essential for organizations. Through a detailed analysis of literature and various studies in business management and information technology, this research addresses several key areas, including process automation and efficiency, product innovation strategies, customer relationship management, market analysis, and strategic decision-making. The aim of this paper is to provide a comprehensive understanding of Artificial Intelligence's techniques impact on business management and to identify best practices and strategies for leveraging technology to achieve business objectives. A survey of 259 businesses in Albania was conducted to assess Artificial Intelligence's role in their management practices and its overall impact. The responses were analyzed and visualized in graphs to highlight significant trends and insights, providing a comprehensive overview of Artificial Intelligence's influence on business management in the Albanian context. During the analysis, Robotic Process Automation (RPA) emerged as one of the most commonly used AI techniques among these businesses.

Keywords – Artificial Intelligence (AI), Business Management, Process Automation, Strategic Decision-Making, AI Techniques, RPA(robotic process automation), CRM

I. INTRODUCTION

In today's rapidly evolving technological landscape, artificial intelligence is having a profound impact on all aspects of business. Analyzing how AI impacts business management has become a crucial and timely challenge for management science. This paper aims to examine and understand the ways in which AI is transforming management practices compared to traditional methods, highlighting both the advantages and challenges associated with this transformation. To understand the role of AI in reshaping business operations and resource management, we will compare different management approaches, with and without technology. By analyzing current work practices versus automated tools such as management software and process automation, we aim to identify the lasting benefits that AI can bring to business management. This study also explores the key role of management in integrating technology, investigating how AI can increase efficiency and effectiveness in processes, positively impacting human and financial

performance within organizations. To gain a comprehensive perspective, we conducted interviews with several companies to understand whether and how they implement AI-driven technologies in their management.

Through questionnaires and direct conversations, we aim to uncover their experiences with AI, including the advantages and challenges they encounter on their journey towards modernized management. Through recent analysis and findings, we strive to provide a clear and well-argued overview of why companies should use AI in their management processes, demonstrating how AI can bring significant improvements in efficiency, productivity, and competitiveness in an increasingly digitalized market. In particular, this paper examines how new digital tools are revolutionizing traditional methods of managing operations, human resources, and business strategies. The paper begins with a review of the stages of the technology cycle, analyzing the fundamental concepts and theories that underpin the impact of AI on business management, while discussing the advantages and challenges that come with integrating AI. Next, we explore process automation and business efficiency, focusing on how AI technologies and automation systems improve operations management. This includes an examination of the challenges and opportunities in implementing automated systems, such as investment costs, resistance to change, and data security concerns. The paper then moves on to innovation and product development, illustrating how AI supports various aspects of product development projects, from collaboration platforms and progress monitoring systems to advanced project management methodologies. We further analyze customer and user relationship management, highlighting the role of AI-driven technologies in improving the customer experience through CRM systems that effectively store and manage customer information. The role of AI in personalizing customer interactions – leveraging data analytics and content personalization tools – is also examined in depth.

Human resource management in technology-driven environments is another focal point, where we discuss the impact of AI on skill development and employee training within organizations. This includes the use of online learning platforms, personalized training applications, and virtual simulations to create more effective learning experiences. Moving to the local business landscape, we present the methodology and findings from our market analysis and study of strategic decision-making in Albania. Here, we detail the insights gathered from questionnaires and interviews with Albanian companies regarding their adoption of AI in business management. During the analysis, we also understand which AI technique is most used in Albania, which is RPA. Finally, we provide a forecast for the future of business management, focusing on the potential impact of AI on management practices. We analyze emerging trends and potential innovations that will shape the way businesses

operate and compete in the evolving digital landscape. Together, these sections provide a comprehensive overview of the transformative role that AI is playing in key areas of business management.

II. METHODOLOGY

This study employs a dual-method approach, using both secondary and primary data sources to provide a comprehensive understanding of AI's impact on business management, with a specific focus on Albania. In the **secondary research phase**, we gathered data from online library databases, industry reports, and academic publications. This data collection aimed to examine existing findings on AI in business, identify key challenges and benefits, and analyze conclusions from previous studies. By reviewing these resources, we gained foundational insights into how AI has influenced business management practices globally. In the **primary research phase**, a targeted study assessed AI technology adoption across various sectors in Albania. We selected a range of companies from both public and private sectors based on their relevance to the study. A structured survey was developed using Google Forms and organized around key themes: business sector information, identifying specific industries and business types; technology and AI adoption, examining the AI tools in use and adoption rates across sectors; challenges in technology use, exploring barriers to AI implementation within organizations; technology's role in management and efficiency, assessing AI's impact on operational efficiency and process automation; and future expectations, gauging businesses' plans for AI expansion and their perspectives on its future role in management.

Through this survey-based approach, we gained insights into AI's current perception, adoption, and impact within Albanian organizations. This methodology aims to present a balanced perspective on AI's role in reshaping business operations and to assess its potential to enhance efficiency and competitiveness in the Albanian context.

III. THE SIGNIFICANCE OF AI IN BUSINESS MANAGEMENT

In today's rapidly evolving digital world, Artificial Intelligence (AI) is transforming how businesses operate and manage processes across various industries. With more companies integrating AI-driven tools, the potential to enhance efficiency, introduce innovative solutions, and make data-based decisions is expanding rapidly. AI empowers businesses to optimize workflows, automate repetitive tasks, and extract valuable insights from large data sets, enabling analyses that were once beyond reach.

3.1. Why AI's Impact Matters

AI has emerged as a game-changer, influencing not only operational processes but also reshaping the competitive landscape. PwC estimates that by 2030, AI could contribute up to $15.7 trillion to the global economy, with sectors like finance, healthcare, and retail experiencing transformative changes [2]. Businesses today face complex demands that require agility and innovative responses. AI's ability to process vast datasets, predict outcomes, and support strategic decision-making has made it essential for businesses aiming to maintain competitiveness and foster growth in an increasingly data-driven market [1]. The adoption of AI technologies significantly enhances decision-making processes and resource management. Advanced analytics and predictive modeling allow companies to forecast trends, identify new market opportunities, and make data-informed decisions. For instance, machine learning algorithms in customer relationship management (CRM) systems improve customer interactions, personalize marketing, and build loyalty. Additionally, AI-driven automation—such as Robotic Process Automation (RPA)—reduces manual workloads, enabling employees to focus on strategic, high-value tasks [1].

3.2. The Importance of Studying AI's Role in Business Management

Understanding AI's impact on business management is crucial for modern organizations aiming to integrate these technologies effectively. With rapid advancements in AI capabilities, organizations must evaluate both the benefits and challenges of AI adoption. AI enables managers to create smarter operational workflows, optimize costs, and manage resources efficiently. However, AI integration also introduces challenges, including data privacy concerns, potential job displacement, and ethical considerations surrounding algorithmic transparency and bias [2]. This study examines how AI reshapes management practices by comparing traditional approaches with AI-enhanced methods. Through this analysis, businesses can develop sustainable strategies for integrating AI technologies, helping managers optimize performance while addressing associated challenges. As AI continues to evolve, understanding its impact on business management is essential for organizations seeking to remain competitive in an increasingly digital market.

IV. THE ROLE OF AI IN TRANSFORMING BUSINESS PROCESSES

As Artificial Intelligence (AI) continues to evolve, it is reshaping fundamental business processes across industries, enhancing both the efficiency and effectiveness of operations. Businesses today are increasingly leveraging AI to automate routine tasks, streamline workflows, and drive innovation,

resulting in more agile and responsive organizations. AI's ability to analyze large datasets, identify patterns, and make data-informed decisions allows companies to optimize operations and develop products that better meet consumer demands. This chapter explores two critical areas where AI is making a substantial impact on business processes: process automation, which enhances operational efficiency, and product development, which fosters innovation and competitiveness. By examining these areas, we gain insight into how AI not only improves current practices but also positions organizations for sustained growth and market relevance in a rapidly changing digital landscape.

4.1. Process Automation and Operational Efficiency

In today's competitive business landscape, Artificial Intelligence (AI) is redefining the efficiency and effectiveness of core business processes. A major application of AI in this realm is Process Automation. By integrating AI-driven tools into workflows, organizations can reduce the time, cost, and resources required for routine, repetitive tasks. This not only improves operational efficiency but also frees employees to focus on strategic roles that require critical thinking and creativity.

Robotic Process Automation (RPA) stands out as a powerful tool within AI-driven automation. RPA uses software robots, or "bots," to automate high-volume, repetitive tasks traditionally performed by humans, such as data entry, customer service interactions, invoice processing, and basic decision-making. RPA operates with high speed and minimal errors, enhancing both accuracy and productivity. For instance, RPA can seamlessly handle data extraction from one platform and input it into another, allowing companies to improve efficiency and reduce human error [3][4].

Beyond RPA, Intelligent Process Automation (IPA) combines RPA with advanced AI capabilities like machine learning and natural language processing (NLP). This enables businesses to automate not only structured but also unstructured tasks that were previously difficult to automate. With IPA, companies can analyze unstructured data, such as emails or customer service logs, and make decisions based on this data. This level of automation allows companies to manage more complex operations requiring language comprehension or decision-making informed by past patterns [4][5]. AI also enhances Business Process Management Systems (BPMS) by integrating predictive analytics, allowing businesses to optimize workflows in real-time. Through continuous monitoring and predictive insights, AI-enhanced BPMS can detect bottlenecks and recommend adjustments, fostering more responsive and resilient operations. This proactive process management reduces operational downtime and enables strategic resource allocation. In high-

volume sectors like logistics and manufacturing, this approach can lead to substantial cost savings and increased output [6][7].

Case Study Example: In the financial sector, RPA is widely used to manage customer interactions, data verification, and compliance tasks. Banks and insurance companies leverage RPA to streamline customer onboarding, automate risk assessments, and generate regulatory reports with high accuracy. By automating these processes, companies reduce processing time, ensure compliance with industry standards, and ultimately enhance customer satisfaction and operational efficiency [5].

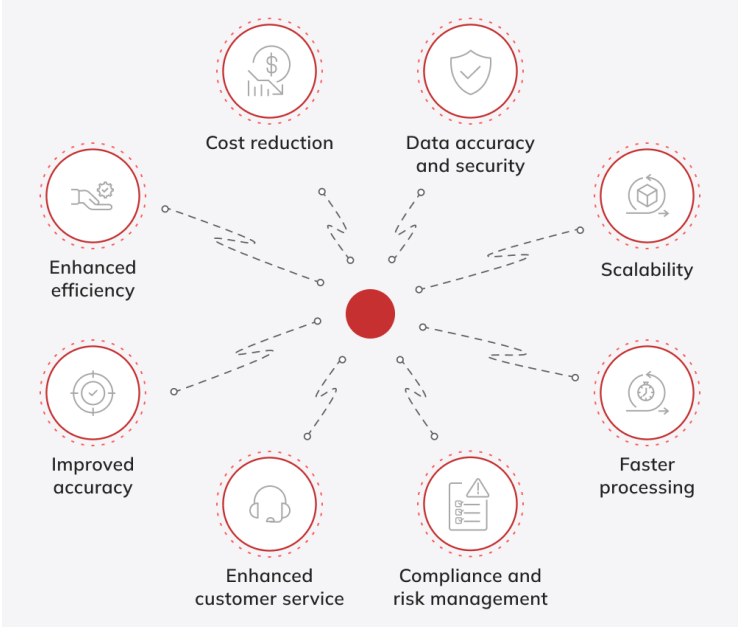

Fig. 1 RPA in Bank Industry [8]

4.2 Innovation and Product Development

AI is transforming operational processes and serving as a key driver of innovation and product development. With AI, companies gain deeper insights into consumer preferences and market trends, enabling them to develop products closely aligned with customer needs. This data-driven approach to innovation is crucial in today's fast-paced markets, where competitiveness often depends on a company's ability to respond quickly to changing customer demands.

Advanced Data Analytics play a central role in product development by enabling companies to collect and analyze large volumes of data from sources

like customer feedback, market trends, and competitor analysis. Machine learning models can identify patterns and predict customer preferences, allowing companies to tailor product development more accurately to meet consumer demands. For example, in the technology sector, user data analysis helps companies prioritize features in new product versions, thereby improving user satisfaction and retention [7][5]. AI also facilitates rapid prototyping and product testing, speeding up the development cycle. Through simulations and predictive modeling, AI can forecast product performance, identify potential design flaws, and suggest improvements before physical prototypes are built. This reduces the time and costs associated with traditional trial-and-error approaches, enabling faster market entry. For instance, in the automotive industry, AI-driven simulations predict vehicle performance under different conditions, reducing the need for extensive physical testing and accelerating development timelines [4][7].

Collaborative Product Development is another area where AI makes a significant impact. AI-powered platforms enable real-time data sharing across departments, enhancing communication and decision-making. These platforms allow engineers, designers, and marketers to work cohesively, ensuring that product development aligns with market needs and business goals. For instance, AI tools in collaborative software can recommend modifications based on historical data, providing team members with actionable insights that improve product quality and reduce development time [6].

Enhancing Competitive Advantage through AI-Driven Innovation: AI enables companies to create and launch products that meet current demands and anticipate future trends. By continuously analyzing market and consumer data, AI helps businesses stay ahead of competitors, allowing them to identify market gaps and introduce innovative products earlier, establishing a first-mover advantage. Furthermore, AI's ability to rapidly process large datasets allows businesses to respond to real-time market shifts, enhancing adaptability in a dynamic economic landscape [7][5].

Case Study Example: In the retail sector, companies leverage AI to predict fashion trends and optimize inventory based on seasonal demands. By analyzing historical sales data, social media trends, and weather patterns, AI systems help retailers determine which products are likely to sell well and adjust stock accordingly. This approach minimizes inventory costs, reduces waste, and maximizes sales potential, giving retailers a competitive edge [5].

V. AI IN CUSTOMER AND HUMAN RESOURCE MANAGEMENT

In modern business, Artificial Intelligence (AI) plays a crucial role in managing customer relationships and human resources. AI-driven tools allow businesses to personalize customer interactions, enhance engagement, and foster loyalty through data insights. In HRM, AI applications streamline recruitment, training, and employee development, enabling companies to attract and retain top talent more efficiently. This chapter explores AI's impact on Customer Relationship Management (CRM) and Human Resource Management (HRM).

5.1 Improvement Customer Relationship Management (CRM

Customer Relationship Management (CRM) has become a cornerstone of business strategy for understanding and meeting customer needs. By maintaining detailed customer information—ranging from contact details to past purchases and preferences CRM systems enable businesses to build and sustain strong customer relationships. Through advanced analytics and reporting, CRM platforms allow companies to gain deeper insights into customer behavior and preferences, enabling them to tailor services and products more effectively to match these needs. This approach not only enhances customer satisfaction but also fosters loyalty, which is crucial for business success in competitive markets [9].

One of the primary functions of CRM is to enable personalized communication. By leveraging data collected through CRM systems, businesses can create targeted offers and messages that resonate with individual customers [10] . This personalized approach enhances the customer experience and strengthens engagement, as clients feel valued and understood. Studies show that personalized interactions foster greater loyalty and trust, both of which are essential for long-term customer retention.

CRM systems also allow companies to manage customer interactions across the entire customer lifecycle—from initial engagement to post-purchase support and loyalty-building. This end-to-end management enables businesses to maintain a full communication history, which sales and customer service teams can access to meet customer needs efficiently. For example, a CRM system can track various touch points such as phone calls, emails, and in-person meetings, creating a seamless experience for the customer and ensuring that teams can address inquiries based on a complete interaction history [11].

Improving Sales and Marketing Effectiveness with CRM

In the Albanian business landscape, CRM usage is gradually increasing, especially among medium-sized and large enterprises. Initially, CRM adoption focused on stabilizing customer relationships, as it allowed companies to organize and track customer data in a more systematic way. CRM systems also contribute to personalized marketing efforts. By storing detailed information on customers' preferences, needs, and past purchases, Albanian businesses can deliver more tailored messages and offers, making interactions more engaging and relevant. This personalization can improve response rates and increase customer satisfaction, as customers receive communications that align with their interests. Beyond relationship management, CRM systems significantly improve the effectiveness of sales and marketing efforts. By analyzing data and generating reports, CRM tools allow businesses to identify trends and preferences among customers, enabling them to assess the effectiveness of their marketing and sales strategies. This data-driven approach empowers companies to refine their strategies to better meet customer expectations and maximize business results. CRM systems drive increased customer loyalty by increasing the quality and responsiveness of customer support. By keeping comprehensive records of interactions and preferences, CRM tools enable businesses to provide personalized services in a timely manner, which helps build trust and long-term relationships with customers[11]. This is especially valuable for Albanian businesses looking to gain a competitive advantage in a market where customer loyalty can significantly impact success [13].

5.2. Impact on Human Resources

Human Resource Management (HRM) as a scientific discipline encompasses the processes of planning, organizing, staffing, leading, and controlling. The resources available to an organization—whether human, financial, physical, or informational must be managed effectively to be utilized efficiently. In the past, the term "personnel management" implied that merely hiring employees was sufficient to meet business needs [14]. Today, employees are seen not just as expenses but as crucial resources akin to capital and other assets, even as the organization's most valuable asset. Human resource managers are responsible for planning, recruiting, selecting, and developing new employees through continuous training and education to adapt to changing demands. Thus, HRM is a process aimed at ensuring that the right people are in the right place at the right time. Training plays a central role in modern HRM and has long been recognized for its importance. As Peter Drucker stated in 1998, managers are uniquely expected to contribute to the vision and capability of their teams. Training is necessary to maintain a qualified workforce that is

technically proficient and equipped for career progression in specialized departments or leadership roles. [15]

Case Example: BKT's Technology-Improvement Recruitment

The National Commercial Bank of Albania (BKT), one of the largest banks in Albania, exemplifies the use of technology in its recruitment and selection processes to ensure accuracy and efficiency. The BKT recruitment process includes [16]:

1. **Job Posting**: BKT posts vacancies on multiple platforms, including LinkedIn, Portal i Pune, the bank's official website, and other recruitment sites, reaching a diverse pool of candidates.
2. **Applicant Tracking System (ATS)**: BKT uses ATS to streamline the application process, receiving, organizing, and filtering applications to identify suitable candidates based on experience and education.
3. **AI-Powered Analysis**: BKT employs AI algorithms to evaluate resumes and cover letters, selecting the best-suited candidates by analyzing their professional experience, education, and specific skills.
4. **Online Assessments and Video Interviews**: After initial screening, candidates complete online assessments and participate in video interviews, which include predefined questions and real-time evaluations to ensure objectivity.
5. **Online Presence Monitoring**: BKT leverages online monitoring tools to gain insight into candidates' social media activity and professional behavior.
6. **Practical Tests and Simulations**: In final stages, candidates participate in practical tasks online, simulating real-world job conditions to verify their skills.
7. **Integration and Training**: Technology facilitates new employees' onboarding through HRIS, where BKT manages documentation, delivers tailored training, and tracks progress during the probation period.

VI. MARKET ANALYSIS AND STRATEGIC TECHNOLOGY ADOPTION IN ALBANIA

In recent years, technology has rapidly permeated various industries in Albania, reshaping business practices and management approaches. This chapter examines the current state of technology adoption among Albanian businesses, focusing on the extent to which AI and other digital tools are integrated into management processes. By conducting a survey across multiple sectors including, finance, IT, small businesses, and household appliance retail this analysis provides insights into how Albanian businesses utilize technology to enhance productivity, efficiency, and customer

engagement. Through both online questionnaires and physical interviews, the study explores the types of technology employed, the benefits perceived by business owners, and the challenges they face. By identifying these key areas, this chapter aims to present a comprehensive view of technology's impact on the Albanian business landscape and provide valuable insights into the opportunities and obstacles present in the local market.

6.1 Insights from the Survey and Market Analysis

Technology has increasingly permeated Albania, influencing various industries and transforming traditional business practices. For this reason, we decided to conduct a real-world study within the Albanian market to understand whether businesses are incorporating technology into their management processes. This study involved 259 businesses across different sectors:

- Financial Sector
- IT Sector
- Electronics and Home Appliance Sector
- Small Businesses

Interviews were conducted in person with representatives from some businesses, while an online questionnaire via Google Forms gathered additional responses. The objective was to understand the impact of technology on business management, focusing on AI technology use, benefits, challenges, and its influence on business efficiency and productivity in the current environment. The questionnaire was structured into five main sections to capture information on the business sector, specific uses of technology in business operations, benefits and challenges of technology adoption, the role of technology in marketing and customer experience, and future technology outlook.

Questionnaire Organization

The initial questions focused on gathering basic information about each business's sector. This was followed by questions aimed at understanding if and how these businesses use technology in management and identifying specific types of technology utilized.

Key Findings

From the responses collected:

- **33%** of businesses use financial management applications.
- **25%** use internal management systems like CRM.

- **27%** do not use technology at all in their business operations.

Since staff management is critical for all businesses, especially those with larger teams, companies were also asked if they use technology or tools to manage their workforce. Here's a breakdown of their responses:

- **36%** still manage their staff using traditional methods.
- **33%** use systems for time tracking and performance, such as Clockify (https://clockify.me/).
- **9%** use tools specifically for employee training.

To understand how businesses handle inventory management (product inflows and outflows), participants were also asked about the systems or methods they use:

- **44%** use financial systems like Navision, Financa 5, Bilanci, or Alpha.
- **41%** still rely on Excel.
- **16%** have no system in place.

The goal of the survey and interviews was not only to see how technology impacts these businesses but also to gauge whether its influence has been positive or negative. When asked about the impact of technology, most respondents stated that it has positively affected their business, improving both staff efficiency and product management.

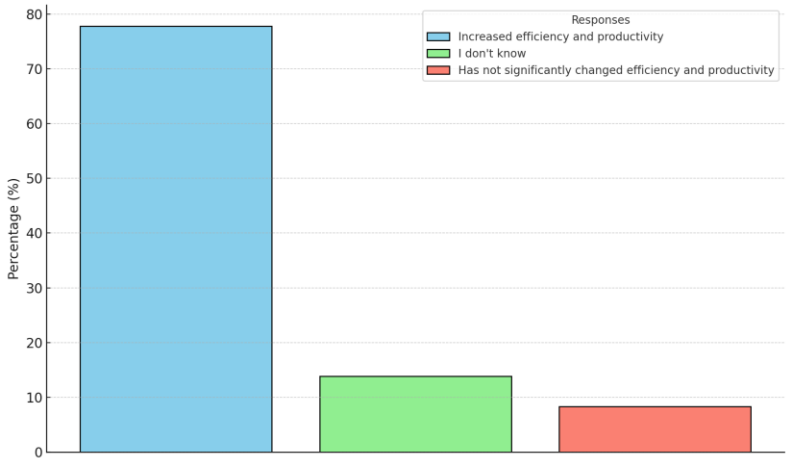

When asked about the types of AI techniques used in their businesses, 60% of respondents indicated that they use Robotic Process Automation (RPA), particularly in financial operations. This includes automating repetitive tasks

such as invoice processing, data entry, and financial reporting, which streamlines workflow and reduces human error. Also 30% of businesses reported using CRM AI to support management functions. Through CRM AI, they enhance customer relationship management by automating customer interactions, personalizing marketing efforts, and analyzing customer data to better predict needs and improve service quality. Together, these AI applications are helping businesses achieve greater efficiency and accuracy in both financial and customer management activities.

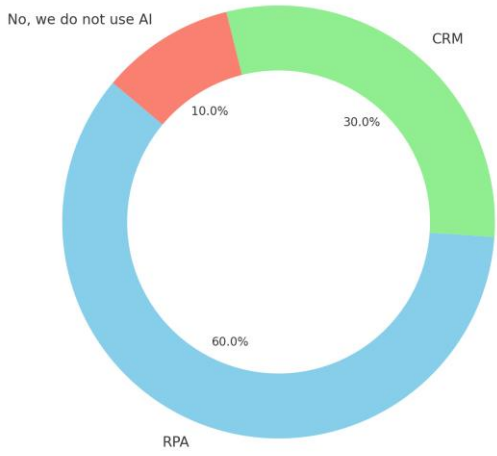

However, despite the positive impact, some business owners expressed concerns, particularly regarding data security and protection. Some are still skeptical about technology's security and reliability, and others find the high costs of implementing these systems prohibitive, as they can be expensive. Technology also presents significant opportunities for enhancing customer service. By utilizing CRM and other customer management tools, businesses can better understand and meet client needs, building stronger customer relationships and loyalty.

6.2 Challenges and Opportunities in Local Adoption

After analyzing the data from personal interviews, we identified key challenges and opportunities in technology and AI adoption among Albanian businesses. Major challenges include high costs, limited resources, data security concerns, and resistance to change due to low digital literacy, especially among SMEs. Also inadequate infrastructure in rural areas restricts technology access, widening the gap between urban and rural businesses.

Despite these challenges, technology presents significant opportunities. Automation and tools like CRM systems enhance efficiency, customer engagement, and market reach, boosting competitiveness locally and internationally. Advanced technologies like RPA support data-driven decision-making and innovation, while cloud computing enables access to global markets and remote collaboration, promoting growth and cross-border trade.

VII. THE FUTURE OF BUSINESS MANAGEMENT USING AI AND TECHNOLOGY

The future of business management is shaped by technology, bringing efficiency, flexibility, and new opportunities. AI and data analytics enable businesses to predict trends, personalize customer experiences, and streamline operations. Cloud computing and social platforms allow seamless collaboration and secure data storage, enhancing information sharing and risk management. Automation reduces repetitive tasks, freeing resources for innovation and growth. For small businesses, technology is a game-changer. AI-driven analytics, CRM, and specialized booking software improve efficiency, customer engagement, and competitiveness. Although challenges like initial costs and data security exist, the long-term benefits of technology adoption, better service quality, cost savings, and growth potential, make it essential for staying competitive in the digital age.

DISCUSSION

This study explored technology integration in Albanian business management, focusing on CRM, ERP, financial tools, and AI like RPA. Findings show technology boosts efficiency and productivity but faces cost and security challenges. CRM enhances customer relationships, while ERP supports data organization and cross-functional collaboration, aligning with global trends in improved business performance.

CONCLUSION

In conclusion, this study shows that technology positively impacts business management by automating processes that would otherwise consume valuable time. As AI advances, business management will face new challenges, but the benefits of integrating technology are clear and continue to grow. This research serves as a guide for Albanian businesses seeking to improve management practices and address challenges effectively. The study reveals that technology is essential for improving efficiency and productivity, maintaining competitiveness, and meeting modern market demands. The increasing use of AI-driven tools, particularly Robotic Process Automation

(RPA), highlights a trend towards automating operations and focusing human resources on strategic growth initiatives.

ACKNOWLEDGMENT

We would like to thank the 259 businesses and their representatives who participated in this study. Their valuable time, insights, and cooperation were essential to the completion of this research.

RECOMMENDATION

The study recommends that businesses invest in lasting technology to improve efficiency and adapt to changes. Training employees regularly on new tools helps boost productivity and lowers resistance to change. Strong security measures are important to protect sensitive data. Using systems to track performance and support training can increase employee motivation, and having a clear technology plan that aligns with business goals supports long-term success. Staying informed about new developments in AI, automation, and data analysis is important for making smart decisions, while using collaboration tools improves teamwork and communication. Regularly checking technology systems ensures they stay useful, can grow with the business, and are prepared for future needs.

REFERENCES

[1] A.Sestino , A. De.Mauro :Leveraging Artificial Intelligence in Business: Implications, Applications and Methods, 2021

[2] Y.Xiong, S. Xia, X.Wang: Artificial intelligence and business applications, an introduction, 2021

[3] V.P.Sriram, K.S. Lakshmi, V. Podile , M. Naved, K.S. Kuma r:5ROLE OF MACHINE LEARNING AND THEIR EFFECT ON BUSINESS MANAGEMENT IN THE WORLD TODAY, 2021

[4] Dumas, M., Fournier, F., Limonad, L., Marrella, A., Montali, M., Rehse, J.-R., Accorsi, R., Calvanese, D., De Giacomo, G., Fahland, D., Gal, A., La Rosa, M., Völzer, H., & Weber, I.: AI-Augmented Business Process Management, 2024

[5] V.Basri: Examining the Impact of Artificial Intelligence (AI)-Assisted Social Media Marketing on the Performance of Small and Medium Enterprises: Toward Effective Business Management in the Saudi Arabian Context. 2020

[6] K.Buntak, M.Kovačić, M.Mutavdžija:APPLICATION OF ARTIFICIAL INTELLIGENCE IN THE BUSINESS,2020

[7] Nosova, S., Norkina, A., Makar, S., Gerasimenko, T., & Medvedeva, O. Artificial Intelligence as a Driver of Business Process Transformation, 2022

[8] https://innowise.com/blog/rpa-in-banking/

[9] R. U.Khan , Y. Salamzadeh , Q.Iqbal, Sh.:YangThe Impact of Customer Relationship Management and Company Reputation on Customer Loyalty: The Mediating Role of Customer Satisfaction, 2020

[10] M. F. Pynadath, T. M. Rofn, S.Thomas: Evolution of customer relationship management to data mining-based customer relationship management: a scientometric analysis, 2022

[11] R. Ahmed, J. Omarein: Fostering Long-Term Customer Relationships by enhancing Customer Experience, 2024
[12] SH.Altarifi: THE IMPACT OF CRM ON MARKETING PERFORMANCE THROUGH INNOVATION CAPABILITY, 2020
[13] E.KALEMAJ: E-Tourism Developments: Technologies Adoption in the Albanian hospitality sector
[14] G. Anwar, N. N. Abdullah: The impact of Human resource management practice on Organizational performance, 2021
[15] M. S. Rao: Peter Druck eter Drucker's Principles, Philosophies, and Pr s Principles, Philosophies, and Practices actices , 2021
[16] https://www.bkt.com.al/